V International Conference on Permafrost in Trondheim, Norway, August 1988

PERMAFROST

PROCEEDINGS VOL. 2

TAPIR

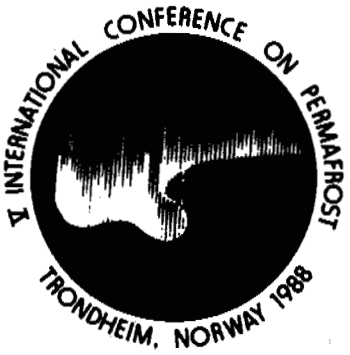

PERMAFROST

Fifth International Conference

PROCEEDINGS VOLUME 2

August 2-5, 1988

Editor:
Kaare Senneset

Organized by
The Norwegian Committee on Permafrost
The Norwegian Institute of Technology

TAPIR PUBLISHERS
Trondheim, Norway

ISBN 82-519-0863-9

Printed in Norway.

CONTENTS

VOLUME 1: SCIENCE

CLIMATE CHANGE AND GEOTHERMAL REGIME

REGIONAL PERMAFROST

PHYSICS AND CHEMISTRY OF FROZEN GROUND, FROST HEAVE MECHANISM

HYDROLOGY, ECOLOGY OF NATURAL AND DISTURBED AREAS

PERIGLACIAL PHENOMENA, GEOCRYOLOGY

VOLUME 2: ENGINEERING

SITE INVESTIGATIONS AND TERRAIN ANALYSES, SUBSEA PERMAFROST

GEOTECHNICAL PROPERTIES, FROST HEAVE PARAMETERS

GEOTECHNICAL ENGINEERING, PIPELINE CONSTRUCTION

ENGINEERING, -PETROLEUM, -MINING, -MUNICIPAL

BOREHOLE INVESTIGATIONS OF THE ELECTRICAL PROPERTIES OF FROZEN SILT

S.A. Arcone and A.J. Delaney

U.S. Army Cold Regions Research and Engineering Laboratory

SYNOPSIS The dielectric constant and attenuation rate of short radiowave pulses in frozen Fairbanks silt have been measured between boreholes 12 m deep and spaced between 4.4 and 17.6 m. The ranges for volumetric ice content and temperature were 44 to 79% and -6.0 (surface, early April) to -0.7°C (bottom) respectively. The pulses lasted approximately 30 ns, had a power spectrum centered near 100 MHz, and were transmitted and received at the same depth. Dielectric constants were determined from the propagation time delay of the leading edge and there was no significant dispersion. Attenuation rates (dB/m) were determined by comparing signal levels received between different borehole pairs and were adjusted for geometric spreading losses. Concurrent borehole dc resistivity measurements allowed estimates of the separate contributions of various loss mechanisms. The results show the dielectric constant to vary between 4.3 and 7.0 and to correlate well with the volumetric ice content, but not with temperature. Average attenuation rates at any particular depth varied between 1.4 and 4.0 dB/m. The lowest values occurred in the sections with the higher ice content. No more than 0.8 dB/m could be ascribed to conductive absorption losses, suggesting that scattering is an important loss mechanism.

INTRODUCTION

Short-pulse radar operating between 50 and 500 MHz is often used for exploration in northern regions (e.g., Annan and Davis, 1976; Davis et al., 1976; Arcone and Delaney, 1984). The freezing of soil decreases the wave attenuation at these frequencies found in the same materials when thawed. Knowledge of the electrical properties of frozen soils, which determines wave velocity and attenuation rate, is thus essential to the interpretation of radar records in northern climates.

The electrical resistivity ρ of frozen soils strongly depends on the mobility of charge carriers along networks of unfrozen water, given poorly conducting minerals. Complex dielectric permittivity ε^* depends on the relative proportions and individual properties of mineral matter, air, ice and unfrozen water (e.g., Hoekstra and Delaney, 1974; Delaney and Arcone, 1984). Grain size and temperature help determine the amount of unfrozen water, which exists near particle surfaces. The water content determines how many channels form (usually a small volumetric percentage is needed to coat all soil particles) and how many voids can be filled with water or ice. Temperature mainly determines the percentage of interstitial water that forms ice; as temperature decreases below 0°C the percentage of unfrozen water decreases (Tice et al., 1978). Electrical properties also depend on frequency, which is controlled by several relaxation processes (Olhoeft, 1977). In this research the bandwidth was sufficiently narrow to avoid such dependence.

Field investigations of frozen soil properties in the 50- to 500-MHz range have not been extensive. Arcone and Delaney (1982a, 1984) and Delaney and Arcone (1984), using fixed frequency and pulse techniques, have found the dielectric constant ε' to vary between 3 and 12 for silt between about -2 and -12°C, with volumetric ice content varying from 0 to over 80%. Annan and Davis (1976) and Annan (1976) have calculated ε' from signal propagation times for clayey soils with high ice content, and found some values less than 3.2, that of pure ice. None of the above works contains data on signal attenuation. Indirect methods such as modeling or low frequency resistivity measurements (e.g., Arcone and Delaney, 1982a) can be employed to estimate attenuation rates.

The objective of this research was to measure in situ the dielectric permittivity of frozen silt and to correlate values with soil temperature and ice content. High ice content silt is common in interior Alaska. The time delays of pulses transmitted between boreholes at a site in Fairbanks, Alaska, and attenuation rates calculated from comparisons of signal loss between different borehole pairs were used to compute the real part ε' of the dielectric permittivity. Measurements of dc resistivity allowed attenuation mechanisms to be estimated. The data reported here are from two years for late March - early April when the ground was entirely frozen.

EQUIPMENT AND DATA PROCESSING

Electromagnetic

A control unit manufactured by the Xadar Company (Electromagnetic Reflection Profiling System, model 1316) operated a pair of borehole antennas manufactured by the GSSI

Company. The unit is intended for radar subsurface profiling with transmit and receive antennas close together, but may be used with the antennas at any separation. The pulse repetition frequency was 50 kHz. The signals received are sequentially sampled to convert the VHF frequencies to the audio range for digital or analog recording over one of several scan lengths, ranging from 43 to 2000 ns. The scans were linearly stacked to reduce incoherent noise and then stored on magnetic tape. An exponential gain was applied over the first quarter of the scan, after which it remained constant. An overall system gain was also used. Data were later transferred to a computer for playback and graphic display.

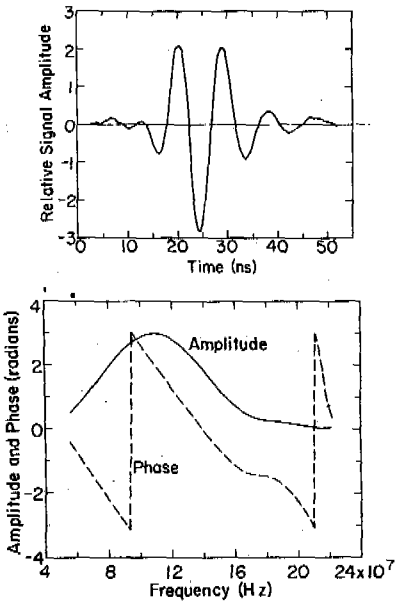

Fig. 1 Typical transmitted wavelet (top) and its associated amplitude and phase spectra.

A typical radiated pulse shape and its associated Fourier spectrum are shown in Figure 1. Both transmit and receive antennas do not radiate uniformly in the radial direction, although pulse shape is maintained in all directions. Measurements made in air revealed that received amplitude could vary as much as 2.6 dB, depending on the azimuthal orientation of the antennas. However, this could cause only a small adjustment in the measured attenuation rate (in dB/m) when divided by the propagation distances. Antenna orientation in the boreholes was inhibited by the attached ropes and cables, but was impossible to determine as the antennas would rotate when being lowered.

Time delay was calibrated by recording pulse transmissions between antennas separated in air at measured distances. The absolute zero time reference for any borehole pair was determined by first measuring the time delay difference t_d between air transmissions over a distance equal to the borehole spacing, and that between the boreholes (both recordings within 1 minute) at the maximum depth of 11.5 m. The borehole separation divided by the free space velocity c = 30 cm/ns was then added to t_d to give the zero time reference. This procedure fixed the position of the absolute time reference on our recordings for both years of measurement. Temperatures recorded throughout the year at 11.5-m depth revealed no seasonal changes, thus verifying an assumption of no dielectric changes at the 11.5-m depth. Yearly calibrations were required to compensate for drift in the zero time reference (approximately 1 ns/hour) because of changes in dc bias levels within the course of a day or between years.

Signal amplitude calibration was determined by the gain settings and signal level recorded for each transmission. Attenuation rates between a borehole pair were determined by comparing the amplitudes received between that pair with those measured between a closer reference pair, for which total attenuation was generally less; 13 combinations of pairs were utilized. The rates are therefore based on relative measurements to eliminate system losses. Absolute calibrations were impossible because of the unknown values of initial signal strength at the antennas.

Resistivity

A string of electrodes was attached to a 3.8-cm-diameter plastic (ABS) pipe and inserted down a separate borehole, which was then backfilled with wet silt and allowed to refreeze. The electrodes were separated by 30 cm and an apparent resistivity ρ_a was computed using the formula for a Wenner array embedded in a homogeneous earth

$$\rho_a = 4\pi a\, V/I \ , \qquad (1)$$

where a is the electrode spacing and V and I are the measured voltage and injected current, respectively. The quantity ρ_a is an integration over a radius of about 0.7a and equals the real resistivity for homogeneous earth. A more complete description of this experiment (including discussions of contact resistance and pipe effects) with data for 12 months is given by Delaney et al. (in press).

Temperature

Temperature T was measured at 30-cm levels using a thermistor probe slowly lowered down a separate borehole filled with ethylene glycol. The thermistor (Omega 400 series) was calibrated to 0.01°C. Readings were made on a battery-operated voltmeter after equilibrium was established at each level. The thermistor was weighted to facilitate lowering. An entire run lasted about 45 minutes.

Electromagnetic Data Reduction

The time delay and peak amplitude of each pulse transmission allowed computation of the complex index of refraction $n^* = n' - in''$ ($i = \sqrt{-1}$) from which $\varepsilon^* = \varepsilon' - i\varepsilon'' = n^{*2}$ could be calculated. Time delays were measured at the leading edge of the wavelet and, with the known borehole separation, determined n'. The position of the leading edge was determined visually to about ± 0.5 ns, which generally

gives an error of less than 0.1 in ε'. The consistency in oscillation periods for all wavelets precluded the presence of dispersion and the possibility that leading edge velocities were not characteristic of the strongest frequency of the wavelets. Only the leading edge could be used because the wavelet length and spectrum in the air reference (centered at approximately 140 MHz) was different than in the ground (100 MHz). The attenuation rate β (dB/m) was computed by comparing the peak received signal strength A_2 for one pair with that for a closer, reference hole pair A_1. After adjusting the ratio A_2/A_1 for geometric spreading losses, β is then found from the formula

$$\beta = 20 \log (A_2/A_1)/\Delta Z \qquad (2)$$

where ΔZ is the difference in separation between the two borehole pairs. The imaginary part of the refractive index is then

$$n'' = \beta c/(8.68 \cdot 2\pi f) = 0.055\ \beta/f \qquad (3)$$

where f is the strongest frequency of transmission (in hundreds of MHz). The components of ε^* are then

$$\varepsilon' = n'^2 - n''^2 , \qquad (4)$$

and

$$\varepsilon'' = 2n'n'' . \qquad (5)$$

The quantity n" proved small enough to allow $\varepsilon' = n'^2$ to within ± 0.04, which is within the error of the time measurement.

Signal attenuation other than geometric spreading is caused by resistive or dipolar dispersional losses, or scattering. Delaney and Arcone (1984) have shown the dipolar component of ε'' to be in the range 0.1-0.2 for very high ice content Fairbanks silt, which at 100 MHz, gives 0.4-0.8 dB/m for an $\varepsilon' = 5$. Attenuation rates due to material resistivity ρ are computed from the formula

$$\beta_\rho = 4.34/c\sqrt{\varepsilon'}\ \varepsilon_o \rho = 1636/\rho\sqrt{\varepsilon'} . \qquad (6)$$

SITE DESCRIPTION AND PREPARATION

The investigation was conducted at the Farmer's Loop Road test facility of USACRREL in Fairbanks, Alaska. The soil type to several tens of meters depth is retransported eolian silt (Péwé, 1958). Previous investigations here (Arcone et al., 1978; Arcone and Delaney, 1982b) have reported values for ground resistivity and the active layer dielectric constant. Generally, volumetric ice content (discussed later) exceeds 50% and active layer depth is 70-100 cm. An organic mat covers the surface. The highest and lowest ground temperatures occur in early spring and late summer respectively.

Six holes (Fig. 2) were drilled to approximately 12-m depth and cased with 3-in. (7.62-cm) diameter ABS plastic pipe, capped and sealed at the bottom. Core samples could not

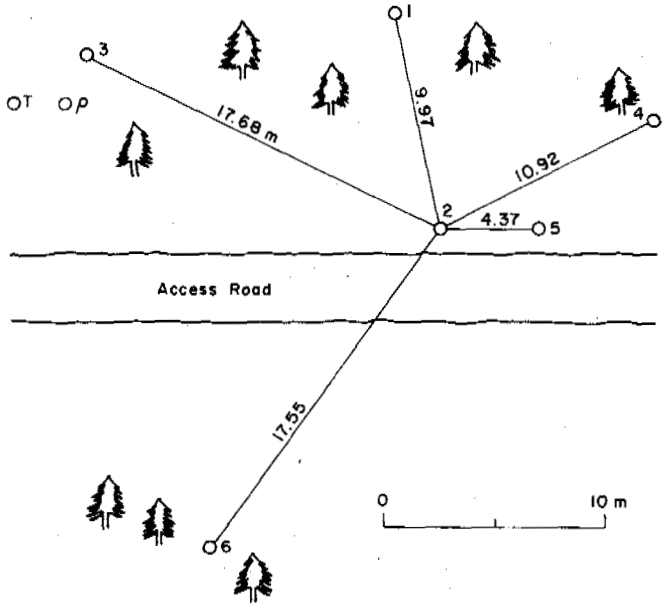

Fig. 2 Borehole layout at the Farmer's Loop Road test facility. T and ρ are the temperature and resistivity electrode string boreholes.

be obtained because freeze-back of the core barrel to the hole wall constantly occurred at the near 0°C temperature of the soil. Consequently, only augered cuttings were obtained from which gravimetric water content was measured. Massive ice was not encountered in any of the holes.

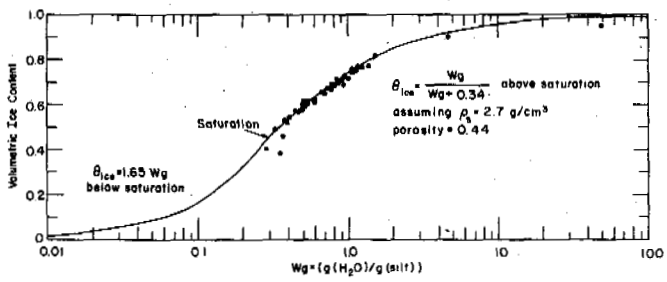

Fig. 3 Calibration data for computing volumetric ice content from gravimetric water content.

Equivalent volumetric ice content was calculated using a calibration curve (Fig. 3) matched to data from cores obtained at a nearby site at Fox, Alaska, and from other studies at Fox and Farmer's Loop Road (Arcone and Delaney, 1982b). The equations for the curves assumed a silt density of 2.7 g/cm^3, a porosity of 0.44 (Hoekstra and Delaney, 1974) and that $\theta_{ice} + \theta_{silt} + \theta_{air} = 1$ where θ is volumetric content. Above saturation, $\theta_{air} = 0$. The volumetric unfrozen water content was not measured in the cores nor considered in the theory. This causes an error of a few percent in the saturation calculations because

several grams of unfrozen water can exist per 100 g of silt (Tice et al., 1978) below -0.7°C, the highest temperature encountered in the boreholes.

RESULTS AND DISCUSSION

Pulse transmissions were recorded at 1-m depth intervals. The antennas were raised simultaneously from a bottom datum plane established by surface leveling. Nine borehole pairs were investigated for ε' and Figure 4 shows a typical record. The two widest pairs (boreholes 2 to 6 and 2 to 3, Fig. 2) gave limited or no discernible signal above the noise level. Generally, transmissions in the top 3 m between each pair were severely affected by the noise generated by the sequential sampling (see Equipment and Data Processing) of nearby FM radio stations, as is evident in Figure 4. None of the inter-borehole paths crossed a third borehole and rarely was an event secondary to the direct transmission observed for any pair but the closest. The correlations between propagation characteristics and ice content are treated statistically because no soil samples were obtained between boreholes.

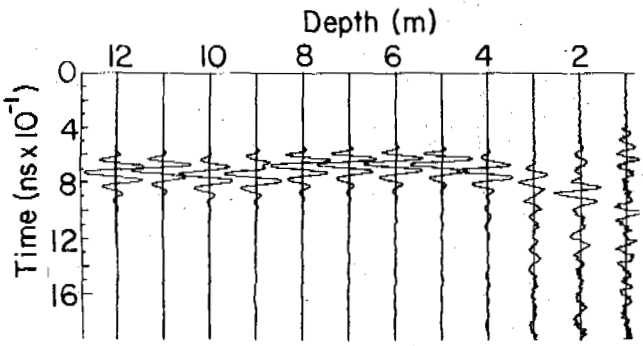

Fig. 4 Typical inter-borehole pulse transmissions, in this case between holes 4 and 5.

Figures 5a and b show the temperature and θ_{ice} profiles. The temperature profile was done on April 4, 1986, with an approximate snow cover of 30 cm and before any extensive thaw periods had begun. Temperature was constant below 6 m at -0.75°C. θ_{ice} varied between 48 and 78% and no formations of massive ice were found in any of the holes. The θ_{ice} profile for hole 6 shows the largest fluctuations. This profile will not be included in subsequent averaging and comparisons as the hole was too distant to receive any transmissions.

Figure 5c compares 1985-86 average values of ε' with the average θ_{ice} at each depth for holes 1 to 5. The lowest values of ε' correlate with the highest ice contents and vice versa. At these high values of θ_{ice}, not

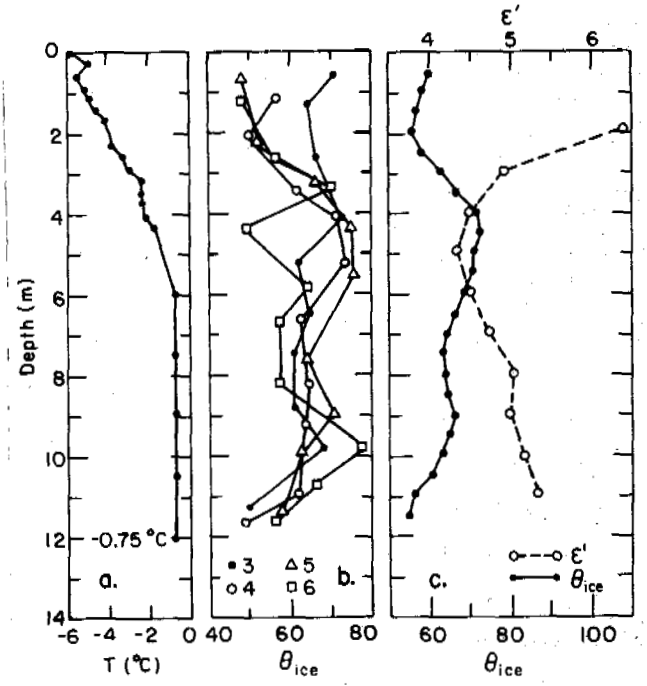

Fig. 5 Temperature (a), volumetric ice (b), and average dielectric constant (holes 1 to 5), and volumetric ice profiles (c).

only have all voids been filled with ice, but the ice volume exceeds the porosity of dry silt. Consequently, samples with greater silt content have the higher values of ε' because of the unfrozen water between or adsorbed on the silt particles. If the value of θ_{ice} were to decrease below saturation, ε' would again decrease because air would continually replace water. Consequently, there is a double-valued dependency of ε' on θ_{ice}.

This double-valued dependency of ε' on θ_{ice} is illustrated in Figure 6, which superimposes the dielectric data of Figure 5c (along with data for holes 4 to 5) on (revised) theoretical curves and other experimental data for frozen silt given by Delaney and Arcone (1984). The solid curve is based on both laboratory and field data taken at temperatures near -7°C. The crossed data points are from Figure 5c and the dark triangles are the averages for just holes 4 and 5, both of which were sampled to calculate θ_{ice}. Either the set of dark triangles or that of crosses agrees well with the previous observations, although the temperature range for the borehole data was -0.75 to -4.0°C. This temperature insensitivity must be related to the only temperature-sensitive component, the unfrozen water, either through a significant reduction in the volumetric fraction of silt at high ice contents, or through a decrease in its own permittivity in the natural state.

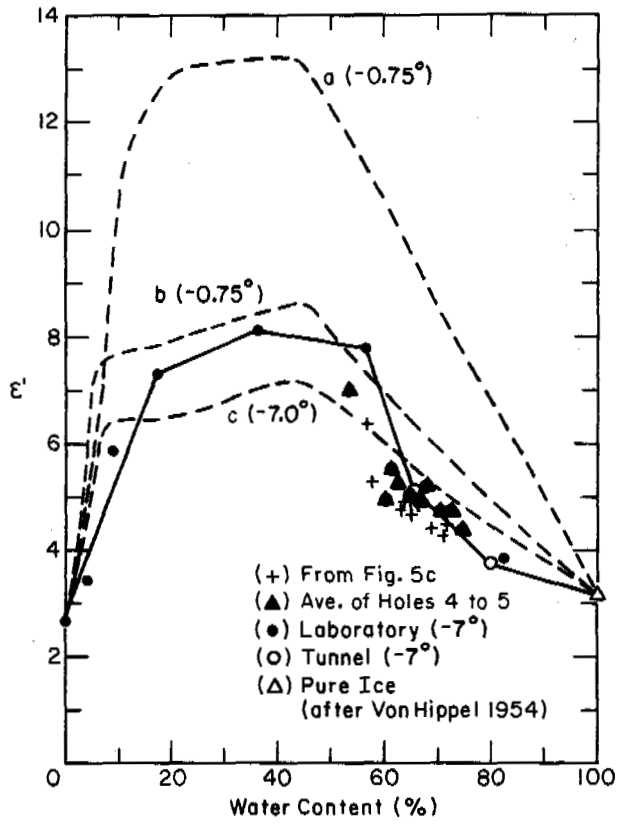

Fig. 6 Dielectric constant vs. volumetric water content data compared with previous investigations and theoretical results (dashed curves - explained in text).

The hypothesis that the temperature insensitivity is due to the reduced volumetric fraction of silt at high ice contents is tested by the theoretical curves in Figure 6 which are derived from a simple volumetrically based dielectric mixing formula:

$$\varepsilon' = \sum_{m=1}^{4} \varepsilon'_m \vartheta_m \quad . \qquad (7)$$

The index m is for the components: ice, unfrozen water, air and dry silt. The ε' values of air, silt and ice are 1.0, 4.0 and 3.2, respectively, the dry sample porosity is 0.44 and the silt density is 2.7 g/cm^3. The unfrozen water is assigned an ε' of 84 at -0.75°C and 60 at -7.0°C (Stogryn and Desargent, 1985), values which alter the previous version of this curve (Delaney and Arcone, 1984) based on a value of $\varepsilon' = 88$. Curves (b) (-0.75°C) and (c) (-7.0°C) assume a capacity for unfrozen water content of 4 g/100 g silt, while curve (a) (-0.75°C) assumes a value of 8. Recent data from Tice et al. (in press) based on nuclear magnetic resonance suggest that 8 (-0.75°C) and 4 (-4 to -7°C) are more appropriate. Thus, the wide separation of curves (a) and (c) near 60% water content means that, theoretically, the reduced amount of silt in high ice content sections is not sufficient to cause the temperature insensitivity that we observe from the data. An overestimate of ε' for supercooled unfrozen water does not seem possible in view of the high permittivities measured on well-mixed laboratory samples (Delaney and Arcone, 1982). More sophisticated models based on structural considerations would give a better match to the data, but are not expected to alter the conclusion of a theoretical temperature sensitivity.

It seems, then, that the reduced temperature sensitivity is due to an inability of the silt to have reached its full capacity for retaining unfrozen water. It is unlikely that ice lens growth has occurred at the expense of the unfrozen water in the already frozen silt in view of the high degree of saturation and the results of Tice et al. (in press). The possibility that not all silt particles ever came in contact with unfrozen water is also unlikely because it is probable that this retransported section originally formed as an aggrading saturated active layer. Therefore, at this time we can only speculate on the possibility of organics or molecular diffusion as agents of reduction in unfrozen water content.

Figure 7a plots resistivity versus depth. The values range from 1000 to over 12,000 ohm-m and are representative of silt to a radial distance of about 20 cm from the electrode string (Delaney et al., in press). Also plotted are the equivalent attenuation rates β_ρ associated with these values. The lowest value (~ 1000 ohm-m) gives a maximum β_ρ of about 0.75 dB/m. Generally, however, most values below the 4-m depth are less than about 0.3 dB/m.

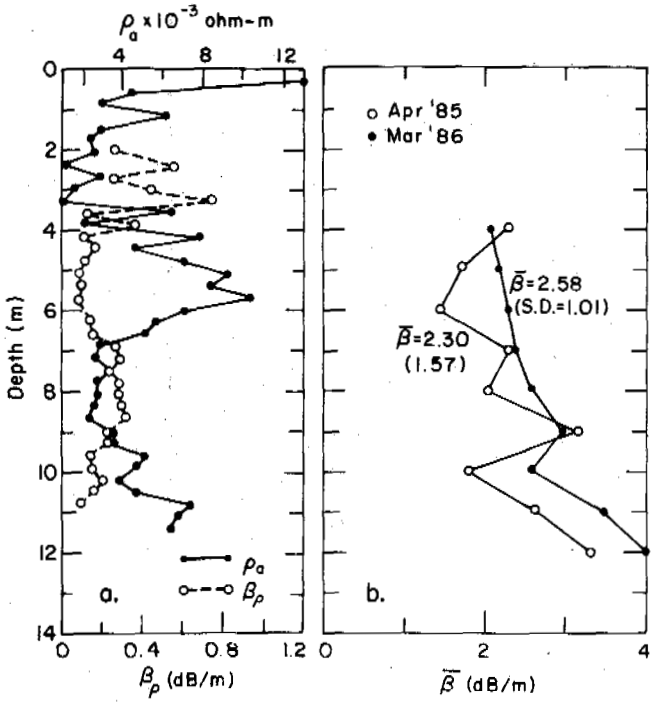

Fig. 7 Resistivity (dc) and its associated signal attenuation rate (a), and average total attenuation rates for two different years (b).

Figure 7b plots the average propagation attenuation rate measured at each depth for April 1985 and March 1986. Average rates are presented to give some compensation for variations due to changes in antenna orientation (0.23 dB/m at most) or to dielectric inhomogeneities near the antennas. Between 10 and 13 comparisons between borehole pairs were used to calculate each point. Averages above the 4-m depth are not given, either because of noise distortion, or because too few signal levels could be read above the noise to give a meaningful average. The few values that could be calculated using borehole 6 are included in these averages. There is a general increase of attenuation with depth, which correlates with the increase in T and ε' with depth and the decreasing θ_{ice} values below 8 m. The minimum average value of 1.40 dB/m is well above the maximum rate of 0.75 dB/m due to conductive losses (Fig. 7a). The lack of dispersion seen in all waveforms (e.g. Fig. 4) suggests that dielectric relaxation is not a significant attenuation mechanism. We are thus left with scattering as the important loss mechanism. The largest values of β seen below 8 m may therefore indicate greater inhomogeneity, as would also the decrease in θ_{ice} from such high values at 4-6 m. The maximum value of 4 dB/m gives n" = 0.22, which supplies an insignificant correction to the calculation of ε' as per eq 4.

CONCLUSIONS

Inter-borehole pulse propagation can be an effective means of generally assessing volumetric ice content in frozen silt. Although ε' does not seem sensitive to temperature in the cases studied, such sensitivity could exist in other silt deposits, depending probably on lithologic or historical factors not currently understood. The double-valued dependency of ε' vs θ_{ice} requires, however, other information to establish if θ_{ice} is greater or less than about 40%. This can be done easily with a non-contact surface or borehole resistivity technique such as double dipole magnetic induction (e.g., Arcone et al., 1978). Values above 1000 ohm-m generally indicate $\theta_{ice} > 40\%$. It is not at all clear that propagation attenuation rates could be used to diagnose the range of θ_{ice} because increasing losses caused by decreasing resistivity may be compensated for by less scattering due to increased homogeneity. The overall average of 2.3-2.6 dB/m found here means that separations greater than 20 m will need more power and more sophisticated signal processing than just stacking to assess ice content with this technique.

REFERENCES

Annan, A P (1976).
Density of ice samples from "Involuted Hill" test site, District of Mackenzie. Report of Activities, Part C, Geologic Survey of Canada, Paper 76-1C, 91-95.

Annan, A P & Davis, J L (1976). Impulse radar sounding in permafrost.
Radio Science, (11), 4, 383-394.

Arcone, S A & Delaney, A J (1982a).
Electrical properties of frozen ground at VHF near Point Barrow, Alaska.
IEEE Trans. on Geoscience and Remote Sensing, (GE-20), 4, 485-492.

Arcone, S A & Delaney, A J (1982b).
Dielectric properties of thawed active layers overlying permafrost using radar at VHF.
Radio Science, (17), 3, 618-626.

Arcone, S A & Delaney, A J (1984).
Radar investigations above the trans-Alaska pipeline near Fairbanks. CRREL Report 84-27, U.S. Army Cold Regions Research and Engineering Laboratory, Hanover, NH, 1-15.

Arcone, S A, Sellmann, P V & Delaney, A J (1978).
Shallow electromagnetic geophysical investigations of permafrost. Proc III Inter Conf Permafrost, (1), 501-507, Edmonton, Alberta.

Davis, J L, Scott, W J, Morey, R M & Annan, A P (1976). Impulse radar experiments on permafrost near Tuktoyaktuk, N.W.T.
Canadian Journal of Earth Sciences, (13), 1584-1590.

Delaney, A J & Arcone, S A (1984).
Dielectric measurements of frozen silt using time domain reflectometry.
Cold Regions Science and Technology, (9), 39-46.

Delaney, A J, Sellmann, P V & Arcone, S A (in press).
Seasonal variations in resistivity and temperature in discontinuous permafrost near Fairbanks, Alaska. Submitted to V Inter Conf Permafrost, Trondheim.

Hoekstra, P & Delaney, A J (1974).
Dielectric properties of soils at UHF and microwave frequencies.
Journal of Geophysical Research, (75), 11 1699-1708.

Olhoeft, G R (1977). Electrical properties of natural clay permafrost.
Canadian Journal of Earth Sciences, 14, p. 16-24.

Péwé, T L (1958).
Geology of the Fairbanks (D-2) Quadrangle, Alaska. U.S. Geological Survey geological quadrangle map GQ-110.

Stogryn, A & Desargent, G (1985).
The dielectric properties of brine in sea ice at microwave frequencies.
IEEE Trans Geoscience and Remote Sensing, (AP-33), 5, 40-48.

Tice, A R, Burrows, C W & Anderson, D M (1978).
Phase composition measurements on soils at very high water contents by the pulsed nuclear magnetic resonance technique. In Moisture and Frost-Related Soil Properties, Transportation Research Board, National Academy of Sciences.

Tice, A R, Black, P & Berg, R (1988).
Unfrozen water contents measurements of undisturbed and remolded soils from the Northwest Alaska Pipeline Company frost heave facility as determined by pulsed nuclear magnetic resonance. CRREL report (in press). U.S. Army Cold Regions Research and Engineering Laboratory, Hanover, NH.

Von Hippel, A R, Ed. (1954).
Dielectric materials and applications.
J Wiley, New York.

PERMAFROST AND TERRAIN PRELIMINARY MONITORING RESULTS, NORMAN WELLS PIPELINE, CANADA

M.M. Burgess

Permafrost Research, Geological Survey of Canada, Energy, Mines and Resources, Ottawa, Canada

SYNOPSIS The 869 km Norman Wells oil pipeline, owned by Interprovincial Pipe Line (NW) Ltd. (IPL), traverses the discontinuous permafrost zone of Northwestern Canada. A fully buried, small diameter (324 mm) line transporting initially chilled oil was designed for operation in the thaw-sensitive terrain along the route. Operation began in April 1985. Monitoring of the thermal regime at thirteen locations along the route forms a major component of a long term cooperative government-IPL permafrost and terrain research and monitoring program. Observations to the end of March 1987 indicate that mean annual pipe temperatures, which range from 0°C to 5°C, are generally >0°C both within the widespread discontinuous permafrost terrain in the north and the sporadic discontinuous permafrost terrain in the south. Mean annual ground temperatures on the right-of-way (ROW) at 1 m depth, several metres from the trench, range from -2° to +4°C and are on average 1.5 degrees colder than mean annual pipe temperatures. Mean annual ground temperatures off-ROW at a depth of 1 m range from -3° to +3°C and are on average 1 degree colder than those on-ROW. Maximum surface settlement observed on the ROW at the sites has reached up to 80 cm outside the trench area, and over 100 cm in the vicinity of the trench.

INTRODUCTION

The Norman Wells pipeline, the first completely buried oil pipeline in the discontinuous permafrost zone of Canada, began operation in April 1985. The 869 km long, 324 mm diameter, pipeline is owned by Interprovincial Pipe Line (NW) Ltd. (IPL) and carries oil south from Esso Resources' Norman Wells, N.W.T. oilfield to Zama, northwestern Alberta (Figure 1). The terrain conditions encountered along the route (Kay et al., 1983) necessitated the development of special design features and mitigative measures in order to minimize terrain impacts (National Energy Board, 1981; IPL, 1982) and to assure pipe integrity under possible conditions of thaw settlement or frost heave. Details of the design are outlined by Nixon et al. (1984), Nixon and Pick (1986), McRoberts et al. (1985), and Wishart and Fooks (1986).

Features selected to limit energy exchange with the surrounding terrain include 1) winter right-of-way (ROW) clearance, prior to construction, generally to 25 m, maximizing the use of previous cutlines, 2) construction in winter, using temporary roads, 3) oil chilled to near 0°C before delivery to IPL; no further refrigeration in passing through three pump stations (kms 0, 336 and 585), 4) small diameter, shallow burial (average depth, excluding roach, 1 m) and generally uninsulated pipe, and 5) wood chip insulation of thaw sensitive slopes. The Norman Wells pipeline was not expected to directly cause "significant thawing of the underlying permafrost" (Nixon et al., 1984) compared to the slow thawing to depths of 6 m resulting from clearing and construction. Hence its general description as an "ambient" ground temperature pipeline.

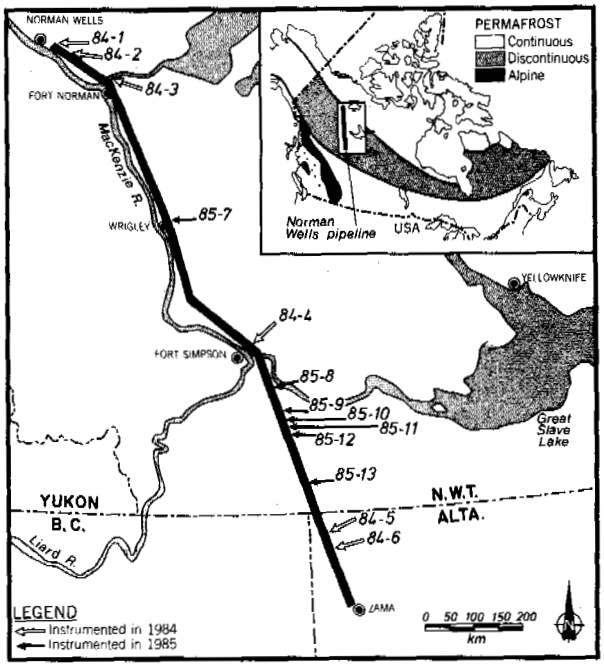

Fig.1 Location of Norman Wells Pipeline and Monitoring Sites

The Norman Wells project provides an important opportunity to observe the behaviour of the pipeline and ROW and to assess the impact of construction and operation of the first, small diameter, buried oil pipeline in permafrost.

This paper discusses observations on 1) the pipe thermal regime, 2) the ground thermal regime, and 3) the surface settlement recorded at 13 joint government and industry monitoring sites from construction to the end of the second year of pipeline operation (March 1987).

PERMAFROST AND TERRAIN RESEARCH AND MONITORING

The long term permafrost and terrain research and monitoring (PTRM) program was established under an Environmental Agreement signed in 1982 between the federal department of Indian and Northern Affairs (INAC) and IPL. A major component of the PTRM program, developed in cooperation with the federal department of Energy, Mines and Resources (EMR), involves the detailed quantification of changes in the ground thermal regime and geomorphic conditions at instrumented sites.

Table I

Site Locations and Descriptions

SITE	NAME	km	DESCRIPTION (at time of establishment)
84-1	Pump Station 1	0.02	Ice-rich silty clay in widespread permafrost
84-2	Canyon Creek		(previously cleared cut line from the 1960s)
	A	19.0	Level terrain, frozen till with low ice content in widespread permafrost
	B	19.3	East-facing permafrost slope with a 1 m insulating wood chip cover
	C	19.6	West-facing permafrost slope with erosion control berms
84-3	Great Bear River		(joint IPL site)
	A	79.2	Stratigraphically complex ice-rich alluvial terrace deposits in widespread permafrost
	B	79.4	Cliff-top lacustrine deposits; aeolian veneer
85-7	Table Mountain		(joint IPL site)
	A	271.2	Ice-rich lacustrine plain (old seismic line)
	B	272.0	Ice-rich lacustrine plain (recent helipad clearing at top of north-facing slope)
	C	272.3	Ice-rich lacustrine plain
84-4	Trail River		(unfrozen terrain after long frozen stretch)
	A	478.0	Unfrozen saturated sands and silts in dune hollow
	B	478.1	Dry sands and silts in dune crest
85-8	Manner's Creek		(rapidly changing permafrost conditions)
	A	557.8	Thin peat, thick (10 m) permafrost
	B	558.2	Thick peat (2.7 m), thin (4 m) permafrost
	C	558.3	Thin peat (1 m), thin (1 m) permafrost
85-9	Pump Station 3	583.3	Unfrozen granular soils after frozen section
85-10	Mackenzie Highway South		
	A	588.3	Transition from recent helipad clearing in unfrozen terrain to
	B	588.7	Thin (3 m) permafrost with 2 m peat cover
85-11	Moraine South	597.4	Thin (4 m) permafrost in recent helipad
85-12	Jean Marie Creek		
	A	608.6	Thin unfrozen peat plateau
	B	608.7	Thick ice-rich peat plateau; 4 m permafrost
85-13	Redknife Hills		
	A	682.2	Frozen (6 m) terrain surrounding large fen
	B	682.4	Frozen (6 m) terrain at edge of fen
	C	682.6	Unfrozen terrain in fen
84-5	Petitot River North		
	A	783.0	Ice-rich peat (3.5 m); 15-18 m permafrost
	B	783.3	Very thick icy peat (7 m); 12 m permafrost
84-6	Petitot River South		
		819.5	Thick (5 m) ice-rich peat; 7 m permafrost

Note: All fences, unless otherwise indicated, are located in terrain newly cleared for the pipeline ROW. Site 85-13 is the only site which has not been set up in the "thermal fence" configuration.

Thirteen principal monitoring sites, shown in Figures 1 and briefly described in Table I, were selected to 1) investigate the terrain response to particular pipeline design features and mitigative measures, including areas of thaw sensitive terrain, frozen/unfrozen interfaces and a wood chip insulated slope, and 2) represent the soil and ground ice conditions along the route. An IPL geotechnical monitoring program involves the instrumentation of 26 slopes; 17 with wood chip insulation. Joint industry- government sites emphasize the study of other terrain conditions.

Thermal instrumentation installed at the PTRM sites has been laid out along one or more "thermal fences". In total there are 23 fences, each of which typically consists of 5 thermistor sensors placed on the external wall of the pipe and a series of 4 boreholes, cased with PVC and instrumented with multithermistor cables. Two 5 m cables (10 sensors, 50 cm spacing) are located within a few metres of the pipe. Two 20 m cables contain 11 sensors spaced every 1 m near the surface and every 2-3 m at depth; one cable is installed on the ROW several metres (4-9) from the pipe, the other is set in the adjacent terrain off-ROW. The establishment of the thermal fences, the instrumentation and the measurement programs are described in detail by Burgess et al. (1986), Burgess (1987) and Pilon et al. (in prep.). Topographic surveys, conducted annually at most fences, record vertical movements in the ground surface to an accuracy of 10 cm over a 20 m x 20 m grid, using 2-3 local benchmarks per site and a 2 m station spacing.

Monthly field trips emphasize the manual acquisition of thermal data for most fences. Automatic loggers (SeaData) also installed at 5 fences record ground temperature cable readings several times daily. The monthly data are published regularly as EMR open file reports (Burgess, 1986 and 1987). Thermal conditions across the ROW are complex especially at sites with different ages and degrees of vegetation removal and of ground surface disturbance. Conditions are dynamic, and may include 1) maintenance activities , 2) stationary or flowing water, 3) changing vegetation cover, as well as 4) variable climatic conditions.

PIPE THERMAL REGIME

Northern section (fences from km 0 to 272)

Permafrost underlies about 75% of the terrain (Kay et al. 1983) and all of the 9 thermal fences in this section. Monthly pipe temperatures recorded over time at the fences from km 19 to 272 (data from the fence at km 0.02 will be discussed separately) fall within the ranges plotted in Figure 2.

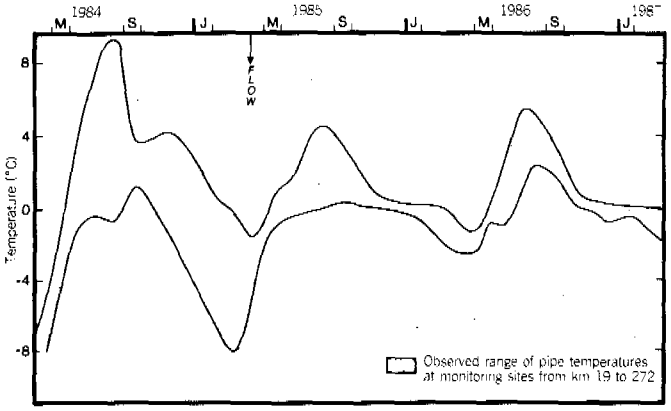

Fig.2 Pipe Temperatures - Northern Section

Pre-flow pipe temperatures (from 5 fences established in 1984) show a wider range and larger annual amplitude than post-flow, reflecting the natural diversity of the adjacent ground thermal regime. Pipe temperatures before flow were generally at any time in close agreement (within 1 degree) at each fence with the temperatures recorded on the ROW at a depth of 1 m several metres from the trench. Individual plots comparing pipe temperature and ROW 1 m ground temperature at each fence are presented in MacInnes et al.(in prep.).

After the pipeline came into operation, differences of 2-4 degrees were commonly observed between pipe temperatures and ROW ground temperatures at 1 m depth. Pipe temperatures at sites with multiple fences, which before flow had differed at a given time by up to 8 degrees from one fence to the next, generally differ by less than 1 degree after flow. Figure 2 also illustrates the warmer winter pipe temperatures observed since oil began flowing.

Table II

Mean Annual Temperatures (Pipe and Ground) and Surface Settlement After 2 Years of Operation

FENCE	(km)	TRENCH AREA		ROW OUTSIDE TRENCH AREA		OFF-ROW
		Mean Pipe Temp. (°C)	Range of Settlement (cm)	Mean 1 m Ground Temp. (°C)	Range of Settlement (cm)	Mean 1 m Ground Temp. (°C)
84-1	(0.02)	-0.2	0 - 60	-0.9*	0 - 80	-2.3
84-2A	(19.0)	0.2	0 - 30	0.1	0 - 20	-1.1
84-2B	(19.3)	0.3	0 - 30	-0.2	0 - 40	-2.5
84-2C	(19.6)	0.4	0 - 20	1.3	0 - 30	-1.0
84-3A	(79.2)	1.2	10 - 50	-1.2	0 - 50	-2.8
84-3B	(79.4)	0.9	0 - 20	0.5	0 - 20	-2.3
85-7A	(271.2)	0.6	10 - 70	0.0	0 - 50	-1.0*
85-7B	(272.0)	0.4	10 - 80	-0.9	0 - 50	-1.4*
85-7C	(272.3)	0.6	20 - 60	-1.6	0 - 30	-1.1*
84-4A	(478.0)	2.4	0 - 50	2.6	0 - 20	1.6
84-4B	(478.1)	2.3	0 - 30	2.9	0 - 30	0.9
85-8A	(557.8)	2.6	10 - 50	-0.3	0 - 30	-0.7
85-8B	(558.2)	2.5	10 - 100+	-0.5	0 - 40	-1.1
85-8C	(558.3)	1.8	10 - 80	-0.4	0 - 60	-0.3
85-9	(583.3)	2.9	0 - 20	3.6	0 - 10	2.5
85-10A	(588.3)	4.8	0 - 50	2.4	0 - 30	1.5
85-10B	(588.7)	4.8	0 - 100+	1.2	0 - 40	-0.6
85-11	(597.4)	3.9	backfilled	2.8	0 - 20	0.1
85-12A	(608.6)	3.4	0 - 70	1.7	0 - 20	0.3
85-12B	(608.7)	3.7	0 - 100+	-0.8	0 - 50	-1.1
84-5A	(783.0)	1.9	N/A	0.4	N/A	0.0
84-5B	(783.3)	1.9	N/A	-0.1	N/A	-0.1
84-6	(819.5)	1.8	N/A	-0.2	N/A	0.0

NOTES:
1) The Trench Area includes the trench and 2 m on either side of the pipe centreline. The ROW Area is the remainder of the surveyed right-of-way.
2) The range of settlement (cm) determined from the surface elevation surveys is defined by the minimum and maximum amount observed. The OFF-ROW is not covered by the survey. 3) Pipe temperatures shown are mean annuals (average of the 5 pipe sensors) calculated for the second year of operation, i.e. April 1986 to March 1987. Calculations were performed by curve fitting to the approximate monthly values, interpolating weekly values and determining 52 week means. 4) Mean annual ground temperatures are the calculated values (same method of calculation as above) for the second year of operation, for the sensor at a nominal depth of 1 m (which is the average depth of cover over the pipe). 5) N/A: not available since a second survey from which settlement could be calculated has not yet been undertaken. 6) * : average of two cables; elsewhere only one ground temperature cable.

Table II presents the calculated mean annual pipe temperatures (using the average of the 5 sensors on the pipe) for each fence during the second year of operation. The calculated mean annual ground temperatures on the ROW, using the 1 m sensor at the deep borehole several metres distant from the pipe, for the same time period, are included in Table II. The 1 m sensor was selected for comparison since this is the average depth of cover over the pipe. (Note: Since the ground temperature cables are in anchored PVC tubes, the absolute depth of the sensors may change as the ground surface heaves or settles; the sensor spacing is however fixed. All references in this paper to 1 m sensor or 1 m depth are thus to ground temperatures at a nominal depth of 1 m.) Mean annual pipe temperatures are between 0° and +1°C at fences along the northern portion of the route. The mean ROW ground temperatures, which are between -2° and +1°C, are on average about 1 degree colder.

Pipe temperatures recorded at the Pump Station site, km 0.02, were variable after start-up. During the first year of operation, when the oil was chilled to about -2°C (Pick, 1986), the mean annual pipe temperature at the fence was about 0.6°C. The delivery temperature has since been -5°C and the mean annual pipe temperature at the fence has dropped to -0.2°C.

Southern section (fences from km 477 to 820)

In this section permafrost underlies approximately 25% of the terrain with numerous frozen/unfrozen interfaces, reaching as many as 15/km (Kay et al. 1983). The range of pipe temperatures recorded over time at the 14 fences located in this portion of the route are plotted in Figure 3. Pre-flow temperatures are not shown since most sites were established in 1985 and only sparse data was gathered at the few 1984 sites.

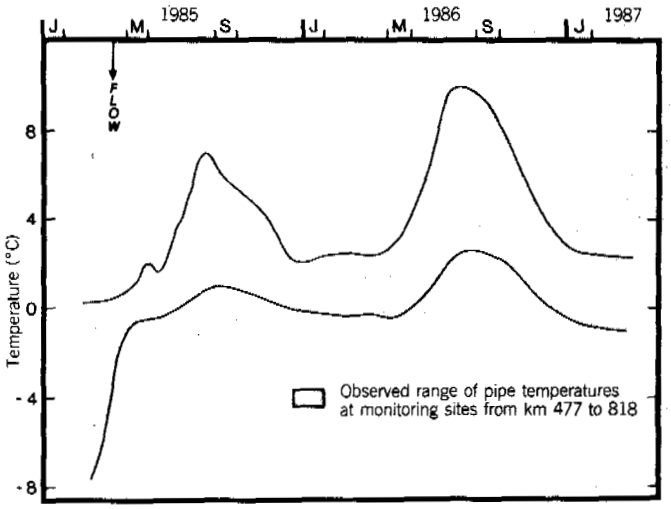

Fig.3 Pipe Temperatures - Southern Section

Winter pipe temperatures have again been conspicuously warmer since the pipeline has been in operation. Table II indicates that all of the monitoring fences, nine of which were originally underlain by permafrost, now have mean annual pipe temperatures well above 0°C and between +2° and +5°C. Mean annual ground temperatures recorded on the ROW several metres from the pipe, and listed in Table II, range from -1 to +4°C. At the permafrost fences mean pipe temperatures are from 1.5 to 5 degrees warmer (average about 2.5) than the mean ROW ground temperatures.

Pipe temperatures at any time are consistently 2-3 degrees warmer at fence 10A (km 588.3) than at fence 9 (km 583.3); mean annual pipe temperatures during the second year of operation

were 2.5°C at fence 9 and 5.0°C at fence 10A. This increase may reflect the increase in oil temperature during pumping at Pump Station 3 which is located between the two fences.

General comments

The mean annual pipe temperatures, in both sections, are on average 1.5 degrees warmer than mean annual ground temperatures at a similar depth on the ROW, several metres from the trench. This temperature difference probably largely reflects the more disturbed terrain conditions in the vicinity of the trench as compared to the rest of the ROW. Depending on the site, the trench may be filled with local or select backfill. Post construction changes have resulted in ditchline depression along a third of the pipeline (IPL, 1986). The subsided ditch may be filled with ponded, or occasionally flowing, water (Wishart and Fooks, 1986). Backfilling of 80 km of trench, with subsidence >20 cm, occurred during winter remedial work in 1986 and 1987.

GROUND THERMAL REGIME

Winter construction generally caused a short term cooling of the ground beneath the ROW. This effect can be seen in the ground temperature isotherms contoured at site 84-1 for September 1984 in Figure 4; temperatures seen at depths below 2 m on-ROW are about 1 degree colder than those off-ROW. The cooling effect can no longer be seen in contours for September 1986 where on-ROW temperatures have gradually increased by up to 2 degrees and are now about 1 degree warmer than off-ROW.

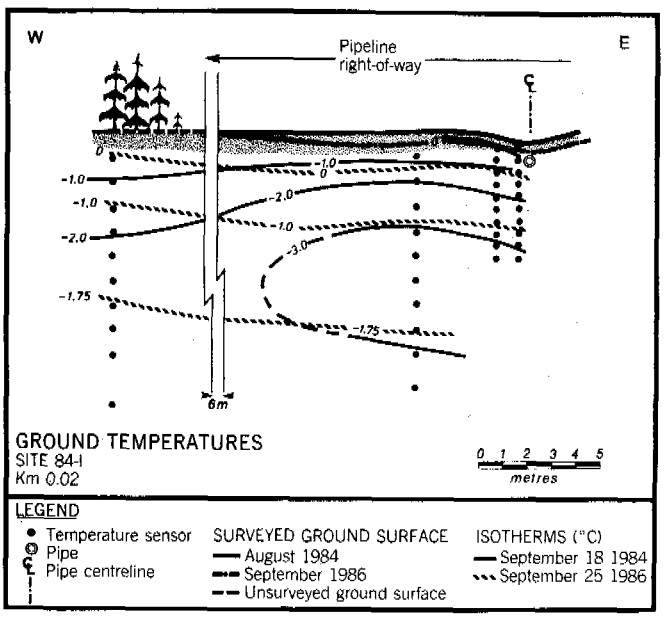

Fig.4 Isothermal Cross-Sections for Site 84-1, km 0.02, September 1984 and 1986

Table II also includes the calculated mean annual off-ROW ground temperatures from the 1 m sensor during the second year of operation. The off-ROW temperatures are generally colder (on average by 1 degree but by as much as 3 degrees) than the ROW temperatures.

At thermal fences in new clearings, whether underlain by permafrost or unfrozen terrain, the ground thermal regime on the ROW after the initial construction cooling has been gradually warming. Increases (up to 2.5 degrees but generally less than 1 degree) in mean annual ground temperatures have been recorded on the ROW from the first year of operation to the second. Ground temperatures at depths below 1 m have generally not reached equilibrium with present near surface conditions.

The ground thermal response in ice-rich terrain and thick ice-rich peat covered sites has been slow due to latent heat effects: mean annual ground temperatures (ROW, 1 m sensor) have generally changed by less than 0.5 degree. Little or no change in permafrost temperatures at depth below 2 m has been observed at these sites (e.g.12B, 5A, 5B and 6). Increases in active layer thickness have been observed; for example, from <1 m to >1.5 m on-ROW at 85-12B. Visual observations indicated that the surface organic soils at 85-12B had undergone considerable scraping and blading during construction and subsequent remedial activities.

Warm thin (1-2 m) permafrost at two southern fences (85-10B and 85-11), both underlain by soils with low ice contents, has disappeared within 2 years of ROW clearance. The thermal regime of two thick permafrost fences in the north, 84-2A and 2C, both underlain by coarse grained till and located in a previous cutline, has been fairly stable since observations began, with active layers ranging from 2 to 6 m. The deeper active layer is observed on the ROW of the west facing slope at fence 2C.

Active layers on the ROW at the end of the 1986 thaw season at newly cleared sites with thick organic soils (greater than 2 m) varied from <0.5 to 2 m, and elsewhere from <0.5 to 2.5 m. Active layers off-ROW at the end of the 1986 thaw season were generally <1 m. Active layers on-ROW have increased (by up to 1 m) since observations began; off-ROW active layers by comparison have generally stayed the same over this period. The active layers quoted here are defined by the maximum depth of penetration of the 0°C isotherm, as measured by the ground temperature cables (may involve interpolation between the 50 or 100 cm sensor spacing and takes any surface settlement into account). The actual thickness of unfrozen material may be greater particularly at sites with fine-grained soil, due to the freezing point depression.

One thermal monitoring fence (84-2B, km 19.3) is located on an east-facing slope insulated with a 1 m cover of wood chips. Data from IPL's instrumented wood chip slopes are also stored on the government data file, but remain proprietary until Jan. 1990 at IPL's request.

During the first summer thaw period following construction, the wood chips at 84-2B underwent a self-heating cycle, with temperatures of up to 15°C recorded at a depth of 0.5 m in the chips. This heat generation, due to microbial decomposition, has been noted in all wood chip

layers during the first summer after placement (McRoberts et al., 1986). This initial self-heating at 84-2B coupled with a winter insulating effect (note in Figure 5, which compares the ground temperature envelope from the uninsulated off-ROW with the envelope from the wood chip covered ROW, the absence of winter cooling beneath the chips), has resulted in an increase in mean annual ground temperature beneath the chips. Current wood chip/ground surface interface temperatures at 84-2B are near 0°C. Ground temperatures beneath the wood chips are not in thermal equilibrium with this interface temperature and are gradually increasing. Mean annual ground temperatures at a depth of 1 m below the chips have increased from -1.5 to -0.5°C during the observation period. Mean annual 1 m off-ROW ground temperatures on this slope by comparison are -2.5°C.

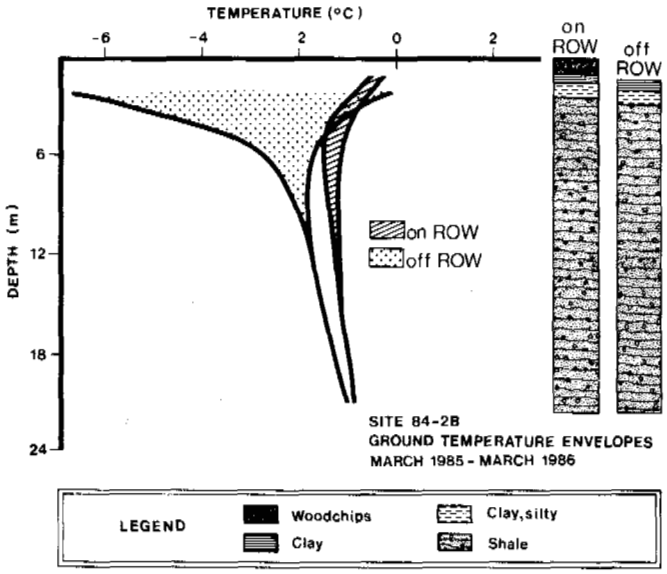

Fig.5 Ground Temperature Envelopes Beneath Wood Chips and Off-ROW at 84-2B, km 19.3.

THAW SETTLEMENT

Surface settlements recorded by the elevation surveys at the thermal fences represent minimum settlements on the ROW, since in all cases the baseline survey was taken following the first thaw season after ROW tree clearance. The range of settlement observed at each site is given in Table II.

In the trench vicinity (2 m on either side of the pipe), the maximum recorded settlement during the limited observation period ranged from 60 to greater than 100 cm in 9 of 20 surveyed fences. Some of this change is likely a result of settlement of the trench backfill which was placed as a frozen and uncompacted berm over the pipe during the winter. Remedial backfill has since been placed in the trench at two fences (85-8C and 85-11) and between fences 85-10A and 10B.

Maximum recorded settlement on the ROW outside the trench area ranged from 50 to 80 cm at 6 of the 20 surveyed fences. A few sites, notably km 0.02 and 79.2, where the originally hummocky terrain was leveled on the ROW and much of the surface organic layer removed across the ROW during construction, have again developed a noticeable hummocky relief (over 50 cm). A contour map of settlement at km 0.02, site 84-1, is shown in Figure 6.

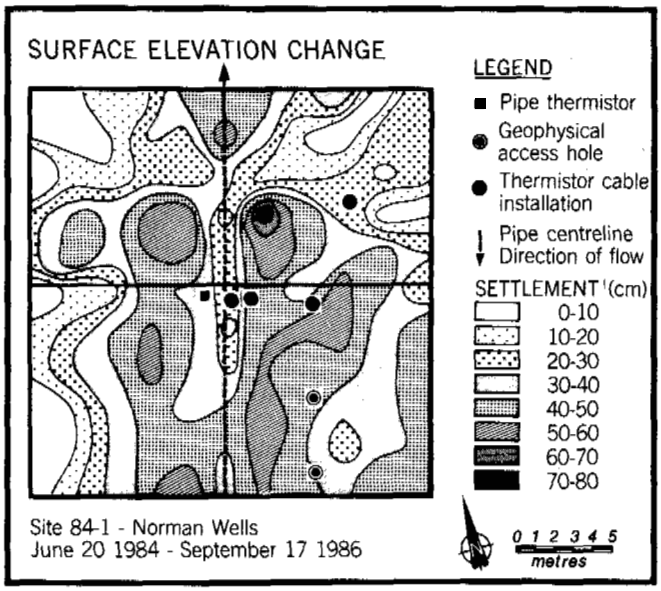

Fig.6 Site 84-1, km 0.02: Contoured Surface Settlement from June 1984 to September 1986.

Only surface settlements are recorded by the PTRM program; monitoring of pipe movements is not included. During the establishment of IPL's geotechnical monitoring program 7 sites were initially selected for thaw settlement monitoring (IPL, 1984). These locations represent worst case situations where thaw settlement beneath the pipe, over a short distance, greater than the design differential thaw settlement (established as up to 0.8 m in mineral soils and up to 1.0 m in thick organics (Nixon and Pick, 1986)) was possible. IPL's visual monitoring program, an integral part of their geotechnical monitoring, had identified an additional 18 locations for detailed thaw settlement investigation by the end of 1986 (IPL, 1986). These areas encompass three thermal fences (84-1, 85-7B and 85-12B) where surface settlements of over 60 cm have been recorded in the trench area and of over 50 cm elsewhere on the ROW. Additional ground temperature instrumentation has been installed by the PTRM program at 5 of these locations.

CONCLUSIONS

The general results summarized below are based on observations gathered at the instrumented thermal fences following two years of pipeline operation. The PTRM is proposed to continue for 5-10 years or until conditions stabilize.

The "ambient" pipeline operates with mean annual pipe temperatures generally above 0°C within both predominantly frozen terrain and unfrozen terrain. Mean pipe temperatures

during the second year of operation ranged from 0 to +5°C. The mean annual pipe temperatures are generally warmer (on average by 1.5 degree) than mean annual ground temperatures on the ROW outside the trench area at a similar depth.

Mean annual ground temperatures on-ROW, at a depth of 1 m several metres from the trench, ranged from -2 to +4°C during the second year of pipeline operation. Mean annual 1 m ground temperatures off-ROW during this period ranged from -3 to +3°C. The mean off-ROW ground temperatures are generally colder than on-ROW, by 1 degree on average. The ground thermal regime on the ROW is generally not in thermal equilibrium with present surface conditions. A warming trend has been observed at most sites from the first to the second year of operation. The thermal response in ice-rich terrain is slow due to latent heat effects. Active layers on-ROW, which currently range from <0.5 m to 2.5 m, have generally increased (by up to 1 m) during the observation period. Off-ROW active layers, generally less than 1 m, have changed relatively little.

At the thermal fence located on a wood chip insulated slope the mean annual wood chip/ground surface interface temperature is currently -0.2°C. Mean annual ground temperatures have increased, e.g. from -1.5 to -0.5°C at 1 m below the interface.

Maximum recorded surface settlement ranged from 60 to over 100 cm in the trench vicinity at 9 of 20 surveyed thermal fences and from 50 to 80 cm on the ROW outside the trench area at 6 of 20 surveyed thermal fences.

ACKNOWLEDGMENTS

The efforts of Kaye MacInnes (INAC) in organizing and coordinating this program require special mention. Many other individuals within INAC, EMR and IPL have provided cooperation, support and assistance: in particular, A. Judge, J. Pilon, V. Allen, W. Pearce, A. Pick, D. Wishart, J. Smith, M. Yerichuk, W. Dunlop, F. Adlem, and B. Gauthier. The PTRM program has been primarily funded by INAC's Northern Affairs program, with contributions from the Northern Oil and Gas Action Program (NOGAP). Additional funding and assistance has been provided by EMR's former Earth Physics Branch, the Geological Survey of Canada and the Federal Panel on Energy Research and Development, IPL Ltd, and the N.W.T. Regional Surveyor's Office.

REFERENCES

Burgess, M M (1986)
Norman Wells pipeline monitoring sites ground temperature data file: 1984-1985. Energy, Mines and Resources Canada, Earth Physics Branch Open File 86-6, 21 pp + app.

Burgess, M M (1987)
Norman Wells pipeline monitoring sites ground temperature data file: 1986. Energy, Mines and Resources Canada, Geological Survey of Canada, Open File 1621, 24 pp + app.

Burgess, M M, Pilon, J A & MacInnes, K L (1986)
Permafrost thermal monitoring program, Norman Wells to Zama oil pipeline. Intl.Soc.Pet.Ind. Bio., Proc.North.Hydrocarb.Dev.Env.Prob.Solv. Conf., Sept. 1985, Banff, Canada, 248-257.

Interprovincial Pipe Line (NW) Ltd. (1982).
Reassessment of plans to minimize terrain damage along the Interprovincial Pipe Line(NW) Ltd. oil pipeline from Norman Wells to Zama. Report to Nat. Energy Board of Canada, 25pp.

Interprovincial Pipe Line (NW) Ltd. (1984).
Post construction monitoring programs for the Norman Wells to Zama pipeline. Report to the National Energy Board of Canada, 29pp + app.

Interprovincial Pipe Line (NW) Ltd. (1986).
Norman Wells Pipeline project. 1986 report on monitoring of construction and operation. Report to Nat. Energy Board of Canada, 107pp.

Kay, A E, Allison, A M, Botha, W J & Scott, W J (1983).
Continuous geophysical investigation for mapping permafrost distribution, Mackenzie Valley, N.W.T., Canada. Proc.4th Intl. Perm.Conf., Fairbanks, Alaska, July 1983, 578-583.

MacInnes, K, Burgess, M, Harry, D, Baker, H, Tarnocai, C, Pilon, J & Judge, A (in prep).
Norman Wells to Zama Pipeline Permafrost and Terrain Monitoring Program: Progress Report 1983-1986.

McRoberts, E C, Nixon, J F, Hanna, A J & Pick, A R (1985).
Geothermal considerations for wood chips used as permafrost slope insulation. Proc.Intl. Symp.Gr.Freez., Japan, Aug. 1985, Vol.1, 305-312.

McRoberts, E C, Hanna, A J and Smith, J (1986).
Monitoring of thawing permafrost slopes: Interprovincial Pipe Line. Nat. Res. Counc. Canada, Proc. Workshops.on Subsea.Perm. and Pipelines in Perm., Nov. 1985, Tech. Memo 139, 133-151.

National Energy Board Canada (1981).
Reasons for decision in the matter of an application under the National Energy Board Act of Interprovincial Pipe Line (NW) Ltd., Supply and Services Canada Cat. No. NE 22-1/1981-1E, 173pp + app.

Nixon, J F & Pick, A R (1986).
Design of Norman Wells pipeline for frost heave and thaw settlement. Nat.Res.Counc.Can. Proc.Workshops Subsea Perm.&Pipelines in Perm. Nov. 1985, Tech.Memo. No. 139, 67-85.

Nixon, J F, Stuchly, J & Pick, A R (1984).
Design of Norman Wells pipeline for frost heave and thaw settlement. Am.Soc.Mech.Eng., Proc.3rd Intl.Offshore Mech. and Arctic Eng. Symp., New Orleans, La., Feb. 12-16, 1984.

Pick, A R (1986).
Norman Wells pipeline project. Nat. Res. Counc. Canada, Proc. Workshops on subsea permafrost and pipelines in permafrost, Nov. 1985, Tech. Memo. No. 139, 61-66.

Pilon, J A, Burgess, M M, Judge, A S, Allen, V S, MacInnes, K L, Harry, D G, Tarnocai, C and Baker, H (in prep).
Norman Wells to Zama pipeline permafrost and terrain research and monitoring program: site establishment report.

Wishart, D M & Fooks, C E (1986).
Norman Wells pipeline project right-of-way drainage control - problems and solutions. Intl.Soc.Pet.Ind.Bio., Proc.North.Hydrocarb. Dev.Env.Problem Solv.Conf., Banff, Canada, Sept. 1985, 209-218.

CONTRIBUTION TO THE STUDY OF THE ACTIVE LAYER IN THE AREA AROUND CENTRUM LAKE, NORTH EAST GREENLAND

M. Chiron and J.-F. Loubiere

Département de Géodynamique des milieux continentaux Université Pierre et Marie Curie, Paris, France

SYNOPSIS The objective of an expedition to northeastern Greenland was to conduct a preliminary study of one of the northernmost karsts in the world. It is located in Komprins Christian Land. We thought it would be interesting to observe the importance of the active layer (mollisol) at the end of the month of July 1983, on a terrace on the west bank of Lake Centrum.

INTRODUCTION

In the summer, at a latitude of 80° north, there is sunlight all the time and the temperatures are above zero. We noted that between July 10th and August 6th 1983 there was a minimum of +1° and a maximum of +14°. There was virtually no rainfall. However the region was swept by extremely high winds. The ground has thawed about several dozen centimeters and this thickness represents the active layer which is a good climatic indicater of the extreme environment. To the best of our knowledge, the only (and very interesting) measurements performed in the area are those conducted by W. Davies during his voyage of June 1960.
Our contribution, comprising several additional measurements, will trace 3 sections which cut through the terraces, the river and the lake.

LOCATION

Our soundings were performed on a large ice-free terrace bordered by two rivers (the Saefaxi Elv to the north and the Clear Water). The source of the two rivers is located in the large inlandsis situated some 40 km upstream to the west. They flow into Centrum Lake down further. The soil, which is composed of polygons of tundra 2 to 15 meters in diameter, consists of about 80% of sand of fluviatile and aeolian origin, while the remaining 20% consists of fine gravel. This surface is situated at an altitude of between 0 and 6 meters above sea level. Hekla Fjord is about 60 km avay.

METHODOLOGY

Two types of soundings were performed : firstly along an axis A, located entirely on the upper terrace, 1700 m in length, in an east-west direction; using shovels we dug four circular holes 60 cm in diameter, 565 m from each other.
Secondly, using a sledge hammer, we drove a round metal bar 2 cm in diameter, 2 m apart along an axis B (74 m in length) and then 45 m apart along an axis C (1125 m in length) until we reached the permafrost.

The first sounding of the cross-section (B axis) was performed in the emerged bed (after the summer flood) of the Clear Water River. The first sounding along the longitudinal section (C axis) was performed below the water level of Lake Centrum.

Observations

On the sandy terrace, 2.5 to 5 m above the lake, the depth of permafrost was found to be 76 cm (soundings 1 and 2 on A axis) and to be 83 cm (soundings 3 and 4 on A axis). Soundings 1 and 2 found that water collected very rapidly, suggesting a badly drained mollisol. Soundings 3 and 4 on the other hand, carried out at a slightly higher altitude, remained dry.

(i) In the permanent river bed, the water had acted as a shield and so the frozen ground was closer to the surface (39 to 40 cm). We believe that the calories supplied by the water (temperature 8.2 on July 13) contributed to the thaw and the formation of mollisol.

(ii) Below the surface of the lake, the ground had thawed over 16 cm (sounding along C axis). The temperature of the water therefore seems sufficient to be able to push back the permafrost at this level, with the formation of a submerged mollisol just below the surface of the river.

(iii) However, the fact that the water is not very deep in the intermittent branch of the river means it does not constitute an insulation layer sufficient to protect the permafrost which is thus pushed back to 60 cm from the surface which is only slightly submerged.

The terrace presented an exposed hill slope to the south (with a slope of 40°). In spite of this exposure, which would have been favourable to a pronounced thaw, we noted that the mollisol was relatively thin over the whole of the hill slope. It was only on the edge of the talus that the mollisol became at all significant, growing from 64 to 112 cm, the largest that we were able to observe in the region (see Figure 4, transverse cut, B axis, sounding 33). This zone has benefitted from the maximum solar radiation in July. We know that the albedo, i.e. the capacity of reflection with regard to solar radiation, varies with the nature of the environment affected by it. During the summer months, as the thin layer of snow has melted, the sandy substratum, which is dark brown in colour, absorbs the heat. This weakness in the action of the albedo synergizes with the exposure and the gradient factors of the site.

CONCLUSION

In this brief note, among the different factors of the geographic milieu influencing the freeze-thaw cycle of the soil, are the part played by the climate of the locality, the vegetation and snow coverage, the nature of the soil and its temporary degree of humidity with without water being present. The importance of another factor is confirmed: the exposure of the site.
We observed this in July 1983. This liquid mass delays the warming and the thawing of the submerged soil. According to our observations, it would seem that the level of water covering the permanently or temporarily submerged mollisol is decisive : the greater the layer of water, the smaller the thickness of the mollisol. For this to be confirmed, additional measurements would have to be made in both summer and winter at different depths in Lake Centrum. Even though quaternary continental carbonate formations of north Greenland are better understood (Adolphe, Loubière 1986), no study has been yet carried out to our knowledge on the lake sedimentation in this region.

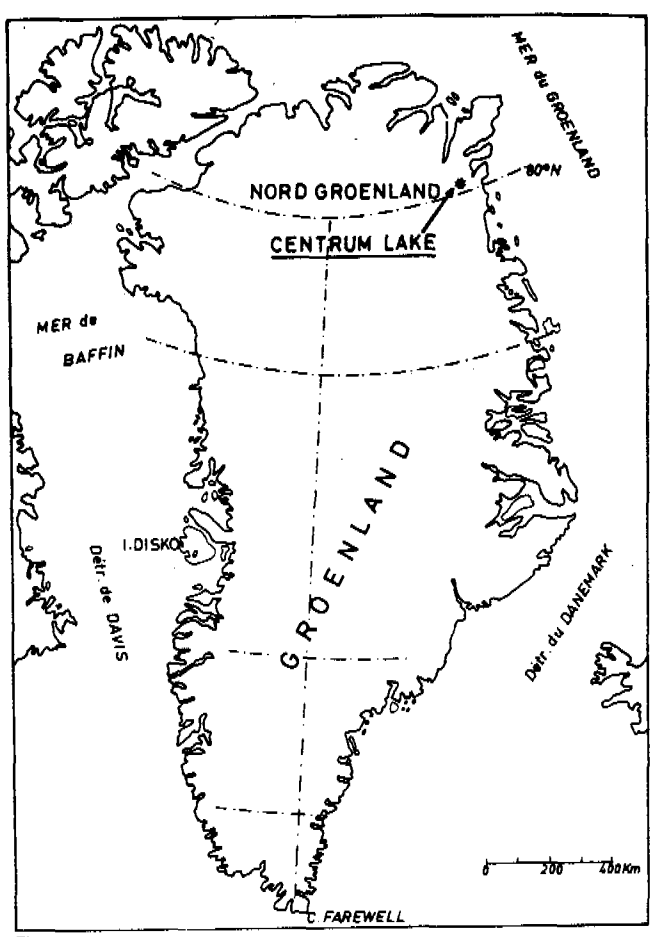

Fig:1
Geographical situation

REFERENCES

Adolphe, J-P, Loubière, J-F (1987). Etude préliminaire sur les calcins du Nord Est Groenland. Symposium Caen Août 86. Pecsi M.,French H.M (Eds): Loess and Periglacial phenomena, Akademia-Kiado, Budapest 1987

Davies, E.W. (1964). Surface Features of Permafrost in arid areas. US Geological Survey, Washington D.C. USA.

Davies, E.W. (1972). Landscape of Northern Greenland. Special Report 164. Cold regions research and engineering laboratory, Hanover, New Hampshire, USA.

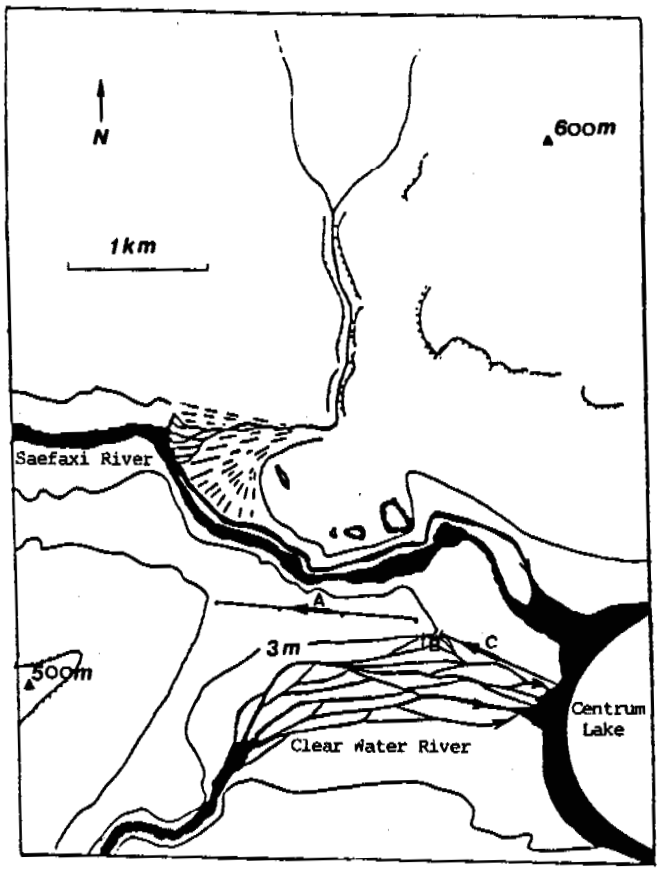

Fig. 2
Location of the soundings

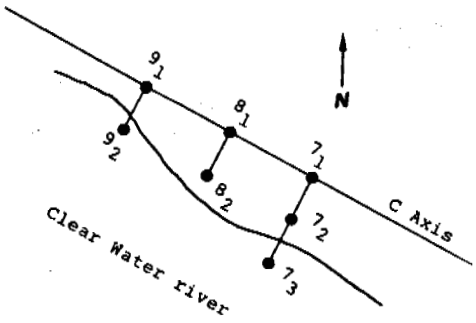

Fig. 3

Schematic showing the location of the soundings 9_2, 8_2, 7_2 and 7_3 parallel to the Clear Water river and perpendicular to the C axis. The soundings 7_3 and 9_2 were performed below the 18 cm of water of the river.

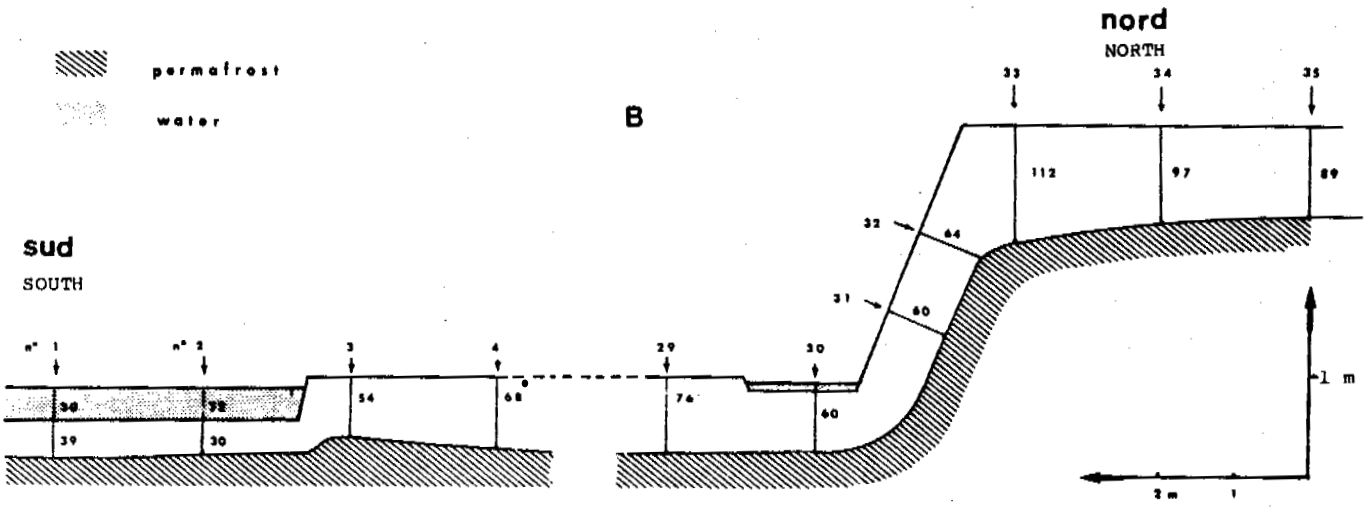

Fig. 4
Cross-section of the edge of the river of the first terrace showing the thickness of the mollisol

TABLE I

N° of soundings	Depth of water, in cm	Distance between the surface and the permafrost, in cm	Observations
1	no water on the surface	76	After 3 to 4 minutes 2 to 3 cm of water collected in the bottom of soundings 1 and 2
2		76	
3		83	Soundings remained dry
4		83	

A axis, oriented east-west, was 1700 in length. The 4 soundings were 565 m from each other (see map showing location).

TABLE II

N° of soundings	Depth of water, in cm	Distance between the surface and the permafrost, in cm	Observations
1	30	39	
2	32	30	The 2 soundings were performed below the waters in the bed of the Clear Water river.
3		54	
4		68	
5		72	
6		70	
7		70	
8		71	
9		69	
10		69	
11		74	
12		72	
13		74	
14		73	
15		73	
16		74	
17		75	
18		76	
19		73	
20		70	
21		73	
22		72	
23		72	
24		69	
25		69	
26		68	
27		67	
28		71	
29		76	
30	12	60	Sounding performed in an intermittent branch of the Clear Water river (see schematic 1)
31		60	
32		64	
33		112	
34		97	
35		89	
36		88	
37		84	
38		83	

The B axis, oriented south-north, was 74 m in length. The 38 soundings were 2 m from each other (see location map).

TABLE III

N° of soundings	Depth of water, in cm	Distance between the surface and the permafrost, in cm	Observations
1	30	46	The first sounding was performed below the waters of Lake Centrum
2		68	
3		65	
4		70	
5		68	
6		66	
7_1		76	Soundings tangential to the Clear Water river (see schematic 1)
7_2		63	
7_3	18	55	
8_1		71	
8_2	0	76	
9_1		63	
9_2	18	57	
10		62	
11		64	
12		68	
13		64	
14		68	
15		68	
16		67	
17		69	
18		69	
19		68	
20		70	
21		69	
22	15	73	Sounding performed in an intermittent branch of the Clear Water river.
23		65	
24		70	
25		76	

The C axis, oriented east-north-east / west-south-west, was 1125 m in length. The 25 soundings were 45 m from each other (see location map).

SEASONAL VARIATIONS IN RESISTIVITY AND TEMPERATURE IN DISCONTINUOUS PERMAFROST

A. Delaney, P. Sellmann and S. Arcone

U.S. Army Cold Regions Research and Engineering Laboratory, Hanover, N.H. 03755-1290 USA

SYNOPSIS Electrical resistivity and temperature were measured in two 12.2-m-deep boreholes in interior Alaska in perennially frozen ice-rich silt and in coarse-grained alluvium. Seasonal temperature and resistivity changes were most noticeable in the upper 6 m at both sites, with resistivity varying more than several thousand ohm-m during the year. Resistivity profiles were compared with lithology, temperature and moisture content. At the alluvium site resistivity and grain size strongly correlated. Values ranging over 10,000 ohm-m occurred with coarse-grained material and values an order of magnitude lower occurred in the fine-grained material section. At the ice-rich silt site, resistivity values were generally lower, but in agreement with values for the fine-grained part of the alluvial section. Lithologic variations in the discontinuous permafrost zone can be as important as the high permafrost temperatures and correspondingly large unfrozen water contents in accounting for significant seasonal resistivity changes in fine-grained sediment.

INTRODUCTION

The electrical resistivity of perennially frozen materials can be a direct indication of material type, permeability, volumetric water or ice content and temperature. Resistivity is usually interpreted from measurements of apparent resistivity using multi-electrode galvanic arrays (Wenner, 1915), low frequency magnetotelluric, wavetilt or surface impedance plane wave methods (e.g., Hoekstra et al., 1974; Arcone et al., 1978, 1979; Koziar and Strangway, 1978) or by magnetic induction and induced polarization techniques (e.g. Sinha, 1976; Hoekstra, 1978). The transient electromagnetic technique has proven useful for studies of thick permafrost (Ehrenbard et al., 1983). It was our intention to observe directly seasonal variations in ground resistivity using a permanent vertical electrode array and to compare the results with temperature and material characteristics.

Vertical arrays were installed at sites of previous geophysical investigations (e.g., Arcone et al., 1978; Arcone and Delaney, 1985). In early April 1985, strings of electrodes, 12.2 m long, were placed in boreholes in gravelly alluvium and in Fairbanks silt where soil type and ice content had been logged. The electrodes were at 30 cm intervals, which allowed vertical profiling at various electrode separations. The temperature holes were within 3 m of the resistivity holes and data were recorded throughout the year.

RESISTIVITY OF EARTH MATERIALS

The resistivity of most earth materials usually falls between 10 and 10,000 ohm-m. The factors that most influence the resistivity of unfrozen earth materials containing nonconductive (i.e., nonmetallic) minerals are free water content, ionic concentration, permeability, porosity and grain size. Conduction is mainly electrolytic along continuous films of water adsorbed on grain boundaries, and through water in pore spaces (Parkhomenkho, 1967). Conductivity (the inverse of resistivity) is proportional to the ionic concentration of the water and the ionic mobility, i.e., the concentration and quality of conducting paths, determined by material textural properties. As temperature drops below 0°C, the resistivity increases as the amount of unfrozen water decreases. This unfrozen water exists in an adsorbed state on the grain surfaces and in a saline condition in the pore spaces (Andersen et al., 1973). Consequently, the amount of fine-grained material in a section and the temperature will strongly control the unfrozen water content. Resistivities greater than 10^4 ohm-m have been encountered when the ground ice content is far in excess of saturation (Hoekstra et al., 1974).

METHODS AND MEASUREMENT TECHNIQUES

Resistivity

Measurements of apparent resistivity were made in vertical boreholes using the Wenner configuration. A Wenner array consists of four colinear, equispaced electrodes. A current I is delivered and received between the outer electrodes, and the resulting potential difference V is measured between the inner electrodes. For this array on the ground surface an apparent ground resistivity ρ_a is computed from

$$\rho_a = 2\pi a \frac{V}{I},$$

where a is the inter-electrode separation. If the array is within the ground (Fig. 1)

$$\rho_a = 4\pi a \frac{V}{I}.$$

This separation is varied to sound into the earth, or held constant to profile. If the ground is homogeneous, ρ_a is the actual ground resistivity ρ. Complicated integral formulations are required to relate layer parameters to ρ_a in the usual case of a horizontally layered earth, and interactive computer programs now facilitate interpretation of soundings made from the surface. Procedures are not available to interpret data for subsurface arrays. Close a separations were used to give readings indicative of the immediate surroundings; the radius of the zone of influence of a particular separation is generally assumed to be about 0.7 a. However, high-resistivity materials may force the current close to the borehole and reduce the depth of investigation (Labo, 1987).

The transmitter used was a Huntec LOPO Mk-3, which has a selectable output impedance to match electrode resistance as variations in ground conditions occur throughout the year. Maximum output current was selected (generally 0.2 to 1.5 A) and recorded for each data station. Potential was measured with a DC digital voltmeter (Fluke 8600A). Potentials were recorded for both cycles of the transmitter output and, during the off-cycle, to check for spurious self-potential readings that may indicate high contact resistance. The average voltage level was used to compute ρ_a for each station.

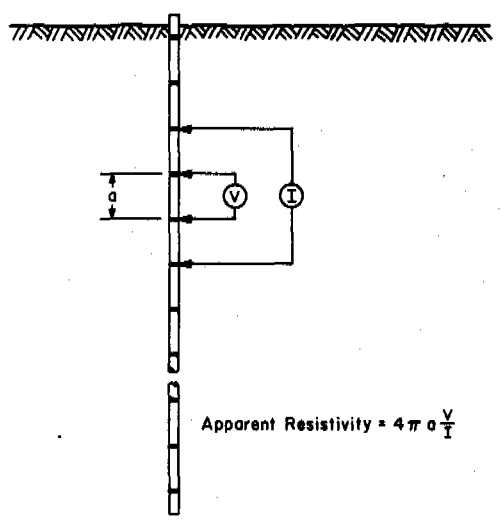

Fig. 1 A schematic drawing of the buried Wenner array.

The electrodes were placed at 30-cm intervals from the ground surface to a depth of 12.2 m and connected to a junction block at the ground surface. Each electrode was made up from several strands of tinned copper wire wrapped around the cable bundle. The cable bundles were armored with spiral wrap polyethylene to prevent damage both during installation and from frost action in the active layer. This bundle was then taped to the outside of a 3.8-cm-diameter (1-1/2-in.) ABS pipe for insertion into the drilled holes. This assured a straight cable array and accurate positioning of the electrodes.

Temperature

Vertical temperature profiles were recorded coincidentally with the resistivity measurements in a 3.8-cm-diameter cased hole filled with ethylene glycol. A thermistor calibrated to 0.01°C was attached to a 15.2-m cable and resistance was recorded with a Fluke 8600A digital multimeter as the thermistor was lowered down the glycol filled hole. Readings were made when the ohm-meter indicated thermal equilibrium at stations every 30 cm for the top 5 m and at 1.5-m increments below that level.

SITES

The study sites contained soils common to interior Alaska on much of the Yukon-Tanana uplands and on the broad Tanana floodplain. The silt site is at the USACRREL field station located off Farmers Loop Road near Fairbanks. It is an area of undisturbed permafrost with a natural black spruce forest and an organic ground cover. The active layer thickness is usually less than 1.0 m. The soil is retransported Fairbanks silt and is frozen deeper than 33 m (Péwé, 1958). Holes for casing installation at the silt site were rotary drilled using compressed air for circulation. Grab samples were obtained during drilling and the casing was backfilled with a silt slurry. Gravimetric water content was measured and converted to volumetric ice content using the calibration discussed by Arcone and Delaney (this volume).

The alluvium site is located near the Chena River on Ft. Wainwright in an area mapped as flood plain sand and gravel (Péwé, 1958). The annual active layer thickness is usually about 1.5 m and the soils are continuously frozen to at least 12.2 m. The 20.3-cm-diameter holes for casing installation were augered to 12.2 m.

RESULTS

Eighteen resistivity and temperature profiles were recorded between July 1985 and September 1986 at both the Ft. Wainwright and Farmers Loop sites. Apparent resistivity was recorded at 38 vertical locations on each recording session. Apparent resistivity results are for an a separation of 30 cm, and we assume that

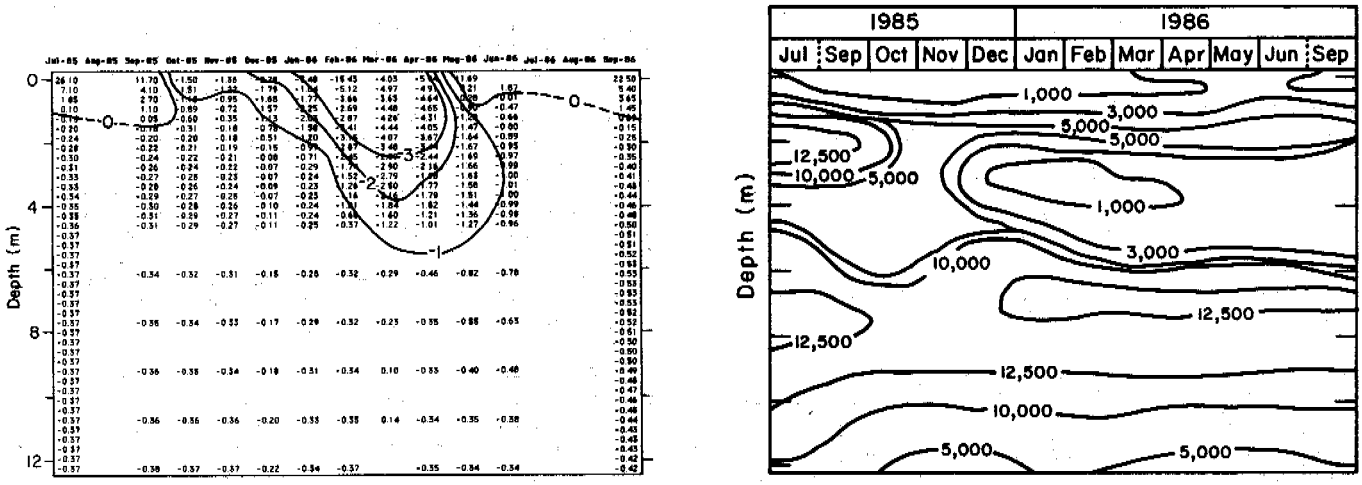

a. Temperature.

b. Apparent resistivity.

Fig. 2 Temperature and apparent resistivity contours as a function of depth for the alluvium site recorded between July 1985 and September 1986.

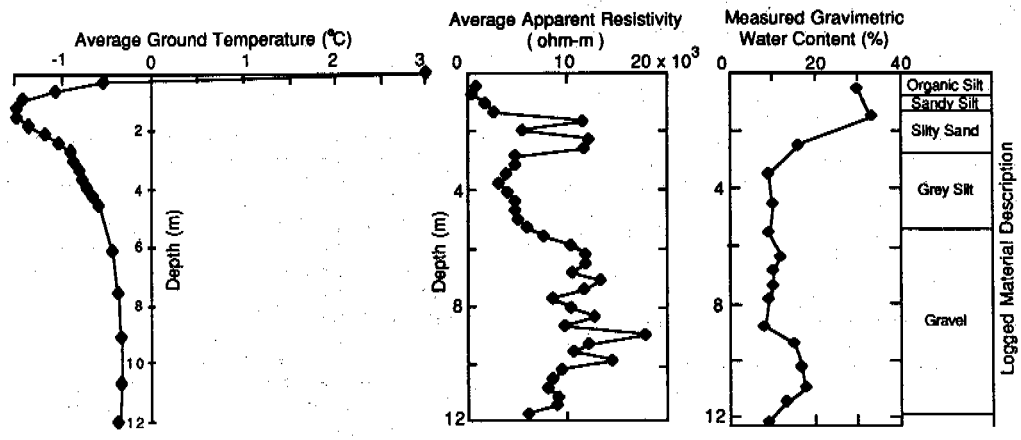

Fig. 3 The average apparent resistivity compared with the average ground temperature and gravimetric soil moisture content as a function of depth at the alluvium site.

material within a radius of 20 cm primarily influences the resistivity data.

Alluvium Site

Contoured temperature data are shown in Figure 2a. The zero degree contour defines the limit of seasonal thaw, which reaches 1.5 m by mid-September. The average temperature at 12.2 m is -0.36°C. All of the temperatures are very consistent at depth. The ρ_a values for the alluvial site are shown contoured in Figure 2b. Apparent resistivity is generally high throughout the year, with most values between 8,000-15,000 ohm-m at depths greater than 3 m. The widest range (92-25,000 ohm-m) occurs in the active layer, which experiences the most variation in moisture content and ground temperature. Values of 3,000-10,000 ohm-m recorded at 2-5 m depth in early December decreased to 700 ohm-m by late February, but did not return to the 1985 summer values. This zone of lower resistivity is shown by the 1000-ohm-m closed contour on Figure 2b. This may seem unusual in view of the lobe of low temperatures seen at this position in Figure 2a; however, what is actually unusual are the high values seen beneath July-October at 3-6 m depth. This zone is associated with the silt section shown in Figure 3, and at this time no logical explanation has been developed to clarify this unusual pattern.

Figure 3 compares the computed average apparent resistivity ($\bar{\rho}_a$) from all recorded measurements with gravimetric water content, with the lithology of samples from a hole drilled near the resistivity string and with average ground temperature. The subfreezing temperatures imply that nearly all the water was frozen except in the silt sections where the fine-grained nature of the soil can pro-

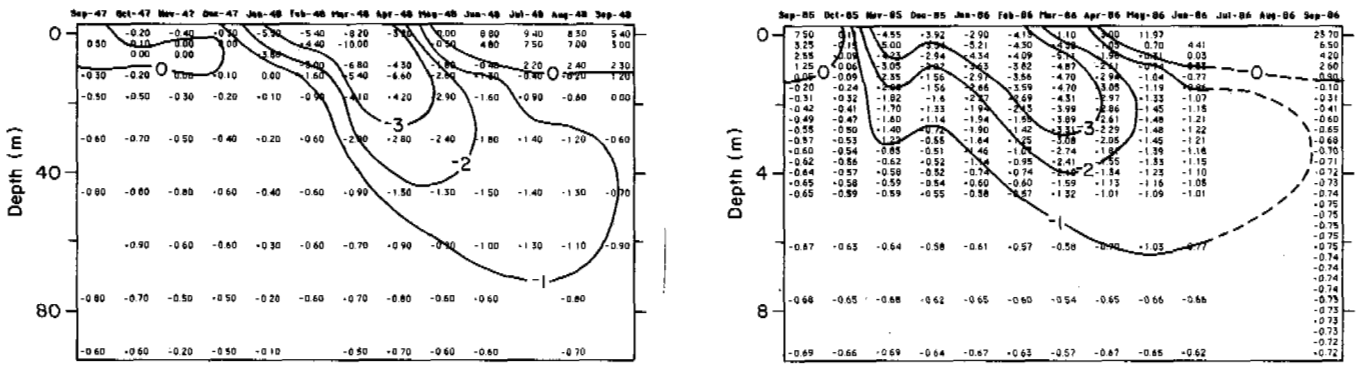

a. 1947-48. b. 1985-86.

Fig. 4 Temperature contours as a function of depth for the silt site.

vide a network of unfrozen water near the grain surfaces. The low $\bar{\rho}_a$ values at the surface are ascribable to the higher temperatures experienced during the summer and to the conductive active layer. The increase of $\bar{\rho}_a$ at the base of the active layer reflects the sharp decrease in average temperature and decrease in silt content. The sharp decrease below 3 m corresponds to the change in lithology back to silt. Below 4 m $\bar{\rho}_a$ gradually increases as the silt content progressively decreased with depth to less than 20% by weight of mineral content at 12 m depth. Arcone and Delaney (in press) have shown organic content generally to be less than 1% of dry weight.

Silt Site

Figure 4 shows temperature data recorded at the silt site for two recording periods. The 1947-48 data were recorded within 60 m of the present installation. Both sets show the average ground temperature to be less than -0.55°C at a depth of 9.14 m. Both the average value and the contours indicate no warming of the permafrost at this site after 38 years. The minimum surface temperature recorded during this study was -6.0°C, recorded on 26 February, and temperatures within 1.0°C of this value occurred within 1 m of the surface through 4 April. This period saw the highest resistivities occurring at the surface.

The ρ_a data are contoured in Figure 5. Lower resistivities of the active layer above 1.5 m are consistent with the higher ground temperatures. Values of 200-500 ohm-m occurred in the active layer at the time of maximum seasonal thaw, and values greater than 10,000 ohm-m occurred at the time of minimum ground temperatures. Below 2 m the readings at any depth show little change with time. Layering can be seen by the contouring, which reveals distinct zones where values less than 3,000 ohm-m occur.

Figure 6 compares average apparent resistivity ($\bar{\rho}_a$) with average ground temperature and volumetric ice content θ_v. The lowest values of $\bar{\rho}_a$ occur above 4 m depth where summer resistivities bring $\bar{\rho}_a$ down to about 1000 ohm-m. Between 4 and 6 m, θ_v is high and $\bar{\rho}_a$ nears 10,000 ohm-m. Despite no significant change in θ_v or T (seasonally as well), between 6 and 10 m, $\bar{\rho}_a$ decreases to around 2000 ohm-m. $\bar{\rho}_a$ then increases near the bottom as θ_v decreases. Previous field studies at this site by Arcone et al. (1978) confirm that values in the 1000 to 3000-ohm-m range are characteristic of this material beneath the active layer. However, laboratory studies of Hoekstra et al. (1974) have shown that Fairbanks silt with varying organic content (up to 10% of dry weight) can range several thousand ohm-m higher than silt without organics. Therefore, it is speculated that the zones of highest resistivity may be zones of higher organic content.

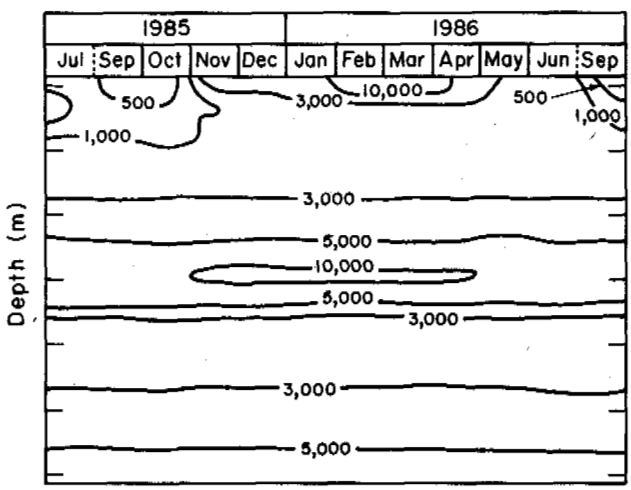

Fig. 5 Apparent resistivity contours as a function of depth for the silt site recorded between July 1985 and September 1986.

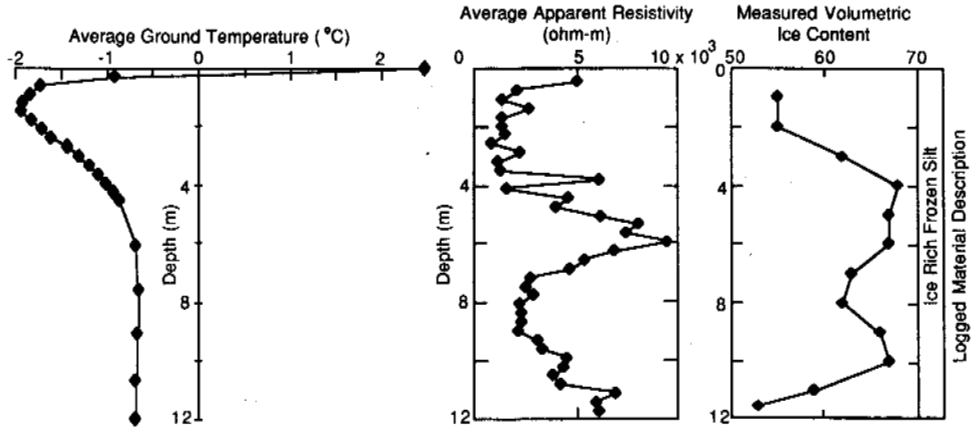

Fig. 6 The average apparent resistivity compared with the average ground temperature and volumetric ice content as a function of depth at the silt site.

DISCUSSION OF ERRORS

Contact Resistance

Two sources of error in determining ρ_a are contact resistance and effects of the borehole itself. Contact resistance results from poor contact between the electrodes and the ground; thus causing intense electric fields around the contact points as current is impeded. The result is an increase in ρ_a as contact resistance adds in series to the ground resistance. Borehole effects are caused by the presence of the borehole itself, which, in this case, is a highly resistive cylindrical column that must be accounted for in the computation of ρ_a.

After the ABS pipe was inserted into the borehole, a thawed silt (or sand) slurry was poured into the annulus between the pipe and the hole wall. The pipe was then rotated and tamped to enforce settling. Since measurements did not commence until mid-July (90 days after installation), we are confident of complete freezeback. If contact resistance is a serious problem throughout the array, then a log-log plot of ρ_a vs $\underline{a}$ separation will have a slope greater than 1. This was not seen in the data recorded using telescoping up-hole and down-hole soundings. Furthermore, general agreement between 30- and 60-cm $\underline{a}$ separation profiles, recorded at the silt site and shown in Figure 7, implies no contact resistance problems. The exact effect of the borehole itself is almost impossible to compute because of the asymmetrical placing of the electrodes (the string of electrodes may not be centered exactly in the hole). Nevertheless, an error was estimated using a theoretical model in which the electrodes are placed at the surface of a two-layer medium, the upper layer of which is infinitely resistive and equal to the pipe column radius (1.9 cm) in thickness, while the lower layer is of resistivity ρ. The computations revealed that at $\underline{a}$ = 30 cm the error is 8.4% at ρ = 500 ohm-m and continually decreases to 0.24% at 15,000 ohm-m. At values less than 500 ohm-m, the error is much more appreciable although within the correct order of magnitude. Such low values of ρ_a were recorded near the surface where surface effect may be more significant than that of the borehole. In any case one may argue that the effect of the borehole must be insignificant because the electrode spacing was so much greater than the borehole radius.

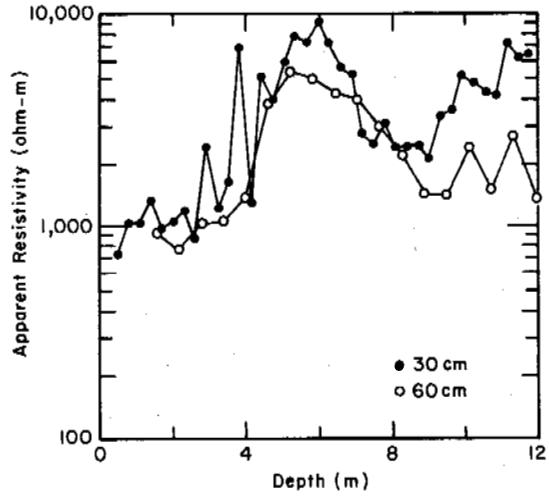

Fig. 7 Resistivity profiles recorded at the silt site using separations of 30 and 60 cm.

SUMMARY AND CONCLUSIONS

The observations provide a good quantitative record of seasonal variations in resistivity and temperature at two sites in the discontinuous permafrost zone. The results also show that apparent ground resistivity can be

measured in situ with permanently installed arrays in perennially frozen soils without significant effects from contact resistance or the presence of the electrode installation. The values obtained correlated well with the lithology at the alluvium site, and showed some unexpectedly high values at the ice-rich silt site in view of the relatively high (> -1.0°C) in-situ temperatures at depth. The general resistivity range at the silt site agrees well with previous research there, which used surface based methods, while the higher values obtained may be indicative of higher organic content. In contrast with the data recorded at the alluvium site, the silt site shows distinct values more consistent with temperature changes below the active layer and greater seasonal variation in the active layer resistivity. The results thus demonstrate that ground based resistivity surveys in interior Alaska can be strongly affected by seasonal variations and large variations in properties and distribution of fine-grained soils.

REFERENCES

ACFEL (1950).
Investigation of military construction in arctic and subarctic regions, comprehensive report 1945-48; Main report and appendix III-Design and construction studies at Fairbanks research area. Tech. Rep. 28, Permafrost Division, U.S. Army Corps of Engineers, U.S. Army Cold Regions Research and Engineering Laboratory, Hanover, New Hampshire.

Andersen, D M, Tice, A R & McKim, H L (1973).
The unfrozen water in frozen soils. Permafrost: Proceedings of an International Conference, 257-288, National Academy of Sciences, National Research Council, Washington, D.C.

Arcone, S A & Delaney, A J (this volume).
Borehole investigations of the electrical properties of frozen silt. Proc. V International Conference on Permafrost, Trondheim, Norway.

Arcone, S A & Delaney, A J (in press).
Investigations of dielectric properties of some frozen materials using cross borehole radiowave pulse transmissions. CRREL report. U.S. Army Cold Regions Research and Engineering Laboratory, Hanover, New Hampshire.

Arcone, S A & Delaney, A J (1985).
Dielectric studies of permafrost using cross-borehole VHF pulse propagation. Proc. Workshop on Permafrost Geophysics, Golden, Colo., CRREL Special Report 85-5, 3-5, U.S. Army Cold Regions Research and Engineering Laboratory, Hanover, New Hampshire.

Arcone, S A, Sellmann, P V & Delaney, A J (1978).
Shallow electromagnetic investigations of permafrost. Proc. III International Conference on Permafrost, (1), 501-507, Edmonton, Alberta.

Arcone, S A, Sellmann, P V & Delaney, A J (1979).
Effects of seasonal changes and ground ice on electromagnetic surveys of permafrost. CRREL Report 79-23, U.S. Army Cold Regions Research and Engineering Laboratory, Hanover, New Hampshire.

Ehrenbard, R L, Hoekstra, P & Rozenberg, G (1983).
Transient electromagnetic soundings for permafrost mapping. Proc. III International Conference on Permafrost, (1), 272-277, Edmonton, Alberta.

Hoekstra, P (1978). Electromagnetic methods for mapping shallow permafrost.
Geophysics, (43), 4, 782-787.

Hoekstra, P, Sellmann, P V & Delaney, A (1974).
Airborne resistivity mapping of permafrost near Fairbanks, Alaska. CRREL Research Report 324, U.S. Army Cold Regions Research and Engineering Laboratory, Hanover, New Hampshire.

Koziar, A, & Strangway, D W (1978). Permafrost mapping by audiofrequency magnetotellurics.
Canadian Journal of Earth Sciences, (15), 10, 1539-1546.

Labo, J (1987).
A practical introduction to borehole geophysics, Geophysical References, (2), 70, Norman Crook, Editor. Society of Exploration Geophysicists, Tulsa, Oklahoma.

Parkhomenko, E I (1967).
Electrical properties of rock. Translated from Russian by G.V. Keller, Plenum Press, New York.

Péwé, T L (1958).
Geology of the Fairbanks (D-2) Quadrangle, Alaska, U.S. Geological Survey Geological Quadrangle Map GQ-110.

Sinha, A K (1976). Determination of ground constants of permafrost terrains by an electromagnetic method.
Canadian Journal of Earth Sciences, (13), 429.

Wenner, F (1915).
A method of measuring earth resistivity, U.S. Bureau of Standards Bulletin 12.

PERMAFROST CONDITIONS IN THE SHORE AREA AT SVALBARD

O. Gregersen[1] and T. Eidsmoen[2]

[1]Norwegian Geotechnical Institute, Oslo, Norway
[2]Norwegian State Railways, Drammen, Norway (formerly of NGI)

ABSTRACT. Permafrost registrations at Svalbard are few, and have so far been restricted to inland areas. This article describes a recent project which has studied permafrost conditions in the shore area of Svalbard. Two representative sites, Longyearbyen and Svea, were chosen for the project. At both sites thermistors were permanently installed in 100 m deep drillholes. The data confirm the previous assumptions of no offshore permafrost and indicate the shore area to be a zone of "warm" permafrost. The data also give some interesting information on the geological history.

INTRODUCTION

With a mean annual temperature of about -6°C, the permafrost in central parts of Svalbard is classified as "cold permafrost". The geological history of Svalbard, however, makes the existence of offshore permafrost unlikely. Therefore, the shore area is believed to form a transition zone between frozen and unfrozen ground, a zone of "warm permafrost". As "warm permafrost" very often presents difficult foundation conditions, it is important to have this problem investigated prior to design of constructions in the shore area.

Previously no observations or analysis have been carried out to investigate this phenomenon. Neither have the few existing shore area constructions given any reliable information on this question.

During the period December 1986 to December 1987 this problem was given considerable attention by NGI, and a project including both temperature measurements and a theoretical analysis was carried out. Recent interest in this problem has grown from increased activity associated with resource prospecting both on Svalbard and its near-shore areas. The possible exploiting of new resources in the Svalbard region will make the shore area a very important zone for the location of different types of constructions such as docks, storage buildings and supply facilities. Also, the shore area is an important region for pipeline crossings.

TEST SITES AND INSTALLATIONS

Two locations were chosen for measurements of temperatures in the ground, Longyearbyen and Svea, see Figure 1. The climatic conditions are much the same at the two locations, with a mean annual temperature of about -6°C. However, the recent geological history is very different at the two locations. At Longyearbyen the shore area is "old land", raised about sea level after the last glaciation, probably a few thousand

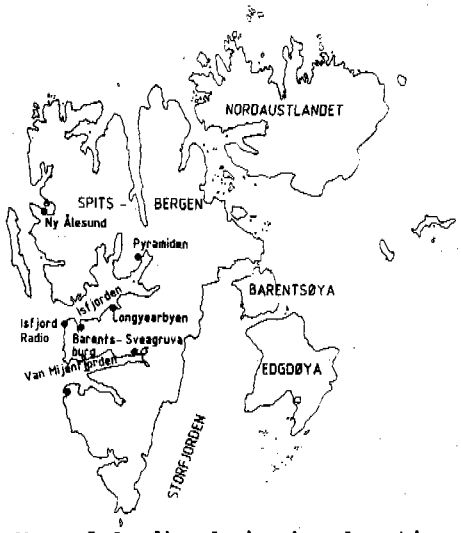

Figure 1 Map of Svalbard showing location of test sites Longyearbyen and Svea.

years ago. The soil profile is one of marine clay and silt overlain by fluvioglacial deposits. The Svea Lowland is "new land", about 700 years old. The area was submerged until surges of the Paula glacier across the van Mijen fjord compressed the seabed sediments and lifted them above sea level, Haga (1978) and Péwé (1981). The locations are shown in more detail in Figure 2.

The temperature measurement programme was based on preliminary theoretical calculations of the thermal conditions. The surface and water temperatures were assumed to be -6°C and +1°C respectively, and the temperature gradient to be 50 m/°C. Thermal conductivities were varied from 1.7 to 1.9 W/mK for clay and from 2.5 to 3.5 W/mK for bedrock. The results of these calculations are presented in Figure 3. The calculations show clearly that temperature measurements must be taken to considerable depths to give the necessary information. For practical reasons the depth was limited to 100 m. The figure also shows that the sea influences the ground temperatures to some 200 m from

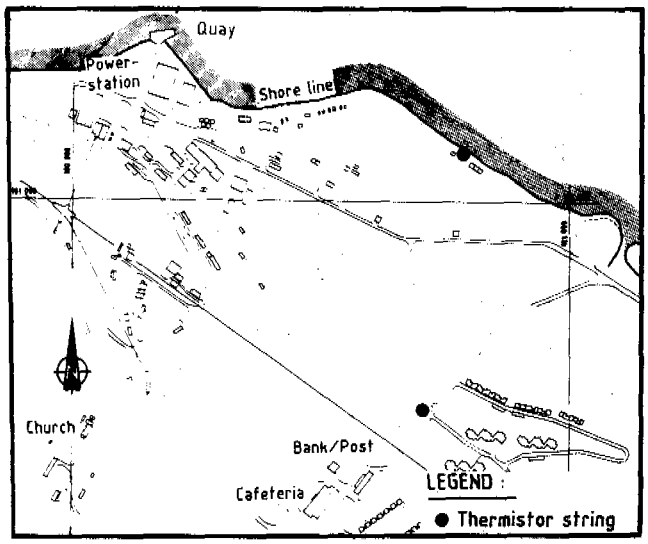

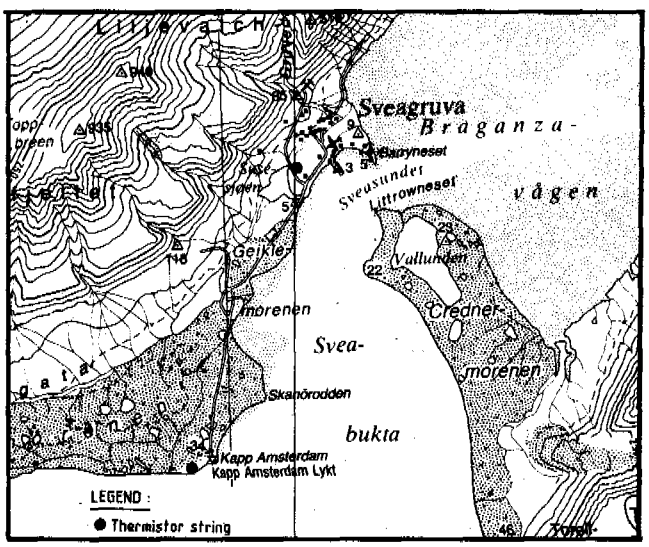

Figure 2 Test sites Longyearbyen (a) and Svea (b) showing locations of thermistor strings.

the shore-line. Reference temperature measurements must therefore be recorded at a distance of 200 m or further away from the shore-line. At Svea the reference measurements were taken some 200 m from the shore-line, and at Longyearbyen some 500 m. The thermistor strings are shown in Figure 3. Four 100 m strings were prepared with thermistors at 10, 15, 20, 30, 40, 50, 75 and 100 m depths. In addition, to obtain a detailed profile of temperatures within the depth interval influenced by annual variations in temperatures and surface conditions, separate 10 m long thermistor strings were prepared for installation in the shore-line at Svea and Longyearbyen, with thermistors placed at depths of 1, 2, 3, 4, 5, 6, 8 and 10 m.

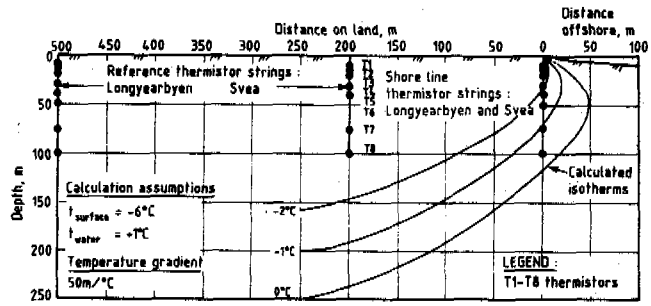

Figure 3 General profile showing results of thermal calculations and location of thermistor strings.

The thermistor strings were installed in predrilled holes. Drilling was performed during the period October to December 1986, using diamond core drill bits of internal diameter 42.5 mm and saline water as a drilling fluid. The temperature of the fluid varied from 0°C to 5°C. The depth to bedrock at Svea was 40 m at the shore-line location and 30 m at the on-land location; at Longyearbyen the depths were > 70 m and 10 m respectively. Drilling of a 100 m deep hole took between 2 and 3 days; all drilling was carried out according to plan, except for the shore-line hole in Longyearbyen which was stopped at a depth of 70.5 m instead of 100 m.

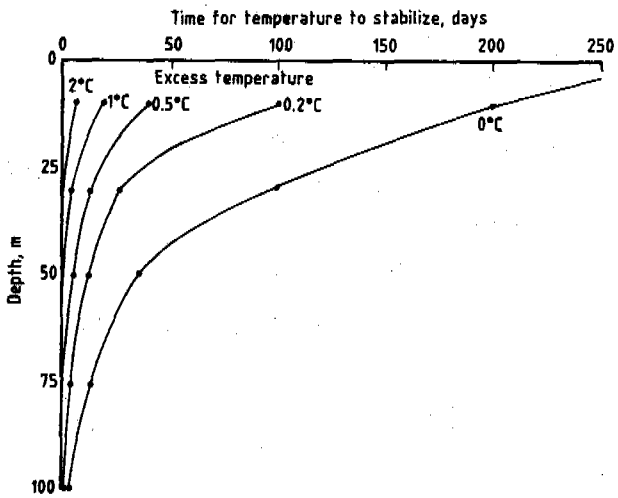

Figure 4 Diagram showing the time for temperature to stabilize after drilling a 100 m deep hole at Svea.

GROUND TEMPERATURE INCREASE DUE TO HEAT FROM DRILLING

The ground temperature around the borings increased during drilling, and measurements were taken to study the temperature stabilization process over the depth profile. Figure 4 illustrates this process for the 100 m deep "on-land" drill hole at Svea. The figure shows temperature increase that are highest near the surface and which diminish rapidly with depth. Consequently dissipation of excess heat takes less time in the lower part of the profile than in the upper part. For example, at a depth of 100 m the excess temperature is equalized 8 days

after completion of drilling, while at a depth of 10 m the time taken is 200 days; an excess temperature of 0.2°C is reached after 3 days at a depth of 100 m and after 100 days at a depth of 10 m. The observations demonstrate clearly that stabilization of temperatures in drill holes takes considerable time (months) and indicate measurements of ground temperature taken shortly after completion of drilling (days or weeks) may not be reliable.

REFERENCE TEMPERATURE PROFILES.

Figure 5 shows the measured temperature profiles at Longyearbyen and Sveagruva. While the reference profiles give a mean temperature of -6.1°C on the surface, the temperature gradients are very different for the two sites. At Longyearbyen the gradient is 30 m/°C while at Svea it is 20 m/°C. Extrapolation of the temperature profiles with depth gives 190 m of permafrost at Longyearbyen and 125 m at Svea. The temperature profile from Longyearbyen shows considerable irregulatities in the upper 30 to 40 m, and a constant average temperature distribution. This is not found at Svea where the profile shows a linear increase with depth. Liestøl (1980) reports typically vertical gradients in previous measurements which he attributes to the warm climatic period between 1920 and 1960.

Thermal gradients of 30 m/°C and 20 m/°C are steep compared to previous measurements at Svalbard, where Liestøl (1980) reports thermal gradients between 50 m/°C and 40 m/°C. The extreme steep thermal gradient at Svea indicates that the thermal regime in this area is not in equilibrium, but in a state of permafrost growth. The likely explanation for this is that the flat area, where the temperature profile is located, was originally submerged. Haga (1978) and Péwé (1981) proposed that surges of the Paula glacier across the van Mijen fjord compressed seabed sediments and lifted them above sea-level to form the present Svea Lowland. The last surge is dated to some 700 years ago.

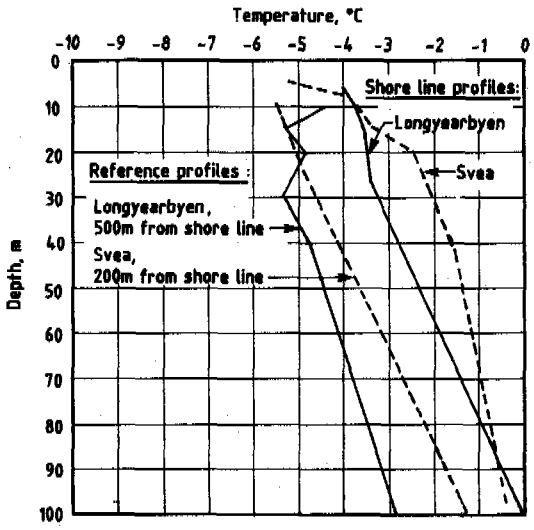

Figure 5 Measured temperature profiles Longyearbyen and Svea.

Simple thermal calculations have been carried out to test out this theory. The analysis assumes that the original surface temperature was 0°C, the temperature gradient is equal to the gradient in Longyearbyen (40 m/°C) and the surface was suddenly exposed to a surface temperature of -6.1°C. Results of the exercise, together with the measured temperature profile, are presented in Figure 6. Theoretically, and for these assumptions, the present thermal gradient is reached 500 years after lifting the area above sea level; however the actual measured temperatures are reached about 1000 years after the uplift of the land. While the calculations do not give full agreement with the measured temperatures, the simplicity of the exercise is such that it is fair to say the calculations fit surprisingly well with the theory.

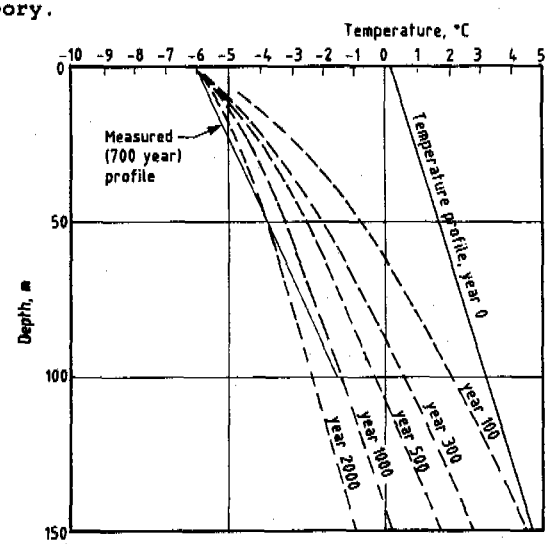

Figure 6 Calculated permafrost penetration for newly exposed land in Svea, as a function with time. Measured temperature profiles (700 years).

TEMPERATURE PROFILES AT THE SHORE LINE

Measured temperature profiles at the shoreline are also presented in Figure 5. Comparing the data from Longyearbyen and Svea, the temperatures reflect the same situation that was observed for the reference profiles. Temperatures at Longyearbyen are considerably lower than those at Svea and, as discussed above, result from the difference in geological history of the two locations. It should also be noted that, as expected, temperatures at the shoreline are much influenced by the heat resource of the sea. At a given depth the shore-line temperature is about 2°C higher than the reference temperature at the same site.

Isotherms are drawn from the measurements of temperature and are presented in Figure 7. The figure shows the shore area to be a zone of permafrost temperatures close to zero. At both sites the permafrost probably extends 30 to 40 m out from the shore-line. It also seems likely that the temperatures at shallow depths (10 to 20 m) are not significantly different for the

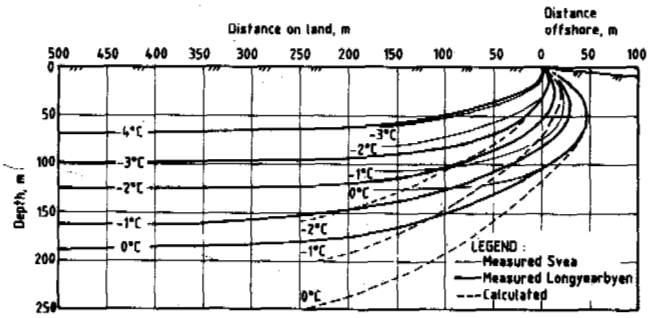

Figure 7 Isotherms, based on measured temperatures and theoretical calculations.

two sites, indicating that at shallow depths the temperature is mainly dependent on local surface conditions such as currents, ice conditions, and shore-line topography.

Results of preliminary calculations of the thermal conditions are included in Figure 7. In the shore area there is a reasonable fit between calculated and measured isotherms. The increasing discrepancy away from the shore-line is due to the incorrect assumption for the reference thermal gradient, 50 m/^{o}C, compared to measured values of 30 m/^{o}C and 20 m/^{o}C. Revised calculations using the correct reference thermal gradient would give a good fit with the isotherms based on measured data.

DISCUSSION

The field observations confirm that the shore area is a zone of warm permafrost. Inside the shore-line the mean temperature is 1-2^{o}C below zero, while outside the shore-line the surface temperature is above zero with transition to permafrost conditions at a few meters depth. It is probable that these conditions are largely representative of the shore zone along entire southern and western coastal areas of Svalbard.

However local conditions will have a significant influence on the temperature conditions at shallow depths, the most important zone for engineering construction. These conditions are currents, ice conditions and shore-line topography. Another important factor influencing the foundation conditions is the soil. At temperatures close to zero special emphasis must also be given to the salinity: With a high salinity the soil can be virtually unfrozen even at temperatures of -2 to -3^{o}C, Gregersen (1983).

The study has shown that geotechnical investigations of a construction site may be restricted to analysis of the local climatic conditions, measurement of the temperatures at shallow depth and analysis of the soil conditions. Such information would be sufficient for foundation design of most constructions when supplemented with the data from the present study. One should, however, bear in mind that thermal conditions, as revealed in the Svalbard shore-line area, are very unfavourable for foundation engineering. It is therefore essential that sufficient and appropriate local investigations be carried out.

CONCLUSIONS

1. Heat accumulation from drilling in permafrost ground can be considerble and may take months to dissipate. Reliable ground temperature profiles are obtained 5-6 months after completion of the drilling operation.

2. Ground temperature profiles reflect the recent geological history of the two areas. Temperature profiles at the 700 year old Svea Lowland are markedly warmer than at the much older land at Longyearbyen. At Svea the thermal conditons in the ground have not yet stabilized. A state of active permafrost growth has been documented.

3. Observations confirm that the shore-line is a zone of warm permafrost, and that with mean temperatures between +1 and -2^{o}C the thermal stability is delicate. From a foundation engineering point of view the shore area can be a difficult zone.

4. Thermal conditions of a land area are primarily a function of the overall climatic situation. The recorded temperature profiles are therefore in general representative of the entire shore zone of the southern and western coastal areas of Svalbard. However local conditions will have a significant influence on the conditions at shallow depth. When evaluating the thermal conditions of an area with respect to foundation engineering, both general knowledge representative of the region and data from a study of local conditions should be used. Such data are for example the local climate, currents, ice conditions, shore-line topography and soil conditions.

ACKNOWLEDGEMENTS

The authors are very grateful to Store Norske Spitsbergen Kulkompani, Svalbard, for their valuable assistance during installation work in the field. The project is supported by Statoil.

LIST OF REFERENCES

Gregersen, O., A. Phukan and T. Johansen (1983)
Engineering properties and foundation design alternatives in marine Svea clay, Svalbard. International Conference on Permafrost, 4. Fairbanks, Alaska 1983. Proceedings, pp. 384-388. Also publ. in: Norwegian Geotechnical Institute, Oslo. Publ. No. 159, 1985.

Haga, Ø. (1978)
A study of the effect of the Paula glacier on the sediments in the inner part of van Mijen fjord. Thesis (in Norwegian). University of Oslo.

Liestøl, O. (1980)
Permafrost conditions in Spitsbergen. Frost Action in Soils, Oslo. Publ. No. 21.

Péwé, T.L., D.E. Rowan and R.H. Péwé (1981)
Engineering geology of the Svea Lowland, Spitsbergen, Svalbard. Frost Action in Soils, Oslo. Publ. No. 23.

CORE DRILLING THROUGH ROCK GLACIER-PERMAFROST

W. Haeberli, J. Huder, H.-R. Keusen, J. Pika and H. Röthlisberger

Versuchsanstalt für Wasserbau, Hydrologie und Glaziologie, ETH Zürich, Switzerland

SYNOPSIS: Rock glaciers are perennially frozen debris masses which slowly creep down mountain slopes. Their ice contains undeciphered information about the evolution of periglacial environments since the last Ice Age. In addition, creep of rock glacier permafrost takes place under practically constant temperatures, stresses and strain rates. Rock glacier flow is therefore a natural large-scale/ longterm experiment on the steady state creep of ice-rock mixtures. In order to study these aspects, a core drilling project has been started on the active rock glacier Murtèl I, Piz Corvatsch, Engadin, Swiss Alps. The drilling operation took place in spring 1987. Borehole temperature at 15m depth is close to -2°C. Permafrost reaches down to the severely fissured and highly permeable bedrock at about 50m depth. Beneath a 3m-active layer, it contains (with increasing depth) pure and massive ice (12m), supersaturated frozen sands with ice lenses (17m), and ice-bearing blocks (18m).

INTRODUCTION

In mountain regions, ice-rich permafrost often occurs within steep, debris covered slopes. With increasing thickness of the ice bearing debris, stresses can build up which trigger the creep of the permafrost. During the process of permafrost creep, the original debris accumulation - for instance a scree slope or a moraine - is slowly deformed. The product of this deformational process is the rock glacier, certainly the most striking phenomenon of mountain permafrost. Based on the evidence now accumulated from geomorphological observations, geophysical soundings, and from geodetic and photogrammetric measurements, rock glaciers can be assumed to flow in a steady-state creep mode under fairly constant stresses, strain rates and temperatures. They contain large amounts of various kinds of congelation ice (Shumskii 1964) - interstitial ice, ice lenses and massive ice - as well as sometimes also buried sedimentary ice from avalanche cones and glacierets. First attempts to model rock glacier flow indicate that the age of most rock glacier permafrost is in the order of 10^3 to 10^4 years, i.e. comparable to the duration of the Holocene time period (Wahrhaftig and Cox 1959, Olyphant 1983, Haeberli 1985, Vitek and Giardino 1987). In order to gain more insight into these aspects, a core drilling project has been recently started in the Swiss Alps. The present contribution briefly describes the concept of the project, the investigated site, the drilling operation and some first results.

CONCEPT OF THE PROJECT

Flow of rock glacier permafrost can be considered to be a natural large-scale and long-term experiment on the creep of rock-ice mixtures. Compared to laboratory tests, this natural experiment has great advantages as well as severe limitations. The greatest advantage is given by the fact that steady state creep obviously takes place, and that boundary conditions vary little over extended time periods, mainly due to the thermal inertia of ice-rich permafrost. It is, however, very difficult to exactly define these boundary conditions; the 3-dimensional distribution of ice content, temperature, stress and strain rate cannot be accurately studied by surface observations and geophysical prospecting techniques alone (Haeberli 1985). As an important step towards at least partially overcoming these problems, it was decided to drill through the permafrost of an active rock glacier, to take core samples from the permafrost table down to bedrock, and to prepare the borehole for long-term monitoring of temperature and deformation. The results of core analysis and borehole observations are expected to furnish basic input data for modelling large-scale permafrost creep (cf. Sayles 1968, Hooke et al. 1972, Haynes 1978, Vyalov 1978, Echelmeyer and Wang 1987).

The ice within rock glacier permafrost is assumed to have formed within nonconsolidated sediments. In contrast to high-mountain firn and glacier ice, it probably originates from frozen groundwater rather than from directly-accumulated layers of atmospheric precipitation. Rock-glacier permafrost could contain information on the evolution of the Alpine environment and so be complementary to the information extracted from high-altitude glacier cores (cf. Oeschger et al. 1978, Wagenbach et al., in press). A number of analyses are therefore planned on the recovered cores in order to investigate the possibilities of reconstructing the past evolution of high-altitude permafrost, as well as of finding paleoenvironmental information on climate, hydrological processes or rock-wall weathering. These analyses will include studies of ice crystals (size and orientation), impurities in the ice (dust, pollen, air bubbles) and isotopes

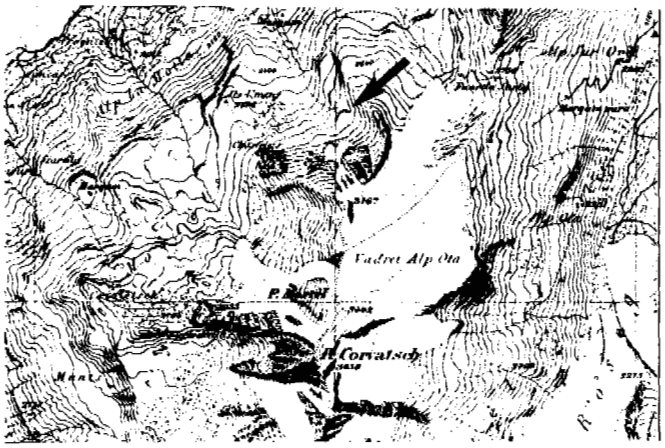

Fig. 1: Position of the investigated site on the "Topographischer Atlas der Schweiz", sheet "Bernina", compiled by Coaz (1850/51). Arrow points to rock glacier Murtèl I, the front of which is already clearly defined. Note that the rock-glacier surface was not covered by remarkable extents of perennial surface ice at the time of maximum glacier extent during the Little Ice Age.

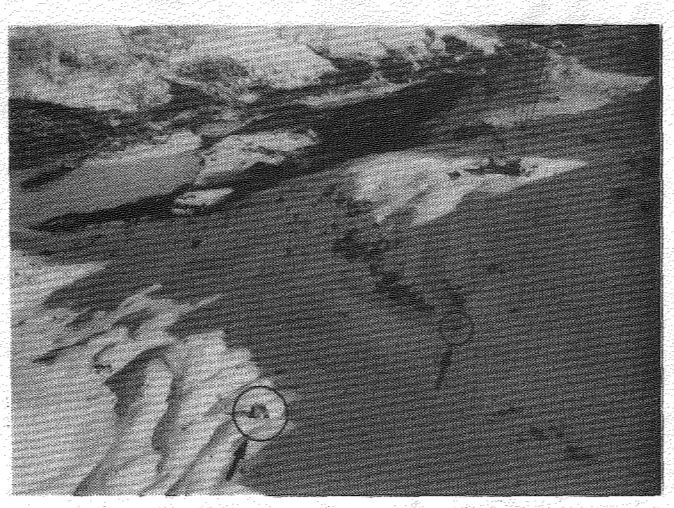

Fig. 2: Active rock glacier Murtèl I from the Corvatsch cable car during core drilling operation. Circles mark the compressor (at the sharp turn of a ski run) and the drilling station (in the center of the rock-glacier surface).

(^{18}O,^{3}H). Attempts will also be made to date the permafrost core, using ^{14}C-measurements on organic remains and flow models.

As a geothermal phenomenon, rock glacier permafrost is closely related to climate and the energy balance at the surface. Thermal conditions within rock-glacier permafrost are governed by climatic influences, as well as by geothermal and frictional heating. Climatic conditions have changed considerably during the past century. It is hoped that the long-term monitoring of borehole temperatures foreseen in this project will provide information on possible warming trends, and on what a future increase in temperature could mean for the thermal and mechanical stability of relatively warm and ice-rich mountain permafrost. General degradation of high-altitude permafrost could cause numerous problems to buildings recently constructed in ice-bearing permafrost (cf. Keusen and Haeberli 1983).

SITE DESCRIPTION

The active rock glacier Murtèl I near Piz Corvatsch, Upper Engadin, Grisons, was chosen as the drill site (Fig. 1). The place is easily accessible from the Corvatsch cable car. The rock glacier itself has developed within a former cirque from north-westerly-exposed scree slopes between 2850 and 2620 m.a.s.l. and shows very pronounced ogive-like transverse ridges (Fig. 2). The steep and approximately 20m-high front is largely free of vegetation and rests on granodiorite bedrock.When first accurately mapped in 1850/51 by Coaz, the rock glacier front and the streamlet emerging from it were very close to where they are today. In addition, the rock glacier surface was portrayed to be completely ice free. Small ice patches from avalanche cones exist today on the scree slopes at the head of the rock glacier.

A number of measurements have been carried out on the investigated rock glacier Murtèl I. Using shallow seismic refraction, Barsch (1973) showed the active layer thickness to be about 2 to 4m with a tendency towards higher values near the front. On the basis of snow temperature measurements, Haeberli (1973) indicated that permafrost is absent in the granodiorite rocks in front of the perennially frozen rock glacier. Barsch and Hell (1976) analysed displacements of surface boulders from aerial photographs taken in 1932, 1955 and 1971. They showed that surface flow is strongly compressing towards the front with average annual displacements being in the order of a few centimeters. Barsch (1977) has already carried out a shallow core drilling to 10.4m depth and he described the recovered material as mostly frozen silty sand with ice lenses. King et al. (1987) have obtained results from geoelectrical resistivity and radio-echo soundings, which agree surprisingly well with those from earlier deep seismic soundings (Barsch and Hell 1976), confirming that the bedrock beneath the rock glacier is overdeepened. From a comparison of the results from the three different sounding techniques applied, it was concluded that the rock glacier permafrost must be very rich in ice and that permafrost thickness should be comparable to bedrock depth which was expected to be around 50m at the drill site.

Fig. 3: Supersaturated sand and gravel frozen to the core catcher. In order to avoid contamination, such core samples were packed and stored separately.

DRILLING OPERATION

Field work started in late April, 1987. In order to recover uncontaminated cores and to minimize thermal disturbance of the borehole, it had been decided to use a triple core-tube system in combination with air cooling (cf. Lange 1973). An Atlas 12-bar screw compressor was therefore installed to deliver air at a rate of 13 m^3/minute through a snow-buried 2-inch tube (cooling) to an air tank for removal of condensed water and then to the heavy hydraulic Longyear-34 rotational core drilling machine. The core material was automatically filled into transparent plastic liners which remained insulated from the cold air circulating between the outer two tubes of the core barrel. The full plastic liners were cut to the appropriate size, closed, marked, packed into plastic bags, stored in a cooler box at -6°C and finally taken down to a deep-freeze facility (-30°C) by helicopter. During the whole drilling operation, mean snow cover thickness on the rock glacier surface slowly decreased from about 1m to a few decimeters.

A shallow experimental hole was first drilled to test the procedure. The boulders of the active layer were penetrated without coring providing air in the borehole could escape and the material was highly porous and permeable. A 6m-casing was installed (Odex-system) at the top of the borehole in order to stabilise the borehole walls at the permafrost table and within the active layer. Cores were taken from immediatly beneath the permafrost table at about 3m depth. Core diameter was 70mm and the outer diameter of the drill was 106mm. The samples came out completely dry, indicating that no melting had taken place during drilling and that the air cooling worked efficiently. The ice was quite heavily broken, however, probably as a result of stress relief. A hard-metal drilling bit was used in ice and ice-rich material. The last 10cm of each individual run were done without air cooling. This allowed the lower end of the core to melt slightly at the periphery, to freeze back to the core catcher (Fig. 3) and, hence, to hold chips of the core material within the plastic liner. A total of about 6m of ice-rich cores were taken in the experimental hole which reached a depth of 21.7m. The samples will be used for pilot analyses of the core material. A plastic tube was inserted to case the hole and a temperature of -1.7°C was measured at the bottom of the hole after thermal stabilization.

At the same time, the machine was moved by some 2m and drilling of the deep hole was begun. Cores were taken beneath 3.6m depth, large boulders usually had to be penetrated by percussion boring, and ice-containing rock was cored using a diamond crown in combination with a double core-barrel since rock cores tended to deform the plastic liners. No casing was used within the well ice-bonded material. Below about 45m however, the borehole became increasingly unstable. The last piece of ice was recovered at 51m within large boulders or severely-fissured rock, the transition between the two appearing to be gradual. Problems with unstable borehole walls continued in bedrock at greater depths. An attempt to inject concrete for stabilisation was not successful, because the injected mass disappeared into what was obviously highly permeable rock. Borehole television and caliper logging indicated that large cavities had formed in the lower part of the hole (Figures 4 and 5). No pressurized water was encountered. At 62.5m,the drilling was stopped within solid bedrock. A complete set of borehole logs was run in the temporarily water-filled experimental hole. However, the high permeability of the subpermafrost rocks made it impossible to fill the deep hole with water for borehole logging. Therefore, the experimental hole was deepened to 40m. Here again, unfortunately, air and water were lost at 32m depth, where a connection with the deep hole had developed in the meantime (air loss occurring from the experimental hole to the deep hole). 84mm diameter plastic tubes for horizontal and vertical deformation measurements were now introduced into the deep borehole down to a depth of 58m, where loose material had obstructed the hole. The inclinometry tubes were firmly anchored in bedrock with concrete; they had been put into a mantle of synthetic tissue in order to prevent loss of injected concrete in the permeable rocks. The upper part of the hole around the inclinometry tubes was filled with water which completely froze in the course of the first night. Thermistors and magnetic rings have been mounted around the tubes. The experimental hole has been equipped with a string of 1-component seismometers and precision thermistors down to a depth of 32m. The drilling operation finished in early July.

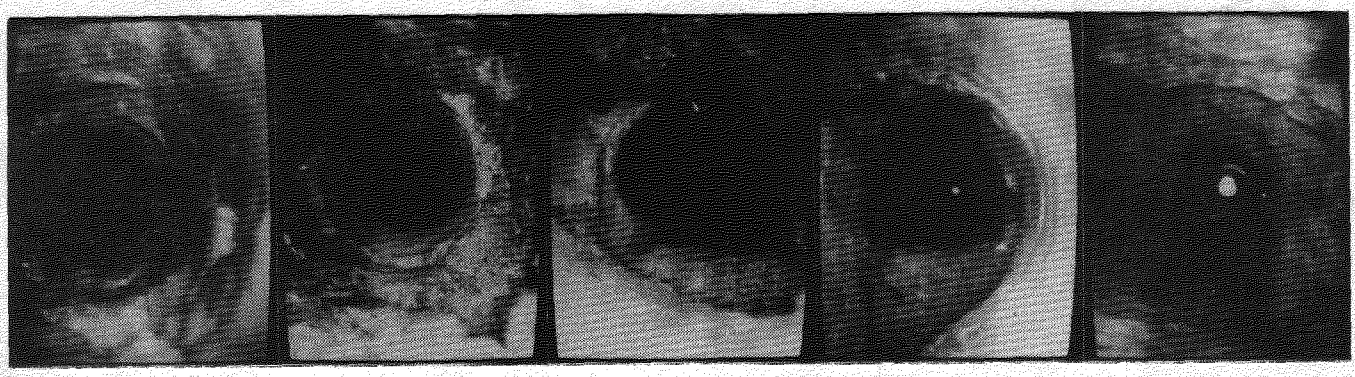

Fig. 4: Five single shots from borehole-TV showing smooth and heavily-iced borehole walls in frozen gravels at about 40m depth (left), irregular borehole geometry in unstable, relatively warm but still ice-saturated blocks and bedrock around 50m, and standing water (reflection from camera lights) in solid non-frozen bedrock at 54m (right).

FIRST RESULTS AND CONCLUSIONS

Figure 5 summarises a few preliminary results. Borehole diameter after drilling is from caliper logging and gives an indication of relative erosional stability. Temperature from borehole measurements in the fall of 1987 has been roughly corrected for thermal disturbances arising during drilling and is assumed to be within less than ±0.2°C of the undisturbed temperature. Stratigraphy is based on a visual, generalised description of the cores. Density was determined by weighing the cores and estimating the amounts of lost material where the samples are contained in plastic liners; from comparison with pure ice and rock samples, it is estimated to be correct within ±10% of the given value. Ice content by volume is from density. Finally, shear stress was calculated as the product of density, acceleration due to gravity, depth and the sine of the average surface slope (10°) measured over a length of 250m, i.e. five times the rock glacier thickness and about half of the total rock-glacier length.

Five main zones can be discerned beneath the active layer:

(1) to a depth of 15m, very pure ice predominates. Average temperature is -2 to -3°C and varies seasonally, density is close to 1 Mg/m^3 and shear stresses increase with increasing depth to a maximum of about 25 kPa.

(2) From 15 to 28m, layers of frozen and highly supersaturated silt, sand and gravel alternate with thick ice lenses. Average temperature is between -1 and -2°C, density is 1 to 1.5 Mg/m^3 and shear stress reaches a maximum of about 50 kPa.

(3) From 28 to 32m, the same material is encountered but without thick ice lenses. Temperature is slightly below -1°C, density increases to nearly 2 Mg/m^3 and shear stress is about 60 kPa.

(4) From 32 to 50m, coarse and saturated frozen rock debris containing layers of frozen sand in places extend down to bedrock at about 50m. Temperature increases towards the melting point at the bottom, where shear stress comes close to 150 kPa due to the high density (2 to 2.5 Mg/m^3) of the material.

(5) In contrast to what can be seen in front of the rock glacier, the bedrock immediately beneath the perennially frozen sediments is highly fissured and permeable. The permafrost base appears to coincide with the uppermost part of the heavily weathered bedrock. At about 54m, more solid and less permeable bedrock exists.

Much refinement of this information can be expected from more detailed measurements and analyses. However, a few general conclusions can be drawn already now. With respect to the fact that there are permafrost-free areas close to the drill site, the borehole temperature at the depth of zero annual amplitude is rather low. Permafrost thickness - as expected from geophysical soundings - is about 50m and the temperature gradient is surprisingly high. This may possibly be due to subpermafrost groundwater flow in permeable rock (cf. Echelmeyer 1987). Ice content decreases systematically with depth as expected, probably leading to the anticipated change in viscosity with depth (cf. Haeberli 1985). The amount of near-surface ice is, however, extremely high. In the upper half of the rock-glacier permafrost, the average ice content by volume is about 80 to 90%, figures comparable to what has been observed in basal layers of (ice) glaciers. It can be assumed that primary and secondary frost heave play an important role in the ice formation within the upper rock glacier layers and therefore largely influence the geometry of talus cones and scree slopes in general. Self-purification effects occurring at the freezing front may have displaced or even eliminated part of the environmental information usually contained in the inclusions and impurities of sedimentary ice. The pronounced layering of the rock glacier permafrost opens up the possibility of investigating the mechanical behaviour of various materials; these materials obviously deform under slightly different stresses and temperatures.

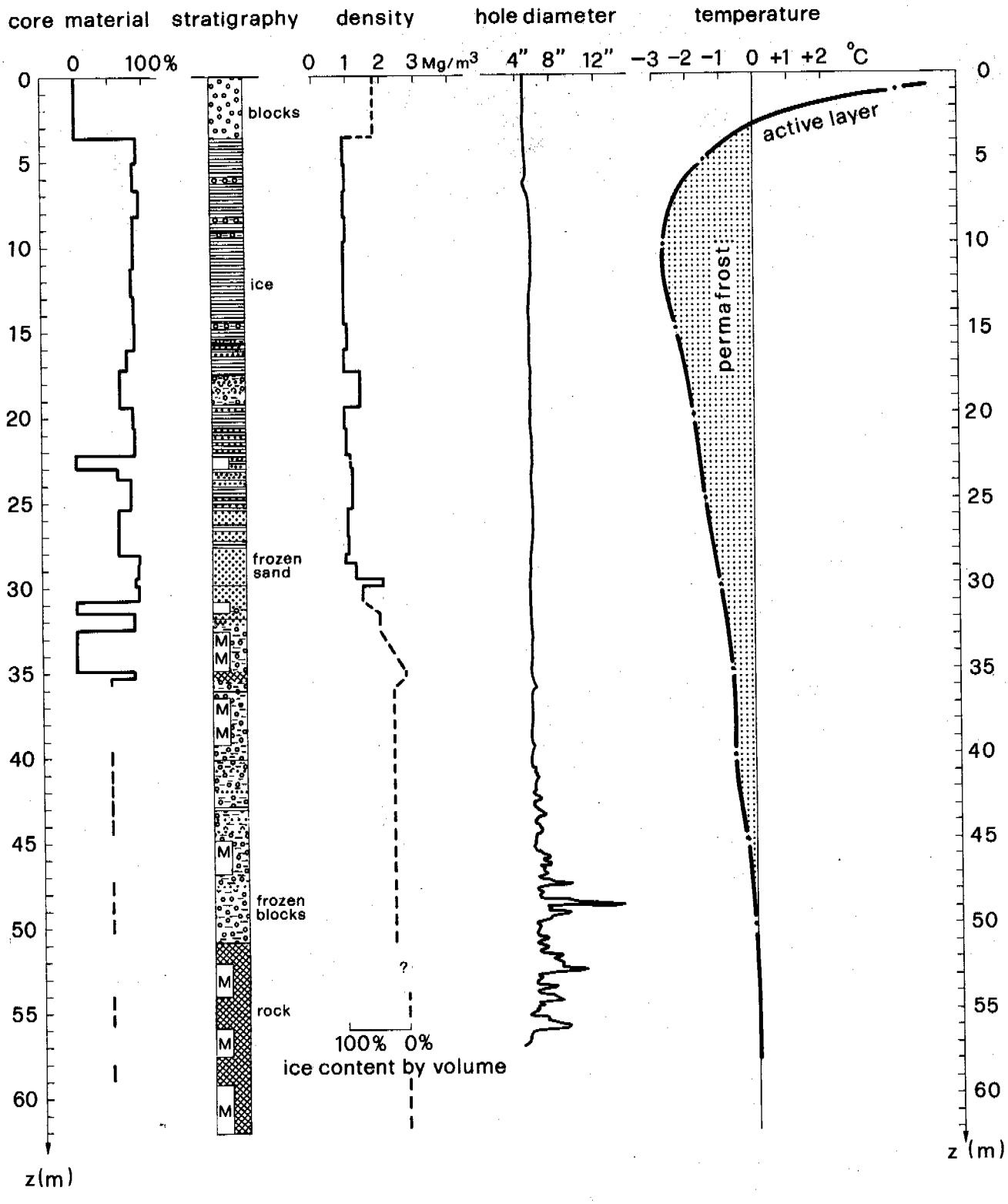

Fig. 5: Recovered core material, core stratigraphy, density and ice content by volume, borehole diameter immediately after drilling, and borehole temperature. M = zones penetrated by hammer ("martello"), dashed lines indicate rough and highly uncertain estimates.

ACKNOWLEDGEMENTS

The drilling work was carried out by Stump Bohr AG, Zürich, with substantial cooperation from the Cable Car Company Surlej - Silvaplana - Corvatsch. The project is being supported by a research fund from ETH Zürich. Bernhard Etter, Paul Gnos, Werner Nobs, Willy Schmid, Daniel Vonder Mühll and a number of other colleagues helped with the planning of the project and the field work. Pamela Alean edited the English of the manuscript. Special thanks are due to Prof. Dr. D. Vischer, director of VAW/ETH, for his constant encouragement and assistance.

REFERENCES

Barsch, D (1973). Refraktionsseismische Bestimmung der Obergrenze des gefrorenen Schuttkörpers in verschiedenen Blockgletschern Graubündens, Schweizer Alpen. Zeitschrift für Gletscherkunde und Glazialgeologie (9), 1 - 2, 143 - 167.

Barsch, D (1977). Ein Permafrostprofil aus Graubünden, Schweizer Alpen. Zeitschrift für Geomorphologie NF (21), 79 - 86.

Barsch, D and Hell, G (1976). Photogrammetrische Bewegungsmessungen am Blockgletscher Murtèl I, Oberengadin, Schweizer Alpen. Zeitschrift für Gletscherkunde und Glazialgeologie (11), 2, 111 - 142.

Echelmeyer, K (1987). Anomalous heat flow and temperatures associated with subglacial water flow. IAHS Publication (170), 93 - 104.

Echelmeyer, K and Wang, Z (1987). Direct observation of basal sliding and deformation of basal drift at subfreezing temperatures. Journal of Glaciology (33), 113, 83 - 98.

Haeberli, W (1973). Die Basis-Temperatur der winterlichen Schneedecke als möglicher Indikator für die Verbreitung von Permafrost in den Alpen. Zeitschrift für Gletscherkunde und Glazialgeologie (9), 1 - 2, 221 - 227.

Haeberli, W (1985). Creep of mountain permafrost: internal structure and flow of Alpine rock glaciers. Mitteilungen der Versuchsanstalt für Wasserbau, Hydrologie und Glaziologie der ETH Zürich (77), 142pp.

Haynes, FD (1978). Strength and deformation of frozen silt. Third International Conference on Permafrost, NRC-Ottawa, (1), 656 - 661.

Hooke, RL, Dahlin, BB and Kauper, MT (1972). Creep of ice containing dispersed fine sand. Journal of Glaciology (11), 63, 327 - 336.

Keusen, HR and Haeberli, W (1983). Site investigation and foundation design asopects of cable car construction in Alpine permafrost at the "Chli Matterhorn", Wallis, Swiss Alps. Fourth International Conference on Permafrost, NAP-Washington, Proc., 601 - 605.

King, L, Fisch, W, Haeberli, W and Waechter, HP (1987). Comparison of resistivity and radio-echo soundings on rock glacier permafrost. Zeitschrift für Gletscherkunde und Glazialgeologie (23), 1, 77 - 97.

Lange, GR (1973). Investigation of sampling perennially frozen alluvial gravel by core drilling. Permafrost Second International Conference, North American Contribution, NAS-Washington D.C., 535 - 541.

Oeschger, H, Schotterer, U, Stauffer, B, Haeberli, W and Röthlisberger, H (1978). First results from Alpine core drilling projects. Zeitschrift für Gletscherkunde und Glazialgeologie (13), 193 - 208.

Olyphant, GA (1983). Computer simulation of rock-glacier development under viscous and pseudoplastic flow. Geological Society of America Bulletin (94), 499 - 505.

Sayles, FH (1968). Creep of frozen sand. USA CRREL Technical report (190), 54pp.

Shumskii, PA (1964). Principles of structural glaciology. Transl. D. Kraus. Dover, New York, 497pp.

Vitek, JD and Giardino, JR (1987). A bibliography on rock glaciers. Oklahoma State University and Texas A & M University, 48pp.

Vyalov, SS (1978). Kinetic theory of deformation of frozen soils. Third International Conference on Permafrost, NRC-Ottawa, (1), 750 - 755.

Wagenbach, D, Münnich, KO, Schotterer, U and Oeschger, H (in press). The anthropogenic impact on snow chemistry at Colle Gnifetti, Swiss Alps. Annals of Glaciology.

Wahrhaftig, C and Cox, A (1959). Rock glaciers in the Alaska Range. Geological Society of America Bulletin (70), 383 - 435.

REMOTE SENSING LINEAMENT STUDY IN NORTHWESTERN ALASKA

Huang, S.L.[1] and N. Lozano[2]

[1]University of Alaska, Fairbanks
[2]University of Mississippi

SYNOPSIS: Landsat images have proven valuable in mapping of regional and local lineaments that control mineral occurrences. An investigation was conducted on Landsat MSS image to explore the feasibility of using spatial filtering techniques for geological structure studies in the Red Dog deposit area. The Red Dog deposit, located in northwestern Alaska, is one of the world's largest zinc deposits. The test Landsat image was processed with several 3-by-3 mathematical filters. Examination of the processed images revealed that a low-pass filter enhanced the subtle linear features in the area best. Major lineaments were traced on the filtered image and the result was compared with existing maps and reports. Not only were the mapped structures comparable to the field observations, but the resulting information also revealed two sets of major structural trends which had not been documented previously.

INTRODUCTION

Remote sensing techniques have been widely utilized to locate geological structures associated with major mineral occurrences. These techniques reduce the size of potential target areas, decrease exploration costs, and furthermore, increase the mineral discoveries. The identification of lineaments on images has an important implication in economic geology. Many mining districts occur along linear trends extending hundreds of kilometers in length. Within the mineralized zones, individual mines are commonly localized by intersecting fracture systems. Landsat imagery is useful for locating both regional structure and local lineaments.

Albert and Steele (1976) demonstrated that there was strong correlation between densities of linear structures and mineral occurrences, such as those found in the McCarthy quadrangle, with approximately 100 mineral occurrences. Metz (1983) conducted a study in the interpretation of linear features of Landsat coverage of Alaska and ratio image analysis of major mineral occurrences to determine characteristics of the alteration zones and local structures. Metz concluded that ratio image analysis could be an effective method of locating alteration zones associated with major mineral occurrences, however, no distinction between types of ore deposits could be made.

In this study, the authors applied a series of mathematical filters to a Landsat multispectral scanner (MSS) image to enhance and identify geological structures in the Red Dog deposit area. The enhancement methods used were of a simple, practical nature and allowed the authors to obtain preliminary information on the linear features which might be related to mineral occurrences.

REGIONAL GEOLOGY OF STUDY AREA

The Red Dog mineral deposit is located in northwestern Alaska (Fig. 1), about 960 km by air from Anchorage, Alaska. Kotzebue, the largest village near the mine, is located 144 km southwest of the deposit. The topography around the mine consists of rolling hills, leading into mountains to the north and the east. The elevation of the mine is 305 m above sea level and the area is within the continuous permafrost zone.

The present mine reserve is estimated to be 77 million metric tons at a grade of 17.1% zinc, 5% lead and 82 grams per ton of silver. The mine life is estimated at nearly 50 years (Giegerich, 1987). At full production, this mine will be the largest zinc mine and one of the lowest cost producers in the western world.

The western Brooks Range and adjacent areas are divided by Mayfield et al. (1983) into four geologic provinces: 1) the DeLong Mountains allochthon belt; 2) the Colville basin; 3) the Schwatka Mountains province; and 4) the Yukon-Koyukuk province. The DeLong Mountains allochthon belt consists of the Endicott Mountains, DeLong Mountains, Lisburne hills, and northern and western parts of the Baird Mountains. In this province the bedrock is composed of sedimentary and, to a lesser extent, igneous rocks that range in age from Ordovician to Early Cretaceous. The rocks occur in a series of stacked thrust sheets, the smallest division of a structural level.

The thrust sheets that exist in the DeLong Mountains allochthon belt contain parts of structurally overlapping sequences. These sequences are composed of sedimentary, metasedimentary and/or igneous rocks. This

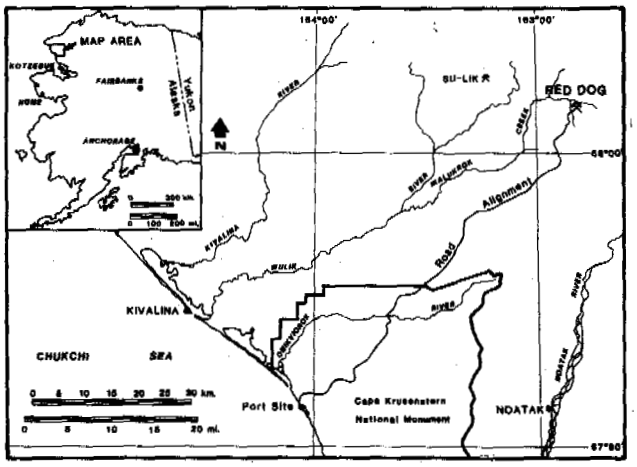

Fig. 1. Location of Red Dog Mineral Deposit (Giegerich, 1987).

region is thought to make up a large synclonorium with strata that dip south or southwest along the north front of the DeLong and Endicott Mountains, and north or northwest along the southern boundary. While many folds have diverse orientations, most axes in the DeLong Mountains generally parallel the westerly or southwesterly physiographic trend of the mountain range and are thought to be at right angles to the principle thrust direction.

The differentiated allochthons in the DeLong Mountains allochthon belt include the Brooks Range allochthon and six other allochthons. The Red Dog deposit is within the Brooks Range allocthon. The host rock consists of black shale, siltstone, and schist of the Early Mississippian to Early Middle Pennsylvanian Kuna formation (Lueck, 1983). The ore is found as sulfide disseminations in the host rock; discordant quartz-rich sulfide veins and stockwork fillings; massive, fine grained, conformable podiform bodies; and barite veins, some of which contain variable amount of zinc, lead, and iron sulfides. The mineralized horizon is overlain by rocks of the Pennsylvanian to Early Triassic Etivluk Group that consist mainly of unsilicified gray, green and red argillites interbedded with radiolarian cherts and thin barite layers of the Permian Siksikpuk formation.

IMAGE ANALYSIS METHODOLOGY

Landsat Data

The satellite image (scene ID 1387-22090) sensed by Landsat 1 on August 14, 1973 was obtained to study the regional geological structures. Multispectral scanners (MSS), the primary sensors aboard Landsats 1 to 3, provided an entire ground coverage of 185-by-185 km square per scene with a ground resolution of 79 m. Reflectance from the

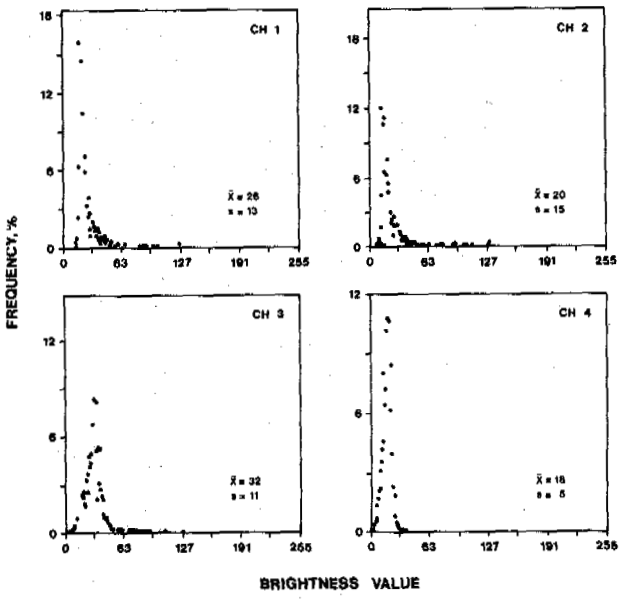

Fig. 2 Histograms of pixel brightness of the target image at four spectral ranges

terrain was separated into four spectral channels. Band numbers 1 to 4 designated images from the MSS system and separated the reflectance in spectral ranges of 0.5 to 0.6 micrometer (green), 0.6 to 0.7 micrometer (red), 0.7 to 0.8 micrometer (near IR) and 0.8 to 1.1 micrometer (near IR), respectively. A subimage of 40.5-by-40.5 km square corresponding to a subscene of 512-by-512 MSS pixels was used in the investigation.

Contrast Stretch

Image processing of the study was performed on a Comtal/3M Vision one/20 image processor, with a VAX 11/750 as the host computer. ELAS (Earth Resources Laboratory Application Software), a geobased information computer program package, was used in conjunction with the Comtal processing functions to extract data from Landsat image.

The initial attempt was to enhance the contrast of the original Landsat image. Fig. 2 shows the spectral radiance (brightness value) distributions of the target image at four spectral ranges. Statistical data indicated that the mean brightness values of the study images ranged between 18 and 32. In order to produce the optimun contrast, the original brightness values of four band images were stretched over the entire range of 256 gray levels according to the normal distribution curves. In the study a false color composite image of the Red Dog deposit area was generated by combining bands 1, 2, and 3 with blue, green, and red as the primary color for each corresponding image.

Lineament Enhancement

Landsat MSS sensors scan reflected electromagnetic waves from the terrain and record the radiance in a digital form. The complex wave of a Landsat image can be separated into its component wavelengths by a mathematical process known as spatial frequency filtering. Filters can be designed to transmit the waves depending on spatial frequency and direction. The common frequency filters applicable are high-pass, intermediate-pass, and low-pass. Low-pass filters are designed to emphasize large area changes in brightness and de-emphasize the local detail on the image. High-pass filters operate just the opposite. For example, a low-pass filter may be implemented by averaging the original brightness values of pixels within the filtered area, and a high-pass filter may be applied by subtracting a low-pass filtered image from the original image (Lillesand and Kiefler, 1987). The direction in which the filter is passed across the image also determines which linear features are enhanced. Lineaments normal to the filter direction are enhanced while those parallel to the filter direction are suppressed.

The image of Red Dog deposit area was filtered using the Comtal's convolver functions at different frequency levels. The convolution process, one of the filtering techniques, has been successful in enhancing the lineaments for geological structure studies. The convolution can be described as follows:

$$O(x,y) = \sum_{u=-a}^{+a} \sum_{v=-b}^{+b} I(x+u,y+v) f(u,v) \qquad (1)$$

where

O(x,y): the output pixel value at (x,y) after filtering;

I(x+u,y+v): the input pixel values surrounding the (x,y);

f(u,v): the filter coefficient.

The sum of all the filter coefficients is generally set to equal unity to avoid shifts in the average value of the image radiance. Filtering is performed with v lines of the image simultaneously. The influence convolution filter may have on an image depends upon the size of the filter and the values of filter coefficients (Lillesand and Kiefer, 1987). In the study, several 3-by-3 convolution filters were implemented to enhance linear features on the images.

The Comtal's convolution routine provided the authors with a real-time filtering process. The standard procedure invoking the convolution routine included the following:

(i) generating a color-composite image;

(ii) determining a convolver input image from the color image;

(iii) activating the convolver filter with a 3-by-3 matrix as shown:

a b a

b c b

a b a

(iv) specifying the filter coefficients interactively by depressing a special function key and rolling the trackball device to relocate the target positions.

Initially, the coefficients a,b, and c were set as 0, 0, and 1, and the target was moved to screen center (255, 255). While the interactivity was enabled, new values of a, b and c were generated, based on the following algorithms:

$$\frac{a}{b} = \frac{Y - 255}{255} \qquad (2)$$

$$\frac{b}{c} = \frac{X - 255}{255} \qquad (3)$$

where

x, y: the target coordinates ($0 \leq x, y \leq 511$).

The Comtal's low-pass filter was implemented as the target was moved into the lower right corner of the image. The low-pass convolution produced relatively constant filter coefficients. As the target was moved into the upper left corner, a high-pass filter with large variation in coefficients was generated. In the study, four types of convolution filters were used to enhance linear features on images of bands 2 and 3. The analysis involved processing images through a set of filters at various frequency levels. The filter, which emphasized linar features best at each frequency level, was chosen interactively while viewing the texture changes of the image. In general, the filtered band 2 image revealed geological structures in greater detail and the processed band 3 image enhanced the stream patterns and terrain features of the area.

The high-pass filter [1.43, -1.67, 1.43, -1.67, 1.94, -1.67, 1.43, -1.67, 1.43] was able to reveal the fine detail of terrain texture, although it suppressed the contrast between the main streams and the tributaries. The low-pass filter [0.10, 0.12, 0.10, 0.12, 0.14, 0.12, 0.10, 0.12, 0.10] was also activated to observe the effect on the image. The result of this low-pass filtering did not indicate any significant improvement. Among the filters tested, an intermediate-frequency filter [-0.01, 0.04, -0.01, 0.04, 0.88, 0.04, -0.01, 0.04, -0.01] was found to best show the linear features. An example of the filtered image is shown in Fig. 3. The filtered image, as compared with the color composite image, shows a better linear trends and less subtle brightness variations.

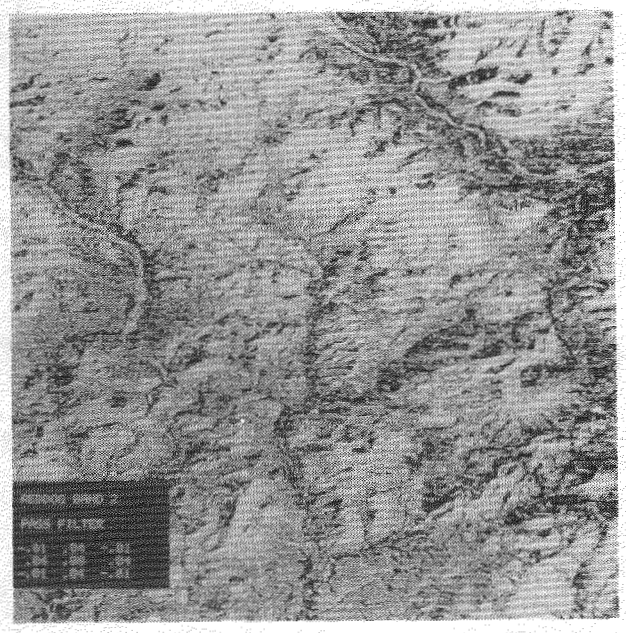

Fig. 3 Frequency filtered image of target area.

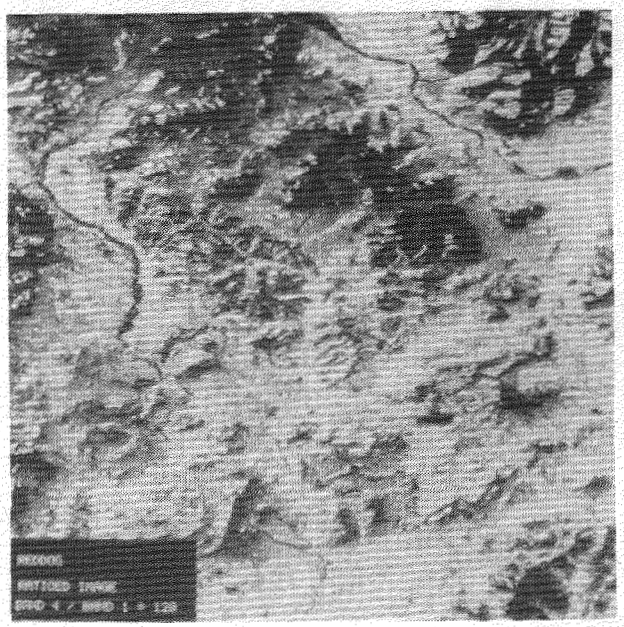

Fig. 4 Ratio image of band 4 to band 1.

Ratio images were also prepared by dividing the pixel brightness value in one band by the corresponding pixel brightness value in another band and the divisions were multiplied by a factor based on a look-up table. The contrast of ratio images was then enhanced by normal contrast enhancement techniques. The rationale for using the ratioing process was to remove the shadowing effect on terrain features. The process provided the authors with a better understanding of the distribution of linear topographic features, such as drainage patterns in the area. In the study, the ratio image of band 4 to band 1 was used to illustrate this advantage. The ratio image, as shown in Fig. 4, enhances the stream pattern and topographic highs.

RESULTS AND ANALYSIS

According to the palinspastic model proposed by Mayfield et al. (1983), the thrust sheets moved northward and collided with the Arctic Alaska plate, which has moved southward, out of the Beaufort Sea, in a counterclockwise motion relative to the North American craton. The Brooks Range was created in the Early Cretaceous period during an orogeny that produced numerous thrust faults with as much as tens of kilometers of displacement.

From the filtered image shown in Fig. 3 and a comparison with the ratio image (Fig. 4), two major linear trends were seen on the satellite image. Fig. 5A summerizes the major lineaments/thrust faults identified on the processed Landsat image. The major thrust faults mapped by Mayfield et al. (1983) are also reproduced and shown in Fig. 5B.

The east-west trend consists of linear features labelled as E, G and I on Fig. 5A and the north-south faults are composed of lineaments of A, B, C and D. The remainder of the thrust faults documented by Mayfield et al. (1983) are not identifiable from the satellite image. These traced lineaments, in general, coincide with the stream courses which tend to follow the weak zones. A less exposed lineament, A, is found on the right edge of the figure. This lineament, when overlapped over a topographic map, shows that it follows one of the tributaries of Wrench Creek. Along the lineament are ridges which parallel this linear feature until it intersects a thrust fault. This lineament appears to continue southward but shifts towards the east.

The north-south lineaments (B and D) also follow stream courses and connect to known mapped, thrust faults. The other major north-south lineament (C) starts at the junction of an east-west lineament and follows a known thrust fault until it reaches a tributary of the Wulik River.

The east-west lineaments were detected and they too follow stream courses. The lineament (E) at the bottom of the map (Fig. 5A) has been mapped as a thrust fault by Mayfield's team, but the other lineaments (F, G, and a branch of H) were not documented. The second east-west lineament (G) follows a stream course on the right edge of the map and continues westward, parallel to a set of ridges. The third east-west lineament (I) begins as a mapped thrust fault, but continues westward, following stream courses and saddles

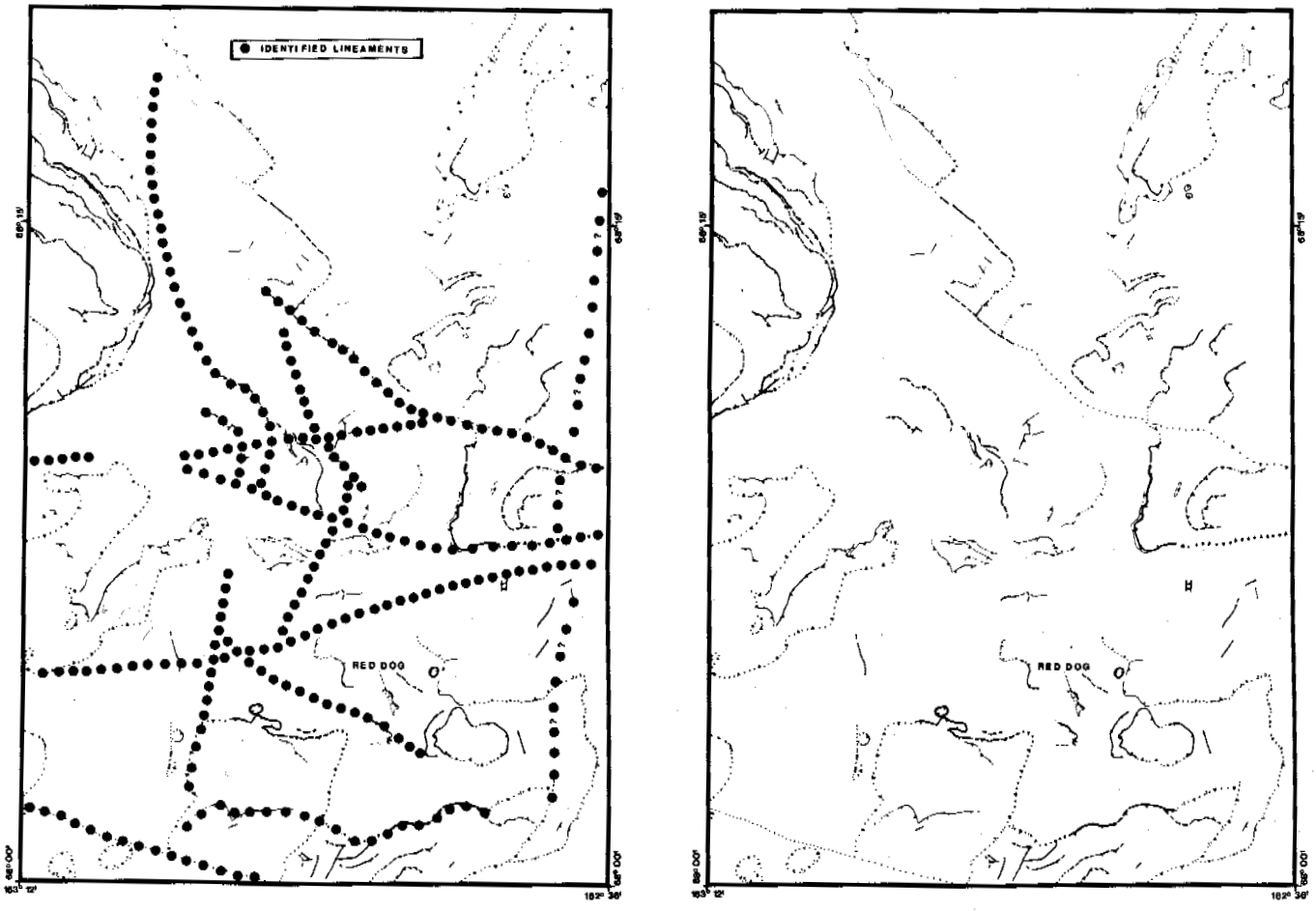

Fig. 5 (A) Major lineaments identified on Landsat image of Red Dog deposit area.
(B) Regional geological structures mapped by Mayfield et. al. in 1983.

until it reaches the Wulik River. This lineament branches out and one of the branches follows a mapped north-west thrust fault. The other follows a stream course which intersects with the Wulik River and is concealed by the alluvial deposit of the Wulik River.

CONCLUSIONS

In summary, conclusions drawn from this study are:

(i) The low-pass filter is most valuable in the enhancement of linear geological features in the Red Dog deposit area, Alaska;

(ii) The filtered band 2 (near IR) image reveals structural lineaments in greater detail while band 3 image enhances stream pattern; and

(iii) Most of the lineaments identified on the image follow stream courses and appear to coincide with a number of the mapped major thrust faults in the region.

ACKNOWLEDGEMENTS

The authors wish to express their gratitude to Mrs. Alice Baergen for her assistance in typing this manuscript and to Mrs. Cathy Farmer for her review of the article.

REFERENCES

Albert, N.R.D. & Steele, W.C. (1976). Interpretation of Landsat imagery of the McCarthy quadrangle, Alaska, U.S. Geological Survey Misc. Field Studies Map MF-773N, Scale 1:250,000, 3 sheets.

ELAS (1984). Earth Resource Laboratory Applications Software - ELAS user's guide, NASA, National Space Technology Laboratories, Earth Resources Laboratory.

Giegerich, H.M. (1987). Progress report on Cominco's Red Dog Project in Alaska, second largest zinc deposit ever discovered: Mining Engineering.

Lillesand, T.M. & Kiefer, R.W. (1987). Remote sensing and image interpretation, 721p, John Wiley and Sons, 2nd Edition, New York

Lueck, L. (1983). Petrologic and geochemical characterization of the Red Dog and other base-metal sulfide and barite deposits in the DeLong Mountains, Western Brooks Range, Alaska, in Master thesis, University of Alaska.

Mayfield, C.F., Tailleur, I.L., & Ellesiek, I. (1983). Stratigraphy, structure, and palinspastic synthesis of the western Brooks Range, northwestern Alaska. U.S. Geological Survey, Open-File Report OF 83-779.

Metz, P.A. (1983). Landsat linear features and mineral occurrences in Alaska. MIRL Report No. 66, University of Alaska-Fairbanks, Alaska.

THERMAL EVIDENCE FOR AN ACTIVE LAYER ON THE SEABOTTOM OF THE CANADIAN BEAUFORT SEA SHELF

J.A. Hunter, H.A. MacAulay, S.E. Pullan. R.M. Gagné, R.A. Burns and R.L. Good

Geological Survey of Canada, 601 Booth Street, Ottawa, Ontario, Canada, K1A 0E8

SYNOPSIS Thick permafrost occurs widely beneath the Canadian Beaufort Sea continental shelf. Over much of the seafloor, the water temperatures are below 0°C. However, in nearshore regions, out to 25 km offshore, seasonal changes in water temperatures occur due to variations in the Mackenzie River outflow. During summer months, warm river water (above 0°C) flows on to the shelf and is in contact with the bottom to water depths of up to 20 m. During winter months, the flow is reduced and the effects of the upwelling of Arctic seawater (below 0°C) on the shelf can be observed in water depths as shallow as 2 m. An active layer at the seabottom is produced by these seasonal changes and the thermal effects reach beyond 10 m sub-bottom.

Between 1977 and 1986, six regional temperature profiles were compiled from the readings of thermistor cables installed in 80 drill-holes on the Beaufort shelf. These data, which were obtained at the end of the winter period, showed the previous summer's warming effect to be at a depth of 7 to 10 m below bottom, with the thermal anomalies attenuating seaward. At one additional shoreline site, both summer and winter sub-seabottom temperature profiles show large seasonally reversing thermal gradients of up to 2°C per metre within the first kilometre offshore. The presence of an active layer should be a consideration in seabottom engineering design in a permafrost regime.

INTRODUCTION

The Canadian Beaufort Sea continental shelf has recently become an area of intense oil exploration activity. Sufficient oil reserves have been established to warrant consideration of plans for future development from offshore wells. Designs for well completions and pipelines are not without technical difficulties due to the presence of ice-bearing permafrost at shallow depths.

The Beaufort Sea shelf is relatively shallow, extending 120 km offshore to a shelf break between 90 and 110 m water depth. Since the shelf was thought not to have been glaciated during the late stage Pleistocene ice advance, Mackay (1972) suggested that extensive permafrost could have accreted beneath the seafloor which, because of sea-level lowering, was exposed as dry land. Hunter et al. (1976, 1978) provided geophysical evidence that indicated the widespread occurrence of ice-bearing permafrost under the Canadian Beaufort Sea shelf, and this has been subsequently confirmed by industry drilling (O'Connor, 1984). Taylor and Allen (1987) have shown, from seabottom temperature measurements seaward of the 25 m isobath, that permafrost conditions presently occur at the seabed over almost the entire outer shelf zone, where the measured seabottom temperatures range from -0.41 to -1.92°C.

The heat transport of the Mackenzie River has a strong influence on the inshore water temperatures on the Canadian Beaufort shelf (Fig. 1), and this in turn affects the distribution of offshore permafrost (Mackay and Mackay, 1974). The Mackenzie factor makes the configuration and thermal history of sub-seabottom permafrost in this region very different from that of offshore permafrost beneath the Alaskan Beaufort Sea shelf (e.g. Swift et al., 1983). This present study focusses on the influence of the Mackenzie River discharge as it affects the nearshore sub-seabottom permafrost configuration out to water depths of 20 m. Studies of this nature may be a necessary consideration in designing nearshore pipeline approaches and shoreline crossings.

The Mackenzie River discharge has a strongly seasonal character. Figure 2 is a generalized flow-rate curve based on an average of four years (1980-1983) observations at Arctic Red River, which is at the apex of the Mackenzie Delta (e.g. Environment Canada, 1982). Characteristically, an abrupt increase in discharge rate occurs in late May or early June, when flow rates can reach ten times that of the winter low. The rate drops off rapidly to about half its maximum during June, and then decreases uniformly throughout the summer. By the end of November the Mackenzie discharge is back to its low winter value. Although no discharge records are available at the mouths of any of the delta channels, it is suggested that the discharge at the seacoast follows the general trend of the curve shown in Figure 2, with perhaps a time delay of some days.

Between 1977 and 1986, a series of end-of-winter temperature measurements of both

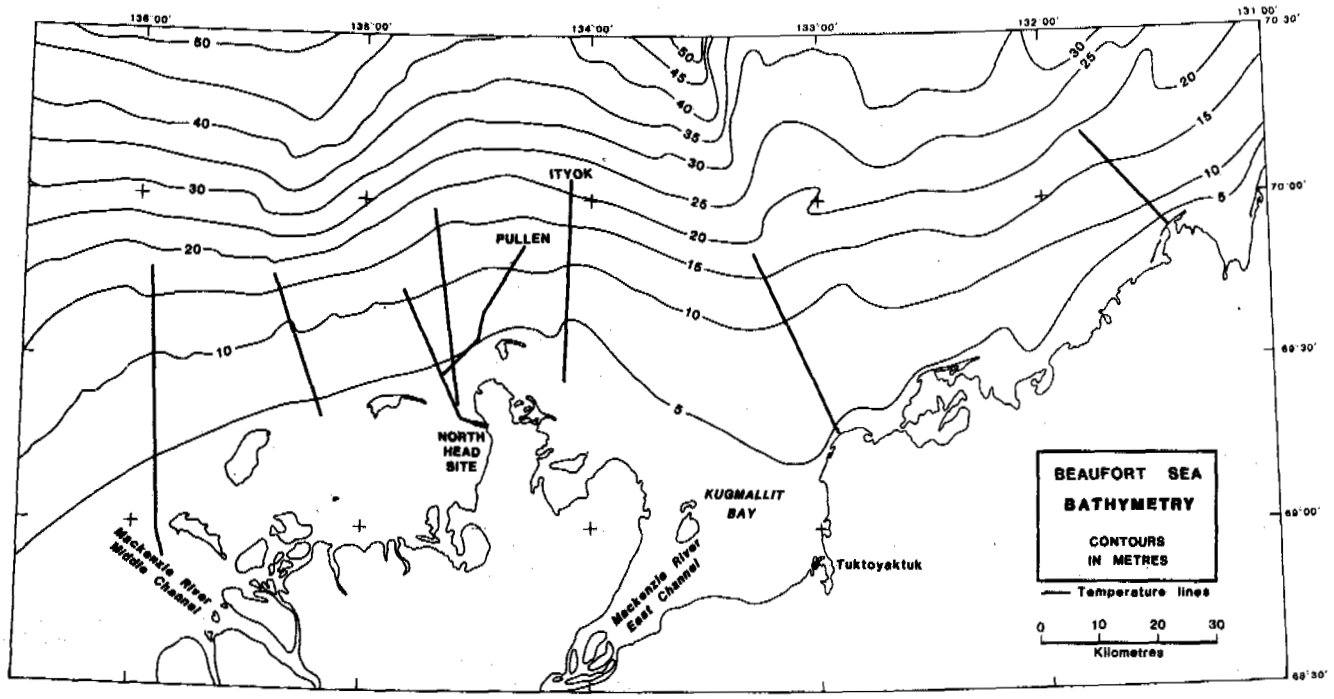

Fig. 1 - Generalized bathymetry of the southern Canadian Beaufort Sea and location of temperature lines.

seawater and the sub-seabottom sediments were made during the month of April. These measurements were made along six regional nearshore to offshore lines in water depths of up to 12 m. Additionally, seawater column temperature measurements were made along these same regional lines in early September 1986. Although the September measurements were not taken at peak discharge (see Fig. 2), these data probably represent the average summertime water temperature sections, and provide a guide as to the range of seabottom temperatures and the temperature structure of the freshwater layer of the inshore area which prevails in the summertime months.

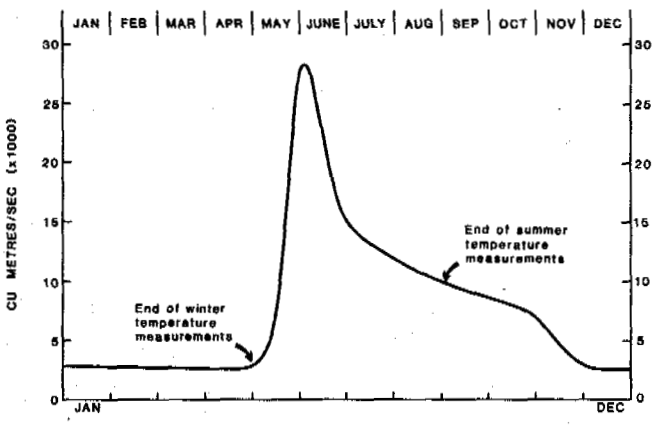

Fig. 2 - A generalized annual discharge curve for the Mackenzie River showing the location in time of winter and summer temperature measurements in the Beaufort Sea.

SUB-SEABOTTOM TEMPERATURE MEASUREMENTS

The locations of the temperature lines are shown in Figure 1. Each line consisted of at least ten thermistor cable installations to depths as much as 40 m below seabottom. Most of the holes drilled for temperature measurements used an hydraulic jet drilling technique (Judge et al. 1976), and thermistor cables were installed in 2.5 cm diameter steel casing. Cables consisted of 12 to 24 thermistors with spacings ranging between 0.75 m and 5 m, resulting in relatively detailed temperature profiles of the immediate sub-bottom. Since hydraulic jet drilling introduces a thermal disturbance into the seabottom, the temperature cables were monitored continually after installation to obtain equilibrium temperature conditions. Depending upon the amount of thermal disturbance, and the nature of the seafloor materials, return to equilibrium (to within 0.1°C, the accuracy of the thermistors) was achieved in time periods between three days and several weeks.

The seafloor materials encountered during drilling consisted of sand, silt and clays of recent and Pleistocene age (O'Connor, 1983). Drilling conditions varied with the type of material, with poorest penetration and hole collapse in loose sand and best drilling in clays, silt and ice-bearing sands.

Wherever possible, temperature profiles of the seawater column were measured; either through the casing or from separate measurements with thermistor cables deployed beneath the sea-ice.

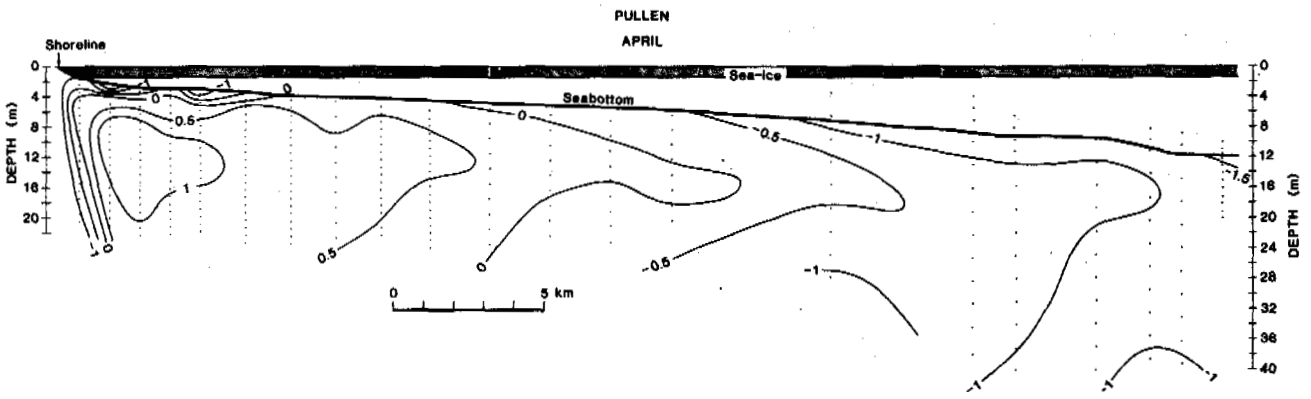

Fig. 3 - Sub-seabottom thermal section for the Pullen line end-of-winter measurements.

Figure 3 shows a representative section of sub-bottom temperatures measured during April for a line near Pullen Island (see Fig. 1 for location). The isotherms are contoured in 0.5°C intervals with a thermistor calibration accuracy of 0.1°C.

In the shoreline area, large vertical and horizontal temperature gradients exist. This area is strongly under the influence of Mackenzie River water since this water is resident on the bottom for the longest period during the summer months. The net effect is shown by the warm bulb enclosed by the +1°C isotherm. Landward, the horizontal gradient at depth indicates the influence of the relatively cold (-8°C) permafrost on shore. The vertical gradient near the seafloor suggests that cold seawater invades the nearshore region in winter-time, mixing with the reduced flow of Mackenzie River water and giving rise to pockets of cold water (even below 0°C) in some areas.

In water depths between 4 and 8 m, isotherms immediately below seabottom are pulled back shoreward, showing the effect of cold water invasion on the seafloor during winter months. The previous summer's warming effect from Mackenzie River water is shown as temperature maxima between 7 and 10 m below bottom. These maxima probably also reflect a cumulative effect of many winter-summer temperature cycles, as well as other less well-known factors such as long-term warming effects or degradation of permafrost at depth, and the rate of coastal erosion and sea-level rise since the last glaciation.

The sub-bottom temperature maxima attenuate with water-depth and distance offshore. Hence, the sub-bottom temperatures at 12 m water depth are almost isothermal.

The nature of the sub-bottom temperature maxima can be seen in Figure 4, which is a compilation of data from all installations on all lines from April observations. In this figure, the maximum observed sub-seabottom temperature is plotted with respect to the water depth at the installation location. Although these data come from widely separated areas of the Beaufort nearshore shelf, a definite trend can be seen. In water depths less than 6.5 m, positive sub-seabottom temperature maxima are observed, usually occurring between 6 and 10 m below seabottom. At these water depths, Mackenzie River water is resident for the longest time during summer months. At water depths beyond 6.5 m, the temperature maxima are below 0°C, indicating a lesser effect of warm Mackenzie River water. Extrapolating the trend line to -1.8°C, cold seawater would be the limiting condition where no thermal maximum would be observed, (i.e. no mixed Mackenzie River water reaches the seabed).

It is unfortunate that no similar sub-seabottom temperature data are available for these water depths for the end-of-summer

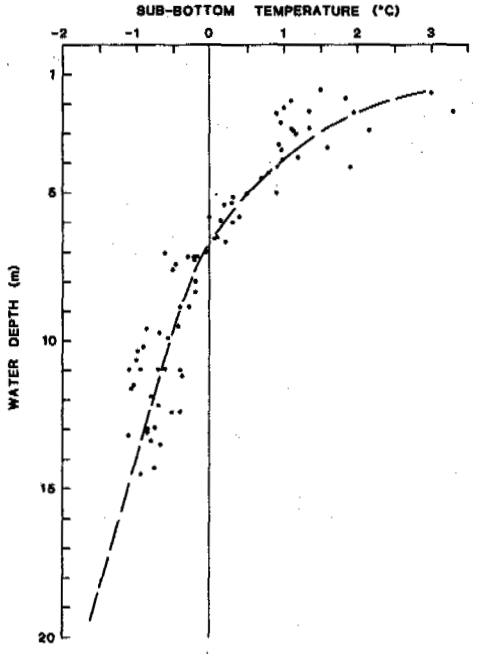

Fig. 4 - A compilation of maximum observed sub-seabottom temperatures vs. water depth for all temperature holes drilled during the end-of-winter period in the Beaufort Sea.

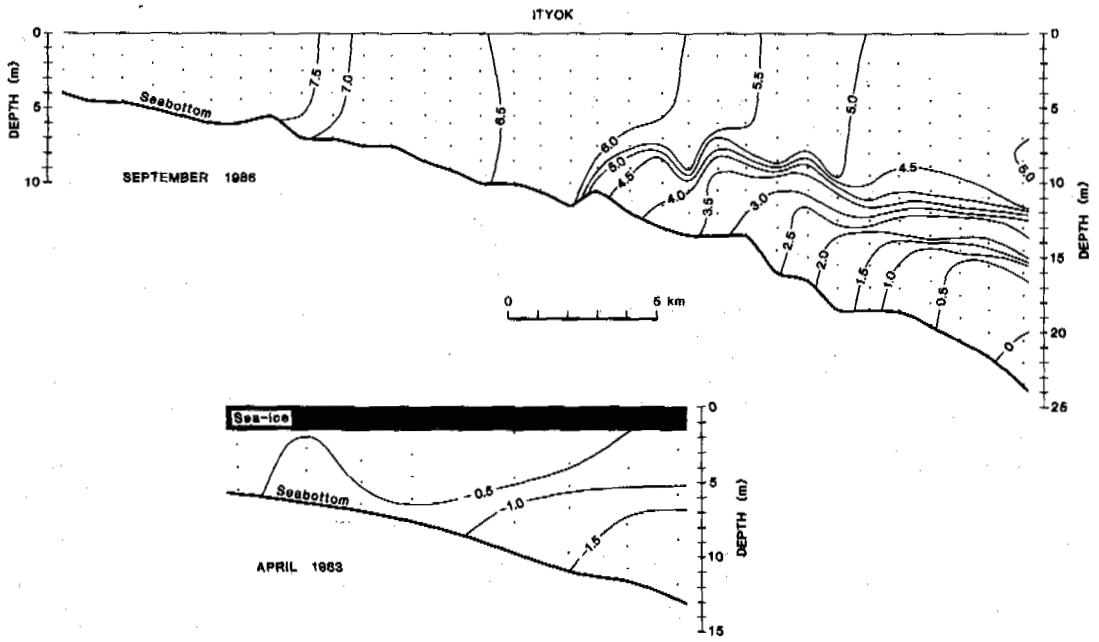

Fig. 5 - A comparison of seawater temperature distribution from onshore to offshore for end-of-summer (upper section) and end-of-winter (lower section) measurements.

period. It is suggested that temperature minima would probably exist beneath the seabottom instead of the temperature maxima observed at the end of winter. Some indications of such a seasonal effect have been observed within a couple of metres of the seabottom beyond the 25 m isobath (Taylor and Allen, 1987).

SEAWATER TEMPERATURE MEASUREMENTS

Measurements of seawater column temperatures have been made for both April and September time periods. A comparison of summer and winter water temperatures is shown in Figure 5 for the Ityok line. The upper section in this figure shows the effect of Mackenzie River water in September. This warm water, at temperatures between +5°C and +7.5°C, forms an upper layer approximately 8 m thick. The river water cools to seaward with a gradient of approximately 1°C per 7.5 km. Between water depths of 8 and 15 m strong vertical temperature gradients exist, probably indicating mixing with cold seawater. From this figure, it is apparent that the seabottom, at water depths less than 8 m, is under the full thermal effect of the Mackenzie River discharge, whereas at water depths between 8 and 20 m, it experiences lower temperatures. It is suggested that this example may be close to the average temperature distribution along the Mackenzie Delta front for the summer period; similar observations and conclusions have also been made by Burgess and Judge (1977). During peak flooding in June the warm fresh-water layer may increase substantially, but in turn this layer is probably much thinner during October and November.

Figure 6 is a compilation of water temperature measurements made at the seabottom along all survey lines for both winter time (April) and summer time (September) conditions for water depths between 2 m and 24 m. The September suite of data clearly shows the thick warm fresh-water layer. Although the temperatures for April are almost entirely below 0°C, a similar trend can be seen with mixed Mackenzie River water extending, as a surface layer, out to 5 m water depth. While the September measurements indicate mixed water at

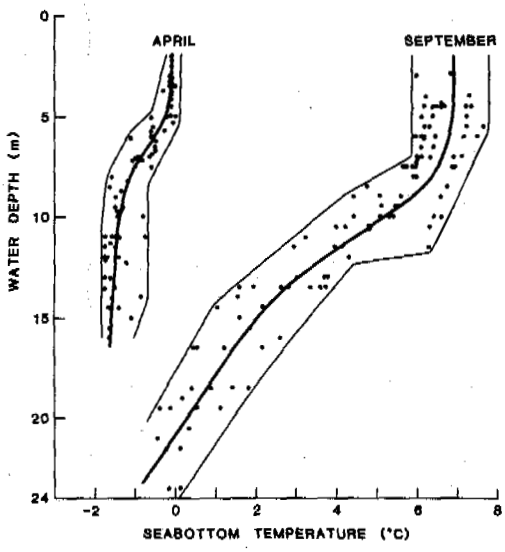

Fig. 6 - A compilation from all survey lines of water temperature measurements made at the seabottom vs. water depth for end-of-winter (April) and end-of-summer (September).

the seabottom to water depths of at least 20 m, the April measurements show that essentially unmixed cold sea water at -1.6 to -1.8°C exists at the seabottom in water depths beyond 8 m. This figure illustrates that a large extent of the nearshore zone is characterized by a layer immediately beneath the seabed experiencing an annual cycle of temperatures above and below 0°C - an active layer.

SHORELINE STUDIES: NORTH HEAD, RICHARDS ISLAND

In an attempt to understand the seasonal variation of permafrost temperatures in the shoreline zone, a survey was carried out at North Head, Richards Island (see Fig. 1) in an area where pipelines may be brought ashore in future oil and gas development.

During the summer of 1985, a series of 10 boreholes were drilled along a line from the shore to 800 m offshore. Thermistor cables were installed and equilibrium temperatures for early September were measured. The site was reoccupied in April of 1986 when 11 holes were drilled along the same line and thermistor cables were re-installed to obtain late winter equilibrium sub-bottom temperatures. The temperature results are shown as thermal sections in Figure 7.

The summertime temperature configuration shown in Figure 7(a) indicates a thin thaw zone above 0°C along the entire section out to 800 m offshore. In the inshore area, at water depths less than 1 m, the thaw zone is less than 0.5 m thick. In deeper water areas (>2 m), the thaw zone increases to 8 m thickness. At the shoreline, across the beach or intertidal zone, the thaw zone is approximately 1 m thick. Between 30 m and 350 m offshore, a large temperature gradient, exceeding 1°C/m, occurs in the first 6 m below bottom. The coldest permafrost (< -7°C) occurs at a depth of 8 m below seabottom in this area while the permafrost at the same depth at the shoreline is relatively warm (-3°C to -4°C).

The configuration of the summertime permafrost temperature regime can be explained by examining the temperature regime in late winter shown in Figure 7(b). In wintertime, 1.5 to 2 m of sea-ice is formed, and at freeze-up the ice freezes to the bottom in the shallowest water areas first. Therefore the nearshore seabottom zone experiences cold temperatures in wintertime for a much longer period than the offshore zone. In the offshore zone, the warm Mackenzie River water (above 0°C) is slowly replaced with mixed fresh and salt water at temperatures slightly below 0°C. Hence, as Figure 7(b) shows, the winter subseafloor temperature gradient in the nearshore zone is as large as the summer gradient (> 1°/m), but the gradient has reversed direction. At distances beyond 200 m offshore the residual summer heating pulse from the warm Mackenzie River water is found at a depth of 10 m below bottom and is indicated by the shoreward bending back of the isotherms. A residual pocket, above 0°C, is indicated at the offshore end of this line. From previous work, this zone is known to extend seaward, as shown in Figure 3.

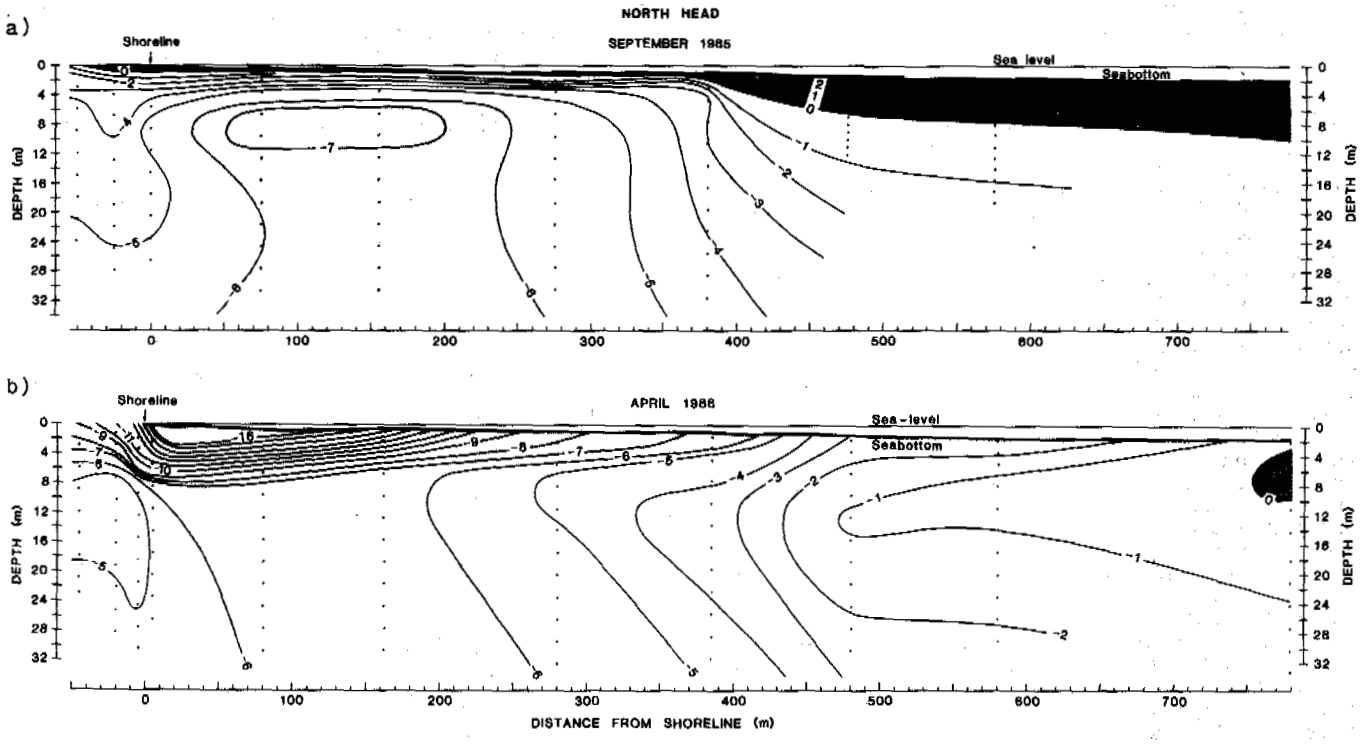

Fig. 7 - Thermal sections at the North Head nearshore test site; (a) end-of-summer and (b) end-of-winter.

In Figure 7 it can be seen that the shoreline permafrost temperatures at depths below 8 m are warmer than those occurring in the nearshore. The shoreline beach and cliff areas characteristically are covered by thick drifts of snow (> 2 m in places) which act as a thermal blanket. This effect is clearly seen in the horizontal gradients at shallow depths which occur across the shoreline area.

Terrain geological studies in these areas have indicated that this particular test site has a relatively stable coastline; that is, no measurable coastal erosion has taken place in the last 30 years (Dallimore et al., 1988). Hence, the thermal effects shown in the nearshore sub-seabottom are probably not indicative of relict permafrost. The major factor appears to be the relatively broad inshore zone of shallow water that freezes to the bottom early in the winter season. This area has the thinnest thaw layer in summer and the largest vertical thermal gradients. It is interesting to speculate on the origin of this zone - do frost heave and ice-lense formation contribute substantially to the development of the shallow water zone? Such a question can be answered only by further detailed studies of ice content and soil type in the first 8 m below seabottom.

It is thought that similar winter and summer conditions prevail in many areas of the Beaufort sea coast where stable shorelines exist. Hence, pipeline landfall designs which interact with, or may cause to change, existing permafrost conditions, must consider horizontal temperature gradients exceeding 15° per kilometre and seasonally reversing vertical seabottom gradients exceeding 1°C/m.

SUMMARY

The seafloor of the nearshore Canadian Beaufort Sea is subjected to annual temperature cycles above and below 0°C as a result of the fluctuating warm freshwater levels of the Mackenzie River. The resulting temperature distribution in the sub-bottom indicates an "active layer" above permafrost which extends out to the 20 m isobath. This active layer effect is most pronounced in shallow water areas and attenuates seaward.

At the coastline, where seawater freezes to bottom in winter, large temperature gradients are developed in the immediate seabottom. During summer months the gradients are reversed. Both summer and winter gradients may be in excess of 1°C per metre.

Construction engineering of bottom-founded structures and pipelines should consider the widespread occurrence of the sub-seabottom active zone.

REFERENCES

Burgess, M. and Judge, A.S. (1977). Thermal observations conducted as part of Beaufort Delta Oil Project Limited's sampling cruise on the M.S. Norwerta, Beaufort Sea, 1976. Geothermal Service of Canada, Earth Physics Branch, Internal Report 77-1.

Dallimore, S.R., Kurfurst, P.J. and Hunter, J.A.M. (1988). Geotechnical and geothermal conditions of nearshore sediments, Southern Beaufort Sea, Northwest Territories, Canada. in Proceedings, Fifth International Conference on Permafrost, Aug. 2-5, 1988, Trondheim, Norway.

Environment Canada. (1982). Sediment data, Canadian rivers 1980. Inland Water Directorate, Water Survey of Canada, 167-168.

Hunter, J.A., Judge, A.S., MacAulay, H.A., Good, R.L., Gagné, R.M. and Burns, R.A. (1976). Permafrost and frozen sub-bottom materials in the Southern Beaufort Sea. Beaufort Sea Project, Technical Report No. 22, Dept. Environment Canada, 174 pp.

Hunter, J.A., Neave, K.G., MacAulay, H.A. and Hobson, G.D. (1978). Interpretation of sub-seabottom permafrost in the Beaufort Sea by seismic methods. Part I. Seismic refraction methods. in Proceedings, Third International Conference on Permafrost, July 10-13, 1978, Edmonton, Alberta, Canada, 514-520.

Judge, A.S., MacAulay, H.A. and Hunter, J.A. (1976). An application of hydraulic jet drilling techniques to mapping of sub-seabottom permafrost. Geological Survey of Canada, Paper 76-1C, 75-78.

Mackay, J.R. (1972). Offshore permafrost and ground ice, Southern Beaufort Sea, Canada. Canadian Journal of Earth Sciences, 9, 1550-1561.

Mackay, D.K. and Mackay, J.R. (1974). Heat energy of the Mackenzie River. in Further Hydrologic Studies in the Mackenzie Valley, Dept. Environment Canada, Environmental-Social Program, Northern Pipelines, Report 74-35, 1-24.

O'Connor, M.J. (1983). Development of a proposed model to account for the surficial geology of the Southern Beaufort Sea. Geological Survey of Canada, Open File 954, 128 pp.

-------. (1984). Distribution and occurrence of frozen sub-seabottom sediments: A comparison of geotechnical and shallow seismic evidence from the Canadian Beaufort Sea. Report prepared for the Geological Survey of Canada, 106 pp.

Swift, D.W., Harrison, W.D. and Osterkamp, T.E. (1983). Heat and salt transport processes in thawing subsea permafrost at Prudhoe Bay, Alaska. in Proceedings, Fourth International Conference on Permafrost, July 17-22, 1983, Fairbanks, Alaska, 1221-1226.

Taylor, A.E. and Allen, V. (1987). Shallow sediment temperature perturbations and sediment thermal conductivities, Canadian Beaufort Shelf. Canadian Journal of Earth Sciences, 24, 2223-2234.

FOUNDATION CONSIDERATIONS FOR SITING AND DESIGNING THE RED DOG MINE MILL FACILITIES ON PERMAFROST

T.G. Krzewinski[1], T.A. Hammer[2] and G.G. Booth[3]

[1]Lakehead Testing Laboratory, Duluth, MN
[2]Dames & Moore, Portland, OR
[3]Cominco Alaska, Anchorage, AK

SYNOPSIS The Red Dog Mine (zinc/lead) project is being advanced by Cominco Alaska Incorporated (CAI) and construction at the mine site began in the winter of 1988. The mill facility for processing the ore into concentrate will be located adjacent to the open pit mine on relatively warm permafrost soil and rock. This paper will summarize the site characteristics and describe the analytical and design techniques utilized to found the various components of the mill facility. The more sensitive facilities will be monitored during the early years of operations to verify that the foundation schemes selected are performing as designed.

INTRODUCTION

Development of the Red Dog Mine will require a tailings dam, water supply dam, mill site, dump areas for waste fill and a series of diversion ditches. The mine and mill facilities are located at Longitude 162° 58' west and Latitude 67° 66' north in northwestern Alaska. During the summers of 1984 and 1985, and the winter of 1987, Dames & Moore carried out geotechnical investigations at the sites and site alternatives for these facilities. This paper summarizes the geotechnical investigations conducted to explore foundation and thermal conditions at the mill site location and provides the foundation design concepts developed to support the mill facilities. The geotechnical investigations carried out are detailed in a previous paper by the author (Krezewinski, Stanley & Moore, 1986).

The investigations were conducted during five separate field explorations, the first being conducted between June 19 and June 30, 1984, the second between August 10 and September 2, 1984, the third between August 7 and August 16, 1985, the fourth on September 19, 1985, and the last being conducted between March 25 and April 1, 1987. Twenty-nine borings were drilled in the vicinity of the mill site. Figure 1 is a Site Plan of the Mill Site which shows the locations of these borings. The boreholes were augered and/or cored to depths ranging from 8 to 113 feet (3 to 38 meters) for the purpose of logging subsurface soil and thermal conditions and obtaining undisturbed soil and rock samples for identification and laboratory testing.

PROJECT DESCRIPTION

A total of 25 buildings and support facilities have been identified by the designers as structures to be constructed in the mill site area at the locations shown on Figure 1. The facilities include ore processing and storage facilities, process water treatment facilities, accomodations, fuel storage, a power plant, roads, retaining walls and various other support facilities. Prior to construction of facilities, the mill site will be excavated down to elevations ranging from 967 to 985 feet (original ground elevations shown on Figure 1). This will place most of the facilities directly on bedrock. However, several of the facilities will be located above bedrock on overburden soils and special design conditions will be required to ensure adequate foundation performance.

FIELDWORK

The field program utilized Central Mine Equipment Company (CME) -55 drill rigs which were transported to the various drill sites by a Bell 205 helicopter. The CME-55's were equipped with both hollow stem auger for drilling and drive sampling overburden soils and wire-line diamond core drilling equipment with an optional refrigerated drilling-fluid unit for coring permafrost and maintaining the core in a frozen state.

Nine of the twenty-nine holes were drilled utilizing refrigerated coring techniques. In ice-rich and ice-bonded permafrost zones, the only way to retrieve undisturbed core samples maintained at their in-situ densities is through the use of refrigerated coring techniques. The recovered core was protected from thawing in the field and the core was transported periodically to Anchorage for frozen storage.

Thermistor strings were installed in 11 of the boreholes to permit future observations of the thermal condition of the soil/rock at boring locations. Each thermistor string was placed in 1.25 inch (3.2 centimeter) I.D. PVC pipe installed to the full depth and filled with a 50/50 mixture of propylene glycol and water. The strings were installed to the bottom of the PVC pipe and the annular space between the PVC pipe and the borehole wall was backfilled with sand. At the ground surface, a short section of 3 or 4-inch

(7.6 or 10.2-centimeter) diameter PVC pipe with a cap was placed over the 1.25 inch (3.2 cm) PVC casing for protection of the thermistor string lead and connection.

LABORATORY TESTING

Soil and rock samples were tested in the Dames & Moore Anchorage laboratory to classify the materials encountered and determine their physical and engineering characteristic. The laboratory testing program included sample inspection, sample photography, soil classification, moisture density measurements, grain-size analyses, Atterberg limits tests, constant head permeability tests, thaw consolidation tests and direct shear and triaxial shear strength tests.

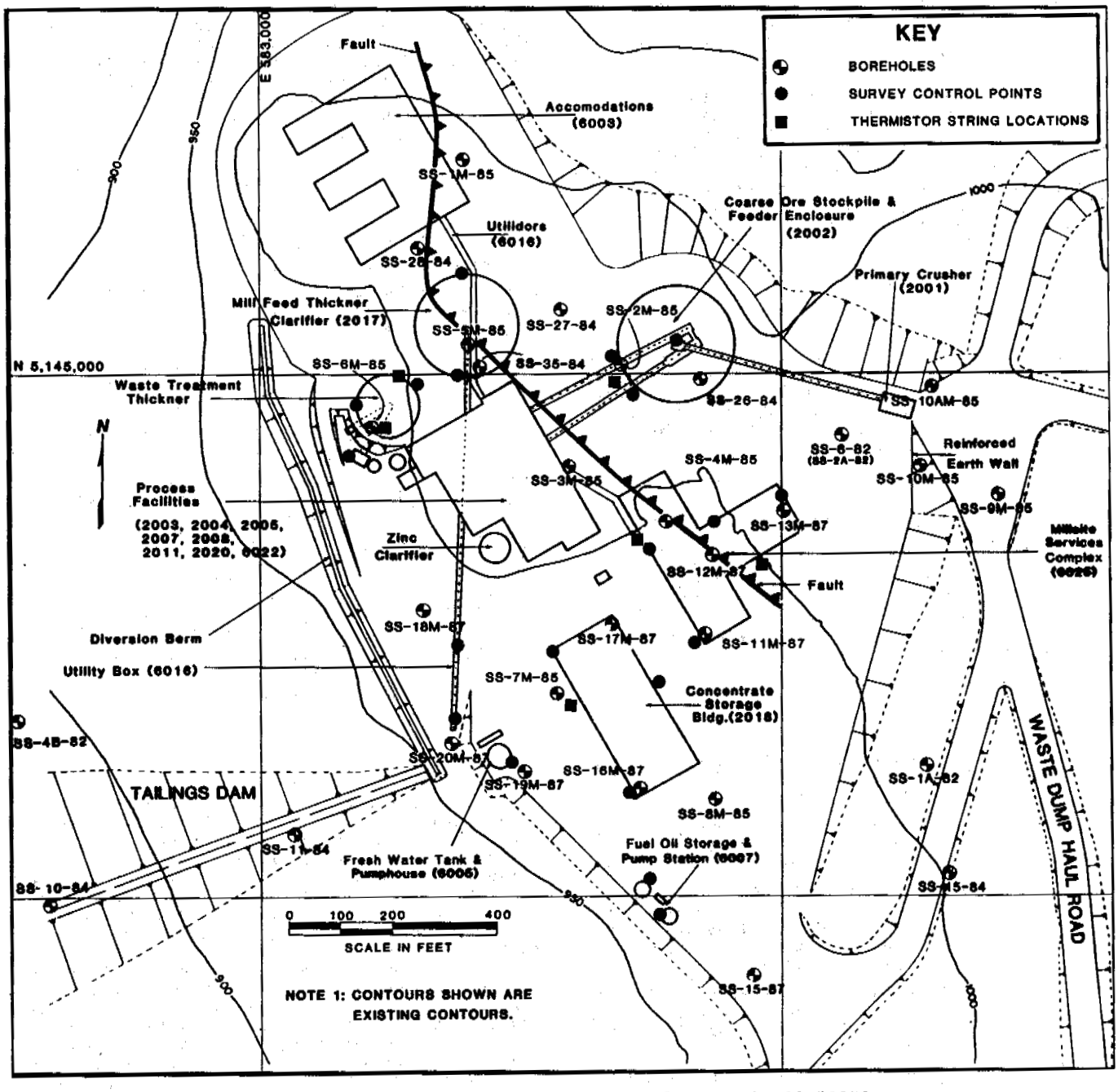

FIG. 1 RED DOG MILL SITE PLAN AND MONITORING LOCATIONS

SITE CONDITIONS

The millsite is located adjacent to both the ore deposit and the tailings dam. The entire site is covered with a low-growing tundra mat. The overburden soils, which appear to be colluvial deposits capped with a thin layer of surficial silts and peat, vary in thickness from 0 to 13 feet (0 to 4.3 meters). The underlying bedrock occurs as two distinct rock formations and appears to be separated by a thrust fault extending through the site. Bedrock to the west of the fault is chert-carbonate while shales and sandstones were logged to the east of the fault. The chert-carbonate is relatively competent, hard, dense, moderately-fractured chert and dolomite.

The shale and sandstone deposits contained numerous clay gouge zones and excess ice down to depths of 20 to 30 feet (6.7 to 10 meters). The fractures and bedding within the chert deposit contained vitronite while vitronite was not logged within the shale and sandstone deposit. The thermistor data at the mill site indicates permafrost temperatures in the 27 to 30°F (-2.8 to -1.1°C) range.

DESIGN CONCEPTS

The present plan at the mill site calls for excavation of 30 to 40 feet (10 to 13 meters) of material from the site for use as borrow in other areas and the founding of the heavier components of the mill on the more competent chert bedrock within the excavated site area.

SITE EXCAVATION AND CONSTRUCTION MATERIALS

Material to be excavated during site grading can be classified into 4 groups, depending on soil constituents and ice content. Table 1 presents the 4 material classifications and characteristics used for categorizing the excavation material.

TABLE 1

CLASSIFICATION CATEGORIES FOR EXCAVATED MATERIAL

Material Group	Material Characteristics
Waste	Surficial/colluvium; high ice and/or organic content; fine grained with little or no rock
Restricted Use	Typically directly beneath waste material; high ice content (10% to 30% by volume); significant gravel content (GM) with little organics
Special Handling	Relatively competent rock containing significant ice (5% to 10% by volume); less than 20% fines
Select Material	Relatively competent rock containing less than 5% ice by volume; less than 20% fines

THERMAL ANALYSES FOR SITE EXCAVATION

Thermal analyses using a computer solution of the Modified Berggren equation (Braley 1984) were performed to evaluate the effect of excavating the site down to design grade. The required parameters for this method of analysis include: local climatological data, thermal properties of the in-situ soil and rock, and surface characteristics which are expressed in terms of an "n" factor. The climatological data includes the mean annual temperature, thaw degree-days and the number of thaw days annually. This information was collected from a variety of sources including previous experience at the mill site. Physical properties of the in-situ soil and rock were determined by laboratory testing of relatively undisturbed samples obtained from subsurface explorations. Table 2 contains a tabulation of the input parameters used in our analysis:

TABLE 2

THERMAL ANALYSIS INPUT PARAMETERS

Environmental Parameters

Mean Annual Temperature (°F)	18 (-7.8°C)
Thaw Degree Days (°F days)	1400 (778°C days)
Thaw Season Length (days)	140

	Material Classification		
Material Properties	Waste	Restricted Use and Special Handling	Select Material
Thaw n	1.7	1.8	1.4
Dry Density(lb/cu ft)	70-90	105-125	146
Moisture (%)	20-30	2-15	2-4
Heat Capacity (BTU/cu ft-°F)	29	27	28
Conductivity (BTU/ft-hr-°F)	0.7	1.1	1.7
Latent Heat (BTU/cu ft)	2600-3000	400-2300	400-850

NOTE: 1 gram/cu cm = 62.4 lb/cu ft
1 BTU = 252.2 gr cal
1 cu ft = 28317 cu cm
1°C = 1.8°F

The analysis was directed at evaluating the thermal response of the site to excavation to design grade and the beneficial effect on the proposed foundations in areas of cut due to thawing and draining of excess ice from the subsurface soil and rock. The analyses included consideration of the extent of the thaw resulting from exposure to both one and two thaw seasons. The two thaw season scenario assumed that significant drainage would occur during the initial thaw season. Although total feeeze-back would then occur during the intervening winter freeze season, the following summer thaw would produce greater thaw depths due to the reduced moisture content (and reduced latent heat) of the previously thawed and drained zone. A summary of the analyses is presented below.

THAW DEPTHS FOR EXCAVATED AREAS

Material Classification	Thaw Depth(ft) 1 Thaw Season	Thaw Depth(ft) 2 Thaw Seasons
Waste Material	4-5(1.3-1.7 M)	5-6(1.7-2 M)
Restricted Use & Special Handling	7-9(2.3-3 M)	9-10(3-3.3 M)
Select Material	9-10(3-3.3 M)	9-10(3-3.3 M)

As the table indicates, allowing the site to thaw prior to construction of facilities is beneficial, since the resulting reduction of excess ice due to thaw and drainage will reduce settlement associated with thaw strain and creep.

FOUNDATION DESIGNS

Several of the mill facilities will be placed on relatively unweathered to slightly weathered bedrock while others will be founded on highly weathered bedrock. Foundation loadings range from lightly loaded prefabricated structures to almost 500 kips (226,799 Kg)/footing and a 100,000 kip (4,535,970 Kg) ore stockpile. Building temperatures range from unheated to a 60°F (15.6°C) heated floor slab with some facilities classified as highly sensitive to settlement.

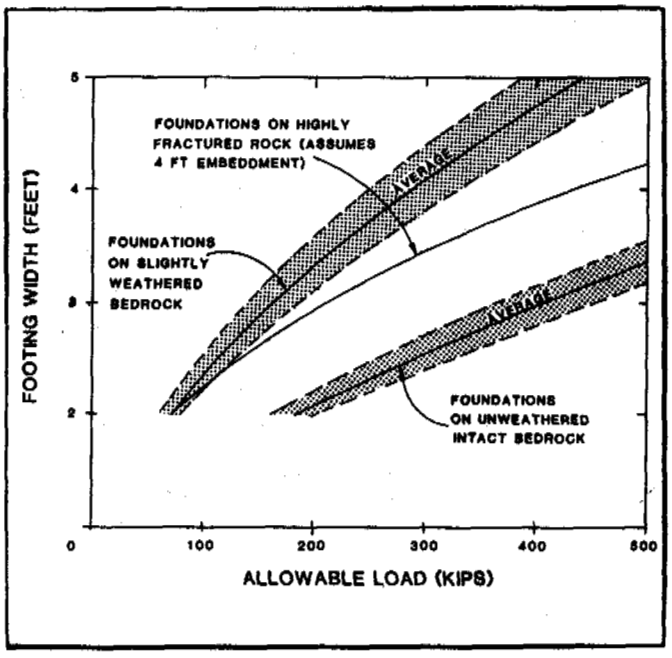

NOTE: 1 meter = 3 feet; 1 kip = 453.6 Kg.

FIG. 2 ALLOWABLE LOAD FOR SPREAD FOOTINGS FOUNDED ON BEDROCK

FOUNDATIONS ON BEDROCK

Based on information obtained from the subsurface explorations, the following facilities will likely be founded on relatively competent bedrock:

- Accomodations
- Primary crusher module
- Primary grinding and mill shop module
- Primary and secondary grinding module
- Tertiary grinding module
- Zinc and lead flotation module
- Lead and zinc dewatering module
- Mill feed thickener/clarifier
- Water treatment module

Most of the above facilities will be supported on spread footings. The bearing capacity analyses considered foundations placed both on relatively level undisturbed foundation rock, and highly fractured rock caused by excavation disturbance. Figure 2 presents curves for general sizing of spread footings, where facilities are to be founded on unweathered to slightly weathered bedrock (Bowles, 1977 and NAVFAC DM-7.2, 1982).

Lateral capacity will be developed by a combination of passive resistance and base friction. Foundations embedded in competent rock and poured neat against the sides of the excavation will develop an allowable equivalent fluid pressure of 700 pounds per cubic foot (11.2 gr per cu cm). If compacted 2-inch (5.1-cm) minus crushed rock is installed adjacent to the footing, an allowable equivalent fluid pressure of 500 pounds per cubic foot (8.0 gr per cu cm) can be achieved. In addition, base friction of one-half times the total vertical dead load is available provided the bottoms of the footing excavations are clean and free of loose rock and soil.

The refrigerated coring performed during the first 1985 investigation revealed that ice is present in the intact bedrock to considerable depth. The occurrence of ice was not common, however, and it appeared to be limited to fillings within joints and fractures. In addition, thermal analysis indicates that allowing the site to thaw prior to construction of the facilities will reduce the amount of excess ice to the depth of thaw as discussed in the previous section. Consequently, we feel that thaw and creep settlement of foundations on rock will generally be less than 1-inch (2.54 cm).

FOUNDATION ON WEATHERED BEDROCK

Based on available subsurface information, the following facilities will be founded partly or wholly on "restricted use" or "special handling" weathered bedrock material:

- Coarse ore stockpile and feeder enclosures
- Concentrate storage building
- Freshwater tank and pump house
- Fuel oil storage and pump station
- Mill site services complex
- Power house module

The foundations for these facilities are designed to either maintain the permafrost in a frozen

state or transmit the loads to the bedrock level or both. Heated and unheated buildings will be founded on spread footings within an insulated pad or on piles, when the buildings can be elevated to allow ambient air flow beneath the structure. In those areas where bedrock is not excessively deep, facilities will either be founded on tip end bearing piles or excavation replacement techniques will be used to transmit loads to the bedrock strata. Examples of facilities with foundations that occur above the level of unweathered bedrock are discussed in the following paragraphs.

Coarse Ore Stockpile and Feeder Enclosures:

This facility consists of an 84-foot (28-meter) high conical pile of coarse ore overlying a double hopper/conveyor system which supplies ore to the mill facilities. The hopper feeders and conveyor system are enclosed beneath the ore pile in a horseshoe arch tunnel gallery constructed of corrugated steel plate with rigid framing which is supported on reinforced concrete footings. The conveyor system will be housed in two 9-foot (3-meter) diameter steel pipes. The ore stockpile is supplied via an overhead conveyor system housed in a 9-foot diameter steel pipe. The overhead system is supported by guyed vertical supports which in turn are supported on spread footings. The vertical columns will support an approximate 100-foot (33.3 meter) span of the conveyor system at about 400 pounds per foot (540 Kg per meter), resulting in a vertical downward load on the order of 40 kips (18,140 Kg) for each support. A protective umbrella will also be supported over the stockpile to reduce dust. A total storage capacity of the coarse ore pile will be approximately 50,000 tons (4,535,970 Kg).

Based on information obtained from subsurface explorations, the proposed facility site is underlain by approximately 12 feet (4 meters) of ice-rich colluvium which, in turn, is underlain by slightly to severely weathered carbonaceous shale with occasional to frequent 1/8 to 1/4 inch (0.3 to 0.6 cm) ice filled fractures to the total depth of the boring (50 feet/16.7 meters). General site excavation will remove the colluvium and about 9 feet (3 meters) on average of the ice-rich bedrock. In addition, thermal analysis indicates that allowing the site to thaw after site excavation and prior to construction will eliminate the excess ice in the bedrock to a depth of 7 to 9 feet (2.3 to 3 meters) and 9 to 10 feet (3 to 3.3 meters) for one and two thaw seasons, respectively.

Considering the beneficial effects of removing the upper ice-rich colluvium and bedrock and the reduction of excess ice due to two thaw seasons, the analysis indicates that the coarse ore pile and the underlying facilities will settle up to 6 inches (15.2 cm) due to creep. This settlement will be greatest at the center of the ore pile and diminish to less than 1 inch (2.5 cm) at the pile edge. The total settlement should occur at an estimated rate of one-half inch (1.3 cm) per year. The analysis assumes that the gallery is supported on spread footings with contact pressures of 10 ksf (4.9 Kg per sq cm) and that subsurface conditions do not vary significantly across the area of the ore pile. Due to the uncertainties associated with the analysis, greater settlements (in excess of 6 inches/15.2 cm) may occur. Therefore, the structures underlying the ore pile will be monitored for settlement by periodic level surveys at selected points along the conveyor and hopper galleries. In addition, a thermistor string will be installed to the west of the concentrate pile between the below ground conveyor galleries. It is anticipated that moderate settlement of the hopper and conveyor systems can be compensated for by periodic adjustment utilizing jacking or shimming methods. Excessive settlement, although unlikely, may require that the galleries be releveled after several years of use.

The vertical columns supporting the overhead conveyor system will be founded on spread footings embedded 5 feet (1.7 meters) into the exposed weathered bedrock (special handling material). As stated previously, the weathered bedrock should experience about 9 feet (3 meters) of thaw if exposed to two thaw seasons. Settlement due to creep can be reduced to tolerable levels if the bearing stresses acting on the lower boundary of the previously thawed zone (9 feet-3 meters) are limited to 2 ksf (1.0 Kg per sq cm). Accordingly, allowable bearing stresses imposed by the spread footing embedded to a 5-foot (1.7 meters) depth will be limited to about 5.5 ksf (2.1 Kg per sq cm). Foundations designed accordingly should experience less than 2 inches (5 cm) total settlement.

Power House Module:

The power house module is located at the southwestern portion of the Process Facility Complex. The power house is considered very sensitive to settlement and will be supported on individual spread footings with a maximum vertical load of about 240 kips (108,860 Kg). Extensive cuts ranging from about 30 to 40 feet (10 to 13 meters) in thickness will be required at the site. As a result, the finished floor of the module will be primarily in bedrock, but the far western portion may lie in special handling material.

The excavation for the power house module will be left open for at least one thaw season prior to construction. This should induce thaw well into the select material. Since the power house module has been classified as very sensitive to movement and since sloping rock strata are present beneath the facility, the structure will be designed for a low allowable bearing value. Footings embedded at least 3 feet (1 meter) below finished grade will be designed using an allowable bearing capacity of 6 ksf (2.9 Kg per sq cm). Foundation constructed as described above will undergo estimated total thaw and creep settlement of less than 1 inch (2.5 cm).

INSPECTION AND MONITORING

Variations in subsurface conditions will probably be encountered during construction. In order to permit correlations between the foundation utilized and the actual conditions encountered with the plans and specifications, a qualified geotechnical engineer will perform daily construction inspections. Observations made during these inspections will include, but not be limited to, the following:

1. Delineating and categorizing excavation material as waste, restricted use, special handling, and select.

2. Proper ground preparation for fill placement. Determining ice-rich zones and/or waste material zones where over excavation will be required.

3. Fill placement procedures and fill density testing.

4. Fill gradation and quality monitoring and testing.

5. Foundation excavations.

6. Installation and initial reading of monitoring instrumentation.

7. Stability of cut slopes, retaining structures and drainage structures.

A monitoring scheme has been developed for several of the mill site facilities, where foundation conditions are difficult and/or sensitive structures are located. Figure 1 includes a site plan showing where thermistor strings and vertical control survey pegs will be installed. The number of monitoring locations shown on the figure are considered to be a minimum; additional survey pegs may also be placed on any of the heated facilities founded above bedrock. In addition to the monitoring points, periodic site inspections will be performed to assess the performance of cut slopes, retaining structures, drainage structures and fill sections. Site inspections during the early and late summer periods (June and September) would provide the most relevant information. All thermistor strings and settlement points will be monitored on a regular basis. The following reading schedule has been recommended for the first two years after installation:

Once in early May, just before breakup
June through September, once each month
Once each in November, January and March

The data will be analyzed as soon as possible after reading during the early stages. Where signs of movement or thermal degradation are detected, the monitoring schedule will be accelerated to refine definition of performance. In this way, remedial measures can be instigated before damage to facilities occurs.

After 2 years, if performance of facilities is satisfactory, the monitoring schedule will be reduced to just a few readings per year.

CONCLUSIONS

The founding of a world class mine's mill facility on relatively warm permafrost soil and rock is within the capabilities of the current state of the practice in arctic geotechnical engineering. Utilizing standard geotechnical analysis techniques and current understanding of the creep phenomenon, buildable foundations for large, heavily loaded facilities on permafrost rock can be designed. The performance data for similar structures is, however, nearly non-existent and a well planned system for monitoring short and long term performance is an important part of design process.

REFERENCES

Braley, W.A. (1984). A Personal Computer Solution to the Modified Berggren Equation. Alaska DOT/PF Report No. AK-RD-85-19, Fairbanks, Alaska

Bowles, J.E. (1977). Foundation Analysis and Design, 2nd Edition, 750 pp. McGraw-Hill, Inc.

Krzewinski, T.G., Stanley, J.M., & Moore, D.W. (1986). Geotechnical Investigation - Cominco's Red Dog Mine Facilities. Proc. Fourth International Cold Regions Engineering Specialty Conference (ASCE), Anchorage, Alaska.

NAVFAC DM - 7.2 (1982). Foundations And Earth Structures - Design Manual. Department of The Navy.

ACKNOWLEDGEMENTS

Acknowledgement is made to Cominco Alaska, Incorporated, for their support during this design effort and for their permission to publish this paper.

ELECTRIC PROSPECTING OF INHOMOGENEOUS FROZEN MEDIA

V.V. Kuskov

Faculty of Geology, Moscow State University, Moscow, USSR

SYNOPSIS To attain the increased efficiency of electrical prospecting of inhomogeneous media it is necessary to develop two- and three-dimensional interpretation apparatus including: a body of mathematics for the solution of direct problems; library of typical models of inhomogeneous media; methodology of experimental work; and interpretation methods. Two-dimensional interpretation procedures for some classes of two-dimensional models are discussed. The principles of interpreting the data of electrical sounding of horizontally-inhomogeneous media have been formulated.

In engineering-geological studies of frozen grounds great role is played by field geophysical methods enabling to promptly survey an area to a required depth. The dependence of specific electrical resistivity of grounds on their lithology, fracturing, moisture content, and temperature makes it possible to apply electrometric prospecting methods to obtain data needed for compiling maps of the permafrost zone. Electric prospecting by the resistivity method (ERM) is of prime importance in such studies due to its sufficient efficiency and simplicity.

The existing interpretation apparatus of electric prospecting rests on the analytical solutions obtained for horizontally and vertically-layered geoelectric models. Permafrost geoelectric profiles are distinguished by their great spatial variability, therefore, actual media cannot often be satisfactorily approximated by such models. Practice has shown that the formalistic use of the one-dimensional interpretation apparatus may lead to grave errors. Two- and three-dimensional interpretation of the ERM is needed to study horizontally inhomogeneous media. The main problems here are:

(1) development of interpretation apparatus permitting solution of direct problems of ERM for horizontally inhomogeneous models;

(2) establishment of a library of typical models of inhomogeneous media;

(3) validation of field work methodology;

(4) development of the principles underlying the ERM data interpretation for inhomogeneous media.

These problems have been studied for several years at the Department of Geocryology, Moscow State University.

Potentialities of analytical methods for solving direct problems of the ERM are limited to studying models with only inhomogeneous electrical conductivity. Numerical methods of mathematical modeling of electric fields in inhomogeneous media such as methods of finite differences, finite elements, and integral equations are commonly employed. The most simple and universal is the finite difference method. It assumes quantization of the model under study and approximate solution of respective boundary problem.

We have developed a body of mathematics and a package of programs for finite-difference simulation of direct ERM problems for two-dimensional models (Bastis and Kuskov, 1985; Kuskov, 1985, 1986). At present, a library of two-dimensional geoelectrical models, most typical of the permafrost regions, is being established. Thus, for instance, very many estimations of longitudinal and transverse curves of vertical electrical sounding (VES) for an escarpment, horst, graben, cylindrical insert of a rectangular cross-section, semi-confined horizon, etc. have been made. We have considered several geometric patterns of these models for various combinations of specific resistivity. The estimation results have been used to compile an album of master curves (Kuskov, 1986).

An analysis of the estimated data and practical experience of the ERM application in inhomogeneous media led to the development of principles underlying the interpretation of the resistivity method data.

While studying two- and three-dimensional inhomogeneous media, a problem arises of choosing efficient observation systems to assist in obtaining information adequate for an unambiguous solution of the inverse problem. We believe that an unambiguous determination of the electric conductivity of a medium necessitates the coincidence of the dimensions of experimental data and the object under study. In other words, in one-, two- and three-dimensional cases we should obtain one-, two-, and three-dimensional functions of apparent resistivity: $\rho_a(r)$; $\rho_a(r,x)$, and $\rho_a(r,x,y)$, respecti-

vely, where r is an array of current electrodes; and x and y are the coordinates of the sounding stations on the ground surface with the y axis directed along the extension of the two-dimensional models. Unfortunately, this assumption has so far been proved only for the one-dimensional case (the Tikhonov's theorem), but the physical sense of soundings allows us to believe in its validity.

Let us consider a case of two-dimensional media. The general principle of solving inverse problems is the minimization of the discrepancy between the observed and estimated data:

$$F(\bar{p}) = \sum_{i,j} \left(\frac{\rho_a^o(r_i,x_j) - \rho_a^e(r_i,x_j,\bar{p})}{\rho_a^o(r_i,x_j)} \right)^2$$

where, ρ_a^o and ρ_a^e are, respectively, the observed and estimated characteristics of a field; i=1, ..., n; j=1,..., m; n is a number of quantization points in sounding curves; m is a number of sounding stations; and $\bar{p}$ is the vector of the selected model parameters. Commensurability of functional values $F(\bar{p})$ with the data accuracy is regarded as a criterion of the termination of the interpretation process. Since the direct problem solution still requires great computing resources, it is necessary to develop methods producing adequate initial approximations for the selection procedure.

Interpretation of sounding data should be carried out in the classes of simplified models. Hence, there is a need to typify the whole wealth of geoelectrical inhomogeneities and to select such classes of models, which, on the one hand, easily approximate real situations, and, on the other, could be described by few parameters. An analysis of the solutions of direct problems makes it possible to develop a system of diagnostic criteria for the selection of the required class of models. A characteristic behavior of some sounding curves usually lays the basis for diagnostics. In our opinion, apparent resistivity (ρ_a (r, x)) profiles should be used to this end.

We have studied apparent resistivity profiles for typical two-dimensional structures. Their analysis has shown that: (1) isolines of apparent resistivities easily approximate the real geometry of a structure; and (2) correlation of resistivities of a model does not practically affect the specific features of structures under study. Here are some examples. Figs.1, 2 and 3 show the ρ_a profiles for the models of an escarpment and an insert. Sounding was carried out in a VES modification.

While comparing Figs. 1 and 2, it becomes obvious that longitudinal VES (ρ_a^I (r,x)) reflect a model geometry better. Profile ρ_a^I (r,x), unlike transverse soundings (ρ_a^{II}(r,x)) does not inherit specific features of an escarpment in an area of expanded arrays r. This property of longitudinal soundings should be taken into account in planning field work.

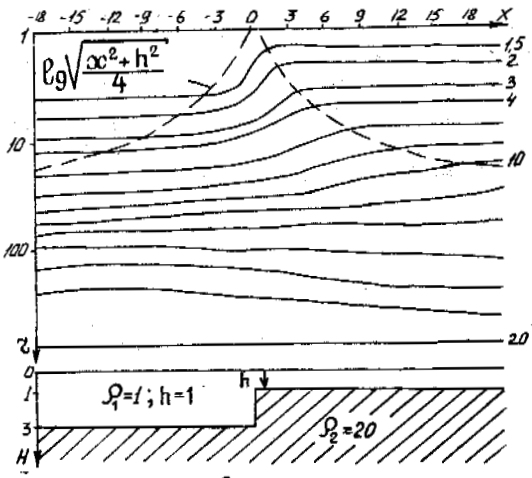

Fig.1 The ρ_a^I(r,x) profile for the model of an escarpment with a high-resistance basement

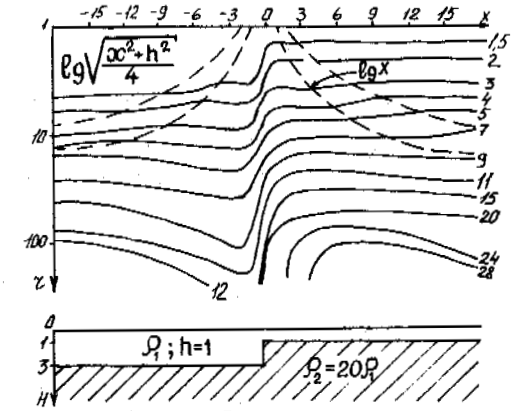

Fig.2 The ρ_a^{II}(r,x) profile for the model of an escarpment with a high-resistance basement

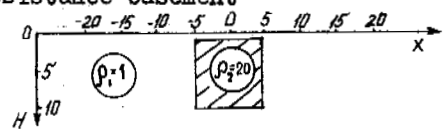

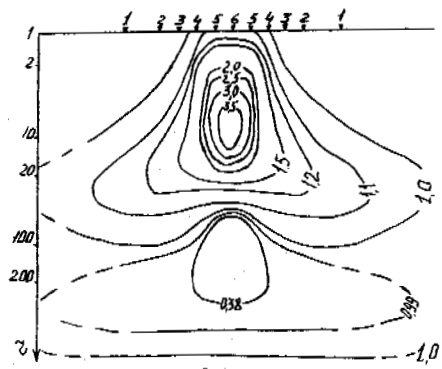

Fig.3 The ρ_a^I profile for the model of a high-resistance insert of rectangular cross-section (top)

When interpreting, one should make the best use of a well-developed, one-dimensional body of mathematics for solving the inverse problems. With this in view, the need is to evolve a theory of distortions. Manifestations of horizontal inhomogeneities on horizontal sounding curves are called distortions, assuming that the interpretation of such curves in the class of horizontally-layered models will be erroneous.

An analysis of the estimated curves for inhomogeneous models has allowed us to make physical classification of distorting effects, based on the pattern of divergencies of normal curves (ρ_a^h), obtained above a horizontally-layered model with parameters corresponding to the position of the VES station in an inhomogeneous model, and the distorted curves above horizontally-inhomogeneous models (Kuskov, 1986). Longitudinal VES curves, irrespective of a model class, are distorted within a limited range of arrays (Fig.4). We called this effect a

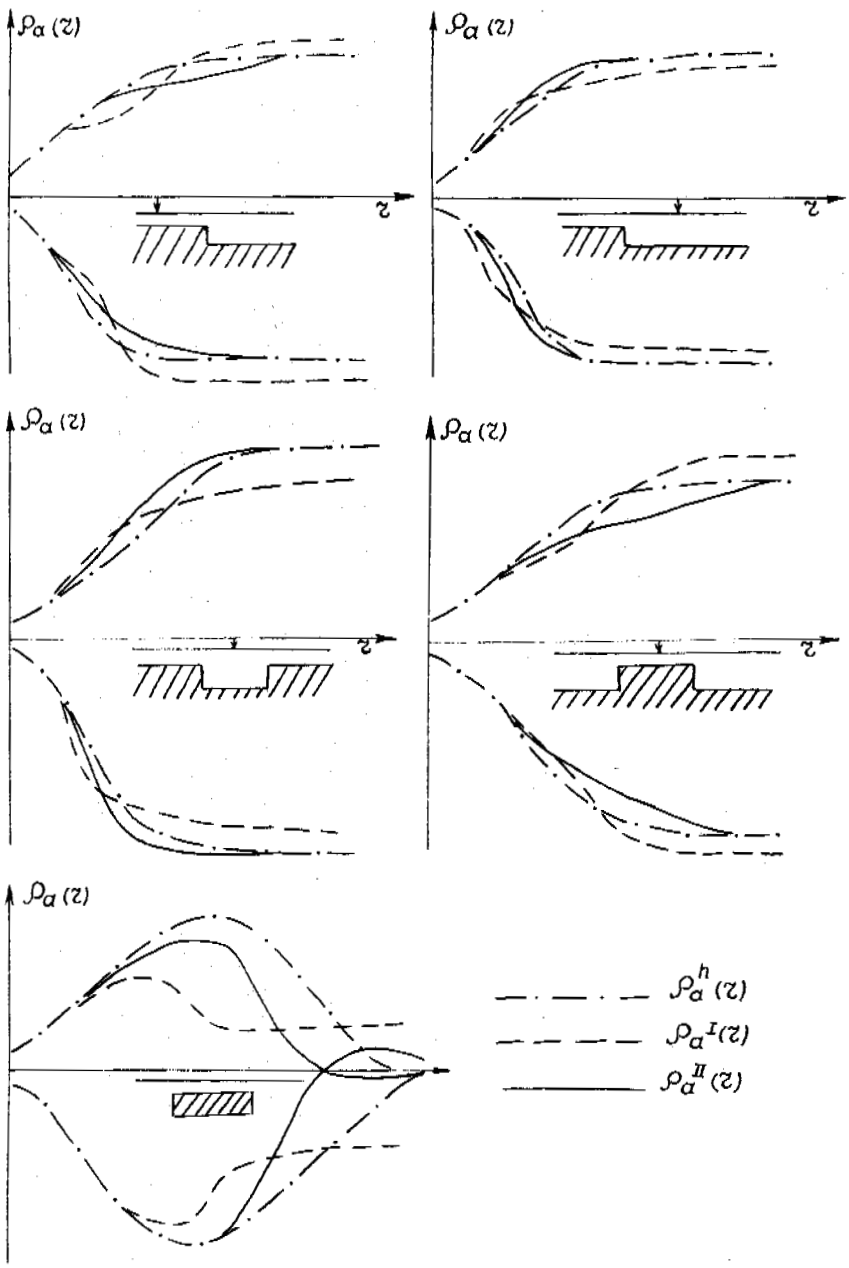

Fig. 4 Distorting effects on the VES curves typical of themodels of escarpment, graben, horst and insert

longitudinal local effect. Transverse soundings are fraught with more complicated distortions that are of similar type in various models. The following two distorting effects can be distiguished: (a) an effect produced by current electrodes when they cross the vertical boundary of the structure being studied. This effect which manifests itself locally on the VES curves has been termed by us as transverse local effect; and (b) an effect, distorting the right branch of the VES curve (we call it asymptotic effect), associated with the occurrence of an inhomogeneity near a measuring electrode.

In the course of interpretation by a one-dimensional scheme the identified distorting effects led to normal errors. Thus, the appearance of one, more seldom, two fictitious layers in a geoelectrical profile is due to local effects, while errors in determination of electrical conductivity of a structure base are associated with an asymptotic effect (Kuskov, 1986). These regularities may be useful in the interpretation practice.

In practice it is important to identify information a fortiori suitable for one-dimensional interpretation. Hence, profiles of apparent resistivities should be used. Areas where ρ_a isolines differ from the horizontal ones are indicative of the distorting effect of inhomogeneities. Having specified the location of an excitation boundary in the profile and following the behavior of isolines, we may identify an area of possible one-dimensional interpretation by the equation $\frac{\partial \rho_a}{\partial x} = 0$. While planning the location of a VES station, an electrode array excluding the curve distortion may be determined from the formula $r = \sqrt{x^2 + h^2}$ where, x is a distance from the sounding point to an inhomogeneity; and h is a depth to its upper edge. In Figs.1 and 2 these anays are divided by a broken line.

In the cases when the application of traditional interpretation methods is impossible, the use should be made of two-dimensional apparatus of interpretation. Therefore, the principles of sounding data interpretation in a class of two-dimensional models are as follows:

- identification of the type of inhomogeneities by using profiles of apparent resistivities;
- analysis of distortions to make the best use of the apparatus of one-dimensional interpretation;
- solution of the inverse problem by the method of selection using the estimated master curves or numerical modeling.

The methodology described remains quite valid for three-dimensional cases.

REFERENCES

Bastis, A.Iy. & Kuskov, V.V.(1985). O chislennom reshenii dvumerno-neodnorodnykh zadach metoda soprotivleniy. Izvestiya AN SSSR, ser.Fizika Zemli (3), 70-76, Moskva.

Kuskov, V.V. (1985). Chislennoe modelirovanie vertikalnykh electricheskikh zondirovaniy v dvumerno-neodnorodnykh sredakh. - Vestnik Moskovskogo universiteta, ser.4 - geologiya, (1), 82-88, Moskva.

Kuskov, V.V. (1986) Matematicheskoe modelirovanie pri izuchenii dvumerno-neodnorodnykh sred metodom VES. Kand.diss., 190 pp. Moskva.

PREDICTION OF PERMAFROST THICKNESS BY THE "TWO POINT" METHOD

I.M. Kutasov

Department of Petroleum Engineering and Geosciences, Louisiana Tech University, Ruston, Louisiana, USA

SYNOPSIS Presented in this paper is a new method which will allow one to predict the permafrost thickness on the basis of temperature measurements in deep wells made after a relatively short shut-in time. This method employs four transient temperature measurements taken at two depths (below the permafrost base) with two calculated static (undisturbed) temperatures at these depths. The geothermal gradient is determined and the position of the permafrost base is estimated. Values of permafrost thickness for 15 Northern Canadian wells have been used to verify the suggested method.

INTRODUCTION

The development of rapid methods of predicting permafrost temperatures and thicknesses is essential to progress in the areas of geophysics, well drilling, oil/gas production, and mining. In some cases, the thickness of the permafrost can be estimated from resistivity, sonic, and surface seismic velocity logs. The permafrost properties sought by borehole logging measurements include the depth of the permafrost base, the type of soil, and the type and amount of material in the pore space. Because deep wells in permafrost areas are usually drilled with a warm mud, there is some unknown degree of melting around the well. Thus, the borehole correction required for log interpretation can become quite large and is often indeterminate. The base of the permafrost can be detected with resistivity and sonic logs. The transition from higher resistivity and velocity readings to lower values can be considered as the base of the permafrost. The electrical resistivities of frozen sediments are affected to a greater extent than are seismic velocities. Seismic velocities may increase by 2 to 10 times in transition to a frozen state, whereas the electrical resistivity may increase by 30 to 300 times in the same temperature interval (Hnatiuk and Randall, 1977). Laboratory data for the electric and acoustic response of frozen soils have shown that the significant variables affecting these parameters are salinity, surface area of soils per unit of volume, temperature, and water content. Thus, the laboratory data should be used to interpret the log response. Since it is difficult to perform such laboratory studies, the temperature logs are commonly used to determine the permafrost temperature and thickness.

When wells are drilled through permafrost, the natural temperature field of the formations (in the vicinity of the borehole) is disturbed and the frozen rocks thaw for some distance from the borehole axis. To determine the static temperature of the formation and permafrost thickness, one must wait for some period after completion of drilling before making geothermal measurements. This is the so-called restoration time, after which the difference between the temperature of the formation and that of the fluid is less than the needed measurement accuracy. The presence of permafrost has a marked effect on the time required for the near-well-bore formations to recover their static temperatures. The duration of refreezing of the layer thawed during drilling is very dependent on the natural temperature of the formation; therefore, the rocks at the bottom of the permafrost refreeze slowly. A lengthy restoration period of up to ten years or more is required to determine the temperature and thickness of permafrost with sufficient accuracy (Lachenbruch and Brewer 1959; Judge 1973; Melinkov et al. 1974; Taylor et al. 1977; Judge et al. 1979; Taylor et al. 1982).

The objective of this paper is to present a new "two point" method which will permit one to determine the permafrost thickness from short-term (in comparison with the time required for temperature restoration) downhole temperature logs.

PHYSICAL MODEL

The slow return to thermal equilibrium in the section of the well within the permafrost creates serious difficulties in determining the permafrost temperature and

thickness. It is clear that in the sections of the borehole below the permafrost, the static (undisturbed) formation temperatures can be predicted from temperature logs taken at relatively short shut-in times. The proposed "two point" method of predicting the permafrost thickness is based on determining the geothermal gradient in a uniform layer below the permafrost zone (Figure 1). Therefore, a lithological profile for the h_2-h_p section of the well must be available. Only four temperature measurements (T_1,T_2) for two depths h_1,h_2) are needed to determine the geothermal gradient. The position of the permafrost base is predicted by the extrapolation of the static formation temperature - depth curve to 0°C (Figure 1). It should be noted that in this paper the permafrost base is defined as the 0°C isotherm. The existence of a more severe climate in the past or the transgression of the Arctic Shoreline results in warming and thinning of the permafrost (Balobaev et al. 1973; Lachenbruch et al. 1982). Due to slow movement of the permafrost base, the temperature field in the section of the well below the permafrost is also disturbed. An approximate equation which permits one to estimate the thickness of the disturbed zone (if the rate of permafrost thinning is known) was presented by Melnikov et al. (1974). Thus the accurate value of geothermal gradient can be determined only from temperature measurements below this disturbed zone. Our experience has shown that if the condition h_1-h_p > 20m (Figure 1) is satisfied, the geothermal gradient can be estimated with good accuracy.

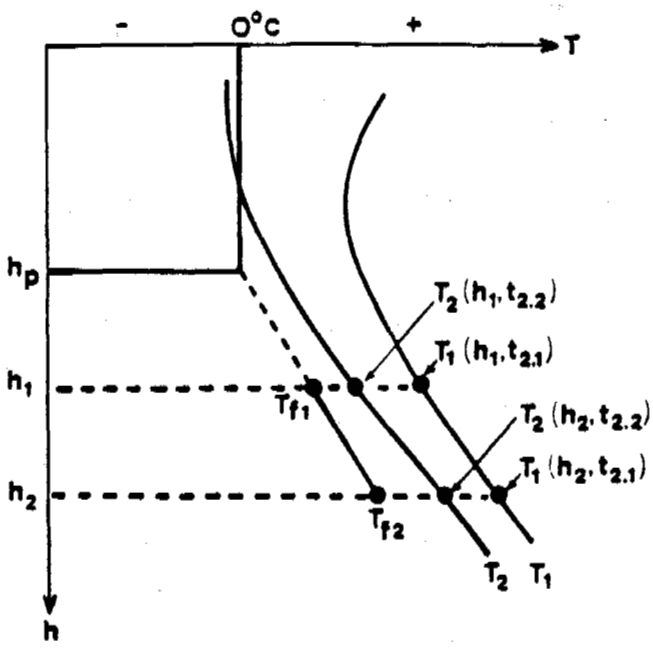

Fig. 1. Permafrost base prediction - - a Schematic Model

WORKING FORMULAS

The mathematical model of the "two point" method is based on the assumption that in deep wells the temperature of drilling mud at a given depth is practically constant during the drilling process (Kutasov 1968; Kutasov 1976). The results of temperature surveys in deep wells have shown that this assumption is valid (Bullard 1947; Lachenbruch and Brewer 1959; Jaeger 1961; Kutasov et al. 1966).

Fluctuations in the formation temperature near the well must first be determined, allowing for the circulation of drilling fluid with a temperature T_m. The following values are given: r_w, the radius of the well; t_1, the circulation time (disturbance time) of the drilling fluid at a given depth; T_f, the formation static temperature; and a, the thermal diffusivity of the formation.

It is well known that the appropriate thermal conduction equation has a solution in integral form, the integral being solvable only by numerical means (Jaeger 1956). We have found that, for moderate and large values of the dimensionless circulation time (t_D>5), the temperature distribution function $T_c(r,t_1)$ in the vicinity of the well can be described by the relation:

$$\frac{T_c(r,t_1) - T_f}{T_m - T_f} = 1 - \frac{\ln r_D}{\ln R_D} \qquad (1)$$

where

$$R_D = 1 + D_o \sqrt{t_D} \quad ; \quad D_o = 2.184$$

$$R_D = \frac{R}{r_w} \quad ; \quad r_D = \frac{r}{r_w}$$

$$t_D = \frac{at_1}{r_w^2}$$

R is the radius of thermal influence and r is the radial distance (the vertical coordinate coincides with the axis of the well). Thus the dimensionless temperature in the wellbore and in formations at the end of mud circulation (at a given depth) can be expressed as:

$$T_{CD}(r_D,t_D) = \begin{cases} 1; & 0 \le r_D \le 1 \\ 1 - \ln r_D/\ln R_D; & 1 \le r_D \le R_D \\ 0; & r_D > R_D \end{cases} \quad (2)$$

where

$$T_{CD}(r_D,t_D) = \frac{T_C(r,t_1) - T_f}{T_m - T_f}$$

To determine the temperature along the well axis $T(0,t_2)$ after circulation of drilling fluid has ceased, we used the solution of the thermal diffusion equation that describes cooling along the axis of a cylindrical body with known initial distribution, placed in an infinite medium at constant temperature (Carslaw and Jaeger 1959).

$$T_D(t_D,n) = 2p\int_0^{\infty} \tau T_{CD}(\tau,t_D)\, \exp(-p\tau^2)\, d\tau \quad (3)$$

where τ is a variable of integration, t_2 is the shut-in time (time between the log and well completion) and

$$T_D(t_D,n) = \frac{T(0,t_2) - T_f}{T_m - T_f}$$

$$n = \frac{t_2}{t_1} \quad ; \quad p = \frac{1}{4nt_D}$$

Here we assume that, for deep wells, the radius of thermal influence is much larger than the well radius and, therefore, the difference in thermal properties of drilling muds and formations can be neglected. By inserting T_{CD} into Equation 3, we obtain

$$T_D(t_D,n) = 1 - e^{-p} + 2p\int_1^{R_D} \tau(1 - \ln \tau/\ln R_D)\, \exp(-p\tau^2)\, d\tau \quad (4)$$

The last integral can be presented as a sum of the two following integrals:

$$I_1 = \int_1^{R_D} \tau \exp(-p\tau^2)\, d\tau = -\frac{1}{2p}\exp(-pR_D^2) + \frac{1}{2p}\exp(-p)$$

and

$$I_2 = -\frac{1}{\ln R_D}\int_1^{R_D} \tau \exp(-p\tau^2)\, \ln \tau\, d\tau$$

Integrating by part and using the substitution $u = \tau^2$, and noting that:

$$\int \frac{\exp(bx)}{x}\, dx = Ei(bx)$$

we obtain

$$I_2 = \frac{1}{2p}\exp(-pR_D^2) - \frac{Ei(-pR_D^2) - Ei(-p)}{4p \ln R_D}$$

Where Ei is the exponential integral (a tabulated function). Inserting values of I_1, I_2, and T_D into Equation 4, we obtain:

$$\frac{T(0,t_2) - T_f}{T_m - T_f} = 1 - \frac{Ei(-pR_D^2) - Ei(-p)}{2 \ln R_D} \quad (5)$$

$$t_D > 5$$

In practice, for deep wells (large t_D and small p) we can assume that:

$$R_D = D_0\sqrt{t_D} \quad (6)$$

and

$$Ei(-p) = -\ln t_D - \ln n - \ln 4 + 0.5772 \quad (7)$$

Introduction of equations 6 and 7 into Formula 5 yields:

$$\frac{T(0,t_2) - T_f}{T_m - T_f} = -\frac{Ei(-\frac{D}{n}) + \ln n - D_1}{\ln t_D + 2 \ln D_0}$$

where

$$D = \frac{D_0^2}{4} = 1.1925$$

$$D_1 = 0.5772 + \ln D = 0.7532$$

If two measured temperatures (T_1,T_2) are available for the given depth with $t_2 = t_{2.1}$ and $t_2 = t_{2.2}$, we obtain:

$$\frac{T_1 - T_f}{T_2 - T_f} = \frac{Ei(-\frac{D}{n_1}) + \ln n_1 - D_1}{Ei(-\frac{D}{n_2}) + \ln n_2 - D_1}$$

Therefore:

$$T_f = T_2 + \gamma(T_1 - T_2) \qquad (8)$$

where

$$\gamma = \frac{Ei(-\frac{D}{n_2}) + \ln n_2 - D_1}{Ei(-\frac{D}{n_2}) - Ei(-\frac{D}{n_1}) + \ln \frac{n_2}{n_1}} \qquad (9)$$

$$n_1 = \frac{t_{2.1}}{t_1} ; \quad n_2 = \frac{t_{2.2}}{t_1} \qquad (10)$$

Thus the well radius and thermal diffusivity of the formation have no influence on T_f, as the unknown parameters T_m and t_D have been eliminated. The quantities r_w and a, however, affect the value of T_f through T_1 and T_2.

We have given the name "two-point" method to the procedure just described for determining the natural formation temperature. In order for this method to be employed, the temperature logs must be performed in a well under unsteady-state thermal conditions.

The disturbance time at given depth is:

$$t_1 = t_d - t_h$$

Where t_d is the total drilling time, t_h is the period of time needed to reach the given depth. The values of t_h can be determined from drilling records. In our case, the drilling records were not available and the following formula was used:

$$t_1 = t_d(1 - \frac{h}{H}) \qquad (11)$$

where h is the given depth, H is the total vertical depth of the well.

To determine the geothermal gradient, one should calculate the static formation temperature at two different depths (Figure 1). From formulas 8-11, one obtains:

$$\text{For } h = h_1 \; ; \quad T_f = T_{f1}$$

$$\text{For } h = h_2 \; ; \quad T_f = T_{f2}$$

Thus the geothermal gradient is:

$$A = \frac{T_{f2} - T_{f1}}{h_2 - h_1} \qquad (12)$$

Finally, the position of the permafrost base (h_p) is estimated by extrapolation (Figure 1).

$$h_p = h_1 - \frac{T_{f1}}{A} \qquad (13)$$

FIELD DATA

Precise temperature measurements taken in 15 deep wells located in Northern Canada (Arctic Islands and Mackenzie Delta) were used to verify the proposed method (Taylor and Judge 1977; Judge et al. 1979). The total depth of the wells (H), drilling time (t_d), shut-in time (time between termination of drilling and logging) for two temperature surveys ($t_{2.1}$ and $t_{2.2}$) and two randomly selected depths (h_1 and h_2) are presented in Table I. The transient temperatures for depths $h = h_1$ and $h = h_2$ at shut-in times $t_2 = t_{2.1}$ and $t_2 = t_{2.2}$ were taken from the previously mentioned references and are also presented in Table I. It should be noted that interpolation was often used to get values of temperature at the same depth for two different shut-in times.

DATA PROCESSING AND DISCUSSION

From Formula 11 and Table I (at $h = h_1$ or $h = h_2$) the parameter t_1 was calculated with an IBM PC and program utilizing the Ei-function for calculation of γ in Formula 9. The formation static temperatures for two depths are determined from Formula 8. A general computer program was prepared to calculate the permafrost thickness from Formulas 8-13: The results of the calculations are presented in Table II. The predicted formation static temperatures (T_{f1},T_{f2}) for two depths (h_1,h_2) are also presented in Table II. Permafrost thicknesses (h_p*) obtained from temperature logs after long shut-in times (t_2*) were compared to those determined by the "two point" method (Table II). Comparison indicates that the proposed "two point" method can be used to predict the permafrost thickness with good accuracy. The accuracy of the suggested method can be improved if more than two depths are selected in the section of the well below the permafrost. In Table III, the values of h_p are presented for six combinations of h_1 and h_2 (four depths). The average value of permafrost thickness is 276.3 m. If one assumes the "exact" value of permafrost thickness (h_p*) for this well is 259 m as determined by the long-time method of Taylor, et al., (Table II) then the proposed short-time method provides a value

with a relative accuracy of 6.5% (compare with 12%, Table II).

It should be noted that, in this example, temperature logs with relatively short shut-in times and drilling time ratios were used. Indeed, for Well 272 the value of $t_{2.2}/t_d = 158/53 = 3$ and the exact value of $h_p^* = 259$ m is obtained at $t_2^*/t_d = 31$, (Table II). It is also clear that the predicted values of the permafrost thickness are very dependent on the accuracy of the temperature logs in deep wells (Table III).

Table I Input data (Taylor and Judge, 1977; Judge, et al., 1979)

Well No.	H m	t_d days	$t_{2.1}$ days	$t_{2.2}$ days	h_1 m	h_2 m	$T_1(h_1, t_{2.1})$ °C	$T_2(h_1, t_{2.2})$ °C	$T_1(h_2, t_{2.1})$ °C	$T_2(h_2, t_{2.2})$ °C
86	3375	240	265	634	325.0	350.0	3.38	2.53	4.45	3.67
155	3925	119	190	431	475.0	500.0	4.69	2.97	5.71	4.32
158	3177	73	82	320	450.0	500.0	3.33	1.69	5.98	4.60
167	4361	179	26	106	152.4	213.4	9.88	6.56	11.87	9.07
168	4000	97	99	491	613.0	652.6	3.91	2.42	5.21	3.82
169	2281	65	104	479	275.0	300.0	3.84	2.31	5.27	3.69
170	1829	28	132	372	381.8	427.6	3.77	3.05	6.27	5.45
175	3845	145	53	440	550.0	575.0	9.35	3.98	10.73	5.41
178	3205	94	23	250	375.0	400.0	5.15	1.70	5.73	2.43
192	3689	188	35	321	149.4	195.1	9.56	4.27	11.11	6.04
193	4704	237	16	62	375.0	400.0	7.74	5.09	8.52	6.12
196	4383	133	41	395	785.0	814.7	3.49	2.13	4.10	2.93
272	3305	53	83	158	335.0	365.8	4.93	3.43	5.73	4.33
274	3295	61	60	135	411.2	456.9	4.36	2.97	5.96	4.53
275	3295	116	8	88	396.2	457.2	9.24	4.48	11.03	6.35

NOTE: Well No. is the Earth Physics Branch (Department of Energy, Mines and Resources, Ottawa, Canada) file number used throughout this paper.

Table II Permafrost thicknesses for 15 Northern Canadian Wells

Well No.	T_{f1} °C	T_{f2} °C	h_p m	h_p^* m	t_2^*/t_d	$\frac{\Delta h_p}{h_p^*} \cdot 100\%$
86	1.78	2.97	288	306	8.7	5.9
155	1.41	3.06	454	445	25	2.0
158	1.00	4.02	433	429	24	0.9
167	3.44	6.47	83	86	17	3.5
168	1.95	3.38	559	577	28	3.1
169	1.78	3.15	242	256	19	5.5
170	2.64	4.98	330	336	105	1.8
175	2.72	4.18	503	502	18	0.2
178	0.98	1.71	341	354	29	3.7
192	2.18	4.12	98	95	15	3.2
193	1.21	2.61	353	341	12	3.5
196	1.85	2.68	719	726	14	1.6
272	1.49	2.51	290	259	31	12.0
274	1.43	3.09	372	358	26	3.9
275	2.40	4.33	320	320	10	0.0

NOTE: (a) t_2^* is the time between drilling completion and latest log.
(b) h_p^* is the permafrost thickness determined from a series of logs (at $t_2 \leq t_2^*$). Temperature measurements within the permafrost zone were used (Taylor et al. 1982).

Table III Permafrost thickness, well 272, $t_{2.1}$ = 83 days, $t_{2.2}$ = 158 days.

h_1 m	h_2 m	$T_1(h_1,t_{2.1})$ °C	$T_2(h_1,t_{2.2})$ °C	$T_1(h_2,t_{2.1})$ °C	$T_2(h_2,t_{2.2})$ °C	T_{f1} °C	T_{f2} °C	A °C/100m	h_p m
335.0	365.8	4.93	3.43	5.73	4.33	1.49	2.51	3.31	290.0
335.0	396.2	4.93	3.43	6.71	5.26	1.49	3.38	3.09	286.8
335.0	426.7	4.93	3.43	7.71	6.13	1.49	4.09	2.84	282.5
365.8	396.2	5.73	4.33	6.71	5.26	2.51	3.38	2.86	278.0
365.8	426.7	5.73	4.33	7.71	6.13	2.51	4.09	2.59	268.9
396.2	426.7	6.71	5.26	7.71	6.13	3.38	4.09	2.33	251.4

CONCLUSIONS

A new method for predicting the permafrost thickness is described. Only two temperature logs taken at relatively short shut-in times are needed to apply this method. Values of permafrost thickness for 15 Northern Canadian wells have been used to verify the "two point" method. Application of the suggested method may reduce the time and cost of permafrost surveys in Arctic areas.

ACKNOWLEDGMENTS

The author wishes to thank Dr. Robert M. Caruthers for his valuable suggestions and Mr. Cuong T. Nguyen for assistance with the calculations.

REFERENCES

Balobaev, V.T., Devyatkin, V.N. and Kutasov, I.M. (1973). Contemporary Geothermal Conditions of the Existence and Development of Permafrost, In Proceedings of the Second International Conference on Permafrost, Yakutsk, Soviet Contribution Washington, D.C., National Academy of Science, 8-12.

Bullard, E.C. (1947). The Time Necessary for a Borehole to Attain Temperature Equilibrium, Mon. Not. R. Astron. Soc. Geophys. Suppl. 5, 127-130.

Carslaw, H.C. and Jaeger, J.C. (1959). Conduction of Heat in Solids, 2nd Edition, Oxford University Press, London, 207.

Jaeger, J.C. (1956). Conduction of heat in an infinite region bounded internally by a circular cylinder of a perfect conductor. Aust. J. Phys. 9, 167-169.

Jaeger, J.C. (1961). The Effect of the Drilling Fluid on Temperatures Measured in Boreholes, J. Geophys. Res. 66, 563-569.

Judge, A.S. (1973). Deep Temperature Observations in the Canadian North, In Permafrost - The North American Contribution to the Second International Conference, Yakutsk, Washington, D.C., National Academy of Science, 35-40.

Judge, A.S., Taylor, A.E. and Burgess, M. (1979). Canadian Geothermal Data Collection--Northern Wells 1977-78, Geothermal Series Number 11, Earth Physics Branch, Energy, Mines, and Resources, Ottawa, 187 pp.

Kutasov, I.M., Lyubimova, E.A. and Firsov, F.V. (1966). Rate of Recovery of the Temperature Field in Wells on the Kola Peninsula, in the collection of papers "Problemy glubinnogo teplovogo potoka" (Problems in the Heat Flux at Depth), Nauka, Moscow, 74-87.

Kutasov, I.M. (1968). Determination of Time Required for the Attainment of Temperature Equilibrium and Geothermal Gradient in Deep Boreholes. Freiberger Forschungshefte, C238, 55-61.

Kutasov, I.M. (1976). Thermal Parameters of Wells Drilled in Permafrost Regions, Nedra, Moscow. 119 pp.

Lachenbruch, A.H. and Brewer, M.C. (1959). Dissipation of the Temperature Effect of Drilling a Well in Arctic Alaska, U.S. Geol. Surv. Bull. 1083-C, 74-109.

Lachenbruch, A.H., Sass, J.H., Marshall, B.V. and Moses, T.H. (1982). Permafrost, Heat Flow and the Geothermal Regime at Prudhoe Bay Alaska. Journal of Geophysical Research, 87, 9301-9316.

Melnikov, P.I., Balobaev, V.T., Kutasov, I.M. and Devyatkin, V.N. (1974). Geothermal Studies in Central Yakutia, International Geology Review, May, 363-368.

Taylor, A.E. and Judge, A.S. (1977). Canadian Geothermal Data Collection - Northern Wells, 1976-77, Geothermal Series Number 10 Earth Physics Branch, Energy, Mines and Resources, Ottawa, 194 pp.

Taylor, A.E., Burgess, M., Judge, A.S. and Allen, V.S. (1982). Canadian Geothermal Data Collection--Northern Wells 1981, Geothermal Series, Number 13, Earth Physics Branch, Energy, Mines and Resources, Ottawa, 153 pp.

THE USE OF GROUND PROBING RADAR IN THE DESIGN AND MONITORING OF WATER RETAINING EMBANKMENTS IN PERMAFROST

P.T. Lafleche, A.S. Judge and J.A. Pilon

Terrain Sciences Division, Geological Survey of Canada, Ottawa, Canada

SYNOPSIS The construction of frozen earth containment dams is becoming an increasingly important element in the development of northern regions. The availability of local materials, a relatively impermeable frozen overburden and naturally low year-round temperatures make the construction of frozen embankments a cost effective technique in permafrost areas. Several such structures, however, have suffered failures in the past. The development of an active layer during the summer season can degrade a dam's ability to retain water. Additionally, sub-dam fluid transport can occur through unfrozen natural topsoil or poor quality bedrock. Degradation of included ice within the dam fill matrix or topsoil can also result in leakage.

The Permafrost Research Group has monitored the performance of several naturally frozen earth dams at the Echo Bay Mines Ltd. Lupin mine, near Contwoyto Lake N.W.T. since 1982. The dams are used to enclose a small watershed which serves as a mine-tailings pond. Initial investigations were undertaken with the use of thermistor strings in short drillholes. More recently, the use of ground probing radar (GPR) has been instrumental in confirming and locating possible zones of containment failure within the dams. The ability of GPR to image the subsurface to depths of several tens of metres is sufficient to resolve the dam structure including voids, sub-dam overburden, bedrock topography, active layer depth and to discriminate between frozen and unfrozen zones within the subsurface. The thermal regime of the dams and underlying natural materials will change considerably over the initial few years after construction. Through comparison of the thermal data and seasonal radar profiles a history for such structures has been developed that will be important for performance evaluation and design of future facilities.

The ground probing radar technique has shown itself to be a viable tool for post-construction monitoring. Similarly, radar surveys can aid in pre-construction site-selection and in establishing dam design requirements.

INTRODUCTION

During late June and September 1986 and April 1987 several ground probing radar (GPR) surveys were undertaken across tailings pond dams at the Lupin Mine site of Echo Bay Mines Ltd. The Lupin site is located in the Northwest Territories, on the northwest side of Contwoyto Lake, about 480 km east of Great Bear Lake. The area is underlain by several hundred metres of permafrost: over five hundred metres of frozen ground was intersected in the development of the mine shaft. The tailings disposal pond at the site (Figure 1) was created by damming a small watershed to create an enclosed storage basin. This basin was designed to hold the tailings output of the mine for several years. Decantation into the natural environment would occur after treatment has reduced the contaminant content to an acceptable level. These containment dams were constructed from locally derived sand and gravel or crushed tailings sand. Several of the dams were lined with an impermeable liner. Typically each dam site was scraped clean of organic material prior to construction of the dams. The frozen nature of the dams and the underlying overburden and bedrock should preclude any fluid transport through or beneath the structures. Several of the dams were elevated and broadened by the addition of gravelly-sand in 1984.

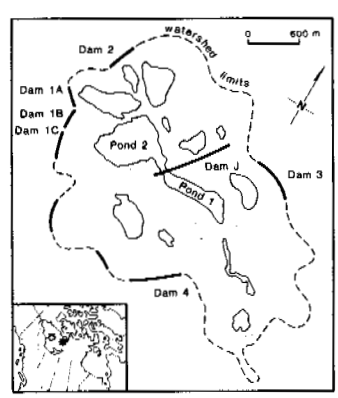

Fig.1. The Lupin Mine tailings facility.

Despite the precautions taken in the design and construction of the dams, leakage of tailings water has been known to occur during the thaw season through or around several of the dams. The purpose of the GPR surveys was to establish if a high resolution geophysical technique, such as GPR , could detect unfrozen zones (taliks) within or below the dams and so reveal a picture of the dam and overburden conditions. Unfrozen zones were thought to be the cause of fluid transport from the tailings pond into the surrounding environment. In addition to the radar surveys, a ground temperature monitoring program has been carried out at the site since 1982. Thermistors are installed in boreholes through four of the dams. Early temperature measuring cables suffered failures but reliable ground temperature data are available from June 1, 1985 to the present date. Temperature data normally are collected several times per month.

The ability of GPR to image the ground to 50 m in some cases allows resolution of the dam structures, sub-dam overburden conditions, bedrock topography and depth of thaw; and to locate unfrozen zones (taliks) within the overburden and uppermost bedrock.

FROZEN CORE CONTAINMENT DAMS

Frozen core containment dams have been used extensively in the Soviet Union for a number of years. The main advantage of these structures is that they are impermeable to fluid flow due to their frozen nature and are relatively cheap to construct as materials can be found locally. Typically the structures are built upon the natural overburden and are less than 50 m in height (Sayles, 1983). Such dams are maintained in an impermeable state either by naturally low local temperatures or through active refrigeration techniques such as the installation of cold air or liquid refrigerant piping. Several instances of dam failure have occurred in the Soviet Union. These usually involve a small area of leakage which rapidly expands due to local melting around the leak site. Causes of potential leakage are insufficient freezing of the dam during construction, degradation of the dam base due to thermal heating by the retained fluid which eventually results in a sub-dam talik, thaw degradation of the reservoir side of the dam embankment, melting arising from high fluid flows at outlet structures or the creation of voids within the dam arising from the melting of large ice pockets inadvertently included in the dam during construction.

GROUND PROBING RADAR (GPR)

The GPR is a fairly new geophysical tool, the first models being commercially available in the mid 1970's. GPR is similar in principle to the reflection seismic method in that a pulse of energy is directed into the ground and the arrival times of reflections from subsurface interfaces are recorded. The main difference between the techniques is that radar uses an electromagnetic as opposed to an acoustic energy source. Radar possesses a much more limited depth of penetration than seismic, typically of the order of 50 m or less, but provides a significant increase in resolution. Subsurface resolution is dependant upon the pulse length and, as such, can be as low as one half a metre. This high spatial resolution can be important in the solution of complex near surface problems. GPR has been found to be most useful in engineering geophysical applications such as the delineation of overburden thickness, permafrost extent and depth (LaFleche and Judge, 1987a), water table depth and ice thickness (Annan and Davis, 1977) or for locating buried cables, pipes (Morey, 1974), fractures (Olhoeft, 1978), voids (Owen and Suhler, 1980), gravels (Davis et al., 1984) and tunnels (Dolphin et al., 1978).

Radar reflections are produced by interfaces between materials of contrasting electrical properties, specifically the dielectric permittivity or electrical conductivity. Common causes of subsurface reflections are material interfaces (overburden-rock, gravel-sand), top of the water table, boundaries between frozen and unfrozen water, voids, fractures and ice lenses. Within the radio frequency band, a large dielectric and conductivity contrast exists between water and most natural geologic materials (Morey, 1974). The ability of a material to retain water within its pore spaces is an important factor for the determination of its bulk electrical properties. As such, the presence or absence of water and its chemistry controls, to a large degree, the subsurface propagation characteristics of the radar pulse. Distinct variations in grain size or rock porosity, and the associated changes in the volume percentage of retained water, will produce radar reflections.

The depth to which a radar pulse will effectively "penetrate" is dependant upon the electromagnetic absorption characteristics of the ground and the amount of energy lost due to reflection, refraction and diffraction effects. In a general sense, the depth of penetration will decrease with increasing water content. Dry, homogenous or frozen materials will offer the greatest potential depth penetration.

The depths to specific reflectors are calculated from a knowledge of the subsurface radar velocity distribution. In air, the radar pulse, typically in the MHz or GHz frequency range, travels with the speed of light (0.3 m/ns). In the ground the pulse travels with a velocity (typically 10 to 50% of the speed of light) which is dependent upon the electrical properties of the material traversed. The radar velocity distribution in the ground can be determined, as in the case of seismic surveys, by a common depth point sounding (CDP).

The low conductivity and low dielectric losses of very high frequency (VHF) electromagnetic waves in frozen ground allow considerable penetration in permafrost. The extent of taliks can be mapped as the sharp contrasts in conductivity and permittivity between frozen and unfrozen zones result in strong reflections from these boundaries.

DAM SITE INVESTIGATIONS

Two dam sites were initially surveyed in June of 1986: Dams 2 and J (Figure 1). Dam J was resurveyed in April of 1987. Both of these dams currently have or have experienced associated tailings water seepage. Borehole temperature data are available for Dam 2. Dam J was only recently constructed in 1985, thus only the details of the construction plans are available. It was built to seal off the primary tailings pond, Pond 1, from the decantation pond, Pond 2, shown in Figure 1. Pond 2 serves as a temporary holding basin before decantation into the environment. The water is treated to remove contaminants during decantation from Pond 1 to Pond 2.

A third site, Dam 1A (Figure 1) was surveyed in late September of 1986 and resurveyed in April of 1987. Borehole temperature readings indicate that a thaw bulb may exist at depth beneath the dam.

Dam 2

Dam 2 (Figure 2) was surveyed with the object of mapping the sub-dam bedrock and overburden competency. Seepage had been observed to occur around the south end of the dam abutment, near the station at 310 m on the radar profile (Figure 3), during previous summer seasons. The core extracted from a drillhole at location 356 m, beyond the end of the profile, had shown indication of substantial fracturing through the first 5 m of bedrock. The source of water transport was thought to be due to the melting, during the thaw season, of ice infilling these fractures. Temperature data indicate that the ground temperature could rise as high as 0°C even at 7 m depth during the period of maximum thaw.

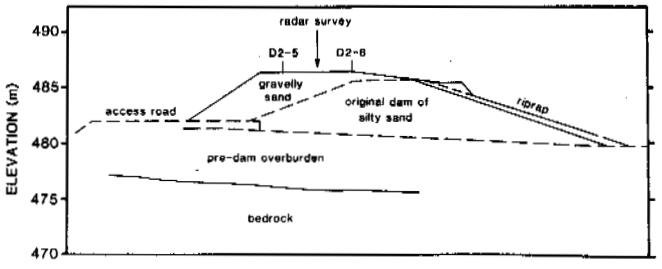

Fig.2. Cross-section of Dam 2.

The dam was profiled from north to south using an A-Cubed Inc. PulseEKKO III radar equipped with 50 MHz antennas. The transmitting and receiving antennas were separated by 4 m and the station spacing was 4 m. The horizontal axis on the radar profiles represents the distance along the dam, while the vertical axis represents travel time (nanoseconds) to a particular reflection event.

The interpretated ground section is shown in Figure 3. The velocity (0.11 m/ns), determined from CDP soundings, can be used to calculate the depths to reflectors 1, 2 and 3 indicated on Fig. 3 (LaFleche et al., 1987b).

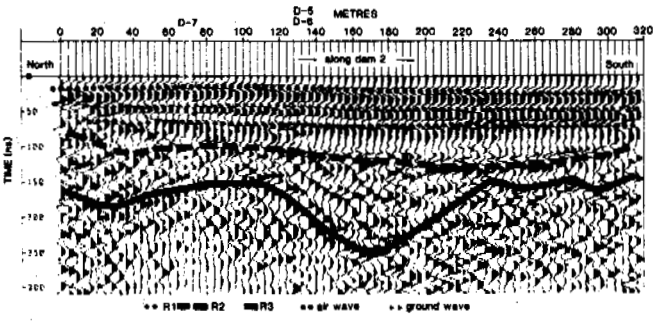

Fig.3. A 50 MHz radar profile and interpreted section for Dam 2 in June of 1986.

Reflector 1 is at a depth of about 2 m appearing to combine the boundary between the new and old dam material and the depth of the active layer. Temperature data from thermistors D-5 and D-6 indicate that the latter should reside between 2 and 3 m. Since both interfaces could be roughly coincident at this time of year it would be difficult to resolve them as separate events. It can however be observed that in many places reflector 1 is represented by a broad double pulse indicative of a complex boundary. The new dam fill which is believed to be gravelly sand should retain much less moisture than the original silty sand. Such an interface should provide a good electrical contrast as indicated by reflector 1.

Reflector 2 is at a depth of about 4.2 m and represents the interface of the silty sand dam fill with the natural silty sand overburden. The natural overburden should contain considerably more frozen water than the dam fill resulting in a strong electrical contrast. The dam fill material was obtained by drying excavated natural overburden material to substantially reduce its water content.

Reflector 3 varies considerably in depth along the profile. It represents the top of the bedrock. A substantial (5 m) dip in the bedrock topography is observed near the middle of the dam (at distance along the profile of 110 to 222 m). Drillholes D-6 and D-7 (Figure 3) indicate bedrock depths of 4.1 and 10.4 m respectively. The depths calculated at D-6 and D-7 from the radar profile are 5.9 and 9.5 m respectively. The discrepency arises from an uncertainty of the true velocity profile. Each layer of dam fill possesses its own radar velocity and thickness and these should be taken into account when calculating the true depth to bedrock.

Strong reflections are observed within the bedrock. These most likely represent included ice within the phyllite; the ice could be present either along cleavage planes or in fractures and joints. The limit of the reflections at depth (Figure 3) is a function of several factors including the gain level, the detection threshold of the instrument and the absorptive characteristics of the subsurface materials. Increasing or decreasing the gain during pro-

cessing will move this apparent boundary either downward or upward. The apparent dip in the base of these reflections is an artifact of the increased thickness of overburden in the central area of the dam. The bedrock material should possess a higher radar velocity than the natural silty sand overburden; the addition of an increased thickness of lower velocity material stretches out the traces in this area yielding a distorted image of the deep structure.

Dam J

Dam J was surveyed with the object of detecting a possible area of seepage through either the dam itself or its base. The dam was originally filled with run of mill (ROM) material to the original land surface (Golder Associates, 1986). This means we should not expect to encounter any layering or large reflectors within the dam itself. An impermeable sand liner was placed on the upstream side. The ROM material is relatively permeable and is unable to support a fluid head across the dam for any period of time. Little permafrost existed naturally at the site as most of the central portion of the dam foundation was originally covered by water in a pre-existing stream bed. This resulted in the material immediately under the central portion of the dam being initially unfrozen.

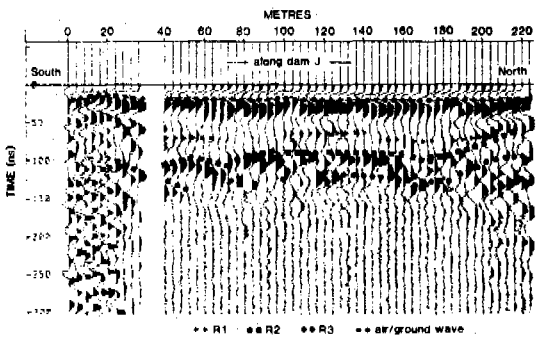

Fig.4. A 50 MHz radar profile along Dam J in June of 1986.

The dam was profiled with the PulseEKKO III radar using the 50 MHz antennas in June of 1986 and April of 1987. The transmitter-receiver separation and the station spacing were 4 m for the June 1986 survey and 2 m for the 1987 survey respectively. A CDP sounding was taken near the north end of the dam. The radar profiles over the dam are shown in Figures 4 and 5. CDP soundings taken in September 1986 and April 1987 indicate that the top layer velocity is 0.14 m/ns.

In the initial survey (Figure 4) the depth of penetration of the radar is quite limited over the dam itself. This is evidenced by the lack of returns at mid to late times at locations 40 m to 200 m along the profile. The high water content and unfrozen nature of the overburden under Dam J limits the penetration of the radar pulse. Note that the rather clean radar traces directly under Dam J are in direct contrast to the profile presented under Dam 2 (Figure 3) where strong reflections are indicated to depth. The traces at either end of Dam J, that is in the areas not originally submerged, exhibit the latter character.

Given these initial survey results, several possible causes of leakage from Pond 1 to Pond 2 were envisaged. These are:

1. Leakage could be occurring directly through the rather thin tailings sand liner.
2. Leakage could be aided by the melting of lake ice included with the ROM material during winter dam construction period.
3. Fluid could be transported through the natural overburden or lake-bottom base which seems to be unfrozen.

Subsequently, the dam was widened and raised in the fall of 1986. The effect of this was to present a wider surface over which to promote freezing. The results of the April 1987 survey (Figure 5) show that radar penetration has increased significantly under the dam itself, suggesting that the ground has frozen considerably over the winter of 1986/87. Figure 6 shows, for comparison, the interpretated section for the September 1987 survey. The interface between the old dam fill and the new fill is clearly visible in the radar profile. The base of the dam can be traced across the old river bed.

Dam 1A

Dam 1A was surveyed with the object of mapping one or more large unfrozen zones (taliks) which

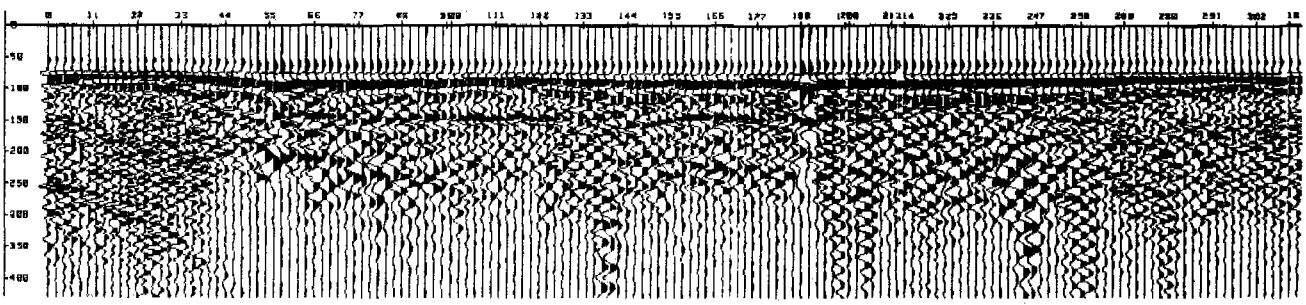

Fig.5. A 50 MHz radar profile along Dam J in April of 1987.

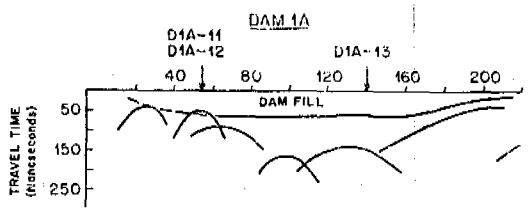

Fig.6. Interpreted section for the profile in Fig.5.

were thought to exist below the dam's base. A small stream originally cut across the middle of the area spanned by the dam. This resulted in the formation of a small floodplain valley and possibly year-round unfrozen zones under the river bed. Thermistors were installed in five drillholes, D1A-1, 10, 11, 12 and 13 (Figure 7). The temperature data for drillhole D1A-13 show that the subsurface remains frozen below a depth of 4 m year-round. Thermistor string D1A-1 indicates a potential thaw depth of 4.3 m. The thermistors in drillholes D1A-11 and D1A-12 indicate that the subsurface material remains unfrozen down to 10 m during the season of maximum thaw and can remain above -2°C down to at least 24 m depth. The thermistors in drillhole D1A-10 indicate that the subsurface can thaw down to about 5 m depth. The temperature data thus show the presence of a talik in the natural overburden beneath the dam at the position of thermistor strings D1A-10, D1A-11 and D1A-12. This dam was surveyed using the 100 MHz antennas in September of 1987 in order to provide the best subsurface resolution. The April 1987 survey employed the 50 MHz antennas. The station interval was 2 m.

The profile along the top of the dam shows strong reflections from the interface between the original silty-sand fill derived from dried overburden material and the gravel-sand material used in elevating the dams. The interface between the dam fill and the original overburden is also evident. The bedrock/overburden interface is not obvious on this profile. The holes drilled from the top of the dam, D1A-11 and D1A-12, indicate that bedrock is at least ten metres deep. This corresponds to a minimum of 220 ns in radar pulse travel time.

The profile along the dam access road (Figure 7) shows three strong reflectors (Figure 8). Reflector R1 represents the interface between the gravelly-sand and dam fill and the original silty-sand dam fill. Reflector R2 represents the interface between the dam fill and the natural overburden. Reflector R3 represents the bedrock interface. Drillhole D1A-10 intersects the bedrock at 5.2 m. The depth to bedrock at D1A-10 as calculated from the radar profile is 5.1 m. Drillhole D1A-1 was unfortunately not logged. The radar profile shows a pronounced dip in the bedrock topography between locations 130 m and 210 m along the profile. This agrees with the drillhole data which indicates that the bedrock interface is substantially deeper, below 10 m, at 166 m.

Generally, returns are recorded to depth along the length of the profile. Two zones showing an absence of deeper reflections are marked on the profile. These are areas of high electromagnetic attenuation which are probably partially to substantially unfrozen. The absorption of electromagnetic energy in the central unfrozen zone has resulted in an extremely weak reflection from the bedrock interface between 170 m and 195 m (as indicated by the dashed line). Furthermore the lower radar pulse velocity associated with this zone has depressed that portion of the bedrock reflector which is visible. The bedrock interface thus appears

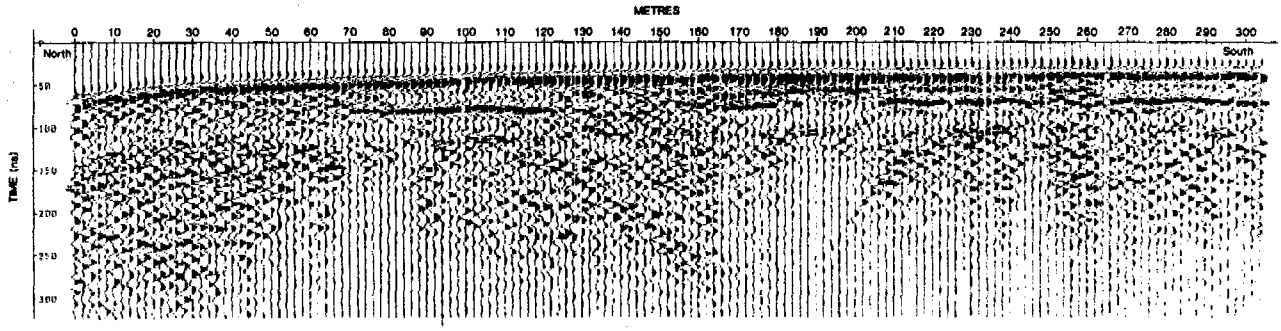

Fig.7. A 100 MHz radar profile along the Dam 1A access road in September of 1986.

Two radar profiles were run at this site, one along the top of the dam and one at a lower elevation along the dam access road containing thermistor strings D1A-1 and D1A-10. The latter profile is shown in Figure 8. Common depth point soundings were taken in both cases. The ground wave velocities at the top of the dam and on the access road are 0.094 and 0.081 m/ns respectively. These are quite similar to the velocity calculated for Dam 2 which is similar in construction to Dam 1A.

slightly deeper than it actually is in this region.

The central thaw zone corresponds with the stream bed leading out of the original watershed, suggesting that a talik existed prior to dam construction. The top of the zone lies at a depth of about 5 m. Thawing of the overlying overburden and dam fill has occurred under locations 180 m to 190 m. The bedrock in drill-

hole D1A-11 was found to be highly fractured and of generally poor quality for the top two metres. Drillhole D1A-12 intersected poor to fair quality bedrock down to 15 m. There exists a potential for fluid transport through the upper portion of the bedrock as in the case of Dam 2.

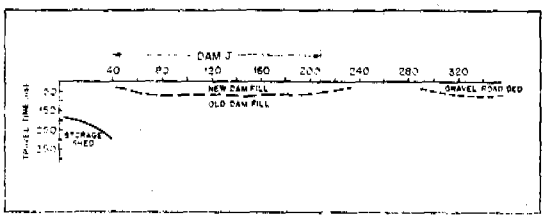

Fig.8. Interpreted section for the profile in Fig.7.

The more northerly thaw zone corresponds to the location where seepage was observed to occur immediately after the dam construction in the fall of 1981.

CONCLUSION

Frozen earth-filled dams and embankments have considerable application in the permafrost regions of the world. The ground probing radar surveys were able to yield considerable information on the dam and sub-dam conditions and performance. This information corresponded well to the subsurface conditions as determined by the dam construction procedures and subsequent drill-coring. The radar has also served to extend our knowledge of the subsurface to areas where little was previously known. Radar surveys should be a powerful technique for pre-construction site investigation and for monitoring both before and after dam construction. Problems, such as those encountered at Dam 2 with the poor quality of bedrock, could be detected in advance and designed around in the construction phase. Two probable thaw zones under Dam 1A were detected in the radar profile. These correspond well with the existing downhole temperature information. Likewise the radar was able to detect the unfrozen nature of Dam J and follow its freezing over time. The major advantage of the radar is that it is able to map the total extent of the thaw zones between drillholes.

Given the changing ground conditions associated with the yearly freeze-thaw cycle, it would be advantageous to monitor the dam conditions with the radar at several times during the year. This, in conjunction with the on-going temperature monitoring program, would allow us to determine the nature of any long term changes at the site. A combined geophysical and thermal history of these sites will be important when considering future developments of this type on permafrost.

ACKNOWLEDGEMENTS

The authors wish to express their gratitude to Echo Bay Mines Ltd. for providing logistic assistance; in particular, Bob Gilroy, Hugh Wilson and Ed Wong. The thermal monitoring program is conducted under contract to EMR-Canada by Geocon Inc. Funding assistance has been provided by the Northern Environmental Directorate of Indian and Northern Affairs Canada.

REFERENCES

Annan, AP, Davis, JL (1977). Impulse radar applied to ice thickness measurements and fresh water bathymetry. Geol. Sur. of Can. Paper 77-1B, 63-65.

Davis, JL, Annan, AP, Vaughan, C (1984). Placer exploration using radar and seismic methods. Expanded abstracts of the 54th Ann. Int. S.E.G. Meeting.

Dolphin, LT, Beaty, WB, Tanzi, JD (1978). Radar probing of Vitorio Peak, New Mexico. Geophysics, 43, 1441-1448.

Fowler, JC (1981). Subsurface reflection profiling using ground probing radar. Mining Engineering, 33, 1266-1270.

Geocon, Inc. (1986). Interim Data Report No. 40906-1-04, submitted to the Terrain Sciences Division, Geol. Sur. of Can.

Golder Associates (1986). Draft report on tailings impoundment area, Contwoyto Lake, N.W.T., submitted to Echo Bay Mines Ltd.

Kovacs, A, and Morey, RM (1985). Impulse radar sounding of frozen ground. US Army Corps of Eng. C.R.R.E.L., Spec. Rep. 85-5, 28-40.

LaFleche, PT, Judge, AS, Taylor, AE (1987a). Applications of geophysical methods to resource development in northern Canada. CIM Bulletin, 80, 78-87.

LaFleche, PT, Judge, AS, Pilon, JA (1987b). Ground probing radar in the investigation of the competancy of frozen tailings pond dams. Current Research, Part A, Geol. Sur. of Can., Paper 87-1A, 191-197.

Morey, RM (1974). Continuous subsurface profiling by impulse radar: Proceedings of the Engineering Foundation Conference on Subsurface Exploration for Underground Excavation and Heavy Construction, Am. Soc. Civ. Eng.

Olhoeft, GR (1978). Surficial mapping and in situ electrical measurements by impulse radar: Am. Geophy. Union. Trans., 59, 1055.

Owen, TE, Suhler, SA (1980). Subsurface void detection using surface resistivity and borehole electromagnetic techniques: Expanded abstracts of the 50th Ann. Int. S.E.G. Meeting.

Sayles, FH (1984). Design and performance of water-retaining embankments in permafrost. Final Proceedings of the 4th Int. Conf. Permafrost, Fairbanks, Alaska, 31-42.

PEAT FORMATION IN SVALBARD

J. Låg

Agricultural University of Norway, 1432 Ås-NLH, Norway

SYNOPSIS For a long time it has been a common testbook declaration that no peatland exists in Svalbard. This statement is, however, not quite correct. In Svalbard many moss species occur which give possibilities for peat accumulation where the growing conditions are sufficient. Peat deposits more than 1 m deep have been found in scattered places. The most remarkable peatlands occur on steep ground. The water released by thawing of the superficial permafrost layer has here percolated downwards on the surface of the still frozen soil, giving bases for a luxuriant growth of mosses. Peatlands occur in the neighbourhood of Grumantbyen at Isfjorden with a gradient of up to 1:1.1, and depths of the peat stratum up to 3 m.

INTRODUCTION

The primary condition for development of peat is a certain production of organic material. Further the decomposition has to go comparatively slowly. Svalbard has an extremely cold climate. Permafrost has been registered down to a depth af 450 m (Liestøl 1977). The rate of decomposition of humus, under these circumstances, is of course very slow.

For a long time it has been a general saying in textbooks that Svalbard has no peatland. This statement is, however, not quite correct. Many of the moss species growing here, produce peat at more southern latitudes. A question now is where in Svalbard we can find sufficient growing conditions for these plants.

According to an international definition the term peatland is used for areas with a surface organic layer of at least 30 cm depth.

PEAT FORMATION IN STEEP SLOPES

The water set free by melting of a surface layer of the soil during summer time moves downwards on the surface of the permafrost in sloping areas. This moving water is as a rule favourable for the vegetation owing to a relatively large content of oxygen and nutrients. In slopes with a good local climate, and with an extra supply of nutrients from dropping of sea birds, the growing conditions can be especially advantageous. After systematically searcing for such localities, peat deposits were found in steep slopes between the outlet of Bjørndalen river and Grumantbyen at Isfjorden. In the years 1977-1979 investigations were carried out. Depth up to 1.1 m, and gradient up to 1:1.1 were noted (Låg 1980).

The study of such curious peatlands has been continued. Because the heat conductivity power is low in the thawed peat, this layer is shallow, and the measurement of the total peat depth is not easy. However, in these landscapes slips and landslides often occur, giving new cuttings in the soil material. In the neighbourhood of Grumantbyen a peat depth of 3 m was measured in 1987.

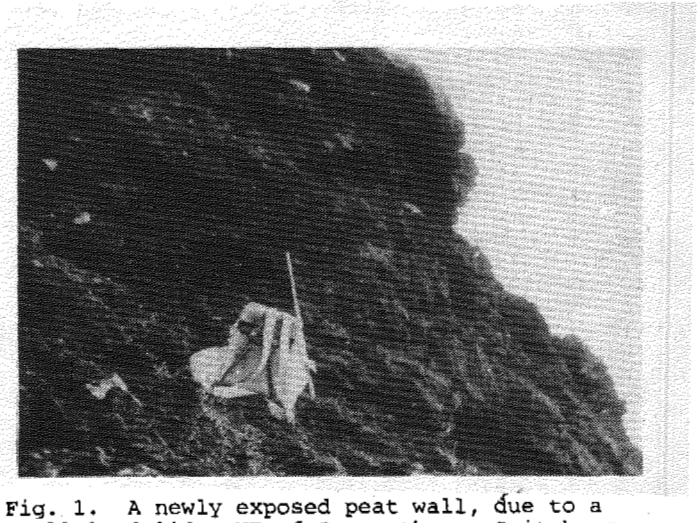

Fig. 1. A newly exposed peat wall, due to a small landslide, NE of Grumantbyen, Spitsbergen. Foto J. Låg, 01.08.1987.

In several other places peat with a steep surface has been found. At Sassenfjorden, in a slope to the northeast of Fredheim, I have measured peat depth of a little more than 1 m. In many places, e.g. at Recherfjorden, Vårsolbukta, Hornsund, and Skansen peat with a depth of 0.3-0.6 m has been discovered.

There is no reason to assume that peat formation in steep slopes occurs only in Svalbard. Similar natural conditions can be found in other places in the permafrost regions. Under a short

stay in Greenland I have noticed such phenomena there (Låg 1981). A Canadian lady, Catherine LaFarge-England, has in a private letter dated 09.06.1987, told that she has found 4 m deep peat, sloping 34°, in Ellesmere Island, around 82°N.

Fig. 2. The steep, relatively smooth slope, has a peat cover, at most places of depths 0.5 - 1.0 m, NE of Grumantbyen, Spitsbergen. Foto J. Låg, 24.07.1986.

A main reason why so few up to now have noticed these curious peat deposits seems to be the traditional way of stating that peatland is to be found in flat areas in the landscape.

PEATLANDS WITH NEARLY HORIZONTAL SURFACE

Scattered small peatlands are not seldom. The Swede Nathorst (1910) tells that in 1882 he discovered peat with a depth of 2 m in Kapp Thordson Peninsula. He mentions 4 other places where he has seen peat, and says that such soil material is not seldom in Spitsbergen. At last he quotes the opinion of another Swede (Gunnar Andersson) that peat formation is not going on any longer here, and consequently that the deposits mentioned are relics.

In Sauridalen, Kapp Thordsen, I have seen a 2 m deep peat deposit at the eastern side of the river. This seems to be the locality reported by Nathorst. (He used the name Renntier-Tal.) The surface was nearly horizontal and had a luxuriant growing moss carpet. The publication of Nathorst seems to be unknown for most of the scientists studying soil conditions in Svalbard.

In the Midterhuken area well decomposed peat rich in nitrogen occurs (Låg 1980). Adventdalen has peat deposits (Låg 1979, Göttlich & Hornburg 1982). The last mentioned authors have performed an age determination, showing the result 4615 ± 45 years. Serebryannyy et al. (1985) have described a 1.7 m thick peat layer in Nordenskiölds Land. An age determination showed approximately 4500 years B.P.

Mires with depths of peat less than 30 cm are of cource quite common (see e.g. Eurola 1971, Plichta 1977).

Fig. 3. Eroded peat deposit. Mitherhuken, Spitsbergen. Foto J. Låg, 23.07.1979.

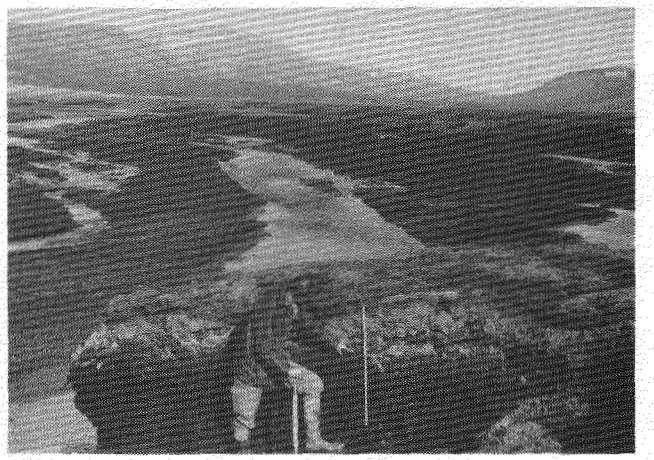

Fig. 4. Peat covered by 0.5 m mineral soil. Adventdalen, north of Mine No. 7. Foto J. Låg 31.07.1983.

NEW REPORTS ON PEAT DEPOSITS IN SVALBARD

When I had discovered the curious peat deposits in steep slopes, I asked scientists who use to travel in the Svalbard region to look for such deposits. Three employees at the Norwegian Polar Research Institute (T. Siggerud,

O. Salvigsen, and T.S. Winsnes) have told about small peatland areas in Karl XII Islands and Herman's Island. Mr. Asbjørn Børset has later visited Karl XII Islands situated around 80° 40'N, and observed peat deposits both there and in the near Broch's Island. So far I have not had the opportunity to visit these places.

REFERENCES

Eurola, S. (1971). The middle artic mire vegetation in Spitsbergen. Acta Agral. Fennica. 123, 87-107.

Göttlich, K. & Hornburg, P. (1982). Ein Zeuge wärmezeitlicher Moore in Adventdalen auf Spitzbergen (Svalbard-Archipel). Telma. 12, 253-260.

Liestøl, O. (1977). Pingos, springs, and permafrost in Spitsbergen. Norsk polar-institutt. Årbok 1975, 7-29.

Låg, J. (1979). Litt om jordbunnsforholdene på Svalbard. (English summary.) Jord og Myr. 3, 99-110.

Låg, J. (1980). Special peat formation in Svalbard. Acta Agric. Scand. 30, 205-210.

Låg, J. (1981). Humus accumulation in steep slopes at the inner part of Søndre Strøm-fjord, Greenland. Acta Agric. Scand. 31, 242-244.

Nathorst, A.G. (1910). Beiträge zur Geologie der Bären-Insel, Spitzbergens und des König-Karl-Landes. Bull. Geol. Inst..... Uppsala. 10, 261-415.

Plichta, W. (1977). Systematics of soils of the Hornsund region West Spitsbergen. Acta Universitatis Nicolai Copernici. Geografia. 13, 175-180.

Serebryannyy, L.P., Tishkov, A.A., Malyasova, Ye. S., Solomina, O.N. & Il'ves, E.O. (1985). Reconstruction of the development of vegetation in arctic high latitudes. Polar Geography and Geology. 9, 308-320.

PERMAFROST GEOPHYSICAL INVESTIGATION AT THE NEW AIRPORT SITE OF KANGIQSUALUJJUAQ, NORTHERN QUEBEC, CANADA

M.-K. Seguin, E. Gahe, M. Allard and K. Ben-Mikoud

Centre D'etudes Nordiques, Cite Universitaire, Quebec, GIK 7P4 Université Laval, Canada

SYNOPSIS The study area is located in the southeastern part of Ungava Bay. The airport site lies in a valley oriented: NW-SE, flanked by steep bedrock ridges partly filled with glacial and marine deposits. Recent governmental policy required the construction of new airports for Inuitian communities of northern Quebec. Construction in a discontinuous permafrost environment requires knowledge of active layer thicknesses as well as lateral and vertical distribution of permafrost, bedrock topography and groundwater regime. With these objectives in mind, five geophysical methods were used to investigate the spatial distribution of permafrost on the airport site. Four methods (electrical resistivity, induced polarization, electromagnetism and refraction seismic) were useful to determine the thickness of the active layer and permafrost and three others (electrical resistivity, refraction seismic and gravimetric) to delineate bedrock topography. Combining the geophysical data, the following results were obtained. The thickness of the active layer ranges from 0.5 to 2.8 m (mean: 1.2), that of permafrost from 1.5 to 20 m (mean: 8), that of the unfrozen layer beneath permafrost 3 to 52 m (mean: 15) and the depth to bedrock from 9 to 66 m (mean: 27). The permafrost underlies 40% of the study area. The physical properties (electrical resistivity, chargeability and density) are obtained for different geological units.

INTRODUCTION

The investigated site is located some 160 km northeast of Kuujjuaq at longitude 66°W and latitude 58°30'N (Fig.1)

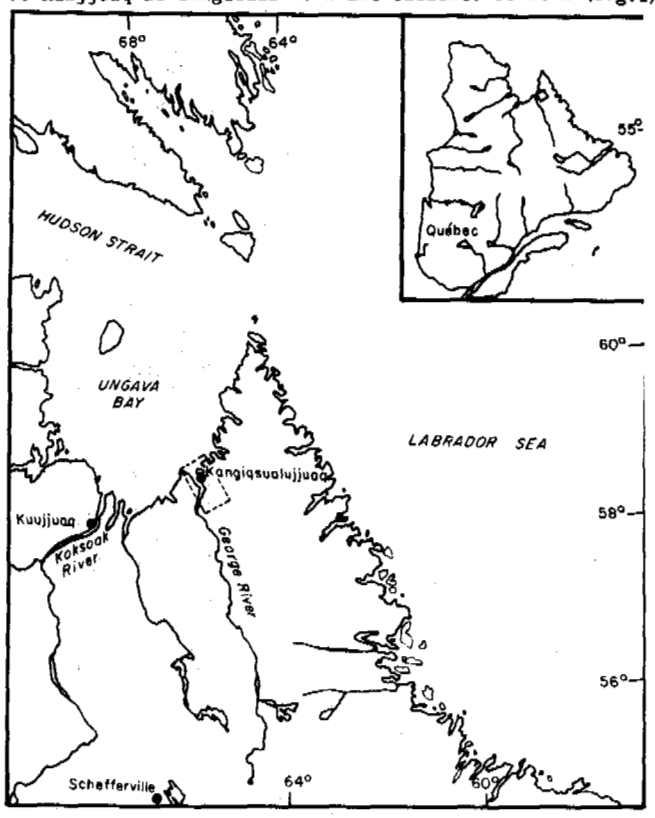

Fig. 1- Airport site location, Kangiqsualujjuaq, northern Quebec.

The planned airstrip site is situated in a glacially scoured valley oriented NW-SE which is bordered by rocky cliffs (Fig. 2).

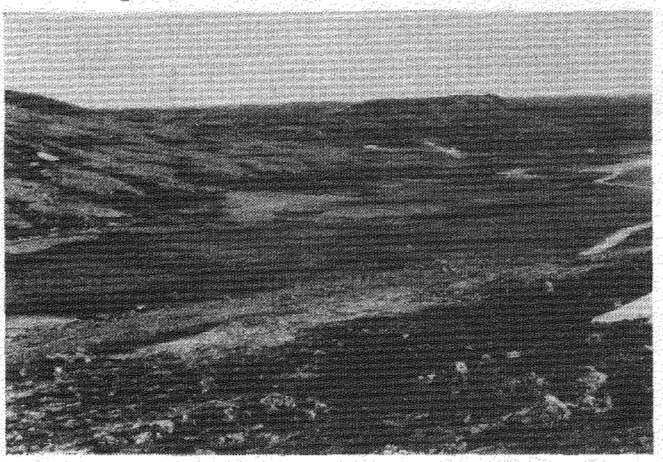

Fig. 2- Typical landscape of Kangiqsualujjaq valley. Valley bottom is in marine sand and gravel and slopes are in bedrock and till. Part of the present airstrip is visible on the right hand side.

A few bedrock outcrops are also present in its central part. The bedrock is mainly composed of granite gneisses; the geological setting is part of the Aphebian Churchill province of the Canadian Shield (Douglas 1968, Bostock 1964, Taylor 1968, 1974). The bedrock is overlain by a compact glacial till of variable thickness. In the valley bottom, till is covered by thick post-glacial, glaciomarine sediments made principally of coarse sands, gravels, and ice-rafted boulders. Occasional clayey silt lenses are also observed through the marine sediments. Therefore the airstrip site is on very heteregeneous sediments which make permafrost conditions very variable, a

picture still made more complex by the discontinuous nature of permafrost. Topography, drainage pattern, vegetation and climatic conditions are described by Ben-Miloud and Seguin (1987). The fine-grained sediments are dispersed on the site but are not always visible on surface. Four main types of surficial deposits are observed in the valley: typical marine deposits of variable grain size and composition, terrestrial deposits (peat) on palsa plateaus and fens, a S shaped glacial marine shoreline and a silty clay permafrost mound. Mean annual air temperature of the nearby village is -5.6°.

Many different aspects were considered in the construction of the airport (Lupien et al., 1984). The main objective was to minimize the impact of permafrost occurrence at the site. Hence, a knowledge of the active layer thickness, lateral and vertical distribution of permafrost, bedrock topography, groundwater regime, local stratigraphy of the unconsolidated sediments is needed. To achieve these goals, geomorphological investigation and mapping of surficial deposits, drainage pattern and vegetation cover were first undertaken (Gahé, 1988). A detailed study of the surficial sediments on the airport site was carried out in 1986 and 1987 by Ben-Miloud and Seguin (1987) and is illustrated in Figure 3. Geophysical applications to permafrost problems on airport sites are scarce. Kawaski et al. (1983) mention briefly the use of geophysical methods on permafrost airport sites in Alaska.

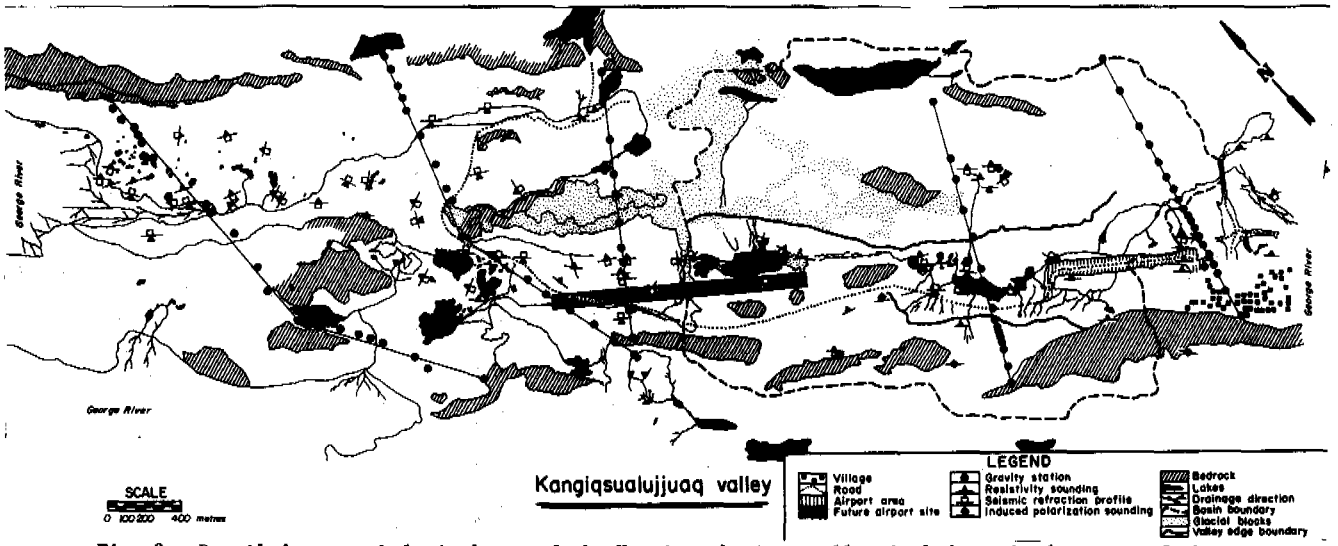

Fig. 3- Detailed geomorpholggical map of the Kangiqsualujjuaq valley including the location of the future airport site and geophysical surveys

Four geophysical methods were used to delineate the boundaries of permafrost: 1) electrical resistivity soundings (ERS) with a Schlumberger array, 2) induced polarization (IP) in the dipole-dipole configuration, 3) electromagnetic (EM) soundings, and 4) seismic refraction (SR). ERS were used for permafrost investigations in the 1940s (Dostovalov, 1947, Ananyan, 1950, Akimov, 1951). The current is circulated in the ground with two electrodes and the potential measured with two others. A graph of the apparent resistivity vs the half separation of the expanding current electrodes allows a quantitative interpretation of the layered media with depth. In the IP method, a current is also injected in the ground with current electrodes, but in addition to the primary potential, a secondary potential drop resulting from induced currents is measured as a function of time. Until recently, the IP method has not been used commonly for permafrost mapping (Brown et al., 1985). When using a dipole-dipole configuration, the potential electrodes are located outside the current electrode pair. The expanding spread is an integer number of the constant separation of the electrode pairs. Pseudo-section plots of apparent chargeabilities which are a measure of the underground induced currents and apparent resistivities lead to the recognition of soil layers characterized by differing electrical properties with depth.

The electromagnetic method works on the principle that the magnetic component of an electromagnetic wave penetrating the ground induces secondary currents in conducting bodies. The currents cause a secondary magnetic field which is detected on surface. Using multiple separations: emitter-receiver and multiple frequencies of emission, the space field distribution measured on surface yields information on the geometry and nature of the conductors at depth. The apparent conductivities measured provide some indications on the distribution of permafrost at depth (Annan and Davis, 1976). The seismic refraction (SR) method is also used to detect underground layers which are characterized by their specific seismic velocities. In order to detect the refracted wave on surface, an increase of velocity with depth is required. Seismic refraction can locate precisely the active layer but is unable to determine the base of permafrost due to a velocity inversion. After correcting for the hidden (low velocity) layers the depth to bedrock can be estimated. In the past, the SR method was used with success to determine the permafrost extent (Roethlisberger, 1961)

Finally, gravimetry was used as a complementary technique to estimate the depth to bedrock considering the large density contrast between the soils (1.92 g cm^{-3}) and bedrock units (2.65 g cm^{-3}). The integrated geophysical results provide a two dimensional and occasionally three dimensional picture of permafrost masses characterized by a variable ice content as well as taliks. In this manner, the top and base of permafrost are accurately outlined underneath the planned airport site. All the specifications to the geophysical equipment used are shown in Table 1.

DEPTH OF THE THAWING FRONT

Some 52 soundings (mainly trenches) were carried out in July 1983 on diferent types of deposits using manual and motorized methods (Lupien et al., 1984) to determine the thaw depth (Table 2). 10 soundings were made at 120 m

TABLE 1

GEOPHYSICAL INSTRUMENTATION USED

ELECTRICAL RESISTIVITY	INDUCED POLARIZATION	ELECTROMAGNETOMETRY	SEISMIC REFRACTION
Resistivity meter: ABEM digital SAS 300 Frequency = 4 Hz Characterics: the emitter circulates a pre-selected current (0.2 to 20 m A) and the receiver coupled to a microprocessor measures the voltage (+ or - 1 or - 500 V). The microprocessor controls the measurements and calculates automatically soil resistances (R= V/I) which are transformed digitally in KΩ, Ω or MΩ. The electrical resistance is read directly.	The induced polarization unit (Huntec) is composed of a Lopo M-3 transmitter and a MK III receiver The characteristics of the transmitter are: - maximum output voltage: 1000 V - maximum current: 1,5 A - resistance range: 100 to 6200 - period of current injection or turn off: 1 ms - period of one cycle 2, 4, 8 or 16 s - ratio of active to passive period 1:1, 1:28:1, 1:67:1, 2:2:1 For the receiver, eleven measurement scales of the primary voltage (Vp) allow a resolution of 0.1% between 10^{-6} and 10 V. Both Vp and apparent chargeabilities (Ma) are measured.	Geonics EM 34-3 of the Slingram type with mobile transmitter and receiver. Multifrequency (0,4, 1,6 and 6,4 KHz) and multiseparation unit (40, 20 and 10m) operating in both horizontal and vertical coplanar configurations. The apparent conductivity is read directly and expressed in millimhos m^{-1}. The selected conductivity scales are 0-3, 10, 30, 100, 300 millimhos m^{-1}.	EGLG Geometrics (model ES-1225) with 12 channels. Record time: 25- 2000 ms. Record size: 8 bits by 1000 sampled points for each channel. Delay time: 0-50 s in increments of 1 ms. Input impedance: 10 000 Ω . Frequency response: 3-1000 Hz; power supply: 11-14 VDC; maximum output signal: 0.35 V; preamplifier gain: 33 db; amplifier gain: 0,6, 12...66 db.

TABLE 2

Active layer (AL) thickness determined by mechanical soundings

Site no.	soundings	Al thickness (m)	w.t. depth (m)	w.c. (%)	soil type
A	28	0.3->1.8	≥1.7	4.6-24.8	sg + b
B	2	0.7-1.2	0.3-0.6	12-31.2	ss
C	2	0.3-0.6	0.2-0.4	14.4-16.8	sg
D	2	0.7-1.1	1.5-1.8	11.1-33.3	ss
E	4	1.5-1.8	0.6-1.1	15.7-19.7	ss + sg
F	1	>3	>3	14.2-26.9	sg
G	9	1.5->3	≥3	1.4-20.4	sg + b
H	3	1.6->3	---	2.8	sg
	52				

A= airstrip, B= apron and surrounding roads, C= buildings, D= communication tower, E= antenna tower, F= meteorological station, G= gravel pit, H= access road, sg= sand and gravel, ss= silty sand, b= blocks, w.t.= water table, w.c.= water content

spacings along the central line of the airstrip and 18 others along two parallel lines located at a distance of 30 m on each side. The depth of the soundings varied between 0.6 and 3 m, some of them reached the thaw front while others were hampered by the presence of boulders or the collapse of the walls caused by a near surface water table. The number of soundings, the thaw depth, the water table depth, the gravimetric water content and the soil type for the sectors considered are shown in Table 2. The general stratigraphical setting is known from surficial geology mapping of the broader surrounding region, including sections in a nearby gravel pit and in sea cliffs. The ground layers detected by the geophysical methods generally coincide with this regional knowledge.

GEOPHYSICAL DETERMINATION OF ACTIVE LAYER AND PERMAFROST EXTENT

a- Electrical resistivity soundings (ERS)

47 ERS measurements were carried out on the airstrip site. The interpretation of the ERS results is carried out with the help of master curves (Compagnie Générale de Géophysique, 1955, 1963, The Rijkswaterstaat, 1969, Seguin and Allard, 1984a, b) or by inversion techniques using a computer program (Zohdy, 1975). Active layer thicknesses determined with the ERS range from 0.5 to 2.8 m (average: 1.2 m) as compared with 0.3 to 3 m with the mechanical soundings. In the active layer, the corresponding resistivity values vary from 400 to 40 000 Ω-m (average: 10 000). According to Lupien et al. (1984) the variation in the thickness is related to the grain size, the finer grained sediments having smaller thaw front depths (Table 2). The thermal properties (conductivity) is apparently a function of grain size. A comparison of the individual thaw front depths obtained with mechanical and ER soundings is generally good considering the fact that the measurements were at slightly different periods of time and that local variations of terrain conditions ought to be considered.

The ERS investigation has indicated that the permafrost is thicker when the sediments are finer grained. The permafrost thickness is 11.5 m in areas overlain by a peat cover. It is 15 m or more underneath a clayey silt permafrost mound. The values of ER are located in the range 35 000 - 150 000 (average 58 000 Ω-m) for these different types of terrain. In addition to the determination of the active layer and permafrost thickness, the depth to bedrock and the stratigraphy of the unconsolidated deposits are also assessed (Seguin, 1974, 1976, Seguin and Allard, 1987, Gahé et al., 1987).

An example is shown in fine-grained sediments. The ERS curve (Fig. 4b) shows the stratigraphy obtained through its interpretation. From bottom to top, it is the following: 1) depth to bedrock (53 m), 2) unfrozen sediments (mainly saturated clayey silt) from 53 to 13 m, 3) similar sediments but frozen (13-1m), and 4) thaw front depth of approximately 1 m. Coring has shown that the ice is lenticular in such materials. A second example is selected adjacent to a raised marine shoreline and

oriented perpendicular to the three main lines on which mechanical soundings were performed (Fig. 4a), i.e. perpendicular to the airstrip axis. The ERS indicates the presence of a 2.5-thick unfrozen surface layer with a corresponding ER value to 5 000 Ω-m. This thickness is 1 to 2 times larger than in clayey silt of the mounds on the peat plateaus. The higher thermal conductivity of sand and gravel mainly explains this difference. The permafrost thickness on this last site is about 10 m with an ER value of 90 000 Ω-m. The ER contrast: active layer-permafrost is 1:18. The texture of the ice in this type of materials is intergranular.

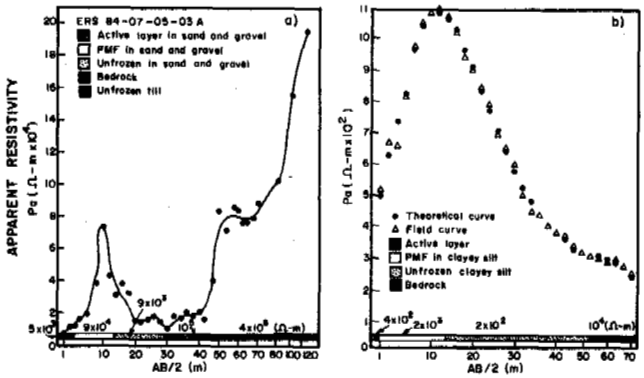

Fig. 4– Typical electrical resistivity soundings: a) in fine-grained sediments, b) in coarse-grained sediments. The diagrams show the apparent resistivity (in ordinate) vs half current electrode separation (in abscissa). The interpreted stratigraphy and the corresponding true electrical resistivities are indicated in parallel to the abscissa.

b– Induced polarization (IP)

When making use of the dipole-dipole configuration with the IP surveys, the depth to the base of permafrost is obtained by calibration of the depth separations on the pseudo-sections into realistic depths which are obtained by comparison with those obtained by ER soundings at the same localities or using formulas for depth calculations which are characteristic of each configuration used (Roy and Apparao, 1971, Roy, 1972, Edwards, 1977, Apparao and Sarma, 1971). For this second type of calibration, the integer n which corresponds to the expanding spread in the dipole-dipole configuration is used to obtain the depth of investigation. The pseudo-sections (Fig. 5) show a variation of permafrost thickness along a 150 m long transect on the central line of the airport. In the pseudo-section, the point of investigation is located midway between the internal current and potential electrodes. The depth of this point is fixed by the intersection of two orthogonal lines (making an angle of 45° with respect to the horizontal) issued from the surface position of the two internal electrodes. The ER pseudo-section shows an irregularity at the base of permafrost which is determined by taking into account the resistivity contrast; the steepest gradient of apparent resistivity contour lines outline the boundary between frozen and unfrozen terrain. The IP pseudo-section shows three zones of low steep chargeability (A, B and C). Zone A is located at the end of line CL and the information is insufficient to arrive at a satisfactory interpretation. Zone C on the chargeability pseudo-section corresponds exactly to the same zone on the resistivity pseudo-section. Zones B and C may be explained by two phenomena: 1) taliks in sand or 2) frozen silty or clayey silt lenses. The last explanation is more probable because permafrost in clayey silt mounds was observed nearby the airstrip site.

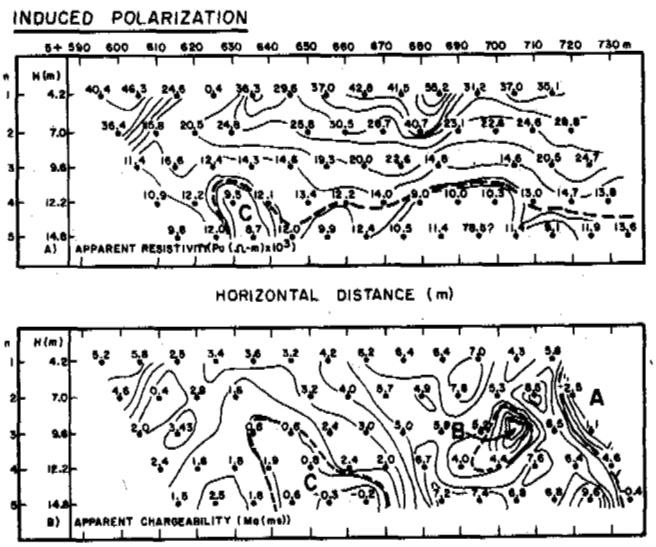

Fig. 5– Electrical resistivity and chargeability pseudo-sections on a portion of the central line of the planned airport. The dashed lines indicate the outline of permafrost. The abscissa represents the horizontal distance along the center line of the projected airstrip (in m) and the double ordinates the dipole-dipole spread integer (m) and the depth of investigation (H) in metres respectively.

The depth of permafrost base varies fr . 2 to 13 m along most of the profile except for stations 5 + 620 and 6 + 630 where it is closer to 10 m (Fig. 5). On both apparent resistivity and chargeability dipole-dipole pseudo-sections, the base of the permafrost is irregular rather than subhorizontal and the chargeabilities yield a somewhat thicker estimate for the thickness of permafrost than the resistivities. Finally, chargeability values are apparently less sensitive to lateral heterogeneities of the soils than electrical resistivities.

In summary, the IP method was very useful to determine the thickness of the active layer, the lateral and vertical extent of permafrost, the stratigraphy and the degree of heterogeneity of the soils.

ELECTROMAGNETIC SURVEYS (EM)

The depths of investigation using EM (34-3) surveys are a function of frequency as well as separation and configuration of the two antennas. Only a semi-quantitative estimate of the depth extent of permafrost may be obtained. This is due to the insufficient number of separations and frequencies used and the difficulties of calculating the penetration depth of the signal. With a coplanar vertical configuration and coils separations of 10, 20 and 40 m, the maximum depths of penetration are 7.5, 15 and 30 m respectively. The estimation of permafrost thickness is based on conductivity contrasts between frozen and unfrozen zones. Accordingly, a decrease in conductivity (7 to 4.5 mmhos m^{-1}) between stations 5 + 000 and 5 + 160 (Fig. 6) indicates that permafrost is thicker (over 15 m) than in the interval: 5 + 160 to 5 + 280 where it is estimated between 7.5 and 15 m. For instance, at station 5 + 640 (Fig. 6), the conductivity values for the three separations are 4.5, 2.5 and 3.3 mmhos m^{-1}. The decrease in conductivity from 4.5 to 2.5 mmhos m^{-1} is caused by the occurrence of a permafrost

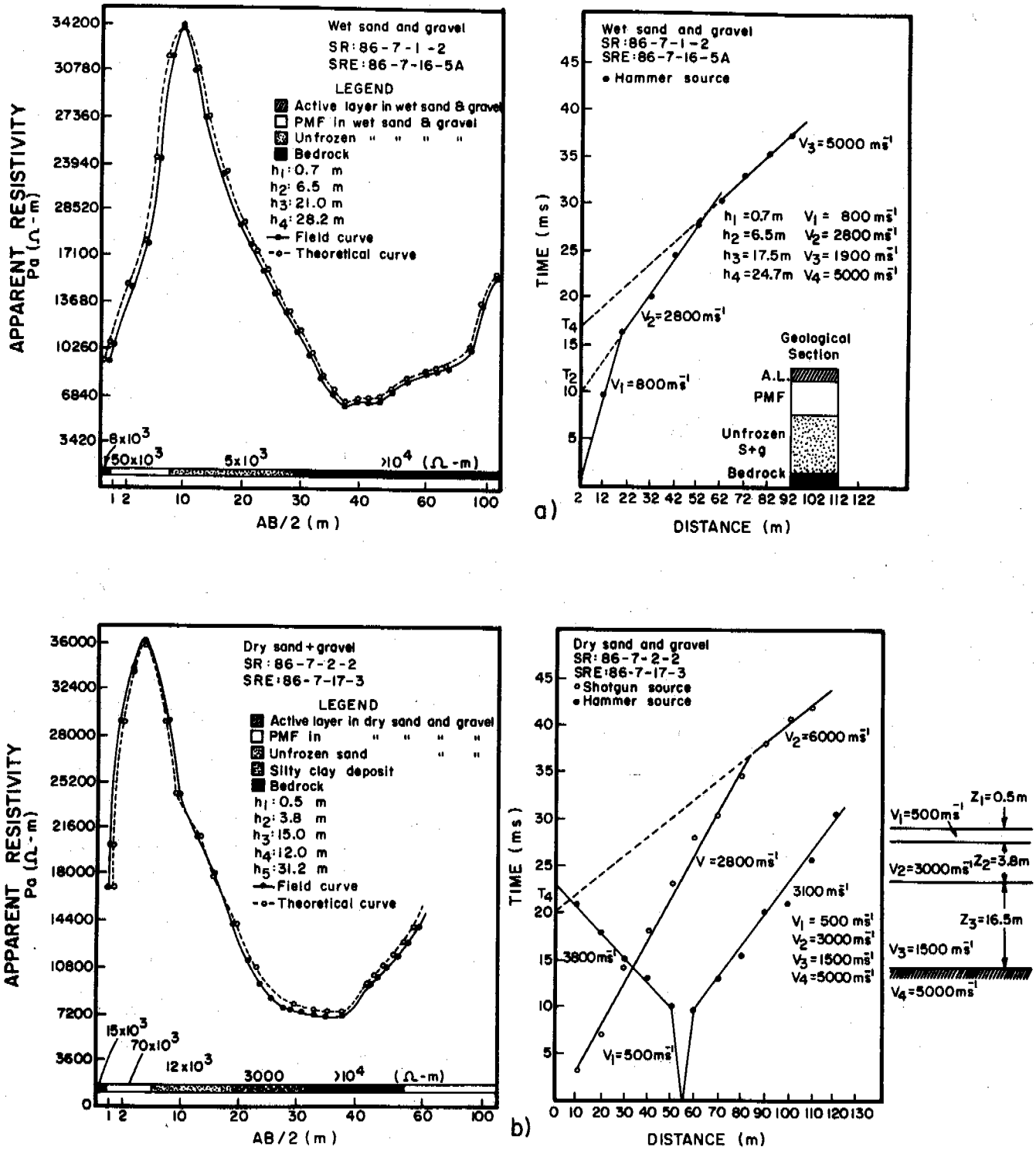

Fig. 7- Selected seismic refraction profiles and electrical resistivity soundings on two specific sites (a and b) of the projected airport.

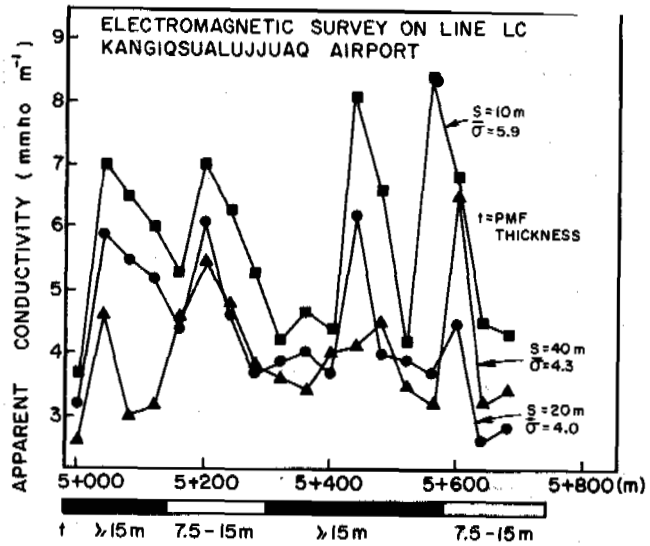

Fig. 6– Electromagnetic profiles (coplanar configuration, EM 34-3) with transmitter-receiver separation(s) of 10, 20 and 40 m. Mean conductivities (σ) are shown and allow a semi-quantitative estimate of the thickness of permafrost. The abscissa represents the horizontal distance and the ordinate the apparent conductivity in mmhos.

layer the base of which is bounded at an approximate depth of 15 m. The increase of conductivity at the 40 m separation suggests strongly that there is no permafrost at depth greater than 15 m. By comparison with the permafrost thicknesses determined by resistivity and chargeability pseudo-sections from the IP survey (Fig. 5) which yielded 10 and 13 m respectively, it is concluded that the permafrost thickness at this station is located between 12 and 15 m. The interpretation of this EM survey indicates that the lower boundary of permafrost is irregular as observed in the resistivity pseudo-section (Fig. 5). Although it gives less detailed results, the EM method is also useful to outline vertical and lateral variations of permafrost and it confirms results obtained with other methods.

SEISMIC REFRACTION (SR)

SR is an ancillary method of confirming the results obtained with other geophysical methods relative to permafrost thickness and a substitute for drilling. The interpretation of the SR profiles was complicated by the occurrence of a low velocity layer generally located between the base of permafrost in the sediments and the deeper bedrock. The true depth to bedrock can be estimated by assuming a realistic value for this low velocity layer (Whitely and Greenhalgh, 1978) and calculating its thickness. An estimate of the velocity of this third layer (below the permafrost base) is obtained from the seismic lines done in unfrozen areas contiguous to the discontinuous permafrost zones characterized by a similar stratigraphy. Thirteen seismic lines were surveyed over the new airport site. All hammer shots were detonated 1 m off the line and when a shotgun source was used, a hole of about 0.65 m below the ground level was dug to insure maximum energy transfer into the ground. Without a knowledge of the velocity inversion, the travel-time graph would be interpreted as a 2 layer structure (Fig. 7).

DISCUSSION OF THE RESULTS AND CONCLUSIONS

Some difficulties are faced in the interpretation of the results obtained with the geophysical methods used. Problems are encountered with ERS measurements in areas of very dry sand and gravel. This is mainly due to large electrode contact resistance and the extremely high resistivity of near surface soils. Quite often the IP method encounters the same difficulties as ERS in dry sand and gravel. Consequently, the moist mass cover and soil water table level are important factors to be considered in the determination of the lateral and vertical distribution of permafrost in marine and fluvioglacial coarse grained deposits. A comparison of the mechanical and geophysical soundings is of the upmost impostance as it provides a good oportunity to verify the precision of the ER and IP soundings in estimating active layer thicknesses. When using the dipole-dipole configuration, IP data are not reliable to outline the active layer boundary; the large electrode spread (>10 m) does not allow a sufficient resolution. The thickness of discontinuous permafrost ranges from 1.5 to 20 (average: 8.1 m) under the new airport site. No drilling through the permafrost is available for ground thruthing but these values are in accordance with many drill holes and thermistor cable data in similar materials available around the village. The thickness is quite variable in sand and gravel. ERS, IP pseudo-sections and EM surveys indicated that permafrost is perforated with taliks and is quite irregular at its base. This situation is explained by the grain size variation of the sediments which influences the physical parameters of the soils (e.g. thermal conductivity) which in their turn control the electrical properties of permafrost terrains. Some of the difficulties related to field conditions are solved through the integration of the various geophysical results. This allowed a more accurate estimate of permafrost distribution as illustrated in the fence diagram (Fig. 8). In the study

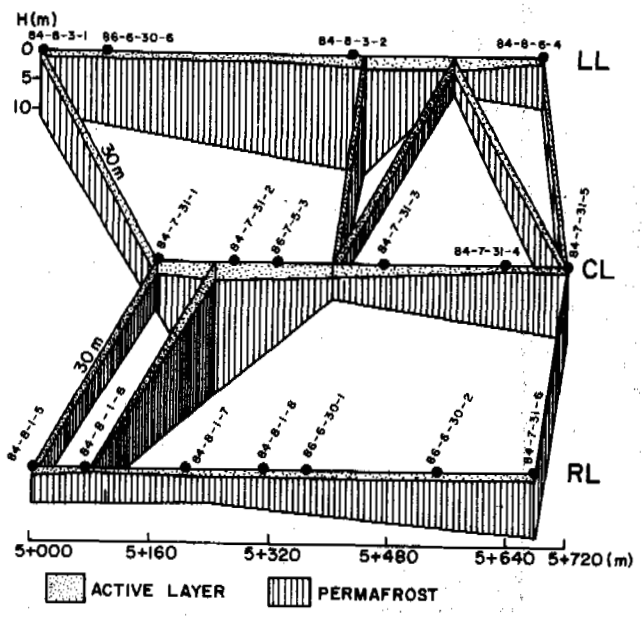

Fig. 8– Fence diagram showing active layer thickness and permafrost distribution under the proposed airstrip according to the integrated interpretation of all geophysical methods.

of the airport site located in a discontinuous permafrost zone, integrated geophysical methods are useful for three reasons: 1) determination of active layer thickness, 2) delineation of horizontal and vertical extension of permafrost, 3) estimation of the depth to bedrock. Optimisation of the combined geophysical results demonstrates that the ERS and SR surveys are most useful to estimate thick active layer depths. In decreasing order of resolution, IP, ERS and EM surveys are the most reliable integrated geophysical methods to outline the horizontal and vertical distribution of permafrost. ER and IP soundings are most appropriate to calculate its thickness while IP and EM methods are the best techniques to determine both its lateral extent and thickness. Depth to bedrock is most accurately defined with integrated ERS, RS and gravimetric methods.

Most of the stratigraphic data are obtained with the ERS methods. The water table level is generally located with a combination of ERS, IP and SR methods. The amount of heterogeneity in the soils is usually evidenced by the parameters: chargeability (IP) and conductivity (EM).

Permafrost investigations are clearly needed for the planning and construction of airstrip and roads in northern Canada. The geophysical methods used in this investigation are complementary tools to geomorphological, drainage and soil studies.

The results are needed: a) to plan and locate an airstrip site, access roads and ancillary commodities, b) to plan infrastructure and geotechnical studies, c) for the choice of nature, type, volume and thickness of construction materials, d) to indicate the areas when an artificial insulating pad could be needed, e) to estimate the volume of bedrock excavation required underneath a thin layer of sedimentary cover. Engineering problems such as blasting, quarrying, crushing and their associated costs can be more easily apprehended with the aid of the geophysical information. In this respect, we think that the sequence of geophysical methods used for this purpose is necessary considering its relatively low cost.

ACKNOWLEDGEMENTS

The authors wish to thank the following persons who contributed to the execution of this study: Claire Beysserias, Christian Bouchard, Jacqueline Bouchard, Jean Desbiens, Alain Fournier, Richard Fortier, Renée Gélinas, Yvan Grenier, Lyne Messier, Florence Nicollin, Yvon Pelletier and Johanne Plourde.

REFERENCES

Akimov, A.T. (1951). The study of permafrost by geophysical and geoelectrical methods in the eastern part of the Bolshezeneskaya tundra. Manuscript Fondy in to Merzlotov AN SSSR.

Ananyan, A.A. (1950). Investigation of the passage of an electric current through freezing and frozen soils. Rukopis Fondy in to Merzlotoved, SSSR.

Annan, A.P. and Davis, J.L. (1976). Impulse radar profiling in permafrost. Geological Survey of Canada, Paper 75-1C, 343-351.

Apparao, A. & Sarma, V.S. (1981). A modified pseudo-depth section as a tool in resistivity and IP prospecting. Geophys. Res. Bull, (19), 187-208.

Ben-Miloud, K. & Seguin, M.-K. (1987). Solution of velocity inversion in seismic refraction surveys with the use of electrical methods in three types of terrains from the Kangiqsualujjuaq valley, Northern Quebec. Comptes Rendus du 55ième Congrès de l'ACFAS, Ottawa, 17 p.

Bostock, H.S. (1964). A provisional physiographic map of Canada. Geol. Surv. Can., Paper 64-35, 24 pp.

Brown, J., Metz, M.C. and Hoekstra, P. (1985). Workship on permafrost geophysics. Golden, Colorado, 23-24 October 1984, CREEL, 118 pp.

Compagnie Générale de Géophysique (1955). Abaques de sondage électrique. Geophysical Prospecting, (3), Suppl. No. 3, 50 pp.

Compagnie Générale de Géophysique (1963). Abaques de sondage électrique/Master Curves for Electrical Sounding. European Association of Exploration Geophysicists.

Dostovalov, B.N. (1947). Electrical characteristics of permanently frozen rocks. Akad. Nauk SSSR, 5, 18-35.

Douglas, R.J.W. (1968). Géologie et ressources minérales du Canada. Partie A, Série de la géologie économique No. 1. Commission géologique du Canada, 50-165.

Edwards, L.S. (1977). A modified pseudosection for resistivity and IP. Geophysics, (42), 5, 1020-1036.

Gahé, E. (1988). Géomorphologie cryogène et géophysique dans la région de Kangiqsualujjuaq. Ph.D. thesis, Université Laval, 210 pp.

Gahé, E., Allard, M., & Seguin, M.-K. (1987). Géophysique et dynamique holocène de plateaux palsiques à Kangiqsualujjuaq, Québec nordique. Géographie physique et Quaternaire (41), 1, 33-46.

Kawaski, K., Gruol, V. and Osterkamp, T.E. (1983). Field Evaluation Site for Ground Ice Detection. Report No. FHWA-AK-83-27, Alaska Dept. of Transportation and Publication Facilities.

Lupien, Rosenberg, Journeaux & Assoc. Inc. (1984). Etude géotechnique, (George River), Report S-84-710, 27 pp.

Rijkswaterstaat, The Neherlands (1969). Standard graphs for resistivity prospecting. European Association of Exploration Geophysicists.

Roethlisberger, H. (1961). Seismic Refraction Soundings in Permafrost near Thulé, Greenland, in G.O. Roasch, edit., Geology of the Arctic, Vol. 2, International Symposium on Arctic Geology. Irst Calgary (Alberta) Proceedings, 1960, 970-981.

Roy, A. (1972). Depth of investigation in Wenner, three-electrode and dipole resistivity methods. Geophysical Prospecting, (20), 329-430.

Roy, A. & Apparao, A. (1971). Depth of investigation in direct current methods. Geophysics, (36), 943-959.

Seguin, M.-K. (1974). The use of geophysical methods in permafrost investigation: iron ore deposits of the central part of the Labrador Trough, northeastern Canada. Geoforum, (18), 55-68.

Seguin, M.-K. (1976). Observations géophysiques sur le pergélisol des environs du lac Minto. Cahiers de Géographie de Québec, (50), 20, 327-364.

Seguin, M.-K. & Allard, M. (1984a). La répartition du pergélisol dans la région du détroit de Manitounuk, côté ouest de la mer d'Hudson, Canada. Canadian Journal of Earth Sciences, (21), 354-364.

Seguin, M.-K. & Allard, M. (1984b). Le pergélisol et les processus thermokarstiques de la région de la rivière Nastopoca, Nouveau-Québec. Géographie physique et Quaternaire, (38), 11-25.

Seguin, M.-K. & Allard, M. (1987). La géophysique appliquée au pergélisol, Québec nordique: historique et développements récents. Géographie physique et Quaternaire, (41), 127-140.

Taylor, F.C. (1968). Operation Torngat, Quebec, Newfoundland-Labrador. In Report of activities; Geol. Surv. Can. Part A, Study 68-1, 149-150.

Taylor, F.C. (1974). Reconnaissance geology of a part of the Precambrian Shield, Northern Quebec and Northwest Territories. Geol. Surv. Can., Paper 74-21, 9 pp and map.

Whitely, R.J. & Greenhalgh, S.A. (1978). Velocity inversion and the shallow seismic refraction method. Geoexploration, (17), 125-141.

Zohdy, A.A.R. (1975). Automatic interpretation of Schlumberger sounding curves, using modified Dar Zarrouk Functions, U.S. Geol. Surv. Bull. no. 1313 E, 41 pp.

D.C. RESISTIVITY ALONG THE COAST AT PRUDHOE BAY, ALASKA

P.V. Sellmann, A.J. Delaney and S.A. Arcone

U.S. Army Cold Regions Research and Engineering Laboratory, Hanover, N.H. 03755-1290 USA

SYNOPSIS Electrical resistivity measurements, at three sites in Prudhoe Bay, Alaska, were made to provide an understanding of marine modification to coastal permafrost, and to evaluate D.C. resistivity techniques for coastal subsea permafrost studies. The measurements were made using Wenner electrical resistivity soundings. Profiles extended 2.8 km offshore and inland beyond the last signs of tundra modification by coastal processes. Offshore measurements were made with a floating cable, and inland measurements were made using driven electrodes. The observations indicate that the electrical properties of permafrost beneath the coastal bluff and adjacent tundra are rapidly modified by coastal erosion and periodic flooding during storms. Along one control line, apparent resistivity changes corresponded with the configuration of the top of ice-bonded permafrost observed by Baker (1987). Modeling supported by the control data permitted a close interpretation of the position of the top of ice-bonded subsea permafrost and provided a range of real resistivities for offshore materials.

INTRODUCTION

Background

Most subsea permafrost formed on the continental shelves when they were exposed during low sea level stands associated with periods of major glacial activity. This permafrost was covered by rising sea level as the glaciers melted. Even though the sea level is now fairly stable, permafrost is still being inundated in some areas of active coastal erosion. Inundation can dramatically change the properties of permafrost due to exposure to salt water and to as much as a 10°C warming in some coastal settings. Along segments of the Beaufort Sea coastline, permafrost is undergoing a significant reduction in strength, thaw settlement, gas hydrate decomposition, and redistribution of free gas. This study establishes some electrical resistivity values for coastal permafrost near Prudhoe Bay, an area undergoing active coastal modification.

Recent studies (Scott, 1975; Corwin, 1983; Dyck et al., 1983; Sellmann et al., 1985) indicate that geophysical D.C. resistivity methods can be used for subsea permafrost investigations. These methods may be best suited for shallow coastal waters where ice-bonded permafrost is expected at shallow depths (<30 m) below the seabed, permitting relatively short, more-manageable electrode arrays. The technique also has potential in areas where seismic methods may encounter problems, such as sediments containing small amounts of natural gas in voids, which greatly attenuate seismic signals. Thus, practical implementation of the D.C. sounding method can complement deeper sounding transient electromagnetic methods for certain areas. Studies by the Earth Technology Corp. (1985, 1986) have suggested that modified transient EM equipment and procedures and magnetic induction might also be used for investigations at shallow depths below the seabed. At present, however, a combination of D.C. and Transient EM is the most practical geophysical approach to obtaining information on the entire offshore permafrost section (Ehrenbard et al., 1983; Walker et al., 1985).

Resistivity data are interpreted by constructing models that generate output similar to observations. Because closed-form inversion solutions are virtually impossible to achieve, computational programs utilizing fast, iterative procedures are now commonly used to produce a layered model to fit the data. These programs often require some preliminary estimates for the resistivity and thickness of each assumed layer. Only a small amount of resistivity data has been correlated with subsurface sections having a known distribution of ice-bonded permafrost, and much of it is proprietary. This lack of resistivity data near shore is also due to the limited experience with shallow penetrating electrical methods in areas of ice-bonded subsea permafrost and is one of the reasons for this study.

Objectives and Approach

The objectives of this study were to establish resistivity values and their spatial variation for coastal permafrost in areas of active erosion, and to understand the influence of erosion and periodic flooding during storms upon those values. Thus we hoped to gain information necessary for the interpretation of electrically based methods. A secondary objective was to evaluate our marine D.C. resistivity surveying equipment for detecting subsea permafrost at shallow depths in coastal waters.

Sites with differing coastal relief and beach configuration were selected in Prudhoe Bay. It was assumed that the general distribution of subsurface materials would be similar at all study sites and that coastal erosion rates were approximately 1 m/yr. Data on land were collected with D.C. soundings made parallel to the shoreline and moved progressively inland to a point beyond any evidence of flooding of the tundra surface. Spacings between soundings on land varied to provide coverage of local relief and features found on the beaches, bluffs, and adjacent tundra surfaces. The farthest-inland soundings were considered references representing subsurface electrical properties not yet modified by coastal processes, and were made on what appeared to be undisturbed tundra surfaces. A floating cable was used to extend the survey lines up to 2.8 km offshore by profiling and sounding. The cable was normal to the shoreline for most of this surveying. Soundings and profiling offshore were done at regular intervals from the beach.

D.C. SOUNDING METHOD

Resistivity was measured using the symmetric Wenner array illustrated in Figure 1. The two outer electrodes provide a path for current I, and the resulting difference in ground potential V is measured between the inner electrodes. For homogeneous ground, the real resistivity ρ in ohm-m is equal to the measured apparent resistivity ρ_a, which is found from the formula

$$\rho_a = 2\pi \underline{a} \frac{V}{I}$$

where $\underline{a}$ is the interelectrode spacing. Over layered earth, ρ_a is also a function of the layer thicknesses and resistivities and so is an apparent quantity. Computational modeling must then be used to interpret the sounding curve.

On land we used copper-clad electrodes driven approximately 15 cm into the ground at $\underline{a}$ spacings up to 50 m. The low resistivity of the thawed active layer and marine sediments on the beach ensured good electrode contact. The marine cable was fabricated by a commercial cabling company and is buoyant. It was 150 m long with eight Wenner $\underline{a}$ spacings ranging from 3 to 46 m. The progressively larger $\underline{a}$ spacings in the Wenner array telescoped out from the end nearest the boat, with the first electrode always in use. The cable utilized simple lead electrodes as described in vonArx (1962).

A regulated current signal was generated by a Huntec transmitter, and potential difference was measured with a Fluke digital voltmeter. The Huntec unit has switch-selectable output impedance, and output current is variable to 1.5 A. In most cases maximum output current was used for the marine surveys. The potential difference was determined by subtracting values read during the *on* cycle from values for the transmitter *off* period. The *off* reading allowed elimination of naturally occurring background potentials.

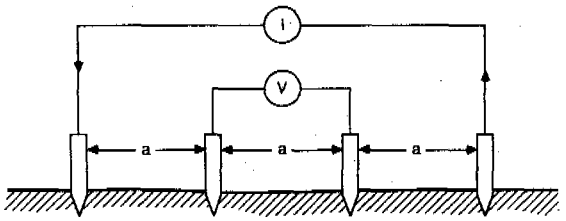

Figure 1. Multi-electrode Wenner array. The electrode separation $\underline{a}$ was varied from 0.5 to 50 m on land and 3 to 46 m offshore.

STUDY SITES

The rates of coastal erosion and associated modification of the cold terrestrial permafrost vary greatly along the Beaufort Sea coastline and depend on material type, coastal relief, and exposure. Three sites were selected for this study in the Prudhoe Bay area and are shown in Figure 2. The Prudhoe Bay area has low coastal erosion rates compared to more western segments of the Beaufort Sea, where rates commonly exceed 5 m/yr (Reimnitz et al., 1985). Rates in Prudhoe Bay are closer to 1-2 m/yr and are probably lower in this area because of the coarser material and lower ground ice volumes in the upper part of the permafrost section. Infiltration of sea water can rapidly influence electrical properties of coarse-grained material if voids are not ice-filled. In general, chemical modification by salt should be much less rapid in fine-grained than in coarse sediment.

Site 1

This site, shown in Figure 2, is situated several hundred meters east of the West Dock in Prudhoe Bay. It has a low bluff about 1.5 m high and a very narrow 1-3 m wide beach. Data for this site are shown in Figure 3. The fresh nature of some of the exposures suggests active erosion. Only a small increase in sea level is required to bring waves in direct contact with the bluff. This low bluff and the adjacent terrain are easily overtopped during storms, as indicated by the large amount of driftwood found more than 100 m inland.

Direct observations (Baker, 1987) of the depth to the top of ice-bonded permafrost offshore, shown in Figure 3, for this line provided ideal control for the marine resistivity observations. Baker's (1987) profile was based on drilling and probing. Water depth data included in the profiles were collected during our resistivity survey.

Site 2

This site is about 3.7 km northeast of the East Dock in Prudhoe Bay (Fig. 2). The tallest coastal bluffs occur here (Fig. 4), ranging from 2 to 3 m in height. The beach is about 6 m wide and is paved with sod blocks that slumped from the tundra surface. The bluff face is actively eroding, with large

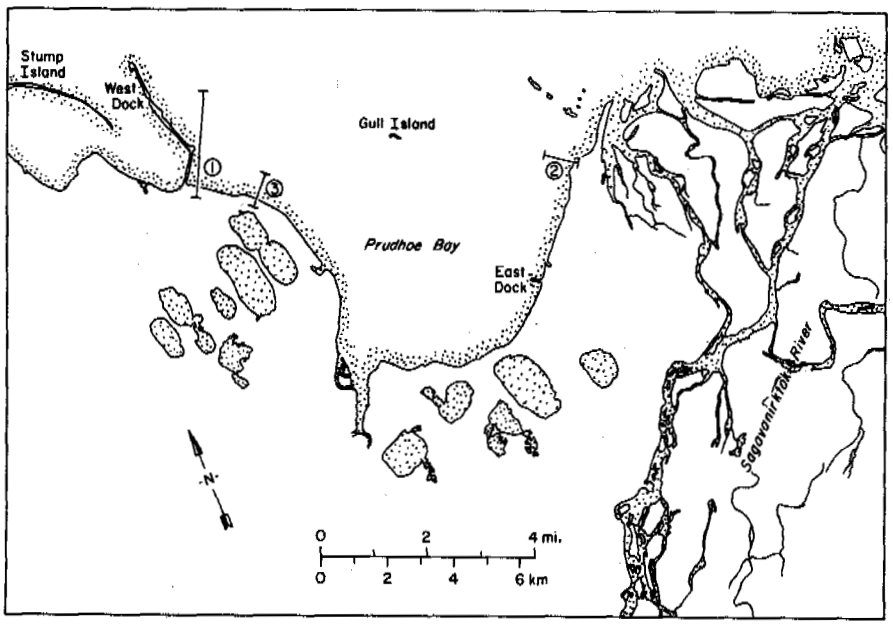

Figure 2. Index map of the Prudhoe Bay area showing the location of our study sites.

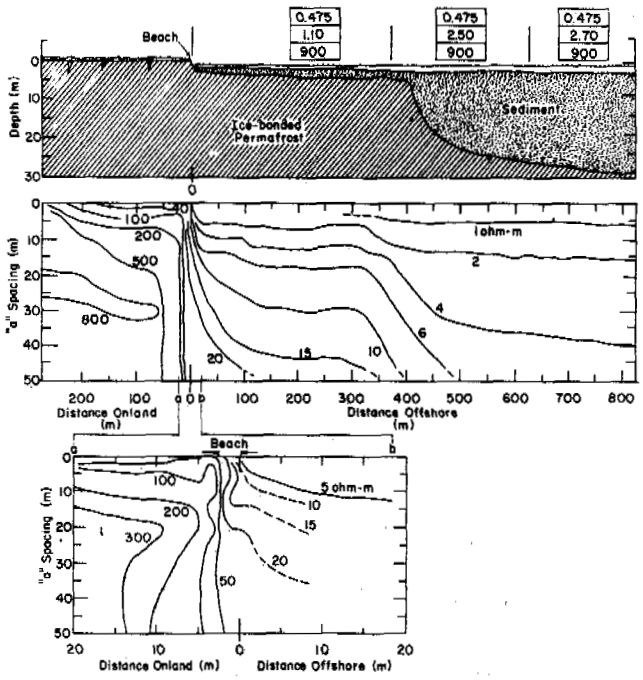

Figure 3. Contoured apparent resistivity data for Site 1 in Prudhoe Bay. Contoured data from an expanded segment of the line that includes the beach are shown in the lower part of the figure. The position of the top of ice-bonded permafrost (after Baker, 1987) is shown in the upper part of the figure as a solid line. The computed depth to the top of ice-bonded permafrost (shown by dots) was calculated using the three-layer models at the top of the figure.

blocks collapsing over fresh exposures. Overtopping of the bluff appears to be very limited with only minor changes in the vegetation patterns near the bluff crest due to salt spray. The materials exposed in the bluff are silty sands, which seem similar for all sites. No information on subsea permafrost was available for Sites 2 and 3.

Site 3

This site is approximately 2 km east of the West Dock (Fig. 2). This location (Fig. 5) is different from the previous sites in that it lacks a coastal bluff. The beach formed between two points of land and grades into the low-lying adjacent tundra. Overtopping of the beach and inland tundra is extensive because of the low elevation of the tundra surface. Driftwood can be found more than 200 m inland.

RESULTS AND DISCUSSION

The soundings on land were all made asymmetrically by expanding the electrodes in one direction parallel to the water's edge at a spacings of 0.5, 1, 2, 3, 4, 5, 7, 10, 20, 30 and 50 m. The marine resistivity data were gathered every 25 m along profiles at fixed a spacings on lines normal to the coast. The offshore a spacings commonly used were 3, 6, 9, 12, 15, 30 and 46 m. In Figures 3-5 the apparent resistivity values are contoured as a function of distance and a spacing. The position of important features such as the coastal bluff, beach, and shoreline are noted. Inserts with expanded scales in the figures illustrate the rapid changes in resistivity seaward of the coastal bluff. No insert was constructed for Site 3 since changes landward were more gradual.

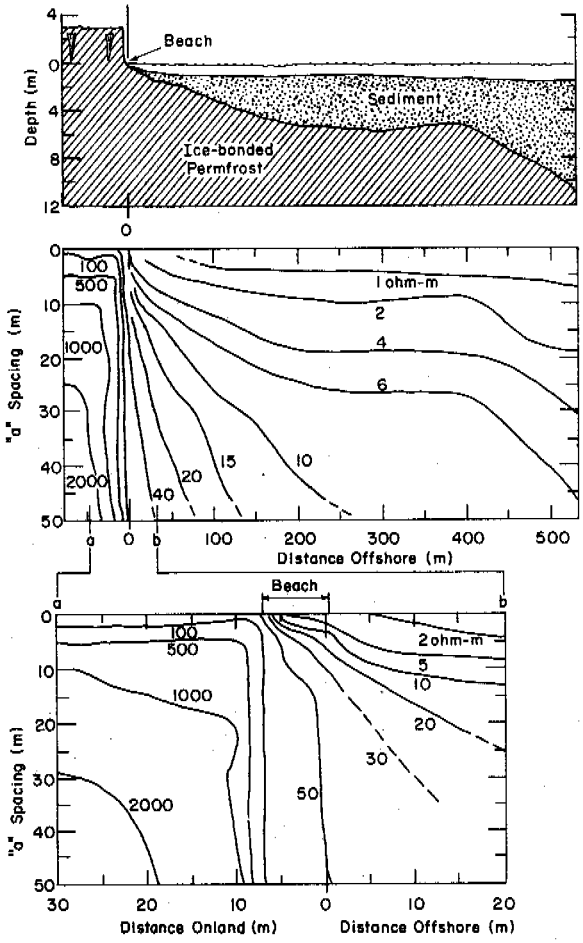

Figure 4. Contoured apparent resistivity data for Site 2 in Prudhoe Bay. Water depth, height of the coastal bluff, and computed depth to the top of ice-bonded permafrost are shown in the cross section in the upper part of the figure. Contoured data for an expanded segment of the line that includes the beach are shown in the lower part of the figure.

Land observations

There are some unique features in the on-land resistivity data that appear related to surface relief, beach width, and potential for surface flooding. The greatest resistivities were observed at Site 2 (Fig. 4), which had the highest bluffs and the least physical indication of flooding or other inland disturbance. A maximum apparent resistivity of 2800 ohm-m was observed 65 m inland of the bluff. The high values and the horizontal disposition of the contours suggest that site 2 has had the least modification. In contrast, Sites 1 and 3 show the influence of past flooding by the significant reduction in near-surface resistivities and the seaward sloping of the resistivity contours. Near-surface resistivities at Site 3 are less than 6 ohm-m more than 175 m inland from the inner edge of the active beach, a distance that corresponds with the inner limit of most recent flooding as indicated by driftwood and other debris. The topography in this area

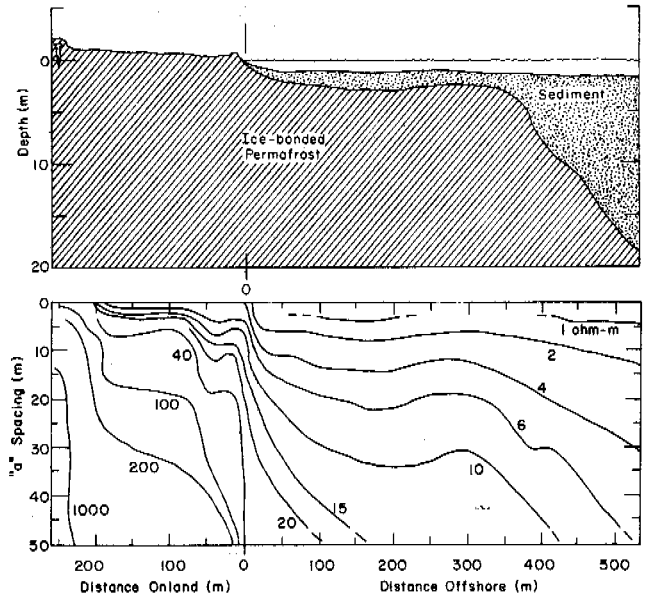

Figure 5. Contoured apparent resistivity data for Site 3 in Prudhoe Bay. Water depth, coastal relief, and computed depth to the top of ice-bonded permatrost are shown in the upper part of the figure.

suggests that coastal flooding may have occurred at this site for many years. Values greater than 500 ohm-m are not found at depth until the inner limit of flooding is exceeded. At the more easterly Site 2, the 500 ohm-m values correspond with the tall bluffs and higher-elevation tundra surface where flooding apparently does not occur.

Seaward Observations

There are some common patterns in all data from seaward of the coastal bluffs. No apparent resistivity values greater than 100 ohm-m were observed at all *a* spacings. The values and trends were similar between the bluffs and the water edge, with no values at the water edge greater than 50 ohm-m at 50-m *a* spacings; most values were less than 40 ohm-m.

Variations in water depth along the study lines were usually less than 1 m, the total depth never exceeded 2 m, and the water resistivity was always about 0.47 ohm-m. The contoured data of Figure 3 demonstrate that these parameters were not sufficient to mask resistivity variations at depth. For example, the larger change in resistivity at depth in Figure 3 occurs in a zone between 300 and 400 m where there is less than a 0.5-m variation in water depth. This small change in water depth cannot account for the more than 6 ohm-m resistivity change seen across the zone at an *a* spacing of 46 m, since earlier field observations and theoretical considerations (Sellmann et al., 1985) have shown that a 0.5-m change in water depth would account for a variation of less than 1 ohm-m. Resistivity changes at the small *a* spacings (3-6 m) are expected for the small changes in water depth (Fig. 3 and 6).

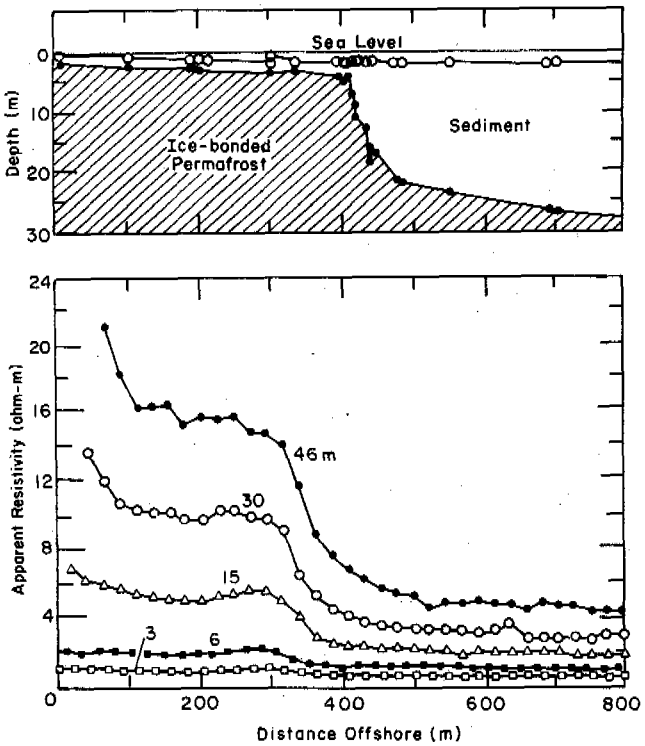

Figure 6. Control data for Site 1 (from Baker 1987) and apparent D.C. resistivity data for five a spacings for a line parallel to the control.

The relatively large variations in resistivity with depth and the configuration of the contours correspond with the shape of the top of ice-bonded permafrost observed in the control section of Figure 3. However, the anomaly in the resistivity data is shoreward of the break (the sharp increase in permafrost depth at 400 m) in the control data. This discrepancy may be caused by our resistivity line being slightly east of the control. The marine resistivity data at the other sites (Fig. 4 and 5) also show similar breaks, which are taken to indicate a sudden increase in depth to the top of the ice-bonded permafrost. The positions of the breaks correspond approximately with the 1.5-m water depth.

There is a noticeable gradient in all the resistivity data that occurs within about 200 m of the beach and appears to reflect changes in the electrical properties of permafrost. This is believed due to warming in the marine environment. Apparent resistivities at our sites fall below 20 ohm-m within the first 100 m of the shore at 46-m a spacings.

Modeling

Modeling of the offshore apparent resistivity data using Baker's (1987) depth profile for Site 1 (Fig. 3, 6) achieved a good fit using three-layer models. The modeling was done using a commercially available resistivity inversion software package (RESIX, Interpex Limited). Three models were used for the best fit and are shown, along with the calculated position of the top of ice-bonded permafrost, in Figure 3. Second-layer resistivity was increased with water depth and distance from shore. A resistivity of 1.1 ohm-m was used when water depths were 1.5 m and less, 2.5 ohm-m for the 1.6-1.8 m range, and 2.7 ohm-m for depths 1.9 m and greater. These resistivities seem logical because of the possibility of salt enrichment of the bed sediments in the shallow water zone when salt is rejected during formation of the sea ice. At greater water depths there would be more chance for mixing and freshening of the bed sediments.

Apparent resistivity data for the other two sites (2 and 3) were interpreted using the models developed for Site 1. The calculated position of the top of ice-bonded permafrost is shown in the upper parts of Figures 4 and 5.

The models for Site 1 indicate real resistivities for the sediment above the ice-bonded permafrost (layer 2) and for the ice-bonded permafrost (layer 3). The model is not greatly influenced by variations in resistivity of the third layer. Resistivity of the ice-bonded permafrost can be varied from 200 to 1000 ohm-m without significant change in the calculated depth to the top of this layer. However, calculated depths of the ice-bonded permafrost are extremely sensitive to changes in the resistivity of the second layer. For example, where the observed depth to the top of the ice-bonded permafrost is 22 m below the seabed, a ± 0.5 ohm-m variation in resistivity providing the best fit can cause a ± 6 m variation in layer thickness. Even though first-layer parameters are also important, they are not a problem since they can be directly measured at the time of a survey.

This equipment and technique prepared for investigations in shallow coastal waters with a maximum electrode spacing of 50 m is limited to operations in water that does not exceed 6-7 m in depth. This is illustrated in Figure 7, which shows 50-m a spacing model resistiv-

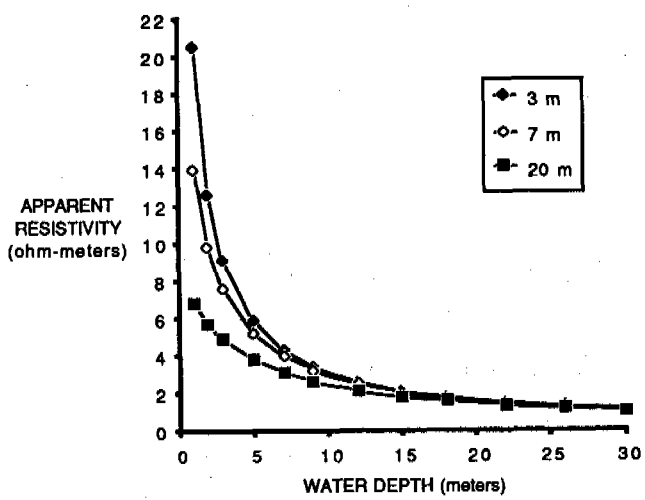

Figure 7. Model resistivity data (50-m a spacing) for various water depths in cases where ice-bonded permafrost is at 3, 7 and 20 m depths beneath the seabed.

ity data as a function of water depth in cases where ice-bonded permafrost at 900 ohm-m is beneath three sediment (2.5 ohm-m) depths of 3, 7 and 20 m. These model parameters used were for conditions similar to those at the Prudhoe Bay sites. The curves show that beyond about a 7-m water depth there is little sensitivity to the total depth of permafrost.

SUMMARY AND CONCLUSIONS

D.C. resistivity data from an arctic coastal setting illustrate the impact of marine inundation on cold permafrost formed on land. The D.C. resistivity technique using a Wenner floating array with maximum electrode spacing of 50 m also appears to provide a tool for understanding the electrical properties and distribution of permafrost in these shallow coastal waters where ice-bonded permafrost may not be more than 30 m below the seabed and where water depths do not exceed 6 to 7 m.

Apparent resistivity observations for Wenner electrode separations up to 50 m made along several cross sections extending from land offshore into Prudhoe Bay have some similar characteristics: (1) resistivities greater than 20 ohm-m were not observed more than 100 m from shore, (2) maximum resistivities at the water's edge were around 50 ohm-m, (3) resistivities greater than 100 ohm-m were not found seaward of the coastal bluffs, and (4) resistivities just inland of the bluff can increase above the seaward values by an order of magnitude. Modeling indicates that real resistivities for the sediment over ice-bonded permafrost ranged from 1.1 to 2.7 ohm-m and that the permafrost may range from 200 to 1000 ohm-m.

Resistivity contour patterns and modeling results correspond well with the drilling and penetrometer observations of Baker (1987); thus this geophysical approach has been useful in this geological setting and appears to have applications for scientific and engineering investigations such as offshore pipeline design and routing. The contours and modeling suggest that a rapid increase in the depth to the top of ice-bonded permafrost seen at the control site also occurs along other study lines in Prudhoe Bay. The position of this zone of noticeable increase in depth to the top of permafrost seems to correspond approximately with the 1.5-m water depth.

The data on changing resistivities within 200-300 m of the coastline may also provide useful information on historical erosion rates.

REFERENCES

Baker, G C (1987).
Salt redistribution during freezing of saline sand columns, with applications to subsea permafrost. Ph.D. Thesis, University of Alaska, Fairbanks, 232 pp.

Corwin, R F (1983).
Marine permafrost detection using galvanic electrical resistivity methods. Proceedings, 15 Offshore Technology Conference (1), 329-336.

Dyck, A V, Scott W J & Lobach J (1983).
Waterborne resistivity/induced polarization survey of Collins Bay, Wollaston Lake. Geological Survey of Canada, Paper 82-11, p. 281-289.

Earth Technology Corp. (1985).
Feasibility investigation of marine electromagnetic system. Contract report for US Army Cold Regions Research and Engineering Laboratory, 24 pp.

Earth Technology Corp. (1986).
Feasibility investigation - Shallow transient electromagnetic (TDEM) system. Contract report for US Army Cold Regions Research and Engineering Laboratory, 22 pp.

Ehrenbard, R L, Hoekstra P & Rozenberg, G (1983).
Transient electromagnetic soundings for permafrost mapping. Proc. Fourth Int. Conf. on Permafrost, Fairbanks: Washington, DC, National Academy of Sciences, 272-277.

Reimnitz, E, Graves, S M & Barnes, P W (1985).
Beaufort Sea coastal erosion, shoreline evolution, and sediment flux. U.S. Geological Survey, Open-File Report 85-380, 1-18.

Scott, W J (1975).
Preliminary experiments in marine resistivity near Tuktoyaktuk, District of Mackenzie. Geological Survey of Canada, paper 75-1A, 141-145.

Sellmann, P V, Delaney, A J & Arcone, S A (1985).
Mapping resistive seabed features using D.C. methods. Proc, of the Arctic Energy Tech. Workshop, U.S. Dept. of Energy - DOE/METC-85/6014, 136-147.

vonArx, W S (1962).
An Introduction to Physical Oceanography, 422 pp. Addison Wesley Publishing Company, Inc.

Walker, G G, Kawasaki, K & Osterkamp, T E (1985).
Transient electromagnetic detection of subsea permafrost, workshop on permafrost geophysics. US Army Cold Regions Research and Engineering Laboratory, Special Report 85-5, p. 106-108.

EM SOUNDINGS FOR MAPPING COMPLEX GEOLOGY IN THE PERMAFROST TERRAIN OF NORTHERN CANADA

A.K. Sinha

Geological Survey of Canada, Ottawa, Ontario, Canada

SYNOPSIS Borehole temperature measurements in several oil and gas wells in the Big Lake area of the Mackenzie Delta, N.W.T., Canada, indicated a relatively sharp decrease in permafrost thickness from about 700 m to about 100 m towards the west, over a distance of 20 km. In an attempt to obtain more detailed information, transient electromagnetic (EM) soundings were made along a 25 km line across the area.

Seventeen central soundings at an average separation of 1.5 km were made on a profile which crossed a channel of the Mackenzie River. At least two loop sizes were used at each station to produce good resolution at both shallow and large depths. The interpretation of EM data indicated an abrupt discontinuity in the electrical parameters at the channel, possibly due to a change in the thermal conditions. West of the channel, the permafrost is less than 100 m thick, and is underlain by 100 - 150 m thick unfrozen sediments (2-5 Ωm). This unfrozen layer thins to about 50 m in the immediate vicinity of the channel. Below this is a moderately low resistivity material (5-8 Ωm) which could be another layer of unfrozen sediments. East of the channel, the permafrost is about 265 m thick increasing eastward to more than 650 m. A thin unfrozen layer (25-50 m) was detected at depths of 70-100 m at all stations east of the channel. Interpretation of the data was complicated by the presence of lateral inhomogeneities and irregularly shaped bodies near the channel.

INTRODUCTION

Electrical and electromagnetic (EM) methods have successfully been used in the past few years for mapping the distribution of permafrost in Alaska and in northern regions of Canada (Daniel et al, 1976; Annan and Davis, 1976; Koziar and Strangway, 1978; Rozenberg et al, 1985). The methods rely on the fact that electrical resistivities of sediments increase significantly when they are frozen (Hoekstra et al, 1975; Olhoeft, 1975). A number of papers have documented case histories on the application of EM methods for detection and delineation of permafrost in northern Canada (Hoekstra and McNeill, 1973; Rossiter et al, 1978; Sartorelli and French, 1982). Sinha and Stephens (1983) used both multifrequency and transient ground EM systems for detection of horizontal interfaces between geological formations in the Mackenzie Delta, N.W.T., Canada, especially the contact between the ice-bonded permafrost and the underlying unfrozen sediments. The tests were made near exploratory oil and gas wells which had been surveyed earlier with temperature and other geophysical logs (Taylor et al, 1982). A comparison of the depths to the interfaces from both systems showed good agreement with well-log data. The effects of lateral inhomogeneities were found to be less with the transient system data. It was also easier and less ambiguous to invert the transient EM field data in terms of a layered model.

Taylor et al (1982) have recently published data on permafrost thickness at several locations in northern Canada based mainly on borehole temperature measurements. They detected anomalous permafrost characteristics in the Richards Island area in the Mackenzie Delta (Figure 1). West and south of Big Lake, the permafrost thickness ranged from over 270 m to more than 600 m in a cluster of holes. But only 15 km WSW of that cluster, the permafrost thickness at a number of holes on the eastern bank of a Mackenzie River channel ranged in thickness from 144 to 275 m. The last thickness value possibly relates to a transitional zone since the permafrost thickness decreases to 217 m in a hole (not shown) about 1 km south. Over much of the permafrost section, the thermal profile is almost isothermal between 0 and -2°C. The base of the ice-

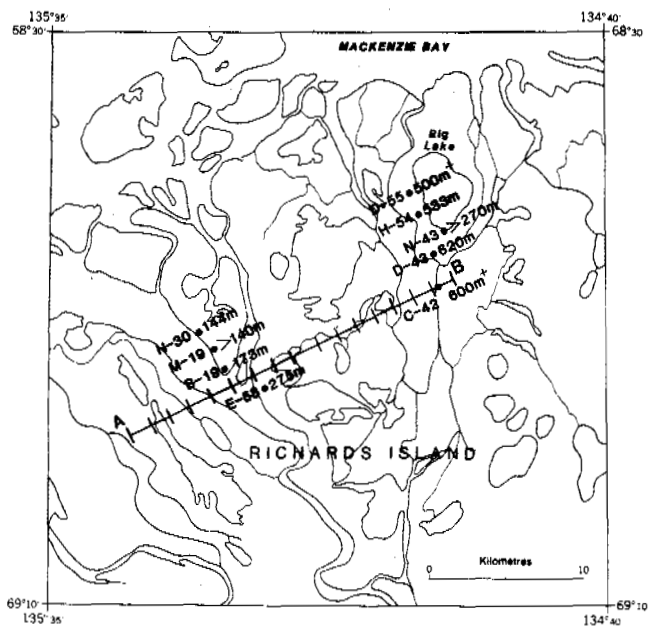

Fig. 1 Location of the survey profile in the Richards Island area, N.W.T. The thickness of permafrost at several exploratory oil and gas wells are also indicated.

bearing permafrost was determined by detecting changes in the electrical and acoustic properties of the sediments. In coarse-grained sediments, the base may almost coincide with 0°C isotherm. In fine grained soil, the freezing characteristics of the soil predominate and the base of the ice bearing permafrost may be several tens of meters above the 0°C isotherm with an underlying transition layer (Osterkamp and Payne, 1981).

Geological Survey of Canada Contribution No. 43287

Judge (1986) provided permafrost thickness values from borehole temperature measurements observed at exploratory wells in the Mackenzie Delta and Arctic Islands along with interpretation of down-hole geophysical logs. Figure 2 adapted from Judge (1986) shows permafrost thickness contours in the Beaufort Sea continental shelf and adjacent Tuktoyaktuk coastlands with contour intervals of 100 m. The greatest permafrost thickness, about 740 m occurs in northern Richards Island. The permafrost thickness drops sharply towards the west from 600 m to less than 100 m within a distance of 15-20 km with the lowest thickness occurring west of the Mackenzie River channel shown by the arrow. The thickness increases again in the SW corner of the map area. The gradient in permafrost thickness indicates the complex subsurface geology and Quaternary history in the area.

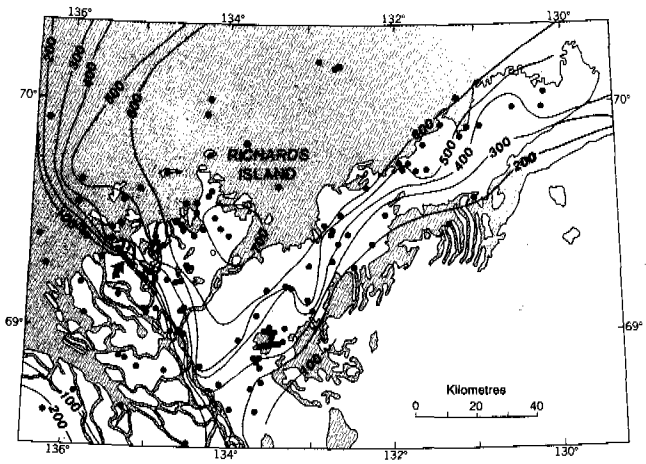

Fig. 2 Contours of permafrost thickness in metres in the Mackenzie Delta and Beaufort Sea Continental Shelf (after Judge, 1986). The arrow indicates the Mackenzie River channel crossing the profile.

Transient EM soundings were made along a line so as to obtain detailed information about the variation of permafrost thickness in the area. The purpose of the survey was to determine if the change in permafrost thickness was gradual from west to east or if there was an abrupt change in permafrost thickness at any location. In the case of the latter possibility, determination of the exact location of the abrupt change was the other purpose of the survey. Seventeen soundings were done on a line oriented at N64°E at an average separation of 1.5 km (Figure 1). The first sounding was done about 7.5 km WSW of the hole Niglintgak B-19 (69°18.2'N, 135°18.3'W) west of the Mackenzie River channel where the permafrost was 173 m thick. This station is designated as Station 1 while Station 17 is the easternmost sounding point. The eastern end of the line ended just south of Big Lake, about 1 km east of the drillhole Taglu C-42 (69°21'N, 134°56.6'W) where the permafrost thickness was over 600 m. It was hoped that systematic determination of permafrost thickness on this line would help in understanding the subsurface geology which might be responsible for such abrupt changes in permafrost thickness.

GEOLOGY OF THE AREA

The Big Lake area located 80 km west of Tuktoyaktuk in the Mackenzie River Delta is a low coastal area extending over 15,000 km^2 and covered by unconsolidated Pleistocene fluvial, deltaic and estuarine sediments up to 100 m thick over much of the Delta (Mackay, 1963). The region is dotted with thousands of lakes and dissected by a network of several large channels and numerous smaller winding channels. Active sedimentation, rapid coastal recession (typical rates of 1 m/year have been observed) and constantly shifting river channels also characterize the area. Pleistocene sediments on Richards Island consist of stonefree sands, silts and clays, silty clays being more common towards the north. During the Pleistocene, much of the Delta was covered by ice sheets; however, the northern part of the Delta was believed to have been unglaciated at least during the late Wisconsinan Glaciation (Forbes, 1980), i.e. for the last 40,000 years. Changes as great as 100 m in eustatic sea level during the glacial period resulted in long periods of emergence and submergence of the Delta. As areas of the Delta were unglaciated throughout the late Wisconsin and subjected to low surface temperatures during periods of emergence, conditions favoured the formation of thick permafrost. Such conditions have persisted in the Delta since deglaciation over 10,000 years ago.

The distribution and extent of permafrost in the Delta is however not simple. The presence of numerous water bodies (the sea, lakes and shifting river channels), the shoreline transgression, past periods of submergence and emergence, glaciation and deglaciation all contribute to make the permafrost distribution rather complex. In the old Delta, the permafrost thickness varies from 90 to 700 m and the temperature ranges from -4 to -9°C (Judge, 1975). In the modern Delta, the sedimentation is active with frequent spring flooding. The permafrost thickness ranges from 0 to 80 m and the temperature is slightly below 0°C.

DESCRIPTION OF THE SYSTEM AND FIELD PROCEDURES

An EM-37 transient EM system, built by Geonics Ltd, Toronto was used for the survey. The system consisted of a non-grounded square loop transmitter lying flat on the surface. A large current with equal time-on and time-off was passed through the loop. The loop size varied from 450 m by 450 m to 70 m by 70 m as detailed below. The larger loop was used for deep soundings while the data from the smaller loop was used to obtain greater resolution at shallower depths. The receiver consisted of a small multi-turn coil that allowed measurement of voltage decay in three orthogonal directions during the time-off period at various time intervals or channels after the current is turned off. For sounding work, only the decay of the vertical component of the induced magnetic field at its centre of the transmitter was measured. The system has been described in detail by Sinha and Stephens (1983).

A sharp termination of the current flowing through the transmitter induces eddy currents to flow in the ground in accordance with Faraday's law. These time-varying eddy currents diffuse laterally and vertically at a rate determined by resistivity and thickness parameters of the ground. The secondary magnetic fields produced by the eddy currents are measured by the receiver at the centre of the loop.

It can be shown that a system with a square loop transmitter and a receiver coil at the centre is equivalent, in the time range employed, to a system consisting of a magnetic dipole transmitter and an electric dipole receiver separated by a distance R equal to $L/\sqrt{\pi}$, where L is the length of the side of the square loop. This allows for use of all theories developed for the latter case while using the first set-up in the field.

During the survey, skidoos were used for laying of the transmitter loop and for movement, in general. At least two transmitter loop sizes were used at each station. The larger loop size was 300 m square west of the river channel where the permafrost was thinner and 450 m square east of the channel where permafrost was thicker, for sounding to depths of 300 m and 600 m respectively. A smaller loop was used at each station to obtain detailed information at shallow

depths. The size of the smaller loop varied from 70-75 m square west of the channel to 150 m square to the east. Two base frequencies of 30 and 3 Hz were used with the system permitting measurement of decay voltages at 30 channels up to a maximum of 70 ms after the current turn-off. The currents in the loop varied from 22-23 A for the larger loops and 25-27 A for the smaller loops.

A correction for the finite turn-off time of the current was applied to the measured decay voltages since the theory was based on an instantaneous turn-off. The turn-off time depends on the area of the loop and the current, and may be read from the transmitter console. The corrected decay voltages are converted to apparent resistivity using equation (3) assuming late time conditions. The late time, defined as the time when the induced current distribution becomes invariant with time, appears relatively quickly in the resistive onshore environments. The field data are plotted on double log sheets with apparent resistivity ρ_a in the ordinate and square root of time on abscissa.

APPARENT RESISTIVITY CONCEPT

Although the decay of the vertical magnetic field component at the centre of the transmitter loop depends on the resistivity and thickness of the subsurface layers, the decay pattern itself is not sufficiently diagnostic for interpretation. Hence, as in most EM systems, the field results are normally presented in terms of apparent resistivity. Ehrenbard et al (1983) illustrated the advantage of presenting the results in terms of apparent resistivity.

Figure 3 shows a plot of the apparent resistivity ρ_a of a homogeneous medium normalized by its true resistivity ρ_1 against the parameter τ_1/R where

$$\tau_1 = \sqrt{2\pi\rho_1 t 10^7} \qquad (1)$$

is a measure of the depth of exploration, t is the time after turn-off and R is the equivalent distance between transmitter and the receiver.

At early time, defined by $\tau_1/R < 2$

$$\rho_a = \frac{2\pi R^4}{3m} E_\phi \qquad (2)$$

At late time, defined by $\tau_1/R > 10$, when the current system has stabilized,

$$\rho_a = \frac{\mu}{4\pi t}\left(\frac{R\mu m}{5tE_\phi}\right)^{\frac{2}{3}} \qquad (3)$$

where

m = Dipole moment of the transmitter in Am2,

μ = Magnetic permeability of the medium in H/m,

E_ϕ = Azimuthal electric field in V/m.

It is obvious from Figure 3 that in early times the apparent resistivity is not a true reflection of the resistivity of the ground. In late time, however, the apparent resistivity approaches ρ_1. Thus it is convenient to use the late time expression of apparent resistivity if the measured time channels are also in late times. In fact,when working onshore, the late time behaviour appears quickly after only a few channels. But in offshore environments when near-surface sediments are extremely conductive, the early time behaviour may persist for many channels. Since the late time commences at $\tau_1/R > 10$, it is easy to show that the time of measurement must satisfy the relation.

$$t > \frac{R^2}{2\pi\rho_1 10^5} \qquad (4)$$

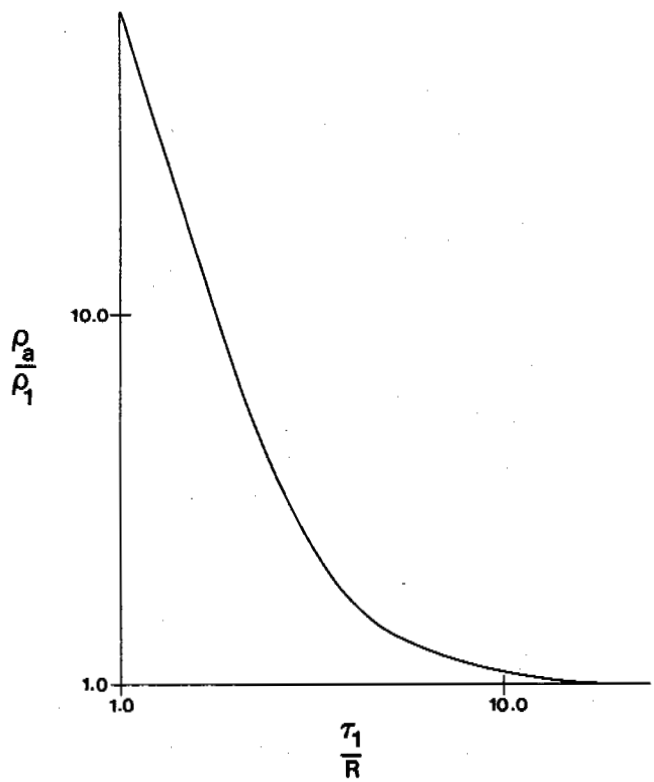

Fig. 3 Plot of normalized apparent resistivity ρ_a/ρ_1 versus τ_1/R for a homogeneous half-space.

INTERPRETATION OF FIELD SURVEY RESULTS

Interpretation of field data in terms of a layered ground consists of two phases. In the first, the apparent resistivity of several possible layered models are computed for the time periods used by the receiver and compared to the field plot of apparent resistivity versus square root of time until a reasonable match is obtained. In the second phase, the parameters of the best-match model form the input to an automatic nonlinear least-squares inversion program for the best model to satisfy the field data (Anderson, 1982). Finally, the response of the model determined by the inversion program is visually compared with the field response and further adjustments may be made in the parameters of the model at this stage.

Figure 4 shows the corrected plots of apparent resistivity at two sounding stations, station 1 in the west and station 15 in the east along with the models with the best match with field data. At station 1, the top frozen layer (281 Ωm) extends to a

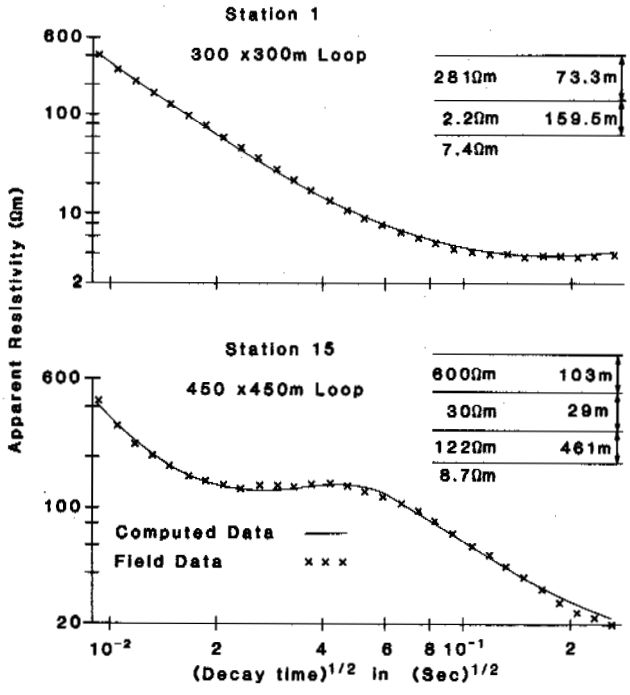

Fig. 4 Plots of field data at stations 1 and 15 in the form of apparent resistivity versus square root of time and their interpretation in terms of a layered ground.

depth of 73.3 m, below which a conductive layer (2.2 Ωm), presumably an unfrozen clay layer exists. A slightly more resistive layer (7.4 Ωm) appears at a depth of 232.8 m. From the resistivity value, the bottom layer appears to be an unfrozen silt or sandstone horizon containing salt water. From Young and McNeill (1984), the second and third layers could be the Nuktuk and Beaufort formations consisting of mud and clay for the former and gravel, sand and mud for the latter formation. At station 15, the apparent resistivity curve looks quite different. Although a thin conductive layer (30 Ωm) detected at a depth of 103 m is possibly unfrozen, the main conductive horizon occurs at a much greater depth of 593 m. Although there are no drill holes near this station, drill hole C-42 located about 1.5 km to the east of station 15 has a permafrost thickness of over 600 m according to temperature measurements. The discrepancy between the two figures may be explained by the fact that the ice-bonded permafrost generally thaws at a shallower depth than predicted by thermal logs because of the presence of electrolytes, but their temperatures may still be below 0°C. The geological section within the permafrost transects mudstone and sandstones of the Beaufort formation.

Figure 5 shows the composite interpretation of the EM soundings on the line. At each station, the data from the large and small loops were jointly interpreted such that the interpreted model satisfies both sets of data. No sounding was done at station 6 on the river channel because of logistical problems. Figure 5 shows that the permafrost distribution on the line falls into two distinct categories. West of the river channel (station 5), the permafrost is relatively thin, generally less than 100 m, underlain by unfrozen sediments. The unfrozen sediments can be divided into two distinct layers, possibly indicating two different sediment types, e.g. clay and sand. East of the river channel, the permafrost thickens, increasing in thickness from 265 m at

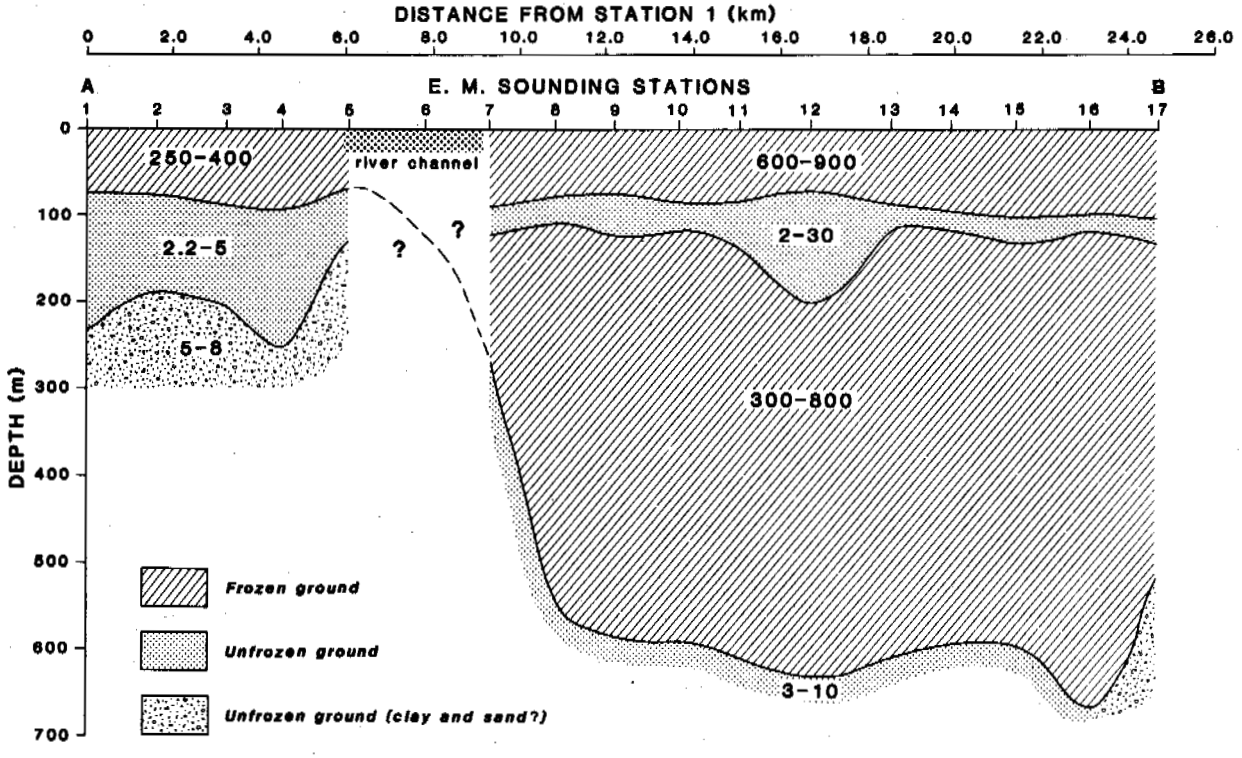

Fig. 5 Composite interpretation of the survey profile in Big Lake area. The resistivities of the layers are indicated in Ωm.

station 7 to about 675 m at station 16, beyond which the thickness drops to 513 m at station 17. An interesting feature at all sounding stations east of the river channel is the presence of a thin layer of unfrozen sediments close to the surface. The layer is thickest under station 12 where it is about 125 m thick and more resistive than at nearby stations. This thin unfrozen layer may reflect a zone which had thawed either due to the proximity of warm lakes or rivers or cover by a former extensive lake and subsequent slow refreezing after drainage of that lake.

The thickness of the permafrost increases abruptly between stations 7 and 8 but stays reasonably uniform east of station 8. At some of the stations, the sounding curves were greatly distorted perhaps implying the presence of lateral inhomogeneities such as taliks forming two- and three-dimensional bodies instead of simple horizontal layers. This could again be due to the very complex recent geological history of the area resulting in very irregular boundaries.

A similar transient EM survey was carried out on a N-S line in 1983 (Rozenberg et al, 1985) SW of Big Lake. One of their sounding stations was located about 1 km WSW of station 16. Rozenberg et al (1985) interpreted the permafrost thickness at their station to be 670 m which agrees well with our interpretation of 675 m at station 16. However, they did not report detecting any unfrozen sediments close to the surface at that station, although they reported detecting unfrozen material at a depth of 30 m, 400 m south of that station. Thus, there is good agreement between their interpretation and our results in that area.

CONCLUSIONS

Deep transient EM soundings were carried out on a 25 km long line southwest of the Big Lake in the Mackenzie Delta, N.W.T., to obtain detailed information where borehole temperature measurements indicated a sharp change in the permafrost thickness. The permafrost was rather thin west of the Mackenzie River channel which forms the present boundary between the modern and the old delta. East of the channel, the permafrost thickness was much greater, of the order of 500 m or more from 2 km east of the channel onward.

At five sounding stations west of the river channel, the permafrost was never more than 100 m thick. Below the permafrost, two conductive layers were detected which could be unfrozen clay and sandy sediments. To the east of the channel, an abrupt change in permafrost thickness was noted at station 7, less than a km from the eastern edge of the river channel, where it was 265 m. The thickness increased to 560 m at station 8, 1.5 km further east from station 7 and stayed reasonably uniform further east. A thin, shallow unfrozen layer was also detected at all stations east of the channel. This layer increased in thickness 8 to 10 km east from the river channel where the sounding curves were rather distorted. The bottom unfrozen sediments east of the channel were quite conductive (3-10 Ωm), suggesting the presence of unfrozen clays, mixtures of clay and silt or the presence of salt water in the pores.

The success of the EM survey in delineating the subsurface conditions in this area down to depths of 700 m proves that such techniques can be used in mapping the distribution of permafrost in areas where permafrost thickness may change rapidly. This type of survey may be extended to offshore areas with minor changes in equipment although the depth of investigation may be somewhat reduced because of the presence of highly conductive near-surface materials.

ACKNOWLEDGMENTS

The author wishes to thank his colleagues L.E. Stephens and D. Gresham of the Geological Survey of Canada and Perry Lanthier of the former Earth Physics Branch for help in carrying out the field survey and preliminary interpretation of the data. Thanks are also extended to Polar Continental Shelf Project for providing logistical help during the field program and to the office of the Energy Research and Development, EMR, for partially financing the field work. Dr. A.S. Judge of GSC suggested the idea of carrying out EM soundings in the area and critically read this manuscript.

REFERENCES

Anderson, W.L. (1982). Nonlinear least-squares inversion of transient soundings for a central induction loop system (Program NLSTCI). Open-File report 82-1129, U.S. Geological Survey, 35 p.

Annan, A.P. and Davis, J.L. (1976). Impulse radar sounding in permafrost. Radio Science, v. 11 (4), 383-394.

Daniels, J.J., Keller, G.V. and Jacobson, J.J. (1976). Computer-assisted interpretation of electromagnetic soundings over a permafrost section. Geophysics, 41, 752-765.

Ehrenbard, R.L., Hoekstra, P. and Rozenberg, G. (1983). Transient electromagnetic soundings for permafrost mapping. Proc. 4th Int. Conf. on Permafrost, National Academy Press, Washington, D.C., 272-277.

Forbes, D.L. (1980). Late Quaternary sea levels in the Southern Beaufort Sea. Current Research, Paper 80-1B, Geological Survey of Canada, 75-87.

Hoekstra, P. and McNeill, J.D. (1973). Electromagnetic probing of permafrost. in Permafrost -- The North American Contribution to 2nd Int. Conf., Yakutsk, Washington, D.C., 517-526.

Hoekstra, P., Sellmann, P.V. and Delaney, A. (1975). Ground and airborne resistivity surveys of permafrost near Fairbanks, Alaska. Geophysics, v. 40 (4), 641-656.

Judge, A.S. (1975). Geothermal studies in the Mackenzie Valley by the Earth Physics Branch. Geothermal Series No. 2, Geothermal Service of Canada, 12 p.

Judge, A. (1986). Permafrost distribution and the quaternary history of the Mackenzie-Beaufort region: A geothermal perspective. Open-File Report 1237, Geological Survey of Canada, 41-45.

Koziar, A. and Strangeway, D.W. (1978). Permafrost mapping by audio frequency magnetotelluric. Can. J. of Earth Sciences, v. 15, 1535-1546.

Mackay, J.R. (1963). The Mackenzie Delta Area, N.W.T. Geographical Branch Memoir No. 8, Dept. of Mines and Technical Surveys, Canada.

Olhoeft, G. (1975). The electrical properties of permafrost. Ph.D. thesis, University of Toronto, Toronto, Canada.

Osterkamp, T.E. and Payne, M.W. (1981). Estimates of permafrost thickness from well logs in northern Alaska. Cold Regions Science and Technology, v. 5, 13-27.

Rossiter, J.R., Strangway, D.W., Koziar, A., Wong, J. and Olhoeft, G.R. (1978). Electromagnetic sounding of permafrost. Proc. 3rd Int. Conf. on Permafrost, v. 1, Ottawa, National Research Council of Canada, 567-572.

Rozenberg, G., Henderson, J.D., Sartorelli, A.N. and Judge, A.S. (1985). Some aspects of transient electromagnetic soundings for permafrost delineation. Workshop on Permafrost Geophysics, CRREL Special Rep. 85-5 (J. Brown, M.C. Metz and P. Hoekstra ed), 74-90.

Sartorelli, A.N. and French, R.B. (1982). Electromagnetic induction methods for mapping permafrost along northern pipeline corridors. Proc. 4th Canadian Permafrost Conf, National Res. Council of Canada, Ottawa, 283-295.

Sinha, A.K. and Stephens, L.E. (1983). Deep electromagnetic sounding over the permafrost terrain in the Mackenzie Delta, N.W.T., Canada. Proc. 4th Int. Conf. on Permafrost, Washington, D.C.; National Academy Press, 1166-1171.

Taylor, A.E., Burgess, M., Judge, A.S. and Allen, V.S. (1982). Canadian geothermal data collection - Northern wells, 1981. Geothermal Series No. 13, Earth Physics Branch, 154 p.

Young, F.G. and McNeill, D.H. (1984). Cenozoic stratigraphy of the Mackenzie Delta, Northwest Territories. Bulletin 336, Geological Survey of Canada, 63 p.

MAPPING AND ENGINEERING-GEOLOGIC EVALUATION OF KURUMS

A.I. Tyurin, N.N. Romanovsky and D.O. Sergeyev

Faculty of Geology, Moscow State University, Moscow, USSR

SYNOPSIS Over the last 10 to 15 years rock streams are more frequently used or treated as a probable base for engineering structures. The present paper is based on the data obtained from the studies of the Transbaikal bald mountain belt where rock streams occupy more than a half of the slope area and are distinguished by large size and complex structure due to geostructural peculiarities of near-surface solid rocks, altitudinal permafrost and climatic zonality, and specific features of the subsurface water flow. The authors have proposed the methods for mapping stable paragenetic complexes of facies (rock stream, deluvial, solifluction, etc.) occurring in a certain area termed "slope segment". Features, which are facies of slope formations, are identified as conventional units within slope segments as a result of engineering-geological analysis. By the combinations of the peculiarities of the structure and movement mechanisms, the features are subdivided into four groups depending on the hazard for engineering development. Based on the studies of the features, the principles of slope segment evaluation have been developed to aid in choosing a proper method for laying a roadbed and working out a set of engineering measures to achieve safe road operation. The procedures which have been elaborated are embodied in the maps of engineering-geologic conditions and engineering-geological evaluation.

For about 200 years rock streams (kurums) have been attracting attention of scientists. Over the last 10-15 years rock streams are more and more often considered as a base for various engineering projects. It should be noted that the problem of constructing on rock streams has always existed. Builders treated and continue to treat rock streams as a complex and incomprehensive phenomenon, trying to by-pass them. In the majority of cases such a practice was a success because, so far, only regions with rock streams of limited extent had been developed. Avoidance of rock streams inevitably incurred additional expenditures. At present, when high-mountain regions where rock streams occupy up to 80 percent of the area are being developed it is impossible to pass them around and construction on them is inevitable.

The present paper is based on the data obtained from the studies of rock streams in the bald-mountain belt of the Transbaikal region. The authors have experience of rock-stream investigation in South Yakutiya based on the cryofacies analysis. Rock streams in this area are formations limited in extent from some tens to a few hundred meters. They occur mainly on the sides of valleys cut in plateaus and have distinct belts of mobilization, transit and accumulation of clastic material. The rock streams in the Transbaikal mountains are different; their features are as follows: (1) they are large and extended down slope; (2) series of alternating rock streams, often different in morphology and genesis, are located, as a rule, on every slope; (3) there is no distinct differention of rock stream belts (of mobilization, transit and accumulation). One rock stream cover may be incorporated into the mobilization belt of the other. This pattern, sometimes complicated by several accumulative belts, may repeatedly occur on a slope; (4) due to a large altitude gradient, a rock-stream slope is frequently characterized by climatic and geocryologic altitudinal zonality; and (5) complex geostructural conditions (topography, diverse and close to the surface solid rock bedding, fault and block tectonics etc.) that lead to complicated paragenetic connections of rock streams and their association with different types of exogenetic processes and phenomena.

The points listed above require a larger scope of methods and procedures as compared with previously used in studying rock streams.

The studies of rock streams in the Transbaikal region have shown that in different parts of the mountains they are differently distributed and differ significantly in morphology. In addition, rock streams have been found to be paragenetically related to certain types of slope formations (accumulations). Cosequently, we have conducted (1) special geomorphological mapping to study in detail the slopes depending on the neotectonic setting, glacial phenomena in the Pleistocene, as well as composition and geostructural features of bedrock; and (2) special mapping of the Quaternary formations connected paragenetically with rock streams deserptium. It has been established that Quaternary formations of eluvial, colluvial, glacial and even aquatic series may (a) serve as a substratum for the formation of rock-stream deserptium; (b) be connected paragenetically with the latter, forming alternating

areas; and (c) exclude the presence of rock-stream deserptium. It has also been established that rock-stream deserptium itself may serve a basis for the formation of other genetic types of Quaternary deposits. These findings allowed us to compile a "Map of Rock Streams" based on a special map of Quaternary deposits. It represents in detail slope formations and especially various rock stream facies and their combinations. The main taxonomic unit of rock stream that was distinguished and studied in the course of special geological surveys was a rock stream facies. The following rock stream facies were identified by common morphology and orientation of the processes that displaced and transformed rudaceous material: "flows of rock streams", net-like rock streams, rock-stream slopes, as well as complicated combinations of flow rock stream forms with areal ones. Therefore, at the first stage of studies of rock-stream facies, three large morphological groups of rock-stream forms were identified: (1) isometric; (2) linear (flow); and (3) net-like. Each comprises different facies distinguished by individual morphological peculiarities of the rock stream body and occurrence in various relief forms. This is due to the fact that the morphology of rock streams is predetermined by their genesis. Geostructural features of slopes are also very important. These are: (1) presence of different kinds of fructure systems and tectonoc fragmentation zones; (2) lithological peculiarities of rocks and orientation of geologic layers relative to the slopes; (3) slope steepness and evolution; (4) dimensions of the drainage system and the associated slope inundation; (5) presence of external sources of rock streams; and (6) the type of unconsolidated sediments which served as a background for rock streams development. With this in view, rock-stream facies within morphological groups were identified based on an obligatory analysis of all the factors involved in rock-stream formation directly on the slope under study.

The next stage of the work was mapping of rock-stream facies. However, large-scale mapping of rock streams is impossible because of their limited size. Many rock streams are only a few meters wide. Rock-stream facies alternate with those of other slope deposits such as, for example, eluvial-deluvial ones, forming a parageneticaly related group of slope facies. Such groups occupy considerable parts of slopes corresponding, in the taxonomic series of landscapes, to the "facies association". The geometric forms of the latter on the slope are often similar to segments; therefore, in this paper they were conditionally termed "slope segments". Thus, as a result of a special geological survey, it were not the boundaries of individual rock streams that have been identified and mapped but the parageneses of slope formations, including also the groups of rock stream facies.

Within the slope segments identified, the percentage of areas occupied by their constituent facies was determined. The map shows the rock stream "coverage" (percentage) in a "segment". which was shaded in color corresponding to the rock stream genesis if it covered more than 50 percent of the segment's area or to the type of slope deposits prevalent in this "segment".

An engineering-geological prediction of the interaction between a rock stream and a road along the entire rock stream slope is not yet feasible. Within the limits of slope segments, an engineering-geological analysis enabled identification of conditional units or features. Most frequently, these are rock stream facies or other types of slope formations. They can also be represented by rock stream subfacies, i.e. by smaller units but still of considerable size. The identification of such features was based upon the following factors: (1) thickness of the rudaceous cover and its relation to the depth of the seasonally thawing layer (STL); (2) presence or absence of a bald-mountain-ice-containing horizon and its thickness" (3) size and shape of rock fragments,and, mainly, the degree of their roundness; (4) density of the structure ("packing") of the rudaceous cover; (5) presence of a layer of inundated, thixotropic fine-grained material in the basement of the STL and/or the same material in a perennially frozen state; (6) presence of water flow from the STL in the rock stream body in summer; and (7) slope steepness.

To evaluate the stability of a segment feature, observations were conducted of the behavior of engineering structures and of the engineering-geological processes and phenomena induced by them. We could then predict undesirable displacements of the rock stream cover under the impact of road construction, such as: sliding of the rudaceous cover down the ice-ground base; plastic deformation of the bald-mountain ice layer; its partial or complete thawing and associated subsidence; visco-plastic deformations of the fine-earth layer; the cover deformations caused by the hydrodynamic head of the STL waters; and fine-earth suffosion and gravitational displacements. Segments with an areal or stream-like (concentrated) patterns of the rudaceous cover movement have been distinguished. The order of the rates of movement and amounts of material displaced have been evaluated for the both, depending on slope steepness, rudaceous cover thickness, and quality of the displacement surface in natural conditions and those of slope cutting. By the specifics of structure and mecanisms of motion, the features of rock stream slopes are subdivided into four groups as to the extent of hazard associated with their engineering-geological development: safe, comparatively safe, hazardous and extremely hazardous.

The safe type of rock stream features and other slope formations is characterized by a fairly stable state of the rudaceous cover; absence of conditions for its catastrophic displacements due to slope cutting; absence of debris movement; and rates of movement, if any, that do not exceeding a few millimeters a year. Construction of roads on such rock streams is safe.

The comparatively safe type of rock stream features is characterized by the fragments with bald-mountain ice of insignificant thickness (up to 0.3 m); unconsolidated structure of debris in the rudaceous cover, etc. Roads

constructed on these rock stream features experience the impact of the rudaceous material that moves at a rate of up to several mm a year. Insignificant, decreasing with time, sibsidence of the roadbed caused by the consolidation of the cover and by thawing of ice lenses also occurs. Rudaceous material fall-outs with a volume of several cubic meters are possible when hollows are cut in a slope. All the unfavorable consequences, incurred through natural and man-induced processes, can be eliminated in the course of routine roadway exploitation.

The hazardous type of rock-stream features is characterized by a complex structure and presence of a 1-2 m-thick bald-mountain ice layer or a layer of water-saturated thixotropic fine-earth (0.5 and more m-thick) at the base of the rock stream. On the whole, the rudaceous cover moves at a rate of 1-3 cm per year. Natural causes (rainfall, hot summer bringing about an increase in STL depth, seismic phenomena, etc.) as well as engineering activity can give rise to catastrophic movements of the rudaceous cover with displacements amounting to several tens of cubic meters. Thermoerosion scours, thermokarst subsidence and other undesirable phenomena, disturbing the stability of structures and requiring specialized, costly repair work, are also possible. Sections of roads built on such rock-stream features can experience considerable subsidence, be washed out, and blocked up with rudaceous material, stopping normal traffic for a certain period of time. The extremely hazardous type of rock-stream features is distinguished by a 2-3 and more m-thick ice-ground layer and great rates of the rudaceous cover movement reaching several tens of cm per year. Large catastrophic movements with debris displacements amounting to several meters are also possible. A section of the road built on such a slope feature may be completely destroyed as a result of catastrophic phenomena associated with thawing or washing out of the ice-ground layer at the base of the roadbed. These phenomena can develop with time and disrupt the use of the road for a long period. Measures aimed at prevention and elimination of the above phenomena demand heavy investments and, in a number of cases, do not guarantee the desired safety.

It should be noted that undisturbed rock-stream slopes rarely preserve traces of active processes. This seeming stability of rock streams is a result of long-term geological processes producing an equilibrium profile. However, specific permafrost-facies structure of rock streams makes them rather unstable if they are disturbed by construction work. It is clearly manifested when mine workings are made in rock streams.

Thus, an engineering-geological evaluation of different kinds of rock streams made by the authors can be used in road designing and construction. Nevertheless, the choice of road variants requires compilation of an evaluation map. But rock-stream features, because of their small size, cannot be plotted on such a map. That is why it has been deemed reasonable to evaluate slope segments as a whole from the engineering-geological standpoint. Large-scale studies of slope segments have proved that in engineering development they vary by preferable methods of laying roadbeds (on shelves, in semi-hollows- semiembankments, in embankments), and also require different sets of engineering measures for their construction and safe operation. It should be emphasized that segments can contain, in different combinations, features of all four groups distinguished by complexity (hazard) for development.

To construct a road reliably and operate it safely, preliminary recommendations aimed at carrying out a number of engineering reclamation measures and/or engineering protection of various structures built on the most hazardous portions of slopes have been worked out. Taking into account the complexity of the above described work and engineering-protection measures, slope segments have been subdivided into four categories: favorable, conditionally favorable, unfavorable and extremely unfavorable for road construction. The category of slope segments is an indirect indication of relative expences needed for laying a road within their limits.

From the engineering-geological viewpoint, a method of road construction is of no principal significance for the slope segments belonging to the first, favorable category since no specific reclamation measures and structures are required to ensure engineering protection of roads.

Laying a roadbed on the slope segments of the second, conditionally favorable for road construction and operation category requires selection of a preferable method (shelf, embankment) and determination of an optimum slope cutting depth in accordance with the rock stream structure and rudaceous cover thickness (Fig.1). A new drainage system must also be envisaged or the natural one preserved. This can be done by laying girder floors over the hollows concentrating subsurface flow, by creating over them a coarse-fragmental "cushion" to preserve the rudaceous cover from colmatage, or by other methods.

The third, unfavorable category of slope segments includes those features construction on which does not ensure safety and durability of structures and their continuous operation without preliminary removal or stabilization of the rudaceous cover (Fig.2). In every concrete case different reclamation measures should be recommended. A set of such measures usually incorporates stabilization of the rudaceous material of rock streams, its removal and laying drainage pipes into the formed hollows or filling them with rubble-gravelly material. Other engineering measures can be employed.

The fourth category comprises slope segments which are extremely unfavorable for development. It includes rock-stream facies as well as glaciers and rock-stream glaciers. The rudaceous cover removal or stabilization will not ensure the stability of structures or their normal operation on such slope segments (Fig.3) and construction will trigger off extremely unfavorable engineering-geologic processes (powerful thermokarst subsidence, thermoerosion,etc.). In addition, the rudaceous cover removal or reliable stabilization on such rock streams is

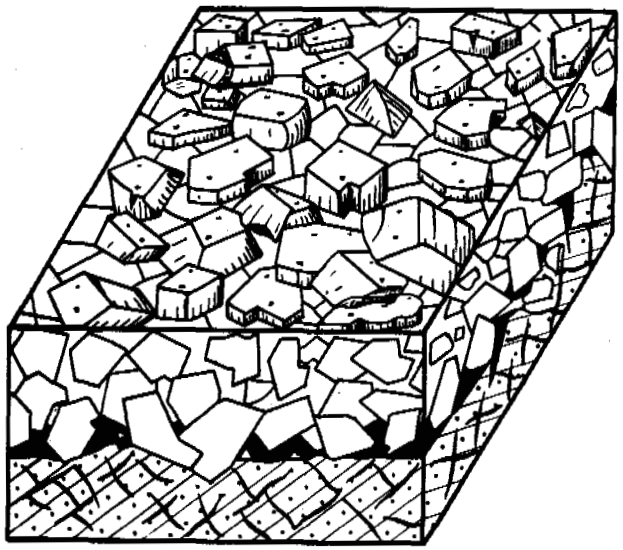

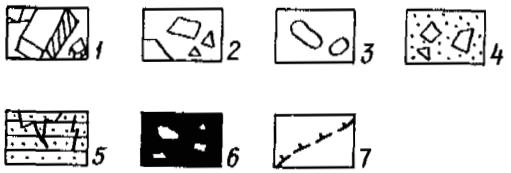

Fig.1 A slope segment of the conditionally favorable category with the rock-stream cover of a heaved rock 1 - blocky material on a rock-stream surface; 2 - rubble-blocky material in the cross-section of a rock stream; 3 - rubble-blocky material of rounded shape in the cross-section of a rock stream; 4 - unconsolidated rudaceous formations with a fine-grained fill; 5 - fractured solid rock ("rock in fragments"); 6 - bald-mountain ice with solid rock fragments; 7 - the upper boundary of perennially frozen rocks.

frequently impracticable due to considerable slope steepness and great thickness of rudaceous formations or bald mountain ice.

The unfavorable man-induced processes occurring on rock-stream slopes due to slope cutting include concentrated water flows from the STL. In the period of snow melting and in the autumn when air temperature often passes 0°C, the STL waters form on the road surface 20-30 cm-thick, small in area and volume icings. On steep roads such icings can make the movement of wheeled vehicles not only difficult and dangerous but completely impossible.

An analysis of engineering-geological characteristics of slopes and natural processes occurring on them coupled with the prediction of the possible man-induced processes have allowed us to compile a "Map of engineering-geologic conditions" and a "Map of engineering-geological evaluation". The former represents all the specific features of the structure of rock streams and their dynamics, whereas the latter

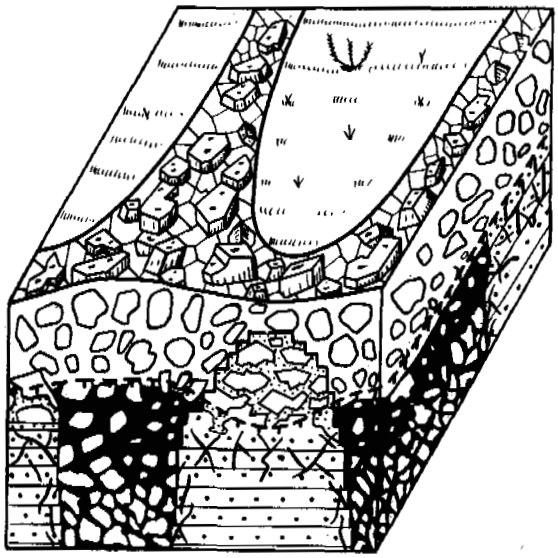

Fig.2 A slope segment of the unfavorable category with fan-shaped rock streams. Symbols as in Fig.1

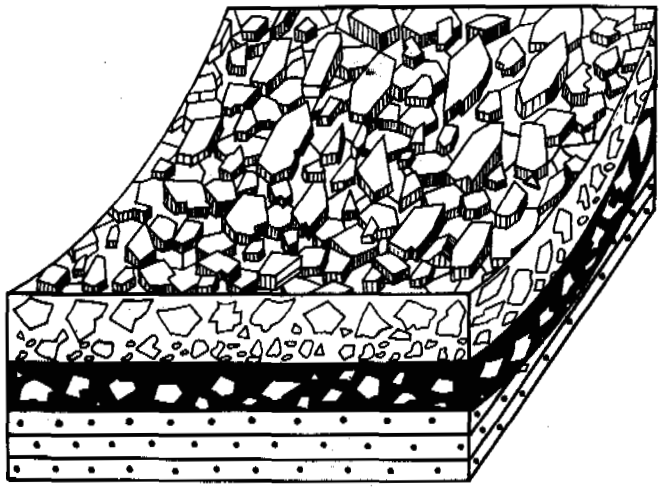

Fig.3 A slope segment of the extremely unfavorable category with fan-shaped cover rock streams. Symbols as in Fig.1

characterizes the category of slope segments from the engineering-geological standpoint. If such maps are fairly simple they can be combined into one map.

DEVELOPMENT AND THAWING OF ICE-RICH PERMAFROST AROUND CHILLED PIPELINES MONITORED BY RESISTANCE GAUGES

R.O. Van Everdingen and L.E. Carlson

The Arctic Institute of North America, Calgary, Canada T2N 1N4
L.E.C. Engineering Ltd., Calgary, Canada T2K 4R5

SYNOPSIS Data from electrical-resistance freezing gauges installed alongside three test sections of chilled, buried pipeline show development of frost bulbs around the pipes; development of increasing ice contents with time; and progressive melting of excess ice and thawing of the ground after the shutdown of chilling.

INTRODUCTION

The Calgary Test Site

In early 1974, the Calgary Frost Heave Test Facility was constructed by Canadian Arctic Gas Study Ltd., to study the potential development of frost heave around chilled, large-diameter pipelines buried in unfrozen, frost-susceptible soils. The initial installation consisted of four pipe sections (CONTROL, GRAVEL, DEEP-BURIAL and RESTRAINED), each 1.22 m in diameter and 12.2 m long, through which refrigerated air at atmospheric pressure could be circulated at a temperature of about -12°C. Additional details of the test installation, site layout, and summaries of test results can be found in Slusarchuk et al.(1978) and Carlson et al. (1982). The latter presented an interpretation of the heave history to the end of 1980.

Operation of the test site started on 20 March 1974. The CONTROL section was removed in the fall of 1977. The facility was taken over by Foothills Pipe Lines Ltd. at the end of 1977. Two additional insulated pipe sections were activated in February 1979. Chilling was discontinued on 24 February 1986 and shortly thereafter the DEEP-BURIAL section was excavated to enable inspection of the frost bulb around the pipe. The remainder of the facility was dismantled in October 1986.

Resistivity Measurements

Installation of electrical-resistance freezing gauges in the test site was to serve two purposes. First, the test site provided an excellent opportunity for testing the long-term performance of this type of freezing detector. As at least some excess ice could be expected to form in the frost bulbs around the chilled pipe sections, the test site also presented a chance to establish whether the growth of ice-rich permafrost would be reflected in a gradual increase in measured resistance values.

FREEZING GAUGES

Instrumentation

Three freezing gauges of the Type II variety described by Banner and van Everdingen (1979) were constructed as shown in Figure 1.

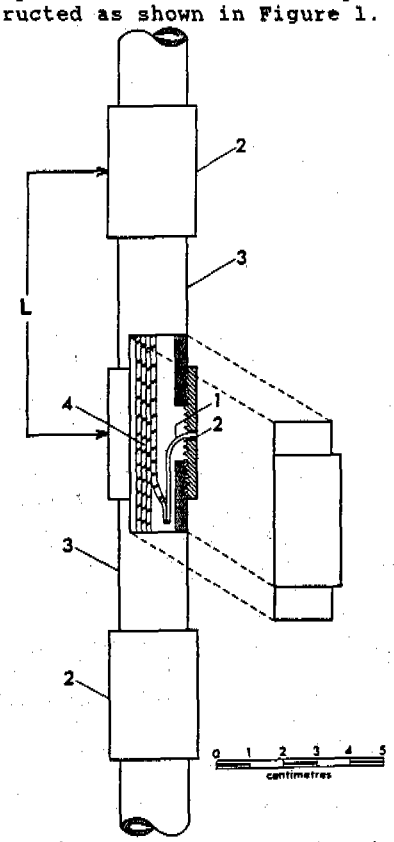

Fig. 1 Freezing gauge construction (after Banner and van Everdingen, 1979). 1 - soldered wire stubs; 2 - galvanized steel pipe couplings; 3 - threaded PVC nipples; 4 - connecting wires. Joints waterproofed with Teflon tape. L - effective electrode interval.

Each gauge carried 52 electrodes, with gaps between adjoining electrodes varying from 10 to 126 mm (effective electrode interval L varying from 60 to 176 mm). The lengths of the gauges ranged from 3.93 to 4.58 m. A special 72-Hz Wheatstone bridge with phase-sensitive detector and automatic gain control was used to measure resistance between pairs of adjoining electrodes on each gauge.

The freezing gauges were installed beside three of the original buried pipe sections (CONTROL, GRAVEL, and DEEP-BURIAL). Each gauge was positioned 1.2 m from the pipe centre line, on the same side of the pipe as the prime thermistor string, but 2.9 m closer to the cold inlet end of the pipe.

Readings were taken approximately weekly from 26 February 1974 until 7 October 1977; monitoring was resumed in May 1985 and continued until late September 1986, to cover the period preceeding and following the shut-down of the chilling plant.

Data Conversion

Readings from the three-digit readout on the ten-turn balancing potentiometer of the Wheatstone bridge were converted to resistance values, using the calibration curve for the instrument. Apparent resistivity values (r) in ohm.metres were then calculated using the equation

$$r = (R * A) / (100 * \log L) \qquad [1]$$

where R is measured resistance in ohms, A is electrode surface area in cm², and L is the effective electrode spacing in mm (see Fig.1). Equation [1] is based on the results of tests using various electrode spacings in containers filled with saturated soil material from the test site, and in a water-filled column.

DISCUSSION OF RESULTS

As the freezing gauge installed in the GRAVEL section provided the most complete record of changes in resistivity during the operation of the test site, the results from this gauge are used as the basis for this discussion.

Resistivity vs. time curves for selected electrode intervals from 0.10 m above to 1.77 m below the base of the pipe, for the two periods of observation (1 March 1974 to 7 October 1977; 9 May 1985 to 28 September 1986), are shown in Figures 2 and 3, respectively. Resistivity vs. depth curves are shown in Figure 4 for selected dates between 1 March 1974 and 24 February 1986 (termination of chilling), and in Figure 5 for selected dates during the thaw period. The progress of initial freezing from 0.20 m above to 1.77 m below the base of the pipe, and the progress of complete thawing in the interval from 1.26 m above to 0.62 m below the base of the pipe, are shown in Figures 6 and 7, respectively, together with 0°C points for the prime thermistor string.

As expected, the effects of seasonal variations in temperature (and in moisture content in the soil) on resistivity were extreme for the upper few electrode intervals, but they were gradually attenuated with depth. The sudden sharp rise in resistivity for each of the deeper electrode intervals some time after the start of chilling on 20 March 1974 (Fig.2) reflects the onset of freezing and the development of the frost bulb around the chilled pipe. After the initial rapid increase, resistivity values continued to rise more slowly for some time, reflecting the gradual decrease in unfrozen water contents as temperatures dropped farther below 0°C.

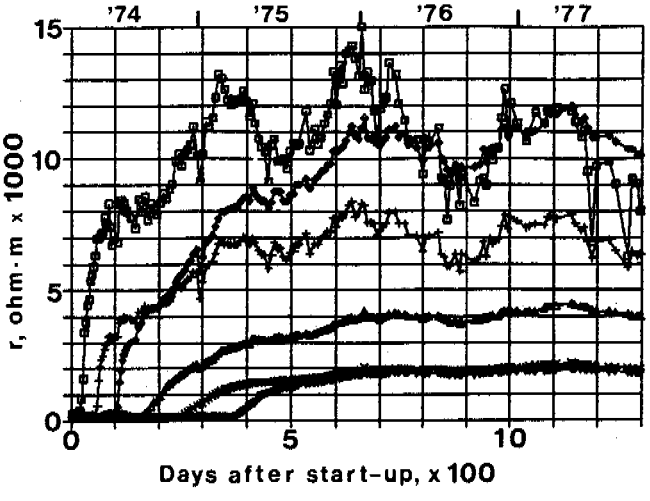

Fig. 2 Resistivity vs. time during freezing, for electrode intervals centred at:
□ +0.10 m; + -0.51 m; ◇ -0.93 m;
△ -1.20 m; × -1.42 m; ▽ -1.77 m,
relative to the base of the pipe.

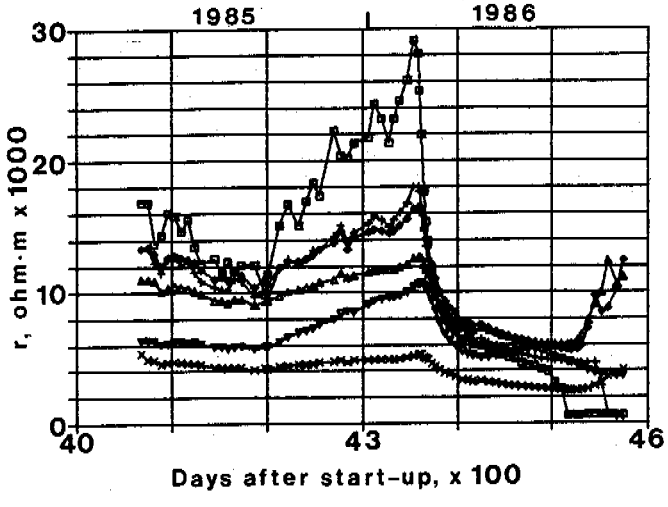

Fig. 3 Resistivity vs. time during thawing, for electrode intervals centred at:
□ +0.10 m; + -0.51 m; ◇ -0.93 m;
△ -1.20 m; × -1.42 m; ▽ -1.77 m,
relative to the base of the pipe.

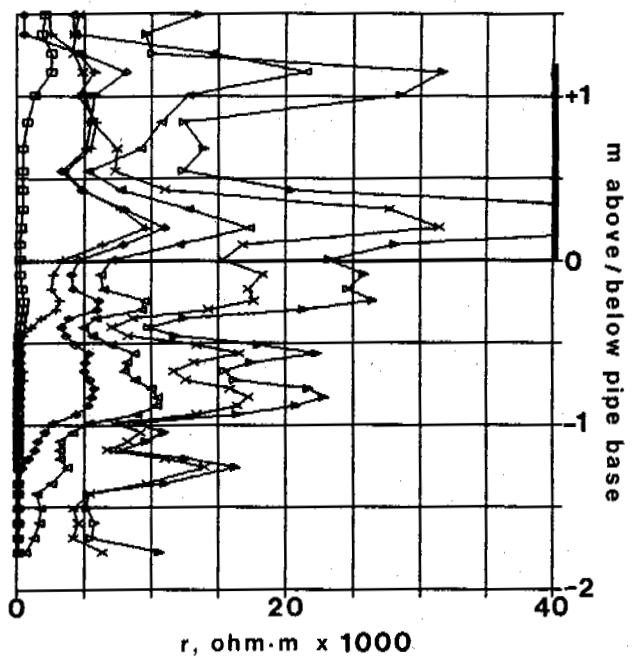

Fig. 4 Resistivity vs. depth during freezing on: □ 1 March 1974; + 9 May 1974; ◇ 24 Sept. 1974: ◁ 30 April 1975; × 9 May 1985; ▷ 24 Febr. 1986.

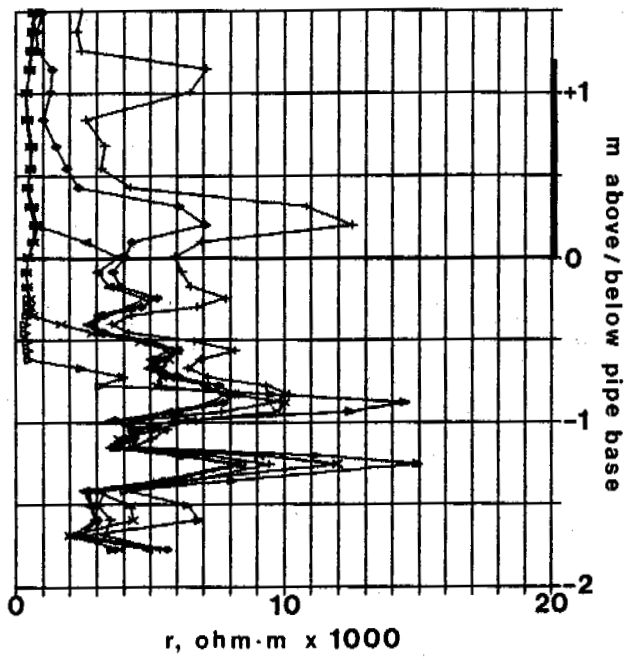

Fig. 5 Resistivity vs. depth during thawing on: + 14 April 1986; ◇ 27 June 1986; ◁ 25 July 1986; × 29 Aug. 1986; ▷ 28 Sept. 1986.

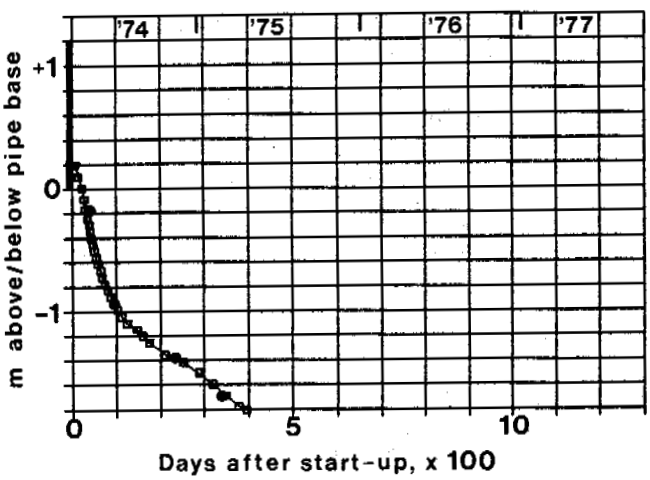

Fig. 6 Penetration of freezing vs. time. Black dots: arrival of 0°C isotherm, based on thermistor readings.

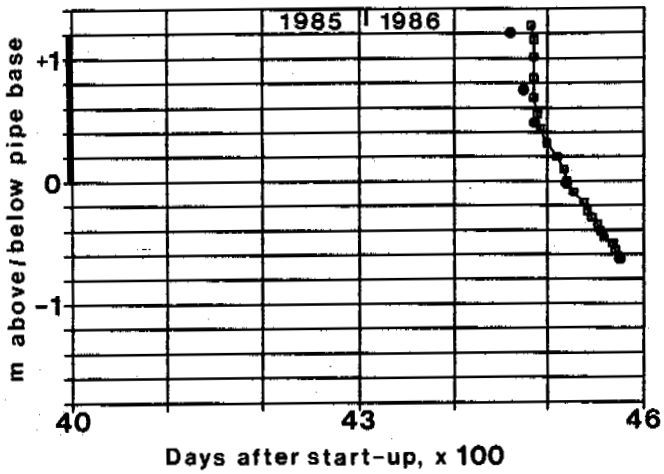

Fig. 7 Penetration of thaw vs. time. Black dots: arrival of 0°C isotherm, based on thermistor readings.

The larger than average increases in resistivity for some of the electrode intervals (e.g curve C in Fig.2; Fig.4) are interpreted as indicative of either the formation of segregated ice and ice lenses or, close to the pipe, the lower unfrozen water contents caused by lower temperatures. The general increase in resistivity values during the period between October 1977 and May 1985 (days 1297 and 4068, Figs.2 and 3) is interpreted as reflecting the formation of additional segregated ice.

The sharp temporary drop in resistivity shown by curves A and B in Figure 2 around day 288 reflects a rise in soil temperature, and hence unfrozen water content, caused by a temporary shut-down of the chilling plant beteen Christmas and New Year's Eve 1974. The effect of the shutdown extended from 1.97 m above to 1.26 m below the base of the pipe. Two similar dips in resistivity shown by the same curves on days 1177 and 1241 (Fig.2) probably have a similar origin. In those instances the effects extended from 1.26 m above to 0.65 m below the

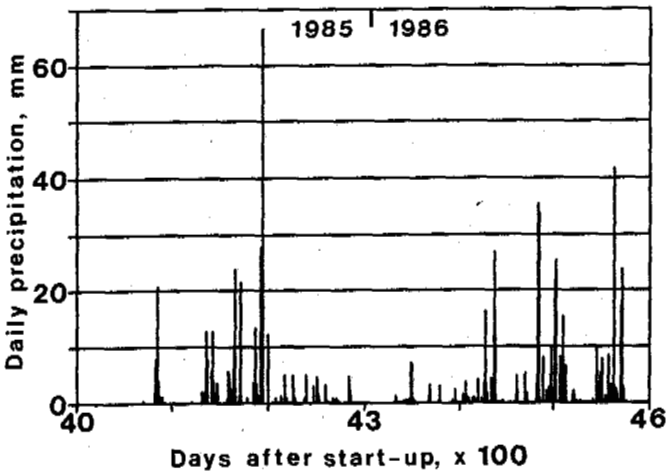

Fig. 8 Precipitation at the University of Calgary weather station near the test site, for the period 9 May 1985 to 28 September 1986.

base of the pipe. A sharp, short-lived dip in resistivity is also shown by curve A in Figure 3 around day 4198 (15 September 1985). It followed a two-day rainfall of 95 mm on 11 and 12 September 1985 (Fig.8). The effect extended from 0.55 m above to 0.29 m below the base of the pipe. As the resistivity at and near the ground surface was not noticeably affected it is likely that the cause was a wheather-related refrigeration problem, rather than the infiltration of rainwater.

The effect of the shut-down of the chilling plant on day 4359 extended to a depth of 0.8 m below the base of the pipe within 24 hours (Fig.3). For the electrode intervals between 1.2 m above and 0.8 m below the base of the pipe, resistivity values dropped at a gradually decreasing rate (reflecting decreasing thermal gradients), which accelerated suddenly into a steep drop from some value between 5000 and 2000 ohm.m to the range for unfrozen soil (between 100 and 500 ohm.m). The time lag between the arrival of the 0°C isotherm and the apparent completion of thawing between 1.3 and 0.5 m above the base of the pipe, indicated in Figure 7, may have been due to a lack of water saturation in that portion of the soil until after the rainstorms of 28 and 29 June 1986 (days 4483 and 4484, Fig.8).

Several of the intervals more than 0.8 m below the base of the pipe showed increases in resistivity after 15 August 1986 (day 4530; curves C and D in Fig.3; curves E and F in Fig.5). The only tentative explanation that can be offered for this phenomenon at this time is that some of the water released during warming of the frozen soil (below 0°C) may have moved and then refrozen to be incorporated into several of the existing ice lenses.

The patterns of changes in resistivity revealed by the freezing gauges in the CONTROL and DEEP-BURIAL sections are similar to that shown here for the gauge in the GRAVEL section. Maximum resistivity values were somewhat lower in the CONTROL section, and somewhat higher in the DEEP-BURIAL section, compared with those for the GRAVEL section. In the DEEP-BURIAL section, the effect of the chilling-plant shut-down extended to a depth of 1.16 m below the base of the pipe within 24 hours.

CONCLUSIONS

Electrical-resistance freezing gauges provide a practical means for monitoring of both natural and man-induced ground freezing.

The onset of freezing is indicated by a sudden rapid increase in the measured resistance (and thus resistivity) values for individual electrode intervals.

Gradual reduction of the unfrozen water content of the soil due to decreasing temperatures after initial freezing is reflected by a slower further increase in resistivity. This effect is strongest close to the chilled pipe.

Progressive development of segregated ice in the soil is indicated by larger than average increases in resistivity.

Thawing is indicated by a return of the resistivity to values for unfrozen soil. During thawing the resistivity drops at an initially rapid, but gradually decreasing rate.

Although variable electrode spacing complicates data conversion, it may be attractive in certain applications.

ACKNOWLEDGEMENTS

Canadian Arctic Gas Study Ltd., Canada Department of the Environment, Foothills Pipe Lines Ltd., and Canada Department of Energy, Mines and Resources have contributed to various aspects of this study at various times.

REFERENCES

Banner, J.A., & van Everdingen, R.O. (1979). Frost gauges and freezing gauges. Inland Waters Directorate, Environment Canada, NHRI Paper No. 3, 18 pp.

Carlson, L.E., Ellwood, J.R., Nixon, J.F. & Slusarchuk, W.A. (1982). Field test results of operating a chilled, buried pipeline in unfrozen ground. Proc. 4th Can. Permafrost Conf., National Research Council of Canada, Ottawa, 475-480.

Slusarchuk, W.A., Clark, J.I., Nixon, J.F., Morgenstern, N.R. & Gaskin, P.N. (1978). Field test results of a chilled pipeline buried in unfrozen ground. Proc. 3rd Int. Conf. Permafrost, National Research Council of Canada, Ottawa, (1), 877-883.

THE ORIGIN OF PATTERNED GROUNDS IN N.W. SVALBARD

B. Van Vliet-Lanoe

Centre de Géomorphologie du C.N.R.S., Rue des Tilleuls – 14000 Caen, France

SYNOPSIS - Different theories exist concerning the cryoturbation process. This paper develops and demonstrates that the dynamics of the most frequently occuring patterned grounds results from differential frost heave. This differential heave is controlled by 1) the drainage and thermal conditions and 2) the **gradient** and the **contrast of frost susceptibility.** Loadcasting and cryostatic pressures are strictly restricted to poorly drained soils characterized by an unstable cryogenic fabric (such as pure silts or silty sand textures) on a base of permafrost or shallow bedrock. The other sediments are normally stable. The translocation of fine particles during melting can promote frost susceptibility in a previous nonsusceptible coarse material. Most of the patterned grounds and cryoturbations can be easily explained by the frost susceptibility gradient related to the prevailing drainage conditions.

INTRODUCTION

Most studies of periglacial phenomena, either active or relict, are usually restricted to the most evident features. But the most common, albeit hidden process acting, in a cold environment is ice lensing. Ice lensing is the motor of frost heave mainly controlled by the drainage and the thermal gradient ; for these reasons, it is the basis to periglacial deformations (i.e. cryoturbations), both on slopes and on flat topography.

The drainage conditions under which patterned ground and cryoturbations can develop is rarely correctly studied in active conditions. Although one can ready find displacement measurements in the litterature, it is very difficult to find information on, for example the autumn position of the water table. It is the reason why we have made a detailed mapping of patterned ground, the late summer conditions in Svalbard being very close to those prevailing at the onset of the frost season.

The cryogenic aggregation or fabric of sediments resulting from ice lensing is important because it is responsible for the enhancement or inhibition of various mechanisms such as load casting by its behaviour (stability) during either or both of the melt and or the freeze-back seasons. This is expressed mainly in the form of induced modifications of the hydraulic conductivity. It has been mentioned in active forms by soil scientists. A micromorphological approach (petrographical analysis of consolidated undisturbed soft samples) allows easy recognition of the traces and, more specifically, of the locations of the ice lenses. This approach permits us :

1) identification of the annual sequence of plastic soil deformations related to frost, and the translocation of particles during melt,

2) identification of the progression of the freezing front by the successive positions of the ice lenses, consecutive to differences in moisture content related to textural composition,

3) and identification of the dominant mechanism behind cryoturbation related to the stability of the cryogenic fabric.

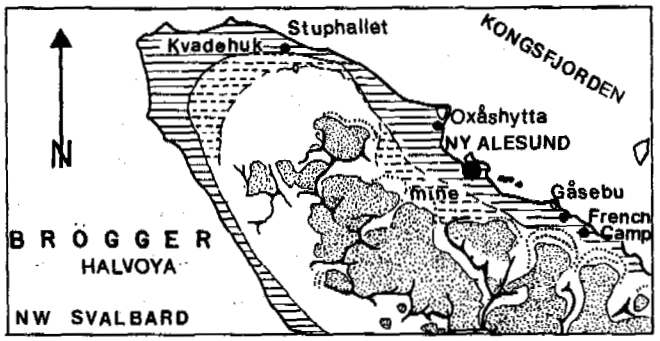

Fig. 1 - Location map of the investigated sites related with the different glaciomarine deposits : holocene (continuous hatching) and preholocene (broken hatching)

THE ROLE OF DRAINAGE QUALITY

Because topography and lithology give a range of both periglacial patterned ground and drainage conditions, a small area located to the Gåsebu house on the northern slope of the Brögger Peninsula was mapped in detail at a reduced scale. The sediments and topography result mainly from the early holocene history (Corbel, 1961 ; about 9000 y. BP) with some recent (± 80 years) aeolian deposits (Van Vliet & Héquette, 1987). Dolomitic limestone bars enclose glacio-marine deposits, which form fossil islands in the Kongsfjord, now stranded by prograding Atlantic sandur (Brossard & Joly, 1986). Other sites were also investigated, Kvadehuksletta, the Stuphallet flat, Oxåshytta and the mining sector of Ny Alesund, but only from a dynamical approach.

Drainage classes were adapted (Van Vliet, 1983) to freezing soils ; they are different from those of the Soil Survey Manual (1965) because the autumn position of the water table and the thermal gradient control the intensity and the shape of frost heave. Knowledge of the spring and summer positions of the water table is inrelevant because most Arctic soils are waterlogged during the melt

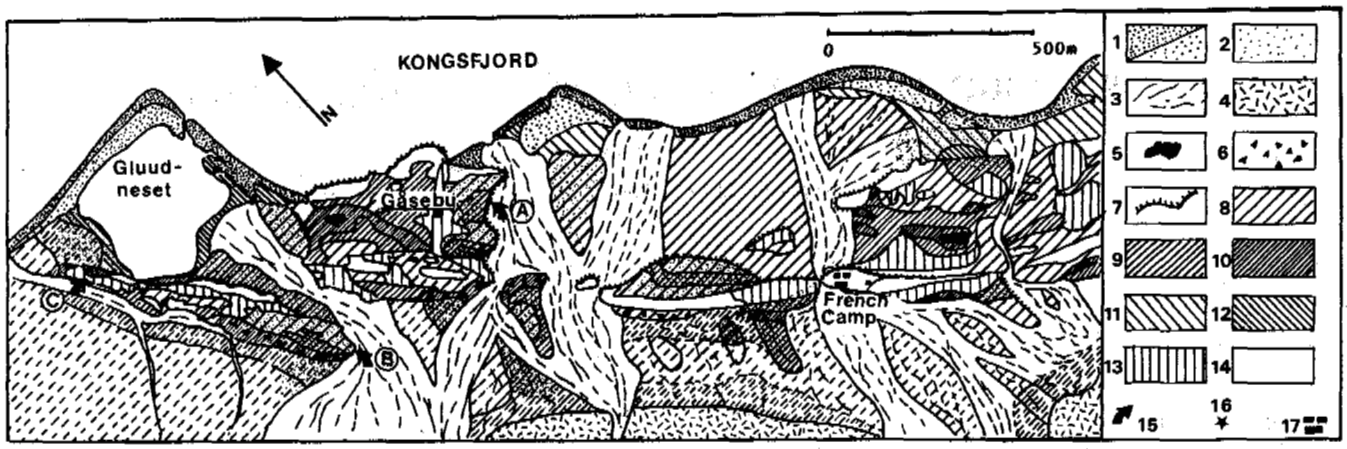

Fig. 2 - Superficial drainage map of the Gåsebu sector, Brogger Peninsula Svalbard - 1a/b. active-inactive beaches ; 2. aeolian sand ; 3. sandur ; 4. morainic arc ; 5. permanent pond ; 6. frost heaved blocks ; 7. cliff ; 8. moderately drained ; 9. imperfectly drained ; 10. poorly drained ; 12-13. moderately to imperfectly drained brackish soils ; 14. limestone outcrop ; 15. investigation sites ; 16. thermal recording station ; 17. buildings

season and drained in summer. Textural conditions depend upon both the level of capillary rise in sediment, its mineralogical composition, its organic content and its cryogenic fabric (interaggregate porosity ; Van Vliet, 1983, 1985).

Five drainage classes were defined (table 1) :

In the first three classes, microrelief remains flat. The most common patterned ground forms are related to class 3, in sediment with an autumn water content close to the field capacity or slightly higher. On the other hand, if drainage improves for topographic or other reasons (texture), low center forms can evolve to high centred ones as sounded by Zoltai & Tarnocaï (1981).

TABLE I

Drainage classes	Morphology
Shallow pound	Palsas
Poorly drained soil with shallow water table at less than 5 cm in sands or with a surficial pF value < 1	Flat mudboil or stone circles, poorly expressed ; low centre polygons, heaved blocs
Imperfectly drained soil with a capillary fringe allowing a stable field capacity in surface (1 < pF < 2.5, excepted in organics)	Most of the patterned grounds associated with a flat microtopography
Moderately well drained soil with a capillary fringe allowing a stable field capacity at 50 cm in depth. Surface pF is usually above 2.5	Hummocky soils, high center patterned ground
Well to extremely well drained soil ; no detectable water table. Profile only slightly humid (normal surface pF > 3)	

This relationship between drainage and related morphology have also been observed at other sites in the Brögger and also in the lower Advental. It has also been recently confirmed by Walker (1985, N.W. Canada).

CRYOTURBATION DYNAMICS IN GASEBU

The lithostratigraphic units affected by cryoturbation in this site consist basically of recent aeolian stratified fine sands, rather silty and humic, resting mainly on an early Holocene littoral complexe whose stratigraphy has been detailed elsewhere (Van Vliet & Héquette, 1987).

In the main profile (site A, fig. 2) three types of profiles exist : - fine stratified sand resting on coarse sands and gravel ; - fine sand resting on humic silts, a former paleosol existing at the top of the lower complex ; - fine sand resting on pink dolomitic silts resulting from the weathering and frost shattering of carboniferous dolomitic limestones. Those three facies coexist in the same drainage conditions in site A. The surface of the fine sand is affected by a net of cryodesiccation fissures whose mesh ranges from 25 cm in poorly drained sites up to 50 cm in well drained ones. On this shallow net rests, a larger net of about 1 m of mesh seaming related to thermal cracking ; it is sensitive to the permafrost table, normally at a depth of 80 cm. Continuous thermal recording performed in this site during the years 1982-1983 has shown 1) a water table position close to the base of surficial fine sand at the freeze-back season and 2) only one effective freeze-thaw cycle each year.

This site shows clearly the role of differential heave in the formation of cryoturbations:

a) The proximity of a water table in depressions influence differential frost heave of various textured sediments : the rigidity of frozen wet surficial horizon induces a flat microrelief and obliges differential heave pressures to develop, mainly in a downward direction. This induces injection of the unfrozen underlying sediment along weakness zones : here in the two nets of fissures, normally open in late summer (Van Vliet, 1983) as shown by presence in it of entire leaves of dryas or willow. This injection occurs little by little, independent of the density or frost susceptibility gradients of the different layers :

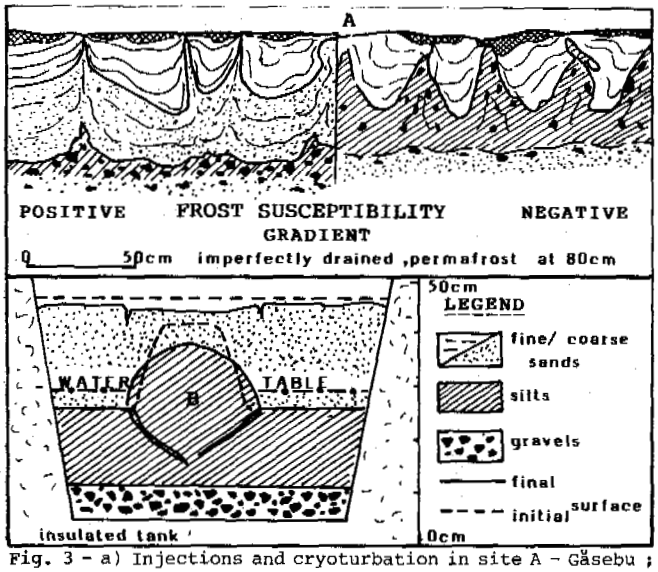

Fig. 3 - a) Injections and cryoturbation in site A - Gåsebu ; b) Injection experiment in Caen Laboratory (25 freeze-thaw cycles)

we have observed at 50 m distance (fig. 3a) injections of silts between prisms of fine sands in two profiles, although in another site it is the coarse sand which appears to be injected. These observations reduce considerably the importance of the load casting.

This surface rigidity has been reproduced experimentally in the Caen laboratory, both in the presence of a slope and in the presence of a flat topography with an high water table (Van Vliet, 1987a). This latter experiment, performed in a medium size cell (fig. 3b), suggested that, in absence of weakness, injections may not occur infine textured sediment on flat topography. Injections were also produced by chance in an earlier experiment (Coutard & Mücher, 1985).

b) At **drained sites**, the differential heave resulting from subtile differences in moisture content related to the microrelief, to a discrete vegetation cover as proposal by Williams (1962), or more commonly to variation of the texture and of the organic content (Tsytovich, 1975 ; Van Vliet, 1986). This differential heave enables the formation of hummocky microrelief as shown in figure 4. Deformation is different from that in poorly drained aera ; the prisms of fine sands defined by the desiccation net evolves to a rugby football shape ; infilling of the fissures produces humic wedges. On the same slope, in the lowest zone, this humic accumulation deforms to a drop-like feature (fig. 4b).

This style of deformation may also be relevant at a larger scale, for example in the infill of trenches of large size polygones. The hummock relief results from the summation of all the stresses accumulated during freezing (cryogenic fabric and differential heaving), at the outset of thawing (refreezing ice ; Mackay, 1983) and by desiccation in summer. This situation is summarized in figure 5. Notice that this sum of stresses is the same as with gilgaï formation in swelling clays (Van Vliet, 1987a).

c) **On slope** the deformation of cryoturbations or hummocks are related to the drainage quality and frostcreep as shown in figure 6 (Van Vliet, 1987b). Supplementary deformations are related to

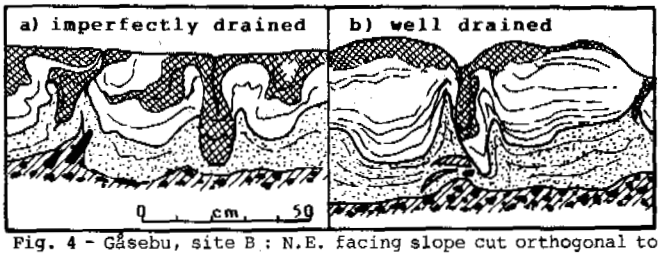

Fig. 4 - Gåsebu, site B : N.E. facing slope cut orthogonal to the slope - a. downslope : flat microtopography - b. upslope : hummocky microrelief

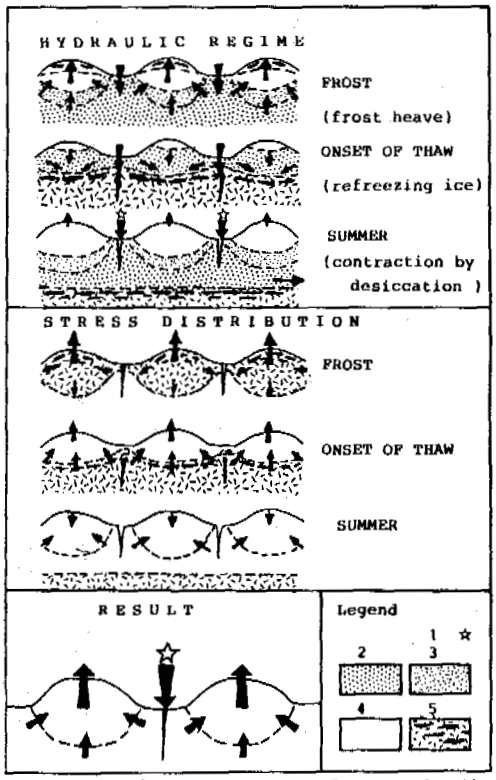

Fig. 5 - Frost dynamics and geometry of stress leading to the occurence hummocky microrelief. Permafrost is not necessary 1) imported matters ; 2) wet ; 3) moist ; 4) dry ; 5) frozen + ice lenses

microslipping over ice lenses (Van Vliet, 1982) which are related to their abundance (Rein & Burrous, 1980 ; Mackay, 1983). In these conditions, the desiccation cracks evolve into pseudo-shear planes.

d) **In thin sections**, the injection patterns show clearly :

1) Preservation of traces of ice lenses after deformation. They occur in both injections or in hummocky soils and suggest the existence of internal pressure during the lowering of the freezing front and an usual absence of liquefaction, even in sand or silt (fig. 7, left),

2) Thin sections also show that injected silts (fig. 7, right) present traces of ice lensing bending in the direction of the less susceptible material.

This is to be expected as the normal behaviour of freezing soils. Moreover, in this very unstable

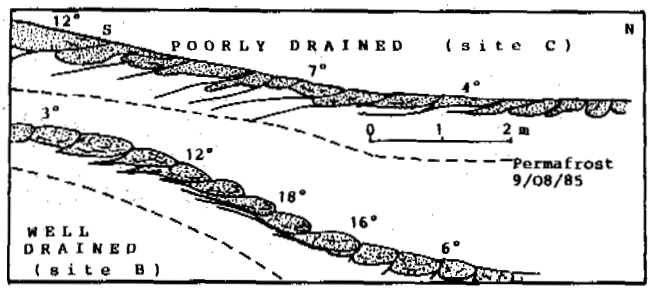

Fig. 6 - Deformation of cryoturbations and hummocks on slope. Gåsebu sites

material, traces of ice are still preserved. This situation has also been reproduced experimentally in Caen.

These observations show that ice lensing occured after the deformations induced by cryostatic pressures which, in turn, were created by differential heave. Liquefaction and load casting were ineffective even in wet soils. The origin of cryoturbation is not to be found in loadcasting theory as proposed by Cegła and Dzułinski (1967) ; Van Den Berghe and Vandenbroeck (1982) or Mackay (1983), although it could exist in some exceptional conditions favouring the destabilization of the cryogenic fabric.

THE FROST SUSCEPTIBILITY GRADIENT

These observations enable one to propose a new theory complementary to that of differential frost heave, as proposed by Sharp in 1942, supported by the observations of Dylikowa (1961) and partially demonstrated by the experiments of Corte (1972) and particularly those of Pissart (1982). In 1985 we proposed this of **frost susceptibility gradient.** If surface material is more frost susceptible than underlying sediment (via difference in clay silt or organic content), **gradient** will be **positive** ; here injections are not able to reach the surface, but deform to a diapiric shape (fig. 9) because of the rigidity of the surface layer caused by frost.

If the surface sediment is less susceptible than the underlying, the **gradient** is **negative** and the injected sediment heaves more rapidly than the surface layer ; it is able to burst through to the surface to form a mudboil as observed by Pissart (1976) on Banks Island (N.W.T. Canada).

The observations made in the other sandy sites of the Brogger follow the same laws(Oxåshytta, Stuphallet, mining zone of Ny Alesund).

This hypothesis, especially in the presence of a positive gradient, can be extended to explain contiguous stone circles as the result of bedrock along cracking patterns (fig. 9).

PATTERNED GROUND IN STUPHALLET AND KVAKEHUK

a) The imperfectly drained site of the **Stuphallet** shows a flat microtopography. In this place, a yellow lagoonal dolomitic sand rests on a thin layer of glacio-marine gravel underlain by a red glacio-marine silty clay : this site presented initially a negative gradient of frost susceptibility.

Irregularities in the surface of the red clay and these of thermal contraction cracks are similar to the Gasebu site, but on a larger scale. At the intersection of the cracks, red clay heaves and finally burst through the surface of the sand. The

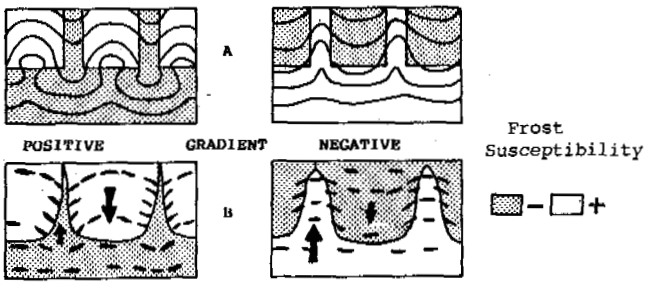

Fig. 7 - Relation between (A) the successive locations the 0° C isotherms (theoretical) controlled by the frost susceptibility and (B) these of the ice lenses observed in thin sections. Dominant heave

heaving of the red clay improves surficial drainage as shown by changes in lichen. Normally, a black cryptogamic crust covers the soil surface. When the clay reaches to within 25 cm of the surface, direct watersupply from the water table is stopped and the crust changes to grey lichen. With times, the interfacial gravel layer burst first, rapidly followed by a central red mudboil. In mature forms, mosses can invade the gravely circle but not the boil.

Micromorphological investigations show that the cryogenic fabric remains stable throughout the red clay profile, even in the surficial horizon. This shows that load casting or convectional theories are unacceptable in this case.

As a conclusion this early Holocene site can easily produce coalescing stone circles or mudboils in imperfectly drained sites in about 9000 freezing cycles.

b) In the vicinity of **Kvadehuk**, in the same age and drainage conditions, mature stone circles can occur. Here, as in other sites on the Brogger, the fine matrix is formed by residual silt (frost shattering and differential dissolution of beach pebbles and rock outcrops in dolomitic limestone) which has been illuviated in depth by melt water and freeze-thaw translocation (Van Vliet, 1983). This feature, demonstrated by Forman and Miller (1984) in this area, produces at depth an highly frost susceptible matrix and in the surface, a dry unconsolidated gravelly layer. In this contrasted situation (experiment at the Caen Station), the differential frost heave of the silt can easily protrude through the surface gravel, enlarge and finally become coalescing. The micromorphology shows the partial conservation in depth of the traces of ice lenses (more or less preserved following the clay content in the matrix) inside the mudboil ; a vesicular horizon occurs at the contact of the stone circle, even in depth, and in the surface 20 cm of the boil ; it results from the local rapid thawing of the material with the consequent collapse of the cryogenic fabric (Van Vliet *et al.*, 1984). As before, it is believed that stone circles the evolution sand mudboil is controlled by drainage variation.

The **contrast** of frost susceptibility acts as an accelerator compared to the Stupphalet site. Moreover, in such contrasted cases, a previously weakness seems unnecessary to produce a boil. The existing contrast may be originally present, inherited from stone frost-jacking (formation of a stone pavement in depression) or produced as in of most of the cases by debris translocation in depth. Here load casting and convectional theories

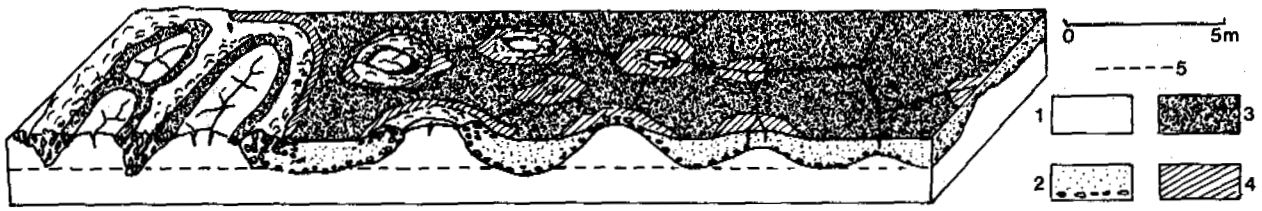

Fig. 8 - Differential heave and growth of the stone circles of the Stuphallet flat - 1. red glacio-marine silty clay ; 2. lagunal gravel and sands ; 3. black cryptogamic crust ; 4. grey lichens ; 5. observed level of the water table (20.9.85)

as proposed by Prestrud and Hallet (1986) are inapplicable.

c) Granulometric analysis undertaken on circles and stripes show a **translocation of clay** at depth as already observed by Schmertmann & Taylor (1965) ; this is not only the result of unsorted accumulation of frost shattering products but results mainly form a preferential translocation of clays in depth of the suspension created by the destruction of cryogenic fabric (Van Vliet, 1985) in surface horizons. A textural accumulation forms above an hydraulic conductivity boundary, in this case the permafrost. This feature occurs also in other sediments like in till (Locke, 1986). Their consequences are :
1) an increase in stability of the cryogenic fabric in depth or downslope position associated with an increase in frost susceptibility,
2) and a lost of fabric stability and of frost susceptibility in the superficial and upslope horizons associated with a propensity to thixotropy and mud flow.

These particle translocations lead progressively to a negative gradient of frost susceptibility. This explains the omnipresence of inactive circles on old Arctic surfaces. The feature becomes inactive when the top of the fines accumulation becomes so deep to escape the injection process.

d) **On slopes**, this sketch remains valuable, as in the case of cryoturbations ; by the progressive creation of negative gradient, mudboil can protrude through a scree surface as on profile nearby Blomstrand peninsula (Herz & Andreas, 1966). These features are particulary common in zones of drainage concentration, leading sometimes to rows of mudboils aligne along the main seepage lines.

CONCLUSIONS

The systematic use of micromorphological techniques leads us to conclude hat differential frostheave is the main mechanism responsible for both cryoturbation and patterned ground genesis.

- The **rigidity of wet surfaces by frost**, already advocated by many authors (Washburn, 1969 ; Shilts, 1973, 1978) is very important, but it is here related with poorly to imperfectly drained soils, with differential heave and cryogenic pressure to explain the evolution of microtopography. The position of the water table in autumn is of prime importance.

- The **role of permafrost is limited** ; it essentially keeps especially in autumn water table in the soil surface vicinity in porous sediments (cryogenic fabric).

- The complementary information given by the **type of frost susceptibility gradient** leads to an easy understanding (fig. 9) of the dynamics of injection and pattern acquisition in soils affected by weaknesses such as thermal or desiccation nets.
- A marked **contrast of frost susceptibility** seems to act as an accelerator. In this case, and if gradient is negative, the sometimes loose character of surficial layer leads to formation of coalescing circles without a necessary net of craks.

- This common sketch of evolution of cryoturbated soils fits very well with the previous observations of Hopkins & Sigafoos (1950) which were amongst the first to show that patterned grounds corresponded to cryoturbations in profiles.

- Our sketch presents also the advantage that it takes into account the textural evolution of a sediment affected by a cryogenic diagenesis and the modifications of its frost susceptibility with aging of the topographical surface.

AKNOWLEDGMENT

This work was financially supported by the french CNRS "GIS-Arctique" and Centre de Géomorphologie where the analytical datas, the experimental researches and the dactylography were performed. We thank the following organisms for their logistical help : the Norsk Polar Institute, the Kingsbay Kull Company, Elf Norge, the french Ambassy and the Compagnie Paquet. We thank also John Mitchell (Ottawa) for improving our translation.

REFERENCES

BROSSARD, Th & JOLY, D, 1986. Le complexe géomorphologique aval des glaciers Loven Est et Central (Spitzberg). Cahiers de Géographie de Besançon, 29, (2), 5-58

CEGLA, J.R. & DZULYNSKI, S., 1970. Systems with reversed density gradient and their occurence in periglacial zones. Acta Univ. Wratisl., Studia geograf., 13, 17-39

CORBEL, J., 1961. Morphologie périglaciaire de l'Arctique. Annales de Géographie, 70, 1-24

CORTE, A., 1972. Laboratory formation of extrusion features by multicyclic freeze-thaw in soils. Bull. Centre Géomorphologie CNRS, Caen, n° 13, 14, 15, 157-182

COUTARD, J.P. & MUCHER, H.M., 1985. Deformation of laminated silt loam due to repeated freezing and thawing. Earth Surface Processes and Landforms, 10, (4), 309-319

DYLIKOWA, A., 1961. Structures de pressions congélistatiques et structures de gonflement par le gel près de Katarzynow près de Lodz. Bull. Soc. Lettres Lodz, 12, (9), 1-23

FORMAN, S. & MILLER, G., 1984. Time dependent soil morphologies and pedogenic processes on raised beaches, Bröggerhalvoya, Spitzbergen Svalbard archipelago. Arctic and Alpine Research, 16, (4), 381-394

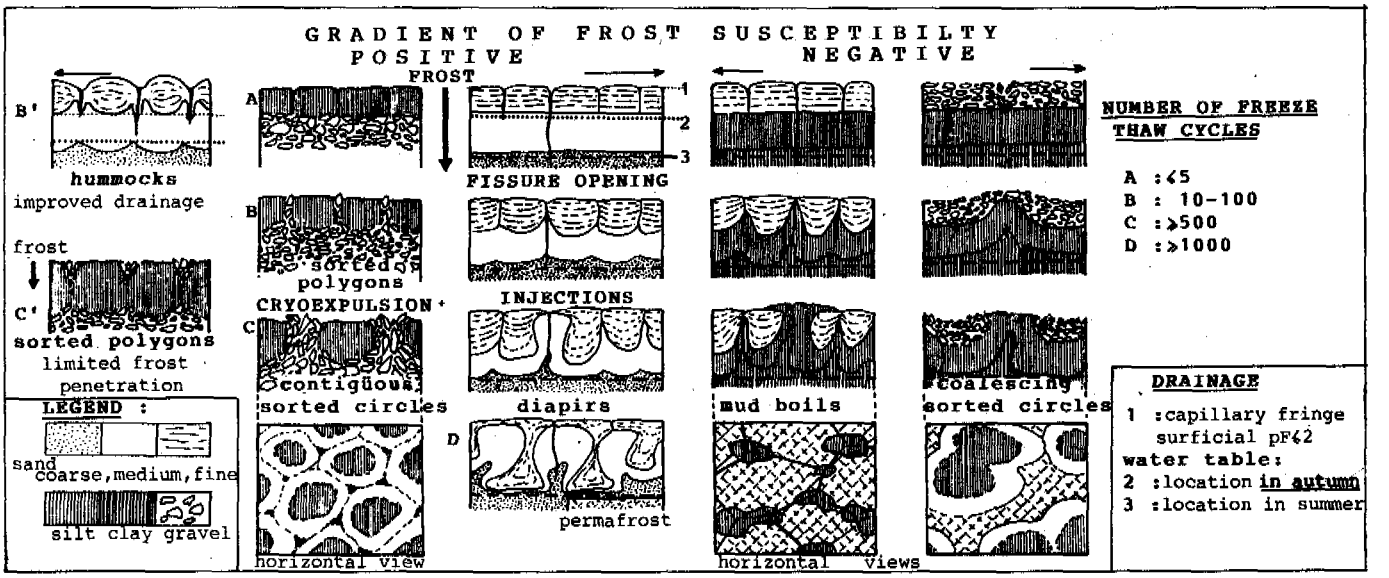

Fig. 9 - General sketch of cryoturbations and patterned ground development

HALLET, B. & PRESTRUD, S., 1986. Dynamics of periglacial sorted circles in Western Spitzbergen. Quaternary Res., 26, (1), 81-99

HERZ, K. & ANDREAS, G., 1966. Untersuchungen zur Morphologie der periglazialen Auftauschicht in Kongsfjordgebiet (West-Spitsbergen). Petersmann Mitt, 110, (3), 190-198

HOPKINS, D.M. & SIGAFOOS, R.S., 1951. Frost action and vegetation patterns on Seward Peninsula, Alaska, US Geol. Survey Bull., 974-c, 51-100

LOCKE, W., 1986. Fine particles translocation in soils developped on glacial deposits, Southern Baffin Island, NWT, Canada. Arctic and Alpine Res., 18, (1), 33-43

MACKAY, J.R., 1983. Downward water movement into frozen ground, Western arctic coast, Canada. Can. Jour. Earth Sc., 20, 120-134

PISSART, A., 1976. Sols à buttes, cercles non triés et sols striés non triés de l'Ile de Banks (Canada, NWT). Biul. Peryglac., 26, 275-285

PISSART, A., 1982. Déformation de cylindres de limon entourés de graviers sous l'action d'alternances gel-dégel. Expériences sur l'origine des cryoturbations. Biul. Peryglac., 29, 219-229

REIN, R. & BURROUS, C., 1980. Laboratory measurements of subsurface displacement during thaw of low angle slopes of a frost susceptible soil. Arctic and Alpine Res., 12, 349-358

SCHMERTMANN, J.H. & TAYLOR, R.S., 1965. Quantitative data from patterned ground site over permafrost. CRREL, Research Report, (96), 76 p.

SHARP, R.P., 1942. Periglacial involution in Illinois. Jour. of Geology, 50, 113-133

SHILTS, W.W., 1978. Nature and genesis of mudboils Central Keewatin, Canad. Jour. Earth Sc., 10, 1053-1068

SIGAFOOS, R.S. & HOPKINS, D.M., 1952. Soil stability on slopes in regions of perennially frozen ground. Highway Research Board, Special Report, (2), 176-192

TSYTOVICH, N.A., 1975. The mechanics of frozen ground. G.K. Swinzow editor, Scripta Books Co, Washington D.C., 152 p.

VANDENBERGHE, J. & VAN DEN BROECK, P., 1982. Weichselian convolution phenomena and processes in fine sediments. Boreas, 11, 299-315

VAN VLIET-LANOE, B., 1983. Etudes cryopédologiques au S. du Kongsfjord, Svalbard. Rapport de la Mission Spitzberg 82, public. interne Centre Géomorphologie CNRS, Caen, 39 p.

VAN VLIET-LANOE, B., 1985a. Frost effects in soils in "Soil and Quaternary Landscape Evolution". J. Boardman edit., 117-158

VAN VLIET-LANOE, B., 1986. Interaction entre activité biologique et glace de ségrégation en lentilles ; exemples observés en milieu arctique et alpin. In "Micromorphologie des sols/soil micromorphology". N. Fédoroff, L.M. Bresson et M.A. Courty édit., AFES, 337-344

VAN VLIET-LANOE, B., 1987a. Le rôle de la glace de ségrégation dans les formations superficielles de l'Europe de l'Ouest. Processus et Héritages. Thèse d'Etat, Univ. Paris I, 796 p.

VAN VLIET-LANOE, B., 1987b. Cryoreptation, gélifluxion et coulées boueuses : une dynamique continue en relation avec le drainage et la stabilité de l'agrégation cryogénique. In "Loess and Periglacial Phenomena". M. Pecsi and H.M. French edit., Akad. Kiado, Budapest, 203-226

VAN VLIET-LANOE, B., COUTARD, J.P. & PISSART, A., 1984. Structures caused by repeated freezing and thawing in various loamy sediments. A comparison of active, fossil and experimental data. Earth Surface Proc., 9, 553-565

VAN VLIET-LANOE, B. & HEQUETTE, A., 1987. Activité éolienne et sables limoneux sur les versants exposés au NE de la péninsule du Brögger Spitzberg du NO (Svalbard). In "Loess and Periglacial Phenomena". M. Pecsi and H.M. French edit., Akad. Kiado, Budapest, 103-124

WALKER, D., 1985. Vegetation and environmental gradients of the Prudhoe Bay region, Alaska. CRREL Report 85-14

WASHBURN, A., 1969. Weathering, frost action and patterned ground in the Mester Vig district, North East Greenland. Meddel. om Gronland, 176, (4), 303 p.

WILLIAMS, P.J., 1959. The development and significance of stone earth circles. Skrift. Norke Videnskaps Akademi 1, Oslo 1, Math. Naturviden. Kl., (3), 3-13

ZOLTAI, S. & TARNOCAI, C., 1981. Some non sorted patterned ground types in Northern Canada. Arctic and Alpine Res., 13, 139-151

THE STATISTICAL ANALYSIS ON FROST HEAVE OF SOILS IN SEASONALLY FROZEN GROUND AREA

Wang, Jianguo and Xie, Yinqi

Heilongjiang Provincial Research Institute of Water Conservancy

SYNOPSIS Based on a large number of experiment results in the seasonal frost areas (from N 36° to N 50.2°), the authors made a statistical analysis about the ultimate frost heave amount and presented a series of relations between the frost heave amount and its main influencing factors. The analytical results show that the ultimate frost heave amount does not increase monotonically with frost index and north latitude, but follows a random normal distribution. The relation between the underground water head before freezing and ultimate heave amount for clayey and sandy soil can be expressed by logarithmic and a linear function, respectively.

INTRODUCTION

The problem of frost heave in seasonal frost areas is one of the anticipative tasks in the field of frozen ground research. In recent years, research on this subject has deepened and the research method has been changed from unitary geographical method to the synthetical study stage, in which frozen ground is regarded as a system related to its structure, environment and function.

During frost heaving the structure of a soil (soil texture, density and water content) and the environment of the system (water supply and various engineering conditions) are subject of random fluctuation. Thus, it is difficult to get the practical indexes (parameters) for engineering with only the method of experimental soil mechanics. In view of this, the authors have made a statistical analysis on a large number of frost heave data observed from prototype engineering structure and observation sites in seasonal frost areas of China with the purpose of : (1) finding the quantitative relations between the characteristic values of frost heave of subsoil of beneath hydraulic structures and the main factors which influence them,(2) establishing the criteria for engineering classification of soils according to their frost heave behaviour, and (3) deriving the analytical equations to necessary for determining frost heave indexes to satisfy the requirements of frost heave forecasting and engineering design.

THE LIMITS AND MAIN PARAMETERS OF THE STATISTICAL ANALYSIS

The sources, types and limits of data

The data are selected from the reports of all previous National Conferences on Hydraulic Engineering and Anti-heave Technics, National Conference on Permafrost and Information Exchanging Network on Anti-heave. Amount which 98% of the data are obtained from the areas between 36 to 50.2 degrees north latitude of China. Frost information concerning alpine conditions is not included.

The principle of collecting data

All the data used in this work have given sources and belong to the same type (e.g., same soil texture, water condition and load). This ensures that the samples be random.

Main items of statistics

(1) The longitude and latitude of observation sites; (2) Soil texture including soil grain size, liquid limit ($\overline{W}_L$), plastic limit ($\overline{W}_p$), plasticity index (I_p) and specific gravity (G_s); (3) Soil classification; (4) Observation time; (5) Freezing index (one-year freezing index (F) or average freezing index ($\overline{F}$) over several years); (6) The conditions of soil water (average water content, W, in before freezing and W' in the period of reaching the maximum frost depth); (7) The conditions of underground water (including the ground water table Z (metres) in pre-freezing period and deepest water table Z' (metres) in freezing period); (8) Freezing thickness, H (metres); (9) Freezing depth (initial frozen thickness), H_M (metres); (10) Ground frost heave amount h (metres); (11) Freezing time T (days) from the date of steady freezing in the ground to the date when the maximum fros depth is reached.

THE STATISTICAL ANALYSIS ON THE REGIONAL REGULARITIES OF FROST HEAVE

The regional regularities of the maximum value of frost heave

The maximum value of frost heave for both clayey and sandy soil obtained from Xinjiang, Qinghai, Gansu, Shanxi, Beijing, Neimeng, Heilongjiang, Jilin and Liaoning were shown in Fig.1 and Fig.2,

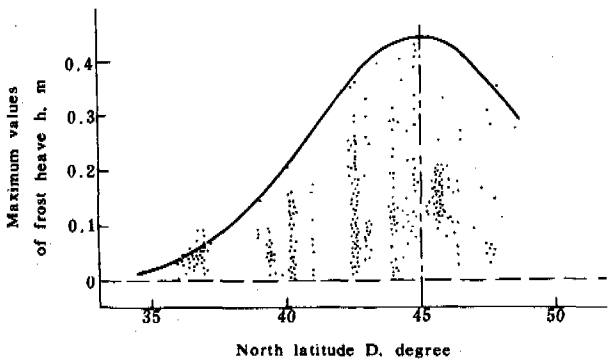

Fig.1 The Maximum Values of Frost Heave vs North Latitude for Clayey Soil

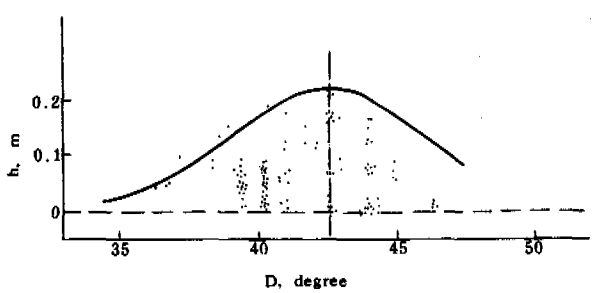

Fig.2 The Maximum Values of Frost Heave vs North Latitude for Sandy Soil

respectively.

These locations are all in the range of 36 to 50.2 degrees north latitude, covering almost the entire seasonal frost area of China.

It is seen from Fig.1 that the envelope of the maximum values of frost heave (h) versus north latitude (D) is of a good random normal distribution with its peak at 45 N. This indicates that although frost heave is the result of comprehensive effect of various factors, frost heave, considered as a ground system behaviour, has the specific property of continuous evolution in time and space. The relation between the maximum values of frost heave and north latitude D for clayey soil can be expressed as

$$h_{D,max} = \frac{1}{\sqrt{2\pi}\sigma_D} EXP[-\frac{(X_D-\mu_D)^2}{2\sigma_D^2}]$$

$$=0.45EXP[-0.63617(X_D-10.0)^2] \quad (1)$$

where $h_{D,max}$ is the potential maximum frost heave in metres, σ_D and μ_D are characteristic constants and have the value of $\sigma_D=0.88654$ and $\mu_D=10.0$ respectively, X_D is the conversion value of the abscissa (equal to 0.2222D) and D denotes the north latitude.

The statistical result for sandy soil is plotted in Fig.2, and shows a similar shape of envelope of the maximum values of frost heave vs north latitude to that seen in Fig.1 for clayey soil. Since the characteristic number σ_D^C for sandy soil is greater than that for clayey soil, the decrease of the maximum values is slower. The relation between the maximum values of frost heave and north latitude for sandy soil can be written as:

$$h^C_{D,max} = \frac{1}{\sqrt{2\pi}\sigma^C_D} EXP[\frac{(X^C_D-\mu^C_D)^2}{2(\sigma^C_D)^2}]$$

$$=0.225EXP[-0.159(X^C_D-21.30^2] \quad (2)$$

where $h^C_{D,max}$ is the potential maximum frost heave for sandy soil in meter, σ^C_D and μ^C_D are the characteristic constants, having the values of $\sigma^C_D=0.1773$, and $\mu^C_D=21.3$ and X^C_D denotes the conversion value of abscissa and $X^C_D=0.5$.

The peak of the envelope of maximum frost heave for sandy soil appears at about 42.5°N.

The relation between the maximum values of frost heave and freezing index

The maximum values of frost heave for clayey soil as a function of freezing index (F) was plotted in Fig.3. The relation between $h_{F,max}$ and F can be written as

$$h_{F,max} = \frac{1}{\sqrt{2\pi}\sigma_F} EXP[-\frac{(X_F-\mu_F)^2}{2\sigma_F^2}]$$

$$=0.45EXP[-0.63617(X_F-2.40)^2] \quad (3)$$

where $h_{F,max}$ is the possible maximum values of frost heave corresponding to a certain freezing index; σ_F and μ_F are characteristic constants, having a value of $\sigma_F=0.88654$, and $\mu_F=2.40$; $X_F=F/650$ is the conversion value of abscissa, and F is freezing index which could be a one-year observation value or the average value over several years.

With the same analysis, the statistical results for sandy soil are depicted in Fig.4. The standard deviation σ for sandy soil is about two times greater than that for clayey soil. This indicates

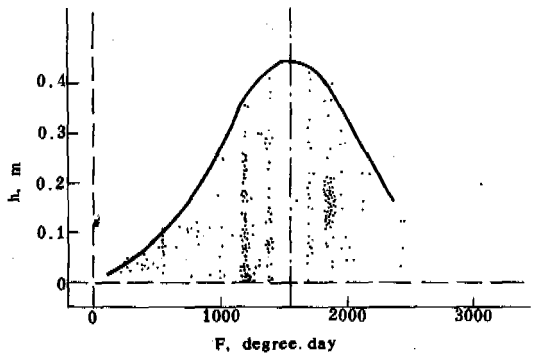

Fig.3 Maximum Values of Frost Heave as a Function of Freezing Index for Clayey Soil

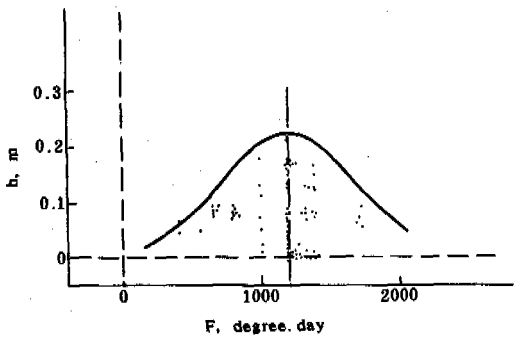

Fig.4 Maximum values of Frost Heave as a Function of Freezing Index for Sandy Soil

that the variation of maximum values of frost heave with F for sandy soil is less sensitive than that for clayey soil. The relation between $h^c_{F,max}$ and F for sandy soil can be expressed as:

$$h^c_{F,max} = \frac{1}{\sqrt{2\pi}\sigma^c_F} \cdot EXP[-\frac{(X^c_F-\mu^c_F)^2}{2(\sigma^c_F)^2}]$$

$$=0.225EXP[-0.159(X^c_F-4.53)^2] \quad (4)$$

where $h^c_{F,max}$ is the possible maximum values of frost heave for sandy soil; σ^c_F and μ^c_F are characteristic constants and have a value of σ^c_F=1.773, and μ^c_F=4.53; and X^c_F=F/265 is the conversion value of abscissa.

It is seen from Figs 3 and 4 (or eqs 3 and 4) that the peak of the envelopes appears at a freezing index of 1560 degree·days for clayey soil and 1200 degree·days for sandy soil, respectively. The two freezing indexes correspond to the latitude of 45°N for clayey soil and 42.5°N for sandy soil, at which the peak of the envelopes of h vs D appears.

In addition, the authors have also made a statistical analysis on the maximum values of frost heave vs frost depth (H_M), frozen ground thickness (H) and average freezing speed (V_f). It is found that the maximum values of frost heave closely follow a normal distribution with all these random variables. This indicates that frost heave of the ground does not always increase with increasing freezing index, frozen ground thickness, frost depth and rate of freezing, but there exist optimum values for producing the maximum frost heave. For clayey soil, the optimum value of frozen thickness H=1.35 m, the optimum value of frost depth H_M=1.15 m, and the optimum value of average freezing speed $\bar{V}_f$=1.10 cm.day. The optimum values D and F can be obtained from the random normal distribution. These values provide a scientific basis for engineering design for frost protection and frost heave forecasting.

THE STATISTICAL ANALYSIS OF FROST HEAVE AND WATER CONCITION

Relation between frost heave and ground water table before freezing

The frost heave behaviour of soils is very sensitive to water conditions. The ground water table before freezing is usually refered to the level observed in the first 10 days for which the ground surface is continually frozen (or average value in this period). The statistical curve of ground water depth Z before freezing vs the maximum value of frost heave for clayey soil is shown in Fig.5. The geographical locations from which the data originated the same as those used in Fig.1. From Fig.5, we may find that with lower ground water table, the maximum

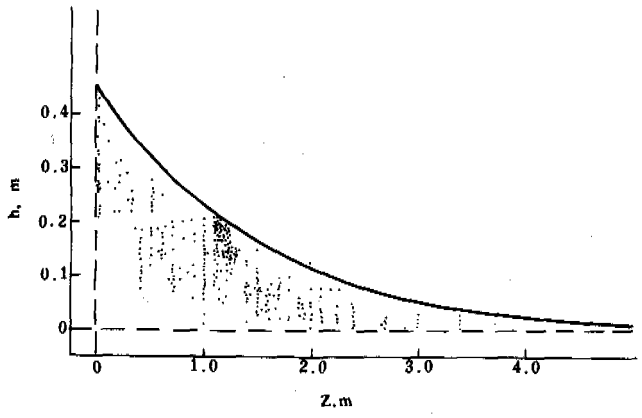

Fig.5 Ground Water Table before Freezing vs Maximum Frost Heave for Clayey Soil

value of frost heave decreases, which can be expressed as

$$h_{z,max} = 0.45\ EXP(-0.7Z) \qquad (5)$$

where $h_{z,max}$ is the possible maximum frost heave corresponding to a certain ground water table before freezing for clayey soil, and Z is the depth of ground water table before freezing in metres.

The same kind of statistical curve for sandy soil is shown in Fig.6 for snady soil ($h^c_{z,max}$). The relation between the maximum values of frost heave and the depth of ground water table before freezing (Z) is linear and can be described by

$$h^c_{z,max} = 0.225-0.107Z \qquad (6)$$

The frost heave of soils is closely related to spatial factors, as well as the function of the factors of soil texture, values of $h_{D,max}$ or $h_{F,max}$ corresponding to D or F can be regarded as the quantitative basis of specifying geographical locations. For the same D or F, although the frost heave changes at random, it is still under the control of the major factor Z.

The statistical analysis on frost heave and ground water condition

The water content before freezing is usually defined as the average water content of frozen soil in the first 10 days of steady freezing period. The statistical analysis indicates that frost heave increases linearly with increasing prefreezing water content (W) and can be expressed as

$$h_{w,max} = 1.333W-0.2 \qquad (7)$$

where $h_{w,max}$ is in metres and W is in decimal fractions.

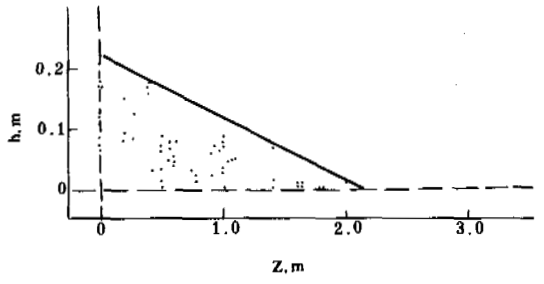

Fig.6 Ground Water Table before Freezing vs Maximum Frost Heave for Sandy Soil

CONCLUSION

(i) Summing the environmental factors influencing frost heave, the north latitued D and freezing index F all conform to the random normal distribution vs the maximum values of frost heave. Thus, in seasonal frost areas, the amount of frost heave may be used as a quantitative basis for sub-dividing geographical regions. When D=45 degrees and F=1560 °C·day, frost heave in clayey soil will have the maximum value. When D=42.5 degrees and F=1200 °C·day, frost heave in sandy soil will have the maximum value. When D or F are larger than those values frost heave will, contradictorily, decrease. This is obviously due to the fact that the freezing rate is greater than the speed of water migration. For clayey soil, the optimum value of freezing rate for producing the maximum frost heave is about 1.10 cm/day.

(ii) Statistical analysis shows that the potential maximum frost heave amount can be well related to north latitude, freezing index, prefreezing ground water table and water content in terms of various mathematical expressions.

ACKNOWLEDGMENT

The authors sincerely thank the persons who provided us various and very useful information and experimental data.

DISCONTINUOUS PERMAFROST MAPPING USING THE EM-31

D.S. Washburn and A. Phukan

Cold Regions Laboratory, Inc. (CRL), Anchorage, The University of Alaska at Anchorage (UAA)

SYNOPSIS This paper outlines the successful use and advantage of employing a combined geophysical induction resistivity survey and drilling program for the delineation of warm, shallow, discontinuous permafrost. A few lines of data are given in building by building detail from a major housing project in Ft. Wainwright, Fairbanks, Alaska. The apparent resistivity signatures of frozen, transitionally frozen, and unfrozen soils are shown. Survey costs are given and success rates are discussed.

INTRODUCTION

A Fort Wainwright, Fairbanks, Alaska, housing project is located in the shallow discontinuous permafrost zone. It lies on an 80 acre (32.4 hectare) site in the Chena River silty, sandy, gravelly alluvium. The 400 unit project has approximately 150 individual buildings that are primarily two story, wooden framed, multiplex townhouses. The design-stage geotechnical site investigation roughly outlined the areas of frozen and unfrozen ground. An inductive resistivity geophysical survey was planned as the most cost-effective means to detect the presence or absence of permafrost on a proposed building by building basis. Such information would help to design more cost-effective foundation systems for the buildings, would help to direct and minimize any additional detailed drilling that would be required prior to construction, and for economic and supply planning purposes, would help to estimate the required number of the more expensive foundation designs for permafrost.

The traditional approach in engineering for locating permafrost under construction projects is to conduct extensive drilling programs. In many cases however, geophysical surveys should be conducted in order to augment the borehole information. The major advantage of a combined geophysical and drilling program is that often more ground can be continuously explored at less cost than with a drilling program alone. For example, Peffer and Robelen (1983) show as much as a 12 to 1 cost advantage with various geophysical methods for studies that are comparable in scope and technique to the effort required for the search of shallow frozen ground in major engineering projects.

Additional considerations for the choice of the inductive resistivity method in general and the Geonics EM-31 in particular for this problem include the following.

- Of the common surface geophysical tools, resistivity can be expected to have the greatest physical property contrast between frozen and unfrozen soils (see Charmichael, 1982; Clark, 1966; or Kawasaki, 1985). Maximizing the target's contrast with its host increases its detectibility and thus increases the chance of success for the survey. For example, at warm permafrost temperatures, Hoekstra and McNeill (1973) show contrasts of about 3 for saturated sandy gravel and of about 1.5 for Fairbanks silt. That is to say, a warm Fairbanks silt permafrost is generally a very detectable 1.5 times more resistive than the same, but thawed silt.

- Seismic contrasts may or may not be sufficient in this project's mostly ice-poor alluvium. Moreover, seismic surveys are generally much slower and more complex to run; require larger crews; have more complex, less durable, less reliable, and more expensive instrumentation; and, are not as qualitatively easy to interpret in the field while underway. With adequate contrasts, seismic methods can however give a much better target definition at depth. But in this shallow case, this is not a governing concern.

- Inductive resistivity methods have at least three times more lateral resolution than the galvanic, or direct current, resistivity techniques. Thus, more detailed data from the nontraditional inductive resistivity method is possible.

- The inductive method uses non-contacting fields coils so that significant time and effort is saved from making four good electrical electrode contacts with the ground for each measurement as is required by the galvanic systems.

- To their disadvantage in very resistive materials, galvanic systems are susceptible to detrimentally high electrode contact resistances, whereas the inductive methods suffer from a reduced sensitivity (see Arcone, 1981). Neither turns out to be a problem for the data found below.

- On this project, all the permafrost that has been drilled was hit at least before a depth of 15 feet (4.6 m). So, for the simple two-layer case of 15 feet (4.6 m) of thawed material over permafrost, the EM-31 receives approximately 35% of its signal from the more resistive permafrost (see Geonics, 1979). Thus, the EM-31 has an adequate depth of exploration.

- The EM-31 weighs about 20 pounds, requires only a one-man crew, and is very easy to operate.

- And, in Anchorage, the EM-31 rents from a local source for 80 $US per day or 350 $US per week, or costs about 10 000 $US. So it is quite affordable.

SURVEY DATA AND RESULTS

The EM-31 was used to detect shallow permafrost along proposed roads, underground utility right-of-ways, and building lines. The goal was to establish the presence or absence of frozen ground under each proposed site so that the proper designs could be planned. This was to be accomplished by measuring the apparent resistivity at each site along lines at 20 foot (6.1 m) station intervals and by using any nearby drillholes from the design-stage geotechnical investigation as ground truth to help control the interpretation. Then, a minimal drilling and trenching program would be planned to check any areas in question and any interpreted hidden frozen zones that lay beneath the proposed structures for further thaw strain and thermal considerations.

Line 8

At first, a 16 acre (6.5 hectare) area, about one fifth of the project, was surveyed. No permafrost was drilled in this area prior to the survey, and consequently none was expected. Appropriately, none is detected by the resistivity survey. The left half of figure 1 shows a typical apparent resistivity line, line 8, over unfrozen predominately silty sands and gravels. Note the 170 ohm-m values for the unfrozen material in this area. Except for a few cultural spikes at stations 5+00 and 1+30 (in feet), note also how relatively smooth and noise-free the data is.

As seen at the start of line 8, the most resistive material encountered in the area is a very distinct, dry deposit of loose, very fine-grained aeolian sands. It has an apparent resistivity of 350 ohm-m. Had the survey been planned and conducted earlier in the pre-design site investigation program, it would have turned out that the resistivity method would have effectively mapped the areal extent of this frost susceptible, F2 to F3, soil thereby saving some of the delineation drilling costs. Furthermore, excavation estimates for its removal from underneath the proposed building sites could have been made from the data. There is no confusion about this relatively resistive material's response being that of permafrost because of its surface expression and correlation with the existing drillhole data. However, as a result of the reduced permafrost to overburden contrast and hence its reduced detectability, a few drillholes would still have been necessary to check if any frozen ground lay hidden underneath the dry sands.

Over the suspected unfrozen ground, we are able to positively establish that no permafrost exists under any of the proposed foundations to within a depth of at least 35 feet (10.7 m). Because cutting line is the most time consuming part of the survey and since little was required here, it took two men only a day and a half to stake and survey the necessary 14 lines in this unfrozen area. This figures to about 50 $US per acre (124 $US per hectare) for acquisition costs, or about the cost of two of the twenty existing auger holes in the area.

Line 20

The right side of figure 1 shows line 20 with the locations of the proposed buildings. It also shows the results of the post-survey, pre-construction drilling at the bottom of the section. Line 20 is an offset extension of line 8. Line 8 station 0+00 is proximal to line 20 station 5+70. The 350 ohm-m, dry aeolian sand hump can be seen centered at station 5+30. From station 4+50 to about 2+90, the data shows the characteristic transition to resistive permafrost, which in this case is frozen sandy gravels and gravelly sands. The anomalous data points at stations 4+40 and 2+80 are due to man-made clutter and can be ignored. At 0+60, the data shows that a low resistivity thaw bulb exists and extends off the beginning of the line. The thaw bulb coincides with an existing road that is located off the end of the line at station 0-70.

The ground conditions under the proposed buildings along line 20 are interpreted to be:

Building 89 - unfrozen
90 - unfrozen
91 - transitional
97 - frozen, and
96 - frozen.

Later drilling confirms the above interpretation except that borehole B-91 is completely unfrozen. Note the heavy frozen bar and the ice description code on the borehole logs in the figure. It turns out that line 20 traverses building 91 near the back of the 70 foot (21 m) deep building, which is also towards confirmed frozen ground, and that BH B-91 was drilled near its front, which is also towards thawed ground. Thus, thawed soils lie to the left and in front of the section and building, and frozen soils lie to the right and behind the building. We therefore maintain

that the interpretation of transitionally frozen soil is correct and that the much more expensive single borehole did not adequately investigate the site. Furthermore, if the foundation was built for being on an unfrozen ground, we would then predict that the back left corner of the building will soon be differentially settling due to thaw consolidation.

Lines 17 and 18

Figure 2 shows two more lines from the same general area having permafrost as line 20. Lines 20, 18, and 17 are all sub-parallel to each other and are separated by about 335 feet (102 m) and 135 feet (41 m) respectively. Buildings 121, 122, 124, and 117 and 118 are all correctly interpreted to lie on frozen ground. Note the apparent resistivity highs and the logs on the figure. Numbers 125 and 119 are thought to lie on transitionally thawed material. But, BH B-125 shows only thawed, moist to saturated, medium sandy gravels and fine gravelly medium sands. And, drilling verifies that building 120 lies on unfrozen ground.

The ragged, irregular response at the ends of lines 17 and 18, particularly from stations 5+20 to 7+20 on line 18, supports a variety of interpretations. None of which have been particularly confirmed or denied at this point. Since some rubbish is found overgrown on the ground in the woods at station 6+40 on line 18 (note the missing data point), the conservative interpretation is that there is more metal junk in the ground at the end of line 18 and that there is some kind of marginal conductor, like an old buried metal pipeline, that runs from line 18 station 5+60 to line 17 station 5+60. The conductor bounds evidence of man's activities on the one side from undisturbed permafrost on the other. A more speculative interpretation says that there is only a little cutural noise at line 18 station 6+40 and that there is on line 18 a very irregular and thermally unstable permafrost margin. A margin that includes a thaw channel at stations 5+60 on both lines 17 and 18. Along these lines of

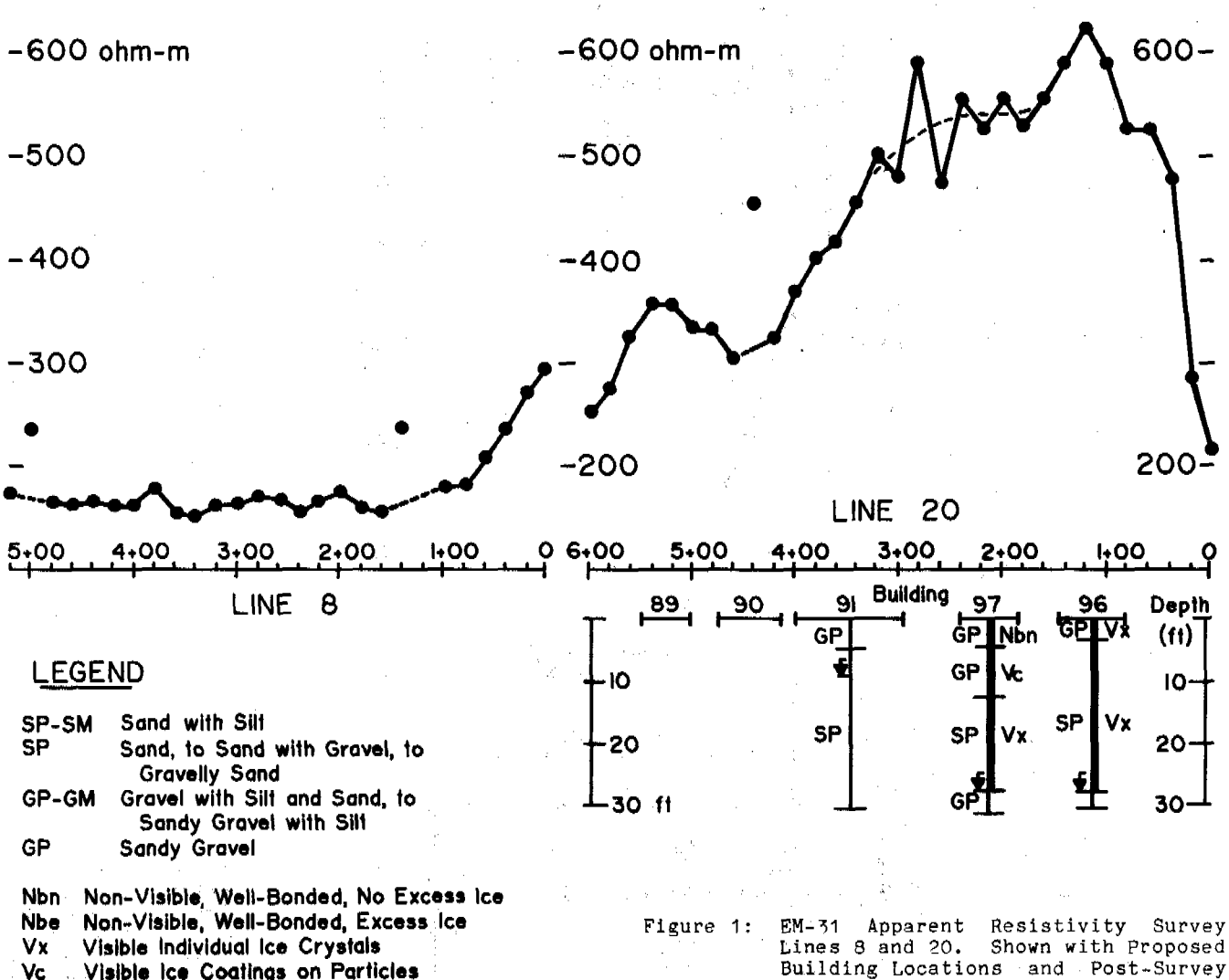

Figure 1: EM-31 Apparent Resistivity Survey Lines 8 and 20. Shown with Proposed Building Locations and Post-Survey Drillhole Logs.

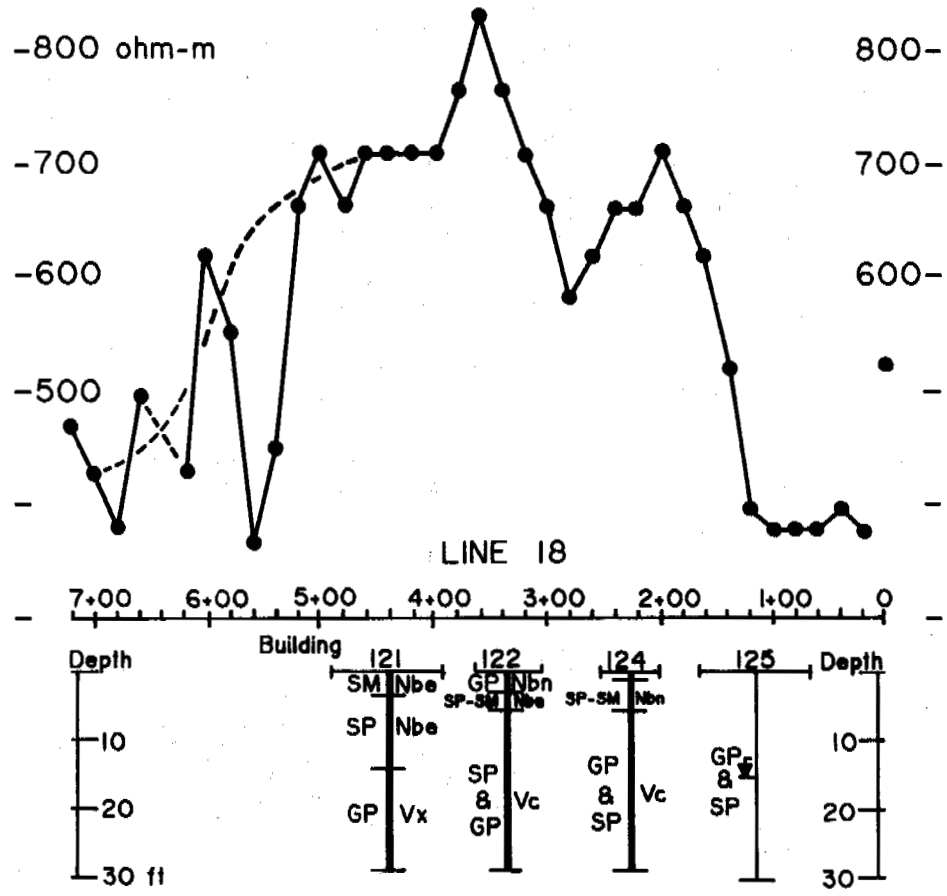

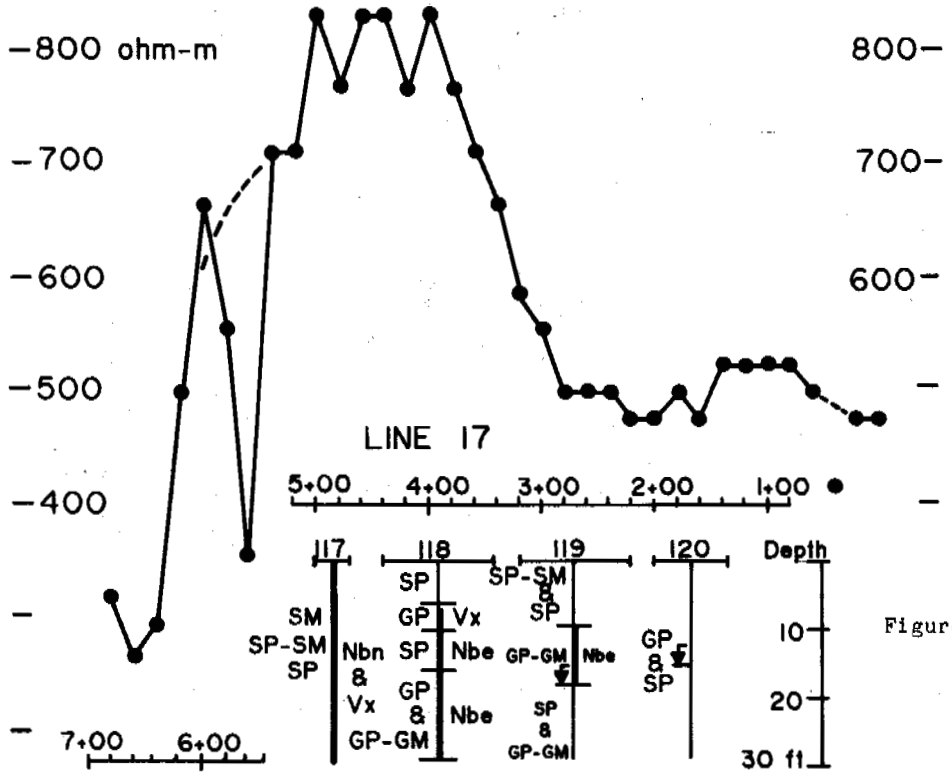

Figure 2: EM - 31 Apparent Resistivity Survey Lines 17 and 18. Shown with Proposed Building Locations and Post - survey Drillhole Logs.

thought, there could also be some thermal degradation of the permafrost under line 18 at station 2+80 which was later missed by either BH B-122 or B-124.

Since the magnitude of the permafrost's apparent resistivity increases from about 550 ohm-m on line 20, to about 700 on line 18, to about 800 ohm-m on 17, the near-surface frozen ground is probably getting either thicker, colder, or icier. Colder and icier are thought to be the more important of the three since the bottom of the permafrost in this area cannot be seen with the EM-31. Note the similarly smooth transition down to the less resistive ground on line 18 at stations 2+00 to 1+20 and on line 17 at stations 3+80 to 2+80. The less resistive unit on line 18 at stations 1+20 to 0+00 and on line 17 at stations 2+80 to the 0+00 is interpreted to be thawed, as stated above, because a similar response was registered over a nearby shallow gravel pit. The apparent resistivity of this unit increases from about 400 ohm-m on 18, to 500 on line 17. Thus, it appears that a gradual lithologic change is taking place. The 400 ohm-m thawed unit on line 18 probably becomes less moist so as to increase its apparent resistivity to 500 ohm-m by line 17 while the permafrost becomes more resistive by line 17 possibly because of an increase of frozen moisture content. A coarsening of the 400 ohm-m unit and an increase of the fines in the permafrost could explain the possible shift in the moisture, and consequently the resistivity. Boreholes BH B-125 and B-120 confirm the interpretation by drilling coarser, drier, sandy gravels with some gravelly sands in B-120. The B-120 sands and gravels have an average moisture content of 3% for the material above the 15 foot (4.6 m) deep watertable. Compare that to an average 13% moisture for the finer material in BH B-125 as described above. And, the borehole logs from the permafrost do indeed show siltier material (GP-GM, SP-SM, and SM) towards the +800 ohm-m line 17 high, particularly in BH B-117. The idea of having colder, more resistive permafrost in the direction from line 20 to line 17 follows from the fact that the edge of the permafrost in the direction perpendicular to lines 17, 18, and 20 is mapped off the side of line 20 away from lines 17 and 18. Thus, one would suspect colder ground inside of and away from the margins of the permafrost. An alternative interpretation to the rise in apparent resistivity of the 400 ohm-m unit on line 18 to 500 ohm-m on 17 is that a deep, resistive permafrost could exist under the unit at a shallower depth under line 17. This is not believed to be the case as a result of the work in the nearby gravel pit, as mentioned above. And as we have already seen, BH B-120 later confirms the interpretation.

Because of the more extensive line cutting that was needed, the acquisition costs in this neighborhood averaged about 1.5 times that of those in the line 8 area example, or about 75 $US per acre (185 $US per hectare). Of the 24 buildings proposed for this one area, we correctly interpreted that all 7 of our unfrozen cases are indeed unfrozen, 10 of our 11 frozen cases were drilled solidly into permafrost, and of the 6 of our transitional cases, 2 are unfrozen, 2 are marginally or transitionally frozen, and 2 are frozen at the drillhole locations. In light of the above discussion about building 91 on line 20, we view our interpretation of the transitional cases as being successful. Significantly, the worst case of calling a site unfrozen when it turns out frozen, has not occurred. As for building 95, the one frozen case in this neighborhood that was found to be unfrozen by the drillhole, it is appropriate here to note that we have since learned from two temperature monitoring holes that are placed near lines 17 and 18 into presumably the coldest ground, that the upper 20 feet (6.1 m) of permafrost averages a warm 31.4°F (-0.3°C) during the summertime when the survey and drilling was done. Since building 95 is very near the margin of the permafrost, but it is definitely completely within the greater than 500 ohm-m contour, and since the permafrost margins are probably warmer than 31.4°F (-0.3°C), we suggest that the drilling action of the auger melted the marginal permafrost which was then logged as being unfrozen. Drilling may not indeed always produce the final word.

Finally, in addition to the main EM-31 mapping program, a few lines were surveyed with the deeper-looking EM-34. The EM-34 is very similar in principle to the EM-31, but it has two larger, more powerful, separable coils (the EM-31 is a single piece of equipment that has a fixed 12 foot (3.7 m) coil spacing) which consequently makes it a little heavier, more complex, and requires a two man crew. The EM-34 was used to determine a depth to the bottom of the permafrost. Depths were needed to estimate what drilling capacity was required to later bore through the frozen ground and to estimate an upper limit of thaw consolidation and settlement. It is estimated from the resistivity data that the permafrost is everywhere something under 60 feet (18 m) thick wherever it was surveyed. One refrigerated corehole has been drilled to date, and there the permafrost is 43 feet (13.1 m) thick.

CONCLUSIONS

Here, as in general, not all high resistivities exclusively indicate permafrost. On this project for example, 350 ohm-m aeolian sands and 500 ohm-m coarse gravels have been described. Both of these exceptions however are easily interpretable and require only a few drillholes to verify. Nevertheless, in all cases on this project, surveyed and drilled permafrost produced a recognizable, generally greater than 500 ohm-m, apparent resistivity high. Eighty proposed building sites were investigated and not once was an area interpreted to be unfrozen when it turned out to be frozen - the worst case. Moreover, the method proved to be over 90% accurate for detecting permafrost. A large part of the success is due in general to the moderately resistive, 200 ohm-m host which provides a good contrast with the frozen ground. A survey in dry, clean gravels would not have been so revealing. But then again, it would not have been as critical to know. This success is

noteworthy in that the permafrost here is quite warm, above 31°F (-0.5°C), and is thus not nearly so resistive and detectable as colder permafrost. This survey was very successful and provided a large amount of relatively inexpensive data that greatly complimented the borehole information. The inductive resistivity method on this project has proven to be accurate, reliable, fast, and very cost-effective.

REFERENCES

Arcone, S.A. (1981). Some field studies of the correlation between electromagnetic and direct current measurements of ground resistivity. Underground Corrosion, ASTM Special Treatment Technical Testing Publication 741, p 92-110.

Charmichael, R.S., ed. (1982). Handbook of Physical Properties of Rocks, vols 1 and 2, 749 pp, CRC Press, Boca Raton, FL.

Clark, S.P., Jr., ed. (1966). Handbook of Physical Constants, 587 pp, GSA Memoir 97, New York.

Geonics Limited (1979). Operating Manual for EM-31 Non-Contacting Terrain Conductivity Meter with Technical Notes, 57 pp, Geonics, Ontario, Canada.

Hoekstra, P. & McNeill, J.D. (1973). Electromagnetic probing of permafrost. Proc. 2nd ICP, p 517-526, Yakutsk, USSR.

Kawasaki, K. & Osterkamp, T.E. (1985). Electromagntic Induction Measurements in Permafrost Terrain for Detecting Ground Ice and Ice-Rich Soils, 195 pp., University of Alaska Geophysical Institute Report UAG 300, Fairbanks.

Peffer, J.R. & Robelen, P.C. (1983). Affordable: Overburden mapping using new geophysical techniques. Pit & Quarry, August 1983.

A DISCUSSION ON MAXIMUM SEASONAL FROST DEPTH OF GROUND

Xu, Ruiqi, Pang, Guoliang and Wang, Bingcheng

Heilongjiang Water Conservancy School, Harbin, China

SYNOPSIS Maximum seasonal frost depth of ground affects the calculation of frost heave, frost heave rate, circumferential force and normal force, which is also the indispensable data for architectural design and construction. But habitually maximum frost depth of ground and the depth of freezing soil layer are confused and without strict distinction.

The paper is for researching and analyzing maximum seasonal frost depth of ground, make clear the criterion of calculating the maximum seasonal frost depth of ground.

Maximum seasonal frost depth of ground directly affects the calculation of frost heave capacity, frost heave rate, normal force and circumferential force, which is indispensable data in the architectural design and construction. However at present the maximum frost depth of ground and the thickness of freezing soil layer are habitually mixed up both at home and abroad, and are not distinguished strictly. For instance, the meteorological station and in and outdoor experiments measured that the frost depth was the thickness of freezing soil layer, not the maximum frost depth of ground.

Whether with theoretical equation or empirical equation, frost heave capacity, water content migration and frost heave rate are all related with frost depth. While adopting incorrect frost depth, the frost heave rate that is counted will be different. Thus the classification of frost heave divided by frost heave rate is influenced.

The seasonal frost depth of ground is different, which has a great influence on the normal frost heave. See fig. 1

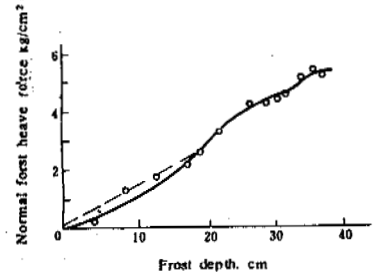

fig.1 the relation between frost depth and normal frost heave

Frost depth increases as the frost heave is increased. When frost depth is at its maximum the accumulating value of the frost heave is the greatest.

The characteristic of frost heave in soil can be reflected by the law that the frost heave capacity and frost heave change along frost depth. See fig. 2.

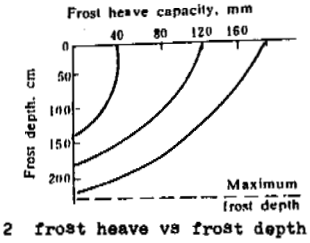

fig.2 frost heave vs frost depth

From the figure we know that the distribution of frost heave capacity along frost depth is uneven. Regarding this phenominon as the total frost heave capacity of the soil surface (namely the accumulating frost heave capacity of the soil surface), the total frost heave capacity on the soil surface increases with the developement of frost depth, not increasing in direct proportion, nor along the total frost depth. The frost heave capacity on the soil surface arrives at its maximum only after frost developing at a certain depth. Though frost depth develops continuously afterwards and at last reaches its maximum frost depth, the total frost heave capacity on the soil surface increases very little and is relatively stable.

The same criterion should be adopted to count the maximum frost depth. The frost penetration, however, whether it is directly measured or calculated and induced from the empirical equation, is different from the practical frost depth value of frost heave mechanism. That frost heave being widely used in various equation directly affects the anti-frost damage measures of hydraulic structures. So it is necessary to achieve unanimity of opinion of frost depth, and to adopt the same standard in order to be in common use.

Frost heave in natural freezing layer is the natural phenominon created by the water and heat in soil fluxing and phases changing below $0^{\circ}C$. A certain point in layer moves upwards along the normal line of the cooling frontal edge, in the meanwhile moves downwards opposite to the direction, so frost heave at certain point in freezing layer is equal in size and opposite in direction. Moving upward makes sublayer press tightly. Under the action of frost, frost depth device is freezing up with freezing soil, which rises upwards accompanying the increase of frost heave capacity and frost heave. See figure 3.

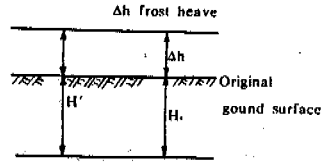

figure 3 frost heave and frost depth

So the value measured by the general meteorological station is the thickness of the freezing soil layer, not the practical frost depth. If the frost depth needs to be achieved, the frost heave capacity must be misused. For instance, an experiment in a foreign university as fig. 4 shows,

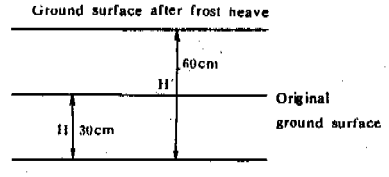

figure 4 an example of frost heave vs frost depth

From the figure we see the appearance before and after freezing. The thickness of freezing soil layer is 60cm; frost heave capacity is 30cm; the maximum frost depth H = 60cm - 30cm= 30cm. Anti-frost measures should be taken with 30cm, otherwise the error is great with 60cm, and its result is foreseeable. From this we can see that it is necessary to achieve unanimity of opinion of frost depth.

REFERENCES

1 Механика мерзлых грунтов «Высшая школа» 1973

2. Soil Physics Japan Muxiachengyi 1982,9

3.Soil Mechanics China Wuhan Hydraulic and Electric College Feng Guodong editor 1984, 8

PRINCIPLES FOR COMPILING AN ATLAS OF SEASONAL FROST PENETRATION, JILIN, CHINA (1: 2000000)

Zhang, Xing, Li, Yinrong and Song, Zhengyuan

Institute of Water Conservancy, Jilin, China

SYNOPSIS For purposes of engineering design an atlas has been compiled to reflect the dynamics of seasonally frozen ground, and particularly the depth of frost penetration in soils under different freezing conditions, variations in the freezing process with time during the freezing season and interannual variation in the depth of frost penetration. In a given geographical region, soil properties and the moisture content of the soil prior to freezing are the major internal factors influencing the seasonal depth of frost penetration, while the thickness of snow cover and the freezing index, which very with latitude and altitute, are the main external factors. The dynamic of frost penetration in seasonally frozen ground is shown in the atlas by the following four parameters: the standard frozen depth (Z_o), the coefficient of variation of frost depth (C_v), coefficient for the influence of snow cover (β) and the elapsed time of the freezing season (T).

INTRODUCTION

The mapping of seasonally frozen ground is a complicated problem because of the variety of natural factors that deeply affect the process and result of ground freezing. At a given site, the position of the freezing front varies with time, the maximum depth of frost penetration differs from year to year; and at any time, the depth of frozen soil can vary by a factor of 2 to 4 within a distance of a few kilometres.

For engineering purpose, it is necessary to know the regime of seasonal freezing processes, i.e., to show the seasonally frozen depth, the process of freezing vs time and the interannual variations in frozen depth each of which is shown in the atlas.

In this paper the authors discuss the principles for compilation of the atlas seasonally frozen ground in Jilin Province, China.

TERMINOLOGY AND CONCEPTIONS

The soil-type classification and terminology are based on the "Regulations for geotechnical tests SDSOI-79" promulgated by the Ministry of Water Conservancy and Electricity, People's Republic of China.

The period of time with a mean air temperature below 0°C is called the freezing season; the number of 10-day periods (T) is called the elapsed time of freezing season.

The freezing index (F_1) is defined as the integrated area of temperature-time curve within the freezing season in °C·10 days.

The period from the beginning of the freezing season to the time of maximum frost penetration is the calculated duration of the freezing season (T_1).

The period of time with mean daily air temperatures below 0°C and the beginning of soil freezing is the pre-freezing period, in which the water content of the soil is defined as the pre-freezing water content (W, %).

The term seasonally frozen depth refers to the maximum value of frost penetration, including frost heave.

STANDARD FROZEN DEPTH

The standard frozen depth is defined as the mean depth of frost penetration in fine-grained inorganic soil with a pre-freezing water content of 25% (W_o—standard pre-freezing water content), observed for several years at a snow-free meteorological observation site (Central Meteorological Bureau, 1979b)

A standard frozen depth is dependent mainly on the freezing index, as controlled by latitude (L) and altitude (H) of the observation site, and is affected by local conditions such as surface cover, hydrogeology and engineering-geology.

The standard frozen depth is a site-specific characteristic determined by statistical analysis of observatory data. It is a basic index in the mapping of seasonally frozen ground.

RELATIONSHIP BETWEEN STANDARD FROZEN DEPTH AND FREEZING INDEX

From statistical analysis of several years data

from 30 observation sites it is known that the standard frozen depth (Z_o, m) is dependent on the freezing index $\bar{F}_1$:

$$Z_o = a_o\sqrt{\bar{F}_1} \quad (1)$$

where a_o —coefficient of the standard forzen depth, known to be 0.115 in Jilin Province; and
$\bar{F}_1$— mean value of freezing index for several years.

At the 30 observation sites,the fine-grained particle content of the seasonally frozen soils ranges from 48 to 78%, in which salt content is 11 to 74%,and the clay content is from 2 to 34%. At 15 sites, the depth of the groundwater table is less than 4 m. Four observation sites are on frost susceptible soils with frost heaving amounts of 10 to 31.5 cm, or 6 to 25% of the maximum frozen depth.

INFLUENCE OF PRE-FREEZING WATER CONTENT ON DEPTH OF FROST PENETRATION

At a snow-free site, as the pre-freezing water content W is not equal to W_o, the mean frozen depth for any year (Z) differs from Z_o, and can be expressed by the following equation:

$$Z = K_w Z_o \quad (2)$$

where K_w— the revised coefficient of water content

$$K_w = \sqrt{\frac{W_o}{W}} = \frac{5}{W} \quad (3)$$

Substituting a_o and k_w in Equation (2), gives

$$Z = 0.575\sqrt{\frac{\bar{F}_1}{W}} \quad (4)$$

Equation (4), although it is approximate theoretically, has proved by comparison with field data to be accurate enough for practical purposes (Zhang, 1983). The water content value used for statistical analysis ranges from 8 to 30%.

VARIATION IN $\bar{F}_1$

Within the Jilin Province, 187000 km² in area, there are 48 observation sites. In addition, data from 20 adjacent sites were used. Thus, in a total area of 260000 km², data from 68 observation sites were used in the analysis; in other words, there were more than 10 observation sites for each 100 cm² on the map (1:2000000). This is dense enough for mapping.

In the mountainous regions, variation in elevation affects the values of $\bar{F}_1$ and Z_o. The Z_o increases by 4 to 7 cm per 100 m increase in elevation.

Jilin Province can be divided into four physical regions east to west.

Region I, the Changbaishan Natural Environment Protected Region, is very mountainous and $\bar{F}_1$ is found to be closely-related to latitude.

$$\bar{F}_1 = -293.5+9.3L+11.7H \quad (5)$$

where L— latitude, in degrees;
H— elevation in 100 m.

The correlation coefficient of Eq.(5) is 0.934.

In Region II, the central-eastern hills,

$$\bar{F}_1 = -665.7+18.2L+13.6H \quad (6)$$

The correlation coefficient of Eq.(6) is 0.838.

Substituting Eq.(5) and (6) into Eq.(1), the relation of Z_o to L and H can be derived.

In principle the formulae Eq.(5) and (6) should be applied only to those areas lower than 1000 m a.s.l.

In Regions III and IV, the Central-western Hills and the Western Plain, the relief is less than 100 m, the distribution of $\bar{F}_1$ mainly depends on latitude,and the observed data of Z_o are applied directly to mapping.

EFFECTS OF SNOW COVER ON THE MEAN VALUE OF SEASONAL FROST DEPTH

An increase in the depth of snow cover will reduce the effect of $\bar{F}_1$ on the seasonal frost depth. So, $\bar{F}_1$ in Eq.(1) should be changed to $\bar{F}_2$, so:

$$\bar{F}_2 = \bar{F}_1 - \beta\sqrt{\bar{F}_1} \quad (7)$$

where β — coefficient showing the effect of snow cover on $\bar{F}_1$,

$$\beta = 0.193 + 0.402\ \bar{H}_x \quad (8)$$

where $\bar{H}_x$— mean depth of snow cover for several years, and can be determined from Eq.(9),

$$\bar{H}_x = \frac{\Sigma H_i}{120} \quad (9)$$

where H_i— daily depth of snow cover during the period from the beginning of November the end of February, in centimetres.

INTERANNUAL VARIATION OF FROST PENETRATION

The depth frost penetration at a any site can vary greatly from year to year. The coefficient of variability (C_v) ranges from 0.04 to 0.27 in

Jilin Province.

Based on analysis of empirical frequency curves from 100 sites within the temperate zone in China (Central Meteorological Bureau, 1979a), it is considered that the third type of Poisson normal distribution curve, with a skewness coefficient (C_s)=0 can be the theoretical distribution curve for the depth of frost penetration (Zhang and Wang, 1981). The C_v value is the index to show the interannual variation of seasonal frost penetration.

It is necessary to examine carefully the observed data to determine the value of C_v seasonaly frost penetration under natural conditions, because any change in position will cause the observed data to vary widely.

Observations at 40 meteorological stations for 25 years show that the thicker the snow cover, the greater will be the value of C_v.

$$C_v = 0.081 + 0.135\bar{H}_x \qquad (10)$$

The correlation coefficient for Eq.(10) is 0.92. In this province, $\bar{H}_x$ is less than 16 cm.

From Eq.(10), it can be shown that if $\bar{H}_x$=0, C_v=0.081. A calculation based on $\bar{F}_1$ shows that the C_v value should be 0.062, however. The fact that two values are close indicates that $\bar{F}_1$ is the major factor in controlling the depth of frost penetration at a snow-free site.

PROGRESS OF FROST PENETRATION VS TIME DURING THE FREEZING PERIOD

The progress of frost penetration can be expressed by Eq.(11).

$$Z_{(t)} = \alpha_{(t)}Z \qquad (11)$$

where $\alpha_{(t)}$ — time-course coefficient of the depth of frost penetration;
t — elapsed time, in 10-day periods; ~~and~~
Z — mean annual value of maximum depth of frost penetration.

In the temperate zone of China, $\alpha_{(t)}$ can be expressed by Eq.(12).

$$\alpha_{(t)} = [3(\frac{t}{T_1})-2(\frac{t}{T_1})^2]m \qquad (12)$$

where, the value of in depends mainly on the pre-freezing water content (W). As W ranges increases from 8 to 30%, m increases from 0.51 to 0.73.

As the duration of freezing season (τ) is less than is 10-day periods depth of frost penetration will continue to increases after the freezing season, but the amount of this increase will not exceed 5% of the annual frost depth. This situation often occurs in regions near the southern limit of the discontinuous permafrost zone. As T<150 days, T_1 is always less than T.

CONTENTS OF THE ATLAS

The atlas includes the following maps:

1. Isopleths of the standard frozen depth (Z_o) for Jilin Province;

2. Isopleths of the coefficient of variation in frost depth (C_v) under natural conditions;

3. Isopleths of the coefficient for the effect of snow cover on depth of frost penetration;

4. Regionalisation of the duration of the freezing season (T) in Jilin Province.

In the accompanying text, curves showing the relationship of Z_o to L and H for defferent natural regions, moisture coefficient and a table showing the $\alpha_{(t)}$ values are presented.

The atlas can be used to predict the frequency of a given depth of frost penetration and the progress of frost penetration.

CONCLUSIONS

The atlas (1:2000000) of seasonal frost penetration for Jilin Province is the result of studies for the compilation an atlas of seasonal frost for the temperate zone of China.

Based on examination and analysis of field observations from more than 100 meteorological stations, it can be concluded that:

(i) The seasonal ground freezing regime can be expresses by the standard value (Z_o), coefficient of variability (C_v), coefficient of snow effects (β) and a time-course coefficient($\alpha_{(t)}$).

(ii) In a given geographical region, soil properties and pre-freezing water content are the two major internal factors that influence the seasonal frost depth, while the depth of snow cover and the freezing index are the major external factors. The mean frozen depth for several years is the basic index to evaluate the quantitative characteristics of seasonally frozen ground. The C_v value reflects the interannual variations, and the coefficient $\alpha_{(t)}$ can be used to express the freezing process.

(iii) The principles suggested above can also be used for compilation of an atlas of seasonal frost depth for the whole temperate zone of China, only some parameters will have to be changed for different regions.

The results demonstrate that the equations suggested can be used to determine the seasonal frost depth and the time-course of freezing penetration for coarse-grained soils with a fines content (<2 mm particles) greater than 50% (Zhang, 1983). However, they are not suitable for the soils influenced by saline ground water.

REFERENCES

Central Meteorological Bureau of China, (1979a). Climatic atlas, China. p.222-223, Cartographic Publishing House.

Central Meteorological Bureau of China, (1979b). Regulations for surface air observation. Meteorological Publishing House.

Zhang Xing and Wang Shiduo, (1981). Statistical characteristics of seasonal frozen ground in Jilin, China. Journal of Glaciology and Cryopedology, (3), 37-46.

Zhang Xing, (1983). Natural freezing penetrative rate of the seasonally frozen ground in the medium temperate zone of China. Pro.2nd Chinese National Conference on Permafrost, p.138-145, Gansu People's Publishing House.

SEGREGATION FREEZING OBSERVED IN WELDED TUFF BY OPEN SYSTEM FROST HEAVE TEST

Akagawa, Satoshi, Goto, Shigeru and Saito, Akira

Shimizu Corporation, Tokyo, Japan

SYNOPSIS Segregation freezing that results in ice lens growth is observed during freezing in saturated and unsaturated porous rocks. The porous rock heaves in a way similar to soil frost heaving, cracking the rock, which has the tensile strength of 1.4 MPa. The heave susceptibility of the rock was found to be lower than that of frost-susceptible soil; however, the rest of the heaving properties appear to be similar. Almost the same segregation temperatures at which the final ice lens segregates are obtained in two tests from the ice lenses' location and temperature profiles, regardless of the water saturation condition of 92 and 100%. However, the heave and water intake properties seem to differ with the water saturation condition. The growth of ice lenses in a porous rock reflects the possibility of weathering by segregation freezing during rock freezing.

INTRODUCTION

Extensive studies of the weathering of rocks due to freeze-thaw cycles have been conducted in the past; however, there has been no general agreement on a weathering process (White, 1976). In one special case of rock weathering, the frost shattering of a frozen porous rock was studied by Fukuda and Matuoka (1982); the data showed a possibility of segregation freezing, which may have resulted in the growth of visible or invisible ice lenses in the rock. Their paper clearly demonstrated the existence of the pore-water pressure gradient in the unfrozen part of the unsaturated rock while freezing.

The existence of the pore-water pressure gradient reveals a possibility of high suction force generation near the freezing front (originally Taber, 1929). The suction force will be caused by segregation freezing instead of in situ freezing (Takagi, 1980). Segregation freezing results in the cracking of the soil skeleton through ice lensing. Obviously, if the segregation freezing takes place in the rock, it results in weathering.

In this paper, the possibility of segregation freezing in porous rock is observed by two open- system frost heave tests, Test A and Test B, using the same kind of rock that was cored from the same area as Fukuda and Matuoka (1982). As a result, segregation freezing in the rock is confirmed by the growth of ice lenses. In this paper the characteristics of the growing ice lenses in a porous rock are also reported, and compared with those of soil freezing.

FROST HEAVE TEST

Test apparatus

Frost heave tests were conducted with the apparatus shown in Fig. 1. The maximum specimen size that can be tested in this apparatus is 30 cm in height and 30 cm in diameter. In these tests, the specimen diameter was reduced to 29 cm to reduce side friction, and height was reduced to 25 cm to make room for NFS (non-frost-susceptible) sand at both ends of the specimen, as shown in Fig. 2. Water sealing of the side wall of the specimen was obtained by a 1-mm-thick, flexible silicone rubber jacket, also shown in Fig. 2.

The temperature of the test specimen was controlled through both the top and bottom pedestals. The temperature of the upper pedestal was controlled by circulating ethylene glycol through the pedestal. The lower pedestal temperature was maintained at a selected positive temperature by controlling the temperature of the water in the pedestal. The water is connected to the pressurized pore water reservoir tank and is supplied to the specimen through the porous plate as pore water. Freezing was initiated from the upper pedestal downward. Between the upper pedestal and the specimen, NFS sand was placed to avoid supercooling and to improve distribution of the overburdem pressure. The space between the acrylic Plexiglas cell and the silicone rubber membrane was filled with gelatine to prevent convective heat transfer. Overburden pressure was applied by an air actuator except for the low pressures of 5 and 7.5 kPa used in Test A. Those two low pressures were applied with weights.

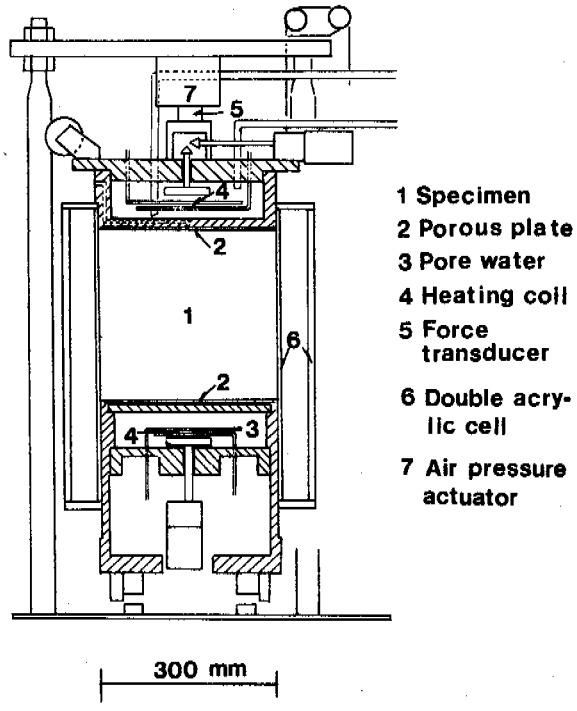

Fig. 1. Frost heave test apparatus.

TABLE I

Physical and Mechanical Properties of the Porous Rock

	Unfrozen Dry (20°C)	Unfrozen Saturated (20°C)	Frozen Saturated (-5°C)	Frozen Saturated (-15°C)	Frozen Saturated (-25°C)
Apparent specific gravity	1.40	1.72	--	--	--
Porosity (%)	37.9		--	--	--
Strength (MN/m^2) Compressive	14.6	6.6	12.0	18.5	26.2
Strength (MN/m^2) Tensile (split test)	1.6	1.4	1.4	4.4	5.7
Tangent modulus (MN/m^2)	4812	3548	2859	2068	3763
Secant modulus (MN/m^2)	4596	3126	3097	3410	6281
Elastic wave velocity (Km/s)	2.45	2.72	3.20	3.67	3.89
Poisson's ratio	0.17	0.28	0.46	0.38	0.42

Since the apparatus was placed in a walk-in type coldroom in which the temperature was maintained at 0±1°C, lateral heat flow to or from the specimen was minimized. The frost heave was measured with a digital deformation gauge that has an accuracy of ±0.001 mm.

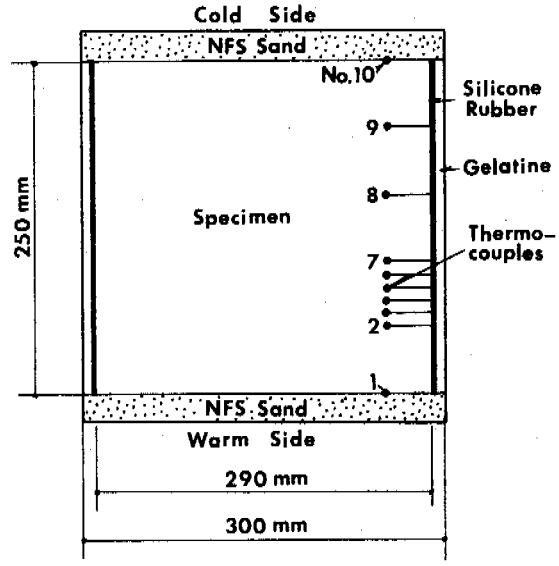

Fig. 2. Specimen configuration.

Since this measuring system has no analog circuit, no drift was expected. The pore water flow was measured with an electrical water depth meter that was installed in the pore water reservoir tank. The tank had a 10-L capacity. The temperature of the specimen was measured with 10 thermocouples that were installed 5 cm into the side of the specimen. The locations of the thermocouples are shown in Fig. 2. All these data were recorded every hour by a computerized data acquisition system.

Sample properties

The material used in this experiment is a rhyolite-welded-tuff that was obtained from an ocean volcanic deposit. This rock is characterized by a cemented structure with air bubble and flow line features. This rock is made up of about 15% by volume of 0.2- to 2-mm plagioclase grains and 0.2- to 1-mm quartz grains such as phenocryst, bonded by 85% vitreous groundmass. The groundmass is strongly modified by diagenesis, and volcanic glass and other minerals are changed to clinoptilolite, chlorite, and montmorillonite.

The physical and mechanical properties of this rock are listed in Table 1 for the convenience of the future discussion of a relation between frost heave force and rock strength.

Test conditions

The test conditions for the frost heave tests are listed in Table 2. The water saturation conditions for the two tests were different. For Test A, the sample was submerged in water for a week, leaving 1 cm of the upper part in air. In this case, the degree of saturation was 92%. For Test B, the sample was submerged in water as in Test A but for 3 months. In this case, the degree of saturation was measured as 100%. The overburden pressure was changed several times from 5 KPa to 0.2 MPa in

TABLE II

Test Conditions

Test name	Water saturation condition (%)	Pressure		Temperature	
		Overburden pressure (KPa)	Pore water pressure (KPa)	Warm (°C)	Cold (°C)
Test A	92	5, 75, 30, 50, 100, 200	3	4.0	-14.5
Test B	100	60, 105, 150, 200	3	4.3	-14.9

Test A and 60 KPa to 0.2 MPa in Test B to observe the influence of overburden pressure on the frost heaving characteristics. Before the frost heave tests, the specimens were maintained at the warm side temperatures, shown in Table 2, for a week to establish uniform initial temperature conditions. Then the cold side temperatures were dropped to those shown in Table 2 for the test initiation. The pore water pressure was set at 3 KPa at the top of the specimen to maintain slight positive gauge pressures throughout it.

TEST RESULTS AND DISCUSSION

During the frost heave tests, both samples heaved as shown in Fig. 3. Segregation freez-

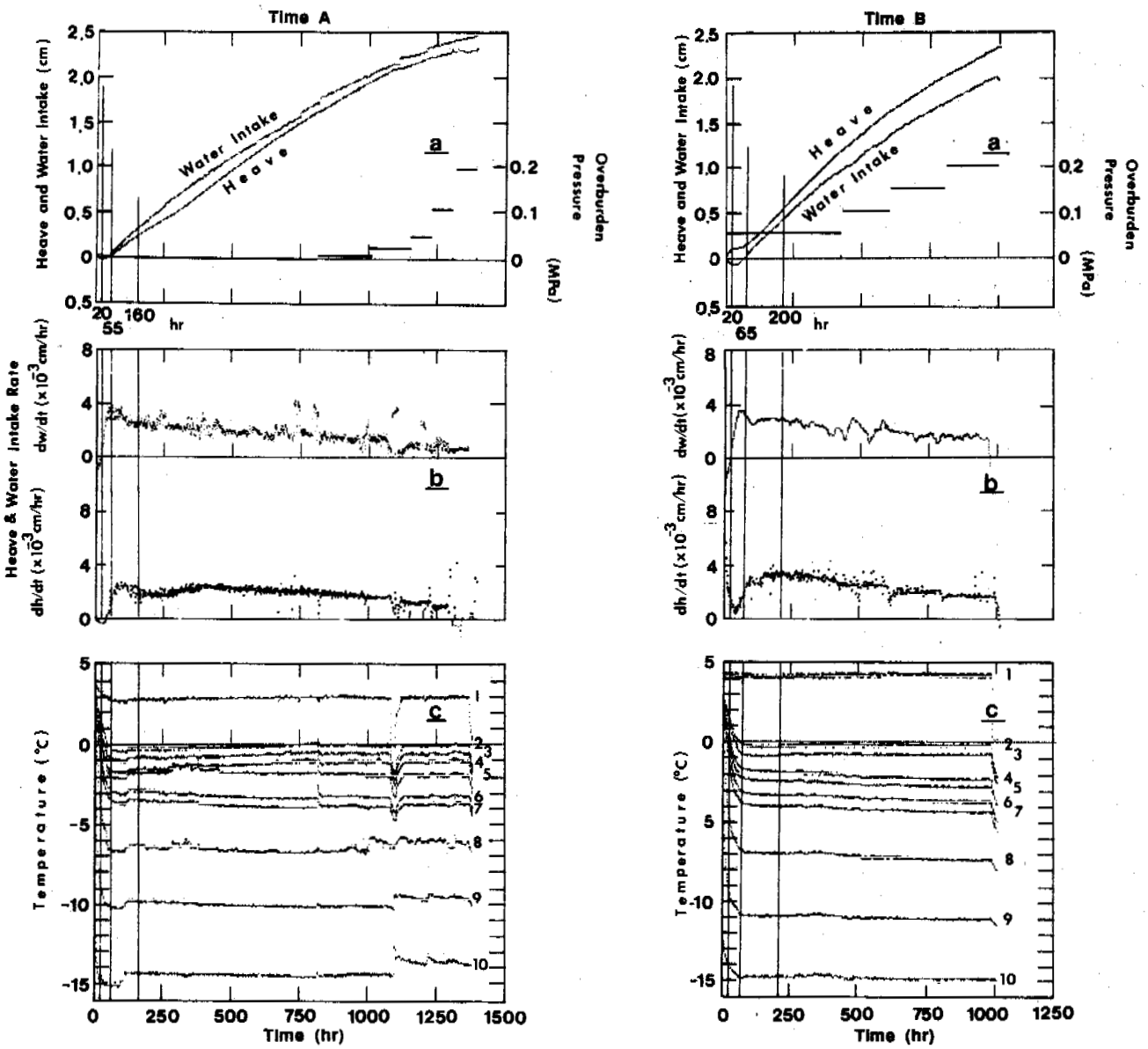

Fig. 3. Heave and water intake characteristics (numbers in [c] are thermocouple numbers).

ing activity in the rock is confirmed by analyzing the heave and water intake curves and the ice lens distribution.

Heave and water intake properties

The heave and water intake curves are shown in Fig. 3a with values of applied overburden pressures. The heave rate and water intake rate are shown in Fig. 3b; they are calculated by subtracting adjacent pairs of heave or water intake data and dividing by the time difference of 1 hour. The specimen temperatures are shown in Fig. 3c. The temperatures were measured with 10 thermocouples installed in the specimens, as shown in Fig. 2.

During the frost heave tests, both samples heaved about 2 cm at 1,000 hours. The heave amount observed in Test A, which used the unsaturated sample, is slightly smaller than than in Test B, which used the saturated sample, although the overburden pressure in Test B was usually larger than Test A. The heave amount observed in Test B is larger than the water intake amount, whereas the inverse relation was observed in Test A. One possible explanation of these properties will be discussed later.

The frost heave and heave rate curves acquired from Test A show that heaving started at time t=55 hours after an initial slight shrinkage. The heave and heave rate curves of Test B show heaving that is similar to that of the saturated frost-susceptible soil observed in a frost heave test conducted with the same specimen size, overburden pressure, and freezing conditions (Akagawa, 1983).

In general, a saturated frost-susceptible soil first shows in situ freezing, expelling pore water if overburden pressure is high. The heave rate due to in situ freezing then decreases sharply as the freezing rate decreases and segregation freezing becomes predominant, increasing the heave rate and drawing the pore-water into the sample. When segregation freezing becomes dominant, ice lenses start to grow following the depth of the zero isotherm, and the heave amount is 9% greater than the water intake amount (Akagawa, in press). The data shown in Fig. 3 may be understood as following the heaving modes found in the soil mentioned above:

(1) A period of predominant in situ freezing. Negative water intake rates were observed in the first 20 hours in both Test A and Test B. These data reveal that in situ freezing was predominant during this period.

(2) A transition period from in situ freezing to segregation freezing. The water intake rates turned positive and increased steeply during the periods of t= 20 to 55 hours in Test A and 20 to 65 hours in Test B. These data reveal that in situ freezing was tapering off and segregation freezing was becoming predominant.

(3) A period of predominant segregation freezing. The ratios of heave rate to water intake rate, (dh/dt)/(dw/dt), at each recorded time seem to be about 1.09 after 55 hours in Test A and 65 hours in Test B, except for a period from t=20 to 380 hours in Test A. These data reveal that segregation freezing was predominant in this period.

From this point of view concerning the heave and water intake properties, it may be said that segregation freezing has been taking place in both unsaturated and saturated porous rock and that expansion due to in situ freezing has also been active in Test B, in at least the first 20 hours of freezing, which used a saturated sample.

Ice lens distribution

After the frost heave tests, both specimens were cut to observe the water content profile and ice lens distribution to confirm the segregation freezing. Results of these observations are shown in Fig. 4a and b. Several visible ice lenses were observed, and their distribution and variation of thickness were found to resemble ice lenses seen in frost susceptible soils; however, there were fewer visible ice lenses in the rock than in the soil. Therefore, the occurrence of segregation freezing, which was revealed by the heave and water intake properties, was confirmed by the existence of the segregated ice lenses.

Additional experimental results of note for the frost heave study are listed below, and are compared to the heave characteristics of the above-mentioned frost-susceptible soil:

Heave rate during segregation freezing

The heave rate of the rock appeared to remain constant at relatively low values such as 0.01 to 0.03 mm/hr shown in Fig. 3b, whereas the heave rate of the frost-susceptible soil, which was observed in a frost heave test using the same specimen size and similar freezing conditions, varied from 0.3 to 0.02 mm/hr as time elapsed (Akagawa, 1983).

The effect of overburden pressure on heave and water intake rate during segregation freezing

The heave and water intake rates at each overburden pressure during segregation freezing are plotted in Fig. 5. As is generally accepted in soil frost heave studies, a higher overburden pressure causes a lower heave rate. The same situation applies for rock heaving.

The effect of unsaturation on frost heaving

In Test A, no heaving was observed during the period between t=0 to 55 hours, but slight heaving was observed in Test B during t=0 to 65 hours, as shown in Fig. 3a. The water intake rate was higher than the heave rate between t=55 to 380 hours in Test A, whereas the rest of the data in Fig. 3b show an inverse relationship between the heave rate and the water intake rate. One possible explanation for the appearance of the heaving in Test B in this period is that the excess pore water, which was locally developed by in situ freezing in the saturated sample, cracked the rock, causing expansion, and absence of the heaving in Test A is thought to be the result of insufficient excess pore water for cracking the unsaturated specimen. This lower heave

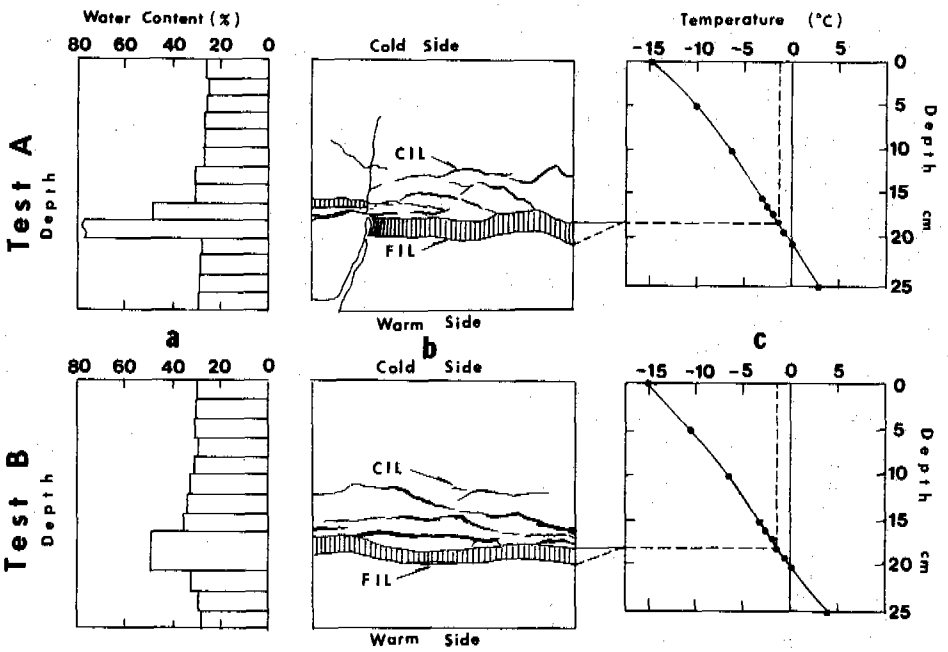

Fig. 4. Ice lens distribution and segregation temperature of the final ice lens (FIL). (a - water content; b - ice lens distribution; c - temperature profile when final ice lens starts to grow).

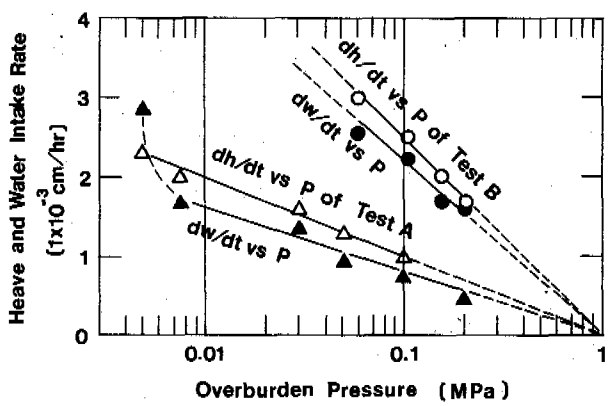

Fig. 5. Effect of surcharge pressure on frost heave rate (dh/dt) and water intake rate (dw/dt) (The triangle and circle data points represent the results for Test A and Test B, respectively. White and black points represent heave rate and water intake rate, respectively).

rate compared to the water intake rate during the early stage of freezing in Test A might be the cause of the higher water intake amount than heave amount in this test.

As shown in Fig. 5, all data agree well with a relation $(dh/dt)/(dw/dt) \simeq 1.09$, except for the water intake rate data for Test A at an overburden pressure of 5 KPa. These unconforming data can be explained by the mechanism of intake water filling the void space of the pores in the unsaturated sample, as mentioned above. The remainder of the data seem to hold to that relation $(dh/dt)/(dw/dt) \simeq 1.09$; however, the heave rate of Test A is lower than that of Test B. This experimental result may reveal that although segregation freezing was taking place predominantly in both the saturated and unsaturated samples, the unsaturated porous rock heaves less by segregation freezing than saturated one does. This behavior is same as that found in soils.

A relation between shut-off pressure and tensile strength

Another interesting result is revealed by extrapolating the relation between heave rate or water intake rate and overburden pressure in Fig. 5 to a higher overburden pressure. As is seen in this figure, heave will cease at an overburden pressure of about 1 MPa, although the shut-off pressure of the final ice lens was expected to be about 1.4 MPa, which is the tensile strength of this sample. This relation may lead to a study of force balance at segregating ice, but several experiments should be done to examine the reliability of the extrapolation, the properties of pore water, and the mechanisms of cracking in the porous rock, for example.

Segregation freezing temperature of the final ice lens

From the sketches of the ice lens distribution for the two tests, the segregation temperatures for the final ice lenses of Test A and B are determined. The depth corresponding to the final ice lens is assumed to be equal to the cold side of the final ice lens. This means that the heave amount for the rest of the ice lenses was negligibly small. Since the final ice lens thickness is about 10 times that of the rest of the ice lenses' total, this assumption may reasonably be accepted as seen in Fig. 4. The time when the final ice

lens started to grow is assumed to be in a period between when the water intake rate is at a maximum and a time when the amount of heave reaches a value equal to the total heave minus the thickness of the final ice lens. These periods are obtained from Fig. 3a and b as t=55 to 160 hours for Test A and t=65 to 200 hours for Test B, because the thickness of the final ice lenses were determined to be 21 mm for Test A and 18 mm for Test B from sketches shown in Fig. 4b. During these two time periods, the temperature profiles seem to be stabilized as seen in Fig. 3c. Therefore, the mean values of each of the two corresponding depths are used as the temperatures when the final ice lenses started to grow and are shown in Fig. 4c. Since the ice lenses have wavy shapes, the depth and temperature of the final ice lens might vary by approximately ±3 mm and ±0.25°C, respectively. From this figure the segregation temperatures of the final ice lenses were found to be -1.45±0.25°C for Test A and - 1.4±0.25°C for Test B. These segregation temperatures are somewhat lower those that of frost-susceptible soils (Konrad and Morgenstern, 1982; Ishizaki, 1985; Akagawa, in press). This tendency may be related to the high tensile strength of the rock compared to that of the soils (Radd and Oertle, 1966; Miller, 1978; Takagi, 1980; Gilpin, 1980; Takashi et al., 1981; Horiguchi, 1987).

Another result acquired from this experiment is the concordance of the segregation temperature of the unsaturated sample and the saturated sample, although the saturated sample heaves more than does the unsaturated sample. This result may reveal that the same value of frost heaving force that cracked the specimen was generated at the place where the ice lens was segregating and the difference in the heave amount may be caused by the permeability of the water path to the segregating ice.

CONCLUSIONS

One weathering process of a porous rock, rhyolite-welded-tuff, was discussed with data obtained from open-system frost heave tests. Both saturated and unsaturated (Sr=92%) samples heaved considerably.

The mode of heaving was viewed from the analogy of the frost heaving properties, heave and/or water intake amount and rate of soil. The heaving observed in the unsaturated sample was interpreted as heaving due to segregation freezing, whereas the heaving observed in the saturated sample was interpreted as due to in situ and segregation freezing. These interpretations were confirmed by observation of the segregated ice lenses that grew by cracking the specimen, which has the tensile strength of 1.4 MPa.

The temperatures at the warm side of the final ice lenses, segregation temperature, in both saturated and unsaturated rocks were determined as -1.45±0.25°C and -1.40±0.25°C from the final ice lens locations and temperature profiles. This similarity of the segregation temperatures and the test results that the unsaturated rock heaved less than the saturated rock implied that the similar values of the frost heave force, suction force in pore water, were generated at the final ice lenses and the permeability of the water path to the ice lens causes the heave amounts to differ.

In conclusion, this particular porous rock is weathered by segregation freezing, which cracks the structure under relatively mild negative temperatures at about -1.4 to -1.5°C, even in a slightly unsaturated condition.

ACKNOWLEDGMENT

The author thanks Dr. S. Kinoshita and Dr. F. Fukuda of the Institute of Low Temperature Science , Hokkaido University, for their valuable suggestions. The author is also indebted to Dr. Y. Nakano, Dr. R. Berg and E. Chamberlain of USACRREL for their comments and stimulating discussions.

REFERENCES

Akagawa, S (1983).
Relation between frost heave and specimen length. Research report of Shimizu Institute of Technology. Tokyo: ShimizuCo (formally presented at 4th Int. Conf. Permafrost).

Akagawa, S (in press). Experimental study of frozen fringe characteristics.
J. Cold Regions Sci. Tech.

Fukuda, M & Matuoka, T (1982). Pore-water pressure profile in freezing porous rocks.
Low Temperature Science, Ser. A, (41), 217-224.

Gilpin, R R (1980). A model for the prediction of ice lensing and frost heave in soils.
Water Resource Research, 16, (5), 918-930.

Horiguchi, K (1987). An osmotic model for soil freezing.
J. Cold Regions Sci. Tech, 14, (1), 13-22.

Ishizaki, T (1985).
Experimental study of final ice lens growth in partically frozen saturated soil. Proc. 4th Int. Symp. Ground Freezing, 71-78.

Miller, R D (1978).
Frost heaving in non-colloidal soils. Proc. 3rd Int. Conf. Permafrost, 962-967.

Radd, F J & Oertle, D H (1966).
Experimental pressure studies on frost heave mechanisms and the growth-fusion behavior of ice. Proc. 2nd Int. Conf. Permafrost, 377-284.

Taber, S (1929). Frost heaving.
Journal of Geology, 37, (1), 428-461.

Takagi, S (1980). The adsorption force theory of frost heaving.
Cold Regions Science and Technology, 3, 57-81.

Takashi, T, Ohrai, T, Yamamoto, H & Okamoto, J (1981). Upper limit of heaving pressure derived by pore water pressure measurements of partially frozen soil.
Engineering Geology, 18, 245-257.

White, S E (1976). Is frost action really only hydration shattering?
Arctic and Alpine Research, 8, (1), 1-6.

SOME ASPECTS OF SOILS ENGINEERING PROPERTIES IMPROVEMENT DURING DAM CONSTRUCTION

G.F. Bianov[1], V.I. Makarov[2] and E.L. Kadkina[2]

[1]Scientific Research Centre of the "Hydroproject" Institute, Moscow, USSR
[2]The Permafrostology Institute, Yakutsk, USSR

SYNOPSIS The paper focuses on upgrading soils engineering characteristics by basic parameters defining their strength, deformation and seepage properties, with change or optimization of grain-size composition and moisture content.

For construction of embankment dams impervious elements sandy loams are used with coarse fractions having a low seepage coefficient and relatively large internal friction angle. In practice the qualitative compaction of soils with coarse fraction (with over 50 per cent of 2 mm and larger fractions of the dry soil mass) presents some difficulties because of the formation of rigid skeleton during compaction which impedes the fine soil filler compaction.

It is a common fact that with the equal amount of compaction applied the soil is compacted most effectively only at the appropriate moisture content called the optimum compaction moisture. In case the soil moisture is below optimum it is wetted before placement into the structure which is usually done without any difficulties. When the moisture content exceeds the optimum value the soil is called overmoist. The moisture content reduction of these soils is quite a problem.

The easiest way is to dry the soil by natural means, in the open air, i.e. to aerate it. Unfortunately this method of soils moisture reduction is only applicable in dry climate regions where the amount of summer precipitations is considerably lower than the evaporated moisture. In the regions with the amount of summer precipitations exceeding the evaporated moisture the aeration does not give positive results, and it may even lead to the soil moisture content increase.

The process of soil drying in specially designed furnaces is not only energy and labour consuming but low productive as well. Generally the moisture content reduction does not exceed 2-3 per cent after drying in furnaces. A more intensive soil drying results in the sharp decrease of the furnace output and higher fuel consumption.

In Japan a method was developed of the clay soil moisture reduction by adding 20 per cent of crushed granite with 15 mm maximum grain size. After mixing the moisture of the initial soil was decreased by 40 per cent due to water absorbtion by the granite fragments (Borovoi, 1957). The drawback of this method is the impossibility of simultaneous regulation of the soil moisture and grain-size composition. It is even more significant in cases of soil and soil mixtures with coarse fractions. The higher the cohesive soils moisture, the greater amount of coarse fractions is needed. But the greater the coarse-grained content of the soil, the smaller amount of fragments may be added. For example, the preparation of soil mixture with given grain-size composition including 3 components, namely: the deluvial sandy loam with pebble, gravel and crushed stone, glacial rubby sandy loam and sand gravel for construction of the Ust-Khantaisk dam cores provided the fine component moisture reduction in the soil mixture only by 1.0-1.5 per cent (Kouperman, Myznikov, Plotnikov, 1977).

The studied literature allows to conclude that at present there is no sufficiently reliable procedure for soil reclamation accepted worldwide, which could considerably change the major compactibility parameters, i.e. the moisture content and grain-size composition.

The Authors' investigations indicate that in general there is a soil reclamation method allowing to change the soil properties so that they achieve some previously prescribed parameters, this method may be called the soil improvement method. It includes the crushing of coarse fraction present or added to the soil (Bianov, Makarov, Kadkina, 1982). After crushing, the coarse fraction amount reduces, resulting in the fine grains increase. The crushed material absorbs moisture from the initial fine soil. After this treatment the soil heterogeneity and fine soil moisture decrease, resulting in higher soil compactibility.

Let us look at the feasibility of this soil improvement method for dam impervious elements construction in various climatic, engineering and geological conditions.

Example N 1. For the Kolym dam core construction the deluvial solifluction deposits were used which are natural sand soil mixture fillers with gruss crushed argillites, aleurolites

and shales fractions. The natural moisture of these soils ranges from 6 to 50 per cent with the coarse fraction (P) amounting to 35-73 per cent by weight, the coarse fractions moisture being 4.9 per cent. The design criteria for dam materials require the soil moisture below 15 per cent and P < 50 per cent, the dry fine soil density in compacted state ρ = 1.65 g/cm^3 for 90 per cent occurence.

Suppose we are to use sandy loam with 20 per cent dry fine soil moisture (W_{dfs}) and P = 35 per cent for dam core construction. To reduce the soil moisture some crushed argillites, aleurolites and shales may be added which are provided from the quarry for dam shoulders material. The crushed stone moisture is below 3 per cent. This mixture is an initial material for improvement and is to be crushed in a given mode. The improved soil is to conform to the design moisture, the grain-size composition and the compactibility requirements.

The fine soil moisture to be obtained upon improvement is calculated by the formula

$$W^*_{fs} = \frac{G_{fs}(\rho_{fs} - \rho_{dfs})\rho_m}{\rho_{fs} \cdot \rho_{dfs}} \cdot 100\% \quad (1)$$

where G_{fs} = 0.8 is the minimum fine soil saturation coefficient allowable for dam core material compaction; ρ_{fs} = 2.75 g/cm^3 is the fine component density (specific weight) of the soil; ρ_m = 1.0 g/cm^3 is the moisture density of the soil.

In compliance with equation 1 for the improved soil material of the Kolym dam core the fine soil moisture is to be W^*_{fs} = 19.3 per cent.

Determination of the soil improvement parameters includes two aspects: estimation of the required additions mass (relations of the initial components of the soil prior to crushing) and the choice of the crushing mode to attain the improved soil.

The relation between the initial components of the soil mixture is calculated by:

$$\frac{X}{Y} = \frac{(W_{dfs} - W_y)\cdot(100 - W_x)}{(W_x - W_{dfs})\cdot(100 + W_y)} \quad (2)$$

where X and Y are the amount of the soil components by weight (for example, sand and clay); W_x and W_y are these components moisture values in per cents.

The condition of the soil moisture calculation is that the soil moisture remains unchanged during crushing, i.e. the moisture of the soil mixture prior to crushing is equal to that of the improved soil material. During crushing the soil moisture content is redistributed due to absorbtion by the crushed products.

$$W_{dfs} = W^* = 0.01\, W^*_{fs}(100-P^*)+W^*_{cs}P^* \quad (3)$$

where W^*_{cs} is the coarse fragments moisture of the improved soil in per cent equal to the coarse fragments saturation.

The experiments proved that argillites, aleurolites and shales fractions available at the Kolym hydropower plant construction site increased their saturation by 2-4 per cent after crushing. For the given case we accept W^*_{cs} = = 7 per cent, P^* = 50 per cent, then W_{dfs}=W^* = = 13.2 per cent, and consequently X:Y = 1:0.8, which means that to attain the soil mixture with 13.2 per cent moisture content it is necessary to mix sandy loam soil with 35 per cent moisture content and P = 20 per cent and the crushed stone with 3 per cent moisture content in the proportion 1:0.8. Thus the prepared mixture will contain 60 per cent coarse fractions which is derived by the formula

$$P_{dfs} = \frac{P_y(W_x-W_{dfs})+P_x(W_{dfs}-W_y)}{100(W_x-W_y)} \quad (4)$$

where P_{dfs} is the coarse fraction amount of the soil mixture by weight, in per cents; P_x and P_y are the coarse fractions amount in each component of the soil mixture by weight, in per cents.

To obtain the improved soil properties with P^*= = 50 per cent from the initial soil with P_{fs}= = 61 per cent the crusher mode is chosen so that 18 per cent of the coarse fraction turn into fine-grained soil.

The soil improvement procedure is as follows. The initial soil (component X) from the quarry is conveyed to the crusher along with the additives in the form of crushed stone (component Y). The crusher produces the improved soil with prescribed parameters: W^* = 13.2 per cent, W^*_{fs} = 19.3 per cent, P^*= 50 per cent. Compacting this soil up to G_{fs}= 0.8 the dry fine component density is achieved equal to ρ_{dfs} = = 1.65 g/cm^3.

Example N 2. For the Rogun dam core the soils including 53 per cent of coarse components with 23 per cent fragments above 80 mm, and up to 37 per cent of fragments above 40 mm were used. The fine soil component moisture is 17 per cent, the fine particles density (specific weight) is 2.7 g/cm^3. The design envisages the following dam core material properties: the dry fine component density ρ_{dfs}= 2.1 g/cm^3, but not below 2.05 g/cm^3, the dry soil density ρ_{ds} = 2.25 g/cm^3, but not below 2.15 g/cm^3, and the soil moisture 11-12 per cent.

Calculation by the formula

$$\rho_{dfs}^{ult} = \frac{\rho_s \cdot \rho_m}{0.01W\rho_s + \rho_m} \qquad (5)$$

shows that the soil with ρ_s = 2.70 g/cm^3 and 11.5 per cent moisture content can be compacted up to ρ_{dfs}^{ult} = 2.05 g/cm^3 at maximum. Still the available soil is to be compacted up to $\rho_{dfs} \geqslant 2.13$ g/cm^3, thus it is to be improved.

As with the example above we calculate the improved soil properties: W^* = 10.1 per cent, W_{fs}^* = 11.5 per cent, P^* = 0.25. The calculations also reveal that no additives are required for the soil improvement. The crushing of 40 mm and above fraction alone will suffice.

At present in the Permafrostology Institute of the Siberian Branch of the USSR Academy of Sciences a testing soil improvement installation is exhibited using a double-drum crusher, the installation is based on the soil mixture preparation procedure suggested by the Authors (Bianov, Makarov, Kadkina, 1982). It is equipped with devices preventing the wet clay soil from sticking to the drums. The soil improvement installation has the productivity of 1 m^3/h per one linear centimeter of the drum length, and the energy consumption is 1 kwt·h/m^3.

The installation operation proves the versitality of this method concerning its applicability to practically all types of initial soils and materials, and the process of soil improvement by crushing, according to experiments, is sufficiently productive, cost-effective and low energy and labour consuming. The experiments indicate that some mechanical energy envolved in crushing is transformed into thermal one increasing noticeably the final soil mixture temperature, which is of particular importance for construction in low temperature conditions.

It is also essential that the soil improvement allows to significantly diminish the dam profile due to high compaction density of the soil mixtures, to reduce the dimensions of impervious elements and transition zones of earth- and rockfill dams comparing with overwetted soil mixtures.

The above examples illustrate the efficiency of the given method of soil improvement. It is a sufficient argument for the unification of embankment dams impervious elements and development of a versatile improvement procedure for various initial soils for these elements.

Recently the Central Asian Branch of the "Hydroproject" Institute has performed development projects of an experimental installation for improvement of overwetted loams with coarse fragments for the Rogun dam core. The project needs further refinment. Still the problem lies with the choice of adequate crusher. The homemade crushers, for example, drum crushers, which are the most suitable for the material to be crushed, have limited inlet and outlet opening parameters.

CONCLUSIONS

An optimization procedure of grain-size composition and moisture content of overwetted clay soils with coarse fragments has been developed and experimentally verified. The crushing of coarse fractions of the soil mixture results in the rock material specific surface and absorbtion increase, the grain-size composition improvement and lower moisture content due to its redistribution among the soil mixture components.

REFERENCES

Bianov G.F., Makarov V.I., Kadkina E.L. (1982). Sposob prigotovlenija gruntovykh smesei. Authors' Certificate N 971991. Bulletin of Inventions, N 41.

Borovoi A.A., editor. (1957). Proektirovanije i stroitelstvo bolshykh plotin. Review of the papers, presented for the 7th and 8th International Congresses on Large Dams, Energia, Moscow, p.63-64.

Kouperman V.P., Myznikov Yu.N., Plotnikov V.M. (1977). Ust-Khantaiskie plotiny. Energia, Moscow, 151 p.

FROST HEAVE FORCES ON H AND PIPE FOUNDATION PILES

J.S. Buska and J.B. Johnson

U.S. Army Cold Regions Research and Engineering Laboratory, Hanover, N.H. 03755-1290 USA

SYNOPSIS The magnitude and variation of forces and shear stresses, caused by frost heaving in Fairbanks silt and the adfreeze effects of a surface ice layer and a gravel layer, were determined as a function of depth along the upper 2.75 m of a pipe pile and an H pile for three consecutive winter seasons (1982-1985). The peak frost heaving forces on the H pile during each winter were 752, 790 and 802 kN. Peak frost heaving forces on the pipe pile of 1118 and 1115 kN were determined only for the second and third winter seasons. Maximum average shear stresses acting on the H pile were 256, 348 and 308 kPa during the three winter seasons. Maximum average shear stresses acting on the pipe pile were 627 and 972 kPa for the second and third winter seasons. The surficial ice layer may have contributed 15 to 20% of the peak forces measured on the piles. The gravel layer on the H pile contributed about 35% of the peak forces measured.

INTRODUCTION

Foundations embedded in frost-susceptible soils can be subjected to large uplift forces resulting from frost heaving of the soils. These forces can cause an upward vertical displacement of foundations that are not embedded below the frost depth or do not have sufficient resistance to counteract heaving forces. In Alaska, H and pipe piles are often used to support buildings, bridges and dock structures. It is important that design engineers know the magnitude of frost heaving forces that can act on foundation piles and how these forces are distributed along the piles. This information is used to determine the tensile strength requirements of a pile and the depth to which a pile needs to be embedded or how it must be loaded to resist heaving forces.

This paper presents the results of a three-year study (1982-85) designed to measure and record the magnitude and distribution of axial strains, as a function of depth, time and temperature, for an H pile and a pipe pile penetrating surficial layers of ice and gravel and embedded in Fairbanks silt with an active layer overlying permafrost.

METHODS AND MATERIALS

Soil Conditions

The study was conducted at the Cold Regions Research and Engineering Laboratory's Alaska Field Station, Fairbanks, Alaska. The test site had been cleared of vegetation and consisted of deep colluvial deposits of slightly organic silts (Crory and Reed, 1965). Soil moisture content was not measured in the fall preceding the 1982-83 measurement program; however, it was observed that the soil deposits were saturated below a depth of about 0.5 m. Soil moisture prior to the 1983-84 winter was found to have 40% water content by weight near the surface and varied from 25% to 29% between the surface and a depth of about 2.4 m.

The thickness of the seasonally thawed or active layer between the piles at the beginning of the winter season was 2.3 m in 1982, 1.6 m in 1983 and 1.6 m in 1984. The soil in the active layer froze to the depth of the permafrost each winter during the study, as illustrated in Figure 1. Frost heaving at the site ranges from 2 to 7 cm during a typical winter.

Two commonly encountered situations for pile installations in Alaska are aufeis buildup around piles near river crossings and the use of gravel backfill around the top of piles. The experimental configuration was designed to allow for surficial ice buildup and the use of gravel backfill. Ice collars of 1.8-m diameter were installed to a thickness of 25 cm during the 1982-83 season and 45 cm during the 1984-85 season around the upper sections of the piles in an effort to measure the adfreeze effects of surface ice deposits (Fig. 1). A 0.6-m-thick by 1.8-m diameter gravel layer was used to replace the original backfill soil around the tops of the piles in August 1983 and left in place through the 1984-85 season (Fig. 1).

The top 3-m section of an H pile (HP10x57, 25.4 cm web, 85 kg/lineal meter) and a pipe pile (30.5-cm I.D., 0.95-cm wall thickness) was instrumented with hermetically sealed weldable strain gauges and copper-constantan thermocouples. These were placed every 15.2 cm along the centerline on both sides of the web of the H pile and on diametrically opposite sides of the pipe pile. Strain gauges

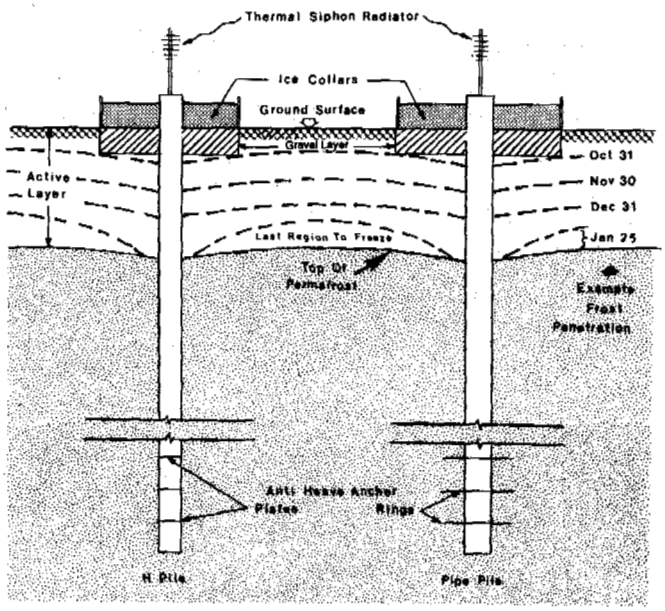

Figure 1. Development of frost penetration at the experimental site.

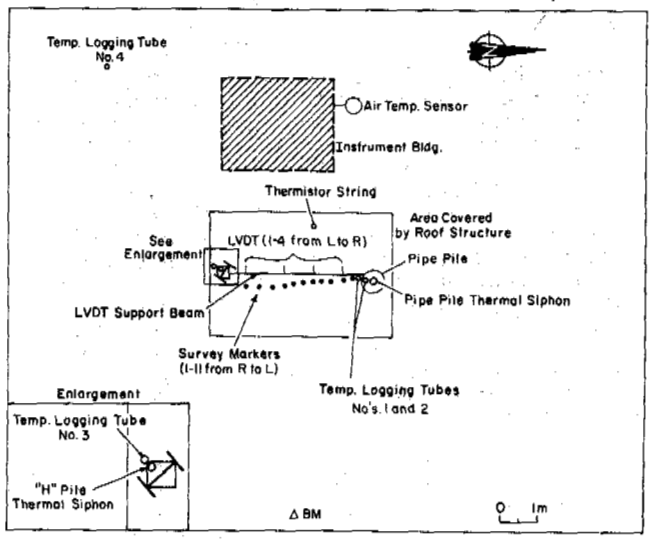

Figure 2. Plan view of the experiment site.

oriented at 90° to the axial direction were interspersed between the axially oriented gauges along the length of the instrumented sections. These we used to measure transverse strains in the piles and to estimate the magnitude of horizontal compressive stresses in the soil acting on the piles (Johnson and Esch, 1985).

Both the H and pipe piles were calibrated in compression prior to installation and in tension at the end of the experiment (Johnson and Buska, in press). After the initial calibration the piles were installed in holes augered to a depth of approximately 9 m. The holes around the piles were backfilled during the week of 31 October 1982 with a saturated sand slurry mixture for the lower 6 m and with native silt at 40% water content by weight for the upper 3 m. Thermal siphon tubes with propane as the refrigerating fluid were installed in both piles to aid in freezing the lower 6 m of backfill slurry and cooling the permafrost, thereby increasing the frost jacking resistance of the piles.

An air temperature sensor was mounted in a protective housing on the north side of the instrumentation hut. Soil temperatures were measured using thermistors spaced every 15.2 cm to a depth of 2.75 m (Fig. 2).

Soil surface heave measurements were made using standard level surveying methods during the 1982-83 season. These measurements indicated that the test piles did not change elevation during the 1982-83 season. Therefore, linear variable displacement transducers (LVDTs) mounted on a beam suspended between the piles were used to measure the ground surface heave during the 1983-84 and 1984-85 seasons (Fig. 2). The stability of the piles was reconfirmed by survey during the 1984-85 season.

Force and Shear Stress Calculations

The magnitudes of frost-heave-induced shear stresses along the soil/pile interface were determined by using the strain measurements to first calculate the internal axial stresses in the piles and the internal axial forces in the piles. The frost-heave-induced shear stresses along the soil/pile interface were then found by dividing the difference in force magnitude between two adjacent gauges by the corresponding pile surface area (Johnson and Esch, 1985).

Due to strain gauge malfunctions, the shear stress at the ice/pile interface over the thickness of the ice collar had to be estimated, by using the flow law for polycrystalline freshwater ice to obtain

$$\tau_c = (\dot{\epsilon}/A)^{1/n}$$

where $\dot{\epsilon}$ is the strain rate in the ice, A is a temperature-dependent constant, τ_c is the shear stress over the thickness of the ice collar and n is a constant determined from experiments (Paterson, 1981; Johnson and Buska, in press). The strain rate in the ice was calculated as the difference between the soil surface displacement rate near the pile and that at the soil/pile interface divided by the width over which soil displacement occurs (assumed to be 1 cm; Penner and Irwin, 1969).

The uplift force on the piles at the ground surface due to the ice collar was calculated as a product of the ice/pile shear stress (τ_c), the pile surface area per lineal centimeter and the ice collar thickness.

The heaving force acting on the piles due to the gravel layer was calculated by subtracting the force acting on the pile at a depth just below the bottom of the gravel layer from the force due to the ice layer (Johnson and Buska, in press).

EXPERIMENTAL RESULTS AND DISCUSSION

There were five major low-tempeature periods during each season when the air temperature dropped below -25°C for several days or more. Ground temperatures throughout the active layer above the permafrost were at or below 0°C by early April for the first winter season and by early January for the last two winter seasons. The temperatures along the H and pipe piles were slightly lower than those in the adjacent undisturbed ground. Temperatures for the pipe pile were generally lower than those for the H pile because of better contact with the thermal siphon at depth. Soil and pile temperatures were lower during the second and third winter seasons because the site was cleared of snow.

Figure 3 shows the soil surface heave for the 1982-83, 1983-84 and 1984-85 seasons. The ground surface displacements of between 2 and 7 cm shown in Figure 3 may slightly underestimate the absolute or maximum accumulated displacements since the measurements were initiated just after the onset of soil freezing. The displacement measurements for 1983-84 indicate that the soil heave was greatest in the vicinity of the pipe pile.

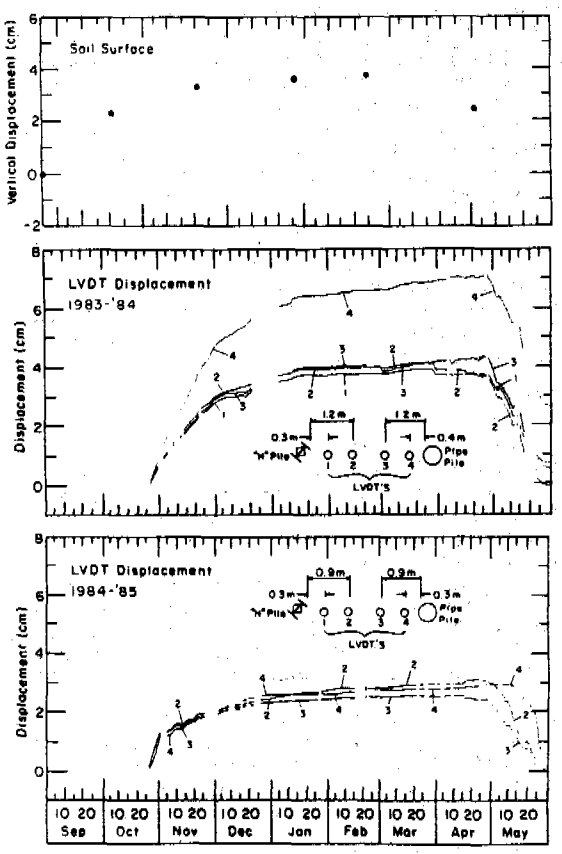

Figure 3. Soil surface heave for the 1982-83, 1983-84, and 1984-85 seasons. LVDT displacements for points 1, 2, 3, and 4 indicate soil surface displacements taken at the locations indicated.

The temperature, shear stress and frost heave force distributions for the H pile are shown in Figure 4 for selected dates during the 1984-85 season. The shaded area shows the shear stress distribution on the H pile. The ice/pile shear stress and the uplift force due to the ice collar are shown above the ground surface or zero depth value. Soil/pile shear stresses due to frost heaving are not uniform along the length of a pile; generally they act from the ground surface to the depth of the maximum force on the pile, and the restraining shear stresses act from the depth of the maximum force on the pile downward until the uplift force is balanced. Uplift soil/pile shear stresses are present in the permafrost throughout the winter season.

Table 1 summarizes the results and Figures 5-7 show the air temperature, ground temperature and pile frost heave force as functions of depth and time for the 1982-83, 1983-84 and 1984-85 seasons.

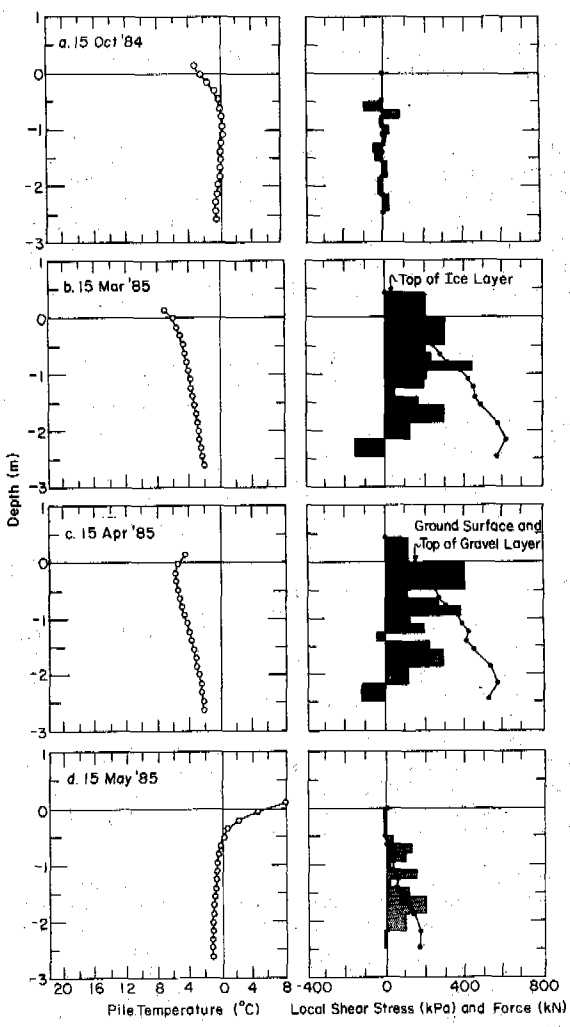

Figure 4. Pile temperature, shear stress distribution (shaded area), and force as a function of depth for the H pile during the 1984-85 season. (a) 15 October 1984; (b) 15 March 1985; (c) 15 April 1985; (d) 15 May 1985.

Table 1. Summary of Maximum Forces and Average Shear Stresses on the H and Pipe Piles.

	H pile			Pipe pile*	
	1982-83	1983-84	1984-85	1983-84	1984-85
Date peak frost heaving force occurred	24 Jan 1983	17 Feb 1984	26 Feb 1985	17 Dec 1983	15 Dec 1984
Depth below ground surface where peak force occurred (m)	2.29	2.21	2.16	1.75	0.94
Peak frost heaving force (kN)	752	790	802	1118	1115
Thickness of active layer between the piles at beginning of season (m)	2.3	1.6	1.6	1.6	1.6
Thickness of ice layer (m)	0.25	---	0.45	---	0.45
Heaving force due to ice layer (kN)**	151	---	118	---	185
Ice/pile shear stress due to ice layer (kPa)**	588	---	255	---	401
Max. average soil/pile shear stress using "boxed-in" (H) surface area of H pile (kPa)***	256	348	308	---	---
Max. average soil/pile shear stress using actual surface area of piles (kPa)***	157	214	190	627	972
Maximum internal stress in pile (MPa)	48.5	51.0	51.7	118.7	118.4
Heaving force due to gravel layer (kN)**	---	280	292	---	---

* The pipe pile results need to be verified by further research (see text).

** The force and shear stresses for the ice and gravel layers had to be calculated indirectly (see text) and may be too high for the ice layer and consequently too low for the gravel layer.

*** Computed using the pile surface areas from the soil surface to the depth of the peak frost-heaving force on the pile.

The peak forces on the H pile were essentially the same, varying by only 29 kN from the average peak force for all three winter seasons. During the study, the pipe pile suffered considerable strain gauge malfunction. The results from the few remaining good gauges are presented in Table 1. The magnitudes of forces and shear stresses on the pipe pile appear too high in comparison with the H pile results and values reported by others. The pipe pile results need to be verified by further research. The ice collars may have contributed 15 to 20% of the peak forces measured on the piles. The forces and stresses resulting from the ice and gravel layers could not be determined directly due to strain gauge malfunctions. The forces and stresses were calculated indirectly and may be too high for the ice layer and consequently too low for the gravel layer.

The forces for both piles generally increased after a decrease in air temperature and decreased after an increase in air temperature. Changes in the forces acting on the piles usually lagged behind corresponding air temperatures from 1 to 8 days, with the longer lag times occurring later in the winter season. In the spring, uplift forces are relieved from the surface down as the ground warms.

The majority of experiments to measure frost heaving forces acting on piles have been conducted on piles embedded in non-permafrost soil. In analyzing the results of those experiments it has been implicitly assumed that once the soil temperature is lower than 0°C (i.e. when the soil is frozen) the soil heave and frost-heaving forces are negligible. The results of our experiments and those of Crory and Reed (1965) indicate that soil heave and frost heave forces continue to be generated throughout the winter even in frozen ground (Figs. 3-7). These effects may possibly be explained by the existence and migration of unfrozen water within the frozen soil. When frozen soil containing both ice and unfrozen water is subjected to a temperature gradient, this causes water to move toward the colder

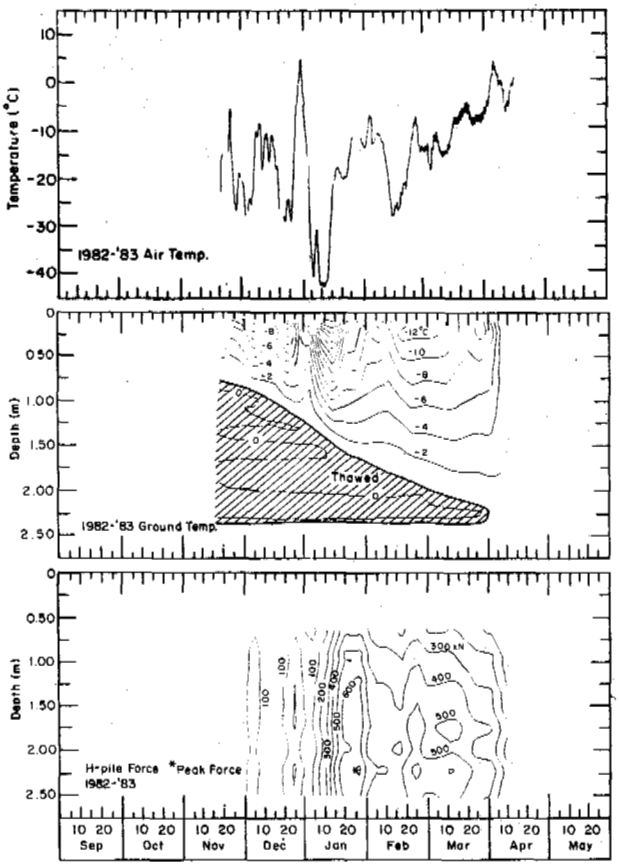

Figure 5. Comparison of air temperature, ground temperature, and H pile frost heave force as a function of depth and time for the 1982-83 season.

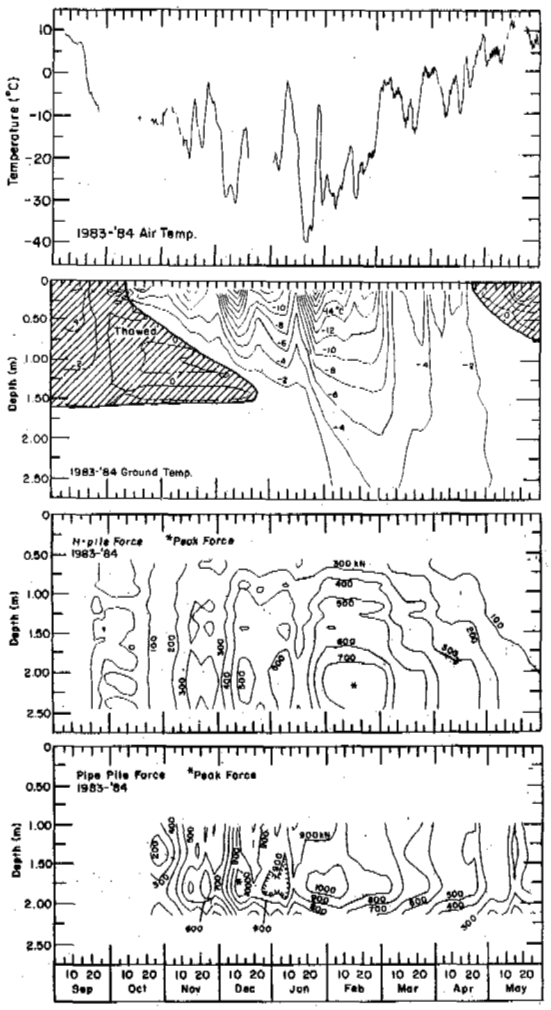

Figure 6. Comparison of air temperature, ground temperature, H pile frost heave force, and pipe pile frost heave force as a function of depth and time for the 1983-84 season.

soil, enhancing ice lens formation and soil heaving (Oliphant et al., 1983). The unfrozen water content-temperature relationship may also explain why the heave forces acting on piles embedded in permafrost respond so rapidly to temperature changes. On cooling, an increase in ice lens growth will contribute to increased heave forces. On warming, the percentage of unfrozen water will increase exponentially as a function of temperature, resulting in a decrease in heave forces.

The depth of maximum heave force might be expected to coincide with the depth where the most rapid freezing is occurring (Johnson and Buska, in press). For non-permafrost soils the depth of most rapid freezing is near the 0°C isotherm. The relationship between temperature and unfrozen water content for frozen soils must be known to estimate the depths of maximum freezing rate over time. The depth of maximum freezing rate is then used when calculating the depth of action for frost heaving stresses over time.

CONCLUSIONS

Calculated forces, as determined from the instrumented piles, indicate that the magnitude of frost-heaving uplift forces acting on a pile increases from the soil surface to a maximum value at depth, and then decreases due to the restraining action of the soil or permafrost on the pile.

The average depths of the maximum frost heave forces were 2.2 m on the H pile and 1.4 m on the pipe pile. The peak frost-heave forces were 802 kN for the H pile and 1118 kN for the pipe pile during the three winters of the study. The maximum internal tensile stresses were 51.7 MPa for the H pile and 118.4 MPa for the pipe pile. The maximum calculated heave

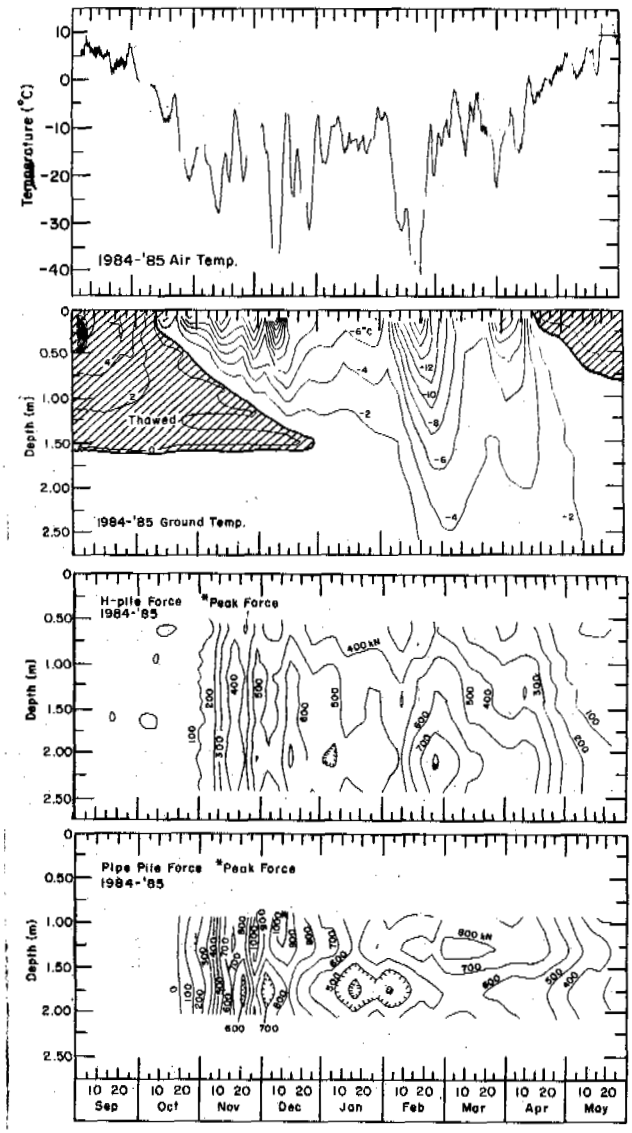

Figure 7. Comparison of air temperature, ground temperature, H pile frost heave force, and pipe pile frost heave force as a function of depth and time for the 1984-85 season.

force that may have been contributed by the ice layers at the top of the piles was 151 kN for the H pile and 185 kN for the pipe pile. The maximum calculated heave force contributed by the gravel layer around the top of the H pile was about 292 kN.

The maximum average soil/pile shear stress computed on the basis of the "boxed in" (H) surface area of the H pile from the soil surface to the depth of peak frost heave force was 348 kPa for the H pile. The maximum average soil/pile shear stress computed using the actual surface areas of the piles from the soil surface to the depth of the peak frost heave force was 214 kPa for the H pile and 972 kPa for the pipe pile. Ice/pile shear stresses due to the ice collars at the tops of the piles were 588 and 255 kPa for the H pile and 401 kPa for the pipe pile.

Maximum heaving forces and shear stresses occurred during periods of maximum cold and soil surface heave magnitude. These forces were not related to the depth of frost for most of the winter, since the soil adjacent to the piles was frozen to the permafrost table, and may be explained by the existence of unfrozen water in the soil. The forces for both piles generally increased after a decrease in air temperature and decreased after an increase in air temperature. Changes in forces acting on the piles usually lagged behind corresponding air temperature changes by several days. Soil surface displacements of 2 to 7 cm were measured at the experiment site.

The important mechanisms that determine the magnitude of uplift heave forces are (1) soil heaving as the driving force, and (2) soil temperature, which controls the unfrozen water content, mechanical properties of the soil and the area of influence of heaving pressures.

ACKNOWLEDGMENTS

Funding for this study was provided by the Alaska Department of Transportation and Public Facilities and by the Federal Highway Administration.

The authors gratefully acknowledge the efforts of C. Rohwer, C. Olmstead, S. Perkins, B. Young, R. Briggs, D. Solie, D. Dinwoodie, M. Sturm, W. Zito, L. Kozycki and D. Haynes. The authors also thank Dave Esch for his contributions to the completion of the project.

REFERENCES

Crory, F E & Reed, R E (1965). Measurement of frost heaving forces on piles. U.S.A. Cold Regions Research and Engineering Laboratory (USACRREL) Technical Report 145.

Johnson, J B & Esch, D C (1985). Frostjacking forces on H and pipe piles embedded in Fairbanks silt. Proc 4th Inter Sym Ground Freezing, Sapporo, (2), 125-133.

Johnson, J B & Buska, J S (in press). Measurement of frost heave forces on H and pipe piles. USACRREL Report.

Oliphant, J L, Tice, A R & Nakano, Y (1983). Water migration due to a temperature gradient in frozen soil. Proc 4th Inter Conf Permafrost, Fairbanks, 951-956.

Paterson, W S B (1981). The physics of glaciers. 20-41. Pergamon, New York.

Penner, E & Irwin, W W (1969). Adfreezing of Leda Clay to anchored footing columns. Can. Geotech. J., (6), 3, 327-337.

A NEW FREEZING TEST FOR DETERMINING FROST SUSCEPTIBILITY

E.J. Chamberlain

U.S. Army Cold Regions Research and Engineering Laboratory

SYNOPSIS A new freezing test for determining the frost susceptibility of soils used in pavement systems is designed to supplant the standard CRREL freezing test. This new test cuts the time required to determine frost susceptibility in half. It also allows for the determination of both the frost heave and thaw weakening susceptibilities and considers the effects of freeze-thaw cycling. The new freezing test also eliminates much of the variability in test results by completely automating the temperature control and the data observations.

INTRODUCTION

Laboratory freezing tests are necessary to accurately characterize the frost susceptibility of soils. This is especially true for borderline granular materials used for the base and subbase layers in roads and runways.

The U.S. Army Corps of Engineers has employed a freezing test (Chamberlain and Carbee, 1981) for more than 30 years. While this test has proven adequate for identifying and classifying frost-susceptible soils, it suffers from several serious defects. Most significant of these are poor temperature control, indeterminate side friction, lengthy test period, lack of thaw weakening index, and provision for only one freeze. Furthermore, the standard CRREL freezing test is conservative and appears to reject many non-frost-susceptible materials as frost-susceptible.

This report discusses the current Corps of Engineers practice for conducting freezing tests on soils, presents a new freezing test designed to replace it, describes test equipment and procedures, and suggests a method for classifying the frost susceptibility of soils based on both frost heave and thaw weakening.

CURRENT FREEZING TEST

The freezing test employed by the Corps of Engineers, often referred to as the CRREL standard freezing test, was developed to evaluate the relative frost susceptibility of soils and granular base and subbase materials used in pavement systems. In the standard test, materials are subjected to a very severe combination of freezing and moisture conditions that are highly conducive to frost heaving. The test does not predict the actual magnitude of frost heave under field conditions, but is designed to provide a relative indication of the potential for frost heave.

Soil samples are generally compacted and frozen from the top down at a constant rate of 13 mm/day for 12 days. The samples are frozen in tapered, acrylic Plexiglas cylinders that are Teflon-lined and lightly coated with silicone grease to reduce side friction. A porous stone at the base and a constant-head water supply provide a source of water 10 mm above the sample bottom. A surcharge of 3.5 kPa is placed on the sample to simulate a 150 mm thickness of asphalt concrete pavement. The samples are frozen in groups of four in a freezing cabinet. The lower boundary temperature is maintained at +4°C throughout the test, while the upper boundary air temperature is lowered once a day in steps to facilitate the average frost penetration rate of 13 mm/day.

The temperatures in the soil samples are measured by thermocouples placed through the cell walls and are automatically recorded by a data acquisition system. Frost heave is observed with displacement transducers and is continuously recorded, along with the thermocouple outputs, on the data acquisition system. Frost depths are determined by plotting the temperature profiles and interpolating the position of the 0°C isotherm. The maximum frost heave rate occurring during the test period is used as an index of the frost susceptibility.

The standard test has several limitations. The test requires too much time (12 days) and is encumbered by manual temperature adjustments. Side friction is not eliminated, particularly with coarser-grained materials. The test does not consider the effects of freeze-thaw cycling. The test is principally an index test for frost heave and does not directly address thaw weakening, which is frequently more of a problem in roads than frost heave. Furthermore, the standard test appears to be conservative, and there is no evidence of direct correlation with field observations.

DEVELOPMENT OF A NEW FREEZING TEST

A new freezing test was proposed (Chamberlain, 1981) to alleviate the problems with the standard test. As a result, the following criteria were established: 1) precise control of boundary temperatures is necessary; 2) radial heat flow must be minimized; 3) side friction must be eliminated; 4) free access to water must be available; 5) freeze-thaw cycling must be specified; 6) the test must be completed in one week; and 7) the test must provide for both frost heave and thaw weakening susceptibility indexes.

The literature was thoroughly reviewed (Chamberlain, 1981) for state-of-the-art practices for determining the frost susceptibility of soils with freezing tests. A multi-ring freezing cell (MRFC) configuration was selected to minimize side friction during freezing while still accommodating the other important factors. The MRFC is not a new development in frost-susceptibility testing; it was used long ago by Taber (1929) and Ruckli (1950). Because of the lack of a moisture seal between the rings and because of soil extrusion between rings during thawing, a rubber membrane was selected to line the inside of the cell.

I also found that precise upper and lower boundary temperature control could be best obtained by circulating a non-freezing liquid from refrigerated baths through plates in intimate contact with the top and bottom of the test sample. Although a constant rate of heat extraction was considered desirable, it was concluded that a constant cold-plate temperature during freezing was a more practical objective and that the heat extraction rates should approximate the rates that occur in seasonal frost regions. A heat flow rate in the range of 50-100 W/m² was selected for the critical period during which the frost heave susceptibility index would be determined. A temperature gradient of approximately 0.04°C/mm was chosen as a compromise between what has been observed in the field and what is technically practical.

I decided that at least two freeze-thaw cycles were required to allow for the effects of changes in soil structure, density, permeability, etc. caused by freezing and thawing. Each freeze-thaw cycle would take 48 hours and each leg of the cycle would be 24 hours in duration. With an allowance for a final 24 hours for conducting the thaw weakening test, the freezing and thawing could be accomplished in one working week.

As a result the upper boundary temperature was selected to be -3°C and the lower boundary temperature +3°C for the first 8 hours of freezing. To assure complete freeze conditioning of the test sample, the top and bottom temperatures are set to -12°C and 0°C, respectively, during the final 16 hours of each freezing leg. Complete freezing is necessary to thoroughly condition the test material with frost action before freezing it a second time. This is necessary because the frost heave rates of materials containing clay fines may be increased significantly by freeze-thaw cycling. The frost heave observations critical to determining the frost heave susceptibility are made at the end of the first 8 hours of freezing. During the first 16 hours of thawing, the temperature of the upper boundary is raised to +12°C and the bottom temperature is increased to +3°C. Both the upper and lower boundary temperatures are set to +3°C during the last 8 hours of thawing to condition the sample at a uniform temperature before the next freeze. The same conditioning temperatures are applied before the first freeze to ensure that the initial temperature conditions are the same for both freeze-thaw cycles. The entire boundary temperature program is illustrated in Fig.1.

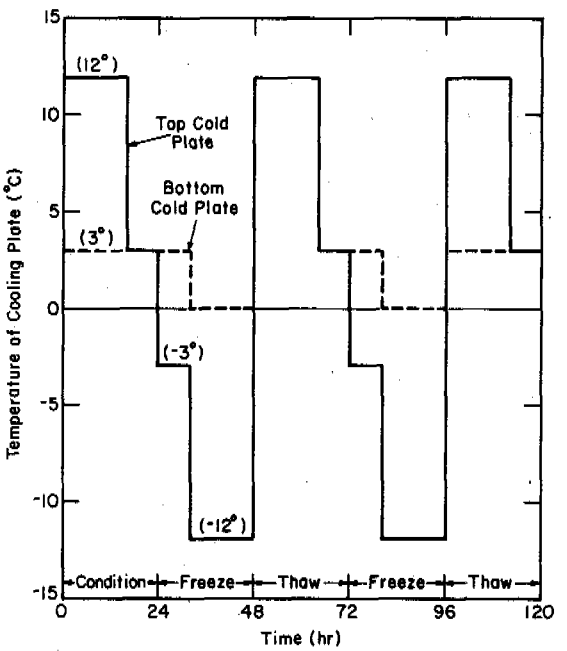

Figure 1. Boundary temperatures for new freezing test.

I decided that a constant head of water should be supplied to the base of the sample through a porous stone. The water table should be maintained about 10 mm above the sample base during freezing to provide a severe condition of water availability. The samples can be soaked before freezing by raising the water table in increments to the top. Theoretically the water table could also be lowered to approximately 1 m below the sample base if a 1-bar air entry value saturated porous stone were placed between the sample and the base plate. The practical maximum distance between the sample bottom and the water table, however, is 0.75 m because of problems in sustaining the continuity of water in the porous stone, in the space beneath it, and in the connecting lines. The water supply can also be shut off to simulate closed-system freezing.

A surcharge of 3.5 kPa was selected as a standard for this freezing test as is used for the standard test. No surcharge would be a more

severe condition, but not one applicable to pavement systems.

To facilitate the determination of the frost depth and the boundary temperatures, thermocouples are placed at intervals along the side of the test sample. More precise thermistor or RTD sensors were not considered because of their higher cost and greater fragility. The thermocouples are sealed to the wall with silicone rubber to prevent water leakage.

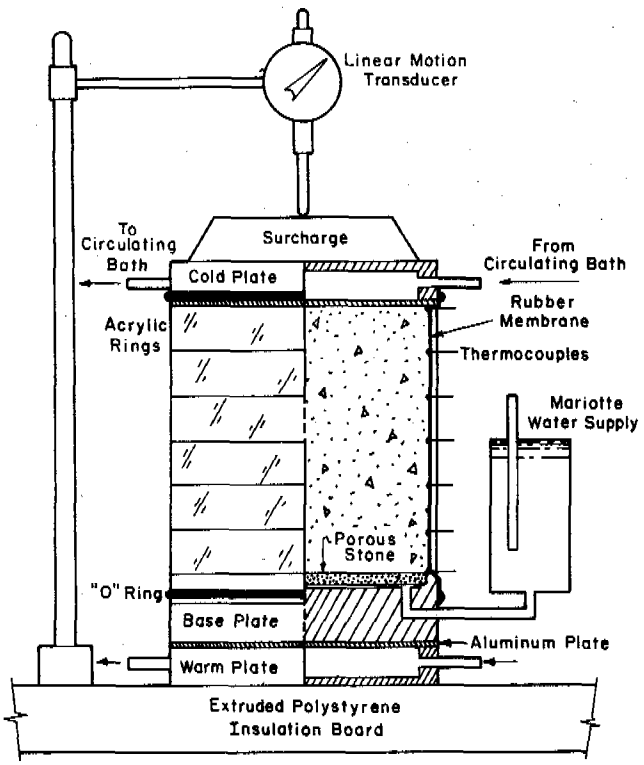

Figure 2. Schematic of new freezing test apparatus

The MRFC test apparatus is illustrated in Fig. 2. The inside diameter of the MRFC is 146 mm and the height 154 mm. Six 25.4-mm-high Plexiglas rings, lined with a rubber membrane, make up the cell. Water is made freely available through a porous base stone from a Mariotte constant-head water supply. Heat exchange plates (cold and warm) are located directly on top of the sample and beneath the water supply base. A solution of ethylene glycol and water is circulated through the cold plates from refrigerated baths to maintain the desired test temperatures. The bath temperatures are controlled with a computer that is programmed with the boundary temperatures shown in Fig. 1. Four samples are frozen together to facilitate replications and productivity. The tests are conducted in a cold room with an ambient temperature just above freezing to limit radial heat flow and to thus ensure a planar freezing zone. Stand-alone setups have also been prepared as shown in Fig.3.

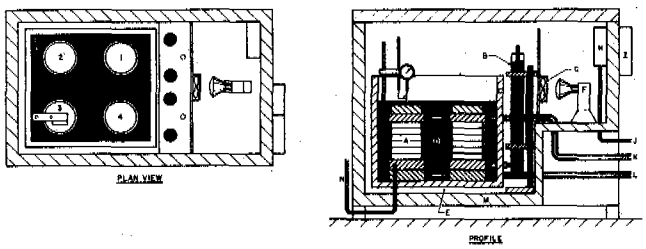

Figure 3. Freezing cabinet assembly for new freezing test.

Dial gages and displacement transducers are arranged on top of each sample to provide records of frost heave and thaw consolidation. The outputs of the displacement transducers and the thermocouples are recorded with a computer-controlled data acquisition system. The same computer is used to control the plate temperatures. The entire data acquisition control system is illustrated schematically in Fig. 4. The data are automatically processed and recorded on a magnetic tape or floppy disk and displayed on a printer. Upon completion of the freeze-thaw cycling, the critical frost heave rates are determined automatically and printed for a permanent record.

The frost heave rates at 8 hours into each freezing leg are considered the critical heave

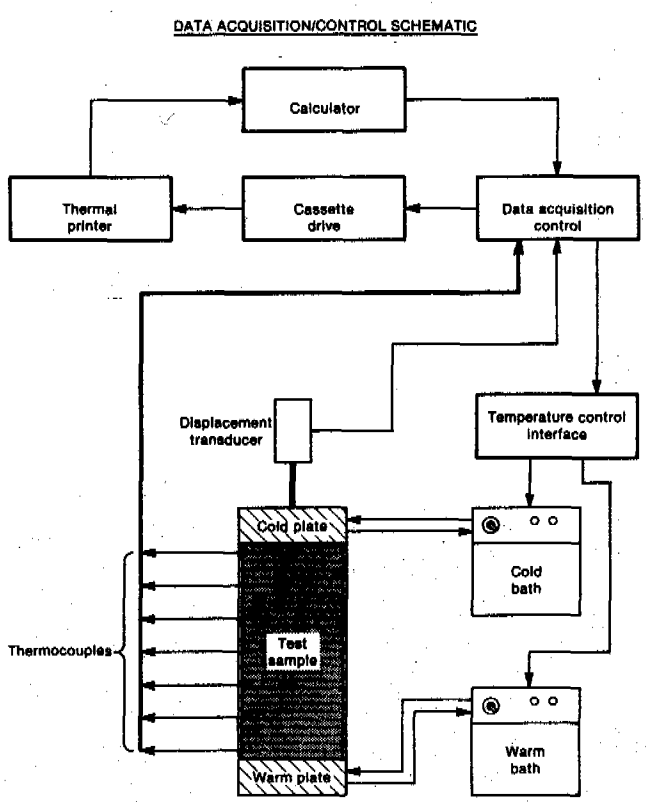

Figure 4. Schematic of the temperature control and data acquisition system.

rates, and they are used to determine the frost-heave susceptibilities of the test materials. The frost-heave susceptibility determined from the first freeze should be used for conditions where freezing is continuous throughout the winter, whereas the frost susceptibility from the second freeze should be used when more than one complete cycle of freezing and thawing occurs. The thaw-weakening susceptibility is determined after the second freeze-thaw cycle with a CBR (California bearing ratio) test. Preliminary frost-susceptibility criteria based on all three of the critical factors are shown in Table I.

Table I. Preliminary frost-susceptibility criteria.

Frost-susceptibility classification	Heave rate (mm/day)	Thaw CBR (%)
Negligible	<1	>20
Very low	1-2	20-15
Low	2-4	15-10
Medium	4-8	10-5
High	8-16	5-2
Very high	>16	<2

VALIDATION OF THE NEW FREEZING TEST

Preliminary tests were made to ensure that the MRFC method of confinement minimized the side friction problem. The rubber-lined multi-ring configuration was first compared with the CRREL Teflon-coated tapered cylinder and wraps made of telescoping plastic film and waxed paper. Fig. 5 shows the results of freezing tests on a frost-susceptible sand with the four methods of confinement. The MRFC and the plastic film and waxed paper confined samples heaved similarly, while the frost heave in the CRREL tapered cylinder was considerably less. Another test series that included a sample with no confinement confirmed that the MRFC method of confinement caused little restraint to frost heave.

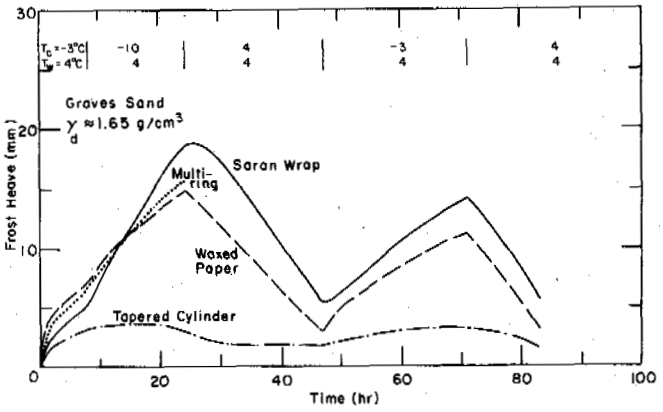

Figure 5. Results of freezing tests with four experimental methods of confinement.

Other studies were made to ensure that the frost front was planar and the heat flow was one dimensional. Split vertical sections of a frozen clay specimen showed nearly linear ice and soil layer features characteristic of one-dimensional heat flow, whereas radial heat flow was observed to be no more than 5 W/m^2. The radial heat flow measurements also showed that the net vertical heat flow was in the range of 50-100 W/m^2 at the end of the first 8 hours of both freezing legs.

The new freezing test was validated with materials and data from field test sections. Six soils from Winchendon, Massachusetts, and three from Albany, New York, were selected for this evaluation. These tests are discussed in detail elsewhere (Chamberlain, 1986). The Unified Soil Classifications and other soil index properties for each of the test materials are given in Table II. Examples of test results for two of the test materials are shown in Fig. 6 and 7. Figure 7 illustrates the importance of the two freeze-thaw cycles. The critical frost heave rate for the second freeze is five times the rate observed during

Table II. Test material index properties.

Material	Percent finer than 0.074 mm	Percent finer than 0.002 mm	Uniformity Coefficient	Liquid Limit (%)	Plasticity Index (%)	Gravity	Soil classification*
Winchendon							
Dense-graded stone	9	6	46.2	-	NP	2.82	GM-GP
Graves sand	48	16	20.8	-	NP	2.70	SM
Hart Brothers sand	31	8	9.1	-	NP	2.76	SM
Hyannis sand	31	3	3.8	-	NP	2.67	SM
Ikalanian sand	48	8	5.2	-	NP	2.70	SM-SP
Sibley till	38	24	22.5	19	4	2.74	SM-SC
Albany							
Taxiway B base	15	10	95.8	-	NP	2.72	SW-SM
Taxiway B subbase	13	8	16.3	-	NP	2.68	GW-GM
Taxiway B subgrade	16	6	2.6	-	NP	2.69	SM

* G - gravel, S - sand, M - silt, P - poorly graded, C - clay, W - well graded.

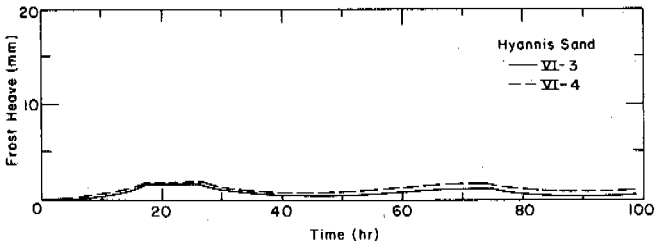

Figure 6. Example of frost heave results with new freezing test; Hyannis sand.

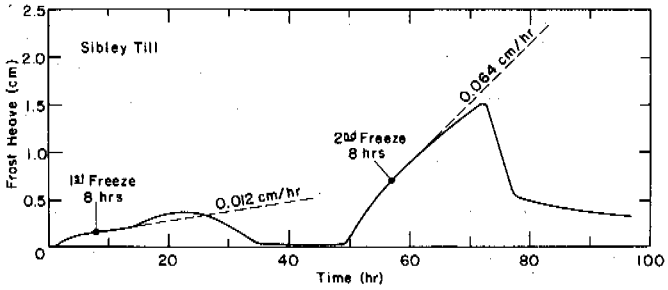

Figure 7. Example of frost heave results with new freezing test; Sibley till.

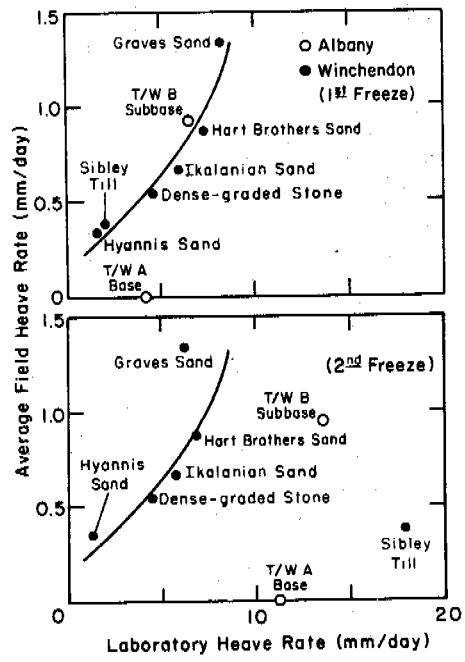

Figure 8. Comparison of average field frost heave rates with laboratory heave rates.

the first freeze. Three additional tests on the same soil yielded similar results. This soil, Sibley till, had 24% finer than 0.002 mm and a plasticity index of 4.

The average frost heave rates for each of the test materials are plotted against the average frost heave rates observed for a two-year period in the field in Fig. 8. There is a strong correlation between the laboratory and field observations of heave rate, especially for the first freeze. The correlation is not on a line of equality, as the laboratory heave rates exceed the field values by a factor of 10. However, it is the intent of this study to use the freezing test qualitatively as an index test, not a quantitative predictor of frost heave in the field. When the heave rate results are plotted for the second freeze (Fig. 7), the correlation between the laboratory and field results is weaker, as the points for two Albany sites and one Winchendon site fall far to the right of the curve fitting the remainder of the data.

The CBR after thawing is correlated with results of pavement loading tests in Fig. 9. It can be seen that there is a strong correlation between the laboratory CBR after thawing and the maximum resilient pavement deflections for a simulated wheel load of 280 kPa that occurred during the thaw period in the field.

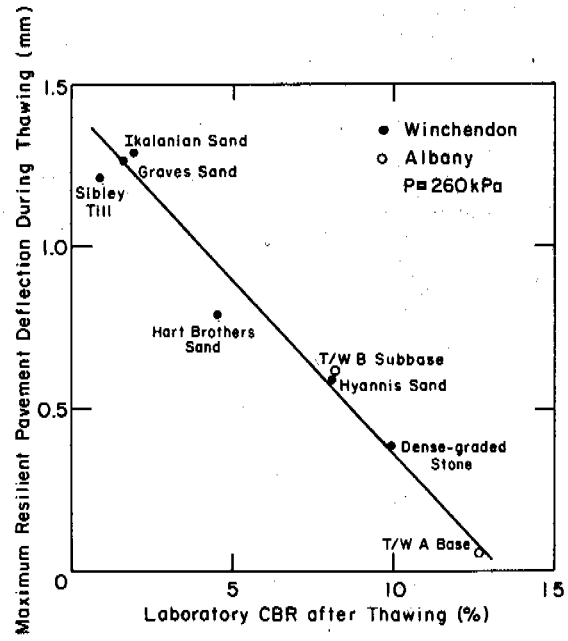

Figure 9. Comparison of maximum pavement deflections for 280-kPa simulated wheel loading in the field with the laboratory CBR after thawing.

DISCUSSION

The importance of conducting a freezing test with indicators of both frost heave and thaw weakening susceptibility has been demonstrated with this series of tests. Comparisons of

Table III. Summary of frost-susceptibility ratings made with new freezing test.

Material	New freezing test: 8-hr heave rate, 1st freeze	New freezing test: 8-hr heave rate, 2nd freeze	New freezing test: Thaw CBR	Range of field observations: Heave rate	Range of field observations: Pavement deflection
Winchendon					
Dense-graded stone	M	M	M	VL-M	M
Graves sand	H	M	VH	L-H	H-VH
Hart Brothers sand	M	M	H	VL-M	H
Hyannis sand	VL	VL	M	N-L	M
Ikalanian sand	M	M	H	VL-M	H-VH
Sibley till	VL	VH	VH	N-VL	H-VH
Albany					
Taxiway A base	M	H	L	N	N
Taxiway B subbase	M	H	M	L	H
Taxiway B subgrade	H	H	VL	L	H

N - negligible, VL - very low, L - low, M - medium, H - high, VH - very high

frost-susceptibility ratings for each of the test materials (Table III) show that the frost-susceptibility classifications based on thaw weakening are either greater than or equal to the ratings based on frost heave, and for the Sibley till material, the thaw-weakening characteristics would definitely control its selection as a road construction material. The importance of conducting two freeze-thaw cycles is not as clearly demonstrated with these tests apart from the observation that freeze-thaw cycling can have a dramatic effect on frost heave rate in the laboratory. The increases in heave rates observed in the laboratory were probably due to changes in permeability caused by freezing. Chamberlain and Gow (1979) showed that freezing can cause large increases in the permeability of soils containing clay fines. The response was different in the field because the freezing and thawing did not reach the water table. Thus, an unconditioned layer of material remained between the water table and the freezing zone.

Because all of the field validation work was done at sites where the water table was very near to the maximum depth of frost penetration, the frost-susceptibility classifications given in Table III are for a severe water availability condition. For other conditions where the water table is deep or there is a coarse drainage layer that interrupts the flow of water into the test material, a closed-system freezing test may be more appropriate.

The test results presented here are for only a limited number of materials and test conditions. For this test to be implemented as a tool for design or compliance, additional tests must be conducted for a wider variety of soil and environmental conditions.

CONCLUSIONS

The determination of the frost susceptibility of soil materials used in pavement systems is more adequate with a freezing test if indicators of both frost heave susceptibility and thaw weakening susceptibility are included in the test matrix. The effects of freeze-thaw cycling can be evaluated by including at least two cycles of freezing and thawing.

The new freezing test described here accomplishes these tasks in a more efficient and precise manner than the currently used standard CRREL freezing test.

Additional validation of the new freezing test is required before reliable frost-susceptibility criteria based on its use can be established and before the test can replace the standard freezing test used by the Corps of Engineers.

REFERENCES

Chamberlain, E J (1981).
Frost susceptibility of soil, Review of index tests. U.S. Army Cold Regions Research and Engineering Laboratory, CRREL Cold Regions Science and Engineering Monograph 81-2., 121 p.

Chamberlain, E J (1986).
Evaluation of selected frost-susceptibility test methods. U.S. Army Cold Regions Research and Engineering Laboratory, CRREL Report 86-14, 56 p.

Chamberlain, E J & Carbee, D L (1981).
The CRREL frost heave test.
Frost I Jord, (22), 55-63.

Chamberlain, E J & Gow, A J (1979).
Effect of freezing and thawing on the peremability and structure of soil.
Engr. Geology, (13), 73-92.

Ruckli, R (1950).
Pavement design and frost susceptibility of road foundations. (In German),
Strasse und Verkehr, (36), 125-134.

Taber, S (1929).
Frost heaving.
Jour. of Geology, (27), 428-461.

THAW SETTLEMENT OF FROZEN SUBSOILS IN SEASONAL FROST REGIONS

Cheng, Enyuan and Jiang, Hongju

Oilfield Construction Design and Research Institute of Daqing Petroleum Administrative Bureau, China

SYNOPSIS The laboratory thaw consolidation tests with undisturbed samples and the in-situ observations on thaw settlements of testing buildings and in-operation buildings were carried out. for investigating the thaw settlement of frozen ground. It is found that the settlement of frozen soils starts with the soil temperature increasing and the relation between the settlement amount and elapsed time of thawing is practically linear. The consolidation settlement tends to be stable in ten days after the soil was completely thawed. The thawing consolidation settlement amount is directly proportional to the applied load. A commonly used formula for predicting the thawing and consolidation settlement was checked by testing 967 samples taken from 11 sites.

INTRODUCTION

In seasonal frost regions, if the soil is frost susceptible, the thaw settlement of foundation will take place during thaw. With a certain level of load on thawing frozen soil, the settlements are caused by thaw as well as compression. Combination of these two kinds of settlements will make the building based on the soil to settle in different extents. As the settlement is greater than the allowable deformation of a building, the building will be destroyed. In order to investigate thaw-settlement behaviour of frozen soils and predict the thaw settlement of actual engineering, the following work i.e., laboratory thaw-consolidation tests with undisturbed frozen soil samples, field observations on thaw settlement of natural ground with or without external loads, and observations on thaw settlement of frozen subsoils beneath actual buildings were performed during 1981-1985.

THE COMMONLY-USED FORMULA FOR CALCULATING THAW-CONSOLIDATION SETTLEMENT

As mentioned above, if there are loads on frozen subsoils, the consolidation settlement will take place in company with thaw settlement during thaw. This total value of the settlements of frozen soils may be calculated with the following formula (Tsytovich, 1962).

$$S = A_0 H + aPH \qquad (1)$$

where A_0 is the coefficient of thaw settlement;

a is the coefficient of consolidation;
H is the thickness of thawing frozen-soil;
P is the total compression stress on the subsoils concerned.

If the values of A_0, a and P vary with the depth, in calculating the total settlement frozen subsoil, it is necessary to divide the frozen soil concerned into several layers. The settlement in i-th layer may be estimated by

$$\Delta S_i = \Delta H_i \ (A_{oi} + a_i P_i) \qquad (2)$$

Then, the total thaw and consolidation settlement is given by

$$S = \sum_{i=1}^{n} \Delta S_i = \sum_{i=1}^{n} \Delta H_i (A_{oi} + a_i P_i) \qquad (3)$$

If external pressure is equal to zero, eq.(3) becomes:

$$S = \sum_{i=1}^{n} \Delta H_i A_{oi} \qquad (4)$$

Eq.(4) is only used to calculate soil thaw settlement in the self-weight.

DETERMINATION OF PARAMETERS A_0, a AND P

The key to use eq.(3) and (4) is to determine the values of A_0 and a at construction site.

Investigation shows that the parameters A_0 and a are closely related to the water content, dry unit weight and structure of frozen soils.

In order to get the values of A_0 and a for foundation design in Daqing region, a series of thaw-consolidation tests were conducted on 967 undisturbed samples. By analyzing the test data, the parameters A_0 and a can be evaluated with water content (W) and dry unit weight (γd) in terms of the following equations (Tong et al., 1985).

In the case of compression after thawed:

$$A_0' = 0.00445W - 0.07015 \quad (5)$$

or $A_0' = 47.724 - 62.504\gamma d + 10.842\ EXP\ (\gamma d)$ (6)

In the case of compression while thawing:

$$A_0' = 0.00586W - 0.1027 \quad (7)$$

or $A_0' = 40.088 - 37.404\gamma d + 4.2288\ EXP\ (\gamma d)$ (8)

Under a load of 200 kPa

$$a = 0.0025W - 0.0179 - 1.93 \times 10^{-24} EXP\ (W) \quad (9)$$

$$a = 0.2202 - 0.1203\gamma d + 0.0012\ EXP\ (\gamma d) \quad (10)$$

Value of H_i in the formulas mentioned above depends upon the thickness total of frozen soil and the evenness of A and a in the frozen soil layer concerned underneath the foundations. If distribution of A_0 and a in all of frozen soil layers is even, then the frozen soil can be treated as one layer, other-wise, the frozen soil should be divided into several layers.

The value of P for each subsoil layer is determined by:

$$P = \frac{P_1 + P_2}{2} + \frac{q_1 + q_2}{2}$$

where P_1 and P_2 are the applied stresses at upper-and lower-surface of each layer, q_1 and q_2 are self-weight pressure on the upper-and lower-surface of each layer, respectively.

APPLICATION CONDITION AND VERIFICATION OF EQUATIONS (3) AND (4)

To test the reliability of eqs (3) and (4), 40 model test foundations were placed in Fangxiao, Oilfield Construction Design and Research Institute of Daqing Petrolem Administerative Bureau and Children's palace test sites with different buried depthes, and their thaw settlements were observed. In addition, laboratory thaw settlement tests on the undisturbed samples from the observation sites were also carried out.

Verification of Eq.(4)

The test results from the laboratory thawing tests on the undisturbed samples from the three test sites were used to calculate thaw settlement with eq.(4). Then, the calculated thaw settlements were compared with the observed values, as shown in Table I.

From Table I, it is seen that the calculated and observed values are very close. Thus, formula (4) can be used to predict thaw settlement in engineering practice with a enough accuracity.

Verification of Eq.(3)

With formula (3) we calculated the total settlements of thawing and consolidation of frozen soils under different loads at the test sites and compared the observed values. The comparison shows that at some test sites, the calculated values are concordant with observed values, as shown in Table II.

The reasons why the observed and calculated settlements are in a good agreement may be:

(i) The soil at the test site are of weak or medium frost susceptibility and are distributed homogeneously.

(ii) The applied pressure on the test foundation is not greater than the compressive strength of the thawed soils, therefore, plastic sliding of the soil beneath the foundation may not take place.

However, for other test sites, the calculated values are discordant with observed values, as shown in Table III.

Note that the compressive strength of thawed soils listed in Table II and III are evaluated according to the Standard of Subsoil and Foundation Design for Industrial and Civil Architecture (GTJ7-74).

From the data in Table III, observed settlements are greater than calculated ones, this may be explained as following:

The soil in the test site is a saturated loam, strong frost susceptible soil. So, its angle of internal friction after thawing will be greatly decreased (Tsytovich, 1962).

Because of moisture migration during freezing, many ice lenses were formed in the frozen soils. After thawing, the water content of the subsoil is very high, about 56.2% in maximum, and the subsoil becomes in plastic-flow state. Therefore, the compression and shear strength of subsoil are very low. As a result, under the action of load, the subsoil beneath foundation will be squeezed out plasticly and the settlement will be much greater. In this case, the field testing condition did not accord with the condition of lateral restraint, under which eq. (3) was drived. That eq.(3) is inapplicable to this case.

By analysing the results observed at the test site, the conditions for the application of eq. (4) are: (1) The value of A_0 should be obtained from the tests on the undisturbed samples taken from the place where settlement needs to be predicted and in the time when frost depth is deepest; and (2) the water content of frozen soil is less than 50%.

The application of eq.(3) requires more conditions. They are: (1) The structure of frozen soil must be massive or laminal; (2) Values of A_0 and a should be less than 0.07 and 0.06 kPa respectively, and (3) the additional stress in subsoil caused by applied load must be less than the compressive strength of the soil after thawing.

TABLE I

Comparison Between the Calculated Thaw Settlements with Eq.(4) and Observed Values

Test site	Frost depth (cm)	Thickness of each layer (cm)	Values of A_o	Total sett. calculated S_c (cm)	Total sett. observed S_o (cm)	Error $\frac{S_o-S_c}{S_o}$
Fangxiao test site	200	45	0.134	6.03		
		30	0.079	2.37		
		35	0.048	1.68		
		40	0.017	0.68		
		50	0.009	0.45		
				=11.21	11.8	5%
Institute test site	195	40	0.111	4.44		
		30	0.108	3.24		
		40	0.0876	3.504		
		40	0.0673	2.692		
		45	0.0733	3.665		
				=17.54	17.9	2%
Children palace test site	165	45	0.178	8.01		
		30	0.142	4.26		
		30	0.114	3.42		
		30	0.081	2.43		
		30	0.073	2.19		
				=20.31	22	7.7%

TABLE II

Comparison Between Calculated and Observed Thaw Settlement at a Test Site

Buried depth of test foundation	(m)	0.5	0.5	1.1	1.1	1.1	1.1
Compressive strength of the thawed soils	(kPa)	98	98	130	130	130	130
Contact pressure on the base of foundation	(kPa)	49	98	49	98	147	196
Total settlement calculated	(cm)	14.7	17.6	7.8	8.4	11.2	12.8
Total settlement observed	(cm)	14.7	16.6	8.3	8.2	11.4	12.9

VERIFICATION THROUGH ACTUAL BUILDINGS

In Daqing region, in order to built apartments as well as to make them into use in the same year, the foundation engineering, including excavation work of frozen soil, should be usually started in March, when the active layer is still frozen. So it is necessary to determine the frost susceptibility subsoils at the site according to the data of engineering geological investigation and then to estimate the allowable thickness of residual frozen soil based on the check of total thaw settlement of the subsoil with values of A_o and a observed.

The observations on total thaw settlement of three five-storey apartments that were build on different typies of frost heave soil were made in order to check eq.(3) through actual buildings. The calculated and observed results are shown in Table IV.

From Table IV, it is seen that the calculated values of thaw settlement is greater slightly than that observed. It is feasible to apply eq. (3) engineering practice from the point of safety view. The difference between the calculated and observed values may be caused by that the observation was started after construction of foun-

TABLE III

Comparison Between Calculated and Observed Thaw Settlement at a Test Site

Buried depth of test foundation	(m)	0.5	0.8	0.8	0.8	1.4	1.4	1.4
Compressive strength of the thawed soils	(kPa)	<50	60	60	60	65	65	65
Contact pressure on the base of foundation	(kPa)	50	50	100	150	50	100	200
Total settlement calculated	(cm)	14.2	9.6	11.9	14.4	2.9	3.8	4.5
Total settlement observed	(cm)	20.0	16.7	19.3	19.5	10.7	14.3	15.3

TABLE IV

Comparison Between Calculated and Observed Settlements of Three Actual Buildings

Items \ Building & Place	No.2 Building in Fangxiao Quarter	No.1-2 Building in Fengshou Quarter	No.3-5 Building in Lixingcun Quarter
Thickness of residual frozen soil H (cm)	46	31	27
Designed load (kPa)	100	100	100
Water content in frozen soil (%)	21.4	23.1	20.1
Coefficient of thaw settlement, A_o	0.023	0.033	0.015
Amount of thaw settlement $S=A_oH$ (cm)	1.058	1.023	0.405
Coefficient of thaw compression, a	0.032	0.036	0.028
Settlement of thaw compression $S=aHP$ (cm)	1.472	1.116	0.756
Total calculated settlement $S=S+S$ (cm)	2.53	2.14	1.16
Observed total settlement S_o (cm)	2.34	2.03	1.07
Error, $\frac{S_o-S}{S_o}$ %	8.1	5.4	8.1

dation before this, some thaw and consolidation settlement had taken place.

CONCLUSIONS

(i) Through laboratory test with great number of undisturbed samples of frozen soil and statistical analysis, the quantitative relationship between parameters A_o and a, and water content as well as dry unit weight were obtained. And also, the adaptability of values of A_o and a had been determined through indoor and outdoor test of thaw consolidation.

(ii) By observing the thaw settlements of three five-storey apartments and lots of model foundations on residual frozen soil layer, it is verified that the method discussed in this paper can be used to predict the thaw settlement of seasonally frozen soils with a good accuracity. But, it can not be used to predict the thaw settlement of the frozen soils with higher frost susceptibility, which compressive strength after thawing is less than applied load.

REFERENCES

Tong Chagnjiang & Chen Enyuan, (1985). Thaw-consolidation behaviour of seasonally frozen soils. Proceedings of 4th Interna-

tional Symposium on Ground Freezing, Sapporo, Japan, p.159-163.

Tsytovich, N.A., (1962). Base and Foundations on Frozen Ground, (Chinese translation). Chinese Industrial Publishing House, p.29-43.

Standard of Subsoil and Foundation Design for Industrial and Civil Architecture(GTJ7-74). Chinese Architecture Publishing House, 1974.

TENSILE ADFREEZING STRENGTH BETWEEN SOIL AND FOUNDATION

Ding, Jingkang, Lou, Anjin and Yang, Xueqin

Northwest Institute, China Academy of Railway Sciences

SYNOPSIS The tensile adfreezing strength tests between soil and foundation are introduced and the results are analysed in this paper. It is pointed that the tensile adfreezing strength is 25% or so greater than the shear adfreezing strength. The behaviours of the tensile adfreezing strength are also analysed in the paper, and the test values of the tensile adfreezing strength taken from laboratory are given.

INTRODUCTION

The adfreezing strength between frozen soil and foundation is the main source of the bearing capacity of pile and anchor-rod in frozen ground and the main element to effect the stability of the foundation. It is also a great requisite parameter for calculating the stability of resisting frost heave of foundation and of resisting fall and slide of the retaining wall. But in the past, the adfreezing strength has been defined as the shear strength between frozen soil and foundation, and from this, a test method has been presented (Cheitovich, 1973) to determine the adfreezing strength by pulling or pushing a pole out of the frozen ground. When designing an engineering, people often assume that the tensile adfreezing strength is equal to the shear adfreezing strength, and use the later for calculating foundation for all the frozen interfaces. Is it proper? And if it suits the practice? There is no evidence by now. In order to solve the above problem and study the behaviour of tensile adfreezing strength, a test is made in laboratory for determining the tensile and shear adfreezing strength between frozen soil and concrete and steel foundations.

EXPERIMENTATION

The tensile test of adfreezing strength between frozen soil and concrete is made by the equipment in Figure 1. The sample is a barrel. Two pieces of steel pipe of 80 mm in diameter and 200 mm in length are adopted for making sample, one for pouring concrete in, another for filling the test soil in. When making a sample, we put the two pipes together and fill the soil into it, then insert a thermocouple in the interface. After this, move the sample into cool room for freezing until it is to be frozen, then put it into the test instrument and keep it in a constant temperature circumstance for 24 hours.

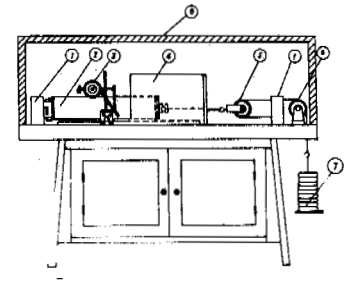

1 Fastening Bass 2 Sample
3 Dial Indicator 4 Safe Cover
5 Moving Block 6 Stable Block
7 Weight
8 Box of Constant Temperature

Fig.1 Equipment for Tensile Adfreezing Strength Test

Then we can start the tensile test.
A constant loading speed is used for the test. The load increment is 98.07 N per hour, i.e. the loading velocity is 1.47 N/cm^2.hr. During the test, keep the sample in constant temperature and measure the temperature and deformation of the interface.
A rectangular sample for shear test is used. The shear box is divided into two parts, one for pouring concrete in, another for filling test soil in. After getting the sample ready, we install a thermocouple in the interface, and then the process of freezing sample and the method of shear test are the same as the tensile test.
The test for determining the tensile and shear adfreezing strength between frozen soil and steel foundation is made by the equipment in

* Jiang Jiazheng and Zhao Cuifeng take part in the test.

Figure 2. The freezing areas of steel sample

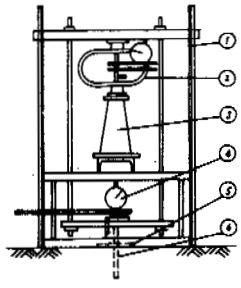

1 Shelf for Loading
2 Dynamometer
3 Jack
4 Dial Indicator
5 Sample for Tension
6 Sample for Shear

Fig.2 Equipment for Tensile and Shear Test

for tensile and shear test are the same. After burying the steel sample and thermocouples into the soil in model trough, we make the temperature of the room decreasing to freeze the model trough. As the model trough is completely frozen, it is covered with soft foam plastic for 24 hours, so that the soil temperature could be more uniform. Then we can start the test. A fast continuous load by jack is taken for the test and one test must be finished in one to two minutes. The soil temperature, stress on the shear interface and the displacement of the steel sample are measured during the test.

RESULTS AND ANALYSIS

Table I and II show the tensile and shear adfreezing strength values obtained by above ways.
From Table I and II we can see that the tensile adfreezing strength is greater than the shear adfreezing strength when the boundary conditions are the same (See Fig. 3).

TABLE I

Tensile and Shear Adfreezing Strength between Frozen Soil and Concrete Foundation

No. of Sample	Water content (%)	Density (kg/m^3)	Temperature (°C)	Destroying strength (kpa)	Destroying creep displacement (mm)	Note
1-2	13.6		-4.6	77.5	0.07	Tension
1-10	12.3	2030	-4.8	97.1	0.02	Tension
1-14	13.2	2050	-5.3	175.5	0.39	Tension
1-15	13.3	1070	-5.0	292.2	0.39	Tension
1-16	11.0	1950	-5.6	126.5	0.18	Tension
1-23	11.3	1950	-5.4	185.3	0.36	Tension
1-8	16.4	2090	-4.5	546.2		Tension
1-9	16.4	2090	-4.7	507.0	0.48	Tension
1-12	20.8	2020	-5.1	526.6	0.35	Tension
1-13	21.1	2000	-4.9	644.3	0.57	Tension
2-1	16.7	1970	-5.5	393.2	0.38	Shear
2-2	16.7	1970	-4.9	435.4	0.50	Shear

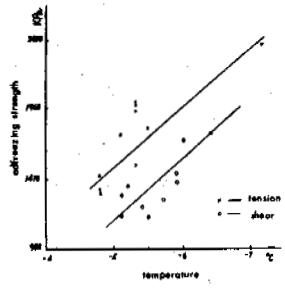

Fig.3 Comparison of Tensile and Shear Adfreezing Strength

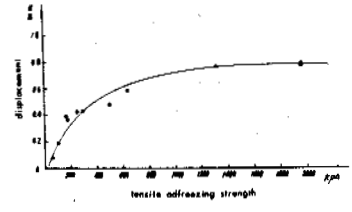

Fig.4 Relationship between Adfreezing Strength and Tensile Destroying Creep Displacement

TABLE II

Tensile and Shear Adfreezing Strength between Frozen Soil and Steel Foundation

No. of sample	Water content (%)	Density (kg/m^3)	Temperature (°C)	Destroying strength (kpa)	Destroying creep displacement (mm)	Note
5-5	15.5	1960	-4.8	1583.8	0.40	Tension
4-3	15.8	2086	-5.5	1820.1	0.45	Tension
4-5	15.8	1080	-5.1	1778.9	0.11	Tension
6-2	15.6	2070	-5.3	2008.4	0.75	Tension
6-3	15.6	2070	-5.3	1564.2	0.52	Tension
6-4	15.6	2070	-5.3	1981.9	0.73	Tension
4-4	15.8	2080	-5.3	1934.9	0.16	Tension
5-1	15.5	1960	-7.2	2426.2		Tension
2-2	15.9	2030	-4.8	1388.6	0.95	Tension
3-2	13.7	2040	-4.8	1372.0	0.81	Tension
1-5	12.7	2030	-11.9	3490.2		Tension
1-4	15.7	2030	-12.5	4116.8		Tension
6-2	15.6	2070	-5.4	1260.1	0.14	Shear
4-2	15.8	2080	-5.1	1348.4	0.65	Shear
5-2	15.5	1960	-5.1	1206.2	1.30	Shear
6-1	15.6	2070	-5.2	1415.1	1.21	Shear
6-3	15.6	2070	-5.5	1193.5	1.39	Shear
6-4	15.6	2070	-5.7	1321.0		Shear
5-4	15.5	1960	-5.9	1503.4	0.65	Shear
4-5	15.8	2080	-6.0	1731.9	1.49	Shear
5-5	15.5	1960	-6.4	1785.8	1.94	Shear
6-5	15.6	2070	-5.9	1442.6	0.59	Shear

Putting together the tensile and shear adfreezing strength which are obtained under the similar water content, we have Fig. 3. It is shown that the tensile adfreezing strength is about 25% greater than the shear adfreezing strength when the temperature are the same.
The features of the interface under tension as following:

(i) the tensile destroying creep displacement of the interface between the frozen soil and foundation is smaller, and generally ranges from fraction of a millimeter to one millimeter (see Table I and II). It increases with the tensile adfreezing strength, and at the end tends to a constant value (see Fig. 4). This value is about 0.8 mm. But the shear destroying creep displacement value is generally greater. The relationship between the shear adfreezing strength and destroying creep displacement is shown in Fig. 5. When the adfreezing strength is less than 2000 kpa the shear destroying creep displacement ranges from a fraction of a millimeter to two millimeter.

(ii) the stress-strain relation tends to be nonlinear when the interface is tensed. It has the behaviour that belongs to the typical brittle materials, i.e. there is no turn on the stress-strain curve (see Fig. 6). However, it is founded from the curve that the interface is yielded when the stress on the interface reaches to the limit, i.e. as the stress keeps on in the limit state,

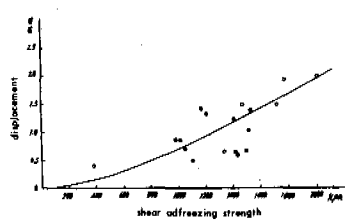

Fig.5 Relationship between Adfreezing Strength and Shear Destroying creep Displacement

the deformation increases quickly. It indicates that the interface has also a behaviour that belongs to the plastic materials.

Except the natures mentioned above, the tensile adfreezing strength is similar to the shear adfreezing strength. Its features depend upon the soil type, water content, temperature, load acting time and foundation material as stated by Ding Jingkang in 1983.
The tests indicate that as the water content of the soil in interface is different, the tensile adfreezing strength is not the same. When the moisture is less than that of the liquid limit of the soil, the tensile adfreezing strength increases with it increases (see Fig. 7).

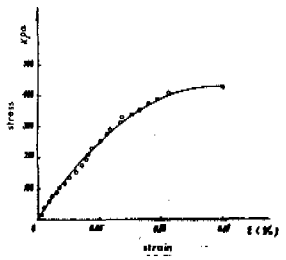

Fig.6 Tensile Stress-Strain Curve of the Interface of Frozen Soil and Concrete Foundation

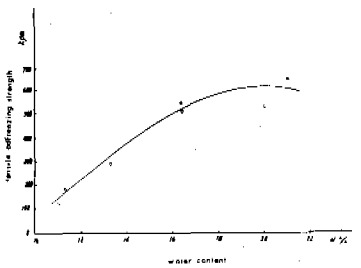

Fig.7 Relationship between Water Content and Tensile Adfreezing Strength

The variation of soil type at the interface will make the contact properties between frozen soil and foundation different, i.e. it will change the number of ice stuck contact point and the features of ice film between frozen soil and foundation, so that the tensile adfreezing strength will be different. After the sample are destroyed it is discovered by the observations to the interface that there is always an ice film not only on the concrete but on the steel foundation as well. It is the features of this ice film that defines the behaviour of the tensile adfreezing strength of the interface.

The test results of the tensile adfreezing strength at different temperatures and loading velocities are listed in Table I and II. One can see from the tables that the tensile adfreezing strength increases with the negative temperatures and decreases with the load acting time. For example, the tensile adfreezing strength between frozen soil and steel foundation, when the temperature on the interface changes from -4.8°C to -12.5°C, ranges from 1583.8 kpa to 4116.8 kpa. If we ignore the difference of the influence of steel and concrete on adfreezing strength, the tensile adfreezing strength ranges averagely from 1800 kpa to 500 kpa when the loading velocity changes from 94 N/Mi./Cm^2 to 0.02 N/Mi./Cm^2.

CONCLUSION

The tensile adfreezing strength between frozen soil and foundation is not equal to the shear adfreezing strength, the former is generally 25% or so greater than the later.

There is a behaviour of brittle materials when the interface is destroyed by tension, and there does not exist residual tensile adfreezing strength.

The tensile destroying creep displacement value of the interface is smaller and the limit value is about 0.8 mm.

That the shear adfreezing strength is used instead of the tensile adfreezing strength for calculating the stability of foundation is tending to be on the safe side. In order to simple the calculating and safety store, that we use the shear adfreezing strength for all freezing interfaces to calculate the stability of foundation is all right.

REFERENCE

Cheitovich, H.A. (1973). The mechanics of frozen ground. 178-183. High School Press. Moscow.

Ding Jingkang (1983). Study on the long-term resistant force of anchor rod in permafrost. Proc. of the Second National Conference on Permafrost of China. 295-303. Gansu People's Publishing House.

Wu Ziwang (1983). The strength and destroying properties of frozen soil. Proc. of the Second National Conference on Permafrost of China. 275-283. Gansu People's Publishing House.

INTERACTION BETWEEN A LATERALLY LOADED PILE AND FROZEN SOIL

L. Domaschuk[1], L. Fransson[2] and D.H. Shields

[1]University of Manitoba, Winnipeg, Canada
[2]University of Luleå, Sweden

SYNOPSIS The paper describes the creep behaviour of a laterally loaded pipe pile, 150 mm square and 1800 mm long, embeded in a frozen sand. Plate load cells mounted along the bearing face of the pile measured the soil reaction forces. Initially the distribution of the reactive forces was nonlinear with depth but as creep of the pile occurred, the forces near the top of the pile decreased, while those further down the pile increased. Ultimately the distribution became linear with depth.

INTRODUCTION

The subject of laterally loaded piles in frozen soil has recently taken on added importance because of such works as construction of above-ground pipelines in permafrost regions and proposed offshore drilling platform construction in the arctic. To date, very few studies of laterally loaded piles in frozen soil have been carried out and the analysis of lateral pile deflections is still in its infancy. To the writers' knowledge, the only frozen soil-lateral pile load test data in the literature are those reported by Rowley et al. (1975) for full scale tests carried out at Inuvik, Canada. Nixon (1984) presented some results of small scale lateral pile load tests that he conducted in ice, which could have application to ice-rich soil.

In the analysis of their test data, Rowley et al. treated the frozen soil as a Winkler foundation with a subgrade modulus, k, that was both load and time dependent. For a fixed time, k decreased with increasing load and for a fixed load, k decreased with time because of the creep behaviour of the soil. To predict the load-deflection relationship, the authors suggested a procedure in which the problem of pressure-creep expansion of a cylindrical cavity was transformed into a pressure-settlement relationship for a strip load which was then used to obtain the pressure-deflection relationship for the pile.

Nixon (1984), and Neukirchner and Nixon (1986) analyzed the Rowley et al. data as well as the Nixon data assuming the soil exhibited secondary creep only. Their solution was based on the premise that after a period of load distribution and adjustment, the pile rotated at a uniform angular rate about some definable point. It was tacitly assumed that the behaviour of the pile changed from that of a flexible pile to that of a rigid pile with time. The solution predicted the changes in pile deflection, the pile moment and the soil pressure along the length of the pile with time.

The purpose of the writers' current investigation is to provide much needed test data on laterally loaded piles in frozen soil under controlled conditions of soil, temperature and load application. To this end, a large-scale experimental model study is being carried out in which the load distribution along the pile length and its redistribution due to creep is measured in addition to the pile deflection. This paper deals with the details of the test equipment and procedure, and some preliminary load-deflection test data.

TEST SET UP

Test Facility

The test facility consists of a pit 2.5 m square and 2 m deep with reinforced concrete walls and floor, 200 mm thick, insulated with 200 mm of rigid insulation on the outside and 100 mm of rigid insulation on the inside. Platecoil panels made from 14 gauge carbon steel and measuring 737 mm by 2108 mm were placed along the sides and the bottom of the pit. The side panels and the bottom panels were interconnected separately to provide two independent flow networks. The pit is housed in an insulated room 5 m square and 3 m high. A 5 hp air-cooled compressor is used to refrigerate the room and a 3 hp air-cooled compressor is used to circulate refrigerant through the platecoil panels. Thermostatically controlled solenoid expansion valves permit independent temperature control of the bottom and side panels. Four vertical strings of thermocouples mounted on long wood stakes were positioned from the centre of the pit to a wall panel to monitor soil temperatures. The thermocouple spacing was 200 mm along each

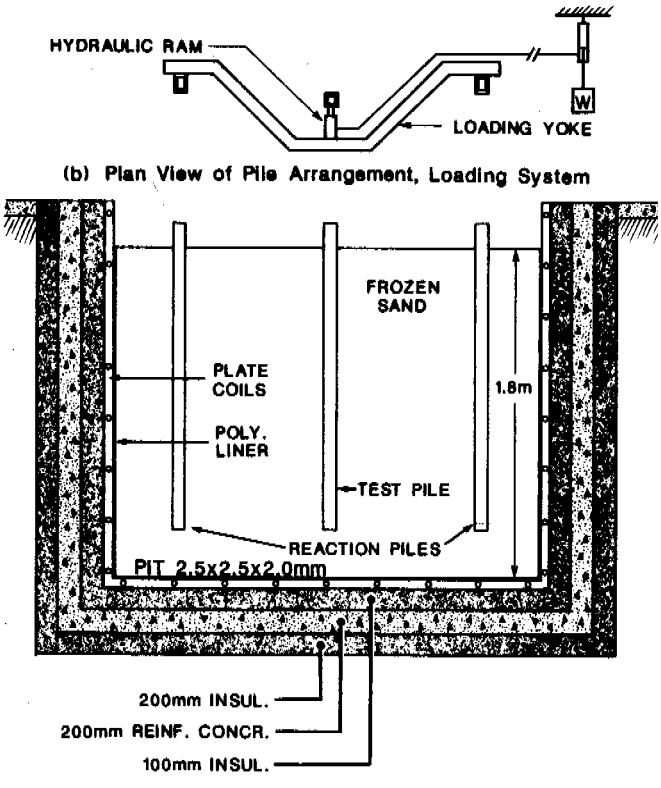

Fig. 1. Test facility: (a) section through pit; (b) planview of pile arrangement and loading system.

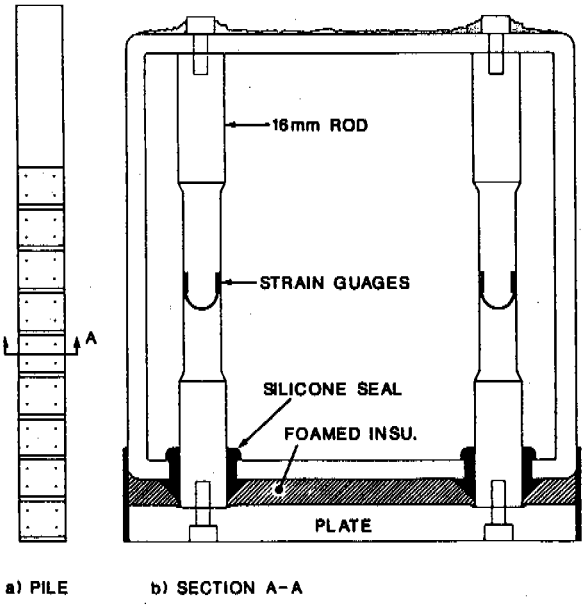

Fig. 2. (a) Instrumented pile; (b) details of plate load cell.

string. A sketch of the test pit is shown in Fig. 1a.

Test Pile

The test pile consisted of tubular pipe, 150 mm square and 1800 mm long with a wall thickness of 6 mm. Nine rectangular plates, 150 mm x 125 mm, and 13 mm thick, were mounted along the front face of the pile by means of bolts that passed through holes in the front face to the back face where they were securely fastened. Four bolts were used for each plate. A 15 mm gap was left between the individual plates and a 13 mm gap was left between the plates and the face of the pile. These spaces were filled with polyurethane foam. The bolts were formed from 16 mm steel rods and were made into load cells by reducing their diameters and mounting two strain gauges on each reduced section. The machined diameters varied from 12 mm for the top plate to 4 mm for the bottom plate in an attempt to maintain approximately the same accuracy in view of the anticipated reduction in reactive pressure with depth. Each plate load cell was calibrated individually. The stiffness of the instrumented pile, EI, as determined from a deflection test, was 2.53×10^3 kNm^2. A sketch of the instrumented pile is shown in Fig. 2.

Soil

A medium sand, the grain size distribution of which is shown in Fig. 3, was placed in the pit. A polyethylene liner, 0.5 mm thick, was used to separate the sand from the platecoil panels in order to prevent adfreeze forces from acting on the panels. A 100 mm layer of wet sand was first placed in the bottom of the pit, two reaction piles and thermocouple strings were positioned in the sand and the sand was allowed to freeze. Sand was then placed in the pit in a loose saturated state

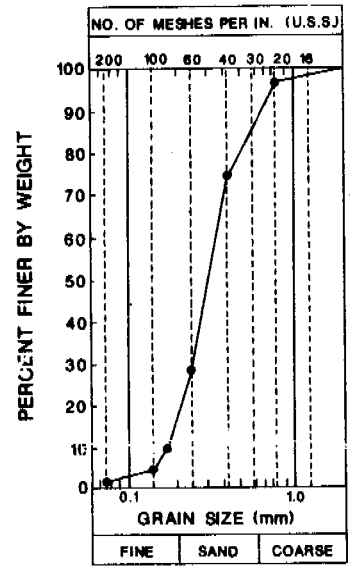

Fig. 3. Grain-size distribution of the sand.

using the following procedure.

A rectangular wetting tank 2.8 m x 0.7 m and 0.6 m high was constructed out of sheet metal. A metal divider was placed 0.4 m from one end so as to create a reservoir. The bottom of the divider was perforated to permit water to flow into and out of the reservoir. The lower half of the remainder of the tank was filled with uniformly graded stone having a maximum size of 38 mm. A sand container 2.4 m long and 0.7 m wide was constructed with a bottom made of expanded steel having approximately 6 mm openings. This container was set inside the tank so that it rested on the surface of the stone layer. Air dry sand was placed in the container to a depth of about 150 mm. Water was then pumped into the reservoir from which it flowed into the stone layer and up into the sand. The level of the water was brought to the surface level of the sand. The water was then drained to a level below the bottom of the sand container leaving the sand in a partially saturated state. The container with the sand was then lifted out of the tank and lowered into the pit which had about a 300 mm layer of cold (0°C) water above the sand in place. The container was lowered just below the surface of the water and the sand flowed out of the container and was thus deposited by sedimentation. Openings were left in the bottom of the container through which the reaction piles and thermocouple strings passed as the container was lowered and raised. Sand was placed to a depth of 1.8 m in this fashion. The final layer of sand was levelled off manually, which caused some disturbance within this upper layer.

Freezing Procedure

The sand was frozen unidirectionally upward. The bottom panels were maintained at a temperature of -30°C, the side panels were closed off, and the ambient air temperature was maintained at 0°C. Thermocouple readings were taken daily. Because the sand had been cooled to near freezing during its placement, it only took about 2 days to bring it to temperatures equal to or less than 0°C. After 16 days, the temperature of the sand varied linearly from 0°C at the top to -30°C at the bottom.

To bring the frozen mass to the intended test temperature of -3°C, the bottom panels were shut off and the side panels and the ambient air temperature were set at -3°C. It was not possible to simultaneously circulate refrigerant through both the side panel circuit and the bottom panel circuit at the same temperature (-3°C) with the particular arrangement of a single compressor and thermostatically controlled expansion values. After a period of several weeks, a steady state temperature distribution throughout the mass was achieved with a slight vertical temperature gradient. This state of the temperature was maintained during the test.

The temperature profiles are shown in Fig. 4 for the following instances: just after the sand had been placed; 2 days after the freezing process had been initiated (all temperature at or below 0°C); and during the test.

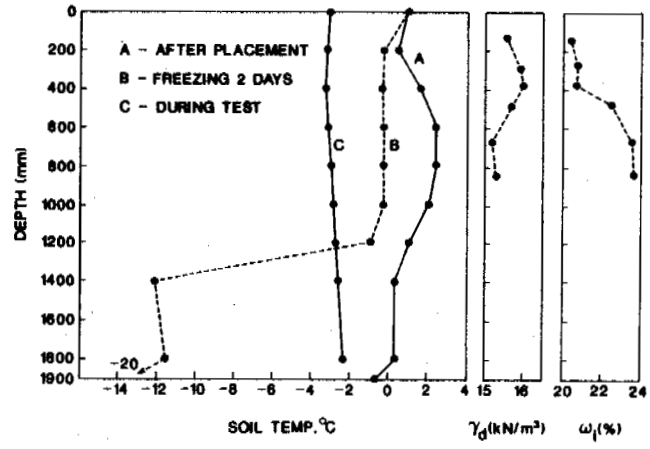

Fig. 4. Temperature profiles in the sand; unit weight and soil moisture profiles.

Densities and ice contents of the sand were determined to a depth of 800 mm after the test had been underway for several weeks. This was done by coring. The data is shown in Fig. 4. The dry densities ranged between 15 and 16 kN/m³ and ice content increased from about 21% near the surface to about 23.5% beyond the 700 mm depth. Some drying of the sand had occurred through sublimation near the surface despite occasional watering of the surface.

Test Pile Assembly

Two piles, identical in section and length to the test pile were used as reaction piles. They were installed before the sand was placed as mentioned previously. The test pile was installed after the sand had been placed and frozen. This was achieved by stacking circular polystyrene discs, 300 mm in diameter and 100 mm thick at the test pile location as the sand was being placed. The discs were subsequently removed, the test pile was put into place and the annular space between the pile and the frozen soil was filled with saturated precooled sand in thin lifts to the top of the upper plate load cell of the test pile. The pile embedment was such that the centre of the first plate load cell was 100 mm below the surface of the sand. The space above the top of the upper plate cell (37.5 mm) was filled with insulation. The back side of the pile was greased before it was installed to prevent the soil from freezing to it. The sides of the pile were left untreated. A yoke was used to transfer the load from the test pile to the reaction piles. The load was applied to the pile through an assembly of dead weights and hydraulic rams (Fig. 1b) and was measured at the pile with a load cell. Pile deflections were measured with an linear variable differential transformer (LVDT).

TEST PROCEDURES AND RESULTS

Reaction Pile Test

The two reaction piles were subjected to a series of short term lateral load tests to obtain an indication of the creep behaviour of the frozen sand and the load capacity of the piles. The piles were jacked toward each other to eliminate the need for a reaction frame. The point of load application and deflection measurement was 80 mm above the sand surface. The loads applied were 20, 40, 60, 80, 100, and 120 kN. Each load was left on until the creep rate had decreased to less than 0.5 mm per day. At the end of the loading stage, the piles were unloaded and the rebound was measured.

The pile deflections and rebound are shown as a function of time in Fig. 5. The deflections

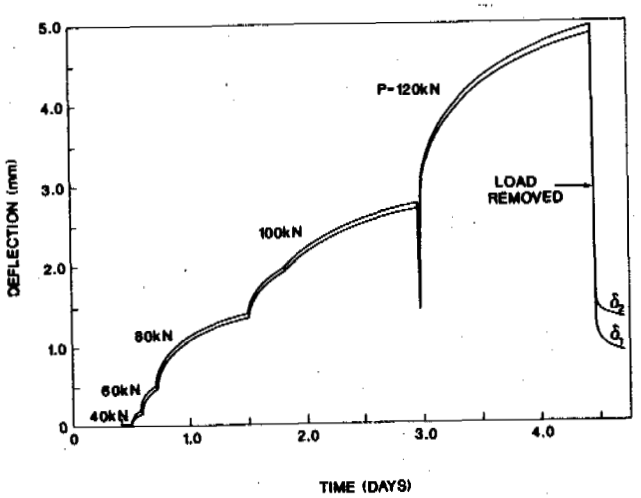

Fig. 5. Results of tests on reaction piles.

were corrected to take into account the distortion of the pile section due to the concentrated force acting on the face of the pile. The piles underwent primary creep under each load increment within the short time intervals used. The total deflection was approximately 5 mm. The rebound following load removal was approximately 4 mm and therefore the permanent creep was only about 1 mm under the given test conditions.

Test Pile

The first load increment applied to the test pile was 35 kN. The point of load application and deflection measurement was 100 mm above the sand surface. Some difficulty was encountered in keeping the load constant because of friction in the hydraulic cylinder to which the dead weight, W, was attached (Fig. 1b). Attempts were made to reduce the friction by such means as wrapping the cylinder with heating coils, attaching mechanical vibrators to the cylinder, etc. The final solution was to periodically bleed off some of the oil within the system so as to cause some displacement of the piston and thus destroy the static friction. This proved to be quite satisfactory and is now done on a daily basis. Unfortunately, this was not done for the first two load increments, and therefore there were some fluctuations in the magnitude of the loads. When the deflection had attenuated, the load was increased to 65 kN.

The results of the first two load increments are included in this paper. The loads and pile deflections are shown as a function of time in Fig. 6. Significant fluctuations in load occurred primarily at the start of each load application and remained essentially constant thereafter. There were corresponding fluctuations in the pile deflections. The deflections generally increased with time at a decreasing rate for each load increment and essentially attenuated in approximately 100 hrs. The attenuated deflection was about 1 mm for the 35 kN load and approximately 3 mm for the 60 kN load.

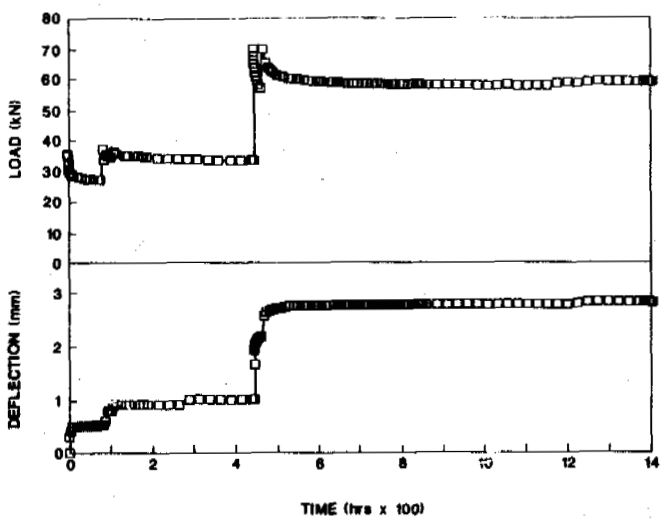

Fig. 6. Loads and pile deflections versus time.

The reactive soil forces recorded for those load cells registering compressive forces are shown plotted as a function of time in Fig. 7. All other load cells registered zero or slightly negative values. Since the load cells were mounted on the front face only, there was no way of knowing the load distribution along the entire pile length. The data indicates that as creep occurred, there was a redistribution of the reactive forces acting on the pile. Generally, there was a reduction in the reactive forces near the top of the pile and an increase in the reactive forces lower down. In the case of the 35 kN load there was a slight reduction in the force registered in the uppermost cell, and a slight increase in the next three lower cells. In the case of the 60 kN load there was a substantial reduction in the uppermost cell, a slight reduction in the next lower

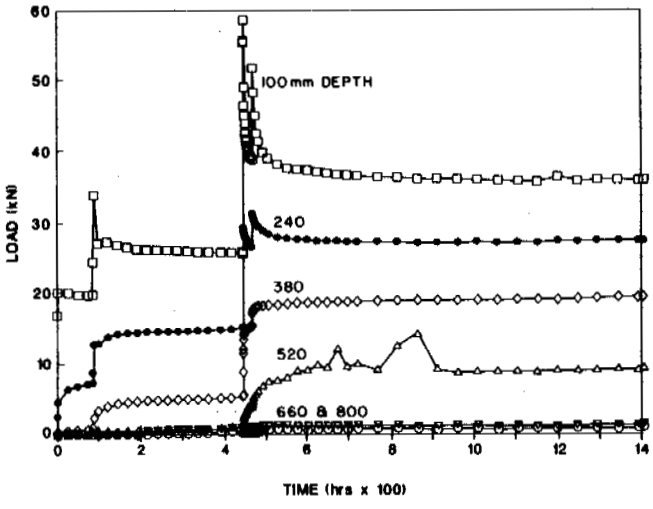

Figure 7. Reaction loads registered by plate load cells.

cell, and a significant increase in the next two lower cells.

The distributions of measured reactive forces with depth are shown in Fig. 8 at the start and at the end of each load application. The distribution indicates that the compressive

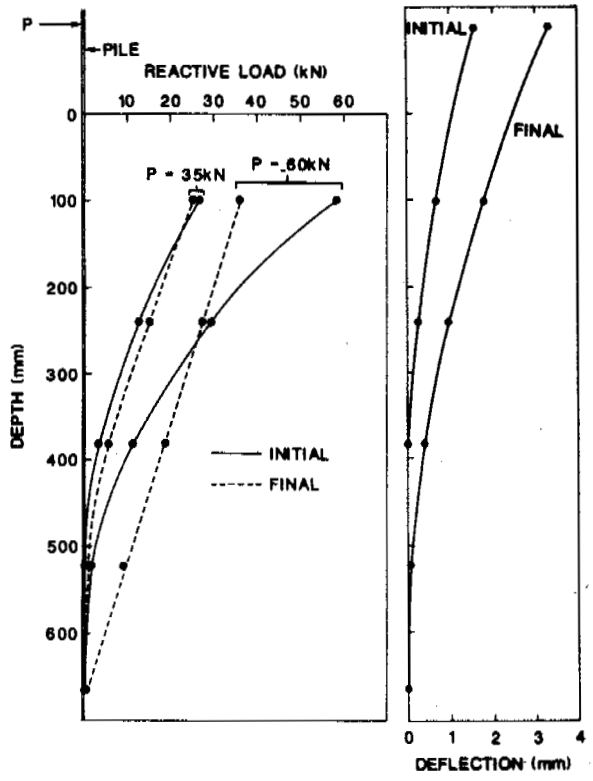

Fig. 8. (a) Distribution of measured reactive forces with depth; (b) Calculated pile deflection profiles

reactive soil forces which acted on the face of the pile extended to a depth of about 520 mm for the 35 kN load and about 660 mm for the 60 kN load, or roughly the upper third of the embedded depth of the pile. As well, with time, the redistribution for both loads tended towards a linear distribution with depth.

The deflection profile of the pile was not measured during the test. An approximate deflection profile was calculated by simply treating the pile as a cantilever beam carrying a series of concentrated known forces consisting of the applied load and the reactive forces measured by the plate cells. The beam was assumed to be cantilevered at the point of zero reactive force. The initial and final deflection profiles thus calculated for the 60 kN applied load are shown in Fig. 8(b). A comparison of the computed deflections of the top of the pile (Fig. 8b) with the measured deflections (Fig. 6) shows very good agreement, lending credence to the assumptions made in computing deflections. The change in deflection curve with time due to soil creep indicates that the maximum bending moment also changes with time. This points out the importance of knowing the redistribution of reactive pressures on a pile due to creep when ascertaining the structural requirements of the pile.

CONCLUSIONS

A new facility has been developed which allows large scale piles to be inserted into frozen soil or ice and then tested under lateral load. The conclusions which can be drawn from the first test in the facility are:

1. A 150 mm square pile embedded in a frozen sand, when subjected to loads of 35 kN and 60 kN, underwent attenuating deflection due to creep of the frozen sand. The total attenuated deflection was approximately 3 mm.

2. The time to attenuation was about 100 hours for each load.

3. Load cells mounted on the bearing face of the pile indicated that the compressive reactive forces acting on the face of the pile extended to a depth of about four pile diameters, or roughly one-third the embedment depth of the pile. The depth to the point of rotation (or fixation) increased slightly with load.

4. The initial distribution of compressive reactive soil forces on the face of the pile was nonlinear with depth.

5. As a result of creep, the distribution of reactive forces became linear with depth.

REFERENCES

Neukirchner, R.J. and Nixon, J.F. (1987). Behaviour of laterally loaded piles in permafrost. Jour. of Geot. Eng., Vol. 113, No. 1, Jan., 1-14.

Nixon, J.F. (1984). Laterally loaded piles in permafrost. Can. Geot. Jour., Vol. 21, 431-438.

Rowley, R.K., Watson, G.H. and Ladanyi, B. (1975). Prediction of pile performance in permafrost under lateral load. Can. Geot. Jour., Vol. 12, 510-523.

ACKNOWLEDGEMENTS

The writers wish to acknowledge the financial assistance provided by NSERC, Ottawa, Canada, and the Swedish American Foundation. As well, special thanks go to Mr. Brian Turnbull and Mr. Ed Lemke, who provided invaluable assistance in setting up the testing facility.

CHOICE OF PARAMETERS OF IMPACT BREAKAGE OF FROZEN SOILS AND ROCKS

A.I. Fedulov and V.N. Labutin

Mining Institute of the Siberian Branch of the USSR
Academy of Sciences, Novosibirsk, USSR

ABSTRACT The paper deals with the technological schemes of breakage of various hard materials including seasonal-frozen soils and ever-frozen rocks by impact load; a change of the parameters of the process, its action and a change in time are shown. The concept concerning the specific per unit length of impact load per unit of length of a blade of a wedge-like tool is introduced.The character of a change of the components of force of breakage, the values of an angle of positioning of the tool, the intensity and the energy-intensity of the process is established. The obtained materials of the investigations are the basis for creating the real working members for practice of breaking and mining of hard materials.

The industrial exploitation of the districts of the East and the North-East of the Soviet Union is associated with mining of considerable volumes of rocks and seasonal-frozen soils as well as ever-frozen ones.
A traditional method of the solution of this problem is the drilling-and-blasting method of loosening followed by loading and transfer of rock mass by the mechanisms of various types, such as excavators, loaders, scrapers and bulldozers, etc. Only to a lesser degree, in some places, the rippers mounted on the tractors are used.
As known the drilling-and-blasting method of mining supposes the specific cyclicity of the process. At the same time the most advanced high-production continuous flow process technology supposes continuity of the process. In fairly hard rocks as well as frozen soils one may perform this only by means of the working members of impact action which may provide the high-efficient flow of the process of breakage. The existing examples in the field of percussion drilling of hard rocks and ores confirm convincingly the reality of this direction.
For designing and projecting the high - production impact devices for breakage, the initial data of the parameters of the effective flow of this process are required. Over a long period of time, under the various conditions, the Mining Institute of the Siberian Branch of the USSR Academy of Sciences conducted the investigations into the impact method of breakage of coals, frozen soils which made it possible to obtain a series of the fundamental results (Nedorezov, 1965, Vikhlyayev, 1969. Fedulov, 1973, 1975, 1977. Fedulov, Polonsky, 1977. Sleptsov,1982). During the investigation of impact breakage of materials, two schemes of loading were considered. The first scheme takes into account the various existing in practice technological processes associated with breakage of specimens of end sizes (oversizes of various rocks, laminated, block materials, etc.), the second one is typical of the technological processes of separation of a layer of a material, its extraction and mining. If the first one is associated with a single action completing with a crack of a specimen, the second one supposes some continuity of the process and in this connection it must possess the high efficiency.
As a result of the analytical and experimental investigations of the process of impact breakage of various hard materials, a number of very important scientifically and practically dependences were established making it possible to approach to the solution of the question about the parameters of the impact devices for these purposes with sufficient validity.
The obtained experimental dependences of some parameters of the impact process (maximum impulsive force, pulse length, maximum depth of penetration per impact) upon the quantity of sequentially delivering impacts against the wedge-like indenter show a fairly sharp change of their values from impact to impact. The character of the graph of the maximum impulsive force representing the curve increasing with a deceleration indicates the change of the properties of the material under the indenter, and makes it possible to draw the important conclusions. One may state that the traditional indices of the mechanical properties of the material characterize only its condition before the first impact and cannot be used in the process of growth of stresses under the tool. On the other hand, clearly the magnitude of the maximum force has the most substantial influence on the process intensity (depth of penetration of the indenter) from the very beginning of the breaking process during the first impacts.
Thus, for evaluating the effectiveness of the impact breakage, it is necessary to use the integral indices characterizing it as a whole and including the process intensity in themselves. Such index may be represented by the energy-intensity of breakage of the

material.
As a result of the experiments with the specimens having the end sizes, it was found that the energy-intensity of breakage considerably depends on the impact energy. For providing the course of the process in the mode of three-dimensional breakage, with enough low energy-intensity, the impact energy and the striker mass must be not less than some minimum values. Upon exceeding the optimal value of the energy, the energy - intensity varies only slightly whereby an increase of the impact power must lead to a growth of crushing capacity.
The process of impact breakage may begin only at a defined value of load falling at a per-unit of the indenter size. In this connection, particularly, for the wedge-like tool, the understanding of "per unit length of impact energy" was introduced.
The values of the impact parameters as to the striker energy and mass should be chosen with due regard for the physico-mechanical characteristics of the material to be broken. Thus, for example, for the efficient flow of the process of impact breakage of the specimens with the end sizes, the "per unit length of impact energy", such as the energy referred to the length of the wedge-like tool blade having , as it has been established, the oriented effect of breakage, must be not below 120-150 J/m $\cdot 10^{-2}$ for most rocks and other hard materials. Our knowledge about the physical essence of the process of impact breakage of materials one layer at a time, at present, reduces to the scheme according to which the breakage of the materials by the working member of impact action between two successive impacts may be divided conventionally into three stages : impact breaking in a zone of penetration of the tool into the material, cutting of a zone with disturbed links produced after it due to arising fracturing, and , at last, cutting of undisturbed material under the action of the force of the movement of the working member. Depending on the speed of the movement, three variants of the values of the indices of the process are possible of which the most favourable variant as regards the breaking intensity, the magnitude of the force of the movement and the specific energy consumptions is the case when the next impact delivers after completion of cutting of the zone with disturbed links. Such frequency of impacts makes it possible to obtain a fairly high speed of the movement at comparatively small tractive forces. The optimal values of the parameters of the process depend on the properties of the medium broken. For example, to provide a desired magnitude of penetration of the wedge-like tool when breaking one layer at a time of a certain thickness of the frozen soil, the per unit length of impact energies of no less than 80-100 J/m $\cdot 10^{-2}$ are required. Based on the values of the per unit length of impact energy obtained during experiments, the minimum value of the impact energy for most practical cases must be not below 800-1000 J.
The principle of the impact breakage one layer at a time has been best widely checked in the frozen soils and the coals.

The experimental investigations into the breakage of the coals were conducted in the Kuzbass opencast collieries, of the seasonal-frozen soils in Moscow, Novosibirsk and Ust-Kamenogorsk, of the ever-frozen rocks in the Zapolyarye mines.
Subjected to the impact breakage were the coals with hardness of 0.8 to 3.0 according to Prof. M.M. Protodyakonov scale, the seasonal-frozen soils of various grain compositions: loamy, light sand loam, gravel, the temperature of the soils varied between -1 to -12°C, the humidity between 16 to 28%. The ever-frozen rocks included 50...60% of hard fractions - gravel and quartizitic boulders in size to 0.3x0.3x0.3 m and had a filler as a loamy light sand, clay, silt and ice (common icing of the rocks ranged from 20 to 30%). The temperature of the frozen mass varied between -7 to -10°C.
The investigations were carried out on the specialized fully dimensional stands developed and manufactured for the specific conditions of the breakage as well as with the use of the base machines (excavator, hard-rock tunneling machine, truck loader) on which the experimental working impact members, such as the pneumatic hammers with energy per blow of 500...1700 J and frequency of blows of 6...15 s^{-1} developed by the Mining Institute of the Siberian Branch of the USSR Academy of Sciences were mounted. The equilateral chisel teeth with the lip angle of 35° were used as a tool.
In the process of the investigation of the breakage one layer at a time of the hard materials, the variable parameters were as follows: the thickness of the layer broken, the energy per single blow, the physico-mechanical properties of the material, the distance between the tools - pitch of breakage, angle of inclination of tool axis to plane of face (angle of attack). According to this, the following magnitudes were determined; the thickness of the broken layer; the cross sections and the length of cuts formed after the passage of the impact working member; the force of the movement of the working member; the normal force acting on the tool from the side of the face; the speed of the movement of the experimental working members; the duration of the tests; the physico-mechanical properties of the material broken.
As a result of the conducted investigations of the process of the breakage one layer at a time of the hard materials using the impact working members, the knowledge of the physical essence of the process under investigation was obtained, and in particular the pattern of the formed trace of the breakage was revealed. The process of the impact breakage one layer at a time is outwardly similar to the process of the cutting, and is followed by the periodic separation of the elements of spalling with the formation of the trace of the breakage, whose cross section has a form similar to the trapezoid. The side surfaces of the trace are inclined to the vertical at the angle of side splitting ψ which decreases with an increase of the thickness of the layer broken (Fig. 1). The cross-sectional area of the trace of the breakage

varied depending on the angle of side split.

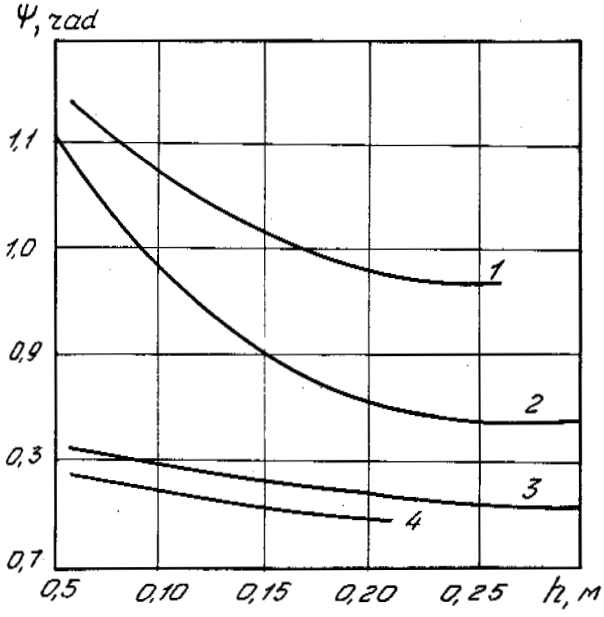

Fig.1 Dependence of angle of split on thickness of layer broken

1 - seasonal-frozen soils; 2 - coal along the bedding; 3 - coal across the bedding; 4 - many-year-frozen rocks

The exterior appearance of the trace of the breakage showed the deformations of breaking-off along the side surfaces and the presence of crumple and shear on its bottom. The share of the side surfaces increased with an increase of the thickness of the broken layer, thus the breakage in thick layers should be recognized more expedient energetically.
The character of the process of the impact breakage of the coal and frozen soil using the doubled tools is mainly similar to the process of the breakage using the single tools with the difference that between the teeth a ridge of undisturbed soil was formed whose height decreased with an increase of the thickness of the broken layer h and with a decrease of the distance between the teeth l (Fig.2).
The horizontal component of the tractive forces increased with an increase of the broken layer thickness from the parabolic law (Fig.3).
When breaking the frozen soils, their physico-mechanical properties and temperature acted on the tractive forces. Thus, when breaking the sandy loams, the magnitude of the horizontal component was less compared to the gravel and loamy soils.
The magnitude of the horizontal component was dependent on the extent of blocking of the trace of the breakage. In case of the ever-frozen rocks for the blocked, half-blocked and free schemes of the breakage, the horizontal component in the relative units accounted for 1:0.5:0.3. These data for the coal presented in Table show that the broken layer thickness influences the distribution of the magnitude of the horizontal component.

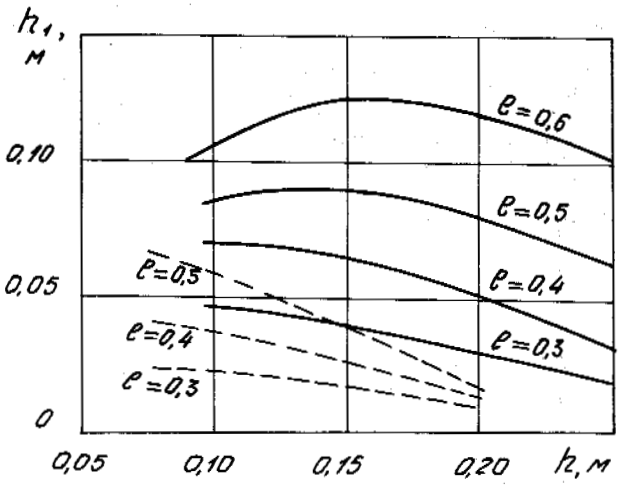

Fig.2 Dependence of ridge height on thickness of layer to be broken and distance between tools

——— - coal across the bedding;
– – – - seasonal-frozen soils

TABLE

Distribution of Forces for Various Breaking Schemes

Thickness of layer to be broken, cm	Form of separation of layer to be broken					
	Blocked	Free	Half-blocked with pitch of breakage l, cm			
			30	40	50	60
	Force P_r, %					
10	100	80	56	70	90	100
20	100	51	56	74	87	97
30	100	38	45	59	73	88

As the investigations show the normal component of the movement force is directed from the face or towards the face, depending on the magnitude of the impact energy, the strength of worked-out soil, the angle of attack and the broken layer thickness. Thus, for the broken layer thickness less than 15 cm, the tendency for expelling of the working member from the broken material was observed, particularly this was marked for more hard soils, low energies of single impact and low angle of attack. The optimal angle of setting of the axis of the working members (angle of attack) ranged from 25 to 30°.
When evaluating the degree of the effectiveness of the breaking process, the index of the

specific energy intensity was used.The total specific consumption of energy was determined by the sum of the consumption of energy for the movement of the working member and the consumption of energy for air, in this case the share of the latter accounted for 25...45% for the seasonal-frozen soils, 60...75% for the coal, up to 94% for the ever-frozen rocks.

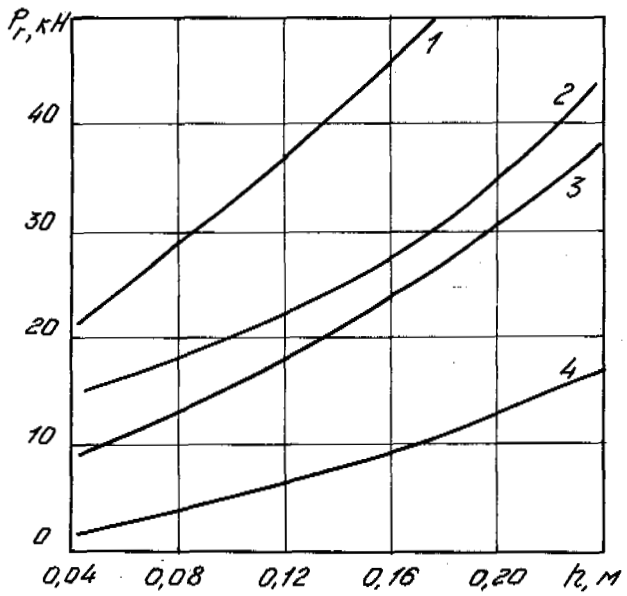

Fig.3. Dependence of horizontal component of force of movement on thickness of layer to be broken:

1 - energy per impact A=1000 J, gravel soil t =-6°C; 2 - A=1000 J, loamy soil, t =-5°C; 3 - A=500 J, sandy loam, t =-3.5°C; 4 - A=1000 J, coal, $\sigma_{compr.}$ = 20 MPa

The specific energy intensity of the breakage one layer at a time of the hard materials by means of the impact working members depends on the energy per impact,the physico-mechanical properties of the material to be broken, the thickness of the layer to be broken (Fig.4), and takes the optimal value at the definite relations of the said parameters.
It decreases to a certain limit with an increase of the thickness of the layer to be broken, whereupon (depending on the conditions of the breakage) it begins either to increase, or remains constant. The increase of the energy of single impact of the working member decreases the magnitude of the specific consumption of energy. When breaking the material using two or several impact tools, the group influence of the tools on the mass to be broken occurs.In this case at defined values of the pitch of the breakage and the thickness of the layer to be separated, the energy intensity of the breakage decreases in comparison to the operation by one tool.
The specific energy - intensity of the impact breakage of the studied hard materials varied between 0.1 and 1.5 kW·h/m^3 depending on their strength. The minimum values were obtained when breaking the coal, and the maximum ones when breaking the ever-frozen rocks.
The coefficient of nonuniformity of the load of the working member varied within 1.3 and 2.5, its values decreased with the increase of the thickness of the layer to be broken.

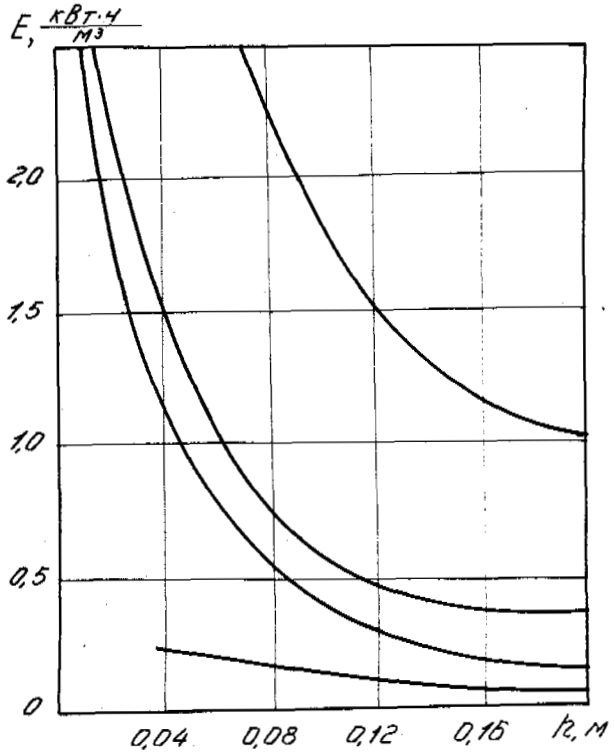

Fig.4. Dependence of specific energy-intensity on thickness of layer to be broken :

1 - A=500 J, n=15 s^{-1}, frozen loamy light sand; 2 - A=500 J, n=15 s^{-1}, frozen loamy soil; 3 - A=1000 J, n=9.5 s^{-1}, frozen gravel soil; 4 - A=1500 J, n=8.3 s^{-1}, ever-frozen rocks

The results of the conducted in-situ experimental investigations of the impact breakage of the coals, frozen soils and rocks show that the effectiveness of the breakage of the hard materials is largely dependent on their physico-mechanical properties, grain composition and temperature (for seasonal-frozen soils and ever-frozen rocks).
According to the obtained data, the ever-frozen rocks have the greatest resistance, which is explained by their relative low temperatures as well as the content of silt and clay in them possessing the high cementing properties at a negative temperature.
The greatest intensity of the impact breakage was attained in the coals and the seasonal-frozen soils and ranged 150 to 200 m^3/h for one impact tool with energy of single impact

1000 J and frequency 9.5 s^{-1}. The intensity of the breakage of the ever-frozen coarse-fragmental rocks obtained during the experiments was 20 m^3/h on the average. This index may be increased at the expense of an increase of the power of the impact device and the drive of the working member.

As one may believe the obtained materials first resulting from our investigations fall into the category of the fundamental results making it possible to judge with any assurance about the possibility and the application of the impact breakage. The data on the per unit length of the impact energy even point to the required levels of the energy of single impact of the device, and hence its possible structural sizes. The tendency for an increase of the per unit length of the impact energy at the expense of a decrease of the width of the tool invariably brings about a decrease of the width of the trace of the breakage and may give rise to difficulties associated with free passage of the impact device through the trace of the breakage. The similar pattern will be observed when increasing the per unit length of the impact energy at the expense of the parameters of the impact device which with other conditions being equal may lead to an increase of its overall dimensions. In this case the tractive forces of the movement (the horizontal component of the tractive forces) sharply increase and the impact breaking process stops.

The obtained results of the conducted in situ experimental investifations showed the outlook of the use of the impact method of the breakage of the hard coals, frozen soils and rocks. For realizing this efficient method of the breakage, the Institute of Mining of the Siberian Branch of the USSR Academy of Sciences has developed and a number of the plants produces in quantity the PN1300 and PN1700 pneumatic hammers which may be mounted on the working equipment of the hydraulic excavators and used for the breakage of the various hard materials including the frozen soils. Based on such impact devices, the experimental models of the working members of the mining machines of various technological purposes have been created.

The bucket of active action for the excavators of structural (with capacity 0.6m^3) and quarry (4.6 m^3) classes have advantageously passed the industrial tests.

The preliminary scientific-engineering developments and the economic designs have shown the possibility of creating the mining machines with the working members of impact action and for underground mining in the conditions of permafrost.

REFERENCES

Nedorezov, I., Fedorov,D., Fedulov,A., Khamchukov,Yu. (1965). Rezanie i udarnoe razrushenie gruntov. Novosibirsk: Nauka Sibirskoe otdelenie, 132 s.

Vikhliaev,A., Kamenskii,V., Fedulov,A. (1969). Udarnoe razrushenie krepkikh materialov. Novosibirsk: Nauka Sibirskoe otdelenie, 158 s.

Fedulov,A., Labutin,V. (1973). Udarnoe razrushenie uglia. Novosibirsk: Nauka Sibirskoe otdelenie, 120 s.

Fedulov,A., Ivanov, R. (1975). Udarnoe razrushenie merzlykh gruntov. Novosibirsk: Nauka Sibirskoe otdelenie. 135 s.

Fedulov,A. (1977). O dvykh skhemakh udarnogo razrusheniia krepkykh materialov. Novosibirsk: Sibirskoe otdelenie, FT PRPI N 6, s. 63-67.

Fedulov,A., Polonskii, G., Karnaukhov,A. (1977). Razrabotka merzlykh gruntov rykhliteliami udarnogo deistviia. Novosibirsk: Nauka Sibirskoe otdelenie. 70 s.

Slepcov,A., Fedulov,A., Labutin,V., Kostyrkin, V. i dr. (1982). Perspektivy sozdaniia potochnoi tekhnologii na osnove udarnogo razrusheniia mnogoletnemerzlykh gornykh porod pnevmomolotom PN1300. Magadan, Kolyma, N 11, s. 7-9.

FROST HEAVE CHARACTERISTICS OF SALINE SOILS AND CANAL DAMAGE

Feng, Ting

Survey and Design Institute of Xinjiang Army Corps of Construction, Shihezi, Xinjiang, P.R. China

SYNOPSIS Canals built on the cold, dry and saline soil regions have been damaged seriously because of frost heave. A lot of frost heave tests on saline soils have been conducted both in the lab and in the field. The test results show that the physical and mechanical properties are becoming worse with the increase in salinity. In particular, a phenomenon analogous to liquefaction may be caused. The freezing point depression and the frost susceptibility of soils depend on the salinity and the chemistry of the salts in the pore fluid. Under low temperature and dry conditions, crystalline expansion will take place in saline soils, especially in sodium sulphate soils. The salinity in pore water will be used to judge the freezing state of saline soils. Water and salts were redistributed after the canal commenced operation. Frost heave was occurred in the inside slope of the canals where salts are leached. The large crystallization expansion occurs in the areas where salt has aggregated, which will speed up damage of canals.

INTRODUCTION

Xinjiang is located in the dry and cold region of the inner continent. The salinization of soils is very serious in most areas of this region. The soils contain sulphates and chlorates with a salinity of 2-10%. The canals built in saline regions are seriously damaged by periodic diversion, and dry periods with frost-thaw action. The investigations showed that almost 100% of the canals built in heavily saline regions were damaged, so that studies of frost heave in saline soil, and the resulting damage to canals are of great significance in dry and cold regions.

NATURAL CONDITIONS AT THE TEST FIELD

Tests were conducted both in the lab and in the field. The first branch canal of No.148 farm and the third branch canal of No.150 farm in Mosuowan reclamation area were selected as the testing sites. These are located in Quaternary alluvial deposits at the southern Zhungeer Basin in the Northern slope of the Tian Mountain. The soil is classified as silty loam with a thickness of more than 13 m.

The annual air temperature at the test sites is 5-7°C on the average. The maximum air temperature is 43°C, and the minumum is -42.8°C. The period when the maximum daily air temperature below 0°C lasts 120-150 days on average. This is an arid area so that agricultural production completely depends on irrigation. For comparison, two testing sites (denoted as site 1 and site 2) were chosen for each of the two test canals. Site 1 is at a saline soil zone and site 2 is at a non-saline soil zone.

PHYSICAL AND MECHANICAL PROPERTIES OF SALINE SOILS

Influence of ions on soil properties

The existence of ions changes the thickness of the diffuse layer around soil particles,thereby influencing the plastic and the liquid limits of soils. Experiments show that the plasticity index of the soil tested decreases with increasing salinity, except for the alkaline soils, as is shown in Fig.1. The soil properties are greatly changed when the salinity Sd is greater than 2%. The physical and mechanical properties mainly depend on the salinity and the salt type. For saline soils, liquefaction will occur and thus its shear strength will tend towards zero, even if its water content is relatively low.

Behavior of swelling and crystallized expansion of saline soils

The swelling and crystallized expansion tests were conducted on the saline soil samples with a dry density of 1.40 g/cm^3. The results show that the amount of swelling is smaller for the chlorate and sulphate soils after soaking in water, but much greater for the carbonate soils. The amount of swelling in the carbonate soil may reach to 2.5-11.8% (see Fig.1).

The crystallized expansion is defined as the volumetric expansion of crystallization caused by the temperature decreasing and concentration of the remaining solution. The formation and the growth of Na_2SO_4-$10H_2O$ after crystallization of the solution with sodium sulphate results in volumetric expansion and damage to the soil texture. The amount of crystallized expansion for the sulphate soil is large, with a maximum of 28%. It increases with increasing sulphate content and decreases with increases in dry density.

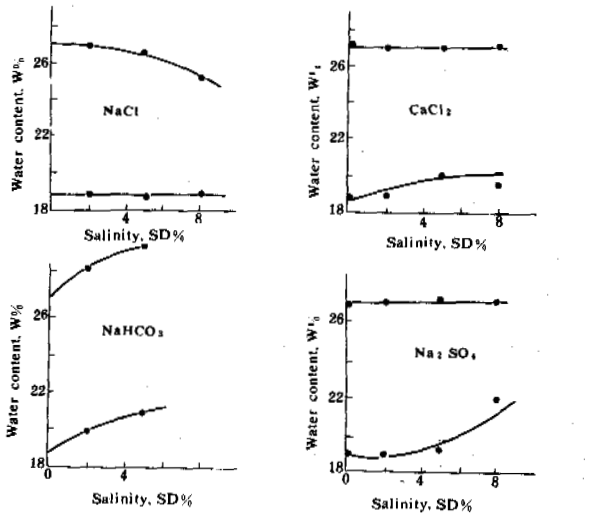

Fig.1 Relations between Salinity, Liquid Limit and Plastic Limit

1 — liquid limit;
2 — plastic limit.

For the sulphate soil with a salinity of 5%, the amount of crystallized expansion is 28.8 and 8.5%, for a dry density, ρ_d, equal to 1.40 and 1.60 g/cm³, respectively. The soils are loosened after being subjected several times to the crystallized expansion. The experiments show that the amount of swelling and crystallization expansion are changed slightly when Sd is greater than 2%, and they are greatly increased when Sd is less than 2% (see Figs.2 and 3).

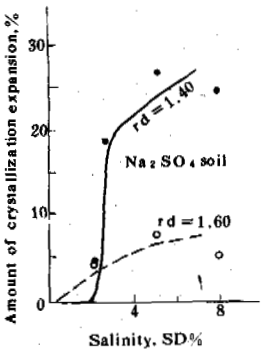

Fig.2 Curves for Crystallization Expansion

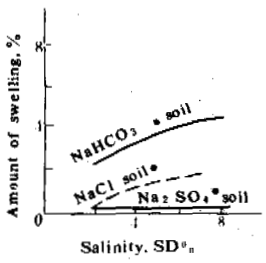

Fig.3 Curves for Swelling after Soaking

Shear strength of saline soils after soaking in water

The salts in the saline soils are dissolved after soaking in water, which results in an increase in the pore size, and a loss of cohesion between soil particles and thus the decrease in the shear strength. The measured values of cohesion, C and the angle of interparticle friction, ϕ for the saturated silty loam with various salinities and a dry density of 1.4 g/cm³ were shown in Table I.

To sum up, different kinds of salts play different roles in saline soils. For the chlorate soil, salt crystallization plays the role of cementing soil particles, thus increasing the shear strength. After soaking, the salts are dissolved and the strength is decreased. With an increase in the chlorate salinity, the plasticity is decreased and moisture retention is increased. If the soil is in a saturated condition for a long time, the phenomenon of liquefaction may readily take place.

For the sulphate soil, salt crystallization will cause expansion and loosening of the soil, and thus decrease the soil strength after drying. After soaking, the salts are dissolved and the strength is decreased. Only at a water content close to the plastic limit the soil strength is higher. The solubility of the sulphate changes greatly with temperature. In Xinjiang region, the climate is dry and the temperature difference is great during day and night, providing a good condition for crystallized expansion of the sulphate. Furthermore, the sulphate soil has a lower solubility. All of the factors mentioned above are extremely harmful to engineering structures. Therefore, the crystallized expansion of the saline soils with higher salinity is a very important factor causing damage to engineering structures in severe cold and arid regions.

WATER AND SALT REDISTRIBUTION AFTER DIVERSION IN CANALS

The key to soluble salt migration in soils is the existence of water. The diversion and drainage of water from the canals, freezing and evaporation of soils cause salts to be aggregated and leached periodically in the soils.

Water redistribution

With the diversion and interruption of water supply and freeze-thaw action, water in the soils is redistributed.

After diversion from the canals, the soils below the infiltration line are in a saturated and leached zone. After cutting off water from the canals, the water content at the surface of the canal is lowered by evaporation and is increased beneath the ground surface. It has its highest value at a depth of 50-60 cm (with the mean value of 20-30%). During freezing, water moves upwards, resulting in a maximum water content of 40-53% at a depth of 30-60 cm, which is in good agreement with the depth of the maximum frost heave ratio observed.

TABLE I

The Measured Values of C and ϕ for the Soils Tested with Various Salinities

Salt	None	NaCl			$NaHCO_3$			Na_2SO_4		
Salinity %	0	2	5	8	2	5	8	2	5	8
C, N/cm^2	0.04	0	0	0	0.49	0	0	0.98	1.37	0.784
ϕ, degree	11.3	5.7	5.0	4.3	7.8	2.9	2.7	4.3	4.0	4.0

Fig.4 shows curves of water content vs depth before and after freezing at site 1 of both No. 148 and No.150 farms, respectively, in 1985-86.

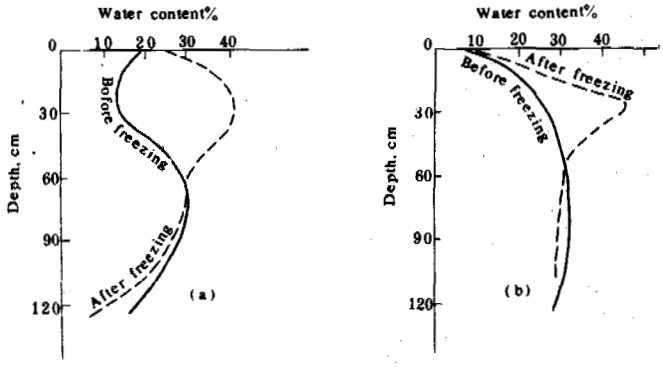

Fig.4 Changes of the Water Content before and after Freezing at Site 1 of Both No.148 Farm (a) and No.150 Farm (b)

Salt redistribution

With the water in canals permeating and leaching, the salts are dissolved. Some salts become aggregated at the outside of the canal and others are transparted to a depth of 50-60 cm. The saturated part of the soil below the infiltration line is the salt leaching zone. The salinity in this zone is lowered to 0.03-0.17%, which is 1/70-1/100 of the value at the outside slope (or the surface of the canal). The distribution of the salinity at the outside slope is triangular with the values higher at the top and lower at the bottom. After freezing, the salt distribution at the inside slope of the canal is made slightly more uniform by water redistribution, and there is a tendency for salt to migrate toward the freezing front (see Fig.5).

In test site 2, the initial salinity is lower, but is higher at site 1. With water flow and leaching actions, almost all of the salts in the soils at the inside slope of the canals at site 1 are leached, with a salinity much less than 0.2%. These soils would be considered non-saline. The salinity at the inside slope of the canals for both sites 1 and 2 are almost the same, which implies that they have a similar freezing behavior.

FREEZING BEHAVIOR OF SALINE SOILS

Freezing behavior of solutions

The solubility of various kinds of salts is shown in Table II. From Table II it can be seen that the solubility of NaCl is very high but is lowered slightly with a decrease in temperature. The solubility of Na_2SO_4 is relatively low, but lowers quickly with decreases in temperature.

TABLE II

The Solubility of the Salts

Salt	Solubility (%) at different temperatures (°C)		
	0	10	20
NaCl	35.7	35.8	36
Na_2SO_4	5	9.0	19.4
$NaHCO_3$	6.9	8.2	9.6

With increases in concentration of the solutions, the freezing point is decreased, especially for the chlorate solution. At low temperature , the solubility of the sulphate solution is very low (5.00%). Even if its initial concentration were higher, the solution would be oversaturated and the salts would precipitate out with decreasing temperature, so that the freezing point depression of the sulphate solution is relatively small. Table III shows the freezing point depression and the frost heaving ratio for the different types of the solutions.

TABLE III

The Freezing Point Depression and Frost Heaving Ratio of Solutions

Solution	Concentration (%)	Freezing point depression (°C)	Frost heaving ratio (ΔV/V)
NaCl	2	-1.0	0.071
	5	-3.0	0.051
	8	-5.4	0.038
	22.4	-21.2	
Na_2SO_4	2	-1.0	
	5	-2.2	0.083
	8	-2.6	0.073
Pure water	0	0	0.09

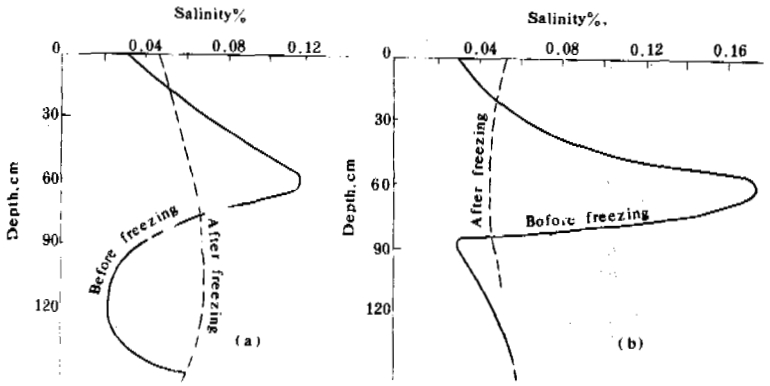

Fig.5 Salinity vs Depth at Site 1 of Both No.148 Farm (a) and No.150 Farm (b)

Frost heaving tests on saline soils

The frost heave tests were conducted in a steel container (40x40x50 cm^3) in which there were four tapered plastic tubes 100 cm in diameter at the top, 130 cm in height and 1040 cm^3 in volume. Insulation materials were wrapped around the outside of the container to ensure unidirectional freezing. Water is supplied from the bottom of the sample during freezing and the soil is frozen under a natural frost penetration rate induced by the temperature controller. The ambient temperature is in the range of from -10 to 0-15°C and the dry density is in the range of 1.2 to 1.40 g/cm^3. The samples are the saturated silty clay.

Fig.6 shows the changes of frost heave with elapsed time for the soils with NaCl and Na_2SO_4. The results show that: (1) The amount of frost heaving decreases with the increase in the salinity. (2) The amount of frost heaving for the sulphate soil is greater than that for the chlorate soil when the salinity is the same. (3) Even though the air temperature drops down to -20°C and the soil temperature down to -9°C, the saline soils with 5% chlorate content are still unfrozen and no water migration occurs. The water content before and after freezing is 30 and 40-50% for the non-saline soils and is 30 and 20-30% for the chlorate soils with the salinity of 5% respectively. (4) Frost heave is relatively low when the temperature is very cold and the freezing index is high. (5) No frost heave was observed for the soils with the NaCl salinity of 5% and 8%. In the tests the soil temperatures are as follows: 0 to -1°C for the non-saline soil, -1 to -2°C for the sulphate soil and -6 to -9°C for the chlorate soil.

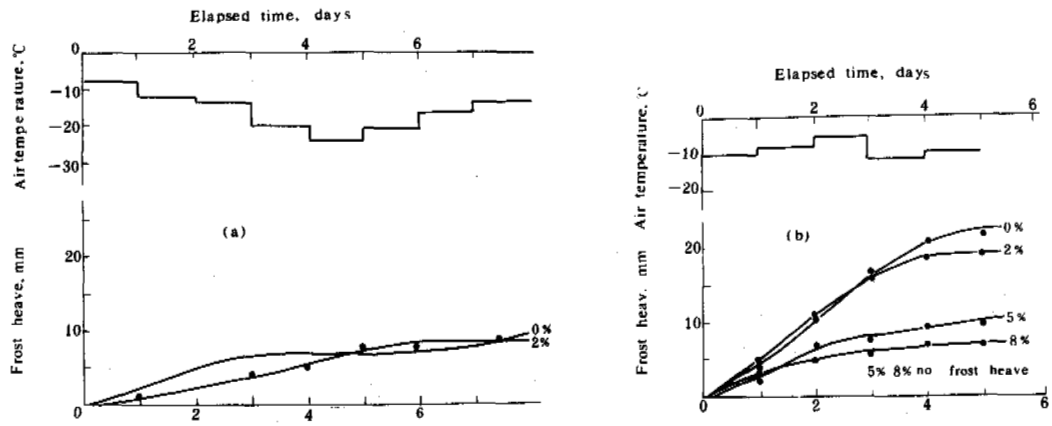

Fig.6 The Frost Heaving Amount vs Elapsed Time for the Soils with NaCl (a) and Na_2SO_4 (b)

Freezing point depression in saline soils

The freezing point depression in the saline soils were determined with thermocouples. The test results are shown in Figs. 7 and 8.

It is seen from Figs.7 and 8 that the freezing point depression for the sulphate soil is lower than that for the chlorate soil. If the salinity is the same, the freezing point depression will be higher when the water content is higher because of the decrease in concentration.There is no obvious inflection point on the curve of the soil temperature vs. the elapsed time for the saline soils with the higher salinity. The test results show that the freezing point depression is closely related to the concentration of the salts in pore water. The relation between freezing point depression and salt concentration for saline loam is shown in Table IV.

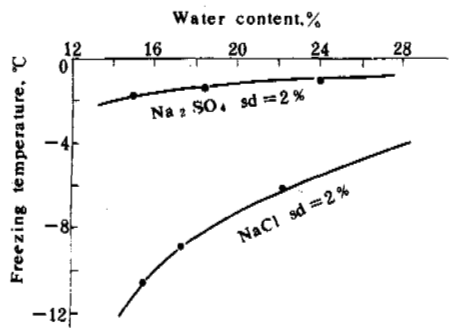

Fig.8 The Freezing Point Depression of the Saline Soils at Different Water Contents

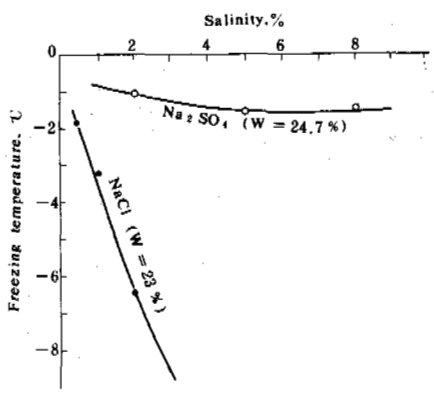

Fig.7 The Freezing Point Depression of the Saturated Saline Soils

The observed values of the salinity and freezing point depression for the two test canals are shown in Table V.

From Table V it can be seen that whether the canal is on the saline soils or not, almost all of the salts in the inside slope have been leached, and the salinity is in the range 0.04 to 0.09% with the mean value of 0.06%. The concentration of the pore water R is in the range 0.27 to 0.24% when W=27-30%. By contrast to Table IV, the freezing point depression is in the range 0 to -0.2°C. Therefore, it is concluded that the freezing point depression of the soils at the inside slopes has no obvious effect whether the canal is constructed in saline soil or not, because of salt leaching. In this case, frost heave is mainly influenced by the freezing rate and the water content before freezing.

TABLE IV

The Freezing Point Depression of the Saline Loam for Various Salt Concentrations

Salt concentration in pore water (%)	0.5	1	3	5
Freezing point depression (°C)	-0.2	-1.5	-1.4	-2.5

TABLE V

Observed Values of Freezing Point and Salinity for the Two Test Canals

Test site			Depth (cm)	Water content (%)	Salinity (%)	Measured freezing front
The first branch canal of No.148 farm	Inside slope	Site 1	30-60	23.8	0.070	-0.013
		Site 2	30-60	24.9	0.056	-0.05
	Outside slope	Site 1	0-30	24.7	2.23	-1.89
		Site 2	0-30	21.7	3.39	
The third branch canal,150 of No.150 farm	Inside slope	Site 1	30-60	23.1	0.063	-0.02
		Site 2	30-60	23.0	0.084	-0.11
	Outside slope	Site 1	0-30	14.3	2.10	-4.90
		Site 2	0-30	23.3	0.410	-0.02

INFLUENCE OF FREEZING RATE ON FROST HEAVE

According to the newest theory (Miller, 1972; Konrad and Morgenstern, 1980) the ice segregation temperature is slightly lower than 0°C which is the freezing point of the pure water. When the soil temperature is much lower than the freezing point depression and the freezing rate is high, water will not be supplied in time so that the amount of frost heave will be lower. The amount of frost heave can reach a maximum only for the following conditions: i.e. the soil temperature is lower than the freezing point and is maintained for a long period of time, and the freezing rate is appropriate for the available water supply.

The observed results of frost heave ratio and freezing rate in the farms of No.148, 150 and 121 were plotted on Fig.9, showing that the heaving ratio is greatly influenced by the freezing rate. The relationship between them can be well described by a hyperbolic function. The heave ratio was suddenly lowered, when the freezing rate was greater than about 1.5 cm/day.

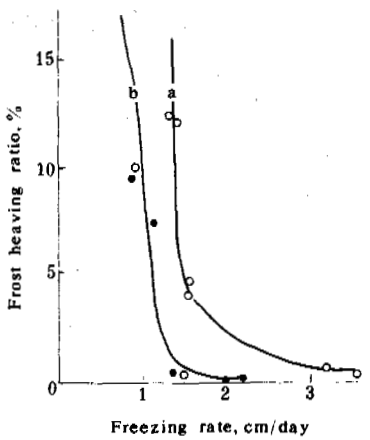

Fig.9 Frost Heave Ratio in the Primary Heaving Zone vs Freezing rate in No.148 farm (curve a) and No.150 and 121 farm (curve b)

CONCLUSIONS

(i) The freezing of saline soils is strongly related to the concentration of salt in pore water. The higher the concentration, the lower both the freezing point depression and the frost heave ratio. The freezing point depression and the heave ratio for sulphate soil are higher than that for chlorate soil when the concentration is the same.

(ii) The amount of frost heave depends on the water content before freezing, freezing rate, salinity, soil temperature, groundwater table and soil properties.

(iii) Because of the higher water maintenance capability, lower soil density, the solubility and the lower plasticity of saline soils, mechanical properties of saline soils are worsened after soaking in water. The soil changes into a slurry after frost-thaw cycles, resulting in sloughing of the canal lining. Therefore, the instability of the base saline soils of a canal is the dominant factor in canal damage.

(iv) Because the original salinity is high, the salts in the saturated zone of the canal embankment are leached after the canal comes into operation, and the pores in the soils are enlarged, leading to an increase in frost heave at the inside slope of the canal and accelerating canal damage. Another reason for canal damage is the crystallization expansion of saline soils in the salt enriched zone at some depth beneath the canal surface.

(v) If the saline soils are kept stable and the salts in soils are not leached, water migration towards the freezing front and frost heave can be completely eliminated because of the presence of the univalent cation chlorate (NaCl, KCl), which maintains a high salinity in the base soil in the range of 3-5%.

ACKNOWLEDGEMENTS

The author is grateful to his colleagues,Messrs Song Jun, Liu Xinping and Li Hao for their participation in this investigation.

REFERENCES

Miller, R.D. (1972). Freezing and heaving of saturated and unsaturated soils. Highway Research Record, No.393, pp.1-11.

Konrad, J.M. and N.R. Morgenstern,(1980). The segregation potential of a freezing soil. Can. Geotech. J., V.18, pp. 482-491.

MECHANICAL PROPERTIES OF FROZEN SALINE CLAYS

T. Furuberg[1] and A.-L. Berggren[2]

[1]SINTEF, Division of Geotechnical Engineering, Trondheim, Norway
[2]Geofrost A/S, Oslo, Norway

ABSTRACT A test series which we performed on a very saline permafrost clay from Svalbard drew our attention to the nexus between pore water salinity and the mechanical properties of frozen saline soil. To further investigate the effect of pore water salinity we have tested three frozen clays with pore water salinity of ~0 g/l, 3 g/l and 33 g/l. Unremoulded samples are used to keep the natural structure of the clays. We have performed both strength and creep tests on the three clays. Unfrozen water content as function of temperature is also determined. For the clay with 33 g/l salinity tests at -3, -5, -10 and -20°C are reported. For the other clays only tests at -5°C are reported. From the test results it is seen that increasing pore water salinity leads to increased unfrozen water content and creep strains and to decreased creep and compressive strength. The influence of salinity on mechanical properties of frozen soil is best accounted for through the unfrozen water content.

INTRODUCTION

Our interest in frozen saline soils was initiated by a test series which we performed on saline permafrost clay from Svea, Svalbard. The Svea clay has a pore water salinity of 50-60 g/l and we discovered that its long term strength was very low compared to other frozen clays. Saline marine clays are common in many areas of Norway, thus a knowledge of the properties of frozen saline soil is needed for ground freezing projects. Relatively few tests on frozen saline soils are reported in the literature, hence we started a test series on artifically frozen clays with different pore water salinities. We tested three clays, Risvollan, Stjørdal and Eberg clay, with pore water salinity of ~0 g/l, 3 g/l and 33 g/l, respectively. When testing soils one may either use remoulded or undisturbed soil samples. Remoulded soil samples are of uniform quality and one may vary a single parameter like salinity, whilst keeping the others constant. The natural structure of the soil is, however, disturbed; we therefore chose to use unremoulded samples. The test series will thus contribute to a database containing results from tests on some typical Norwegian clays. By comparing the results from tests on clays with different salinities, we hoped to determine the influence of pore water salinity on the mechanical properties of frozen clay.

We performed both strength and creep tests. Unfrozen pore water content as a function of temperature was also determined. A selection of the tests performed are presented in this paper. For Stjørdal clay results from tests at different temperatures are given. For the other clays only tests performed at -5°C are presented.

TEST PROCEDURE

Artifically frozen samples were cut from 54 mm cores. The samples were frozen, with no access to water, in a freezer at -26°C. Permafrost clay was cored with an 3" auger. The samples were trimmed on a lathe to a height to diameter ratio of 2. For triaxial tests the samples were clad in a rubber membrane sealed to top and bottom pieces by O-ring seals. For uniaxial tests the samples were given a thin coating of kerosene to keep the ice from sublimating.

The strength tests were performed in a Geonor press with 50 kN capacity. The most commonly used strain rate was 1% min^{-1}. The creep tests were performed in a triaxial creep apparatus. The equipment is described by Berggren (1985). Radial stress is applied by pressurizing the cell fluid. Constant axial stress is produced by an air pressure actuator with constant air pressure. The air pressure is regulated manually to correct for sample cross-section increase during the test. All mechanical tests were performed in a cold room.

Unfrozen water content is determined by two methods, both in an adiabatic calorimeter and by the nuclear magnetic resonance method. These tests were performed at the Division of Refrigeration Engineering, The Norwegian Institute of Technology, and at the US Army's Cold Regions Research and Engineering Laboratories, respectively.

MATERIAL DATA

The Svea clay is a permafrost clay of marine origin. Its pore water is almost twice as saline as seawater and the clay holds thick vertical seams of fresh ice. The clay is dark brown with a relatively high content of organic matter. Risvollan-, Eberg- and Stjørdal clay are marine clays with varying salinity.

A summary of material data is given in Table I.

As undisturbed samples are used, a range rather than one single value is given for some of the parameters. The data include results from the entire test series, not only the tests presented herein. For Svea clay the data are based on the soil excluding thick ice lenses, total values are given in parenthesis.

TABLE I Material Data for the Tested Clays

Material	Contents				Unfrozen strengths		
	w(%)	(%)<2μm	S(g/l)	H(%)	s_u(kPa)	a(kPa)	tanφ
Svea clay	30 (45-50)	24-56	50-70 (20-40)	5	40	-	-
Stjørdal clay	30	25-40	33	1	45-55	10	0.65-0.70
Risvollan clay	35-40	35-50	~0	0	10-25	25	0.50
Eberg clay	57-69	52-83	3	0	11-14	5-10	0.5-0.6

w = water content, <2μm = clay content, S = salinity, H = organic matter, s_u = undrained shear strength, a = attraction, φ = internal friction angle.

TEST RESULTS

The results from the uniaxial compression tests at a strain rate 1% min^{-1} are given in Table II. Strength is defined as peak axial stress. The strength values given are mean values of results from several tests.

TABLE II Compressive Strength.

Clay	T (°C)	Strength (kPa)	No. of tests
Stjørdal	- 3	240	1
	- 4.5	515	2
	- 5.1	528	2
	- 9.5	1490	3
	-19.45	3200	2
Eberg	- 5.05	2630	2
Risvollan	- 5.5	3100*	4
Svea	- 4.8	847	3

Strain rate $\dot{\varepsilon}$ = 1% min^{-1}.
* Risvollan clay; strain rate $\dot{\varepsilon}$ = 1.6% min^{-1}.

Data for the creep tests are given in Tables III to VI. Investigations showed that confining pressure does not influence creep properties of the clays. Unconfined and confined creep tests are therefore reported together in Figures 1A to 1W.

TABLE III Data for Creep Tests on Stjørdal Clay.

Test	Depth (m)	Clay (%)	Salt (g/l)	W_o (%)	σ_I (kPa)	$\sigma_{II}=\sigma_{III}$ (kPa)	θ (°C)	Plot
KRYP6A	8.2	40.3	34.0	29.8	150	0	3.0	B
KRYP6B	8.3	-	-	30.9	145	0	3.1	C
KRYP6C	8.4	46.4	41.0	31.4	170	0	3.0	B
KRYP6D	8.5	30.7	32.0	31.1	160	0	3.0	B
KRYP6E	8.6	34.5	-	28.9	175	0	3.1	A
KRYP3A	9.2	22.2	33.0	30.8	180	0	3.3	A
ST5K1	7.2	28.2	-	30.5	319	0	4.1	F
ST5K2	7.6	25.2	-	29.4	319	0	4.2	F
ST5K3	7.5	27.2	-	28.6	205	0	4.1	G
ST5K5	6.3	37.7	-	35.9	490	0	4.8	E
ST5K6	6.2	31.1	-	29.1	258	0	4.4	G
KRYP9B	8.3	39.3	32.0	29.7	400	0	5.0	D
KRYP9C	8.4	43.0	32.0	32.8	450	0	5.1	E
KRYP9E	8.6	-	-	28.7	380	0	5.2	D
KRYP7A	8.2	42.7	33.0	31.9	370	0	5.1	D
KRYP7C	8.4	39.9	32.0	30.9	315	0	5.2	E
ST10K1	7.5	30.3	-	30.2	485	0	7.7	H
ST10K2	7.7	25.4	-	31.1	655	0	8.7	I
ST10K3	7.1	31.7	-	30.9	485	0	8.7	I
ST10K6	6.3	43.7	-	35.5	905	0	7.9	H
ST10K7	6.7	23.6	-	28.7	600	0	8.4	I
ST20K2	6.4	38.4	-	33.9	1580	0	19.2	J
ST20K6	6.1	30.9	-	29.4	1370	0	19.1	J

W_o = initial water content, σ_I = axial stress, σ_{II} = confining stress, θ = positive value of negative test temperature.

TABLE IV Data for Creep Tests on Svea Clay.

Test	Depth (m)	Clay (%)	Salt (g/l)	W_o (%)	σ_I (kPa)	$\sigma_{II}=\sigma_{III}$ (kPa)	θ (°C)	Plot
S51B	1.8	31.3	41.0	46.5	481	0	5.4	S
S51F	2.6	44.1	36.8	46.8	302	0	5.3	U
S51G	2.8	49.1	33.2	52.4	395	0	5.6	S
S53B	3.2	36.5	30.2	58.0	1180	797	5.6	S
S53C	3.4	24.1	32.0	50.3	1091	797	5.3	T
SVEA12	3.6	42.7	-	50.4	300	0	4.9	W
SVEA13	3.0	48.5	34.5	45.2	200	0	5.1	V
SVEA15	1.4	41.3	-	47.2	400	100	4.5	W
SVEA16	1.6	42.7	33.0	45.0	300	0	3.7	W
SVEA17	1.8	38.0	-	40.0	600	300	4.8	U

TABLE V Data for Creep Tests on Eberg Clay.

Test	Depth (m)	Clay (%)	Salt (g/l)	W_o (%)	σ_I (kPa)	$\sigma_{II}=\sigma_{III}$ (kPa)	θ (°C)	Plot
BKR54	2.98	58	2.2	62.5	1300	0	5.3	K
BKR55	2.99	66	1.8	65.4	1100	0	5.3	L
BKR56	2.99	66	1.9	64.4	1330	0	5.2	M
BKR57	3.19	52	-	68.5	1250	0	5.2	K
BKR58	3.42	69	2.9	64.2	1000	0	5.2	L
BKR59	4.42	72	3.9	64.1	900	0	5.2	M
BKR510	4.18	83	-	64.4	900	0	5.5	N

TABLE VI Data for Creep Tests on Risvollan Clay.

Test	Depth (m)	Clay (%)	Salt (g/l)	W_o (%)	σ_I (kPa)	$\sigma_{II}=\sigma_{III}$ (kPa)	θ (°C)	Plot
T51A	3.15	-	~0	40.7	1477	0	4.9	O
T51B	3.25	35.8	~0	44.2	1938	0	5.2	O
T51D	3.40	57.1	~0	34.4	2462	0	5.3	P
T51E	3.50	45.2	~0	37.4	2557	0	5.3	P
T53A	3.45	40.8	~0	35.4	2563	797	4.7	Q
T53B	3.55	19.6	~0	42.8	3120	797	4.5	Q
T53C	3.65	31.7	~0	38.7	2990	797	-	R
T53D	4.15	29.9	~0	36.6	2993	797	5.2	R

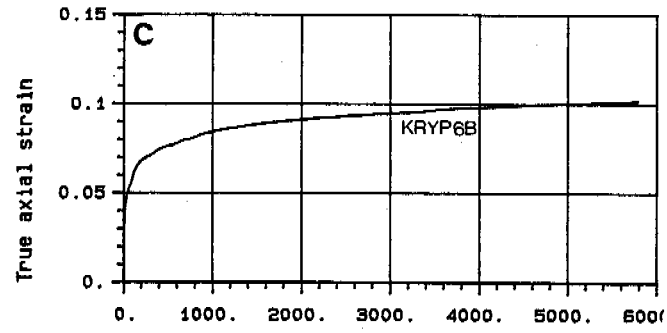

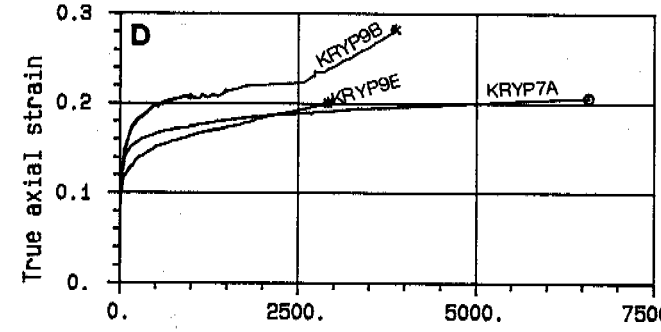

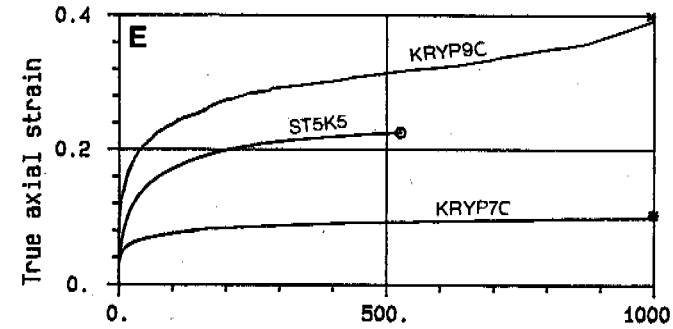

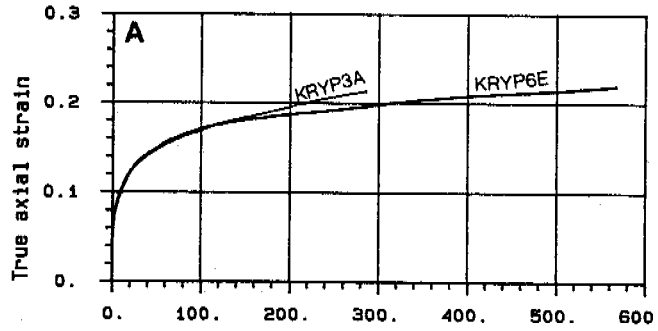

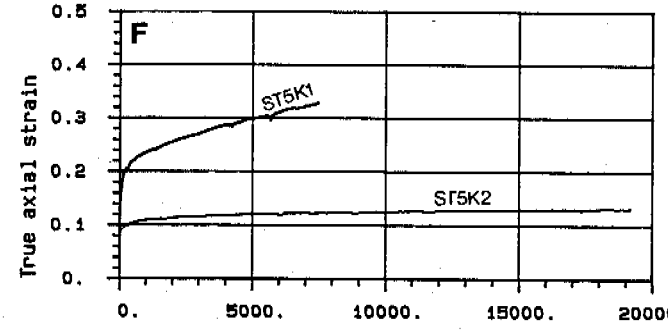

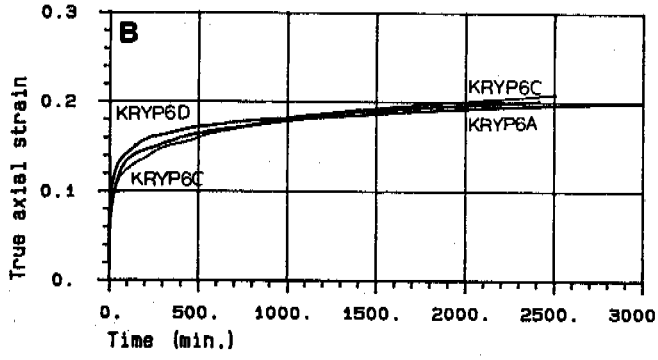

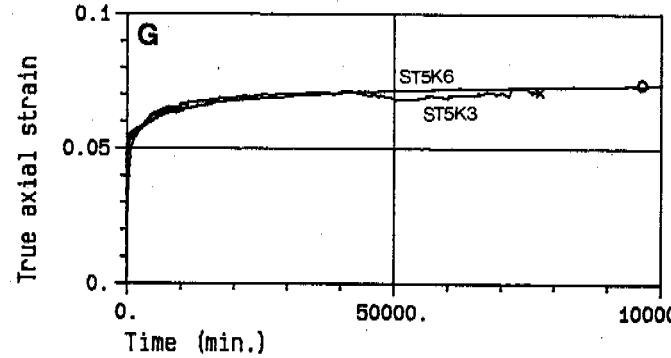

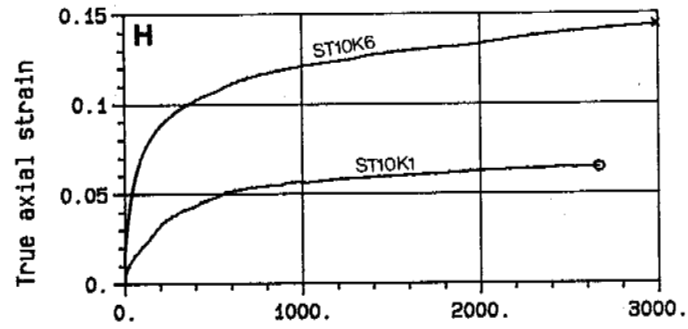
H
ST10K6
ST10K1
True axial strain
0.15
0.1
0.05
0.
0.
1000.
2000.
3000.

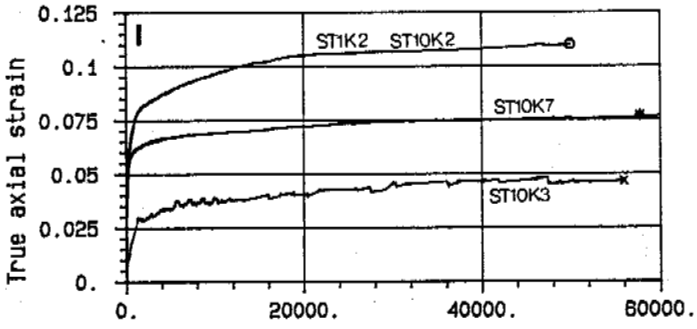
I
ST1K2 ST10K2
ST10K7
ST10K3
True axial strain
0.125
0.1
0.075
0.05
0.025
0.
0.
20000.
40000.
60000.

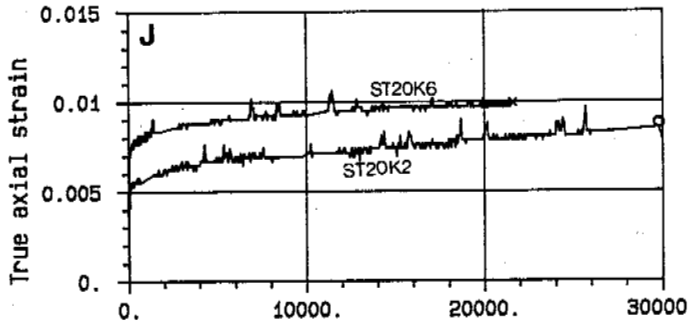
J
ST20K6
ST20K2
True axial strain
0.015
0.01
0.005
0.
0.
10000.
20000.
30000.

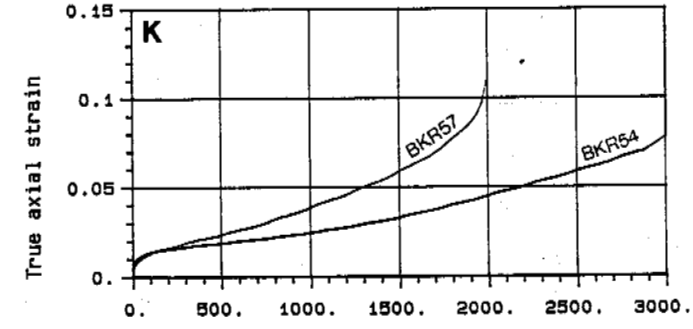
K
BKR57
BKR54
True axial strain
0.15
0.1
0.05
0.
0.
500.
1000.
1500.
2000.
2500.
3000.

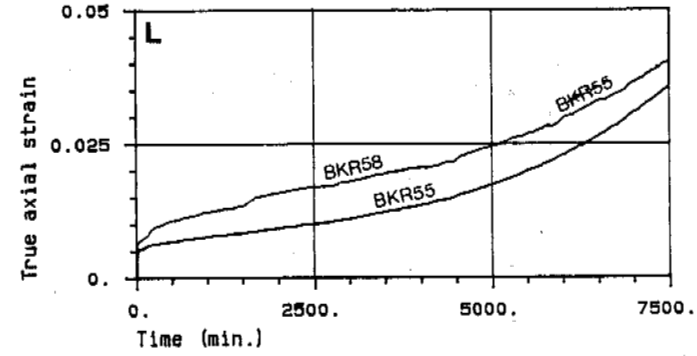
L
BKR55
BKR58
BKR55
True axial strain
0.05
0.025
0.
0.
2500.
5000.
7500.
Time (min.)

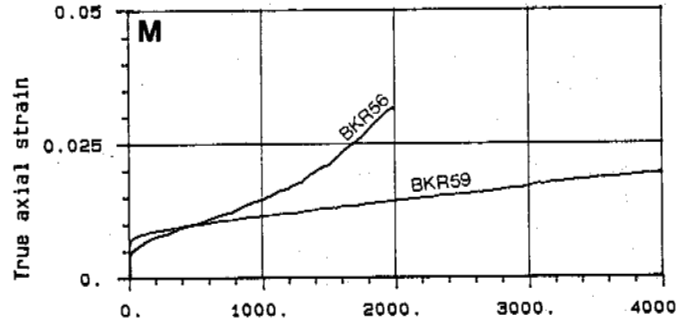
M
BKR56
BKR59
True axial strain
0.05
0.025
0.
0.
1000.
2000.
3000.
4000.

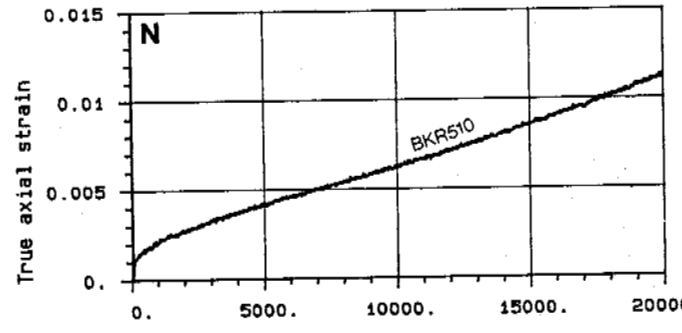
N
BKR510
True axial strain
0.015
0.01
0.005
0.
0.
5000.
10000.
15000.
20000

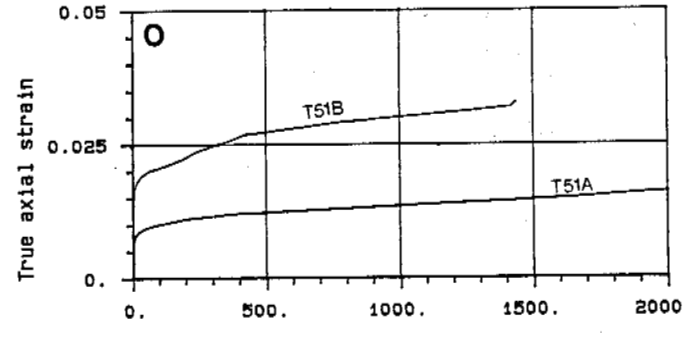
O
T51B
T51A
True axial strain
0.05
0.025
0.
0.
500.
1000.
1500.
2000.

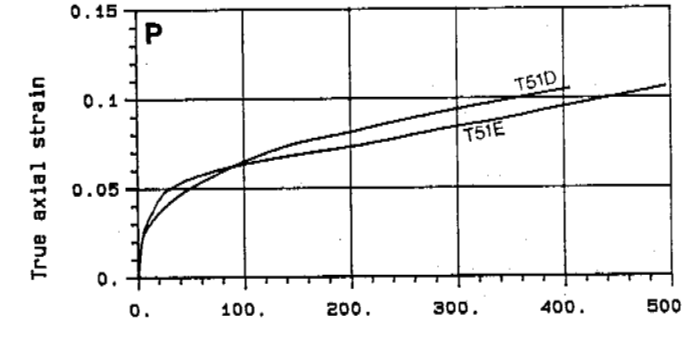
P
T51D
T51E
True axial strain
0.15
0.1
0.05
0.
0.
100.
200.
300.
400.
500.

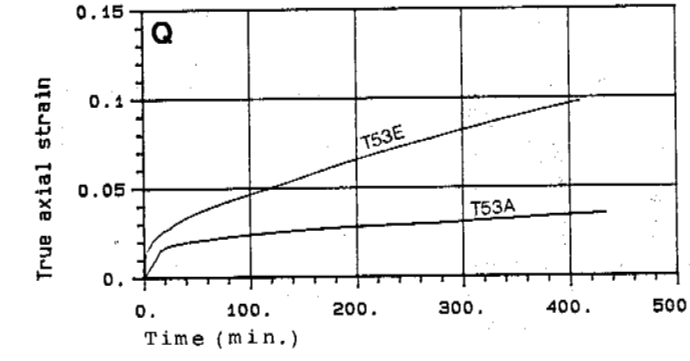
Q
T53E
T53A
True axial strain
0.15
0.1
0.05
0.
0.
100.
200.
300.
400.
500.
Time (min.)

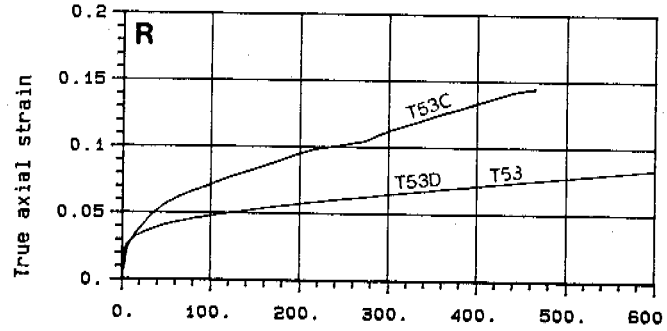

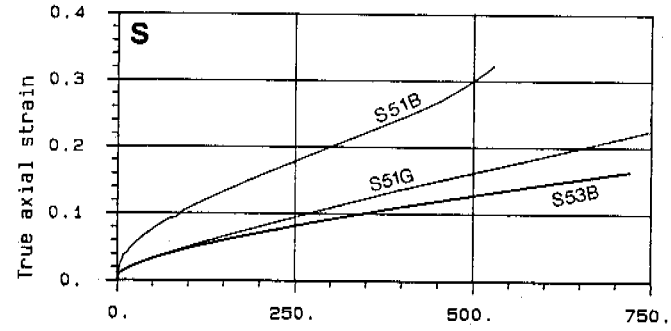

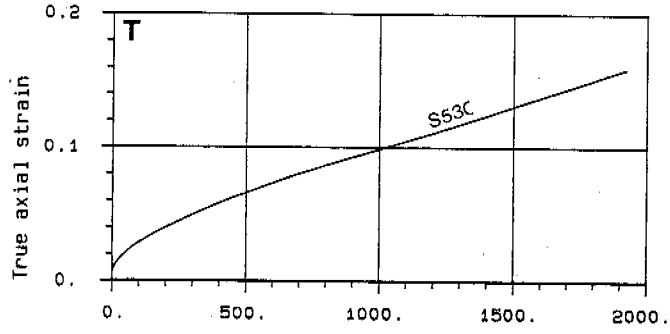

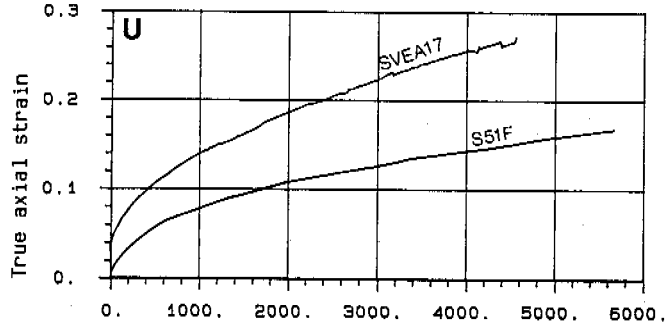

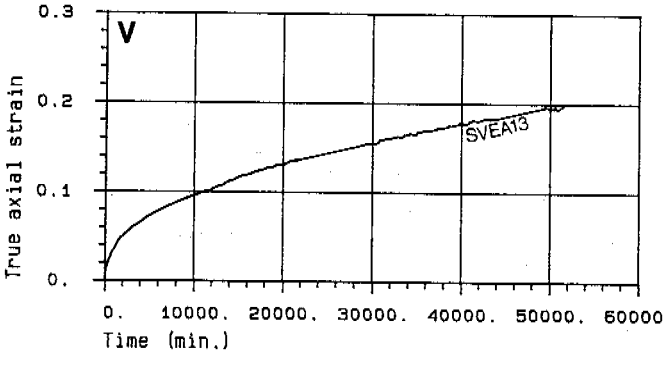

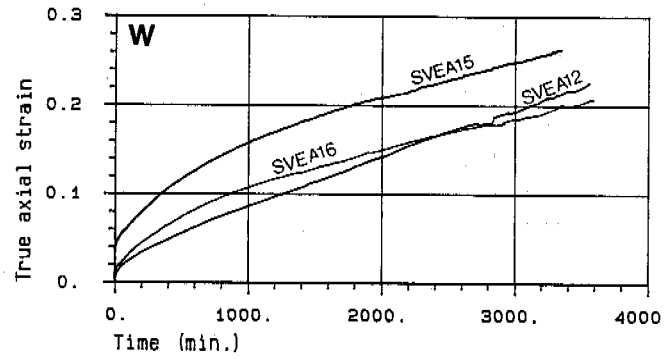

Figs. 1A to 1W Creep Tests. True Axial Strain Versus Time.

Unfrozen water content as function of temperature is given in Figure 2.

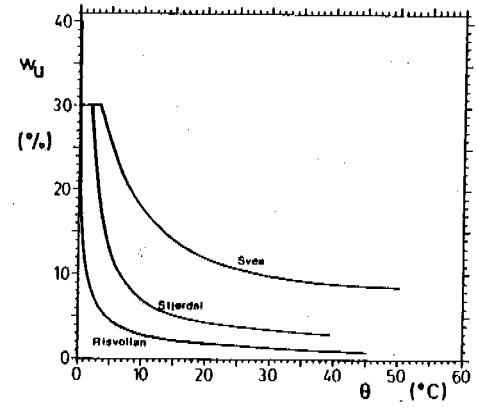

Fig. 2 Unfrozen Water Content as Function of Temperature. After Berggren (1983)

STRENGTH AND DEFORMATION PROPERTIES

The tests are interpreted according to Berggren's model, Berggren (1983). Deformation is computed from the strain equations (1), (2) and (3).

Total strain:

$$\epsilon = \epsilon_p + \epsilon_s \qquad (1)$$

Strain in the primary creep period:

$$\epsilon_p = \frac{1}{r_f}\left[\frac{\sigma}{\sigma_\theta}\right]^i \ln\left[\frac{t}{t_o}\right], \quad 1 = t_o < t \leq t_p \qquad (2)$$

Secondary creep strain:

$$\epsilon_s = \frac{1}{r_f}\left[\frac{\sigma}{\sigma_\theta}\right]^i \left[\frac{t}{t_{pf}}\left[\frac{\sigma}{\sigma_\theta}\right]^j - 1\right], \quad t > t_p \qquad (3)$$

ϵ = engineering strain

ϵ_p = strain in primary creep period

ϵ_s = strain in secondary creep period

t_p = primary creep period

t_{pf} = t_p extrapolated to a fictious failure

j = exponent

σ_θ = temperature dependent reference stress

r_f = the creep number, r, extrapolated to a fictitious failure

i = exponent

t_o = 1 hour, introduced to avoid initial calculation problems.

The temperature dependent reference stress σ_θ may be determined from compression tests at the correct temperature or from unfrozen water content tests by Equation (4).

Temperature dependent reference stress:

$$\sigma_\theta = \sigma_u \left(\frac{W_s}{W_u}\right)^u \qquad (4)$$

σ_u = σ_θ extrapolated to a fictitious thawed state when $W_u = W_s$

u = exponent

W_s = moisture content at 100% saturation

W_u = unfrozen water content.

If the secondary creep stage develops, it will just be a matter of time before failure occurs. Therefore creep strength is taken to be the upper stress limit for primary creep.

Creep strength:

$$\sigma_L = \sigma_\theta \left[\frac{t_{pf}}{t_p}\right]^{(1/j)} \qquad (5)$$

The traditional way of presenting creep tests on frozen soil is by plotting true strain versus time. True strain, $\epsilon = \Delta h/h$, is therefore plotted in Fig. 1, even if the Berggren model is based on engineering strain, $\epsilon = \Delta h/h_o$. The error made by using true strain curves instead of engineering strain curves, for determining parameters for the Berggren model, is relatively small. The parameters given in Table VII are, however, determined from engineering strain plots. The parameters are also based on all tests performed, not only the selected number of tests presented in this paper.

TABLE VII Creep Parameters for Use in the Berggren Model. Parantes Indicates Uncertain Values. After Berggren (1983)

Clay	t_o (h)	i	r_f	j	t_{pf} (min)	u	σ_u (kPa)
Stjørdal	1	3.8	13.7	9.9	6.0	1.7	130
Eberg	1	(4.1)	(15.0)	6.8	1.9	-	-
Risvollan	1	7.1	54.4	4.9	7.2	1.2	300
Svea	1	1.5	4.6	4.1	5.9	6.4	360

In figure 3 creep strength at -5°C is plotted against design period.

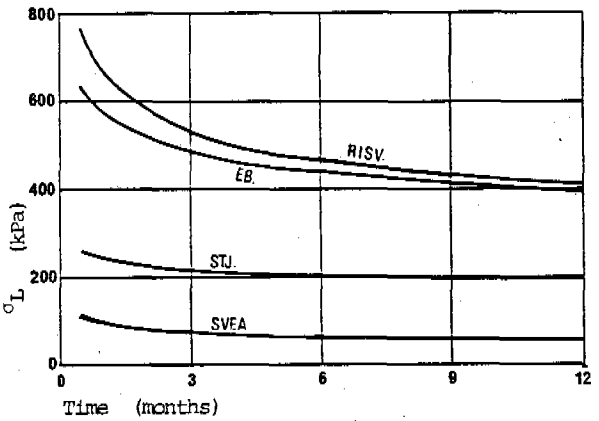

Fig. 3 Creep strength σ_L, versus design period. Temperature -5°C

The four clays accumulate different creep strains during design periods of equal length. Creep strains for a design period, or a primary creep period of 12 months at -5°C, are given in Table VIII.

TABLE VIII Creep Strains Accumulated During a 12 Months Primary Creep Period. Temperature -5°C

Clay	Stjørdal	Eberg	Risvollan	Svea
Primary creep strain (%)	0.9	0.03	~0	3.3
Salinity (g/l)	33	3	~0	50-60, soil 34, total

COMMENTS

In the Berggren model dependency of amount of unfrozen water is exchanged for the temperature dependency. This is done because the water phase is believed to govern the long-term behaviour of the frozen soil whilst the ice governs the short-term behaviour of the soil. No simple mathematical formulation of the unfrozen water content-temperature curve is found. For nonsaline soils a linear logarithmic formulation might be used, but this will not apply if the soil is highly saline. Results from the unfrozen water content

tests should therefore be used directly when determining the temperature dependent reference stress, σ_θ.

As seen from Fig. 2, the amount of unfrozen water increases with increasing salinity. The most saline clays were therefore expected to be the weakest clays. As seen from Table II, this is not quite true. The Svea clay has considerably higher compression strength than the slightly less saline Stjørdal clay. We believe that this is due to the vertical fresh ice seams in the clay, acting as reinforcement when the clay is subjected to rapid loading. From Fig. 3 it is seen that the creep strength of Svea clay is far less than the creep strength of Stjørdal clay. The difference between the creep strengths of the two clays are larger than one would expect from the difference in total salinity of the clays. In the Svea clay, however, the salt is concentrated in the pores in the soil, 50-60 g/l, whilst the ice seams are fresh. This is probably the reason for the Svea clay's low creep strength.

It is difficult to quantify directly the influence of pore water salinity on strength of frozen soils. Results presented by Ogata (1983) clearly show that the relative strength reduction caused by increasing salinity is different for different types of soils. Our tests indicate that the relative strength reduction caused by increasing salinity is not the same for compression and creep strength. In our opinion the influence of salinity on strength of frozen soil is best accounted for through the use of unfrozen water content-temperature curves for determining the temperature dependent reference stress.

A comparison of the creep strengths determined by Berggren's model to creep strengths determined by other methods, shows that the Berggren model gives relatively low creep strengths. This is due to the fact that the model only allows stresses resulting in primary creep. The creep strains accumulated in the same design period are different for different clays. From Table VIII it is seen that the creep strains are strongly dependent on pore water salinity. The most saline clays accumulate largest creep strains. As for creep strength, the influence of salinity on creep strain is accounted for through the unfrozen water content.

CONCLUSIONS

Creep strains and unfrozen water content increase with increasing salinity of the clay, whereas creep and compressive strength decrease with increasing salinity. The relative strength reduction as salinity increases is not equal for creep and compression. This makes it difficult to quantify the influence of salinity on frozen clay strength directly. In our opinion the influence of salinity on strength and deformation properties is best accounted for through the relationship between the unfrozen water content and mechanical properties of clay.

REFERENCES

Berggren, A-L. (1983). "Engineering creep models for frozen soil behaviour". Dr. of Engineering thesis at the Norwegian Institute of Technology.

Berggren, A-L. and Furuberg, T. (1985). "A new Norwegian creep model and creep equipment". Proceedings ISGF85 Hokkaido University, Sapporo, Japan, pp. 181-185.

Ogata, N., Yasuda, M. and Kataoka, T. (1983). "Effects of salt concentration on strength and creep behaviour of artifically frozen soils". Cold Regions Science and Technology 8 (1983) pp. 139-153.

DECREASED SHEAR STRENGTH OF A SILTY SAND SUBJECTED TO FROST

G.P. Gifford

Union College, Schenectady, N.Y.

SYNOPSIS A unique direct simple shear device is described. The device is used to quantitatively assess the thaw-weakening of a soil. A relationship between void ratio and simple shear strength of a silty sand is established. The device is used with a specimen mold, a frost cabinet, and auxiliary instrumentation to establish a relationship between void ratio and post-thaw simple shear strength of the soil. The resulting relationship between void ratio and post-thaw shear strength indicates the soil has weakened due to freeze and thaw. The causes of weakening are increased void ration due to moisture migration during freezing and weakened planes at the location of previous ice lenses. During shear, suspected motion of the thaw-freeze interface and flexibility of the reinforced membrane prove shear was not performed at constant volume. Therefore, it cannot be categorically stated that the post-thaw shear strength is less than the prefreeze strength at all magnitudes of void ratio. However, the device shows great promise for quantitative assessment of thaw-weakening.

INTRODUCTION

The phenomenon of frost heave and subsequent thaw of soils can cause engineering problems. Present solution techniques are expensive and often based on past experience with little or no scientific basis. A more thorough understanding is required to develop economical design techniques. This paper reports the use of a device which employs the simple shear test mode on unfrozen and thawed soil samples.

The device was developed at Worcester Polytechnic Institute and modeled after the simple shear device of the Norwegian Geotechnical Institute as reported by Bjerrum and Landva (1966). The dimensions of the shear sample are ideal for measuring the shear resistance in a highly anisotropic material, such as a soil sample containing melted ice lenses.

As reported by Bishop (1971), the shearing resistance of a saturated soil is inversely proportional to water content when all other factors are equal. During thaw a soil contains "thaw-weakened" zones with little or no ability to resist shear. Alkire (1983) assumes that some form of metastable cluster structure develops in a loose silt during freeze and thaw, and collapses under load. Little is known regarding the magnitude of strength change caused by this metastable structure.

The objective of this report is to demonstrate a new device capable of assessing the shear strength of a silty sand subjected to frost action. To this end the device was used to develop a relationship between void ratio and shear resistance for a frost-susceptible soil, both before and after thermal conditioning. The test data is statistically analyzed, and a best fit empirical equation is developed relating void ratio to shear strength. The primary thermal conditioning variables which were purposely varied during freeze are rate of heat extraction, thermal gradient, and cycling of freeze-thaw. The effects which these variables have on the post-thaw shear strength are discussed.

EQUIPMENT EMPLOYED DURING THIS RESEARCH

The direct simple shear (DSS) device consists of a specimen mold and top cap assembly. The device, shown in Fig. 1, is discussed in detail by Gifford (1984), and is briefly reviewed here.

The specimen mold consists of twenty tapered and interlocked split acrylic discs. As recommended by Shen et al (1978), a maximum height to diameter ratio of 1:8 is utilized to maintain relatively uniform shear strain distribution.

The mold is lined with a tapered rubber membrane which is laterally reinforced with nylon thread. This membrane is employed during DSS testing to prevent leakage and provide lateral support of the sample.

The top cap assembly is used to apply normal and shear stress to the thawed sample through the roughened porous stone. The heating element thaws the top of a previously frozen specimen to produce a thaw-weakened DSS test sample. The elevation of the top cap assembly is variable, to enable a series of DSS tests to be performed on each previously frozen specimen.

The frost cabinet and auxiliary instrumentation are discussed by Gifford et al (1983) and reviewed here. In order to simulate frost action in the field, the cabinet is equipped

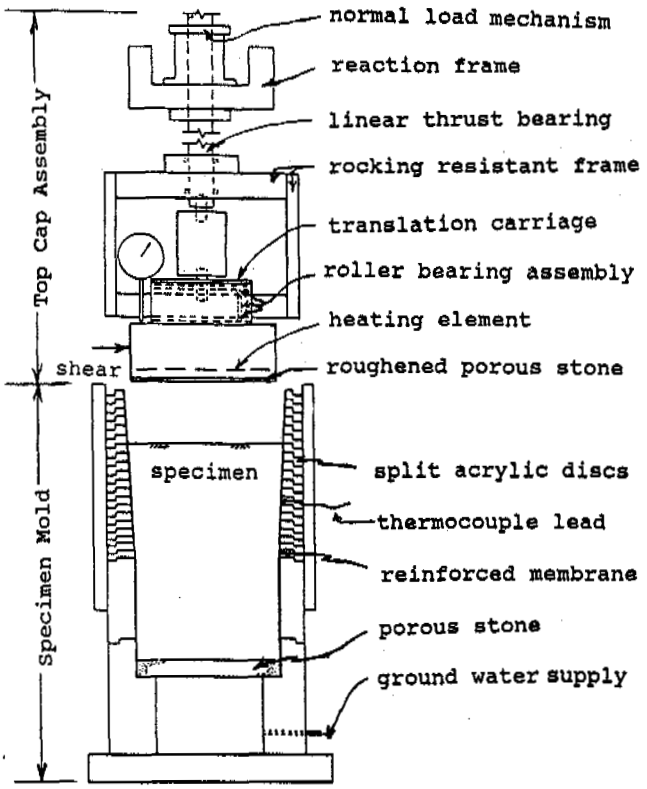

Fig. 1 The Direct Simple Shear Device

with two independent refrigeration units. Vermiculite insulation helps develop the desired thermal gradient. Temperature of the specimen is monitored with thermocouples placed along the outside of the membrane.

During thermal conditioning a plate placed on the specimen prevents sublimation and provides a stable base for the heave measurement system. Heave and moisture migration are monitored electronically. Data from periodic readings of temperature, heave, and moisture migration are recorded by a data acquisition system.

After the desired thermal conditioning, the specimen is frozen throughout to 20°F (-7°C) and the top cap positioned for thawing the uppermost sample. After thaw, air is bled from the sample and the membrane is clamped to the top cap. Water movement is prevented laterally by the membrane, downward by the still frozen subsoil, and upward by the top cap. During shear, constant sample height is maintained by manually adjusting the normal load.

After shear the entire sample is removed for moisture content determination, and the still frozen specimen top shaved to a horizontal plane. The remaining specimen is frozen throughout before the next thaw and shear.

An alternate base is used with the top cap assembly to perform DSS tests on unfrozen soil. A pore pressure transducer in the base allows analysis of test data.

PRESENTATION AND DISCUSSION OF RESULTS OF DSS TESTS ON UNFROZEN IKALANIAN SAND

The results of undrained DSS tests performed on unfrozen soil are presented and discussed in this section. Also presented is a description of the research program employed. The purpose of the prefreeze portion of this research is to establish a best fit relationship between void ratio and undrained shear strength which is compared to a similar relationship from post-thaw test results.

The DSS tests were performed over a wide range of void ratio, e. After each test the entire sample was used to determine moisture content, w. The average void ratio for all samples was calculated from w assuming saturation.

Uniform stress and strain distribution on the sample boundaries is assumed valid. Therefore, average values of both shear stress, τ, and normal stress, σ_n, are assumed equally distributed throughout the sample.

The soil utilized during this research is termed Ikalanian Sand. Index, compaction, and permeability test results are presented in Table I, along with associated ASTM test specifications.

TABLE I

Results of Index, Compaction, and Permeability Testing of Ikalanian Sand

Index Property:		
Specific Gravity (D-854):		2.68
Liquid Limit (D-423):		N.P.*
Plastic Limit (D-424):		N.P.
Particle Size (D-421):		
%weight finer than:		
No. 4	(4.76mm)	100
No. 10	(2.00mm)	99
No. 20	(0.84mm)	96
No. 40	(0.42mm)	88
No. 60	(0.25mm)	77
No. 100	(0.149mm)	61
No. 200	(0.074mm)	36
0.02mm		9
0.005mm		2
0.001mm		1
Compaction Testing (D-698):		
Maximum Dry Density (KN/m³)		18.6
Optimum Moisture Content (%)		13.0
Permeability Testing (D-2434):		
k (cm/sec)	5.7×10^{-5} at e =	0.51
k (cm/sec)	1.1×10^{-4} at e =	0.75

*N.P. indicates non plastic

Since in-situ frost-susceptible soils often become saturated during thaw, and highway design tests often use saturated samples (i.e. CBR); all samples used in this research program were saturated. Failures related to thaw-weakening are shallow in nature so a low magnitude of initial normal stress, σ_{no}, was used for all

tests. Three test series were performed on saturated samples of Ikalanian Sand and designated SX, SIK, and NM.

The SX test series consists of nine tests. The samples were prepared by pouring air-dry soil into standing de-aired water in the membrane.

After consolidation air was bled from the system, and the membrane clamped to the top cap. Water was allowed to percolate up through the sample from a constant head water supply for at least 24 hours.

During these DSS tests constant volume and constant pore pressure were insured by maintaining constant elevation of a water level in a standpipe which was attached to a drain line from the sample. The water level was held constant by adjusting the normal load. Knowledge of the hydrostatic head due to the water level yielded the pore pressure within the sample and consequently allowed effective stress analysis of test data. Basic drainage calculations were performed which indicated that the shear rate was slow enough to allow complete dissipation of excess pore pressure. These tests were, in fact, constant volume quasi-drained tests in that moisture content and pore pressure remained constant during shear.

The SIK test series consists of six tests. To insure saturation the sand was boiled prior to use and poured into standing de-aired water in the membrane. This series was performed prior to the installation of the pore pressure transducer. Therefore, initial pore pressure magnitude was assumed equal to that portion of the initial normal stress applied to the sample after all drain lines were closed. The initial effective normal stress, σ_{no}', is equal to the difference. During shear, the change in pore pressure was assumed equal to the change in normal stress required to maintain constant sample height.

The NM test series consists of five tests. Sample preparation and test procedure were identical to the SIK test series except that a pore pressure transducer was employed to monitor pore pressure during consolidation and shear.

Stress paths in the τ versus σ_n' stress space were plotted for all tests. With the exception of very loose samples, the stress path touches and moves along a failure envelope. The arc tangent of this τ/σ_n' ratio yields the effective angle of internal friction, ϕ'. Furthermore, it may well be argued that the point of tangency adequately defines failure, and the magnitude of shear stress at this point is the undrained shear strength, τ_f. This failure criterion was employed for 16 tests.

The stress path of very loose samples is erratic and does not move along a failure envelope. The magnitude of shear stress at the first peak in the stress path was adopted as failure. This failure criterion was employed for four samples which possessed void ratios of 0.91, 0.88, 0.83, and 0.73.

Fig. 2 shows the e versus τ_f data with a best fit natural logarithmic curve. The data scatter

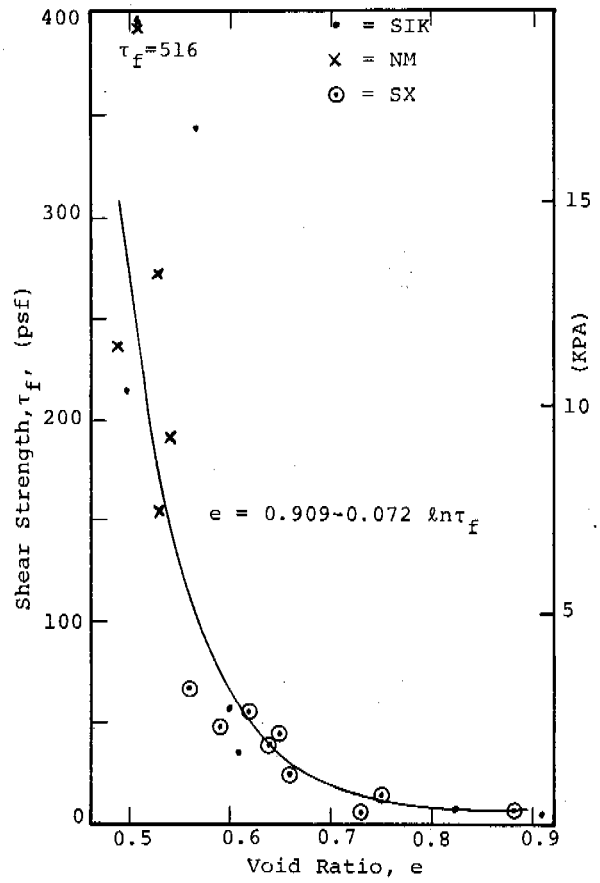

FIG. 2 e Versus τ_f for Unfrozen Ikalanian Sand

appears reasonable for samples looser than e = 0.59, but for samples denser than e = 0.59 the scatter is larger. The data scatter is due to partial drainage during shear caused by volume change associated with flexibility of nylon-reinforced membranes. The error of measured shear strength due to flexibility decreases with shear resistance.

Since thaw-weakened shear resistance is expected to be low, the large magnitude errors from tests on dense samples are of little concern. The discussion above, coupled with the other device related problems, enhanced employment of a different failure criterion for thaw-weakened samples.

PRESENTATION AND DISCUSSION OF RESULTS ON THAW-WEAKENED IKALANIAN SAND

The DSS results obtained from tests performed on Ikalanian Sand which was thermally conditioned in the frost cabinet are presented and discussed.

Three thermal conditioning variables were purposely varied to study how they effect the degree of ice lensing and ultimately the post-thaw shear strength. They are rate of heat

extraction, thermal gradient, and cycling of freeze-thaw. To control other variables, one soil was used at approximately the same prefreeze void ratio, and each specimen was subjected to the same overburden prior to thermal conditioning. With the exception of specimen FTS-6, all test specimens employed open water supply systems, and were initially capillary saturated. Test FTS-6 employed a closed water supply system and was initially fully saturated.

All specimens except FTS-7 were subjected to one freeze-thaw cycle. Test FTS-7 was subjected to two cycles as follows. After the desired thermal conditioning, the specimen was frozen throughout to 20°F (-7°C). Then the temperature of the upper portion of the frost cabinet was incrementally raised to 34°F (1°C), and the lower cabinet portion set at 30°F (-1°C). The thaw cycle lasted 130 hours. The specimen was then frozen from the top downward by a large temperature drop of the upper cabinet portion so as to minimize freezing from the thaw-freeze interface upward.

The rate of heat removal is directly related to the rate of frost front penetration. The rate of frost front penetration was varied throughout the research program and each individual test.

The thermal gradient, defined as the change in temperature per unit length of specimen height, was varied throughout the entire test program.

The rate of frost penetration into each specimen was scheduled in increments and varied for each test, so that nearly horizontal zones of varying degrees of ice segregation would develop. Table II presents a summary of the thermal conditioning, and the prefreeze specimen characteristics; as well as moisture migration and heave data for the six freeze tests performed on Ikalanian Sand. The corrected heave was calculated by subtracting the heave due to nine percent volume expansion of pore water upon transformation to ice from the total heave.

Because of the difference in thermal conductivity of the acrylic mold and soil specimen unidirectional frost front penetration, thus horizontal ice lensing was suspected. During rapid freezing, if the 32°F (0°C) isotherm penetrates the mold more quickly than the soil, an arched 32°F (0°C) isotherm will develop within the specimen. If the depth of frost penetration is then held constant, the isotherm would become horizontal after some time, but ice segregation might be smeared throughout the arched zone. One specimen, FTS-9 was purposely removed from the frost cabinet after only three DSS tests to visually inspect a suspected ice lens. Examination of the collected data indicates that heave of 0.15 in. (0.38 cm) occurred as the depth of frost penetration increased from 4.2 in. (10.7 cm) to 4.5 in. (11.4 cm). An ice lens, 0.12 in. (0.3 cm) thick, was found within this depth, and extended horizontally completely across the specimen. This observation proved that horizontal ice lensing can purposely be induced with this equipment.

Knowing the moisture migration history of the specimen, it is conceivable to expect zones of high post-thaw moisture content and low post-thaw shear resistance at the location of ice lenses. Attempts to correlate the moisture migration and shear resistance with thermal history were inconclusive and are further discussed by Sage and D'Andrea (1983).

In order to simulate field conditions during thaw and post-thaw shear, the top cap was placed on the frozen specimen and a normal stress of

TABLE II

Summary of Freeze Tests on Ikalanian Sand

	FTS-3	FTS-4	FTS-5	FTS-6	FTS-7	FTS-9
Initial Dry Density, KN/m^3	17.59	17.75	17.92	18.12	18.03	17.68
Initial Moisture Content, %	18.4	19.1	18.8	17.0	17.5	18.8
Initial Void Ratio	0.49	0.48	0.47	0.46	0.47	0.49
Initial Percent Saturation, %	100.0	100.0	100.0	100.0	100.0	100.0
Duration of Test, hours	2186	116	63	62	515	156
Number of Freezing Cycles	1	1	1	1	2	1
Number of Freezing Increments	14	2	1	1	2	3
Ground Water Conditions	OPEN	OPEN	OPEN	CLOSED	OPEN	OPEN
Maximum Frost Depth, cm	10.7	8.9	13.5	11.7	11.4	13.0
Max. Rate of Frost Pene. cm/day	2.29	12.80	199.90	51.31	188.98	28.19
Aver. Rate of Frost Pene. cm/day	0.13	1.83	5.13	4.06	3.00	1.98
Mini. Rate of Frost Pene. cm/day	0.00	0.56	0.36	1.24	2.74	0.76
Aver. Thermal Gradient, °C/cm	0.22	0.26	0.35	0.31	0.28	0.26
Depth to Water Level, cm	21.6	21.6	21.6	0.0	21.6	21.6
Maximum Frost Depth, cm	10.7	8.9	13.5	11.7	11.4	13.0
Total Moisture Migration, cc	442.5	206.5	81.9	0.0	3.3	324.5
Total Heave, cm	3.0	1.5	0.5	0.3	0.3	2.3
Corrected Heave, cm	2.8	1.3	0.0	0.0	0.0	2.0
Aver. Moist. Transfer Rate cc/day	4.92	42.77	31.30	0.0	0.0	49.98
Aver. Heave Rate, cm/day	0.03	0.25	0.0	0.0	0.0	0.3

approximately 150 psf (7.2 KPa) was maintained during thaw. As thaw commenced, air was bled from the sample and the membrane was sealed and clamped around the top cap. As thaw continued, the nine percent volume loss caused by ice transformation to water required that the normal stress be continually adjusted to maintain 150 psf (7.2 KPa).

As the desired depth of thaw was approached, the heating element was turned off and a DSS test performed. During shear the elevation of the top cap was maintained constant by adjusting the normal load as required. Pore pressure was not monitored; and furthermore, the preshear pore pressure was not known. Therefore, a total stress analysis was the only means available for data interpretation, and a somewhat arbitrary point on the total stress path must define failure.

To this end, a statistical analysis was performed on prefreeze DSS test data. The values of shear strain, δ, at τ_f were plotted against void ratio. A best fit line was calculated via the least squares method and the equation of the line is:

$$\delta = 100\ (e - 0.49) \qquad (1)$$

As expected, strain at failure increases with void ratio. The post-thaw shear strength of Ikalanian Sand, τ_{pt}, is herein defined as the measured shear resistance at the strain calculated from Equation 1 utilizing the appropriate void ratio.

Fig. 3 shows the e versus τ_{pt} data for 23 of the tests performed on thermally conditioned Ikalanian Sand with a best fit natural logarithmic curve. The six data points which are circled exhibited minimal shear resistance and were not used to establish the best fit curve. Data from all 23 tests were grouped in this figure, because at a given void ratio little variation of τ_{pt} was perceived, regardless of the rate of freezing, open or closed water supply system, or number of freeze-thaw cycles to which the specimen was subjected. Also included in Fig. 3 is the best fit curve from prefreeze data.

Examination of Fig. 3 reveals the following. At a particular void ratio a saturated sample of unfrozen Ikalanian Sand possesses an undrained shear strength which is greater than that of a thawed sample at the same void ratio. It appears that thaw-weakening is caused by two effects. First, the additional water which migrates into the soil during freeze causes an increased void ratio of the sample upon thaw. This increased void ratio would cause a decreased shear strength along the prefreeze curve if the soil had not been previously frozen. The fact that the loss of strength is more than that due to the increase of void ratio is attributed to the fact that the soil was frozen. As the soil grains separate due to freezing pore water and ice lensing, and

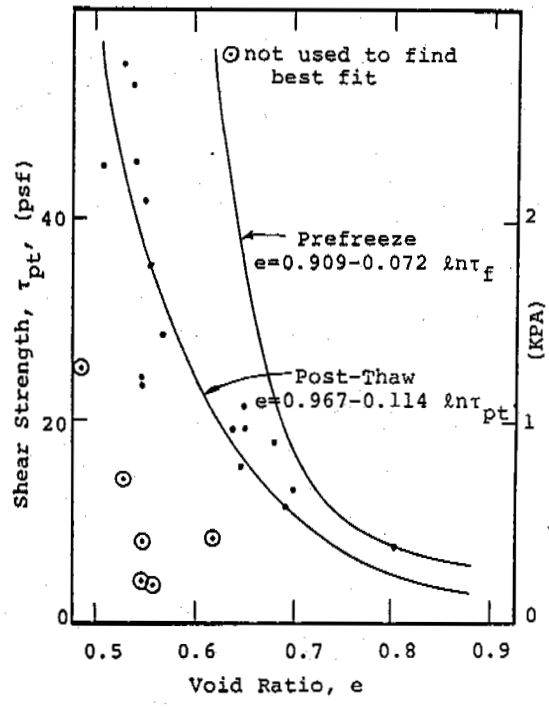

Fig. 3 e Versus τ_{pt} for Thaw-Weakened Ikalanian Sand

subsequently converge during thaw, weak planes develop within the specimen. The weakness of these planes is detected by the DSS device.

The DSS device shows promise as a useful tool to evaluate the post-thaw shear strength of a previously frozen soil specimen.

A problem of the device has to do with the latent heat built up in the top cap during thaw. Because of the nine percent volume decrease associated with phase transformation of ice to water, the normal load applied to the closed system decreases as thawing progresses. Consequently, the magnitude of change of normal stress caused by continued thaw and/or by soil behavior subject to undrained DSS testing is not distinguishable. This is the reason the strain oriented failure criterion was adopted. Furthermore, it is not possible to correct the test data, because of the variable amount of heat present during each test. Since shear resistance is a function of the effective normal stress, it cannot be categorically stated that the difference between prefreeze and post-thaw relationships presented in Fig. 3 is solely due to thermal conditioning.

Another complicating factor has to do with the measured moisture content. There was a time lag of about ten minutes between execution of the DSS test and sampling for moisture content determination. Continued thaw during this time may have caused a change of moisture content, thus void ratio, of the bulk sample.

Undrained DSS tests were performed on thawed samples at various levels within the specimens. Profiles of moisture content and post-thaw shear

strength with depth are presented by Gifford (1984). The profiles accentuate the anisotropic soil shear strength which is expected in a previously frozen soil column. The DSS test mode is geometrically ideal to investigate the shear resistance at the thaw-weakened zones of limited vertical extent.

CONCLUSIONS

As demonstrated herein, this unique direct simple shear device can be used to evaluate the post-thaw shear strength of a frost-susceptible soil. This pioneering use of the DSS test mode is particularly useful to assess the shear resistance at weakened zones of a previously frozen soil column. Even though the results presented are inconclusive, a new method of quantitatively measuring both the prefreeze and post-thaw shear strength of soil is introduced.

The following conclusions were reached:

1. The incorporation of a pore pressure transducer into the alternate DSS test device is useful, in that effective stress analysis of test data is available.

2. As presently designed, the DSS device is less effective in assessing the strength of a thaw-weakened soil utilizing total stress analysis.

3. Use of this DSS device lends itself to examination of the anisotropic zonal nature of thaw-weakened soil; especially considering previous studies which used conventional test methods.

4. Based on test results presented herein, the following behavioral characteristics are noted specifically for Ikalanian Sand:

a. The undrained shear strength of saturated Ikalanian Sand decreases with increased void ratio.
b. Under appropriate conditions, frost heaving of Ikalanian Sand produces ice lensing and subsequent zones of high moisture content after thaw. Furthermore, these zones exhibit undrained DSS strength magnitudes which are greatly reduced from the prefreeze strength.
c. The post-thaw DSS strength of Ikalanian Sandis independent of the rate of frost penetration, the water supply system (open or closed), and the number of freeze-thaw cycles to which it had been previously subjected.
d. The post-thaw DSS strength of Ikalanian Sand is less than that of the unfrozen saturated soil at an equivalent void ratio.
e. Thermal conditioning which causes an increase in localized moisture content produces a weakened plane within the Ikalanian Sand upon thaw. Therefore, thaw-weakening is produced not only by the increased moisture content (i.e. void ratio) and decreased residual stress, but also from grain separation on some plane.

ACKNOWLEDGEMENTS

The research described has been partially supported by the United States Department of Transportation, Office of University Research,and their contributions are gratefully acknowledged. The views presented herein, however, are those of the author. Thanks are also extended to the Massachusetts Department of Public Works Frost Research Station for supplying the Ikalanian Sand used during this research.

REFERENCES

Alkire, B. D., and Morrison, J. M., (1983). "Change in Soil Structure Due to Freeze-Thaw and Repeated Loading," Transportation Research Record #918, pp. 15-22.

Bishop, A.W., (1971). "Shear Strength Parameters for Undisturbed and Remolded Soil Specimens," In Stress-Strain Behavior of Soils, Proceedings, Roscoe Memorial Symposium, Cambridge University, Cambridge, England, pp. 3-58.

Bjerrum, L. and Landva, A., (1966). "Direct Simple Shear Tests on a Norwegian Quick Clay," Geotechnique, Vol. 16, No. 1, pp. 1-20.

Gifford, G. P., (1984). "Assessment of Shear Strength Loss of a Silty Sand Subjected to Frost Action," Dissertation Presented to the Faculty of Worcester Polytechnic Institute, Worcester, Ma., in partial fulfillment of the requirements for the degree of Doctor of Philosophy.

Gifford, G. P., D'Andrea, R. A., and Sage, J. D., (1983). "A Device for the Evaluation of Thaw-Weakening of Frost-Susceptible Soil," Transportation Research Record #918, pp. 10-15.

Sage, J. D., and D'Andrea, R. A., (1983). "Shear Strength Characteristics of Soils Subjected to Frost Action," Final Report DTRS 5680-C-00035, Department of Transportation, Washington, D. C., 143 pp.

Shen, C., Sadigh, K., and Hermann, L., (1978). "An Analysis of NGI Simple Shear Apparatus for Cyclic Soil Testing," Dynamic Geotechnical Testing, ASTM STP654, pp. 148-162.

THEORETICAL FROBLEMS OF CRYOGENIC GEOSYSTEM MODELLING

S.E. Grechishchev

All-Union Scientific Research Institute of Hydrogeology and Engineering Geology, Moscow, USSR

SYNOPSIS Cryogenic natural-territorial complexes (NTC) - geosystems - are considered as natural objects of mathematical modelling for the purposes of geocryologic prediction. A functional thermodynamic model of NTC is suggested, in which cryogenic physical-geologic processes are considered as strains of rocks that are a lithogenic basis of NTC.

Considerable complexity of natural geocryologic systems is specified by interaction of many processes of the lower class, including the processes in biota; therefore, the only solution of the problem of geocryologic prediction is mathematical modelling.

For the construction of a mathematical model of some natural object according to the principles of systematic approach it is necessary to perform the following operations: determination of the object of modelling (object of prediction), formalization of the statement of prediction problem, ascertainment of factors-reasons in a well-grounded plan, choice of model organization.

The problem of distinguishing uniformly functioning natural bodies, the choice of which as a modelling object is expedient, is for the last 20 years studied in detail by landscape science, in the framework of which the study has been developed of natural-territorial complexes (NTC) - "homogeneous, able to self-regulation natural systems, connected with the outer medium through energy and mass transfer" (Sochava, 1974). There in NTC close interconnections are realized between heat and moisture circulation in rocks, their lithology and place in the relief, climate and vegetation (Sochava, 1974; Krauclis, 1980; Shvetsov, 1973).

Soil and vegetation are usually accepted by specialists in physical geography to be a part of NTC or geosystem. The rocks that occur beneath the soil layer, are actually not considered that is reflected in the term "inert basis" (Krauclis, 1980).

But this view should not be considered valid. Investigations carried out in the north of West Siberia by statistical methods have proved that there is a correlation between appearance of NTC and its lithogenic base to a considerably higher depth. Melnikov (1981) determined, for instance, that NTC appearance for sites correlates with lithogenic base to the depth of seasonal freezing-thawing layer, for stows it correlates with lithogenic base to the depth of annual heat storage and for tracts - to the depth of erosional cut.

The data above indicate that NTC should be considered as the whole complex of surface conditions (vegetation, soil cover, soils) and underlying lithogenic base to their correlation depth. As NTC are geosystems connected with the outer environment through energy and mass exchange, then such a correlation speaks for self-organizing accompanied by homeostasis. In this case homeostasis area of cryogenic NTC should coincide with lithology variations observed in natural conditions and also soil moisture and temperature with the same biota composition.

The NTC definition suggested includes, as characters, the following two important circumstances. First, the main character is homogenity criterion, on this basis a system is singled out as a homogeneous natural body, and this is an area of its homeostasis. Second, homeostasis boundaries are a natural limit beyond that thermodynamic stability of the system is lost. So a suggested interpretation of NTC is a synthesis of ideas about NTC as an energy and mass exchange system with concepts developed by Shvetsov about thermodynamic stability of soil association.

The aim of geocryologic prediction and hence simulation is to determine a change of geocryologic conditions in time within natural-territorial complexes for a given period. In this case geocryologic conditions are as follows: temperature, total moisture content, soil ice content, ice body availability, thickness of freezing and thawing layers, cryogenic physical geological processes (thermokarst, heaving, fracturing, solifluction etc.). It should be noted that under energetical (thermodynamic) approach cryogenic physical geological processes are considered in a generalized view as motion (migration, deformation) within and at the border of soil complex.

The energetical approach to the analysis of NTC functioning allows to make its functional thermodynamic model.

To formalize the aim of geocryologic prediction, NTC should be considered as a certain area D with one relation, constituted by rocks that are a lithogenic base of NTC with the boarder line L, that is the soil surface. Within the D area there is area D_1 with one and many relations and with the temperature lower than 0°C (seasonally and perennially frozen ground) with boarderline L_1. In its turn there is a subarea with many relations D_2 of ice bodies with the boarderline L_2 within the area D_1.

Formalizing of "cryogenic physical geological process" notion is not difficult if to take account of its definition as a "morphogenetic process". Such a definition is interpreted by the deformation (motion) vector $\vec{U}_L$ notion of the surface L, that is a boundary meaning of the deformation vector $\vec{U}$ of the whole area D. Thus cryogenic processes can be formalized as deformation vector $\vec{U}$ (including ruptures-fractures) in the area D. This is one of the main differences of the suggested functional model variant from analogous models in physical geography and other related sciences. To identificate the types of cryogenic processes basing on vector $\vec{U}$ jointly with boundaries L_1 and L_2, occurring in soil, it is necessary to elaborate the criteria of identification (i.e. a certain analyzing block in the model).

Considering the above mentioned, the aim of geocryologic prediction can be formalized as a determining of t (temperature), w (total moisture content), $\vec{U}$ (deformation) and boundaries L_1 and L_2 depending on coordinate $\vec{x}$ and time τ in the area D + L.

When selecting factors that affect changes of geocryologic conditions of NTC, a formalized definition of geocryologic prediction aim should be considered. In particular, factors should not be considered with a period of variation essentially more (trend ones) or essentially less (short-period ones) than a predicted one. Changes of world ocean level, climatic fluctuations (as climate is a mean value for a 30-years period), tectonic movement, glaciation etc. relate to trend changes. Daily fluctuations of meteoelements refer to short-period changes.

One of the main purposes of geocryology is studying the factors that influence the process of geocryologic conditions change. They are presented in a number of generalising works (Principles of permafrost predictions, 1974; Pavlov, 1979; Grechishchev, Chistotinov, Shur, 1984 etc.). With regard to this a physical-geographical axiom by Shvetsov (1973) is a very useful one according to it geocryologic conditions are determined by interaction of three components: climate, ground composition and its place in the relief. The following groups of factors, affecting geocryologic conditions should be singled out: hydrometeorologic, composition and properties of soil cover, relief, composition and properties of ground, human activities. The latter includes any changes of heat and mass exchange, relief, soil cover, caused by human activities (construction and operation of engineering structures).

To make a functional (mathematical in future) NTC model it is reasonable to subdivide the above mentioned groups of factors into two subgroups: factors depending on the processes within D + L area (i.e. in grounds, constituting NTC) and factors that do not depend on the process inside the area. A list of factors, affecting NTC geocryologic conditions with allowance for formalized aim of geocryologic prediction is given in Table 1.

Design of a functional cybernetic NTC model can be carried out on the basis of different principles.For instance, it can be made on the basis of classifying the factors valid for the input to the area D. But the complexity of such a model is too high. That is why a rational organizing principle should serve a basis of a model.

As the purpose of geocryologic prediction is to determine changes of thermal and moisture conditions of rocks (physical processes) and development of cryogenic physical geological processes (mechanical processes), then a model should reflect a connection between thermal physics and mechanics, i.e. to refer to a class of thermodynamic models. As far as such NTC, according to definition, is a system open to energy and mass, then a model should reflect energy and mass exchange.

Thus NTC model should base on the principle of energy and mass exchange of the area D + L with the outer environment. Moreover mass exchange will mean only moisture exchange as for the main types of cryogenic NTC the other components of mass exchange are not significant eolian redeposits of sand and dust soils) or can be considered in a different way (for instance, snowstorm transport of snow can be taken into account with a certain coefficient, constant for each NTC and depending on relief and surface roughness).

Relative to the fact that there the input of NTC system must be energy and mass, their balance on the surface L should be considered. This approach to thermophysical aspects of landscapes is common and in conformity with permafrost zone it is well presented in Pavlov's work, 1979. As far as heat, entering the soil is the most interesting aspect of heat balance for us, then the main equation of heat balance will be as follows:

$$Q = Q_c - (Q_c A + I_{ef} + P + LE), \qquad (1)$$

where Q - heat, entering the soil; L - moisture evaporation heat; the rest are given in Table 1.

Components of heat balance in equation 1 depend on conditions on the surface L, that allows to write this equation in the following generalized way:

TABLE 1

Factors Affecting Geocryologic Conditions of NTC

Groups of factors	Factors, depending on the processes within the area D + L	Factors, that do not depend on the processes within the area D + L
Hydrometeorologic	Evaporation from the surface L of the soil and by soil covers (E); convective heat flow (P); effective radiation (I_{ef}); cover albedo (A); wind velocity at the height of 1 m; soil temperature (t_L); soil moisture (W_L); surface water inflow (Γ)	At the height of 2 m above L; total radiation (Q_c); precipitation (O); air temperature (t_{air}); humidity (W_{air})
Composition and properties of soil cover (Π)	Thickness of the cover, density (of the snow cover) or specific biomass (of vegetation cover); relative phytomass area; vegetation extinction; transparency of water layer; soil cover roughness; heat conduction, heat capacity, vapour and moisture conductivity (of snow, water or technogenic cover) etc.	
Relief	Surface outline (L)	
Composition and properties of rocks (G)	Thermophysical (heat conduction, heat capacity); mechanical (deformation, strength, thermal expansion, swelling etc.); mass exchange (moisture conductivity, water yielding capacity from the surface etc.)	Lithology, granulometric composition, water-physical properties (plastic limit, moisture capacity etc.)
Technogenic (human)		Heat inflow to the ground from engineering structures (ΔQ_T); disturbances of soil cover under constructing and operating these structures ($\Delta\Pi_T$); a change of surface water inflow under artificial irrigation or drainage (ΔM_T); a change of surface profile (foundation pits, embankments) - ΔL_T

$$Q = Q\,(Q_c,\ t_L,\ w,\ \Pi,\ L) \qquad (2)$$

Mass (Moisture) balance on the surface L can be considered in the analogous way. Moisture balance equation solved for moisture mass, entering the soil or leaving it can be written in the form:

$$M = O + \Gamma - (S + E) \qquad (3)$$

where M - moisture, entering the soil, S - surface run off, the rest are given in Table 1.

Components of water balance in equation (3) also depend on conditions on the surface L, that can be given in the following generalized form:

$$M = M\,(M_c,\ t_L,\ w_L,\ \Pi,\ L) \qquad (4)$$

where $M_c = O + \Gamma$ - total moisture inflow to the surface L.

When making a functional (and on its basis a mathematical) model of NTC it is essential that factors, valid inside the area D + L and affecting factors-reasons in the way analogous to feedback, can be summed up with the latter. This condition is significant, as most relations in NTC system are not linear. Energy and mass increments satisfy this requirement. So, assuming that balance relationships (2) and (4) satisfy expansion into series conditions let's write them down as increments:

$$\begin{aligned}\Delta Q &\approx \Delta Q_c + \frac{\partial Q}{\partial t_L}\Delta t_L + \frac{\partial Q}{\partial w_L}\Delta w_L + \frac{\partial Q}{\partial \Pi}\Delta\Pi + \frac{\partial Q}{\partial L}\Delta L \\ \Delta M &\approx \Delta M_c + \frac{\partial M}{\partial t_L}\Delta t_L + \frac{\partial M}{\partial w_L}\Delta w_L + \frac{\partial M}{\partial \Pi}\Delta\Pi + \frac{\partial M}{\partial L}\Delta L\end{aligned} \qquad (5)$$

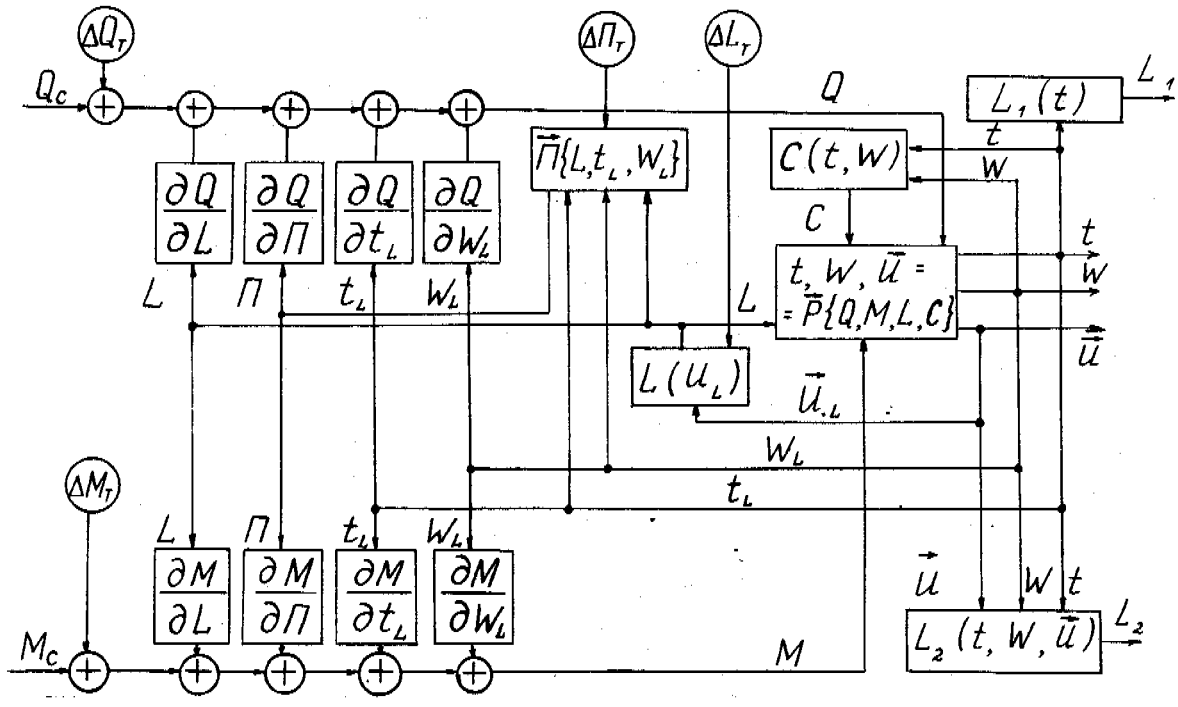

Fig. 1 Functional model of cryogenic NTC for geocryologic predictions.

The following notes should be made to the balance equations (5). The first equation is a transformation of the heat balance equation (1). Calculations, based on this equations, are considered in some works, to be difficult ones as the heat value Q, entering the soil, is small if compared with Q_c, namely it is a small difference between large numbers. This, in some cases, can bring about a considerable error in determining Q. Accordingly, a change to the soil surface temperature when calculating is made on the basis of air temperature. Then, instead of the first of equations (5) another one is taken, namely:

$$\Delta t_{\mathcal{L}} \approx \frac{\partial t_{\mathcal{L}}}{\partial t_{air}} \Delta t_{air} + \frac{\partial t_{\mathcal{L}}}{\partial w_{\mathcal{L}}} \Delta w_{\mathcal{L}} + \frac{\partial t_{\mathcal{L}}}{\partial \Pi} \Delta \Pi + \frac{\partial t_{\mathcal{L}}}{\partial \mathcal{L}} \Delta \mathcal{L} , \quad (6)$$

where t_{air} - is air temperature.

The use of the latter equation instead of the heat balance equation does not affect the construction of a general functional model. Later on incremental signs will be omitted.

Soil covers: vegetation, snow, water and human (for instance, asphalt) are very important for energy and mass exchange of landscapes. Composition and properties of vegetation cover depends on the relief, temperature, soil moisture and time (phytocoenosis age); of snow cover - on the relief (snow blowing off the elevated places and its accumulation in the depressions) and vegetation; water depth - on the relief and so on. In a general case dependence between soil cover composition and properties can evidently be represented as a certain temporary operator

$$\Pi = \Pi\{t_{\mathcal{L}}, w_{\mathcal{L}}, \mathcal{L}\} \quad (7)$$

Processes of heat and moisture redistribution and deformation development within the area D + L under known heat and moisture flows at the area boundary, its outline and soil properties can be described by thermoreology equations of frozen ground (Grechishchev, Chistotinov, Shur, 1984) that can be symbolically given as a certain operator

$$t, w, \vec{u} = P\{Q, M, L, C\} \quad (8)$$

Boundary outline L depends on deformation vector at the boundary, i.e.

$$L = L(\vec{U}_L). \quad (9)$$

Soil properties depend on its temperature and total moisture content, that can be given as:

$$C = C(t, w). \quad (10)$$

Notations in equations (7)-(10) are given in Table 1.

Equations (5)-(10) form a closed system. They are graphically shown in the scheme of Fig. 1, that represent functioning of NTC and can be called a functional model of NTC. It refers to a class of simultation thermodynamic models and is composed of the following, united by feedback and feedforward, blocks: relief, composition and properties of surface covers (biota, snow and technogenic covers etc.), composition and properties of NTC to the depth of its correlation with the surface covers. At the input to the model there are factors of energy exchange (climate energetic components: radiation or air temperature above and geotermic gradient or mean temperature of the higher NTC rank) and mass exchange (precipitation and hydrologic regime), at the output of the model there are thermal moisture conditions and cryogenic physical geological processes. There on the scheme possible increments are also given for heat, moisture, surface covers and relief, caused by technogenic reasons (see Table 1).

The main advantage of a functional model is that it makes visible the whole complex of processes occurring in a natural object and contributing to a better understanding of prediction aim. Besides, it allows to combine deterministic physical mathematical models with empirical relations, obtained from direct observations for the regime of separate NTC components without physical analysis of their interrelations.

Investigation of soil complex functioning can be carried out with the offered functional thermodynamic model. In particular, its analysis, allows to concretize a principle notion of thermodynamic stability of natural geocryologic bodies, that can be defined as a return of the system, after outer impact, to the homeostasis area that is the area of equilibrium in phase space of characters. If after an outer (technogenic, for instance) impact a system does not return to a homeostasis area, then it means a loss of equilibrium. In this way the value can be determined of permissible outer impacts on NTC, that is required for determining the purposes of environment protection, for instance.

One of the future problems in mathematical modelling is the problem of model stability due to a great number of factors and to a probabilistic character of the initial data, obtained in the process of regional investigations. A possible way to solve this problem is development of optimal mathematical models, to minimizing calculation errors.

REFERENCES

Grechishchev, S.E., Chistotinov, L.V., Shur, Y.L. (1984). Osnovy modelirovaniya kriogennykh fiziko-geologicheskikh protsessov. M., Nauka, 230 s.

Krauklis, A.A. (1980). Eksperimentalnoye landshaftovedenie. Novosibirsk, Nauka, 320 s.

Melnikov, E.S. (1981). K razvitiyu metodologicheskikh osnov regionalnoi inzhenernoi geologii. Inzhenernaya geologiya, N 6.

Osnovy merzlotnogo prognoza pri inzhenerno-geologicheskikh issledovaniyakh. M., Izd-vo MGU, 1974, 432 s.

Pavlov, A.V. (1979). Teplofizika landshaftov. Novosibirsk, Nauka, 320 s.

Shvetsov, P.F. (1973). Obshchie polozheniya. V knige: Osnovy metodiki inzhenerno-geokriologicheskikh prognozov pri razvedke mestorozhdenii tverdykh poleznykh iskopaemykh. M., Nedra, s.10-20.

USE OF GEOTEXTILES TO MITIGATE FROST HEAVE IN SOILS

K. Henry

U.S. Army Cold Regions Research and Engineering Laboratory, Hanover, N.H. 03755-1290 USA

SYNOPSIS One potential use of geotextiles is horizontal placement in soil above the water table to act as a capillary break or barrier to mitigate frost heave. A capillary break works because larger pore sizes and/or wetting angles of the material than surrounding soil result in lower unsaturated hydraulic conductivity and lowered height of capillary rise of water. This reduces frost heave by limiting the rate of upward water migration.

Five series of open-system, unidirectional frost-heave tests were run in which three nonwoven polypropylene geotextiles were tested for their ability to mitigate frost heave. Certain fabrics were successful in reducing frost heave by as much as 85%. Test results also indicate that the optimum fabric thickness required to mitigate frost heave is a function of soil type as well as properties of the geotextile.

INTRODUCTION

Frost action in soils poses significant problems for highway and airport pavements. The advent of the use of geotextiles in pavement sections offers the possibility of mitigating frost effects. Certain geotextiles can be placed horizontally in the soil above the water table to reduce upward water migration under freezing conditions.

The presence of a capillary break in frost-susceptible soil can, in certain cases, reduce frost heave by reducing the height of capillary rise of ground water and by reducing the upward migration of water under tension gradients when the capillary break is not saturated. It is hypothesized that geotextiles with comparatively large pore sizes and fibers that are hydrophobic can be successfully used as capillary breaks.

The laboratory investigation currently under way at CRREL is attempting to show that properly chosen geotextiles will behave as capillary breaks when placed in frost-susceptible soil and to better define the characteristics important to a geotextile's ability to mitigate frost heave. To date, only nonwoven polypropylene geotextiles have been tested because they performed comparatively well in preliminary tests.

PREVIOUS WORKS

The placement of layers of clean sands and gravels in frost-susceptible materials has been known to reduce frost heave (Rengmark, 1963; Taivainen, 1963). It is thought that when placed above the water table and below the depth of frost penetration, coarse material reduces frost heave by breaking the capillary path and thereby reducing water available at the freezing front (e.g. Rengmark, 1963). The saturated hydraulic conductivities of many geotextiles are similar to clean medium to fine sands (Bell et al., 1980), which suggests their use as capillary breaks due to pore sizes. In addition, some fabrics consist of fibers that have a lower affinity for water than soil particles, which is likely to enhance their ability to reduce capillary rise.

In a laboratory study conducted by Allen et al. (1983) in which five geotextiles were tested by placing them in samples of frost-susceptible soil and freezing the samples, they stated that the geotextiles that reduced frost heave the most were either relatively thick and permeable* as well as somewhat hydrophobic or were "strongly hydrophobic." The "hydrophobicity" of the materials was evaluated based on the casual observation of water on the surface of these materials (Allen, 1986). One geotextile that was described as being made of hydrophilic material actually increased frost heave compared to the reference sample (Allen et al., 1983). Allen et al. (1983) did not discuss the results in terms of pore characteristics such as pore size distribution in the various fabrics compared to the pore or grain size distribution of the soil. A survey of manufacturers' literature revealed that the AOS** of the

* No actual values of permeability for specific fabrics tested were published; however, it is implied that they ranged from 0.1 to 0.01 cm/sec (Allen et al., 1983). These values of permeability are comparable to those of clean sand.

** AOS, or apparent opening size (also referred to as equivalent opening size or EOS), is defined as the number of the U.S. standard sieve with openings closest in size to the largest openings in the geotextile (CW-02215, 1986).

Table I. Engineering properties of geotextiles as manufactured.

Geotextile	Construction and Material	Thickness (cm)	Hydraulic K Conductivity (cm/sec)	Equivalent Opening Size (mm)
Fibertex 200	Needle-punched polypropylene	0.19	0.15	0.15
Fibertex 400	Needle-punched polypropylene	0.38	0.3	0.15
Mirafi 600x	Woven polypropylene	0.01	0.1-0.85	
Typar 3401	Heat-bonded polypropylene	0.038	0.03	0.23-0.15

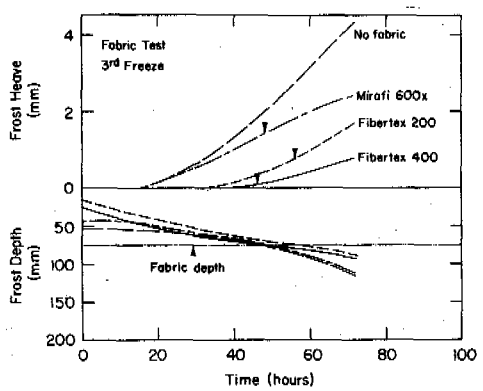

Figure 1. Results of standard CRREL frost-heave tests conducted on Dartmouth sand with three different geotextiles (modified after Chamberlain, 1986).

best- and worst-performing fabrics was essentially the same, indicating the inadequacy of AOS as an index of pore characteristics and the need for a measure of pore size distribution of the fabrics to better examine their effect.

Hoover et al. (1981) examined the ability of geotextiles to act as interlayer reinforcement in the construction and maintenance of roadway sections. Mirafi 140, a heat-bonded polypropylene fabric was found to reduce heave in open-system laboratory freeze-thaw tests. Although Hoover et al. (1981) did not discuss the fabric's pore characteristics, consultation with the manufacturer indicates that the fabric has a coefficient of permeability of 0.05 cm/s, which is on the order of that of a medium to fine sand (Lothspeich, 1988). The sample that heaved the least had two layers of fabric -- each located at a 1/3 point in the sample. The fabric also improved all stability and strength parameters of the soils in the laboratory.

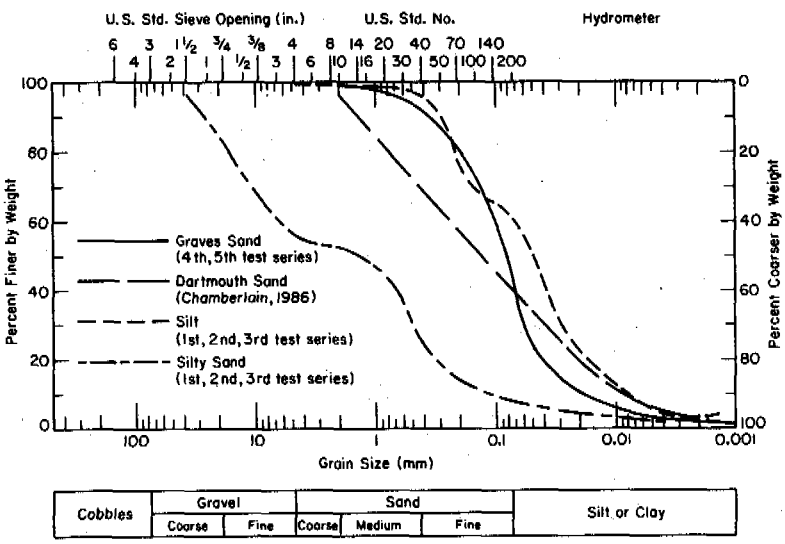

Figure 2a. Grain size distribution curves of soils used in frost heave tests.

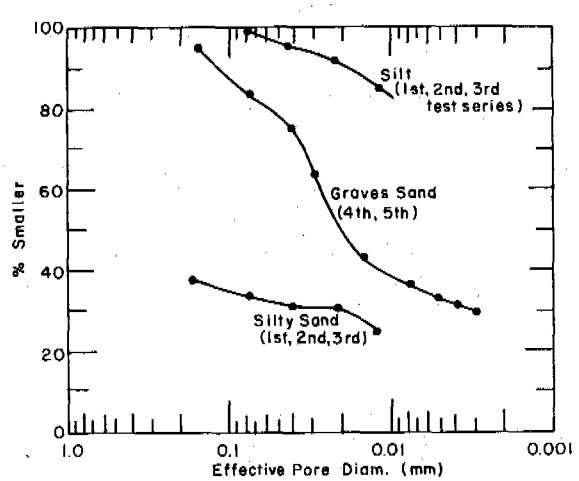

Figure 2b. Pore size distributions of soils used in frost heave tests, based on soil moisture characteristic determination.

Experimental results of standard CRREL frost-heave tests on silty soil with three different polypropylene geotextiles inserted at mid-height in soil samples are presented in Figure 1 (Chamberlain, 1986). The engineering properties of the fabrics tested in this series, as well as tests in the present study, are listed in Table 1. Since Fibertex 200 and 400 are identical except for thickness, these preliminary results indicate the significance of fabric thickness in ability to mitigate frost-heave (bear in mind, however, that the fabrics are compressed when placed in the sample mold). Pore size distributions of the fabrics and soils used were not determined in these tests. Grain size distribution of the soil used is shown in Figure 2a.

EXPERIMENTAL PROGRAM

Five series of open system, unidirectional frost-heave tests were run in which nonwoven geotextile fabrics were tested for their ability to mitigate frost heave. The procedure followed is known as the CRREL Standard Frost Heave Test, where the rate of frost penetration is approximately 12.7 mm/day. See Chamberlain and Carbee (1981) for complete test details and Table II for test series and sample descriptions.

In the first three test series, soil specimens were contained in tapered Plexiglas cells, 15.2 cm in length with a 14.0 cm inner diameter at the bottom and a 14.6 cm inner diameter at the top. The purpose of the taper was to minimize side friction during frost heave. In the last two test series, sample containers consisted of 15.2-cm-diameter cylinders made up of six Plexiglas rings lined with rubber membranes. This sample mold has been found to be more effective than the tapered molds in reducing side friction during frost heave (Chamberlain, 1987). Sample height before freezing was 15.2 cm.

Based on results of previous work, Fibertex 400 and Typar 3401 were the geotextiles selected for the first three laboratory trials. Both of these fabrics have the same permittivity, defined as hydraulic conductivity divided by thickness; however, Fibertex 400 is ten times as thick as Typar 3401. Both fabrics, being composed of polypropylene fibers, are hydrophobic. The Fibertex is needle-punched and the Typar is heat-bonded, and as such, it is likely that porosities and pore size distributions are very different (Christopher and Holtz, 1985). The Fibertex and Typar were both tested in the same silt and the Fibertex was also tested in a silty sand.

The first frost-heave test series was a reference series run on four soils without fabrics. The second and third series utilized two heaving soils from the first series with geotextiles placed at midheight. A total of five samples with geotextiles were tested in the first three test series; no duplicate samples were tested due to a shortage of soil material. After these initial tests, it was decided to investigate further the effect of fabric thickness on frost heave. The fourth and fifth test series were replicate tests that utilized a frost-susceptible sandy silt (Graves sand) with zero, one, two, and four abutting layers of Fibertex 200 inserted at midheight of the samples.

Table II. Test series and sample descriptions for laboratory frost-heave tests utilizing geotextiles inserted at midheight as capillary barriers.

Test Series	Sample Configuration
1 (reference for series 2 and 3)	1 - Silt, no fabric 2 - Silty sand, no fabric
2	1 - Silt with Typar 3401
	2 - Silt with Fibertex 400
	3 - Silt with 2 layers Fibertex 400
	4 - Silty sand with Fibertex 400
3	1 - Layered sample: silty sand and silt separated by Fibertex 400
4 & 5 (duplicate tests)	1 - Graves sand, no geotextile
	2 - Graves sand, 1 layer Fibertex 200
	3 - Graves sand, 2 layers Fibertex 200
	4 - Graves sand, 4 layers Fibertex 200

Grain size analyses and pore size distributions (calculated from soil moisture characteristics) for the soils used are presented in Figure 2. In all cases, the geotextiles meet U.S. Corps of Engineers filter fabric design criteria for the particular soil tested (CW-02215, 1986). The design was done in an effort to minimize potential clogging of fabric during sample saturation prior to freezing and is a factor that should be considered in any field installation of geotextiles for such purposes.

It is noted that about 10-1/2 hours after the fifth frost heave test series was begun, a very rapid freeze of all four samples occurred (within one hour) due to a malfunction in one of the glycol temperature baths. The samples were subsequently thawed, and the test was restarted about 57 hours after the test was originally started. The results of the tests may have been affected by this initial freezing of the fabrics.

In all tests, the location of the fabric in the samples was at midheight; this is approximately 6-7 cm above the water table. However, the optimum location of geotextiles being used

as capillary breaks with respect to water table height and depth of frost penetration should be determined. Ongoing work at CRREL is considering these factors. Results should be available later.

RESULTS AND ANALYSIS

The results of the first three frost heave test series are presented in Figures 3, 4, and 6. Fibertex 400 appears to be capable of reducing frost heave in the silt and silty sand tested as well as in a two-layered sample where the fabric separated two soils.

Typar 3401 had an almost identical effect in reducing heave of the silt as did Fibertex. These results indicate that capillary behavior is influenced by thickness, pore structure, and hydrophobicity.

Considering factors that affect capillarity, the height of capillary rise (h_c) in a tube is:

$$h_c = \frac{2\ T_s\ \cos\alpha}{R\ \gamma}$$

where

T_s = surface tension of liquid,
R = radius of the tube,
γ = unit weight of the liquid, and
α = contact angle between the liquid and the tube.

This relationship clarifies the role of surface properties in the capillary behavior of geotextiles. Although the soil and geotextile pore geometry is much more complex than that of a tube, it is obvious that when a geotextile has a wetting angle greater than that of soil particles, the geotextile experiences less capillary rise. The surface properties of fibers are affected by the polymers used as well as by the manufacturing process; unfortunately, not much is known about the wetting angles of engineering fabrics (Bell et al., 1980). Some measure or index of wetting angle would be useful to this research and, ultimately, to the proper selection of fabrics for use as capillary breaks. The threshold pressure (discussed below) divided by some characteristic pore size may be such an index of wetting angle of geotextiles.

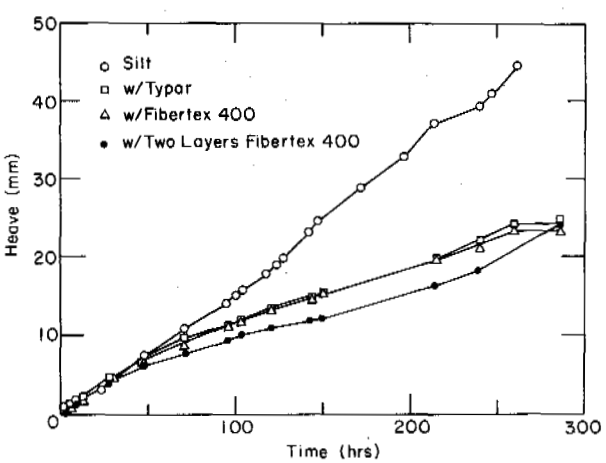

Figure 3. Effect of geotextiles on the frost heave of a silt.

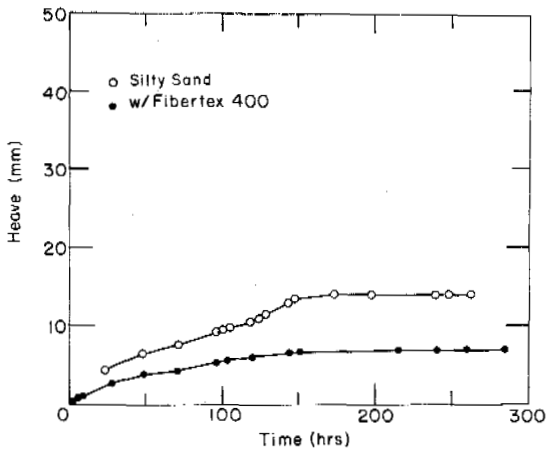

Figure 4. Effect of a geotextile on the frost heave of a silty sand.

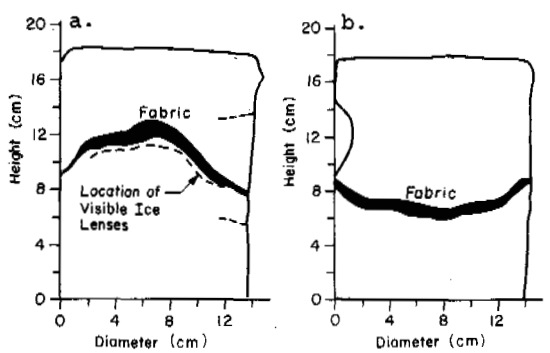

Figure 5. Fibertex 400 in frozen silt; a) Two layers and b) one layer.

Relatively large pore sizes and wetting angles result in low unsaturated hydraulic conductivity of a layer and thus would inhibit the upward migration of water under freezing conditions. If this is the case, the fabric behaves as a low permeability clay layer with respect to frost heave -- that is, the rate of water flow upward is too low to optimally feed a growing ice lens. In unsaturated hydraulic conductivity tests run on Fibertex 400, at a desaturation pressure of 1.5 kPa, the hydraulic conductivity was 5×10^{-5} cm/sec, and at a desaturation pressure of 8.9 kPa, the fabric

was so dry that no moisture was in contact with the porous cups to give pressure readings (Henry, 1987). This is an extremely rapid rate of decrease in hydraulic conductivity with suction when compared with typical silty soils. A typical silt would have an unsaturated hydraulic conductivity of about 10^{-6} cm/sec at 10 kPa. Thus, these geotextiles could limit the rate of upward water migration and reduce frost heave in unsaturated flow conditions in freezing soils.

A strongly hydrophobic fabric may tend to trap water above its surface and cause "ponding" problems. Allen et al. (1983) report that a "threshold pressure" of 7.5 cm of water was required to initiate flow through a particular melt-bonded polypropelene fabric. (The threshold pressure, being related to pore size and fiber wettability, also provides an indication of hydrophobicity [Allen et al., 1983].) Allen (1986) reported ponding problems on the same fabric when draining under low positive pressures.

Based on results of Chamberlain (1986), the variation of fabric thicknesses was expected to have more of an effect on the heave than is demonstrated in Figure 3. There were too many variations in experimental parameters and too few tests to draw any definite conclusions yet. When the frozen samples were sliced in half vertically, it could be seen that the double layer of Fibertex 400 had moved upward in the sample and that an ice lens was present just beneath it. This was different from the usual observation that the fabric remained relatively horizontal or even slightly concave within the sample (see Figure 5).

Figure 6 shows the interesting result of having Fibertex 400 reduce heave in a layered soil specimen. In this case a coarser, marginally frost-susceptible silty sand was separated by the geotextile from a more frost-susceptible silt. This test result indicates that there is a possibility of using geotextiles with marginal base course material and a frost-susceptible subgrade to act both as a separator and a capillary barrier.

The results of the fourth and fifth frost heave tests are shown in Figures 7 and 8. One of the most interesting results is that one layer of Fibertex 200 had no effect on the amount of heave, whereas two layers appreciably moderated frost heave. The pore size distribution curve for Graves sand reveals that 100% of the pore sizes in the soil are finer than the AOS (apparent opening size) of the Fibertex 200 (0.125 mm); thus, capillary barrier behavior is likely. In work done by Chamberlain (1986), one layer of Fibertex 200 did mitigate heave (see Figure 1); however, a different soil was used in that test. The soil used in these tests and the soil used by Chamberlain (1986) are both classified as sandy silt according to the Unified Soil Classification System (see Figure 2 for the grain size distribution curves). The AOS of Fibertex 200 is less than the D_{85} (the sieve size for which 85% of the soil remains) of both soils -- this being the design criteria of the

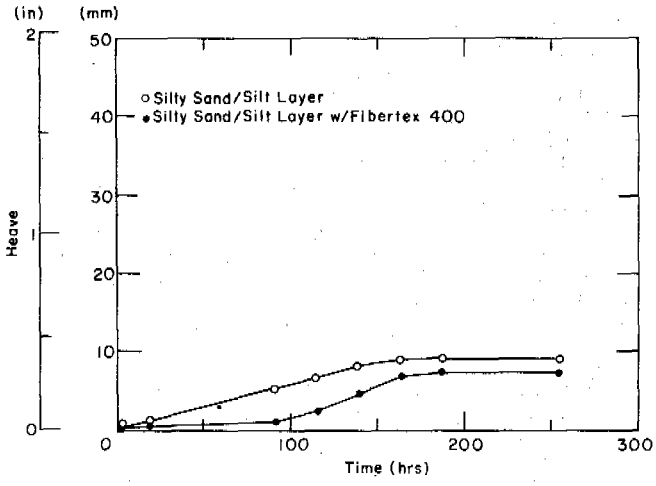

Figure 6. Effect of geotextile on frost heave of layered silty sand/silt sample.

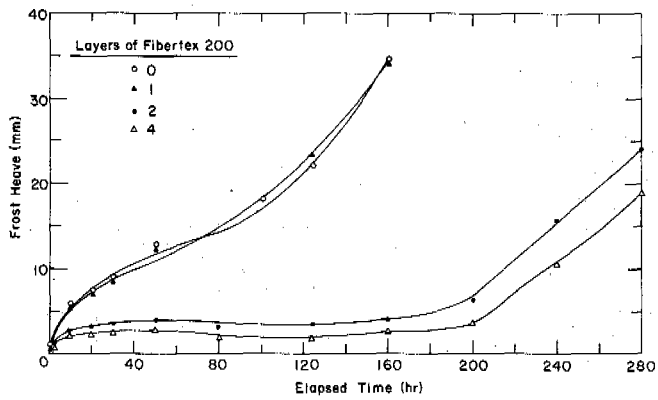

Figure 7. Effect of Fibertex 200 on the frost heave of Graves sand (fourth test series).

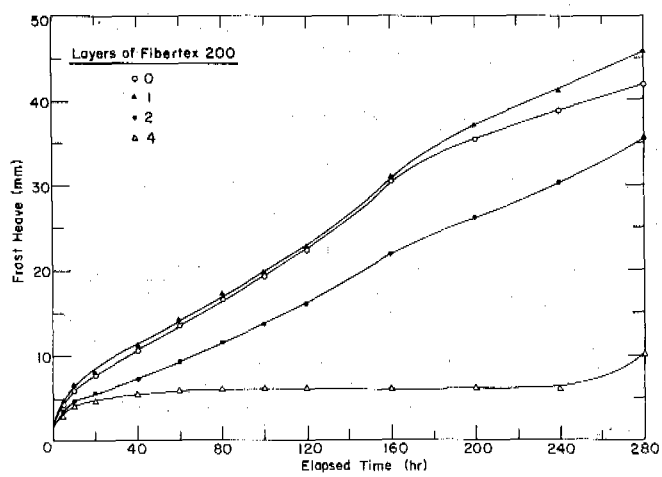

Figure 8. Effect of Fibertex 200 on the frost heave of Graves sand (fifth test series).

U.S. Army Corps of Engineers for filter fabrics used in this soil type (CW-02215, 1986). Other than the published AOS value, no information is available on the pore size distribution of Fibertex 200. If the actual range of pore sizes in the fabric were known, it would be possible to determine if a soil would be likely to clog the fabric as well as to compare the pore size distributions of the soil and fabric. It is possible that the Graves Sand, which has more fines near the AOS of the fabric than the Dartmouth Sand, has enough fines to substantially fill voids in one layer of fabric, and thus reduce its capillary break behavior.

Two layers of Fibertex 200 reduced heave by about 85% in the fourth test series and by only 25% in the fifth test series. In addition, four layers of fabric were more effective frost-heave mitigators in the fourth series than the fifth. The anomalous test conditions of the fifth test series have already been noted above. The freezing of the saturated fabric may have changed the pore structure or otherwise degraded the fabric.

CONCLUSIONS

Based on the current test results and their analysis, the following conclusions are made:

1. Certain nonwoven polypropylene geotextiles show promise for use as capillary breaks in mitigating frost heave when placed horizontally above the water table. Factors that are likely to contribute to their success in laboratory tests include pore size, pore distribution, pore structure, and the hydrophobicity of the fibers.

2. Fabric thickness can significantly affect the ability of a fabric to mitigate frost heave. There appears to be an optimum thickness of fabric to reduce frost heave. This varies with soil type.

3. When Fibertex 400 separated two frost-susceptible soils, it reduced heave in a laboratory test. This suggests the possibility of using geotextile both as a separator and as a capillary break with a marginal base course and a frost-susceptible subgrade.

4. Future work should try to better define the roles of fabric characteristics such as pore size and pore size distribution of the fabric compared to pore size distribution of the soil fiber type (wetting angles), permeability, and placement in the soil body in determining capillary break behavior when placed in particular soils. Possible degradation due to clogging and freezing should also be studied. Work is ongoing at CRREL to better define geotextile characteristics and field conditions that may influence capillary behavior.

REFERENCES

Allen, T (1986).
Personal communication, Engineer. Washington State Department of Transportation, Olympia.

Allen, T, Bell, J R & Vinson, T S (1983).
Properties of Geotextiles in Cold Regions Applications, Transportation Research Report 83-6, 275 pp. Transportation Research Institute. Oregon State University, Corvallis.

Bell, J R, Hicks, R G, Copeland, J, Evans, G L, Cogne, J J, Mallard, P, Jahn, S & Lewis, M (1980).
Evaluation of Test Methods and Use Criteria for Geotechnical Fabrics in Highway Applications, FHWA Report 80-021, June. Federal Highway Administration. Washington, D.C.

Chamberlain, E J (1987).
A freeze-thaw test to determine the frost susceptibility of soils, US Army Corps of Engineers Cold Regions Research and Engineering Laboratory, Special Report 87-1, January, 90 pp.

Chamberlain, E J (1986).
Personal communication, Research Civil Engineer. US Army Cold Regions Research and Engineering Laboratory, Hanover, N.H.

Chamberlain, E J & Carbee, D L (1981).
The CRREL Frost Heave Test, USA. Frost i Jord, November (22) 53-63.

Christopher, B R & Holtz, R D (1985).
Geotextile Engineering Manual, Federal Highway Administration, FHWA-TS-86-203. National Highway Institute, Washington, D.C.

CW-02215 (1986).
Geotextiles Used as Filters, Civil Works Construction Guide Specification, Dept. of the Army, Corps of Engineers.

Henry, K S (1987).
A Laboratory Investigation of the use of Geotextiles to Mitigate Frost Heave and a Case Study of Potential Causes of Frost Heave, Master's Thesis, Civil Engineering Department, Northwestern University, Evanston, Ill., 155 pp.

Hoover, J M, Pitt, J M, Handfelt, L D & Stanley, R L (1981). Performance of Soil-Aggregate-Fabric Systems in Frost-Susceptible Roads, Linn County, Iowa. Transportation Research Record (827) 6-14.

Lothspeich, S (1988).
Personal communication, Civil Engineer, Mirafi, Inc., Charlotte, N.C. 28224.

Rengmark, F (1963).
Highway Pavement Design in Frost Areas in Sweden, Highway Research Record No. 33, 137-150.

Taivainen, O A (1963).
Preventive Measures to Reduce Frost Heave in Finland, Highway Research Record No. 33, 202-216.

Roth, H (1977).
Filter Fabric for Improving Frost Susceptible Soils, Proceedings, International Conference on the Use of Fabrics in Geotechnics, Ecole Nationale des Ponts et Chausses, Paris, April, (1) 23-28.
Department, Northwestern University, Evanston, Ill., 155 pp.

VOLUME OF FROZEN GROUND STRENGTH TESTING

L.N. Khrustalev and G.P. Pustovoit

Laboratory of Engineering Geocryology, Faculty of Geology,
Moscow State University, Moscow, USSR

SYNOPSIS An optimization approach to determining the volume of frozen ground strength testing is described which involves minimization of the costs of such testing and of possible losses due to its insufficent volume. A derivation is given for the analytic relationship connecting optimal volume of testing with its cost, construction project cost, and variability of permafrost characteristics. This relationship can form the basis of survey planning.

One of the fundamental principles of engineering geology is the principle of feed-back (Rats, 1973). It demands that the solution of a geological problem should be made taking into account the aims and results of the corresponding engineering problem solution. In recent years, increasing importance is attached to the methods for controlling the quality of geotechnical systems. For this reason the quality factors of the system to be constructed, which are determined from the appropriate model, should be taken into consideration in engineering-geologic investigations. It is these which can and should ensure the feed-back mentioned above.

With these considerations in view, we are going to examine a specific (but very important) problem of engineering geology that arises in any investigations: determination of the volume of ground testing. The approach we suggest here is general enough and can be applied to any testing, both of frozen and unfrozen grounds. However, the problem being very complicated, there is no general solution of it available in complete form that can be used in practice. Such a solution has been obtained by us in application to the use of permafrost, when characteristics of ground strength have the controlling influence on the quality and stability of structures. We shall try not to restrict the generality of our exposition, but the final result that can form the basis of survey planning is given for the particular case mentioned above and reflected in the title of our paper.

The purpose of testing commonly consists in estimating the mean value of a characteristic x of the ground in a statistical population (an engineering-geologic element) and in providing the uncertainty of that estimate which does not exceed a fixed value with a fixed probability. If n trials have been made, the testing results are sampling mean x_0 and sampling variance σ^2, the error being estimated using the random quantity

$$\varepsilon = \sqrt{n}\,(x - x_0)/\sigma \qquad (1)$$

The methods in use for statistical processing of testing results are based on the assumption of the normal distribution law for characteristics of the ground. In that case the random quantity (1) has Student's t-distribution, and the number of trials can be found from the equation

$$\sqrt{n} = \frac{t_{n-1}(\alpha)}{\delta} \cdot \frac{\sigma}{x_0}\,, \qquad (2)$$

where $t_{n-1}(\alpha)$ is quantile of the t-distribution with n-1 degree of freedom corresponding to the confidence coefficient α; and δ is relative error in determining the characteristic to be ensured with probability α.

The last factor in the equation becomes known only when data have been obtained and processed, that is, a volume of testing depends on its results. One can break this vicious circle by using the method of successive approximations consisting of a multistage correction of survey planning in the course of work.

It has been suggested, for instance, to recalculate the mean value of the characteristic under study as new data come in, stopping the trials when the mean has been stabilized (Maslov, 1968). However, to do this one needs to establish a continuous link between the laboratory and the field unit, a condition that cannot always be satisfied. The most natural procedure seems to be the practice of a multistage survey in which the volume of testing at a subsequent stage is determined from the results obtained at the previous one. Probably, better schemes of successive approximations can be devised but, when considered within the framework of deterministic or "semiprobabilistic" concepts usually adopted in design, all such procedures encounter the hardly surmountable obstacle related to indeterminacy of the first factor in the right-hand side of equation (2).

The question of confidence coefficient α

guaranteeing the accuracy and reliability of design indices remains open so far. The design codes in force in the USSR recommend the value $\alpha = 0.85$ for permafrost. Some authors propose to relate this quantity to the type of construction and survey stage (Kagan,1973) and point out specific probability values, substantiating them with construction practices. One has to admit, however, that in all cases the confidence probability is actually assigned. One may even assert that the established approach based on the determination of confidence intervals and subsequent use of deterministic theoretical values of characteristics in design practice is incapable of a justified assignment of the probability.

Indeed, a confidence probability is an inevitable consequence of the artificial replacement of random quantities by deterministic theoretical values and in principle it cannot be obtained as a result of any kind of measurements because it depends on the purpose of such measurements. However, there is a one-side connection only between surveys and their final objective - the structure to be errected, namely: the output data of surveys with a fixed reliability (confidence probability) are the input ones for the structure design project. But data reliability is an input parameter for the surveys and cannot be determined unless through the reliability of the final result, i.e. the structure stability. However, this reliability cannot be estimated by using the deterministic approach. Therefore, the necessary feed-back is absent, thus making it impossible to ensure the reliability of the input data.

When that fact is realized, this leads to a different approach based on probabilistic concepts and economic criteria. Its essence, as noted by Rats (1973), can be summarized in the following question: "How much will the guarantees cost us and what do we risk if our guarantees are broken?" The word "guarantee" here refers, not to accuracy of the data, but to stability of the structure, and the necessary feed-back is prvided, not by an artificial confidence probability, but by actual economic indices: survey cost and the cost of possible losses due to insufficient volume of testing. By minimizing the sum of these quantities,

$$C_s + C_l \longrightarrow \text{minimum} \qquad (3)$$

one can determine a volume of testing that is economically optimal.

The arising optimization problem is attractive due to its apparent simplicity; solutions having been tried many times. As far as we know, however, not a single attempt has resulted in a closed solution free of artificial restrictions (such as normative reliability levels etc.), which are essentially equivalent to assigning a confidence probability in arbitrary manner. The cause of this is as follows.

Stability of structures is affected by a great many random factors, many of them being dependent on time; thus, the temperature regime of the foundation plays the controlling role in construction on permafrost. Consequently, even when the accuracy and reliability of geologic data are identical, structures built in different natural conditions have differing degrees of stability guarantee. The loss cost also varies, being probabilistic in nature in addition to this. The relation between the accuracy of basic data, stability guarantee, and loss cost is indirect. It depends on processes, both deterministic and random ones, that take place during interaction of foundation soil with the structure and the environment. For this reason it is impossible to provide a sound estimation of losses outside of a consistent probabilistic approach to the description of the "foundation-structure" system. Such an approach,as developed by the present authors, permits a sound formulation and solution of the optimization problem (3). We now examine the basic ideas and results of that approach.

First of all, we have to admit that any stability criterion formulated is a condition imposed on random functions of time, such as loading on the foundation, its temperature, carrying capacity, and strain. A violation of that condition, called failure of the system, is a random event which may or may not occur during a given interval of time with some probability. The probability of failureless functioning of a system regarded as a function of time interval is termed the life function. The function has the value one for an infinitesimal interval of time and tends to zero when the interval indefinitely increases.

The life function depends on all parameters (both deterministic and stochastic) that control structural stability. When a methematical (stochastic) model of a system is being built, less significant parameters are identified and discarded, while the remaining ones are used to construct a parameter-complex with the help of a stability criterion; this is termed safety characteristic and is another argument in the life function (the first being the time).

Thus, for example, when permafrost is used as foundation (according to principle I), the stability criterion is the carrying capacity of the foundation, which must always remain greater than the load on it. The normalized strength margin (the difference between the carrying capacity and the load divided by the square root of the variance of that difference) which is a random function of time must be positive. A peak in this function towards the negative region means failure of the system, while the probability of the absence of such peaks determines the life function. The safety characteristic is the mathematical expectation of normalized strength margin which is constructed from the mathematical expectations of basic quantities (regarded as random functions), their variances and spectral characteristics. The form of the life function $P(\tau, \gamma)$ and the method for calculating the safety characteristic γ were obtained by us (Khrustalev and Pustovoit, 1984, 1985; Pustovoit, 1986), the latter paper giving more exact results, according to which

$$P(\tau,\gamma) = \exp\left[-\frac{\tau}{2.5\gamma}\exp\left(-\gamma^2/2\right)\right]. \qquad (4)$$

The life function is a quantitative measure of the guarantee that a structure will be stable under unfavorable random excitations. This

measure has a merely mathematical meaning however. The corresponding measure invested with economic content has been called risk cost by us. It is defined as the mathematical expectation of loss due to premature failure of the foundation and is expressed through the time derivative of the life function (the latter taken with the minus sign is the probability density of the time interval until the first failure). The meaning of risk cost is sufficiently exactly reflected in its name. When stability (and the safety characteristic) increases the cost decreases, but the initial expense (foundation construction, preparation of the foundation base etc.) increases. The sum of the initial cost of the structure and risk cost is called the reduced total cost and we expect it to be a minimum at some value of the safety characteristic. Investigations show that this is the case. The value of safety characteristic (and the corresponding design solution) that provides the least reduced total cost is optimal from the economic point of view. Any departure from it causes unjustified expenses: either during construction (strength margin is unjustifiably increased) or during use (premature repairs and reconstruction due to low stability).

We have obtained a general equation for the optimal safety characteristic which, however, is little convenient for routine practical calculations. In the particular case indicated (principle I), the specific form of function (4) has permitted considerable simplifications, representing the equation in the form

$$(0{,}5+\nu^2)\gamma_0^2+2\nu\gamma_0-\ln\frac{E\nu}{5-62.5/\tau_e}=0 \qquad (5)$$

: γ_0 desired optimal value of safety characteristic; ν is the combined coefficient of variation that incorporates variability in the carrying capacity and loads; E is an economic coefficient characterizing relative cost of base and foundation; τ_e is the duration of structure use, in years. The method for calculating the coefficients E and ν from basic design cost information is described in the papers mentioned above.

The results obtained have served as a basis for solving problem (3), central to our paper, which we can at last consider. Let us return to expression (1) and the notation introduced there. After surveying, we insert sampling mean x_0 into the calculation and get from equation (5) the optimal value of safety characteristic γ_0 corresponding to the least reduced total cost C_m. But the population mean x which will act on the structure is different from x_0, hence the actual value of safety characteristic γ will be different from γ_0 and the corresponding value C from C_m. Since C_m is the least possible cost of the structure designed for conditions determined by x_0, we have $C > C_m$ no matter what are the signs of $x-x_0$ or $\gamma-\gamma_0$ We explain: if $\gamma > \gamma_0$, that means that the geological conditions have turned out to be "better than we thought" and we had designed too costly foundations - the total cost has increased due to initial cost; if $\gamma < \gamma_0$ that would mean that the conditions have turned out to be "worse than we thought", and the stability is lower than designed - the cost has increased due to risk cost. In either case the difference $\Delta C = C - C_m$ means extra cost (losses) because of inaccurate knowledge of soil characteristics.

Consider the above total cost as the function $C(x)$. In that case $C_m = C(x_0)$, and the loss ΔC is a function of the difference $x-x_0$. If we expand that function into Taylor's series and substitute variable ε for x according to (I) we shall have

$$\Delta C(\varepsilon)=\sum_{k=2}^{\infty}\frac{1}{k!}C^{(k)}\left(\frac{\sigma}{\sqrt{n}}\right)^k\varepsilon^k \qquad (6)$$

where $C^{(k)}$ is the k-th derivative of $C(x)$ at point x_0. The series begins with the second-order term, because x_0 is a point where the reduced total cost is at a minimum, hence $C^{(1)} = 0$.

Since ε is a random quantity, the cost of possible losses due to insufficient volume of testing should be defined as the mathematical expectation of (6):

$$C_1=\int_{-\infty}^{\infty}\Delta C(\varepsilon)\,f(\varepsilon)\,d\varepsilon, \qquad (7)$$

where $f(\varepsilon)$ is the distribution density of random quantity (1), that is, the t-distribution.

As can be seen from (6), the integral can be calculated by summing the series composed of the moments of the distribution. We can restrict ourselves to the first term of the series, because all odd moments of the t-distribution are zero, while the second term (corresponding to k=4) already differs from the first by a factor of order $(4n)^{-1}$. One can now write down the loss cost as a function of volume of testing n:

$$C_1 = C^{(2)}\sigma^2\,\frac{n-1}{2n(n-3)}. \qquad (8)$$

The dependence of survey cost on n is straightforward (it can be taken linear, for instance), so problem (3) is fully determined. Naturally, the difficulty mentioned above still remains: σ and x_0 can be determined only after trials. It is involved in the problem itself and cannot be obviated except by the method of successive approximations. In the case of multistage surveys $C^{(2)}$ and σ should be calculated based on testing results obtained at the preceding stage (these quantities at the first stage can be determined by analogs - we are entitled to consider that there is

always some information on the subject of study); in such a case in expression (8) they should be regarded as independent of the desired size n of the subsequent stage. Substituting (8) in (3), differentiating with respect to n, and equating the derivative to zero, we obtain an equation from which to determine the optimal volume of testing n:

$$\frac{dC_s}{dn} = C^{(2)} \sigma^2 F(n), \qquad (9)$$

where

$$F(n) = \frac{n^2 - 2n + 3}{2n^2(n-3)^2} \approx \frac{1}{2n^2}\left(\frac{n-1}{n-3}\right)^2 \qquad (10)$$

The existence and uniqueness of the solution follow from the fact that when $n > 3$, function (10) monotonically decreases from infinity to zero, while all the other quantities in (9) are positive. Of course, non-integer values of n should be rounded. If (9) yields a value of n that is smaller than the volume of testing at the preceding stage, further survey is not reasonable economically.

To sum up, the general solution of the basic problem is given by (9). We have confined our consideration to the case of testing a single ground characteristic in order not to encumber the logic with more technicalities. The problem is easily extended to cover the multidimensional case: (9) is then replaced by a set of equations in the unknowns $n_1, n_2, \ldots$, volumes of testing for various ground characteristics. The solution could be found because we have succeeded in establishing a feed-back: from cost and structure stability guarantees to surveys. The feed-back has turned out to be complex enough, in terms of the derivative $C^{(2)}$ which concentrates in itself all information on the interaction of base grounds with the structure and the environment, in addition to incorporating economic indices. This complexity is partly the reason why it has for so long been not possible to get the solution to this problem, although the relevant ideas floated in the air, so to speak: the problem seems to be genuinely nontrivial and requires nontrivial methods to solve it.

Let us consider at last the better developed particular case (principe I). Here the main object of testing is strength characteristics of permafrost controlling a structure stability and function (4). Using equation (5) and the relation between reduced total cost and its second derivative at the minimum, we express the latter in terms of known (computable) parameters. Denoting the derivative in the left-hand side of (9) by C_1 (cost of a single trial), we get the equation

$$n\frac{n-3}{n-1} = \frac{\sigma}{x_0}\sqrt{\frac{C_0}{C_t}\cdot\frac{E\gamma_0}{2\nu}}, \qquad (11)$$

where C_0 is the innitial cost of the structure, γ_0 is the root to (5).

The reader should pay attention to the general character of the relationship between the cost of a structure and optimal volume of testing: $n \sim \sqrt{C_0}$, i.e. to the fact that volume of testing increases less rapidly than the cost. Therefore, the larger the structure the smaller is the cost of surveys in the sum total of expeditures. This should be kept in mind by those dealing with economics of construction. The remaining parameters in the right-hand side of (11) relate the optimal volume of testing to a great number of regional and local factors: climate and ground conditions, constructional peculiarities, economic indices of construction, etc. All these factors should be taken into account when planning surveys in the permafrost zone. Equation (11) should serve here as a specific instrument of calculation.

REFERENCES

Kagan, A.A. (1973). Raschetnye pokazateli fiziko-mekhanicheskikh svoistv gruntov, 144 pp. Leningrad: Stroiizdat.

Khrustalev, L.N.(1979). Tekhniko-ekonomicheskiy raschet optimalnoi glubiny predpostroechnogo ottaivaniya vechnomerzlykh gruntov pod zdaniem. - Osnovaniya, fundamenty i mechanika gruntov, 3, 19-22.

Khrustalev, L.N. & Pustovoit, G.P. (1984). O naznachenii koeffitsienta nadezhnosti pri raschete vechnomerzlykh osnovaniy sooruzheniy. - Osnovaniya, fundamenty i mekhanika gruntov, 5, 21-23.

Khrustalev, L.N. & Pustovoit, G.P. (1985) Naznachenie koeffitsienta nadezhnosti pri raschete vechnomerzlykh osnovaniy sooruzheniy s chisto ekonomicheskoi otvetstvennostyu. - Osnovaniya, fundamenty i mekhanika gruntov, 2, 20-22.

Maslov, N.N. (1968). Dlitelnaya ustoichivost' i deformatsii smeshcheniya podpornykh sooruzheniy, 159 pp. Moskva: Energiya.

Pustovoit, G.P. (1986). Prognoz ustoichivosti zdaniy, vozvodimykh s sokhraneniem vechnomerzlogo sostoyaniya gruntov osnovaniya. V knige: Trudy Severnogo otdeleniya NII osnovaniy, vyp.5, 28-34. Syktyvkar.

Rats, M.V. (1973). Strukturnye modeli v inzhenernoi geologii, 214 pp. Moskva: Nedra.

MECHANICAL FROZEN ROCK-FILL PROPERTIES AS SOIL STRUCTURE

Ya.A. Kronik, A.N. Gavrilov and V.N. Shramkova

Branch Research Laboratory for Engineering Cryopedology in Power Plant Construction (BRLECPPC),
Kuibyshev Civil Engineering Institute, Moscow, USSR

SYNOPSIS Physical and mechanical properties of this qualitatively new material-ice-rock (stone) system differ from those of the components forming it, that dry rock fill and ice. The results of the experemental laboratory and field researches of the deformation and strength propertyes of the frosen coarse-grained soils are discussed in this topic. Deformation characteristic of the rock-fill relationship nomograms of the temperature and ice content to be used in the engineering work are set in this report too.

INTRODUCTION

When hydraulic structures are built in the Far North such material as coarse-grain soil is used which, however, gets saturated with ice when moisture penetrates it. Ice saturation may take place in a natural way-through condensation of moisture from interstitial pore air, through infiltration of atmospheric precipitation which is observed, for instance, in rock-earthfill dams, or it is formed artificially by pouring water as, for instance, in building port hydraulic structures. The degree of natural ice saturation of coarse-grain soil may vary widely being caused by anizotropy of the material as well as by its being placed into the structure body in stages.

Physical and mechanical properties of this qualitatively new material - ice-rock (stone) system - differ from those of the components forming it, that is dry rock fill and ice. This should be taken into consideration in designing and building hydrotechnical structures in the North.

The object of the researches carried on was to study the effect of the degree of ice saturation and negative temperature on deformative and strength characteristics of the ice-rock material.

MECHANISM OF SUPPORT

Experimental researches were conducted both in the BRLECPPC and at the Kolima hydrostation now under construction, the Kolima biotite granite serving as the material for studies. In studying deformability under laboratory conditions homogeneous gruss-gravel mixture with fraction diameter of 3-5 mm was used while in evaluating strength a mixture formed by crushing larger pieces of biotito granite with fraction diameter of 3-10 mm was tested. The density of hard particles (ρ) of the soil tested was within 1,44 - 1,50 t/m^3 with porosity index (e) varying from 0,43-0,48. The degree of ice content (G_i) varied from zero (air-dry mixture) to 1 (ice-rock mixture), negative temperatures (θ) - from zero to -21°C below zero, which corresponds to the data of field observations of thermo-regime of embankment dams built in the Far North. Under field conditions deformability of rock fill was estimated having fraction diameter up to 1m and more, and density (ρ) of 2,2 t/m^3. For this purpose a pilot embankment was built on the site of the Kolima hydrostation.

To define deformative properties of the material under laboratory conditions compression devices were used placed in the working section of the climatic chamber of KTK-800. Strength properties of frozen coarse-grain soils were studed using direct shear apparatus GGP-30 placed in the gallery of the control meararing apparatus in the dam of the Kolima hydrostation. The experiments were conducted in the method described in (Vjalov S.S., 1978) which implies carrying on a series of tests under conditions of rapid shear to define "instantaneous" strength (τ_i) followed by a series of tests in applying direct shear loading in stages, with $\Delta\tau = 0{,}1\,\tau_i$, the time of load application on each stage (Δt) being 24 hours. Prolonged strength (τ_p) for each test is defined by design using the point where direction of the straight line of the graph of dependence of shear deformations (δ) on acting stress $\sigma = f(\tau)$ in coordinates $\ln\tau - \ln\delta$ Maximum vertical stress (σ) was 0,9...

Analysis

The analysis of the results of testing deformative properties of frozen coarse-grain soil under compression conditions allowed to use fractional-linear relationship (Tsytovich N.A. and other, 1981) to describe the development of deformations in time, vertical stress being variable:

$$\varepsilon(t,\theta,G_i,\sigma) = \delta(\theta,G_i)\frac{t}{T^*(\theta,G_i)+t}\sigma^{\beta(\theta,G_i)} \qquad (1)$$

where ε - relative deformation, t - time, σ - acting stress, δ, T^*, β - empirical parameters depending, in general case, on θ and G_i (3).

The dispersion analysis made showed that the influence of ice content (G_i) tells on the values of all the three empirical parameters while temperature (θ) essentially effects only (δ) parameter. The character of the relationships $\delta = f(\theta)$, $\delta = f(G_i)$ and $T^* = f(G_i)$, $\beta = f(G_i)$ is shown in Fig.1 (a,b,c ,d) and for their description relationships (2) - (4) are offered:

$$\delta = K - \beta' \left(\frac{|\theta|}{B}\right)^{\rho} \qquad (2)$$

$$T^* = T_o + T_\infty \frac{G_i}{A + G_i} \qquad (3)$$

$$\beta = VG_i^2 + FG_i + \beta_o \qquad (4)$$

where $K, \beta', \rho, T_o, T_\infty, A, V, F, \beta_o$ -empirical parameters; dimension coefficient; $B = 1^\circ C$.

It should be noted that the parameters in expression (2) depend on G_i. The experimentally obtained relationships $K = f(G_i)$, $\rho = f(G_i)$ and $\beta' = f(G_i)$ are shown in Fig.1 (e,f,g)

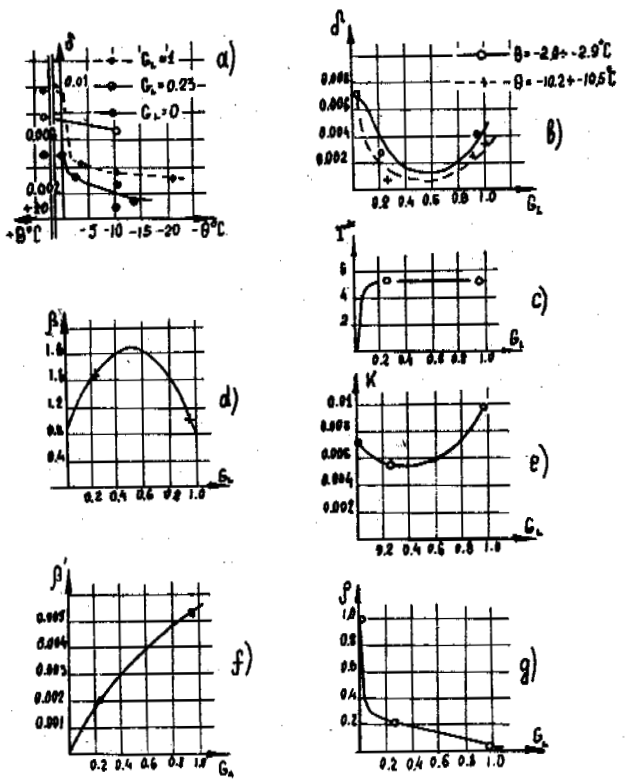

Fig.1 Dependence of deformative reological parameters of gruss soils on temperature and degree of ice saturation.

The influence of G_i upon strength properties of frozen gruss-gravel soil - internal friction angle (φ) and specific cohesion (C) at various temperatures and different modes of loading is shown in Fig.2.

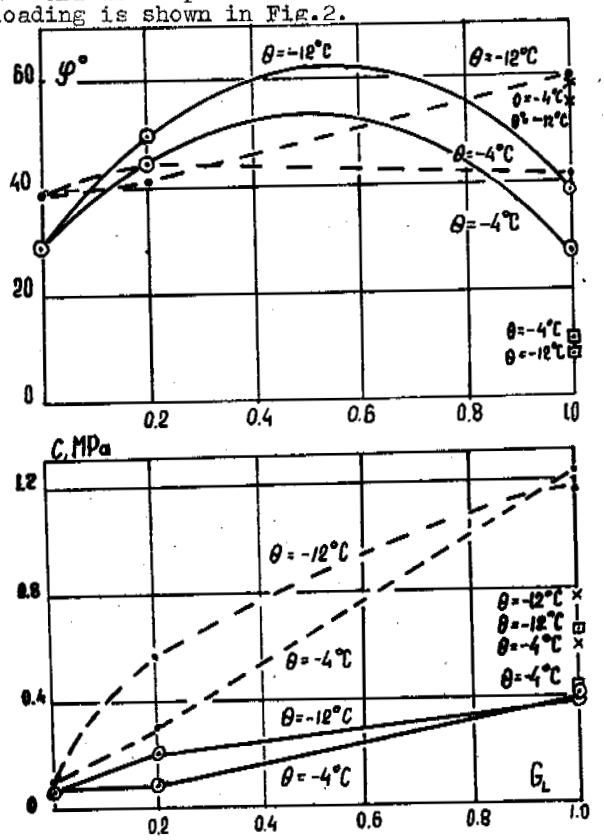

Fig.2 Dependence of strength properties of gruss-gravel soils on ice content
—o— - prolonged strength
—o— - prolonged strength of ice at $\theta = -4^\circ C$ and $-12^\circ C$ respectively
——— instantaneous strength
—·—·— instantaneous strength of ice at $\theta = -4^\circ C$ and $\theta = -12^\circ C$ respectively

The analysis of the results obtained shows that increasing ice content leads to greater values of specific cohesion (C) and that the effect of ice content (G_i) on the internal friction angle (φ_p) in studying prolonged strength is nonambiguous; it increases with G_i growing up to 0,4-0,5 and then it falls down to values of φ_p when $G_i = 0$ The reduction of temperature θ contributes to the increase of φ_p and C_p values of frozen gruss-gravel soils. Data of ice tests made following the same method are presented, for comparison, in Fig.2.

Such a character of the effect of ice content (G_i) on deformative and strength properties of ice-rock materials is obviously due to cryogennic texture of the samples. In deep through freezing of not fully water-saturated coarse-grain soil a film (crust) texture is formed.

The development of ice-cementing bond presents repacking of coarse-grain soil particles, which reduces deformability (Fig.1B) and raises strength and increases values φ_p and C_p

With all-side three-dimensional freezing of fully water-saturated soil basalt texture is formed. Contacts between fractions are broken and in this case strength and deformative properties of ice are primarily responsible for mechanical properties of ice-rock material, which results in increased deformability parameter δ and reduced φ_p . Specific cohesion with increased G_i continues to grow which indicates that the strength of ice-rock system has increased as a whole owing to involving into work not only separate parts but also the ice formed.

The results of laboratory researches allow to evaluate qualitatively general regularities of the behaviour of ice-rock materials in varying thermo-moisture regime, time and acting stress. To obtain design mechanical characteristics of frozen rock mass one should make use of the results of field observations of pilot embankments or of large scale field tests. Thus, as a result of processing the data of field observations of the pilot embankment deformations (Tsytovich N.A. and other, 1983) and of taking into account the regularities of soil deformation obtained in laboratory experiments (Fig.1) values of reological parameters of expressions (1), (2), (3) for real rock mass were found which are presented in Table 1.

To decrease labour-taking engineering calculations a nomogram was built using the parameters obtained for defining the value of relative deformation, taking into account the degree of ice content, negative temperatures, acting stress and time factor shown in Fig.3.

The degree of creep was defined using expression:

$$C_K = \left[K - \beta' \left(\frac{|\theta|}{B}\right)\right] \frac{t}{T^* + t} \qquad (5)$$

TABLE I

Values of empirical coefficients of expressions (1) - (3)

G_i	K	β'	ρ	T^*	β
0	0,0657	0,00031	1,0	0,15	0,336
0,2	0,0479	0,0178	0,218	8,85	0,707
1,0	0,0859	0,0479	0,0531	9,91	0,475

Calculations were made by specially prepared programme in Fortran language for computer ES-1033. The solution was analyzed with the help of a grapher in standard "Grafor" method. The nomogram presented here is of grid nomogram class with equally spaced scales along coordinate axes. It gives a 10-20-fold saving of labour and time for calculations. With its help using field observation data of ice formation and temperature regime of various real rockfill hydrostructures, settlements were calculated and the results were compared with the data of settlements observed in the field. This comparison indicates that the design forecast sufficiently well agrees (with discrepancy unto 15%) with the data of field observations. Fig.4, as an example, presents a design forecast of

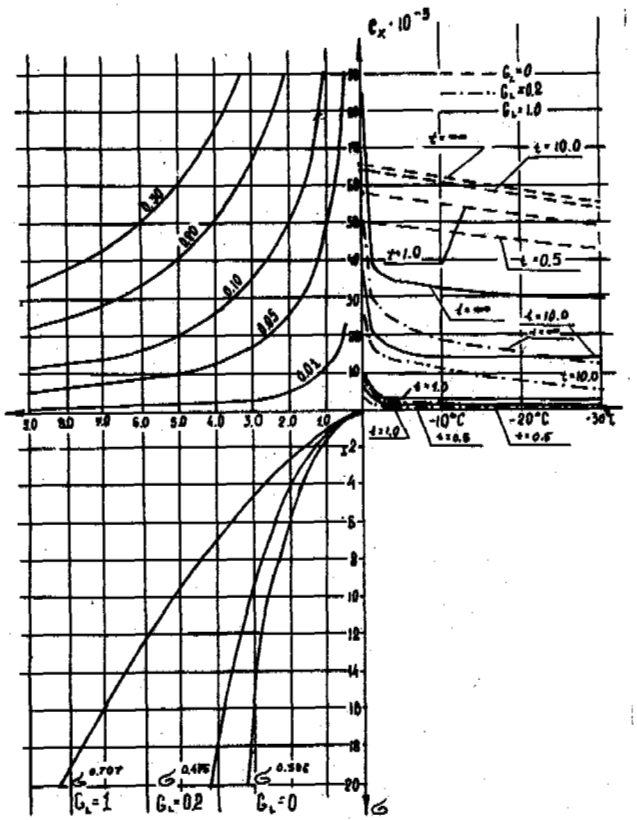

Fig.3. Nomogram for defining relative deformations of rock mass

settlement made with the help of a nomogram for a real rockfill structure and the settlements observed using the data of control-measuring devices. Design parameters are given in Table 2.

TABLE 2

Design parameters for estimating structure settlements

NN of stages	Stage duration (in years)	G_i	θ°C	σ MPa	Notes
I stage	0,26	0	0	0,099	ρ=2,2 t/m^3 h=4,5 m
II stage	0,25	0	0	0,054	ρ=1,2 t/m^3
III stage	0,75	1,0	-5	0,099	
IY stage	0,5	0	0	0,054	Layer is assumed to have thawed, water-saturated
Y stage	0,5	0	0	0,054	ρ=1,2 t/m^3

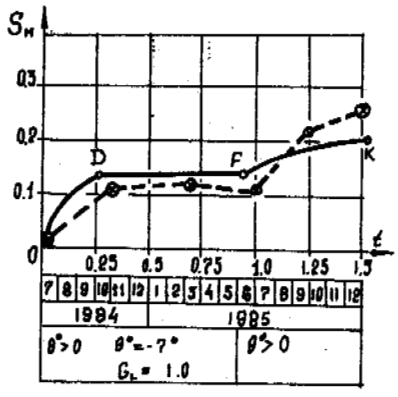

Fig.4. Structure settlements
— —●— - design forecast data
——o—— - data given by control-measuring apparatus

All the above allows to recommend that the described method, nomograms as well as the obtained deformative reological characteristics of rock mass should be used for preliminary evaluation of the deformative behaviour of embankment structures,

REFERENCES

Vjalov, S.S. (1978). Reologicheskye osnovy mehaniky gruntov. Moskva. Vystchaja shkola. str.448 (in Russian).

Tsytovich, N.A., Kronik Ya.A., Gavrilov A.N. and Vorobyov E.A. (1981). Mechanical properties of frozen coarse-grained soils. Engineering Geology, 18 p.47-53. Elsevier Scientific Publishing Company, Amsterdam-Printed in The Netherlands.

Tsytovich, N.A., Kronik Ya.A., Gavrilov A.N., Demin I.I. (1983). Prognoz termonaprjagenno-deformirovannogo sostojanya gruntovyh soorugenij metodom konechneh elementov. Problemy geokryologii. Moskva. Nauka. str.44-56.

A STUDY OF FROST HEAVE IN LARGE U-SHAPED CONCRETE CANALS

Li, Anguo

Northwest Institute of Water Conservancy, Ministry of Water Resources and Electric Power, Yangling Town, Shanxi, People's Republic of China

SYNOPSIS Based on the data obtained from observations in an experimental canal and a test site during the three cold seasons, the freezing and the frost heave behaviour of the subsoils beneath large U-shaped concrete canals were analyzed and the methods for predicting the frost depth and the heaving rate are presented. It was found that frost heave will not occur if the water content in the subsoils before freezing, is not greater than 15.1% and the normal frost heave force will be negligible if it is not greater than 17.3%. The normal frost heave force determined by a pressure transducer was 1.8 times greater than that determined by a dynamometer, on the average, and was 5.5 times greater in completely confined conditions than in lining-confined conditions. After revision, values of the normal frost heave force are suggested for engineering design under the same conditions.

INTRODUCTION

To study the freezing and the frost heave behaviour in subsoils beneath large U-shaped concrete canals and to study the feasibility and the methods for the design and the construction of the linings, an experimental canal was built in Shanxi in 1981 and a site for observing frost heave of different buried plates (10, 30 and 50 cm in diameter) was set up nearby. The experimental canal was located on the loess terrace, on the east bank of the Qian river with a northeast trend and without snow cover in winter so that the slopes, whether facing the sun or not, were observable. The soil was classified as a silty clay with the ground water table at about the 20 m depth. The size of the test section of the canal was: 5.1 m in depth, 7.17 m in width at the top, sides having a 3.2 m radius and 10° slope of the bottom. The lining was built with spray concrete with a thickness of 10 cm and cross flexible seams every 2 m. On the southern bank of the canal, there was a site used for determining air temperatures, precipitation, ground temperatures and frost depth. The water content of the subsoils was obtained by drilling and sampling. The amounts of frost heave (or thaw settlement) in the subsoils and the displacements of canal lining were determined by dial gauges. The normal frost heave force was determined by both a pressure transducer (set up in a completely confined pattern) and a dynamometer (set up in completely confined and lining-confined patterns). All of the instruments were set up normal to the surface at the observation points and calibrated before using. The observation period lasted for three cold seasons and all of the data showedalmost the same regularity.

FREEZING BEHAVIOUR OF CANAL SUBSOILS

In the U-shaped canal, each observation point had its own slope orientation and degree of direct sunshine, so that each point had its own difference between ground surface temperature and air temperature in winter. According to the observations, the ratios η_i of the accumulated negative temperatures (the sum of the absolute values of temperatures in the period from the start of the cold season to the day of maximum frost depth) at the surface of each observation points to the freezing index (the sum of the absolute values of mean daily air temperature during the cold season), are shown in Table I and contours of this ratio, below the canal, at a particular times, are shown in Fig.1.

TABLE I

Values of η_i and α_i at Each Location Within the Canal

position	Sol	S1	S2	S3	S4	S5	
η_i	4.00	3.45	2.55	2.58	2.81	3.27	
α_i	2.66	2.95	2.46	1.96	2.34	2.28	
position	0	N5	N4	N3	N2	N1	No1
η_i	3.28	2.58	1.73	1.03	1.01	1.25	1.95
α_i	3.22	2.15	2.06	1.31		1.30	2.45

The distribution pattern of frost depth was in good agreement with that of surface temperature patterns. The frost depth was relatively deep at the southern slope which had a longer freezing period and relatively shallow at the northern slope which had a shorter freezing period

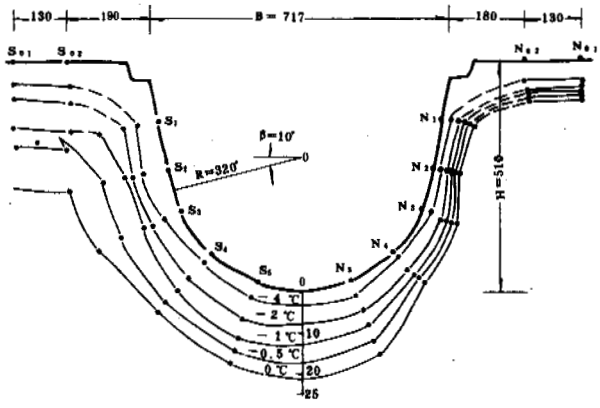

Fig.1 Contours of Ground Temperature Ratios, η_1
(Jan 23, 1983, at 7 o'clock)

and which usually underwent freezing at night and thawing during the day. The frost depth at the southern bank of the canal was greater than that at the northern bank.

The relationship between the maximum frost depth and the accumulated negative temperature at the surface and that between the maximum frost depth and the freezing index could be expressed respectively by:

$$h = \alpha_i \sqrt{Ii} \qquad (1)$$

$$h = \alpha_i \sqrt{\eta_i F_o} \qquad (2)$$

where h — the maximal frost depth, cm;
Ii — the accumulated negative temperatures at surface, °C day;
α_i — the coefficient of frost depth, cm·°C$^{-\frac{1}{2}}$ day (see Table I);
F_o — the freezing index, °C day;
η_i — the temperature ratio (see Table I).

FROST HEAVE IN THE SUBSOILS OF THE CANAL

Analysing the amount of frost heave on a cross section of the canal

Observations during three years showed that the amount of frost heave at each observation point of the canal was not directly proportional to the frost depth, but mainly depended on the moisture condition of the subsoils. Where the water content was higher , there was a greater amount of frost heave, and vice versa. In order of the amount of frost heave going from high to low the positions were: S5, 0, S4 and N5 in the first year. S1 and S2 in the second; S3 and N4 in the third.

It is well known that frost damage in a canal lining is mainly caused by the differential frost heave, which was expressed by a differential coefficient (K) defined as the ratio of the difference in the amount of heave between two points adjacent to each other, to the distance between the two points, expressed as a percent. The results showed that the locations with maximum frost heave were at 0 and S5 and the locations with the maximum value of K were at N5 in 1981 and 1983. An exception was the location S4, which had both the maximum heave and the maximum K, in 1982. Although the differential coefficient of frost heave was greater at locations with the greater amount of frost heave, the locations with the maximum frost heave was not coincident with the location of the maximum differential coefficient. Therefore, in the frost heave resistance design of canal linings, using the single parameter, i.e.the maximum frost heave, is not safe and another parameter,i.e. the maximum differential coefficient should be added.

Relationship between frost heave and water content in subsoils

Frost heave is caused by the phase change of water during freezing which results in volumetric expansion. Thus the water content in subsoils is a dominant factor for frost heave. According to the data taken from observations, the relationship between the heaving rate (defined as the ratio of the amount of frost heave to its corresponding frost depth, %) and the water content in the subsoils before freezing and the relationship between the heaving rate and the water content of the subsoils during the freezing period could be expressed by a statistical method as follows:

$$\eta = 0.3638\ (W1-15.07) \qquad (3)$$

$$\eta = 0.5857\ (W2-17.15) \qquad (4)$$

where η — the heaving rate, %;
W1— the water content of subsoils before freezing, %;
W2— the water content of subsoils during the freezing period, %.

From equations (3) and (4) it can be seen that when the water content in subsoils is 15.07% before freezing (Wo1) and 17.15% in the freezing period (Wo2), respectively, the heaving rate is equal to zero and no frost heave occurred in the subsoils. Both of the water contents mentioned above are slightly lower than the plastic limit, Wp (18.4% on the average) and could be expressed by

$$Wo1 = 0.82\ Wp \qquad (5)$$

$$Wo2 = 0.93\ Wp \qquad (6)$$

Equations (3) and (4) could be used for the prediction of frost heave in the same type of subsoils in a closed system and equations (5) and (6) could be used for the prediction of the water content at which frost heave occurs. To prevent construction from frost damage, the following measures should be taken: draining, cutting off any water supply and lowering the

water content in the subsoils.

Residual deformation of frost heave

The amount of frost heave could disappear completely in some situations, but usually it is only recovered partially during the thawing period by thaw settlement , and so there is some residual deformation. If the deformation caused by frost heave disappeared completely in the thawing period, the lining would be safe. Otherwise, frost damage will be produced by the accumulated residual deformations, so the value of the residual deformation should be the third parameter in the anti-frost design of canals. Table II shows the maximum frost heave and the values of the residual deformation determined at the site.

It can be seen that residual deformation existed everywhere. Where there was a great amount of frost heave, there was a great amount of residual deformation, but there was no direct correlation between the two. The ratio of the residual deformation to the amount of frost heave tended to increase with an increase in the elevation of the observation point (from point O to S1). It implies that the residual deformation not only depends on the maximum frost heave, but also depends on the canal section and the slope. The steeper the slope, the higher was the residual deformation. For the U-shaped canal, the deformation caused by frost heave was not totally recovered. Even though its value was very low, frost damage still could occur after the canal came into operation for a long period, so that anti-frost heave measures should be taken.

NORMAL FROST HEAVE FORCE

Forming and developing processes of normal frost heave force

The normal frost heave force is defined as the force acting vertically on the bottom of the canal lining produced by frost heave in the subsoils. Obviously, if there is no frost heave during subsoil freezing, or if the canal lining could be deformed freely a normal frost heave force would not be produced. However this situation is seldom met in practice. Fig.2 shows the normal frost heave pressure vs.the elapsed time determined by the pressure transducer with a plate diameter of 30 cm. It can be seen that the normal frost heave pressure was negative at the initial stage of soil freezing because of soil shrinkage, increased with an

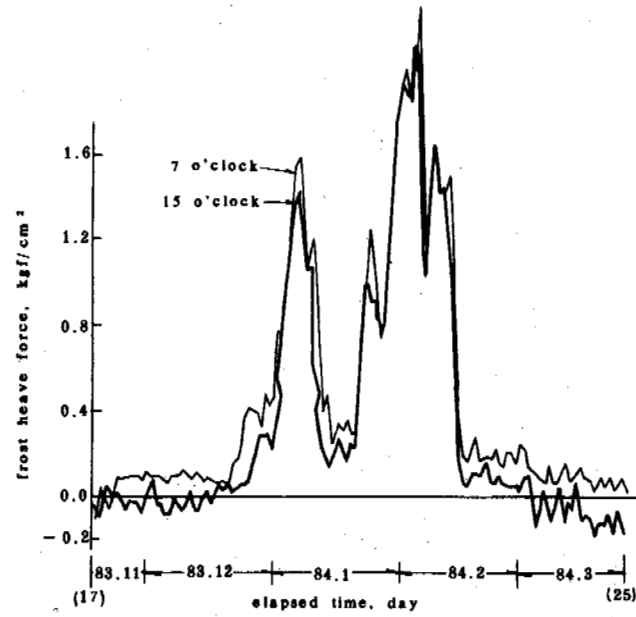

Fig.2 Frost Heave Pressure vs. Elapsed Time as Determined by a Pressure Ttansducer

TABLE II

Maximum Frost Heave and Maximum Residual Deformation*

position		S1	S2	S3	S4	S5	O	N5	N4
Δhmax	1981	1.30	0.99	1.03	3.29	9.43	11.94	8.78	0.91
	1982	6.40	7.08	3.78	8.24	7.60	7.41	6.29	1.93
	1983	5.89	3.42	1.50	5.54	14.00	11.02	11.23	1.64
ε	1981	0.81	0.78	0.30	1.28	5.01	3.55	3.10	0.10
	1982	5.09	6.33	2.89	4.28	2.36	1.73	1.88	0.75
	1983	4.88	1.96	1.03	2.21	7.47	5.51	9.12	0.40
ε/Δh	1981	62.31	79.19	29.13	38.91	53.13	29.73	35.25	10.99
	1982	79.53	89.41	76.46	51.94	31.05	23.35	29.89	38.86
	1983	82.85	57.31	68.67	39.89	53.36	50.00	81.21	24.39

* Δhmax — maximum of frost heave,mm;
ε — residual deformation, mm.

TABLE III

Maximum Normal Frost Heave Pressure in Different Locations of the Canal, kgf/cm²

position	S1	S2	S3	S4	S5	O	N5	N4
by transducer completely confined	1.71	0.98	1.22	1.08	1.64	1.77	1.21	0.29
by dynamometer completely confined	0.97	0.86	0.41	1.28	0.92	0.90		
by dynamometer lining-confined-like		0.11		0.12	0.25	0.11	0.37	0.02

increase in frost depth after continuous freezing occurred, reached a maximum after the maximum frost depth occurred, decreased sharply in the thawing period, and finally dropped down to a negative value lower than the values in the initial stage of subsoil freezing.

Distribution of normal frost heave force along the cross section of the canal

From Table III it can be seen that the locations with the normal frost heave pressure from high to low are as follows: O, S5, S1 in the first; N5, S2, S3, S4 in the second; N4 in the third and N1, N2, N3 with the values equal to zero. Under completely confined conditions, the normal frost heave force determined by the pressure transducer was 1.8 times higher than that determined by the dynamometer, on the average. When the dynamometer was used, the normal frost heave force under the completely confined condition was 5.5 times higher than that under the lining-confined condition, on the average.

Factors affecting normal frost heave force

The factors influencing the normal frost heave force could be the following: frost heave factors of the subsoils including soil properties, water content, temperature and freezing rate; and the deformation factors of the lining plates, including structure, type of lining plates and their section size, etc.

1) influence of moisture condition of subsoils on normal frost heave force

In the closed system, the normal frost heave force increased with an increase in the initial water content greater than that initiating frost heave. For a plate diameter plate of 30 cm, the relationship between the maximum normal frost heave pressure and the water content before freezing could be expressed by

$$\sigma = 0.2127\ (W1-17.28) \qquad (7)$$

Where σ is the maximum normal frost heave pressure, kgf/cm².

The water content of the subsoils before freezing was 0.94 times the plastic limit.

2) influence of heaving rate on the normal frost heave force

In the closed system, the normal frost heave pressure increased with an increase in the heaving rate of the subsoils. The relationship between them could be expressed by

$$\sigma = 1.164\eta 0.793 \qquad (8)$$

Where η is the heaving rate, %.

3) influence of the area of the test plate on normal frost heave force

The relationship between the normal frost heave pressure and the area of the test plate could be expressed by

$$\sigma = \sigma_o + \frac{\alpha}{\Omega} \qquad (9)$$

Where σ — the determined value of the normal frost heave pressure, kgf/cm²;
σ_o — the frost heave pressure of the soil column under the test plate, kgf/cm²;
Ω — the area of the test plate, cm²;
α — the coefficient, kgf, which is the frost heave force of the soil body surrounding the confined soil column.

Based on the determined values of the normal frost heave force with different areas of the test plates at the site, equation (9) could be written in the following form:

$$\sigma = 0.3568 + \frac{62.875}{\Omega} \qquad (10)$$

From equations (9) and (10) it can be seen that σ_o is equal to 0.3568 kgf/cm², which is the normal frost heave pressure without the influence of the surrounding soils.

Adopted values of normal frost heave force

The values, shown in Table III, of the normal frost heave pressure were obtained by different methods. The values, σ_i, determined by the pressure transducer were greater than their true values so they could be used in engineering design until they are revised. First, considering the confined condition, the values of σ_i, shown in Table III, should be divided by 5.5

TABLE IV

The Revised Values of the Normal Frost Heave Force σ_{oi}, kgf/cm^2

position	Stop	S1	S2	S3	S4	0	N5	N4	N3
σ_{oi}	0	0.249	0.143	0.178	0.157	0.258	0.176	0.042	0

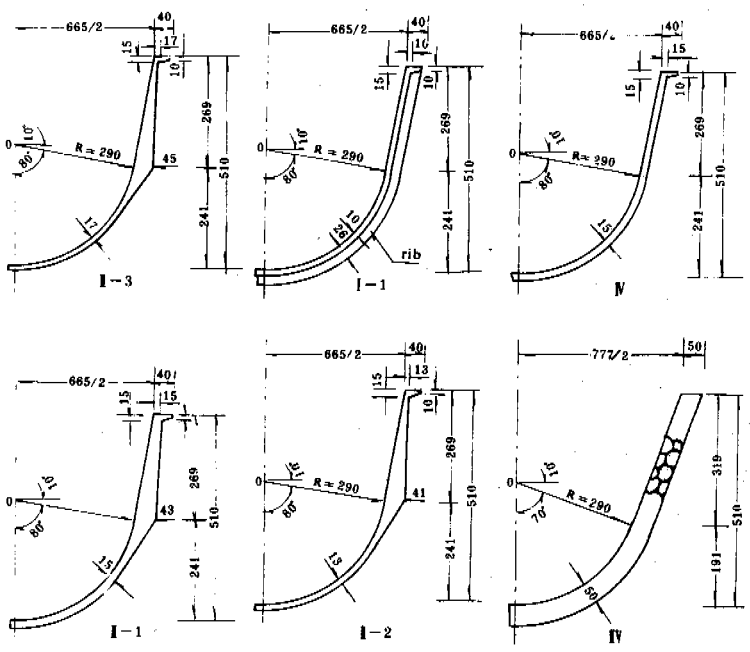

Fig.3 The Sectional Drawing of Different Types of Canal Lining

for the revistion from the completely confined pattern to lining confined patternaccording to the analysis mentioned pre previously. Second, considering the area of the test plate σ_i should be divided by 1.249 to delete the influence of the area of the test plate because σ/σ_o equals to 1.249 in equation (10) when the plate diameter is 30 cm. After the revision mentioed above, the values σ_{oi}, shown in Table IV, are those determined by the pressure transducer and without the influences of the plate area and the confined conditions so that they could be used in engineering design.

ANTI-FROST DAMAGE EFFECTIVENESS OF DIFFERENT TYPES OF LINING

Fig.3 shows the type and the size of the linings. Cracks in the lining plates were checked for,4 times from 1982 to 1984. The results showed that cracks occurred in all of the sections of the concrete canal to different degrees (except for the stone canal section) and the crack rate tended to increase year by year. The cracks were distributed horizontally from 1 to 3 m beneath the top of the canal and the crack width was less than 0.5 mm. The displacement at the location of the cracks could not be observed. The order of the crack rate, from high to low, in th different types of lining shown in Fig.3, was as follows: type IV(50% in slope facing south and north)>type I-1(28.6% in slope facing north and 19% in slope facing south) > type II-3 (28.6% in slope facing north and 7.1% in slope facing south). The resistance to frost damage of the different types of the lining was in the following order: type IIV (the stoned lining) was the best, type II (the concrete lining),the second best (among which, type II-3 was better), type I the third best and type IV the worst.

CONCLUSIONS

(i) The distribution of both frost depth and frost heave observed along the cross section of a canal lining was nonuniform. For similar canal conditions, the frost depth at different locations could be calculated by equation (1) or (2) according to whether the data are air temperatures or ground surface temperatures. The heaving rate could be calculated by equation (3) or (4) according to the water content in the subsoils.

(ii) Where the water content in the subsoils, before freezing, was less than 15.07%, frost heave did not occur, and where it was less than 17.28%, the normal frost heave force was negligible. the ratio of the two water contents mentioned above to the plastic limit was 0.82 and 0.94, respectively.

(iii) The dominant design parameters for frost heave resistance in canal linings should be the maximum frost heave, the differential coefficient of frost heave and the residual deformation.

(iv) The value and the distribution of the normal frost heave force depends on the magnitude of the frost heave in the sub soils and the deformation of the lining plates. The values of the normal frost heave force changed with the determination method. The values determined by the pressure transducer were 1.8 times higher than those determined by the dynamometer, on the average, and the values determined in the completely confined pattern were 5.5 times higher than those determined in the lining-confined pattern, on the average. The influence of the area of the test plates on the normal frost heave pressure could be expressed by equation (10) and the values of the normal heave pressure, shown in Table IV, could be used for engineering design if the conditions are the same.

(v) Cracks occurred in each type of canal lining and the crack rate tended to increase year by year. Type II lining was better than type I and type IV was the worst.

(vi) In the large U-shaped concrete canals, the lining was not only uplifted but also displaced to the inside at the slope facing north by the frost heave forces, and the displacement caused by frost heave was not totally recovered and so frost damage occurred. Measures for preventing frost heave in subsoils should be taken into account in the design and construction of canals.

REFERENCES

Cheng Xiaobai, (1980). Discussion on the simple method for calculating the normal frost heave force at the bottom of foundations. J.of Water Conservancy and Electric Power (2).

Orlov, B.O. (1962). Frost heave in fine-grained soils. Moscow, Publishing House of Sciences

Tong Changjiang and Cuan Fennian, (1985). Frost heave in soils and prevention of frost damage in structures. Publishing House of Water Conservancy and Electric Power.

FROST HEAVING FORCE ON THE FOUNDATION OF A HEATING BUILDING

Liu, Hongxu

Heilongjiang Provincial Institute of Low Temperature Construction Science, Harbin, China

SYNOPSIS In order to investigate the frost heaving force on the foundation of heating building, an experimental heating building with various test foundations was constructed at the Yanjiagang Frozen Ground Field Station nearby Harbin, Northeast China. Frost heaving force on the test foundations was observed for three winters from 1982 to 1985. The test results thaw that the frost heaving forces on the foundations of a heating building are much smaller than that on the similar foundations at a natural test site, which are not heated. Based on the test results, emperical equations for calculating the frost heaving forces on footings or pile foundations of a heating building were presented.

INTRODUCTION

Many investigations on frost heaving forces at natural sites in permafrost and seasonal frozen areas have been carried out (Liu, 1983; Tong, 1983), but only a few studies are concerned with the frost heaving force on the outside of foundations of the heating buildings. This subject had been intensively investigated by the author and his colleagues through an experimental heating building at the Yanjiagang Field Station nearby Harbin, Northeast China, for three winters from 1982 to 1985. This report is the summary of this work.

FIELD EXPERIMENT

Site conditions

The test site for the experimental heating building is located at the Yanjiagang Frozen Ground Field Station, which is about 30 km southwest to Harbin. It is on the first terrace of the Sonhua River and has a thick layer of the Quaternary river and lake deposits.

The maximum frost depth at this site is about 155 cm. The subsoil beneath the experimental building is loam, with an average plastic limit of 20% and liquid limit of 35%. The amount of frost heave occured at this site is 30.9 mm in maximum and 17.5 cm in minimum, with an average heaving ratio of 20%,belonging to a high frost susceptibility.

Construction of the experimental building

The experimental heating building is composed of four rooms, with a total area of 61.75 m^2, as drown in Fig.1. It is supported by eight piles with a diameter of 40 cm by 10 m long (denoted as M1,M2,...M8 in Fig.1). These piles are also used as the anchoring piles for the four test foundations A,B,C and D (see Fig.1). To determine the ground temperature and thaw depth of the subsoil beneath the test building, 27 sets of thermal couples (No.1-27) and 11 detectors of frost depth (No.28-38) were embedded around the building foundations, as shown in Fig.1.

Foundations A and C are square footings with a dimention of 100x100 cm and a layer of 50-cm-thick underlying sand pad. Foundation B is a strip footing with the dimention of 100 cm long by 60 cm wide. It was embedded 50 cm deep below natural ground surface on a 50-cm-thick sand pad. To eliminate the frost heaving force on the ends of the strip footing, subsoils around both ends of the footing were replaced with coarse-grained sand in a volume of 130 cm long by 30 cm wide and by 300 cm deep. Foundation D is a grounding pile, which is 40 cm in diameter by 155 cm long.

For comparison, three seperate foundations a, b and d, which are similar to the test foundations A, B and D, respectively, were constructed at the test site nearby the testing building where no effect were induced by the heating.

TEST RESULTS

The variation of daily mean air temperature (θ_d), frost depth (H), frost heave amount (Δh) and ground water table at the test site from November 1982 to June 1983 were shown in Fig.2. The in-door monthly mean air temperature (θ) of each room of the experimental heating building for three winters from 1982 to 1985 was listed in Table I. The observed values of the total frost heaving force on each pair of comparative foundations A and a, B and b, D and d and foundation C in two winters of 1983-1985 were illustrated in Figs. 3, 4, 5 and 6, respectively. Variation of the frost depth and thaw depth beneath these foundations and at the test site were also plotted in these figures.

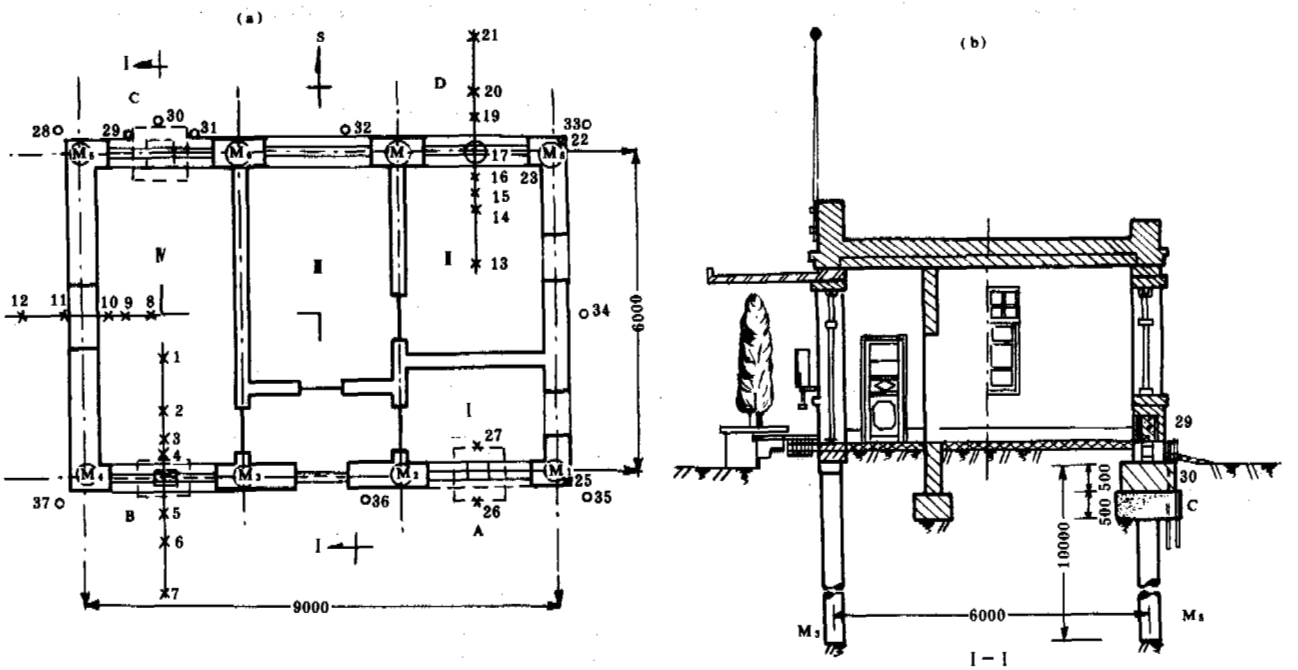

Fig.1 Drawing of the Experimental Building: (a) air view; (b) I-I section
X—thermalcouples (No.1-27), O—detectors for frost depth (No.28-38)

TABLE I

Monthly Mean Air Temperature (θ, °C) Inside of Each Room of the Test Building

Month	θ, °C in various years and rooms											
	1982-1983				1983-1984				1984-1985			
	I	II	III	IV	I	II	III	IV	I	II	III	IV
11	20.5	18.7	15.8	14.3	17.7	16.8	13.2	10.5	14.1	14.8	13.7	11.2
12	17.8	17.7	13.5	11.4	13.0	15.5	11.4	9.1	16.8	13.2	12.6	9.7
1	16.6	18.4	14.1	12.2	12.9	14.2	8.5	9.3	18.3	11.8	11.4	9.1
2	17.9	19.0	15.1	12.4	15.7	19.7	14.2	11.5	18.4	12.4	11.3	8.3
3	19.0	20.5	17.4	16.8	17.0	20.6	16.4	13.3	16.6	13.2	12.3	9.3
4	20.0	21.8	20.0	19.0	19.7	20.6	17.8	17.2	15.7	15.9	15.9	12.9
5	22.0	23.6	21.5	19.6	22.0	21.7	20.5	20.5	-	-	-	-
Room average	19.2	20.0	16.8	15.1	16.9	18.4	14.6	13.1	16.7	13.5	12.9	9.8
Building average	17.7				15.7				13.2			

Note: I — Administrating room, II — Dormitory,
III — Office, IV — Monitoring room.

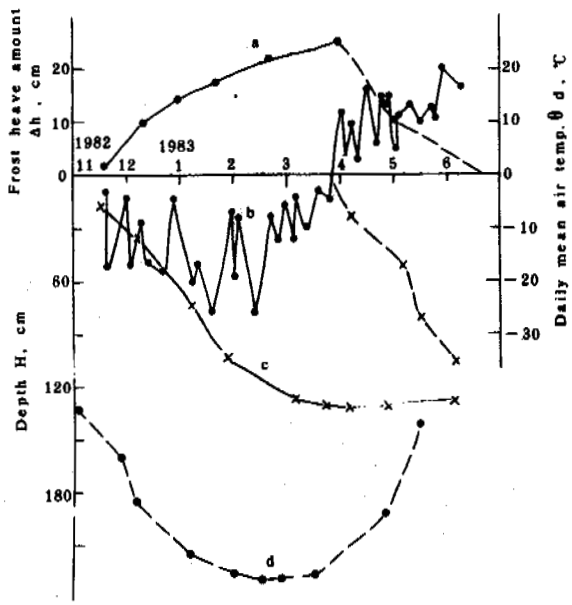

Fig.2 Variation of Frost Heave (a), Daily Mean Air Temperature (b), Frost Depth (c) and Ground Water Table (d) with Time for the Natural Test Side

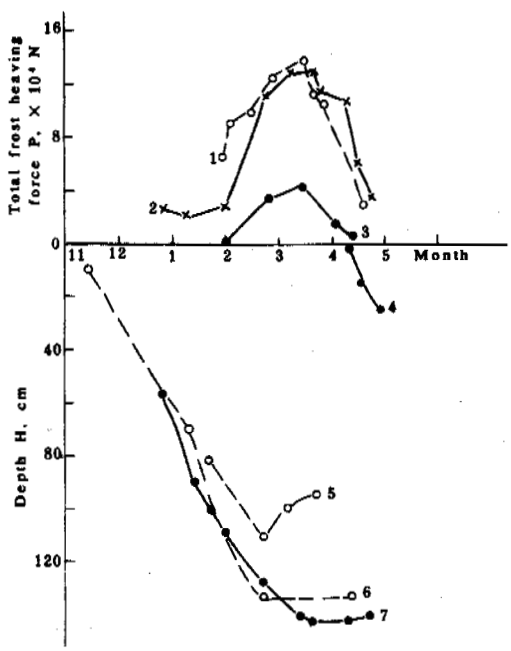

Fig.4 Variation of Total Frost Heaving Force and Frost and Thaw Depthes for Foundations B and a:

1,2 — Foundation b in 1983-1984 and 1984-1985;
3 — Foundation B in B 1984-1985 ;
4 — Thaw depth at the test site in 1983-1984;
5,6 — Frost depth determined by thermalcouples No.4 and 5 in 1983-1984;
7 — Frost depth at test site in 1983-1984.

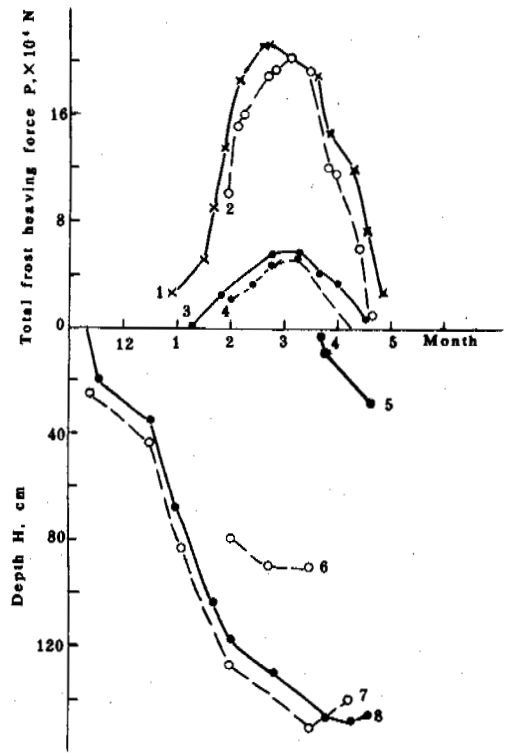

Fig.3 Variation of total frost heaving force and frost and thaw depthes for foundations A and a:

1,2 — Foundation a in 1983-1984 and 1984;
3,4 — Foundation A in 1983-1984 and 1984-1985;
5 — Thaw depth at the natural test site in 1984-1985;
6,7 — Frost depth determined by thermalcouples No.27 and 26; in 1984-1985;
8 — Frost depth at test site in 1984-1985.

ANALYSIS AND DISCUSSION

It is seen from Figs.3 to 6 that the frost heave forces on foundations a,b and d are much greater than that on foundations A,B,C and D. It means that the frost heaving forces acting on the outside surface of the foundations of a heating building are much smaller than that on the foundations at a natural site, which are not heated. This is due to the fact that none or only a little of the subsoils inside the heated foundations were frozen.

Note that the total frost heaving force measured on foundation D is the smallest one ($<2\times10^4$N) among those values of frost heave force measured of the four testing foundations, as shown in Fig.5. This is accounted for: (a) This foundation is on the sunny side of the building, so that the frost depth of the subsoils around the foundation is substantially reduced; (b) Their was a certain length of the pile foundation below the deepest frost front, which provided a certain amount of anchoring force against frost heave due to the friction between pile and soils.

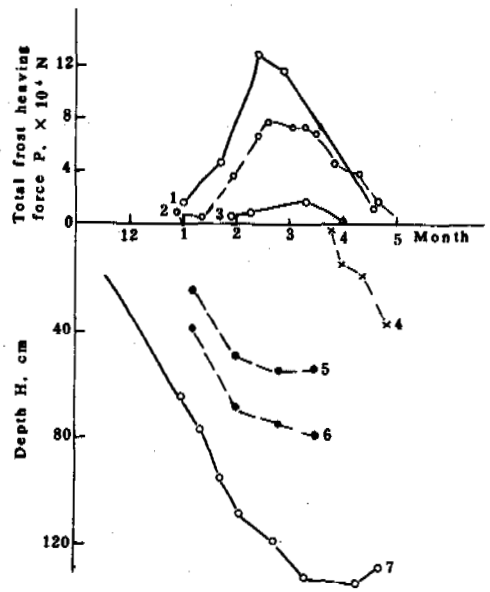

Fig.5 Variation of total frost heaving force, frost depth and thaw depth for foundations D and d:

1,2 — Foundation d in 1982-1983 and 1983-1984;
3 — Foundation D in 1984-1985;
4 — Thaw depth at the test site in 1982-1983;
5,6 — Frost depth determined by thermalcouples No.17 and 18 in 1984-1985;
7 — Frost depth at test site in 1982-1983.

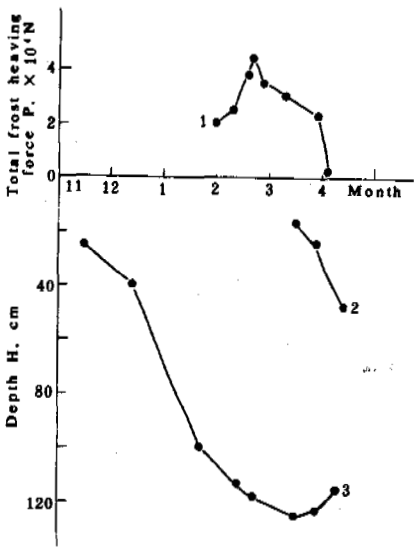

Fig.6 Variation of total frost heaving force (1), thaw depth (2) and frost depth (3) for foundations C in 1984-1985

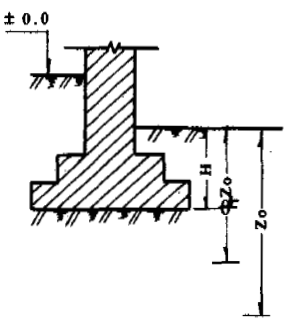

Fig.7 Scheme of a Buried Shallow Foundation

It is seen from Fig.4 that the maximum frost heaving force per unit length observed on the strip footing (foundation B) is about 4.3×10^4 N/m. It usually can not be balanced by the weight of a one-floor building, but can be balanced by a two-floor building with a two-brick-thick wall and a few windows. In the sense of this, the possibility of suffering frost damage for the latter is much lower then that for the former.

It is seen from Figs.3 and 4 that the total frost heaving force on the pile foundation is slightly greater than that on the strip footing (about 5.6×10^4N for the former and 4.3×10^4N for the latter) at the same buried depth. However, the former load applied on the foundations by the building weight per unit base area is much (2.5-3 times) greater than the latter. That is to say using pile or column foundation is favourable in taking its weight to balance frost heaving force. Furthermore, the contact area with frost susceptible subsoils is much less for pile or column foundation than for strip footing. It means that the possibility of suffering uneven frost heave is much lower for the former than for the latter. It is, therefore, concluded that using pile or column foundation instead of strip footing is favourable in prevention of frost damage.

In calculating the frost heaving force on the foundations of the outside wall of heating buildings, basides the effect of heating on the frost depth of base soil, the distribution of frozen soil around the foundations should also be considered. For the foundation of a concave wall (shady corner), not only the frost depth of its base soil is shallow, but also only one quater of its surrounding subsoil (i.e., outside of the foundation) is possible to produce frost heave. Whereas, for the foundation of a convex wall (sunny corner), not only the frost depth of its base soil is deeper, but also about three

quarters of its subsoil will be able to produce frost heave. For the foundation beneath the straight section of a wall, its situation of suffering frost heave is between the above two cases.

Based on the test results, the total normal frost heave force (P_H) on the shallow foundation of a heating building with its buried depth less than maximum frost depth can be evaluated by

$$P = m_v \cdot m_H P_e \qquad (1)$$

where P_e is the normal frost heaving force on a similar foundation which is placed in the natural site; m_H is the heating-effect coefficient reflecting the distribution of frozen soil around a heated foundation and has the values of 0.25, 0.5 and 0.75 for concave, straight and convex wall, respectively; and m is the heating-effect coefficient related with the frost depth beneath the foundation. It is estimated by

$$m_v = \frac{\psi_T Z_o - H}{Z_o - H} \qquad (2)$$

where ψ_T is a coefficient related to the effect of heating on frost depth, Z_o is the so-called standard frost depth and H is the embedded depth of the foundation (Fig.7).

The total tangential frost heaving force on a pile foundation can be evaluated by

$$P_H = \psi_T m_H P_e \qquad (3)$$

in which the subsoils have the same meaning as above.

CONCLUSIONS

1. The circular or square (pile or column) foundation had a higher ability of anti-frost heave than strip footing.

2. The planar configuration of a heating building should be designed as simple as possible so as to greatly decrease the difference in the effect of heating on the foundations beneath outside wall of the building.

3. Increasing the weight of a foundation (e.g., constructing two-floor buildings rather than one-floor buildings) is an effective measure of anti-frost heave.

ACKNOWLEDGEMENTS

The author is grateful to his colleagues,Messrs Zhou Youchai, Wang Gongshan and Li Kun for their contributions to this study.

REFERENCES

Liu Hongxu, (1983). Calculation of frost-heaving forces in seasonally frozen subsoils. Proceedings of 4th International Conference on Permafrost, Washington, D.C., National Academy Press.

Tong Changjiang and Yu Chongyun, (1983). Research on the frost-heaving force of soils, Proceedings of 4th International Conference on Permafrost, Washingtou, D.C., National Academy Press.

FROST HEAVE IN SALINE-SATURATED FINE-GRAINED SOILS

B.T.D. Lu, M.L. Leonard and L. Mahar

The Earth Technology Corporation, 3777 Long Beach Boulevard,
P.O. Box 7765 Long Beach, 90807 USA

SYNOPSIS

This study investigated the effects of salinity on the frost heave characteristics of four fine-grained soils through a series of laboratory tests on specimens prepared at various combinations of salinity, temperature, temperature gradient, overburden stress, and density. The water intake and heave versus time results of specimens frozen from top down at freezing rates representative of arctic field conditions indicated that increasing salinity, overburden stress and temperature gradient would decrease frost heave potential of otherwise highly frost susceptible fine-grained soils. Since grain size is a key factor in the formation of segregated ice lenses, and the soils tested had grain size characteristics more optimal for lens growth than many arctic soils, it is quite probable that there should exist a wide variety of soils with limited frost heave potential for construction use in the arctic offshore environment.

INTRODUCTION

Although considerable work has been conducted regarding frost heave characteristics of soils, very limited data deals with the frost heave nature of saline-water-saturated material (Chamberlain, 1983). The presence of saline pore fluid significantly alters the freezing and water migration mechanisms and will, therefore, alter the frost heave process.

The study described here was conducted as part of a Joint Industry Research Program (The Earth Technology Corporation, 1983 and 1985) to provide fundamental data for designing arctic exploration and production islands.

The specific objectives of the frost heave study were to assess the effect of salinity on the frost heave behavior of a known frost-susceptible soil, evaluate the effects of overburden pressure and temperature gradient on the frost heave behavior of saline soil, and gage the effect of soil gradation on the frost heave response of saline soil. To meet the objectives, a laboratory frost heave test program was performed on specimens of four fine-grained soils including Manchester silt, sandy silt, clayey silt, and a mixture of arctic clay and silt samples. Tests were performed on specimens at various salinity, temperature, temperature gradient, overburden pressure, and duration combinations.

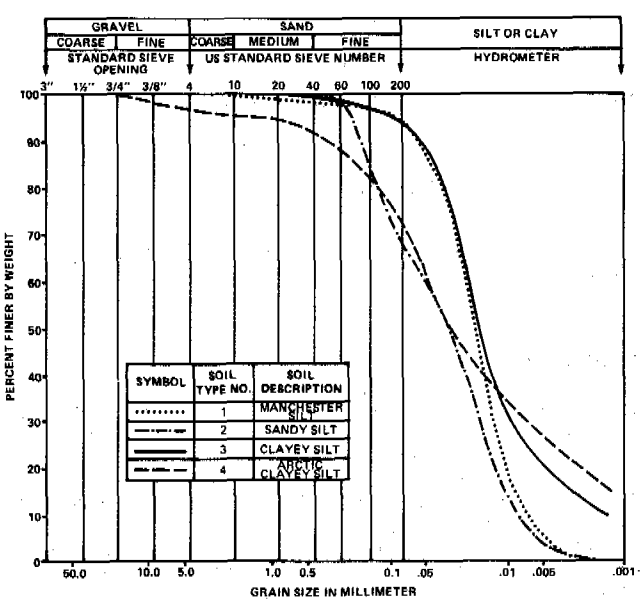

FIGURE 1. GRAIN SIZE DISTRIBUTIONS–FROST HEAVE TEST SOILS

Test Materials

Four fine-grained soil types were used in the testing program. Grain size curves for the four different materials tested are shown in Figure 1. As shown in Table I, a majority of the tests were performed on soil type 1 - Manchester silt, which was selected because it exhibits high frost heave potential when saturated with fresh water (Kaplar, 1974). Soil type 2 (sandy silt) and soil type 3 (clayey silt) were prepared by adding specific amounts of sand and clay to Manchester silt, respectively. Soil type 4 is an arctic clayey silt which was reconstituted from bag samples of silt and clay remaining from a previous arctic offshore drilling program.

TABLE I.
Summary of Test Program

Test No.	Soil Type	γ_{dry} (g/cm^3)	S (g/ℓ)	T_t (°C)	T_b (°C)	T_f (°C/cm)	σ'_v kPa	t (hrs)
1	1	1.63	0	-0.2	-0.9	0.07	3.5	198
2	1	1.60	30	-1.5	-2.4	0.09	11.0	75
3	1	1.68	10	-0.4	-1.6	0.11	3.5	113
4	1	1.64	0	-0.1	-1.4	0.12	3.5	216
5	1	1.62	24	-1.0	-2.0	0.09	3.5	28
6	1	1.64	15	-0.7	-2.0	0.12	3.5	164
7	1	1.65	20	-1.0	-2.4	0.13	3.5	92
8	1	1.61	0	-1.5	-5.8	0.41	3.5	93
9	1	1.61	19	-1.9	-8.7	0.65	3.5	72
10	1	1.62	10	-2.3	-9.7	0.70	3.5	96
11	1	1.65	10	0	-8.1	0.77	69.0	117
12	1	1.66	10	0	-8.4	0.80	34.5	96
13	1	1.61	10	-1.5	-8.4	0.66	20.7	76
14	3	1.61	10	-2.4	-8.5	0.58	3.5	103
15	4	1.80	26	-1.8	-8.2	0.61	3.5	70
16	2	1.68	0	-1.6	-8.3	0.64	3.5	72
17	3	1.61	20	-3.2	-8.7	0.52	3.5	95
18	2	1.70	10	-1.6	-8.8	0.68	3.5	74
19	2	1.70	20	-1.2	-8.6	0.70	3.5	68

Note: (1) Soil type 1 = Manchester silt; soil type 2 = sandy silt; soil type 3 = clayey silt; and soil type 4 = arctic clayey silt

(2) γ_{dry} = dry density; S = salinity; T_t = temperature at top of specimen; T_b = temperature at bottom of specimen; T_f = steady state temperature gradient; σ'_v = overburden pressure; and t = test duration.

EQUIPMENT AND PROCEDURES

The frost heave test apparatus consists of a 9.8 cm I.D. by 15.6 cm O.D. cylinder, instrumented along the sides with thermistors. Details of the frost heave cell design and operation are presented by Mageau and Sherman (1983). Figure 2 shows a schematic diagram of the test apparatus, thermistor arrangement, and freezing and insulation provision.

The cell is insulated with 7.6 cm of polyurethane foam to minimize radial heat flow into the sample. During testing, the cell is placed in a temperature-controlled environment (industrial refrigerator). The temperature in the cold room is maintained as close to 0.3°C above the freezing point as possible. External coolant circulating baths supply a glycol-water mixture to the heat exchangers at adjustable preselected temperatures, allowing any desired gradient to be applied. Earlier testing during the research had shown very similar results when freezing specimens upward and downward. The coolant baths are capable of maintaining refrigerant temperatures to within ±0.02°C.

During each test, measurements of vertical displacement (heave), water intake, and temperature are recorded. Vertical heave is measured using a dial gage accurate to ± 0.0025 mm. Water intake is measured by reading a burette accurate to ±0.2 mℓ. Waterproof and pressure resistant thermistors, calibrated prior to the test program in a zero point calibration box, are used for temperature measurements

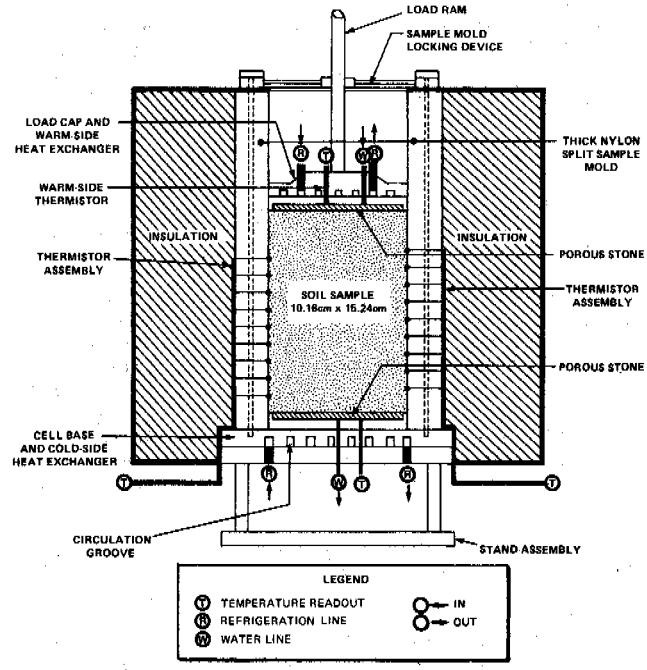

FIGURE 2. FROST HEAVE CELL DIAGRAM

accurate to within ±0.1°C, with ±0.01°C repeatability.

Sample Preparation

Specimens for soil types 1, 2 and 3 were prepared in 2.5-cm lifts in a compaction mold using a 4.5-kg hammer dropping at a height of about 45.7 cm. The surface of each lift was scarified prior to placing the next lift.

The soil type 4 specimen was prepared by a slurry consolidation method. The soil slurry was prepared by thoroughly mixing the soil with enough saline water to produce a slurry with a water content in excess of the liquid limit of the soil. The slurry was then consolidated in a specially designed consolidometer under a surcharge of about 173 kPa for 5 days prior to testing.

Saturation, Consolidation, and Isothermal Equilibration

The frost heave cell was assembled in the refrigerator. The specimens (except the arctic soil specimen) were saturated with solution of the desired salinity. The specimens were saturated from the base with the top drain line open. During saturation, the specimens were subjected to the desired overburden pressure. Gravity flow gave degrees of saturation between 90 and 100 percent overnight for all samples except the clayey silt, which required a pressure of about 7 to 10 kPa on the incoming water line to accelerate the saturation process. Whenever a pressure was added to the incoming water line, an equivalent additional surcharge load was applied to the sample via the top piston and dead weight system. After closing the bottom plate drainage line, the specimen was allowed to set for 3 to 4 hours to stabilize pore

pressures. After saturation/consolidation, the top and bottom heat exchanger plates were connected to the refrigeration bath, set at 0.3°C above the pore-fluid freezing point. Coolant was circulated for several hours to induce a uniform temperature in the specimen.

Freezing Procedure

For the seven tests performed having cold side temperatures of 1 to 2°C below the freezing point, nucleation was induced by supercooling the base of the sample at -15 to -17°C while monitoring the change in height and base plate temperature. As soon as any change in height was observed, the circulation lines were disconnected from the -15 to -17°C bath and reconnected to the refrigeration baths, which were preset to give the desired boundary temperature for each test. For the remaining 12 tests performed having cold side temperatures of 5 to 7°C below the freezing point, nucleation inducement was not required.

Temperature readings for top and bottom plates and cell sidewalls were recorded periodically along with change in height and water intake or expulsion. Data were typically recorded at times of 0, 1, 5, 10, 20, and 30 minutes; and 2, 4, 8, 16, and 24 hours, and twice daily thereafter. Tests were continued for 4 days or until the rate of frost heave appeared to reach steady state.

After completion of the test, the specimen was removed from the cell and examined. The location of the final ice lens, if any, and frost front were measured. The moisture content of both frozen and unfrozen parts was obtained for most specimens. Salinities of the frozen and unfrozen parts were determined for several samples by electrical conductivity methods.

TEST RESULTS

The results of this study are summarized in Table II and evaluated in the following sections.

Vertical Heave and Water Intake

Figure 3 presents typical example plots of water intake and vertical heave versus time.

Each plot follows a typical pattern of decreasing water intake and heave with time. During the tests, the plots were continually updated. When the rate of heave became constant (slope of heave versus time plot not changing) or heaving stopped, the test was ended. The slopes of the curves during this steady-state period were calculated and recorded as the water intake velocity and heave rate. For tests ending prior to 100 hours, the heave versus time curve was extrapolated at the steady-state slope to 100 hours.

Observed Frost Penetration and Ice Lens Formation

Visible ice lenses were observed in only three specimens (Test Nos. 14, 15, and 17). For Test No. 14 (clayey silt), the ice lens was about 0.25 cm in thickness and located 14 cm from specimen bottom. The ice lenses observed in Test No. 15 (arctic clayey silt) were concentrated in a zone about 1.0 cm thick, located 13 cm above sample bottom. Instead of a thin, continuous ice layer, this zone contained many small, discontinuous ice lenses. An ice lens, 0.5 to 0.75 cm thick, was noted at 14 cm above the bottom of the clayey silt specimen (Test No. 17).

Frost penetration distances for samples with clear frozen/unfrozen boundaries were measured with a scale accurate to 0.25 cm. They ranged from 8.1 cm in Test No. 1 to nearly 15.2 cm in Test No. 19 (Table II).

TABLE II
Summary of Test Results

Test No.	Soil Type	D_f	h_s	$\dot{h}_s$	T_f	V_s	SP
1	1	8.1	1.04	1.8	0.07	1.1	-
2	1	-	0.00	-	0.09	-	0.0
3	1	-	1.27	4.0	0.11	3.9	3.5
4	1	14.0	1.42	7.0	0.12	4.5	5.5
5	1	-	0.05	-	0.09	-	0.0
6	1	-	1.12	2.2	0.12	2.5	2.3
7	1	-	0.89	18.5	0.13	15.0	-
8	1	-	1.12	4.3	0.41	5.3	10.5
9	1	-	0.66	7.8	0.65	9.7	-
10	1	-	0.56	3.8	0.70	5.3	5.3
11	1	-	0.20	3.6	0.77	1.6	2.8
12	1	11.9	0.30	3.9	0.80	2.5	4.8
13	1	-	0.36	6.0	0.66	3.9	9.1
14	3	14.2	0.81	6.0	0.58	5.6	10.2
15	4	13.5	1.17	12.8	0.61	12.5	5.0
16	2	13.7	0.66	3.1	0.64	7.7	-
17	3	14.5	0.48	6.5	0.52	6.1	12.3
18	2	12.7	0.53	7.0	0.68	5.3	10.1
19	2	11.7	0.30	3.6	0.70	2.5	5.1

Notes: D_f = observed frost penetration distance, cm; h_s = total heave in 100 hours, cm; $\dot{h}_s$ = steady state heave rate, 10^{-7} cm/sec; T_f = steady state temperature gradient, °C/cm; V_s = steady state water intake velocity, 10^{-7} cm/sec; SP = calculated segregation potential, 10^{-6} cm^2/sec °C

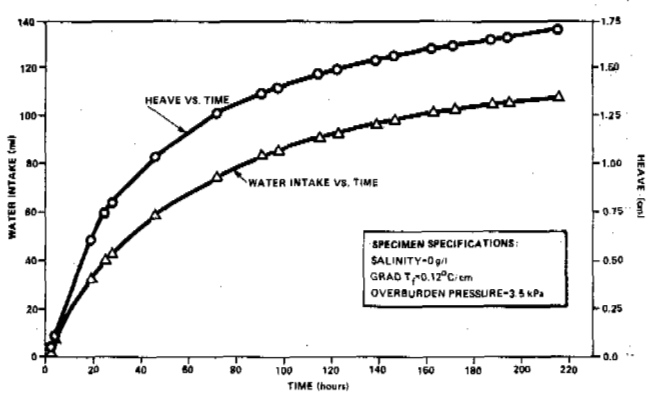

FIGURE 3. TYPICAL HEAVE AND WATER INTAKE VS. TIME, TEST NO.5

Effect of Salinity on Heave

For Manchester silt, the effect of salinity on heave at 100 hours test duration is demonstrated in Figure 4A . At shallow temperature gradients (0.09 to 0.13°C/cm), the Manchester silt saturated with distilled water heaved 1.42 cm in 100 hours. With 10 g/ℓ salinity, the heave reduced to 1.27 cm which is about 89 percent of the distilled water sample heave. For salinity increased above 10 g/ℓ, the heave progressively reduced. Above a salinity of 20 g/ℓ, the 100-hour heave suddenly dropped to nearly zero. At 24 g/ℓ salinity, the heave at 100 hours was 0.05 cm (Test No. 5), and at 30 g/ℓ, no heave was measured after 75 hours. In the latter test, heave shutoff may have resulted from a combination of overburden pressure (11 kPa versus 3.5 kPa in other tests) and salinity. For steeper temperature gradients (0.41 to 0.70°C/cm), the effect of salinity at lower concentrations (0 to 20 g/ℓ) was similar to that at shallower gradients. However, the salinities tested at the steeper temperature gradients were not high enough to reduce heave to zero.

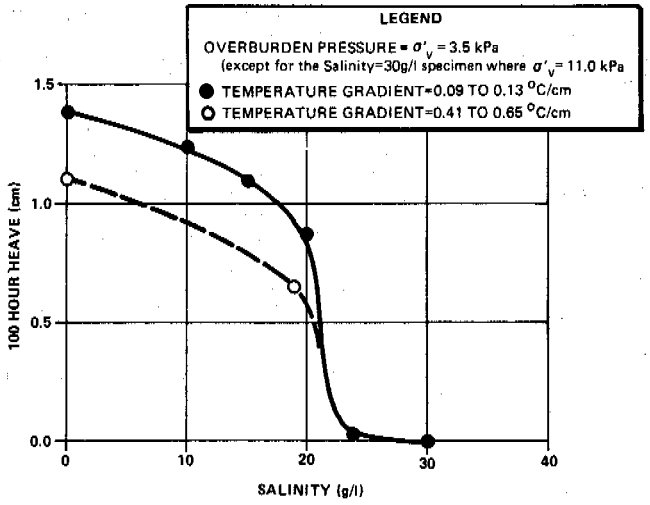

(A) MANCHESTER SILT

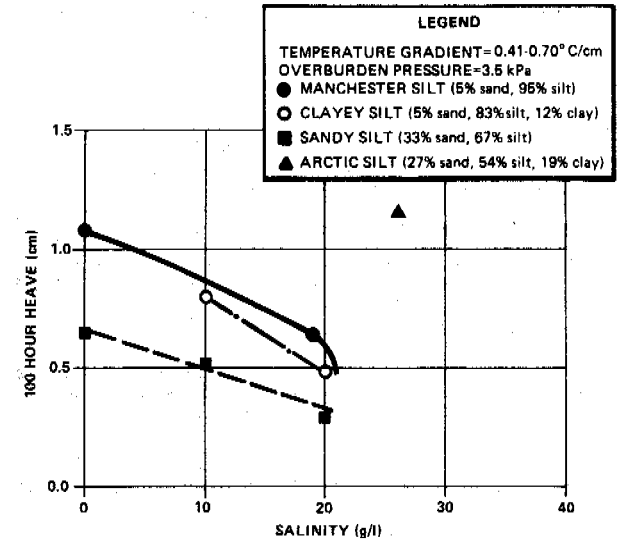

(B) ALL FOUR SOIL TYPES

FIGURE 4. FROST HEAVE STUDY-SALINITY EFFECT ON HEAVE AT 100 HOURS FOR VARIOUS SOIL TYPES

As shown in Figure 4B, both clayey silt and sandy silt exhibited the same trend of reduced heave at higher salinities. Although heave "shutoff" salinities were not reached for clayey silt and sandy silt, the percent reductions in heave with salinity within the range of salinities tested were greater than for Manchester silt (40 to 50 percent compared to 35 to 40 percent). Heave at 100 hours was reduced to less than 0.5 cm for both soils at 20 g/ℓ salinity. It would be expected that, at slightly higher salinities (25 to 30 g/ℓ), nearly zero heave would occur.

Effect of Overburden Pressure on Heave

Test Nos. 11 to 13 tested the effect of overburden pressure on the heave potential of highly frost-susceptible Manchester silt. As with non-saline samples, increased overburden pressure reduced the heave observed for Manchester silt with 10 g/ℓ salinity (Penner and Ueda, 1977; Konrad and Morgenstern, 1983). Heave at 100 hours reduced by more than 42 percent as overburden pressure increased from 20.7 to 69.0 kPa (Table II). The greatest reduction in the heave occurs in the 0 to 20.7 kPa range.

Effect of Soil Gradation on Heave

The test results in Table II show that the sandy silt (33 percent sand, 67 percent silt) heaved less than the more fine-grained soils at each salinity level. Also, clayey silt heaved slightly less than Manchester silt.

The one arctic soil specimen (27 percent sand, 54 percent silt, 19 percent clay) tested gave unexpected high heave despite a post-test salinity of 26 g/ℓ in the frozen portion of the sample (Test No. 15). The arctic soil specimen was prepared by slurry consolidation which may have caused heave results differing from those of all other samples prepared by wet tamping.

Also, the clay content in the arctic clayey silt is significantly higher than that in the other three soils. Thus, the higher frost heave potential may be a result of either higher clay content or specimen preparation method. Further investigation is needed to confirm this.

An increase in the coarse fraction content tends to decrease heave, as expected. For samples tested at 0 g/ℓ salinity, the addition of 33 percent fine-medium sand to the Manchester silt reduced the frost heave at 100 hours by about 40 percent, while at salinities near 20 g/ℓ, the reduction was about 55 percent. More testing of granular soils with varying fines contents would be needed to establish clearer relationships between gradation and frost heave potential.

Effect of Temperature Gradient on Heave

For freshwater Manchester silt specimens, a temperature gradient increase from 0.12 to 0.41°C/cm reduced heave by 22 percent (Figure 4A). A similar effect is shown for specimens saturated with saline (20 g/ℓ) pore fluid.

Effect of Salinity on Water Intake Velocity and Steady-State Heave Rate

For Manchester silt specimens tested at shallow temperature gradients (less than 0.16°C/cm), a substantial decrease in water intake velocities occurs with increasing saline contents (Table II). The trend is quite similar to that observed for 100-hour heave versus salinity (Figure 4A).

Water intake velocities also decreased substantially with increasing salinity for sandy silt specimens. At 20 g/ℓ saline content, the water intake velocity was down to 2.5 x 10^{-7} cm/sec compared to 7.7 x 10^{-7} cm/sec for the nonsaline specimen (a reduction of about 67 percent).

Steady-state heave rates were also observed to decrease with increasing salinity for both Manchester silt and sandy silt (Figure 5). The reduction in heave rate from that for nonsaline samples was nearly 70 percent for Manchester silt at 15 g/ℓ salinity and about 55 percent for the sandy silt at 20 g/ℓ salinity.

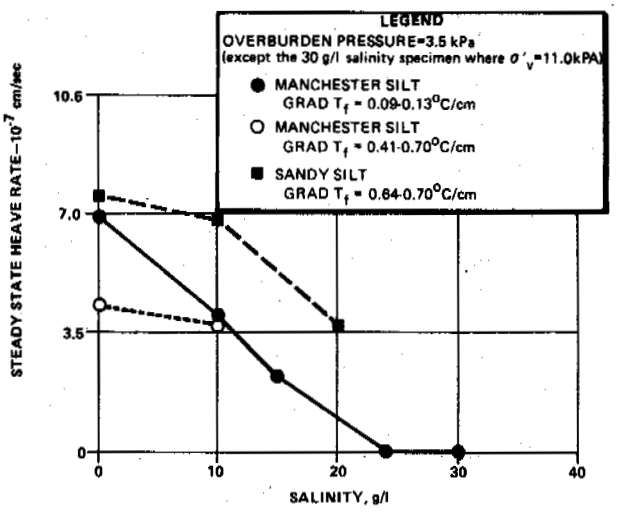

FIGURE 5. SALINITY EFFECT ON STEADY-STATE HEAVE RATE

DISCUSSION

Although considerable effort has been put forth to understand the frost heave phenomenon, the effect of salinity on frost heave behavior has received limited attention. Chamberlain (1983) studied the influence of salinity on two soils, Morin clay and Dartmouth sand. For Morin clay saturated with distilled water, Chamberlain found steady-state heave rates of 2.3 x 10^{-7} cm/sec, which compares well with the heave rate of about 0.7 x 10^{-7} cm/sec found here for Manchester silt. Increasing the salinity to 34.6 g/ℓ reduced the Morin clay heave rate by about 60 percent compared with a 40 percent reduction associated with an increase to 20 g/ℓ for the Manchester silt. Similar percent reductions in heave at 100 hours were observed for both material types, for the same increase in salinity. For Dartmouth sand (4 percent gravel, 56 percent sand, and 40 percent silt and clay), Chamberlain reported a 75 percent reduction in heave rate and a 49 percent reduction in heave at 100 hours associated with pore-fluid salinity increasing from 0 to 35.7 g/ℓ. He also demonstrated the marked differences in moisture content profiles of samples with and without salinity. The results of moisture content and salinity measurements after the tests in this program also confirmed such findings.

A mechanistic theory of ice lens formation and a method for evaluating frost heave behavior in fine-grained soils has been developed by Konrad and Morgenstern (1981, 1982, 1983, 1984). The method relates the rate of heave under steady-state conditions to the potential to develop segregated ice, termed the "segregation potential" (SP) which equals the ratio of the heave rate, h_s to the temperature gradient, T_f.

Values of segregation potential were determined for the present testing program, and are tabulated in Table II. The results indicate the segregation potential decreases with increasing salinity. The observed effect of salinity on segregation potential is very similar to that on heave after 100 hours, previously shown in Figures 4A and 4B.

The effect of steady-state temperature gradient on segregation potential is also shown on Table II, where it can be observed that segregation potential decreases with increasing temperature gradient. The effect of overburden pressure on segregation potential for saline (10 g/ℓ) Manchester silt specimens shows decreasing segregation potential with increasing pressure.

Konrad and Morgenstern (1983) developed the following relationship to account for the effect of overburden pressure, P_e, on SP:

$$SP = SP_o \, e^{-aP_e}$$

where SP_o is the segregation potential for zero overburden pressure and "a" is the empirical constant.

When applied to a best fit of test results for saline (10 g/ℓ) Manchester silt specimens, the above analysis yields values for SP_o = 0.57 x 10^{-6} $cm^2/sec°C$ and a = 1.04 kPa^{-1}.

Such a relationship can be used for predicting the frost heave under field conditions from laboratory tests at zero or low overburden pressures. The expected frost heave of homogeneous soil in the field may be estimated over a wide range of overburden pressures and salinities from the results of relatively few laboratory tests using the method presented by Konrad and Morgenstern (1983), provided that the following apply:

1) The salinity and density of the soil sample used in laboratory testing are essentially the same as that existing in the field.

2) The freezing characteristics reflect the conditions at the onset of the formation of the final ice lens (i.e., a "quasi" stationary frost front).

3) The suction at the frost front is relatively small (i.e., warm plate temperatures close enough to 0°C to ensure a small length of unfrozen soil).

SUMMARY OF RESULTS AND CONCLUSIONS

The effects of the various parameters on frost heave test results can be summarized as follows:

- Increased salinity decreased the heave at 100 hours test duration.
- The frost heave potential of the highly frost-susceptible Manchester silt effectively "shut off" at saline contents above about 24 g/ℓ.
- Few significant ice lenses formed in the saline-water-saturated silt soils subjected to freezing conditions that are generally optimum for segregated ice formation in such soils.
- At salinities of 10 to 20 g/ℓ, the heave (at 100 hours) was substantially reduced (by 38 to 54 percent) from that observed for nonsaline-saturated specimens.
- The arctic soil, formed by a composite of silt and clay specimens from the Beaufort seabed, heaved considerably despite what was considered to be a saline content of 26 g/ℓ. Due to the difficulties encountered during testing, there is some degree of uncertainty in salinity determination.
- At increased overburden pressures, the frost heave potential of Manchester silt at 10 g/ℓ salinity was significantly reduced (42 percent reduction in heave between 20.7 and 69.0 kPa).
- Addition of only 33 percent fine-medium sand to the Manchester silt resulted in substantial reductions in heave potential at salinity levels of 0, 10, and 20 g/ℓ. The heave reductions were in the range of 40 to 55 percent.
- Heave at 100 hours was considerably lower at temperature gradients of 0.59 to 0.79°C/cm than at small temperature gradients (less than 0.16°C/cm). Heave reductions ranged from about 22 to 60 percent depending on salinity.
- Salinity increases generally decreased steady-state water intake velocities, heave rates, and segregation potential.

The water intake and heave versus time results of specimens frozen from top down at freezing rates representative of arctic field conditions indicated that increasing salinity, overburden stress and temperature gradient would decrease frost heave potential of otherwise highly frost susceptible fine-grained soils. Since grain size is a key factor in the formation of segregated ice lenses, and the soils tested had grain size characteristics more optimal for lens growth than many arctic soils, it is quite probable that there should exist a wide variety of soils with limited frost heave potential for construction use in the arctic offshore environment.

REFERENCES

Chamberlain, E.J. (1983). Frost heave of saline soils. Proc. Fourth International Conference on Permafrost, Fairbanks, Alaska, 121-126.

Kaplar, C.W. (1968). New experiments to simplify frost susceptibility testing of soils. Highway Research Record, No. 215, 48-59.

Kaplar, C.W. (1974). Feezing test for evaluating relative frost susceptibility of various soils. Technical Report 250, U.S. Army Corps of Engineeris, Cold Regions Research and Engineering Laboratory, Hanover, New Jersey, 37 p.

Konrad, J.M. & Morgenstern, N.R. (1981). A mechanistic theory of ice lens formation in fine-grained soils. Canadian Geotechnical Journal (17), 473-486.

Konrad, J.M. & Morgenstern, N.R. (1982). The segregation potential of a freezing soil. Canadian Geotechnical Journal (18), 482-491.

Konrad, J.M. & Morgenstern, N.R. (1983). Prediction of frost heave in the laboratory during transient freezing. Canadian Geotechnical Journal (19), 250-259.

Konrad, J.M. & Morgenstern, N.R. (1984). Frost heave prediction of chilled pipelines buried in unfrozen soils. Canadian Geotechnical Journal (21), 100-115.

Mageau, D.W. & Sherman, M.B. (1983). Frost cell design and operation. Proceedings Fourth International Conference on Permafrost, Fairbanks, Alaska, 6 p.

Ono, N. (1975). Thermal properties of sea ice IV. Thermal constants of sea ice. Draft Translation 467, U.S. Army Corps of Engineers, Cold Regions Research and Engineering Laboratory, Hanover, New Hampshire.

Penner, E. & Ueda, T. (1977). The dependence of frost heaving on load application - preliminary results. Proceedings International Symposium on Frost Action in Soils, University of Lulea, Sweden.

Penner, E. & Ueda, T. (1978). A soil frost-susceptibility test and a basis for interpreting heaving rates. Proceedings Third International Conference on Permafrost, Edmonton, Alberta, Canada, Volume 1, 721-778.

Tart, R.G., Jr. (1983). Winter constructed gravel islands. Proceedings Fourth International Conference on Permafrost, Fairbanks, Alaska.

The Earth Technology Corporation (1983). Geotechnical considerations for design of arctic exploration and production islands. Phase I report.

The Earth Technology Corporation (1985). Geotechnical considerations for design of arctic exploration and production islands, Phase II report.

EFFECT OF VARIABLE THERMAL PROPERTIES ON FREEZING WITH AN UNFROZEN WATER CONTENT

V.J. Lunardini

U.S. Army Cold Regions Research and Engineering Laboratory, Hanover, NH, USA

SYNOPSIS While many materials undergo phase change at a fixed temperature, the variation of unfrozen water with temperature causes a soil system to freeze or thaw over a finite temperature range. Exact and approximate solutions are given for conduction phase change of plane layers of soil with unfrozen water contents that vary linearly and quadratically with temperature. The temperatures and phase change depths are found to vary significantly from those predicted for the constant temperature (Neumann) problem. The thermal conductivity and specific heat of the soil within the mushy zone varied as a function of unfrozen water content. The effect of specific heat is negligible and the effect of variable thermal conductivity can be accounted for by a proper choice of thermal properties used in the constant thermal property solution.

INTRODUCTION

The theory of conductive heat transfer with solidification has been largely confined to materials that change phase at a single temperature. The best known problem is that of Neumann and its solution has been widely used for the freezing of soils, Neumann (1860), Berggren (1943), Carslaw and Jaeger (1959). However, for media such as soils, the phase change can occur over a range of temperatures, Anderson and Tice (1973), Tice et al. (1978), Lunardini (1981a). At any temperature below the normal freezing point, there will be an equilibrium state of unfrozen water, ice, and soil solids. Figure 1 shows the geometry for a semi-infinite soil mass, initially at a temperature above freezing, that freezes due to a constant surface temperature held below freezing. The phase change is assumed to occur within temperature limits of T_m and T_f, representing minimum and maximum phase change temperatures.

Figure 2 shows a sketch of the unfrozen water, ξ, as a function of temperature for a typical soil. At T_f the water is all liquid, while at T_m, the free water is all frozen. There may be a residual amount of unfrozen bound water, denoted by ξ_f, which will remain even at very low temperatures. It is assumed that for $T < T_m$, unfrozen water may exist but no phase change will occur. The region $T_m \leq T \leq T_f$ is called the zone of phase change or the mushy zone. In this region water can solidify to ice with unfrozen water and ice coexisting. As $(T_f - T_m) \to 0$, the phase change will approach the Neumann problem often used for coarse-grained materials such as sands and gravels. The form of the ξ function

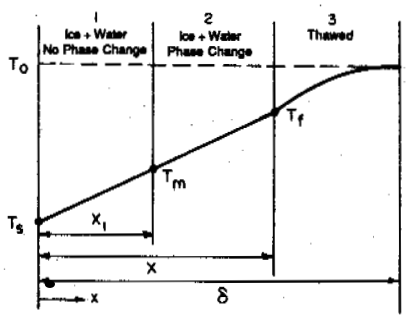

Figure 1. Geometry for solidification with a phase change zone.

for soils can be expressed by different functional relations. The simplest relation is a linear one

$$\xi = \xi_o + \frac{\Delta\xi}{\Delta T_m} (T - T_f) \qquad (1)$$

where $\Delta\xi = \xi_o - \xi_f$ and $\Delta T_m = T_f - T_m$

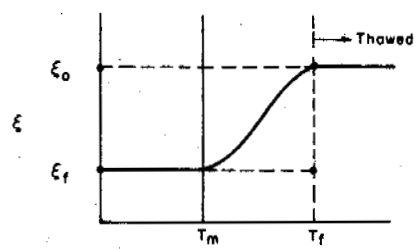

Figure 2. Unfrozen water versus temperature.

A relation which can closely model the data and is easy to manipulate analytically is a quadratic function

$$\xi = \xi_o + \frac{2\,\Delta\xi}{\Delta T_m} (T - T_f) + \frac{\Delta\xi}{\Delta T_m^2} (T - T_f)^2 \qquad (2)$$

The thermal conductivity and the specific heat, within the mushy zone, are functions of the unfrozen water and may be represented by

$$k = k_u - \frac{(k_f - k_u)}{\Delta\xi} (\xi - \xi_o) \qquad (3)$$

$$C = C_u - \frac{(C_f - C_u)}{\Delta\xi} (\xi - \xi_o) \qquad (4)$$

These properties are functions of the particular unfrozen water function, Frivick (1980). Equation 3 gives k-values close to those of the geometric mean for the parameters of this study. Within the fully frozen region (zone 1) it is assumed that the thermal properties are constant and equal to the frozen values while for the thawed region (zone 3) the properties are constant and equal to the thawed soil values.

Tien and Geiger (1967) and Ozisk and Uzzell (1979)

used an unfrozen liquid content which varied with position within the two-phase zone but did not deal with soil systems. Cho and Sunderland (1974) found a solution for the freeze of a material with thermal conductivity varying linearly with temperature and with a single phase change temperature.

BASIC EQUATIONS

For a small volume within the mushy zone, energy will be conducted in and out of the volume and latent heat will be released during solidification; the problem is one of conduction with a distributed energy source. The governing equations were derived by Lunardini (1985, 1987). The energy equation is

$$\frac{\partial}{\partial x}\left(k\,\frac{\partial \theta_2}{\partial x}\right) = C\,\frac{\partial \theta_2}{\partial t} - \frac{\ell\,\rho_d}{(T_f - T_m)}\,\frac{d\xi}{d\theta_2}\,\frac{\partial \theta_2}{\partial t} \tag{5}$$

Thermal conductivity and specific heat in region 2, for the linear ξ case, are

$$k = k_o(1 + \beta_1\,\theta_2) \tag{6a}$$

$$C = C_o(1 + \beta_2\,\theta_2) \tag{6b}$$

For the mushy zone with variable thermal properties $k_o = k_u$ and $C_o = C_u$, however, k_o, C_o can be any values if the thermal properties in region 2 are constant.

In the mushy zone the following transformation is used.

$$\psi = \frac{1}{k_o}\int_0^{\theta_2} k(\theta_2')\,d\theta_2' \tag{7}$$

For linear ξ the function ψ can be evaluated explicitly.

$$\psi = \theta_2 + \frac{\beta_1}{2}\,\theta_2^2 \tag{8}$$

$$k = k_o\sqrt{1 + 2\beta_1\psi} \tag{9}$$

The most general case is a problem with 3 regions as shown in Figure 1. The equations for the three regions are

$$\frac{\partial^2 \theta_1}{\partial x^2} = \frac{1}{\alpha_1}\,\frac{\partial \theta_1}{\partial t} \tag{10}$$

$$\theta_1(0,t) = \phi \tag{10a}$$

$$\theta_1(X_1,t) = 1 \tag{10b}$$

$$k_1\,\frac{\partial \theta_1(X_1,t)}{\partial x} = k(X_1)\,\frac{\partial \theta_2(X_1,t)}{\partial x} \tag{11}$$

$$\sqrt{1 + 2\beta_1\psi}\,\frac{\partial^2 \psi}{\partial x^2} = \frac{\partial}{\partial t}\left[F_1\psi + F_2(1+2\beta_1\psi)^{3/2}\right] \tag{12}$$

$$\psi(X,t) = 0 \tag{12a}$$

$$\psi(X_1,t) = 1 + \beta_1/2 \tag{12b}$$

$$k_o\,\frac{\partial \psi(X,t)}{\partial x} = k_3\,\frac{\partial \theta_3(X,t)}{\partial x} \tag{12c}$$

$$\frac{\partial^2 \theta_3}{\partial x^2} = \frac{1}{\alpha_3}\,\frac{\partial \theta_3}{\partial t} \tag{13}$$

$$\lim_{x\to\infty} \theta_3(x,t) = -\phi_o \tag{13a}$$

$$\theta_3(x,0) = -\phi_o \tag{13b}$$

$$\theta_3(X,t) = 0 \tag{14}$$

Exact solutions for the three-zone problem with variable thermal properties have not been found. Approximate solutions can be obtained using the heat balance integral, however, before doing this it is useful to examine the simpler two-zone problem. If the surface temperature, T_s, is greater than or equal to the minimum phase change temperature then a completely frozen zone will not exist. Thus we need only examine regions 2 and 3.

TWO ZONE PROBLEMS

The two-zone problem is simpler than the three-zone case and will lead to results that can simplify the need for the full three-zone problem. The linear unfrozen water case will be examined for both variable and constant thermal properties while the quadratic water content case will be evaluated only for the constant property problem. This will be shown to be adequate for the general problem.

Linear Unfrozen Water Function

Variable Thermal Properties

Equations (12-14) are valid for this case except that the boundary condition (12b) becomes

$$\psi(0,t) = \phi + \frac{\beta_1\phi^2}{2} = P \tag{15}$$

An approximation to the solution may be obtained with the heat balance integral method which has been adapted to problems of freezing in soils systems by Lunardini (1981b, 1982, 1983) and Lunardini and Varotta (1981). The equations are well known and will not be derived here, the interested reader can consult Lunardini (1981a). Referring to Figure 1, Equations (12) and (13) become

$$\int_0^X \sqrt{1 + 2\beta_2\psi}\,\frac{\partial^2 \psi}{\partial x^2}\,dx = \frac{d}{dt}\left[\int_0^X \left[F_1\psi + F_2(1+2\beta_1\psi)^{3/2}\right]dx - F_2 X\right] \tag{16}$$

$$-\alpha_3\,\frac{\partial \theta_3}{\partial x}(X,t) = \frac{d}{dt}\left[\int_X^\delta \theta_3\,dx + \phi_o\delta\right] \tag{17}$$

For the heat balance integral Eqs (13a,b) become

$$\theta_3(\delta,t) = -\phi_o \tag{14a}$$

$$\frac{\partial \theta_3(\delta,t)}{\partial x} = 0 \tag{14b}$$

Quadratic temperature profiles are assumed for ψ and θ_3 since experience has shown that they yield good results for the heat balance integral method.

$$\psi = \left(1 - \frac{x}{X}\right)\left[\frac{2\lambda_o}{\delta - X}\,x + P\left(1 - \frac{x}{X}\right)\right] \tag{18}$$

$$\theta_3 = \phi_o\left[\left(\frac{\delta - x}{\delta - X}\right)^2 - 1\right] \tag{19}$$

In order to simplify the algebra the following parameters are defined

$$X = 2\gamma\sqrt{\alpha_3 t} \tag{20}$$

$$\delta - X = BX \tag{21}$$

The solution of Eqs (16) and (17) is straightforward but tedious; the algebraic manipulations are given in

Lunardini (1987). The parameters γ and B can be found from the following equations.

$$\gamma^2 = \frac{1}{B(\frac{B}{3} + 1)} \tag{22}$$

$$K\, Q_1\, B(\frac{B}{3} + 1) = [F_1(\frac{A}{2} + \frac{K}{3}) + F_2(Q_2 - 1)]\alpha_3 \tag{23}$$

where

$$Q_1 = \frac{\sqrt{N}}{2} + \frac{A}{4K}(\sqrt{N} - 1) + \frac{M \ln Q_3}{2\sqrt{2\beta_1 K}}$$

$$Q_2 = \frac{\sqrt{N}}{4}[N + \frac{3}{2}M + \frac{A(N-1)}{2K}] + \frac{3M^2 \ln Q_3}{8\sqrt{2\beta_1 K}}$$

$$Q_3 = \frac{\sqrt{2\beta_1 K} + \beta_1(2K + A)}{\sqrt{2\beta_1 K} + \beta_1 A}$$

Constant Thermal Properties

The constant thermal properties solution follows from the preceding case if $\beta_{21} \to 0$, $\beta_1 \to 0$, $\alpha_0 = \alpha_2$, $\sigma_0 = \sigma$, $\lambda_0 = \lambda$.

$$(B - \frac{2\lambda}{\phi})(B+1) - (1 + \frac{\lambda}{2B})(1+\sigma)\,\alpha_{32} = 0 \tag{24}$$

The parameter γ is again found from Eq (22). For this case an exact solution is possible by using a similarity transformation, as was shown by Lunardini (1985).

Quadratic Unfrozen Water Function

With a quadratic unfrozen water function, it is not possible to find a closed form solution for variable thermal properties. Thus a heat balance approximation will be used for constant thermal properties. The equations for region 2, using Eq (2), are

$$\alpha_2 \frac{\partial^2 \theta_2}{\partial x^2} = \frac{\partial}{\partial t}[(1+2\sigma)\theta_2 - \sigma\,\theta_2^2] \tag{25}$$

$$\theta_2(X,t) = 0 \tag{25a}$$

$$\theta_2(X_1,t) = 1 \tag{25b}$$

$$k_2 \frac{\partial \theta_2}{\partial x}(X,t) = k_3 \frac{\partial \theta_3}{\partial x}(X,t) \tag{25c}$$

The heat balance integral form of Eq (25) is

$$\alpha_2 [\frac{\partial \theta_2}{\partial x}(X,t) - \frac{\partial \theta_2}{\partial x}(0,t)] = \frac{d}{dt}\int_0^X [(1+2\sigma)\theta_2 - \sigma\theta_2^2]dx \tag{26}$$

Eq (17) is still valid for region 3. The temperature profile for region 3 is again Eq (19) while that for region 2 is assumed to be

$$\theta_2 = (1 - \frac{x}{X})[\frac{2\lambda}{B}\frac{x}{X} + \phi(1 - \frac{x}{X})] \tag{27}$$

The parameter γ is found from Eq (22) and the equation for B is

$$(\phi B - 2\lambda)(B+3) = \alpha_{32}\{(\frac{\lambda}{B} + \phi)[1 + 2\sigma - \frac{3\phi\sigma}{5}] - \frac{2}{5}\frac{\sigma\lambda^2}{B^2}\} \tag{28}$$

The two zone solutions can be compared by considering some specific cases. Consider a typical soil with properties suggested by Nakano and Brown (1971). The results of several cases are summarized in Tables I and II. Cases 1-3 in the tables show that the effect of specific heat variation is not important and can be neglected. However, case 4 indicates that the thermal conductivity can cause 15-25% variations in the rate of growth of the freezing zone. Case 5 uses average values of k and C within the mushy zone and the effect of variable properties can be accounted for by using the constant property solution with the average of the fully frozen and fully thawed thermal properties. Cases 4 and 6 show that the heat balance approximation is within about 7% of the exact solution. This verifies the acceptable accuracy of the heat balance integral method. The effect of the different unfrozen water content functions can be deduced from cases 4 and 7 of Table II. The growth rate for the quadratic water function lags that of the linear water function by about 9%. This was also noted by Lunardini (1985). The quadratic unfrozen water function will be more accurate for an actual soil and is presented in graphical form as Figures 3-5 for the 2-zone problem.

Table I. Effect of thermal properties on freeze of soil with average properties, linear ξ.

Case	C_o	k_o	β_1	γ	% Diff.	Comment
1	0.63	0.0058	0.431	0.3988	-	variable k,C.
2	0.63	0.0058	0.431	0.3996	0.2	C=0.63, constant
3	0.54	0.0058	0.431	0.4016	0.7	C=0.54, constant
4	0.54	0.0083	0	0.4575	14.7	constant k,C*
5	0.585	0.0071	0	0.4126	3.5	constant k,C**
6	0.54	0.0083	0	0.4277	7.2	exact solution*

$T_o = -T_s = -T_m = 4°C$, $\xi_o = 0.2$, $\xi_f = .0782$, $\rho_d = 1.68$ g/cm^3
$k_f = .0083$ cal/s-cm°C, $k_u = .0058$, $C_f = .54$ cal/cm^3-°C
$C_u = .63$, $S_T = 0.1539$, $\phi = \phi_o = 1.0$ Case 1: $\beta_2 = -0.1429$
* $k_2 = 0.0083$ $C_2 = 0.54$ $k_3 = k_u$ $C_3 = C_u$
** $k_2 = (k_f + k_u)/2 = 0.0071$ $C_2 = (C_f + C_u)/2 = 0.585$

Table II. Effect of thermal properties on freeze of soil with extreme property variations, linear ξ.

Case	C_o	k_o	β_1	γ	% Diff.	Comment
1	0.63	0.0058	1	0.4626	-	variable k,C
2	0.63	0.0058	1	0.4607	-0.4	C=0.63, constant
3	0.315	0.0058	1	0.4696	1.5	C=0.315 constant
4	0.315	0.0116	0	0.5671	22.6	constant k,C*
5	0.473	0.0087	0	0.4726	2.2	constant k,C**
6	0.315	0.0116	0	0.5304	14.7	constant k,C* exact solution
7	0.315	0.0116	0	0.5226	13.0	constant k,C* quadratic ξ.

k_f=.0116 cal/s-cm-°C, k_u=.0058, C_f=.315 cal/cm^3-°C, C_u=.63
$S_T = 0.1539$ $\phi = \phi_o = 1$ Case 1: $\beta_2 = -0.50$
* $k_2 = 0.0116$ $C_2 = 0.35$
** $k_2 = (k_f + k_u)/2 = 0.0087$ $C_2 = (C_u + C_f)/2 = 0.473$

THREE ZONE PROBLEMS

Since the variable property case can be adequately handled by an appropriate constant property solution, only the constant property problem will be examined.

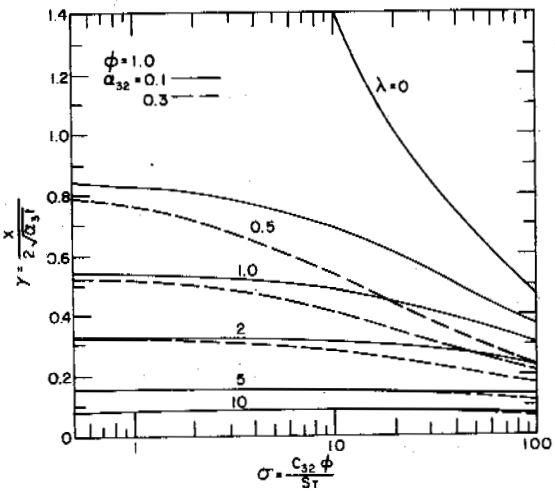

Figure 3. γ vs σ, quadratic ξ, two zone problem, $\phi = 1$, $\alpha_{32} = 0.1$, 0.3.

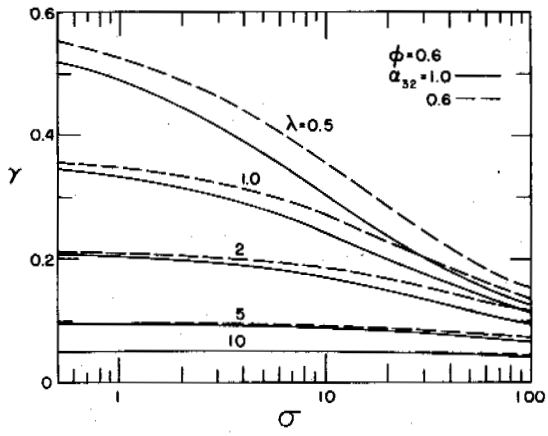

Figure 4. γ vs σ, quadratic ξ, two zone problem, $\phi = 0.6$, $\alpha_{32} = 0.6$, 1.

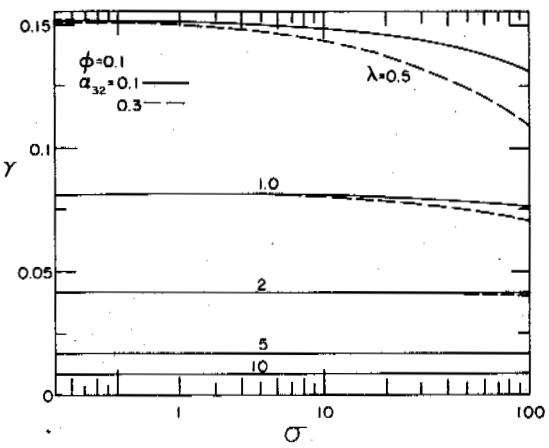

Figure 5. γ vs σ, quadratic ξ, two zone problem, $\phi = 0.1$, $\alpha_{32} = 0.1$, 0.3.

Linear Unfrozen Water Function

The similarity method was used by Lunardini (1985) to obtain an exact solution to this problem. The solution is found with two phase change parameters η and γ, defined by

$$X_1 = 2\eta\sqrt{\alpha_1 t} \tag{29}$$

$$X = 2\gamma\sqrt{\alpha_3 t} \tag{30}$$

The parameters η and γ are found from the simultaneous solution of two equations. Lunardini (1985) showed that this solution approached the Neumann solution as the phase change zone decreased. The thaw/freeze interface can greatly exceed the value for the Neumann solution if phase change occurs over a finite temperature zone.

Heat Balance Integral Solution

The heat balance integral equations for the three zone problem are as follows

$$\alpha_1\left[\frac{\partial\theta_1(X_1,t)}{\partial x} - \frac{\partial\theta_1(0,t)}{\partial x}\right] = \frac{d}{dt}\int_0^{X_1}(\theta_1-1)dx \tag{31}$$

$$\theta_1(0,t) = \phi \tag{31a}$$

$$\theta_1(X_1,t) = 1 \tag{31b}$$

$$\frac{\partial\theta_1(X_1,t)}{\partial x} = k_{21}\frac{\partial\theta_2(X_1,t)}{\partial x} \tag{31c}$$

$$\alpha_2\left[\frac{\partial\theta_2(X,t)}{\partial x} - \frac{\partial\theta_2(X_1,t)}{\partial x}\right] = (1+\sigma)\frac{d}{dt}\left[\int_{X_1}^{X}\theta_2 dx + X_1\right] \tag{32}$$

$$\theta_2(X,t) = 0 \tag{32a}$$

$$\theta_2(X_1,t) = 1 \tag{32b}$$

$$\frac{\partial\theta_2}{\partial x}(X,t) = k_{32}\frac{\partial\theta_3}{\partial x}(X,t) \tag{32c}$$

$$-\alpha_3\frac{\partial\theta_3}{\partial x}(X,t) = \frac{d}{dt}\left[\int_X^{\delta}\theta_3 dx + \phi_o\delta\right] \tag{33}$$

$$\theta_3(\delta,t) = \phi_o \tag{33a}$$

$$\theta_3(X,t) = 0 \tag{33b}$$

$$\frac{\partial\theta_3}{\partial x}(\delta,t) = 0 \tag{33c}$$

Quadratic temperature profiles were assumed for the three regions with a straightforward solution to Eqs (31-33). The results are given below.

$$\gamma^2 = \frac{1}{B\left(\frac{B}{3}+1\right)} \tag{34}$$

$$\eta^2 = (1-R)^2\gamma^2\alpha_{31} \tag{35}$$

$$(\phi-1)(3-\eta^2) - (6+\eta^2)\left[(1-R)k_{21}\left(\frac{1}{R} - \frac{\lambda}{B}\right)\right] = 0 \qquad (36)$$

$$1 - \frac{2\lambda R}{B} - \frac{(1+\sigma)}{3} R\, \alpha_{32}\, \gamma^2 \left(3-2R + \frac{R^2\lambda}{B}\right) = 0 \qquad (37)$$

These four equations can be easily solved for η and γ.

Table III shows that the approximate solution is in error by less than 6% when compared to the exact solution.

Table III. Comparison of exact and HBI solutions. Linear ξ, and constant k, C.

Case	T_m (°C)	Exact Solution η	Exact Solution γ	H.B.I. Solution η	H.B.I. Solution γ	% Diff. η	% Diff. γ
1	-4	0.0617	0.3029	0.0622	0.2938	0.8	-3.1
2	-2	0.1135	0.2576	0.1150	0.2411	1.3	-6.4
3	-1	0.1376	0.2272	0.1390	0.2168	1.0	-4.6
4	-.5	0.1492	0.2106	0.1505	0.2050	0.9	-2.6
5	-.1	0.1571	0.1946	0.1595	0.1958	1.5	0.6

T_o=4°C, T_s=-6, T_f=0°C, k_1=0.00828 cal/s-cm °C, k_2=0.00703 k_3=0.00578, C_1=C_2=C_3=0.165 cal/cm^3 °C, S_T=0.0605

Quadratic Unfrozen Water Function

The equations for the quadratic unfrozen water relation are identical to Eqs (31-33) except that Eq 32 is

$$\alpha_2\left[\frac{\partial\theta_2}{\partial x}(X,t) - \frac{\partial\theta_2}{\partial x}(X_1,t)\right] = \left[\frac{d}{dt}\int_{X_1}^{X}\{(1+2\sigma)\theta_2 - \sigma\theta_2^2\}dx + (1+\sigma)X_1\right] \qquad (38)$$

Quadratic temperature approximations were used. The solution is given by Eqs (34-36) with the mushy zone equation given by

$$1-2z - R^2\,\alpha_{32}\gamma^2\left\{\frac{z-2}{3} + \frac{1+\sigma}{R} - \frac{\sigma}{15}(2z^2 - 7z+18)\right\} = 0 \qquad (39)$$

Case 1 of Table 3 was evaluated for the quadratic ξ and it was found that η = 0.0572 and γ = 0.2730. These values differ from the linear ξ approximation by about 8%. Graphical solutions for the quadratic ξ, three zone problem are shown in Figs 6-8 for typical soil parameters.

CONCLUSIONS

The mathematical model used assumed the latent heat to be a source of energy distributed throughout the volume of a soil with phase-change temperature limits of T_f and T_m. This contrasts with the Neumann problem wherein the latent heat is totally released at the upper phase change temperature T_f. A comparison of the exact solution for the former case showed that it converged to the Neumann solution as (T_f-T_m) approached zero. Thus the model is based on sound physical principles.

The effect of variable specific heat on the rate of phase change is negligible for the cases examined, thus it is acceptable to use an average specific heat value in the mushy zone. Variation of the thermal conductivity with water content is significant and can cause 15-25% change in the rate of freezing of the soil. The constant

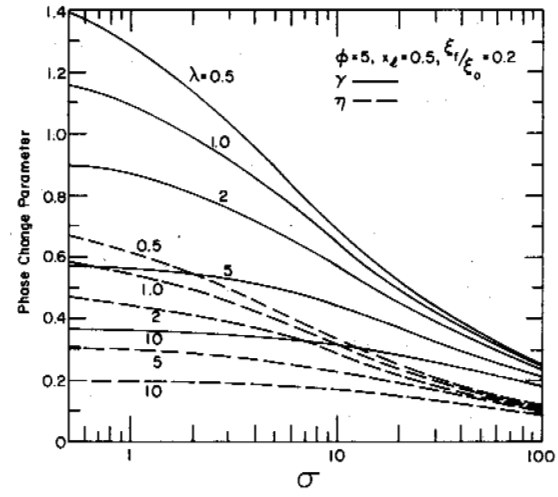

Figure 6. Quadratic ξ, three zone solution, ϕ=5, x_ℓ=0.5.

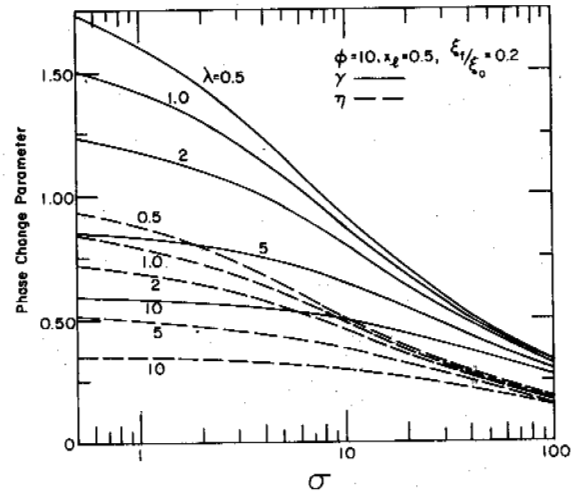

Figure 7. Quadratic ξ, three zone solution, ϕ=10, x_ℓ=0.5.

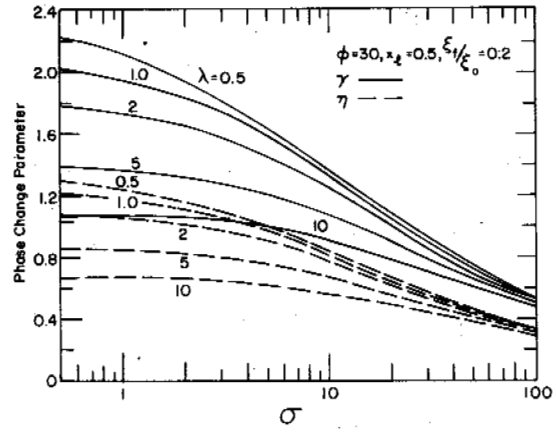

Figure 8. Quadratic ξ, three zone solution, ϕ=30, x_ℓ=0.5.

property solution, with average values of the thermal properties in the mushy zone, gives a solution which is quite close to that for the variable property solution. It is acceptable to use the much simpler, constant property solution with average thermal properties to compensate for the actual variable thermal conductivity.

A series of graphs are presented of the constant property, three-zone problem for typical ranges of soil parameters. These graphs allow rapid predictions to be made for the freezing of soils with an unfrozen water content that is a function of temperature and variable thermal properties.

REFERENCES

Anderson, D.M. and A. Tice (1973) "The Unfrozen Interfacial Phase in Frozen Soil Water Systems." In Analysis and synthesis. Ecological Studies, vol. 4, eds., A. Nodos et al., New York: Springer-Verlag, pp. 107-124.

Berggren, W.P. (1943) "Prediction of Temperature Distribution in Frozen Soils." Transactions, American Geophysical Union 24(3):71-77.

Carslaw, H.S. and Jaeger, J.C. (1959) Conduction of Heat in Solids, Clarendon, Oxford.

Cho, S.H. and Sunderland, J.E. (1974) "Phase Change Problems with Temperature-Dependent Thermal Conductivity," J. Heat Transfer, V. 96, (2), pp. 214-217.

Frivik, P.E. (1980) "State-of-the-Art-Report, Ground Freezing: Thermal Properties, Modelling of Processes and Thermal Design," ISGF, pp. 354-373.

Lunardini, V.J. (1987) "Freezing of Soil with an Unfrozen Water Content and Variable Thermal Properties," CRREL Rept 417, Hanover, NH.

Lunardini, V.J. (1985) "Freezing of Soil with Phase Change Occurring Over A Finite Temperature Zone," Proceedings, 4th Int. Offshore Mechanics and Arctic Engineering Symposium, Vol. II, pp. 38-46, American Society of Mechanical Engineers.

Lunardini, V.J. (1983) "Freezing and Thawing: Heat Balance Integral Approximations," J. Energy Resources Tech., vol. 105(1), pp. 30-37.

Lunardini, V.J. (1982) "Freezing of Soil with Surface Convection," Proceedings of Third International Symposium on Ground Freezing, USACRREL, Hanover, NH, pp. 205-212.

Lunardini, V.J. (1981a) Heat Transfer in Cold Climates, Van Nostrand Reinhold Company, New York.

Lunardini, V.J. (1981b) "Phase Change Around a Circular Cylinder," J. Heat Transfer, vol. 103, no. 3, pp. 598-600.

Lunardini, V.J. and R. Varotta. (1981) "Approximate Solution to Neumann Problem for Soil Systems," J. Energy Resources Tech., vol. 103, no. 1, pp. 76-81.

Nakano, Y. and J. Brown (1971) "Effect of a Freezing Zone of Finite Width on the Thermal Regime of Soils," J. Water Resources Research, vol. 7, no. 5, pp. 1226-1233.

Neumann, F. (ca. 1860) Lectures given in 1860s. See Riemann-Weber. Die partiellen Differential-gleichungen. Physik (5th ed., 1912), 2:121.

Ozisik, M.N. and J.C. Uzzell (1979) "Exact Solution for Freezing in Cylindrical Symmetry with Extended Freezing Temperature Range", J. Heat Transfer, vol. 101, pp. 331-334.

Tice, A.R., C.M. Burrows and D.M. Anderson (1978) "Phase Composition Measurements on Soils at Very High Water Content by the Pulsed Nuclear Magnetic Resonance Technique." Moisture and frost-related soil properties. Transportation Research Board, Nat. Acad. Sciences, pp. 11-14.

Tien, R.H. and Geiger, G.I. (1967) "A Heat Transfer Analysis of the Solidification of a Binary Eutectic System", J. Heat Transfer, Ser C, ASME, vol. 89, pp. 230-234.

NOMENCLATURE

$A = 2\lambda_o/B$
$B = (\delta - X)/X$
C = specific heat, cal/cm^3-°C
$C_{ij} = C_i/C_j$
C_o = arbitrary value of specific heat for constant property mushy zone, otherwise $C_o \equiv C_u$
$F_1 = (1+\sigma_o - \beta_{21})/\alpha_o$
$F_2 = \beta_{21}/(3\alpha_o\beta_1)$
k = thermal conductivity, cal/s-cm-°C
$k_{ij} = k_i/k_j$
k_o = any specified constant conductivity mushy zone value of k, otherwise $k_o \equiv k_u$.
$K = P-A$
ℓ = latent heat of fusion of water, cal/g
$M = 1 - A^2\beta_1/(2K)$
$N = 1+2\beta_1 P$
$P = \phi + \phi^2\beta_1/2$
$R = 1 - n\sqrt{\alpha_{13}/\gamma} = 1-X_1/X$
$S_T = C_3(T_f - T_s)/(\rho_d \ell \Delta\xi)$

t = time
T = temperature
T_f, T_m = maximum and minimum phase change temperatures
T_o, T_s = initial and surface temperatures
x = Cartesian coordinate
x_ℓ = volumetric water fraction
X, X_1 = phase change interface for T_f, T_m
z = $R\lambda/B$

α = thermal diffusivity = k/C
$\alpha_{ij} = \alpha_i/\alpha_j$
$\alpha_o = k_o/C_o$
$\beta_1 = k_{fu} - 1$
$\beta_2 = C_{fu} - 1$
δ = temperature penetration depth
$\theta = (T_f - T)/(T_f - T_m)$, dimensionless temperature
$\lambda = \phi_o k_{32}$
$\lambda_o = \phi_o k_{30}$
ξ = ratio of unfrozen water mass to soil solid mass
ξ_o, ξ_f, ξ_s - values of ξ at T_f, T_m, T_s
ρ_d = dry unit density of soil solids, g/cm^3
$\sigma = C_{32}\phi/S_T$
$\sigma_o = C_{30}\phi/S_T$
$\phi = (T_f - T_s)/(T_f - T_m)$
$\phi_o = (T_o - T_f)/(T_f - T_m)$

Subscripts

1,2,3 - regions of soil
f,s,u - frozen, surface value, and thawed value

DEVELOPMENT AND APPLICATION PRACTICE OF METHODS FOR PRELIMINARY THAWING OF PERMAFROST SOILS IN FOUNDATIONS

E.S. Maksimenko

Northern Affiliate, Research Institute for Foundations and Underground Structures, USSR's State Building Committee, Vorkuta, USSR

SYNOPSIS Varieties of methods are examined; methods for calculating basic electric thawing parameters, viz. duration and power expenses, are discussed according to frozen-soil conditions and the chosen thawing regime; technical specifications and fields of application. Some new thawing methods are described.

A highly important measure for reducing deformations in the foundations of buildings and structures erected on permafrost soils proves to be a preliminary thawing of these soils to a design depth. Preliminary thawing enjoys a particularly large-scale application in construction projects on areas with an irregular and deep occurence of the top surface of permafrost soils.

The size of the areas and depths for preliminary thawing are to be calculated according to the specific frozen-soil conditions, the size of the structure to be erected, the intensity of its impact on foundation soils, as well as the implemented method of foundation construction. Preliminary thawing depths for buildings up to 24 m wide are, as a rule, 10--20 m, for large industrial objects they may attain 40 m (Maksimenko, Ponomarev et al., 1986).

Among the fairly great number of different methods of preliminary thawing the ones that have become particularly widespread are hydro-, steam- and electric thawing.

The first two secure a high thawing rate in well-filtering large-skeletal soils, but are little effective in thawing finely-dispersed sediments.

Applicability of electric thawing methods is practically not restricted by the type of the soils to be thawed; therefore, in the Vorkuta industrial district, where clayey soils are widespread, the entire volume of work for preliminary thawing has been executed with the use of electricity. In recent years these methods have been successfully used also in other regions - Western and Eastern Siberia (Urengoiskaya and Neryungrinskaya thermal power stations). Not least important in this were such factors as the use of electricity required for carrying out numerous general construction jobs, a sufficiently simple technology and the possibility of controlling the thawing process.

The principal varieties of electric thawing methods are: the use of various electric heaters and a direct passage of alternating electric current through the soil mass being thawed with the aid of electrodes.

Heaters and electrodes are to be set up at the area to be thawed in the majority of cases at the spices of equilateral triangles in the preliminarily drilled holes. The spacing of holes will be appointed according to calculation results with respect to the duration of soil thawing and electricity expenses, i.e. the main parameters determining the efficiency of the method.

Since in the majority of cases preliminary thawing is achieved on areas with permafrost soils of non-fusing type, to reduce electricity consumption various measures are taken to confine heat releases solely to occurence depths of the soils to be thawed. In the use of electric heaters this is achieved by placing the heating parts directly inside the frozen mass and in the use of electrodes - by covering with electrically non-conductive varnishes or paints the upper surfaces of thawed soils cutting across the frozen mass.

Of all the versatility of electric heater designs (Maksimenko, 1982) particularly widespread in thawing practice have become ohmic heaters (Boiko, 1975) which are noted for low material consumption and simplicity in manufacture. The power of such heaters is determined by the applied voltage (usually not above 40 V) and the diameter of the branches subject to a condition that the density of the current flowing in it should not exceed 1.5 A/mm^2 (Maksimenko, 1982). An optimal operating regime of ohmic heaters corresponds to a length power 1.0-1.8 kW/m. A further increase of power will lead to significant evaporation of soil moisture from the soil mass being thawed, which is accompanied by an increase of thermal resistance of the soil around the heater and a decrease of the thawing rate.

Ohmic heaters belong to constant-power heaters for which the duration of thawing (electric power supply) is to be calculated according to the formula (1) obtained by approximating the analytical solution of the problem of heat conduction for a linear source of heat in a boundless massif (Carslaw, Jaeger, 1964).

$$\tau_1 = 1.59 \cdot R^2 (\sigma \cdot w/a \cdot P_1)^{1/2} \qquad (1)$$

where τ_1 is duration, s; R is the radius of thawing (radius of the zone of thawed ground around the heater), m; σ is latent heat of ice melting, kJ/kg; w is the ice content of frozen soil, kg/m^3; a is the temperature conductivity of thawed soil, m^2/s; P_1 is the length power of the heater, kW/m.

Specific electric power consumption per unit volume of prepared soil for constant-power heaters is to be calculated according to the formula

$$q_1 = P_1 \cdot h \cdot \tau_1 / (\pi \cdot R^2 \cdot H_0), \qquad (2)$$

where q_1 is electric power consumption, kJ/m^3; h is the length of the heating part of the heater, m; H_0 is the depth of preliminary heting, m.

Application of electric heaters for preparing foundation soils is characterized by the following indices: under 2-4 m spacing of heaters the thawing duration varies within one-two months, the specific electric power consumption amounting to 40-90 kWhr per 1 m^3 of prepared foundation area (Maksimenko, 1984).

Direct passage of alternating electric current through the soil mass being thawed (electrode method) is essentially simpler technologically, since we may use as electrodes metallic pipes, reinforcement rods etc. which do not call for special treatment. The duration of thawing (c) of soils by means of the electrode method is described by a semi-empirical formula

$$\tau_2 = D \left\{ 0.5\left(1 - \frac{\rho_M}{\rho_T}\right)^2 \left[\left(\frac{R}{r_0}\right)^2 \cdot \left(\ln \frac{R}{r_0} - 0.5\right) - \left(\frac{r}{r_0}\right)^2 \left(\ln \frac{r}{r_0} - 0.5\right) \right] + \left(\frac{\rho_M}{\rho_T}\right)\left(1 - \frac{\rho_M}{\rho_T}\right) \times \left[\frac{(R^2 - r^2)}{r_0^2} \right] \ln \frac{R}{r_0} + \left(\frac{\rho_M}{\rho_T}\right)^2 \delta \left(\ln \frac{R}{r_0}\right)^2 \right\} \qquad (3)$$

where

$$D = 1.03 \cdot 10^3 \left[\left(\ln \frac{h}{H_0}\right)^3 + 5.18 \right] \rho_T^2 \cdot r_0^2 \cdot \sigma \cdot w / V^2;$$

$$\delta = li\,(R/r_0)^2 - li\,(r/r_0)^2;$$

ρ_M, ρ_T is the specific electric resistanance of soil in the frozen and thawed state, respectively, Ohm·m; r is the radius of the hole inside which an electrode is placed, m; r_0 is the electrode radius, m; V is the voltage between the electrodes, usually equal to 380 V; the rest of the symbols are the same as those in the formulae (1) and (2).

The specific electric power consumption per unit volume of prepared soil under the electrode method is to be calculated according to the formula

$$q_2 = 10^{-3} \cdot h \cdot V^2 \tau_2 \frac{(1/\rho_M + 1/\rho_T)}{(4R^2 H_0 \ln \frac{R}{r_0})}, \qquad (4)$$

where q_2 is electric power consumption, kJ/m^3.

The above varieties of electric thawing methods differ not merely in the character of heat conduction in the soil mass thawed (heat from the heater finds its way into the soil through the borehole walls, whilst under the electrode method it is generated directly in the soil) but also by the dynamics of the thaing process proper, i.e. by the dependence of the thawing radius on the duration of electric power supply. When using heaters (cf. figure, curve 1) the thawing rate attunates with time, which is explained by an increase of thermal resistance of the thawed soil zone, interfering with heat transfer from the heater to the boundary of phase transitions, i.e. the front of thawing. Under the electrode method, with and increase of the thawed zone volume the thawing rate increases (curve 2), which is associated with a decrease of electric resistance of the soil between the electrodes and, correspondingly, with an increase of heat release inside the soil mass being thawed.

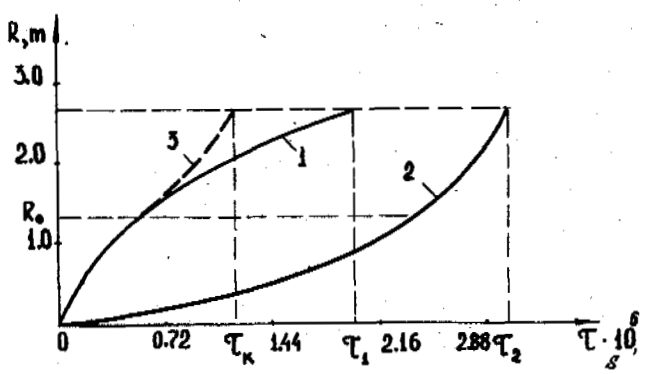

Fig. Thawing radius R versus duration for different methods of electric thawing

A significant improvement of technico-economic indices of electric thawing has been made possible by the use of a combination method developed recently (Maksimenko, 1984), which is a synthesis of the positive properties of the above-described varieties.

Thawing of soils by the combination method involves the use of the same electric heaters

as current receivers with a variable, two-stage power supply regime. At the first stage voltage is supplied to the current receivers in accordance with the specifications of the electric heaters used. In this case the thawing radius versus time coincides with curve 1. Upon attainment of the R_0 value (cf. figure) corresponding to the equality of thawing rates achieved separately by the heaters and by the electrode method the first stage is over. At the second stage, voltage, mostly 380 V, is supplied to the adjacent current receivers, using them as electrodes for a direct passage of electric current through the soil (curve 3).

Reduction of thawing length and of electric power consumption under the combination method is achieved: at the first stage - due to a higher rate of thawing by the use of heaters for an insignificant thermal resistance of the thawed zone and, correspondingly, insignificant reserves of heat accumulated in this zone; at the second stage - due to a high rate of electrode thawing for a sufficiently well-developed process and concentration of heat releases inside the soil mass being thawed.

Beginning from 1984 the combination method of electric thawing has been intensively introduced in the city of Vorkuta, where during the first three years alone it was used in the construction of 15 industrial and civil projects and is at present being mastered by the builders of the Urengoiskaya thermal power station and the Tikhii community centre. As compared to the design solutionsproviding for the use of ohmic heaters for soil thawing, it was possible to more than double improve the main technico-economic indices: volume of borehole drilling to accomodate heaters, metal consumption in fabricating current receivers, electric power consumption. Correspondingly, the cost of preparing 1 cu.m of foundation soil was twice reduced. It is to be underlined that on these projects while using the combination method the thawing depth did not, understandably, change (15-22 m), similarly as did the volumes of prepared soil. Only the spacing of current receivers increased from 2.2-3.5 m to 4.0-4.5 m. In the case of objects with great depths of preliminary thawing, while preserving the design thawing duration within one-one and a half months, the spacing of current receivers can be increased to 5.0-7.0 m.

The length of the first stage of soil thawing by the use of the combination method is to be calculated after the formula (1) by substituting R_0 values in it, and that of the second stage - after the formula (3) by preliminarily substituting r for R_0.

The value of R_0 is dependent both on the specific frozen-soil and technological parameters: spacing of current receivers, their geometrical dimensions, the magnitude of applied voltage, the power of electric heaters used at the first stage. Moreover, in appointing technological parameters it would be feasible to secure the possibility of using the same sources of electric power (transformers) for power supply of current receivers at both the stages, i.e. to appoint the power of the heater equal to that of the electrode at the termination of the thawing process (power consumed by the electrode increses with the thawing radius).

Using the solution of the problem of electric resistance between coaxially arranged infinite and finite cylinders (Iossel, Kochanov, et al., 1981), the formula for calculating heater power (kW) can be represented in the form

$$P = \frac{\pi \cdot r_0 \cdot \mu \cdot V^2}{\rho_T \left(1 - \frac{0.87 \cdot \mu r_0}{R}\right)}, \qquad (5)$$

where $\mu = 0.637 + 0.554 \cdot (h/2\,r_0)^{0.76}$; the other of the symbols are the same as in the previous formulae.

The value of R_0 will be calculated from the formula:

$$R_0 = r_0 \cdot \exp\left(A - \sqrt{A^2 - B^2}\right), \qquad (6)$$

where

$$A = B + C; \qquad B = \frac{\rho_M}{\rho_T} \cdot \frac{\ln \frac{r_0}{R}}{(1 - \rho_M/\rho_T)};$$

$$C = \frac{1.31 V^2}{\rho_T \left[\left(\ln \frac{h}{H_0}\right)^3 + 5.18\right] \sqrt{\frac{a \cdot \tau \cdot wP}{h}} \cdot \left(1 - \frac{\rho_M}{\rho_T}\right)}$$

The duration of soil thawing by the use of the combination method will be calculated after the formula (7) and specific electric power consumption - after the formula (8).

$$\tau_k = \tau_1 + \tau_2; \qquad (7)$$

$$q_k = \frac{P\tau_1 + \frac{0.25 \cdot 10^{-3} \pi h V^2 \tau_2}{\ln(R/r_0)} \cdot \left(\frac{1}{\rho_M} + \frac{1}{\rho_T}\right)}{\pi R^2 \cdot H_0} \qquad (8)$$

where τ_1, τ_2 is the duration of the first and second stage calculated according to the formulae (1) and (2) for the respective parameter values, s; q_k is electric power consumption, kJ/cu.m.

Experience in using electric thawing methods

in the Vorkuta industrial district and in other regions enables us to give the following characteristic of the field of applicability of these methods.

The use of electric heaters is not controlled by the frozen-soil conditions of the areas to be thawed, and the technico-economic indices of the said method are principally determined by the ice content of the soils, their thermal-physical properties and the chosen thawing regime (heater power, thawing radius).

The application efficiency of the electrode method is, moreover, dependent on the electric properties of the soils. Frozen soils are endowed with a significant specific resistance and the process of electrode thawing proceeds rather slowly. The length of thawing, particularly in large-skeletal soils, may be as long as several months. Furthermore, by virtue of the natural inhomogeneity of the soil mass with respect to electric resistance there arise at the initial stage local heating zones the growth of which accounts for a significant non-uniformity of heat releases. Therefore, a rational field of application for the electrode method prove to be the sectionally homogeneous clayey grounds with a specific electric resistance in the frozen state up to 100 Ohm·m.

The above drawbacks of the electrode method significantly less affect the efficiency of the combination method because the passage of electric current through the soil mass occurs with the presence in the latter of sufficiently developed zones of thawed soil around the current receivers. Its application is not restricted by dispersion of the soils, but solely by the specific resistance in the frozen state - 300-400 Ohm .m.

The above-described methods for preliminary thawing, for all their universality and technological advantages, call for the presence in the construction area of electric power which is not always available in required amounts in the areas of pioneer construction, particularly oil and gas fields. To deal with such conditions there has been developed the energetically autonomous method involving a direct burning of liquid fuel in the boreholes (Maksimenko and Pavlichenko, 1986). We may use as fuel petroleum- and oil-containing wastes of machine building, straw oil, masout, etc.

The method is realized in the following manner. Placed in a borehole preliminarily drilled to the requisite thawing depth is an inventory pipe of 80-100 mm diameter with a welded bottom, into which fuel is poured and a perforated tubular air conduit of 25-50 mm diameter is lowered. Setting the fuel on fire is achieved by means of a lowered wick with air supplied into the borehole from a compressor.

As fuel burns up, there occurs an automatic movement of the zone of principal heat releases (flame) over the depth of the layer being dealt with. Heat is conveyed into the soil mass being thawed around the borehole through radiation and a convective heat exchange between gaseous combustion products and borehole walls.

This method is notable for a sufficiently unsofisticated production technology and a possibility of controlling the rate of fuel burning (through air supply) and of the number of burns-through in a borehole, and by the length of operating stages. The combined field and laboratory tests on the new method have pointed to a sufficiently high efficiency in the use of fuel (0.5÷0.8), as determined by the ratio of heat spent on thawing frozen soil to the calorific value of the fuel (Maksimenko and Pavlichenko, 1986).

In conclusion we would like to point out that a preliminary thawing of permafrost soils in foundations significantly extends the possibilities of construction reclamation of northern areas and of the use of numerous methods of foundation design. Moreover, the thawing process proper and the construction properties of thawed soils are well controllable, thus enabling practically any preset reliability of the foundation to be secured for the entire service period.

REFERENCES

Boiko I.V. (1975). Preconstruction thawing of permafrost soils in the foundations of buildings and structures in Vorkuta. - In: Materials on Construction Problems in Vorkuta. Komi Book Publishers, p. 9-15, Syktyvkar.

Iossel Yu.Ya., Kochanov E.S., Strunskii M.G. (1981). Calculation of electric capacitance. Energoizdat Publishers, p.288, Leningrad.

Carslaw, H, Jaeger, J. (1984). Conduction of heat in solids, 2nd Edition, 488, Oxford.

Maksimenko E.S. (1982). Recommendations for the use of electric heaters in thawing permafrost soils. N.M.Gersevanov Research Institute for Foundations and Underground Structures, p.26, Moscow.

Maksimenko E.S. (1984). Combination method for electric thawing of permafrost grounds and foundations. "Bases, Foundations and Soil Mechanics", № 6, p.21-23, Moscow.

Maksimenko E.S., Ponomarev V.D., Sorokin V.A., Fedoseev Yu.G. (1986). Determination of deformation characteristics of permafrost soils by using the method of test thawing. "Bases, Foundation and Soil Mechenics", № 6, p.21,22, Moscow.

Maksimenko E.S., Pavlichenko S.A. (1986). Estimating the efficiency of using liquid fuel for preliminary thawing of foundation soils. - Proc. N.M.Gersevanov Research Institute for Foundations and Underground Structures, issue 85, p.15-21.

SECONDARY CREEP INTERPRETATIONS OF ICE RICH PERMAFROST
Secondary Creep, Permafrost Soils, Creep of Ice

E.C. McRoberts

Hardy BBT Limited, Edmonton, Alberta

SYNOPSIS Secondary creep interpretations of samples of ice rich permafrost soils at temperatures from -0.8°C to -4.0°C are presented. The data are compared to recently published summaries of ice creep. It is found that for temperatures below -2.0°C ice creep data constitutes a good upper bound or conservative relationship for permafrost soil creep rates. At warmer temperatures samples of ice rich permafrost exhibit faster secondary creep rates.

INTRODUCTION

A secondary creep model can offer a realistic interpretation of load-deformation response of ice and ice-rich permafrost soils, for example, Roggensack (1977), McRoberts et al (1978), Morgenstern et al (1980), and Savigny and Morgenstern (1986). In addition, secondary creep models provide a reasonably straightforward method of predicting load-deformation response for a wide variety of design requirements in permafrost, i.e., Nixon and McRoberts (1976), Nixon (1978), and Morgenstern et al (1980). This paper reports on secondary creep interpretations of undisturbed samples of natural permafrost obtained at several sites in the Mackenzie River Valley. Upper bound correlations relating secondary creep rate to applied stress are provided. While the greater part of the data considered are based on unconfined tests, confined tests are also reviewed. As appropriate, secondary creep correlations are compared with published data on flow laws for ice.

SECONDARY CREEP

The creep response obtained by step loading a frozen sample of ice or ice-rich permafrost soil can exhibit three distinct states; primary, secondary, and tertiary creep. At high stress levels the secondary creep stage is transitory with deformations passing quickly into a tertiary phase, the onset of which denotes failure. At low stresses, and depending upon test duration, a secondary creep stage may not be reached. The test data considered here are well described by secondary creep behaviour. The form of the flow law for secondary creep takes the form (see McRoberts et al 1978)

$$\dot{\varepsilon} = A\, \sigma_d^n / (1-T)^m \quad \ldots\ldots\ldots\ldots\ldots\ldots\ldots\ldots 1$$

where A, m, and n are constants determined by testing, $\dot{\varepsilon}$ is the secondary creep rate, σ_d the applied deviator stress, and T is the temperature. In some cases, Equation 1 takes a bilinear form, see Equation 3.

There has been considerable discussion on the magnitude of exponent, n, in Equation 1. Nixon and McRoberts (1976) considered creep data for ice and reported a range of n from near 1.0 up to 4.0 as a function of temperature and shear stress level. More recently Morgenstern et al (1980) and Sego and Morgenstern (1983) report that n converges on 3 for ice. This is in agreement with Paterson and Budd (1982) who conclude that n = 3 for glacial ice. As noted by McRoberts (1982), low n values reported by Nixon and McRoberts (1976) were influenced by low shear stress, relatively warm tests on well-strained glacial ice with preferentially oriented ice crystal structure. McRoberts (1982) reported a best fit n = 3.2 for artificially prepared ice with randomly oriented crystal structure.

Creep data for ice rich permafrost soils support a value of n = 3. Roggensack (1977) reported creep tests on undisturbed samples of ice-rich fine-grained glaciolacustrine soil and reported a bilinear flow law. However by eliminating certain data he defined a flow law with n=2.75. McRoberts et al (1978) tested ice-rich glaciolacustrine silts and reported a bilinear flow low with n = 3.0 at low stress. However at higher stresses, where creep response was dominated by samples which ultimately reached tertiary creep, an exponent value of 6.0 was reported.

The magnitude of the exponent m in Equation 1 accounts for temperature effects. McRoberts et al (1978) used an m value of 1.8, based on correlations with ice as reported by McRoberts (1982). Nixon (1978) provided a re-analyses of the McRoberts et al (1978) data and used a value of m = 2 for a reference temperature of -2.5°C. Creep data for ice reported by Morgenstern et al (1980) is presented in the form of log A, versus log (1-T) following Nixon and Neukirchner (1984), see Figure 1. The slope of log A, versus log (1-T) defines the m parameter, which for ice appears to be m = 2 for T = -1°C and m = 1 for T colder than -2°C.

SAMPLE DESCRIPTION

The creep test data reported by Roggensack (1977),

McRoberts et al (1978), and Savigny and Morgenstern (1986) as well as additional data reported here are all for icy permafrost soils obtained in the Mackenzie River Valley between Fort Simpson and Norman Wells NWT. The test data discussed here is referred to as B, E, G and P Series, from Northern Engineering Services Company Ltd. (1977), the data from Roggensack (1977) as R series, and from Savigny and Morgenstern (1986) as S series. The B series samples were described in detail by McRoberts et al (1978). The E series samples were obtained by horizontally coring in the headscarp of a large landslide in close proximity to the site discussed by Roggensack (1977). The G series were obtained from the same boreholes reported by Savigny and Morgenstern (1986). The P series are peat samples obtained from an elevated peat bog in the Fort Simpson area. Table 1 summarizes the index properties of the samples tested. A list of the water (ice) content data is given for each sample in Table 2 as well as in McRoberts et al (1978) for B samples.

TABLE 1

Properties of Test Samples

Sample Series	Sand (%)		Silt (%)		Clay (%)		L.L. (%)		P.I. (%)		USC
B	1	11	53	79	17	38	31	60	16	26	ML or MH
E	0		55	76	24	45	38	48	16	26	CI
G	0	42	50	63	7	50	48	59	15	35	MH, ML or CH
P	Fibrous Woody Peat										

The B samples consisted of a finely banded stratified ice with sub-parallel bands of visible ice from 5 to 20 mm in thickness separated by soil layers of equivalent thickness. The E samples, obtained by horizontally coring in ice-rich glaciolacustrine soils, have the same general water content range as the B samples, but have an entirely different ice structure. The ice in the E samples exists as substantial veins up to 80 mm thick oriented at varying angles to the main axis of the sample. The G cores obtained by vertical sampling of fine grained glaciolacustrine clay have lower water contents of typically 22% to 30% with one sample at 74%. Visible ice was usually present in the form of thin lenses and inclusions even in the lower water content samples. The P series samples had considerable visible ice with water (ice) contents ranging from 410% to 2000%.

Details of laboratory equipment and testing procedures are discussed by McRoberts et al (1978). In all cases creep interpretations were done using large size computer derived plots of temperature versus time, strain versus time and log strain rate versus log time. The average creep rate of the sample could then be easily determined from the slope of the straight line segment of the strain-time curve. The creep rate so obtained was then compared against the log $\dot{\varepsilon}$ versus log t to check that a secondary creep stage had been reached. An example of the type of plot used to derive strain rates for all tests quoted here is given in Figure 2. In this particular test, primary creep ended at about 3.0×10^4 min. For the next 3.0×10^4 min. a secondary rate of $\dot{\varepsilon} = 9.09 \times 10^{-1}$/year was calculated at a temperature of -1.2°C. A rise in temperature to -1.0°C then resulted in a second period of secondary creep at a rate of 1.12×10^{-1}/year. Typical strain time plots for some 30 B series samples are given as Figures 1 to 7 in McRoberts et al (1978).

A limited series of tests were conducted with confining pressures of from 28 to 276 kPa using jacketed samples and either air, mineral oil, or a weak methanol solution as cell fluid, see McRoberts et al (1987). The R series had a light mineral oil as cell fluid, no membrane, and a light coat of ice sprayed on the sample as a jacket. No penetration of oil into the sample was reported. S series samples were unjacketed.

Test temperatures ranged from -0.8°C to -4.0°C and with the majority at -1.0°C and -3.0°C. Testing duration varied depending upon stress level. For samples that resulted in creep rupture the test duration ranged from 1×10^1 to 2×10^4 min. Long-term tests at low stress levels ranged in durations from 2×10^4 to 2×10^5 min. In certain cases, tests were terminated after significant test durations but before a secondary creep stage, as evidenced on a log $\dot{\varepsilon}$ - log time plot was reached. Such tests are separately identified.

SECONDARY CREEP INTERPRETATIONS

Basic data for each sample tested are given either in Table 2 or by McRoberts et al (1978). The greater part of the creep data is for temperatures near -1.0°C. All B,E,G and P series data was first grouped together using $m = 2.0$ to a reference temperature of -1°C using Equation 2, McRoberts et al (1978), see Figure 3. A cross superimposed on the series symbol indicates the creep test terminated in creep rupture. A vertical line denotes that the sample was tested in a confined condition. A best fit upper bound line to all data was obtained by judgment to be:

$$\dot{\varepsilon} = (4.0 \times 10^{-7} \sigma_d^{3.0} + 2.16 \times 10^{-14} \sigma_d^{3.0}) / (1-T)^{2.0} \quad \ldots 2$$

This relationship exhibits a marked bilinear form. The exponent $n = 6$ is heavily influenced by samples that ultimately failed. Many samples at stress levels above 400 kPa did not fail, but may well have done so for sufficiently long test durations. A best fit average line to these data using statistical methods has not been obtained, but would clearly result in significantly lower creep rates than those predicted by the upper bound relationship of Equation 2.

Figures 4, 5 and 6 consider three temperature ranges of B,E,G and P series data at average reference temperatures of -1.0, -2.5 and -3.5°C, respectively. As ice data reported in Figure 2 suggest a variation in m as a function of temperature an $m = 2$ was used for the soil data between -0.5 and -1.5°C and an $m = 1$ for colder data. All samples which failed were eliminated in Figures 4,5 and 6. Figure 4 suggests the flow law for ice is slightly non-conservative and an upper bound consisting of the first term of Equation 2 is a good fit to the warm soil data. For soil data between -2.0 and -3.0°C the ice data is a reasonable upper bound. The data colder than -3.0°C is solely B series data and the greater part of the data suggests creep rates somewhat less than ice. Various attempts were made to quantify reasons for the scatter apparent in the data by considering index properties, soil classifications and so forth. However, no

orderly pattern was found. It is possible that ice structure and the favourable orientation of ice lenses with planes of higher shear stress may play a role.

The soils considered here confirm a flow law with n of 3 at lower stresses. At higher stresses n can become greater than 3 for frozen soils and a bilinear flow law has been presented in this study, Equation 3. While it might be argued see Savigny and Morgenstern (1986) that the secondary creep interpretation should not be applied to stress levels which result in failure it is important to note that transient creep rates at higher stress levels will be higher than that predicted by an n of 3. This factor may be important in a variety of design considerations.

Equation 2 is not viewed as being a realistic upper bound relationship for soil data colder than about $-1.5^{o}C$. For soil temperatures colder than $-2.0^{o}C$ and for shear stress levels less than about 400 kPa the upper bound of soil behaviour follows the flow law for ice. That is:

$$T<-2.0^{o}C;\ \dot{\varepsilon} = 6.1x10^{-8}\sigma_d^{3.0}/(1-T)^{1.0} \quad . \ . \ . \ . \ . \ 3$$

For warm soil, the first term of Equation 3 applies, that is:

$$-0.8>T<-1.5^{o}C;\ \dot{\varepsilon} = 4.0x10^{-7}\sigma_d^{3.0}/(1-T)^{2.0} \quad . \ . \ 4$$

The domain between these two temperatures has not been studied further but it may be realistic to extrapolate Equation 4 to $-2.0^{o}C$.

The load deformation interpretations made in this study have assumed that all soil deformation results from creep of the ice matrix. As discussed by Brodskaya (1962), Tsytovich (1975) and more recently by Nixon and Lem (1984) frozen soils may exhibit a volumetric strain or consolidation effect. Some proportion of the creep response measured in the tests reported here may be influenced by consolidation. It might be speculated that consolidation could result in the slightly greater creep of ice rich soils compared to ice creep at the $T = -1.0^{o}C$ reference temperature, i.e., Figure 4.

R AND S SERIES TESTS

In this study short duration 1A to 6A tests of the R series and unacceptable rated S series tests have been eliminated from any comparisons. If R and S series tests are corrected to $-1.0^{o}C$ (test range -0.7 to $-1.95^{o}C$) the comparison, not shown here, is reasonable. However, almost all R and S series data are for cell pressures from 69 to 621 kPa. It was speculated in Northern Engineering Services Company Ltd. (1977) and more recently by Nixon and Lem (1984) that an all-round or confining pressure may influence creep rate by pressure melting. The theoretical basis for pressure-melting effect in ice has been presented by Edlefsen and Anderson (1943). The effect ranges from $0.008^{o}C$/atm to $0.09^{o}C$/atm. Radd and Ortle (1973) have confirmed the $0.09^{o}C$/atm case for the case where ice pressure changes but water pressure remains constant. If this factor is applied to creep tests a decrease in strain rate would be expected for unconfined tests, due to the equivalent temperature increase. This was observed in the R series tests although an increase in creep rate; see Roggensack (1977) was expected on changing from a confined to unconfined stage.

Figure 7 presents all confined B,G,R and S series tests with and without the melting point factor applied, and corrected to a reference temperature of $-1.0^{o}C$. All B,E,G,P,R,S series data with temperatures between $-0.5^{o}C$ and $-1.5^{o}C$ and using the pressure melting correction factor for confined tests, are collated in Figure 8. Most R series data correct close to the upper-bound relationship, Equation 5.

Consolidation effects and the lack of a cell membrane may cause faster creep rates for R and S series tests. Higher confining pressure may promote volumetric straining due to consolidation. It may also be speculated that the lack of a membrane in the R and S series tests in which cell pressures were applied by paraffin could have resulted in enhanced creep.

CONCLUSIONS

Laboratory techniques are capable of measuring creep rates of down to about 5×10^{-3}/year. Long-term testing would benefit from the ability to measure deflections to at least 2 to 5×10^{-5} cm.

Most samples exhibited a secondary creep mode of deformation; however, in some tests creep rates were still decreasing at the end of the test. Samples exhibited a creep response similar to that of ice even with water (ice) contents as low as 22% to 25%. Soils with such water contents are capable of undergoing thaw settlement suggesting that excess ice is present in the soil skeleton. This suggests that even small volumes of ice exert a dominant influence on creep response. While the creep data presented and reviewed here is consistent, there is considerable variation in the creep response at a given stress level. Such variation might be expected keeping in mind that natural samples have been tested. The data considered here confirm a secondary creep flow law for ice with $n = 3.0$. At higher stresses a bilinear flow law with $n = 6.0$ may be appropriate in certain design applications. The data suggests that the creep rate for permafrost soils at temperatures of $-1.5^{o}C$ or warmer can creep faster than ice. At temperatures colder than $-2.0^{o}C$ ice creep data constitutes a good upper bound to soil creep. The soil data also supports an $m = 2$ for temperatures near $-1.0^{o}C$ and $m = 1$ for temperatures below $-2.0^{o}C$.

Creep tests undertaken with substantial cell pressures apparently accentuate creep rate. This may be due to pressure melting or consolidation effects. It can be speculated that for the warm soils tested that portion of the creep response faster than ice at the same temperature may be a consolidation effect.

REFERENCES

BRODSKAYA, A.G. 1962. Compressibility of frozen ground Izd-vo Akad.Nauk.SSR

EDLEFSEN, N.E. and ANDERSON A.B.C. 1943. Thermodynamics of soil moisture. Hilgardia, Vol.15, pp.31-298.

MCROBERTS, E.C. LAW, T.C. and MURRAY, T.K. 1978. Creep tests on undisturbed ice-rich silt. 3rd. Int. Conf. on Permafrost. Edmonton, Alberta, Canada, pp.540-555.

MORGENSTERN, N.R., ROGGENSACK, W.S. and WEAVER, J.S. The behaviour of friction piles in ice and ice-rich soils. 17(3), pp.405-415.

NIXON, J.F. 1978. Foundation design approaches in permafrost areas. Can. Geotech. J., 15(1), pp.96-112.

NIXON, J.F. and LEM, G. 1984. Creep and strength testing of frozen saline fine-grained soil. Can. Geotech. J., 21(3), pp.518-529

NIXON, J.F. and MCROBERTS, E.C. 1976. A design approach for pile foundations in permafrost. Can. Geotech. J., 13(1) pp.40-57

NIXON, J.F. and NEUKIRCHNER, R.J. 1984. Design of vertical and laterally loaded piles in saline permafrost. Third Internation Symposium Cold Regions Engineering Edmonton, Alberta.

NORTHERN ENGINEERING SERVICES COMPANY LTD. 1978. Interim report on creep testing of permafrost soils. Northern Engineering Services Company Ltd., Calgary, Alberta 1977.

PATTERSON, W.S.B. and BUDD , W.F. 1982. Flow parameters for ice sheet modeling. Cold Regions Science and Technology, 6 pp.175-177.

RADD, F.J. and ORTLE, D.H. 1973. Experimental pressure studies of frost heave mechanisms and the growth-fusion behaviour of ice. North American Contribution, 2nd Int. P.F. Conf., Yakutsk, pp.377-384.

ROGGENSACK, W.D. 1977. Geotechnical properties of fine-grained permafrost soils. Unpub. Ph.D. Thesis, Univ. of Alberta, Edmonton, Canada.

SAVIGNY, K.W. and MORGENSTERN, N.R. 1986. Creep behaviour of undisturbed clay permafrost. Can. Geotech. J., 23(4), pp.515-527.

TSYTOVICH, N.A. 1975. The mechanics of frozen ground. McGraw Hill.

TABLE 2

Test Data

B Series					E Series					G Series					P Series				
1	2	3	4	5	1	2	3	4	5	1	2	3	4	5	1	2	3	4	5
115	200	138	-1.0	4.3E-2	81	14	0	-3.0	4.6E-4	22	207	0	-2.0	6.8E-2	1000	414	0	-3.0	2.7E0 *
93	14	276	-1.0	2.0E-3	78	69	0	-3.0	2.0E-3	26	138	0	-2.2	2.1E-2	729	207	0	-2.3	2.3E-2
55	414	138	-1.1	4.4E-2				-1.2	1.9E-2	30	69	0	-2.2	2.8E-3	908	564	0	-2.3	8.1E0 *
107	276	138	-1.1	8.0E-1	144	413	0	-1.0	9.8E+1	24	138	0	-1.0	3.3E-2	542	35	0	-2.8	6.1E-4
118	207	69	-1.0	2.7E-1	44	103	0	-2.2	6.7E-3	22	69	0	-2.2	1.7E-2	683	69	0	-2.9	3.0E-3
120	138	69	-1.1	5.6E-2	74	280	0	-2.4	2.5E-1	28	414F	0	-1.8	1.1E+1	567	138	0	-2.9	2.4E-2
79	14	0	-1.3	1.1E-3*				-2.9	1.5E-1		276	0	-1.9	1.8E-2	558	690	0	-2.7	1.1E+2
112	414	138	-0.7	5.5E0	26	138	0	-2.9	4.0E-3	21	276	138	-1.8	5.4E-2	1077	104	0	-2.3	1.6E-2*
92	35	0	-0.8	3.4E-3*				-1.5	6.8E-3	22	138	0	-1.9	5.1E-3	864	690	0	-2.3	3.4E+1
110	276	138	-3.3	9.8E-1*	50	413F	0	-1.0	1.9E+1	22	207	0	-2.0	7.6E-1*	531	414	0	-1.7	1.1E+1
111	207	138	-3.1	8.1E-1*	118	34	0	-2.7	1.8E-3*	26	158	138	-0.8	2.8E-2	570	721	0	-0.7	2.4E+2
						104	0	-1.8	6.6E-2*	30	138	0	-1.2	2.3E-2	725	1380F	0	-0.7	5.7E+3*
					87	138	0	-2.5	1.3E-2*	74	138	0	-1.2	9.1E-2	549	138	0	-1.4	1.6E-2
					254	276F	0	-0.8	1.9E0				-1.0	1.1E-1		138	0	-1.3	2.1E-2
					96	69	0	-2.5	4.8E-3*	30	69	0	-1.2	3.3E-2	652	69	0	-1.9	2.0E-2
					131	207	0	-1.0	4.2E-1	23	207	0	-0.8	7.5E-3	748	1380F	0	-0.8	2.9E+3*
					114	138	0	-1.1	8.3E-2	23	138	0	-2.8	1.7E-2	482	138	0	-1.2	5.3E-2
					151	207	0	-1.0	8.3E-1*						409	69	0	-1.3	1.8E-2
					67	414F	0	-1.0	2.6E0						448	414	0	-1.1	4.0E+1
					53	69	0	-0.9	1.6E-2						496	690	0	-0.9	1.4E+2*
					65	69	0	-0.9	1.3E-2						181	69	0	-2.7	9.7E-4
					62	689F	0	-1.0	2.2E+2							69	0	-2.8	6.8E-4
					37	200	0	-3.0	2.1E-2						1988	34	0	-2.2	1.9E-3
					47	207	0	-2.5	2.8E-2										
					59	689F	0	-1.0	3.3E+2										

1. Water content (%) 2. Deviator Stress (kPa) 3. Confining Stress (kPa) 4. Temperature (^{o}C)
5. Strain Rates (yr^{-1}), (4.3E-2 = 4.3 x10^{-2})

F Denotes sample failed * Denotes sample may still be in primary creep stage.

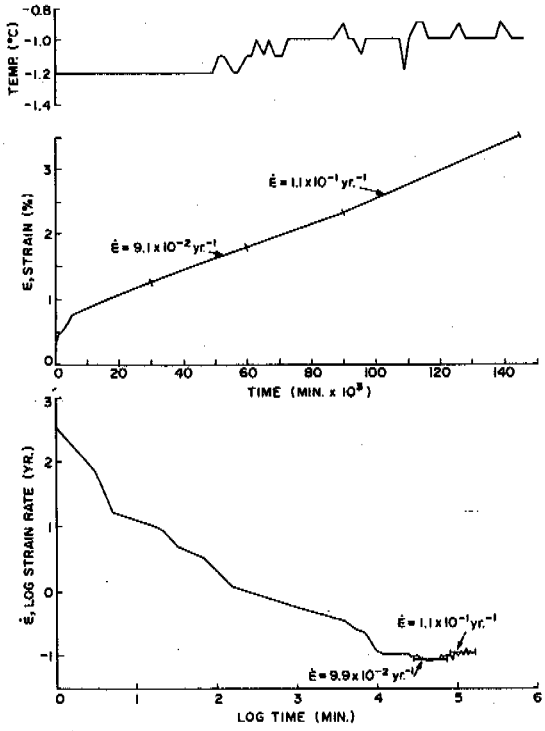

Fig. 1 Typical Test Data and Interpretation

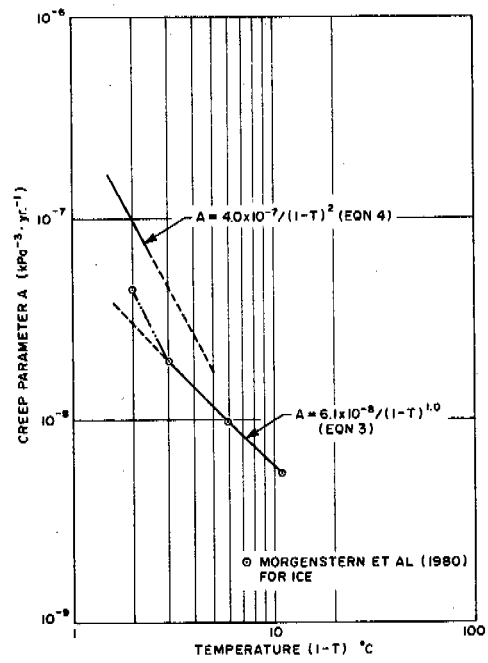

Fig. 2 Creep Data for Ice Compared with Upper Bound Soil Data

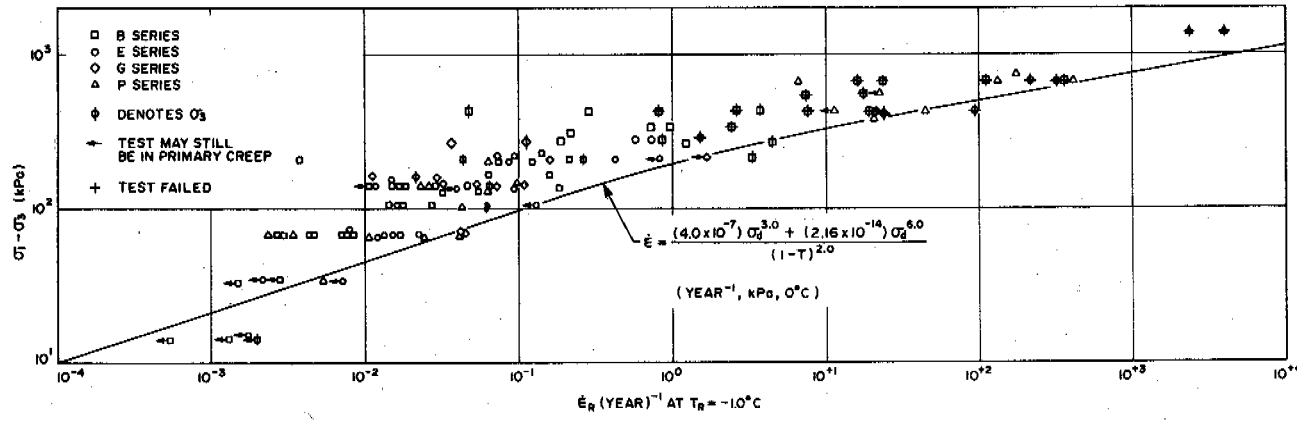

Fig. 3 B,E,G,P Series Data at Reference Temperature (T_R) of -1°C

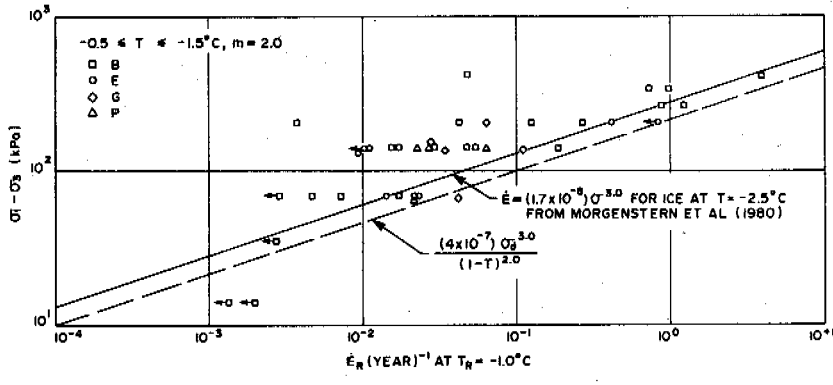

Fig. 4 B,E,G,P Series Data

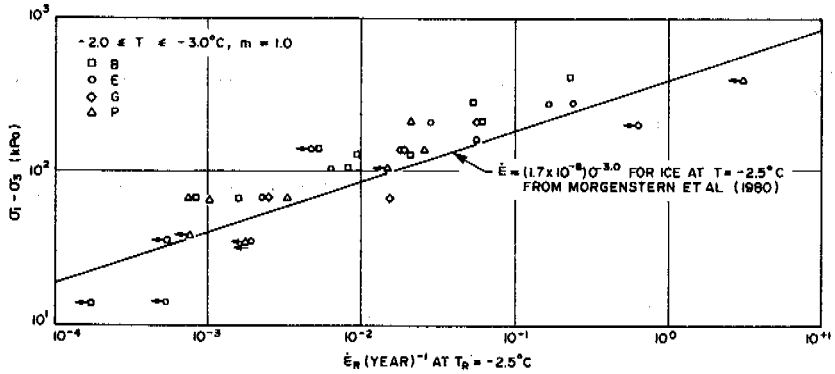

Fig. 5 B,E,G,P Series Data

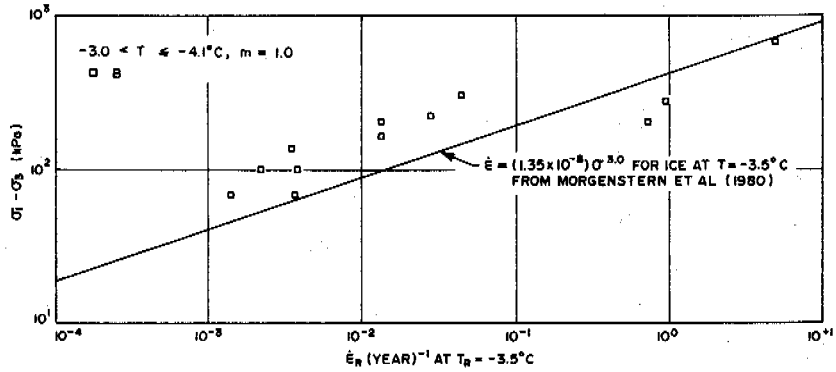

Fig. 6 B Series Data

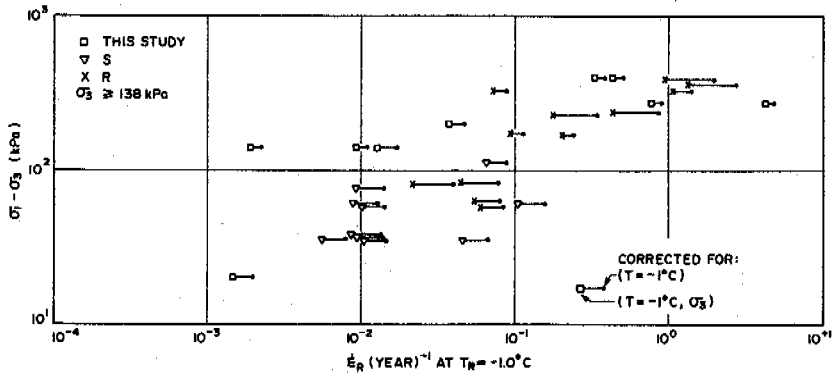

Fig. 7 Confined Test Data with and Without Pressure Melting Correction

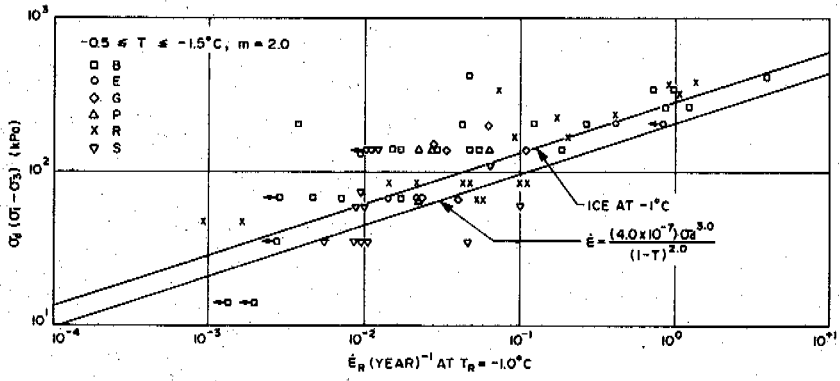

Fig. 8 All Series Data $-0.5 \leq T \leq -1.5°C$

PHASE RELAXATION OF THE WATER IN FROZEN GROUND SAMPLES

V.P. Melnikov, L.S. Podenko and A.G. Zavodovski

Institute of Northern Development, Sibirian Branch of the USSR Academy of Sciences, Tyumen, USSR

The kinetics of phase relaxation of pore water is considered to be one of the most important and complicated aspects in the problem of moisture crystallization in grounds. The kinetics of phase relaxation of the water in capillary-porous systems was the subject of numerous investigations (Anderson, 1978; Ershov, 1979; Grechishev, 1980; Chistotinov, 1973; Lishtwan, 1985). According to the data available, deceleration of moisture crystallization, i.e. a slow relaxation, is observed after the equilibrium temperature was established (fig.1).

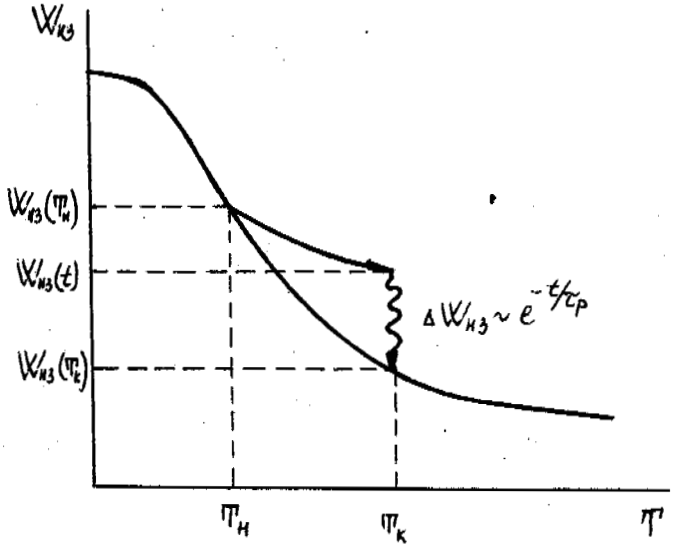

Fig.1 Non-equilibrium Crystallization of the Water in capillary - porous media

Analitical expression has been proposed, which describes moisture phase relaxation:

$$\frac{dW_{H3}(t)}{dt} = -\frac{1}{\tau_p}\left[W_{H3}(t) - W_{H3}(T)\right] \quad (1)$$

where $W_{H3}(t)$ is the non-equilibrium amount of unfrozen water at a time t; $W_{H3}(T)$ is the equilibrium amount of unfrozen water at a temperature of the environment T; τ_p is the phase relaxation time.

Deceleration of water crystallization is caused by such kinetic factors as high viscosity of the water in capillary-porous systemes, low probability of nucleation due to the destruction of the ice-like structure of water near the interphase boundary, slow interaction between the mineral framework and water and slow changes in rock structure and texture during water crystallization (Ershov et al, 1979; Chistotinov, 1973; Nesterov et al.,1984; Grechishev et al., 1980).

It is known, however, that notable structure changes are associated only with the water, adsorbed by the surface of a substrate (one or two monolayers) (Halle, Wennerstrom, 1981), which makes up but a small portion from the total amount of water in water-saturated grounds.

In porous systems with partial moisture contents water is noted to dispense in clusters, joined with each other by surface liquid films and micropores (Heifetz, 1982). The kinetics of water crystallization in such systems is strongly dependent upon random nucleation of separate clusters, the rest of the bulk liquid remains in the non-equilibrium overcooled state. The influence of the kinetics of supercooled water spontaneuos crystallization on phase relaxation of water was not analized in detail.

Thus, the proposed mechanisms of non-equilibrium water crystallization in porous systems (Ershov et al., 1979; Chistotinov, 1973; Nesterov et al.,1984; Grechishev et al., 1980) require more thorough investigation.

The analysis of experimental data on the relaxation time of water revealed that, as a rule, data were obtained through calorimetric measurements of the samples with a characteristic size $l \geq 0{,}005$ m. It was found difficult to establish and control the iso-

thermal regime of water crystallization, fitting to these samples (Kalve, Pratt, 1963). Even small thermal gradients contribute a lot to the heat flow, due to the transient processes of the temperature re-distribution over the sample's bulk. According to the data (Nesterov, Danielyan et al., 1984), the τ_p value in quartz sands, clay minerals, peat and ground, irrespective of cooling conditions of a sample, varies from some instants to 45 minutes, influenced by the dispersity and chemical-mineralogical composition of the environment.

It was shown (Lishtwan et al., 1985) that phase relaxation in peat samples, once the equilibrium temperature was established, can durate for two hours. It was also established (Grechishev et al., 1980) that temperature deformations in clay samples last for ten days after the isothermal regime was established. This thermal retarded effect is associated with slow phase relaxation of ground water (Grechishev et al., 1980).

It is thus necessary, first, to measure phase relaxation time of the water in grounds with high moisture content, taking into account the effect of transient thermophysical processes, and, second, to perform the analysis of a probable influence of spontaneous crystallization on the kinetics of the isothermal phase relaxation of the water in grounds with low moisture content.

The analysis was done of the kinetics of water crystallization for a number of disperse systems: quartz sands of different dispersity (63-71 mkm; 63-140 mkm), kaolinite, montmorillonite. The analysis was carried out by the methods of scanning calorimetry and NMR, taking into account transient thermophysical processes. For the solution of the first task measurements were taken at the negative temperature of the environment $T_{env.} = -10°C$ in order to eliminate the effect of spontaneous crystallization, for experiments have shown that in case of spontaneous crystallization the life-time of metastable state $\tau_* \ll 1$ s. The efficiency of nucleation in montmorillonite samples with moisture content W = 60-75% was studied in order to evaluate the contribution of water clusters spontaneous crystallization to the kinetics of the isothermal ground crystallization.

Calorimetric measurements reported were obtained with Perkin-Elmer quick-responce scanning microcalorimeter DSC-2 with the time constant 0.5 s in the absence of a sample. NMR- measurements were carried out with the coherent relaxometer with operating frequency of 30 MHz (Kibrik, 1980). The advantage of NMR-measurements is that transient thermophysical processes inside of the measuring cell do not distore the results of kinetic measurements of phase composition.

Relaxation times of the temperature τ_T were estimated for every sample through a standard procedure, described by Kalve (1963). The wall temperature of the measuring cell, containing a sample, was abruptly changed (with the velocity of 80°C/min) by 2-3°C and the dynamics of the heat flow q was studied in the absence of phase transition processes. Under these conditions the heat flow $q \sim \Delta T$ represents the kinetics of thermal relaxation within the sample, where ΔT is the temperature difference between the sample and the cell. The obtained values of the relaxation time of the temperature τ_T in the absence of phase transition processes do not exceed 10 s, which is several orders of magnitude higher than the time constant of the calorimeter DSC-2.

The estimation of relaxation times in waterin clay minerals and quartz sands was done with applying the techniques, described by Nesterov et al. (1984). A container with a sample was placed into the measuring cell at the constant negative wall temperature of -10°C. After some initial supercooling and decay of metastability a self-recorder registered the peak value of crystallization (fig.2), characteristic for the majority of the samples.

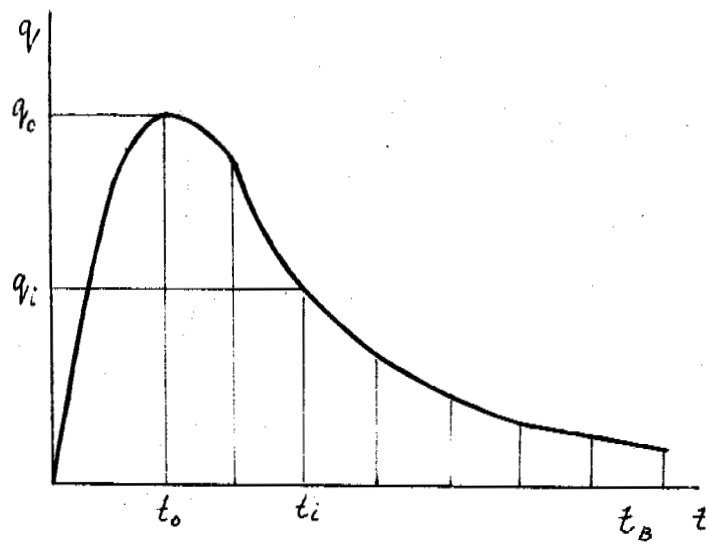

Fig.2 Thermogram of Crystallization

To determine the relaxation time of water the sloping part of the thermogram was divided into sections at arbitrary equal time spans and interpreted in terms of a well known method (Nesterov et al., 1984), taking into account thermal relaxation of the sample. The initial moment of temperature relaxation was assumed to correspond to the peak value. The process was investigated up to the time τ_B, when the deviations of the registered curves from the basic line were less than 2% as compared with the peak value. A special estimation revealed that at time intervals following τ_B no more than 10% from the total amount of water, participating in crystallization was crystallized, which made up less than 2% from the absolute total moisture content. For all samples of quartz sand, montmorillonite and kaolinite with moisture content from 25 to 50% at -10°C the times τ_p, evaluated by the method (Nesterov et al. 1984), do not exceed 20 s.

The measurements of τ_p, obtained by the

authors, differ significantly from the literature data on τ_p (Nesterov et al., 1984). Thus, according to Nesterov et al. (1984), τ_p = 800 s, whereas according to the authors' results, τ_p = 20 s. The particular feature of our experiments is that samples, much smaller in size as compared with those decribed in literature, were investigated, and measurements were carried out with Perkin-Elmer quick-responce scanning microcalorimeter DSC-2.

In order to analyze the discrepancies discovered the dependence was studied of τ_p from the amount of the sample, packed into the calorimeter cell. As is seen in table I an increase in τ_p is observed with increasing in the amount of the sample. The bottom line of table I presents data on τ_T for the same sample. As it can be seen from table I, the τ_T value also increases with quantity increasing of the sample, which is true for all investigated masses of $\tau_p > \tau_T$.

To our know, the main contribution to the obtained values of τ_p is given by the temperature relaxation processes and water phase change with characteristic times not exceeding 20 s.

TABLE I

Relaxation Times τ_p and Temperature τ_T as a Function of the Sample's Mass

M, mgm	14	23	33	46	67	94	99	103
τ_p, s	21,5	23,5	24	26	27,5	45	57	65
τ_T, s	10	10	10,5	11	10,5	20	22,5	24

Additional information on phase composition of moisture and the kinetics of ice formation in quartz sands and montmorillonite was obtained through the NMR-method. Phase composition of moisture was determined by the techniques, described by Tice et al. (1978). Thus obtained equilibrium diagram of the phase composition of montmorillonite is presented in fig.3. Fig.4 presents the dynamics of mass change in unfrozen water during its crystallization in montmorillonite. The analysis of the kinetic curves revealed that the phase composition of pore water remains unchanged after the isothermal regime was established.

So, the results of kinetic measurements on water crystallization, obtained through microcalorimetry and NMR, show that at -10°C the relaxation time of the phase composition of the total amount of water in capillary-porous media do not exceed 20 s.

Through NMR-techniques a long-term (within several days) phase relaxation of water was investigated in montmorillonite samples of characteristic size 0.01 m and with moisture

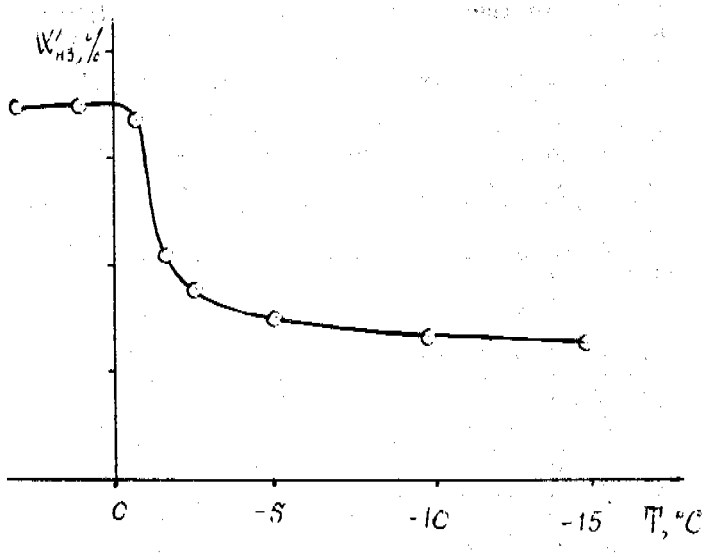

Fig.3 Equilibrium Diagram of Unfrozen Water Content in Montmorillonite with Moisture W = 70%.

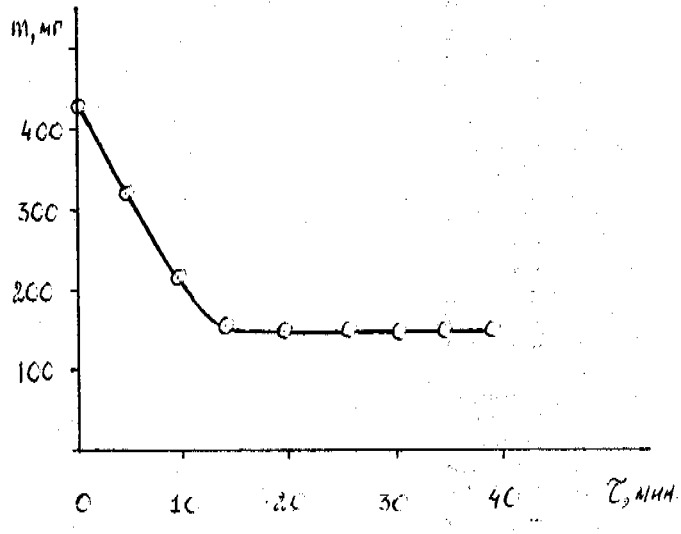

Fig.4 Dynamics of Mass Change of Unfrozen Water in Montmorillonite with W = 70% at T = -10°C

content of 25-120% at -10°C. As follows from the data obtained thermal equilibrium between the environment and the sample was established, as a rule, in an hour. Afterward unfrozen water was not subjected to any changes beyond the scope of measurement errors. After an hour the maximum deviation of unfrozen water content from the equilibrium value does not exceed 10%. Afterward the phase composition of water remains unchanged for 13 days. The results obtained revealed the absence of long-term changes of water composition in

frozen grounds at -10°C. According to our data, the period, at which the equilibrium phase composition of water during moisture-saturated grounds freezing is established, does not exceed 20 s, after the equilibrium was established between the environment and the sample. In case of large samples with high moisture content long-term transient processes are seemed to be conditioned by the temperature re-distribution over the sample's bulk.

In case of partial moisture content pore water exsists in the form of clusters. It appears to lead to a notable increase in the life-time of non-equilibrium supercooled water. In fact, the experimental results on the life-time of metastable supercooled samples with moisture content $\leqslant$ 45% revealed that the life-time of metastable water at -70°C exceeds 8 hours. In general it means that in case of partial moisture content and at temperatures $T_{mean} \geqslant -7°C$ the process of total crystallization may be decelerated due to a significant life-time of separate clusters of non-equilibrium supercooled water.

To estimate the mean (τ_*) value of the life-time of a supercooled water cluster the efficiency J_* of nucleation was determined for montmorillonite with moisture content 60-75% at - 56°C. It was established that $J_* \sim 10^6 s^{-1} m^{-3}$ at T = -5,6°C.

With the help of correlation (Franks, 1985)

$$\tau_* = \frac{1}{J_* \cdot V} \qquad (2)$$

the mean life-time of a fixed size cluster could be estimated. Thus, the τ_* value exceeds 10 days at T = -5,6°C and at the size of 100 mkm.

This latter proves that deviations in the kinetics of thermophysical changes in grounds within upper horizons of the cryolithozone may be, in many cases, conditioned by cyclic temperature changes (Melnikov, 1987).

REFERENCES

ERSHOV, E.D. et al. (1979). Fazovyi sostav vlagi v merzlih porodah. Moskovskyi Gosudarstvennyi Universitet, Moskwa.

CHISTOTINOV, L.V. (1973). O relaksacionnom haraktere kinetiky kristallizacii vlagy v gornih porodah. Sbornik "Problemi geokriologii", Sibirskoe Otdelenie Akademii Nauk SSSR.

FRANKS, F. (1985). Voda i vodnie rastvori pri temperaturah nije 0°C. Naukova Dumka, Kiev, 338s.

GRECKISHCHEV, S.E, CHISTOTINOV, L.V, SHUR, Y.A. (1980). Kriogennie phisikogeologicheskie processi i ih prognoz. Nedra, Moskwa, 328s.

HALLE, B, WENNERSTROM, H. (1981). Interpretation of magnetic resonance data from water nuclear in heterogeneous systems. J.Chem.Phys., V.75,(4), 1928-1943.

HEIFETZ, L.I, NEIMARK, A.V. (1982). Mnogophaznie processi v poristih sredah. Himia, Moskwa.

KALVE, E, PRATT, A. (1963). Mikrokalorimetria Inostrannaya Literatura, Moskwa.

KIBRIK, G.E. (1980). Moduliator impulsnogo spektrometra yadernogo magnitnogo rezonansa. (3). P.T.E.

LISHTWAN, I.I, BROVKO, G.P, DAVIDOVSKYI, P.I. (1985). Issledovanie fazovogo sostava vodi v torfe kalorimetricheskim metodom. Ingenernaya Geologia, Nauka, (4),s.114-120.

MELNIKOV, V.P. (1987). Electrophyzicheskie issledovaniya merzlih porod. Nauka,Moskwa

NESTEROV, I.I, DANIELIAN, Y.S, YANITSKYI, P.A, GALIEVA, V.N. (1984). Neravnovesnaya kristallizacia vlagi v merzlih gruntah. Dalnevostochnoe Otdelenie Akademii Nauk SSSR, t.277, (4), s.928.

TICE, A.R, BURROUS, C.M, ANDERSON, D.M.(1987). Composition measurements on soils at very heit water contents by pulsed Nuclear Magnetic Resonance Tecnique. Trans.Res. Bord., 16-20, Washington.

STANDARD METHOD FOR PILE LOAD TESTS IN PERMAFROST

R.J. Neukirchner

Dames & Moore, Golden, Colorado, USA

Synopsis: The completion of a pile load test in permafrost involves the expenditure of considerable time and money. Documented pile load test programs have been completed using a variety of methods; however, no accepted, uniform set of test procedures exists. The American Society for Testing and Materials (ASTM) is developing a standard method for conducting axial compressive pile load tests in permafrost. This paper outlines the proposed standard test method. It presents the key permafrost-related aspects of the test method and discusses the rationale used in their development.

INTRODUCTION

The practice of engineering is based in large part on the ability to predict the behavior of materials in response to applied loading conditions. Engineers often rely on the results of laboratory and field tests on test materials and/or systems to describe the behavior of real materials and/or systems. In order to ensure the reliability and repeatability of the results of these tests, standard testing methods are used. One of the major functions of the American Society for Testing and Materials (ASTM) is to assist in the development, documentation and distribution of standard test methods and procedures. ASTM has, in 1986, established Subcommittee D18.19, Frozen Soil and Rock, to address the key issues associated with the identification, classification, evaluation and testing of frozen earth materials.

The subcommittee is currently developing a "Standard Method of Testing Individual Piles in Permafrost Under Static Axial Compressive Load". Before the standard test method is adopted, it must be reviewed and adopted by the current subcommittee, by committee D-18 on Soil and Rock and, finally, by the overall membership of ASTM. This paper presents the key permafrost-related aspects of the proposed test method as well as the rationale used in its development.

BACKGROUND

The completion of a pile load test program in permafrost involves the expenditure of considerable time and money. Documented pile load test programs have been completed using a variety of methods. These programs, many of which are listed in Table 1, have been designed and carried out by leading engineers and organizations without the benefit of an agreed upon, standard test method or procedure. Each test program has added to the overall state-of-the-art regarding the behavior of pile foundations in permafrost. The various procedures used and test results obtained have enabled the validation of theories on permafrost behavior and the development of current analytical procedures. Valuable lessons have been learned from each program.

The development of a standard test method will build on the lessons learned to enable future test programs to proceed with the knowledge that, if carefully planned and executed, the data they produce will be reliable and repeatable and will allow for a realistic assessment of actual pile behavior.

In the development of any such test method, however, conflicts between theory and practice exist. The desire for scientific purity and precision are opposed by the limited time and funds which invariably exist; compromises must be made. The proposed test method represents compromises between the desired and the achievable.

PILE LOAD TEST OBJECTIVES

The proposed test method will provide data on the behavior of the test pile in its environment. The test results, in themselves, will not directly provide or confirm design criteria for actual piles. Inherent differences between short term and long term behavior of frozen materials, physical differences between the test pile and the actual pile and differences in the test pile environment (air and ground temperatures) and the design conditions for the actual pile must first be evaluated and accounted for. The load test data must be analyzed in light of the above.

A satisfactory method for testing piles in permafrost must provide reliable data on the behavior of a loaded test pile which can be used to predict the behavior of actual piles under actual load conditions. The test data must be adequate to describe the similarities and to evaluate the differences between the test pile and the actual piles. The test data must be suitable for use with existing analytical techniques and must be reliable.

TABLE 1 - PARTIAL LISTING OF PUBLISHED PILE TEST DATA

Source	Pile Type	Effective Pile Diameter(m)	Installation Procedure	Type of Loading	Test Duration (hr)
Vyalov (1959)	Wood	0.035		Static	650-9000
	Concrete	0.10-0.22	Driven	Static	1000
	Wood	0.035		Incremental	120/load
Crory (1963)	Wood	0.15-0.25	Slurried	Incremental	24/load
	Steel Pipe				
	Steel H				
Dokuchayev and Markin (1971)	Concrete	0.40	Driven	Static	360
Johnston and Ladanyi (1972)	Steel Rod	0.15	Grouted	Static	1500
Rowley, Watson, Ladanyi (1973)	Wood	0.46	Slurried	Incremental	24/load
Vyalov (1973)	Concrete	0.16-0.25	Driven	Incremental	720-1600
Goff (1974)	Steel Pipe	0.30	Slurried	Static	0.1-48
Luscher, Black, McPhail(1983)	Steel Pipe	0.45	Slurried	Incremental	72/load
Manikian (1983)	Steel H, Steel Pipe	0.27-0.45	Driven	Incremental	0.25-720/load
Dipasquale, Gerlek, Phukan (1983)	Steel H	0.25	Driven	Incremental	0.5-12/load
Nixon (1988)	Steel Pipe	0.14	Slurried	Incremental	50-160/load

In order to facilitate the extrapolation of the test data to the design of actual piles, the test pile and the actual piles should be made of similar material, have a similar shape and size, and be installed with similar procedures and equipment.

In order to correctly analyze the test data, the environmental conditions (ground and air temperatures) during the test must be recorded to allow comparison to design environmental conditions.

Test data which describe both the time-deflection (creep) and ultimate (failure) load behavior of the test pile must be developed in order to allow the prediction of the creep behavior and ultimate load capacity of the actual piles. The test data must be developed through the use of carefully designed, installed and calibrated measurement systems.

In order to provide test data which can be reliably used to predict actual pile behavior, the test method must minimize the impact of short term effects. Such short term effects include dissipation of lateral stresses which occur during pile freeze-back and minimization of the effect of "load history" on incrementally loaded piles.

The standard method of testing described herein has been developed to address the issues listed above and to provide reliable, consistent data on the behavior of loaded test piles which can be used effectively by qualified engineers to adequately predict the behavior of actual piles.

TEST PILE INSTALLATION

Following is a summary of the key requirements included in the section headed "Test Pile Installation". The requirements are aimed at insuring that the performance of the test pile is representative of the behavior of the actual piles and that an adequate evaluation of the ground thermal regime can be made.

The installation procedure used for the test pile should be similar to that anticipated for use in the actual pile installation. The pile similarities should encompass specifications, material, equipment and also, by inference, site conditions. For driven piles, procedures for pre-drilling, soil warming and pile driving should be similar for the test pile and the actual piles; the test pile driver should have a similar ratio of delivered energy to pile mass as the driver to be used for actual pile installation. For slurried piles, the type of drill rig for the test pile should be similar to that to be used for actual pile installation; the slurry material, its gradation and placement procedures should be similar to those to be used for actual pile installation.

The test pile must be installed in a manner to eliminate contact with the soil in the design active layer. Pile sleeves or casings can be used. For slurried piles, greases and friction-reducing materials may be acceptable for this purpose.

The engineer must specify a procedure for addressing end-bearing. Acceptable procedures would include measurement (strain gages or pressure cell), elimination (provide compressible layer or void space below the pile tip) or analytical evaluation of end-bearing resistance.

Ground temperature monitoring devices must be installed adjacent to the test pile surface and monitored periodically prior to and during testing. A minimum of three measurement points is required. For piles greater than 3m in length, spacing of measurement points at 1.5m spacings is recommended.

TABLE 2
Minimum Test Delay Times
Delay Time (Days after Freezeback)

Ground Temperature	>-5°C	<-5°C
Soil Type		
Ice or Ice-Rich Soil	2	3
Course-grained soil	10	14
Fine-grained soil (including silty sands)	14	21

Pile testing must be delayed until freezeback has occurred and until lateral pressures generated during freezeback have dissipated to a nominal level. Temperature measurements will be used to determine when freezeback occurs. Lateral stresses, according of Ladanyi et al (1987), will be at a maximum after pile driving or freezeback and will dissipate slowly with time at a rate dependent on soil type, temperature, pile geometry and initial lateral stress. Minimum delay times, after freezeback, proposed in the test method are shown in Table 2.

APPARATUS FOR APPLYING LOADS

Following is a summary of the key requirements included in the section titled "Apparatus for Applying Loads". The requirements have been developed to insure accuracy of load application and overall test safety. The requirements are consistent with past pile load test procedures and are based on procedures included in ASTM D-1143, the equivalent standard procedure for piles in thawed soils.

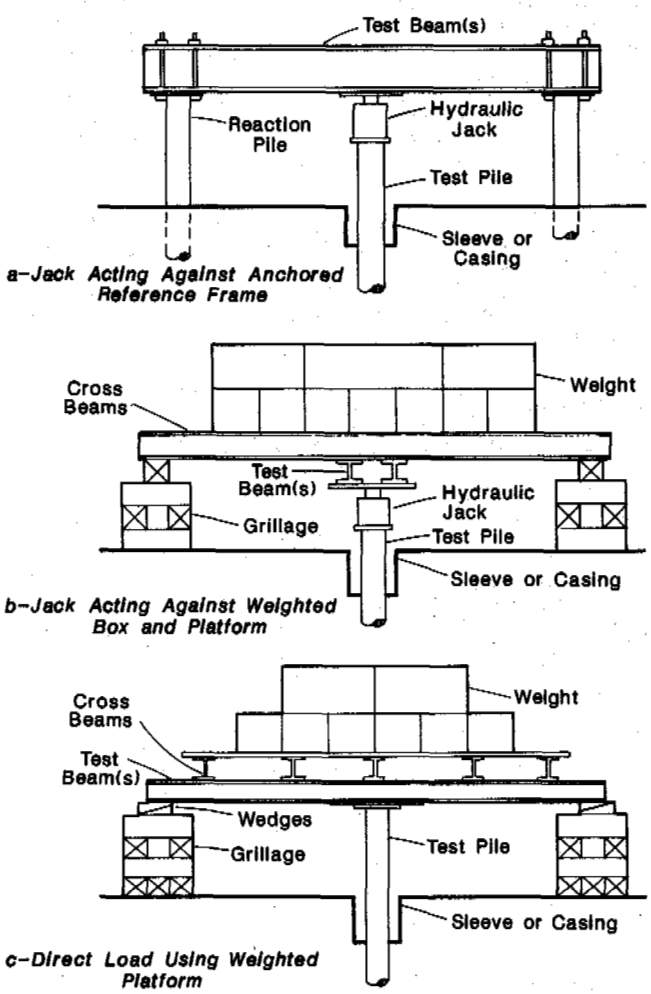

Figure 1 – Acceptable Loading Systems

Load Application may be accomplished by direct load or through a mechanical or hydraulic system. Loads may be generated by known weight, or by jacking against a dead load or a structural framework. Figure 1 shows three examples of acceptable loading systems. Accuracy of the loading system must be maintained to within two percent of the minimum applied load. Because of the duration of the tests, load certainty, or reliability, must be provided. Jacks must be accurately calibrated at expected test temperatures; load accumulator devices may be required.

APPARATUS FOR MEASURING MOVEMENT

Following is a summary of the key requirements included in the section titled, "Apparatus for Measuring Movement". The requirements have been developed to provide for the acquisition of reliable data suitable for use in the analysis of test pile behavior..

A primary and a secondary system must be provided for the measurement of axial pile top movements. The primary system must have an accuracy of 10^{-4} in (2.5×10^{-4}cm); the secondary system must have an accuracy of 10^{-2} in (2.5×10^{-2}cm). The secondary system is provided as an overall check on the primary measurement system.

The reference beam system must be designed and constructed to minimize unaccounted for movements. The systems must provide adequate structural stability and must be shielded from wind, precipitation and direct sunlight. Each reference beam must include a temperature measurement point which is to be periodically monitored during each test. Prior to a test, readings of air temperature versus deflection of the reference beam system must be made and used as a basis for developing a deflection correction for reference beam temperature.

Incremental strain measurements or intermediate pile movement measurements are not mandatory but are included as optional requirements in the proposed standard. Either system would allow an assessment of pile load distribution with time and depth. The measurement of lateral pile top movement is also included as an optional requirement.

LOADING PROCEDURES

Following is a summary of the key requirements included in the section headed "Loading Procedures". The standard defines pile failure as the onset of an accelerating creep rate or incremental deflections which increase with subsequent, uniform time increments. Careful, periodic measurements of load, pile top movement, ground temperature and reference beam temperature must be recorded in order to allow for proper evaluation of the pile behavior.

The standard defines a Base Test Load as the applied load acting on the test pile in the context of the then-existing ground temperatures which is equivalent to the actual pile design load. In order to convert a Base Test Load to a design pile load, or vice-versa, the engineer must account for differences in ground

temperature during the test period and design conditions as well as differences in diameter and/or length between the test pile and the design pile. Published relationships between soil strength, or creep, and temperature may be used to adjust the Base Test Load to the design pile load.

The current test procedure requires the engineer to establish a tentative relationship between pile load and time to failure. A relationship such as that developed by Vyalov (1959), as illustrated in Figure 2, may be used. The tentative relationship will be used to select a short-term failure load for the test pile and may be used in the analysis of load test data. The procedure for loading piles is given as follows:

- The test load should be applied in a continuous, uniform manner until the test load is achieved. The load should be applied quickly (5-10 min.) but not at a rate which will cause rapid, progressive failure of the pile during the loading process. Impact loads are not permitted.
- The test load should be held at its designated value until either pile failure occurs or a "uniform" creep rate is obtained. If failure does not occur, loads must be maintained for a minimum of three days. Prior to the load test, the engineer must establish criteria for defining what constitutes a "uniform" creep rate for the particular test conditions.
- After either pile failure or uniform creep occurs, the applied load should be removed as quickly as possible and rebound deflection measurements shall be taken.
- The test pile shall remain unloaded for 24 hours before a subsequent test load, if required, is applied.

TEST PROCEDURE

Following is a summary of the key requirements included in the section headed "Test Procedures". The test procedures make use of the Base Test Load and the tentative relationship between strength and time established, as described above, by the engineer.

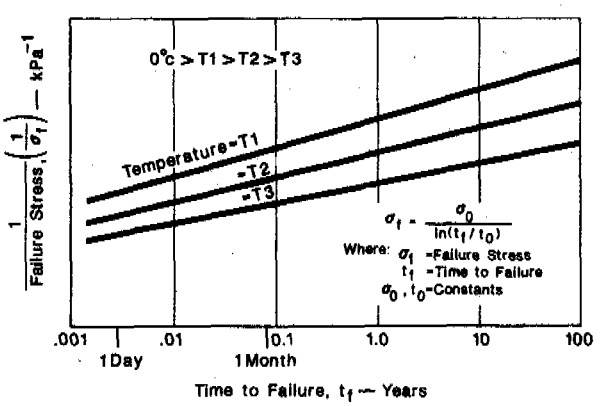

Figure 2 - Vyalov Relationship Between Failure Stress and Time

The proposed standard contains three acceptable test procedures - Standard, Alternate and Confirmation Test Procedures. Other acceptable procedures may be added in the future as either new data, new analytical procedures or new design needs dictate.

The Standard Test Procedure is the basic procedure for testing piles in permafrost. It is applicable to all soil and ground temperature conditions and should be used where no other pile test data for similar conditions in the same area are available. The procedure requires the testing of two piles; each pile will be loaded with two test load increments as listed in Table 3. A creep load increment and a failure load increment will be applied to each pile. The Standard Test Procedure will yield two pile failure load data points and at least two pile creep load data points for use in subsequent analysis of test data.

The Alternate Test Procedure is equivalent to the Standard Test Procedure as regards its area of applicability. It may be a more useful procedure in non-ice rich soils. The Alternate Test Procedure requires the testing of three piles; each pile will be loaded with one test load increment as listed in Table 3. Either a failure load or a creep load increment will be applied to each pile. The Alternate Test Procedure will yield two pile failure load data points and at least one pile creep load data point for use in subsequent analyses of test data.

The Confirmation Test Procedure may only be used in areas where other pile test data for similar conditions are available; it can be used specifically to confirm existing pile design criteria. The Confirmation Test Procedure requires the testing of one pile; the pile will be loaded with two test load increments - a creep load increment and a failure load increment - as listed in Table 3. The data from each test load increment must

TABLE 3
Acceptable Pile Test Procedures

Procedure	Pile No.	Load No.	Load Type(1)	Load Level
Standard	1	1	C	100% Base Test Load
		2	F	Failure in 6-12 hrs.
	2	1	C	200% Base Test Load
		2	F	Failure in 3-5 days
Alternate	1	1	F	Failure in 3-6 hrs.
	2	1	F	Failure in 3-5 days
	3	1	C	100% Base Test Load
Confirmation(2)	1	1	C	100% Base Test Load
		2	F	Failure in 24 hrs.

Note

(1) C=Creep Load; F=Failure Load
(2) For use in areas where other pile load test data are available

be compared, in the field, to the predicted creep rate and the predicted failure time. If either the actual creep rate is greater than the predicted creep rate or if the time to failure is less than the predicted time to failure, a second pile must be tested. The second pile, if required, would be loaded as described in Table 3 for the Standard Test Procedure, test pile number 2.

During each test load increment, measurements of load, axial movement and reference beam temperature are to be taken and recorded at specified time intervals. These readings must be taken as nearly simultaneously as possible. Ground temperatures must be measured at least once a day during each test load increment.

The test procedures described above are designed to provide adequate data for analysis by a qualified engineer or practitioner. Each test procedure has been set at a minimum level in order to encourage the organizations responsible for the installation of pile foundations in permafrost areas to conduct such test programs. For large, new facilities or for areas with unusual or complicated subsurface conditions, the test procedures described above should be expanded to include additional test piles in order to provide additional failure load and creep load information. In particular, longer duration creep load tests should be conducted in order to provide a better basis for assessing long term behavior of the actual piles.

SUMMARY

ASTM is developing a standard test method for individual piles in permafrost under a static, axial, compressive load. This test method, which must be approved by the overall membership of ASTM, will provide a standard method for carrying out load tests on piles in permafrost.

The test method includes requirements for test pile installation, for the apparatus for applying loads, for the apparatus for measuring pile movement, for pile loading procedures and for the pile test procedures.

The development of the proposed test method has taken into account the lessons learned in previous pile test programs. The test method, when adopted, will enable future test programs to proceed with the knowledge that the data they produce should be reliable and repeatable and should allow for a realistic assessment of actual pile behavior.

REFERENCES

Crory, F.E., (1963) "Pile Foundations in Permafrost", Proceedings International Conference on Permafrost, Lafayette, Ind., pp 467-472.

Dipasquale, L., Gerlek, S. and Phukan, A., (1983) "Design and Construction of Pile Foundations in the Yukon-Kuskokwim Delta, Alaska", Proceedings of the Fourth International Conference on Permafrost; Fairbanks, National Academy of Science Press, pp 232-237.

Dokuchayev, W. and Markin, K., (1971) "Pile Foundations in Permafrost", in Russian, Gostroyizdat, 143 pp.

Goff, R.D., (1974), "Pile Foundations in Arctic Areas," Preprint, ASCE National Structural Engineering Meeting, Cincinnati, 26 pp.

Johnston, G.H. and Ladanyi, B. (1972) "Field Tests of Grouted Rod Anchors Embedded in Permafrost", Canadian Geotechnical Journal, Vol. 11, No. 4, pp. 531-553.

Ladanyi, B. and Guichaqua, A. (1986) "Time Dependent Bond Regain in Driven Piles in Permafrost," Proceedings of the International Conference on Deep Foundations; Beijing, Vol. 1, pp. 2164-2169.

Luscher, U., Black, W.T. and McPhail, J.F. (1983) "Results of Load Tests on Temperature Controlled Piles in Permafrost", Proceedings of the Fourth International Conference on Permafrost; Fairbanks, National Academy of Science Press, pp. 756-761.

Manikian, V. (1983) "Pile Driving and Load Tests in Permafrost For the Kuparuk Pipeline System," Proceedings of the Fourth International Conference on Permafrost; Fairbanks, National Academy of Science Press, pp. 804-810.

Nixon, J.F. (1988) "Pile Load Tests on Saline Permafrost at Clyde River, N.W.T.", Canadian Geotechnical Journal, Vol. 25, No. 1.

Rowley, R.K., Watson, G.H., and Ladanyi, B. (1973) "Vertical and Lateral Pile Load Test in Permafrost," Proceedings, Second International Conference on Permafrost, Yakutsk, North American Contribution, pp. 712-721.

Vyalov, S.S., (1959) "Rheological Properties and Bearing Capacity of Frozen Soils", Translation 74, U.S. Army Cold Regions Research Engineering Laboratory, translated 1965, 219 pp.

Vyalov, S.S., (1962) "Strength and Creep of Frozen Soils and Calculations in ice-soil Retaining Structures", U.S. Army Cold Regions Research Engineering Laboratory, Translation 76, 301 pp.

Vyalov, S.S, (1978) "Long Term Settlement of Foundations on Permafrost", Proceedings, Third International Conference on Permafrost, Edmondton, Alta., Vol 1, pp. 898-903.

CRYOGENIC HEAVE UNDER FREEZING OF ROCKS

V.L. Nevecherya

Moscow Geological Prospecting Institute

SYNOPSIS The main regularities of cryogenic heave of rocks in time and area, obtained in perennial studies, are given in the work. A new technique was used, asserting that cryogenic heave within homogeneous sites, distinguished by zonation, is considered to be a stochastic (random) process that allows the probability theory and statistical methods to be widely used for a reliable determination of this process parameters. Seasonal heaving is estimated to regularly transform into perennial one in neoformation of permafrost. Nevertheless, a cyclic process of seasonal heaving becomes progressive, which results in gradual rise of freezing rocks. The intensity and irregularity of heaving in an area sharply decreases with the growth of freezing depth.

INTRODUCTION

Regardless of perennial investigations, cryogenic (frost) heave under seasonal and perennial freezing of rocks has been so far insufficiently studied. Inadequate consideration of this process has a harmful impact, especially in the seasonal freezing-thawing layer (SFL--SML), which results in freezing deformations of various constructions and primarily linear ones (railways, motor roads pipelines, irrigation channels, communication lines, etc.). These deformations do not have catastrophic effects, but they cause considerable losses to national economy, due to their multiplicity. Active development of the north and east territories of the country where dust-clay oversaturated soils with deep seasonal freezing-thawing predominate, has made a further study of cryogenic processes necessary. That is why special attention was paid to cryogenic heave of rocks when studying these areas. The results of perennial investigations (1958-1986), made by the author to develop the technique and to study cryogenic heave in different regions of the country, are given briefly in this report. As a process of cryogenic heave under seasonal freezing is a bit different from that under perennial one, they should be first considered separately.

MECHANISM OF SUPPORT

Before considering cryogenic heave under seasonal freezing of rocks, it should be noted that by the beginning of the 70s a tendency of permafrost zone development has been changed. Vast areas are involved in economic development instead of small ones. A trend in cryogenic heave investigations has also been changed since conditions for construction were not everywhere favourable. The main efforts are focused on revealing the intensity of cryogenic heave manifestation in an area when developing these territories. Consequently, for studying cryogenic heave in soils (SFL--SML) a new methodology, different from those accepted before, has been worked out to study and predict this process, based on the idea that cryogenic heave is considered to be a stochastic (random) process, that allows to widely use the probability theory and statistical methods to estimate it in time and area.

Analysis

It is known that seasonal cryogenic heave, causing general freezing of heaving rock, is a complex natural process that occurs in certain engineering-geological conditions and is caused not only by the rock composition, but also by thermal-physical and physical-mechanical regularities of the rock (SFL--SML) freezing. Special and time varisbility of the main engineering-geocryological parameters results in the change of intensity of cryogenic heave for different cites, within considerable limits and in some homogeneous sites it is not uniformly manifested in area but as a random (stochastic) process. Thus, when estimating cryogenic heave manifestation of the territory, above all its zoning (typifying) is made according to this manifestation intensity. With this aim in view a classification has been worked out that helps to correlate cryogenic heave processes with the main natural factors, specifying them: soil (SFL--SML) composition, moisture before freezing and freezing temperature regime (Nevecherya, 1973). Depending on the combination of these factors, all the variability of cryogenic heave through the intensity of its manifestation should be subdivided into four types: I -- rather intensive; II -- intensive; III -- weak; IV -- hardly manifested. The type of cryogenic heave based on the intensity of its manifestation is determined by comparative estimation of natural factors according to the classification (Table I). For a typifying unit an engineering-geological subdivision is accepted that is characterized

by homogeneous factors mentioned above and different from combination of these factors for another subdivision. At the scale of 1:100,000 - 1:200,000, a natural complex (micro-area) singled out during engineering-geocryological survey is accepted to be a typification unit. At the small-scale zoning, an engineering-geological area and engineering-geological region are taken for the typification unit.

In 1965 this technique used for the zoning the Siberia according to the intensity of heave manifestation in soils (SML) for high-way engineering (Nevecherya,1966). In 1980 the area between the rivers Pur and Nadym (West Siberia) the zoning was made according to the intensity of SFL--SML cryogenic heave and a map was compiled to a scale of 1:100,000 and for the same areas to a scale of 1:25,000 (Geocryological Conditions, 1983).

In 1986 the map of the USSR territory zoning was compiled together with Belopukhova E.B., based on the intensity of cryogenic heave manifestation in soils of seasonal thawing--seasonal freezing layers, to a scale of 1:7,500,000. According to the legend, 9 subdivisions of the areas are made due to the intensity of cryogenic heave manifestation and the area of frost-susceptible soil spreading within the district.

The reliability of the area subdivision and the accuracy of boundaries put on the map is confirmed to a certain degree by actual data and the data of many authors on the progress in deformation of different structures, caused by soil heaving.

Thus, as a result of zoning, we obtain a qualitative estimate of the territory based on the intensity of cryogenic heave manifestation. To determine quantitative parameters of cryogenic heave and their change in time and area within the typified areas (sites), the following methods are used. When it is possible to carry out the work for one or more years within the typified area, heave measuring plots are made and regime observations are carried out. When making studies within a spring-summer season, the value and intensity of heaving is determined on the basis of the technique suggested by the author and heaving is estimated with the value of the frozen heaving rock subsidence under thawing.(Nevecherya,1976). Since cryogenic heave manifests itself as a random process within homogeneous sites, then for a reliable determination of its parameters a heave measuring testing ground is made on the regime-studying plot, where 30 heave-measuring devices of different constructions are set up, according to a certain scheme that allows to define the nature of heaving show in area and to obtain data enough for statistical treatment. The height of marks position relative to a specially put bench-mark, not subjected to heaving, is determined by the levelling before freezing (at the moment of maximum SML) and in spring by the end of snow melting before thawing. The difference between measurements gives the value of total heaving in these points in a winter season. The depth of SFL--SML is measured with cryopedometers, probes or by drilling probe wells. With the data obtained the mean by depth intensity of cryogenic heave is determined. To study cryogenic heave by depth, a differential heave-measuring -shaped device is used, and to determine the value of tangential forces of heaving a -shaped tie rod with a load gosge is used. On the site temperature wells are made and snow-sticks are put. To study the tendency of heaving parameters change during development, stationary plots within the sites of disturbed conditions and also the sites with specially disturbed conditions have to established.

TABLE I

Lithological composition of soils	Temperature coefficient of freezing degr./sm					
	Favourable for heaving, q - 0.10 - 0.15			Unfavourable for heaving q > 0.15 or q < 0.10		
	$CW_{cr} < W_{bw} \leqslant W_f$	$W_{ht} < W_{bw} \leqslant W_{cr}$	$W_{bw} \leqslant W_{ht}$	$W_{cr} < W_{bw} \leqslant W_b$	$W_{ht} < W_{bw} \leqslant W_{cr}$	$W_{bw} \leqslant W_{ht}$
Loam, dust	I*/	I	III	II	III	IV
Clay, dust	I	I	III	II	III	IV
Sandy loam, dust	I	II	III	II	III	IV
Loam	I	II	III	II	III	IV
Sandy loam	I	II	III	II	III	IV
Sand, dust	I	II	III	II	III	IV
Clay	I	II	IV	III	III	IV
Fine sand	II	III	IV	III	III	IV
Rock debris (coarse) with 30 per cent clay-dust filler	II	III	IV	III	III	IV
Peaty soil	II	III	IV	III	IV	IV
Rock debris (coarse) with clay-dust filler from 10 to 30 per cent.	II	III	IV	III	IV	IV
Medium-size sand	III	III	IV	III	IV	IV

Note: I-IV - numbers come for the type of cryogenic heave according to the intensity of its manifestation, given above.

W_{bw} -- pre-winter moisture of soil (SFL--SML).

W_f -- full moisture capacity

W_{ht} -- heaving threshold moisture, according to Kudryavtsev B.A.

W_{cr} -- critical moisture according to Sumgin M.I. and Tsytovich N.A. (Nevecherya, 1973).

The data on the total amount of heaving and mean intensity of cryogenic heave, obtained in observations on the proving ground using accelerated technique, can be considered as random values, due to a randomness of cryogenic heave or as realisation of a random function during the analysis of the process intensity dependence on space and time coordinates. That is why corresponding mathematical methods are used for the treatment of these observations (Nevecherya, 1978). Without discussing the technique of the data treatment in detail, it should be noted that to determine spacial irregularity of cryogenic heave manifestation, an auto-correlation function is used, characterizing a change of interdependence of heaving value with a distance growths between two measurement points. An auto-correlation chart gives the idea of frost mounds nature in an area while the correlation radius value, with the function value equal to zero, characteristizes dimensions of a separate frost mound. The radius value allows to obtain a real meaning of irregularity coefficient and a module of heaving relative irregularity. The irregularity coefficient value can be determined in the following way. Correlation radius determines the length of a separate frost mound. In an extreme case heaving summarized value is equal to a maximum one in the centre of the frost mound and to a minimum one at the edge. Consequently, the irregularity coefficient is equal to a difference between these values, divided by a half of correlation radius. So we obtain maximum value of irregularity coefficient that should be considered when estimating heaving capacity of the territory. Treatment of the perennial observations by means of the above mentioned technique helped to reveal the following regularities of the seasonal cryogenic heave. First of all it was found out that cryogenic heave of soils (SFL--SML) under natural conditions is a steady process of annual surface ascending and descending, its parameters changing within comparatively narrow limits or being practically unchanged. Separate frost mound centres are hardly ever displaced from year to year. This is confirmed by the data obtained and also by the fact that correlation radius, being very characteristic of the plot, remains almost unchanged for years. It should be noted that the correlation radius increases a bit with a growth of heaving mean value, that is the dimensions of a separate frost mound expand somewhat with the increase of the heaving total value. Particular meaning of the heave total value at a point is not constant. It changes from year to year but there is no trend in it. The intensity of these changes are considerably determined by the type of natural conditions. There, within the natural complexes where soil moisture, the depth of SFL--SML and conditions of freezing change a bit from year to year, the value of heaving at a point changes within a very narrow interval. Changes of the mean, for the proving ground, value of the heaving total amount are also small. Tundra, forest tundra and taiga the increase or decrease of the mean for the proving ground, value of the heaving total amount if compared with a previous season is observed in the case when a corresponding increase or decrease of SFL--SML thickness is marked. Estimation of this factor impact has demonstrated that an average, over depth heaving intensity that does not depend on the depth of SFL--SML, is a more stable, in-time value, characteristic of a given cryogenic type. This has allowed to obtain a formula for determining a summarized value of heaving over the thickness of SFL--SML. As a whole for the above-mentioned zones the mean over-depth heaving intensity is characterized as follows: 6 -- 10 per cent and more for SFL soils come for the plots with a very intensive manifestation of cryogenic heave, 3 - 6 per cent come for plots with an intensive manifestation and 1 - 3 per cent come for the plots with a weak manifestation of cryogenic heave. There in the forest steppe and steppe zones average over-depth heaving intensity changes considerably depending on the pre-winter moisture content. Accordingly, the technique was worked out for determining pre-winter moisture of soils before freezing on the basis of perennial data on the nature of moistening in this area (Nevecherya, 1966) and for determining moisture content based on the data of separate measurements in the summer-autumn season (Nevecherya, 1965). It has been defined that a correlation radius and, consequently, the dimensions of single frost mounds under heaving of SFL soils averages 10 metres, from 15 to 8 m. The size of the frost mounds under heaving of SML soils amounts to 6-8 m. with the exception of cites with medallion-like spots, where correlation radius amounts to 3-4 m., which coincides with the dimensions of medallion-like spots in plan. So, the established type of cryogenic heave corresponds in nature to one of the three types of the sites, singled out due to the intensity of cryogenic heave. Thus, the data obtained within one-two winter periods can be considered as an averaged characteristics of cryogenic heave of the territory. According to the first-year observations, it is possible to determine a minimum number of heave-measuring marks, basing one self on a given reliability and accuracy of heaving mean value. It should be noted that when developing the territory the established type of cryogenic heave considerably changes, but as far as an average by depth intensity of heaving for SML soils does not change, then the data obtained for natural conditions can be used for predictions when estimating soil cryogenic heave.

It has also been defined that under neoformation of permafrost (PF) a seasonal cryogenic heave regularly transforms into a perennial one. Separate seasonal frost mounds turn into growing frost mounds in proper conditions. It is confirmed by the fact that dimensions of growing frost mounds in plan in the first years are equal to those under very intensive seasonal cryogenic heave manifestation. Neoformation of PF is as a rule accompanied by its heaving. In the southern part of a permafrost zone with a considerable thickness of a snow cover it is cryogenic heave that makes for the formation of a short-term permafrost and PF neoformation. Elevation of the surface as a result of heaving brings about notable decrease of the snow-cover thickness, which makes for a sudden cooling of ground in winter. Particularly intensive heaving is observed with a growing of perennial segregated mounds and heaving ridges, convex-hillocky and large-hillocky pest lands and also string bogs. To reveal the dynamics of cryogenic heave under perennial freezing, constant observations were organised to watch mounds

growing and heaving areas of elevation using special marks and bench marks. Observations were initiated in 1971-72 years and are being continued todate. To determine the age of the mounds and consequently average heaving rate, the method was used of field comparative interpretation of aerial photographs (AFI) for different years (Geocryological conditions, 1983). It has been determined that under perennial soil freezing cryogenic heave manifests itself as a seasonal (cyclic) one, i.e. it lasts for a certain period each year. The start of the heaving period and its duration is determined by the depth of perennial freezing and intensity of winter cooling our of soils, that actively shows itself under heave segregation mounds growth. Cryogenic heave rate decreases sbruptly with the permafrost thickness. Thus in the year of the mound formation, i.e. when seasonal freezing turns into perennial one, the rate of cryogenic heave amounts to 200-250 mm per year. With a growth of permafrost thickness from 1.5 mm to 3 mm the rate decreases from 130 to 60 mm per year. With permafrost thickness below the mound being 8 mm and other favourable conditions, cryogenic heave rate amounts to 7-10 mm/y. In permafrost and rare permafrost island zone the growth of separate frost mounds in unfrozen layer ceases, the thickness of newly-formed PF being 10-15 mm. A change of height is noted of such mounds within 10-30 mm over the years caused by displacement of the PF lower boundary in heaving soil with a change of heaving mound thermal state in some winter seasons. With a constant increase of soil temperature, an elevation takes place of the PF lower surface, causing the mound settlement with the rate of 60-200 mm per year and then its failure. Cryogenic heave with an areal PF formation is also noted, but its rate is markedly lower than with frost mound growth. In permafrost island zone it amounts to 5-15 mm/y. It should be noted that when developing the territory, the intensification of perennial cryogenic heave is often observed and frost mound growth is resumed that in natural conditions does not occur.

CONCLUSION

Thus, cryogenic heave manifests itself as a limited process under seasonal and perennial ground freezing. However, when seasonal freezing transforms into perennial one, cryogenic heave turns from a cyclic process into a cyclic progressive, and that brings about gradual elevation of some layers and the freezing ground surface to a considerable height. It should be taken into consideration when making geological and geomorphological investigations in permafrost zone. Heaving irregularity occurring under seasonal freezing causes various ice content of the upper 10-15 m thickness of PF homogeneous as to composition and total moisture.

REFERENCES

Geologicheskiye uslovia Zapadno-Sibirskoi gazonosnoi provintsii. (1983). Izd-vo "Nauka", Sibirskoye otdelenie, Novosibirsk, 199 s.

Metodicheskie rekomendatsii po prognozu izmereniya inzhenerno-geologicheskikh uslovii i razvitiya criogennykh protsessov pri lineinom stroitelstve v severno-tayozhnoi zone Zapadnoi Sibiri (1976). Nauchn, red. Nevecherya V.L., M., VSEGINGEO, 44 s.

Nevecherya V.L., (1965). O metodike rascheta predzimnei vlazhnosti gruntov yuga Zapadnoi Sibiri. V kn.: "Izvestiya SO AN SSSR", vyp. 3, N 10, 134-139, Novosibirsk.

Nevecherya V.L. (1966). K voprosu prognosirovaniya predzimnei vlazhnosti gruntovykh osnovanii zheleznykh dorog Zapadnoi Sibiri. V kn.: "Merzlotnye issledovaniya". Vyp. 5, 100-111, Moskovskii Universitet, Moskwa.

Nevecherya, V.L. (1966). K raionirovaniyu Zapadnoi Sibiri po intensivnosti protsessov puchino-obrazovaniya v gruntakh. V kn.: "Materialy VIII Vsesoyuzn. mezhved. soveshch. po geokriologii, vyp. 3, 53-59. Yakutsk.

Nevecherya, V.L. (1973). K metodike raionirovaniya territorii po intensivnosti proyavleniya protsessov puchinoobrazovaniya v gruntakh. V kn.: "Uskorennye metody inzhenerno-geologicheskogo izucheniya nefte-gazonosnykh raionov Zapadnoi Sibiri na osnove landshaftnoi indikatsii. Trudy VSEGINGEO, vyp. 62, 21-27. Moskwa.

Nevecherya,V.L., Goralchuk M.I. (1978). Nekotorye zakonomernosti sezonnogo putcheniya gruntov v severotayozhnoi zone Zapadnoi Sibiri. V kn.: Krigennye protsessy. 177-188. "Nauka", Moskwa.

EFFECTIVE LIFE IN CREEP OF FROZEN SOILS

V.R. Parameswaran

Department of Materials Science and Engineering, Northwestern University, Evanston, IL 60208 USA

SYNOPSIS

A new method to predict the onset of failure in the creep of frozen soils is suggested. By this technique an effective life longer than that predicted from the time to reach minimum creep rate or the time of transition from steady state to accelerating creep, can be obtained during the performance of a structure prior to ultimate failure. Using a personal computer to monitor the performance of the foundation, a warning signal can be activated prior to the onset of failure.

INTRODUCTION

Bearing capacities of foundations in permafrost areas are governed by the strength and creep of frozen soils. A pile foundation for instance, bears the load due to the structure mainly by the adfreeze bond strength at the pile-soil interface, and partly by end bearing. If the ground can be assumed to consist essentially of one type of soil considered homogeneous, the above two factors can be combined to calculate the total bearing capacity ϕ as:

$$\phi = \tau_{ad} A_{ad} + \sigma A_b \qquad (1)$$

where τ_{ad} is the shear strength of the adfreezing bond at the pile-soil interface, A_{ad} is the adfreezing interfacial area, σ is the long term strength of the soil in compression and A_b is the end bearing area of the pile tip. Thus the important parameters that govern the bearing capacity are: the long term adfreeze bond strength between a pile and the soil (τ), and the long term strength of the soil under compression (σ). The objective of any good design is to arrive at suitable (or allowable) values of the stresses τ and σ, so that they are not exceeded in practice.

The soil around the pile is under a constant load creep condition, and the pile is continuously being displaced at a rate (although imperceptibly small) that depends on the applied load, temperature, physical characteristics such as grain size, ice content, porosity etc. of the soil, surface characteristics of the pile, and several other factors. In practice, based on an allowable settlement to occur during the anticipated life of the structure, an allowable rate of pile displacement or settlement is calculated. The stress corresponding to this allowable displacement rate has to be determined in order to arrive at the number of piles required to support a structure.

Three different approaches to obtain the allowable stresses τ and σ, were reviewed earlier (Parameswaran, 1985a, 1986). In one approach, stress obtained by extrapolation of the results from rate controlled tests carried out at higher rates, to a lower allowable displacement rate, is always much higher than that obtained from constant load creep tests carried out at the lower displacement rates. In the second method, the allowable stress is determined from a plot of applied stress vs the minimum or steady state creep rate observed in creep tests, neglecting the instantaneous displacement and primary creep. In the third method proposed by Vyalov (1959, 1962) the failure time t_f (defined as the time at which secondary or steady state creep ends and tertiary or accelerating creep starts) is related to the applied stress τ at the pile-soil interface, by an equation:

$$\ln \frac{t_f}{t_o} = \frac{\tau_o}{\tau} \qquad (2)$$

where t_o and τ_o are characteristic constants for the soil under consideration. (In the case of creep tests carried out on frozen soil material in the form of samples of cylindrical or other shape, the shear stress τ in equation 2 is replaced by the compressive or tensile stress σ). From a plot of $\ln (t_f)$ vs 1/(stress), the allowable stress for an expected life is calculated.

All the three methods underestimate the allowable life of a structure in frozen soil under a given load, because, in general, frozen soils creep with a prolonged tertiary creep region. A much longer failure time extending into the early part of tertiary creep region can be chosen by a method proposed recently for determination of failure time in creep in any material (Parameswaran, 1987). The method is based on the premise that failure time in creep can be taken as the time at which the straight line from the origin to the point corresponding to the displacement (or strain) on the creep curve becomes a tangent to the curve. At this point, the slope of the line, which is equal to the total displacement or strain divided by the elapsed time since the beginning of a test, is also a minimum. In this paper, results from several creep tests carried

*Formerly Senior Research Officer, Institute for Research in Construction, National Research Council of Canada

out in the permafrost laboratories of the Institute for Research in Construction, on piles embedded in frozen soils as well as those carried out on cylindrical samples of frozen soils, are analyzed and it is shown that the effective life of a structure can be increased by at least 50% more than that based on Vyalov's definition of failure time.

ANALYSIS OF TEST DATA

Experimental methods and materials used for model pile tests and creep tests in frozen soils were described in earlier papers (Parameswaran, 1979, 1985b). Figures 1 and 2 show typical creep curves where the displacement and displacement rate of a pile embedded in a frozen soil and subjected to a constant load, are plotted as a function of time, in (a) and (b), respectively. Similar creep curves for a cylindrical sample of frozen sand (Figure 3) show the variation of strain and strain rate respectively, with time. The times denoted by t_1 and t_2 in these figures represent the beginning and end of the secondary or steady state creep region. Although engineering creep curves obtained by plotting the variation of displacement or strain with time show a pseudo-steady-state region (as in Figures (a) of 1 to 3), strictly speaking there is not a truly steady state region where the rate of displacement or strain remains constant for the period t_1 to t_2. The rate of displacement or strain decreases continuously until it reaches a minimum at t_m, after which it increases, as shown in the Figures (b) of 1 to 3. The failure time t_f used by Vyalov in equation (2) is the same as t_2 in Figures 1 to 3. It may, however, be more accurate to use t_m instead of t_2, although this reduces the effective life of the structure considerably.

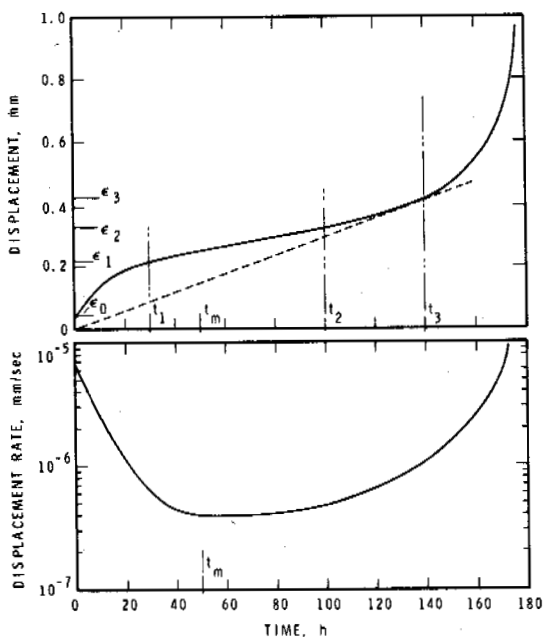

FIGURE 1 Typical creep curves for a steel pile in frozen sand at -2.5°C
(stress: 0.215 MPa, moisture content: 14%)
(a) Variation of displacement with time
(b) Variation of the rate of displacement with time

The time t_3 corresponds to the point on the creep curve at which the straight line from the origin is a tangent to the curve. The slope of a line from the origin to any point lying on the creep curve is given by the total displacement at that point divided by the elapsed time, and this slope is a minimum at the point corresponding to t_3. As pointed out earlier (Parameswaran, 1987) it will be convenient to use the time t_3 instead of t_2 or t_m, as the failure time for calculating the optimum stress in the design of foundations for structures in frozen ground. This will give a much longer effective life of a structure built on perennially frozen ground.

An error in estimating the failure time t_3 is likely to have a somewhat greater effect than an error in estimating t_m, as the former is in the tertiary or accelerating creep region, where the creep rate increases much faster with time than in the vicinity of t_m. However, as frozen soils under stresses usually encountered in the field (1 MPa) exhibit a prolonged tertiary creep region, preventive measures can be taken prior to the onset of actual failure of a structure.

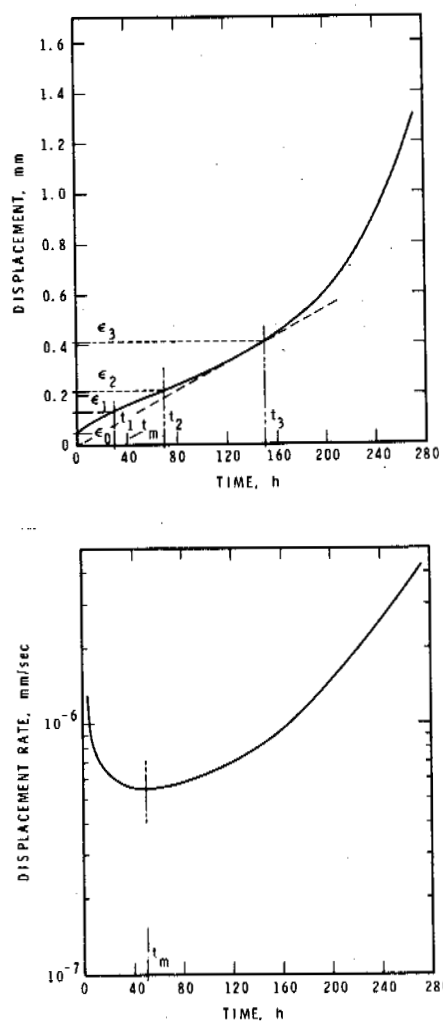

FIGURE 2 Creep curves for a wood pile in frozen silty clay at -6°C
(stress: 0.315 MPa, moisture content in soil: 40%)

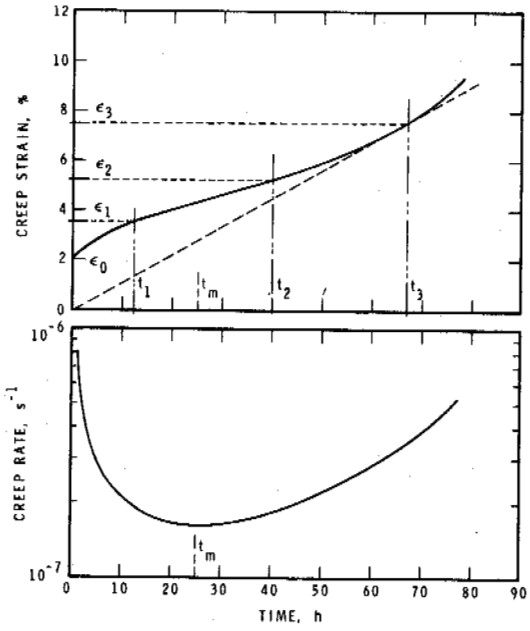

FIGURE 3 Typical creep curve for a frozen cylindrical sand sample at -10°C (stress: 6.4 MPa, moisture content of sample: 20%)
(a) Variation of axial strain with time
(b) Variation of strain rate with time

The displacement of a pile can be monitored continuously as a function of time by a device such as a linear variable differential transformer, and the data stored using a suitable data logger and a microcomputer. The slope at each instant, calculated automatically by dividing the total displacement by the elapsed time, can be compared with previous values. The instant at which this ratio starts to increase significantly after reaching a minimum value can be determined by the computer, and a warning signal can be issued to take preventive measures to avoid catastrophic failure. This method has been used successfully in laboratory experiments on creep of frozen soils and on model pile foundations in frozen soils.

The times corresponding to the various points along the creep curves (such as those shown in Figures 1 and 2) for model piles frozen in various soils and subjected to constant loads are given in Table I. The table also shows the temperature and stress at the pile-soil interface during each test. Table II is similar to Table I except that the data shown there are obtained from creep curves (such as that shown in Figure 3) for cylindrical samples tested under constant uniaxial compressive stress. It is evident from these tables that the failure time as defined by 't_3' is much longer than that defined by 't_m' (the time to attain the minimum creep rate) or 't_2', the time for transition from stage 2 to stage 3 creep. The ratio (t_3 / t_2) has a value of about 1.5 in most cases, and the ratio of (t_3 / t_m) is larger than 2 in most cases. This shows that at a particular temperature and stress, the useful life predicted for foundations of structures built in perennially frozen ground could indeed be enhanced by considering the time t_3 as the failure time instead of t_m or t_2. Alternatively, for a structure designed for a lifetime of t_2, the limiting or allowable stress on a pile foundation can be increased due to the extended failure time, thereby resulting in some savings.

TABLE I
TYPICAL CREEP DATA FOR PILES IN FROZEN SOILS (REF. FIG. 1 AND 2 FOR TIMES t_m, t_2, t_3)

Test No.	Material	Temp. °C (±0.2)	Stress MPa	Minimum Creep rate mm/S	Time to Reach Min. Creep Rate t_m, S	Time at the End of Stage II t_2, S	Time t_3, S	t_3/t_2	t_3/t_m
36	Wood Pile in Sand	-6	0.447	5.6×10^{-8}	2.52×10^{5}	8.28×10^{5}	1.44×10^{6}	1.74	5.71
42	"	-2.5	0.285	2.5×10^{-7}	9.00×10^{5}	1.58×10^{6}	2.38×10^{6}	1.51	2.63
30	Wood Pile in silty soil	-2.5	0.544	4×10^{-6}	3.60×10^{4}	6.12×10^{4}	8.64×10^{4}	1.47	2.40
75	Wood Pile in clay	-6	0.365	5.5×10^{-7}	1.26×10^{5}	2.52×10^{5}	5.4×10^{4}	2.14	4.29
79	Creosoted wood pile in clay	-6	0.442	9.7×10^{-8}	2.16×10^{5}	7.20×10^{5}	1.44×10^{6}	2.00	6.67
41	Steel Pipe Pile in Sand	-6	0.447	2.5×10^{-6}	7.92×10^{4}	9.36×10^{4}	1.33×10^{5}	1.42	1.68
37	"	-2.5	0.215	3.9×10^{-7}	1.80×10^{5}	3.60×10^{5}	5.04×10^{5}	1.40	2.80
51	"	-2.5	0.175	1.1×10^{-5}	5.76×10^{3}	1.19×10^{4}	1.91×10^{4}	1.60	3.32
20	Concrete Pile in Sand	-2.5	0.238	6.7×10^{-7}	2.16×10^{5}	3.60×10^{5}	4.68×10^{5}	1.30	2.17
65	Concrete Pile in Silty Soil	"	0.221	2.5×10^{-7}	9.00×10^{4}	1.98×10^{5}	3.06×10^{5}	1.55	3.40

TABLE II
TYPICAL CREEP DATA FOR CYLINDRICAL SAMPLES OF FROZEN SOILS

Test No.	Material	Temp. °C (±0.2)	Stress MPa	Minimum Creep rate s^{-1}	Time to Reach Min. Creep Rate t_m, S	Time at the End of Stage II t_2, S	Time t_3, S	t_3/t_2	t_3/t_m
35	Frozen sand (20% ice)	-10	7.45	9.0×10^{-7}	2.27×10^4	3.60×10^4	5.40×10^4	1.50	2.38
36	"	"	8.65	1.8×10^{-6}	1.01×10^4	1.62×10^4	2.52×10^4	1.56	2.50
38	"	"	6.48	1.6×10^{-7}	9.00×10^4	1.44×10^5	2.41×10^5	1.67	2.68
39	"	"	6.72	6.5×10^{-7}	2.34×10^4	3.60×10^4	5.40×10^4	1.50	2.31
21	"	-3	2.37	8.7×10^{-9}	5.40×10^5	1.19×10^6	1.80×10^6	1.51	3.33
26	"	"	3.32	1.1×10^{-7}	1.69×10^5	2.16×10^5	3.24×10^6	1.50	1.92
27	"	"	3.11	9.1×10^{-8}	1.26×10^5	2.16×10^5	3.24×10^6	1.50	2.57
47	Frozen clay (50% ice)	-10	3.50	2.8×10^{-6}	5.40×10^3	8.28×10^3	1.80×10^4	2.17	3.33
48	"	"	2.10	7.6×10^{-3}	1.08×10^4	1.44×10^4	4.68×10^4	3.25	4.33
49	"	"	3.17	1.8×10^{-5}	2.52×10^3	3.24×10^3	5.40×10^3	1.67	2.14
19	"	"	0.78	1.7×10^{-8}	1.44×10^5	3.46×10^5	5.40×10^5	1.56	3.75

CONCLUSIONS

A new concept of failure time in the creep of frozen soils extending into the tertiary creep regime is proposed. According to this concept, the failure time can be taken as that point on the creep curve at which the slope of the straight line joining the origin (which is equal to the total displacement up to that time divided by the elapsed time) is a minimum, and the line becomes a tangent to the curve at that point. Data from several creep tests of loaded piles in frozen soils as well cylindrical samples of frozen soils under compression were analyzed, and it was shown that the failure time so estimated is 1.5 to 2 times larger than the conventional failure time defined as the time to reach minimum creep rate in the secondary creep region or the end of the steady state creep regime. This extended failure time thus prolongs considerably the useful life of structures built in permafrost areas. The method can also be used to determine the onset of failure by creep of a foundation in frozen soil, and to take preventive measures prior to onset of catastrophic failure.

ACKNOWLEDGEMENTS

The research reported in this paper was carried out at the Institute for Research in Construction, National Research Council of Canada. Colin Hubbs conducted most of the tests reported here, Douglas Bright and Harold Dahl interfaced the creep tests with a desk top computer through an automatic data logger, and Doug Scott did the illustrations. The author appreciates their help and extends his sincere thanks to all of them.

REFERENCES

Parameswaran, V.R. (1979). Creep of model piles in frozen soils. Canadian Geotechnical Journal, Vol, 16, p. 69.

Parameswaran, V.R. (1985a). Attenuating creep of piles in frozen soils. Proceedings of Session: "Foundations in Permafrost and Seasonal Frost", ASCE Spring Convention, pp. 16-28.

Parameswaran, V.R. (1985b). Effect of alternating stress on the creep of frozen soils. Mechanics of Materials, Vol. 4, p. 109.

Parameswaran, V.R. (1986). Bearing capacity calculations for piles in permafrost. Proceedings, Fourth International Conference, Cold Regions Engineering, Anchorage, Alaska, pp. 751-759.

Parameswaran, V.R. (1987). Failure time in creep. Mechanics of Materials, Vol. 6, pp. 89-91.

Vyalov, S.S. (1959). Rheological properties and bearing capacity of frozen soils. (Izdatel 'Stvo Akademii Nauk SSR, Moscow), U.S. Army Cold Regions Research and Engineering Laboratory Translation No. 74, 219 p.

Vyalov, S.S. (editor) (1962). The strength and creep of frozen soils and calculations for ice-soil retaining structures. (Izdatel 'Stvo Akademii Nauk SSR, Moscow), U.S. Army CRREL Translation No. 76, 301 p.

HORIZONTAL FROST HEAVE FORCE ACTING ON THE RETAINING WALL IN SEASONAL FROZEN REGIONS

Shui, Tieling and Na, Wenjie

Heilongjiang Provincial Institute of Water Conservancy, Harbin, China

SYNOPSIS Based on the studies of developmental process and distribution along a retaining wall of horizontal frost heave force acting on the wall, this paper presents a simplified chart of stress distribution of the horizontal frost heave force to determine the value of maximum horizontal frost heave force, and provides a design basis for the safety operation of the retaining wall in seasonal frost regions. According to the distribution characteristics of the horizontal frost heave force, the affected scope of horizontal frost heave force in the soil at the back of the retaining wall and the proposed fill section for the protection of frost hazard can be identified.

NATURAL CONDITIONS OF THE TESTING SITH

The tested soils in the test site are heavy silty loam.The physical properties of the soil samples taken from different depths are shown in Table I. The mean air temperature at the Harbin Frozen Ground Test Site is 3.5 degree Centigrade. The lowest temperature is -38.5 degree Centigrade, and maximum freezing index is 2371 degree-days. The frost depth, groundwater table and the maximum frost amount at the test site from 1982 to 1986 are shown in Table II.

TABLE II

Frost Depth,Groundwater Table and Maximum Frost Heave Amount at the Test Site From 1982 to 1986

Yrs Items	1982-83	1983-84	1984-85	1985-86
Frost heave amount (mm)	142	170	161	286
Frost depth (cm)	150	160	154	134
Groundwater depth (cm)	140-300	110-340	90-297	60-260

DEVELOPMENTAL PROCESS AND DISTRIBUTION OF HORIZONTAL FROST HEAVE FORCE

When it is in the double direction freezing state,the freezing line in soil at the back of a retaining wall transits from straight line paralled to the top of the wall near ground surface to curce, then to straingt line again parallel to the base of the wall (Fig.1).

TABLE I

Physical Properties of the Soil Tested Taken From Different Depths

Soil classification	Sampling depth (cm)	Composition of soil grain (%) >.05 (mm)	.05-.005 (mm)	<.005 (mm)	Plastic limit W_p (%)	Liquid limit W_L (%)	Plastic index I_p	Specific gravity
Heavy silty loam	0-40	17.5	62.5	20.0	23.8	39.5	15.7	2.67
Heavy silty loam	40-250	16.0	64.0	20.0	21.5	34.6	13.1	2.69

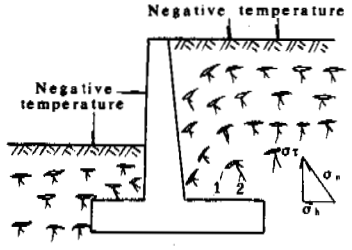

Fig.1 Horizontal Frost Heave Force Acting on the Retaining Wall Under Two-directional Freezing

1— ice lenses, 2 — direction of frost heave force,
σ_n — frost heave force,
σ_t — tangential frost heave force,
σ_h — horizontal frost heave force.

Frost heave force (σ_n) is always normal to the freezing line front. Horizontal component, σ_h of σ_n is the horizontal frost heave force discussed in this paper.

The developmental process of horizontal frost heave force acting on the retaining wall can be divided into four stages: a) Formation stage. With the change of temperature from plus to minus, the soil at the back of the retaining wall begins to freeze and generates the horizontal frost heave force σ_h. This stage generally lasts from the middle October to late November. b) Increase stage. Negative temperature falls continuously, and freezing depth increases. The horizontal frost heave force increases gradually and reaches its maximum value. This stage is from December to March. c) Decaying stage. When the weather becomes warmer, the thawing of the soil initiates. The horizontal frost heave force decreases gradually, which occurs in late March. d) Disappear stage. When the soil is completely thawed, the frost heave force will disappear accordingly (Xu, 1983).

Fig.2 shows the variation of the horizontal frost heave force (σ_h) acting on the unit area of the retaining wall with different exposed height (h) observed at the test site in two winters of 1984-1985 and 1985-1986, respectively.

The distribution of horizontal frost heave force along the height of the retaining wall is approximately triangular. With the increase in frost depth, σ_h increases almost linearly, and after reaching its maximum value at a certain depth, it decreases with increasing depth. The distribution of horizontal frost heave force along the depth measured in the winters of 1984-1985 and 1985-1986 were shown in Fig.3 and 4, respectively.

The occurence time of maximum σ_h acting on the retaining walls with different heights is not synchronous.

PRESSURE CHART AND AFFECTED SCOPE

Check of stability and strength of the retaining wall should be made according to the maximum value of σ_h occured on the wall concerned. It is, however, impossible and impractical to give out so many pressure charts for the walls with different height. It is advised to design the wall according to the pressure chart with the envelope of the maximum value of σ_h measured from 1984 to 1986, which can be simplified as a trapezoid, as shown in Fig.5. The simplified chart can be divided into the exposed and buried parts. The maximum value of σ_h appears at the section located from 1/2 to 2/3 of the exposed height of the wall (from B to C). The value of σ_h at the base of the exposed part (D) is about 60 percent of the maximum value; while at the maximum frost depth (E) the value of σ_h equals to zero. The maximum frost depth (Hm) beneath the wall is 110 cm from the natural ground surface.

The pressure chart proposed above is suitable only when the height of the wall is as 0.8 to 1.2 times high as the local maximum frost depth and the soil at the back of the retaining wall is heavy silty loam. Table III shows the comparison between the designed and the measured value of σ_h. For the heavy silty loam fill material with large frost heave at the upper part and null heave at the base, it is proposed to take the maximum value of σ_h of 0.25 MPa as the design value for the retaining wall. According to the process of temperature variation in filling soil and the pressure chart of σ_h, the affected scope of σ_h on the back of the retaining wall can be determined. In practical engineering the affected scope can be considered as the fill section for the protection of the frost heave. The simplified fill section behind the wall can be determined as follows: Identifying E at 2/3 of the height of the exposed wall from the top and drawing a horizontal line from E to D, let ED equal to the maximum frost depth Hm. From F at the base of the wall at which the buried depth is the same as the maximum frost depth Hm, drawing a horizontal line to G. let FG equal to the half of Hm. Then, from A at the top of the wall, making BAC equal to 40°, drawing a straight line to intersect with GD at C (see Fig.6). The area of ACDG is the scope of effect of horizontal frost heave force. Within the area the fine-grained soil needs to be replaced to prevent frost damage.

CONSLUSIONS

The amount and distribution of horizontal frost heave force acting on the lateral surface of a retaining wall have a close relationship to the height of the wall exposed and change with the development of frost penetration. The maximum value of σ_h acting on the different parts of the retaining wall does not occur synchronously. For a fully-restricted low retaining wall with

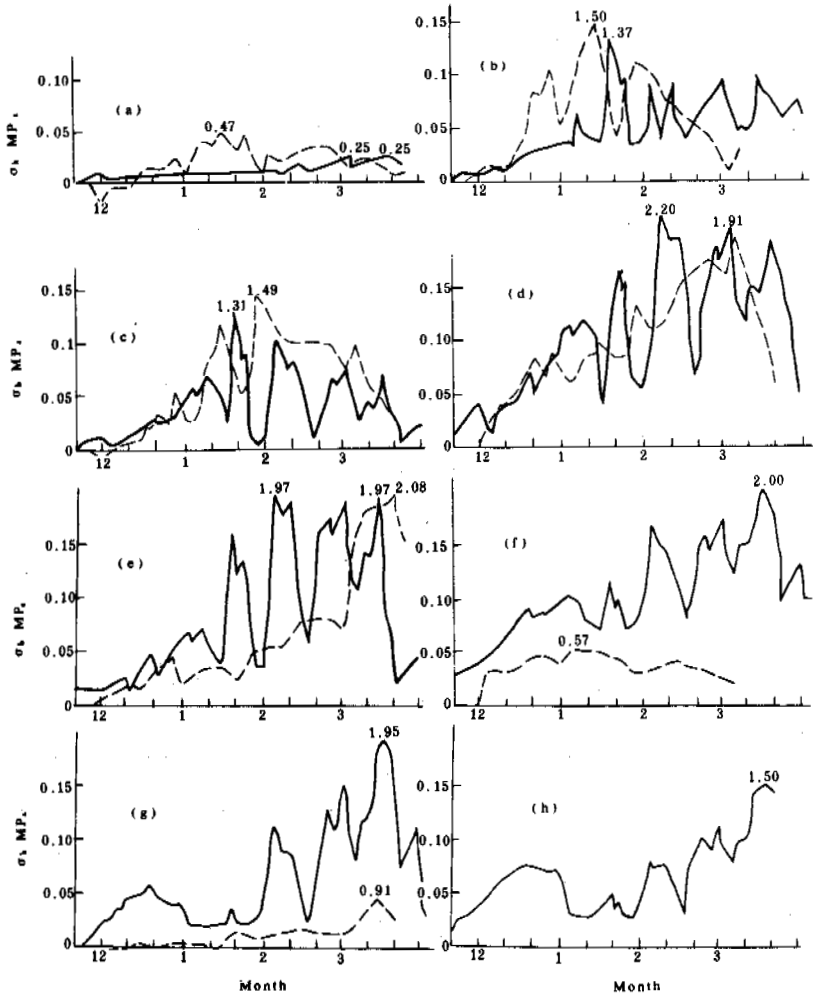

Fig.2 Variation of Horizontal Frost Heave Force with Time for the Retaining Walls with Exposed Height of:

(a) 0-20 cm,(b) 20-40 cm, (c) 40-60 cm, (d) 60-80 cm, (e) 80-120 cm, (f) 100-120 cm, (g) 120-140 cm and (h) 140-160 cm, respectively, and in two winters of 1984-1985 (solid line) and of 1985-1986 (broken line).

TABLE III

Comparison Between the Designed and Measured Value of σ_h

Exposed height of the wall h (cm)	Measured value of σ_h (MPa)		Designed value of σ_h (MPa)
	1984-1985	1985-1986	
20	0.025	0.047	0.06
40	0.137	0.150	0.125
60	0.131	0.149	0.185
80	0.220	0.191	0.25
100	0.197	0.208	0.25
120	0.200	-	0.25
140	0.192	0.091	0.205
160	0.150	-	0.15

backfill of heavy silty loam with large frost heave at the upper part and null heave at the lower part, the retaining wall can be designed according to that the maximum value of σ_h is equal to 0.25 MPa and occurs at 2/3 of the height of the wall exposed. The pressure chart can be drawn by means of the simplified method presented in this paper.

ACKNOWLEDGEMENT

Thanks are extended to Mr.Jiang Liqiang and Mr. Li Dashan for their help in this study.

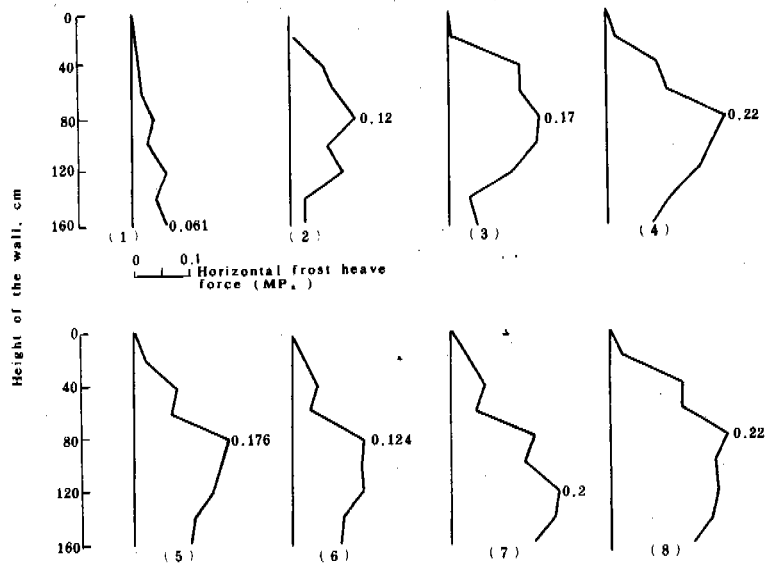

Fig.3 Distribution of σ_n along the Height of Retaining Wall Observed on the Date of: (1) Dec.10, (2) Jan.7, (3) Jan.19, (4) Feb.4, (5) Feb.26, (6) March 4, (7) March 18 and (8) the maximum value in the winter of 1984-1985.

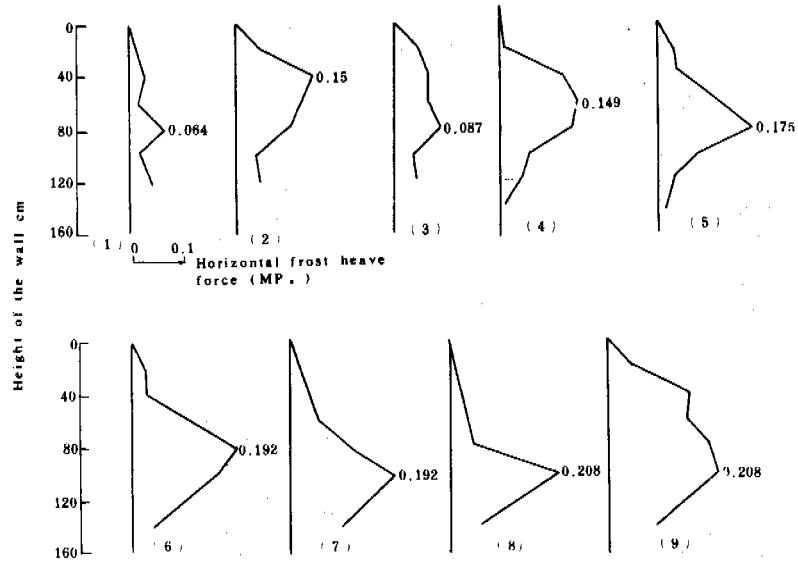

Fig.4 Distribution of σ_h along the Height of Retaining Wall Observed on the Date of: (1) Dec.16, (2) Jan 14, (3) Jan.24, (4) Jan.28, (5) Feb.24, (6) March 6, (7) March 13, (8) March 20 and (9) the maximum value in the winter of 1985-1986.

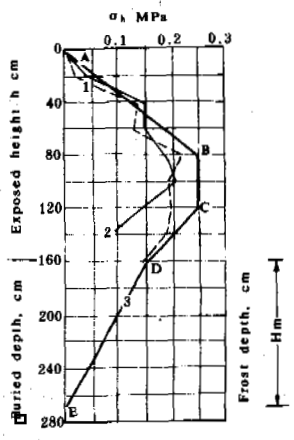

Fig.5 Simplified Pressure Chart of σ_h along the Retaining Wall

1 — observed in 1984-1985,
2 — observed in 1985-1986.

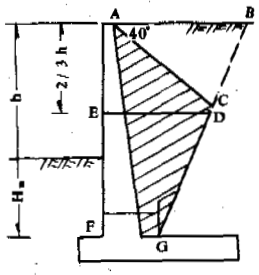

Fig.6 Fill Section behind a Retaining Wall

REFERENCE

Xu Shaoxin, (1983). On frost heave force in foundation. Proceedings of the Second National Conference on Permafrost, 229-232, Gansu Publishing House, Lanzhou, China.

DYNAMIC LOAD EFFECT ON SETTLEMENT OF MODEL PILES IN FROZEN SAND

D.L. Stelzer and O.B. Andersland

Departement of Civil and Environmental Engineering, Michigan State University, East Lansing, Michigan 48824 USA

SYNOPSIS Small cyclic loads superimposed on a sustained pile load will, in some frozen ground situations, increase pile settlement rates to levels which significantly lower their design capacity. To provide more information on this problem, model pile tests were conducted to determine the influence of cyclic load frequency and load amplitude on displacement (settlement) rates in frozen sand. Experimental results showed that cyclic loads significantly increased model pile displacement rates over those observed for the sustained load. The measured displacement (creep) rates were essentially independent of frequency for small cyclic loads superimposed on a sustained load in the range of 0.1 Hz to 10 Hz. Data analysis suggests that creep theory, with an experimental creep parameter and known loads, can be used for prediction of the increase in pile displacement rates.

INTRODUCTION

Small cyclic loads superimposed on a static pile load will, in some frozen ground situations, increase pile settlement rates and significantly lower their design capacity. this situation may arise for piles in perennially frozen ground which are used to support vibrating machinery (turbines, power generators, or compressors) or traveling loads (cranes or fork lift trucks). Pile design criteria normally limit shaft stresses at the pile/frozen soil interface to values which will give no more than 25 mm pile displacement during the service life of the structure. Small cyclic loads, 5 percent of the long-term sustained load, will accelerate settlement (displacement) rates of piles embedded in frozen ground (Parameswaran, 1984). An increase in pile surface roughness (addition of corrugations or lugs) will increase adfreeze bond strength for both short- and long-term loads (Thomas and Lusher, 1980; Andersland and Alwahhab, 1983; Ladanyi and Guichaoua, 1985). The basic mechanisms by

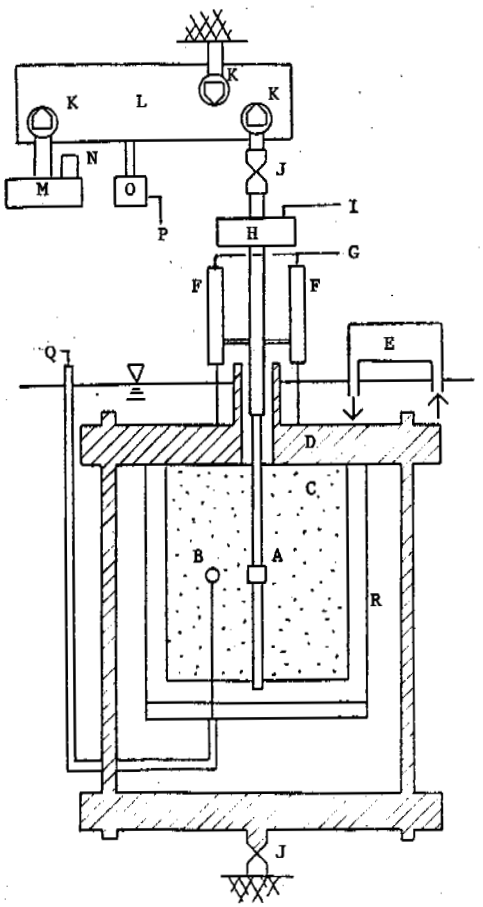

A - MODEL PILE
B - THERMISTOR
C - FROZEN SAND
D - SOIL RESTRAINT
E - COOLANT CIRCULATION
F - DISPLACEMENT TRANSDUCERS
G - DISPL. & TIME RECORDING
H - FORCE TRANSDUCER
I - FORCE RECORDING
J - 360 DEGREE PIVOT
K - RINGS ON KNIFE EDGES
L - LEVER ARM
M - STATIC WEIGHT
O - ELECTRODYNAMIC SHAKER
P - DYNAMIC LOADING CONTROLS
Q - TEMPERATURE RECORDING

FIG. 1 EXPERIMENTAL SYSTEM FOR MODEL PILE TESTS.

which small cyclic loads increase pile settlement rates and a suitable theory for estimation of this increase remain unknown.

To provide more information on this problem, experimental tests have been conducted to determine the dependence of model pile displacement rates in frozen sand on several controlled variables. These variables included cyclic load amplitude, frequency of load application, static load, sand density, ice volume fraction, temperature, and pile surface roughness. After initial rupture of ice adhesion at the pile/frozen soil interface, the load was supported primarily by interaction between the frozen sand and protrusions (lugs) on the model pile. Melting of ice and water movement away from high pressure points, accompanied by a breakdown and formation of new bonds between the ice and soil grains, permits adjustment or movement of particles interacting with pile surface protrusions. The result is a time-dependent displacement (creep) which appeared to be dependent primarily on the static load. Application of a dynamic load increased displacement rates for all dynamic load amplitudes at the various frequencies.

EXPERIMENTAL PROCEDURES

Model Pile Set-up

A plain 9.52 mm steel bar with one 1.59 mm high lug, embedded in a frozen sand specimen (Fig. 1), served as a model pile section suitable for dynamically loaded pull-out tests. The leading edge of the lug was perpendicular to the pile shaft. The frozen sand represents frozen slurry which is used to fill the annulus around piles in the field. The washed, uniformly graded, silica sand (particle size range of 0.420 mm to 0.595 mm) was combined with distilled water to form 152 mm diameter by 152 mm high frozen specimens with the model pile embedded vertically in the center. Preparation procedures gave an average void ratio close to 0.581 with an ice matrix density close to 0.892 gm/cu cm. Sample freezing was permitted longitudinally along the pile with the temperature allowed to stabilize at -14 °C. After removal from the mold, the frozen sample, model pile, and reaction plate were enclosed within a rubber membrane to prevent contamination by the coolant fluid. The sample and pile were then attached to the restraint bracket of the static and dynamic loading system within the empty coolant tank. A refrigerated ethylene glycol/water coolant mixture was pumped into and circulated through the coolant tank for immediate and subsequent temperature control during testing. A thermistor embedded in the frozen sand (38 mm from lug) permitted temperatures to be monitored as required.

Test Procedure

Prior to testing, three displacement transducers (LVDT) and a force transducer were mounted near the top of the model pile. Additional insulation was placed on top of the coolant tank and around the pile connections so as to minimize any temperature fluctuations.

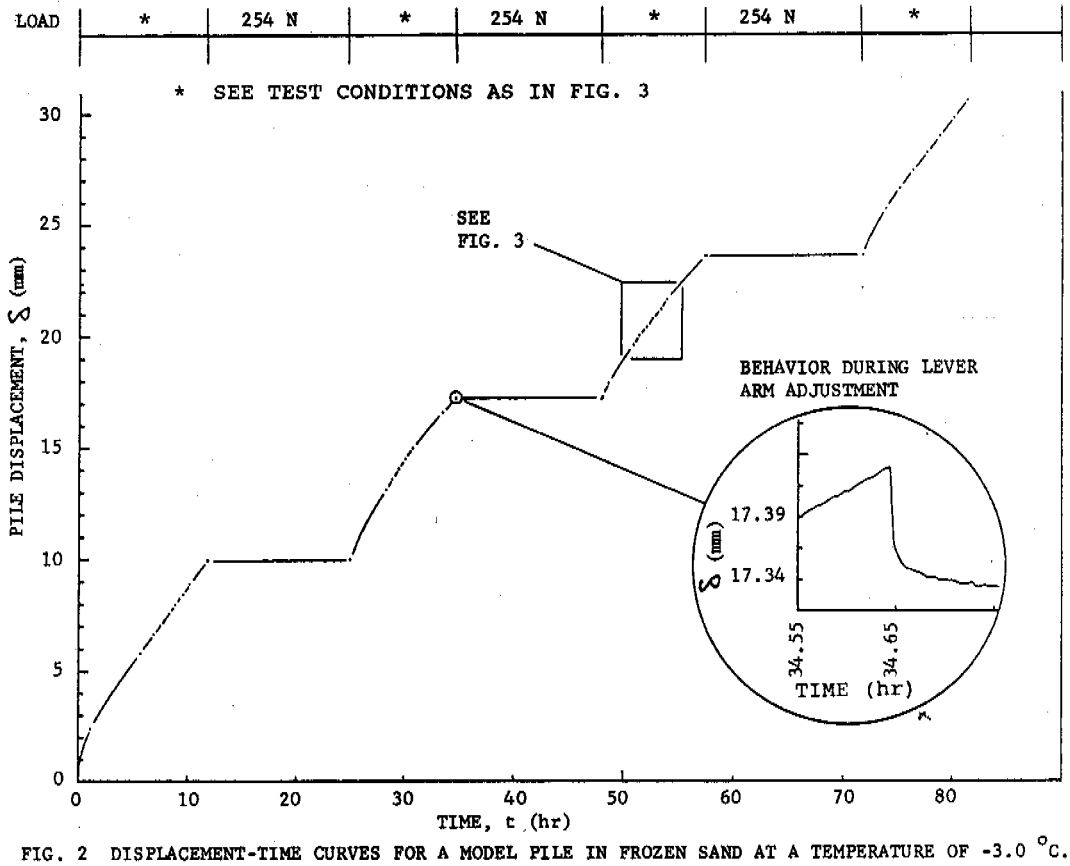

FIG. 2 DISPLACEMENT-TIME CURVES FOR A MODEL PILE IN FROZEN SAND AT A TEMPERATURE OF -3.0 °C.

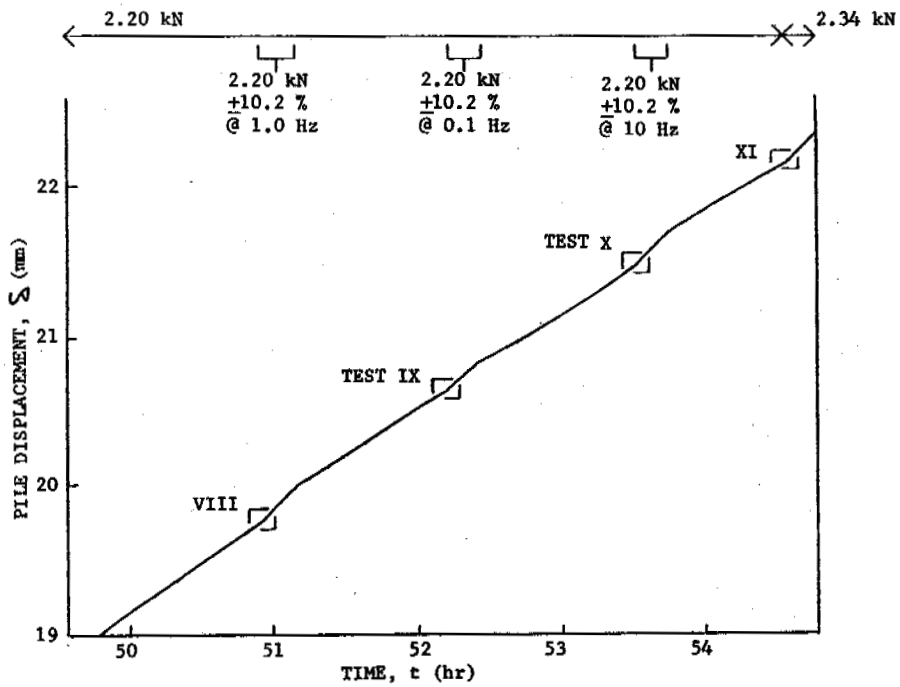

FIG. 3 DISPLACEMENT-TIME CURVE FOR A MODEL PILE IN FROZEN SAND SHOWING THE RELATIONSHIP FOR TESTS VIII THROUGH XI ON SAMPLE 92.

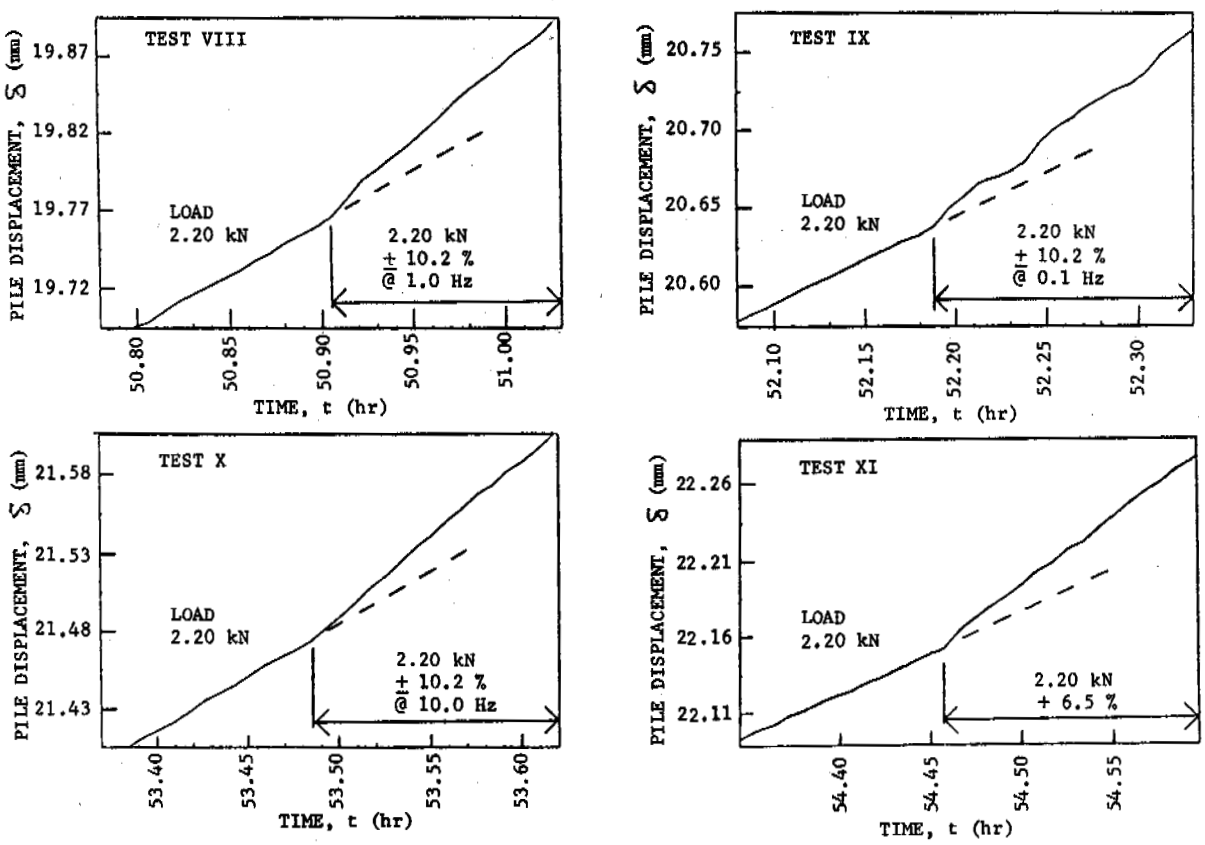

FIG. 4 DISPLACEMENT-TIME CURVES FOR A MODEL PILE IN FROZEN SAND, TESTS VIII THROUGH XI, SAMPLE 92.

The coolant, loading system, pile, and frozen sand were allowed to stabilize at -3.0 ± 0.1°C. The desired static load was then placed on the pile through the lever system illustrated in Fig. 1. Displacement, temperature, and force were recorded relative to elapsed time of test. The static load was maintained until pile movement slowed to essentially a constant displacement rate (Fig. 2). A dynamic force, with the desired wave form, frequency, and force amplitude, was generated by the electrodynamic shaker attached to the lever arm (Fig. 1). This force, monitored by the load cell, was transferred to the top of the model pile thru very stiff connections. Overall results for several tests on one sample are illustrated in Fig. 2. The periods of low load (254 N) which follow each high load (2.20 kN) were necessary to reset the lever arm (Fig. 1). Dynamic loading during the third period of high stress in Fig. 2 is illustrated in Fig. 3. Each dynamic loading period was preceded by and followed by a longer static load period to allow return to a nearly constant displacement rate. Careful monitoring during 0.100 mm displacement before and after the start of a dynamic load provided data such as illustrated in Fig. 4. This technique gave data least effected by other variables for observing the dynamic load effect on displacement rates.

EXPERIMENTAL RESULTS

Model pile displacements were recorded as a function of time for several variables. Results presented in this paper include the influence of static loads, dynamic loads, and frequency. The effects of soil dry density, ice fraction, pile surface roughness, and temperature, are to be covered in a subsequent paper. A typical displacement-time curve involving one sample and several tests is illustrated by the overall curve in Fig. 2. Loads are included at the top of Fig. 2. At about 7 mm displacement after initial loading or 3 to 4 mm after each lever arm adjustment, primary creep decreased to a nearly constant rate and dynamic load tests were started. On a larger scale, a test series is shown in Fig. 3 with detailed information in Fig. 4 for about 0.100 mm displacement immediately before and after application of the three dynamic and one static load changes. Best fit straight lines over the 0.100 mm displacement, immediately before and after a load change, gave average displacement rates during that period of time. Test XI in Fig. 4, showing the effect of a 6.5 percent increase in static load on the displacement rate, has been included for comparison.

A comparison of displacement rates, measured immediately before and after a load change, did not always clearly show the effect of a test variable. To illustrate the effect's magnitude, the ratio of displacement rate after dynamic loading to that immediately before the load change was used. These normalized displacement ratios have been plotted against frequency in Fig. 5 for a static load of 2.2 kN and include three different groups of superimposed dynamic loads. The dynamic load was a sine curve waveform with a single peak value equal to the percent of static load given in Figs. 5 and 6. Lines connecting individual data points in Fig. 5 represent several series of tests similar to the series shown in Fig. 3. During dynamic loading at 1.0 Hz and 6.2 Hz, motion of the static weight (Fig. 1) placed small additional loads on the model pile. Since these forces could not be accounted for, data at the test system frequencies of 1.0 and 6.2 Hz have been omitted in Fig. 5. The pile-soil resonant frequency, as described by Schmid (1969), should be much higher than the 10 Hz attainable with equipment available for this study. Three levels of dynamic loading, at frequencies between 0.1 Hz and 10 Hz, provided a range of increased displacement rates.

DISCUSSION

Frequency Effect

The experimental data, summarized in Fig. 5, shows that model pile displacement rates in frozen sand were essentially independent of frequency in the range of 0.1 Hz to 10 Hz. This behavior is in agreement with work reported by Schmid (1969) for model brass piles embedded in dry, uniformly graded, quartz sand with the same particle size range. Schmid (1969) reported a pile-soil resonance at about 50 Hz with a relatively flat peak in his load versus frequency curve. This curve, with a relatively flat response, suggests frequency independence above and below resonance. The smaller model steel pile and stiff frozen sand used in this study should give a higher resonant frequency and its displacement should be relatively frequency independent for 0.1 Hz to 10 Hz. Observed resonant frequencies close to 1.0 Hz and 6.2 Hz were clearly due to the loading system since they could be altered by changing the loading arm set-up.

Load Amplitude Effect

An increase in dynamic load amplitude significantly increased pile displacement rates over rates observed for sustained loads (Fig. 5). Comparisons show rate increases roughly in proportion to increase in load amplitudes, i.e., the rate was approximately doubled when load amplitude was doubled. Since several tests were run on one frozen sample, a creep rate measured just prior to application of the dynamic load might differ from rates for subsequent tests on the same sample. To compare tests performed at different initial creep rates, the ratio $\dot{\delta}_2 / \dot{\delta}_1$ was plotted against $\dot{\delta}_1$ as shown in Fig. 6. Data for each of the three best fit lines corresponds to a given dynamic load amplitude. The small negative slopes may show the effect of starting tests at various displacement rates before secondary creep was fully attained. Points on the left in Fig. 6 would be closer to the minimum or secondary creep rate. In addition, 4 shaded data points (indicated by a slash) represent displacement rate increases for a small static load increase. For a dynamic load amplitude equal to a static load increase, the dynamic rate increase always appeared as some fraction of the static rate increase. The observed model pile behavior suggested that displacement rate increases might be related to creep behavior.

Creep Interpretations

The approximate long-term time-dependent portion of displacement (settlement) for a model friction pile in a frozen soil under a constant load at a constant temperature can be represented by the creep equation in the form

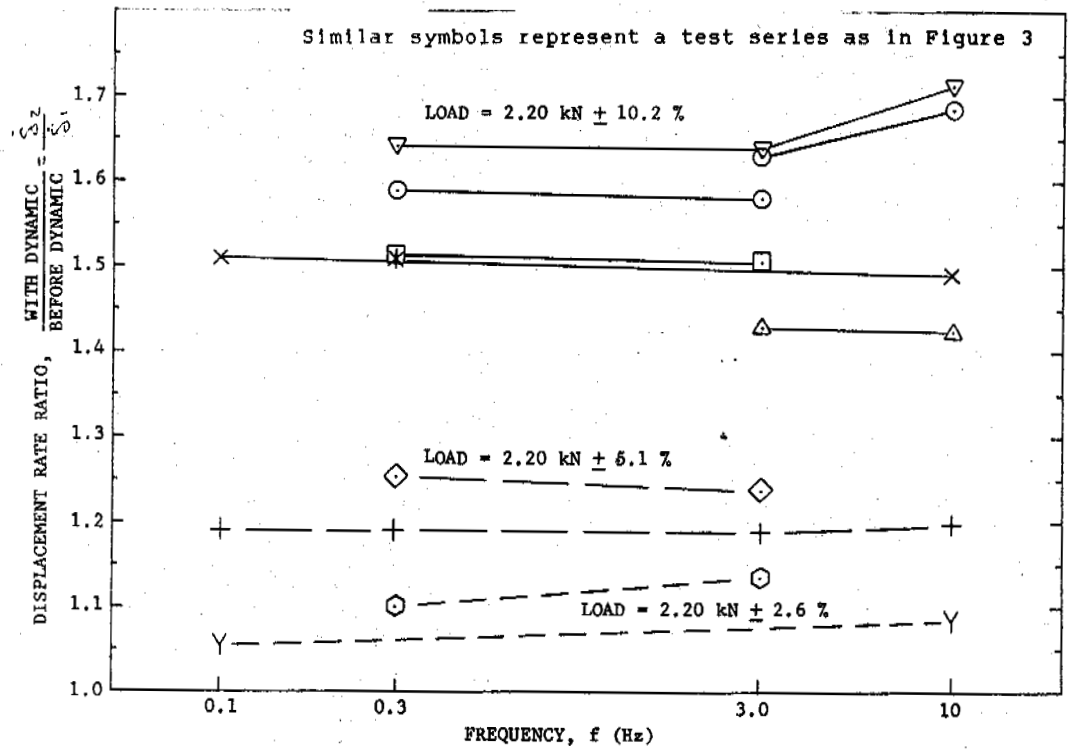

FIG. 5 DYNAMIC LOADING EFFECT ON DISPLACEMENT RATES (NORMALIZED) VERSUS FREQUENCY.

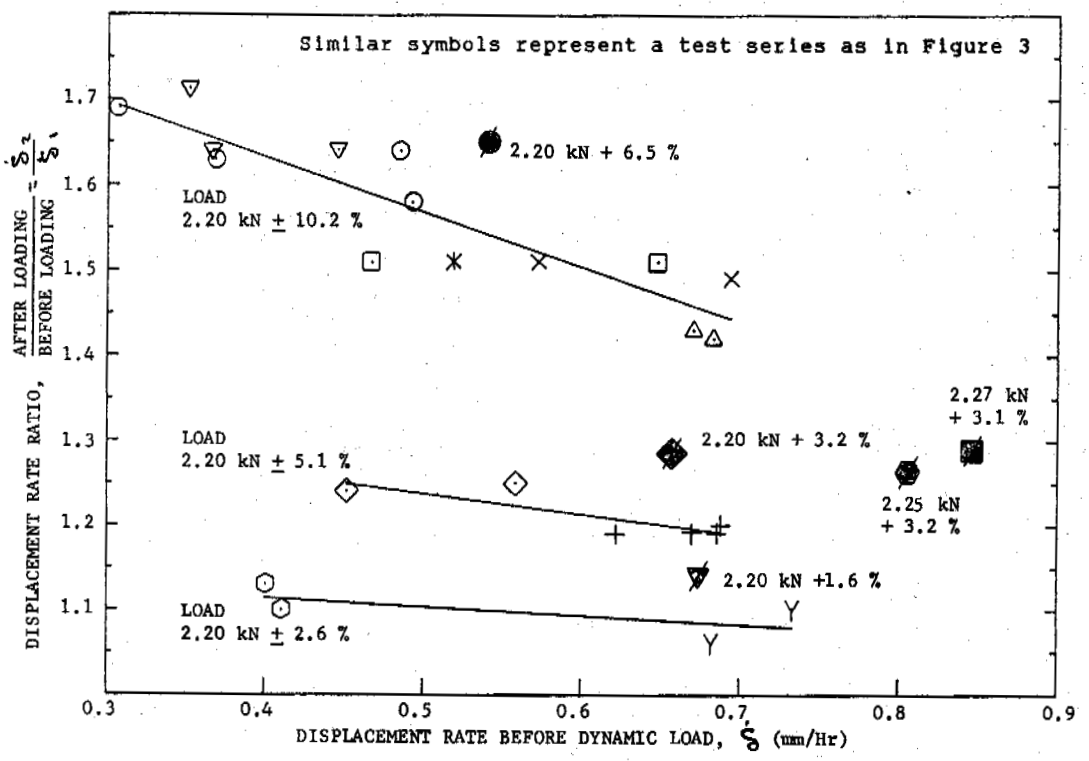

FIG. 6 DISPLACEMENT RATE RATIO VERSUS DISPLACEMENT RATE BEFORE DYNAMIC (±) AND STATIC (+) LOADINGS.

$$\dot{\delta} = \dot{\delta}_c \left(\frac{P}{P_c}\right)^n t \qquad (1)$$

where $\dot{\delta}_c$ is a reference creep rate corresponding to the proof load P_c, P is the pile load, t is time, and n a creep parameter. The model pile load can be readily converted to a shear stress by dividing by the pile surface area. Differentiation of equation (1) with respect to time gives the displacement (creep) rate $\dot{\delta}$. For a small increase in load, with other variables constant, the ratio of displacement rates can be expressed in terms of the initial load P_1, the new load P_2, and the creep parameter n, thus

$$\frac{\dot{\delta}_2}{\dot{\delta}_1} = \frac{\dot{\delta}_c (P_2 / P_c)^n}{\dot{\delta}_c (P_1 / P_c)^n} = \left(\frac{P_2}{P_1}\right)^n \qquad (2)$$

Equation (2) may also be obtained from the relationship representing primary creep. Applying equation (2) to the rates represented in Fig. 4, test XI, with $\dot{\delta}_1$ = 0.540 mm/hr, $\dot{\delta}_2$ = 0.892 mm/hr, P_1 = 2.20 kN, and P_2 = 2.20 + 0.065(2.20) = 2.34 kN gives n = 8.13. Similar computations can be made for the other static load increase data points shown on Fig. 6 with good agreement and an average n close to 8.22.

With frequency effects very small or negligible, and load change taken equal to the dynamic load amplitude, calculations with equation (2) using P_2 = (static load + dynamic load amplitude), P_1, $\dot{\delta}_1$, and $\dot{\delta}_2$ as before, give an average value of n = 4.20 for all dynamic loads. Examination of Fig. 6 shows a decrease in the displacement rate ratio ($\dot{\delta}_2 / \dot{\delta}_1$) with an increase in displacement rate immediately before dynamic loading. The slower $\dot{\delta}_1$ values correspond more closely to secondary creep. For the same loads (P_1 and P_2), the creep parameter n changed, i.e., n appears to increase from about 3.1 to 5.5 as $\dot{\delta}_1$ decreased. Available information indicates that n does not change for a static load increase applied to the model pile. The range in n values provides an estimate of the magnitude of the displacement rate changes for dynamic loading.

CONCLUSIONS

1. A technique has been developed for measurement of displacement rate changes due to dynamic loads superimposed on statically loaded model piles. For small static load increases and nonresonant cyclic loading this method appears to be suitable for determination of a creep parameter n.
2. Model pile displacement rates in frozen sand were observed to be essentially independent of frequency for small dynamic loads superimposed on a large static load in the range of 0.1 Hz to 10 Hz.
3. Cyclic loads significantly increased pile displacement rates over those observed for a sustained load. The magnitude of rate increase was shown to be dependent on amplitude of the cyclic load.
4. Creep theory appears to be suitalle for prediction of the change in pile displacement rates due to a small cyclic load. The method does require use of loads and a reduced creep parameter n determined experimentally following procedures outlined in this paper.

ACKNOWLEDGMENTS

The authors wish to express their appreciation to the National Science Foundation for their support of this research project.

REFERENCES

Andersland, O.B., and Alwahhab, M.R.M. (1983) Lug behavior for model steel piles in frozen sand. PERMAFROST, Proceedings 4th International Conference, National Academy Press, Washington, D.C., p. 16-21.

Ladanyi, B., and Guichaoua, A. 1985. Bearing capacity and settlement of shaped piles in permafrost. Proceedings, 11th International Conference on Soil Mechanics and Foundation Engineering, A.A. Balkema, Boston, Vol. 3, p. 1421-1427.

Parameswaran, V.R. (1984) Effect of dynamic loads on piles in frozen soils. Proceedings, 3rd International Cold Regions Engineering Specialty Conference, Canadian Society for Civil Engineering, Montreal, Canada, Vol. I, p. 41-52.

Schmid, W.E. (1969) Driving resistance and bearing capacity of vibro-driven model piles. PERFORMANCE OF DEEP FOUNDATIONS, American Society for Testing and Materials, Special Technical Publication 444, p. 362-375.

Stelzer, David (in preparation, 1988). Cyclic load effects on model pile behavior in frozen sand. Ph.D Dissertation, Michigan State University, East Lansing, Michigan.

Thomas, H.P., and Luscher, U. (1980) Improvement of bearing capacity of pipe piles by corrugations. Collection of papers from a U.S. Soviet Joint Seminar, Leningrad, USSR.

TANGENTIAL FROST-HEAVING FORCE OF THE REINFORCED CONCRETE PILE AND CALCULATION OF PREVENTING IT FROM PULLING UP DUE TO FROST HEAVE

Sun, Yuliang

Water Resources Committee of Songhua-Liao Basin, Ministry of Water Resources and Electric Power, P.R.C.

SYNOPSIS Tangential frost heaving force against the pile and the frictional resistance in soil are important indexes in pile design to prevent it from pulling up by frost heaving. In order to study these forces the field tests for the pile with different diameter and embeded depth and foundation plate size carried out by the author. The reinforcement meters were used for measuring heaving force. This paper will put emphasis on description of measuring results of tangential frost-heaving force, the extent to which frost heaving is distributed within the extent of broaden plate and its role in preventing pile from pulling up due to frost heaving. In addition, based on these results the computation of pile stability against pulling up due to frost heaving is discussed also in these paper.

IN-SITU TESTS

Shuangliao and Gongzuling pile foundation in-situ test fields were constructed in 1983 and 1984, respectively, both of them are situated in the western area of Jilin province in P.R.C. In the area every year from Nov. when it begins to freeze-up till late May of the next year frozen layer thaws up, the freeze-thaw period lasts about half a year. In these fields, the maximal frozen depth is 1.45 m, before soil is freeze-up the underground water level is 1.2-1.3 m below the ground surface. The soil properties of these fields are different: the soil of Shuangliao field is low-liquid limit clay and contains sifty sand layer below 0.8 m. Yet the soil of Gongzuling field belongs to middle-liquid limit clay. The maximal frost heave is 10-12.7 cm in Shuangliao and 10-17.7 cm in Gongzuling. In-situ dynamometric piles are reinfoced concrete ones, which are single pile anchored. There are two modes of foundation anchoring, one is bore poured pile, the other is big-headed anchoring pile. There are 11 dynamometric piles in Shuanliao field, and so are in Gongzuling, yet in the late, two of the piles are installed for frictional resistance tests. In-situ dynamometric instruments adopted are reinforcement meters. The dynamometric system consists of three parts: A. anchoring part, pouring pile and big-headed anchoring pile are adopted in order to fix dynamometric equipments; B. dynamometric part, the dynamometric section is formwork lining poured reinforced concrete pile, the length of which is equal to the maximal frozen depth in the local area; C. dynamometric elements, this are reinforcement meters, the lower ends of the meters are fixed on the anchoring foundation, the other ends are fixed to the pressure transfer plates on the top of the piles. Under the action of tangential frost heaving, reinforcement meters are in tensile condition. The system structure is shown in Fig. 1. Each measuring time the electric resistance ratio and the resultant electric resistance is measured, according to the difference of the two above values the tangential frost heaving force is derived.

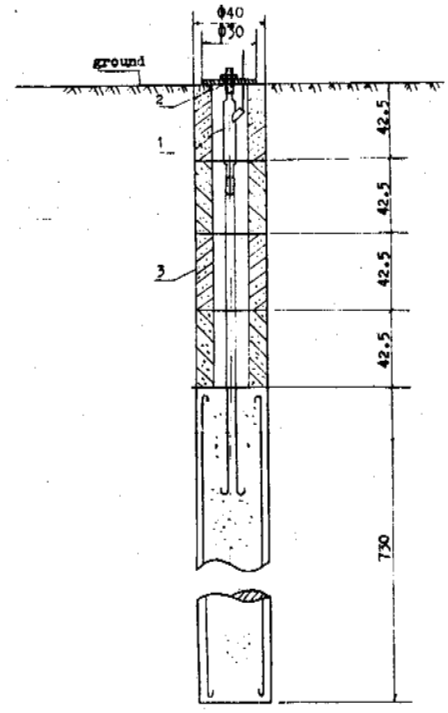

Fig.1 Reinforcement Meter Dynamometric System
1--Reinforcement Meter, 2--Pressure Transfer Plate, 3--Dynamometric Section

In order to eliminate the effect of synthetic factors upon the dynamometric system, non-stress meters were included and both the temperature and the non-stress meter correction were conducted to the measuring quantities. The results of this two corrections are close, their difference is within 1.33 KN, shown in lines 1 and 2 Of Fig. 2.

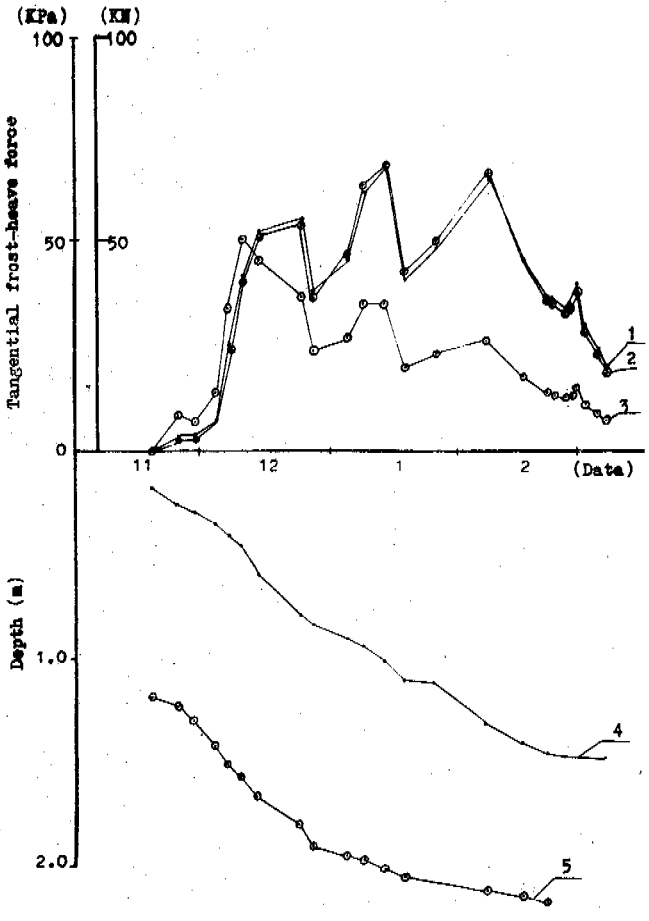

Fig.2 Process Lines of Tangential Frost Heaving Force, Frozen Depth and Underground Water

1--Total frost heaving force with temperature correction (KN)
2--Total frost heaving force with non-stress meter correction (KN)
3--Unit tangential frost heaving pressure (KPa)
4--Frozen depth (cm)
5--Underground water level

TANGENTIAL FROST HEAVING FORCE AND PULLING-UP RESISTANCE

The Development of Tangential Frost Heave Force

In the early freeze-up stage, the tangential frost heaving force develops rapidly and the unit tangential frost heaving pressure reachs the maximal value at the frozen depth of 0.4 m. After entering the middle stage of the development, the tangential frost heaving force increases continuously and reachs its maximum. However, due to the effects of temperature increasing and decreasing and other factors, the velocity of frozen depth development is larger than that of frost pulling-up force, hence the unit tangential frost heaving force tends to decrease. In the late stage of freeze-up period as the rates of frozen depth and frost heaving are slowed down, the force decreases gradually until it is disappeared completely (see Fig.2). In-situ tests indicate that the time when tangential frost heaving force reachs its maximal value, generally speaking, is not coincide with the time of maximal frozen depth (H_m), but at the time of $(0.5\text{-}0.7)H_m$. Therefore, in the calculation of unit tangential frost heaving force the value of frozen depth one should take is not its maximum, but its corrections mentioned previously.

The Effect of Pile Diameter on the Tangential Frost Heaving Force

The test results indicate that the effect of the pile diameter to the force value is not significant. This is due to the fact that the inhomogeneity of frost heave is more notable than pile diameter to influence tangential frost heaving force. For instance, the inhomogeneous frost heaving of surrounding soil, the separation of the pile surface from the frozen layer, the crack in ground surface and so forth all can influence the force obviously. In engineering practise the pile diameter usually is 0.4-0.6 m, the effect of pile diameter can be ingnored.

The Effect of the Density of Backfill

The density of backfill influence the tangential frost heaving directly. This is apparent in the results of 1983-1986 in Shungliao field (see Table 1.) The test data of first year are lower than that of late two years because of the fact that in the first year the surrounding backfill is still loose with comparatively large voids and the strength of freze-bond with pile surface is comparatively weak. It was discovered also that there were cracks along the boundary of the pile and the backfill, and this, of course, is another important factor to decrease the force value. Comparing the results of late two years, the measured force values were still increasing, however, the increment is not notable. It can be deemed that after three years sinking, the den density of backfill already became stable. Therefore, the data of 1985-1986 can be chosen for the calculation.

The Determination of the Design Value of the Tangential Frost Heaving Force

There are many factors which can influence the tangential frost heaving force of pile foundation. Therefore, in the same field the tested force values are vary from pile to pile. Furthermore, for the same pile the maximal values and the time when the maximum occurs are not the same in different years. For instance, for pile No.3 of Gongzuling field on Dec. 19 of

TABLE 1

The Dynamometric Results of Shuangliao Test Field

Pile No.	1983-1984		1984-1985		1985-1986	
	Total (KN)	Unit (KPa)	Total (KN)	Unit (KPa)	Total (KN)	Unit (KPa)
1	18.9	10.7	37.1	27.9	50.9	40.1
2	22.8	14.1	82.7	51.7	99.7	58.8
3	13.5	7.7	30.2	22.7	40.4	48.9
4	10.8	12.8	40.8	34.3	66.8	60.1

For the convenience of comparison, the obtained data of tangential frost heaving force and the frictional resistance in the two fields in recent years are listed in Table 2 for select in calculation. There are 7 piles from Shuangliao, 9 from Gongzuling, amounts to 16 piles.

In Table 2, the maximal total force of Shungliao field occurs at pile No. 3, the maximal unit force at pile No. 4; in Gongzuling, however, the maximal total force at pile No. 8, while the maximal unit force at pile No. 9. The maximal total and unit forces do not occur at the same pile, which is on account of the effect of frozen depth. Since the time when the maximum occurs are different, the corresponding frozen depth are changing also, as a result, value of unit force is influenced. In general cases, the maximum of tangential frost heaving force often occurs in the early freeze-up stage (see line 3 of Fig. 2). From line 3 one can see that the maximal unit force occurs in the early stage, the minimum in the late stage. Hence, one should not take the unit force at either of above two stages as criteria to determine the force value. Since in the early stage, the total force corresponding to the unit force is not the maximum, and in the late stage the unit force is the minimum, however, the design desired data is the maximum of the total force. In order to solve this contradiction, the reductive coefficient of the frozen depth is derived based on the frozen depth data corresponding to the maximal total force. As mentioned previously the time when the maximal tangential frost heaving force occurs is at the frozen depth of (0.5-0.7)Hm, where Hm--the maximal frozen depth or the standard frozen depth in local area. Let's take 0.7Hm as

TABLE 2

Maximal Value of Tangential Frost Heaving Force

Pile No.	Gongzuling Field		Shuangliao Field	
	Total (KN)	Unit (KPa)	Total (KN)	Unit (KPa)
1	70.1	32.6	50.9	40.1
2	73.2	34.4	35.8	28.2
3	83.1	41.1	79.7	50.3
4	35.0	14.9	66.8	60.1
5	58.4	39.7	53.2	41.8
6	53.0	24.7	56.3	43.8
7	69.3	52.2	46.0	29.1
8	83.9	43.7		
9	68.5	58.9		

frozen depth, in the area of above fields the frozen depth after correction is Hz=1.0 m. From this, the calculated unit forces in Shungliao and Gongzuling are 56.8 KPa and 52.4 KPa, respectively. The design value can be taken as p=60 KPa.

Frictional Resistant Force of Pile Foundation

The in-situ observed data of limit frictional resistant force of pile foundation are few. In order to determine the force value range, we study the pulling-up resistant according to stability calculation of piles and in-situ test data. For the poured pile, in the case of no top load, the limit equilibrium of pulling-up resistance can be proved by the formula: (Wang,1983):

$$T=\pi D\sum h_i f_i + 0.9W$$

where T--pulling-up force, KN,
D--diameter of the pile, m,
h_i--the depths of every surrounding soil layer, m,
f_i--the limit frictional resistant forces between every surrounding soil layer.

and the pile surface, KPa,
W--the weight of pile itself, KN, for the underwater part, take float weight.

For pile No.3 of Shungliao field we computed the limit pulling-up frictional resistant force. The diameter of pile No.3 is 0.45 m with embeded depth of 9 m. According to the test data, from Jan. 13,1986, the pile was pulled-up gradually, till Jan. 31 the total pulling-up amounted to 6 mm. On the basis of the two different frozen depths on Jan. 13 and Jan. 31, the calculated results are as follows: the frozen depth on Jan. 13 is 0.9 m, pulling-up force is 72 KN, frictional resistant force f_1=4.5KPa; the frozen depth on Jan. 31 is 1.12 m, pulling-up force is 79.7KN, frictional force f_2=6.4 KPa. In order to obtain the pulling-up frictional resistant force, the pull-out tests were carried out at Gongzuling field. The tested two piles are with diameter of 0.6 m and embeded depth of 9 m. In order to exploit the normal frost heave force to pull-out the pile, a reinforced concrete plate with a diameter of 1 m was fixed onto the top of the pile. The lower surface of it was against the ground, therefore, pile shaft was pulled-out by the normal frost heaving force. According to the measured pulling-out force, the calculated pulling-up frictional resistances are f_3=9.02 KPa, f_4=7.30 KPa, respectively. Comparing the frictional resistance f_1 with f_2 in Shuangliao field, $f_1 < f_2$. From the dynamometric and deformation measurement results one can see that the pulling-up amount of pile foundation on Jan. 13 was 3 mm, did not reach its limit, till Jan. 31 the pulling-up amount was 6 mm, and the pulling-up force of the pile had already reached its limit. Therefore, it is rational to take the value of f_2, that is, the design frictional resistant force is taken as f_p=6 KPa. With the tangential frost heaving force and the limit frictional resistance, the pulling-up stability analysis of pile foundation can be carried out acording to the corresponding criteria.

CONCLUSIONS

The test results of tangential frost heave force of Shuangliao and Gongzuling can be applied to bore-poured reinforced concrete piles whose embeded parts in frozen layer are required to be formwork poured. In order to avoid the effect of normal frost heaving, it is not allowed to construct crossgirders linking pile shafts in the frozen layers or on the ground surface. The reinforcement bars should stretch to the lower end of the pile in order to meet the pulling-up strength requirements. From the results, we can draw the conclusions as follows:

(1) The reinforced concrete piles at Shuangliao and Gongzuling fields are formwork poured within the frozen depth, hence the values of tangential frost heaving force is determined when the pile surface is comparitively smooth. As the average frost heaving rate of the local areas is 6.9-12.2%, the design value of unit tangential frost heaving force is τ_p=60 KPa, which can be refered to for pulling-up design of pile foundation under similar situations.

(2) Under the local conditions, the design value of limit frictional resistant force is 6-7 KPa. The value is obtained by longterm in-situ frozen pulling-up and pulling-out tests, therefore, it is valuable in practice.

(3) For measuring the tangential frost heaving force, the dynamemetric system with reinforcement meter is quite simple and durable.

REFERENCES

Wang Tianqing, 1983. Guide Book of Norm and Standards for Architecture in China and Abroad. Heilongjiang Science and Technology Publishign House.

BEHAVIOUR OF LONG PILES IN PERMAFROST

A. Theriault and B. Ladanyi

Northern Engineering Centre, Ecole Polytechnique, Montreal, Canada

SYNOPSIS Loading axially a long pile in permafrost results in a transient redistribution of stresses along its shaft due to time-dependent displacements characterizing frozen soil creep. Until now, finite element or finite difference methods had to be used for simulating the behaviour of such piles. In this paper, an analytical solution for the same problem is presented and its predictions are compared with some published data obtained by a numerical calculation method and by a direct observation of model piles.

INTRODUCTION

The piles used as foundations in permafrost soils are generally made of concrete, wood or steel. While concrete piles are usually considered to be rigid with respect to the soil, pile compressibility has to be taken into account in the design of slender steel or timber piles.

Pile compressibility produces a stress distribution along the pile that varies with time and displacement. A numerical solution has been presented by Nixon and McRoberts(1976) for a pile embedded in frozen soil. For piles in unfrozen soils, analytical solutions, based on the lateral shear modulus concept, have been published by several authors (Cambefort, 1964; Coyle and Reese, 1966; Cassan, 1966; Murff,1975, 1980; Randolph and Wroth, 1978; Alpan, 1978; Silvestri et al.,1986; Murff and Shapery,1986), while, for piles embedded in an ideal elastic soil mass, numerical solutions have been obtained by Poulos and Davis(1968) and Mattes and Poulos(1969).

In this paper, an attempt is made to extend some of these solutions to piles in frozen soils. The proposed solution accounts for creep properties of the soil surrounding a pile, in addition to the pile-soil interface behaviour and pile properties normally considered by solutions used for unfrozen soils. Similarly, the solution can account for slip along any portion of the pile-soil interface, which takes place after a certain shear displacement. As a result, the theory can evaluate changes in pile stress and deformation, as well as pile-soil interface shear stresses with time at any position along the pile.

The results obtained by the proposed theory are then compared with those found earlier by the finite difference procedure (Nixon and McRoberts,1976) and those measured on model piles (Zhigul'skiy,1966).

THEORY

It is known that for slender piles in permafrost under service conditions, only a very small fraction of the applied axial load is transfered to the pile base. The theory presented here neglects the base resistance; however, its effects can be taken into account easily, as shown by Thëriault (1988).

Consider a cylindrical open ended pile embedded in permafrost (Fig.1), with radius r, embedded length D, and Young's modulus E. The equivalent axial modulus of the pile, E_p, can be calculated from

$$E_p = E\, A_p/\pi r^2 \qquad (1)$$

where A_p is the true area of the pile cross section. Vertical equilibrium of a section of the pile, dz, gives

$$dP + 2\pi r\tau dz = 0 \qquad (2)$$

where P is the axial load, τ is the shear stress along dz, and z is the depth. Since the average axial stress in the pile, σ, is related to P by

$$dP = \pi r^2\, d\sigma, \quad \text{one gets} \qquad (3)$$

$$d\sigma/dz + 2\tau/r = 0 \qquad (4)$$

In addition, considering that the elastic shortening, dw_z, of the length dz of the pile is given by

$$dw_z = -(\sigma/E_p)dz \qquad (5)$$

Equation (4) becomes

$$d^2w_z/dz^2 - 2\tau/rE_p = 0 \qquad (6)$$

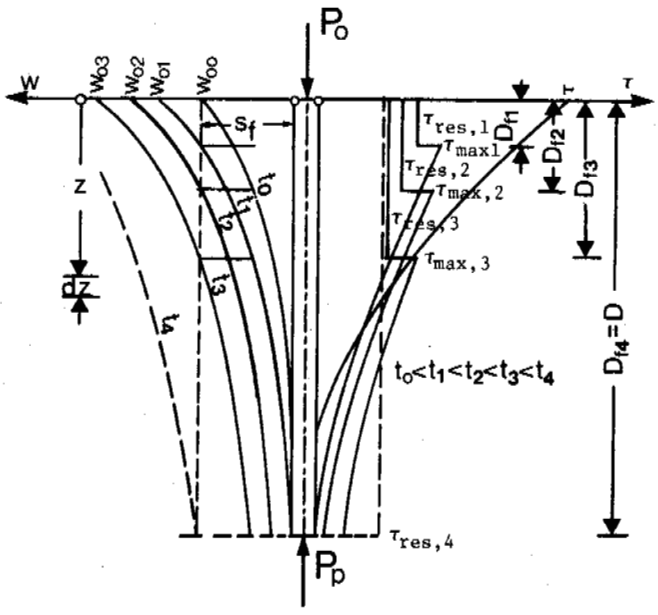

Figure 1. Schematic variation with time of pile settlement and the corresponding shear stresses along the shaft.

This differential equation can be integrated if the variation of τ along the pile shaft is specified. A usual assumption made in unfrozen soil mechanics, is that τ is a linear function of the shear displacement at the soil-pile interface, s, attaining a peak value, $\tau = \tau_{max}$, when a slip occurs at a given limiting displacement, s_f. After the slip, τ either remains constant, or falls to its residual value, τ_{res}.

In evaluating τ, most present theories limit themselves to the mobilization of bond at the pile-soil interface, neglecting the deformations of the surrounding soil. However, as shown by Johnston and Ladanyi(1972) for piles in frozen soils, and by Frank (1974), and Randolph and Wroth (1978) for piles in unfrozen soils, this relationship can be established easily, using the model of concentric cylinders in simple shear.

Using this model and assuming a power-law stress-strain rate relationship for frozen soil in simple shear

$$\dot{\gamma} = \dot{\gamma}_c (\tau/\tau_c)^n \tag{7}$$

where τ_c and $\dot{\gamma}_c$ are reference shear stress and shear strain rate, respectively, Johnston and Ladanyi(1972) obtained for a pile of radius r, and for no-slip condition, the following relationship between the settlement rate, $\dot{s} = ds/dt$ and the shear stress τ along the shaft

$$\tau = \tau_c \dot{s}^{1/n} \left(\frac{n-1}{\dot{\gamma}_c r}\right)^{1/n} \tag{8}$$

Since, for long term, when creep displacements are much larger than instantaneous ones

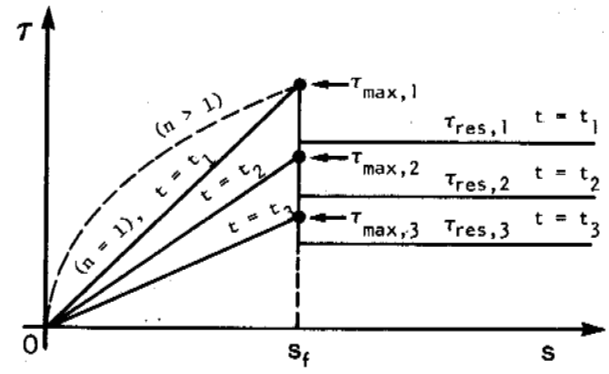

Figure 2. True (n > 1) and assumed (n = 1) mobilization of bond strength τ with shear displacement s and time t, for a pile in permafrost.

$$\dot{s} \approx s/t \tag{9}$$

Equation (8) can be written as

$$\tau \approx \tau_c (s/t)^{1/n} \left(\frac{n-1}{\dot{\gamma}_c r}\right)^{1/n} \tag{10}$$

If, instead of simple shear information, one wants to use the results of triaxial compression creep tests, then, assuming the validity of the von Mises law, it can be shown (Ladanyi, 1972) that in the above equations $\dot{\gamma}_c$ should be replaced by

$$\dot{\gamma}_c = 3^{(n+1)/2} \dot{\varepsilon}_c \tag{11}$$

with $\tau_c = \sigma_c$, where $\dot{\varepsilon}_c$ and σ_c are creep parameters in the triaxial compression creep law

$$\dot{\varepsilon}_e = \dot{\varepsilon}_c (\sigma_e/\sigma_c)^n \tag{12}$$

where $\dot{\varepsilon}_e$ and σ_e are the von Mises equivalent strain rate and stress. Note that σ_c contains the effect of temperature and confining pressure, as shown by Ladanyi(1972). Sego and Morgenstern (1985) have shown the validity of Eq.(7) for ice-rich soil and polycrystalline ice.

In addition, if one wants to use Eq.(10) for also representing the primary creep, this can be done, under a time-hardening assumption, by replacing in Eq.(10) the time t by an appropriate time function, say t^b, in which case $\dot{\varepsilon}_c$ in Eq.(11) becomes $(\dot{\varepsilon}_c/b)^b$, where $b \leq 1$, (Ladanyi,1975). Finally, Eq.(10) can then be written in a general form

$$\tau = \sigma_c (s/r)^{1/n} \left(\frac{n-1}{3^{(n+1)/2}}\right)^{1/n} (b/\dot{\varepsilon}_c)^{b/n} t^{-b/n} \tag{13}$$

Equation (13) shows that, for any given time t = const., τ is a nonlinear function of s. If there is no slip between the pile and the soil, $s = w_z$, and substitution of τ from Eq.(13) into Eq.(6) gives

$$d^2 w_z/dz^2 - M w_z^{1/n} = 0 \tag{14}$$

where M is a time-dependent coefficient.

Unfortunately, integration of Eq.(14) proved to be very difficult, so another way of solving the problem, similar to that used in unfrozen soils, had to be taken. In the latter, it is usually assumed (Fig.2) that for $w_z < s_f$, the mobilized shear stress is linearly related to the shear displacement at the pile-soil interface, such that, for $w_z < s_f$,

$$\tau = (s/s_f)\,\tau_{max} \qquad (15)$$

For $s = s_f$, $\tau = \tau_{max}$, but for $s > s_f$, $\tau \leq \tau_{max}$, eventually falling to $\tau_{residual}$, when the adhesion bond is broken (Fig.2), (see also Murff, 1980).

Under these conditions, Eq.(6) can be integrated, and several appropriate solutions are readily available in the literature. In order to use these solutions for a pile in frozen soil, the aging theory of creep can be applied, as done by Murff and Shapery(1986). In this particular case, this consists in expressing only τ_{max} in Eq.(15) as a function of time and temperature, and in finding solutions for a series of increasing time intervals. For any given time, ($t = t_i > 0$), and for a given soil temperature, Eq.(13) gives the value of $\tau_{max,i}$, corresponding to the critical (slip) displacement, $s = s_f$:

$$\tau_{max,i} = \sigma_c (s_f/r)^{1/n} \left(\frac{n-1}{3^{(n+1)/2}}\right)^{1/n} (b/\dot{\epsilon}_c t_i)^{b/n} \qquad (16)$$

Since, for $s < s_f$, $s = w_z$, substituting Eq.(15) into Eq.(6), the latter becomes

$$d^2w_z/dz^2 - N^2 w_z = 0 \qquad (17)$$

where

$$N^2 = (2/rE_p)(\tau_{max,i}/s_f) \qquad (18)$$

In Eq.(18), $(\tau_{max,i}/s_f)$ represents a shear reaction modulus, which is a function of time and temperature. The well known solution of Eq.(17) is

$$w_z = C_1 \exp(Nz) + C_2 \exp(-Nz) \qquad (19)$$

and from Eq.(5), the axial stress in the pile is

$$\sigma_z = -E_p N[C_1 \exp(Nz) - C_2 \exp(-Nz)] \qquad (20)$$

where C_1 and C_2 are integration constants to be determined from the boundary conditions. The particular solutions have the following form.

(1) No slip solution ($w_o \leq s_f$)

If it is assumed that there is no slip between the pile and the soil, Eqs.(19) and (20) can be solved by introducing the boundary conditions $\sigma_z = \sigma_o = P_o/\pi r^2$ at $z = 0$, and $\sigma_z = 0$ at $z = D$. This yields (e.g., Farmer, 1975)

$$w_z = (\sigma_o/E_p N)\left[\frac{\cosh N(D-z)}{\sinh (ND)}\right] \qquad (21)$$

$$\sigma_z = \sigma_o \left[\frac{\sinh N(D-z)}{\sinh (ND)}\right] \qquad (22)$$

The settlement of the pile head is then, at $z = 0$,

$$w_o = (\sigma_o/E_p N) \coth (ND) \qquad (23)$$

giving w_z in terms of w_o

$$w_z = w_o \left[\frac{\cosh N(D-z)}{\cosh (ND)}\right] \qquad (24)$$

At the moment when slip starts at $z = 0$, w_z is given by Eq.(24), in which $w_o = s_f$.

(2) Slip-everywhere solution ($w_z > s_f$)

As the other extreme, when slip has taken place along the whole pile length, and τ has dropped to its constant residual value, τ_{res}, Eq.(17) becomes

$$d^2w_z/dz^2 - (2/rE_p)(\tau_{res}/1m) = 0 \qquad (25)$$

where $(\tau_{res}/1m)$ is the new shear reaction modulus, constant along the pile, but depending on time and temperature, because τ_{res} usually represents a fraction of τ_{max}.

Integrating Eq.(24) and respecting the boundary conditions that at $z = 0$, $w_z = w_o$ and $dw_z/dz = -\sigma_o/E_p$, yields

$$w_z = w_o - (z/E_p)[\sigma_o - \tau_{res}\, z/r] \qquad (26)$$

and

$$\sigma_z = \sigma_o - 2\,\tau_{res}\, z/r \qquad (27)$$

In fact, Eq.(26) is valid only when the displacement at the pile base has also attained the critical value, i.e., $w_D = s_f$ at $z = D$. In that instant, the settlement of the pile head will be

$$w_o = s_f + (D/E_p)[\sigma_o - \tau_{res}\, D/r] \qquad (28)$$

Note that, under field conditions, τ_{res} will tend with time to a finite value, affected by gravity stresses and generally increasing with depth. A solution for such conditions in unfrozen soil was obtained by Silvestri et al. (1986).

(3) Partial-slip solution ($w_o \geq s_f$)

In that case, it is assumed that slip has occurred down to the depth $z = D_f$ (Fig.1), while there is no slip along the rest of the pile length, $(D - D_f)$. The boundary conditions for Eqs.(19) and (20) are then: $w_z = s_f$ at $z = D_f$, and $dw_z/dz = 0$ at $z = D$. This gives for the portion of the pile below the zone of slip ($D_f < z \leq D$),

$$w_z = s_f \left[\frac{\exp(NZ) + \exp N(2D - z)}{\exp(ND_f) + \exp N(2D - D_f)}\right] \qquad (29)$$

and

$$\sigma_z = E_p N\, s_f \left[\frac{\exp N(2D - z) - \exp(Nz)}{\exp(ND_f) + \exp N(2D - D_f)}\right] \qquad (30)$$

The critical depth where slip occurs, D_f, can be found by satisfying the axial stress equilibrium at $z = D_f$, i.e., by making Eq.(27) equal to Eq.(30):

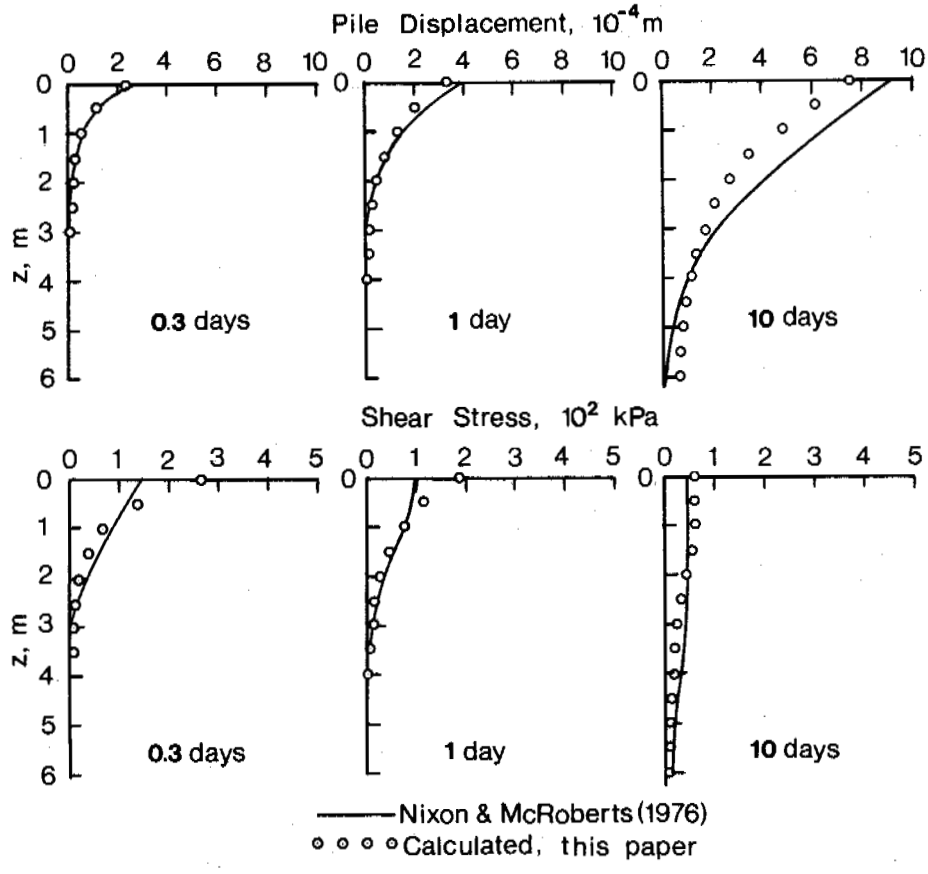

Figure 3. Displacements and shear stresses for a 6.1 m long timber pile in permafrost, obtained by the finite difference method (Nixon and McRoberts, 1976), and by the proposed analytical solution.

$$\sigma_o - (2\,\tau_{res}\,D_f)/r + E_p N s_f \left[\frac{\exp(ND_f) - \exp N(2D-D_f)}{\exp(ND_f) + \exp N(2D-D_f)}\right] = 0 \qquad (31)$$

Once D_f is known, the values of w_z and σ_z at any depth along the pile can be determined for any given values of the applied load and time.

Value of s_f

Similarly as for piles in unfrozen soils, the value of critical slip displacement, s_f, for piles in frozen soils depends on the shape and roughness of the pile shaft, and on the method of pile installation. For very rough cast-in-place piles in a frozen varved soil, Johnston and Ladanyi(1972) found s_f to be of the order of 20 to 30 mm. These values are not much different from those found for piles in unfrozen soils (Vesić, 1976). For driven piles, s_f value may be also a function of the pile diameter. On the other hand, in small scale shear box tests with frozen sand against smooth metallic surfaces, Thériault(1988) has found for s_f a value of about 0.4 mm.

CALCULATION PROCEDURE

Settlements

For predicting the time-dependent settlement of a compressible pile, embedded in frozen soil and loaded by a constant load, P_o, the following procedure is suggested:

(a) For a given time, $t = t_i > 0$, and for known values of E_p and s_f, determine $\tau_{max,i}$ from Eq.(16), and $N = N_i$ from Eq.(18).

(b) Determine D_f from Eq.(31).

(c) If $D_f \leqslant 0$, calculate w_o from Eq.(23), by taking increasing time intervals, until $w_o = s_f$.

(d) If $D_f > 0$, calculate w_o from Eq.(28) by substituting D_f for D. As D_f increases and τ_{res} decreases with time, w_o will also increase until it attains its final finite value given by Eq.(28). From that instant on, only settlement rate can be determined, if $\tau_{res} = f(\dot{e})$ is known.

Clearly, as mentioned, for pile sections located between $D_f < z \leqslant D$, the time settlement is given by Eq.(29).

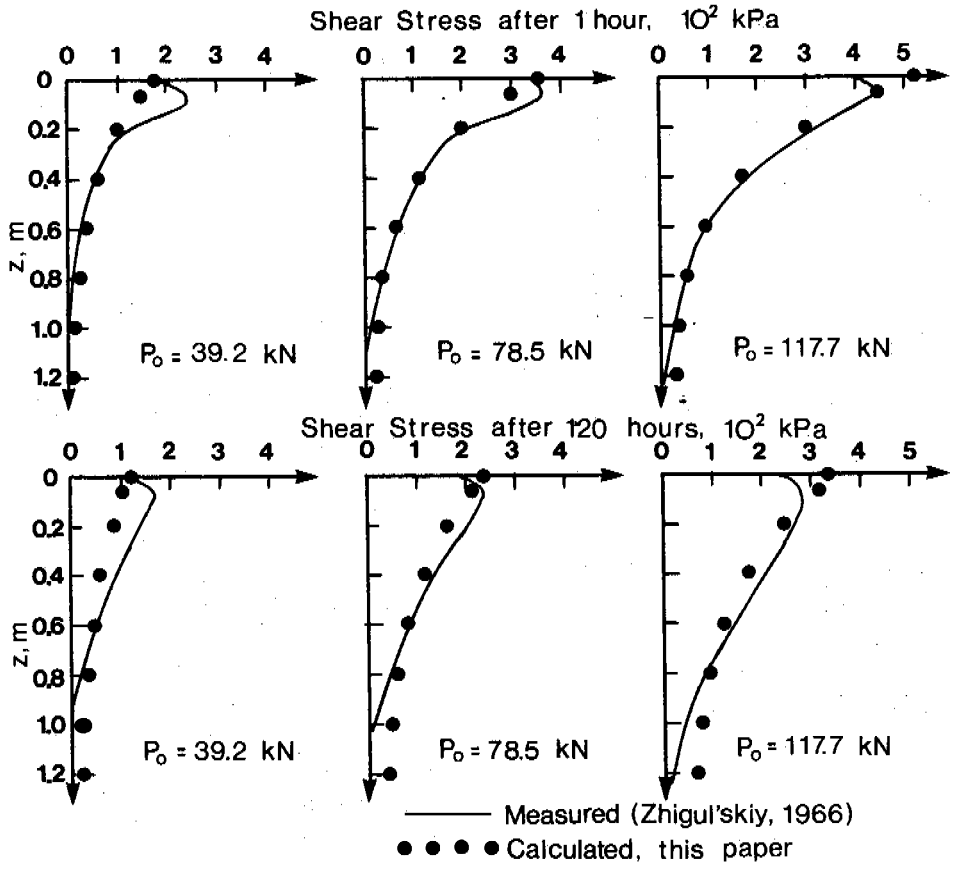

Figure 4. Short- and long-term shear stresses along the shaft of a 1.20 m long model tubular pile, obtained by direct measurements (Zhigul'skiy, 1966), and calculated by the proposed analytical solution.

Axial stresses in the pile

(a) Before slip ($D < D_f$): use Eq.(22).

(b) For partial slip ($0 < D_f < D$): use Eq.(30).

(c) For complete slip ($D_f = D$): use Eq.(27).

Clearly, because $N = f(\text{time})$, there is a continuous axial stress redistribution for any given P_o value.

Tangential stresses along the pile

In the region where $w < s_f$, one gets from Eq.(15):

$$\tau = w_z(\tau_{max}/s_f) \qquad (32)$$

enabling to calculate τ :

(a) Before slip ($D < D_f$), from Eq.(21).

(b) For partial slip ($0 < D_f < D$), from Eq.(29).

(c) For complete slip ($D_f = D$), $\tau = \tau_{res}$.

A program in BASIC is available for these calculations.

COMPARISON WITH PUBLISHED DATA

As no complete case histories on the field behaviour of compressible piles in permafrost have been published to date, the predictions by the proposed theory have been compared with two published studies: one involving a numerical solution (Nixon and McRoberts, 1976), and another one presenting the results of observations on model piles (Zhigul'skiy, 1966).

Nixon and McRoberts (1976) have used the finite difference procedure to simulate the behaviour of a compressible pile embedded in an ice-rich soil or ice. As no slip was allowed at the pile-soil interface, they used the Johnston and Ladanyi (1972) theory for taking into account the soil creep, as in this paper. They also assumed a zero point resistance. The pile characteristics were: D = 6.1 m, r = 0.1525 m, E_p = 8.3 GPa (timber pile), and the pile was loaded by P_o = 188 kN. The ice-rich soil at a temperature of -2°C, was characterized by: b =

1, n = 1.72, and σ_c = 47.6 kPa at $\dot{\varepsilon}_c$ = 1.9×10^{-8} min^{-1}. A slip displacement of 0.4 mm was assumed in the calculation.

Figure 3 shows a comparison between the finite difference solution (full lines) and the proposed analytical solution (points) for three different times after load application. A reasonably good agreement can be seen in both the displacements and the shear stresses along the shaft.

A second comparison is based on the test results on model piles, published by Zhigul'skiy(1966). His tests were made on tubular open-ended aluminium piles embedded in frozen sand. The pile characteristics were: D = 1.20 m, r = 0.103 m (wall thickness 3 mm). As no properties of the frozen sand used in the tests have been reported by the author, some typical values of parameters, found by Thériault(1984) for a similar frozen fine sand ("Joliette Sand"), have been used in the calculation. For the test temperature of -3.2°C, these are: b = 0.67, n = 4.0, and σ_c = 1390 kPa at $\dot{\varepsilon}_c = 10^{-5}$ min^{-1}. As before, it was assumed that s_f = 0.4 mm.

Figure 4 shows the results of the comparison for both short-term (t = 1 hour) and long-term (t = 120 hours) tests, and for the applied loads of 39.2, 78.5, and 118 kN, respectively. The agreement between the observations (full lines) and the predictions (points) is seen to be quite reasonable, keeping in mind that the properties of frozen sand used in the tests, and the value of s_f had to be taken from other sources.

CONCLUSION

A complete analytical solution for an axially loaded compressible pile, embedded in frozen soil is presented. The solution accounts for creep properties of the soil, in addition to the usual pile-soil interface behaviour, including slip. Comparison between stresses and displacements predicted by the proposed solution, and those obtained earlier by a numerical procedure and by a direct observation on model piles, respectively, shows a satisfactory agreement. It is noted that all necessary calculations can be made on a PC, using BASIC, or can be programmed for a pocket calculator.

ACKNOWLEDGEMENT

This work was financially supported by the grants A-1801 and G-1566 (B. Ladanyi) of the National Science and Engineering Research Council of Canada.

REFERENCES

Alpan, I. (1978). Das Last-Setzungverhalten des Einzelpfahles (Load-Settlement Behaviour of a Single Pile). Bauingenieur, Vol.53, pp.293-298.

Cambefort, H. (1964). Essai sur le comportement en terrain homogène des pieux isolés et des groups de pieux. Annales ITBTP, Vol.17, no.204, p.1492.

Cassan, M. (1966). Le tassement des pieux: synthèse des recherches récentes et essais comparatifs. Sols-Soils, No.18-19, pp.43-52.

Coyle, H.M. and Reese, L.C. (1966). Load Transfer for Axially Loaded Piles in Clay. J.of Soil Mech.& Found.Div.,ASCE, Vol.92, No.SM2, pp.1-26.

Farmer, I.W. (1975). Stress Distribution along a Resin Grouted Rock Anchor. Int.J.of Rock Mech.& Mining Sci., Vol.12, No.11, pp.347-351.

Johnston, G.H. and Ladanyi, B. (1972). Field Tests of Grouted Rod Anchors in Permafrost. Canad.Geotech.J., Vol.9, pp.176-194.

Ladanyi, B. (1972). An Engineering Theory of Creep of Frozen Soils. Canad.Geotech.J., Vol.9, pp.63-80.

Ladanyi, B. (1975). Bearing Capacity of Strip Footings in Frozen Soils. Canad.Geotech.J., Vol.12, pp.393-407.

Mattes, N.S. and Poulos, H.G.(1969). Settlement of Single Compressible Pile. J.of Soil Mech.& Found.Div.,ASCE, Vol.95, SM1, pp.189-207.

Murff, J.D. (1975). Response of Axially Loaded Piles. J.of Geotech.Engrg.Div.ASCE, Vol.101, GT3, pp.356-360.

Murff, J.D. (1980). Pile Capacity in a Softening Soil. Int.J. of Numer.& Analyt.Meth. in Geomech., Vol.4, pp.185-189.

Murff, J.D. and Schapery, R.A.(1986). Time Dependence of Axial Pile Response. Int.J.of Numer.& Analyt.Meth. in Geomech., Vol.10, pp. 449-458.

Nixon, J.F. and McRoberts, E.C.(1976). A Design Approach for Pile Foundations in Permafrost. Canad.Geotech.J., Vol.13, pp. 40-57.

Poulos, H.G. and Davis, E.H.(1968). The Settlement Behaviour of Single Axially Loaded Incompressible Piles and Piers.Geotechnique, 18,pp.351-371.

Randolph, M.F. and Wroth, C.P.(1978). Analysis of Deformation of Vertically Loaded Piles. J.of Geotech.Engrg.Div.ASCE, Vol.104, GT12, pp.1485-1488.

Sego, D.C. and Morgenstern, N.R.(1985). Punch Indentation of Polycrystalline Ice. Canad.Geotech.J., Vol.22, pp.226-233.

Silvestri, V., Chapuis, R.P. and Soulié, M. (1986). Prediction of Axial Capacity of Long Piles in Soft Cohesive Soils. Proc.3rd Int. Conf.on Numer.Methods in Offshore Piling, Nantes, France, pp. 191-200.

Thériault(Guichaoua), A. (1984). Capacité portante des pieux tronconiques et crénelés. Mémoire M.Sc.A., Ecole Polytechnique, Montréal, 111p.

Thériault, A. (1988). Capacité portante des pieux dans le pergélisol. Thèse Ph.D., Ecole Polytechnique, Montréal, 350p.

Vesić, A.S. (1977). Design of Pile Foundations. Transp.Res.Board Monograph, NRC,Washington, 68p.

Zhigul'skiy, A.A. (1966). Experimental Investigation of the State of Stress and Strain in the Soil around a Pile. Proc.8th Conf.on Geocryology, Yakutsk, USSR, Part 5, pp.211-223, (In Russian).

INVESTIGATION ON TANGENTIAL FROST HEAVING FORCES

Tong, Changjiang[1], Yu, Chongyun[1], and Sun, Weimin[2]

[1]Lanzhou Institute of Glaciology and Geocryology, Academia Sinica, China
[2]Institute of Daqing Oilfield Construction Design and Research

SYNOPSIS The tangential frost heaving force acting on the lateral surface of foundations depends upon the composition and moisture condition of the soil, freezing rate and foundation material. Test results show that silty soil and loam may create the maximum tangential frost heaving force. The tangential frost heaving force increases with increasing moisture content, negative temperature and freezing rate of soils and the roughness of the surface of foundations. The tangential force also increases with the rise of the groundwater table. The tangential force varies with the foundation material. It has a maximum value for concrete piles and lower values for steel and wood piles. Test results also show that the tangential frost heaving force does not depend upon the diameter of piles. The design values of tangential frost heaving forces, which were determined based on the susceptibility of soils, are also given in this paper.

INTRODUCTION

In the last 50 to 60 years, extensive researches on tangential frost heaving forces acting upon lateral surfaces of foundation piles in the freezing process have been conducted by many investigators. Since 1965, the authors have carried out a lot of experiments on this subject both in the laboratory and at field stations. In addition, plenty of data on frost heaving forces were obtained by the Wangjia Field Test Station of Heilongjiang Provincial Institute of Water Conservancy, the Qingan Field Test Station of Heilongjiang Provincial Institute of Traffic Science and the Yanjiagong Field Observation Station of Heilongjiang Provincial Institute of Low-Temperature Construction Science. Some achievements have been made in the study on the formation and development of the tangential frost heaving force and its influencing factors. Design values of tangential frost heaving stresses have been proposed. Further research, however, is still needed for better understanding of the mechanism of formation of the force and the interaction between foundations and frozen ground, as well as stress distribution in frozen ground. This paper discusses some of the test results obtained by the authors and other investigators.

DISCUSSION

Distribution of Tangential Frost Heaving Stress on Lateral Surface of a Pile

The experimental results show that the distribution of tangential frost heaving stress on the lateral surface of a pile is extremely non-uniform during the process of freezing. The peak value of the stress moves down with the penetration of the frost front and reaches its maximum value when the frost front drops down to the 2/3 of the maximum penetration depth, as is shown in Fig.1 (Tong and Guan, 1985a). The variation of tangential frost heaving stress at different depths is closely related to soil moisture, temperature and the volume of moisture migration. During the whole process of freezing, each layer of soil experiences four stages: initial freezing, active freezing, cooling and super-cooling. Tangential frost heaving pressure increases chiefly in the 1st and 2nd stages, and decreases in the 3rd and 4th stages.

Influence of Soil Characteristics on Tangential Frost Heaving Stress

Under similar thermal and moisture conditions, a decrease in grain size leads to an increase in tangential frost heaving stress. The magnitudes of the stress for various types of soil are in the order of: silty loam>loam>clay gravel>medium sand>coarse sand (Fig.2). The value of the stress for saturated coarse sand with 98% grains larger than 0.1 mm is 95% less than that for the saturated sandy loam. If the content of the grains smaller than 0.1 mm is over 30-50% in sand and gravel, the value of the stress for the soil is about 50% greater than that for the pure sand and gravel.

Influence of Soil Moisture on Tangential Frost Heaving Forces

The experimental evidence shows that in a closed system, the tangential frost heaving stress for clayey soils increases with an increase in water content as the water content is greater than the plastic limit, and finally reaches the value of the tangential stress for ice, as is shown in Fig.3.

For water contents ranging from Wp to Wp+17, the

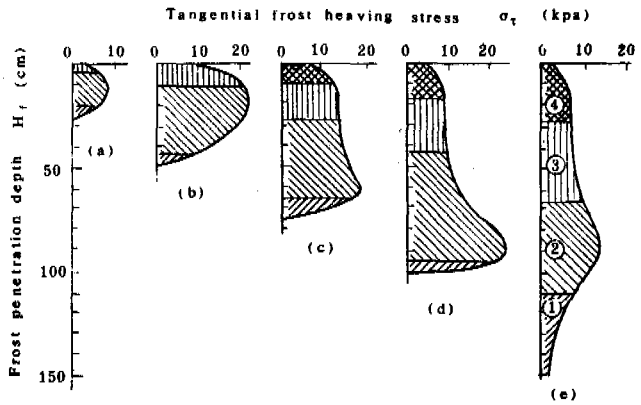

Fig.1 Variation of Tangential Frost Heaving Pressure at Different Depth with Time:

(a) Oct.25, (b) Nov.10, (c) Nov.25, (d) Dec.10, (e) Dec.20.
Range of temperature:
1. 0-- -0.5°C, 2. -0.5-- -5°C,
3. -5-- -10°c, 4. -10°C.

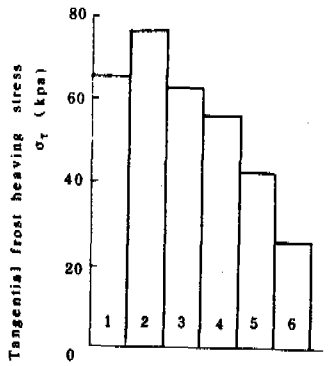

Fig.2 Comparasion of the Tangential Heaving Pressure Among Different types of Soil:

1--loam, 2--silty loam, 3--clay, 4--gravel, 5--medium sand, 6--coarse sand.

increase in the tangential frost heaving stress (σ_τ) with water content can be approximately formulated as the following:

$$\sigma_\tau = \alpha (W - Wp) \qquad (1)$$

where α is an empirical coefficient and Wp is the plastic limit of the soil.

When the water content is between Wp+17 and Wp+60, the tangential frost heaving stress decreases with the increase in water content and finally closes the value of the tangential stress for ice (about 200 kPa) after W is greater than Wp+60.

Influence of Soil Temperature on Tangential Frost Heaving Stress

It has been shown experimentally that the tangential frost heaving stress increases as soil temperature drops (Fig.4). As the temperature drops from freezing point to -5°C, the stress sharply increases and reaches about 60-70% of its maximum value. In the range of temperature from -5°C to -10°C, the increase in the stress with decreasing temperature slows down and,with the temperature below -10°C, the stress tends to be constant. The tangential frost heaving stress as a function of temperature for cohesive soils can be expressed by

$$\sigma_\tau = a|\theta|^b \qquad (2)$$

where θ is the soil temperature in degrees Celsius below zero, a and b are empirical parameters.

In addition, the frost penetration rate has a strong influence on the tangential frost heaving stress. The statistical analysis on experimental data shows that the slower the frost front moves,

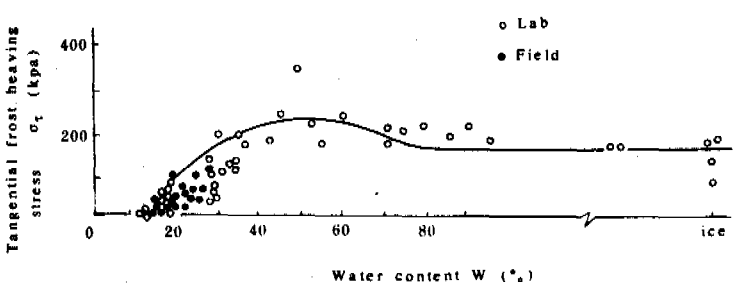

Fig.3 Tangential Frost Heaving Stress vs Water Content

the less the tangential frost heaving pressure increases (Fig.5). At a frost penetration rate (Vf) ranging from 0.9 to 1.0 mm/hr., the growth rate of tangential frost heaving stress ($\xi_\tau = d\sigma_\tau/dt$) is close to zero. The relationship between them can be described by the following equation:

$$\xi_\tau = m\ Vf^n \qquad (3)$$

where m and n are empirical parameters depending upon soil characteristics and moisture.

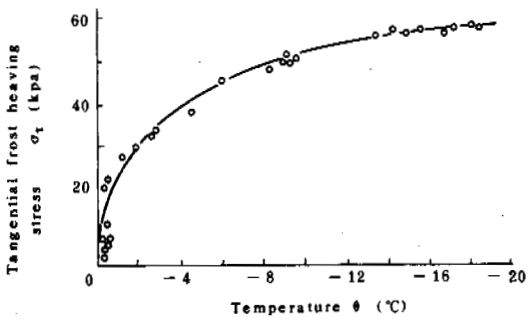

Fig.4 Tangential Frost Heaving Stress vs. Temperature

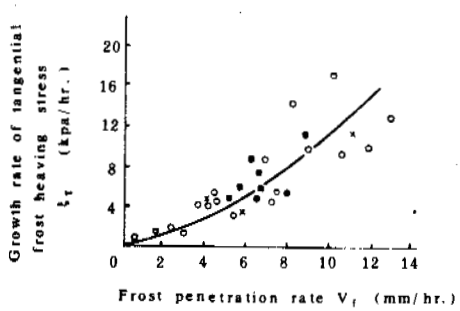

Fig.5 Influence of Frost Penetration Rate on Tangential Frost Heaving Stress in Clayey Soils

Water content: ○ W=16.8%; × W=17.8%; ● W=17.1%; ■ W=20.2%; □ W=18.2%.

Relation Between the Radius of Piles and Tangential Frost Heaving Force

The experiment results[1)] show that the influence of pile radius on tangential frost heaving stress is insignificant (Table I), only that the value of the stress on a pile of smaller diameter is slightly higher.

1) Heilongjiang Provincial Institute of Traffic Science, Study on tangential frost heaving force on reinforced concrete piles of highway bridge in strong frost susceptible soils (unpublished)

TABLE I

Values of Tangential Frost Heaving Stress for Piles of Various Diameters

Diameter of pile (cm)	50	75	100	125
Tangential frost heaving stress (kPa)	66	68	56	58

Tangential Frost Heaving Force on Piles of Different Materials and with Different Surface-Roughness

Tangential frost heaving forces on piles made of different materials depend on adfreezing strength between the piles and the frozen ground. The smoother the surface of a pile, the smaller the value of the force. The experimental results show that the ratio of the force on piles made of wood (circle), steel (without treatment of the surface) and plastics to that on concrete piles is approximately 0.89: 0.75:0.43. Thus, the amending coefficients corresponding to the following common types of materials and surface-qualities are taken as: common precast concrete pile --1.0, smooth steel pile --0.7, and wood pile coated with anti-corrosive oil--0.9.

Antiheaving Effect of Coating Materials

3 types of coating materials, i.e., asphalt, residuum, and industrial vaseline, were tested (Tong et al., 1985b). The results show that coating the surface of piles with the oils 1--2 mm thick causes a remarkable decrease in tangential frost heaving forces on the piles (Fig.6). After 15 frost-thaw cycles, the values of the stress on the piles treated with residuum and vaseline are still much less than that on the uncoated piles (<33 kPa), though some of them have been pressed out. However, the value for the piles treated with asphalt is very close that for the uncoated piles. The most efficient coating materials are oils such as residuum and vaseline. Coating the concrete piles with them can reduce the values of tangential frost heaving forces by 70-80%.

Determination of Tangential Frost Heaving Stress for Foundation Design

It is a general approach to determine the design values of tangential frost heaving stress through field experiments. This is a reliable method but consumes much money and time. Under the particular conditions in China, the design values (Table II) presented on the basis of statistical analysis of indoor and out-door experimental data and the data from engineering practice have been proved acceptable. The determination of the design values in this table is based on the composition of soil, the water and ice contents and the variation of ground-water level. To make the table more conveniently to be used in site

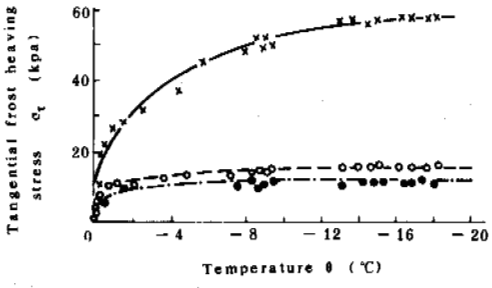

Fig.6 Tangential Frost Heaving Stress on Concrete Piles Coated with Different Kinds of Oils vs.Temperature

× uncoated ○ coated with residuum
● coated with vaseline

exploration and evaluation, the authors identified the texture and physico-mechanical parameters of frozen soils with frost heaving and classified the frost susceptibility of soils as the following: negligible, low, medium, high and very high, for which the corresponding frost heaving ratios are: <1%, 1-3.5%, 3.5-6%,6-12%, >12% respectively. Since the values in Table II are given based on a comprehensive consideration of frost heaving on precast concrete piles at temperatures below -10°C under natural frost conditions, the amendments can be made according to the average temperature of the ground from the surface to 2/3 of the maximum frost penetration depth and the pile material and surface condition (Table III and IV) (Tong., 1985c).

ACKNOWLEDGEMENTS

The authors gratefully thank the co-workers of Heilongjiang Provincial Institute of Water Conservancy and Heilongjiang Provincial Institute of Low-Temperature Construction Science and Institute of Daqing Oilfield Construction Design and Research for their contribution of a great deal of experimental data. The assistance received from Mr. Huang He and Prof. Zhu Yuanlin is sincerely appreciated.

REFERENCES

Changjiang Tong and Fongnian Guan, (1985a), Frost heaving and prevention of frost damages to constructions. China Water Conservancy and Power Press.

Changjiang Tong, Yaqing Wang and Jingshou Liu, (1985b), Effect of antiheaving coating on frost heaving. Collected Papers on Permafrost Studies on Qinghai-Xizang Plateau, Academia Press, China.

Changjiang Tong, (1985c), Tangential frost heaving force of soils and their classification. Collected Papers on Permafrost Studies on Qinghai-Xizang Plateau, Academia Press, China.

TABLE II

Design Values of Tangential Frost Heaving Stress

Frost susceptibility classification		Non	Weak	Medium	Strong	Very strong
Frost heaving ratio (%)		<1	1-3.5	3.5-6	6-12	>12
Texture of frozen soils		massive	mini-layered mini-reticulate	layered	specked	based
Ranges of water content (W) and saturation degree (Sr)	clayey soils	W<Wp	Wp<W≤Wp+7	Wp+7<W≤Wp+17	Wp+17<W≤Wp+34	W>Wp+34
	sandy soils and gravel	---	Sr<0.5	0.5<Sr≤0.8	Sr>0.8	
Minimum distance from ground water table to frost front Z (M)	clayey soils	Z>2.0	1.6<Z≤2.0	1.3<Z≤1.6	1.0<Z≤1.3	Z<1.0
	sandy soils and gravel	Z>1.5	1.2<Z≤1.5	1.0<Z≤1.2	0.5<Z≤1.0	Z<0.5
Tangential frost heaving stress (kPa)	clayey soils	<30	30-60	60-100	100-160	160-300
	sandy soils and gravel	---	<20	20-100	100-200	

TABLE III

Temperature-correction Coefficients

Ground temperature (°C)	-4	-3	-2	-1
Correction coefficients	1	0.8	0.5	0.3

TABLE IV

Correction Coefficients for Different Pile Materials

Materials	Rough stone	Precast concrete pile	Wood pile coated with anti-corrosive oil	steel pile
Correction coefficients	1.3	1.0	0.9	0.7

STRESS-STRAIN BEHAVIOUR OF FROZEN SOILS

S.S. Vyalov[1], R.V. Maximyak[2], V.N. Razbegin[2], M.E. Slepak[2] and A.A. Chapayev[2]

[1]Moscow Civil Engineering Institute, Moscow, USSR
[2]Gersevanov Research Institute of Bases and Underground Structures, Moscow, USSR

ABSTRACT In practice, predicting the stress-strain behaviour of frozen soil loaded by a locally distributed pressure is the most usual problem of engineering geocryology. In this paper some experimental results are given, which have been obtained recently from both microscopic and macroscopic investigations of frozen soil deformation and failure under a rigid plate as well as from uniaxial compression tests. A mathematical model is proposed and discussed to describe the basic peculiarities of frozen soil mechanical behaviour. An analytical solution of plane strain problem has been found using simplified modification of model proposed. This modification can also be regarded as the partial variant of strain-hardening theory. Calculation results are given which compare well with experimental data.

INTRODUCTION

Up to present, only a few works are known dealing with an experimental study of plate problem in frozen soils (Berezantchev, 1947, Vyalov, 1959, Maximyak, 1985). Physical peculiarities of soil behaviour under a loaded rigid plate were firstly investigated by S.S.Vyalov (1959), who described a set of interdependent physico-mechanical processes associated with plate indentation, among them local phase transitions, unfrozen water migration, cracks nucleation and other ones. This paper develops earlier investigations to achieve a better understanding of various structure deteriorating processes comparative role under various loading conditions. A mathematical model of new type is proposed to describe the basic of revealed peculiarities, including microcracking influence and elastoviscoplastic effects at the variable loading regimes.

TESTING METHODS AND RESULTS

Experiments were carried out with a disturbed clay of fixed density and water content, confined into the steel shoot of 100x300x150 mm. Soil was freezing at the fixed temperature during about 100 hours. After that, a constant load was applied through a rigid rectangular steel plate 100x30 mm and 3 mm thickness. Load values were choosed over a range 1.3-13.0MPa. Corresponding test continuties were from several days to several seconds. Quasi-instant strength value (3.75 MPa) had been previously determined in uniaxial compression tests with the same soil.

Structure changes were studied both by visual observations and by investigations of microscopic section of representative soil areas. Resulting soil density, temperature and water content were also measured in the various points through the volume.

Plate settlement in time was fixed by usual way and the typical results are shown on Figure 1.

Generally, a frozen soil under a loaded plate deforms like a multicomponent system with phase transitions and component relative movements occuring. Near the plates foot a zone of compressed soil usually named as "soil core" is obtained where soil density increases and a high local pressure occurs on the particle contacts. This leads to an ice melting and the unfrozen water migration to the less stressed outlying zones where it freezes once again. Correspondingly, soil temperature was found to decrease nearby the plate and to increase at the remote areas due to latent heat of phase transitions. Visually, there are no ice layers within the core zone whereas a fan-like system of such layers is obtained around it.

Depending on the loads level, the various types of structure deteriorating processes are to be prevailing one.

When a load is high enough, a soil under the plate fails its bearing capacity in time, that can be neglected for practice. Pure brittle failure takes place characterized by macroscopic cracks initiating instant growth and merging, as it is shown on Figure 2. Microstructural analyses show the initial imperfections leading role in the failure process. The intrinsic soil cracks, cavities, inclusions and so on initiate stress concentration and unlimited cracks development up to the full destruction.

At first, macroscopic cracks of 45° incline were observed under the plate ends. Then a

fan-like system of such cracks was formed, added by vertical cracks, reaching free soil surface. The average macroscopic cracks length slightly exceeded the plate width (30 mm). No essential changes were found in soil density and water content distribution (see Figure 3).

When a load is still high but unsufficient for instant failure (e.g. 6.5 MPa in our tests) plate settlement grows up with time very intensively (see curve 1 on Figure 1). Microstructural analyses as well as visual observations give an evidence of macroscopic crack nucleation under the plate end at the first moment. During a following viscoplastic flow, initially opened cracks are closing gradually, but microcracks of new type occur and intensively propogate due to viscoplastic deformation development. A new formed set of microcracks has a strong influence on the flow rate which increases with microcracking. In the test discussed settlement rate value finally reached 0.8 mm/sec. Corresponding soil state should be evidently regarded as a damaged one.

Typical settlement-to-time curves fixed under a moderate loads also are presented on Figure 1 ("2" - σ=4.0 MPa, "3" - σ = 3.3 MPa). In this experiment settlement rate values reached correspondingly 2,8·10-2 and 6,5 mm/min. A mixed type of failure takes place which characterized by essential development of both viscoplastic and brittle structure deteriorations through a soil volume. The set of microcracks tends to be a regular one with a preferable cracks orientation formed in accordance with the maximum shear stress directions.

Long-term plate indentation under a small loads goes on without essential ruptures. Only a limited number of isolated cracks occurs which infinitesimal summarized area as well as low cracks density in any representative soil volume allows to ignore cracks influence on the mechanical behaviour. Pure viscoplastic flow takes place. Typical settlement-to-time curve at the such loading conditions is shown on Figure 1 (line "4"). It has been obtained from the test, when the average plate stress σ = 1.7 MPa acted till 34 days. Up to the end of this test a water content in core zone under the plate decreased from 0.30 initially to 0.27. In outlying areas water content reached finally the value 1.34. Gradual disappearance of ice layers in the core zone can see clearly on Figure 4. Soil density has increased to 1.73 g/cm^3 in core zone and was approximately constant (1.7 g/cm^3) in outlying areas. Generally, core zone extended with time.

Proceeded from mentioned above it can be concluded that peculiarities of stress-strain behaviour of frozen soil are determined mainly by interaction of structure reorganization processes of brittle and viscoplastic types. Depending on stress level, each of them can be prevailing one. It should carefully be taken into account by any complete theoretical model to predict mechanical behaviour of frozen soils.

By usual methods of continuum mechanics, to calculate a plate settlement under a certain load, the stress-strain-time relationships need to be known, which usually established in the laboratory sample tests. Their equal validity is supposed at the every point of homogeneous soil volume.

The set of creep curves, which has been obtained in uniaxial compression tests is shown on Figure 5. Tested soil was the same with that used in the plate experiments.

The following peculiarities should be noted generally:
- instant failure of brittle type is obtained, if stress applied is high enough;
- up to the instant strength value if fading or unfading with time viscoplastic flow takes place depending on the level of stress applied
- it is suitable to present the full deformations as the sum of quasi-instant and creep parts, each of these can include both reversable and irreversable components (see Figure 6);
- all of three successive creep stages - primary ($\ddot{\varepsilon} < 0$), secondary ($\ddot{\varepsilon} \simeq 0$) and tertiary ($\ddot{\varepsilon} > 0$) creep is generally observed in frozen soils;
- the resulting strain value depends strongly on changing stress history.

MATHEMATICAL MODEL

To describe mentioned peculiarities the mathematical model early proposed by the authors (Razbegin, 1983, 1985) is developed here. The graphic illustrations of this model by help of standard rheological elements is shown on Figure 7. Here the block "1" simulates a quasi-instant elastoplastic behaviour; "2" - presents viscoelastoplastic deformations developing in time.

Changing rate of viscoelastoplastic behaviour is connected with the element "2-2" which simulates a non-linear (strain rate)-to-(active stress) relationship. An "active" stress is defined as the difference between total stress applied and viscoelastic due to viscoelastic deformations growth. As it was established in special unloading tests, the values of viscoelastic moduli were not to be a constant till viscoplastic flow. Their changes are caused by the intensive microcracking through a soil volume. To illustrate this a system of breaking springs is introduced into the element "2.1". Before the constitutive equations will be set up for model proposed, note the quasi-instant plastic deformations can take of great importance if the dynamic effects are significant, but under a static load applied their influence is neglectable.

Then it can be written down:

$$\varepsilon_{ij} = \varepsilon^{e}_{ij} + \varepsilon^{ve}_{ij} + \varepsilon^{vp}_{ij} \qquad (1)$$

$$\varepsilon^{e}_{ij} = E^{e}_{ijkl}\,\sigma_{kl} \qquad (2)$$

$$\varepsilon^{vpe}_{ij} = \varepsilon^{ve}_{ij} + \varepsilon^{vp}_{ij} \qquad (3)$$

$$\varepsilon^{vpe}_{ij} = F_{ij}(\tau_{kl}) \qquad (4)$$

$$\tau_{ij} = \sigma_{ij} - p_{ij} \qquad (5)$$

$$\dot{\varepsilon}_{ij}^{ve} = E_{ijke}^{ve}(\Omega)\,\dot{P}_{ke} \qquad (6)$$

$$\dot{\varepsilon}_{ij}^{vp} = \dot{\lambda}\,\frac{\partial \Phi(P_{ij}, \varepsilon_{vp})}{\partial P_{ij}} \qquad (7)$$

$$\Omega = \int_{\beta,\gamma,\alpha} \ell(\alpha,\beta,\gamma)\,d\alpha\,d\beta\,d\gamma \qquad (8)$$

$$\dot{\ell} = \dot{\nu}\,\frac{\partial \Phi_\ell(R(P_{ij},\alpha,\beta,\gamma), \mathcal{Æ}(\ell, \chi_k))}{\partial R} \qquad (9)$$

$$R(P_{ij},\alpha,\beta,\gamma) = R(K_I, K_{II}, K_{III}, E_{ijke}^{ve}) \qquad (10)$$

Here

ε_{ij}, ε_{ij}^e - total strains;
ε_{ij}^{ve}, ε_{ij}^{ve} - quasi-instant strains;
ε_{ij}^{vp}, ε_{ij}^{ve} - viscoelastoplastic strains;
ε_{ij}^{vp} - viscoelastic strains;
E_{ijke}^e - viscoplastic strains;
σ_{ij}, τ_{ij} - quasi-instaneous elastic modulus;
- total stress;
- "active" stress (the difference between total stress applied and viscoelastic resistance; viscoelastoplastic strain rate is defined directly by this tensor value);
P_{ij} - viscoelastic stress;
$\dot{(\cdot)}$ - symbol of in-time derivative;
E_{ijke}^{ve} - viscoelastic modulus (are changed due to microcracking);
Ω - damaging parameter (is introduced for taking into account microcracks dedeloped; one can be regarded as the average volume of microcracks continuum at a certain point of soil media);
$\ell(\alpha,\beta,\gamma)$ - scalar damaging function (presents an average length of plane, narrow microcracks being placed perpendicularly to the vector $\bar{n}(\beta,\gamma)$
α - an angle between cracks direction and fixed coordinate system in the plane of the crack; this function is determined in any point through a soil volume);

In respect of Figure 7, equation (2) describes the behaviour of element "1" and eqs (3)-(10) - that of element "2".

(4) - an (active) stress)-to-(viscoelastoplastic strain rate) relationship.

In the most general case:

$$\dot{\varepsilon}_{ij}^{vpe} = F_1(I_1,I_2,I_3)\delta_{ij} + F_2(I_1,I_2,I_3)\tau_{ij} + F_3(I_1,I_2,I_3)\tau_{ik}\tau_{kj} \qquad (11)$$

where F_1, F_2, F_3 - functions of the stress tensor invariants.

For the following, an assumption can be made in accordance with known experimental data (Vyalov, 1986): $F_i = F_i(I_1, J_2)$ where J_2 - the second invariant of deviatoric stress tensor, and

$$\dot{\varepsilon}_{ij}^{vpe} = \left(a I_1^b + \frac{c_1(\sqrt{J_2})^b}{1 + d\left(\frac{I_1}{\sqrt{J_2}}\right)}\right)\delta_{ij} + \frac{c_2(\sqrt{J_2})^b}{1 + d\left(\frac{I_1}{\sqrt{J_2}}\right)}\,S_{ij} \qquad (11)'$$

where a, b, c_1, c_2, d - soil parameters.

Usually a volume strains increment due to only hydrostatic pressure is neglectable. The ratio ($c_1/c_2 = C$) is a dilatancy coefficient. Up to the starting of intensive microcracks growth $C = C(\Omega)$ appears to be a constant, rising essentially after it.

($\bar{\kappa}$) is the equations accepted as in the usual plasticity theory to describe irreversable part of viscoelastoplastic strain increments. A plastic potential surface supposed to be the same with a yield surface being placed at the viscoelastic stress space (not at the total stress space). Analogical assumptions has been early made in (Ivlev, 1971; Zaretcky, 1983). Figure 8 shows a possible form of the yield surface. Eqs (9), (10) are a kinetic ones for the damaging parameter. A general thermodynamical force $R(P_{ij},\alpha,\beta,\gamma)$ is introduced to describe a growth of any individual crack. Crack length increment assumes to be fully irreversable and corresponding function of mechanical energy dissipation assumes to be homogeneous of degree 1 in respect of this increment. One can be written down consequently:

$$\Phi_\ell(R) = 0;\quad d\Phi_\ell = 0 \qquad (12)$$

$$\Phi_\ell = R - (R_0 - \mathcal{Æ}(\ell, \chi_k))$$

$$\begin{cases} \dot{\ell} = A\dot{R} + B\dot{\chi}_k,\ A = \left(\frac{\partial \mathcal{Æ}}{\partial \ell}\right)^{-1};\ B = A\frac{\partial \mathcal{Æ}}{\partial \chi_k},\ \dot{R} > 0 & (13) \\ \dot{\ell} = 0,\ \dot{R} \le 0 & (14) \end{cases}$$

Here R_0 - an initial threshold for microcracks development starting; $\ell^* = \ell - \ell_0$ - an initial increment of crack length; $\mathcal{Æ}$ - hardening function on the cracks length and some additional parameters.

In general case $R(P_{ij}, \ell, \alpha, \beta, \gamma)$ looks intricate enough. For a plane-strain conditions it becomes

$$R = (K_I^2 + K_{II}^2)(1-\nu^2)/E \qquad (15)$$

$$\begin{cases} K_I = P_n\sqrt{\pi\ell},\ P_n < 0 & (16) \\ K_I = 0,\ P_n \ge 0 \end{cases}$$

$$K_{II} = \tau\sqrt{\pi\ell} \qquad (17)$$

$$P_n = \frac{P_{11}+P_{22}}{2} + \frac{P_{11}-P_{22}}{2}\cos 2\alpha + P_{12}\sin 2\alpha \qquad (18)$$

$$\tau = \frac{P_{11}-P_{22}}{2}\sin 2\alpha + P_{12}\cos 2\alpha \qquad (19)$$

where K_i -stress intensity factor to describe the stress distribution nearby the cracks top.

Scalar function $\ell(\alpha,\beta,\gamma)$ seems to be sufficient for taking into account the main features of microcracks continuum. At the beginning this function should evidently be a constant from point to point through a soil volume and for any α,β,γ when initially isotropic, homogenous soil is regarded. In the plain-stress case $\ell=\ell(\alpha)$ and $R(\rho_{ij},\ell,\alpha)$ relationship is determined by (15)-(19)

To represent the microcracking influence upon the viscoelastic modulus values, an integral parameter $\Omega=\int_0^{\pi}\ell(\alpha)d\alpha$ is introduced. Generally, cracks length distribution becomes essentially to depend on cracks direction. So an induced anysotropy of mechanical properties would take place. To describe this, the higher statistical moments of function need to be used.

The set of constitutive equations (1)-(10) is complete if the usual balence equations as well as geometrical limitations is written down additionally.

The mathematical model proposed may be used succesfully for predicting the most essential peculiarities of frozen soil mechanical behaviour. Among them nonlinearity of viscoelastoplastic flow, which changing rate is defined by total stress applied, viscoelastic resistance, and by current state of soil structure, controlled by irreversable part of viscoelastoplastic strain and the damaging parameter; loading history influence the resulting stress-strain state; returning creep under unloading and so on.

SIMPLYFIED MODEL MODIFICATION

When a long-term structure settlement and stability is interested on and loads applied are not too high, changing with time to a small degree, simplyfied modification of model proposed can be suitable for practical calculations.

For this conditions, ignoring possible unloading microcracking and loading history influence and regarding the total creep strain as the only parameter to control current structure state of soil one can be adopted a reduced set of constitutive equations which form is the same as that in the strain-hardening theory.

General form of strain-hardening theory equations is:

$$\dot{\varepsilon}_{ij}=f_{ij}(\sigma_{kl},q_1,\dots,q_n), \qquad (20)$$

where $q_1,\dots,q_n$ - hardening parameters.

In (Slepak, 1982(a)) (20) was concretized in form:

$$\dot{\varepsilon}_{ij}=(\dot{\gamma}_i/2\tau_i)(\sigma_{ij}-3\nu\sigma_m\delta_{ij}/(1+\nu))$$
$$\dot{\gamma}_i=a(\tau_i/a)^{1/m\alpha}/\bar{\gamma}_i^{(1-\alpha)/\alpha} \qquad (21)$$

Here $\bar{\gamma}_i=\int_0^t\dot{\gamma}_i\,dt$

δ_{ij} - Kroneker's symbol;
σ_m $\dot{\gamma}_i$ - average hydrostatic pressure;
- strain rate intensity;
τ_i - tangential stress intensity;
a,m,α - parameters;
ν - lateral deformations coefficient.

To get (21) some additional assumption has been adopted. Particularly, hydrostatic pressure influence is not taken into account for shear deformations development; ν is assumed to be constant, so, the shear and the volume strain-to-time curves are similar. Nevertheless, (21) successfully describes the basic reological effects in frozen soils. In principle, these equations can be used also when loads applied change in time. Based on the set (21) an analytical solution has been obtained for a plate settlement under the plane strain loading conditions. For this, the settlement was presented in the form of multiplication of time-dependent functions with functions depending on coordinates only (Slepak, 1982(b)). Using the results (Vyalov,1986) it can be written down for a displacement of central point of absolutely flexible plate loaded by any certain law P=P(t)

$$s(t)=2^{(1-m)/m}NB\left\{\int_0^t[P(t)]^{1/m\alpha}dt\right\}^{\alpha}$$

$$N=\frac{\omega(\lambda\frac{\pi}{2})(m-\nu)\left(\frac{2}{\sqrt{3}}\sqrt{1-\nu+\nu^2}\right)^{(1-m)/m}}{I^{1/m}(1-m)a^{1/m}}$$

(22)

$$\lambda^2=\frac{1}{m}\left[1+\frac{\nu}{1-\nu}\left(1-\frac{1}{m}\right)\right]$$

$$\omega(\lambda\varphi)=\begin{cases}\sin(|\lambda|\varphi)/|\lambda|, & \lambda^2>0\\ \operatorname{sh}(|\lambda|\varphi)/|\lambda|, & \lambda^2<0\\ 1, & \lambda^2=0\end{cases}$$

$$I=4\int_0^{\pi/2}\cos\varphi[\omega'(\lambda\varphi)]^m d\varphi$$

Here B - plate width.

Parameters in eqs (22) had been estimated in uniaxial compression tests. For the frozen Chegan clay at -5°C temperature it was found that $\nu=0{,}31$; $a=19{,}2$ kg·hour$^{m\alpha}$/cm^2; $m=0{,}34$; $\alpha=0{,}25$ The results of special plate test when pressure applied was $p=17{,}5$ kg/cm^2 are shown on Figure 10. One can see on the Figure calculated and experimental results are compared well.

REFERENCES

Berezantsev, V.G., 1953. Soil resistance to locally distributed loads under a constant temperature below 0°C. (in Russian, in: Materialy po laboratornym issledovaniyam merzlyh gruntov, No 1, Moscow, AN SSSR.

Ivlev, D.D., Bychovcev, G.I., 1971. Theory of hardening plastic bodies (in Russian), Moscow, Nauka.

Maximyak, R.V., Kutvitskaya, N.B., Chapayev A.A., 1985. Behaviour of frozen soil under plate (in Russian), in: Povysheniye nesuschey sposobnosty osnovaniy pri uchete izmeneniy stroitelnych svoistv gruntov vo vremeni. Moscow, Stroyizdat, p. 25.

Razbegin, V.N., 1985 Thermodynamical approach to models building of soil rheological behaviour and long-term strength. (in Russian), in: Povysheniye nesuschey sposobnosty osnovaniy pri uchete izmeneniy stroitelnych svoistv gruntov vo vremeni. Moscow, Stroyizdat, p. 47.

Razbegin, V.N., Vyalov, S.S., 1985. Long-term failure of soils as a thermodynamical process, in: Proc. X ICSMFE, San-Francisco, A.A. Balkema/Rotterdam/Boston, pp. 625-628.

Slepak, M.E., 1982(a) About construction of frozen soil rheological constitutive equations (in Russian), in: Tezicy dokladov IV simpoziuma po reologii gruntov, Samarkand, pp. 152-153.

Slepak, M.E., 1982(b) Settlements and stress-strain state of plastic-frozen soil in the base of centrally loaded pile (in Russian), in: Reologiya gruntov i ingenernoye merzlotovedeniye, Moscow, Nauka, pp. 154-158.

Vyalov, S.S., 1959. Rheological properties and bearing capacity of frozen soils, Moscow, AN SSSR (in Russian).

Vyalov, S.S., 1986 Rheological fundamentals of soil mechanics, Elsevier.

Zaretsky, Yu.K., Schebolev, A.G., 1983. A mathematical model for the viscoplastic deformation of frozen soils, in: Proc. 4th Int. Conf. Permafrost, Fairbanks, v.1, pp. 1457-1462.

ILLUSTRATIONS

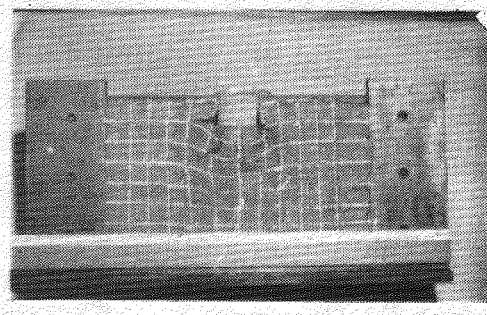

Fig.2. Quasi-instant failure (general view)

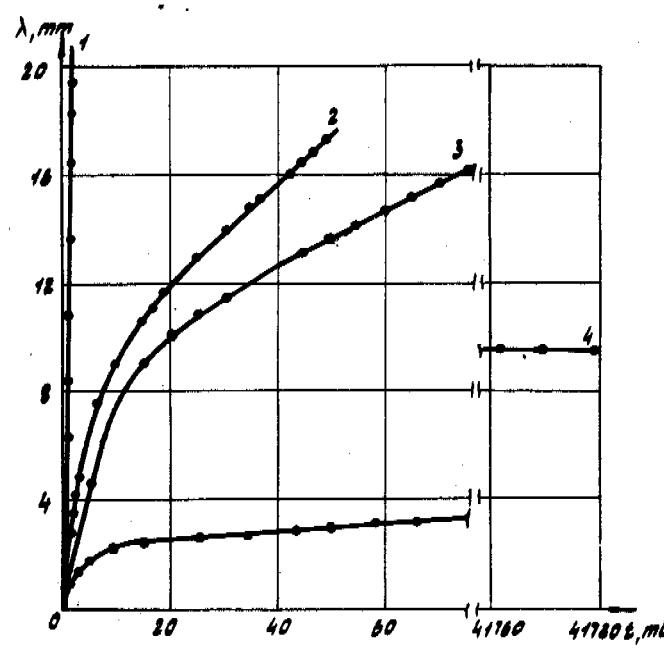

Fig.1. Plate settlement in-time development under the various loads applied: 1 - 6,5MPa; 2 - 4,0MPa; 3 - 3,3MPa; 4-1,6MPa

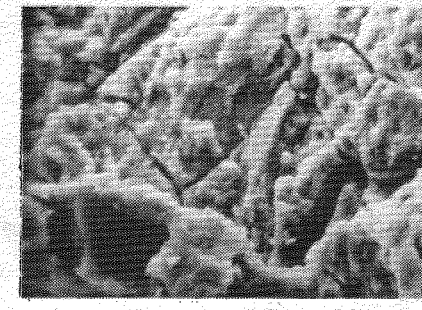

Fig.3. Quasi-instant failure (microstructural view)

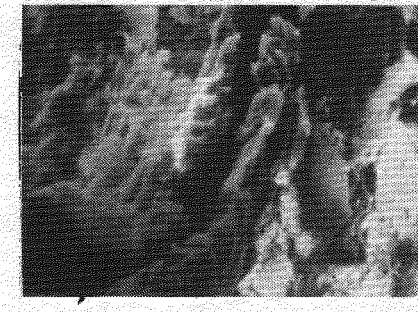

Fig.4. Microcracking due to viscoplastic flow

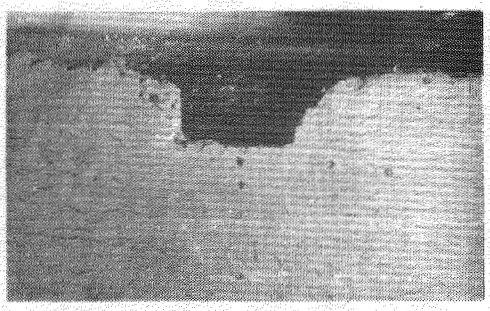

Fig.5. Long-term loading; =1,36MPa, t=34days

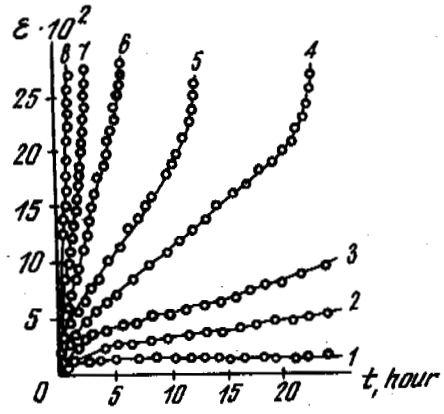

Fig.6. Creep curves in uniaxial compression tests under constant stresses, MPa:
1 - 0,75; 2 - 1,0; 3 - 1,25; 4 - 1,45;
5 - 1,5; 6 - 1,65; 7 - 1,9; 8 - 2,25.

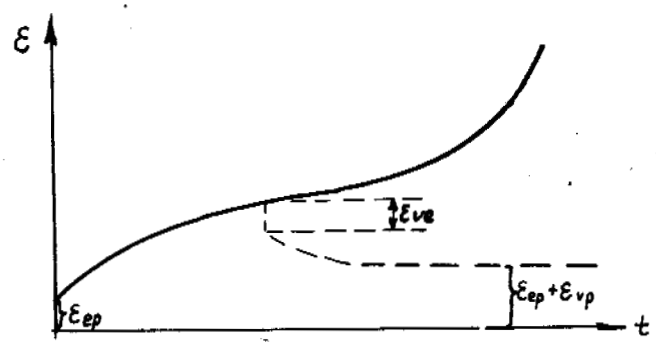

Fig.7. Idealized creep curve (with unloading)

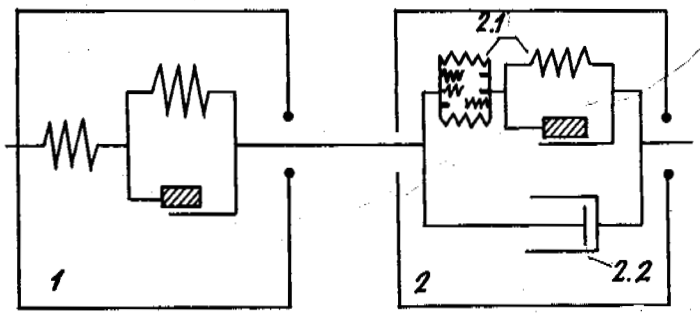

Fig.8. Rheological elements illustration to model proposed.

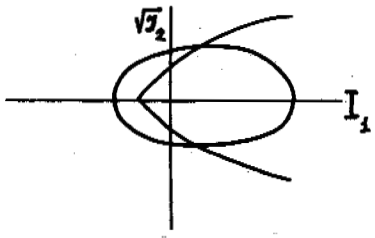

Fig.9. Yield surface.

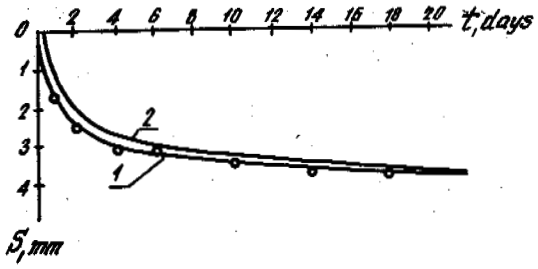

Fig.10. Plate settlement: 1 - experimental, 2 - calculated.

FROST HEAVING FORCES ON FOUNDATIONS IN SEASONALLY FROZEN GROUND

[1]Xu, Shaoxin

Heilongjiang Provincial Research Institute of Water Conservancy

SYNOPSIS All three types of frost heaving forces, i.e., tangential, normal and horizontal, are examined in this paper. The results of laboratory and field experiments show that the three types of frost heaving forces have not only the same physical meaning but also a similar process of generation and development. Consequently, the values of the three types of forces can be examined and estimated from each other.

INTRODUCTION

In seasonal frost areas, freezing ground exerts heaving forces on the foundations of structures when frost heave of the ground is restrained by the foundation. Based on the difference in the form of restraint, frost heaving forces are generally classified as three types: tangential frost heaving force, horizontal frost heaving force on the lateral surface of a foundatin, and normal frost heaving force acting vertically on a foundation. Considering the physical basis of their generation, all three forces are caused by the restraint to volume expansion or heave of the soil due to the phase-change of moisture to ice. Further analysis of laboratory and field experiment data indicates that the three types of frost heaving forces not only have the same physical basis but also are similar with regard to the combined action of temperature, moisture and stress fields in the generation and development of the forces. In similar foundation soils some close relationships exist among the three types of frost heaving forces. This means that empirical examination and estimation of the three types of forces from each other can be made.

DISCUSSION

Tangential Frost Heaving Force on Pile Foundations

The adfreezing bond strength between a pile and the surrounding frozen ground is a prerequisite for the generation of tangential frost heaving forces on the lateral surface of a pile. The volume expansion due to the phase-change of water-to-ice in the surrounding soil is the source of the force. The weight of a pile, applied load and compressibility of the underlying unfrozen soil are the main factors influencing the magnitude of the tangential frost heaving force.

A literature survey shows that most of the experimental investigations on the tangential frost heaving force on piles focused on the influence of moisture, temperature and properties of the pile material. Without any doubt, a clear understanding of the generation, development and variation of the force can be attained with the method of monofactor analysis. In engineering practice, however, the requirement for preventing the frost uplift of a pile foundation is that the tangential frost heaving stress must be less than the adfreezing strength.

Investigations show that the magnitude of the tangential frost heaving force on a pile depends chiefly on the frost-heave susceptibility of the surrounding soil and the degree of the pile's restraint to frost heave. In considering the stability of a pile subjected to frost uplift for design, the following formula is generally used as the stability criterion:

$$\sigma_T \cdot S \leq P + G + f \cdot S_1 \qquad (1)$$

where σ_T is the tangential frost heaving stress;
P is the applied load on the pile;
G is the weight of the pile;
f is the friction between the pile and unfrozen soil;
S is the surface area of the section of the pile in contact with the frozen soil layer;
and S_1 is the surface area of the section of the pile in contact with the unfrozen soil layer.

If the right side in eq.(1) is greater than $\sigma_T \cdot S$, then the magnitude of the tangential force depends on the frost heaving potential of the surrounding soil. In this case, the buried pile foundation restricts the upward frost heave deformation of the surrounding soil body. According to laboratory and field experiments, the radius of influence (1) is approximately equal to the frost depth H (see Fig.1).

If a loading plate with the same cross-section as the pile is used to restrain fully the frost heave deformation of the underlying soil, then the angle of the frost heaving stress in the subgrade is generally regarded as 45°; that is, the radius of influence (1) of the stress is also equal to

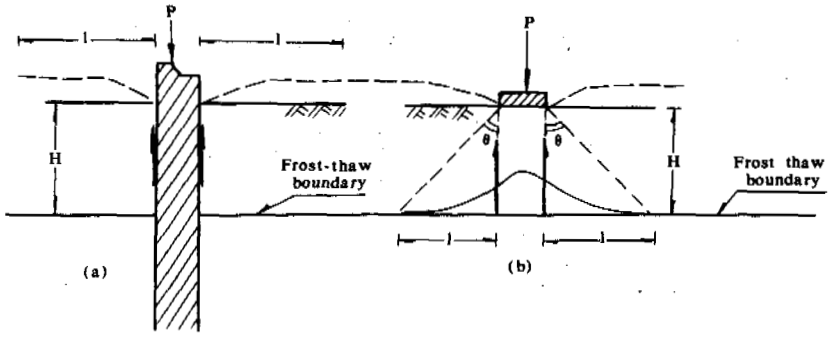

Fig.1 Frost Heave Around a Pile (a) and Under a Loading Plate (b)

frost depth H. The temperature, moisture and stress fields for the above two cases are quite similar, so that frost heave of the surrounding soil subjected to a pile's restraint is very similar to that of the subgrade soil around the edge of a loading plate subjected to the plate's restraint. As a result, the total frost heaving forces for the two cases should be roughly equal. For comparison, the total tangential frost heaving forces on a series of model piles and the total normal frost heaving forces on a series of loading plates with the same diameters as the piles, were measured at Wangjia Frozen Soil Field Station (where the soils are of medium frost susceptibility).The observed values were shown in Table I.

TABLE I

Observed Values of Total Tangential Frost Heaving Force on a Series of Piles and Total Normal Frost Heaving Force on Loading Plates with the Same Diameters as the Piles

Diameter (cm)	50	75	100	125
Total tangential frost heaving force on a pile (x10 N)	14.9	19.4	26.4	35.7
Total normal frost heaving force on a loading plate (x10 N)	15.7	21.6	27.5	36.8

It can be seen from Table I that the values of the two types of frost heaving forces for a certain diameter are very close. Therefore, the tangential frost heaving force on piles can be estimated from the values of normal frost heaving force measured on loading plates heaving the same diameters as the piles and under the same freezing conditions.

Normal Frost Heaving Force on Plate Foundations

Many experimental investigations to determine values of normal frost heaving forces on plate foundations have been conducted in recent years. Since the test plates are all small and the boundary conditions are quite different in these investigations, the measured values of the force are so different that they could not be used in engineering practice. Although there are many factors influencing normal frost heaving force, they can be classified in two groups, i.e., natural conditions and engineering conditions. The natural conditions are the prerequisites for the generation of the force and can be divided into:

(i) Soil characteristics--mineralogical components, particle composition, unit weight, permeability of the underlying soil, and compressibility of the unfrozen soil layer;

(ii) Moisture conditions--water content and dissolved salt content in soil, groundwater level, etc.;

(iii) Thermal conditions--freezing index, thermal properties of soil, frost penetration rate, ground thermal regime,etc.

The engineering conditions which are basic to the magnitude of normal frost heaving force include foundation shape and size, buried depth, applied load, and degree of restraint to frost heave of the subgrade.

For engineering purposes, the magnitude of the normal frost heaving force depends chiefly on the degree of the foundation's restraint and natural conditions. If frost heave of the underlying soil is restricted only by the load applied on the foundation, then the normal frost heaving force is equal to the applied load. If a foundation is fully restrained to frost-heave displacement, the magnitude of the normal frost heaving force depends on the base area of the foundation and the compressibility of the underlying unfrozen soil layer. Based on statistical analysis, Tong and Yu (1983) presented an empirical formula concerning the relationship between the loading plate area and normal frost heaving pressure. To experimentally investigate the normal frost heaving force as a function of loading plate areas, frost heave tests were per-

formed at Wangjia Frozen Soil Field Station on a series of plates with results as shown in Fig.2.

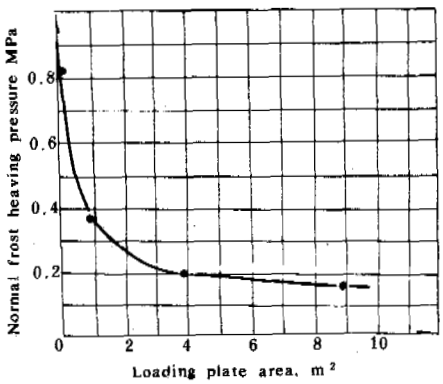

Fig.2 Loading Plate Area vs Normal Frost Heaving Pressure

It can be seen from Fig.2 that the normal frost heaving pressure increases with decrease in plate area. The reason why higher normal frost heaving pressures were measured on smaller plates is that, while freezing, the plate was subjected to a so-called "additional" normal frost heaving pressure resulting from frost heave of the soil beyond the edge of the plate. This additional pressure decreases with an increase in plate area. The ratio (in percent) of the field-measured and calculated "additional" frost heaving pressures, σ_a , to the total pressures, σ_t , on plates with different areas are presented in Table II.

TABLE II

Ratio (in percent) of the Additional Normal Frost heaving Pressure (σ_a) to Total Normal Frost Heaving Pressures (σ_t) on Loading Plates with Various Areas

Plate areas (m^2)	0.01	0.25	1.0	4.0	9.0	25.0	100
σ_a/σ_t (%)	99#	90.7*	76.3*	60.3*	45.2*	31.5*	18.3*

* measured # calculated

The normal frost heaving force on a small plate is produced mainly by the frost heaving stress in the surrounding soil and conveyed to the plate by means of the strength of frozen soil. In a similar way, the tangential frost heaving force on a pile is also caused by the frost heaving stress in the surrounding soil and conveyed to the pile by means of the adfreezing strength between the pile and the soil. Therefore, the two types of frost heaving forces can be mutually examined and evaluated.

It can be seen from Table II that the effect of the surrounding soil on the normal frost heaving force decreases with increasing plate area. The total normal frost heaving force finally tends to be the so-called pure normal frost heaving force without any "additional" effect. The magnitude of the "pure" normal frost heaving force is dependent upon the compressibility of the underlying unfrozen soil. Its maximum value cannot exceed the ultimate strength of the soil.

Horizontal Frost heaving Force Acting on Retaining Walls

It is well known that at air temperatures below 0°C, the backfill behind a retaining wall experiences freezing in two directions. Isotherms in the fill are shown in Fig.3. Upward frost heave of the upper portion of the fill does not result in large forces acting on the wall. But,

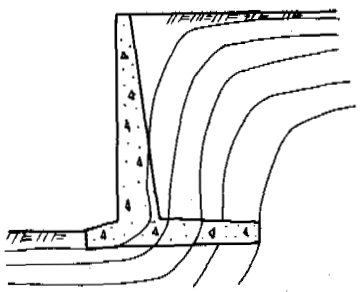

Fig.3 Isotherms Behind a Retaining Wall

due to the wall's restraint it will be subjected to horizontal frost heaving forces. The magnitude of the horizontal force, like tangential and normal frost heaving forces, depends on the degree of restraint and the natural conditions of frost heave. When frost penetration is relatively shallow, the horizontal frost heaving force on a elastic, thin retaining wall can be calculated based on the displacement of the wall. Behind a regid retaining wall, frost heave of the fill is fully restrained by the wall and the displacement of the wall is close to zero. In this case, the horizontal frost heaving pressure is equal to the normal frost heaving pressure under full restraint. Its maximum value cannot exceed the ultimate stength of the frozen soil.

When the isotherms in the soil behind a low retaining wall (i.e., its height is close to the frost penetration depth) are curved lines and the frost heaving force is normal to the isotherms, then the distribution of horizontal frost heaving pressure on the wall can be quite variable. If the back fill is cohesive soil and the groundwater level is below the ground surface, then the distribution of pressure on the wall is as shown in Fig.4, where h is the exposed height of the wall, H is the maximum frost depth, and B is the point at which the maximum pressure occurs.

For a high wall with freezing occurring in two directions, the distribution of horizontal pres-

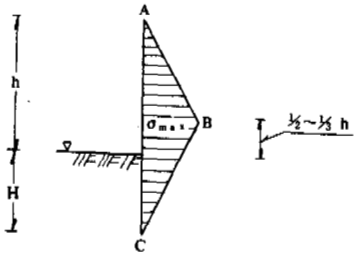

Fig.4 Distribution of the Horizontal Frost Heaving Pressure on a Low Retaining Wall

sure on the wall can be represented as shown in Fig.5. In this case, the maximum pressure occurs within section BC where the isotherms are parallel to the wall. Points B and C represent major changes in direction of the isotherms.

For a rigid high retaining wall with its backfill fully restrained and assuming the same frost depth, the maximum horizontal frost heaving pressure is equal to the pure normal frost heaving pressure.

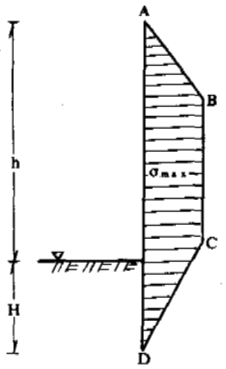

Fig.5 Distribution of the Horizontal Frost Heaving Pressure on a High Retaining Wall

CONCLUSIONS

(i) The tangential, normal and horizontal frost heaving forces have not only the same physical basis but also many similar characteristics. The magnitude of all three types depends chiefly on the associated engineering conditions and natural factors. Suitable experimental values for these forces should be chosen for design based on previous engineering practice.

(ii) The tangential frost heaving force acting on a pile foundation is caused chiefly by the frost heave of the surrounding soil body. It can be estimated or examined by comparing it with the normal frost heaving force acting on a loading plate having the same cross-sectional area as the pile.

(iii) The normal frost heaving pressure on a plate foundation decreases with an increase in plate area. Because of the substantial influence of frost heave in the surrounding soil, the normal frost heaving pressure measured on a small loading plate should not be used in engineering practice. The pure normal frost heaving pressure can be considered as the total normal pressure for a large plate, but its maximum value cannot exceed the ultimate strength of the underlying soil.

(iiii) The distribution of horizontal frost heaving pressure on a retaining wall depends on the height of wall. Its maximum pressure is not greater than the pure normal frost heaving pressure, for the same frost depth.

REFERENCE

Changjiang Tong and Chongyun Yu, (1983).Research on the frost heaving force of soils. Proc. 4th Intern. Conf.Permafrost, pp.1273-1277, Washington D.C. National Academy Press 1983.

ON THE DISTRIBUTION OF FROST HEAVE WITH DEPTH

Zhu, Qiang

Water Conservancy Department of Gansu Province, China

SYNOPSIS The distribution of frost heave with depth is of great importance in areas which experience seasonal frost. Based on the field experiments carried out in Gansu Province since 1979, this paper classifies the heave distribution into 4 types: high heave ratio layer occuring in the upper, lower and middle part of the frozen soil and heave distributed with relative evenness in the frozen soil. The relationship between distribution patterns and water-soil conditions is discussed and an explanation using the principle of water migration is presented. The concept of so-called "major heave layer" is correct only in the closed freezing system. In the open system various types of heave distribution may occur depending on the water supply conditions. The author also provides a mathematical model to verify the effect of ground water on the heave distribution.

INTRODUCTION

In areas which experience seasonal frost, the distribution of frost heave with depth is of great importance for determining the depths of foundations and the thickness of sand-gravel required for subsoil replacement. In the past, it was assumed that more than 2/3 of the heave is concentrated in the upper 1/3 to 1/2 part of the frozen soil, in the so-called "major heave layer". Some investigators in construction engineering have presented data to prove the existence of this type of distribution and derived design criteria for shallow foundations. Since late 1970's, however,investigators in the field of hydraulic engineering, such as wang (1980), Zhu (1981) have pointed out that there are different types of heave distribution according to soil and ground water conditions. The "major heave layer" type is only a special case under specific conditions. To date there is no unanimity of views on the classification of the heave distribution types and their relations to soil and ground water conditions.

In Gansu Province, China, under the Anti-Frost Heave Measures for Canal Lining Program, field experiments to study seasonal frost heave under various soil and ground water conditions have been carried out extensively since 1979. Based on the data from these experiments, this paper summarizes four frost heave distribution types and their relations to soil and ground water conditions. A mathematic model of coupled heat and moisture transfer is applied to verify the conclusions of the experiments and the effect of ground water on the heave distribution.

EXPERIMENTAL RESULTS

The field experiments are carried out at the Zhangye Frost Heave Station, the Daman Main Canal, the Minqin Testing Canal and the Ginghui Main Canal. Each site is characterized by different soil and water conditions. Based on the 312 sets of data obtained at these sites,it was determined that the actual heave distributions can be classified into four types depending on the position of the high heave ratio (HHR*) layer. These include heave distribution where: a) the HHR layer located at the upper half of the frozen soil, b) the HHR layer at the lower half of the frozen soil, c) the HHR layer is located in the middle half of the frozen soil and d) heave is distributed with relative evenness. These four types referred to as type A, B, C and D respectively. Among them, A and B are the most common making up 80% of the 312 sets of data. A brief account of the conditions of the test sites and heave distributions at each site are given in the following sections.

Zhangye frost heave station

The soil at the Zhangye Station can be divided into five types:heavy silty loam,sandy loam,fine sand and loam and sandy loam overlain by a coarse sand layer. The ground water table at each site are artificially controlled at depths of 1, 1.5 and 2.5 m, respectively. A total of 15 testing units consisting of combination of soils and ground water conditions were instrumented to measure frost penetration, soil temperature,soil moisture and heaving. The results from the experiments can be seen in Table I. The results indicate that when the ground water table is close to the surface, such as in unit 100-1,2,3 and 150-1,2,the heave distributions belong to type B, regardless of soil type. An example of this type of heave is shown in Fig.1. For deeper ground water conditions, the main distribution type is A. For the loam and sandy loam covered with coarse sand, the distribution mainly belongs to type B despite the varying ground water

* Heave ratio equals to $\Delta h/\Delta H$, where Δh and ΔH represent the heave and the thickness, respectively, of the same layer.

TABLE I

Heave Distribution Types in Zhangye Frost Heave Station

Unit number	Numbers of distribution types Total	A	B	C	D
100-1 to 5**	15		15		
150-1,2,4,5	6		6		
250-1,2	3	3			
250-4,5	4		4		

**The number before dash denotes the water depth in cm, the number after dash denotes soil types:

1—heavy silty loam; 2—sandy loam; 3—sand; 4—loam under coarse sand; 5—sandy loam under coarse sand.

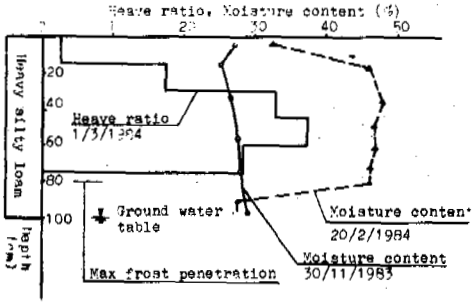

Fig.1 Distribution of Heave Ratio and Water Content of Unit 100-1 in Zhangye Frost Heave Station

depth ranging from 100 to 250 cm.

Daman main canal

This is a concrete lined canal with subsoil mainly consisting of clay and heavy silty loam, replaced to various depths by sand-gravel. The ground water table varied from 0.5 m at the beginning of winter to 1.5 m at the end of winter. Table II summarizes the results and indicate the heave distribution is mainly type B, which amounts to 71% of the data observed. It is apperent in the data from the north facing slopes that heave distribution is also effects by position relative to the ground water table. The shorter the distance between freezing front and the ground water table, the higher the heave ratio. An example of test result from Daman Main Canal is shown in Fig.2.

Ginghui main canal

The ground water table at the Ginghui Main Canal is deeply seated, so the freezing process is similar to a closed system. The subsoil is a

TABLE II

Statistics of Heave Distribution Types in Daman Main Canal

Location of heave measurement	Numbers of distribution types Total	A	B	C	D
NS* upper haef	20	10	2	1	7
NS* lower half	20		12	3	5
bottom	22		21	1	
SS** lower half	23		21	2	
SS upper half	25		23	2	

* NS: north facing slope, that is the sun-exposed side and is warmer.
**SS: south facing slope, that is the shade side and is colder.

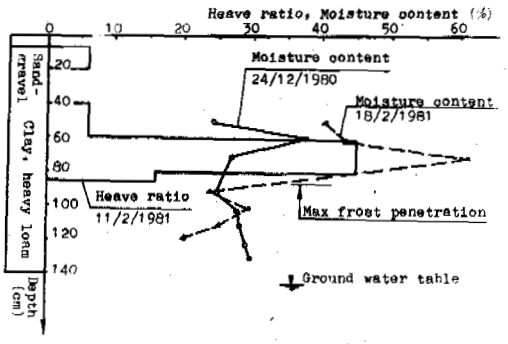

Fig.2 Distribution of Heave Ratio and Water Content of Point No.04 in Section No.2, Daman Main Canal

TABLE III

Statistics of Heave Distribution Types in Ginghui Main Canal

Location of heave measurement	Numbers of distribution types Total	A	B	C	D
WS* upper half	19	17		2	
WS lower half	30	30			
bottom	10	7			3
ES** lower half	30	18		2	10
ES upper half	20	17	1		2

* WS: west slope, the colder side.
**ES: east slope, the warmer side.

loess with vertically developed fissures allowing rapid downward drainage. The results are shown in Table III. The results indicate that over 80% of the site are characterized by type A heave distribution. This type of heave is

very predominant on the colder west slopes where it makes up 96% of the total (Fig.3).

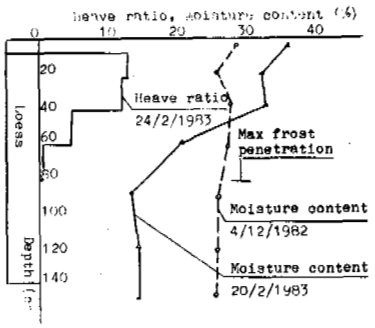

Fig.3 Distribution Curve of Heave Ratio and Water Content of WS Lower Half in Section No.1, Ginghui Main Canal

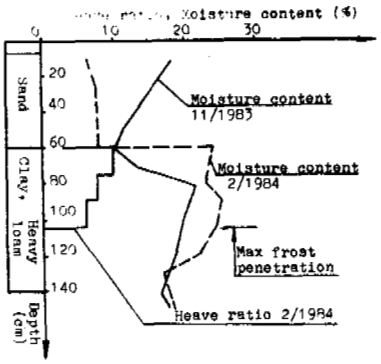

Fig.4 Distribution of Heave Ratio and Water Content of South Facing Slope in Section No.2, Minqin Testing Canal

Minqin testing canal

The depth of ground water table of the Minqin Testing Canal is about 4 m under the canal bottom. The soil is heavy silty loam and silty clay with poor drainage capability. The data are shown in Table IV. When no replacement by sand takes place, the distribution types are mainly A and D. In the case of replacement by sand, the distribution mainly belongs to type B. A typical example of experimental results from a site with subsoil replacement by sand is shown in Fig.4.

TABLE IV

Heave Distribution Types in Minqin Testing Canal

Location of heave measurement	Numbers of distribution types Total	A	B	C	D
without subsoil replacement					
NS upper half	6	1	2	1	2
NS lower half	8	7			1
bottom	8	3		4	1
SS lower half	8	2			6
SS upper half	12	4			8
With subsoil replacement by sand					
NS upper half	4		4		
NS lower half	4		3		1
bottom	4		3	1	
SS lower half	4		4		
SS upper half	4		4		

HEAVE DISTRIBUTION VERSUS SOIL-GROUND WATER CONDITIONS

In order to have a thorough understanding of heave distribution at each site, it is necessary to study the change of soil moisture profiles during freezing. In the case of deeply seated ground water table, we can see from the soil moisture profile shown in Fig.3 that a high moisture content zone corresponding to the HHR layer is present in the upper part of the frozen soil. This zone is caused by the increase of moisture which occurs during freezing. Under this layer, the moisture content decreases and a de-watering zone is present corresponding to a low or non-heaving layer. The de-watering is due to two mechanisms: 1) as a result of seepage from the canal, the moisture in the upper part of subsoil is greater than that in the lower. The moisture transfers downward under the gradient of moisture content and the gravity force, which is the main mechanism of de-watering in the well drainage capability soil; 2) since ground water table is quite deep, the source of water migration during freezing can only originate from the moisture redistribution in a thin zone beneath the HHR layer. According to the observed data, the thickness of de-watering layer affected by the redistribution is about 30 to 50 cm. If it is assumed that all of the moisture causing 5 cm heaving originates from this layer, a loss of 8% water content in the lower 40 cm can be expected. In areas with shallowly seated ground water tables, no de-watering in the moisture profile is observed. On the contrary, the freezing front approaches closer to the ground water table, the soil moisture content increases rapidly as a result of water movement from the water table. Moisture content exceeding 100% (by weight) were measured in the frozen soil below Daman Main Canal invert. Based on the results from Zhangye Frost Heave Station, correlation curves of the heave ratio versus ground water depth have been determined. The equations for the curves for each soil type is given below.

heavy silty loam $\eta=60.5\exp(-0.0146Z)$ (1)

sandy loam $\eta=284/Z + 0.2$ (2)

fine sand $\eta=65.2/(Z-10) + 0.15$ (3)

where η is heave ratio, in percentage; Z is the distance between the ground water table and the freezing front in cm.

When the subsoil is partially replaced by sand and/or gravel, no water migration occurs in the upper layer and the second mechanism of de-watering mentioned previously does not occur. De-watering resulting from gravity force may occur depending on the drainage capacity of the original subsoil. If the soil is very heavy and the drainage is poor, such as in the case of Minqin Testing Canal, the moisture content in the original soil is large enough to support the water migration, then a HHR layer will appear directly below the sand-gravel layer, as shown in Fig.4. When the ground water is shallow, existence of a upper sand-gravel layer does not change the upward water supply at all, thus the HHR layer will appear in the lowest part of the frozen soil, as shown in Fig.2.

MATHEMATICAL MODEL

Besed on the unsaturated soil water movement, Zhang and Zhu (1983) have determined a numerical-analytical method for solving the coupled heat and moisture transfer equations. Using this method, the heave distribution of a silty loam under shallow and deep ground water conditions has been calculated and is shown in Fig.5. The Figure shows that heave distribution differs significantly according to different ground water conditions, this pattern corresponds closely to the experimental results.

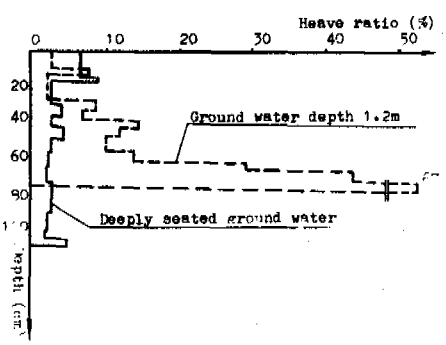

Fig.5 Results of Heave Distribution for a Silty Loam under Shallowly and Deeply Seated Ground Water, as Calculated According to Method Presented by Zhang and Zhu (1981)

CONCLUSION

(i) The result of this paper indicate that various types of the frost heave distribution may exist rather than one single type.

(ii) The heave distribution observed at four field sites may be classified into four types. When the ground water is shallowly seated, the heave distribution is characterized by the high heave ratio layer occurred in the lower half of the frozen soil (Type B), When the local ground water is deeply seated and the soil has a good drainage capability, the heave distribution is characterized by the high heave ratio layer occurred in the upper half of the frozen soil (Type A), when the soil is heavy, the heave distribution is characterized by the high heave ratio layer in the middle half of the frozen soil (Type C) or by heave being distributed with relative evenness (Type D). Among these distribution types, Type A and Type B are most commonly occurred.

(iii) When the upper soil is replaced by sand and/or gravel, the high heave ratio layer will generally occur in the lower half of the frozen layer (Type B). When the ground water is deeply seated, high heave ratio layer will occur directly below the sand-gravel layer in the top of the original soil material. When the ground water is shallowly seated, high heave ratio layer will occur in the lower part of the frozen soil,close to the ground water table.

(iv) The heave ratio observed in the layer near the ground water table is much greater when the high heave ratio layer is in the lower half of the frozen layer (Type B) than when it is in the upper half of the frozen layer (Type A).

ACKNOWLEDGEMENT

The author would like to thank Fu Shining,Wang Zhongjing, Wu Fuxie and Huang Janlan for their contributions to the testing and data processing. This work was supported by the Water Conservancy Department of Gansu Province.

REFERENCES

Wang, X. (1980). A study on the freezing and heaving under different ground water depth and soil conditions. J. of Glaciology and Cryopedology, Vol.3, No.2.

Zhu, Q. (1983). Frost heave characteristics of the concrete canals and the measure of replacing soil in Gansu Province. Proceedings of 2nd National Conf. Permafrost (selection), Lanzhou.

Zhang, S. and Zhu, Q. (1983). A study on the calculation of frost heave. Proc. 4th Int. Conf. Permafrost, Fairbanks.

TRIAXIAL COMPRESSIVE STRENGTH OF FROZEN SOILS UNDER CONSTANT STRAIN RATES

Zhu, Yuanlin[1] and D.L. Carbee[2]

[1]Lanzhou Institute of Glaciology and Geocryology, Academia Sinica, Lanzhou, China
[2]U.S. Army CRREL, Hanover, NH 03755, U.S.A.

SYNOPSIS Triaxial compressive strength tests were conducted on remolded, saturated Fairbanks silt and Northwest sand taken from Alaska under various constant strain rates ranging from 5.27×10^{-7} to $9.84\times10^{-4}s^{-1}$ and confining pressures up to 3.43 MPa at -2°C. The average dry densities of the samples tested were 1.20 g/cm³ for silt and 1.52 g/cm³ for sand, respectively. It was found that within the range of confining pressure employed the maximum deviator stress, $(\sigma_1-\sigma_3)_m$, for the silt did not vary with σ_3, i.e., its angle of internal friction $\phi=0$ and its shear strength τ=cohesion C. For a given temperature and dry density, the value of C increased with increasing strain rate. However, the maximum deviator stress for frozen sand increased significantly with increasing σ_3; and the increase was not linear, indicating that at a given temperature and strain rate, the values of C and ϕ for frozen sand depended upon the range of normal stress σ. At the temperature tested and $\dot{\varepsilon}_1=1.04\times10^{-4}s^{-1}$, the values of C and ϕ for the sand varied as follows: C=1.62 MPa and $\phi=22.8°$ for $\sigma\leq3.1$ MPa, and C=2.30 MPa and $\phi=12.1°$ for $\sigma\geq3.1$ MPa. The test results also showed that the axial failure strain for silt was independent of σ_3, but varied with $\dot{\varepsilon}_1$. It changed abruptly at a strain rate of about 10^{-4}-$10^{-5}s^{-1}$, indicating that a transition of deformation mode occured at this strain rate. Whereas, the failure strain for sand increased with increasing σ_3. The initial tangent modulus of frozen silt and sand seemed to decrease slightly with increasing hydrostatic pressure, presumably owing to the pressure-melting of ice. Significant dilation at larger strains was observed for the sand samples, but not for the silt samples.

INTRODUCTION

The design of stable underground structures in cold regions and artificially frozen-ground supporting structures requires the knowledge of strength and deformation behaviour of frozen soils under the action of both confining (hydrostatic) pressure and vertical load, i.e., at a complex stress state. In the past two decades, therefore, more attention has been paid to the research on the stress-strain behaviour of frozen soils under triaxial stress. While many researchers have studied this subject from various aspects, detailed studies are still required to gain a better understanding of the subject.

The objective of this study was to investigate the effect of confining pressure and strain rate on the stress-strain behaviour of disturbed, frozen saturated Fairbank silt and Northwest sand. The testing temperature was -2°C. The average dry densities of the samples tested were 1.20g/cm³ for the silt and 1.52 g/cm³ for the sand, and their corresponding water content were 42.7% and 25.3%, respectively. The desired confining pressures and cross-head speeds employed are shown in Table I.

MATERIAL AND SPECIMEN PREPARATION

Material

The material used in this investigation are a remolded Fairbanks Fox tunnel silt (FTS) and a remolded Northwest (Irvine) sand (NWS) taken from Alaska. The grain size distribution curves and physical properties of the materials are shown in Fig.1 and Table II.

TABLE I

Confining Pressure and Cross-Head Speed Used

	Silt samples	Sand samples
Confining pressure (MPa)	0, 0.49, 0.98, 1.96	0, 0.98, 1.96, 3.43
Cross-head speed (mm/min)	10, 1, 0.1, 0.01, 0.005	1

Specimen preparation

The samples tested were made by using a gang mold, machined from acrylic plastic, which has a capacity of forming 19 cylindrical specimens at one time. The details of specimen preparation (including compacting, saturating, freezing and trimming) were described by the authors (1987). By using the dual source γ-ray technique with the help of J. Ingersoll, it is known that the distribution of density and moisture along the specimen length was quite uniform.

In order to prevent the pressurizing liquid per-

TABLE II

Physical Properties of the Materials Tested

Material	Plastic limit (%)	Liquid limit (%)	Plastic indix (%)	Specific gravity	Organic content (%)	Specific surface area (m^2/g)
FTS	34.2	38.4	4.2	2.680	5.5	35.0
NWS	—	—	—	2.710	—	—

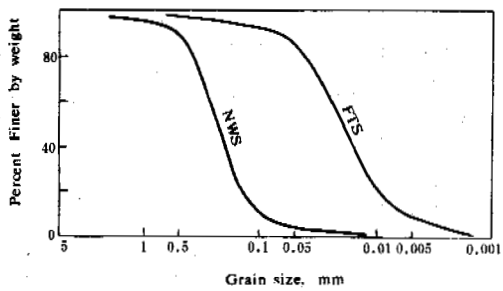

Fig.1 Grain Size Distribution Curves

meating into a specimen and ice sublimation during a test, each specimen was sealed with a piece of rubber membrane and steel end caps. The nominal size of the prepared specimens was 70 mm in diameter by 152 mm long.

TESTING PROCEDURE AND APPARATUS

The triaxial constant cross-head speed compression tests were conducted on a screw-driven universal testing machine in a cold room, which allowed specimens deforming under various constant cross-head speeds. All specimens were tempered and pressurized at the desired temperature and confining pressure for at least 24 hours before testing. The axial force acting on a specimen during the movement of cross-head was measured through a multi-range load cell with an accuracy of 0.5% of full scale. The deformation was measured with a DCDT (direct current displacement transducer), having a sensitivity of 2.5×10^{-4}mm. The confining pressure,which was provided by a compressor and transmitted to the specimen through a 50% by weight glycerol-water solution, was measured with a PLC pressure transducer. The temperature of the working liquid in triaxial cell (taken as the temperature of specimen after reaching equilibrium) was measured with a thermistor positioned inside the cell. The measurements showed that the temperatures were held constant with a fluctuation of less than ±0.05°C. The volume change of a specimen during a test was measured with a volumetric tube.

TEST RESULTS

The curves of deviator stress $(\sigma_1-\sigma_3)$ vs axial strain (ε_1) for FTS and NWS under various σ_3 and strain rates $(\dot{\varepsilon}_1)$, are presented in Fig.2 and 3, respectively. As is commonly defined,

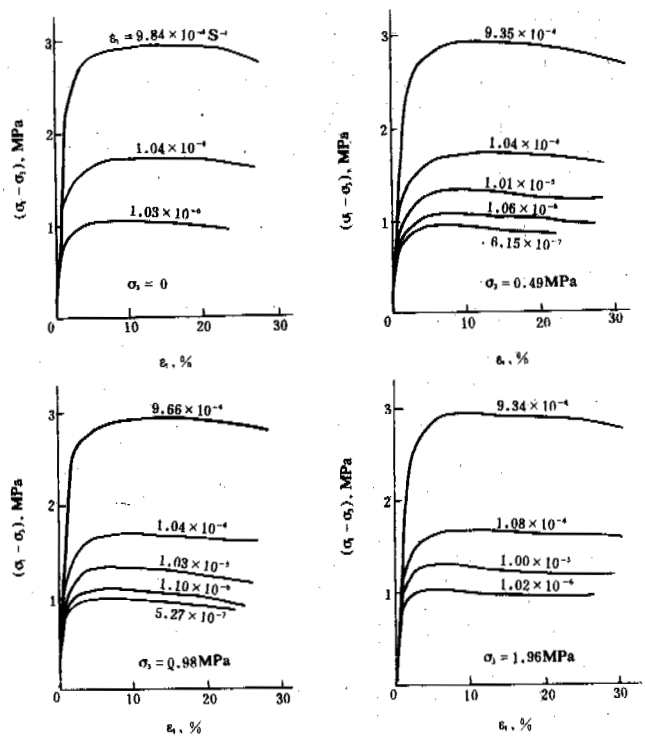

Fig.2 Curves of Deviatoric Stress vs Axial Strain for FTS

the peak of the $(\sigma_1-\sigma_3)$ vs ε_1 curves is defined as the failure of the specimens, so that the deviator stress corresponding to the peak is defined as the deviatoric peak (maximum) strength $(\sigma_1-\sigma_3)_m$, and the axial strain and elapsed time at $(\sigma_1-\sigma_3)_m$ represent the strain at failure (ε_1m) and the time to failure (t_m), respectively. The test results of $(\sigma_1-\sigma_3)_m$, ε_1m, t_m and initial tangent modulus E_i, together with test conditions, ε_1 and σ_3, are summarized in Table III.

TABLE III

Summary of the Test Results and Conditions

Sample number	Applied strain rate, $\dot{\varepsilon}_1$ (s^{-1})	Confining pressure, σ_3 (MPa)	Maximum deviator stress, $(\sigma_1-\sigma_3)_m$ (MPa)	Axial strain at failure, ε_{1m} (%)	Time to failure, t_m (min.)	Initial tangent modulus, E_i (MPa)
	Fairbanks Silt					
F243	9.84×10^{-4}	0	2.79	10.33	1.75	430
F242	1.04×10^{-4}	0	1.71	10.38	16.2	580
F244	1.03×10^{-6}	0	0.97	3.84	620	530
F227	9.35×10^{-4}	0.49	2.75	9.37	1.67	500
F228	1.04×10^{-4}	0.49	1.64	9,40	15.0	500
F236	1.01×10^{-5}	0.49	1.15	3.67	60.5	380
F230	5.16×10^{-6}	0.49	1.06	3.43	111	440
F237	1.06×10^{-6}	0.49	0.97	4.07	638	410
F229	6.15×10^{-7}	0.49	0.94	4.00	1084	350
F235	9.66×10^{-4}	0.98	2.67	10.43	1.80	560
F233	1.04×10^{-4}	0.98	1.70	10.75	17.2	480
F232	1.03×10^{-5}	0.98	1.18	3.77	60.9	560
F234	1.10×10^{-6}	0.98	0.95	3.43	520	390
F231	5.27×10^{-7}	0.98	0.94	3.31	1047	390
F239	9.34×10^{-4}	1.96	2.84	10.37	1.85	480
F238	1.08×10^{-4}	1.96	1.66	10.61	16.32	460
F241	1.00×10^{-5}	1.96	1.19	3.03	50.5	480
F240	1.02×10^{-6}	1.96	0.94	4.09	668	380
	Northwest Sand					
N250	1.02×10^{-4}	0	4.84	3.48	5.67	980
N247	1.04×10^{-4}	0.98	6.09	10.67	17.2	960
N245	1.04×10^{-4}	1.96	6.76	11.36	18.2	940
N246	1.04×10^{-4}	1.96	6.59	13.70	22.0	920
N249	1.05×10^{-4}	3.43	7.41	12.96	20.5	790

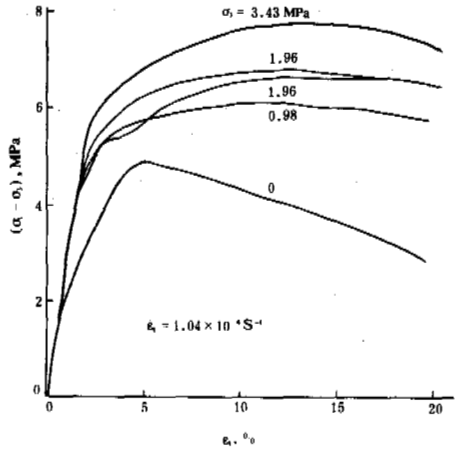

Fig.3 Curves of Deviatoric Stress vs Axial Strain for NWS

DISCUSSION

Effect of confining pressure on the stress-strain behaviour of frozen soils

It is seen from Fig.2 that all of the deviatoric stress-strain curves for a certain strain rate and various σ_3 are quite similar. It means that confining pressure does not significantly affect the deviatoric stress-strain behaviour of frozen silt. All of these curves have a wide "plateau", indicating that the silt samples behaved as a typical ductile (plastic) failure mode under various σ_3, i.e., the samples underwent plastic flow after a small quasi-elastic strain (<1%), and no visible cracks were observed on the surface of the specimens until axial strain up to 30%. However, it was found that confining pressure has a strong effect on the stress-strain behaviour of frozen sand. It is seen from Fig.3 that the sand samples behaved as a typical brittle failure as $\sigma_3 \approx 0$; whereas both the plasticity and strain hardening of the sand samples remarkably increase with increasing confining pressure. This is due to the fact that the interparticle friction and particle interlocking play a more important role in strengthening the sand samples as σ_3 is increased (Andersland and AlNouri,1970; Chamberlain et al., 1972; Sayles, 1974).

Deviatoric peak strength

A plot of the reciprical of deviatoric peak strength, $1/(\sigma_1-\sigma_3)_m$, vs strain rate in semi-logarithm, under various σ_3 for FTS is shown in Fig.4. It is clear from this figure that the

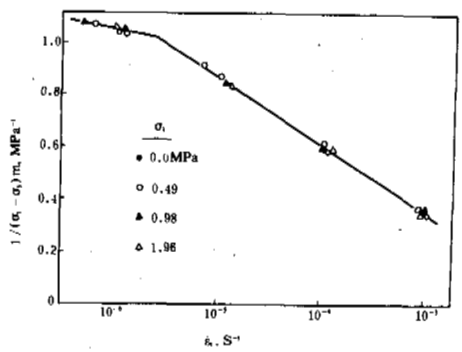

Fig.4 Plot of $1/(\sigma_1-\sigma_3)_m$ vs log $\dot{\varepsilon}_1$ for FTS

variation of $(\sigma_1-\sigma_3)_m$ with $\dot{\varepsilon}_1$ for the silt does not depend upon σ_3. Thus, the peak strength, $(\sigma_1-\sigma_3)_m$, as a function of strain rate, for frozen silt under various σ_3, can be described by the following equation which is similar to the uniaxial compressive strength equation presented by the authors (1984):

$$(\sigma_1-\sigma_3)_m=\frac{\beta\sigma'}{\beta+\sigma'\ln(\dot{\varepsilon}_1'/\dot{\varepsilon}_1)} \qquad (1)$$

where $\dot{\varepsilon}_1'=2.6\times10^{-6}s^{-1}$ is a reference strain rate corresponding to the deflection point of the curve in Fig.4, $\sigma'=0.98$ MPa is the deviatoric peak strength for $\dot{\varepsilon}_1=\dot{\varepsilon}_1'$, and β is the reciprical of the slope of $\ln\dot{\varepsilon}_1$ vs $1/(\sigma_1-\sigma_3)_m$ curve and has a value of 9.1 MPa when $\dot{\varepsilon}_1\geq\dot{\varepsilon}_1'$ and 28.8 MPa when $\dot{\varepsilon}_1\leq\dot{\varepsilon}_1'$.

From Fig.4 the deviatoric peak strength as a function of strain rate for the silt can be also described by the following expression which is similar to Vialov's strength-loss equation:

$$(\sigma_1-\sigma_3)_m=\frac{\beta}{\ln(B/\dot{\varepsilon}_1)} \qquad (2)$$

where parameter B has a value of $2.5\times10^{-2}s^{-1}$ when $\dot{\varepsilon}_1\geq2.6\times10^{-6}s^{-1}$ and 10^7s^{-1} when $\dot{\varepsilon}_1\leq2.6\times10^{-6}s^{-1}$. Note that the independent variable in eq.(2) is strain rate, but not the time-to-failure as is in Vialov's equation.

The deviatoric peak strength as a function of time to failure, t_m, for FTS under various σ_3 was plotted in Fig.5 in logarithm. It is explicit that the variation of the peak strength, $(\sigma_1-\sigma_3)_m$, with time to failure for the silt is not dependent upon σ_3 and can be evaluated by a power-law expression:

$$(\sigma_1-\sigma_3)_m=\sigma''(t_m'/t_m)^{\alpha} \qquad (3)$$

where $t_m'=110$ min is a reference time-to-failure corresponding to the deflection point of the curve in Fig.5, $\sigma''=1.02$ MPa is the peak strength for $t_m=t_m'$, and α is the slope of the curve in Fig.5 and has a value of 0.23 when $t_m\leq t_m'$ and 0.04 when $t_m\geq t_m'$.

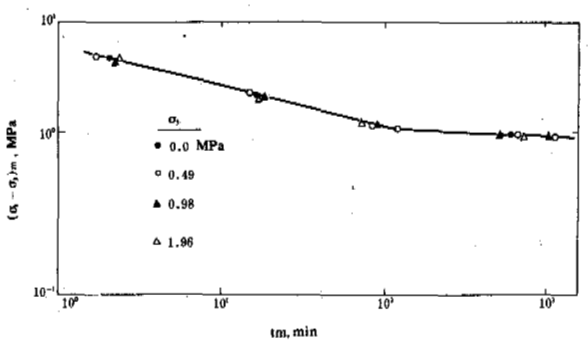

Fig.5 Log-log Plot of $(\sigma_1-\sigma_3)_m$ vs t_m for FTS

Shear strength

The Mohr-circles and envelopes for FTS under various strain rates were plotted in Fig.6, in which the tensile Mohr-circles were plotted based on the authors' tension test data (1986). Explicitly, the angles of internal friction, ϕ, for the silt within the range of confining pressure employed under various strain rates are all equal to zero. Thus, the Coulomb equation for

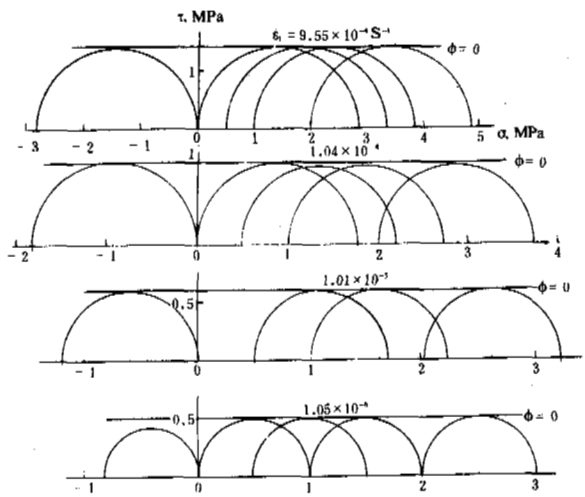

Fig.6 Mohr-circles and Envelopes for FTS

frozen silt is reduced to

$$\tau = C = (\sigma_1 - \sigma_3)_m / 2 \qquad (4)$$

i.e., the shear strength (τ) for frozen silt equals to its cohesion (C), which is equal to a half of the maximum deviator stress.

Similar results were reported by Chamberlain (1972) on a glacial till at -10°C. Ouvry (1985) reported that the maximum deviatoric stress for frozen clay even decreased slightly with increasing confining pressure at various temperatures and strain rates. This is due to the fact that the pressure-melting of ice in frozen soils increases the thickness of unfrozen water film around soil particles, and thus decreases their interparticle friction and cohesion.

For a given temperature the cohesion (C) of a soil varies with strain rate. The values of C for FTS at -2°C under various strain rates were given in Table IV.

TABLE IV

Values of Cohesion C for FTS at -2°C

$\dot{\varepsilon}_1(s^{-1})$	9.55×10^{-4}	1.04×10^{-4}	1.01×10^{-5}	1.05×10^{-6}
C(MPa)	1.39	0.84	0.59	0.48

The Mohr-circles and envelope for NWS at a strain rate of $1.04\times10^{-4}s^{-1}$ were plotted in Fig.7, in which the tensile strength data were from Bayer (unpublished). Obviously, the shear strength of frozen sand can be evaluated by the general form of Coulomb equation:

$$\tau = C + \sigma tg\phi \qquad (5)$$

However, it is seen from Fig.7 that the envelope is not a straight line, but a broken-line within a certain range of normal pressure, σ. Therefore, the values of C and ϕ in eq.(5) is dependent upon the range of normal pressure for a given temperature and strain rate. The values of C and ϕ obtained graphically from Fig.7 are as follows: C=1.62 MPa and ϕ=22.8° when $\sigma \leq 3.1$ MPa, and C=2.30 MPa and ϕ=12.3° when $\sigma \geq 3.1$ MPa. The latter value of ϕ is very close to the value (ϕ=12.4°) obtained by Parameswaran et al. (1981) on frozen medium sand under similar strain rate.

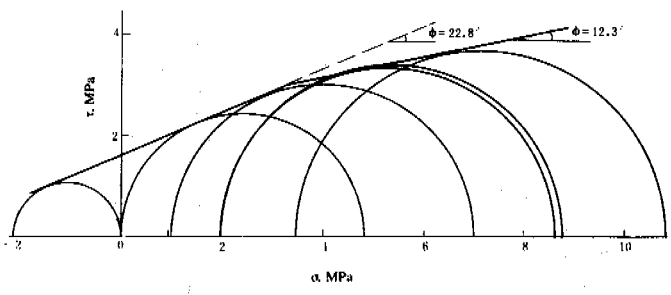

Fig.7 Mohr-circles and Envelope for NWS

Based on the geometric relation of Mohr-circles and their common tangent, the values of C and ϕ can be also determined analytically (thus, more accurately) in terms of the following relations (Terzaghi and Peck, 1968):

$$\frac{(\sigma_1-\sigma_3)_m}{2} = a + \frac{(\sigma_1+\sigma_3)_m}{2} \cdot tg\alpha \qquad (6)$$

$$\sin\phi = tg\alpha \ , \quad a = C\cdot\cos\phi \qquad (7)$$

where parameters a and $tg\alpha$ can be determined from the data shown in Fig.8 by linear regression analysis. The values of C and ϕ for NWS obtained from the test data in terms of eq.(6) and (7) are as follows: C=1.61 MPa and ϕ=22.6° when $\sigma_3 \leq 0.98$ MPa and C=2.26 MPa and ϕ=12.2° when $\sigma_3 \geq 0.98$ MPa. They are very close to those obtained graphically from Fig.7.

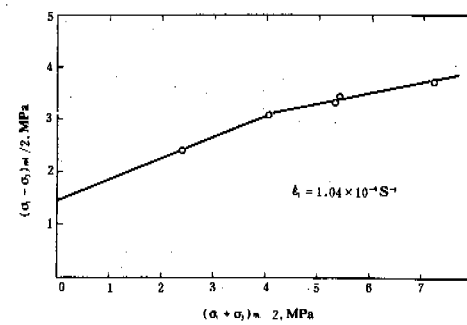

Fig.8 Plot of $(\sigma_1-\sigma_3)_m/2$ vs $(\sigma_1+\sigma_3)_m/2$ for NWS

Axial strain at failure

The variation of axial strain at failure ($\varepsilon_1 m$) with strain rate for FTS under various σ_3 was shown in Fig.9. An abrupt change of the failure strain with strain rate for the silt was observed occuring at a strain rate between 10^{-5} and $10^{-4}s^{-1}$. Whereas, the failure strains remain almost the same for both $\dot{\varepsilon}_1 > 10^{-4}s^{-1}$ and $\dot{\varepsilon}_1 < 10^{-5}s^{-1}$, with the averaged values of 10.2% for the former and 3.7% for the latter. This might imply that a transition of the mode of defromation for the silt occured at this strain rate. A similar phenonmena for sand was observed by Baker et al. (1981) at a strain rate of $3\times10^{-4}s^{-1}$.

Fig.10 shows the failure strain as a function of σ_3 for both NWS and FTS at a strain rate of $1.04\times10^{-4}s^{-1}$. It is seen that the failure strain for silt is independent of σ_3, but it increases with increasing σ_3 for sand (especially at lower confining pressures), accounting for

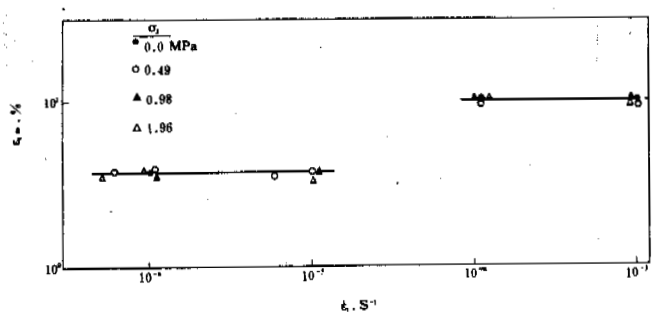

Fig.9 Variation of Axial Strain at Failure with Strain Rate for FTS

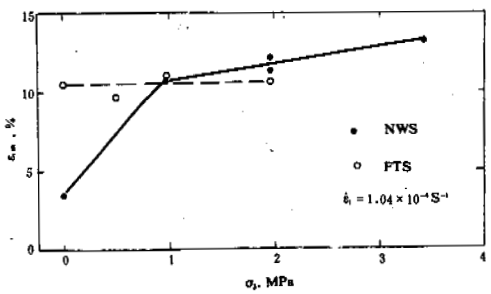

Fig.10 Axial Strain at Failure vs Confining Pressure

the increase in interparticle friction of coarse-grained soil under the effect of confining pressure.

Initial tangent modulus

The variation of initial tangent modulus (E_i) with strain rate for FTS under various σ_3 was illustrated in Fig.11. It is explicit that the initial tangent modulus for the silt does not vary with strain rate at the test conditions. It has an average value of 460 MPa at the test temperature (-2°C).

Fig.12 shows the variation of E_i with σ_3 for both NWS and FTS. It is seen from this figure that the initial tangent modulus for the medium sand is about twice as great as that for the silt at the given temperature and strain rate. The initial tangent moduli for both sand and silt decrease slightly with increasing confining pressure, owing to the pressure-melting of ice in frozen samples.

Volumetric strain

The volumetric strain ($\Delta v/v_o$) vs axial strain curves for both NWS and FTS are plotted in Fig. 13. As was expected, the coarser grained NWS underwent remarkable dilation as observed by Chamberlain et al. (1972) for Ottawa banding sand under high confining pressures. A small amount of volume decrease ($|\Delta v/v_o| < 0.1\%$) was observed at the beginning of deformation for

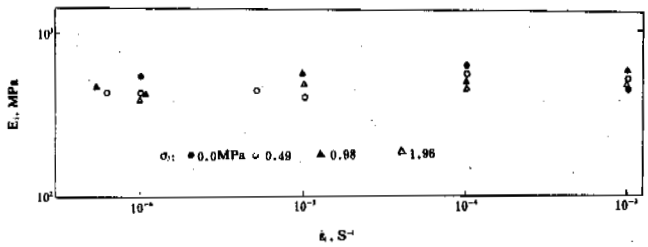

Fig.11 Initial Tangent Modulus vs Strain Rate in Logarithim for FTS

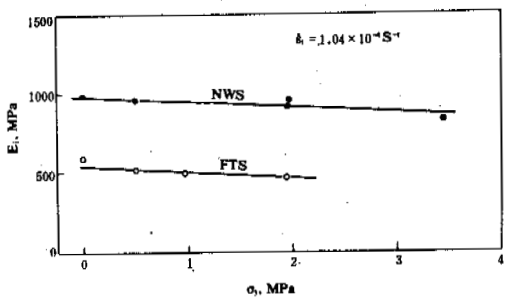

Fig.12 Initial Tangent Modulus vs Confining Pressure

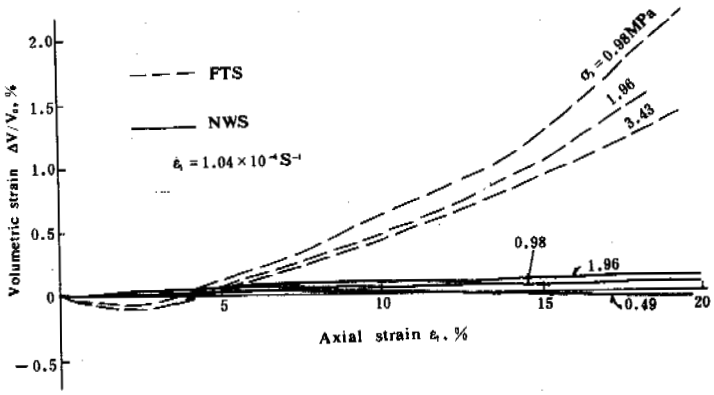

Fig.13 Volumetric Strain vs Axial Strain

the sand. This can be attributed to the closure of air voids in the samples, for which ice saturation degree is relatively lower. Almost no dilation or contraction was observed for the finer grained FTS under various σ_3 employed.

Fig.13 also shows the influence of confining pressure on the volumetric strain curves. The dilation for the sand samples was gradually suppressed as confining pressure was increased.

CONCLUSIONS

It can be concluded from this investigation that:

(i) Confining pressure does not affect the deviatoric stress-strain curves for frozen silt, but significantly increases the plasticity and strain hardening of frozen sand within the range of confining pressure employed.

(ii) The angle of internal friction (ϕ) is equal to zero for frozen silt; it varies with the range of σ_3 for frozen medium sand: $\phi=22.6°$ when $\sigma_3 \leq 0.98$ MPa and $\phi=12.2°$ when $\sigma_3 \geq 0.98$ MPa.

(iii) A sudden change of the axial strain at failure with strain rate was observed occuring at a strain rate between 10^{-4} and $10^{-5}s^{-1}$ for frozen silt at -2°C, indicating that a transition of the mode of deformation and/or failure may occur at this strain rate.

(iv) The axial strain at peak stress does not depend upon confining pressure for frozen silt, but increases with increasing confining pressure for frozen sand, especially at low confining pressure.

(v) The initial tangent modulus of frozen soil is not dependent upon strain rate, but slightly decreases with increasing confining pressure because of the pressure-melting of ice. It has an average value of 460 MPa for silt and 960 MPa for medium sand at -2°C.

(vi) Remarkable dilation in triaxial compression was observed for the coarser grained soil, but almost no volume changes were measured for the finer grained soil.

ACKNOWLEDGEMENTS

This study was sponsored by the U.S.Army Corps of Engineers at the Cold Regions Research & Engineering Laboratory. The authors wish to express their appreciation and thanks for the technical advice and instructive discussion from Dr. A. Assur, Messrs W. Quinn, E. Chamberlain, F. Sayles, D. Cole, Dr. M. Mellor and Dr. Y.C. Yen. We also would like to thank Messrs J. Bayer, J. Rajkowski, J. Ingersoll and G. Durell for their technical support and instrumentation assistance. Thanks are also given to Dr. T.H.W. Baker for review of this paper.

REFERENCES

Andersland, O.B. & Alnouri, I. (1970), Time-dependent strength behaviour of frozen soils. Jnl Soil Mech. Fdns Div. Am. Soc. Civ. Engrs 96, SM4, 1249-1265.

Baker, T.H.W., Jones, S.J. & Parameswaran, V.R. (1981), Confined and unconfined compression tests on frozen sand, Proceedings of Fourth Canadian Permafrost Conference, p. 387-393.

Bayer,J., Investigation into compression and tensile strength of frozen sand and silt, USA CRREL Technical Note (unpublished).

Chamberlain, E.J., Groves, C. & Perham, R. (1972), The mechanical behaviour of frozen earth materials under high pressure triaxial test conditions, Geotechnique, Vol. 22, No.3, p.469-483.

Ourvy, J.F. (1985), Results of triaxial compression tests and triaxial creep tests on an artificially frozen stiff clay, Proceedings of the 4th International symposium on Ground Freezing, Vol.II, p.207-212.

Parameswaran, V.R. & Jones, S.J. (1981), Triaxial testing of frozen sand, Journal of Glaciology, Vol.27, No.95, p.147-156.

Sayles, F.H. (1974), Triaxial constant strain rate tests and triaxial creep tests on frozen Ottawa sand, USA CRREL Technical Report 253.

Zhu, Y.L. & Carbee, D.L. (1984), Uniaxial compressive strength of frozen silt under constant deformation rates, Cold Regions Science and Technology, 9(1984), 3-15.

Zhu, Y.L. & Carbee, D.L. (1986), Tensile strength of frozen silt, Journal of Glaciology and Geocryology, Vol.8, No.1, P. 15-28.

Zhu, Y.L. & Carbee, D.L. (1987), Creep and strength behaviour of frozen silt in uniaxial compression, USA CRREL Report 87-10.

LONG TERM SETTLEMENT TEST (3 YEARS) FOR CONCRETE PILES IN PERMAFROST

B.A. Bredesen[1], O. Puschmann[1] and O. Gregersen[2]

[1]Selmer-Furuholmen Anlegg a.s, Oslo, Norway
[2]Norwegian Geotechnical Institute, Oslo, Norway

SYNOPSIS. Prefabricated concrete piles in drilled holes have been used for foundations for heavy concrete buildings at Svalbard. The pile bearing capacity calculations were based on North-American experience. The test was carried out in order to gain own experience in local soil conditions. The test site in Longyarbyen was chosen close to future building sites where we anticipated poor ground conditions. See Fig. 2.

We also wanted to test the performance of cast-in-place reinforced concrete piles. The tested cast-in-place pile with anti freeze agents and 15% shorter length had the same settlements as the pre-fabricated grouted piles and they can be recommended for future construction projects.

The objective was to establish the load settlement curve for long term loads for that specific soil and the prevailing permafrost temperatures. The settlements are compared against curves of settlements in ice and ice rich silty soils from Nixon and McRoberts. See Fig. 12.

The long term settlement for 40 t load, was 0.5 mm per year (12.5 cm in 25 years).

Fig. 1 Photo of pile loading system

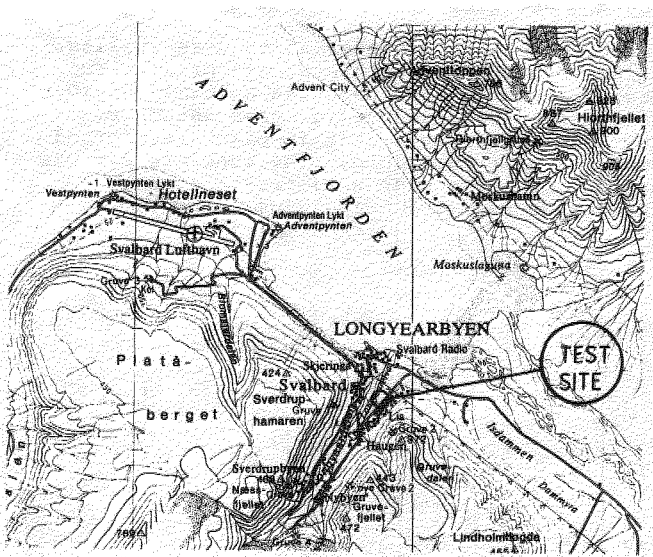

Fig. 2 Location of test site

SOIL CONDITIONS

The soil conditions at the test site are shown on Fig. 3. The top layer which consists of sand and gravel, has a varying thickness over the area. The investigations showed a variation from 2.5 m to 6.0 m. Underneath, to a depth of more than 10 m, the soil consists of a sediment of silt and clay. The amount of fines is gradually increasing with depth. High water content indicates zones of ice rich material. The salinity is low, from 0.8 to 1.6 grams/litre, i.e. the sedimentation took place in brackish water.

TEST PROCEDURE

We wanted, to the greatest extent, to duplicate the pile installations of the constructed buildings at Longyarbyen. These are without frost heave protection.

The frost action in the active layer has influence on the performance of the piles. However, because of the stability of the test structure only one of the test piles was given frost heave protection to a depth of 100 cm.

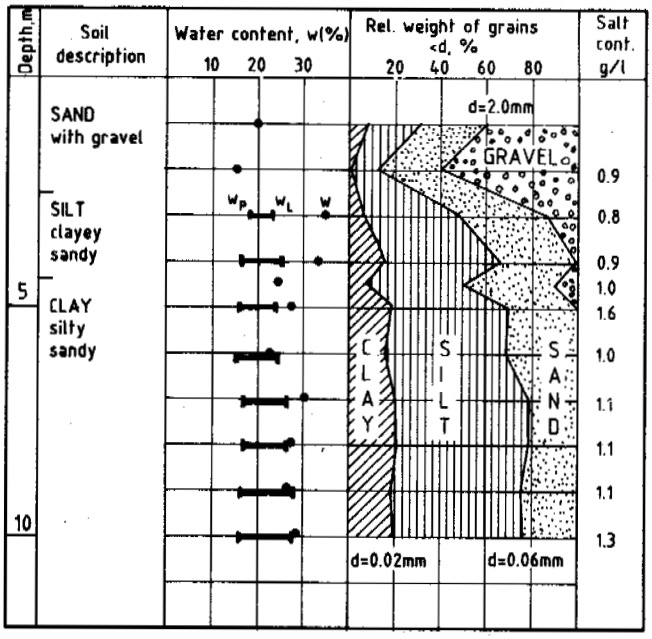

Fig. 3 Soil profile at test site

The test was performed in full scale. The 3 piles were positioned in a triangle 600 cm apart. See Fig. 4.

Three holes with diameter 35 cm were drilled, using an air track with downhole drill. Two prefabricated piles, Hercules H420, 7 and 10 m long, were installed using cement-sand grout. The third pile was a cast-in-place reinforced concrete pile, 6 m long. The concrete mix was a special concrete with anti freeze agents. (Rescon Nonset 400). See Figs 5 and 7.

The drilling took place 83-10-27 and 83-10-28. The piles were grouted 87-11-07 at +16°C. A concrete slab on top of the 3 piles was cast and was loaded with gravel after 10 weeks 84-01-19.

To avoid end bearing, piles 1 and 3 were installed with a cushion of styrofoam. Pile 2 was installed with a load cell to register end bearing.

The test was run 3 years using 40 t load per pile and 1 year using 60 t load. However, for 60 t load the test structure got a sidesway making the settlement measurements impossible.

MEASUREMENTS

The reference pile for settlement measurements was constructed using a prefabricated concrete pile with a special protection in the active layer. See Fig. 6.

The settlements were read using Wild N3 precision niveller from two sides of each pile and with 12 readings for each settlement number. The two measurements were done from 2 different instrument positions (see Fig. 4), and they corresponded very well. The measuring accuracy is within 0.04 mm.

The temperature measurements were read using thermocouples with digital termometer Jenway tc 2000 type 8015 and copper/constantan wire.

The first 2 years settlements and temperatures were recorded 4 times a year.

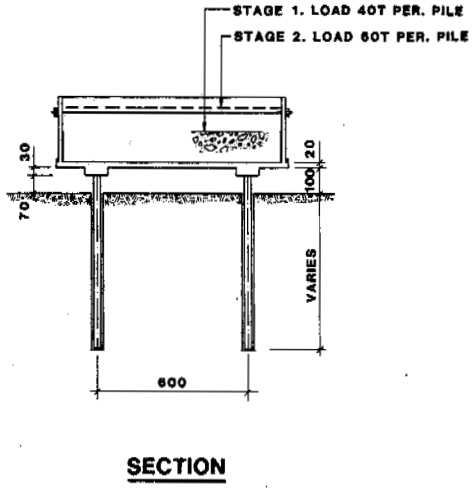

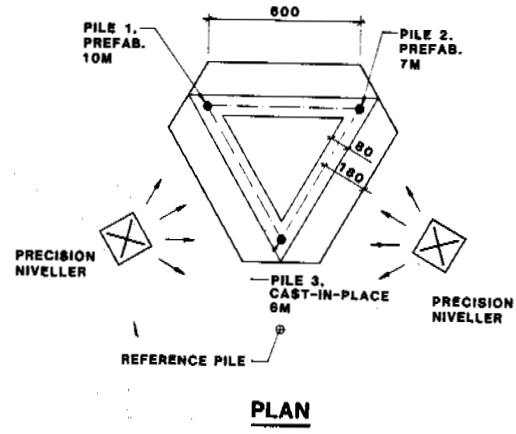

Fig. 4 Pile loading system

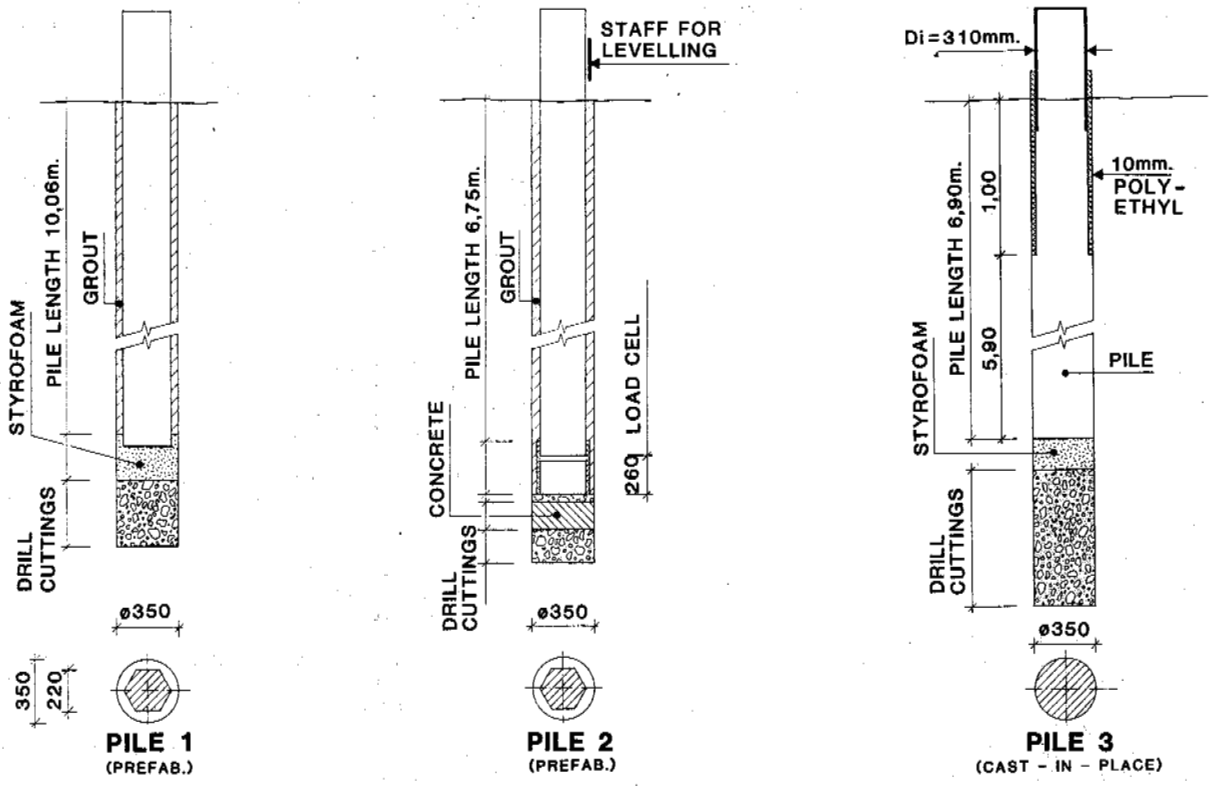

Fig. 5 View of tested piles

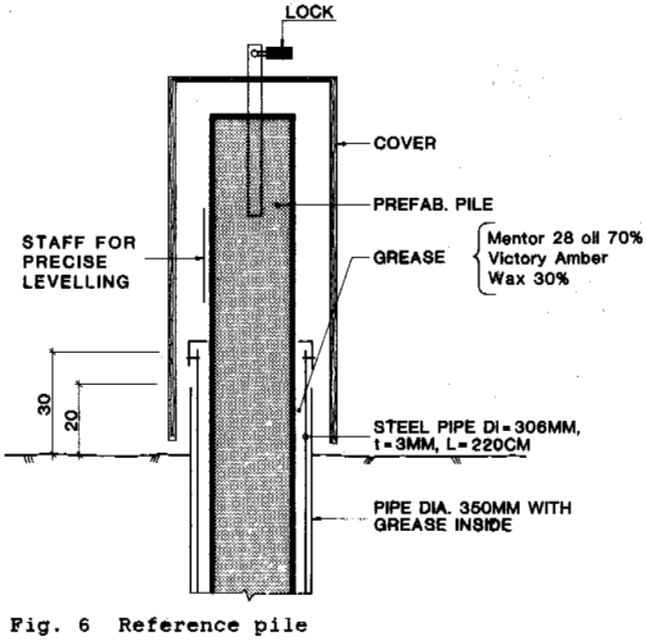

Fig. 6 Reference pile

1983 - FREEZE-BACK

The piles were installed 7 November 1983 at air temperature ÷16°C. The ground temperatures during freeze-back is shown in Fig. 8, and the position of the thermocouples is shown on Fig. 7. The cast-in-place concrete (Rescon Non-set 400) cures at freezing temperatures. A laboratory test after 7 days at ÷5° to ÷8°C in a freezer gave cube compression values 27 MPa for the concrete. For cast-in-place piles with air temperature ÷16°C, the curing of the concrete above ground will govern the time for loading the piles. The heat from the curing did not seem to effect the freeze-back time much. Both types of piles could have been loaded after 3 weeks at that time of the year. The loading was applied after 10 weeks.

1984 - LONG TERM SETTLEMENT INCLUSIVE COMPRESSION OF THE PILE

Concrete is a compressible material and the first year the settlement of the piles in the permafrost was partly caused by the elastic and permanent compression of the concrete pile. The total pile cap settlement of 2.1 mm per year is

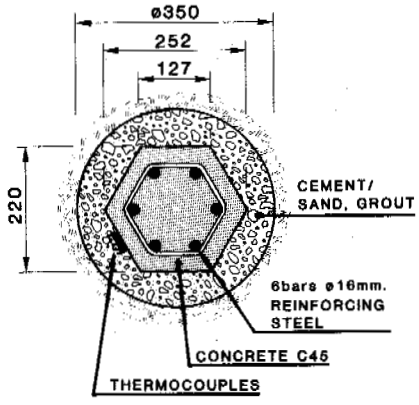

PREFAB. CONCRETE

PILE 1 AND 2

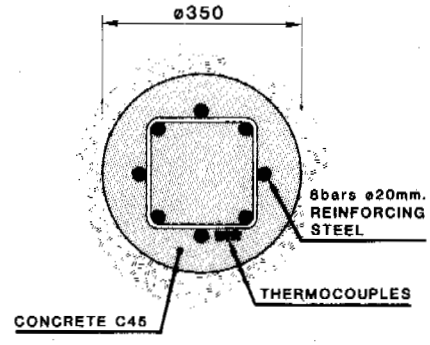

CAST - IN - PLACE CONCRETE

PILE 3

Fig. 7 Cross section of tested piles

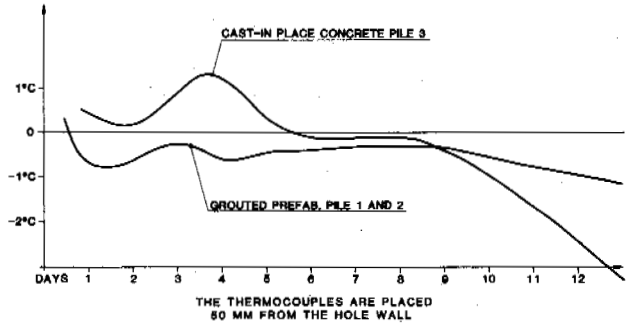

Fig. 8 Freeze-back temperatures at 4 m depth

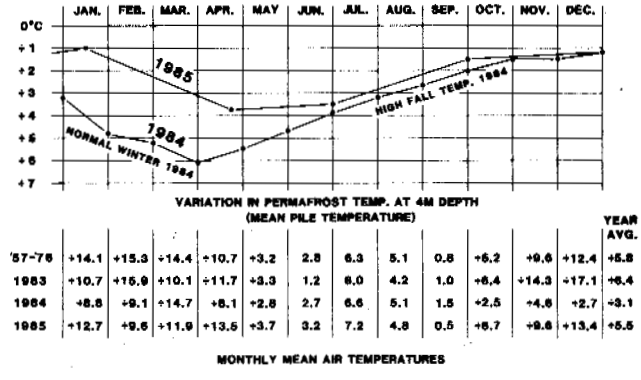

VARIATION IN PERMAFROST TEMP. AT 4M DEPTH
(MEAN PILE TEMPERATURE)

													YEAR AVG.
'57-'76	+14.1	+15.3	+14.4	+10.7	+3.2	2.8	6.3	5.1	0.8	+5.2	+9.6	+12.4	+5.8
1983	+10.7	+15.9	+10.1	+11.7	+3.3	1.2	6.0	4.2	1.0	+6.4	+14.3	+17.1	+6.4
1984	+6.8	+9.1	+14.7	+8.1	+2.8	2.7	6.6	5.1	1.5	+2.5	+4.6	+2.7	+3.1
1985	+12.7	+9.6	+11.9	+13.5	+3.7	3.2	7.2	4.8	0.5	+6.7	+9.6	+13.4	+5.5

MONTHLY MEAN AIR TEMPERATURES

Fig. 9 Temperature observations

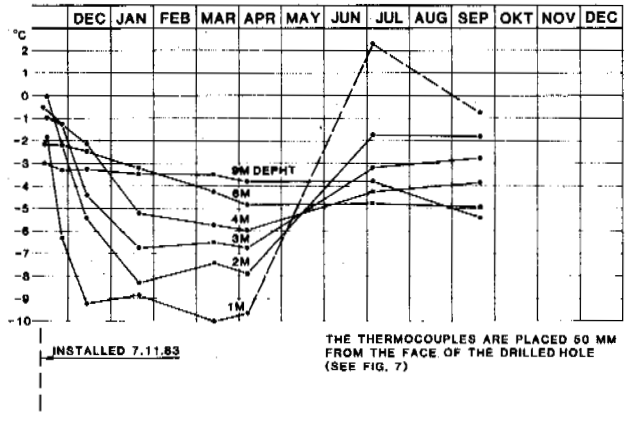

Fig. 10 Temperature observations 1984

partly caused by compression of the pile material as the load gradually is transferred from the ground surface to the permafrost along the pile. It takes time for the forces to be transferred down to the bottom of the pile and the bottom of the pile may only be partially loaded. See Fig. 11.

The first day the 40 t load is applied, the compression acts only on the upper meters of the pile. The modulus of elasticity compares well with the measured 1 day compression values (Fig. 11) 23 September 1986.

The compression of the pile itself is reduced as time pass and one would expect decrease in settlement for the late months of 1984. However, this trend is counterbalanced by increased settlement due to increasing thaw depth.

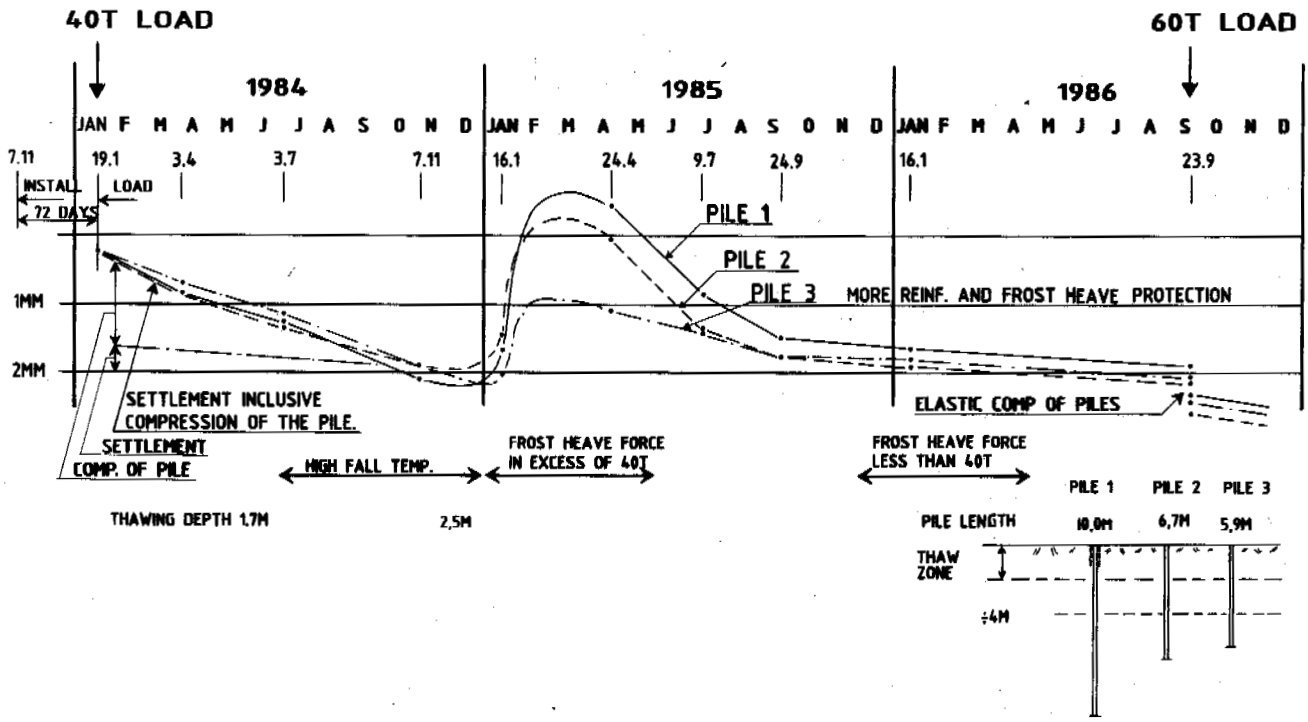

Fig. 11 Pile cap settlements

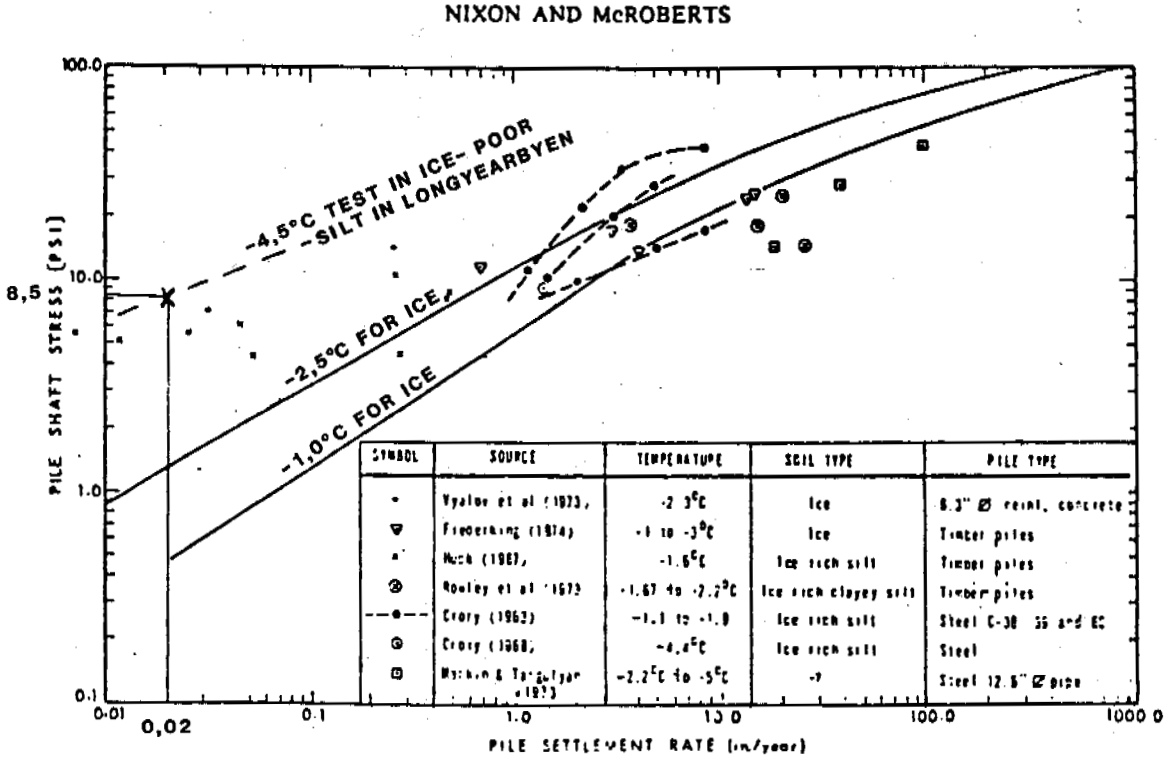

FIG. 9. Review of pile load test data $T = -1$ °C to -2.5 °C (1 psi = 6.9 kN/m²; 1 in./year = 2.54 cm/year).

Fig. 12 Diagram from Nixon and McRoberts (see reference list) Supplemented with test data from Longyarbyen

1985 - FROST HEAVE

The concrete in the piles do not transfer tension so only the reinforcing bars must transfer the frost heave force in excess of the 40 t load. That is the reason why the settlement curve has a humpback the winter 1985. See Fig. 11.

The fall temperatures of 1984 was extremely high (see Fig. 9) and resulted in temperatures at ÷1.5°C at 4 m depth during freeze up and thawing to 2.5 m depth. The frost heave force must have been in excess of 40 t acting on the 35 cm diameter pile and 250 cm length. Pile no. 3 had insulation on length 100 cm and have more reinforcing steel and therefore got less frost heave.

1986 - LONG TERM SETTLEMENT

The summer/fall temperatures of 1985 was normal and resulted in a frost heave force less than 40 t. The settlement curve for 1986 with 0.5 mm per year therefore depicts the long term settlement with maximum thaw depth of approximately 1.5 m. This totals 12.5 cm in 25 years. See Fig. 11.

EVALUATION OF TEST DATA

1. For 40 t load and mean pile shaft stress 0.06 MPa the long term settlement for piles 600 cm long is 0.5 mm per year (1986). Then the frost heave forces are not acting on the piles. The mean temperature at depth 4 m is ÷4.5°C over that time. See Fig. 10.

   The ground is an ice poor silt, and for comparison the settlement data is plotted into the curves from Nixon and McRoberts for ice rich silt in Fig. 12.

2. The cast-in-place pile is slightly better than the slurried piles. The cast-in-place pile and the slurried piles have the same settlement rate when the cast-in-place pile has 15% less surface area.

3. The first year the pile cap settlement was 2.1 mm without frost heave influence. This includes elastic and permanent compression of the concrete pile itself.

4. The increase of pile length from 675 cm to 1006 cm did not reduce the settlement rate. The reason most likely is that because the concrete is highly compressible the bottom of the long pile is only partially loaded. On the other hand the prefabricated pile is partially eccentric in the hole and the quality of the grouting could be less effective on long piles.

5. The settlement curve has been affected by frost jacking. The calculated frost heave force is 54 t. Calculated adfreeze bond stresses is 0.16-0.20 MPa.

   The calculated average adfreeze bond stress during frost heave is higher for the cast-in-place pile (0.20 MPa) than for the slurried prefabricated piles (0.16 MPa). This indicates better quality for this concrete with anti freeze agents.

   Frost heave protection should be considered for building purposes to avoid differential settlement. The protection could be wrapped around the pile to break the adfreeze bond or the ground surface could be insulated to reduce the thawing depth.

6. The use of cast-in-place piles can be recommended. The cast-in-place pile and the slurried prefabricated piles had very similar settlement characteristics. The mix design for the concrete with anti freeze agents (Rescon Nonset 400) and the slurry design were sufficient to transfer the forces. The same slurry mix is used for previous pile installations at Longyarbyen. The use of cast-in-place piles is preferable to withstand lateral forces applied above ground because the column above ground then can have the same cross section as the drilled hole. Cast-in-place piles can also be heavily reinforced for lateral forces.

7. The slurry mixture cement, filler, sand 4:2:10 used for the prefabricated piles did transfer the forces very well. 23 September 1986 the piles were given additional loading of 20 t, resulting in approximately equal elastic deformation 0.4 mm for all piles. The thawed depth then was approximately 150 cm. The time between measurements was 24 hours.

8. For 60 t loading the test rigg got a sidesway so the measurements had to be terminated. The maximum thawing depth then was 1.50 m. For 40 t loading and maximum thawing depth 2.50 m the test rigg was stable.

9. End bearing for Pile 2 was not readable for this small settlements.

REFERENCES

Crory, F.E. (1982). Piling in Frozen Ground. American Society of Civil Engineers. Proceedings, Vol. 108, No. TC1, pp. 112-124.

Ellingbø, O. and J.A. Finstad (1976). Peler i permafrost. Hovedoppgave. Norges tekniske høgskole. Institutt for geoteknikk og fundamenteringslære. 2 vols.

Ladanyi, B. (1980). Field Tests of Foundations in Permafrost. Litterature review. Report prepared for National Research Council. Canada.

Nixon, J.F. and E.C. McRoberts (1975). A design approach for pile foundations in permafrost. Canadian Geotechnical Journal, Vol. 13, No. 1, pp. 40-57.

Phukan, A. (1985). Frozen Ground Engineering. Prentice-Hall, Englewood Cliffs, N.J. 336p.

TANGENTIAL FROST HEAVING FORCE ON REINFORCED CONCRETE PILES OF HIGHWAY BRIDGE

Dai, Huimin and Tian, Deting

Institution for Heilongjiang Provincial Highway and Transportation Research, Harbin, China

SYNOPSIS Experiments and their results on tangential frost heaving force for the reinforced concrete piles of highway bridges, the conditions and parameters of stabilization on anti-heaving, and the method and corresponding coefficients to emend the standard frost depth of soils are chiefly described.

INTRODUCTION

Frost failures have been widely existed in bridges and culvert engineerings in the northern regions, China. With the investigations on some reinforced concrete piles, we found there were more than forty meters of beam bridges within approximate 1000 meters being subjected to the frost failures in varying degrees (Photo 1 and 2). Normal transportation, as a consequence, has been influenced and so heavy losses have been suffered. For this reason, it has been determined to be one of the primary research items since 1981. Experiments have been made intensively on the magnitude of Tangential Frost Heaving Forces; Parameters and Method of the Checking Calculation on Anti-heaving stabilization in the Pile Foundation Designs; Method and Corresponding Coefficients to Emend Standard Frost Depths for 5 years. And these results have been passed by the technical appraisal, which was sponsored by the Ministry of Communications in Harbin, August, 1985. All of the achievements have been taken into "JTJ 024-85 (Ministry of Communication, 1985). The Standard Specifications of Foundation of Highway Bridge Operations and Designs of People's Republic of China.

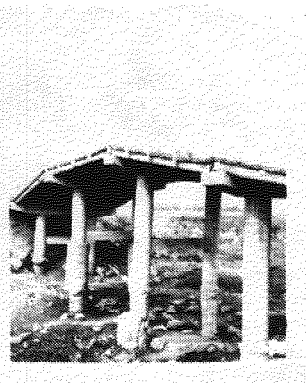

Photo 1 Ji Xinggou Bridge

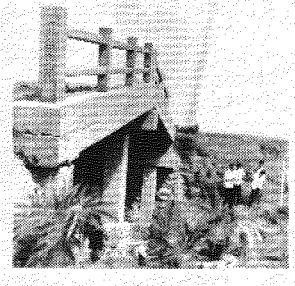

Photo 2 Red Star Bridge

EXPERIMENTS ON TANGENTIAL FROST HEAVING FORCES

In-situ Tests

There are 28 piles for mechanical testing in total, five of them have a diameter of 25 cm, and three-d37 cm, two-d50 cm, two-d75 cm, thirteen-d80cm,two-d100 cm, and one- d 125 cm, respectively.

Fully restrained steel frame against reversed compression were used here, in which there are transverse girders, anchor piles, test piles and mechanical testing apparatus.

The results are shown in Table I.

TABLE I

Results From IN-situ Tests

Item	Frost heaving ratio of subsoil (%)			Unit tangential frost heaving force (kpa)		
Year	82-83	83-84	84-85	82-83	83-84	84-85
No.						
1	25.9	25.0	26.3	216	223	220
2	25.9	25.0	26.3	226	231	232
3	25.9	25.0	26.3	202	221	144
4	16.4	16.4	15.9	156	159	161
5	16.4	16.4	15.9	173	179	176
6	16.4	16.4	15.9	170	180	158
7		3.4	4.8		84	134
8		3.4	4.8		99	144
9		3.4	4.8		49	56
10	8.6	8.0	8.7	45	47	59
11	8.6	8.0	8.7	43	37	51
12	8.6	8.0	8.7	43	41	51
13	8.6	8.0	8.7	35	34	38
14	8.6	8.0	8.7	23	21	27
15	8.6	8.0	8.7	37	23	30
16	8.6	8.0	8.7	23	30	37
17	9.3	9.4	9.6	58	60	66
18	9.3	9.4	9.6	43	46	58
19	9.3	9.4	9.6	44	52	56
20	9.3	9.4	9.6	59	55	58

Note: Nos.1-9 testing piles were built in Qing-an Experimental Field, and Nos.10-20 in Wan-jia.

TABLE II

Results From Model Tests

Geometric scales	Total tangential frost heaving force, KN	Maximum unit tangential frost heaving force, kpa	Average unit tangential frost heaving force, kpa
1:2 ———	26.3	381	84
1:4	4.0	430	50
1:10	1.06	86	32

TABLE III

Results From Rating Calculations to Frost-heaving Bridge Piles

Experiment No.	Structrual style	Designation of soil	Whether frost heave appears	Unit tangential frost heave force, kpa
1	Double-column type of concrete piles; λ=8.8 m	Clay at the depth of 0-6 m; coarse sand at 6-8.4 m; gravel sand at 8.4-8.7; clay under 8.8 m	No	<181
2	Wide slabs, two-6 m spans: double-column concrete piles d-80 cm, λ=8.8 m	Clay 0-8.8 m	No	>179
3	Wide slabs, two-6 m spans; double-column concrete piles, d=70 cm, λ=6m	Silty sand at 0-7 m; mid-sand at 7-9 m; stiff clay at 9-16 m	Yes	>108
4	Wide slabs, three-6 m spans; double-column concrete piles, d=70 cm, λ=14 m	ditto	No	<236
5	Wide slabs, six-6 m spans; double-column concrete piles, d=70 cm, λ=12 m	Clay at 0-5.5 m; silty sand at 5.5-8.5 m; mid-sand under 8.5 m	Yes	>193
6	Half long-lived bridge with five-6 m spans; quadruple-column type of row of piles, d-50 cm, λ=14 m	Silty and at 0-14 m	Yes	>174
7	Wide slabs, two-6 m spans; tricolumn concrete piles; d=70 cm, λ=8 m	Clay at 0-3 m; middle coarse sand under 3 m	Yes	>155
8	Half long-lived bridge with two-6 m spans; quadruple-column concrete piles, d=50 cm, λ=14 m	Clay at 0-3 m; silty sand and fine sand at 3-14 m	Yes	>169
9	Wide slabs, two-6 m spans; double-column concrete piles, d=70 cm, λ=14 m	Clay at 0-14 m, mid-sand at 14-15 m	Yes	>229
10	Wide slabs, seven-6 m spans; quadruple-column concrete piles, section-0.3x0.4 m, λ=10 m	Clay at 0-3.5 m, sandy pebble to 4.5 m; clay to 5.5 m; sandy pebble to 5.8 m; clay to 6.3 m; sandy pebble to 11.1 m	Yes	>177

Note: λ is the embeded depth of piles.

Laboratory model tests

The model tests were performed with three geometric scales, i.e., 1:2; 1:4; and 1:10. Table II indicates the results.

Rating calculations to frost heaving bridge piles

According to static equilibrium, the rating calculations were made to some frost-heaving bridge piles as follows (Table III).

To sum up, an analytical curve of average unit tangential frost-heaving force vs. ratio of subsoil frost heave is constructed (Fig.1).

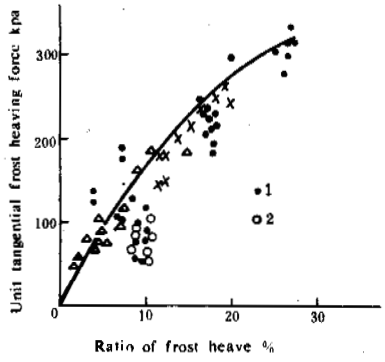

Fig. 1 Unit tangential Frost-heaving Force as a Function of Ratio of Frost Heave

.: Data from Qing-an; O: from Wan-jia; X: from rating calculations; Δ: from Long-feng Experimental site, Daqing (Institute for Heilongjiang Low Temperature Architecture, 1981)

As consistent with Fig.1 and the five-grade classification which we have put forward for seasonal frost soil in highway bridge and culvert, suggested values of tangential frost-heaving force for the reinforced concrete piles are given, as shown in Table IV.

For the purpose of being clear on the effect of pile diameter on the tangential frost heaving force, the field tests were completed under the same freezing condition. However, there are very little influences of pile diameters on unit tangential frost - heaving forces, it can be seen in Table V.

TABLE V

Values of Unit Tangential Frost Heaving Force vs. Pile Diameter

Diameter of testing piles, cm	50	75	100	125
Unit tangential frost heaving force, kpa	66	58	56	58

ACTION OF TANGENTIAL FROST HEAVING FORCE ON PILE FOUNDATION

When frost heave of whole bodies of piles occurs, i.e.,

$$T > P + G + F \qquad (1)$$

Pile's Being Pullen Apart

$$\frac{T - P - G_1 - F_1}{A} > R \qquad (2)$$

Where T is the total tangential frost heaving force, in KN; P is the dead load acting on single pile, in KN; G is its own weight of pile body, in KN; and F is friction resistance of unfrozen soils on piles. G_1 is its own weight of pile body above the separated position, at which a pile is pullen apart, in KN; F_1 is the

TABLE IV

Magnitude of Unit Tangential Frost-heaving Force Proposed

Classification of soils	Non-heaving soil	Weak-heaving soil	Medium-heaving soil	Strong-heaving soil	Severe-heaving soil
Ratio of frost heave (%)	0-1	1-3.5	3.5-6	6-13	13
Unit tangential frost heaving force, kpa	0-15	15-50	50-80	80-160	160-240

Note: 1. For precast bridge pile with smooth surface it needs multiply by 0.8;

2. Values in Table IV are the means under true frost penetration, so emendation must be made while a standard frost depth is provided;

3. Values within a particular range as above can be obtained through interpolation.

friction resistance of the unfrozen soils above the separated position, in KN; A is the sectional area of the separated section, in m^2 (the sectional area of tensile reinforcement when the reinforced concrete is concerned); and R is the ultimate tensile strss of materials, in kpa.

CALCULATION ON ANTI-HEAVING STABILIZATION OF PILE FOUNDATION

Conditions of the anti-heaving stabilization

Based on the analysis of tangential frost-heaving force on pile foundation mentioned above, the two basic conditional equations (3) and (4) must be taken into consideration simultaneously, and only so, the stabilization against frost heave would be assured for the reinforced concrete piles inseasonal frost regions,

$$P + G + F \geq K.T \qquad (3)$$

$$\sigma = \frac{K.T - P - G_1 - F_1}{A} \leq [\sigma] \qquad (4)$$

Where K is the assurance coefficient of structure with the value of 1.2 for statically determinate structures, or 1.3 for statically indeterminate structures; σ is the theoretical stress for a checked section, in kpa; and $[\sigma]$ is the allowable stress of materials, in kpa.

Determination of total tangential frost-heaving force

When the measured frost depth is available, then

$$T = \tau_a \cdot U \cdot H_p + \tau_1 \cdot U \cdot H_{p1} \qquad (5)$$

if not (and with the presumption of no ice formed in river beds during winter), then

$$T = \tau_a \cdot U \cdot Z_o \cdot C_{zo} \qquad (6)$$

Where τ_a is unit tangential frost-heaving force of soils, in kpa; U is the circumferential length of a pile, in m; H_p is the measured frost depth, in m; τ_1 is the unit tangential frost-heaving force of ice, in kpa; H_{p1} is the thickness of ice layer from field measurement, in m; Z_o is the standard frost depth in a certain region, in m, and C_{zo} is a coefficient for emending standard frost depth.

Determination of friction resistance for the frost heaving bridge piles

In order to solve this problem, we have made quite a few experimental studies and analyses as follows:

1. We adopted some intermediate-and small-sized bridges in severe heaving soils, for which we calculated their depths of pile embedment by means of the trial-and-error procedure with different coefficients, then we could find which coefficient is the most conformable to the practice.

2. Chosing the different coefficients for the checking calculations on frost-heaving bridge piles, we are able to find out which coefficient is mostly in accord with the practical situation of frost heave.

From above, a formula is established to determine the frictional resistance of a frost-heaving pile.

$$F = 0.40\Sigma\tau_i L_i \qquad (7)$$

Where τ_i is the ultimate frictional resistance of each soil layer under the freezing front, acting against the sides of piles, in kpa; L_i is the thickness of each layer of soils, in m.

Determination of the dead weight of the pile body

The effects of the dead weight of the pile body have come to an end far before the test on its vertical supportability of a pile is proceeded with. In other words, the T_i value obtained from the tests, i.e., the so-called ultimate frictional resistance of soils around bored pile, provided by "The Standard Specifications of the Foundation of Highway Bridge Operations and designs of People's Republic of China", much obviously, is totally resulted from the external load (or test load), no effects from the dead weight of the pile body involved again. Hence, the entire weight of a pile should be taken into account during the calculation on the frictional resistance against a frost-heaving pile (the floating volumetric weight used for the soil that lies both below the freezing front and the level of under ground water).

EMENDATION OF STANDARD FROST DEPTH OF SOILS

From looking into the large amount of data collected and the test results on frost heave susceptibility for a varity of soils, it is indicated that there is such a fairly close relationship between the frost depth and its own frost heave susceptibility. The frost depth gets smaller with increases of its frost heave susceptibility (see Fig.2)

Based on the aforementioned and the further analyses, we consider it is reasonable and therefore permissible to put forward for the variation of emending coefficients for standard frost depths against frost heave ratio as shown in Fig.3.

Subsequently, according to such a linear enveloping relation, the emending coefficients to standard frost depth can be determinated by the equation,

$$C_{zo} = 1 - Kd \qquad (8)$$

Where Kd is frost heave ratio of subsoil in decimal.

Considering the convenience to practical application of calculation by the equation (8), we sug-

TABLE VI

Magnitude of Emending Coefficients to Standard Frost Depth

Classification of soils	Non-heaving soil	Weak-heaving soil	Medium-heaving soil	Strong-heaving soil	Severe-heaving soil
Emending coefficient	1.0	0.95	0.9	0.85	0.75

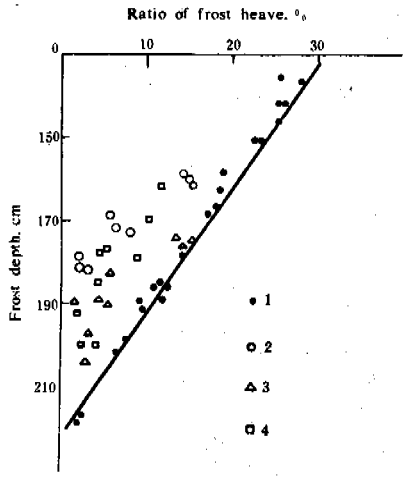

Fig.2 Graph of Frost Depths as a Function of Frost Heave Susceptibility:

· — Clay; o — Fine sand;
Δ — Coarse sandy soil, and
□ — Clay-gravel.

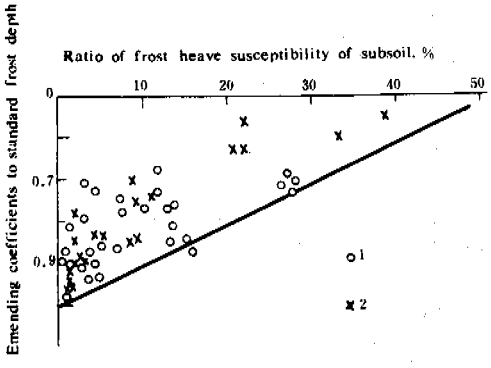

Fig.3 Variation of Emending Coefficients with Frost Heave Susceptibility of Subsoil:

o — Data from Qing-an Experimental Field;
X — From Kaiyuan Experimental Field, belonging to Institution for Lian-ning Provincial Water Conservancy (Wang Xirao, (1980).

gest the specific magnitude of emending coefficients to standard frost depth (Table VI).

CONCLUSION

(i) The unit tangential frost-heaving forces for the reinforced concrete piles, were obtained from the in-situ tests on 28 tested piles with different diameters, experienced for 3-5 years. Moreover, it has already got througn the supplement and proof by the rating calculation to frost heaving bridges. Therefore, the results could be trustworthy.

(ii) Concerning the reinforced concrete bridge piles built in the strong and extra strong frost heaving soils, the tangential frost heaving forces are frequently their control load. So checking calculation on Anti-heaving heaving stability must be given in the process of designing, proceeding by means of the procedure with its formula and parameters set forth in this paper.

(iii) The methods and coefficients for emendation to standard frost depth were also from a large amount of in-situ tests. Hence, it is quite certain for them to be used.

REFERENCES

Institution for Heilongjiang Low Temperature Architecture, etc.: "Deciding on the Magnitude of Tangential Frost Heaving Force in Design, (1981), p.1-5.

Ministry of Communications: "JTJ024-85, Standard Specifications of the Foundation of Highway and Bridge Operations and Designs of the People's Republic of China", the People's Communication Press, (1985), p.63.

Wang Xirao, (1980), Experimental Studies on the Freezing and Frost Heave Susceptibility under Different Underground Water Level and Different Soils, in collection: "Journal of Glaciology and Geocryology", Vol.2, No.3, p.40-45.

PERFORMANCE OF TWO EARTHFILL DAMS AT LUPIN, N.W.T.

S. Dufour[1] and I. Holubec[2]

[1]Geocon Inc. (Lavalin Inc.), Yellowknife, Northwest Territories, Canada (now with International Development Research Centre, Ottawa, Ontario, Canada)
[2]Geocon Inc., (Lavalin Inc.), Regina, Saskatchewan, Canada

SYNOPSIS Several earthfill dams were constructed to enclose a watershed and form a mine tailings pond in a cold permafrost area with relatively poor subsurface conditions. Foundation materials included frozen sands and fractured bedrock which would be difficult to seal should they thaw. The only construction material available locally was a pervious sand. A frozen core dam with liner was designed to maintain the foundation sands and fractured bedrock frozen, and hence watertight. The frozen core and foundation ensure that contaminants do not escape from the pond and that seepage pressures do not cause internal instability of the structure. While predictions of the ground thermal regime evolution showed that frozen conditions would be maintained, very little published data was found to document the behaviour of frozen dams over cold permafrost.

An extensive monitoring programme was initiated shortly after the construction of the earth dams to document the evolution of the thermal regime within the earthfill structures.

This paper discusses the results of four years of monitoring the thermal regime in the embankment and its foundations at two dam sections, each on different thermal conditions. The first section corresponds to the location of a 5 m deep talik while the second section is located over virgin cold permafrost.

INTRODUCTION

The Lupin Gold Mine is located on the west shore of Contwoyto Lake, Northwest Territories, at about 65° 47' North, 111° 12' West, or approximately 380 km northeast of Yellowknife and 1300 km north of Edmonton (see Figure 1). The mine site is about 150 km north of the treeline in an area characterized by low relief, a poorly developed drainage pattern, numerous shallow lakes and cold permafrost.

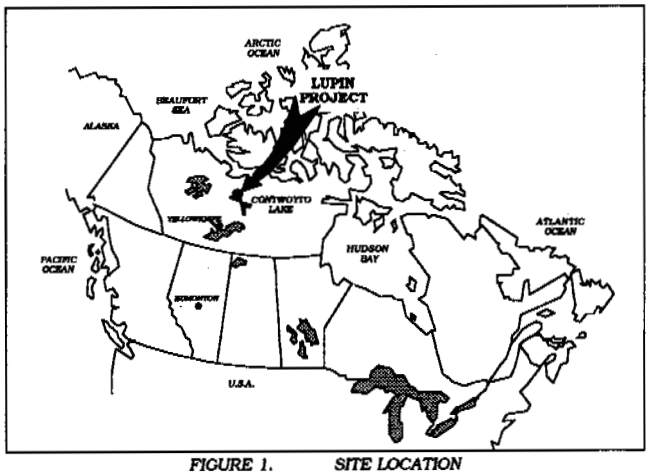

FIGURE 1. SITE LOCATION

Several mill tailings and effluent retention dams were built during the 1981 summer season. The mill complex was completed for the first gold bullion to be cast in May 1982 and impoundment started at that time.

This paper discusses the thermal changes in two of the dams and their performance in general from construction in 1981 to the Fall of 1987. The continuous thermal monitoring was possible because of the owner's interest in detailed monitoring of the dams and the assistance of the Government of Canada.

BACKGROUND INFORMATION

Geology and Geomorphology

The Contwoyto Lake area lies within the Upland unit of the Kazan physiographic region of the Canadian Shield. The area was glaciated during the Pleistocene Epoch and evidence of two ice movement periods are reported (Blake, 1963 and Tremblay, 1976). The thin overburden is predominantly a silty sand till occasionally overlain by glaciofluvial and glaciolacustrine sand and gravel deposits. Eskers and abandoned beaches are common landforms but relatively impervious clays and silts do not occur near the Lupin Mine. Bedrock belongs to the Yellowknife Supergroup of the Archean Epoch. The rock consists of a mixture of low grade metamorphosed argillite, siltstone,

slate, greywacke and quartzite, generally phyllite (Tremblay, 1976).

Relief at the site is generally low. Elevations in the project area range between 470 and 505 m above mean sea level. The rolling ground surface is marked by numerous rock outcrops and block fields.

The area has numerous shallow lakes and marshy depressions. The drainage pattern is disorganized and poorly defined but ultimately, streams lead to Contwoyto Lake.

Climate

The mean annual air temperature at Contwoyto Lake is -12.1°C. Monthly mean daily temperatures are shown on Figure 2. Freezing temperatures may occur during any month of the year. On average, there are 280 days with frost (daily minimum temperature 0°C or lower). The average freezing and thawing indices are estimated as 5100 and 685°C-days, respectively. About the end of September, snow falls and ice forms on lakes. Normally, snow melts by the end of June except where it drifts, and ice break-up on Contwoyto Lake does not occur before the second week of July.

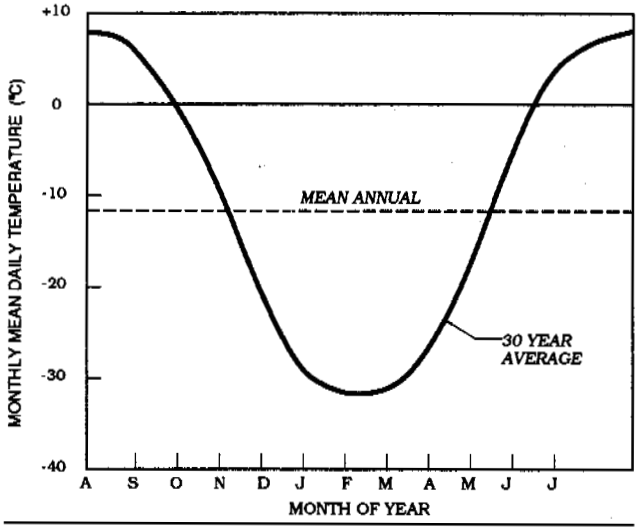

FIGURE 2. MONTHLY MEAN DAILY TEMPERATURES, CONTWOYTO LAKE, NWT

The freezing and thawing indices have averaged 5094 and 821°C-days respectively during the period 1982 to 1987. Indices for each season are:

Year Aug 1-Jul 31	Freeze °C-days	Thaw °C-days
81-82	4979	-
82-83	5707	767
83-84	4604	1049
84-85	5293	800
85-86	5190	702
86-87	4788	788

The mean yearly total precipitation is 275 mm half of which falls as snow (Environment Canada, 1975). The summer months (mid-June to August) have the greatest precipitation with most rainfall in the form of a faint annoying mist (Tremblay, 1976).

DESIGN

Site Selection

The toxicity of the tailings effluent and the fragile northern environment necessitated careful selection of the tailings disposal site. The tailings pond was to be designed for total impoundment of tailings, mill effluent and precipitations (rain, runoff and snow meltwater) during the first years of its life until treatment requirements would be established.

The most suitable site for a tailings pond was found about 4.5 km from the plant. The 614 ha watershed was formed by damming the intermittent outlet of the basin at Dam 1A and five saddles which connected at various elevations with adjoining watersheds (see Figure 3).

The tailings slurry is conveyed from the plant by heat traced pipeline. The slurry is discharged in the northeast sector of the tailings area and solids are not expected to accumulate against the dams in the northwest and west sectors. Hence, good quality water retaining dams are required. It should be noted that Internal Dam J, shown on Figure 3, was built in 1985 as a new water management plan was implemented.

Dam Section

The stratigraphy along the dam alignments basically consists of a thin organic layer, up to 45 cm thick, underlain by sandy till and bedrock. A typical log is shown on Figure 4. The till ranges in thickness from zero at rock outcrops to an estimated 7 m at valley bottoms. The till is a silty sand with gravel and contains occasional cobbles and boulders.

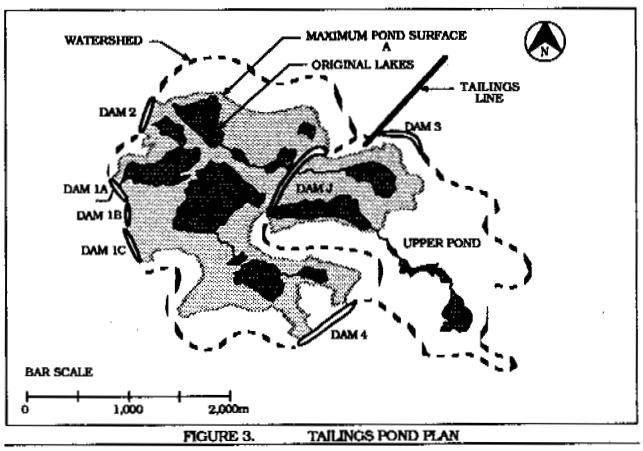

FIGURE 3. TAILINGS POND PLAN

The covered bedrock is generally competent phyllite with a frost-weathered (fractured) zone extending 1.5 to 3 m deep.

The silty sand dam foundation and the thin overburden cover on fractured bedrock could pose substantial seepage and stability problems for a water-retaining dam on an unfrozen foundation. In view of the cold permafrost regime, it was deemed that seepage could be mitigated with a frozen dam core and foundation. The thermal aspects are discussed in the next subsection.

Because of the short construction season and to spread capital outlay, stage building of the dams was to be implemented. In 1981, the stage I dams were built to elevation 485 m from selected and compacted thawed silty sand overburden with an impermeable liner on the upstream side (Figure 5). The valley floor was at approximately el. 478 and 480 m at Dams 1A and 2 respectively. The liner was provided to stop seepage through the dams during the first few years until the foundation permafrost aggraded into the dam core. The second dam stage, to elevation 486.5 m, was built in August 1984 with random borrow end-dumped from the crest on the downstream side. The two largest dams, 1A and 2, are about 8.5 and 6.5 m high respectively at the present. It is now planned to maintain this configuration for the remainder of the projected mine life. Details of the construction are described by Dufour et al. (1988).

Thermal Aspects

The soil and rock are permanently frozen. The thickness of the active layer varies from 0.60 m in thickly vegetated areas to about 2.5 m in barren areas. Few ice lenses were found in the frozen ground foundation material. The largest ice layer observed was 80 mm thick; others were smaller than 25 mm. The measured undisturbed mean annual ground temperature is about -9°C. At the time of construction, thaw beneath the intermittent creek at Dam 1A is believed to have reached through the overburden and fractured bedrock, to sound rock at a depth of 4 to 5 m. The initial ground temperatures of the talik were not measured. It is also estimated that in thermally undisturbed areas at all dams, perhaps 2 m of the foundation sand had thawed by the end of construction which included organics stripping.

Case histories of low head water retaining structures on permafrost are scarce in the literature (Johnston, 1969; Fulwilder, 1973; Roy et al., 1973; Biyanov, 1975). The only relevant case history is from the Crescent Lake Dam near Thule, Greenland (Fulwilder, 1973) which shows a similar dam under similar climatic conditions froze completely in two winters.

The scarcity of applicable case histories and the importance of developing and maintaining a frozen core led to the implementation of a ground temperature monitoring programme.

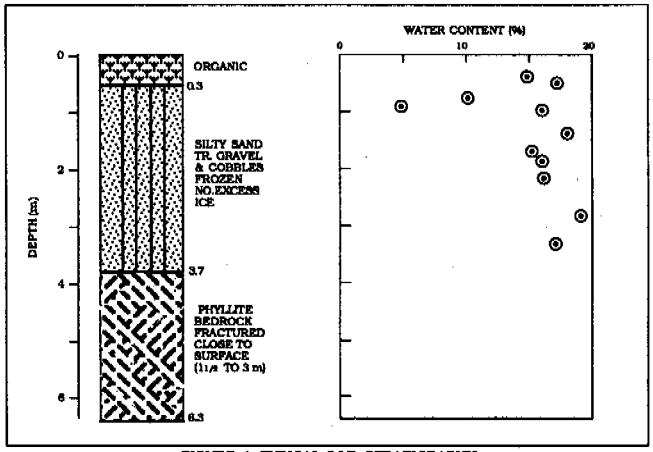

FIGURE 4. TYPICAL SOIL STRATIGRAPHY

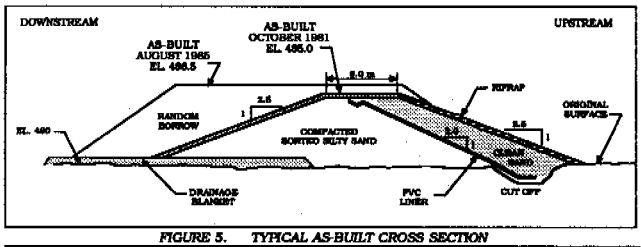

FIGURE 5. TYPICAL AS-BUILT CROSS SECTION

PERFORMANCE

General

Mill tailings and effluent production began in May 1982. The water level fluctuations in the lower tailings pond for the period May 1, 1982 to December 1987 are shown on Figure 6. The peak in 1983 corresponds to spring runoff followed by summer evaporation. During the summers of 1985 and 1986, water was siphoned from the pond over Dam 1A to be discharged in the environment. The water quality was at acceptable standards for discharge to take place and thus avoid raising the dams which were at minimum freeboard.

Several sets of thermistor strings were installed in May 1982, April 1983, October 1983, April 1985 and August 1987 as described in Dufour et al. (1988). Current thermistors are installed to depths varying between 15 m and 25 m at the two sections discussed below.

Locations of the thermistor strings are shown on Figures 3, 7 and 8. Two sections of interest were instrumented: Dam 2 which was built on virgin permafrost and the part of Dam 1A which was built over the basin outlet. In July 1982, the creek section of Dam 1A became important when seepage took place through the talik, located beneath the creek, and appeared on the downstream toe of the dam. Immediately, two long thick silty sand aprons were placed on the upstream and downstream sides of the dam to lengthen the seepage path. It is believed, based upon piezometric observations during drilling, that most of the seepage took place through the upper 2 m of bedrock which

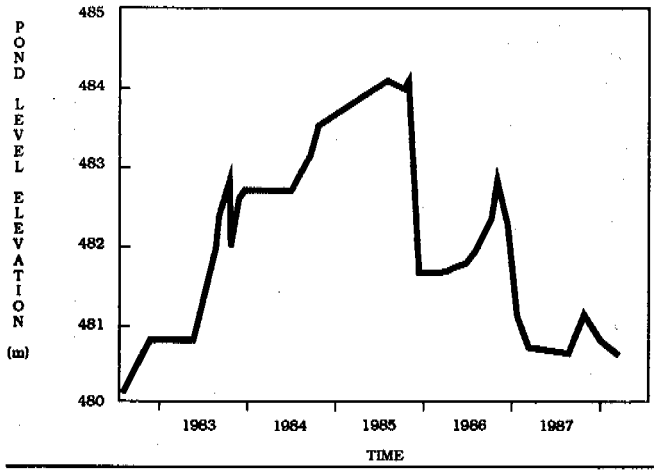

FIGURE 6. TAILINGS POND WATER LEVEL

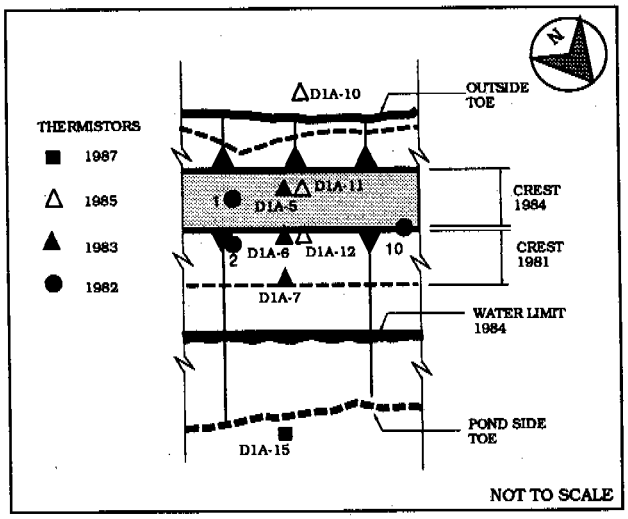

FIGURE 7. THERMISTOR STRING LOCATIONS - DAM 1A

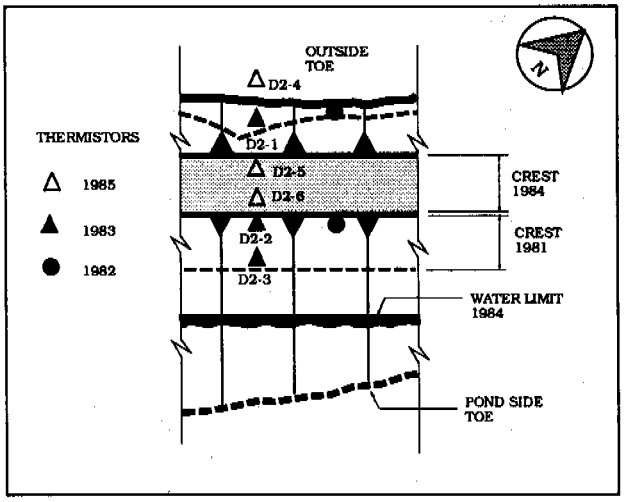

FIGURE 8. THERMISTOR STRING LOCATIONS - DAM 2

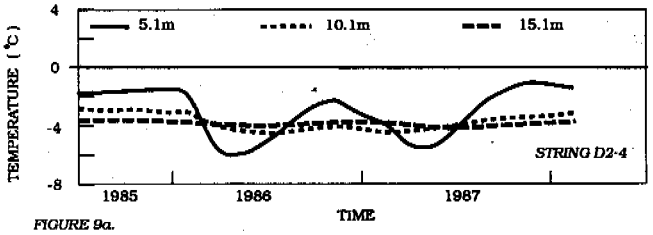

FIGURE 9a.

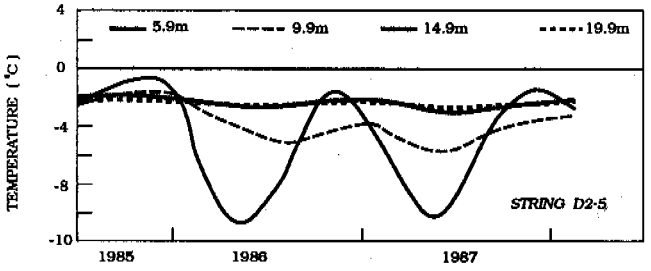

FIGURE 9b.

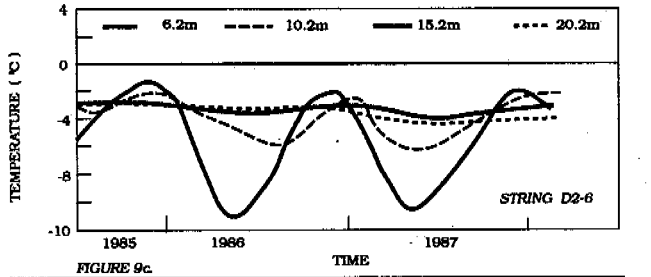

FIGURE 9c.

FIGURE 9 = TEMPERATURE VS TIME, DAM 2

is highly fractured. It should be noted that both the upstream and downstream toes of Dam 1A were kept clear of snow (which normally drifts to about 2 m deep) through the winters of 1983-84 and 1984-85.

GROUND TEMPERATURE OBSERVATIONS

Dam 2

The fill and the thawed top part of the foundation soils froze completely during the first winter. At mid-summer 1982, thermistors showed a dam core temperature of -1°C at elevation 482.5 m. By the summer of 1987 the temperature at the same location was down to -3°C, see Figure 10.

The evolution of the ground temperatures is shown on Figures 9a to 9c. The deep sensors beneath the core (strings D2-5 and D2-6) show a cooling trend since construction, see figures 9b and 9c. Both the cold permafrost regime and the level of water impoundment affect the ultimate steady-state ground temperature. The three components of Figure 9 also show that seasonal variations are felt to a depth of about 18 m. This is significant in that dam fill temperatures (0 to 6 m deep) vary too much for making reliable year to year

comparisons with only a few years data. The entire thermal regime must be considered.

The 1986 pond drawdown and consequent withdrawal of the pond away from the crest appears to have caused a 0.4°C temperature drop at 20 m beneath the dam crest (elevation 466 m), see Figure 9c.

Figure 10 illustrates the isotherms during August 1987. The critical part of the foundation beneath the core, the silty sand and fractured rock, is colder than -5°C and the dam core itself is clearly subject to great annual temperature variations. A natural lake some 100 m downstream of the dam probably influences the position of the -4°C isotherm.

A series of ground probing radar surveys calibrated on the thermistor strings indicated that all of Dam 2 and its foundation are well frozen (Laflèche et al., 1988).

Dam 1A - Creek Section

Figures 11a to 11d show the evolution of the ground temperatures at the section of Dam 1A located over the former talik. It is also useful to relate the underground patterns surveyed by ground probing radar to the thermistor results to understand the complex thermal regime (see radar survey results this conference in Laflèche et al., 1988).

Based on preliminary thermistor readings and seepage observations during the summer of 1982, it is believed that the dam fill froze during the first winter (1982-83) but not the foundation talik. Ground temperature readings taken in 1983 show that the foundation was just below 0°C at the top and just above 0°C at bedrock (not illustrated herein).

All curves on Figure 11 show a cooling trend, hence gradual freeze-back of the talik (8.5 to 12.5 m deep at D1A-11 and -12; to about 6.5 m deep at D1A-10). An exception is the 3.9 m deep sensor at D1A-10, the downstream toe, where a talik remnant remains. Heat flow trends indicate this remnant will eventually disappear. There is a marked decrease in ground temperature after the pond water was drawn down in 1985. At thermistor D1A-12, 18 m beneath the crest, the ground temperature decreased from -1.5 to -2.2°C (Figure 11d). It is interesting to note that the foundation beneath the dam crest did not have a large seasonal fluctuation until 1985 (pre-1985 data not reported herein). This is attributed to the unfrozen soil and bedrock reducing the depth of seasonal temperature variations and thus having a warming influence on the overlying soil. The depth of zero seasonal variations is about 18 m.

The talik at the instrumented section froze back during the winter of 1984-85, four years after construction. There is little doubt that snow clearing at the dam toes played a large role in the rapid freeze-back of the talik. The lowering of the pond instead of

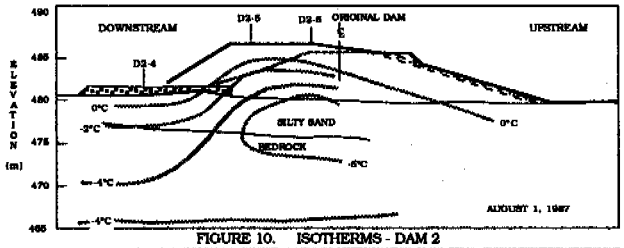

FIGURE 10. ISOTHERMS - DAM 2

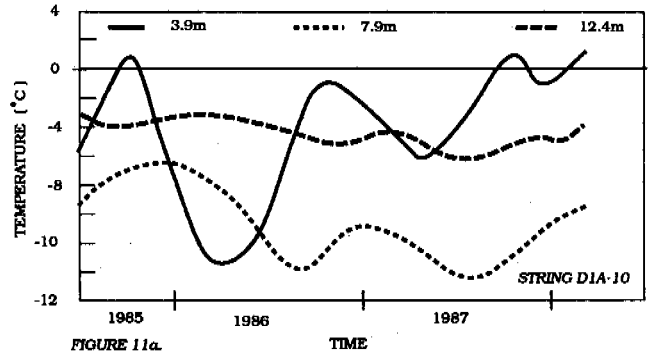

FIGURE 11a.

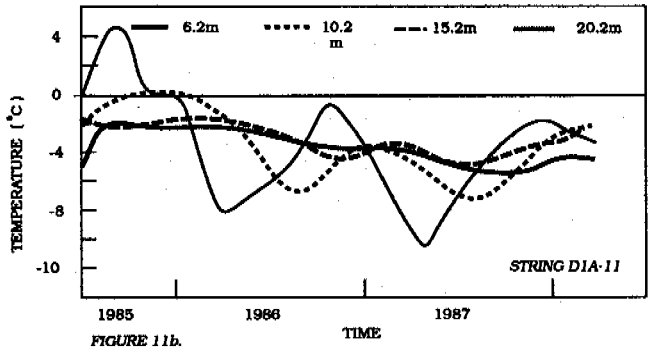

FIGURE 11b.

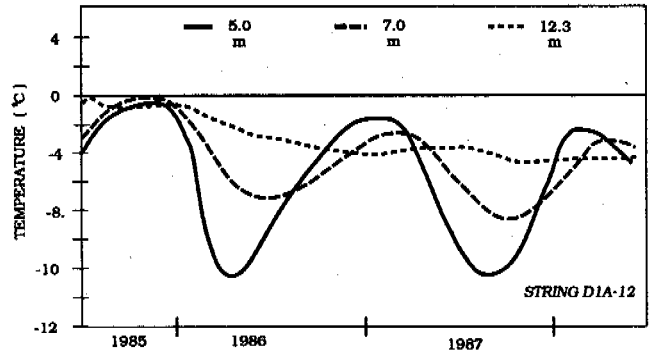

FIGURE 11c.

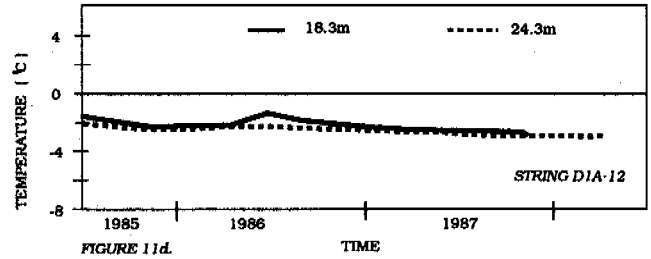

FIGURE 11d.

FIGURE 11. TEMPERATURE VS TIME, DAM 1A

the raising of the dams was also timely and beneficial for freeze-back of the talik.

The isotherms shown on Figure 12 illustrate the thermal regime as of September 1987. The dam fill is comfortably below 0°C although within the depth of large seasonal variations. A bulb colder than -5°C extends from the downstream area into the central dam foundation where the talik used to be. Readings discussed above show this bulb is still expanding (cooling). The -3°C isotherm does not go far beneath the upstream shell which was influenced by the former talik and the relatively warm pond water. The new thermistor string (D1A-15), added to the section in August 1987, shows the 0°C isotherm is about 4 m deep and the -1°C isotherm some 10 m deep. The data suggests the freezing point in the pond might be depressed at least to -0.3°C.

CONCLUSIONS

The results of the ground temperature monitoring at the Lupin tailings dams show the feasibility of the frozen core concept for watertightness in a cold permafrost regime. By utilizing a frozen core, the construction can be inexpensively carried out using local earth materials which would be permeable in the unfrozen state. The fill itself froze permanently in the first year even where a talik was present. The talik froze back in the fourth winter after construction with the help of snow clearing. The unscheduled drawdown of the pond the summer following the winter during which the talik froze back has also had a positive effect upon cooling of the dam foundation.

At Lupin the pond water level has changed drastically in the first five years operations. When at minimum freeboard, the water was higher than the bottom of the active layer and the PVC liner helped to stop seepage. In the design of an unlined frozen core dam, great care must be taken to ensure that the impounded water level will not be higher than the active layer on the dam crest or its abutments. In addition it should be noted that even intermittent creeks can have significant taliks beneath them. Taliks are preferred seepage paths and, under certain circumstances, could cause serious instabilty when not recognized and dealt with.

The evaluation of the thermal regime at any section requires deep thermistors and several years of data because of the large depth of seasonal variations. It was shown that although frozen fill conditions were achieved early and although shallow depth temperatures appear to be similar from year to year, a stable thermal regime was not reached six years after construction. The many factors influencing the dams' thermal regime include: climate, snow cover and pond level. The snow was cleared during two winters to successfully assist freeze-back of the talik at Dam 1A. It is not believed snow removal will be required again. The timely drawdown of the pond (carried out instead of dam raising) has allowed the dam and its foundation to cool further.

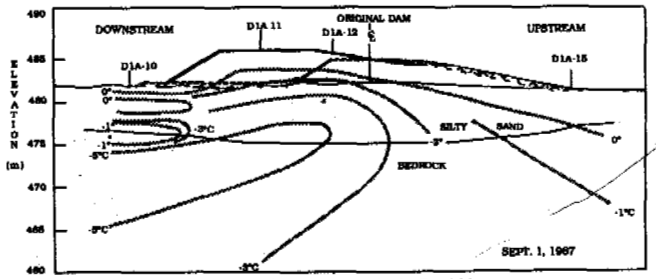

FIGURE 12. ISOTHERMS - DAM 1A

ACKNOWLEDGEMENT

The authors wish to gratefully acknowledge the cooperation and assistance of all Echo Bay Mines Ltd. environmental and corporate staff. This research was supported in part by contracts from the National Research Council of Canada and Energy, Mines and Resources Canada. Dr. Alan Judge of the Geological Survey of Canada is to be thanked for his support of the work.

REFERENCES

Biyanov, GF (1975). Dams on permafrost. 234pp. U.S. Army, CRREL, Draft Transl. TL 555.

Blake, WJr. (1963). Notes on glacial geology, northeastern District of Mackenzie. 12pp. Geol. Sur. of Canada, Paper 63-28.

Dufour, S, Judge, AS, Laflèche, P (1988). Design and Monitoring of Earth Embankments over Permafrost. Proc. 2nd Int. Conf. on Case Hist. in Geotech. Eng., St-Louis, Miss., U.S.A.

Environment Canada, Atmospheric Environment (1975). Canadian Normals, Temperature, 1941-1970. Volume 1-SI, 198pp. No. U.S.C. 551-582 (71), Downsview, Ontario.

Fulwilder, CW (1973). Thermal regime in an Arctic earthfill dam. Proc. 2nd Int. Conf. on Perm., Yakutsk, U.S.S.R., North Am. Contribution, U.S. National Academy of Sciences, 622-628.

Johnston, GH (1969). Dykes on permafrost, Kelsey Generating Station, Manitoba. Can. Geot. Jour. (6), 2, 129-157.

Laflèche, PT, Judge, AS, Pilon, JA (1988). The the use of ground probing radar in the design and monitoring of water retaining embankments in permafrost. This Proc. V Int. Conf. on Perm., Trondheim, Norway.

Roy, M, Larochelle, P, Anctil, C (1973). Stability of dyke embankments at mining sites in the Yellowknife area. 78 pp. Dept. of Indian and Northern Affairs, Ottawa, Ontario, Canada. ALUR Rpt. 72-73-31.

Tremblay, LP (1976). Geology of northern Contwoyto Lake Area, District of Mackenzie. 56pp. EMR Canada, Geol. Sur. of Canada, Memoir 381.

ROADWAY EMBANKMENTS ON WARM PERMAFROST PROBLEMS AND REMEDIAL TREATMENTS

D. Esch

Alaska Department of Transportation – Research Section, Fairbanks, Alaska, USA

SYNOPSIS Monitoring studies on eight experimental road embankment sections constructed on warm (0° to -1° C) permafrost in the interior of Alaska, have provided a basis for design-life performance predictions. Experimental features evaluated have included insulation and peat layers, toe berms, air convection cooling ducts, thermosyphons, solar screens, and geofabric reinforcement. Thermal adjustments and surface movements of these embankments have continued to occur over the full design life. It has been concluded that the majority of long-term embankment problems occur as a result of excessive net warming of the side-slopes. The greatest reductions in thawing and movements came from solar screens and snow control sheds on the side-slopes.

INTRODUCTION

Road embankment performance studies on "warm" permafrost, defined as having an average temperature above -1° C were initiated near Glennallen, Alaska in 1954 when five highway cross-sections were instrumented to record surface and subsurface temperatures. Paving was first placed on the roadway at these sites in 1957 and observations continued until 1960 (Greene et al., 1960) The study at Richardson Highway Mile 130 demonstrated that in spite of the dark asphalt surface and the fact that average annual air temperatures were as high as -3° C, full annual refreezing was occurring beneath the paved roadway surfaces, and average roadway surface temperatures were similar to those at undisturbed permafrost sites. The primary thermal effect of the roadway surface was that of greatly increasing the seasonal variations in surface temperatures, which resulted in a much thicker active layer beneath the road. The active layer thickness at the study sites averaged 2.0 m beneath the gravel roadway surface and 3.1 m after the pavement was placed in 1957.

The first North American installation of subgrade insulation over warm permafrost, using extruded polystyrene foam, was constructed near Chitina, Alaska in 1969 (Esch, 1973). Temperature, settlement, and thaw depth monitoring work has continued at the Chitina site through 1987. The data have demonstrated that warming of the roadway slopes, caused by the combined effects of summertime heating of the exposed gravel, and the wintertime insulating snow cover, is the primary problem with both insulated and uninsulated embankments on warm permafrost. These observations have since been confirmed at four other Interior Alaska sites, where additional records of roadway and slope surface temperatures have been made (Esch, 1983).

In summary, the roadway side-slope surfaces have been found to generally become much warmer than either the travelled roadway surface or the adjacent undisturbed ground surfaces. In all cases studied in warm permafrost areas, the slope surfaces have averaged significantly warmer than 0° C and have warmed to average up to +5° C. As a result, progressively deeper annual thawing of the permafrost occurs and taliks develop beneath slope and ditch areas, causing slope area settlements and ultimately resulting in a loss of lateral and vertical support for the roadway itself (Esch, 1983; McHattie, 1983).

Surface and Air Temperature Observations

Highway pavement and side-slope mean annual surface temperatures, and freezing and thawing season n-factors measured at Interior Alaska sites on warm permafrost are summarized by Tables 1 and 2. As can be seen from these summaries, the average annual pavement surface temperatures have ranged from 3.1° to 4.4° C above the average air temperatures, while the embankment slope temperatures have averaged from 4.0° to 7.7° C warmer than the air. Annual air temperatures for most of the paved highway system in the Interior of Alaska are represented by two long-term recording sites located at the University of Alaska near Fairbanks and at Big Delta, located about 150 km east of Fairbanks. Data for these sites from 1931 through 1986 are shown by Figure 1, which indicates several multi-year periods of warmer than normal average air temperatures. Since pavement temperatures exceed average air temperatures by 3 to 4° C, there is the

TABLE 1 - Road Surface and Slope Surface Annual Temperature Averages for sites in Interior Alaska.

		Annual Average Temperatures (C°)		
Site	Period	Air	Roadway	Slope
Chitina	1971-72	-4.5°	-1.4°	-0.6°
Canyon Creek	1975-77	-4.6°	-1.1°	+2.9°
Bonanza Creek	1975-79	-2.7°	+0.5°	---
South Slope	"	"	---	+5.0°
North Slope	"	"	---	+1.9°
Peger Road	1982-83	-3.3°	+1.1°	---

TABLE 2 - Side-Slope n-Factors for Alaskan Sites.

Site	Period	Slope & Height	Slope-Face Bearing	n-Freeze	n-Thaw
Chitina N	1971-72	3:1 2.1 m	S 30° W	0.70	1.38
Canyon Ck	1974-77	3:1 1.4 m	S 45° W	0.39	1.37
Bonanza Ck South Slope	1975-79	2:1 7.0 m	S 10° E	0.45	1.72
Bonanza Ck North Slope	1975-79	2:1 7.0 m	N 10° W	0.40	1.02

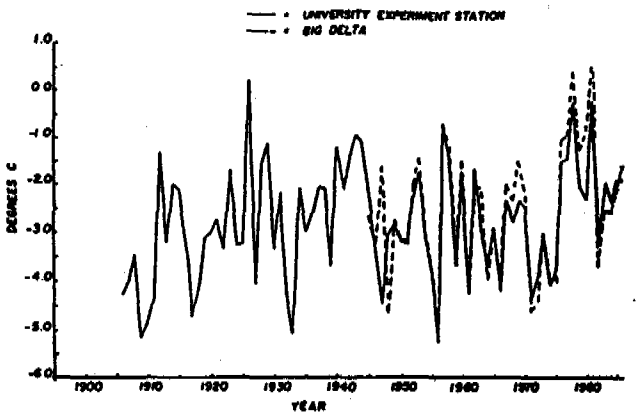

FIGURE 1. Interior Alaska mean annual air temperatures at Fairbanks (UES) and Big Delta (After Juday, 1983).

potential for average annual pavement temperatures to rise above 0° C. This would be expected to result in progressively deeper thawing and talik development beneath the pavement. Due to the elevated temperatures typical of roadway slopes, there is almost a certainty that average slope temperatures will rise well above 0° C and that destructive annually deepening thawing will always occur beneath the embankment slopes on warm permafrost.

Current forecasts of global warming trends expected as a result of the increasing atmospheric concentration of carbon-dioxide and methane also should be considered in the thermal design of embankments. Kellogg (1983) has summarized possible future global and arctic mean surface temperatures, as shown by Figure 2. These forecasts indicate a warming trend expected for the Arctic of roughly 1° C every 10 years. As most of Alaska falls into the sub-arctic climate zone, a rise of 1° C every 10 to 20 years appears possible and embankments which are presently thermally stable may not always remain so.

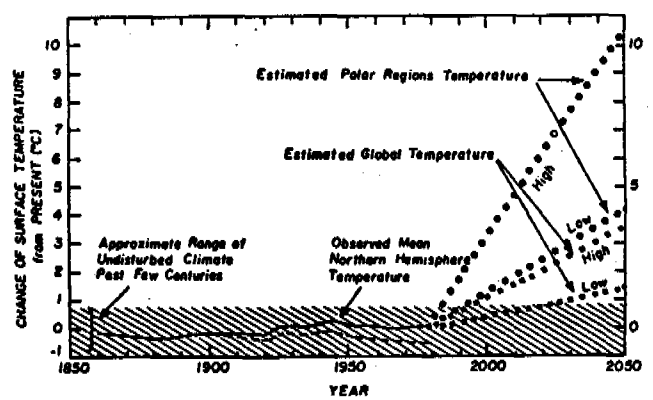

FIGURE 2. Past and future changes of global and Arctic mean surface temperatures (After Kellogg, 1983).

EMBANKMENT PROBLEMS

As inferred by the previous discussions of air, roadway surface, and side-slope temperature trends, various problems must be anticipated in the design of embankments over thaw-unstable permafrost soils. The term "thaw-unstable" soils refers to permafrost soils with higher moisture contents in the frozen state than the soil can retain after thawing. Such soils will drain, consolidate, and compress after thawing. Thaw-stable (low moisture content) permafrost soils, by contrast, will compress and yield elastically after thawing, but do not generally present significant embankment stability problems. Gravels, sands and inorganic loessial silts are frequently found in a thaw-stable state, in Interior Alaska. Unfortunately, thaw-unstable permafrost conditions occur more often than not, and some embankment instability must nearly always be anticipated.

Embankments on permafrost typically require corrective maintenance either because of excessive settlements of the top surface or because settlement movements of the side slopes result in lateral spreading and cracking of the embankment (Fig. 3).

Five different thermal problems which can lead to embankment distress and failure should be considered in embankment design work, as discussed in the following sections:

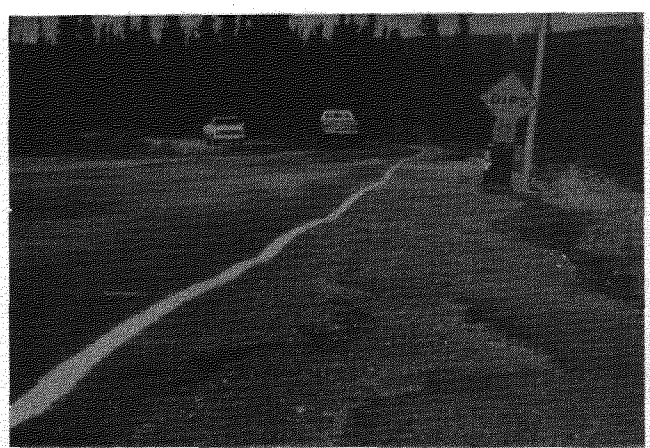

FIGURE 3. Embankment failure from settlements, lateral spreading and cracking from thaw beneath slopes and shoulders.

Massive Subsurface Ice

The worst situation for thaw-instability of embankments results from the occurrence of massive near-surface ice deposits, since thawing of ice results in a total lack of support. Annual thaw-settlements must then be anticipated until either additional thermal resistance is added to the embankment or the ice has entirely melted away. A second problem of embankments overlying ice is that the creep rate of ice under shear stress is much higher than that for frozen soil, and creep movements may lead to excessive settlements even if there is no thawing of the ice.

Inadequate Thermal Resistance

Surface settlements from permafrost thaw and consolidation beneath a roadway can result from three different problems. The first and most obvious is that of inadequate thermal resistance to protect the underlying permafrost from the maximum annual thaw zone. The prediction of thaw depths beneath paved surfaces can be done easily with acceptable accuracy by using the modified Berggren calculation method, (Braley, 1984) as well as by more elaborate methods. However, for the discontinuous permafrost areas of Alaska, where seasonal thawing indices are as high as 2000° C days, seasonal thaw depths exceeding 6 meters must be anticipated when embankment materials are gravels with relatively low moisture contents. For more typical embankments con-

structed with silty gravels over organic silt foundation soils, annual thaw depths fall within the range of 2.5 to 4.5 m. By using polystyrene foam insulation, the annual thaw depth can be reduced to less than 2 m (Esch, 1973; 1983).

Heat Gains from Flowing Water

Water flowing through the active layer beneath the embankment can cause thawing in excess of that expected from heat conduction from the road surface. In practice, it is very difficult to design for the heat input of flowing water beneath an embankment. The designer would need to know the temperature, time, history, source, flowrate, and flow direction of each water source, as well as the permeability of the embankment and foundation soils. Roadways are usually designed to avoid ponding and longitudinal flows by providing drainage culverts through the embankment at appropriate locations. Beyond these water control efforts, embankment designers typically ignore the potential for heat gain from flowing water. Observations indicate to the author that concerns over thawing from temporarily ponded or flowing water have been overstated in the past, and that this is generally a minor factor in poor embankment performance.

Net Surface Warming

In general, subsurface temperatures tend to average nearly the same as the overlying road surface whenever the active layer soil conductivities are reasonably similar in the frozen and thawed states. Therefore, whenever surface temperatures average significantly higher than 0° C the annual thaw depth will exceed the annual depth of refreezing. Residual thaw zones or "taliks" will then develop beneath the roadway. After this process starts, additional heat enters the ground each year and causes additional thawing of the permafrost, and an unending annual cycle of thawing and roadway settling begins to occur.

As stated previously, paved road surface temperatures in Interior Alaska have averaged approximately 4° C warmer than the mean annual air temperature. Mean annual air temperatures in this region typically range from -1° to -5° C, resulting in pavement surfaces which average very close to, or slightly above 0° C. A series of unusually warm years such as occurred between 1976 and 1981 (Fig. 2) would therefore be expected to result in talik development and progressive settlement of many of the roadway sections constructed over permafrost. Observations of instrumented roadway sections during this period have shown net warming and talik development at some sites and not at others. If the climate of the Arctic warms by several degrees as predicted over the next half century, then progressive talik development and roadway settlement distress must be anticipated throughout the Interior Alaska. Some minor changes in average surface temperature can be achieved by using light-colored aggregates or white painted surfaces, but generally the designer must design for the surface albedo of the available paving aggregates.

Side-Slope Warming

The final problem to confront the designer is that of excessive warming of the embankment side-slopes. The consequences of removing the natural surface vegetation mat and thereby causing accelerated thawing of the underlying permafrost have been widely reported. The placement of a thin gravel embankment on top of the organic mat will result in the same effect by compression, thereby altering the summertime thermal balance, reducing evapo-transpiration cooling, and accelerating permafrost thaw. The embankment must taper to zero thickness at the toe of the slope and the sloped surfaces also typically result in increased solar heat gain on at least one side of the fill. The embankment slopes also have a thickened snow cover due to drifting and to plowing from the road surface. All of these factors combine to cause the slopes to become much warmer than a road surface which is maintained free of snow in winter. The typical embankment slope is inclined toward net warming and progressive thawing even if north-facing. All embankment slopes monitored in warm permafrost regions have demonstrated mean surface temperatures significantly warmer than 0° C, and have resulted in annually deepening thaw zones and talik development. The results of thawing beneath the slopes are downward and outward slope movements and ultimately the lateral spreading and cracking failure of the roadway surface (Fig. 3). However, in spite of the almost universal thaw-progression and talik development beneath the roadway slopes, roadway surface failure by spreading and longitudinal cracking is a maintenance problem on less than 20% of roadways on warm permafrost. The most thaw-unstable permafrost soils appear to result in the most severe spreading failures, but the critical soil conditions have not yet been defined.

REMEDIAL TREATMENTS

When faced with the multitude of potential embankment problems and failure mechanisms in warm discontinuous permafrost areas, the designer has several options. The first (and most frequently used) is simply to admit that excessive embankment movements and distress are going to occur, and build a structurally adequate but thermally inadequate embankment; requiring the maintenance engineer to repair the distress as it occurs. Structural adequacy for carrying maximum truck loadings will require no more than 1 m of fill thickness. By frequent maintenance patching and leveling, passable paved roadways can be achieved under the worst permafrost conditions. The most cost-effective approach for thermally inadequate road embankments may be to maintain a gravel-surfaced roadway for a number of years following construction. The routine regrading required to remove potholes and corrugations also serves to level sags and to fill cracks as they occur. Gravel surfaces also typically result in slightly decreased annual thaw depths as compared to paved surfaces, reducing the magnitude of annual settlements. However, the maintenance costs required for higher traffic levels and speeds frequently mandate an asphalt paved surface and require the design engineer to consider a number of alternatives for minimizing roadway distress from thaw-unstable permafrost foundations. Ten different remedial treatments which have been used and evaluated by the Alaska Department of Transportation are discussed below:

Subgrade Insulation

In 1969, the first expanded polystyrene plastic foam insulated roadway over permafrost in North America was constructed at a site near Chitina, Alaska (Esch, 1973). The first insulated airfield was also constructed in 1969 at Kotzebue, Alaska. Since that time six additional highways, totaling 2.94 km, and four airfield runway sections have been similarly insulated. These sections have generally performed quite well, with full annual refreezing beneath the paved surfaces even though the underlying permafrost temperatures are as high as -0.3° C (Esch, 1986). However, insulation has not controlled progressive permafrost thawing beneath the side-slopes at any site, and some lateral spreading and cracking has occurred in the shoulder areas at some of these sites.

Peat Underlays

In 1973, a 90 m length of roadway, located in a permafrost cut section southeast of Fairbanks on the Richardson Highway, was constructed using a 1.2 to 1.5 m thick layer of peat as a thermal underlayer (McHattie, 1983). Peat is of particular value as a thermal protection layer over permafrost because its frozen conductivity may be twice its thawed conductivity. As a result, peat acts to increase heat flow out of the ground during freezing and to reduce heat flow into the ground during the thawing season. The net results of peat's conductivity change and its high latent heat are to reduce the thaw depth and to cause the mean annual temperature of the underlying permafrost to be significantly lower than that of the overlying road surface.

At the study site the peat showed a significant benefit in causing net long-term heat removal, and in preventing talik development beneath the roadway. A similar adjacent roadway section constructed without peat resulted in net warming and talik development (Fig. 4), accompanied by progressive settlement of the road surface. Beneath the side-slope and ditch areas, however, the peat underlayer was of no significant thermal benefit, and talik development has been progressive and rapid (Fig. 4). Site data indicate that temperatures at the underlying permafrost surface have been lowered by approximately 0.5° C by the peat placement.

This study has served to demonstrate the thermal advantages of both artificially placed and naturally occurring peat layers beneath embankments. The benefits of the peat are maximized when it is located high in the active layer and as near to the surface as practical. However, roadway strength considerations generally require that peat layers be covered by at least one meter of fill thickness because of the low elastic modulus of this material.

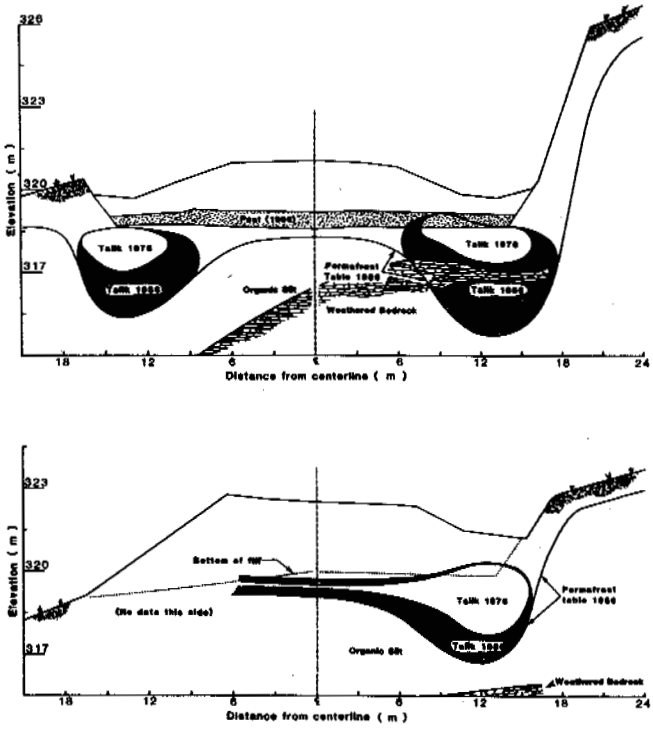

FIGURE 4. Permafrost thaw depths and taliks beneath normal and peat-insulated embankments.

Embankment Berms

Soil berms, placed to protect the lower embankment slopes from accelerated thawing, have been extensively used and investigated in Alaska. These berms are typically constructed of silty soils which result in a reduced seasonal thaw depth as compared to gravels. The performance of 1.8 m thick berms at Parks Highway sites near Fairbanks has been reported by (Esch, 1983). Monitoring of berms movements over the 12 year period following construction has demonstrated that such berms are of very minor value in retarding embankment movements (Fig. 5). In effect, berms perform much the same as the roadway side-slopes, and also create additional surface areas at temperatures averaging well above 0° C. The berms at the Bonanza Creek site have resulted in net warming and talik development in the lower slope areas, and have settled so that the original 1.8 m berm height has been reduced by 30% to 50% in 12 years. These berms also progressively moved outward by 0.5 to 1.0 m as a result of embankment spreading forces, indicating that they are of little or no value in resisting such movements. The use of plastic foam insulated berms was also investigated at this site, and insulation reduced the berm movements only slightly. Soil waste materials were used as a thin (0.7 m) berm at a road site over tundra in the Atigun valley on the Dalton Highway. Although underlaid by cold (-4° C) permafrost, the berms at this site resulted in rapid thawing and settlement, and the development of thaw-ponds alongside the roadway after 2 to 3 years. Long-term projections for the Bonanza Creek site indicate the same problem may eventually occur at that location.

A recently completed study of the effects of periodic snow removal from berm areas (Zarling, 1987) demonstrated that the mean annual surface temperature of the top of a berm could be lowered to approximately 0° C by this method, thereby retarding or eliminating the progressive annual thawing which occurs beneath berms which remain snow-covered in winter.

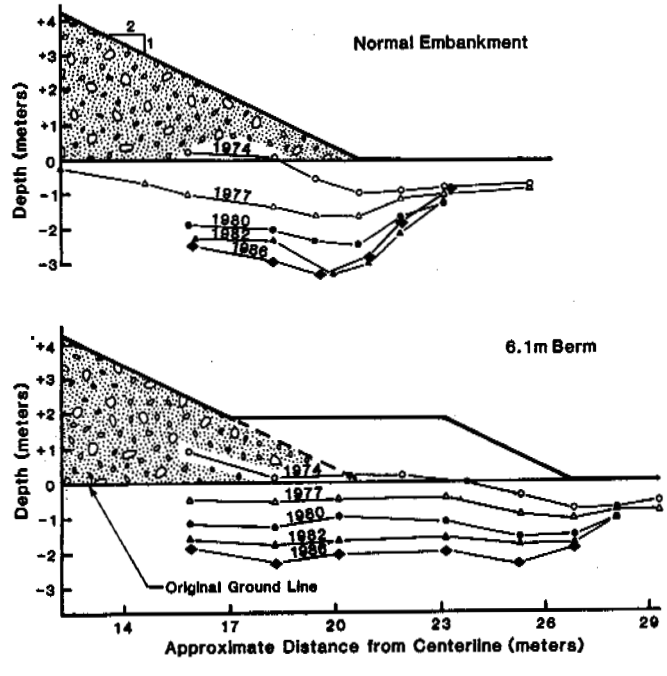

FIGURE 5. Thaw depths beneath lower embankment slopes with and without berms at Bonanza Creek roadway site.

Air-Cooling Ducts

The use of corrugated metal pipes as natural convection air-cooling systems to remove heat and refreeze embankment side-slope areas in winter, has been investigated at two sites in Alaska (Esch, 1983; Zarling, 1987). Criteria for design of these systems are now being evaluated based on the performance of an installation of 0.6 m diameter ducts on the Alaska Highway near Gardiner Creek. The duct system inlets are elevated to just above the maximum snow level, leading to nearly horizontal 22 to 45 m long heat exchange sections buried parallel to the roadway in embankment toe berms. The warmed air exits from vertical exhaust stacks up to 3.5 m in height. Such systems have demonstrated some significant cooling and stabilizing effects but have also been adversely affected by minor settlements which caused localized water ponding within the ducts. This ponding restricts the air flow and the resultant cooling performance. In construction, care must be exercised to properly locate these ducts, to prevent water entry and ponding from minor duct settlements.

Thermosyphon Devices

Thermosyphons are sealed tubes which contain both gaseous and liquid phases of some compound such as ammonia, freon, propane or carbon-dioxide. These devices, also occasionally called "heat pipes", "thermotubes", and "thermopiles" serve as efficient heat exchangers between the air and the subsurface soils. They function only when the top (radiator) portion is cold enough to cause condensation of the internal gas. The condensate then flows down the tube and re-evaporates upon contact with any portion being warmed by the surrounding soil. Under optimum winter conditions of heat transfer the entire thermosyphon will be cooled to the temperature of the ambient air, causing the freezing and cooling of the soils surrounding the buried portion. These devices have been successfully installed in inclined boreholes beneath permafrost related settlement areas on the Bethel, Alaska airport runway (McFadden, 1985) and on Farmers' Loop Road near Fairbanks. An installation on the Hudson Bay Railway in Ontario as reported by Hayley (1983) will also be of interest to the reader. By properly designing for and installing these devices, a significant refreezing and lowering of the temperature of permafrost may be achieved during the winter season. However, the designer must still anticipate and allow for the maximum seasonal thawing since thermosyphons are inactive whenever the air temperature exceeds the subsurface soil temperatures.

Reflective Surfaces

The benefits of different colored aggregates and of white and yellow paint in lowering roadway surface temperatures were intensively studied on Peger Road in Fairbanks (Berg, 1985). The benefits of white paint applied to roads with settlement problems were also studied and reported by Reckard (1985). In the Peger Road study, the surface temperatures were recorded for a two year period on seven different surface treatments, which included white and yellow paint, and rock chip-seals, with white marble, normal aggregate, and dark basalt aggregates. At this site the white painted roadway section had a mean annual surface temperature of -0.5° C compared to normal pavement at +1.1° C and air at -3.3° C. Two problems with painted surfaces were observed. The paint was very slippery during rain, as compared to normal pavements, and also wore away rapidly under high traffic so that annual repainting would be required. This treatment method would be effective in reducing thaw depths and lowering surface and subsurface temperatures on low-volume roads, but could only be used safely for sections where stopping and turning movements were not required. In wintertime it was observed that white-painted sections would also frequently accumulate surface frost while adjacent normal pavements would not.

Slope Coverings

Because of the extreme warming of roadway slopes, and the related problems of settlement, lateral spreading and cracking which result, some extreme solutions are justified in severe problem areas. The most extreme, passive treatment possible is to totally protect the slopes from solar radiation and also to prevent any snow from accumulating on the surface in winter. To evaluate the benefits of this treatment, a section of the Bonanza Creek experimental road embankment was covered with wood framed snow shed/solar screen structures (Fig. 6). Temperatures, thaw depths, and movements of the covered and normal embankments slopes were observed for two years and recently reported by Zarling and Braley (1987). Thaw depth observations demonstrated that the sheds were able to control and reverse the progressive thawing trends common to all other normal, insulated and bermed slopes. The mean annual slope surface temperatures were reduced from a normal slope value of 3.9° C to a value of -2.3° C beneath the sheds. The mean annual air temperature during this period was -3.4° C, indicating that the desired result had been achieved, with slope surfaces cooled by 6.2°C on a yearly average.

FIGURE 6. Snow shed/solar screen structures installed at Bonanza Creek test site.

Embankment Reinforcement with Geotextiles

The potentials for controlling the sags, dips, and cracks in roadways which are distressed from thawing permafrost are being evaluated a series of field trials of geofabric reinforced embankments. These studies, funded by the Alaska Department of Transportation, have investigated the effectiveness of different types and strengths of reinforcement for spanning subsurface voids, and for preventing lateral spreading and cracking of embankments on thaw-weakened foundations. Testing has demonstrated that very high strength plastic grid and strap materials can support embankments and span voids as wide as 2 meters, although allowance must be made for considerable

initial surface deformation (Kinney, 1986). Voids created by thawing ice masses wider than 2 meters, or located along the edges of the embankment where anchorage of the reinforcement on both sides of the sag is not possible, will continue to create problems even with this approach. The reinforcement of embankments by using one or more layers of geotextile to prevent spreading and cracking appears to hold the most promise, and several field evaluations are currently underway to test this approach.

Preliminary Thawing or Excavation of Thaw-Unstable Layers

Active and passive pre-thawing methods may be effectively used to thaw and consolidate unstable permafrost layers prior to construction. The thaw-acceleration effects of stripping organic layers and of applying thin gravel pads with darkened surfaces and surface coverings have been investigated and reported by Esch (1984). Pre-thawing for a period of only one or two thawing seasons prior to construction can greatly reduce future thaw-related settlements from shallow ice-rich permafrost layers. However this method will not provide much benefit when deep subsurface ice deposits exist. Settlement problems may also be avoided by excavation and replacement of ice-rich foundation soils. This method is occasionally used when problem soils are limited to shallow depths and time is not available for more economical pre-thawing operations. Large bulldozers with rippers are effective at excavating frozen soils. This operation is most efficiently done when air temperatures are slightly below freezing to avoid the obvious thaw-related water and traction problems.

SUMMARY AND SUGGESTIONS ON THE "IDEAL" EMBANKMENT DESIGN

In the design of road embankments on warm permafrost, many structural and thermal considerations should be taken into account, and several design alternatives are available. Embankment top surfaces may become too warm and side-slope surfaces are almost certain to warm greatly, followed by talik development along both sides of the roadway. Embankments on thaw- unstable permafrost are likely to remain in some state of motion for an indefinite period. None of the 15 road embankment sections monitored by the Alaska Department of Transportation have ever reached a state of stability in temperatures or in resistance to movement.

If first costs were not a critical factor, the "ideal" embankment for warm permafrost may be one which has nearly vertical slopes which do not accumulate snow, and the slopes should also be shielded or screened from the summer sun. The road surface would be separated thermally as far as possible from the subgrade soils. This could be achieved by insulation; or by allowing air to circulate through a system of ducts or through a porous layer somewhere beneath the pavement. By these means the embankment would tend to approach the mean annual air temperature rather than some elevated temperature as now occurs. The embankment might also be reinforced with geo-fabrics to resist lateral spreading. While these treatments might not all be feasible, they are suggested to guide the designers thoughts toward implementing the results of road embankment research for warm permafrost conditions.

REFERENCES

Berg, R (1985). Effect of Color and Texture on the Surface Temperature of Asphalt Concrete Pavements. Alaska Department of Transportation (DOT) Research Report, AK-RD-85-16.

Braley, W A (1984). A Personal Computer Solution to the Modified Berggren Equation. Alaska DOT Report, AK-RD-85-19.

Connor, B (1984). Air Duct Systems for Roadway Stabilization over Permafrost Areas. Alaska DOT Report, AK-RD-84-10.

Esch, D C (1973). Control of Permafrost Degradation Beneath a Roadway by Subgrade Insulation. Proc. Permafrost - 2nd Intl. Conf., 608-622.

Esch, D C (1983). Evaluation of Experimental Design Features for Roadway Construction over Permafrost. Proc. Permafrost - 4th Intl. Conf., 283-288.

Esch, D C (1984). Surface Modifications for Thawing of Permafrost. Alaska DOT Report, AK-RD-85-10.

Esch, D C (1986). Insulation Performance Beneath Roads and Airfields in Alaska. Alaska DOT Report, AK-RD-87-17.

Greene, G W, Lachenbruch, A & Brewer, M (1960). Some Thermal Effects of a Roadway on Permafrost: Geological Research, 1960, U.S. Geological Survey Professional Paper 400-B, B141-B144.

Hayley, D W, et al (1983). Stabilization of Sinkholes on the Hudson Bay Railroad. Proc. Permafrost - 4th Intl. Conf., 468-473.

Juday, G P (1983). Temperature Trends in the Alaska Climatic Changes Record. Proc. Conf. of Potential Effects of Carbon Dioxide Induced Changes in Alaska; Misc. Publ. 83-1, Sch. of Agr., Univ. of AK Fairbanks, 76-91.

Kellogg, W W (1983). Possible Effects of Global Warming on Arctic Sea Ice, Precipitation, and Carbon Balance. Proc. Conf. on Potential Effects of Carbon Dioxide Induced Changes in Alaska; Misc. Publ. 83-1, Sch. of Agr., Univ. of AK Fairbanks, 59-66.

Kinney, T C (1986). Tensile Reinforcement of Road Embankments on Polygonal Ground. Alaska DOT Report, AK-RD-86-29.

McFadden, T (1985). Performance of the Thermotube Permafrost Stabilization System in the Airport Runway at Bethel, Alaska. Alaska DOT Report, AK-RD-86-20.

McHattie, R L & Esch, D C (1983). Benefits of a Peat Underlay Used in Road Construction on Permafrost. Proc. Permafrost - 4th Intl. Conf. 826-831.

Reckard, M K (1985). White Paint for Highway Thaw-Settlement Control. Interim Report, Alaska DOT Report, AK-RD-85-16.

Krzewinski, T G & Tart, R G. Thermal Design Considerations in Frozen Ground Engineering. ASCE Monograph.

Zarling, J P & Braley, A W (1987). Thaw Stabilization of Roadway Embankments Constructed Over Permafrost. Alaska DOT Report, FHWA-AK-RD-87-20.

REMEDIAL SOLUTIONS FOR PIPELINE THAW SETTLEMENT

J.E. Ferrell[1] and H. P. Thomas[2]

[1]Alyeska Pipeline Service Company
[2]Woodward-Clyde Consultants, 701 Sesame Street, Anchorage, Alaska 99503 U.S.A.

SYNOPSIS

Because of the elevated temperature of the oil, the trans Alaska pipeline was buried only in soils which were initially thawed or thaw stable. Application of this criterion resulted in burial of some 600 km of the line. Starting two years after startup, several short segments of the buried line were identified which were experiencing thaw settlement. In response to this, a suite of remedial solutions was developed to address the range of conditions along the alignment. These included overburden relief, underpinning, relevelling, grouting, ground freezing, remoding and rerouting. The paper describes these remedial solutions and their application, and summarizes several case histories.

INTRODUCTION

The trans Alaska pipeline cuts across the breadth of the State of Alaska starting from the barren northern arctic coastal plain at Prudhoe Bay and terminating in the southern ice-free port of Valdez. In its 1287-kilometer length, the warm oil pipeline traverses both continuous and discontinuous permafrost, and non-permafrost regions in the extreme southern end (see Figure 1). The operating temperature for the 122-cm-diameter pipe varies from 62°C for receipt of the oil at Prudhoe Bay to 49°C at the Valdez Terminal facility. The pipeline is operated by Alyeska Pipeline Service Company. At the present time, the pipeline is transporting 238,000 cubic meters of crude oil per day or 24 percent of the total USA domestic oil production. It is important to minimize disruption of this production.

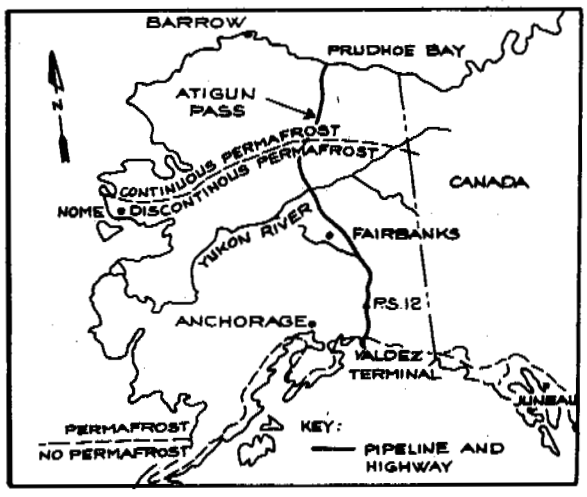

Fig. 1. Route of Trans Alaska Pipeline

During the design and construction phases, extensive soil investigations were performed to assure that the pipe foundation material would support the warm pipe during operation. Over 8000 boreholes were drilled and 600 test pits were excavated to evaluate the foundation conditions. Extensive analysis of the data was performed to determine the safest and most economical routing. During the pipe ditch excavation, a continuous foot-by-foot log was recorded to further assure the integrity of the design. Where these soil investigations indicated that the resulting thaw strains would be too severe for a buried pipe, the pipe was elevated on a pile foundation. In a few cases where an aboveground pipeline was not practical due to avalanche or environmental factors, the pipe was buried either heavily-insulated or lightly insulated with an active mechanical refrigeration system. At the end of construction, the pipeline consisted of 611 km of buried pipe and 676 km of aboveground pipe. Even with the extensive soil investigations, small ice-rich areas were undetected in the continuous and discontinuous permafrost zones. These ice-rich areas became evident as the thaw bulb started to grow after the start of oil flow in mid-1977 (Thomas & Ferrell, 1983). A typical thaw bulb cross section is shown in Figure 2.

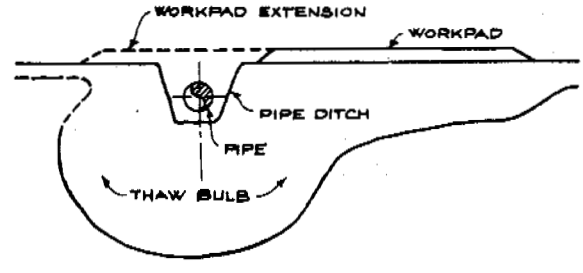

Fig. 2. Thaw Bulb Cross-Section

EARLY REPAIRS

In 1979, after two years of operation and a period of rapid thaw bulb growth, two oil leaks occurred in the buried pipe at Mileposts (MP) 166 and 734. At MP 166, the pipe had settled 1.2 m over a 120-m span as a result of thawing of massive ice in bedrock in a high mountain pass area and, at MP 734, the pipe had settled 1.7 m over a 90-m span as a result of thawing of an ice-rich "permafrost island" in an otherwise thawed environment (Johnson, 1981). The leaks were contained by full-encirclement sleeves welded to the pipe with the annulus between the pipe wall and the sleeve filled with cement grout.

Figure 3 shows the sleeve installed at MP 166. These sleeves allowed oil flow to resume. However, because they could not tolerate future pipe movements, pipe settlement had to be arrested. Based mainly on availability of contingency stockpiled material and equipment, expedient repair designs were implemented due to time constraints. Both designs consisted of piles to carry the pipe loads, downdrag loads and other loads which could result in further pipe movement.

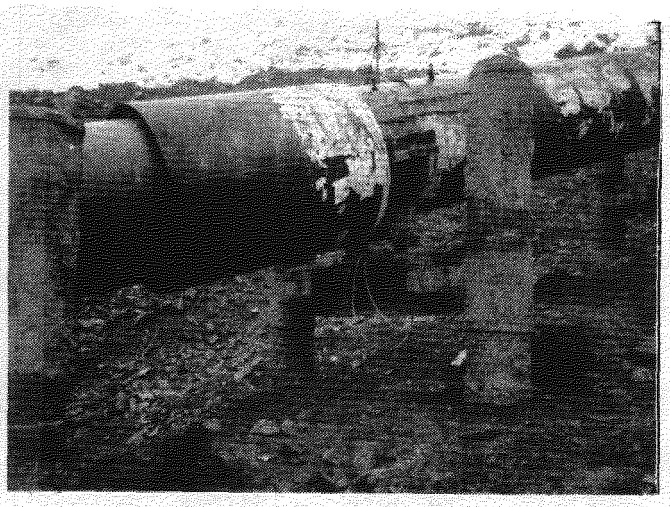

Fig. 3. Underpinning Piles Supporting Sleeved Pipeline at Milepost 166

BELOWGROUND STABILITY PROGRAM

Concurrent with repair of the two leaks, a line-wide extensive geotechnical investigation was initiated to locate other buried pipe segments which could also be experiencing thaw settlement but which had not yet damaged the pipe sufficiently to cause leaks. This investigative program identified additional settled segments in the years from 1979 to 1988. Ten of these have been successfully stabilized, beginning in 1980, before severe pipe damage occurred, and an additional segment is proposed for repair in 1988. The balance of the settled segments had only minor pipe strains and are being monitored via settlement monitoring rods affixed to the top of the pipe, instrumented pigs, and remote sensing (McDevitt and Cole, 1988). The necessity for a repair was determined by calculating pipe curvature change from the as-built pipe profile to the present pipe profile determined from a closely-spaced top-of-pipe survey (Simmons and Alto, 1988).

Defined as that value of pipe curvature corresponding to onset of buckling, critical buckling curvature (K_{cr}) is based on results of full-scale pipe buckling testing (Bouwkamp & Stephen, 1973). If a value of 85 percent or more of K_{cr} was measured, Alyeska has proceeded to stabilize the settled pipe by one of several measures. Both the stabilized and non-stabilized settlement areas are being monitored on a regular basis. Data from the stability monitoring program have shown that the thaw bulb growth as of 1988 is slow and little additional pipe movement is occurring.

As part of the early belowground stability investigation, available construction geotechnical information and operation data were evaluated. As questioned segments were identified, monitoring rods were installed on top of the pipe and instrumented soil boreholes were drilled along-side the pipe. If the rods revealed a settled area or the soil data and thermistors identified ice-rich permafrost, a more-detailed geotechnical investigation was initiated to determine the foundation parameters. However, the repair design was often delayed because the results from further drilling and soil testing could use up several weeks of the short construction season. It became evident that, if a conceptual repair design could be identified early on, the investigation program could be better focused and investigation and repair designs could thereby proceed on parallel courses. It was decided in 1981 that a suite of feasible repair designs from which Alyeska could pattern the geotechnical investigation would reduce investigative cost and design time and facilitate implementation of remedial measures. These Repair Contingent Designs could also identify required materials (especially long-lead items) and required soils information for implementation.

In 1982, Woodward-Clyde Consultants was retained to summarize experience to date and develop new conceptual designs which could satisfy the aforementioned criteria. The goal of the designs was to assure uninterrupted throughput, low risk of pipeline damage, controlled restraint on the exposed buried pipe, and be the most economical with the inherent risks. These designs would also be constrained by weather, river breakups, permits, and availability of men, material, and equipment. Since their development, these contingent designs have significantly sped investigations, evaluation, and repairs.

REMEDIAL SOLUTIONS, THEIR APPLICABILITY, AND CASE HISTORIES

The optimal remedial solution for a given pipe segment depends on a number of factors. Especially important among these are (1) the amount of pipe settlement and resulting state of pipe curvature at the time the problem is identified, and (2) the potential for future pipe settlement and its rate.

As shown in Table 1, an urgent situation is one where pipe curvature is close to buckling and rapid additional settlement is expected. In such a situation, the optimal remedial solution would probably be one which quickly arrested pipe settlement or relevelled the pipe (relieved pipe strains). If the settlement and pipe strains could not be alleviated, the problem area could be bypassed with a reroute. For another segment where pipe strains are not presently severe, a more measured response such as mitigating the cause of the thawing might be appropriate. If thaw strains were high but future thaw settlement was not expected, relevelling the settled pipe is appropriate. Lastly, where settled segments are identified with low pipe strains and no or little future settlement, Alyeska has elected to perform periodic level surveys of the rods attached to the buried pipe.

Following review of a large number of possible remedial solutions, Alyeska adopted the following contingency designs, based on technical feasibility, likelihood of success, relative economics, and ease of construction. Once these concepts were adopted, investigative costs have dropped from about 35 to about 10 percent of the repair cost. Usually a combination of the following contingent designs have been utilized by Alyeska. Table II summarizes the applications of the concepts.

Overburden Relief

As the oil-filled pipe tries to span over a developing settlement zone of finite length, it behaves like a beam and the weight of the soil backfill on top of the pipe comprises a major part of the load it must carry. For this reason, settled pipe has been observed to rebound significantly as a result of removing pipe backfill. Early experience with this was at MP 416 (see Figure 4) and 720 in 1981 when cover was removed from above the pipe. At MP 720, 1.8 m of cover was removed over a length of about 46 m which resulted in the pipe springing up 37 cm with associated reduction in pipe strains. Small amounts of rebound have also been observed at other sites.

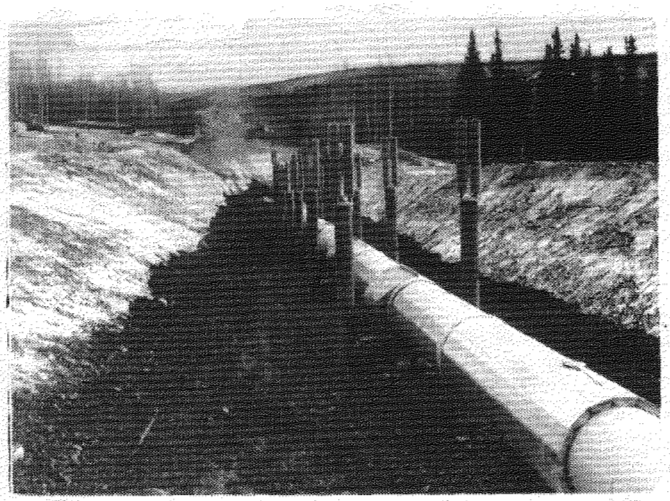

Fig. 4. Unburied and Pile-Supported Pipeline at Milepost 416

Most effective for spans of 15 to 75 m, overburden relief can be used in conjunction with relevelling (see later discussion) and may be temporary or permanent. Since the pipe often needs to be uncovered to establish survey targets and inspect it for possible wrinkles, the additional cost of providing overburden relief may be small. If sufficient ground slope is available, surface drainage may be permanently directed away from the excavation as was done at MP 416. In flat terrain with a high water table, the excavation can be regraded using lightweight backfill.

Underpinning

The principle of underpinning is to limit further pipe strain by supporting the pipe at discrete points. As mentioned earlier, after sleeves were placed on the pipe at MP 166 and 734 in 1979, the pipe was underpinned using Vertical Support Members (VSM's) and Alyeska standard aboveground support hardware (see Figure 3). Even though cover depths were reduced at both sites, the weight of the backfill was still a significant portion of the load which the VSM's had to support. Also, because the warm pipe remains in contact with the soil, the thaw bulb continues to grow and causes additional downdrag loads on the VSM's. Thermal devices could be used in the VSM's, but their effectiveness is limited by the coupled proximity of the warm pipe. At MP 200.2, underpinning was utilized to stop further pipe settlement. At this site, the piles also supported a crossbeam which was used as a reaction surface to jack against for relevelling the pipe to reduce curvature. As an additional benefit, the piles were used as temporary soldier piles for a braced excavation to expose the pipe in the active river channel.

Relevelling

The principle in relevelling is to relieve pipe distress by bringing the pipe into a shape with less severe bending conditions. In practice, this is done by first removing the overburden from the pipe and then lifting the pipe at discrete points using sidebooms or pressurized air bags. The pipe is lifted up to its original profile or possibly above to allow for continued settlement. Finally, a lean mix grout bedding is placed beneath the pipe. (The pipe may or may not be reburied.) Careful control is required during the lifting and, because the pipe is generally in compression, lateral restraint must be maintained throughout the process.

As relevelling is not a thermal solution, the thaw bulb continues to grow and this could require a second cycle of lifting to be done in the future. At MP 720 (see Figure 5), the pipe was lifted 10 cm higher than its original profile to allow for future settlement. Alyeska has found that relevelling is best used where pipe settlement is nearly complete and, like most of the other available techniques, it may be difficult to use in river crossings. However, relevelling has been utilized by Alyeska in seven of the ten repairs performed between 1980 to 1987. First used in 1986, the pressurized air bag lifting technique (see Figure 6) appears to be especially cost-

TABLE I

REMEDIAL SOLUTIONS MATRIX

Pipe Curvature K	Potential for Future Settlement	Objective	Possible Remedial Solutions
High (>85% K_{cr})	High	Arrest pipe settlement and relieve pipe strain	Reroute, relevel and underpinning, remode
High	Low	Relieve pipe strains	Overburden relief, relevel
Low	High	Arrest pipe settlement	Underpinning, maintain permafrost
Low	Low	Monitor pipe settlement	Periodic monitoring surveys

TABLE II

SUMMARY TABLE - THAW SETTLEMENT PROBLEMS AND SOLUTIONS
1980 - 1988

Milepost (Date)	Area	Depth of Cover (m)	Pipe Settlement (m)	Span (m)	% of Critical Curvature (K_{cr})	Potential for Future Settlement	Repair Solutions	Throughput Loss?	Remarks
167.2 (6/80)	Atigun Pass	2	0.76	152	N/A (low)	High	Drainage, grouting, ground freezing.	No	Thermal erosion problem - maintain permafrost.
416 (8/81)	Fairbanks	2	0.95	146	83% (60% after rebound)	High	Overburden relief, A/G remode, underpinning.	No	Remoded pipe is fully restrained.
720 (9/81)	Tonsina	1.7	0.46	55	64% (<50% after rebound)	Low	Overburden relief, relevelling using sidebooms.	No	Ground surface regraded. Pipe elevation raised 10 cm higher than original profile.
168.4 (4/82)	Atigun Pass	2	1.76	76	170%	Low	Relevelled using sidebooms.	No	
200.2 (3/83)	Dietrich River	3.5	0.91	44	180%	High	Pile underpinning and cable supports. Relevelling by jacking against cross beam.	Slight flow reduction	Located beneath active river channel. Later replaced by MP 200.6 reroute.
730.2 (3/83)	Tonsina	3	0.61	122	140%	Low	Relevelling using sidebooms.	No	Unsettled pipe haunches were lowered slightly to improve curvature.
46 (10/83)	North Slope	3	0.76	67	150%	Low	Relevelling using sidebooms.	No	Little further settlement expected.
200.6 (11/84)	Dietrich River	4.6	4.6	81	>200% est.	High	Remode to A/G, reroute around area.	6-day shutdown	Beneath active river channel, pipe was never exposed.
601 (9/86)	McCallum Creek	3	0.79	46	160%	Low	Relevelling using airbags.	No	No remaining permafrost.
158 (10/86)	Atigun River	4	1.07	46	120 to 160%	Low	Relevelling using airbags.	No	No remaining permafrost. In active floodplain.
167.4-167.6 (7/88)	Atigun Pass	2	0.9-1.0	91-122	60 to 70% est.	High (15 cm/yr.)	Relevel, repair damaged insulation, improve drainage.	None expected	Proposed work for 1988. Pipe has 50-cm-thick insulation broken by settlement.

effective and promising as it significantly reduces labor and equipment expense.

Fig. 5. Lifting the Operating Pipeline with Sidebooms at Milepost 720

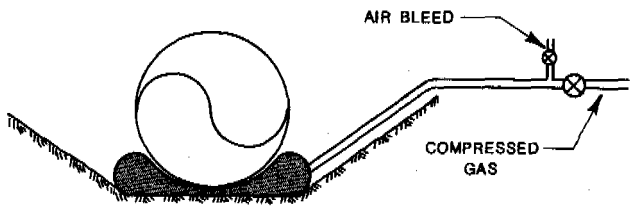

Fig. 6. Air Bag for Pipe Lifting

Grouting

Grouting can be used for soil improvement or for actual pipe lifting. At MP 167 (Atigun Pass) where convective thawing was a problem, grouting was effectively used to (1) create a barrier to groundwater flow (seepage cutoff), and (2) to reduce the permeability of pervious soils in the thaw bulb.

Although it has not yet been used by Alyeska for pipe lifting, displacement grouting appears to be a promising relevelling technique, especially in areas with difficult access such as river crossings. For its use, a closely-spaced array of top-of-pipe survey points would be required to assure control of the lift operation.

Ground Freezing

Refrigeration may be used to refreeze the thaw bulb or to keep the thaw bulb from increasing in size. Both mechanical and passive techniques have been utilized. Mechanical refrigeration is mainly useful as a temporary measure. Free-standing thermosyphons or heat pipes are the passive technique Alyeska has used. First used as a remedial measure before oil flow at MP 723 (Heuer et al, 1981), Alyeska has constructed several heat pipe test sections in different types of terrain. In one test section where closely-spaced heat pipes were installed on either side of a buried segment, pipe settlement was halted and some minor rebound was noted.

At MP 167, Alyeska used a 350-kW portable freezing plant to circulate chilled brine through 268 vertical freeze pipes installed on both sides of the pipeline (see Figure 7). To maintain the recreated frozen zone, 133 heat pipes were then installed, one in every other freeze pipe (Thomas et al, 1982). In addition, heavy pipe insulation is generally required and groundwater flow velocities need to be negligible or reduced to less than about 2 m/day by means of grouting. At MP 167, there was 60 cm of insulation surrounding the pipe and, as mentioned previously, groundwater flow was controlled by water shut-off grouting.

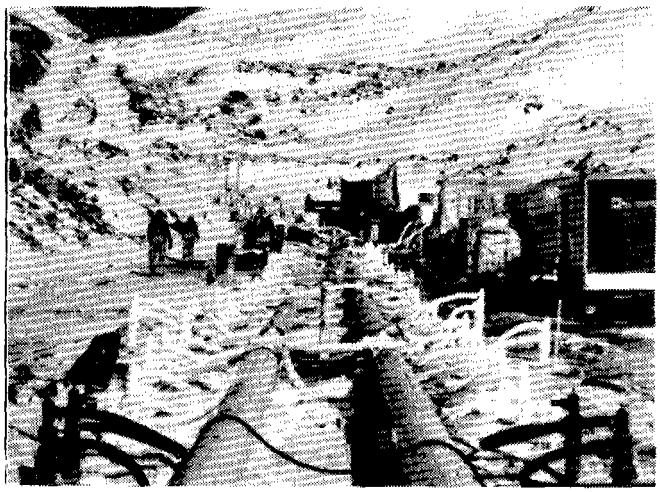

Fig. 7. Ground Freezing at Milepost 167

Remoding

The elevated construction mode used to support nearly half of the pipeline was specifically designed for traversing ice-rich permafrost areas. Because it decouples the warm pipe from the frozen ground, remoding to elevated could appear to be an obvious solution to a pipe settlement problem. However, because raising the pipe profile 3 m (or more) generally requires a shutdown of the pipeline or a tricky stopple and bypass operation, Alyeska has opted for remoding only as a last-resort solution.

Remoding to aboveground was used at MP 416 where the pipe was pile-supported at its rebounded profile and the ground surface was excavated to 60 cm below the bottom of pipe (see Figure 4). This in effect remoded the pipeline without interrupting the oil flow. Most of the pipe settlement (thawing permafrost) areas are also areas of high ground water. MP 416 was unique in this respect in that it was in a sidehill situation and the excavation could be drained. The remoded pipe eliminated heat flow into the remaining permafrost and allowed the piles with their heat pipes to refreeze the ground for pile support. The pipe was securely fastened to the support beams and is fully restrained.

At MP 200.6, further addressed in the following section, the buried pipe was remoded to

aboveground and rerouted around the problem area using typical Alyeska designs and hardware.

Rerouting

An alternate solution may be to bypass an especially-severe problem area. Depending on ground conditions in the area, the reroute could be in the buried or elevated mode. The reroute requires a shutdown or stopple and bypass and is usually justified only in response to a problem not amenable to other solutions. The MP 200.6 repair (see Figure 8) is an example of a reroute because of high pipe strain rates and the difficulty of adequately arresting further settlement. Simmons and Ferrell (1986) have described this repair in detail.

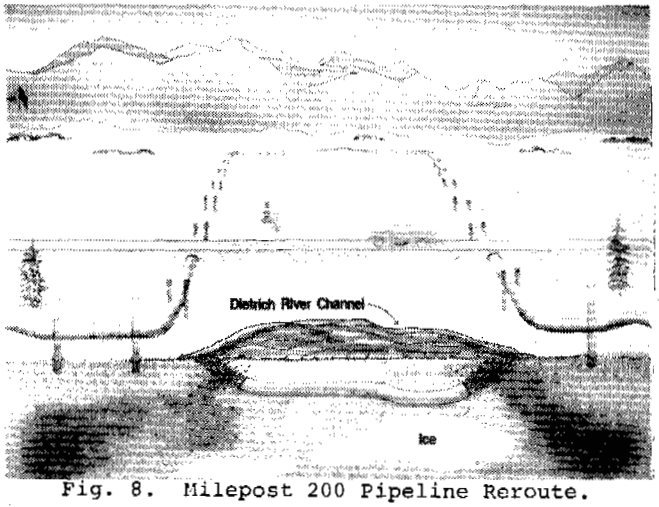

Fig. 8. Milepost 200 Pipeline Reroute.

CONCLUSIONS

- Even with a very extensive subsurface investigation program, occasional sporadic occurrences of ice-rich permafrost may be undetected in otherwise initially-thawed or thaw-stable areas.

- In view of this, it is highly desirable to have a variety of remedial solutions for pipe thaw settlement developed for buried segments of a warm pipeline constructed in arctic and/or subarctic regions.

- No single solution is likely to be best for all situations. The optimal solution will depend on pipe settlement/ curvature, local permafrost characteristics, anticipated pipe settlements/settlement rates, topographic setting, logistics and other factors.

- Based on Alyeska's operating experience, overburden relief followed by relevelling using pressurized air bags appears to be one of the more successful and economical remedial techniques.

- As a result of Alyeska's settlement monitoring program, ten 50- to 150-m-long buried segments have been stabilized on the trans Alaska pipeline since 1980. Nearly all of these stabilization projects have been carried out without interrupting the oil flow. Other buried segments are being monitored regularly for possible future remedial action.

- The pipeline segments that have been stabilized since the first repairs in 1979 amount to less than 0.2 percent of the 611 km of buried pipeline.

ACKNOWLEDGEMENTS

The authors wish to thank Alyeska, the operator of the trans Alaska pipeline, for permission to publish this paper and the Owners of TAPS for their concurrence. We also thank colleagues who reviewed draft versions of the paper for their helpful comments and suggestions.

REFERENCES

Bouwkamp, J.G. and Stephen, R.M. (1973), "Large Diameter Pipe Under Combined Loading," ASCE Transportation Engineering Journal, August.

Heuer, C.E., Krzewinski, T.G. and Metz, M.C. (1981), "Special Thermal Design to Prevent Thaw Settlement and Liquefaction," Proceedings of Fourth Canadian Permafrost Conference, Calgary, Alberta, March 2-6.

Johnson, E.R. (1981), "Buried Oil Pipeline Design and Operation in the Arctic - Lessons Learned on the Alyeska Pipeline:" 37th Petroleum and Mechanical Conference, Dallas, Texas.

McDevitt, P.G. and Cole, G.E. (1988), "Profiling the Trans Alaskan Pipeline Buried Pipe Using the Heath TSI Pipe Locator," Proceedings of API Pipeline Conference, Houston, Texas, April 26-27.

Simmons, G.G. and Ferrell, J.E. (1986), "Alyeska Reroutes Trans-Alaska Pipeline at MP 200," Proceedings of Fourth International Conference on Cold Regions Engineering, ASCE, Anchorage, Alaska, February 24-26.

Simmons, G.G. and Alto, J.V. (1988), "Calculation of Pipeline Curvature by Polynomial Approximation Using Discrete Monitoring Points," International Conference on Pipeline Infrastructure, ASCE, Boston, Massachusetts, June 6-7.

Thomas, H.P., Johnson, E.R., Stanley, J.M., Shuster, J.A. and Pearson, S.W. (1982), "Pipeline Stabilization Project at Atigun Pass," Proceedings of Third International Symposium on Ground Freezing, Hanover, New Hampshire, June 21-24.

Thomas, H.P. and Ferrell, J.E. (1983), "Thermokarst Features Associated with Buried Sections of the Trans-Alaska Pipeline," Proceedings of Fourth International Conference on Permafrost, Fairbanks, Alaska, July 17-22.

A FROZEN FOUNDATION ABOVE A TECHNOGENIC TALIK

I.E. Guryanov

Permafrost Institute, Siberian Branch of the U.S.S.R. Academy of Sciences, Yakutsk, U.S.S.R.

SYNOPSIS A study is made of the combined influence of an unfrozen area that has formed in the permafrost surrounding a warm pit shaft and of hollow box foundations ventilated with outdoor air during the wintertime, upon the temperature regime and load-carrying capacity of the bases of surface pit buildings. The feasibility of a stable, frozen base that is bounded or partially supported by an unfrozen area, is demonstrated. Data on the reliability and economical profitableness of structural-and-technological designs of foundations are given.

The range of problems concerning the building of pit surfaces in the Far North involves structures for which - when the thawing of the bases is not acceptable - it is also unfeasible to retain earth materials in the frozen state. Such a kind of projects are headgear buildings (headframes). Under the action of the warm pit shaft there forms a vertical talik below them, throughout the depth of the shaft within the permafrost. If the headframe is supported by earth materials which, while thawing, subside or lose their strength, then the necessity of maintaining them in the frozen state, combined with the inevitable formation of a talik, means that conventional methods of retaining the permafrost are inapplicable.

Experience has shown that the use of the foundations outside of the unfrozen area leads to an increase in weight of socle structures which overlap the talik as well as in the scope of construction work on the building. Cooling collars such as fore-shafts (Novikov, 1959) failed also to provide the expected effect in an attempt to get the base frozen. In the case of keeping technologically needed warm underground spaces, it evidently becomes necessary to have available the foundations for the structure as a whole, with a high spatial rigidity and high thermal lag that provides for a constantly frozen state of earth materials at the footing. Piles or pier foundations with a surface cellar and deep box foundations (Fig. 1) exemplify alternative methods for laying the foundations for headframes when construction work is proceeding by the principle I СН иП II-18-76. In contrast to the variant of a surface cellar that forms a temperature field at the footing close to a natural field, box foundations which are ventilated with outdoor air during the wintertime, are also examined as being a factor of controlling the temperature regime of permafrost by considering an example of structural developments as done by this author in the design of a northern mine.

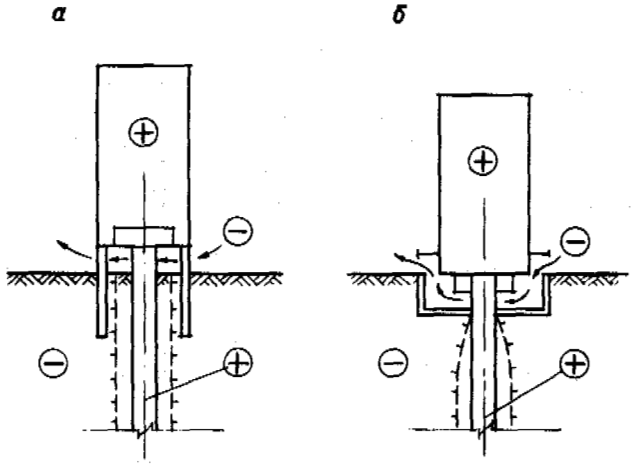

Fig.1 Schemes for Tower Headframe Building Foundations and Their Thermal Interaction with Permafrost. The + and - signs refer to the ambient temperature.
a - piles foundations with a surface cellar;
b - hollow ventilated foundations.

In view of the complexity of the general formulation and crudeness of initial data, the problem of heat exchange between the foundation and earth materials is visualized by dividing it into two problems which are solved independently but are related by boundary conditions and results, namely (a) heat exchange in the foundation, and (b) heat exchange in earth materials. Solutions of both problems are obtained by iteration.

We replace the three-dimensional problem of heat exchange by a two-dimensional, axisymmetrical problem, in order to perform computations on a medium-scale computer, which leads to some overestimation of the calculated temperature of earth materials and to a relevant reserve of load-carrying capacity of the base. Rectangular foundations and equivalent round foundations

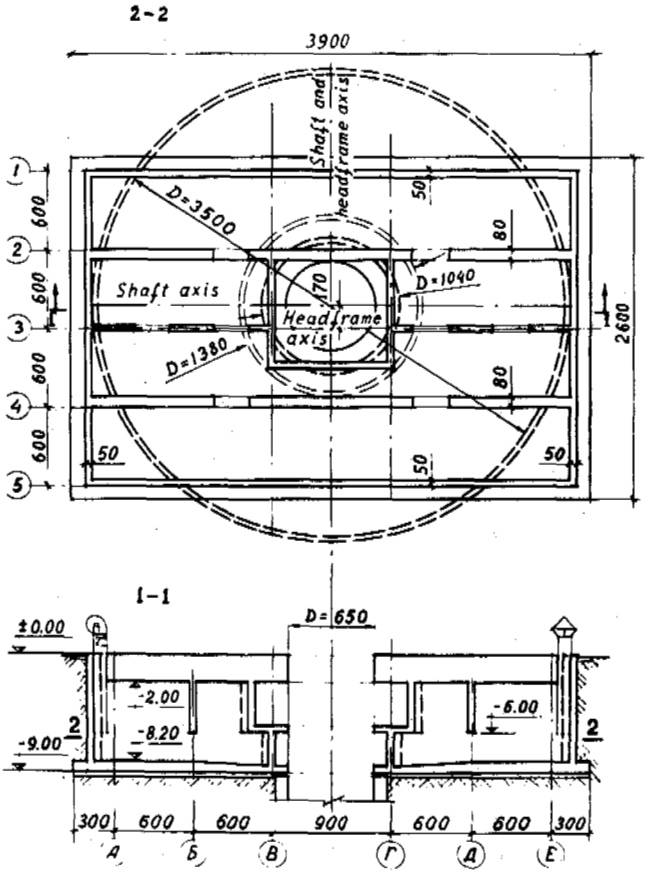

Fig.2 Box Foundation of Headframe No. 1 and its Calculated Scheme (dashes) in the Axisymmetric Problem of Heat Exchange.

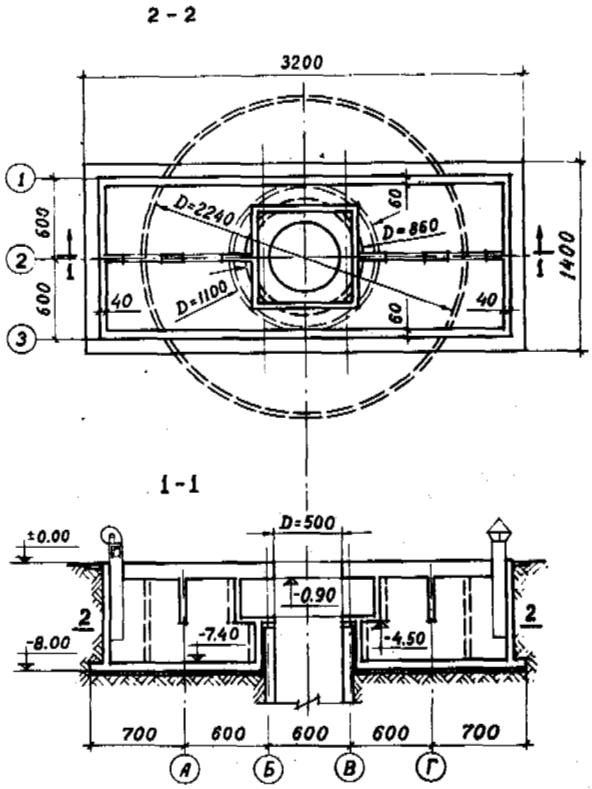

Fig.3 Box Foundation of Headframe No. 2 and its Calculated Scheme (Dashes) in the Axisymmetrical Problem of Heat Exchange.

for headframes No. 1 and No. 2 of the mine indicated are shown in Figs 2 and 3, respectively, and their geometrical characteristics are given in Table I.

TABLE I

Outer Surface F and Volume V of Headframe Foundations

Variant	Headframe No. 1		Headframe No.2	
	F, m^2	V, m^3	F, m^2	V, m^3
Rectangular	1 930	1 145	998	564
Round	1 980	1 136	996	563

The structures are supported by permafrost suglinoks of 0.17 total moisture content having a layered-latticed cryogenic structure. The thermal characteristics of earth materials were taken according to СНиП II-18-76; the initial temperature was -1.3°C throughout the calculated depth of the foundations. The solution of the problem of heat exchange between the building and its base was constructed with a seasonal change of the kind of boundary conditions. A warm period (from 16 April to 15 October) corresponds to the warming of the base due to the contiguous headframe spaces, while a cold period (from 16 October to 15 April) corresponds to the cooling of the base due to mechanical ventilation of the underground spaces with outdoor air.

Boundary Conditions for the Warm Period

During a warm period of the year underground spaces of headframes should be tightly closed, and conduction through protection structures together with radiation and convection in the air volume of a hollow foundation are the factors of heat losses into the base. Convective heat exchange is brought about by the vertical walls of the cellar on the side of the shaft that is ventilated with a warm air, with the resultant effect defined by the function (Gräber et al., 1958):

$$Nu = 0.1(Gr \cdot Pr)^{1/3}, \qquad (1)$$

where Nu, Gr, and Pr are the Nusselt, Grasshof and Prandt criteria. Function (1) holds true when $Gr \cdot Pr > 2 \cdot 10^9$ but is also applicable for the foundations considered, for which $Gr \cdot Pr \geqslant 16.3 \times 10^{10}$, Subject to the Nusselt criterion

$$Nu = \alpha_к \ell / \lambda \ , \qquad (2)$$

where $\alpha_к$ is the heat transfer coefficient, $W/(m^2 \cdot K)$; ℓ is the height of the wall; and λ is the coefficient of heat conduction of air, $W/(m \cdot K)$; function (1) yields the expression for the coefficient of convective heat transfer which is independent of the size of the underground space:

$$\alpha_к = 0.1\lambda \left[q(\theta_п - \theta_в)/(\theta_в \cdot \nu^2) \cdot Pr \right]^{1/3} , \qquad (3)$$

where ν is kinematic viscosity of the air, m^2/s; q is free fall acceleration, m/c^2; and $\theta_в$ and $\theta_п$ are the air temperature and the wall surface temperature, K, respectively.

In doing the calculations, the temperature was averaged for each month, with the values of the coefficients of convective heat transfer for the cellar for the entire warm period being the following: through radiation - $\alpha_л$ = = 1.49 $W/(m^2 \cdot K)$, and through convection - $\alpha_к$ = = 2.15 $W/(m^2 \cdot K)$. The total heat resistance

$$R_o = (\alpha_л + \alpha_к)^{-1} = 275 \ m^2 \cdot K/kW,$$

is by an order of magnitude lower than the resistance to heat transfer to the protection structures. Therefore, only conductive heat exchange was simulated on the computer, with the introduction, however, of an additional "equivalent" protection layer, whose heat conduction was determined from the total heat resistance of the undergound spaces, while heat capacity was additive for the mass of all the foundation structures within the space (see Figs 4 and 5).

For the onset date of the warm period, the mean temperature of the "equivalent" layer is equal to the air temperature in the cellar. On the inner surface of the layer the temperature is due to contiguous technological volumes (+10°C). The air temperature within the pit shafts that heat the footing on the sides, is +7°C for headframe No. 1 and +2°C for headframe No. 2, with the coefficient of convective heat transfer on the headframe surface being α = 17.4 $W/(m^2 \cdot K)$.

Boundary Conditions of a Cold Period

Temperature calculations and ventilation heat measurements are matched by successive approximations. To begin with, we assume that the mean rise in air temperature while moving through the underground space is 20% of the value of its subzero temperature; then we calculate the heat exchange between the foundation and earth materials in the first approximation. The results of the calculation, viz. temperature fields at the footing, allow us to determine the monthly mean temperature gradients $\Delta\theta/\Delta z$ and heat flows within earth materials at the foundation footing, on the whole (Table 2). The tabular values of heat flows are determined from the expression

$$w = -\lambda_м \cdot \Delta\theta/\Delta z \ ,$$

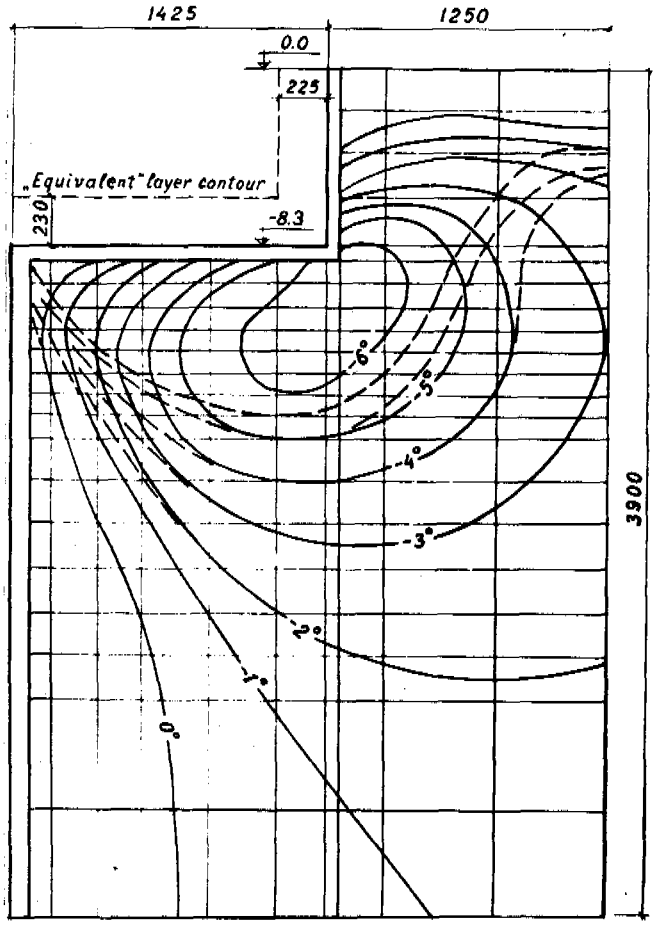

Fig.4 Calculated Temperature Field at the Base of Headframe No. 1 for mid-October; dashes denote the siotherms for April.

where $\lambda_м$ = 1.75 $W/(m \cdot K)$ is the coefficient of heat conduction of frozen ground, and Δz is the interval between the points at which the temperature was measured, m.

Stabilization of the temperature regime of earth materials at the foundations begins not later than during 10 years of exploitation of the structures, and there is only a minor difference between the subsequent temperatures of earth materials over a 1-year cycle for a 30-year period of forecasting. Therefore, the Table 2 data correspond to every year within the interval indicated.

We determine the total heat losses into the ventilated underground space from the foundation earth materials and from the headframe building for the period of a single air exchange to be t = 7.56 min for the cellar and t = 6.59 min for headframes No. 1 and No. 2, with the throughput of the fans being given. Heat losses of earth materials through the axisymmetrical foundation with its outer surface F (Table 1) for a period t, estimated as $Q_м = -w_c Ft$, are given in Table 3. The table also presents heat losses from the headframe rooms into the hollow foundation $Q_в$, as determined

TABLE 2

Calculation of Heat Flows at the Headframe Bases (1st Approximation)

Headframe	Parameters	November	December	January	February	March
	$\Delta\theta/\Delta z$, K/m	4.26	5.67	5.69	4.38	2.07
No. 1	w, W/m^2	-7.46	-9.92	-9.96	-7.66	-3.62
			w_c = -7.72 W/m^2			
	$\Delta\theta/\Delta z$, K/m	4.55	6.06	6.17	4.93	2.63
No. 2	w, W/m^2	-7.96	-10.61	-10.81	-8.64	-4.60
			w_c = -8.52 W/m^2			

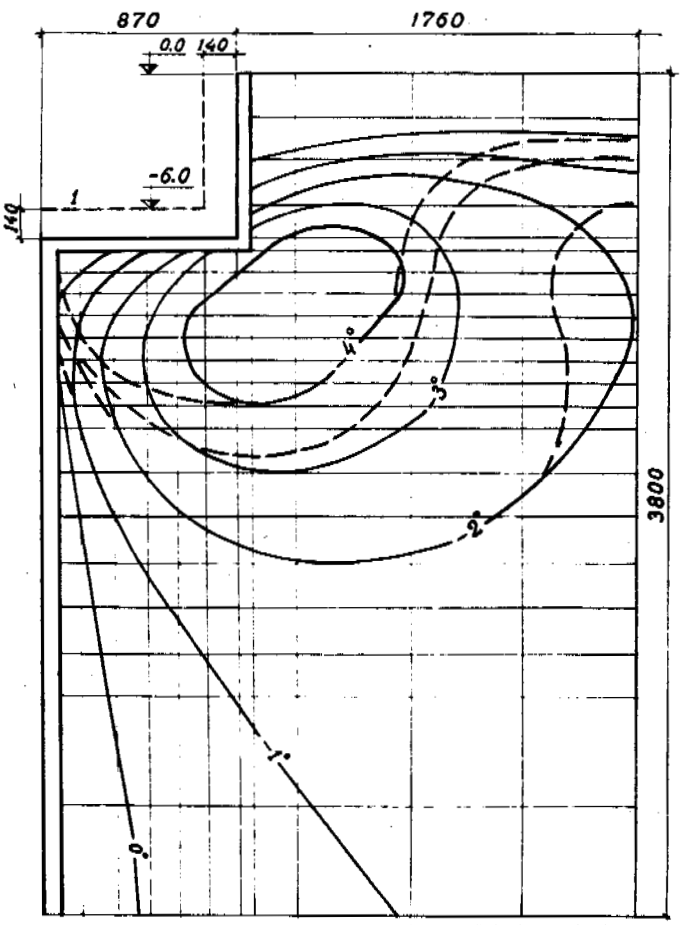

Fig.5 Calculated Temperature Field at the Base of Headframe No. 2 for Mid-October; dashes denote the isotherms for April. I - contour of the "equivalent" layer.

by normalizing methods of construction heat engineering, as well as the temperature difference averaged over the time interval of a single air exchange in the volume V_1: $\Delta\theta = (Q_н + Q_в)/c\gamma V_1$. Unlike the СНиП II-3-79 technique, taking into account the non-stationarity of heat exchange at the time of cooling of the inner foundation structures with a volume of 400 and 72 m^3 of headframes No. 1 and

TABLE 3

Parameters of Heat Exchange in Ventilated Underground Spaces

Headframe	$Q_н$, MJ	$Q_в$, MJ	V_1, m^3	$\Delta\theta$, °C	$\Delta\theta''$, °C
No. 1	6.93	8.45	2 400	4.43	5.06
No. 2	3.36	2.85	774	5.53	5.84

No. 2 increases the temperature differences in the air to a value $\Delta\theta''$. In order to render the temperature of the air surrounding the foundation from inside more exact, it is necessary to specify more exactly the coefficient of heat transfer that is originally taken the same as that in the shaft. Heat transfer from the cellar floor is considered to be a total one, owing to the forced horizontal movement of the air and free convection vertically because the cooled surface of the foundation plate faces upward. Heat transfer in the case of forced flow round the plate is characterized by the Merkel function (Shorin, 1947):

$$Nu = 0.0568 Pe^{0.78}, \qquad (4)$$

where Pe is the Peclét number. Hence, from (2) and (4) the coefficient of convective heat transfer in the case of forced air cooling along the length ℓ = 35 m for the foundation of headframe No. 1 is $\alpha_в = \lambda \cdot Nu/\ell$ = 0.56 W/(m^2·K).

Free air convection, with the values of the Grashof and Prandtl numbers being $2\cdot10^7 < Gr\cdot Pr < 1\cdot10^{12}$, is described -, according to M.A.Mikheev (Shorin, 1952) - by a function of the form (1) with the coefficient 1.35. Therefore, as in the case considered above, with the actual value of $Gr\cdot Pr = 5.9\times10^9$, the size of the vertical convection zone are not involved in describing the process, and the value of the coefficient of convective heat transfer by formula (3) with a correction of 1.35 is α_c = 5.38 W/(m^2·K).

On the other hand, according to results repor-

ted by Griffits and Davies (Shorin, 1947), the coefficient of convective heat transfer in the air of horizontal plates, with their heated surfaces facing upward, is

$$\alpha_c = 2.15(\theta_n - \theta_в)^{0.25} \approx 5.58 \text{ W/(m}^2\cdot\text{K)}.$$

Because both estimates of free convection do not differ significantly, the total coefficient of convective heat transfer on the inner surface of the foundations is taken to be: $\alpha = \alpha_в + \alpha_c \approx 6.0$ W/(m^2·K).

The more precise boundary conditions permit us to calculate the temperature fields at the headframe bases in the second approximation as well as the relevant heat flows at the foundation footing (see Table 4).

stability of a natural permafrost situation, are specified at the upper edge of the region (Guryanov and Demchenko, 1984). Temperature fluctuations of earth materials are attributable to the influence of the shaft and the headframe and are quite unusual because of a lateral heat source and the absence of the seasonally unfrozen layer. October has been taken as the calculated month for which the temperatures of earth materials are the greatest. Temperature fields at the base of the headframes in October as well as for the coldest month (April) are presented in Figs 4 and 5. The figures show that the permafrost boundary undergoes seasonal variations only at the center of the foundations but remains unchanged in its principal part that produces a conic surface within the mass along the shaft.

TABLE 4

Calculation of Heat Flows at the Headframe Bases (2nd Approximation)

Headframe	Parameters	November	December	January	February	March
	$\Delta\theta/\Delta z$, K/m	2.51	4.53	5.18	4.37	2.40
No. 1	w, W/m^2	-4.39	-7.93	-9.06	-7.65	-4.20
			w_c = -6.65 W/m^2			
	$\Delta\theta/\Delta z$, K/m	3.17	5.13	5.73	4.87	2.84
No. 2	w, W/m^2	-5.55	-9.00	-10.04	-8.53	-4.97
			w_c = -7.62 W/m^2			

The difference in values of heat flows of the 1st and 2nd approximations (Tables 2 and 4) leads to changes in the calculated temperature of the forced air by not more than 0.3°C, which does not exceed the accuracy to which it is specified and controlled. Therefore, the 2nd approximation boundary conditions are final.

Calculated Temperature Regime of Earth Materials

The solution of the problem of conductive heat transfer in earth materials has been carried out numerically by a method of heat balances, with proper account of phase transformations of ground moisture at 0°C. The vertical cross-section of a cylindrical calculated region is rectangular in shape with a hollow at the origin of coordinates corresponding to the foundation configuration. Separation into calculated blocks near the foundations is shown in Figs 4 and 5. The depth (89 m) and the radius (107 m) of the calculated region rule out the heat flows outwards.

In the foregoing discussion, we have described the boundary conditions for contact with the foundation. The coefficient of convective heat transfer and the temperature in the shaft (3rd-kind boundary conditions) are specified for the contour of the supports. The surface temperature of ground and snow (1st-kind boundary conditions), verified via a calculation for

The calculations have established that beneath the footing of box foundations which are ventilated with cold outdoor air, there forms a zone of stable subzero temperatures as low as -6°C at the base of headframe No. 1 (Fig. 4) and -4°C at the base of headframe No. 2 (Fig. 5). Toward the end of the warm period the zone of unfrozen ground immediately at the footing of the foundations expands as much as one-third of its size. However, most of the footing area (more than 80%) is constantly supported by frozen earth materials with low subzero temperature, i.e., with a given ventilation regime the conditions for surface and melt water infiltration into the base of the headframes and along the shafts are ruled out.

Load-Carrying Capacity of Headframe Bases

Estimating the load-carrying capacity of the bases is complicated by a multitude of factors, namely the nonuniform temperature field, irregular variation of the characteristics of earth materials, and arbitrary duration of the loads. Therefore, bearing in mind the predominance of clayey ground with low internal friction, our consideration has incorporated only one, generalized characteristic of frozen ground, viz. the equivalent, marginally long bond C. Table 5 gives the calculated values of the bond taking into account experimental results on earth materials at -3°C as well as the functional dependence of their strength on temperature according to СНиП II-18-76.

TABLE 5

Equivalent Bond of Earth Materials as a Function of Temperature

θ, °C	-0.3	-0.5	-1.0	-1.5	-2.0	-3.0	-4.0	-5.0	-6.0
C, kPa	160	240	340	420	480	600	680	760	840

The main load-carrying structures of box foundations which ensure their bend stability at the time of thawing of the central zone of the base, are longitudinal wall beams of the foundations along axes 2 and 4 of headframe No. 1 (Fig. 2) and along axes 1 and 3 of headframe No. 2 (Fig. 3). The beam structures predetermine the investigation of the load-carrying capacity of the bases for plane deformation and, hence, the transition to actual dimensions of the foundations. Plane deformation in the presence of an axisymmetrical temperature field is advantageous as the approximation that underrates the load-carrying capacity.

The load-carrying capacity of headframe bases was investigated numerically along trajectories of marginal shears of a discontinuous solution of the problem of plasticity theory for a wedge. This solution yields the expression for limiting distributed load normal to the side of an acute-angle wedge with the opening 2α (Rabotnov, 1979):

$$q = 2C(1 - \cos 2\alpha). \qquad (5)$$

The characteristics of the defining equations of the problem (sliding lines) lie in the field of solutions at the angle of 45° to the side of the wedge. The bisectrix of the angle 2α is the discontinuity line of normal stresses. The opening angles of the calculated wedge have been determined from the slope of the zero isotherm: $\alpha = 36°40'$ for headframe No. 1 and $\alpha = 40°50'$ for headframe No. 2.

Calculated schemes for foundations are presented in Figs 6 and 7. The diagrams of limiting shear stresses τ_{np} calculated from the actual temperature of earth materials as well as equivalent bond according to Table 5, are constructed along the sliding lines marked at 1 m intervals horizontally, starting from the edge of the foundation footing. The character of the diagrams indicates that the nonuniformity of the stress field within the ground mass is lower as compared with the nonuniformity of the temperature field.

Diagrams of limiting pressures q, equal to the vertical projection of increments of total stresses on the characteristics, are plotted in Figs 6 and 7 for the total load-carrying capacity of the bases /1/ and for additional pressures /2/ as the differences of the load-carrying capacity and own weight of earth materials. Their values were used for calculating the limiting pressures for equal-sized rectangular diagrams which average curvilinear, -total q_{c1} and additional q_{c2} ones (Table 6).

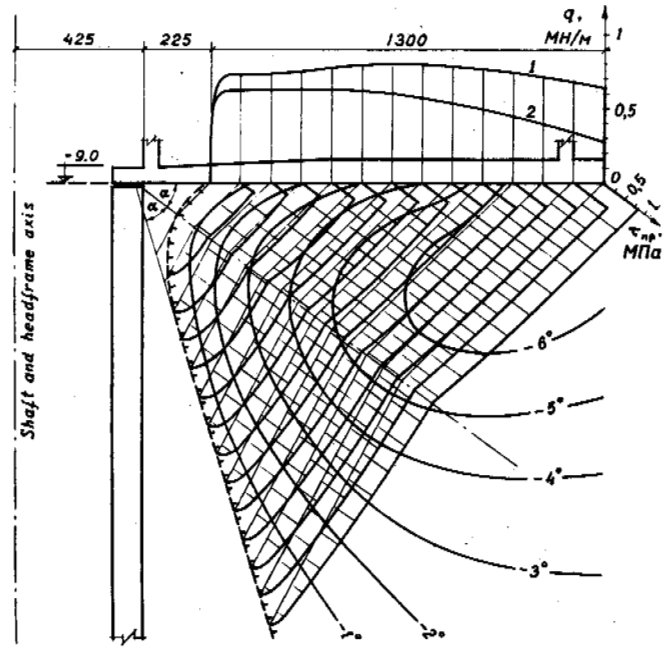

Fig.6 Calculated Scheme for Limiting Equilibrium in Earth Materials of the Base of Headframe No. 1.
The diagrams of limiting shear stresses are plotted at the sliding lines, and the diagrams of limiting pressures are plotted along the foundation footing.
1 - total limiting pressure;
2 - additional pressure.

TABLE 6

Calculated Pressures Below Foundation Footing of Headframes, kPa

Headframe	q_{c1}	q_{c2}	$\bar{c}$	q	p	m	k
No. 1	755	538	593	845	330	0.89	1.63
No. 2	778	586	518	885	180	0.88	3.25

On inserting the mean equivalent bond of the base $\bar{c}$ as the ratio of total resistence to shear along the characteristics to their length, it is easy to find, using formula (5), the theoretical value of limiting load q on the base

for a stripe of a breadth of 1 m.

In Table 6 the quantity $m = q_{cr}/q$ is the measure of closeness of the calculated scheme to its theoretical analogue and, while being less than unity, is also the safety coefficient of limiting pressure. The values of $I - m$ are twice as small as root-mean-square departures of the calculated diagrams τ_{np} from theoretical ones, i.e., numerical solutions on the characteristics possess a convergence margin. The reliability of the foundation-base system is evaluated by the ratio of limiting pressure q_{cz} to mean stress p beneath the footing of the support zone from constant and temporal loads: $k = q_{cz}/p$. In comparison with the mean coefficient of reliability (Table 6) its values from marginal pressures at the edge of the talik (Figs 6 and 7) predetermining the overall limiting state, are higher: $k = 2.67$ and $k = 3.78$. Thus, schematization of the calculations that combines solutions of the problems of a different dimensional representation is justified in view of the high values of the reliability coefficient.

Table 7 compares the total cost estimates of two variants of foundations that were worked out in the design of an underground mine.

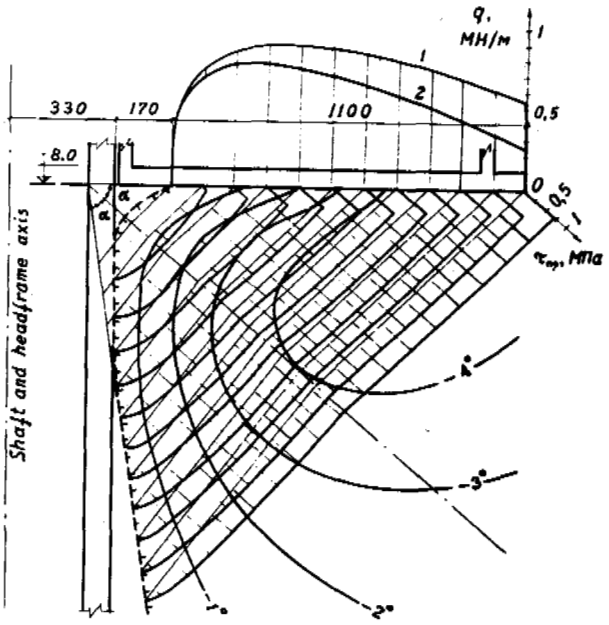

Fig.7 Calculated Scheme for Limiting Equilibrium in Earth Materials at the Base of Headframe No. 2. For explanations refer to Fig. 6.

TABLE 7

Capital Outlays for Construction of Foundations, Thousands of Roubles

Headframe	Piles foundations	Box foundations
No. 1	3 413.9	1 002.6
No. 2	382.4	359.3

For the mine as a whole, box foundations of the headframes guarantee a decrease in investments by 2 434.4 thousands of roubles as well as in annual exploitation costs by 100 thousands of roubles. However, whereas for headframe1 weighing 173 MN the increase in cost of the foundations is very substantial, or by 3,4 times, then for headframe No. 2 weighing 53 MN it is only 6% because for light-weight headframes, the desired increase in the volume of ventilated underground spaces becomes unprofitable.

CONCLUSIONS

1. Structures of box foundations, ventilated with the outdoor air during the wintertime, guarantee the required temperature regime of the permafrost at the base as well as its stability. These are advantageous foundations because loads on the base are transmitted directly by the load-carrying box of the cellar, and the lower stages of the cellar lie at technological levels, without the need to lift them, which is needed in the case of a surface ventilated cellar.
2. During a warm period of the year, the thawing of earth materials at the footing is ruled out, owing to the large own mass of the cooled foundations which is advisable to increase round the periphery of the footing.
3. The permafrost that is bounded or partially supported by an unfrozen zone, are able to serve as a safe base, provided that the temperature stability, in conjunction with the configuration of the frozen mass at the base of the structure, is determined by the strctural-and-technological design of the foundations. With such an approach, the stability of the base and the reliability of the foundations are both guaranteed.

REFERENCES

СНиП II-18-76. (1977). Osnovaniya i fundamenty na vechnomerzlykh gruntakh, 46 p., Moscow: Striizdat.

СНиП II-3-79. (1979). Stritel'naya teplotekhnika, 32 p., Moscow: Striizdat.

Gräber, G., Erk, S. and Grigull, W. (1958). Osnovy ucheniya o teploobmene, 566 p., Moscow: Izd. inostr. liter.

Guryanov, I.E. and Demchenko, R.Ya. (1984). Merzlye grunty pri inzhenernykh vozdeistviyakh, 106-116, Novosibirsk: Nauka.

Novikov, F.Ya. (1959). Temperaturny rezhim merzlykh gornykh porod za krepyu shakhtnykh stvolov, 98 p., Moscow: Izd. AN SSSR.

Rabotnov, Yu.N. (1979). Mekhanika deformiruemogo tverdogo tela, 744 p., Moscow: Nauka.

Shorin, S.N. (1947). Teploperedacha, 227 p., Izd.min.kom.khoz. (1952), Ibid. 339 p., Gosstriizdat. Moscow-Leningrad.

ASSESSMENT OF KEY DESIGN ASPECTS OF A 150 FOOT HIGH EARTH DAM ON WARM PERMAFROST

T.A. Hammer[1], T.G. Krzewinski[2] and G.G. Booth[3]

[1]Dames & Moore, Portland, Oregon
[2]Lakehead Testing Laboratory, Duluth, Minnesota
[3]Cominco Alaska, Anchorage, Alaska

SYNOPSIS Recently a 150 foot (50 meter) high earth dam embankment was designed to be built in an area underlain by relatively warm permafrost. Since few earth dams of this size have been constructed on permafrost, special design details and a positive performance monitoring scheme were incorporated in the design. This paper presents some design parameters, criteria and aspects unique to warm permafrost environment. Primary site selection and the geotechnical investigations are also covered in the paper.

INTRODUCTION

Development of the Cominco Alaska, Incorporated (CAI) Red Dog Mine will require the construction of a sea port with port facilities, a 54 mile long access road between the port and the ore deposit, and the mine facilities which include a tailings dam, water supply dam, mill facilities and waste containment areas for waste material. In 1982, a preliminary boring program was performed for the purpose of selecting mine support facility locations. With this data, the location of the tailings dam was selected. From June through August, 1984, Dames & Moore carried out the second of several geotechnical investigations at the proposed sites as well as investigated site alternatives for the Red Dog Mine facilities. During 1984, the tailings dam was investigated with a boring and testing program performed to obtain design level geotechnical data (Dames & Moore, 1984). A 150 foot high earth tailings dam embankment was subsequently designed. Incorporated into the design was the fact that the dam was to be built on relatively warm permafrost (Dames & Moore, 1987). The design included instrumentation of the dam to monitor performance of the embankment throughout its design life. Figure 1 is a detailed site plan of the tailings dam embankment and its associated seepage collection dam.

GEOLOGY

The Red Dog Mine project site is located at approximately Latitude 67° 66' north and Longitude 162° 58' west in the De Long Mountains of northwestern Alaska. Elevations in the site area range from 750 feet (250 meters) above MSL along Red Dog Creek to more than 2,000 feet (667 meters) above MSL on the western side of Red Dog Valley.

The northeast-trending De Long Mountains include extensively deformed, late Paleozoic to Mesozoic sediments deposited during a transgressive-regressive cycle in a large intracontinental basin. Near-shore clastics and open marine carbonates were deposited from Devonian to early Mississippian times. In the late Mississippian, an extreme carbonate platform containing a large black shale basin (including the Red Dog Deposit) developed. Turbidite flows, tuffaceous sediments and volcanic rock indicate tectonic and magmatic activity also occurred during this time. Stable marine conditions existed from the Pennsylvanian through the early Jurassic and resulted in the formation of shales, cherts, and limestones. Extensive tectonic activity occurred from the Jurassic to the late Cretaceous. Thick flysch sequences accumulated in the newly formed basins and troughs. The detritus was from systectonic volcanoes and the uplifted Paleozoic rocks. Afterwards, several periods of over-thrusting occurred, whereby plates of near-surface rocks were thrust over each other. The cumulative northward displacement exceeded 150 miles (265 Kilometers) in the region. These thrust plates were highly deformed by tight folds and low-angle thrusts. These events, along with erosion, resulted in the formation and topography of the De Long Mountains.

The proposed tailing dam on South Fork Red Dog Creek is underlain by interbedded Cretaceous shale and sandstone. The dark grey to brown sandstone appears as boudins (or "sausage" shapes) within the dark gray shale matrix. Slickensides are common throughout the formation in this area.

GEOTECHNICAL INVESTIGATIONS

The general area where the tailings dam embankment will be constructed was first drilled in 1982 when three borings were advanced at the locations indicated on Figure 1. In 1984, 10 additional borings were advanced within the footprint of the dam for the purpose of obtaining design level subsurface data. Both vertical and inclined boreholes were augered and/or cored to depths ranging from 30 to 150 feet

(10 to 50 meters) for the purpose of logging subsurface soil and thermal conditions, measuring in-situ soil and rock permeabilities, and obtaining undisturbed soil and rock samples for identification and laboratory testing.

SITE CONDITIONS

The proposed location of the tailings dam will be across the south fork of Red Dog Creek approximately 1,100 feet (367 meters) upstream (south) from the confluence with the main branch of Red Dog Creek. The site plan on Figure 1 contains contour lines which show general topographic and drainage features of the area. Bedrock outcrops are present along the west side of the creek.

Vegetation at the site consists mainly of a low growing, well-drained tundra mat with low bush vegetation growing near and along the creek. Bedrock outcrops and exposed colluvial soils are present along the steeper areas and alluvial deposits are exposed within the creek channel.

SUBSURFACE CONDITIONS

The borings revealed that a similar general subsurface profile exists throughout the site, which can be described as follows. The three borings on the west side of the creek, but not within the creek floodplain (SS-5-84, SS-6-84 and SS-7-84) revealed a profile consisting of 1/4 to two feet (8 to 60 cm) of Peat or organic silt over five to seven feet (1.7 to 2.3 meters) of highly weathered bedrock which graded more competent with depth. The weathered zone (upper eight feet-2.7 meters) contained a large quantity of excess ice (to 60%).

The two borings within the creek floodplain (SS-8-84 and SS-12-84) encountered a four to eight foot (1.3 to 2.2 meter) alluvial layer above the bedrock. The alluvium at boring SS-8-84 was cleaner (GP) than that found in SS-12-84 (GM), which is to be expected since SS-8-84 was within the present creek channel while SS-12-84 was slightly to the south of the existing creek channel.

The three borings on the east side of the creek (SS-9-84, SS-10-84 and SS-11-84) revealed a profile consisting of zero to four feet (6 to 1.3 meters) of peat and organic silt over four to fifteen feet (1.3 to 5 meters) of colluvial soils over weathered bedrock which graded more competent with depth. Going upslope (east) the peat and colluvial layers decreased in thickness.

The bedrock encountered in all the borings consisted of gray/black shales interbedded with sandstone. Joints and fractures generally filled with calcite were present in the rock. Numerous gouge zones were also present throughout the bedrock strata, but appeared to be discontinuous within the site area drilled.

The near surface soils were frozen in all boreholes drilled. The soils above the competent bedrock surface generally contained visible ice which occurred as individual ice crystals or inclusions, ice coatings on particles, as random or irregularly oriented ice formations, or as ice lenses greater than one-inch (2.5 cm) thick. The percentage ice, by volume, ranged from 4% to 60% (soils on the west side of the creek contained a much higher percentage of ice than the soils located on the east side). Borings SS-8-84 and SS-12-84 are located within the creek's thaw bulb and were found to be unfrozen below a depth of about 30 feet (10 meters) and eight feet (2.7 meters) respectively. Some visible ice was noted within the intact bedrock above a depth of about 30 feet (10 meters) but the frozen bedrock generally did not contain visible ice.

LABORATORY TESTING

Soil samples were tested to classify the soils encountered and determine their physical and engineering characteristics. The laboratory testing program included sample inspection, sample photography, soil classification, moisture-density measurements, mechanical and hydrometer grain-size analyses, Atterberg limits tests, constant head permeability tests, thaw consolidation tests and direct shear and triaxial shear strength tests.

FOUNDATION MATERIALS

Soils: Three classifications of soils were encountered across the site which are 1) surficial silts and organics, 2) colluvial soils, and 3) alluvium. Since all surficial silts and organics will be stripped prior to placement of the fills, properties of those materials were not determined. A battery of laboratory tests were performed on the colluvial and alluvial soils, the highly weathered bedrock and embankment material (Borrow) to determine the average physical and engineering properties.

THERMAL CONDITIONS

A total of ten thermistor strings have been installed at the tailings dam site for the purpose of monitoring ground temperatures. The data indicates the area is underlain by very warm permafrost with temperatures on the east abutment ranging from about 30°F to 31.5°F (-0.3 to -1.1°C). The west abutment ground temperatures are somewhat colder (27°F/-2.8°C at depth) which is probably due to the more northerly exposure of the west abutment. Two thermistor strings located in the creek floodplain indicate the creek's thaw bulb is about 60 feet (20 meters) deep.

DESIGN CONSIDERATIONS

Several design concerns were identified relative to specific site conditions. They were the extreme climatic conditions, the poor properties of the near-surface foundation materials and the availability of construction material.

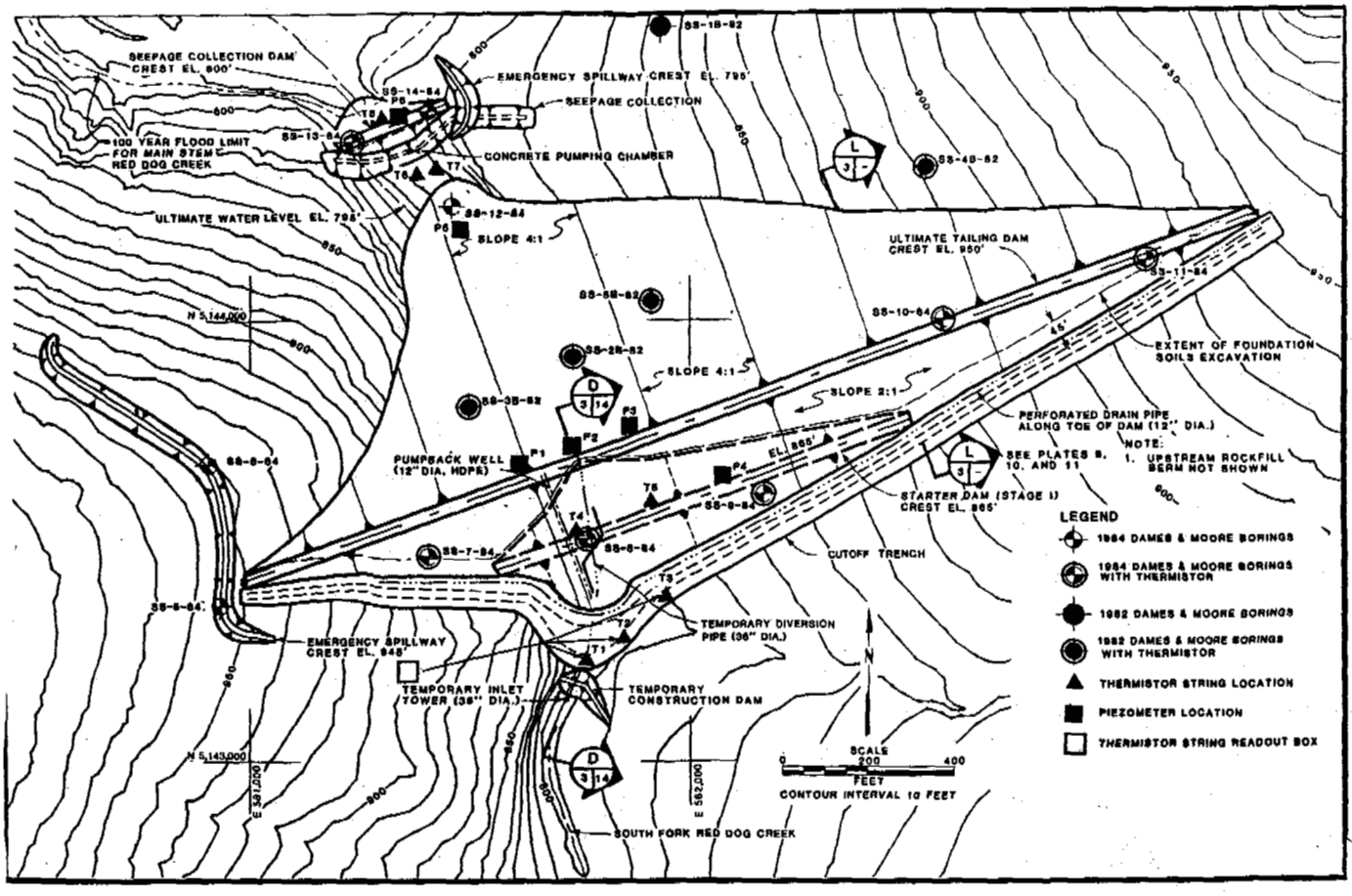

FIG. 1 TAILINGS DAM SITE PLAN AND INSTRUMENT LOCATIONS

Climatic conditions at the site dictate that a strict construction schedule be followed. Foundation excavation and backfilling for starter dam, seepage collection dam and cutoff trenches, as well as construction of the temporary diversion dam will be completed during the winter construction season which normally runs November to May. The fill placement and compaction for various components of the tailing dam will be performed during winter months, which dictates that careful quality control procedures must be followed.

Because the stability of the tailing embankment section may be affected under thawing conditions, certain design features had to be considered. Near-surface soil and highly weathered shale foundation material contain ice and, when thawed, will have relatively low strength and high compressibility. Should thawing occur, excess pore pressures may be experienced during the time immediately following loading induced by embankment placement. Thus, either the embankment section will require relatively gentle side slopes or the near-surface soils and upper, ice-rich shales must be removed.

Adequate borrow for construction of the embankment was located and is therefore not a major concern. However, suitable impervious core material was not available in significant quantities, so a synthetic liner design was utilized to control seepage loss through and beneath the dam. The synthetic liner will cover the upstream face of the dam and will also be extended into a trench cut into rock to minimize seepage under the embankment. A 100-mil-thick high density polyethylene liner was selected for use as the impermeable liner. As a safety factor against the unlikely situation where leaks formed in the liner, a filter drain was designed along the entire upstream slope so any seepage through the liner and into the filter drain will be removed by pumpback wells.

The dam was designed to be constructed in six stages as illustrated on Figure 2. To minimize the impact of thaw strain or creep settlement, Stage 1 was designed to be constructed on a foundation excavated to competent bedrock. If settlement was allowed to occur along the upstream face of the dam, damage and/or rupture of the liner could occur.

A knowledge of the thermal regime of the tailing dam and impoundment area is necessary for proper design in a permafrost zone. The tailing dam has been designed with a synthetic liner covering the upstream face, as well as with a cutoff trench through the upper foundation materials,

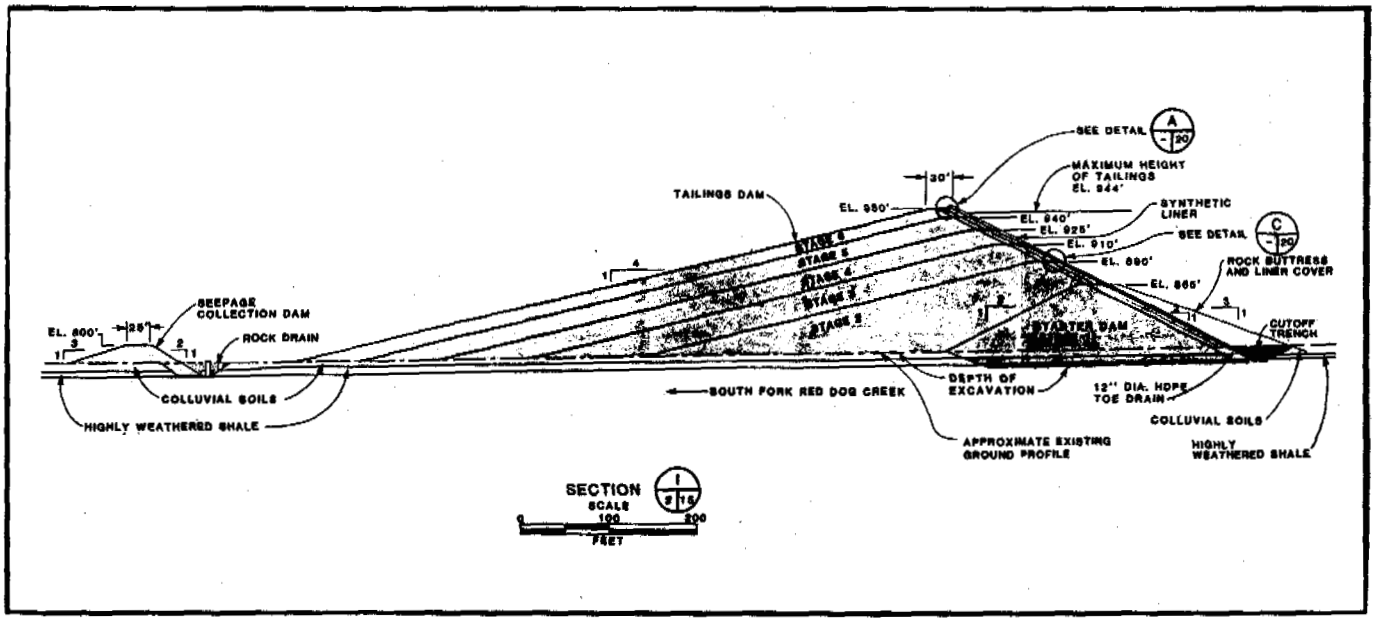

FIG. 2 TAILINGS DAM SECTION STAGED TO MAXIMUM HEIGHT

and thus is considered to be a relatively impervious dam constructed over a permafrost foundation. For this type of construction, it was anticipated that thaw penetration would be mainly downward below the reservoir and the upstream slope, and laterally from the reservoir into the structure and foundation. Furthermore, permafrost conditions will gradually advance into the dam section over the life of the operation. Modeling the thermal regime is complex due to the interaction of many factors, combined with the fact that some phenomena affecting the thermal state such as seepage volumes and heat input from tailings are not well defined. These thermal changes are further complicated by the proposed stage construction of the dam which may occur over a period of ten years or more.

Because of the anticipated permafrost degradation, seepage underflow was an important consideration. A seepage analysis was performed under the conservative assumption that a non-frozen zone will exist beneath the cutoff extending to a depth of 50 feet (17 meters). The seepage analysis considered the presence of non-frozen zones within the streambed prior to dam construction. Based on the maximum calculated seepage flows from material underlying the tailings pond bottom, a toe drainage pipe system was incorporated into the design.

ENGINEERING ANALYSIS

The stability of the proposed tailing dam was evaluated for static and seismic conditions using the computer program STABL2. Stability analyses were performed on critical sections of the dam to determine the minimum width of foundation excavation required and to evaluate different slope configurations for various stages of dam construction. Based on these analyses, it was computed that the starter dam (upstream and downstream faces) and the upstream face of the main dam could be safely constructed at a slope of 2:1 with varying degrees of soil excavation. Similarly, the downstream face of the main dam could be safely constructed at a slope of 4:1.

The soil properties outlined earlier were used in the analyses. A design horizontal earthquake acceleration of 0.05g was used for the dynamic analyses.

Excess pore fluid pressures are expected to develop in the foundation soils with placement of embankment fill. This increase in pore fluid pressure is related to the height of fill by the single parameter R_u. An R_u value is defined as the ratio between: 1) the total pore water pressure, and 2) the wet unit weight of a material times the height of material above the point under consideration. For these analyses, the excess pore pressure developed during thawing was taken to be equivalent to 66% of the total height of fill in areas where construction of the dam will be over ice-rich colluvial soils.

The two loading conditions considered in the analyses were 1) end-of-construction, and 2) long-term. For the first condition, seepage from the thawing ice-rich soil and any seepage through material underlying the dam and impoundment is considered sufficient to accelerate local thawing of the foundation materials. For long term conditions, it was assumed all excess pore pressure had dissipated and the foundation material had fully consolidated.

In later stages of the embankment, fill material will be placed over ice-rich foundation material. To predict settlement, it was estimated that the total ice content of an average 15-foot

thick soil/highly weathered shale horizon within the foundation area was about seven percent. The tundra and surficial soils were considered as being removed. Total thawing within the subsurface profile will result in about one foot (30 cm) of estimated subsidence due to the dissipation of the melted ice. Greater subsidence are expected in subsurface profiles containing higher ice contents. Subsidence of as much as two feet (60 cm) or more may be expected in some locations within the foundation area.

Hydrologic and hydraulic analyses were completed to assist with the design of the seepage collection system, the tailing dam and associated emergency spillways. The U.S. Army Corps of Engineers generalized computer program Flood Hydrograph Package (HEC-1) was used to develop inflow hydrographs, peak flow rates, runoff volumes, and to route hydrographs through the reservoir (U.S. Army Corps, 1981). A similar program for analysis of water surface profiles (HEC-2) was utilized to evaluate spillway flow characteristics (U.S. Army Corps, 1982).

INSTRUMENTATION

The long-term stability of both the seepage dam and the tailing dam is dependent upon assumed pore water pressures in the foundation material, the position of a phreatic surface in the embankment, if any, and permafrost conditions. High excess pore pressure and/or permafrost degradation beneath the embankment could influence the long term stability of the dam. Therefore, it was considered important that the tailing embankment be instrumented so that deviations from anticipated behavior of the embankment could be detected and appropriate measures be designed to compensate for such deviations. Piezometers and thermistors were specified to be installed in the dams to monitor subsurface water levels and temperature variations to verify the design assumptions. Pressure-type piezometers were specified to monitor seepage and pore pressure buildup within the potentially weak foundation soils and to monitor the phreatic surface within the rockfill embankment.

Measurement of the subsurface temperature variations before and after construction of the starter dam and subsequent embankment raises will be evaluated by installing thermistor strings to depths of about 100 feet (33 meters) below the base of the dam. The thermistor strings will be installed in sealed PVC pipe casing filled with silicon.

Figure 1 illustrates the locations of the instruments scheduled for installation within the embankment.

SUMMARY

The design of a 150 foot high tailing dam embankment at Red Dog was complicated by the fact that poor foundation conditions and fragile permafrost is present across the site. Due to the complexity of the hydrology, the predicted general degradation of permafrost within the impoundment, and staged construction, a quantitative analysis of the thermal performance beneath the embankment could not provide reliable results. Rather, simplified thermal procedures were utilized to predict permafrost aggradation into the dam section by the time the ultimate dam section is constructed. Liner tears, larger than anticipated flows through the underlying rock beneath the cutoff trench, or other factors could significantly alter the predicted thermal regime. Therefore, a positive monitoring scheme was developed to detect any deviations from the assumed thermal and hydrologic conditions as early as possible, so corrective measures could be instigated in a timely manner.

REFERENCES

Dames & Moore, 1984, Report of Geotechnical Investigation for the Red Dog Mine Tailings Dam, prepared for Cominco Alaska, Inc, December 3, 1984.

Dames & Moore, 1987, Design Report, Proposed Tailings Dam, Red Dog Mine Development for Cominco Alaska, Inc, July 1, 1987.

U.S. Army Corps of Engineers, 1981, Hydrologic Engineering Center, User's Manual, Flood Hydrograph Package, HEC-1.

U.S. Army Corps of Engneers, 1982, Hydrologic Engineering Center, User's Manual, Water Survace Profiles, HEC-2.

ACKNOWLEDGEMENTS

The project described in this paper was performed as part of the Red Dog Mine development project in Northwest Alaska. The authors wish to acknowledge Cominco Alaska, Incorporated, for permitting the authors to use the data presented in this paper as well as Cominco's project representatives, Mr. Tony Vecchio and Mr. Jerry Booth, who assisted us and monitored our work throughout the project.

PERMAFROST SLOPE DESIGN FOR A BURIED OIL PIPELINE

A.J. Hanna and E.C. McRoberts

Hardy BBT Limited, Alberta, Canada

SYNOPSIS The Interprovincial Pipe Line from Norman Wells, NWT to Zama, Alberta traverses many permafrost slopes. The paper reviews the slope stability design approach for this buried oil pipeline and presents a range of design parameters. A summary of the design configurations is also provided.

INTRODUCTION

During April 1985, Interprovincial Pipe Line Limited began delivery of oil through the 300 mm diameter Norman Wells pipeline 868 km south to Zama, Alberta. Discontinuous permafrost occurs over a large proportion of the pipeline route varying in thickness up to 50 m. The pipeline is fully buried but the properties of Norman Wells crude allow the oil to be discharged at -2° C thereby restricting thermal input into the surrounding soil. A description of this project has been provided by Pick et al (1984).

From Norman Wells south the pipeline parallels the east bank of the Mackenzie River for 500 km, crossing many tributary creeks and rivers. While the route was located so as to avoid major areas of known instability, permafrost slopes were unavoidable. In total over 165 slopes were identified as requiring geotechnical evaluation and site specific design response. The purpose of this paper is to present background information and the design methodology used in slope stability evaluations for the Norman Wells pipeline.

OVERVIEW OF DESIGN APPROACH

The slope stability design process began with the classification of likely failure modes. Following terminology established by earlier studies of permafrost slope failures (McRoberts, 1978), a matrix relating likely failure modes with thermal condition was developed, Table I. For frozen slopes, shear through permafrost is associated with specific geological conditions (McRoberts and Morgenstern, 1974) that were largely avoided by the pipeline. Conventional slope stability analysis methods and control measures were adopted for unfrozen or non-permafrost slopes and are not considered further. The major part of the design effort was therefore directed towards assessing thawing permafrost slopes. Skin flows or planar movements can develop as an active layer forms or penetrates deeper than normal beneath the thermally disturbed permafrost right of way (ROW). Excess pore pressures develop at the thaw front and can lead to unstable conditions depending upon rate of thaw, ice content, type of soil and slope inclination. As thaw proceeds deeper into the slope, two dimensional effects can be considered as a "thaw plug" develops. This thaw plug is confined by undisturbed permafrost terrain adjacent to the ROW. Ditch backfill placed during winter construction operation may also become unstable and is another form of a thaw plug.

TABLE I

Failure Modes

Failure Modes	Thermal Condition: Frozen	Unfrozen	Thawing
Skin/Planar	O	X	X
Plug	O	O	X
Ditch Backfill	O	X	X
Deep Seated	X	X	O

X-possible condition. O-unlikely condition.

While this paper concentrates on the geotechnical methods and procedures used for analytical design, other elements of the design approach were important and are considered briefly as follows. Slope design began during alignment location and where possible and practical, the centreline was located on previously cleared slope segments that had already experienced geothermal disturbance and thawing. In addition, areas of known instability were avoided and field reconnaissance was undertaken to check slopes for signs of instability or thermal erosion. All major permafrost slopes were drilled as well as a representative selection of other slopes. The slope catalogue, terrain analyses, and general knowledge of the route was relied on to establish likely soil and ice conditions in slopes which were not drilled. It was later possible to confirm these assumptions to some extent during the

construction phase through inspection of ditch walls. The permafrost soils encountered were subdivided into three major soils groups permitting a generalization of important soils properties for stability analyses.

The analytical design phase had two basic components which were to: (1) determine which slopes should be stable, and (2) establish practical mitigation techniques for potentially unstable slopes. It was also recognized that several aspects of the construction phase were an important component of the slope design approach. Firstly, a series of clearing and construction specifications were developed which would help to minimize the impact in sensitive terrain. Secondly, during construction it was anticipated that close monitoring of actual conditions as encountered in the pipeline ditch and in cuts would, if required, allow for design refinements and changes if necessary. It was recommended as an integral part of the design approach that once the pipeline went into operation a monitoring program should be instituted and contingency plans for remedial action should be available.

SOIL TYPES AND DESIGN INPUTS

The permafrost soils along the Norman Wells pipeline were subdivided into three broad categories as follows:

Ice Rich Clay (IRC)

Frozen glaciolacustrine silts, clayey silt and silty clay soils, fine grained colluvium or slope wash derived soils were classified as being ice rich clay. Such soils typically have water contents greater than 25 to 30%, plastic limits from 17 to 25%, and liquid limits between 35 and 70%. Thaw settlement tests on these soils indicate that at water contents of less than 20 to 24% little, if any, thaw settlement will occur. IRC soils are rarely encountered with water contents less than the 20 to 24% range within the depth of influence of geothermal effects caused by disturbance of the terrain. There was no ice poor clay category adopted for design purposes. In some slopes, high water contents in the order of 50% or greater, visible ice contents greater than 30 to 50% and thick ice lenses were encountered.

A summary of direct shear tests on initially frozen ice rich clay samples that were thawed when sheared, is given in Table II. Triaxial test data from some of these sites established lower bound strength parameters, c' = 12 kPa and $\phi' = 27.5^{\circ}$. Roggensack (1977) presented triaxial data of c' = 6.9 kPa and $\phi' = 26.5^{\circ}$ for silty clay from the Mountain River area and c' = 3.5 kPa and $\phi' = 34^{\circ}$ from the Fort Simpson region. All direct shear testing was undertaken at extremely low strain rates and at in situ normal stresses. For these tests a cohesion intercept was always obtained. This cohesion intercept would not be expected in normally consolidated clay soils. However, the influence of one or more freeze-thaw cycles is to densify the soil, impart some

TABLE II

Summary of Ice Rich Clay
Direct Shear Test Results

Location	c' kPa	ϕ' Deg.	c_v cm^2/s
IPL	3.5	26.5	
Sans Sault Test Site	3.5	30.5	1.5×10^{-3}
Hanna Creek	4.1	26.7	5.0×10^{-3}
Billy Creek	6.9	24.5	2.5×10^{-3}
Great Bear River	3.5	26.0	6.0×10^{-3}
Willowlake River	4.1	27.5	7.0×10^{-3}
Martin River	3.5	24.5	2.5×10^{-3}
East Simpson Crossing	2.5	30.5	7.0×10^{-3}
Naylors Landing	1.7	29.0	6.0×10^{-3}
Design Value	3.5	24.5	2.5×10^{-3}

degree of fabric and to impose a stress history of over-consolidation (Nixon and Morgenstern, 1973). Therefore, the laboratory observation of a cohesion intercept is reasonable and can be relied on in the field. Design strength parameters, c' = 3.5 kPa and $\phi' = 24.5^{\circ}$ were selected for IRC soils.

In order to undertake an analysis of excess pore pressure effects, the coefficient of consolidation (c_v) is required. A summary of test results is given in Table II following interpretation methods presented by McRoberts et al (1978).

Ice Poor Till (IPT)

These tills are dense soils with water contents typically less than 10 to 15%. Thaw settlement tests indicate that tills with these low water contents will not settle on thawing and, in fact, exhibit a minor tendency to swell. In some frozen slopes a minor component of dense frozen sands or silty sands can occasionally be encountered. For analysis purposes these well draining soils were considered equivalent to ice poor till. All strength data for till has been assembled on Figure 1, with the average strength line established for design indicated. Data for c_v

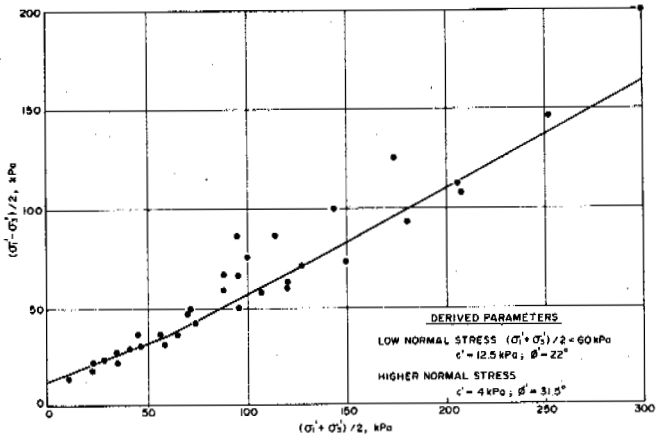

Figure 1. Strength data for ice poor till

varies over a wide range from as low as 4×10^{-4} cm^2/s to a high of 2×10^{-2} cm^2/s. An average c_v is in the range of 5×10^{-3} to 1×10^{-2} cm^2/s.

Ice Rich Till (IRT)

An intermediate category of ice rich till was adopted for design purposes. This classification was used for till soils which have some visible ice and higher water (ice) contents.

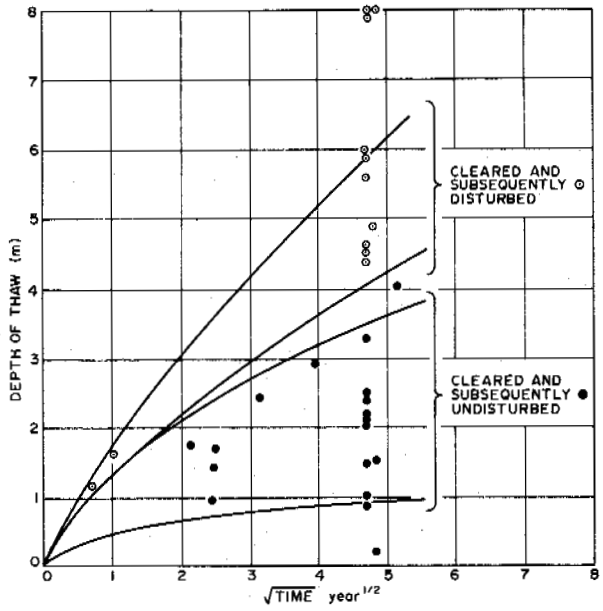

Figure 2. Thaw degradation beneath cleared areas

Depth of Thaw Observations

A fundamental component of stability analyses is the thaw depth following tree clearing and construction. Field observations from the central Mackenzie Valley (Figure 2) indicate moderate degradation for a disturbed slope (i.e., complete removal of vegetation and severe damage to the surface mat) and the expected thaw depth is about 4 to 6 m in 25 years. A relatively undisturbed slope (removal of trees only) may thaw from about 1 to 4 m in 25 years, and in some instances, the permafrost does not appear to degrade at all. Therefore, it is desirable for the pipeline to be constructed with a minimum amount of ground surface disturbance. More detailed interpretation indicates that the width of the disturbed ROW influences thaw depth. This is in accordance with theory, although the effect is difficult to quantify because of uncertainty in the permafrost temperature. Available data (Figure 3) indicates that limiting the ROW width can reduce the long-term thaw depth. Figure 4 presents the design thaw depth progression used for the 13 m wide ROW selected for construction on ice-rich slopes.

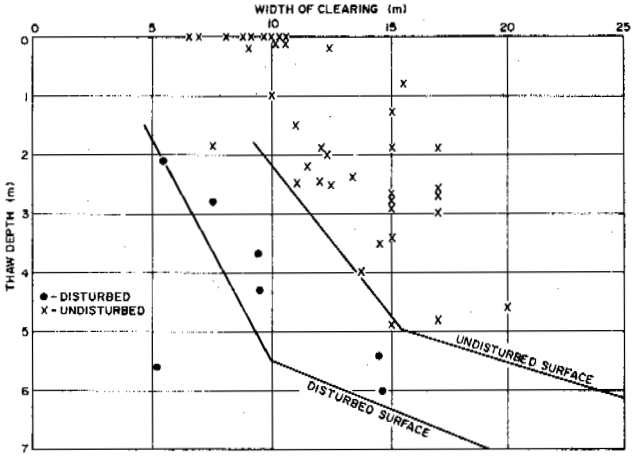

Figure 3. Thaw depth versus width of clearing

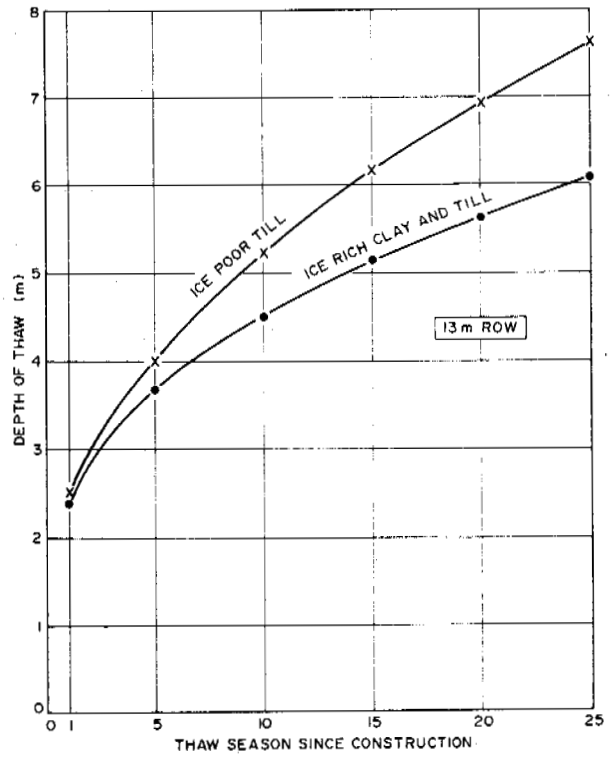

Figure 4. Design thaw progression

Failures in Thawing Slopes

During the late 1970's a detailed program of field investigation, laboratory testing and analyses of thawing slopes was undertaken in the Mackenzie River Valley. As part of this study five slopes, which had failed in a skin flow or planar mode due to a variety of surface disturbance effects, were investigated, Table III. All these slopes are IRC category and from 13° to 19° in inclination. Once failure began, slope angles in the order of 8° to 12° were formed. Adjacent slopes, in what appeared on a visual basis to be identical soils, were stable on inclinations of 4° to 10°. These data taken together suggest that slopes in the order of

TABLE III

Summary of Skin Flow Failures

Site	Disturbance Effect	Slope Angle (Degrees)		
		Initial	Failed To	Adjacent Stable
Sans Sault	Pipeline test installation, winter construction, mechanical tree clearing	16	11	9
Hanna Creek	Forest fire with deep burn in dry surface organics	16	10-12	4
Billy Creek	Ground fire and toe erosion	19	10	10
Martin River	Highway ROW clearing and springthaw traffic	13	9	6
Naylors Landing	Hand clearing of trees for navigation marker Mackenzie River	18	8	10

8^{o} to 10^{o} or less are likely to be stable as long as gross disturbance to the surface cover is avoided.

Pore Pressures in Till

For IPT soils, the low water (ice) contents and the tendency of the soils to actually swell during thaw settlement tests, suggest that low pore water pressures would be encountered in thawing slopes. Piezometers and standpipes were installed in boreholes drilled during the slopes investigation programs in existing thaw bulbs of depths from 1.0 to about 5.0 m. Figure 5 plots all observed data in terms of the pore pressure ratio m, as defined in Figure 5, versus the depth of thaw, d. This data indicates that in most cases very low pore pressure conditions were observed.

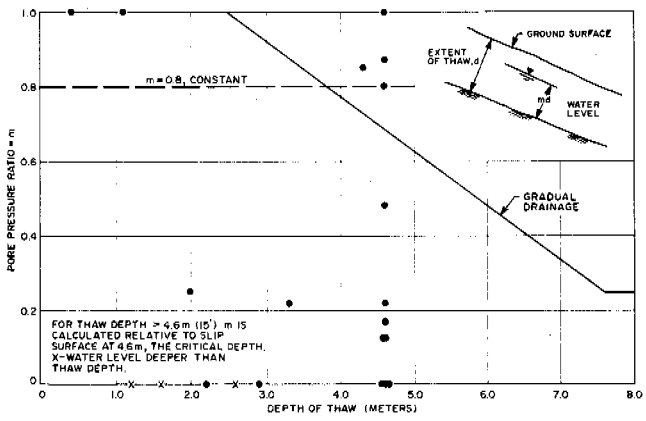

Figure 5. Pore pressures in thawed till slopes

SLOPE DESIGN

A major design decision was to establish the cut-off angle, below which thawing would not result in unstable slopes. Several factors had to be considered. Firstly, the impact of construction disturbance and ROW width was judged to be relevant. It was felt that a 13 m ROW, with hand clearing of trees and minimal surface disturbance would support steeper slopes than a 20 m ROW with complete removal of surface organics and insulating layer. Secondly, the desirable factor of safety (FS) for static loading conditions was in the range, 1.25 to 1.5. Seismic loading was also considered, by applying a 12% horizontal acceleration, and a pseudostatic factor of safety equal to or greater than unity was judged necessary. As thaw proceeds, a transition from infinite slope to thaw plug mechanism had to be considered. The relative influence of moderate effective cohesion, for example c' = 3.5 kPa for IRC, was important at shallow thaw depths. The influence of excess pore pressure generation became less with subsequent thaw seasons (McRoberts et al 1978). Finally the empirical evidence from a range of failed slopes had to be considered.

The long shallow or planar nature of a thawing slope in a cleared pipeline ROW can be readily analyzed by an infinite slope method. For thawing slopes in soils such as ice poor tills the conventional form of the analysis, Equation 1, Figure 6 can be used. In IRC and IRT slopes, excess water pressures generated by thawing of the frozen soil must be incorporated into the appropriate form of the equation to obtain Equation 2, Figure 6 (McRoberts, 1978). For the thaw plug case, where a cleared ROW of finite width is considered, there will be increased side shear resistance along the edges of the thaw bulb corresponding roughly to the width of the ROW. This increased resistance can be incorporated into the infinite slope stability equation, to produce a more general form, Equation 3, Figure 6 (McRoberts, 1978).

An example of the application of this method is as follows. Consider an IRC slope with design parameters as summarized in Table II, and refer to Figure 6 for terms and equations. For a badly disturbed surface, the geothermal analysis indicated $\alpha = 6.1 \times 10^{-2}$ cm/s$^{1/2}$ compared to a value of $\alpha = 3.4 \times 10^{-2}$ cm/s$^{1/2}$ where about 240 mm of peat cover is left

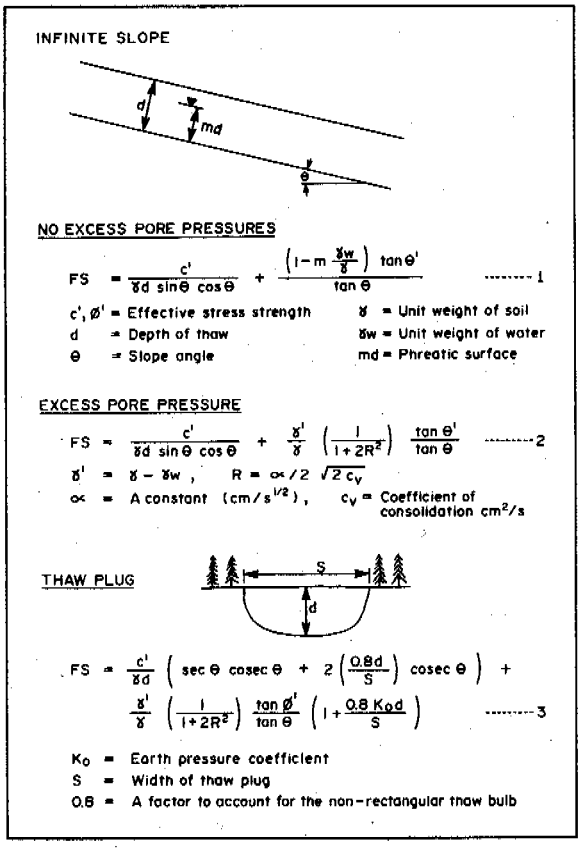

Figure 6. Thaw stability analysis

intact. For a c_v of 1 x 10^{-3} cm^2/s, the R value ranged from 0.34 to 0.61. In the immediate vicinity of the pipeline ditch it is clear that some significant disturbance will be caused. Accordingly, a value of R=0.47 was selected for the first thaw season in IRC slopes. Other design inputs were a thaw depth of 2.4 m and a ratio γ'/γ= 0.5. For the infinite slope equation an FS of 1.47 is predicted for a 9° slope. Assuming c' = 0 the FS = 1.0. With subsequent thaw seasons thaw proceeds deeper according to Figure 4. The influence of c' becomes less, but is more than offset by thaw plug effects and a reduced equivalent R value.

The initial design configuration considered a 13 m ROW and limited surface disturbance. A cut-off angle of 9° was adopted for IRC slopes. This value was consistent with experience on, or adjacent to, documented skin flow failures. As the design evolved, construction practice requiring a wider ROW and peat removal was accommodated. For a wider ROW and complete peat removal the cut-off angle for IRC slopes was reduced to 7°. A summary of the design cut-off angles is presented in Table IV.

The stability of the backfill in the pipeline trench was also considered. It was anticipated that either backhoes or wheel ditchers would be used to excavate the pipeline ditch. Material excavated by backhoe was likely to be larger and more irregularly

TABLE IV

Cut-Off Angles for Thawing Slopes

Construction Condition	Non Insulated			Backfill	
Peat Removal ROW Width	Nil to 20 m	Complete 13 m	Complete to 20 m	Backhoe Spoil	Wheel Ditcher Spoil
Soil Category					
IRC	9	8	7	4	7
IRT	13	12	11	7	10
IPT	18	18	17	10	14

sized than ditcher spoil. Maintaining a stable ditch configuration was required in order to prevent lateral retrogression of thawing permafrost and for drainage and erosion control. Design cut-off angles established for excavated spoil used as ditch backfill are given in Table IV.

Pipeline ROW segments with inclinations greater than the cut-off angles required mitigative action. In some IRC slopes ground ice contents were sufficiently high that the design recommendation was to essentially eliminate thaw below the naturally occurring active layer. Otherwise, the mitigative design tolerated some thaw as long as minimum factors of safety were obtained. A variety of solutions were considered, including a gravel/synthetic insulation sandwich, wood chips and a wood chip/synthetic insulation sandwich. Design procedures for such a method were developed by McRoberts and Nixon (1977). The method accounts for the retarding influence of insulation on the rate of thaw and excess pore pressure generation and the surcharge effect from a free draining layer, such as gravel, increasing the mobilized effective shear strength.

Wood chips were selected as the primary design mode for several reasons as documented by McRoberts et al (1985) who also presented the geothermal considerations involved with wood chip design. Heat generation within the wood chips was recognized in predicting the geothermal performance of the wood chip insulation.

The slope stability design proceeded using the infinite slope method, as modified for insulation effects by McRoberts and Nixon (1977). An FS of at least 1.5 was required and the thickness of wood chips necessary to maintain a minimum FS of 1.5 over a design life of 25 years was obtained, see insert to Figure 7. For example, for a 12° IRC slope a 600 mm thickness of wood chips was predicted for the case of a 13 m ROW with no peat removal and with an average of 150 mm peat assumed present. The design predictions allowed for variations in construction practice. These modifications were based on the predicted increase in depth of thaw consequent upon increases in ROW width and peat removal. For example, if a 600 mm wood chip thickness is required for the "13 m ROW + Peat" case, the predicted maximum allowable

thaw depth is 2.4 m. For the "Peat Removal + 20 m ROW" case, Figure 7, 1000 mm of wood chips are required to maintain the same depth of thaw below the wood chips.

In some instances mitigative action was also necessary where cross-slope grading was required to provide a level working surface for pipeline installation operations. Side hill cuts were designed to 2.5 horizontal:1.0 vertical in unfrozen or ice poor soil. Cuts were made vertical in ice rich terrain. Some longitudinal slopes had side cuts and if the slope required insulation the wood chips were ramped up and over the side cut.

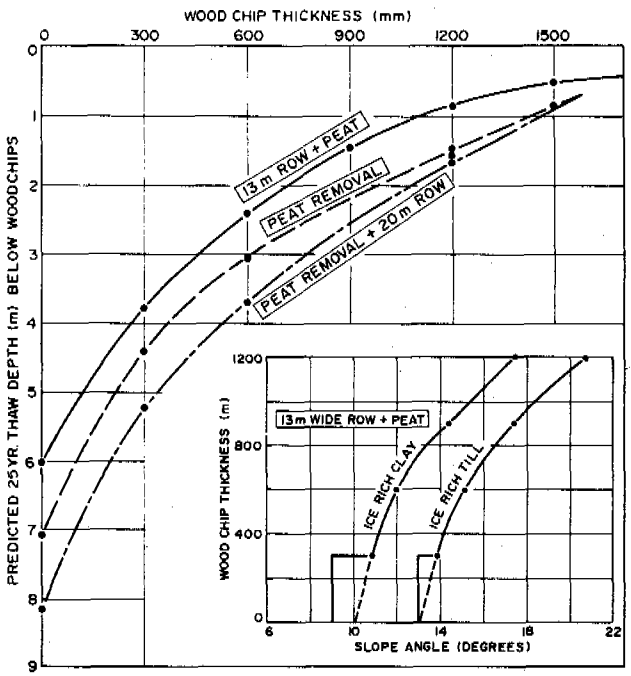

Figure 7. Design insulation requirements

Mitigative measures in the form of select granular backfill, ditch plugs, surface diversion berms and breaks in the backfill mound were used to control potentially adverse drainage conditions along the ROW. Seeding and fertilizing was another important means of reducing erosion potential.

CONCLUDING REMARKS

The slope stability design for the Norman Wells Pipeline Project incorporated geothermal and stability analyses as well as empirical information on previously failed slopes. The stability analyses were based upon the infinite slope theory which was modified to incorporate the effects of pore pressure generation and dissipation, the effects of a thaw plug and a layered profile, accounting for the surcharge and insulating effects of the wood chips. The design itself presented some restrictions to construction practice, such as a narrower ROW, and also provided for field design changes if these restrictions could not be satisfied. Finally, the design stipulated some ground temperature and pore pressure monitoring.

In the spring of 1985, construction of this first fully buried oil pipeline in permafrost terrain was completed. Slope stability designs and wood chip surface insulation continue to provide thermal protection to permafrost slopes susceptible to instability due to thawing. To date, the performance of slopes has been satisfactory with the exception of minor erosion problems and the stability of side cuts aggravated by non-adherence to design specifications. The majority of the wood chip insulation has performed as assumed in the design. Some heat generation persisted on a localized basis on certain slopes (Pick, 1987), however, these situations have been rectified.

REFERENCES

McROBERTS, E.C., FLETCHER, E., & NIXON, J.F. (1987). Thaw consolidation effects in degrading permafrost. Third Intl. Conf. Permafrost, Vol 1, pp 694-699.

McROBERTS, E.C., HANNA, A.J., & SMITH, J. (1986). Monitoring of thawing permafrost slopes: Interprovincial Pipe Line. NRCC Tech. Memo 139, pp 133-151.

McROBERTS, E.C. (1978). Slope stability in cold regions. Geotechnical engineering for cold regions. McGraw Hill Book Co., Editors: Andersland, O.B. and Anderson, D.M.

McROBERTS, E.C., & MORGENSTERN, N.R. (1974). Stability of slopes in frozen soil, Mackenzie Valley, N.W.T., Vol II, pp 554-559.

McROBERTS, E.C., & NIXON, J.F. (1977). Extensions to thawing slope stability theory. Proceedings Second Intl. Symposium on Cold Regions Engineering, University of Alaska.

NIXON, J.F., & MORGENSTERN, N.R. (1973). The residual stress in thawing soils. Can. Geot. Jnl., Vol. 10, p. 571.

PICK, A.R. (1987). Use of wood chips for permafrost slope stabilization. CSCE Centennial Conf., Montreal, May 19-22, 1987.

PICK, A.R., SANGSTER, H., & SMITH, J. (1984). Norman Wells pipeline project. Proc. ASCE/CSCE Third Intl Conf. on Cold Regions Engineering. April 4-6, Edmonton, pp 11-18.

ROGGENSACK, W.D. (1977). Geotechnical properties of fine-grained permafrost soils", Ph.D. Thesis, University of Alberta, Alberta.

A METHOD FOR CALCULATING THE MINIMUM BURIED DEPTH OF BUILDING FOUNDATIONS

Jiang, Hongju and Cheng, Enyuan

Oilfield Construction Design and Research Institute of Daqing Petroleum Administrative Bureau

SYNOPSIS A method for calculating the minimum buried depth of building foundations in seasonally frozen ground is presented. The method is based on the principle that the frost heave deformation of a foundation should not exceed the allowable deformation of the building. The method has been applied to the design of four experimental buildings with satisfactory results.

INTRODUCTION

When the buried depth of a building foundation constructed in seasonally frozen ground is less than the maximum frost penetration, a frozen layer will occur under the foundation. If the soil is frost susceptible, the overlying building foundation will be lifted due to frost heaving of the ground. Observations have shown that frost penetration under a building foundation is variable; hence, the amount of frost heave of the subsoil beneath the foundation may be non-uniform, resulting in differential deformation of the building. When this exceeds the allowable deformation, the walls of the building will tilt, with possibly permanent demage resulting.

The maximum thickness of frozen ground under a foundation, for which the frost heave deformation does not exceed the allowable deformation of the building, is defined as the allowable thickness [d] . The minimum buried depth (h) of a foundation in consideration of frost heave is defined as the difference between the calculated frost penetration (H) and the allowable thickness [d] of frozen layer beneath the foundation, i.e.,

$$h = H - [d] \qquad (1)$$

CALCULATED FROST DEPTH OF SUBSOILS

The calculated frost depth of subsoil refere to the maximum actual frost depth of the soil under foundation after construction of the building. Based upon field observations for many years, this may be estimated by

$$H = m_h \cdot \psi_T \cdot Z_o \qquad (2)$$

where m_h--an empirical coefficient dependent upon the frost susceptibility of the soil;
ψ_T--influence coefficient of heating in buildings on frost depth; and
Z_o--the so-called standard frost depth in the construction area [1].

The values of m_h and ψ_T can be determined from Tables I and II.

TABLE I

Values of the Coefficient m_h in eq.(2)

Frost-susceptibility		m_h
Non	$\eta \leq 1\%$	1.1
Weak	$1\% < \eta \leq 3.5\%$	1.0
Medium	$3.5\% < \eta \leq 6\%$	0.98
High	$6\% < \eta \leq 12\%$	0.9
Very high	$\eta > 12\%$	0.85
Non-frost-susceptible fine sand:		
Saturated	$H_w \leq 1.5$m	0.85
Wet	$1.5\text{m} < H_w \leq 2.5$m	1.0
Slightly wet	$H_w > 2.5$m	1.2

Note: (1) H_w--groundwater level before freezing;
(2) η --frost heave ratio of subsoil.

TABLE II

Values of the Coefficient ψ_T in eq.(2)

Relative height of building floor above ground surfact Δh, cm	Values of ψ_T	
	At the corner of peripheral wall	At the middle of peripheral wall
≤ 30	0.85	0.7
$=75$	1.0	0.8
>75	1.0	1.0

Note:(1) When monthly mean temperature in building is lower than 10°C, ψ_T=1 for heated buildings; ψ_T=1.1 for unheated buildings.
(2) The dividing of the corner and the middle of a peripheral wall is the same as

stated in the Standard of Foundation Design in Industrial and Civil Architecture (TJ7-74).

(3) The values in this table are incorporated in the modified version of Standard of Foundation Design in industrial and Civil Architecture 1985.

METHOD FOR CALCULATING THE ALLOWABLE THICKNESS OF FROZEN LAYER UNDER BUILDING FOUNDATION

Based on our investigation, the allowable frozen layer thickness, [d], under a building foundation can be calculated by

$$[d] = \frac{[\Delta s]\ (1+\bar{\eta})}{\bar{\eta}\cdot\lambda} \qquad (3)$$

where [Δs]--the allowable deformation. For a one-story brick building, [Δs] is taken as 10 mm; for a multi-story building, [Δs] is 15 mm.

$\bar{\eta}$ --the mean frost heave ratio of subsoils concerned. It can be determined from in-situ observational data, or from Fig.1 if there are no data.

λ --a coefficient to account for the effect of load on the frost heave. It is determined from Fig.2.

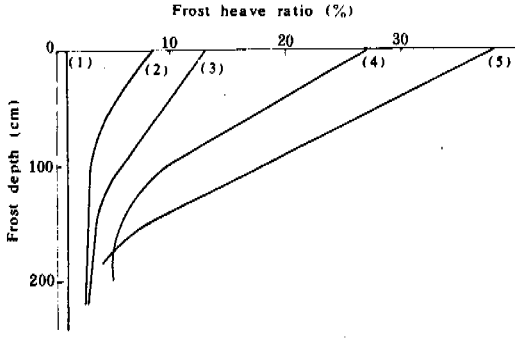

Fig.1 Distribution of Frost Heave Ratio Along Frost Depth for the Subsoil of:
(1) non-frost heave, (2) weak frost heave, (3) medium frost heave, (4) high frost heave, and (5) very high frost heave.

CALCULATION OF THAW SETTLEMENT OF THE FROZEN LAYER BENEATH FOUNDATION ALLOWED IN WINTER

Field observations of experimental foundations

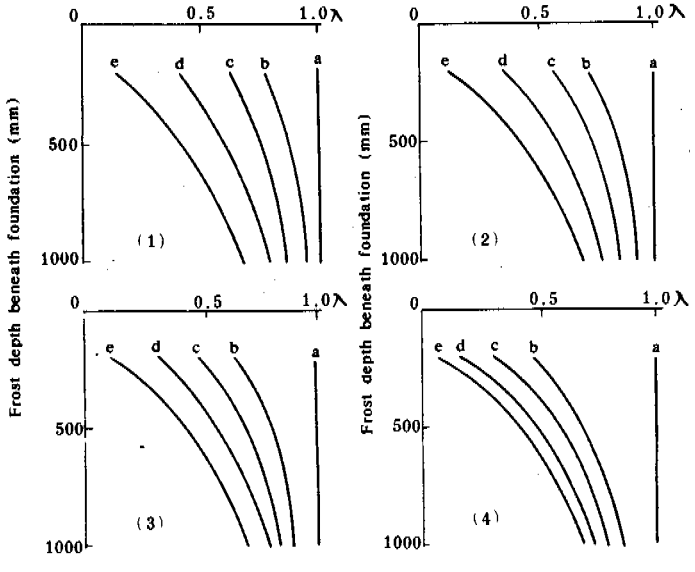

Fig.2 The Coefficient vs. Frost Depth Beneath Foundations with Various Applied Loads:
a--0 kPa, b--30 kPa, c--80 kPa, d--130 kPa, and e--180 kPa for: (1) weak, (2) medium, (3) high, and (4) very high frost susceptible subsoils.

have shown that the subsoils beneath the foundations settle due to thawing after experiencing frost heave in winter. After the frozen layer under a foundation completely thawed, the level of the foundation base was not the same as before frost heave, but was lower. For foundations with the same buried depth and similar soil conditions, the higher the applied load, the less the frost heave deformation, but the greater the thawed settlement. The tests also showed that the greater the frost-heaving ratio of the soil, the more the thawed settlement is, when the applied load is the same. Because the amount of thaw settlement under foundations is greater than the frost heave, the design of a foundation should be based not only on determination of the allowable thickness of frozen soil under the foundation from eq.(3), but also on the thaw settlement of the frozen layer estimated from the following criterion

$$[\Delta s] \geq \Delta s_p = \beta \cdot [d] \qquad (4)$$

where Δs_p is the ultimate thaw settlement of the frozen layer underneath the foundation, and β is the so-called "thaw settlement ratio", defined as the ratio of $\Delta s_p/[d]$ in percent. The value of β may be determined from Fig.3.

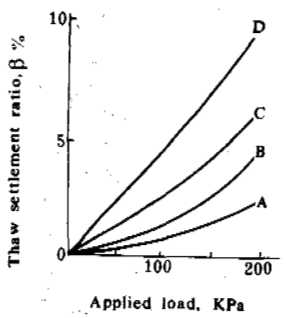

Fig.3 Thaw Settlement Ratio β vs. Applied Load for:

(A) weak, (B) medium, (C) high, (D) very high frost susceptible subsoil.

VERIFICATION OF THE METHOD

Although eqs.(1) and (3) were developed from reasonable assumptions, and the parameters used were determined from field tests, the reliability in engineering practice must be verified.To this end, four experimental one-story brick houses were designed with the above method, constructed in the summer of 1984 and put into use in November of the year. The deformations of the houses were measured periodically. In addition, 36 experimental buildings constructed before 1984 were also checked according to the equations. The results of observations and calculations showed that all of the buildings(either one-story or multi-story) for which the foundation buried depth conformed to the above method, had no cracks or damage.

CONCLUSIONS

(i) Observations on experimental buildings showed that the actual deformation was less than the calculated value. Therefore, based on this, the proposed method for calculating the minimum buried depth of foundation in consideration of soil susceptibility is reliable.

(ii) In calculating the minimum buried depth of foundations by the proposed equations, the change of frost susceptibility of subsoil due to an increase in wather content and/or a rise of the water table during operation of the building should be taken into consideration.

(iii) The proposed method for calculating the minimum buried depth of foundations in seasonally frozen subsoil considers not only the freeze-thaw susceptibility of subsoils but also other various factors so as to make the determined minimum buried depth reasonable.

(iiii) Compared to other available design methods, the buried depth of foundation determined by the proposed method is 40-90 cm less, i.e., a reduction of 20-50% in routine design depth. As a consequence, the cost of foundation engineering can be greatly reduced.

REFERENCE

Standard of Foundation Design in Industrial and Civil Architecture (TJ7-74). Chinese Architecture Publishing House, 1974.

PROTECTION OF WARM PERMAFROST USING CONTROLLED SUBSIDENCE AT NUNAPITCHUK AIRPORT

E.G. Johnson and G.P. Bradley

Department of Transportation and Public Facilities, State of Alaska

SYNOPSIS The selected alignment for the Nunapitchuk Airport required that it be constructed over virgin tundra underlain by warm permafrost consisting of massive ice and ice-rich silt. If not adequately considered, the resulting thaw would cause settlement differentials of several m. The concept of controlled subsidence was used to reduce such settlements to a tolerable level. The design included 1.22 m of embankment with 0.15 m of insulation board placed 0.61 m from the surface. Thermal calculations using iterations of the Modified Berggren Equation indicated that the settlement could be as much as 0.15 m in 20 years in the underlying permafrost. Embankment construction was completed the spring of 1985. As of September 1987, no thaw had occurred in the underlying permafrost as predicted by the initial calculations. It appears that the embankment is performing as designed.

INTRODUCTION

Nunapitchuk is an Eskimo village of approximately 350 residents located along the shore of the Johnson River approximately 40 km west-northwest of Bethel, Alaska. No roads service Nunapitchuk and prior to the construction of the airport, the nearest airport was a 6 km boat or snow machine trip. During spring breakup and fall freeze-up travel was severely limited, making the delivery of freight and mail very unreliable. Medical emergencies had to be evacuated to Bethel by helicopter during these periods.

CLIMATOLOGY

The climate is more marine than continental which tends to lessen the daily temperature extremes. The nearest weather station is at Bethel from which the following data were recorded. During June and July the temperature rises noticeably under the influence of warmer continental air. Extreme air temperatures recorded ranged between -47° C in January and 32° C in June. The average last day of freezing is May 30 and the average first day of freezing is September 9. The annual mean air temperature is -1.7° C. Annual precipitation averages 0.43 m with August, the wettest month, averaging slightly over 0.15 m. Snow fall averages 1.25 m per year with a maximum amount of 1.46 m recorded in January 1952.

GEOLOGY AND TOPOGRAPHY

Nunapitchuk is located in the southeast portion of a major physiographic division of Alaska termed the Yukon-Kuskokwim Lowland, which is a portion of a vast delta formed by the Yukon and Kuskokwim Rivers (Figure 1). Pleistocene delta deposits comprised of silt and sand, and Holocene floodplain alluvium deposited by the Kuskokwim River are the two main contributors to the surficial geology in the vicinity of

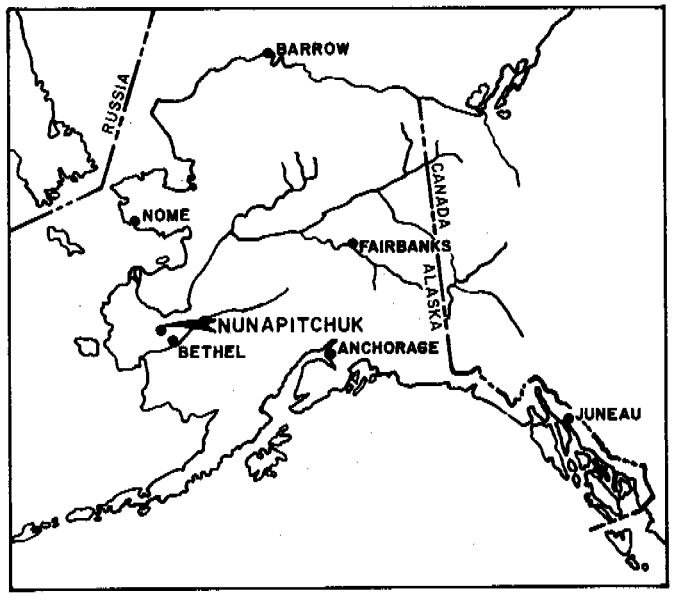

Figure 1 Location Map

Nunapitchuk. A water well, drilled near the Bethel airfield, encountered 130 m of predominately frozen deltaic sediments. Nunapitchuk has been mapped as lying in the area underlain by continuous permafrost.

The Nunapitchuk Airport is located approximately three-quarters of a mile northeast of the village on the north side of the Johnson River (Figure 2). The airport is situated on some of the only high ground in the area that contains sufficient room to develop an airport facility. Even so, the average airport elevation is less than two m above the surrounding lakes and sloughs.

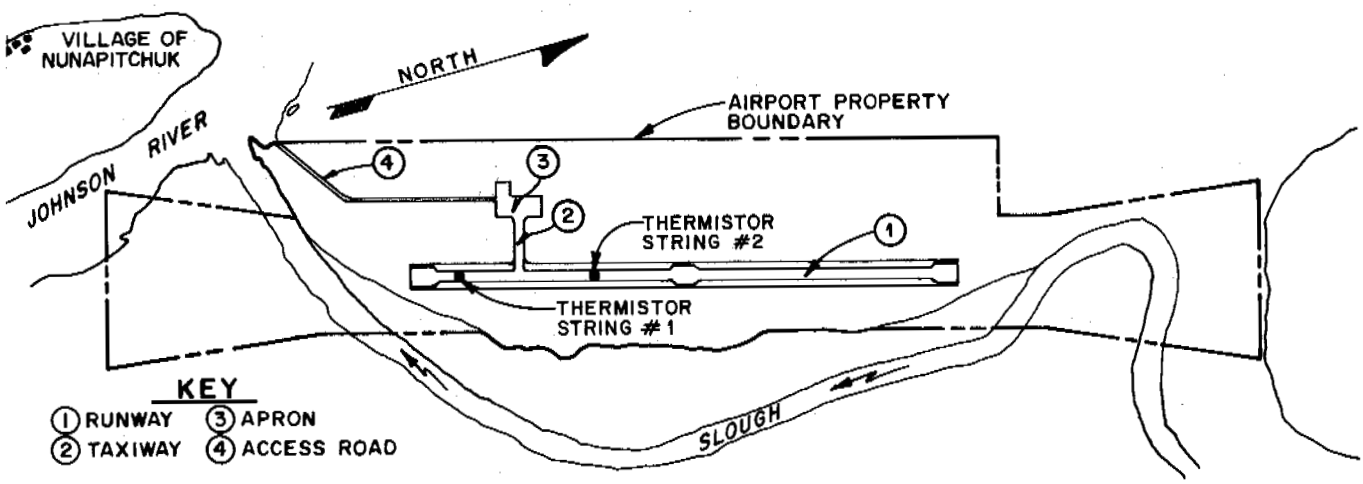

Figure 2 Airport Layout

SOILS

A subsurface field investigation of the proposed alignment was conducted in February and March of 1983 by personnel from the Alaska Department of Transportation and Public Facilities (DOT/PF) Materials Section (Pavey, 1983). Five test holes were placed along the alignment of the proposed embankments. The holes were advanced using a Mobile B-24 auger drill. The test holes were sampled using modified Shelby tubes - standard Shelby tubes with carbide chips brazed to the tip to provide cutting teeth. A fifth test hole was drilled with solid flight auger. Samples were taken from the auger flights.

Frost polygons were evident along the northern and southern thirds of the runway alignment. Test holes advanced along the alignment encountered a layer of frozen organics that overlaid ice or silt and ice combinations containing an estimated 50% or more visible ice. The silt and ice also contained organic matter. Figure 3 provides a profile of an example test hole.

A subsequent field investigation was conducted in November, 1983 to locate a suitable source of embankment material. The nearest site was identified on a gently rolling barren plain approximately 10 km northeast of the proposed airport (Figure 4). The usable portion of the borrow site contained sand to silty sand that was perennially frozen a varying depths below the active layer. However, the relatively low moisture content and silt content as well as the laboratory compaction test results indicated that this site was the most viable for use as embankment fill on the project.

DESIGN

The scope of the project included embankment construction of a 36.6 by 762 m runway safety area, a 12.2 by 621 m taxiway, a 30.5 by 61 m aircraft parking apron, and a 4.3 by 366 m access road (Figure 2). All embankments were designed to be constructed by overlaying the natural ground cover. Due to ice rich materials below the surface of the proposed

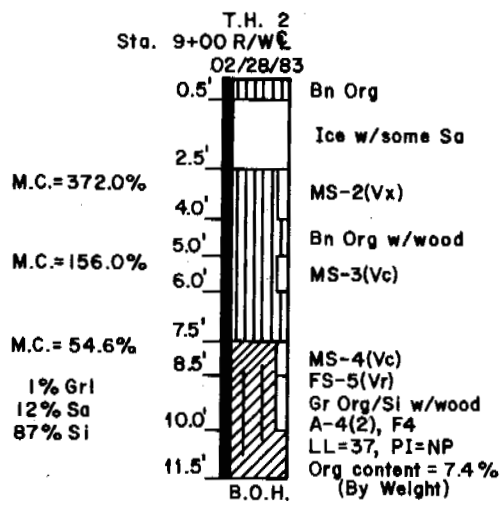

Figure 3 Test Hole

embankments, special design considerations were employed. Several embankment solutions were initially evaluated: 1) 1.2 m of silty sand material, 2) embankment with 0.10 to 0.15 m of insualtion, and 3) embankment with a passive refrigeration system (thermosyphons) without insulation.

To estimate the long term settlement for the various design alternatives the thermal portion of a roadway life-cycle costing computer program developed by Woodward-Clyde Consultants (Kulkarni et al., 1982) for the Alaska Department of Transportation and Public Facilites was used. The program uses iterations of the Modified Berggren Equation (USA Army, 1968) for multiple years, taking into account the amount of thaw consolidation and embankment settlement that will occur in a given year. To do this, the program calculates the settlement based on the input of initial and final void ratios and subtracts the settlement from the thickness of the consolidating layer. The thermal properties of the consolidated layer are adjusted to account for the change in moisture content. The program also calculates any talik that may form

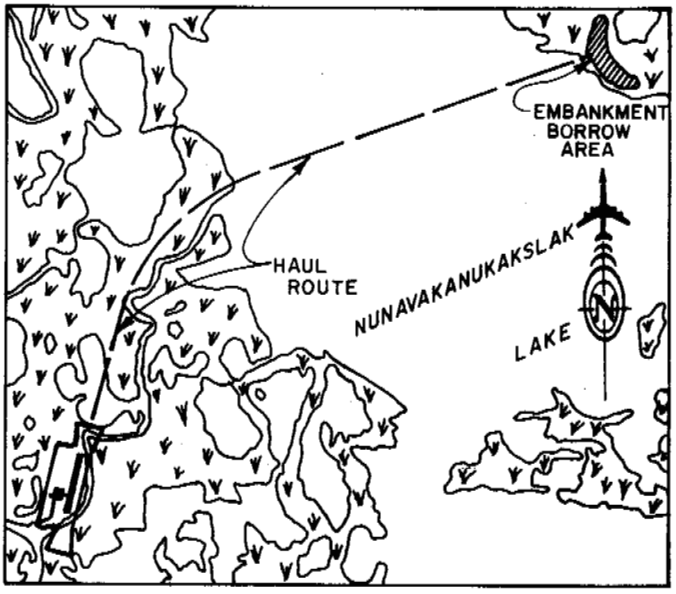

Figure 4 Borrow Area and Haul Route

in the thawed permafrost from one year to the next and inputs into the calculations as a thawed layer.

In the absence of air temperature at the site, air temperature data recorded at the Bethel Airport (Alaska DOT/PF, 1982) 40 km east-southeast of Nunapitchuk was used as input to the program. The average freezing index for Bethel is 1957°C-days with and average air thawing index of 1371°C-days which results in an average annual temperature of -1.7° C. A surface n-factor of 1.4 was chosen based on back-calculated results for gravel surfaced runways (Esch, 1984).

Two subsurface conditions were analyzed and were selected to provide a range of expected thaw settlements. The first included a subsurface soil permafrost with 67% moisture content with an estimated strain of 50% upon thawing (Nelson, et al., 1983). The other included a layer of pure ice as would be found in the ice wedges. Both were overlain with 0.5 feet of peat. The silty sand and sand embankment was to be constructed in the frozen condition with a 40% moisture content and an estimated 25% consolidation upon thawing. Thermal properties of the soils were based on data developed by Kersten, 1949. Calculations were performed for the conservative sand embankment alternative. The design alternatives were evaluated for each condition: 1) no insulation, 2) 0.10 m of insulation, and 3) 0.15 m of insulation. Figures 5 and 6 show the results of the calculations with cumulative embankment settlement plotted versus time in years. These show that for the uninsulated section the expected settlement was 3.7 m in 20 years; for 0.10 m insulation board, 0.24 m; and 0.15 m of insulation board, 0.15 m. The thermosyphon alternative was assumed to experience negligible settlement.

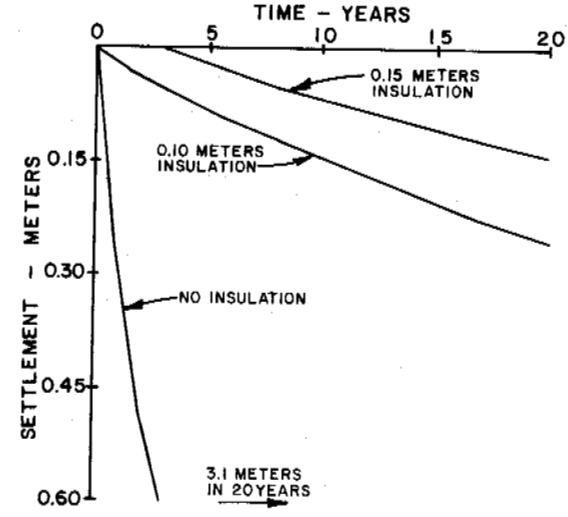

Figure 5 Embankment Settlement Due to Underlying Silt Permafrost Thaw

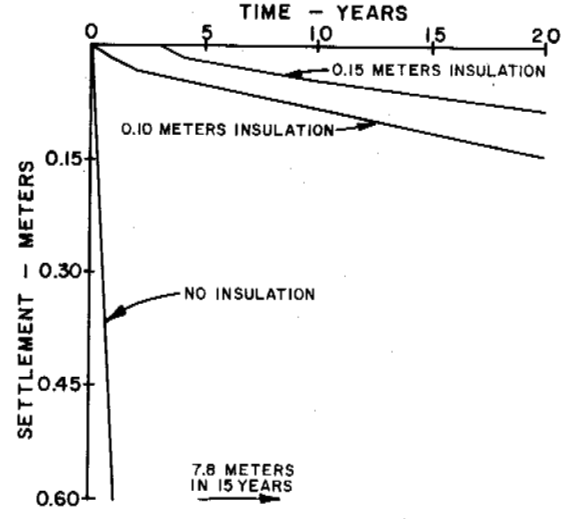

Figure 6 Embankment Settlement Due to Underlying Ice Thaw

After cost estimates and 20 year settlement rates for the three proposed solutions were assembled, a minimum 1.22 m embankment section with 0.10 m of insulation board placed 0.61 m below the top of the finished subgrade was selected as the basic bid for the project. An additional 0.05 m of insulation was bid as an additive alternate. The basic bid had an estimated quantity of insulation board of 3,512 m^3 with an additive alternate potentially adding another 1,755 m^3.

Since access to the borrow area was across lakes and sloughs, the embankment had to be constructed in the winter. Because of this and the anticipated long term settlements, an insulation board with a minimum density of 37.64 Kg/m^3 and a minimum compressive strength of 418.8 kPa was specified. The insulation

board was also required to have a maximum water absorption 0.6% by volume (ASTM D2842-69) and a maximum thermal conductivity of 0.030 cal/m-hr-^{o}C.

To monitor embankment settlement, settlement platforms were intalled to rest on the natural ground prior to construction of the embankment. Each was fitted with a center rod driven 4 m into the natural ground for reference.

Prior to the placement of the first lift of material over the original ground, snow was removed down to the existing vegetative mat (tundra). During snow removal, specifications required the contractor to utilize low ground pressure equipment in order to minimize any damage to the tundra. Any consolidation or tearing of the tundra would reduce its insulative value thus allowing a faster degradation of the underlying permafrost.

Since the embankments were to be constructed during the winter, it was anticipated that frozen chunks of material would be incorporated into the embankments. However, the size of the chunks were specified not to exceed 0.45 m in any dimension with a 0.15 m layer of unfrozen material placed directly below and above the insulation. The purpose of the lower 0.15 m lift of unfrozen material was to provide a level surface with continuous bearing for placement of the insulation boards. The upper unfrozen 0.15 m lift would reduce the damage from frozen material as it was placed on the insulation.

It was anticipated that the frozen chunks of material incorporated in the embankment could not be initially compacted to maximum density. To account for the expected settlement of the embankment material upon thawing, it was specified that the contractor construct all embankments 0.31 m higher than finish subgrade elevations shown on the plans. If the 0.31 m of consolidation was not realized, then new grades and elevations were to be established in the field by the Engineer.

Since moisture control for the embankment material would be difficult during the winter months, the specifications required that the contractor route his earthmoving equipment over the frozen embankment material in an effort to break and compact the frozen chunks. Compaction testing was waived on embankment material placed during freezing weather. However, material placed above the insulation board was required to be compacted when thawed using the necessary equipment to achieve a minimum of 95% laboratory density.

After completion and acceptance of the embankments to finish subgrade, the design called for the construction of a 0.15 m lift of crushed aggregate surface course to be placed over the runway, taxiway, access road and apron. Material required for the aggregate surface course had to be obtained from a source over 200 km from the project. Barging of the material provided the only viable means of transporting the aggregate surface course material.

Due to the favorable bids on the basic contract which included 0.10 m of insulation board, the additive alternate of 0.05 m of additional insulation board was also awarded. The total bid for the project was $2,917,810.00 (USA).

CONSTRUCTION

After the tundra and surrounding sloughs and lakes had frozen sufficiently (early February 1985) to support earthmoving equipment, the contractor off loaded his equipment from the barge and proceeded to construct a 10 km haul road from the borrow area to the airport. Minimal work was required for the haul road as the smooth slough and lake ice provided excellent road surfaces and the tundra between was level enough that only minor grading was necessary.

On February 25, the contractor began hauling and placing the embankment three days after commencing the stripping of unusable material from the borrow area. The size of the frozen silty-sand chunks placed in the embankment beneath the insulation board were generally kept below 0.45 m in any dimension as required in the specifications. The chunks larger than 0.45 m in any dimension were bladed off to the embankment slopes. The 0.15 m of material placed directly below and above the insulation was not entirely thawed as required by the specifications due to the variations in moisture content of the silty sand and the mixing of frozen and unfrozen material at the borrow area during stockpiling. However, enough unfrozen material was available beneath the insulation board to ensure a good bearing surface. Above the insulation board the first lift of material placed had to be increased in thickness from the specified 0.15 m to approximately 0.45 m. This prevented the frozen chunks from shoving the insulation board during placement.

The insulation board used in the project was Dow Chemical Company Stytrofoam HI 60. Due to the large quantity of insulation board required and the arctic winter conditions in which it had to be placed, the contractor obtained 0.08 by 0.61 by 2.4 m boards rather than the standard 0.05 by 0.61 by 2.4 m boards. By reducing the insulation to two layers rather than three, the manual labor was 30% less and the chance of damaged boards was reduced.

During this first phase of construction, the weather was typical for the winter months at Nunapitchuk. Temperatures varied from -37 ^{o}C to 3^{o} C. The construction of the embankment and insulation was started in March 19, 1985 with completion on April 10, 1985. The frozen material above the insulation was allowed to thaw and then graded and compacted before placement of the aggregate surface layer.

INSTRUMENTATION

To monitor and evaluate the performance of the runway embankment, two thermistor strings were installed in the fall of 1985. The strings were fabricated in such a way that the point at which the string penetrated the insulation was 1.22 m away from the point at which the measurements were to be taken. To do this and

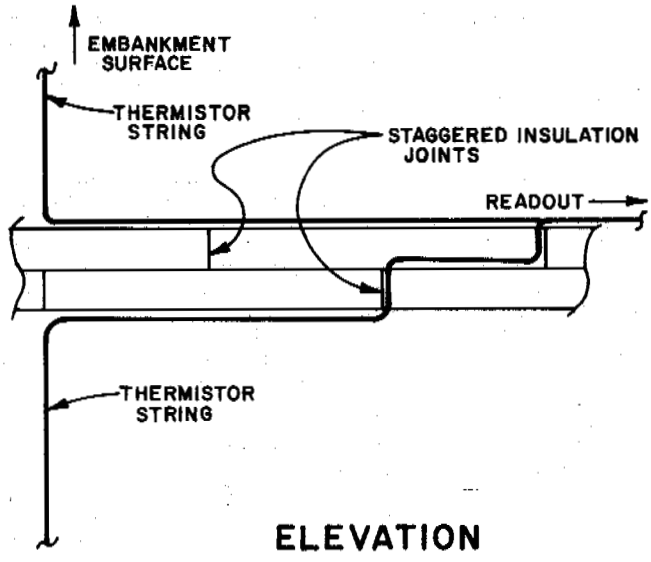

Figure 7 Thermistor Detail to Prevent Thermal Short Through Insulation

measure the temperatures above the insulation, a cable was constructed with two ends - one above the insulation and one below (Figure 7). This was to prevent a thermal short through the insulation from occuring at the point of interest. In each cable 13 YSI 440034 thermistors were used.

To install each cable, the silty sand above the insulation was removed exposing six of the upper layer 0.075 m thick boards of insulation which were removed. This exposed one complete board of the lower layer of insulation which was also removed. The underlying silty sand layer was totally frozen, indicating that no thaw had occurred through the summer of 1985.

A 1.5 m boring was then drilled adjacent to the edge of the removed insulation panel with a Surveyor Drill. The adjacent boards of 37.64 Kg/m^3 insulation were able to support the drill stand and down pressure from the blade of the tractor without noticeable compression. The lower end of the thermistor string was placed in the hole and run along the surface of the exposed silty sand to the other edge of the panel and brought up through the joint (Figure 7). The lower board was replaced and the cable run across the lower insulation layer to the next joint and up to the surface of the insulation. The upper end of the cable was placed along the top of the insulation back to the boring and brought to the surface of the embankment as the hole was backfilled. The cable was then extented to the edge of the embankment in a trench along the top of the insulation, ending in a multiple position switch.

EVALUATION

Figure 8 shows the temperatures of thermistor string No. 2 on April 21 and October 15, 1987. The output switch on string No. 1 could not be located and it was later learned that it had

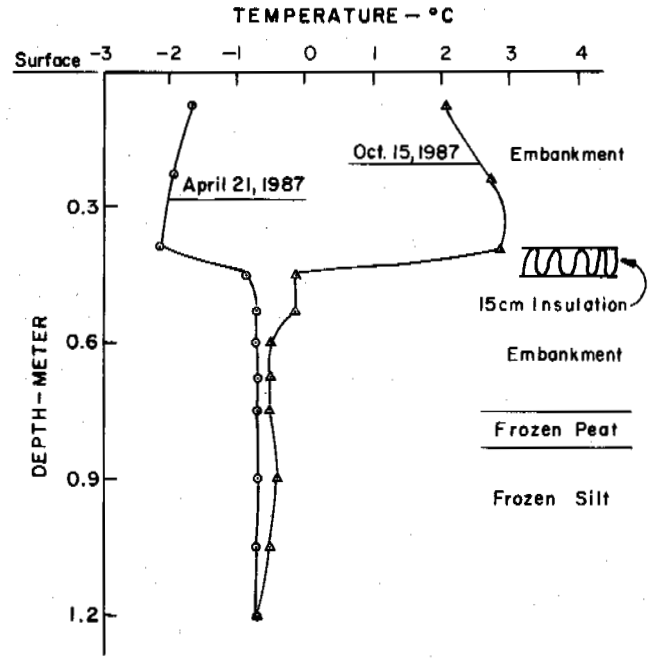

Figure 8 Embankment Temperature Profiles

been destroyed during construction. The May readings on thermistor string No. 2 show the silty sand embankment to be completely refrozen both above and below the insulation. The October readings also show no thaw below the insulation. Two test pits were dug and the thaw below the insulation was measured in both to be 0.10 m. Calculations using the thermal properties for the silty sand indicated a thaw depth of 0.15 m. If the sand is assumed to settle 25%, these numbers are in reasonable agreement.

CONCLUSIONS

At this point in time, it appears that the concept of controlled subsidence (Berg, 1971) or allowing limited settlements of an insulated embankment over the life of the project and re-leveling the surface as needed, will be successful.

ACKNOWLEDGMENTS

The authors would like to thank V. S. Rader for his help with the thermal calculations and T. R. Ottley for performing the materials investigation.

REFERENCES

Alaska Department of Transportation & Public Facilities, (1983), Nunapitchuk Airport Staff Report, Internal report.

Alaska Department of Transportation & Public Facilities, (1984), Nunapitchuk Airport construction plans and specifications.

Alaska Department of Transportation & Public Facilities, (1985-86), Daily & weekly construction reports.

Berg, R.L., (1971), Controlled subsidence of embankments on permafrost, Paper for Advanced Foundation Engineering Class, University of Alaska, Fairbanks.

Esch, D.C., (1986), Evaluation of insulated highway and airport embankments. Alaska Department of Transportation and Public Facilities Report No. AK-RD-86-34.

Kersten, M.S., (1949), Thermal properties of soils. Univ. of Minnesota, Engineering Experiment Station, Bull. 28.

Kulkarni, R., Saraf, C. Finn, F., Hilliard, J. and Van Til, C., (1982), Life cycle costing of paved Alaskan highways, Vol. I & II., Alaska Department of Transportation & Public Facilities, Report No. AK-RD-83-6.

Nelson, R.A., Luscher, U., Rooney, L.W. and Stramler, A.A., (1983), Thaw strain data and thaw settlement predictions for Alaskan soils, Proceedings of the Fourth International Conference on Permafrost, Fairbanks, pp. 912-917.

Pavey, D.R., (1983), Centerline and borrow materials report for Nunapitchuk Airport, Alaska Department of Transportation and Public Facilities.

U.S. Departments of the Army and Air Force, (1966), Arctic and Subarctic construction -calculation methods for depths of freeze and thaw in soil. TM-5-852-6.

THERMAL PERFORMANCE OF A SHALLOW UTILIDOR

F.E. Kennedy, G. Phetteplace, N. Humiston and V. Prabhakar

Dartmouth College, Hanover, New Hampshire, USA

SYNOPSIS The thermal performance of a shallow burial utilidor design in central Alaska was studied by both field measurements and an analytical (finite element) model. Temperatures within the utilidor and in the soil surrounding it were monitored from mid-1985 until mid-1987. The utilidor interior temperatures remained well above 0°C even in the coldest weather and soil beneath and adjacent to the utilidor remained unfrozen. The pattern of ground freezing in the immediate vicinity of the utilidor was significantly affected by heat flowing from the utilidor, but ground temperatures more than about 6 m from the utilidor were relatively unaffected. The transient finite element analysis gave very good predictions of soil temperatures in the utilidor region.

INTRODUCTION

A common method of utility distribution, especially in cold climates, is the utility corridor, or utilidor. The utilidor could contain water and sewer pipes, electric and telephone cables, and pipes for high temperature water or steam and condensate. In very cold regions, such as Alaska, measures must be taken to keep the utilidor's interior temperatures above freezing and to limit heat loss from the utilidor during winter. These measures could include insulation of the utilidor and inclusion of steam traces to heat the water and sewer piping.

Utility corridors can be built either above or below ground. Buried utilidors have a distinct thermal advantage in severe climates. High construction costs, however, along with high groundwater levels, interference with existing utilities, or the presence of permafrost may prevent the deep burial of utilidors. Excavation in permafrost is costly and problems could occur if a heated utilidor was placed in such soils. One of the few analyses of buried utilidor performance in a permafrost region was that of Zirjacks and Huang (1983), which described an underground utilidor in Barrow, Alaska. Excavation of the permafrost for that utilidor required considerable blasting. Although the utilidor was insulated and heated by hot water, utilidor air temperatures frequently dropped below 0°C during cold weather.

An alternative to above-ground or deep burial utilidor designs is a shallow burial design in which the bulk of the corridor is below ground but its top cover is at or above ground surface level. While the initial cost of construction of the shallow burial design would be much less than that of the more typical deep burial design, problems could occur due to exposure of the top of the utilidor to extreme climatic conditions. One such shallow utilidor has recently been constructed in interior Alaska, where the outside air temperature could drop to as low as -50°C in winter. The purpose of this work was to study the thermal behavior of that utilidor. A preliminary analysis of the utilidor which had been done prior to construction (Phetteplace, et al.,1986) indicated that temperatures below freezing could occur within the utilidor during the coldest winter months. That analysis prompted the designers to add extra insulation around the concrete utilidor and to add an uninsulated steam trace inside the utilidor which would heat the interior when necessary. The purpose of the present study was to 1) determine whether those measures were successful in keeping utilidor temperatures above freezing and whether the steam trace was, in fact, required, and 2) study the soil temperatures around the utilidor to see what effect the heat sources in the utility corridor had on those temperatures. The location of the 0°C isotherm which separates frozen from unfrozen soil was of particular interest.

The work involved two phases: 1) a field study involving instrumentation of the utilidor with sensors to measure actual heat flows and temperatures, and 2) a numerical model of the thermal performance of the utilidor and surrounding soil. The thermal analysis was used to calculate temperatures where sensors could not be placed and to predict accurate temperature profiles in the soil surrounding the utilidor.

UTILIDOR SYSTEM AND INSTRUMENTATION

The portion of the utilidor system being studied contains all utilities with the exception of electrical power lines, which are overhead. The utilidor is over 2 kilometers long and was constructed in 1984 and 1985 in an area of interior Alaska which lies in a discontinuous permafrost zone (Williams, 1970). The soil at that location is predominantly gravel, covered by a thin (< 25 cm) layer of peat. The groundwater level at the site is approximately 2.5 m below grade and all utilidor excavation was well above that level.

The utilidor is a rectangular concrete tunnel with a 250 cm by 80 cm interior cross section.

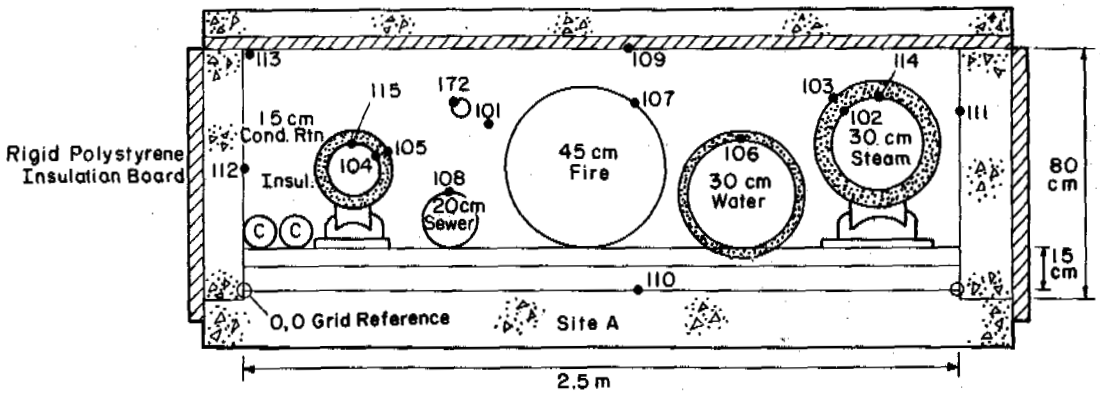

Figure 1. Cross section of utilidor at site A, showing placement of temperature sensors. All numbers refer to thermocouples except 114 and 115, which are heat flow sensors.

The 15 cm thick walls of the utilidor have 5 cm of extruded polystyrene insulation on their exterior surface; the 10 cm lid is lined with 5 cm of extruded polystyrene insulation and 1.25 cm of plywood on its interior surface. The 20 cm thick base of the utilidor is uninsulated. The pipes and conduits within the utilidor are supported at regular intervals by supports which keep the pipes at least 15 cm above the concrete floor. Figure 1 shows a cross section of the utilidor at one of the sites studied.

The steam, condensate and water pipes within the utilidor are insulated. The 30 cm. diameter steam pipe is covered with 5 cm of fiberglass insulation. The condensate pipe (15 cm diameter) is wrapped with 3.75 cm of fiberglass insulation. The 30 cm water pipe is insulated with 3.75 cm of polyisocyanurate. The fire (water) and sewer pipes are uninsulated. An uninsulated 2.5 cm steam trace was also installed within the utilidor to heat the utilidor in the event that below freezing temperatures were encountered in its interior. Thermostatic control was used on each segment of the steam trace to reduce energy consumption. The steam trace was not activated during the course of this study.

During the construction, two sections of the utilidor and the soil around those sections were extensively instrumented with thermocouples and heat flow sensors. About fifteen thermocouples and two heat flow sensors were installed within the utilidor at each of the two sites. The locations of the thermocouples and heat flow sensors within the utilidor at site A are shown in Figure 1. In addition to the instrumentation within the utilidor, over fifty thermocouples were positioned in the soil around the utilidor at each site and two more thermocouples were used to monitor the outside air temperature. The locations of soil thermocouples at site A are shown in Figure 2. The soil thermocouple strings were implanted in the summer of 1985 and, while drilling holes for those thermocouples, frozen ground was encountered at depths ranging from 2 to 3.5 m. Several of the thermocouple locations were in the frozen ground. All thermocouples were made with 20-gage copper constantan thermocouple wire and were read to a resolution of approximately ± 0.1°C. The heat flow sensors had a sensitivity of 63 W/m2 mv.

The sensors at each of the two sites were monitored continuously by an automatic data acquisition system. The main component of this system was located in the mechanical room of a building served by the utilidor. The thermocouples were connected to a waterproof "extender chassis" at each site. These converted the analog signals from the sensors into digital signals. The digital signals were transmitted via a multiconductor communication cable from each extender chassis to the main frame data acquisition system. Since site A was approximately 225 meters from the mechanical room where the data acquisition was located and the other site was over 300 meters away, such a system greatly reduced the cost of extending the much more expensive thermocouple wires. Another reason for using this system was the ability of the extender chassis to operate in the extreme environmental conditions found within the utilidor system.

The data acquisition system was microprocessor controlled and fully programmable. This allowed for a great deal of flexibility in data acquisition. Data were recorded on magnetic tape for ease of transfer to our computer for reduction and analysis. Data also could be printed on site by the data acquisition system to allow for periodic inspection of utilidor and data acquisition system operations.

Data acquisition began at both sites in August 1985 and were collected nearly continuously until July 1987.

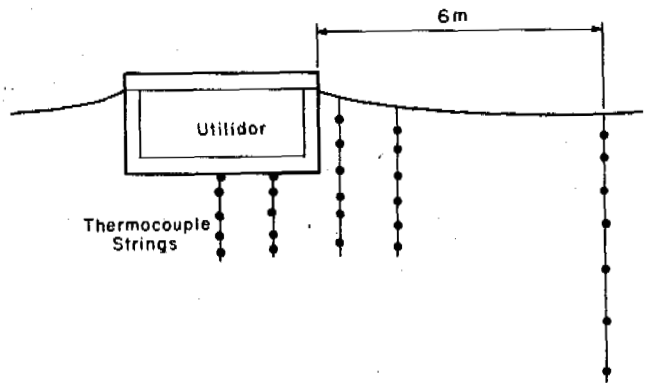

Figure 2. Buried thermocouple cable locations.

TEMPERATURE MEASUREMENTS

Temperature and heat flow data were collected throughout the winter of 1985-86 and 1986-87. Due to space limitations only a small portion of the data is presented here.

The winter of 1985-86 was unusually mild at the utilidor site in central Alaska, with outdoor temperatures at the utilidor site averaging above normal and seldom dropping below -30°C. The variation in outdoor temperature during the period 7 December 1985 to 21 January 1986 is shown in Figure 3, based on temperatures measured daily at midnight and noon. Considerable variation in air temperature is evident, especially during December 1985. The utilidor interior temperatures at each of the instrumented sites were found to be much higher than outside air temperatures. Figure 3 shows the air temperature inside the utilidor at site A during the same 1 1/2 month period. It can be seen that the interior temperatures at this site were quite stable throughout the period, generally remaining between 35°C and 40°C. Interior temperatures at the other site (site B) were also stable but were lower, ranging from 13°C to 16°C in a cool corner of the utilidor and to 25°C nearer the steam pipe. The lower temperatures at site B were due to the fact that site B was nearer the end of the steam distribution circuit, so steam temperatures were lower there and the steam and condensate pipes were smaller. In addition, site B was relatively far from a warm manhole, whereas a nearby warm manhole seems to have contributed to warmer utilidor temperatures at site A.

The relative stability of the utilidor temperatures was also maintained during the winter of 1986-87, which was more severe than the one preceding it. Plots of outdoor air temperature and utilidor air temperature at site A are shown in Figure 4 for the period 2 March to 18 March 1987. Despite large variations in outdoor temperatures, which reached as low as -37°C, the utilidor air temperature remained quite stable at between 34°C and 39°C at site A. Again, temperatures inside the utilidor at site B were lower, reaching a minimum of 12°C on a night in early March that was one of the coldest nights of the year. It was apparent from the measurements that, even in the coldest weather and at the coldest site instrumented, the utilidor interior remained well above freezing without the need for a steam trace.

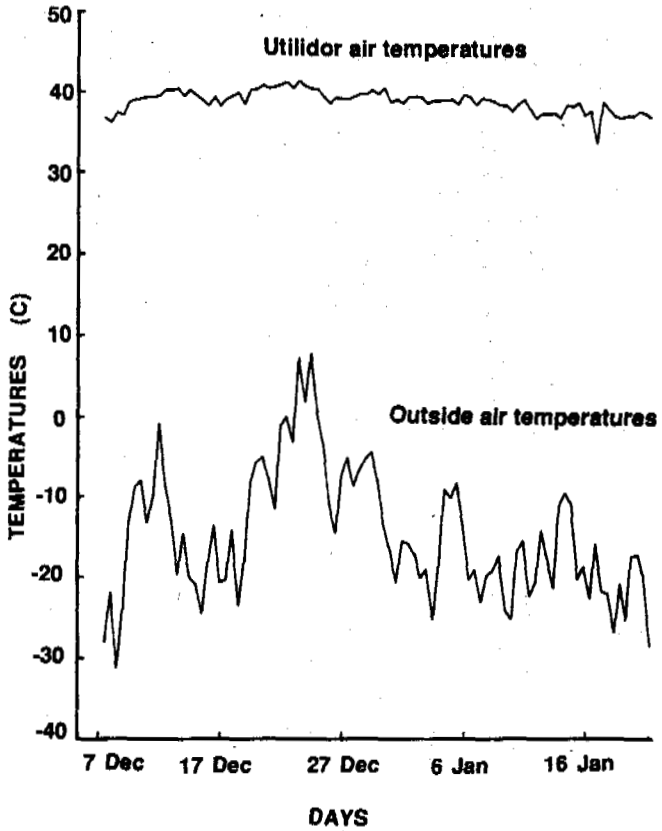

Figure 3. Measured outside air temperatures and utilidor air temperatures at site A during period from 7 Dec 1985 to 21 Jan 1986. Readings taken daily at 00:30 and 12:30.

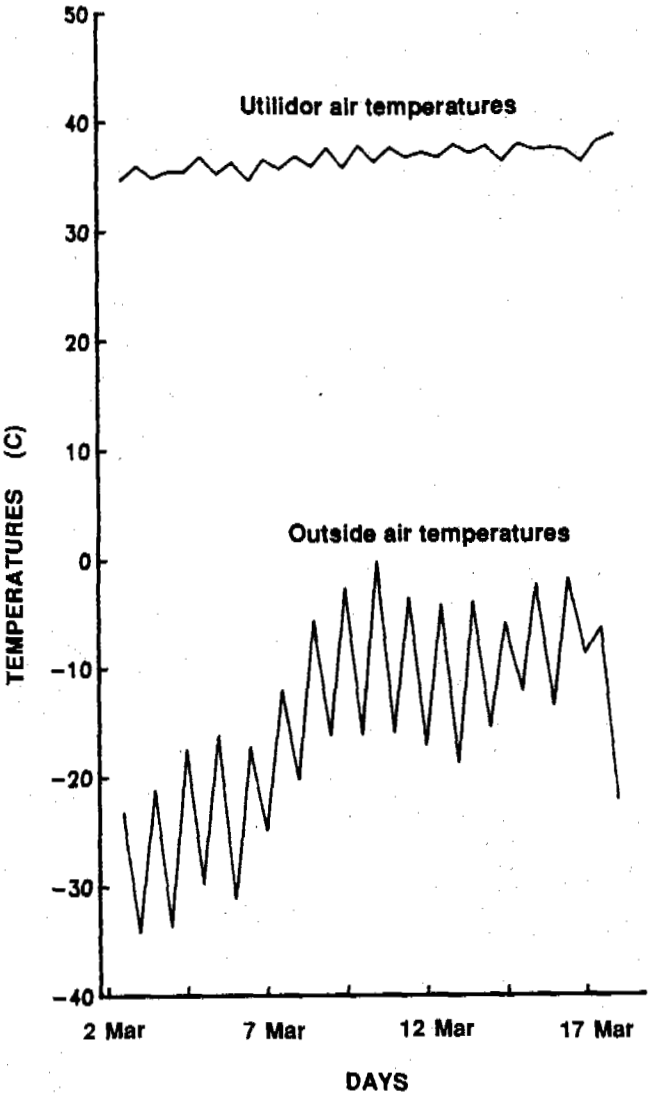

Figure 4. Measured outside air temperatures and utilidor air temperatures at site A during period from 2 Mar 1987 to 18 Mar 1987. Readings taken daily at 00:12 and 12:12.

A study of the utilidor interior temperatures and heat flow measurements showed that both steam and condensate return pipes contributed heat to the utilidor interior, with the heat flow from the steam pipe being about 25% greater than that from the condensate pipe at site A. There was slightly more heat flow from the steam pipe at site B than at A, even though the steam pipe temperature was lower at site B, but there was substantially less heat flow from the much cooler and smaller condensate pipe at site B.

Considerable heat from the utilidor flowed into the surrounding soil, as was evident from measurements of soil temperatures. The thermocouple data were used to construct isotherms in the soil region around the utilidor and examples of the isotherms are shown in Figures 5 and 6. The dashed lines in Figure 5 are isotherms determined from measured soil temperatures at site A on 12 December 1985, while isotherms at the same site on 12 March 1987 are shown in Figure 6. It should be noted that the isotherms were constructed only in the region enclosed by the 50 thermocouples shown in Figure 2, so they don't extend deeper than about 4 m below the ground surface and don't include the soil immediately adjacent to the utilidor. By comparing the December and March data it can be seen that the 0°C isotherm was at a greater depth later in winter, but no freezing was observed in the soil beneath the utilidor even late in winter. Similar results were noted at site B, although the soil temperatures were slightly lower beneath the utilidor at site B. It is apparent from the isotherm spacing that there was a substantial amount of heat flowing radially outward from the utilidor and upward toward the colder ground surface at both sites.

Monitoring of all of the soil thermocouples began late in the summer of 1985 just after the utilidor went into operation. With two exceptions, all of the thermocouples showed an increase in temperature during the August-September period and the ones that had been implanted in frozen ground had increased to above 0°C by the end of August. Two of the thermocouples that had been implanted in frozen soil at site B. however, remained at a constant temperature of -0.3°C throughout the two-month period just after installation. Those thermocouples were located 2 m laterally from the utilidor at 3.5 to 4 m depth. After heat from the utilidor started reaching the two thermocouples, though, in late September 1985, those two temperatures started rising slowly and had reached above 0°C by the end of November. They never again dropped below 0°C during the remainder of the two-year study. It should be noted that the soil drill had encountered difficulty penetrating the frozen ground to depths greater than 3.75 m at that location. Based on these observations, it was concluded that there had been a small patch of permafrost at that location, beginning at a depth of just over 3 m, but it thawed when heat from the utilidor reached it. None of the other soil thermocouples showed indications of being in permafrost either before or after the utilidor was in operation. There was very little settlement of the utilidor of the soil around the utilidor. Comparison of soil temperatures from the summer of 1985 with those measured in the summer of 1987 showed that locations within 3 m of the utilidor were warmer by at least two degrees in 1987 than they had been at the time of utilidor construction two years earlier.

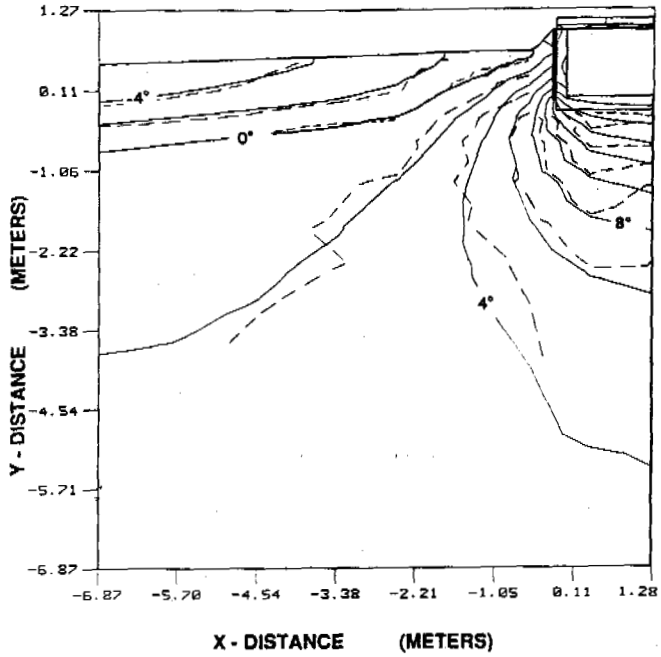

Figure 5. Isotherms in soil around utilidor at site A on 12 Dec 1985. Dashed lines were determined from thermocouple readings at 00:00. Solid lines are based on finite element model predictions.

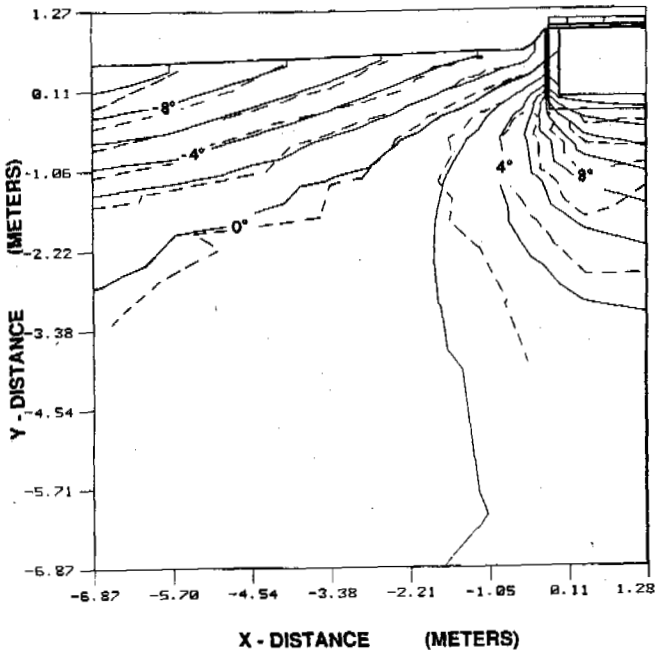

Figure 6. Isotherms in soil around utilidor at site A on 12 Mar 1987. Dashed lines were determined from thermocouple readings at 00:00. Solid lines are based on finite element model predictions.

Temperatures at a control cable located 6 m from the utilidor were less affected by the presence of the utilidor, but were very slightly higher in July 1987 than they had been in August 1985.

Although the measured data provided considerable information about temperatures and heat flows in and around the utilidor, more information was desired, especially in those locations where instrumentation hadn't been installed. This information was obtained from an analytical model of heat transfer in the region of the utilidor.

ANALYTICAL STUDY

Analytical Procedures

The finite element method was chosen for this analysis of temperatures in the region surrounding the utilidor. A preliminary study of the temperature distribution was carried out early in the utilidor design phase (Phetteplace et al., 1986). Although that analysis proved useful in the design of the utilidor, its temperature predictions did not strongly agree with data measured after the utilidor was constructed. The preliminary analysis was a steady state analysis and it used boundary conditions and soil properties that were only rough estimates. It was concluded that a transient thermal model was necessary in order to achieve improved accuracy (Phetteplace et al., 1986). In the present study a transient analysis was run, with effects of soil freezing included.

The finite element program used here was Thermap, a code that was developed at Dartmouth and had proven to give good temperature predictions for a wide variety of heat conduction problems (Glovsky, 1982). The program was modified for this project to account for latent heat effects in melting and freezing (Prabhakar, 1987). The phase change algorithm used in the modified code was an efficient form of an equivalent heat capacity scheme developed recently by Hsiao and Chung (1986).

Before applying the program to the utilidor problem, an extensive numerical study was made of the effect of soil properties and boundary conditions on soil temperatures in a one-dimensional heat transfer situation near the utilidor (Prabhakar, 1987). The soil whose thermal properties gave the best approximation to the measured temperatures in the soil near the utilidor was a coarse-grained soil with 10% moisture content and a dry unit mass of 2.2 g/cm3. That soil type agrees well with soil prevalent at the utilidor site. Properties of such a soil were tabulated by Lunardini (1981).

The finite element mesh used in the final utilidor analysis for site A is shown in Figure 7. It included 424 nodes and 387 elements. Fifty-one of the nodes were at the same locations as buried thermocouples and they are shown by circles in Figure 7. Because of symmetry, only half of the utilidor and the soil on that side were studied. The boundary conditions included: zero heat flux conditions on right and left sides, convection to ambient outside air at the top surface of the utilidor, measured thermocouple readings as prescribed temperature boundary conditions on the inside wall of the utilidor and the top surface of the snow-covered ground, and an assumed constant temperature

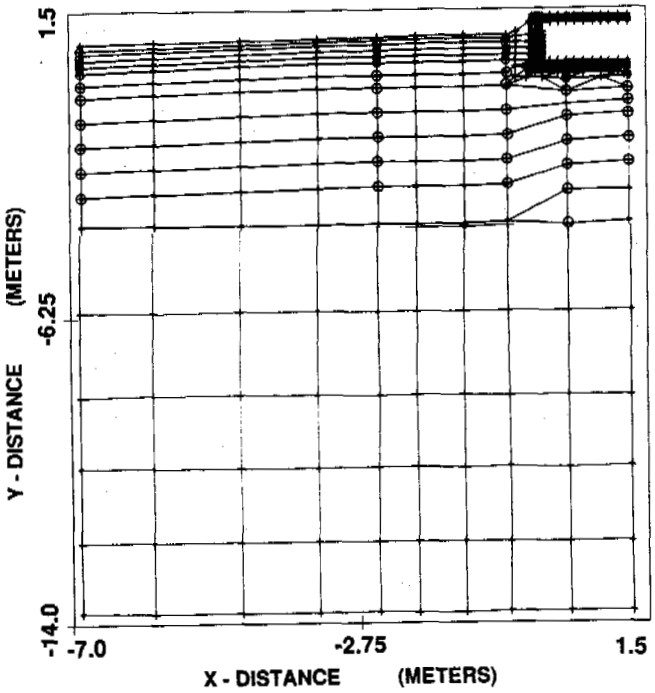

Figure 7. Finite element mesh for thermal analysis of utilidor and surrounding soil. Circles indicate thermocouple locations.

boundary at a depth of 15 m below the ground surface.

A transient analysis was run using the measured soil temperatures at the beginning of a 6-week test period as initial conditions. During the transient analysis the constant temperature conditions at the ground surface and utilidor wall, along with the ambient air temperature, were changed regularly to correspond with measured values. Time steps for the transient analysis were chosen to insure that the freeze front did not skip over any elements during a single time increment.

Analytical Results

Computed temperature distributions at site A are shown by the solid lines (isotherms) in Figures 5 and 6 for two representative days, 12 December 1985 and 12 March 1987, respectively. Comparison of the measured and predicted temperatures shows very good agreement, not just on those two days but throughout the time periods studied (Prabhakar, 1987). In general, predicted temperatures differed by less than 1°C from measured values and the locations of the 0°C isotherm were nearly exactly the same as those determined from measured temperatures. In fact, the only temperatures which differed by more than 0.7°C from measured values were those for several thermocouple locations directly beneath the utilidor, and the exact locations of those thermocouples is questionable because the thermocouple cable was disturbed during construction. Agreement with measured soil temperatures was much better for these transient

analyses than had been the case for the earlier steady-state analysis (Phetteplace, et al. 1986).

The isotherms presented in Figures 5 and 6 offer convincing evidence that no freezing occurs in the soil beneath or adjacent to the utilidor, irrespective of outdoor air temperature or time of year. The analysis predicts that soil temperatures reached 2°C or higher at depths down to at least 15 m in the region within 6 meters of the utilidor at site A. These temperatures would have a very significant effect on the annual patterns of freezing and thawing of the soil in that region.

CONCLUSIONS

The measurements and predictions of this work showed that temperatures within and around this shallow utilidor did not drop below freezing at the sites instrumented, even during the cold winter weather in central Alaska. The presence of a large steam pipe, even though it was insulated, kept utilidor interior air temperatures above 30°C throughout the year at site A and above 10°C at the colder site, site B. A steam trace placed within the utilidor for emergency heating of the corridor proved to be unnecessary. Temperatures in the soil beneath and adjacent to the utilidor were also kept above 0°C by heat conducted from the warm utilidor. Soil temperatures beneath the utilidor at site A increased to above 2°C to depths of at least 15 m, preventing any freezing of that soil. There was evidence that a small patch of permafrost was initially present at a depth of slightly over 3 m near the utilidor at site B. Whereas the temperature at that location had been constant at about -0.3°C for an extended period at the time of utilidor construction, once heat from the utilidor reached that region the temperature increased slowly to above 0°C and remained above freezing throughout the remainder of the two-year study. At lateral distances of 6 m from the utilidor the ground froze to depths of greater than 3 m during the winter, but even there the soil temperatures were slightly influenced by heat conducted from the utilidor and at greater depths the temperature remained above 0°C.

The transient finite element analysis used to predict temperatures around the utilidor proved to be quite accurate. Predictions of soil temperatures and 0°C isotherm location agreed very well with measured values. At present the analysis relies on the specification of measured utilidor wall temperatures as time-varying boundary conditions. Since those temperatures are not usually known a priori to the designer, the program is currently more useful as an analysis tool than as an aid in design. A more complete study of heat transfer within the utilidor is planned, with the goal being a better understanding of heat transfer coefficients from the various heat sources, such as steam pipes. This would eliminate the need for measured utilidor temperatures and would increase the effectiveness of the program as a utilidor design aid.

ACKNOWLEDGEMENTS

The authors acknowledge and thank the following persons for their contributions: S. Lederman of the U.S. Army Corps of Engineers Alaska District, whose cooperation and knowledge of the study sites were invaluable; H. Barger, Eielson Energy Engineer, who was instrumental in obtaining funding and monitoring the data collection system; and, finally, the U.S. Air Force for providing the funding for the field study.

REFERENCES

Glovsky, R.P. (1982). Development and Application of Thermap. Master of Engineering Thesis, Thayer School of Engineering, Dartmouth College, Hanover, NH.

Hsiao, J.S. and Chung, B.T.F. (1986). An Efficient Algorithm for Finite Element Solution to Two-Dimensional Heat Transfer with Melting and Freezing. ASME Journal of Heat Transfer (108), 462-464.

Lunardini, V.J. (1981). Heat Transfer in Cold Climates, Van Nostrand Reinhold, New York

Phetteplace, G., Richmond, P. and Humiston, N. (1986). Thermal Analysis of a Shallow Utilidor., Presented at 77th Annual Conference of International District Heating and Cooling Association, Asheville, NC.

Prabhakar, V. (1987). Heat Transfer from Utilidors. Master of Engineering Thesis, Thayer School of Engineering, Dartmouth College, Hanover, NH.

Williams, J.R. (1970). Ground Water in the Permafrost Regions of Alaska, U.S. Geological Survey Professional Paper # 696

Zirjacks, W.L. and Hwang, C.T. (1983) Underground Utilidors at Barrow, Alaska: A Two-Year History. Proc. 4th Int'l Conf on Permafrost, National Academy Press, Washington, DC, 1513-1517

CONSTRUCTION OF HYDROS IN COLD CLIMATE: ACHIEVEMENTS AND PROBLEMS

L.I. Kudoyarov[1] and N.F. Krivonogova[2]

[1]The V.V. Kuibyshev MISI, Moscow, USSR
[2]The B.E. Vedeneev VNIIG, Leningrad, USSR

SYNOPSIS Specific features of hydros under design, construction and operation in cold climate are considered to demonstrate the advances and urgent problems in estimating engineering geocryological conditions of their foundations; lay-out and design solutions ensuring safe performance of embankment and concrete dams built on frozen and thawing foundations are looked into.

Water power resources of the Soviet North are estimated to be 1,400 TWhr which accounts for 37% of the total USSR hydro power resources. The severe climate, complex engineering geological conditions (to a large extent determined by geocryological situation), lack of material bases in the uninhabited regions together with transport problems are responsible for difficulties in the development of the northern hydro power engineering. On the other hand, these very factors have stimulated the drive for finding new promising and economically effective solutions related to the design and construction of hydros in the Soviet North. The engineering geological conditions are aggravated primarily due to the evolution of permafrost. At the valley stretches wedging into rock formation the transforming role of cryogenesis shows up as the occurrence of upheaved zones in the rock masses with inferior physico-mechnaical properties. Widespread on the steep slopes of the dam abutments and forebay portions of the reservoirs are stone streams revealing their instability caused by the excavation and change of rock thermal conditions in the process of construction. When dealing with semirocks distinguished for high ice content and non-uniform cryogenic structure one may expect the rapid rise of deformability and loss of strength at their thawing, non-uniform thermal settlements and thermokarst manifestations. Besides, valley slopes may contain the beds of weak argillaceous rock or there may be slide-induced displacements suspended by permafrost. It is quite natural, therefore, to foresee the loss of local or general stability of the slopes or activation of slides at the change of thermodynamic conditions. This possibility is duly allowed for by the specialists implementing innovative designs which ensure the stability of slopes and reduce seepage losses. Many hydraulic structures are designed to be built on loose frozen formations different from one another not only by the consituent rocks but, what is more important, by the cryogenic structure and properties. If this is the case, the frozen-type hydraulic structure is adopted. This type of structure is considered to be the best from the safety and environmental points of view, though if the fouhdation is formed by the thick strata of clastic rocks their thawing is unavoidable and, therefore, the foundation treatment procedure must be based on the detailed consideration for the rock behaviour in the process of thawing. All this conditions the selection of the damsite, layout and design of the structures and the relevant construction techniques.

Experience gained in creating designs of dams, power houses, spillways and other structures, both being elaborated and already realized, enables the lay-out problems to be solved for practically all climatic, topographic and geological conditions.

In so doing, the lay-out solutions adopted are meant not only to make for smooth operation of structures built on heterogeneous thawed-frozen foundations with time-dependent properties but to do as little harm as possible to the easily injured northern nature. The heaviest and most heat-releasing structures are advisable to be constructed either in the talik zones or on the frozen rocks undisturbed by upheaval. In this case special attention should be paid to the treatment of foundations, especially if the latter are formed mostly by argillaceous rocks. This is important since at the year-round construction the large number of operations is performed at subzero air temperatures which results in freezing of thawed rocks and hence in the change of their conditions and properties. To control this process is one of the most vital tasks which need to be substantiated by comprehensive scientific studies prior to construction.

Also of primary importance in the hydraulic engineering of the Extreme North is the elaboration of new scientifically sound construction schemes. Numerous investigations in this field, including those performed with participation and under guidance of the authors, have demonstrated that as far as water retaining structures are concerned one of the most promising directions is the application of construction schemes permitting of easy control of heat exchange processes. Construction of dam shells using rockfill does not involve any difficulties. Its excavation, transportation and placement in ungraded conditions are done in the same manner as outside the Northern Climatic Zone. Rockfill can be placed in the shells in high lifts or in layers with subsequent compaction. When using morainic soils which have nearly optimum composition the dams can be constructed either by dry methods or by dumping the soil into water. These techniques were repeatedly tested in practice and proved to be good from the design and construction points of view.

Advisable to be constructed in the North are embankment dams built from soil and mixed (soil and non-soil) materials with shells made of ungraded stone and impervious elements made of local soil materials or realized in the form of steel diaphragms, steel membranes, asphaltic and precast concrete diaphragms. Also recommended are embankment dams having impervious elements in the form of ice-soil walls and "frozen curtains" created and main-

tained with the aid of air, fluid and steam-and-fluid set-ups. In the latter case the design of the contact zone between an impervious element and a thawed-frozen foundation liable to non-uniform deformations needs special consideration.

As is well known, embankment dam foundation settlements and self-compaction of soil in the construction and post-construction periods shall not cause hazardous deformations of impervious elements, drains, transition zones and rigid members of other structures linked to the dam body. Neither concentrated seepage paths nor dangerous piping zones shall appear in the dam.

Proceeding from the above considerations the "Code for designing embankment dams in the Northern Climatic Zone" recommends the design density of soil to be adopted so that the design settlements of different parts of the dam would be close to each other by absolute value, whereas relative settlements of the crest in the operation period would not exceed 2-2.5% of the dam height at a given cross-section. The above recommendation pertains to the embankment dams to be constructed from soil materials only.

Experience shows that in the construction of thawed-type embankment dams it is not feasible to build a core or membrane entirely of thawed soils; the only possible design is a pie-like structure formed by interstratified zones of thawed, frozen and cooled below $0^{\circ}C$ saline soils. That is why to meet the requirements on permissible settlements it is necessary to regulate temperature conditions of impervious elements and determine, with or without the allowance made for salinity, the ultimate temperature conditions at which the settlement rates and values are well within the allowable limits both in the construction and post-construction periods. Multi-purpose studies on the method of construction of the Kolymskaya temporary and stationary dams have made it possible to refine the requirements on soil materials and techniques of their placement in the dam body. The construction procedure modified accordingly enabled optimum temperature conditions to be maintained so that the core could be kept in thawed condition as early as at the construction stage. This, in turn, resulted in uniform deformations at the consolidation of all parts of the structure thereby ensuring its safe thermal stress-strain state. Long-term investigations of the temperature condition changes and ice formation in rockfill shells of the Kolymskaya, Vilujskaya and Khantaiskaya dams permitted of assessing the effect of these processes on the thermal stress-strain state of the dam and controlling them by placing surface soil layers of predetermined grain-size composition and thickness.

Loamy soils on the major part of the USSR North-East are known for high ice and silt contents, which determines the scarcity of soil material suitable for constructing impervious elements. It looks promising, therefore, to make the latter from non-soil materials, e.g. from steel. In particular, impervious diaphragms can be made from steel plates or low carbon steel piles of more than 10-12 mm thickness. Given an anticorrosive vynil, epoxy, bitumen or asphaltic coating such elements may last 200 years. To provide for joint deformation of the diaphragm and the shells it is most reasonable to ensure its free contact with the sides through the medium of bitumen keys.

The dams with steel membranes may be recommended at high heads. Their advantage resides in the shell being dry to the downstream water level. This increases the shell seismic stability, whereas the membrane attains greater freedom of deformations collaborating with the shell, which contributes to the safety and relaxes the requirements on material placement. Construction of dams with steel seepage control elements is best suited to the conditions of the North.

When designing the Adychanskaya power plant to be constructed under extremely severe conditions, among other versions the dams with steel diaphragms have been suggested. In this case, due to severity of climate, the steel structures are proposed to be bolt-connected. Owing to exceptional transportation difficulties the volumes of outside materials have to be cut short. Consequently, a precast concrete diaphragm has been suggested. The diaphragm parts (5-7 kg plates) can be made of concrete protected with heat-and-dampproof mats, of impregnated concrete and lightweight concrete. The design of joints sealed with cold-resistant materials permits of some deformation. At small heads such dams turn out to be preferable to all other kinds of "dams of the North".

The version with an asphaltic concrete diaphragm considered in several design projects of northern dams, is being realized at the Boguchanskaya dam construction. It features the following special merits: an easy-to-realize design admitting of complex mechanization with the use of standard road-building equipment; small quantities of outside materials (bitumen up to 8%), high waterproofness and deformability of the material even at marked settlements of the dam body (resting on thawing ice-rich foundation) and at seismic effects.

The extreme severity of Magadan district known for occurrence of thick strata of permafrost rocks calls for maximum adaptability of a heat-accumulating power structure to the existing natural complex.

Of much practical and theoretical interest in the construction of natural and artificial ice-soil impervious elements (by forced or gravity water delivery) is the ascertainment of relationship between temperature conditions of the rocks, seepage rate and self-healing of cracks and pores with ice (i.e freezing up of the seepage paths). The latter process is seemingly governed by the character and degree of cracking, porosity, ice content and ice ladeness of the rocks as well as by the rigidity of temperature conditions.

Soils are maintained in frozen condition by natural cold or by artificial cooling with air, fluid and steam-and-fluid set-ups used to create "frozen curtains" in the dam body and part of the foundation.

There also exists a theoretically substantiated procedure for constructing impervious elements by dumping frozen soils in cold water or placing them in dry condition and then pouring with water. It has been found that consolidation of such soils proceeds better than that of thawed soils and their further freezing is easier. The new techniques have been tested in practice and look very promising for power construction in the Soviet North-East.

In view of extremely irregular northern river discharges of great concern are the problems of their passing especially in the construction periods. These problems need further studies. The radically new design solutions being suggested are not yet approved for practical uses and hence require comprehensive mechanical and hydraulic investigations to optimize the designs of hydroelectric plant water conveyance structures. Almost all major types of concrete dams, with exception of arch and multi-arch ones, have been realized in the USSR regions characterized by severe climatic conditions.

Experience gained in design, construction and operation of concrete dams located in these regions shows that their stresses, strength and durability depend greatly on temperature effects. All other things being equal, it leads

to a somewhat greater volume of concrete in such dams as compared to those constructed in mild climatic conditions.

As far as concrete volume is concerned, the main types of concrete dams on rock foundations built in the USSR are quite comparable with the best specimens of foreign dams realized under more favourable conditions. It can be positively stated that for mass concrete conventional gravity dams the concrete consumption of 0.76-0.77 m^3 per ton (force) of hydrostatic pressure is a limiting value from the strength considerations. This value can be reduced only if the dam design envisages an upstream face membrane, preliminary compression of concrete, arrangement of widened intercolumnar joints or large longitudinal recesses, etc.

The specific consumption of concrete at the Zeyskaya mass concrete buttress dam practically equals that at the Ust-Ilimskaya mass concrete gravity dam but is well over the specific consumption at the Itaipu dam being constructed in Brazil-Paraguay. It is likely that the construction of a mass concrete buttress dam under rigorous climatic conditions can be cost-effective if it results in 15-20% reduction of the material consumption capacity as compared to a mass concrete gravity dam (to compensate for the higher unit job price of concreting which rises due to the increase of concrete consumption at the deepened portions). For cost-effective mass concrete buttress dams the specific consumption of concrete should be 0.60-0.65 m^3 per ton (force) of hydrostatic pressure.

The relative steel consumption at the existing native dams and at the Sayano-Shushenskaya arch-gravity dam which is under construction is, on the average, around 10 kg/m.

Among most promising dams planned to be constructed on good rivers of Siberia and Soviet Far East, providing the engineering-geological conditions are favourable, is a gravity dam of composite profile built of compact concrete or heat-insulated polymer concrete with the crest and core made of stiff lean concrete. The compact or polymer concretes ensure waterproofness of the dam and protect it from season variations of the ambient air temperature. Besides, they form the main (seepage-control) element of the structure.

One of the problems encountered at the construction of concrete dams in severe climatic conditions is the performance of grouting operations to provide grout curtains in the foundation and to seal the joints.

So far the elaboration of joint grouting techniques at subzero temperatures amounted to the selection of special cold-resistant grouts and different ways of warming the joints. Grouting of construction joints preceeded by hydrodefrosting is considered to be promising. This method has been tested at the Zeyskaya and Sayano-Shushenskaya dams and, according to the investigation results, proved to be rather simple and inexpensive.

In the construction of dams on soils susceptible to settling under thermal effects, where the foundation should be kept frozen, a frozen-up dam with cooling system ensuring its integrity is required. Arrangement of thermoinsulating curtains cutting off frozen concrete dams from reservoirs presents some difficulties. In this case thermohydroinsulating facings of and impervious membranes in the concrete dams and other reinforced concrete structures appear to be rather effective. The dams so protected can be built of low-cement concrete with relaxed requirements on waterproofness, frost and crack resistance.

The designs are elaborated of highly reliable and durable impervious membranes and complex thermohydroinsulating facings of asphaltic lightweight concrete, foam plastics and foam asphalt with reinforced concrete and glass-reinforced plastic enclosure. Also elaborated are the designs of deformation joint sealings and methods for design calculation of plastic thermohydroinsulating facings.

A 200 m^2 experimental strip of such facing has been constructed and tested for 3 years at the Andizhanskaya dam. The tests have demonstrated that in plastic lightweight asphaltic concrete even 2-3 mm cracks and joints undergo self-healing thus restoring waterproofness of the facing. The tests of embankment facings on the Barents Sea and Sea of Okhotsk and thermohydroinsulating facings at the Vilujskaya dam conducted for 10 years have confirmed high reliability of thermohydroinsulation and its protective enclosure.

Construction of hydraulic structures in cold climate is a complicated task which calls for innovative organizational, technological and design solutions.

STUDY OF SOME GEOTECHNICAL ASPECTS EFFECTING CONSTRUCTION IN GLACIAL REGIONS OF HIMALAYAS

D.S. Lalji and R.C. Pathak

Dte of Engg (Def R&D Orgn), Kashmir House, New Delhi, India

SYNOPSIS The higher morphogenic tracts of lofty snow bound Himalayas possess the largest glacier resources in the world, outside the Polar regions. Besides the perennial ice cover, vast reaches of Himalayas come under periglacial environment. Due to unique orographical features of the Himalayas, the lithotectonic zones like Pir Panjal, Great Himalayas and Trans Himalaya ranges receive maximum snow precipitation whereas Zanskar and Ladakh ranges almost receive no snow-fall. In the Western Himalayas, the snow fall pattern is primarily governed by Western Disturbances. In the present paper terrain evaluation, pavement and foundation construction problems of the permafrost and periglacial regions have been attempted. Icing phenomenon, de-icing techniques and the freeze-thaw cycles have been highlighted. The salient geomorphological and geotechnical expressions have been studied with a veiw especially to analyse cold region construction problems.

INTRODUCTION

The remote high-altitude areas of North Western tracts of most enchanting Himalayas inherit some of the largest glacier and permafrost resources in the world. The unique orography and the litho-tectonic structure of the lofty regions of Himalayas exposes a varied and vivid type of geotechnical studies under varying seasonal environment. Besides the perennial ice cover, vast reaches of Himalayas come under periglacial snow cover. Notwithstanding with the fact that human spatial pattern, flora and fauna is sparse in the extreme- ly cold regions, the bare essential need of communications means like tracks, pavements, shelters etc. poses a gigantic task especially under adverse climatic conditions. The problems are further aggra- -vated by the presence of numerous devastating and active snow-ice avalanches.

In the present study the various geomorpholo- gical and geotechnical expressions have been looked into with a view to analyse the identified cold region problems and offer some viable solutions to keep up the normal functional aspects of the populace. The terrain evaluation of the region, the de-icing techniques and foundation parameters of the periglacial and permafrost regions have been highlighted. The construction techniques of pavements and suitable type of habitats alongwith essential supporting services are discussed and suitably presented in the paper after thorough ground checks and physical reconnainances with the helps of large scale topographical survey maps.

REVIEW OF LITERATURE

The inaccessible, unapproachable and hostile terrain of the Himalayas poses challenging tasks in carrying out geotechnicalstudies and maintaining communications. However, undeterred by the cold climatic hazards, Indian Scientists and geotechnical engineers have accepted the challenges and have made commendable progress and tackled permafrost engineering problems with success. The meteorological and environmental effects have been studied in detail by the weather scientists (Pradhan et.al.,1977). The effect of vege- tation and slope stability aspect of peri- glacial regions of Western Himalayas have been analysed (Pathak,1987)(Pathak et.al, 1987). The snow and ice technology of snow bound regions have been amply studied by the author (Lalji D.Singh et.al.,1977). Deicing and anti-icing problems of the roads and pavements have been attempted since early seventies by the scientists of Snow & Avalanche Study Establishment (SASE) and engineers of Border Roads Organi- sation (BRO). The various techniques of de-icing praticed by the above organisat- ions have been presented (Annual SASE Report 1974-75, 1980-81).

Vombatkere (1985) has studied the long term behaviour of glacial ice and also has organised for construction of a bailey bridge at the altitude of 5580 m (1986). Freeze-thaw cycle (Pathak et.al. 1987) and frost-heaving has been studied for pavement construction etc. In somewhat similar scenario Dayal(1985) has reported a frost action study for trasmission line routes between Labrador and Newfound-

land, Canada. Also, terrain evaluation and geotech- nical appreciation has been accounted for by the above author for the same region (Dayal, 1980).

One of the main reasons for instability in glacial soils seems to be the loss of buttressing support by the ice, coupled with excessively high regimes of ground water. Another potentially unstable situation is the one often associated with solifluction sheets or lobes widely encountered in periglacially modified terrains (Eyles, 1983). The shelters made of corrugated gulvanised iron sheets, containerised version, on ground or on sledges , have been time tested. The habitats have been even tried in Antarctic regions and are found very useful under the severe climatic hazards. The authors even recommend the above shelters for other permafrost regions of the world.

TERRAIN EVALUATION AND CLIMATOLOGY

The Himalayas display fantastic variations of geology, geomorphology, climate and vegetation. The lithotectonic zones of Western Himalayas exhibit unique orographical features. The Southern side of the Himalaya is humid with luxuriant flora whereas the Northern side is arid, barren and wears a look of desert. The Pir Panjal, Great Himalaya and Trans Himalaya ranges receive more snow precipitation whereas Zanskar and Ladakh ranges are almost bare coming under low pressure belt of Western disturb- ances mainly responsible for snow precipi- tation. The glacial region is generally above the snow line around 4500m. The study area which is situated in the Northern part of Jammu & Kashmir (J&K) is shown in Fig.1. A typical permafrost glacier region has been depicted at Fig. 2, the base of which is around 4200 m. Outside the permafrost regions fall the periglacial areas which also poses the similar problems of extreme cold effects. A good knowledge of terrain characteristics eventually determines the evolution and geotechnical aspects of periglacial landform.

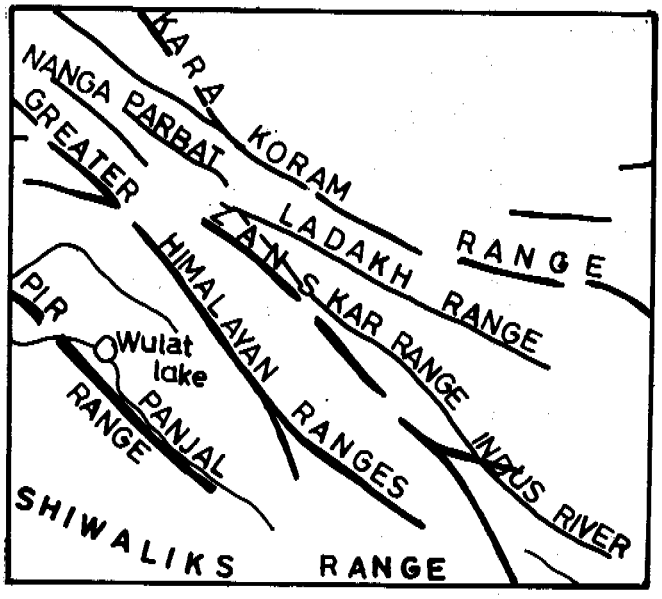

Fig. 1 Lithotectonic Zones of Himalaya

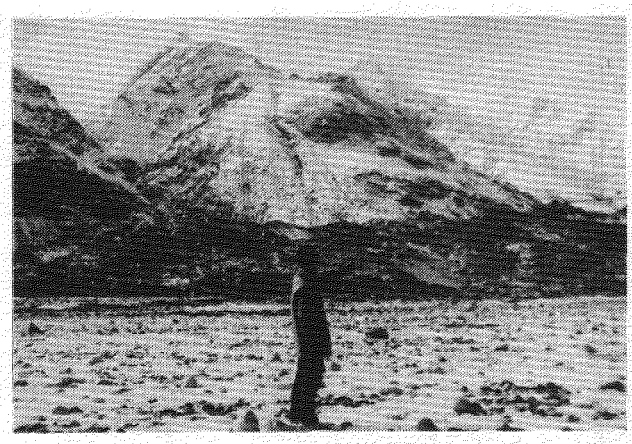

Fig. 2 A Typical Glaciated Region.

In the winter and most part of the year the water bodies in these regions are frozen. Only during summer, snow and ice melts and high flood level is recorded in the valley rivers. The safe tracks and roads have been constructed generally along the river and foothills of the valley mountains. The path is sometime encountering snow and ice avalanches and passes at a height of 5600 m. The glaciated region experiences artic type climate which is primarily governed by the orography. The orographical features could also be obsevered in Fig-1. De-icing and snow clearance is very often required in the area.

DE-ICING

Good amount of work all over the world has been done for de-icing operations by adding chemicals to control ice and snow conditions. Anti-icing techniques, using uncrushed rock salt, coal dust and use of abrasive material is also prevalent. Imminent among them are the several investigates and agencies (Allied chemical, 1958; Brohm and Edwards, 1960; Schneider, 1960). Most commonly used chemicals are sodium chloride and calcium chloride. In the present scenario authors have used urea also in addition to the above two salts in early seventies for de-icing purposes. Primarily using chemicals the eutectic composition i.e. concentration of the solution that possess the lowest freezing point, is important. The eutectic temperature i.e. temperature at the eutectic point is of relevance. Calcium chloride water system remains liquid at temperatures as low as -51°C, which is only -21°C in case of sodium chloride. A comparative chart

of sodium chloride, calcium chloride and urea are drawn at Fig. 3(a). Fig 3(b) represents the melt rate comparison between coaldust with soil as anti-icing measures. It was observed that melt rate of sodium chloride is more than the calcium chloride and 60% melting is achieved within 90 minutes time interval. Though initial melt rate of calcium chloride is faster because of

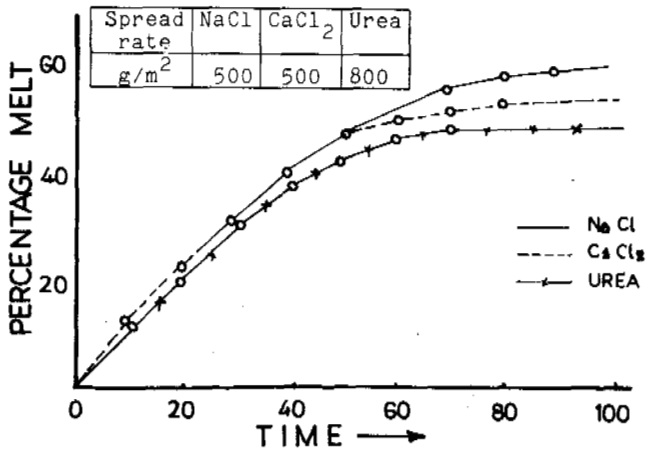

Fig. 3 (a) Melt Rate of Ice Using Chemicals

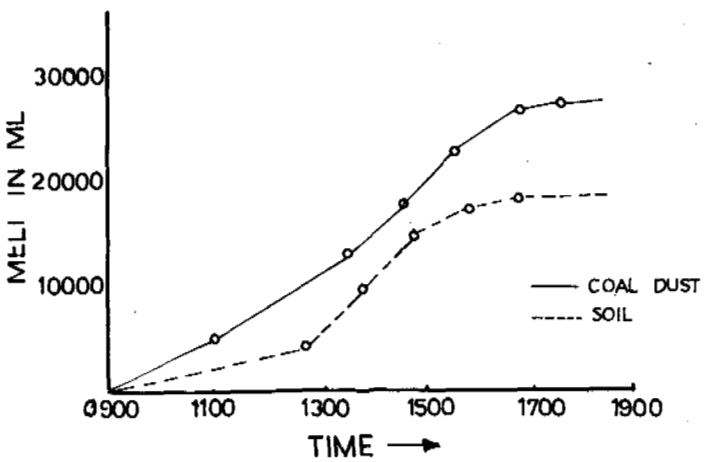

Fig. 3 (b) Melt Rate with Coal Dust And Soil

its exo-thermic reaction, imparting additional heat energy. For achieving similar results, almost double spread rate of urea has to be used. In Fig. 4, a vehicle loaded with container is shown passing through after deicing operation.

In Fig. 5, a Jonga vehicle is approaching the bridge constructed at the height of 5580m on the glacier. Deicing trials with sodium chloride using salt spreader was compared with the mannual spreading rate at the critical stretches in J&K under minimum temperature condition of -17°C. Use of coal dust and abrasives is effective when adequate heat is received from solar

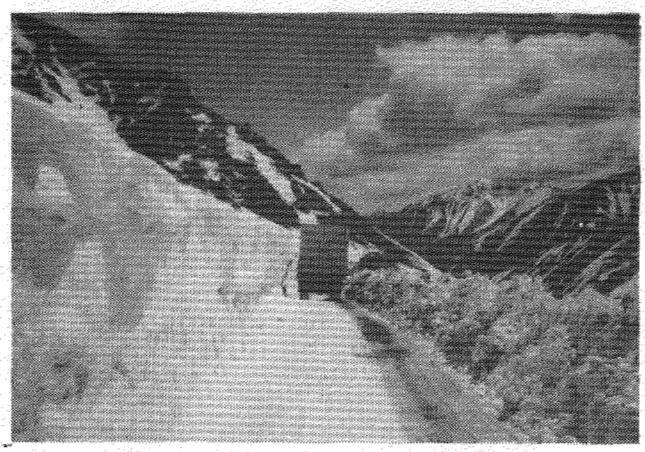

Fig. 4 Transportation of a Container After Deicing operation

radiation. Anti-icing techniques using un-crushed rock salt has been found quite

Fig. 5 A Jonga Crossing Bridge at ht of 5580 m

effective in controlling the ice formation along the side drains and in the mouth of culverts. (Refer Fig. 6)

CONSTRUCTION OF PAVEMENTS

Tracks and roads are the most vital arteries of an efficient communication system. Frost susceptability of the perma- frost regions, subgrade soil condition and freeze-thaw cycle pheno-menon of the periglacial environment plays a very significant role for design and construction of the pavment. As is generally observed in the mountainous tract the roads/tracks passes through saddles/peaks of at places but normally it is along the foothills or near the bed of the valley. Some of the salient factors viz, periglacial solifluxion, frost susceptability, freezing index and depth of frost penetration is discussed below alongwith the practical experience and new line of approach adopted in Indian conditions of Western Himalayan Region.

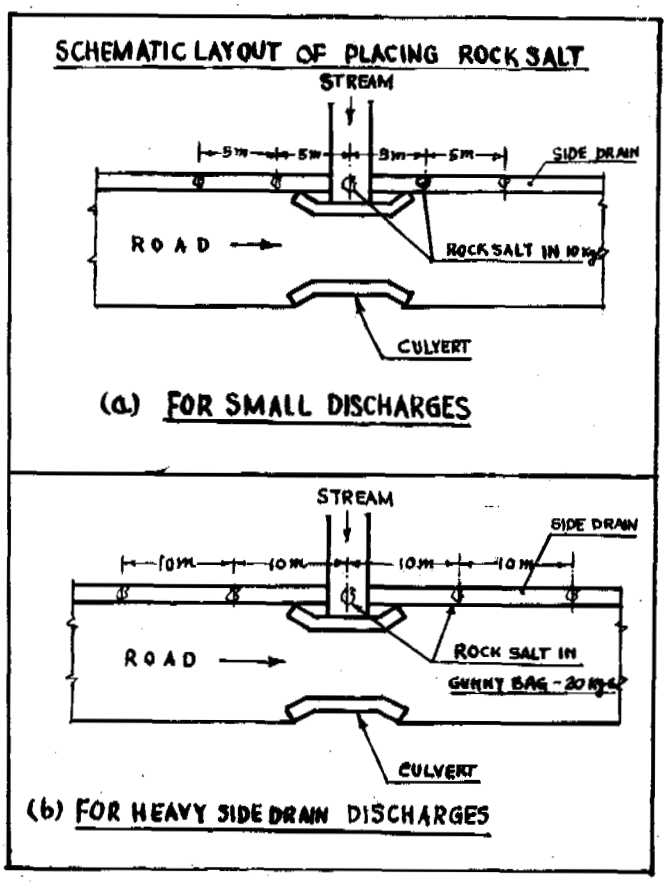

Fig. 6 Layout of Placing Rocksalt

The road construction activity is of recent origin in the study area which comprises mainly of Shyok-Nubra valley and Indus valley Zones. Since road communications are still developing in this region, most part of pavement is WBM type and runs through dry river bed and lower foot hill slopes. Black topped portion exist in comparatively in habited areas. As has been observed earlier, the area experiences severe winter onslaught during 3 to 4 months (Nov-Mar). When the maximum temperature is also at subzero near the glacier area. The area is essentially experiencing glacial and periglacial climatic conditions. Andersland et.al.(1978), Phukan (1985) and Chamberlain (1986) have amplyanalysed the geotechnical problems of frost-heave, periglacial solifluction, frost-susceptability etc.

The mechanical analysis of frozen/unfrozen soil has been done in the laboratory to ascertain its frost susceptability and also CBR Values found out. The data thus obtained has been further evaluated by monograph suggested by Chamberlain (1986). The soil is found to be marginally suscptible only as sand percentage is more than silt. These results are tabulated in Table-I. The frost penetration depth, proposed by Aldrich and Painter (1953) alongwith freezing index is presented in Table-II. The The values of frost penetration observed and computed for three experimental stations are in reasonable agreement. The base thickness of the pavement has been determined by the method of reduced subgrade frost penetration as suggested by Lobacz et.al. (1973). The active layer exists upto 1m depth from top surface in the glacierized region of Nubra valley.

Apart from the icing methods cited before by chemical means, the following practical approach has been resorted to for most of the length of road stretch in the Shyok-Nubra valley and Ladakh region (J&K).

i) Realignment of the route has been done to avoid icing formation.
ii) The surfacial small channels have been diverted away from the road towards valley side.
iii) Wherever possible culverts/bridges have been constructed to avoid small channels/river-icing features.
iv) At some places earth-boulder embankments also have been used to avoid ground icing phenomenon.
v) On the main valley glacier, only pedestrian tracks have been able to construct at the first instance due to presence of many crevasses.
vi) A peculair patch of glacier tongue, 90m width, crosses the road at site of 5530m altitude, which was initially tackled by imbedding boulders/glacial till on the pavement portion. Since the boulders and other debris materials had recurrent sinking due to thermal regime, a bailey bridge was later constructed at this site to finally over come this difficulty. (Refer Fig. 5)

TABLE-I

Soil Classification for Frost Susceptability (Subgrade Soil - CRREL, 86-14)

Location (samples)	Type of Soil	Mechanical Analysis %passing by weight I.S. Sieve			CBR Value Unsoaked	CBR Value soaked	Frost Susceptability
		4.75 mm	2.36 mm	75 micron			
Station 'A' (Altitude 5500m)	SW - SM S-Sand W-Well-graded M-Silt	73.70	56.08	10.54	7 6	12.0 12.5	L-M (Low to medium) As per CRREL report 86-14 Table for Silty gravely sand, p.p.47 Density-2.05 MC(%)-8.0
Station 'B' (5530m)	SW - SM	68.53	50.57	8.99	6 5	13.0 14.0	

TABLE-II

Freezing Index and Frost Penetration Depths

Location	Freezing Index	Depth of Frost Penetration (m) Computed	Observe
Site A (Alt. 5600 m)	500	1.0	0.9
Site B (Alt. 4300 m)	400	0.8	0.6
Site C (Alt. 4500 m)	300	0.7	0.5

Geotechnical Construction Measures

Generally the road alignment is chosen to avoid difficult stretches and water bodies. A bailey bridge designed and constructed over a Pass of altitude 5603m is the highest improvised bridge in the world (Vombatkere, 1985; 1986). The movement of the ice body recorded is negligible. A typical valley road is depicted at Fig. 7. To reduce the frost action, the following measures have been taken :

i) Clean sand or non-frost susceptible soil (NFS) has been put to replace the susceptible soil.
ii) Additional drainage measures have been considered for unexpected wet areas which are a potential source of moisture migration

iii) In the valley, low cost roads on morainic soil has been constructed.

iv) To cater for loss of buttressing ice support, cross drainage has been provided at places.

v) Due to low brittleness of glacial sandy tills, slope failures are very less. Slopes of 2.5 to 1 is generally suitable and provided.

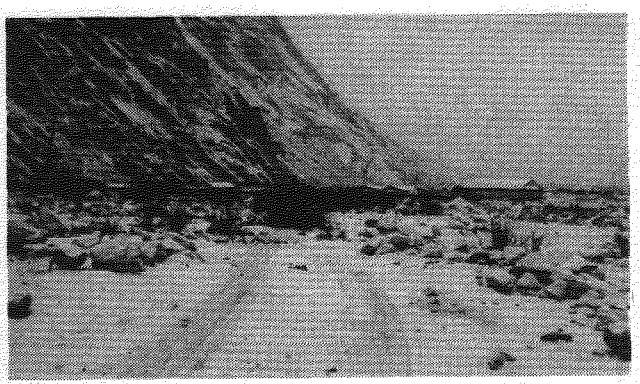

Fig. 7 A Valley Road Track

PLANNING OF SHELTERS

Durable shelters are pre-requisites for the cold regions to withstand the onslaught of wind, snow load etc. Adequate insulation is desirable to keep the inside temperature comfortable. Good amount of research and development has been done towards this end to achieve the desired results. In the Western countries the type of shelters or habitats used are box and cylinderical containers placed above ground, partially buried or totally underground etc. In Indian scenario all these types may not besuitable due to its difficult means of communication and environmental effects. In the present context the Indian scientists have used portable high altitude shelters and containerised modules for various types of accommodation required apart from arctic tentages and low foundation temporary shelters etc. The materials of the habitats used are generally prefabricated aluminium alloy, prefabricated fibre reinforced plastic or glass material (FRP or GRP), FRP sandwitched panels having insulation and fire resistant phenolic foam have been used and found suitable. The components designed and used are light and helicopter-portable. The roof has slope of 15° to 30° on either side to cater for snow loads. The total infrastructure is designed to withstand 100 to 150 kmph of wind speed. In Fig. 4, a loaded container accommodation is shown being transported on a lorry 3 tonner over a permafrost region.

Foundation of the shelters in high altitude area poses peculiar problems. Digging on glacier ice is very difficult. Taking into account all such odds, the foundation generally has been prepared on morainic till soil with small crib-piers and on timber grillage. This also is helpful in minimising differential or unequal settlement due to melt freeze or gradual glacier movement phenomenon. In permafrost regions, foundations are generally placed below the frost penetration depth or active layer. The major consideration to be taken into account are depth of supporting soil strata structure, thermal regime of ground, level of moisture content causing shrinkage/swelling of soil, problems of ice masses and proper drainage. In the present context of rocky and coarse sandy soil ice lenses formation is very less, therefore, normal shallow foundation upto a depth of two-third of frost penetration has been taken for construction purposes. At some places foundations have been laid by cutting ice/snow to about one metre depth. A bottom course of wire netting, corru- gated iron sheets and then cross members of wooden sleeper grillage has been provided to cater for even distribution of super structure load. Leaving a hollow space underneath the superstructure and grillage foundation minimises differential settlment and active layer action. A conventional type of step foundation has been provided for a high altitude shelter made of corru- gated gulvanised iron sheets with transverse and vertical steel truss members as depicted in Fig. 8. About 0.8 m to 1 m deep foundation is considered adequate to withstand the load of super structure. A bottom course of 15 to 20 cms of clean sand has been used to nullify frost heaving action. Calcium chloride is mixed in cement in suitable proportion forproper bondage. In all high altitude structures a small entrance is made before the main module for acclimatisation purposes. At the place of damp proof course level an insul- ation cloth-/material is placed and then flooring has been constructed. Apart from the indigenous improvisations, Indian National Building code also has been adhered to during constructions as far as possible. Suitable drainage has been provided especially in saturated glacial till areas.

Fig. 8 Temporary Shelter of Corrugated Sheets

ESSENTIAL SERVICES

At high altitude in extremely cold climatic conditions, the supporting services like water supply, cooking, power generation, sewage and human waste disposal becomes a difficult problem. Since prevailing low pressure hinders in normal cooking, tinned and semi-pre-cooked food has been found quite useful and recommended. For water, melting of ice and snow has to be resorted in suitable ice melting equipments. Ablution and sewage poses special feature. Use of polythene bags etc. for human waste disposal is quite common.

Some new design of incinerators are being used for sewage disposal which also acts as anti-pollution device. In the Indian conditions for heating of small cabins special type of kerosene burners with exhaust pipes are in use.

CONCLUSIONS

The lofty mountains of Western Himalayas are replete with numerous glalcier and poses tremendous challenges for keeping open and maintaining the vital lines of communications. To construct shelters, pavements and provide essential services for thinly populated permafrost and periglacial regions, is all the more a gigantic task in adverse climate conditions. However, appreciating the terrain characteristics, geomorphology and geotechnical expressions, the following few salient conclusions have been arrived at :-

i) Analysis of terrain evaluation, orography and synoptic weather system, western disturbances, help in appreciation of precipitation and deduction of geotechnical parameters.

ii) Deicing by mechanical means using chemical salts has been found very effective for road ice melting. Rock salt in gunny bags is useful for controlling ice formation in the side drains during early winter periods.

iii) Use of clean sand or non frost susceptible soil and proper drainage are considered very suitable for minimising frost action and periglacial soli-fluxion.

iv) Proper leveling of glacier moramic soil with timber grillage or crib foundations has been tried with success. Foundations on dug-in glacier ice with bottom course of geotextiles, corrugated galvanised iron sheets and timber grillage cross members have been found functional.

v) Precooked food, speical kerosene burners for heating and incinerator type sewage disposal techniques have been found very effective.

ACKNOWLEDGEMENTS

Authors are very grateful to the higher authorities of Defence Research & Development Organisation (DRDO) and various Establishments/Institutions for providing all facilities to carry out this study. Special thanks are due to Shri SS Gulati and Shri GP Nautiyal for excellent secretarial assistance.

REFERENCES

Aldrich, H.P. and Painter, H.M. (1953). Analytical studies of freezing and thawing of soils. Tech Report 42, ACFEL, U.S.A.

Allied Chemical (1958). Calcium Chloride. Bull. No 16, Tech. and Engg. Ser. Ind. Chem. Div. Morristown, N.S.

Andersland, O.B. and Anderson, D.W. (1978). Geo-technical Engineering for Cold Regions. Mc Graw Hill Book Co., New York, U.S.A.

Annual Reports of SASE (1980-81), Manali, India.

Brohm, D.R. and Edwards, H.R. (1960). Use of Chemicals and abrasives in Snow and Ice removal from highway Res. Board, NAS-NRC Pub., 761, Washington D.C.

Chamberlain, J. Edwin (1986). Evaluation of selected Frost-susceptability Task Methods. CRREL Report 86-14 (U.S.A.).

Dayal, U. (1980). Terrain Evaluation and Geotechnical studies for 800 miles long transmission line routes. Proc. 6th S.E.A. Conf. on Soil Engg. Taipei, China.

Dayal, U. (1985). Estimation of heaving and frost forces on Transmission Tower Foundations. Indian Geotechnical Conf. (I.G.C.-85), Dec 16-18, Roorkee, India.

Eyles, N. (1983). Glacial Geology, Pergamon Press Toronto, Canada.

Lalji D. S., Sharma, S. S. and Upadhyay, D.S. (1977). Gap in know how on Snow and Avalanche Technology. P.P. 163-171. Int. Workshop on Ice, Snow and Avalanche, Manali, India.

Lobacz, E.F., Gilman, G.D. and Hermon, F.B. (1973). Corps of Engineers, Design of Highway pavements in Areas of seasonal frost. Proc. of Synp. on Frost Action on Roads, Oslo, P.P. 142-152.

Pathak, R.C. (1987). Geotechnical Aspects of Snow-pack stability of Himalayan Region. Proc. of Int. Sym. on Avalanche Formation, Movement and Effects. IAHS, Pub. No 162. Davos, Switzerland.

Pathak, R.C., Rao, A.P.R. (1987). Some Applied Geo-morphological aspects of Slope stability of Himalayan Region - A case study. Int. Sym. on Geomorphology and Environmental Management, Allahabad University, Allahabad, India (In Press).

Phukan, Arvind (1985). Frozen Ground Engineering Prentice Hall, Inc. New Jersey (U.S.A.).

Pradhan, S.K., Upadhyay, D.S. and Lidoo, P.N. (1977). Climatology of Jammu and Kashmir. P.P. 19-33. Int. Workshop on Ice, Snow and Avalanche, Manali, India.

Personal Communication with Col. S.S. Sharma and other scientists of Defence Research & Development Organisation and B.R.O. (1986-87).

Schneider, T.R. (1960). Eidgenossische Institut fur schnee-und Lawinenfurschung, Weissfluhjoch, Davos, Switzerland.

Vombatkere, S.G. (1985). On the long term behaviour of glacial ice under moving traffic load - A case study. Journal of glaciology, Vol-31, no 109, P.P. 169.

Vombatkere, S.G. (1986). Bridge Resting on an ice body at high altitude. A.S.C.E. Journal, Vol-112, No 2 June 86, U.S.A.

A SUBGRADE COOLING AND ENERGY RECOVERY SYSTEM

E.L. Long and E. Yarmak Jr.

Arctic Foundations, Inc., Anchorage, Alaska, USA

SYNOPSIS The Kotzebue Senior Citizen's Cultural Center had experienced foundation distress due to thaw settlement since construction in the summer of 1975. The structure was originally constructed with a conventional foundation (i.e. heated crawl space) on gravel fill over ice-rich permafrost. A mechanical refrigeration system utilizing 20 horizontal copper loops was installed in 1976 to circulate a cooled glycol/water mixture beneath a layer of polyurethane insulation. Due to operational difficulties, this system only slowed the permafrost degradation and subsequent settlement of the structure. In the summer of 1986, the mechanical system was converted to a two-phase thermosyphon with parallel evaporators and a common external condenser using carbon dioxide as the working fluid. Each of the 20 existing copper loops is utilized as an evaporator. The heat removed from the subgrade is used to preheat make-up air for the ventilation system. Existing mechanical refrigeration equipment was utilized to provide back-up refrigeration capability. Without energy input, the subgrade cooling system now has the capacity to withdraw five times the heat of the mechanical system. Subsequently, the progression of thaw beneath the structure has been reversed.

INTRODUCTION

The village of Kotzebue is located in northwest Alaska at the north end of the Baldwin Peninsula between Kotzebue Sound and a substantial lagoon. To the east and south of the lagoon, low hills dominate the landscape of the peninsula. West of the lagoon, a gravel spit exists upon which the majority of the village's development is clustered. The entire Baldwin Peninsula lies within the region of continuous permafrost with the depth to the base of permafrost being approximately 73 meters in the Kotzebue area (Brown and Péwé, 1973; Ferrians, 1965).

The gravel and sandy gravel deposits that form the Kotzebue Sound side of the spit are generally 9 to 12 meters in depth and are underlain by fine-grained deposits of sand, silt, clay and organics. The soils in the hills to the east and south are predominately ice-rich fine grained deposits. The transition zone between the coarse grained spit deposits and the fine grained ice-rich deposits is interfingered with varying quantities of all the soil types found in the area and generally is capped by a tapering strata of granular soil.

Early structures in Kotzebue were small and used conventional footings on the gravelly soils near the beach where they experienced few foundation problems. As the village grew, the size of the structures increased and new construction was forced east where the surficial granular deposits were thinner and frequently interbedded with fine-grained lagoon sediments, organics and some ice. Even on the better portions of the spit, as the size of the structures increased, settlement became a problem as the thaw bulbs penetrated through the granular soils into the ice-rich fine grained material.

The Kotzebue Senior Citizen's Cultural Center (originally named the Kotzebue Pioneer Home) is sited east of the main village near the transition zone between the gravel and fine-grained deposits. The main portion of the structure is a hexagon with 18 m long sides. Two residential wings are attached to the south and southwest sides of the hexagon and a short mechanical wing is attached on the northeast side. The single story structure is founded on continuous footings with concrete stem walls approximately 1.4 m high. The crawl space beneath the floor is heated by the underfloor utilities. The original foundation design did not provide for maintaining the permafrost beneath the structure. The structure is shown on Figure 1.

In the fall of 1974, the immediate area of the building site was stripped of organics down to in situ granular soils. In the spring and early summer of 1975, the site was filled with 1 to 2 m of compacted granular material to form a level building pad (Abbott, 1975). The total depth of gravel averaged 2.5 m over frozen sand, silt and organics. By August 1, 1975, when the subfloor was installed, the south and southwest wings had settled as much as 5 cm.

EXPLORATION

Initial exploration of the site was conducted in 1973 with 23 borings over the general site area. The majority of the holes were to a depth of 4.6 m, however, three borings were

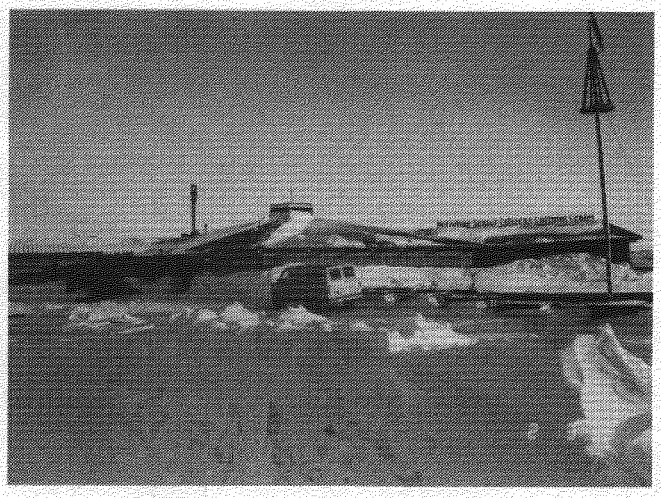

FIGURE 1
Kotzebue Senior Citizen's Cultural Center

made to depths of 12 and 17 m. Moisture contents of less than 30 percent were reported except for a 1-m ice lens in the southeast corner of the area at a depth of 1 to 2 m.

Following the observed settlement in August 1975, seven holes were put down around the structure with depths varying from 3 to 4.6 m. In January 1976, four additional holes were put down to approximately 15 m in depth taking continuous undisturbed samples which were shipped in the frozen condition to Cold Regions Research and Engineering Laboratory (CRREL) at Fairbanks, Alaska and Hanover, New Hampshire for analysis. The primary tests conducted were water content, gradation analysis, density determinations, and thaw consolidation.

SETTLEMENT ANALYSIS

Early settlement while the structure was under construction was attributed primarily to the thawing of seasonally frozen soils. It was also possible that consolidation of loose gravel fill and compressible soils not stripped from the site may have contributed to the problem (Abbott, 1975). The boring data obtained in January 1976 for CRREL indicated that much of the soil to a 15 m depth had moisture contents well in excess of 30 percent. Three of the 4 holes had strata with water contents well over 90 percent, while the fourth hole had strata with water contents in excess of 60 percent.

CRREL estimated that total settlements at the boring locations were expected to be 10 to 20 cm with thaw to 6 m, 20 to 30 cm with thaw to 9 m, and 45 to 60 cm with thaw to 15 m (Crory, 1976). As a result of the CRREL study, the State of Alaska Division of Buildings elected to mechanically refrigerate the entire foundation to maintain the permafrost. This option was one of five alternatives offered by CRREL. Plans and specifications were prepared and forwarded to the contractor.

MECHANICAL REFRIGERATION

Four loops of copper tubing were installed around the perimeter of the foundation while 16 loops were installed in the bottom of the crawl space. The loops varied from 107 to 391 m in length with a total combined length of 4400 m, of which 3450 m are beneath the heated floor space. The 2.2 cm outside diameter copper loops (spaced 0.45 m center to center) were buried beneath 7.6 cm of sand, 7.6 cm of spray applied rigid closed cell 2-component urethane foam, and covered in turn with a layer of spray applied fireproofing.

Refrigerated ethylene glycol was pumped through the coils having been cooled with two 11 kw capacity compressor/chiller packages. Initial freezeback was to be accomplished with both compressors running. Following initial freezeback, the second unit would serve as back-up. Eight fan coil heat transfer units (unit coolers) in two groups of four were connected in parallel to provide outside air cooling when ambient air temperatures dropped below -12°C. Switchover from the refrigeration/chiller unit to the unit coolers was performed automatically.

In September 1981, a review of the operational history of the refrigeration system was performed and it was determined that the mechanical system had been operating with less than 100 percent of all subsystems properly functioning. The building manager indicated that hiring properly trained personnel to operate the system was a major problem. The turnover rate for operators was so high that new operators were almost always being trained. The refrigeration system, with its subsystems, was a complicated operation which required continual monitoring and maintenance to function properly. This amount of "Tender Loving Care" could not be obtained from short term operators. Because the system was located in a somewhat remote city in Alaska, there were often delays involving ordering and delivery of repair items and scheduling of repairmen. Of course, any time the system was inoperative, subgrade warming and thawing took place.

It was estimated that the mechanical system cost $2300.00/month to operate in the summer and $1200.00/month in the winter (1981 costs). Assuming 4½ months of summer operation and 7½ months of winter operation, the total annual operating cost for the mechanical system was $19,350.00 (U.S.) in 1981. Additionally, periodic re-leveling was still being performed as settlement continued at a slower rate.

In 1983, the State of Alaska turned the operation of the Kotzebue Pioneer Home over to the Kotzebue community where it became the Kotzebue Senior Citizen's Cultural Center managed by Maniilaq Corp. In June 1984, Maniilaq advertised for a re-design of the refrigeration system. The system accepted was a conversion of the circulating glycol soil cooling system to a two-phase passive system (thermosyphon) which used the existing mechanical refrigeration and unit cooler system as back-up.

EVALUATION OF MECHANICAL SYSTEM

The total heat transfer through the floor was estimated using temperature measurements acquired on June 26 & 27, 1984. After the total heat transfer was known, the pressure drop through the system and the performance of the unit coolers was estimated.

The old system performance has been approximated by combining an equation which defines a row of infinite circular holes at equal depth and equal spacing in a semi-infinite solid, and an equation which defines a row of infinite circular holes in midplane of an infinite plate (Heuer, 1985), as shown in Figure 2.

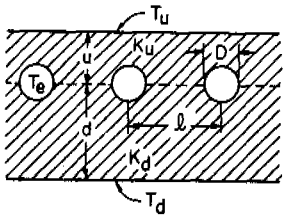

$$R_u = \frac{\ell n\left[\left(\frac{2\ell}{\pi D}\right) \operatorname{Sinh}\left(\frac{G_u \pi u}{\ell}\right)\right]}{G_u \pi K_u N}$$

$$G_u = 2\left(\frac{q_u}{q_u + q_d}\right)$$

d, u > D

FOR R_d OR G_d TRANSPOSE u's AND d's

$$q_{ud} = q_u + q_d = \frac{T_u - T_e}{R_u} + \frac{T_d - T_e}{R_d}$$

NOMENCLATURE:

- d = Downward Distance to Heat Source
- D = Diameter
- K = Thermal Conductivity
- ℓ = Spacing
- N = Length
- q = Heat Flow Rate
- R = Thermal Resistance
- T = Temperature
- u = Upward Distance to Heat Source

SUBSCRIPTS:

- d = Downward
- e = Evaporator
- u = Upward

FIGURE 2
Determination of Soil Thermal Resistance

The average rate of heat removal from the floor and the ground was found to be 25 kw with the coils at -4.4°C. There are 20 loops, so the average heat flux per loop was 1.25 kw.

The performance of the air cooled unit cooler was determined by knowing the heat flux and the temperature difference between the air and glycol. The overall thermal conductance of the unit cooler using glycol was calculated as 0.93 kw/°C. The manufacturer predicted a conductance of 5.20 kw/°C when using R-22 as the refrigerant condensing in a unit cooler.

The average monthly air temperature in Kotzebue reaches a minimum of -20°C. At this temperature, the glycol would be cooled 6.1°C with the compressor off and one unit cooler operating. If the two unit coolers were operated in parallel, the glycol would be cooled to -4.4°C. The use of the system without the compressor was practical only when the air temperature was below -15°C.

CO_2 PASSIVE REFRIGERATION

The passive refrigeration system was designed to remove heat from the underlying soil during the winter so that the depth of thaw in the summer will be acceptable. Also the permafrost would be brought back up to the seasonal frost depth. The system was designed to use carbon dioxide as the primary refrigerant. The carbon dioxide evaporates in the underfloor tubing and the vapor flows to the primary and heat reclaim condenser units, where it condenses and flows back down to the underfloor tubing. This cycle continues as long as the temperature beneath the floor is warmer than outside ambient air temperture (Long, 1963; Bunchko, et al, 1973).

With a maximum crawl space temperature of 21°C, an annual depth of thaw was calculated to be 1.1 m using the Modified Berggren equation.

The primary condenser was custom manufactured using finned radiators that are normally fitted to commercially available two-phase thermosyphons and is shown on Figure 3. The conductance of the primary condenser system is 3.6 kw/°C at an average winter air velocity of 6.0 m/sec (Zarling and Haynes, 1985). The conductance of the heat reclaim condenser (Figure 4) is 1.6 kw/°C when providing 2.4 l/sec of make-up air to the ventilation system.

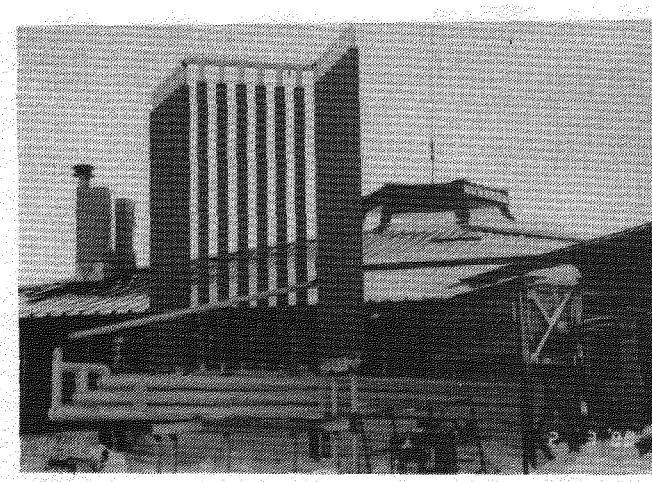

FIGURE 3
Primary Condenser and Liquid Accumulator

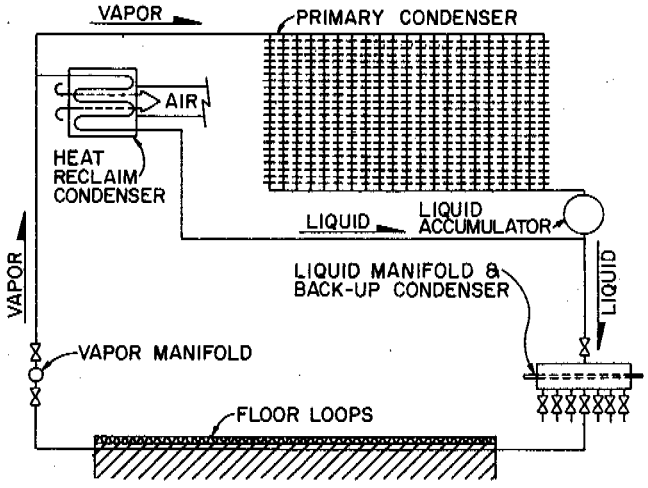

FIGURE 4
Schematic of Passive Carbon Dioxide System

A schematic diagram of the passive carbon dioxide system is shown on Figure 4. Valves have been provided to permit isolation of any one loop in case a leak should develop. A coriolis type mass flow meter and a pressure gauge were installed in early February 1988 to accurately monitor the heat flow of the entire system as well as the individual loops.

Heat transfer permits over 200 kw through the passive system alone. Once the permafrost has recovered to the seasonal depth of thaw, annual cooling will be 470 x 10^6 kJ for an average rate of approximately 22 kw. The heat transfer available to preheat the make-up air for the Senior Center ventilation system will be 140 x 10^6 kJ for an average rate of preheating of 7.7 kw.

BACK-UP CONDENSING SYSTEM

The back-up condensing system can make use of the two existing 11 kw unit packages to provide refrigeration during the summer months if it should ever be required. The compressor/chiller packages utilize R-502 refrigerant. The R-502 is condensed in the compressor section by evaporating R-22 which is condensed in the existing unit coolers located outside the structure. By utilizing R-22 instead of pumped glycol, the conductance of the unit coolers has been increased more than five times. The evaporating R-502 in the chiller section condenses the R-12 which then evaporates in the back-up condenser condensing CO_2. The back-up condenser also serves as a manifold to feed carbon dioxide condensate to each of the 20 copper loops under the floor. All condensate transport is by gravity feed and no pumps are required. The circuits for the back-up condensing system are shown on Figure 5. Note that R-12, R-22, and R-502 are fluorocarbon refrigerants. Each refrigerant was selected for its performance over specific temperature and pressure ranges. The R-22 and R-12 systems

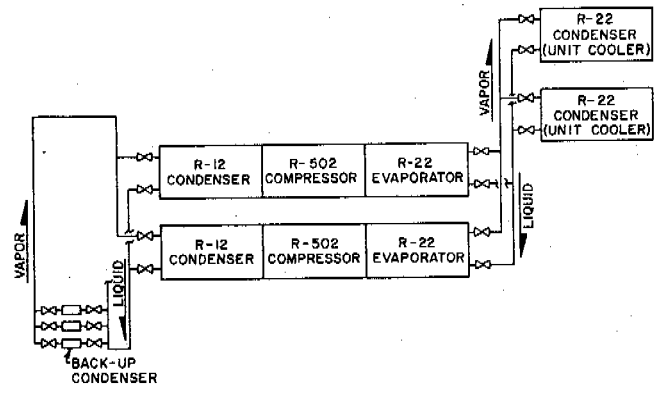

FIGURE 5
Schematic of the Back-Up Condensing System

are operating as thermosyphons while the R-502 vapor is compressed and re-expanded for cooling of the chiller.

CONCLUSIONS

The passive system used to replace an active glycol system has stopped the degradation of the permafrost and within a few years will effect complete recovery of the permafrost. Operational and maintenance costs on the passive system are nil compared to the mechanical system. Preheating of make-up air will further reduce the utility cost of the Kotzebue Senior Citizen's Cultural Center.

The successful conversion of a mechanical refrigeration system to a passive (thermosyphon) system offers another alternative to the high maintenance and energy requirements of mechanical systems.

REFERENCES

Abbott, R.D., Bestwick, L.K. (1975). Preliminary Subsurface Investigation, Differential Settlement, Kotzebue Pioneers Home, Kotzebue, Alaska. Shannon & Wilson, Inc., Fairbanks, Alaska.

Brown, J.E. and Péwé, T.L. (1973). Distribution Of Permafrost In North America And Its Relationship To The Environment: A Review, 1963-1973. Proc. 2nd Int'l Conf. Permafrost - North American Contribution, 71-100.

Buchko, N.A., Onosovskiy, V.V., and Sokolov, V.S. (1973). Liquid-Vapor Heat Transfer Devices Of The 'Long' Thermo-Pile Type For Cooling And Freezing The Ground When Building In Regions With Harsh Climates. Proc. 2nd Int'l Conf. Permafrost - USSR Contribution.

Crory, F.E. (1976). Final Report on Foundation Investigation for Kotzebue Pioneer Home, Kotzebue, Alaska. CRREL, Hanover, New Hampshire.

Ferrians Jr., O.J. (1965). Permafrost Map of Alaska. U.S. Geological Survey, Washington D.C.

Heuer, C.E., Long, E.L., and Zarling, J.P. (1985). Passive Techniques for Ground Temperature Control. Thermal Design/Considerations In Frozen Ground Engineering. ASCE, 72-154.

Long, E.L. (1963). The Long Thermopile. Proc. 1st Int'l Conf. Permafrost. Nat'l Academy of Sciences, 487-491.

Zarling, J.P. and Haynes, F.D. (1985). Thermosyphon Devices and Slab-On-Grade Foundation Design. State of Alaska, Dept. of Transportation and Public Facilities, Report No. AK-RD-86-16.

LONG TERM PLATE LOAD TESTS ON MARINE CLAY IN SVEA, SVALBARD

T. Lunne[1] and T. Eidsmoen[2]

[1]Offshore Soil Investigation Section, Norwegian Geotechnical Institute, Norway
[2]Norwegian State Railways, Drammen, Norway (formerly of NGI)

SYNOPSIS Six instrumented footings have been installed to depths varying between 1.2 and 2.2 m in the saline Svea clay in order to measure the in situ long term creep rate. The shallowest plates are loaded to about 50 kPa and the warmest measured temperature just below the plates are - 2.5 to - 3° C resulting in a maximum creep rate of 2 - 2.5 mm/month, which is significantly less than what was predicted based on laboratory tests. The deepest plates are given a maximum load of 134 kPa. The warmest measured temperature is - 4.5° C and the corresponding maximum creep rate is 4 mm/months, which is close to what was predicted.

INTRODUCTION

Creep behaviour of foundation permafrost soil at Svalbard has so far been estimated based on laboratory tests on obtained samples (Furuberg and Johansen, 1983). Using creep laws (e.g. Ladanyi, 1972) allowable footing stress has then been worked out based on the results of the laboratory tests and assumed ground temperatures. For Svalbard most efforts have been concentrated on the saline Svea clay. In order to improve our knowledge about the in situ creep behaviour of Svea clay it was decided to carry out a series of long term plate load tests with different foundation depths and stress levels. The characteristics of the Svea clay are described by Gregersen, Phukan and Johansen (1983).

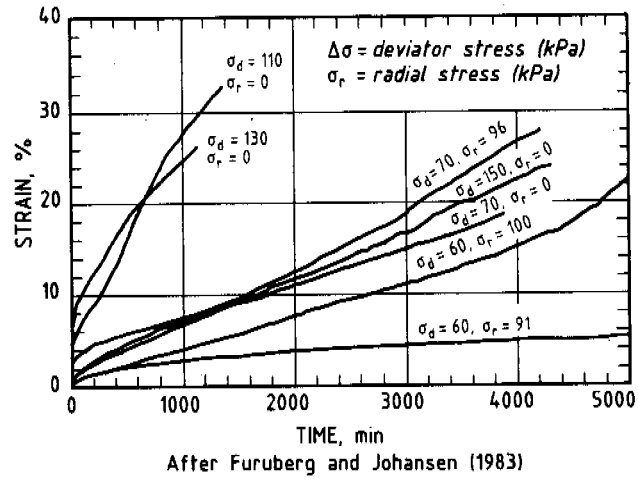

Fig. 1. NTH's creep tests on Svea clay at -3°C (after Furuberg and Johansen, 1983).

TEST SITE AND SOIL CONDITIONS

The test site is located at Svea on Svalbard. The Svea clay is a marine clay with a salt content of about 35 g/l and with up to 10 mm thick icelenses oriented both horizontally and almost vertically.

Laboratory creep tests have been carried out on Svea clay at temperatures of -5°C and -3°C (Johansen, 1981, Furuberg and Johansen, 1983). The tests are mostly carried out on unconfined samples, but some tests are done with a cell pressure. Fig. 1 summarizes the tests done at a temperature of -3°C. Table 1 includes the interpretation of the test results from Furuberg and Johansen (1983) using the creep model of Ladanyi (1972) or Vyalov et. al (1966). It must be emphasized that there is quite a spread in the data. Close to the location of the plates a permafrost station has recorded air temperature and ground temperature down to 3 m below the soil surface over the last ten years (Bakkehøi, 1982). Bakkehøi and Bandis (1987) have presented 5-days medium temperature in air and in the depth interval 0.0-2.5 m below ground level. Fig. 2 shows an example of these data for 1984.

Table 1. Interpretation of creep tests at -3°C and -5°C

	t = -5°C	t = -3°C	Formula
n	7.7	3.1	$\dot{\epsilon} = \dot{\epsilon}_{co}(\frac{\sigma_f}{\sigma_c})^n$
σ_c (KPa)	250	46	
$\dot{\epsilon}_{co}(min^{-1})$	10^{-5}	10^{-5}	

n = dimensionless exponent, dependant on soil type and temperature
σ_c = constant, dependant on soil type and temperature
$\dot{\epsilon}_{co}$ = constant dependant on soil type, but independant on temperature.
$\dot{\epsilon}$ = rate of strain
σ_f = applied stress (kPa)

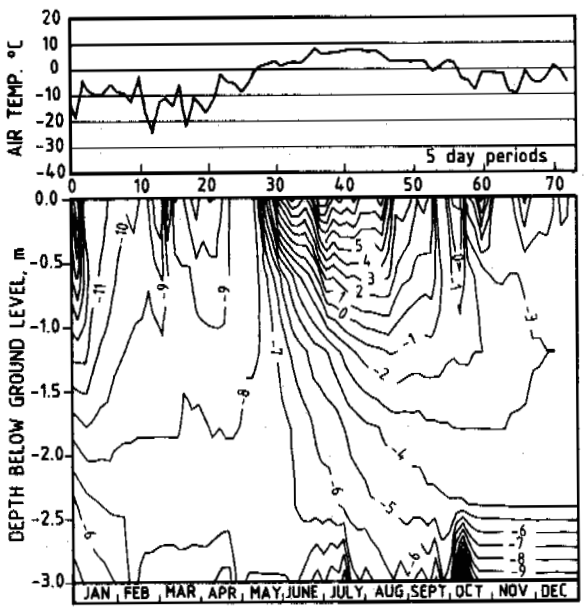

Fig. 2. Temperature recorded at NGI permafrost station in 1984.

FOUNDATIONS AND SETUP OF PLATES

The footings or plates are placed in two groups of three with center distance of 5.8 m as shown on Fig. 3. A hole was digged using a machine to the desired foundation level for each footing. The bottom of each hole was levelled off with a thin gravel layer 50 to 200 mm thick. A 1 m diameter, 22 m thick steel plate was placed directly on the gravel layer followed by an isolation layer of styrofoam (HD 300). As shown in Fig. 4 stiffened steel columns (ϕ 200 m)

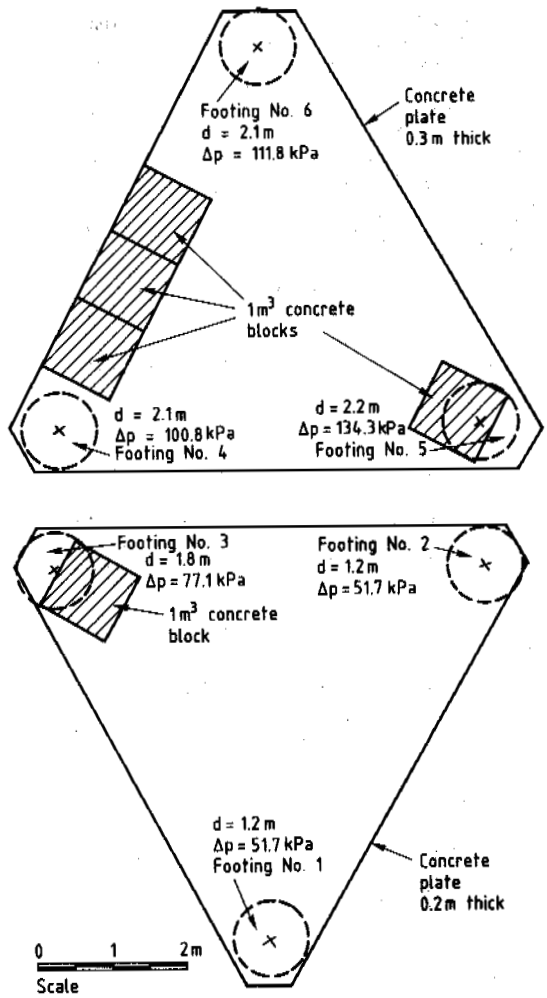

Fig. 3. Arrangement of footings or plates.

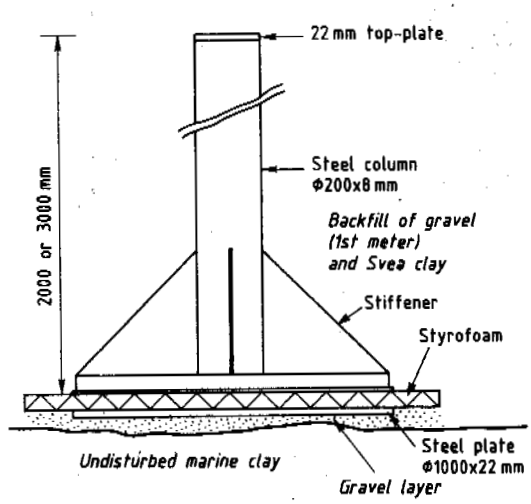

Fig. 4. Details of footing.

where placed on top of the styrofoam. The steel columns were lubricated with gear oil and a plastic sheet placed around it in order to reduce frost heave forces. On top of the columns a triangular concrete plate was cast which constitutes part of the load on the footings. For the shallow footings (2 to 1.2 m depth and 1 to 1.7 m depth) the concrete plate was 200 mm thick. For the deeper footings (2.1-2.2 m) the thickness of the concrete plate was 300 mm. Gravel was used to fill back about 1 m above the footing, the rest of the excavated hole was filled up with the original Svea clay. The footings or plates were installed in November 1986 and the concrete plates cast in December 1986.

INSTRUMENTATION

Fig. 5 shows schematically the foundation depth for each footing and the location of the thermistors and the settlement gauges.

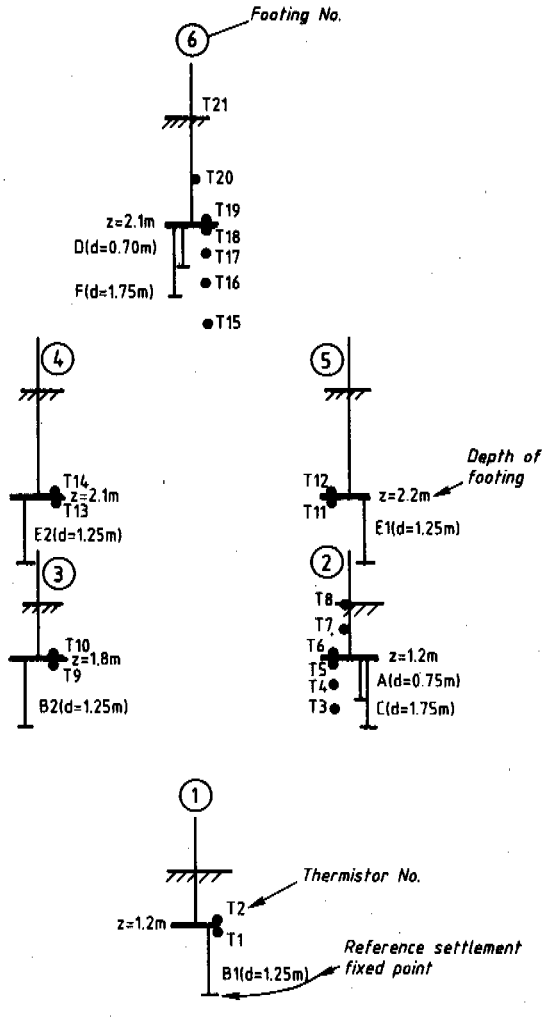

Fig. 5. Footing depths and locations of thermistors and settlement gauges.

Footings No. 1 and 6 (see Fig. 5) have settlement gauges relative to 0.75 m and 1.75 m below the plate. All the other footings have settlement measurement gauges relative to 1.25 m below the plate. The settlement measurement system consist of an inner rod with a tip of diameter 50 mm which is anchored at required depth. First a hole with a diameter of 70 mm was drilled and then the 50 mm diameter tip was frozen into the bottom of the hole by a mixture of sand and water. Outside the inner rod is mounted a protection tube from 0.25 m above the tip to 0.25 m above the footing. The protection tube is filled with oil to prevent the inner rod from freezing. An outer tube is fixed to the footing. Between the outer tube and the protection tube there is no connection. As the plate settles relative to the fixed point, settlements are read using the NGI precision settlement gauge system. Outside the plates a fixed point is anchored to a depth of 6 m below ground level (adaption after Bozozuk et al, 1963). As a check on the precision settlement gauges, settlements of each plate can also be measured by levelling relative to the fixed point.

As shown in Fig. 5 a number of thermistors (NTC-type from Fenwal Electronics) were installed at various depths below ground level. The thermistors are read using an ordinary voltmeter.

The bottom of the steel plate for foundation no. 6 is equipped with two earth pressure cells, (Geonor vibrating wire type), one in the centre and one 0.25 m from the center.

LOADING

After the footings were installed and the concrete plates cast final loading were delayed until the ground temperatures reached a normal level. On the 25th April 1987 additional load was put on using 1 m^3 concrete blocks as shown in Fig. 3. This resulted in calculated average contact stress for each plate as shown on Fig. 3.

MEASUREMENTS

Measurements have been taken at 2-6 weeks intervals since April, 1987.

Temperatures

Fig. 6 shows the maximum recorded temperature just below the plate for all footings in the observation period as a function of depth. As a reference the range of max. temperatures from the nearby permafrost station are included. It can be observed that the temperatures just below the footings fall well within the range of measured values from the permafrost station over the period 1978 - 1984. In Fig. 7 the

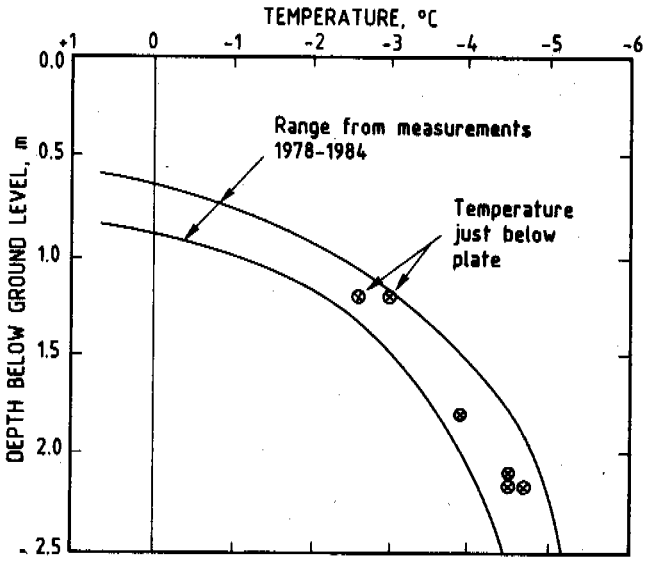

Fig. 6. Temperatures recorded just below footings compared with warmest 5 day medium temperatures for period 1978-1985.

temperature just below each plate have been plotted as a function of time.

Settlements

Fig. 8 shows the settlements as measured by the precision settlement gauges. Clearly one of the settlement gauges - F do by some reason not function properly. This is confirmed by the check levelling which was carried out 4th September. On Fig. 8 we have also marked the maximum settlement rate in mm per month, and at what time it occurs. As expected this to a large extent coincides with the maximum temperatures as recorded just below the plates. From Fig. 8 it can be observed that after November 1987 there are no settlements for any of the plates. In fact plates 1 and 6 show a small heave. The reason for this may be that some frost heave forces have acted on the steel columns even if precautions were taken to prevent this (see Chapter 3).

Earth pressures

As mentioned before plate 6 was equipped, with two earth pressure cells, one in the centre and one 250 mm from the centre. The

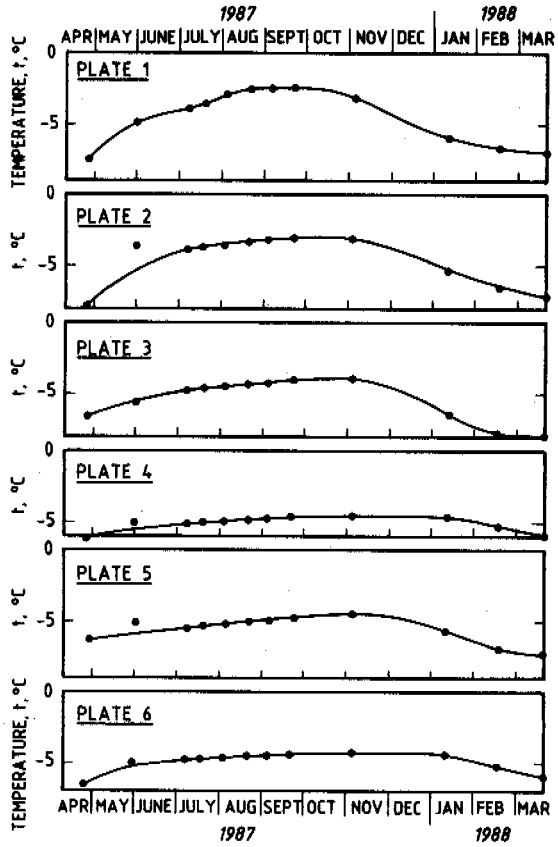

Fig. 7. Maximum observed temperatures vs. depth.

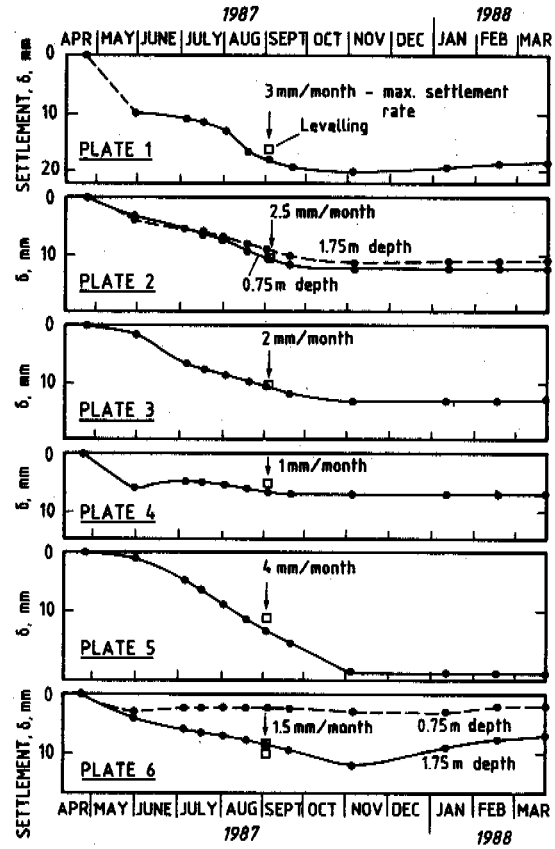

Fig. 8. Recorded settlements.

measured earth pressures have varied little with time and average values up to November 1987 are 144 kPa for the middle of the plate and 137 kPa from center of plate. The theoretical average contact pressure below plate no. 6 is 145 kPa which agree reasonably well with the measured values and confirm that the computed additional stresses are correct. After November 1987 there is a significant reduction in the measured earth pressures. A tentative explanation is, as mentioned in the last section, that frost heave forces have acted on the steal columns.

COMPARISON BETWEEN MEASURED AND COMPUTED SETTLEMENT RATES

Prior to loading of the plates the maximum creep rate of each footing was predicted Lunne (1987) based on the following:

a) A ground temperature profile from the measurements at the nearby permafrost station (Fig. 6).

b) Creep parameters from the tests carried out by Furuberg and Johansen (1983) and Johansen (1981). For temperatures between - 3°C and - 5°C, linear interpolation has been used for the parameters n and σ_c.

c) Stress distribution with depth according to elastic theory (Janbu, 1971).

Decrease in temperature with depth was taken into account by dividing the soil below the plates into layers of 0.2 m thickness. For each layer the strain rate, $\dot{\varepsilon}$, has been computed from the formula given in table 1. The total strain rate has then been computed by summation. The calculations show that the creep settlements are virtially confined to the upper 0.4 m below the plates.

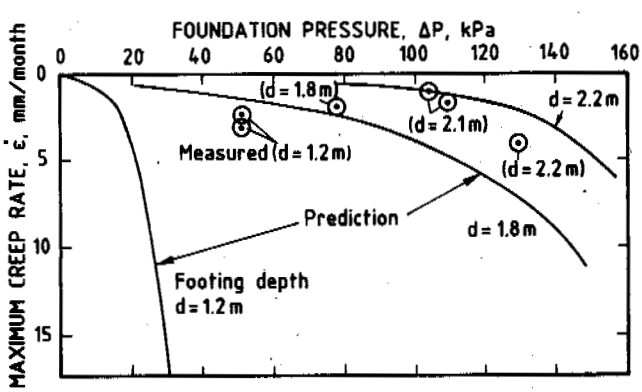

Fig. 9. Comparison between predicted and recorded settlements.

Fig. 9 compares predicted and recorded settlement rates for all plates. It can be observed that for the deepest plates (2.2 and 1.8 m depth) the measured and predicted settlements compares reasonably well. For the two shallowest plates (1.2 m depth) the predicted settlements are much larger than the observed settlements. This may indicate that the laboratory creep parameters determined from the highest temperatures of - 3°C are possibly unreliable and some additional laboratory tests on samples taken immediately below the plates should be performed at temperatures of - 3°C to - 4°C. The present stress level will be kept for one more year, then it will be considered to increase the stress level for all footings.

SUMMARY AND CONCLUSIONS

Six footings have been installed to depths varying between 1.2 and 2.2 m in the saline Svea clay in order to measure the in situ long term creep rate.

The footings have been instrumented so that temperature at various depths above and below the plates can be measured. For one of the footings contact stresses are also measured. Settlements of the footings are measured by precision settlement gauges relative to fixed points 0.75 to 1.75 m below the plates.

The two shallowest plates (1.2 m depth) are loaded by additional vertical stresses of 52 kPa. The warmest temperature below these plates are measured to be -2.5 to -3°C and the corresponding maximum creep rates are 2 - 2.5 mm/months, which are significantly smaller than what was predicted based on laboratory tests.

The three deepest plates (2.2 m depth) are loaded by additional vertical stresses of 100 to 134 kPa. The warmest temperatures in the soil below these plates are measured to be -4.5°C and the corresponding maximum creep rates are 1-4 mm/months (increasing with increasing stress), which is reasonably close to what was predicted based on laboratory tests.

ACKNOWLEDGEMENT

The project described herein is part of a research program supported by Statoil. The authors wish to acknowledge Store Norske Kullkompani, Spitsbergen (SNSK) for assisting with logistical support and following up the measurements.

REFERENCES

1. Bakkehøi, S. (1982)
Datainnsamling på permafroststasonen i Svea, Svalbard Frost i jord, publ. Nr. 24, Oslo.

2. Bakkehøi, S. and C. Bandis (1987)
A preliminary analysis of climatic data from the permafrost station at Svea, Spitzbergen Frost i jord nr. 26, Oslo.

3. Bozozuk, M., G.H. Johnston and J.J. Hamilton (1963)
Deep bench marks in clay and permafrost areas. In Field testing of soils, ASTM Sp. Tech. Pub. No. 322, p. 265.

4. Gregersen, O., A. Phukan and T. Johansen (1983)
Engineering properties and foundation design alternatives in marine Svea clay, Svalbard. International Conference on Permafrost, 4. Fairbanks, Alaska 1983. Proceedings, pp. 384-388. Also publ. in: Norwegian Geotechnical Institute, Oslo, Publ. No. 159, 1985.

5. Furuberg, T. og T. Johansen (1983)
Svealeira sin mekaniske styrke. Rapport til NTNF. NTH Rapport No. F-83.03.

6. Janbu, N. (1971)
Grunnlag i geoteknikk. Tapir forlag, Trondheim.

7. Johansen, T. (1981)
Krypforsøk på Svealeire. Rapport til NTNF. NTH Rapport F.081.05.

8. Ladanyi, B. (1972)
An engineering theory of creep in frozen soils. Canadian Geotechnical Journal Vol. No. 1, pp. 63-79.

9. Lunne, T. (1987)
Arktisk geoteknikk og fundamentering. Forutberegnede krypsetninger for platebelastningsforsøk i Svea. Intern Rapport 52704-5. 20. januar, 1987.

10. Vyalov, S.S. et. al (1966)
Methods of determining creep, long term strength and compressibility characteristics of frozen soil. Nauka Moscow Nat. Res. Counc. of Canada. Techn. Trans. 1364 Ottawa, 1969.

MELIORATION OF SOILS OF CRYOLITHOZONE

O.V. Makeev

Institute of Soil Science and Photosynthesis USSR, Academy of Sciences, Pushchino, Moscow Region, USSR, 142292

SYNOPSIS Effective complex melioration of soils with frost in the profile is possible if a simultaneous control of the two processes, namely frost and soil formation is ensured. A number of soils of cryolithozone due to the permafrost effect as a factor of soil formation specific cryogenic features, horizons and regimes, thus forming new types of soils, the most peculiar of which are cryogenic frozen ones.

Specific character of melioration techniques is increased from the south to the north in the cryolithozone.

The melioration technology of the following ecologo-meliorative groups of tundra soils: frozen tundra mineral gley, frozen tundra bog (peat) gley, coldgenic tundra soils of the bottoms of dried -up thermokarst lakes, coldgenic tundra floodplain and frozen tundra surface-gley; as well as recultivation of the soils destroyed by excavations; phytomelioration of the frozen tundra surface-gley soils are described in the present paper. The data on effective melioration are also presented.

In the northern hemisphere the formation of soils and soil cover is greatly affected by their annual freezing and thawing (Makeev, 1981). The greatest effect is observed in the northern regions where the soil profile often rests on permafrost.

Frost as a factor of soil formation accounts for a number of soil properties including the formation of their taxons. These soils are considered by us to belong to a big taxonomic group - massif of freezing-thawing or short-term trawfrost soils including megaformations of cryogenic and noncryogenic soils (Makeev, 1986). The megaformation of the freezing-thawing cryogenic soils includes the soils formed mainly in the high northern and southern latitudes as well as in the corresponding zones of mountain systems. The genesis development and functioning of such soils are greatly affected by negative temperatures resulting in phase transformation of soil moisture into ice and vice versa. These soils are to have one or several specific cryogenic horizons in their profiles and to develop under conditions of cryogenic (thermal, water, biological, etc.) regimes. During this process both cryogenic and noncryogenic horizons are destroyed and their parts can move in various directions.

The freezing-thawing soils unaffected by the soil cryogenesis, i.e. without profile properties, content, solum and regime characteristics belong to the megaformation of the freezing-thawing noncryogenic soils. They include, for example, all the soils with a short-term and shallow soil profile freezing (sand rubble, etc.).

The mefaformation of the cryogenic soils includes two formations: frozen and coldgenic ones.

The frozen formation consists of the freezing--thawing cryogenic soils, the profile of which is resting on permafrost rocks, being reached by the layer of seasonal thawing during winter time. Thus, these soil are called overfrozen ones. Their average temperature is negative.

Melioration of the following soils from the formation: frozen tundra mineral gley, frozen tundra bog (peat) gley and frozen tundra surface-gley, - is discussed in the present paper.

The coldgenic soil formation includes the soils, the profile of which does not rest on the permafrost, and they have no contact with the seasonal freezing layer. The presence of cryogenic properties, horizons and regimes in these soils is due to their lingering and deep seasonal freezing the degree of which depends not only on climatic conditions but also on granulometric content and some other factors. According to literature data they are shown to be in the frozen state not less than 5 months. Their mean temperature is positive.

Melioration of the following soils from the formation: coldgenic tundra gley on the bottoms of dried-up thermokarst lakes and coldgenic tundra floodplain, - is discussed in the present paper. The above-mentioned frozen and coldgenic soils of the cryolithozone have the most exhibited complex of specific features connected with the frost that results in specific techniques of their melioration. Effective melioration of the soils with the frost in the profile is possible under simultaneous control of the two complex processes: frozen and soil forming, however the task is simplified when the techniques coinside.

The techniques of controlling the frozen process in the soil grounds according to V.A.Kydryavtsev and E.D.Ershov (1969) are subdivided into four groups: a) changing the outer heat exchange; b) controlling heat exchange by changing the content and properties of the meliorated thicknesses; c) changing the temperature regime and heat state of the

meliorated thicknesses by using additional sources and runoffs of heat, and d) controlling temperature conditions in the rocks deposited lower than the meliorated thickness. The techniques of controlling soil forming process during soil melioration outside the cryolithozone are rather well grounded (Kovda, 1985).

Melioration of the soils with the frost in the profile is scientifically based on the estimation of the necessary level of soil heat provision which can be energetically evaluated as a part of annual heat exchange spent on heating the soil surface at its positive temperatures $Q_{t\ 0}$. This part of heat energy plays the main role in soil formation and vital activity of organisms. Its increase or decrease leads to a change both in the soil formation direction and soil bioproduction. Hydrotechnical as well as nonhydrotechnical techniques are used for this purpose. An artificial change both in heat and water regimes of the soils provided by all the techniques results in the increase of soil bioproduction. Therefore, it is rightfull to speak about hydrothermal meliorations when these techniques are applied in complex. However, in the majority of cases hydrotechnical meliorations and among them -drainage occupy the leading place.

The nonhydrotechnical techniques include

1. Snow meliorations providing control of snow accumulation and snow drive away. The effect of snow on the depth of freezing and thawing is many-sided. Due to its high albedo it has a cooling effect and being a thermal insulator in warms the soil by decreasing efficient irradiation. At a small thickness of the snow cover its cooling effect prevails over the warming one. Accordingly, complete snow detention with the formation of snow drifts provided due to small field areas, in the forest zone also preserves soil from strong and deep cooling and freezing, sharply spring warming up to a great depth and increases the amount of snow melting water. After heavy snow winters the snow drive away is required, it provides a sharp decrease of heat spent on snow evaporation, an additional input of heat into soil and good soil loading with moisture. In the region of Vorkuta the snow drive away provides the positive heat flow into the soil by 20-30 days earlier. In the areas with the near-to-surface ice deposit in the rocks the snow drive away combined with water drain from the surface prevents the appearance of thermocarst. Snow can be removed mechanically or by intensive thawing. Prolongation of the vegetation period results in from the snow drive away.

2. Application of various covers for soil surfaces (heat-light- and moisture insulating) is one of the main components of the thermal soil melioration. Coverage with synthetic films decreases the amount of heat spent on evaporation and heat emission coefficient, detains long wavelength infrared irradiation and increases heat provision coefficient of the seasonal-thawing layer. It results in the increase of heat accumulation in soil (temperature is increased by 6-8°C) and soil seasonal thawing. Effective irradiation can be decreased by covering the soil with the film before snowfall, the soil freezing being delayed by 2-3 weeks. Additional thermoinsulation after the snowfall can be provided with cheap wastes in the form of sawdust, peat, moss and artificial snow. In Yakutiya foam coverage gives the positive effect (it increases average temperature of the rocks by 1.3°C and the depth of thawing is decrea ed 3-6 times - Gavrilova, 1978). Covering with an ice-air layer or foam-ice of 35cm thickness at -20°C decreases the soil freezing 5 times, i.e. 40 cm instead of 2 m (Merzlotovedeniye, 1981). This group of techniques also includes colouring the soil surface (blackening, or whitening). Weakly-moisture-permeable covers (mulch, synthetic films) decrease the amount of heat spent on phase transformation of moisture.

3. The increase of soil roughness by its surface loosening allows to decrease albedo by 20-30% and to increase absorption of short wavelength light energy, the coefficient of heat conductance being considerably changed as compared with heat capacity. It probably results in the decrease of soil temperature. The opposite effect, i.e. the increase of the surface layer temperature, can be obtained by soil packing.

4. Subsoil tillage provides stubble preservation and in the arable layer it leads to the appearance of the cavities filled with air which in their turn decrease heat emission.

5. Application of row plant growing under row orientation from the north to the south has a heatting effect, since the total soil surface is increased and greater amount of solar energy will be absorbed.

6. Earthing of the frozen bog (peat) gley soils. In Magadan region (Korekovtsev, Orlovskaya, 1984) application of 200-300 m^3/ha of sand -ice alluvium provided the increase of the thawing depth at an average by 40%, +5°C isotherm reached the depth of 60 cm as compared with 35 cm in the control.

7. Rational forest concervation and field-protecting forestry preserve the soil from extreme winter cooling, decrease inefficient heat expenditures spent on ice thawing and evaporation from soil. Coulisses of perennial grasses and stubble preservation can be additionally used. Culturtechnical practice includes wood vegetation clearance, hassock cutting off and stone removing.

8. Placement of agricultural fields on downwind, flat slopes protecting from the north decreases soil cooling.

9. Application of fertilizers including those increasing cold hardness and frost endurance of plants: nitrogen ones - ammoniacal and ammoniacal-nitrate forms; phosphorus ones - simple superphosphate, containing sulfur; microelement ones molybdenum and nickel forms. In the regions with cryarid soils it is necessary to apply microelements, increasing crop drought-resistance. The soils with high acidity require liming.

10. Phytomelioration of soils. For this purpose it is necessary to select plants and grow new varieties adapted to the conditions of the extreme north as well as to use the productive local grasses on pasture and hay lands. Due to possible day and night photosynthesis with the absorption of not only visible but also infrared rays the amount of the organic matter synthetized under these conditions can be compared with that synthetized in a mild climate.

In the tundra zone the majority of the techniques

mentioned above can be often used together with the hydrotechnical meliorations. Forest conservation and field -protecting forestry are included in the techniques mentioned above for the zones beginning, mainly, from forest-tundra one and southward.

The technology of cryolithozone soil melioration is the most specific in the tundra zone and it will be discussed below, however a number of its elements can be applied in more southern parts of the cryolithozone on the soils with the frost in the profile.

This technology has been developed in energy detail for the groups of soils where drainage plays'a leading part (Makeev, Vasilevskaya and al., 1981; Proektirovanie meliorativnykh system na Dal'nem Vostoke, 1984). Let us consiger the technology of the following soils:

1. Frozen tundra mineral gley soils, the profile of which is resting on permafrost with visible ice, have the depth of seasonal thawing of up to 1.5 m and the heat provision of 20.000 kcal/m^2 year. The soils are of loamy, often medium loamy mechanical content characterized by poor water permeability and frequent thixotropy. Their excessive water stores are due to underground ice lenses and overfrost vadose water. They are situated on the slopes of the over-floodplain terraces. Agricultural development can result in the formation of thermokarst.

II. Frozen tundra bog (peat) gley soils, the profile of which is also resting on permafrost, have, however, the depth of seasonal thawing of 0.4-0,8m and heat provision of 15.000 kcal/m^2 year. The soils have a peat horizon badly decomposed on the top and well decomposed at the bottom. Mineral ground of various mechanical content often thixotropic underlays this horizon. Excessive water stores are the same as in the soils of the first group, but they include gravity supported water formed during snow melting in the seasonal thawing layer. The soils are situated on the depressed district of the over-floodplain terraces. The threat of thermokarst is great.

Melioration of the soils of the Ist and 2nd groups have to be carried out in two steps. During the first step (3-4 years) the thawing of the underground ice is carried out to obtain an even layer of the seasonal thawing, 0.8 and 0.6 m thick in the Ist and 2nd groups, respectively. This aim is achieved by constructing an open network of canals being placed at 100-200 m distance from each other in accord with agricultural needs. Taking into account possible thermokarst the depth of the canals should be not less than 1.4-1.6 m. The beginning of ice melting is provided by sheet preparing, then as far as the thawing proceeds the repeated (not less than three times during the warm period) ridging of a thick network of furrous at a depth of the thawing layer is carried out. The excessive water is removed from the thermokarst depressions which are then planned. It prevents the thermokarst formation during application of soils after melioration. During the 2nd step a drainage network is reconstructed and an irrigation one is built for sprinkling. In the soils of the 2nd group 400-500 m^3/mm of mineral ground per ha should be applied to the arable area.

Building of the roads and hydrotechnical constructions is carried out during both the steps. It is prohibited to remove the soil cover from the routes in order to decrease the threat of thermokarst.

III. Coldgenic tundra gley soils of the bottoms of dried-up thermokarst lakes. Permafrost is absent there but the soils have a tendency towards aggradation. The depth of the seasonal thawing is 1.5 m, heat provision 20.000-25.000 kcal/m^2 year. According to the mechanical content the soils are loessial silt clay loam. The bottoms of shallow lakes have flat slopes.

Melioration of the soils of the 3d group should be realized by the construction of canals for water discharge from the thermokarst lakes, control over the overgrowth of the lake bottoms with productive arctic perennial grasses including their undersowing Arctagrostis broad-leaved, in particular. Liming and application of mineral and organic fertilizers are required. The yield reaches 30-35 c/of hay per I ha (Shvirst, 1984).

While operating the drainage systems some measures should be taken to prevent possible frost aggradation and flooding of the dried-up lakes with spring floods. After degradation of meadow associations it is necessary to flood the lakes and to begin using the bottoms of other ones (grass-fallow system of landscape rotation).

IV. Goldgenic tundra floodplain soils. They exhibit no permafrost, the depth of the seasonal thawing is 1.5 m, heat provisi n, 25,000-30,000 kcal/m^2 year. The majority of these soils except those situated in the floodplain depressions has high water permeability. The soils are systematically flooded with spring waters and heated with high table ground waters. This group of soils occupies the river floodplains. Thermokarst is absent.

Melioration of the soils of the 4th group should be carried out together with flood control, prevention of water stagnation and lowering of the ground water table. For this purpose a network of canals is built, depressions with no runoff are filled with earth and the surface is levelled. Selected closed drainage systems may be required. As a result, 50-70 c of high quality fodder per ha is obtained (Andreev, 1984).

In the frost regions of the North the soils destroyed by excavations are recultivated and applied for agricultural needs (Papernov, Zamoshch, Zakar, 1983). The technology preventing the thermokarst processes is developed. According to it, the total thickness of the potentially fertile soil, drainage layer and deposits from silt basins applied to the recultivated surface must be greater than the depth of their seasonal thawing.

Under conditions of the East-European tundra in the region of Vorkuta according to the method suggested by the Institute of Biology of the Komi Branch of the USSR Academy of Sciences the phytomelioration of the frozen tundra surface-gley soils is successfully carried out with application of relatively low fertilizer rates. This method consists of virgin soil reclamation by discing for cutting the plant cover and for mixing it with the soil. Then local grass mixtures are sowed and hay-mowing is annually carried out. The application of this method resulted in the development of about 5.000 ha of the frozen

tundra surface gley in the Vorkuta region. The hay harvest of the meadow-foxtail grass mixture and cane-type canary grass was 15-20 c/ha and up to 100 c/ha, respectively (Zaboeva, Rubtsov, 1985).

CONCLUSION

In the regions of the Extreme North of the USSR mainly under conditions of the perennial cryolithozone there are about $6 \cdot 10^6$ ha of agricultural lands (Nosov, Vashanov, 1984). Their effective application greatly depends on melioration. Hydrotechnical and nonhydrotechnical techniques of complex melioration can be applied taking into account the specific character of soils: cryogenic frozen and coldgenic ones.

The data on productivity given above allow to predict high efficiency but only in case when the quality of melioration is drastically increased. Such negative consequences of melioration as secondary salinization during excessive irrigation, secondary swamping and an increase of the freezing depth as well as the corresponding measures should be considered while designing melioration systems. It is well known that the subarctic soils can be greatly destroyed under the anthropogenic effect therefore special techniques of soil conservation are required.

LITERATURE

Andreev N.G. (1984). Osnovnye napravleniya razvitiya kormoproizvodstva v raionakh Krainego Severa. V Knige: Sel'skoe i promyslovoe khozyaistvo Krainego Severa. Sektsiya pochvovedenie i agrokhimiya. Novosibirsk, Sibirskoe otdelenie Vsesojuznoi Academii Sel'skokhozyaistvennykh Nauk (VASKHNIL). str, 64-66.

Gavrilova M.K. (1978). Klimat i mnogoletnee promerzanie gornykh porod. Novosibirsk, Nauka, str. 214.

Zaboeva I.V., Rubtsov M.D. (1985). Zemel'nye resursy Bol'shezemel'skoi tundry i ikh ispol'sovanie. - V knige: Problemy pochvennogo criogeneza. Syktyvkar, Komi filial Akademii Nauk SSSR, str. 6-7.

Kovda V.A. (1985). Pochvennyi pokrov, zemledelie i melioratsiya. Preprint, Pushchino, Nauchnyi Tsentr Biologicheskikh Issledovanii (NTsBI) Akademii Nauk SSSR, str. 25.

Korekovtsev A.S., Orlovskaya K.V. (1984). Vliyanie teplovoi melioratsii na svoistva bolotnykh merzlothykh pochv Magadanskoi oblasti. V knige: Sel'skoe promyslovoe khozyaistvo Krainego Severa. Sektsiya pochvovedenie i agrochimiya, Novosibirsk, Sibirskoe otdeleniye VASKHNIL), str.27-29.

Kudryavtsev V.A., Ershov E.D. (1969). Printsipy upravleniya merzlotnym protsessom - V sbornike: Merzlotnye issledovaniya, vypusk IX, Moskva, Moskovskii Gosudarstvennyi Universitet, str. 156-157.

Makeev O.V. (1981). Fatsii pochvennogo cryogeneza i osobennosti organizatsii v nikh pochvennykh profilei. Moskva, Nauka, str. 88.

Makeev O.V. (1986). Sovremennaya kontseptsiya pochvennogo cryogeneza, evolutsiya criogennykh pochv v Golocene i problemy melioratsii pochv s merzlotoi v profile. V knige: Evolutsiya i vozrast pochv SSSR. Pushchino, NTsBI Akademii Nauk SSSR, str. 37-46.

Makeev O.V., Vasilevskaya V.D., Volkovintser V.I., Elovskaya L.G., Zaboeva I.V., Ignatenko I.V., Kovalev R.V., Stepanov A.N., Gershevich V.D. (1981). Plodorodie i ratsional'noe ispol'zovanie pochv Krainego Severa (tundrovaya i lesotundrovaya zony). - V sbornike: Znachenie pochvennykh issledovanii v reshenii Prodovol'stvennoi programmy (doklady General'nogo simposiuma VI s'ezda Vsesouznogo obshchestva pochvovedov), Tbilisi, str. 130-147.

Merzlotovedenie (1981). Moskva, Moskovskii Gosudarstvennyi Universitet. str. 229.

Nosov S.I., Vashanov V.A. (1984). Osnovnye napravleniya ratsional'nogo ispol'zovaniya i okhrany zemel'nykh resursov Severa. V knige: Sel'skoe i promyslovoe khozyaistvo Krainego Severa. Sektsiya pochvovedenie i agrokhimiya. Novosibirsk, Sibirskoe otdelenie VASKHNIL, str. 17-19.

Papernov I.M., Zamoshch M.N., Lazar A.Ya. (1984) Osnovnye printsipy, metodika i resul'taty eksperimental'nykh issledovanii technogeneza i rekultivatsit uslovlyakh Severo-Vostoka. V scornike: Biologicheskie problemy pochv Severa, Chast' I, Magadan. str. 293-294.

Proektirovanie melioralivnykh sistem na Dal'nem Vostoke (1984). Posobie Ministerstva vodnogo khozyaistva SSSR, Vladivostok, str. 87.

Shvirst A.T. (1984). Issledovaniya po sozdaniju senokosov na termokarstovykh ponizheniyakh v subarcticheskoi zone Chukotki. V knige: Sel'skoe i promyslovoe khozyaisstvo v raionakh Krainego Severa. Sektsiya pochvovedenie i agrokhimiya. Novosibirsk, Sibirskoe otdelenie VASKHNIL, str. 107-108.

EMBANKMENT FAILURE FROM CREEP OF PERMAFROST FOUNDATION SOILS

A CASE HISTORY

R. McHattie and D. Esch

Alaska Department of Transportation, Research Section, Fairbanks, Alaska, USA

SYNOPSIS A road section 10.6 meters in height was constructed in 1975 over warm silt permafrost soils near Fairbanks, Alaska, and was observed to have settled very noticeably after several years of service. Borings were made and inclinometer and temperature logging casings were installed early in 1983 along with reference markers for vertical and lateral movement observations. Measurements since that time have indicated that creep movements are occurring in the frozen foundation soils which contain large massive ice deposits. Embankment surface settlements have averaged 30 cm per year since construction, and measurement points located 9 m outside the embankment toes have been uplifted at a rate of 7.5 cm per year. Inclinometer readings have shown that lateral creep movements of the frozen foundation soils are occurring at depths greater than 13 meters, even though seasonal thawing reaches to a depth of only 6.4 m. Measurements indicate the permafrost foundation soil temperatures to be very close to -0.4°C.

To raise and level the roadway in this area to its original height, the embankment was reconstructed in 1987 using wood chips as lightweight fill for replacement of a portion of the embankment soils. By this means, it was possible to raise the road surface to its original elevation while actually reducing the total overburden load on the foundation soils by about 20%. New monitoring equipment has since been installed to monitor the behavior of the reconstructed embankment. Results of all previous monitoring studies are discussed, along with costs and alternatives considered for repair of this embankment.

BACKGROUND

In 1975, the Alaska Department of Highways completed a section of the Parks Highway on new alignment across the Alder Creek valley, approximately 13 km west of Fairbanks, at latitude 64° 52' North. The valley-bottom soils were perennially frozen, ice-rich silts with frequent occurrences of massive subsurface ice. Because of concerns over permafrost thawing and resulting roadway settlements, the two shallow cut areas required at each side of the valley were insulated with polystyrene foam and were extensively instrumented and monitored as reported by Esch (1983). The road embankment across the valley bottom had a total length of 500 m and varied from 3 to 11 m in height. To improve the thermal stability, initial road construction was not permitted until the start of the 1973-74 winter freezing season, and "toe-stabilization" berms 6 m wide by 1.8 m thick were also constructed on both sides of the 2:1 embankment slopes.

By 1980, excessive movements of the embankment were apparent on both sides of the valley. In 1982, the decision was made to survey, instrument, and monitor the movements in the area of the greatest apparent settlements, which by that time had exceeded 2 meters in elevation change. Movement reference points, an inclinometer casing, and a temperature monitoring casing were installed. Observations were made several times over the following 3 years. Because the maximum settlement area had created a vehicle safety hazard due to shortened sight-distances, the roadway was reconstructed to its original elevation in 1986 using wood chips as a lightweight fill-replacement material. Sufficient rock-fill was removed from the embankment and replaced with wood chips so that a significant overall reduction in embankment weight was achieved, as will be described later. The embankment settlements were determined to be caused by plastic creep displacements of the ice-rich permafrost foundation soils, as discussed herein. Creep movements had not previously been considered a problem for roadway embankments.

SITE AND SOILS DESCRIPTIONS

The Alder Creek valley is a short, U-shaped valley surrounded by low hills. The valley-bottom creek has a low flow-rate and is carried beneath the roadway by a 3 m diameter structural steel plate culvert. The valley-bottom soils were investigated with several auger borings during the roadway design stage, and found to consist of gray, slightly organic, perennially frozen silts with deposits of massive subsurface ice. Moisture contents in the silt generally ranged between 25 and 50%. Extensive moisture content and ice occurrence data were obtained from the six borings made through the 3 m thick roadway fill for temperature monitoring cable installations at the two nearby insulated embankment sites (Figure 1). All six of these instrumentation borings encountered massive ice, generally at depths between 6 and 14 meters below the new road surface. One pre-construction boring had also been made in 1972 within 15 m of the maximum settlement area, and encountered only ice at depths of 2.3 and 6.0 m below the original ground surface, with layered ice and silt below that depth. From inspection of these borings one might conclude that over half of the subsurface "soils" in this valley between depths of 3 and 9 m consisted of ice masses, with an average ice layer thickness of 3.7 m.

Vegetation in the Alder Creek Valley consists primarily of small, stunted, black spruce trees to 5 m in height, with a ground surface cover of sphagnum moss. The climate in this area is typical of the dry interior of

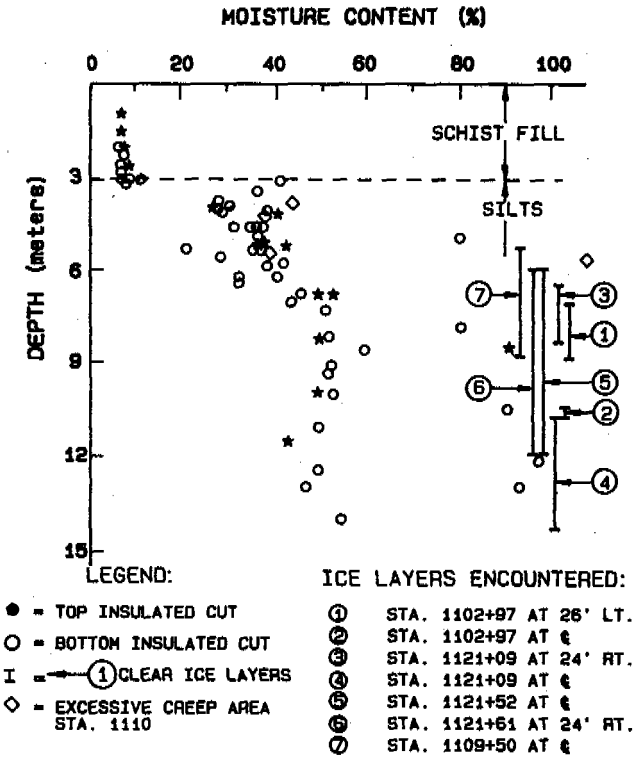

FIGURE 1. Subsurface moisture contents and ice layers in Alder Creek valley borings.

Alaska, with short, warm summers and long, dry winters. Freezing and thawing indices at the Fairbanks airport recording station average approximately -3000 and +1800° C days, respectively. The mean annual air temperature is -3.3° C. Precipitation averages 0.28 m/yr, including the water equivalent of 1.5 m of total snowfall. Permafrost temperatures typically range between 0° and -1° C. Two thermocouple and thermistor strings were installed in nearby undisturbed forest sites in 1975 to monitor subsurface temperatures away from the influence of the roadway. Temperatures at a depth of 9.1 m at these undisturbed sites, which were located approximately 200 m east and west of the area of maximum embankment settlements, are shown by Figure 2. A significant (1°C) air temperature warming trend has been observed in Interior Alaska over the past 11 years, primarily as a result of unusually warm winters. However, the effect of this warming on subsurface temperatures has been small.

DESIGN AND CONSTRUCTION OF EMBANKMENTS

Because of the high subsurface ice contents, various precautions were taken to increase the stability of the embankment in this area during the original construction. In preparation for the fill placement, all trees and brush were hand-cleared and laid on top of the moss cover to avoid any thermal disturbance which would initiate thawing. The contractor was then required to place an initial 1 m thick layer of rock-fill at the start of the 1973-74 winter. This initial layer was occasionally cleared of snow during the winter to maximize seasonal cooling and refreezing of the active layer. Commencing at the start of the 1974 thawing season, the embankment was constructed to final grade, using weathered schist as the primary fill material. Silt toe berms 6.1 m wide by 1.8 m thick were constructed on both sides of the embankment to retard

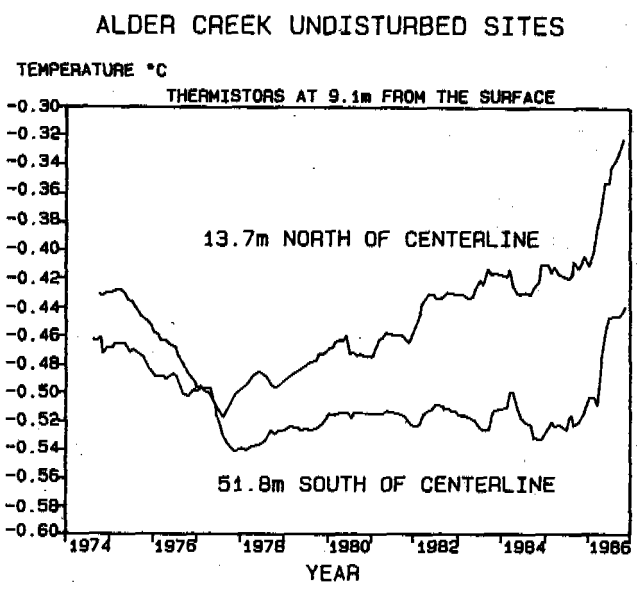

FIGURE 2. Permafrost temperatures at 9.1 m depth in undisturbed forest areas. (six month running averages).

thawing at the toes of the main embankment and to provide some added support against rotational slope movements. The wet densities of the rock and silt fill materials were approximately 2100 and 1750 kg/m^3, respectively. The slopes and toeberms were seeded and the roadway paved in the summer of 1975 to complete the original construction.

INSTRUMENTATION AND MONITORING

Soil auger borings were made through both shoulders of the embankment in October of 1983, and extended to depths of 14.3 and 15.2 m. The borings were made at the point of maximum embankment settlement, located near roadway station 1110 (one station = 30.5 m or 100 feet). The term "roadway station" as used in the text and figures of this report indicates the site location along the roadway centerline as measured from the start of the project (=Station 0). Both borings indicated that the original ground beneath the embankment was still in a frozen condition 10 years after the start of construction. At this location and time, roadway surface settlements were in excess of 2.4 m, yet no cracking or shear displacements were noted in the pavement structure, which was still in excellent condition. This fact was the first indication that plastic flow movements might be occurring in the permafrost foundation soils.

An "Inclinometer" casing was installed in the boring through the east shoulder of the roadway embankment, and extended to a depth of 13 meters. The inclinometer probe is a device which is lowered down a grooved casing and which indicates the tilt of the casing at selected intervals of depth. By taking repeated measurements over intervals of time, the change in the lateral position of the casing can be measured, and subsurface movement patterns can be determined. A second boring directly across the roadway, 4.9 m west of the centerline, was used for installation of a 2.4 cm diameter plastic pipe which extended to a depth of 13.9 m. The pipe was filled with ethylene glycol and subsequently used for logging the subsurface temperatures by means of a thermistor probe.

To provide for accurate monitoring of vertical and lateral movements of the embankment and the adjacent soil surface, a total of 33 movement references were installed at lateral intervals of approximately 3 m. Pavement surface references were 3 cm-long survey nails driven into the asphalt pavement. Side slope and adjacent soil movement reference points consisted of 25 cm long bolts extending up from the centers of 25 cm square aluminum plates which were buried slightly beneath the soil surface. Movement reference points were installed in July of 1983 and surveyed at the end of the thawing seasons in 1984, '85, and '86. Uplifting of the soil surface outside of the embankment area was observed by installing movement reference plates as far as 9 m out from the toe of the embankment slope into the undisturbed forest on each side of the roadway. Experience has indicated that the monitoring plates should have been extended to at least 20 m outward from the toe of slope, while the inclinometer casing should have been installed to a much greater depth, perhaps to 30 meters or more. The initial (1975) and final (1986) embankment cross-sections are shown by Figure 3 at Station 1110.

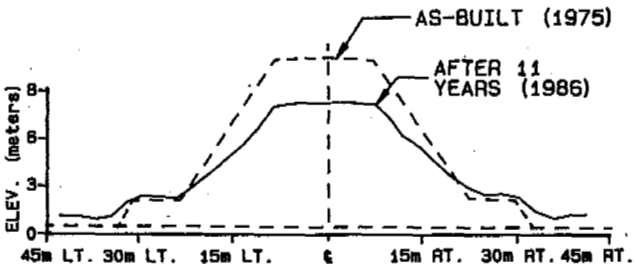

FIGURE 3. Initial (1975) and 1986 embankment cross-sections at Station 1110 (maximum creep area).

TEMPERATURE AND MOVEMENT OBSERVATIONS

Several subsurface temperature profile measurements were made to determine the maximum depths of freezing and thawing within the embankment. These data for 1984 (Figure 4) indicate that the maximum freeze and thaw depths were both approximately 5.9 m, and that embankment and foundation soils below that depth had remained frozen. This observation was further confirmed by the fact that water inside the casing was found to be frozen at the 5.9 m depth on all occasions when attempting to make inclinometer measurements. Thawing of the inclinometer casing was required to allow lowering the inclinometer probe down the casing. Permafrost foundation temperatures during 1984 were found to be approximately -0.2° C at the original ground surface and -0.4° C at a depth of 4 m.

Elevation surveys of the roadway centerline in the Alder Creek area were made in 1982 and again in 1985. These data were used to prepare plots of the centerline profiles (Fig. 5) and of changes in embankment height since construction (Fig. 6). It can be observed from these plots that excessive embankment settlements were common throughout this area, particularly at locations 60 to 100 m north and south (right and left respectively in Figures 5 and 6) of the creek bottom. At these locations the embankment heights had been reduced by 18 to 20% by settlements between 1975 and 1982. It is probable that the valley-bottom permafrost soils were slightly colder than in the areas slightly up-slope. This may explain the reduced creep settlements in the valley-bottom areas. The large 3 m diameter culvert which carried Alder Creek beneath the road embankment

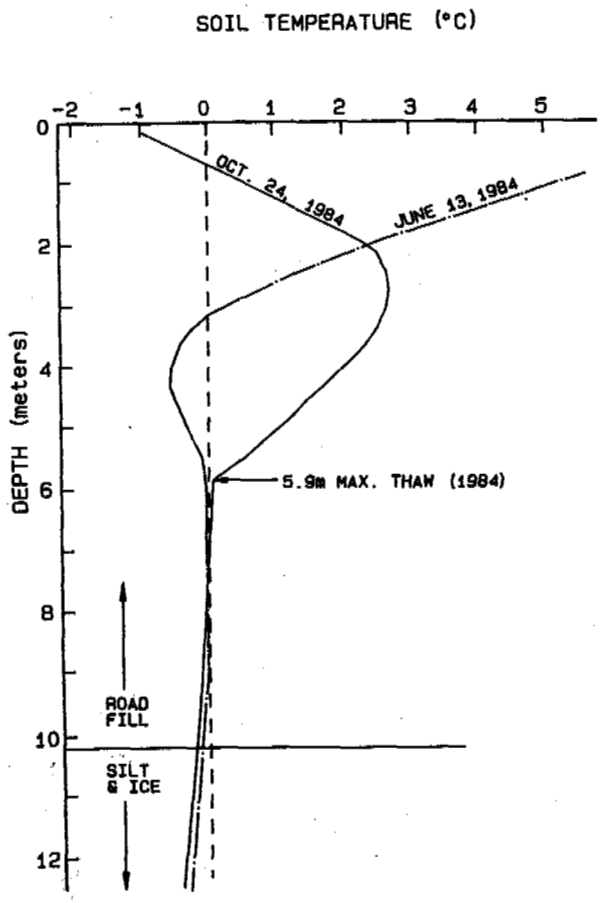

FIGURE 4. Subsurface temperature-depth profiles beneath east shoulder of roadway.

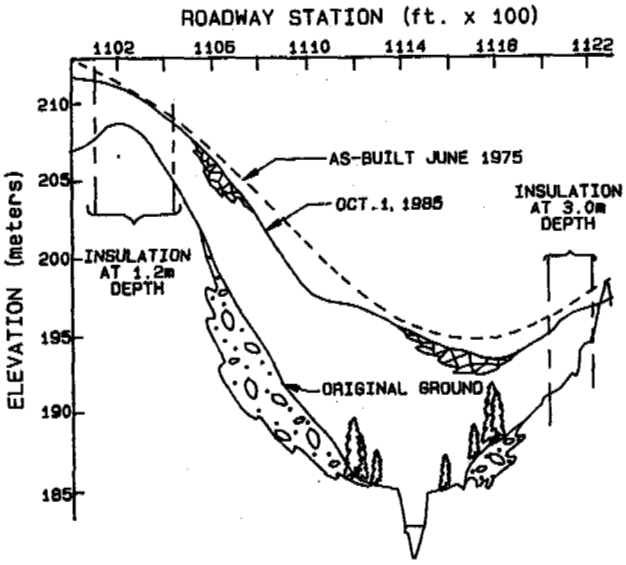

FIGURE 5. Road centerline elevation profiles in 1975 and 1985 across Alder Creek valley.

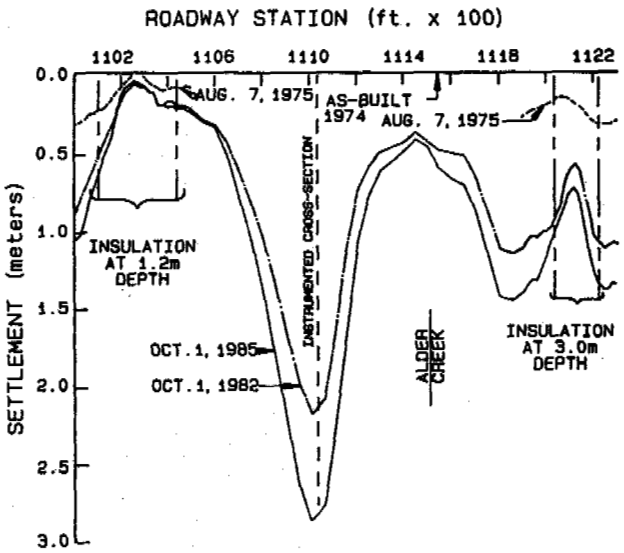

FIGURE 6. Settlements along road centerline across Alder Creek valley from 1975 to 1985.

was also found to act as an aircooling duct and resulted in a lowering of temperatures in the soils surrounding the streambed.

Vertical and lateral movements of the embankment survey reference points are shown by Figure 7. It is apparent from these plots that the downward movements of the center of the embankment correspond to upward and outward movements in the adjacent undisturbed permafrost soils beneath the surrounding forest. The roadway centerline in this area is oriented North, 11° East. The east facing (or right side) embankment slope would be expected to be slightly warmer than the opposite (left) or west facing side. However, except for some apparent localized thaw-related settlements in the right side berm area, the embankment settlements and adjacent soil uplifting have occurred very symmetrically. Movements have progressed in nearly equal annual increments. The seasonality of the movements and the movement rates prior to the 1982 surveys have not been established. However, by comparing the total settlements since construction with current rates, it is apparent that the settlement rate has declined over time. The 1985 total settlements appear to be the result of initial vertical movement rates of 0.36 m/year in 1975 and a reduced rate of 0.25 m/year by 1984. This decline in rates may be explained at least in part by the resultant decrease in the total effective embankment height, from 8.84 m in 1975 to 6.61 m in 1985.

Inclinometer measurements were taken on several dates between October of 1983 and December of 1985. Lateral movements of the embankment and foundation soils at different depths are shown by Figure 8. The pattern of these movements suggests that the maximum movement zone is at some depth below the bottom of the casing (13.5 m).

Stresses beneath an embankment on an elastic foundation may be estimated by using typical vertical pressure distribution charts. The initial vertical pressure increase at the center of the base of the embankment was calculated to be 220 kPa. The initial resulting incremental pressure increases along centerline, at

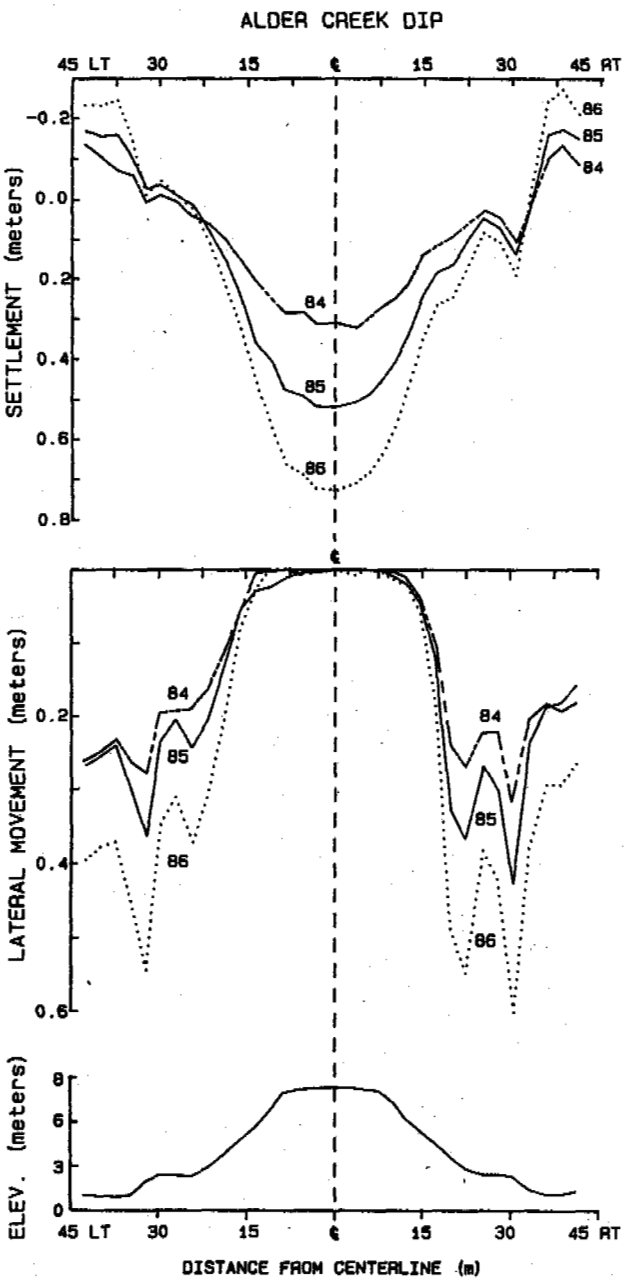

FIGURE 7. Vertical and lateral movements of road, embankment slopes, and adjacent forest structures at Station 1110.

depths of 6 and 12 m below the road surface were calculated to be 211 and 180 kPa, respectively. However, plastic flow within the permafrost foundation soils, and changes in the geometry of the embankment and nearby ground surface would cause stresses to vary from those determined for the initial "elastic" loading condition. Further analysis of the compressive and shear stress states would require finite-element analyses and is beyond the scope of this report. The reader is encouraged to apply his own creep analysis procedures and to test the results against the site data contained herein.

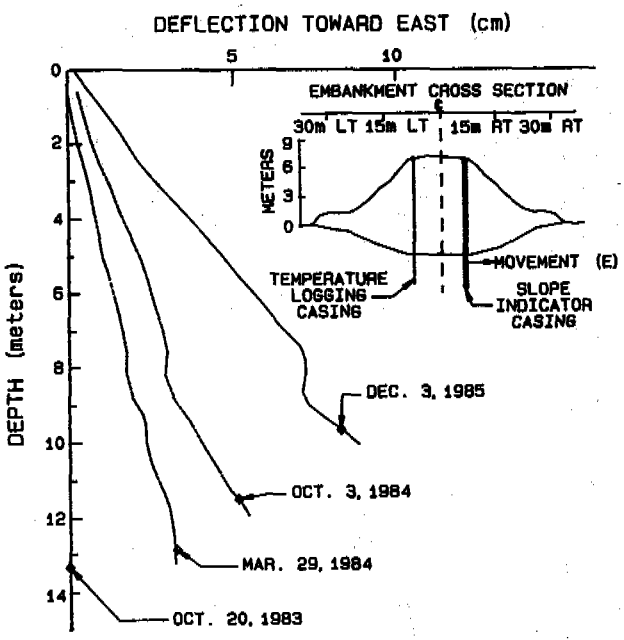

FIGURE 8. Lateral soil movements at various depths along vertical inclinometer casing.

Repair and reconstruction of the embankment was found to be necessary by 1985 to restore grades and sight-distances. In the redesign stage, creep movements were considered likely to continue at the 1985 rate unless the weight of the embankment could be reduced or the temperature of the foundation lowered considerably. The potential for cooling the permafrost foundation with thermosyphons was rejected based on costs, and the decision was made simply to design for a reduction of at least 10% in the embankment pressure beneath the road centerline. Settlements in this area on both sides of the creek suggest that the creep movements are roughly proportional to the embankment pressure.

Two alternative fill replacement materials were considered. These were molded expanded polystyrene foam blocks, and wood chips. Economic comparisons led to selection of the wood chip material and to the final embankment design. In the design analyses the chips were conservatively assumed to have a maximum wet density of 800 kg/m^3, and the desired 10% load reduction was based on this value. The top 3.3 m of the embankment was scheduled for excavation (average depth) and removal prior to the wood chip placement. The chips were tapped with a structural layer of gravel and pavement which totaled 1.1 m in thickness; including a 5 cm thick hot asphalt pavement surfacing. A thickness of 1.2 m of fill was provided to cover the sides of the wood chip layer to retard air and water entry which might accelerate decay.

RECONSTRUCTION OPERATIONS

Repair of the subsidence area on the south side of Alder Creek was undertaken in the late fall of 1986, as part of the general rehabilitation of a 40 km long section of the Parks Highway. Construction at the site began in mid-October, 1986, the removal of the upper 3.3 m of the existing rock fill over a length of 275 m of roadway (Stations 1105 to 1114). The purpose of the late season construction was to ensure that minimal heat would be introduced into the underlying permafrost soils through air temperature exposure or through the placement of warm fill materials. Wood chips were placed in 30 cm lifts and brought to grade using the compactive effort provided by the normal trafficking of dumping and spreading equipment. Wood chip layer thicknesses were varied as needed to restore the roadway surface to the original (1975) elevations, with a maximum of 5.8 m of chips placed within the area of greatest settlement.

A total of about 18,600 m^3 of wood chips were used to fill the subexcavated volume. This construction represented the first placement of such a lightweight fill in Alaska. Wood types used in the fill included wood species such as spruce and birch, which are indigenous to the Fairbanks area. At the start of chip production, trees selected for chipping were "green" wood but this proved unsatisfactory since the live growth did not chip as easily as partially dried deadwood, and stockpiles of this green wood material soon had to be ventilated because of heat build-up. Re-evaluation of the possible wood chip sources resulted in selection of relatively dry standing fire-killed trees from a local 1984 forest fire area. The chips were produced by a commercial wood chipping machine and were similar to those used in decorative landscaping work. Chips averaged about 2 x 2 x 1/2 cm in size and were purchased at a price in place of US $23.60 per cubic meter. Production data indicated that this material could be produced for a price of $12 to $18 per cubic meter in future work.

After the wood chips and the temporary wintertime driving surface had been placed in mid-November of 1986, the fill was allowed to settle until the resumption of construction for the 1987 season. For estimation purposes, a chip post-construction consolidation factor of 10% has been suggested by Washington and Oregon state highway engineers, who have utilized wood chips as a lightweight fill for swamp crossings. It was found that the wood chip surface had settled slightly more than 0.3 m over a 6 month period. Considering a wood chip fill of 5.8 m or less, a 0.3 m consolidation would roughly agree with the 10% estimate previously indicated. It is recognized however that some of the apparent consolidation may in fact be continuing embankment creep. The final in-place density of the chips was estimated at 322 kg per cubic meter, and resulted in an overall embankment pressure reduction of approximately 20%.

The final pavement design analysis over the wood chips was done based on dynamic field falling-weight deflectometer (FWD) testing and on analysis based on elastic theory. A dynamic elastic modulus of 20.7 m Pa was calculated for the chip fill layers based on the FWD test data and used in the final pavement thickness design analysis. The final pavement structural section overlying the wood chips included, from top downward, 5 cm of asphalt pavement, 15 cm of asphalt treated basic course, 15 cm of crushed gravel subbase, and 76 cm of selected schist rock borrow. Lightweight geotextile layers were placed to separate the rock and gravel borrow layers and to prevent mixing of the roack borrow and wood chip layers. The geotextile was added during construction because mixing problems were observed during fill placement over the chips.

SUMMARY

Embankment settlements averaging 0.3 m per year have been observed over a 10 year period for a roadway embankment originally 10.5 m in height. The foundation soils at the site consist of perennially frozen silts with massive ice layers. The ice masses are estimated to exceed 50% of the total subsurface volume below a depth of 2 to 3 m. Permafrost temperatures at this depth were measured at -0.4°C. Reconstruction of the embankment was done in 1986 to restore the roadway to the original elevation after total settlements of 3 m had occurred.

A wood chip fill was used in the reconstruction to increase the fill height while lowering the effective pressure on the foundation soils by 20%. The wood chip layer had a maximum thickness of 5.8 m, and was capped on the top and sides by 1.1 and 1.2 m of fill, respectively. Performance monitoring of the new embankment will be done to record the benefits and problems of this treatment.

REFERENCES

Esch, D.C. (1983) "Evaluation of Experimental Design Features for Roadway Construction Over Permafrost," Proceedings, Permafrost - Fourth International Conference, pp. 283-288.

CONSTRUCTION OF EARTH STRUCTURES IN PERMAFROST AREAS BY HYDRAULIC METHODS

P.I. Melnikov, Chang, R.V., G.P. Kuzmin and A.V. Yakovlev

Permafrost Institute, Siberian Branch of the USSR Academy of Sciences, Yakutsk, USSR

SYNOPSIS A perspective technology is proposed in the paper of constructing earth structures in permafrost areas. Results of full-scale tests are presented.

Until recent time the economic expediency and technical possibilities of constructing earth structures (dams, roads, foundations and others) in permafrost areas by a method of hydraulic deposition is determined by availability of unfrozen or thawed grounds.
Hydraulic working of unfrozen earth is usually carried out from taliks below a river bed or a lake or from surface quarries. Volumes of unfrozen earth in taliks below the rivers and lakes are, as a rule, not large. Use of surface quarries is possible after a lengthy preparation period as long as is given in the Recommendations ... (1974), 6-15 months. In this case considerable areas are withdrawn from land-tenure. Besides, open working may become a cause of intensive thermokarst development. All this leads to construction of earth structures in permafrost areas by hydraulic deposition in a very limited number of cases and is used mainly for construction of dams and tailing dumps according to the data by Kuznetsov et al. (1968) and Biyanov (1975).
In this connection the Permafrost Institute of the Siberian Branch of the USSR Academy of Sciences proposes a new technology of hydraulic deposition of earth structures based on underground hydraulic working of the earth from permafrost through boreholes. Borehole hydraulic working is notable by small amount of stripping, simplicity of equipment used and technological flow process. Stripping consists of boring wells through which the permafrost is worked. The boreholes within the plot being worked are disposed in a chess-board order. Distance between the wells is determined by the chamber dimensions and interchamber pillars. The volume of earth obtained from one chamber depends on the properties and thickness of disperse deposits whose approximate values are given in Fig.1. When the peculiarities of the borehole hydraulic working are considered, there should be introduced, in our opinion, a yield coefficient expressed by a ratio of the total volume of earth

$$\sum_{i=1}^{n} Vi$$

withdrawn from all the wells on a given plot and the area of this plot S :

$$k = \sum_{i=1}^{n} Vi/S$$

Coefficient k may serve as a criterion for the technico-economical calculations.

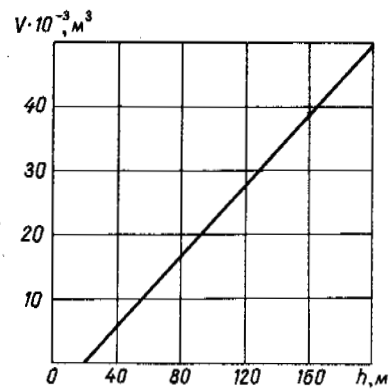

Fig.1 Dependence of the earth volume delivered from one borehole on the thickness of Quaternary deposits

Physics of the process taking place during hydraulic working of permafrost come to the following. Ice cementing bonds of permafrost are weakened or completely disturbed as a result of thermal exposure to water. Destruction of the earth structural bonds after thermal exposure to water is possible with hydraulic monitor jets. In this case, depending on the water temperature and jet pressure, earth destruction takes place in frozen condition at one or another stage of its strength decrease or in thawed condition. Purely mechanical destruction of permafrost due to its high momentary strength requires very high pressure jets, as is shown in a work by Goldin et al. (1980). Washout of permafrost with weakened structural ties is carried out with low pressure water jets

acting through an air medium. In this case low water level must be maintained in the working.
If warmed pond water is available its thermal energy should be used. A large effect is obtained from this in non-bound earth when a washout is a result of filling the cavity with warm water. In this case the cavity roof shape is regulated by the change in water level.
A scheme of hydraulic deposition on a dam is shown on Fig.2. Earth disintegrated by water is delivered to the surface as a hydraulic mixture by a hydraulic elevator, an air-lift, an immersion pump or by forcing out with water or air.

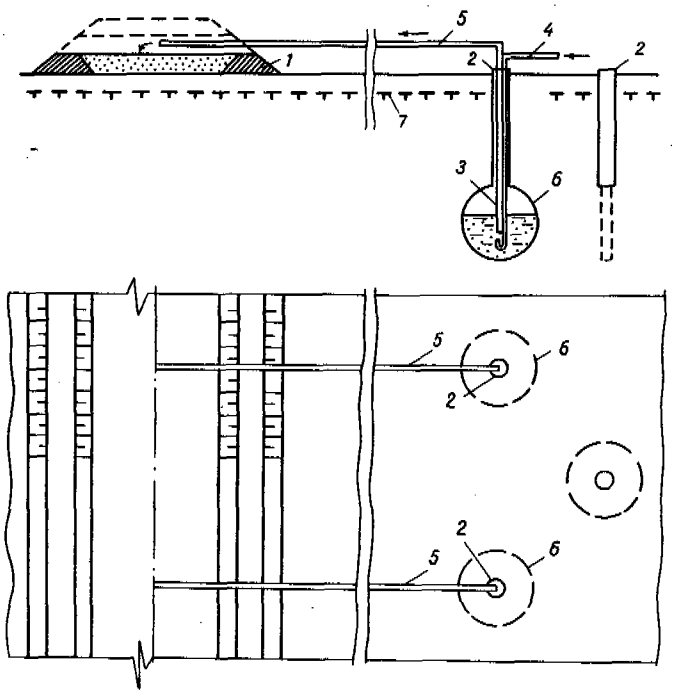

Fig.2 Scheme of an earth dam hydraulic deposition

1 - diking stop prisms; 2 - borehole; 3 - working column; 4 - water supply pipe to the device working parts; 5 - pulp line; 6 - underground cavity boundary; 7 - division boundary between frozen and unfrozen earth.

The sequence of carrying out preparation work and hydraulic working process is shown on Fig.3. The deposit is developed as follows. First, a borehole (1) is drilled to the top boundary of the productive layer and then cased with pipe (2), the space beyond the case being filled with mud (3) and frozen. Then a borehole (4) is drilled to the layer bottom. Preparatory work is completed by lowering a hydraulic unit into the borehole (4).
In the hydraulic elevation method of the pulp supply and jet washout (Fig.3) the hydraulic installation consists of a supply arrangement - a hydraulic elevator (5) co-axial water pipe (6), pulp line (7) and a device for the earth washout - a ring sprayer (8) with a water supply hose (10). In this case uniform washing out of the cavity walls is obtained by moving the sprayer along the vertical face.

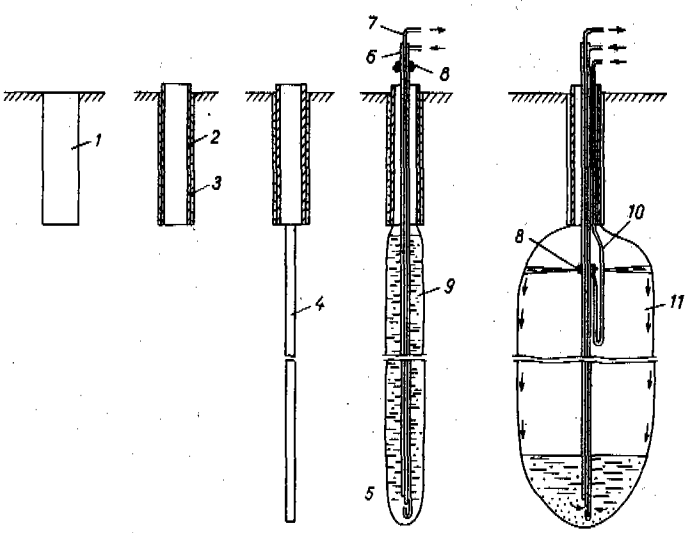

Fig.3 Technological scheme of borehole hydraulic working

1,4 - borehole; 2 - casing pipe; 3 - filler; 5 - hydraulic elevator; 6 - water pipe; 7 - pulp line; 8 - sprayer; 9 - water; 10 - hose; 11 - cavity

In a method of an air-lift delivery which can combine only with a method of washing out of permafrost by thawing, the hydraulic installation consists of a pulp line, an air supply pipe to the lower part of the pulp line and a water supply pipe to the cavity. Water is supplied to the hydraulic installation from natural ponds or from specially built reservoirs.
Pilot experiments have been carried out on plots of similar type composed of fine and medium grain sands, of massive cryogenic structure about 30 m thick with layers of vegetative remnants, supes and gravel-pebble material. Soils contain scrub and tree debris. The volumetric mass of the earth changes from $1.79 \cdot 10^3$ to $1.94 \cdot 10^3$ kg/m^3 and moisture varies within 0.19-0.29. Natural earth temperature at 20 m depth at two plots was minus 2.4 °C and at two others - minus 1.5 °C. The seasonal thaw layer reached 2.6 m. These earths are comparatively easily washed out by a thermal erosion method and are well transported by water. Average particle size is 0.26 mm. The fall velocity of these particles in stagnant water, specified by the hydraulic diameter size, equals 2.7 cm/s. Thermo-physical specifications of earth: thermal conductivity in frozen and unfrozen state 2.45 and 2.21 W/(m K); heat capacity in frozen and unfrozen state 1.18 and 1.59 kJ/(kg K).
Hydraulic borehole working was carried out in four wells. In three of them jet washout

and hydroelevator method of pulp lift was tested. In one well permafrost washout with hydraulic thawing was carried out by filling the cavity with warm water, the pulp being delivered by an air-lift. The following technological equipment was used for permafrost washout and pulp delivery: pumps of 80-100 m^3/h capacity and 50-80 m head, 168 mm diameter pipes for water supply to the hole and 108 mm - for pulp delivery. The hydraulic equipment installation and preparation for work was carried out with the help of a 6.3 t truck crane.

A total of about 5000 m^3 of earth were delivered from four boreholes and used for filling a dike and a road bed. Total cost of the earth working was 3.3 rub/m^3. The working costs will be considerably lower when thick permafrost deposits are worked and high efficiency pressure head forming mechanisms are used.

The proposed technology for constructing earth structures in permafrost areas shows high effectiveness and expediency of its practical application. But full-scale use of this technology requires higher capacity installations and studies of the technology peculiarities of hydraulic deposition into the structures.

REFERENCES

Bijanov, G.F. (1975). Plotiny na vechnoi merzlote. Moskva, Energiya, str. 175.

Goldin, J.A., Petrosyan, L.P. and Smorodinov, M.I. (1980). Issledovanie gidravlicheskogo sposoba razrousheniya merzlogo grunta. Osnovaniya, fundamenty i mekhanika gruntov, (1), 21-22.

Kuznetsov, G.I., Oushakova, V.K. and Shatrok, N.D. (1968). Rezultaty naturnykh obsledovanii rjada khvostokhranilisch v raionakh Vostochnoi Sibiri. Trudy V soveschaniya-seminara po obmenu opytom stroitelstva v sourovykh klimaticheskikh ousloviyakh. Krasnoyarsk, vyp. 1.

Rekomendatsii po proizvodstvu rabot sposobom gidromekhanizatsii pri soorujenii zemlianogo polotna v raionakh vechnoi merzloty. Moskva, VNII transp. str-va, 1974, str. 88.

STORAGE TANK FOUNDATION DESIGN, PRUDHOE BAY, ALASKA, U.S.A.

B. Nidowicz[1], D. Bruggers[2] and V. Manikian[3]

[1]Harding Lawson Associates, Anchorage, Alaska, U.S.A.
[2]Harding Lawson Associates, San Francisco, CA, U.S.A.
[3]ARCO Alaska, Inc., Anchorage, Alaska, U.S.A.

SYNOPSIS A Crude Oil Topping Unit (COTU) was constructed in Prudhoe Bay, Alaska to provide aviation fuel, gasoline and diesel to North Slope clients. Recently, ARCO Alaska, Inc. redesigned the storage tank farm with the addition of a new 4290 cubic meter welded steel tank and the relocation of two existing 790 cubic meter tanks. Subsurface soil exploration and laboratory testing programs were performed to determine the soil properties at the site. The thermal behavior of two Arctic foundation designs was analyzed using a two-dimensional finite element computer program.

The initial design for support of the 38 degree C crude oil tank consisted of AISC W24 by 68 beams spaced on 1.2 meter centers in order to provide a 61.0 cm air space between the bottom of the tank and the top of the gravel pad. The beams were underlain by 22.9 cm of insulation.

The initial tank foundation design was revised because of the high cost of structural beams and the availability of a fin-fan oil cooler in the plant. The final design incorporated the use of the fin-fan oil cooler to reduce storage tank temperature, and involved founding the tank bottom on a sand cushion underlain by 22.9 cm of insulation placed directly on the gravel pad. The temperature criterion for the storage oil was set at 1.7 degrees C for the winter months (November - May).

To confirm this design, additional thermal modeling was conducted using the new criterion. The results indicated that the maximum thaw penetration depth, below the center line of the tank, was 1.3 meters. This depth is above the organic and ice-rich soils. A thaw-settlement of less than 5 cm was predicted, an acceptable condition.

This paper discusses the alternate design modes investigated and the results of the thermal analysis.

INTRODUCTION

The COTU Fuel Storage facility, at Prudhoe Bay, Alaska, is located west of the ARCO Operations Center and consists of ten steel tanks. The tanks are presently supported on gravel pads, typically 1.5 meters thick, and are surrounded by gravel containment berms.

Due to the increased demand for product, additional tank capacity was needed at the facility. ARCO Alaska, Inc. designed a new 4290 cubic meter tank with a diameter of approximately 24 meters and a height of 9 meters. ARCO also planned to remove two existing tanks and replace them with two larger tanks having diameters of 12 meters and heights of 8 meters. Replacement of the tanks necessitated removing the existing tanks, recompaction and placement of additional fill, and construction of the new tanks.

Two significant design considerations for foundations on the North Slope of Alaska are the continuous permafrost and the annual freeze-thaw cycles of the active layer. Conventional shallow spread footings do not perform well because of frost heave from the active layer and the large potential for creep failure in the ice-rich permafrost. At-grade heated structures are acceptable only if founded on a non-frost susceptible fill pad and the permafrost integrity is maintained. Pile foundations are commonly used on the North Slope, but they are expensive. It is advantageous to use gravel since it is abundant in the Prudhoe Bay area.

The objective of this study was to design a cost-effective foundation that would preserve the ice-rich permafrost beneath the tanks throughout the life of the tanks. To provide data for use in design, seven borings were drilled and sampled to depths ranging from 5.5 to 8.5 meters. Selected samples were tested to measure their moisture content, dry density, particle size, specific gravity, Atterberg limits and freezing point depression.

PHYSICAL SETTING

The Prudhoe Bay area is located on the Arctic Coastal Plain, a geologic province bounded on the north by the Beaufort Sea and on the south by the foothills of the Brooks Range (Wahrhaftig, 1965). Several sea level fluctuations due to various glacial epochs have occurred along the Arctic Coastal Plain during

the last 100,000 years. These advances and retreats of the shoreline have alternatively flooded and exposed significant portions of the North Slope.

The Arctic Coastal Plain is mantled by unconsolidated deposits of the Gubik Formation (Black, 1964) consisting of lenses and mixtures of sand, gravel, silt and clay. Though mainly of marine origin, the Gubik formation has also been modified by alluvial, lacustrine, eolian and frost processes.

The principal soil types in the Prudhoe Bay area are fluvial sand and gravel deposited by the Kuparuk-Sagavanirktok River Systems during the last retreat of the Brooks Range glaciers. The sand and gravel are overlain by wind-blown deposits and usually a thin surface mantle of organic soils and tundra vegetation.

The Prudhoe Bay region has an arctic coastal climate. The mean annual air temperature is -13 degrees C (Walker et al., 1980). Mean monthly temperatures range from 17 degrees C in July to -31 degrees C in February.

Permafrost underlies the entire Arctic Coastal Plain. The bottom of the permafrost in the Prudhoe Bay area is approximately 600 meters below the surface (Brown and Péwé, 1973). Thawing during summer months usually does not extend deeper than about 30 cm in undisturbed tundra areas.

SITE CONDITIONS

Test borings show that most of the tank site area is covered by gravel fill of varying thickness. Research of published geologic maps and aerial photographs indicates that the surface conditions beneath the gravel fill consist of a gently undulating ground surface supporting typical tundra vegetation of grasses, sedges, mosses, and low shrubs. The general area is characterized by poor surface drainage, many low marshy areas and shallow wind oriented lakes up to several hundred acres. The site lies at an elevation of about 9 to 12 meters above mean sea level.

Based on the test borings, it was determined that the three tank sites have similar soil profiles. In general, sandy gravel fill, approximately 1.5 meters thick, was found to overlie ice-rich, nonplastic sandy silt and silty sand to depths of 4 to 6 meters. Beneath these soils, sand and gravel extend to the depths explored. Massive ice, in the form of ice lenses and wedges, was commonly encountered within the ice-rich soil.

The fill typically contains 31 to 64 percent gravel, 31 to 56 percent sand, and 5 to 12 percent silt. The moisture content of the fill averages about 8 percent. According to the Unified Soil Classification System, the fill is classified as GP-GM or SP-SM. This fill is representative of Prudhoe Bay area gravel.

The ice-rich soil had moisture contents that varied between 30 and 350 percent, with an average of about 140 percent. The coarse-grained sand and gravel underlying these soils was ice-poor, and had moisture contents ranging between 11 and 36 percent. The freezing point depression of the samples tested varied between -0.1 C to -0.4 C.

DESCRIPTION OF COMPUTER CODE

Computer Code FROST2B (CRREL, 1984) was used to model the thermal regime beneath the heated fuel tanks. FROST2B is a two-dimensional computer code that uses a nodal domain integration model of heat and soil-water flow coupled through isothermal soil-water phase change. The program can be used to analyze two-dimensional freezing/thawing problems where known information is sufficient to supply the necessary modeling parameters, boundary conditions, and initial conditions. The key assumptions used in the thermal analysis of the program are:

1. Heat transport in freezing soils occurs due to conductive and convective processes and follows the general equation of heat transfer in solids and liquids. Additionally, the heat transport equation is nonlinear, as the thermal conductivity and heat capacity of the soil-water-air-ice mixture is a function of ice and water content in a freezing and thawing soil. A volumetric fraction proportion equation is used to describe the thermal conductivity and heat capacity of soil-water-air-ice-mixture as a function of the volumetric content of each composing constituent.

2. Soil-water phase change is assumed to occur isothermally in a partially saturated soil element. The phase change model that couples the heat and soil-water transport models is based on the apparent specific heat capacity model whereby the latent heat effects of freezing water are lumped into the transient heat capacity term of the heat transport equation.

3. Unfrozen zones are nondeformable, and in freezing zones or frozen zones, deformation is due to ice segregation or lens thawing only.

4. Constant parameters, such as porosity, remain constant with respect to time; i.e., freeze-thaw cycles do not modify parameters.

5. Hysteresis effects are negligible.

6. Saline exclusion processes are negligible.

7. Freezing and thawing processes in a two-dimensional medium occur such that there are no internal shear or stress forces developed between different zones.

DESCRIPTION OF THE BASIC MODEL

The model selected consists of a 2.4-meter-high supporting gravel pad with 2 horizontal: 1 vertical (2H:1V) side slopes. The pad is underlain with a 30.5-cm-thick organic layer overlying about 4.6 meters of ice-rich soil overburden. The mechanical and thermal properties of the soils the model consists of were obtained from the laboratory tests and

proprietary data obtained on similar Prudhoe Bay area soil types. The soil properties used in the analysis are presented in Table I. In all but two simulations, a layer of insulation, either 15.2 or 22.9 cm in thickness, was located 30.5 cm beneath the gravel pad surface.

TABLE I.
Soil Properties

Property	Embankment Gravel	Organic	Overburden
Density (kg/m^3), γ_d	1,922	801	1,458
Porosity, θ_s	0.3	0.7	0.45
Initial Volumetric Ice Content	0.099	0.699	0.449
Thermal Conductivity, K (W/mK)	5.23	2.91	2.09
Volumetric Heat Capacity, C (J/kg-K)	2.89	1.55	1.55
Freezing Point of Water, °C	0.	0.	0.
Salinity, PPT	0.	0.	0.
Thaw Strain (%)	3	30	30

Mean monthly air temperatures were obtained for a 9-year period (1970-1978) for the ARCO Air Field at Prudhoe Bay, Alaska (Walker et al., 1980). Figure 1 shows the best fit sinusoidal curve to these data. Since ground surface temperatures are required, the air temperatures must be modified. To modify the air temperatures, the energy exchange at the surface must be calculated. This requires knowledge of several mechanisms including: 1) conduction through snow cover, if it exists, 2) solar (short wave) radiation, 3) long wave radiation, 4) evapotranspiration, and 5) convection to the atmosphere (Lunardini, 1981 and Miller, 1975). Unfortunately, sufficient data were not available to allow for the development of the heat transfer coefficients required to calculate the ground surface temperatures.

To estimate the ground surface temperatures, actual surface temperatures were obtained (Figure 1) and a sinusoidal ground surface temperature curve was developed from the data. Although a constant correction was applied throughout the year, it is recognized that the difference between the air and ground curves is not a constant (Auld, et al., 1978 and Lunardini, 1978).

The initial temperatures used at various locations within the model are discussed next. Initial internal tank temperatures were fixed at either 37.8 degrees C or 54.4 degrees C. Outside the perimeter of the tank, the ground surface temperature curve, T(2), was used.

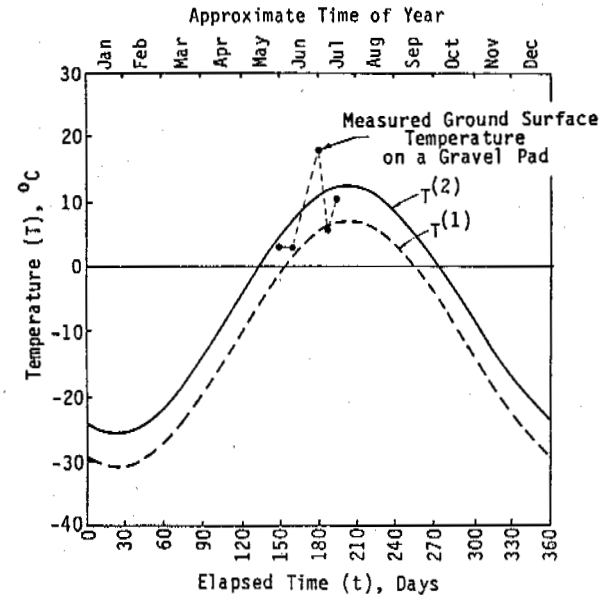

NOTES:

1. Average Air Temperature, $T^{(1)}$, obtained from nine-year temperature record at Prudhoe Bay, Alaska.
$$T^{(1)} = 18.9 \sin \frac{2\pi}{360}(t-117) \quad -12$$
2. Average ground surface temperature, $T^{(2)}$, includes estimated effects of solar radiation.
$$T^{(2)} = 18.9 \sin \frac{2\pi}{360}(t-117) \quad -6.5$$

Fig. 1 Air and Ground Temperatures

Initial pad surface temperatures beneath the tank were varied as follows:

1. Fixed at either 37.8 degrees C or 54.4 degrees C.

2. Allowed to equal the average air temperature, T(1), defined on Figure 1.

3. Fixed at either 37.8 degrees C or 54.4 degrees C for the months of November through May and allowed to equal the average air temperature for the months of June through October.

4. Computed by the model assuming a tank floor temperature of 54.4 degrees C.

5. Fixed at 1.7 degrees C or 4.4 degrees C for the months of mid-September through mid-May and allowed to equal the average air temperature plus 8.3 degrees C for mid-May through mid-September.

Because the pad surface beneath the tank is shaded from the effects of solar radiation, the air temperatures were used instead of the ground temperatures. A fixed-temperature boundary condition of -10 degrees C was assumed at the bottom of the model. This temperature approximates the equilibrium permafrost temperature on the North Slope (Brown and Péwé, 1973).

ANALYSIS AND RESULTS

Using the different thermal criteria previously discussed, thirteen computer simulations were performed. Ten of the simulations modeled a tank supported on a raised beam foundation. The remaining three simulations modeled the tank on an on-grade foundation. The simulations were performed for a design life of 20 years. A summary of the results is presented in Table II. All references to pad surface in this discussion refer to the area directly beneath the tank. The major findings of the simulation are as follows:

1. For all cases analyzed, the location of the thaw front stabilizes between 1 and 5 years.

2. Using the conservative assumption that the pad surface temperature equals the tank floor temperature (37.8 or 54.4 degrees C), we found that the thaw front penetrates the ice-rich soil below the fill with or without insulation.

3. When the pad surface temperature is set equal to the ambient air temperature and no insulation is used (simulation 4), the thaw front penetrates through the gravel pad, but equilibrates at the top of the ice-rich organic layer. If 15.2 cm of insulation is placed in the gravel pad (simulation 6), the thaw front remains within the insulation.

4. The thaw front is limited to a maximum depth of approximately 50.0 cm below the insulation for a beam foundation underlain by 15.2 cm of insulation when the computer program is allowed to determine the pad temperatures (Simulation 1).

5. For an on-grade foundation and when the pad temperature is varied during the summer and winter months (Simulations 11, 12, and 13), the thaw front can be maintained within about 1.2 meters below the bottom of the insulation.

6. Extending the insulation 61 cm beyond the tank perimeter is not sufficient to prevent deep thawing of the outer pad area.

FOUNDATION DESIGN

Using the results of the thermal analysis, we selected two foundation systems. One system is to found the tanks on a 15.2-cm-thick timber deck that is supported on AISC W24 by 68 beams spaced on 1.2-meter centers as shown on Figure 2. This foundation system will result in a 61.0-cm air space between the bottom of the tank and the top of the gravel pad. Located beneath the tank is 15.2 cm of insulation placed 30.5 cm below the top of the gravel pad surface.

TABLE II.
Computer Simulation Results

Computer Simulation Number	Insulation Thickness cm	Initial Gravel Pad Surface (Beneath Tank) Temperature °C	Foundation Type	Maximum Depth of Thaw at Tank Center, Meters		Thaw Settlement At Tank Center, cm	
				One Year	Five Years	One Year	Five Years
1	15.2	Determined by Computer	Beam	0.9	0.9	2.4	2.4
2	None	54.4	Beam	4.5	5.5	67.1	97.5
3	15.2	54.4	Beam	7.9	4.3	15.2	67.1
4	None	Ambient Air	Beam	2.1	2.5	6.4	7.6
5	15.2	37.8	Beam	2.2	3.5	6.4	45.7
6	15.2	Ambient Air	Beam	0.3	0.3	1.2	1.2
7	15.2	Ambient Air: June-Oct 37.8: Nov-May	Beam	0.9	2.6	2.4	15.2
8	22.9	37.8	Beam	1.4	2.0	3.1	22.9
9	22.9	Ambient Air: June-Oct 37.8: Nov-May	Beam	0.3	0.3	1.2	1.2
10	15.2	Ambient Air: June-Oct 54.4: Nov-May	Beam	0.9	1.7	2.4	5.2
11	15.2	4.4: Mid Sept.-Mid May Ambient Air +8.3: Mid May-Mid Sept.	Grade	0.9	1.4	2.4	4.3
12	15.2	4.4: Mid Sept.-Mid May Ambient Air +8.3: Mid May-Mid Sept.	Grade	0.8	1.2	2.4	3.7
13	22.9	4.4: Mid Sept.-Mid May Ambient Air +8.3: Mid May-Mid Sept.	Grade	0.6	1.1	1.8	3.4

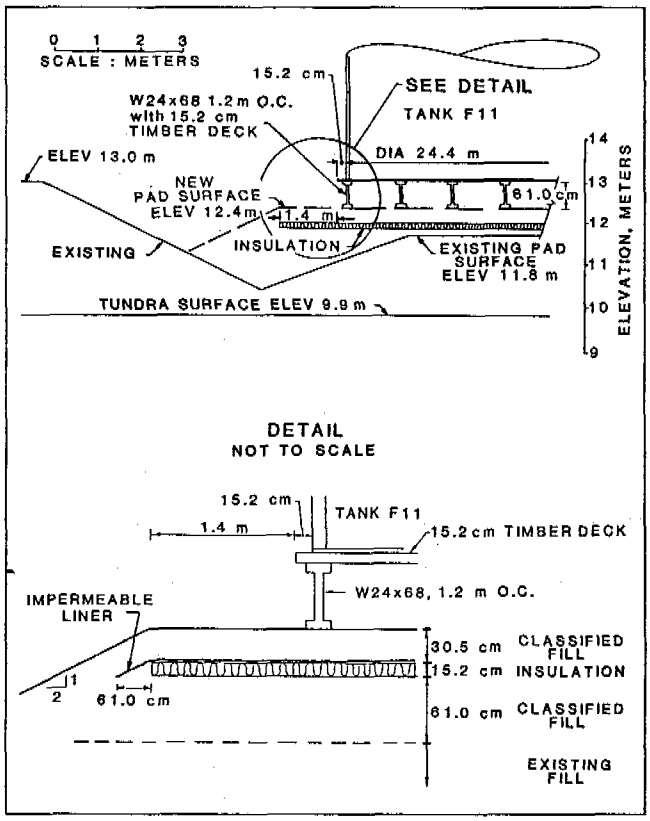

Fig. 2 Steel Beam Support Design

The results of the thermal simulation for this design (Simulation 1) are shown on Figure 3. To keep the area beneath the tank perimeter frozen, the design (Figure 2) shows 1.5 meters of insulation extending outward from the tank.

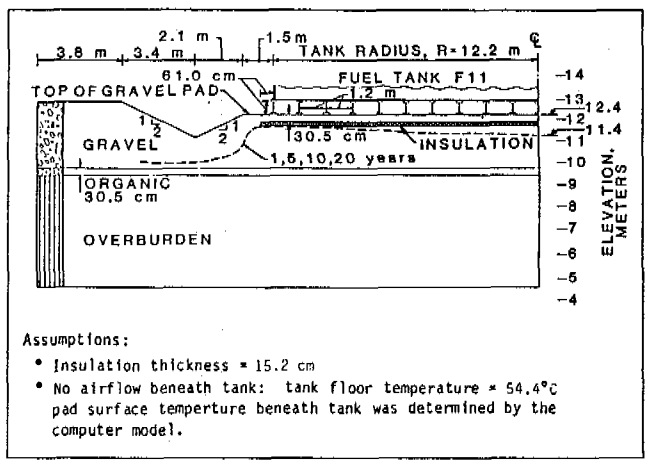

Fig. 3 Results of Thermal Analysis for Steel Beam Design (Simulation 1)

Since snow buildup, i.e. drifting, may impede air flow beneath the tank during the winter months, the effects of warmer temperatures were investigated. In Simulation 7, the pad temperatures were changed to equal ambient air from June through October and 37.8 degrees C from November through May. The results indicated that these warmer temperatures would cause a substantial depth of thaw. Using 22.9 cm of insulation and the same temperatures (Simulation 9), the thaw front stabilizes within the insulation as shown in Figure 4.

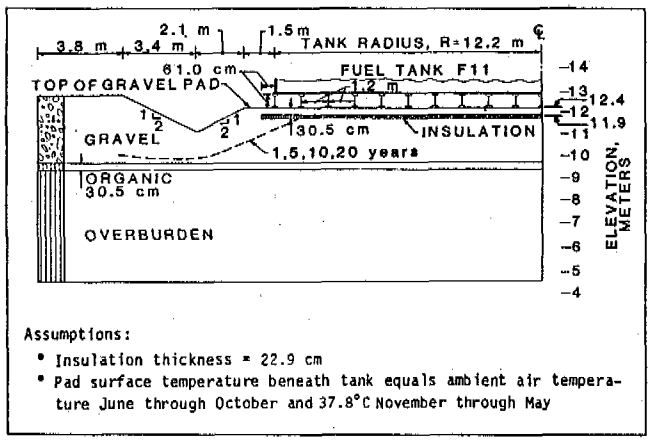

Fig. 4 Results of Thermal Analysis for Steel Beam Design (Simulation 9)

The other system of foundation support is to place the tank directly on the pad surface, as shown on Figure 5. Insulation is located 30.5 cm below the gravel pad surface. To prevent a large thaw bulb from developing beneath the tank, the fluid in the tank must be chilled to at least 4.4 degrees C from mid-September through mid-May, and modified to equal the

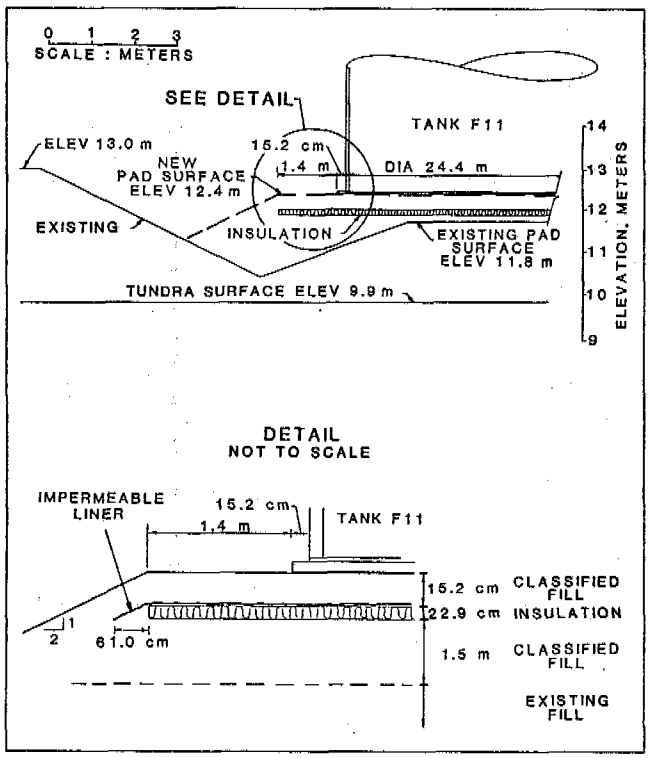

Fig. 5 Pad Support Design

outside ambient air temperature plus 8.3 degrees C from mid-May through mid-September. This will be accomplished by adding a cooling system to the tank inflow lines.

The results of the computer analysis indicated that 15.2 cm of insulation (Simulations 11 and 12) would provide satisfactory designs. However, due to the relatively low cost of the additional insulation, it was decided to use 22.9 cm of insulation as an additional factor of safety.

The results of the thermal analysis performed on this design (Simulation 13) are shown on Figure 6. Like the beam design, to keep the outer area frozen, the design (Figure 5) shows the insulation extending 1.5 meters outward from the tank.

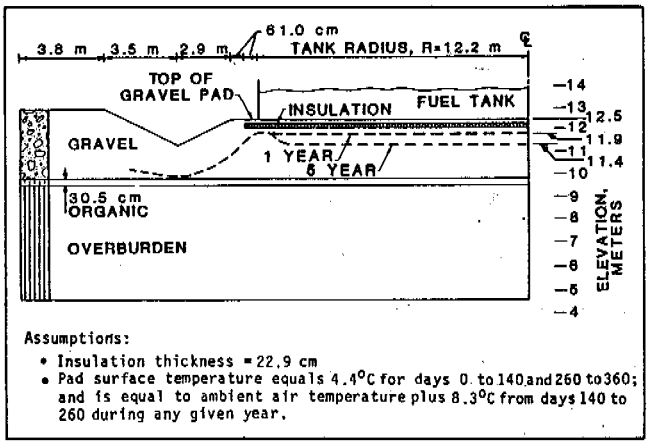

Fig. 6 Results of Thermal Analysis for Pad Support Design (Simulation 13)

DESIGN CONSIDERATIONS

To prevent frost heave, the gravel pad was constructed of classified fill consisting of sand and gravel containing less that 5 percent by weight passing the No. 200 sieve size. The fill was compacted to a minimum of 95 percent maximum dry density as determined by the ASTM Method D 1557 laboratory test procedure.

The insulation was installed on a smooth, level bearing surface with the joints staggered and overlapped to prevent cold leaks, and extended a minimum of 1.5 meters in all directions beyond the tank perimeter. FOAMGLAS cellular glass insulation, as manufactured by Pittsburgh Corning Corporation, was used. Although the thermal properties of this insulation are not as good as fiberglass, it was selected for its long-term stability. Specifically, it does not break down when immersed in oil. An impermeable barrier, resistant to degradation from petroleum products, was placed on top of the insulation for protection against fuel spills.

CONCLUSIONS

Warm fuel storage tanks can be constructed on the Alaskan North Slope using the design concepts presented within this paper. Depending upon the fluid temperatures and pad thickness, the tank can either be placed directly on the gravel pad or elevated. Instrumentation should be installed at the time of construction to allow for continual monitoring of ground temperatures and settlements.

ACKNOWLEDGEMENTS

The permission of the COTU Owners to publish this paper is gratefully acknowledged. Appreciation is extended to ANVIL Corporation, project consulting engineers.

REFERENCES

Auld, et al. 1978. Pad foundation design and performance of surface facilities in the Mackenzie Delta. Proceedings of the Third International Conference on Permafrost. Vol. 1, pp. 765-771.

Black, R.F. 1964. The Prudhoe Bay Field. Proceedings of the geological seminar on the North Slope of Alaska. pp. LI-LII.

Brown, R.J.E. and T.L. Péwé. 1973. Distribution of permafrost in North America and its relationship to the environment: a review, 1963-1973. Permafrost, Second International Conference, North American Contribution.

CRREL. 1984. FROST2B - A Nodal Domain Integration Model of Two-Dimensional Heat and Soil-Water Flow Coupled by Soil-Water Phase Change. Hanover: Cold Regions Research and Engineering Laboratory.

Lunardini, V.J. 1981. Heat Transfer in Cold Climates. Von Nostrand Reinhold Co., New York.

Lunardini, V.J. 1978. Theory of N-factors and correlation of data. Proceedings of the Third International Conference on Permafrost. Vol. 1, pp. 40-46.

Miller, T.W. 1975. The surface heat balance in simulations of permafrost behavior. ASME paper 75-WA/HT-66, November.

Wahrhaftig, C. 1965. Physiographic divisions of Alaska: a classification and brief description with discussion of high latitude physiographic processes. USGS Professional Paper 482.

Walker, D.A., et al. 1980. Geobotanical Atlas of the Prudhoe Bay Region, Alaska. Report 80-14. Hanover: Cold Regions Research and Engineering Laboratory.

STUDIES OF PIPELINE INTERACTION WITH HEAVING SOILS

S.Yu. Parmuzin[1], A.D. Perelmiter[2] and I.Ye. Naidenok[2]

[1]Faculty of Geology, Moscow State University
[2]All-Union Research Institute for Construction of Major Pipelines, Moscow, USSR

SYNOPSIS Vertical displacements of underground pipelines due to nonuniform heaving of freezing soils give rise to additional stresses in the pipe walls. The intensity of displacement in each specific cross-section of a pipeline depends not only on the magnitude of soil heaving at the base, but also on the operation of the pipeline - soil system, and can be determined from the equilibrium of forces that favor or resist pipe displacement. These forces are expressed as functions of the "effective" depth of soil freezing equal to the difference of depths at which pipe displacement begins and ends. Three principal cases have been considered. In the first case freezing occurs only from the soil surface, in the second - only from the pipe surface, and in the third - soil is freezing simultaneously from the soil surface and from the pipe walls. For these cases, a technique has been developed for calculating a pipeline displacement in different cross-sections along its length at any moment of time starting from the beginning of soil freezing. The correctness of this method has been corroborated by laboratory experiments on models and by comparison with field data.

Vertical displacements of underground pipelines due to heaving of freezing soils give rise to considerable stresses in the pipe walls. The magnitude of these stresses depends on variations in soil heaving along the pipeline. Hence strength calculations require knowledge of the magnitude of possible pipeline displacement in each specific cross-section.

Analytical determination of pipeline displacement due to its interaction with frost-susceptible soils presents a complex problem which has not yet been solved in exact formulation. This paper suggests an approximate engineering solution of displacement problem based on calculations of "effective" depth of freezing soil controlled by the difference of freezing depths where pipeline displacement begins and ends. Pipeline displacement begins at such a depth of freezing layer for which the forces favoring displacement exceed those resisting the motion. Motion will terminate either when the freezing process ends or when the forces resisting displacement exceed those causing that displacement.

Depending on the temperature regime of the pipeline and surrounding soil, three basic cases of interaction are possible:

(1) the pipeline lies within the layer of seasonally freezing soil and its temperature is little different from the temperature of the host soil;

(2) the pipeline lies in unfrozen soil and its temperature is below zero at least during some portion of the year. Soil freezing occurs from the pipe surface and, depending on pipeline temperature, seasonal or long-term freezing haloes form;

(3) the pipeline lies in unfrozen soil that experiences freezing both from the soil surface and pipe walls.

In the first of these cases, there is no pipeline displacement until the freezing front has reached the upper pipe generatrix. When the freezing front has reached the upper pipe generatrix, the soil begins to freeze together with the pipeline surface. The layer of frozen soil that has become attached to the pipe may drag the pipeline with it when it is displaced upwards under the action of relative normal forces of frost heaving P_n (Fig.1a). This can occur

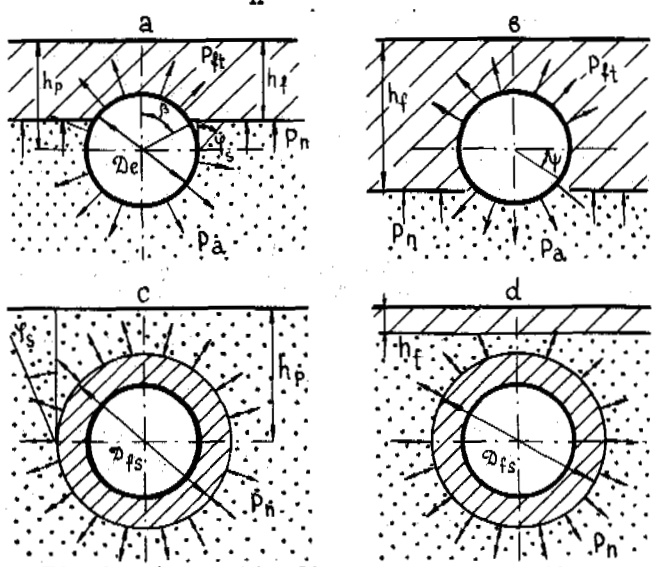

Fig.1 Schematic diagram of forces that act on the pipeline

when the resultant q_{ft} of specific freezing-together forces (P_{ft}), applied to the pipeline surface in the freezing-together zone, exceeds the total weight of the pipeline with the transported item q_p, the weight of unfrozen soil above the pipe in the pockets, and the shear strength of the unfrozen soil (q_{sh}) at the segment from the pipe half-diameter to the bottom of the frozen soil, as well as forces of soil adhesiveness at the lower pipeline generatriz q_a. If the adhesion forces are greater than the rupture strength of unfrozen soil (q_r), then the pipeline displacement occurs together with the soil that has stuck to the pipe and the value of q_r is taken into account in the calculations. Apart from the loads mentioned above, one should include the intensity of vertical load (q) in a cross-section due to the adjoining pipeline segments.

Up to the time when the depth of soil freezing has reached the depth of pipeline axis (h_p), the condition for displacement to begin is written in the form

$$q_{ft} - q_1 - q_s - q_p \pm q = 0 \qquad (1)$$

Here q_1 is equal to the smaller of two values, q_a and q_r. The resultant of specific freezing forces is determined, as has been shown by Perelmiter et al. (1981), from

$$q_{ft} = \frac{1}{2} K_{ft} D_e^2 \frac{t_{min} \sin(\frac{\pi}{T_w} \tau)}{h_f} \left(\frac{1}{2}\beta - \frac{1}{4}\sin 2\beta\right) + \qquad (2)$$

$$+ P^{\circ}_{ft} D_e \sin\beta,$$

where

$$\beta = \cos^{-1} 2 \frac{h_p - h_f}{D_e},$$

K_{ft} is a coefficient of proportionality having the dimension MPa . deg^{-1}; P°_{ft} denotes specific forces of freezing together at 0°C; D_e is the external pipe diameter; t_{min} is the mean monthly temperature of soil surface during the coldest month; T_w is the duration of the winter period, τ is the time from the beginning of freezing to the beginning of displacement; h_f is the depth of frozen layer at time τ.

Formula (2) is derived on the assumptions that temperature changes linearly with depth, the temperature change at the soil surface during winter time is described by a harmonic function, and the specific forces of freezing depend linearly on soil temperature.

The quantities q_a, q_r, and q_{sh} are, determined from the following relations (Perelmiter et al., 1981):

$$q_a = \frac{\pi}{4} P_a D_e, \qquad (3)$$

$$q_r = \sigma_r^{lt} D_e, \qquad (4)$$

$$q_{sh} = g\rho\left(h_f - \frac{1}{2}D_e\right)D_e + 0{,}107\, g\rho D_e^2 + \qquad (5)$$

$$+ \frac{1}{4}\rho g D_e^2 \cos^2\beta \operatorname{tg}\varphi_s + \frac{C D_e \cos\beta}{\cos\varphi_s}$$

where P_a denotes specific forces of adhesion between unfrozen soil and pipeline; σ_r^{lt} is the limiting long-term strength of unfrozen soil for tension; g is the acceleration due to gravity; ρ soil density above the pipe; φ_s is the angle of internal friction for unfrozen soil; C the adhesive force of unfrozen soil. The values of adhesion and long-term strength of unfrozen soil are given in a number of publications (Vetrov and Kondra, 1972; Rekomendatsii... , 1983; Sirota, 1980). The forces q_{ft} and q_{sh}, as can be seen in (2) and (5) are the functions of time τ and of freezing depth h_f. Knowing the dependence of h_f on τ, one can find from (1) the time when the pipeline began to move and the minimum depth of freezing (h_f^{min}) at which that motion will begin. Subsequently, the pipeline and the surrounding soil move together. Pipeline motion terminates on reaching the maximum of soil freezing (h_f^{max}). The difference between h_f^{max} and h_f^{min} is equal to the "effective" thickness which causes pipeline motion (Δ) in the cross-section considered.

$$\Delta = (h_f^{max} - h_f^{min}) K_h \qquad (6)$$

where k_h is the coefficient of soil heaving equal to the ratio of heaving amount at the free surface of soil to the maximum freezing depth; it is determined experimentally.

If calculation by (1) shows that pipeline motion does not occur before the freezing front has reached the depth of pipeline axis, one should examine the equilibrium of forces for $h_p \leq h_f \leq h_p + 0.5\, D_e$ (Fig.1b).

In that case normal forces of heaving q_n which begin to act directly on the pipe are added to the loads that cause the motion. The forces that resist motion decrease, because $q_{sh} = 0$. The condition for equilibrium of forces that act on the pipeline is written in the form

$$q'_{ft} + q'_n - q'_1 - q_p \pm q = 0. \qquad (7)$$

Normal heaving forces under this condition are determined from

$$q'_n = \frac{1}{2} K D_e^2 \left(\sin\Psi - \frac{1}{4}\sin 2\Psi - \frac{1}{2}\Psi\right). \qquad (8)$$

The coefficient of proportionality K is 0.6 MN/m^3 for soils of medium heaving capacity

and 1.0 MN/m^3 for those of strong heaving capacity (Kiselev, 1971).

The force q'_{ft} is determined from (2) when $\beta = \frac{\pi}{2}$.

The forces q'_a and q'_r are determined from

$$q'_a = P_a D_e \left[\frac{1}{2}\left(\frac{\pi}{2} - \Psi\right) + \frac{1}{4}\sin 2\Psi\right]; \qquad (9)$$

$$q'_r = \sigma'^{ft}_r D_e \cos\Psi, \qquad (10)$$

where $\Psi = \sin^{-1} 2\frac{h_f - h_p}{D_e}$.

The magnitude of displacement is found, as in the preceding case, from (7) knowing h_f as a function of τ.

As freezing proceeds, when $h_f > h_p + 0.5\,D_e$, the pipeline is acted on by q_n, q_p, and q only. The equilibrium of forces is written as

$$q_n - q_p \pm q = 0. \qquad (11)$$

The quantity q_n is for this case found from

$$q_n = 0.107\,K\,D_e^2 + K\,D_e\,h_2 \qquad (12)$$

where h_2 is the thickness of frozen soil under the lower pipe generatrix.

An experiment was carried out to test the method for calculating the thickness of the layer at which displacement begins. Three 1-m long steel pipe segments 26, 17, and 9 cm in diameter and a wall thickness of 0.6 cm were put in the frozen zone at a depth of 22 cm from the upper generatrix to the soil surface. The soil at the testing site was represented by silty loam and had the following characteristics: weight humidity 23%, ρ = 0.00146 kg/cm^3, φ_s = 15°, C = 0.014 MPa. Groundwater table was at a depth of 30 - 60 cm prior to freezing. Such soils are classified as strongly frost-susceptible. To shield the sealed butt ends of pipes from the action of heaving forces when soil was frozen on to the ends, these were insulated with two layers of polyethylene. The freezing depth was determined by frost-depth meters of the Danilin system. Observations of pipe motion were made by the geodetic method. Experimental investigations have shown that vertical pipeline motion began in all the three cases much earlier than the time when the frost depth reached the pipe axis. The minimum thickness of frozen soil $h^{min}_{f(ex)}$ at which the motion of test pipes began in the experiment, the comparison with the calculated values $h^{min}_{f(c)}$, as well as the calculated time from the beginning of freezing until the beginning of motion τ_c, are given in Table 1.

The presence of snow does not affect the value of $h^{min}_{f(c)}$, as was to be expected, but just increases the time from the beginning of freezing until the beginning of motion.

Table 1

Experimental data and calculated displacement of experimental tubes

Experimental data		Calculated values		
D_e, cm	$h^{min}_{f(ex)}$, cm	$h^{min}_{f(c)}$, cm	τ_c (hours)	
			with snow	without snow
26	25	25.3	173	94.5
17	24	24.2	158	86
9	23	23.2	145	79

The operation of pipelines with a negative temperature put into unfrozen soil is accompanied by the formation of frost haloes around them. Along the perimeter of this halo heaving forces arise that have the direction along the normal to the surface of freezing (Fig.1c). The active part of relative normal heaving forces P_n, causing pipeline displacement, is situated along the lower semicircle of the cylindrical freezing surface. The heaving forces developing on the upper semicircle of the frozen cylinder are counterbalanced by the overlying unfrozen soil when there is no freezing of soil from the surface, and hence are equal to the weight of that soil acting on the frozen cylinder.

Pipeline motion is in that case prevented by: the total weight of the pipe with the transported item and soil frozen on to it (q_{pfs}) the resistance of unfrozen soil above the pipe(q^c_s), as well as the force of friction (F_{fr}) of frozen soil around the pipe with the surrounding unfrozen soil due to the fact that the horizontal component of frost-heaving forces gives rise to compaction ("wedging-out") of the surrounding unfrozen soil. It is also necessary to include the force (q) due to the influence of the adjoining parts of the pipeline.

The vertical component of friction force causing pipe motion is determined by

$$q^c_n = P_n \cdot D_{fs} \qquad (13)$$

where D_{fs} is the diameter of soil frozen on to the pipe.

The quantity P_n, which depends on the composition, texture and properties of the soil, on freezing conditions, etc., varies within a wide range and is determined experimentally, whereas q_{pfs} and q^c_s are determined from

$$q_{pfs} = q_p + \frac{\pi}{4} g\rho\left(D^2_{fs} - D^2_e\right) \qquad (14)$$

$$q^c_s = g\rho D_{fs}\left(h_p - 0{,}39 D_{fs}\right) + g\rho h^2_p \operatorname{tg}\varphi_s + \frac{C h_p}{\cos\varphi}. \qquad (15)$$

The force arising from the friction between the frozen soil around the pipe and the unfrozen soil is determined as the sum of friction forces arising from the horizontal components of frost-heaving forces acting on the lower and upper semicircles of the frozen cylinder.

The force of friction is determined from the following formula (Perelmiter and Parmuzin, 1981):

$$F_{fr} = [P_n D_{fs} + \xi_o g \rho D_{fs} (h_p - \frac{1}{4} D_{fs}] tg \varphi_s \qquad (16)$$

where $\xi_o = tg^2 (45° - \frac{\varphi_s}{2})$.

From the equation

$$q_n^c - q_{pfs} - q_s^c - F_{fr} \pm q = 0 \qquad (17)$$

one can find the minimum value of D_{fs}^{min}, and so the thickness of soil frozen on to the pipe at which pipeline motion begins. Heaving will terminate simultaneously with freezing; the diameter of the frozen cylinder will then be equal to D_{fs}^{max}.

The value of effective frozen-layer thickness controlling pipeline motion in the cross-section considered is equal to

$$h_{ef} = \frac{1}{2} (D_{fs}^{max} - D_{fs}^{min}) \qquad (18)$$

The magnitude of displacement can then be found from (6).

A number of experiments have been made on the model to substantiate the proposed model for the interaction between the pipeline and the frost-susceptible soils that are freezing from the pipe wall and to determine pipe motion as a function of frost-halo thickness (heaving coefficient). A pipe of diameter 7.6 cm and wall thickness 0.3 cm was put into a metal box 4.05x1.5x1.6 m in size that had been filled with heavy loam (ρ = 0.00202 kg/cm^3). The distance from the soil surface to the upper generatrix of the pipe was 12 cm. The pipe ends were either clamped in hinges or remained free in different experiments. Cold air of temperature -60°C, -30°C, and -20°C was pumped into the model pipe. Soil freezing from the pipe walls took place under the conditions of a free system, i.e., water flow occurred from below. Water level in the device was at a depth 28-32 cm. Soil humidity varied within the range 23 to 27 percent. Soil temperature was measured with resistance thermometers clamped rigidly relative to the pipe; vertical pipe motion was determined at eight points along the length. Measures were taken to prevent displacement sensors from being frozen to the frost-halo soil. Fig.2 shows experimental results for the case of unclamped pipe ends. It can be seen that the rate of freezing significantly affects the magnitude of pipe displacement. In all cases, the magnitude of displacement is a linear function of the frozen layer depth above the pipe. Hinge clamping of the ends diminishes displacement at the middle of the pipe. In that case, the heaving coefficient varied within 0.14 to 0.21 for different freezing rates.

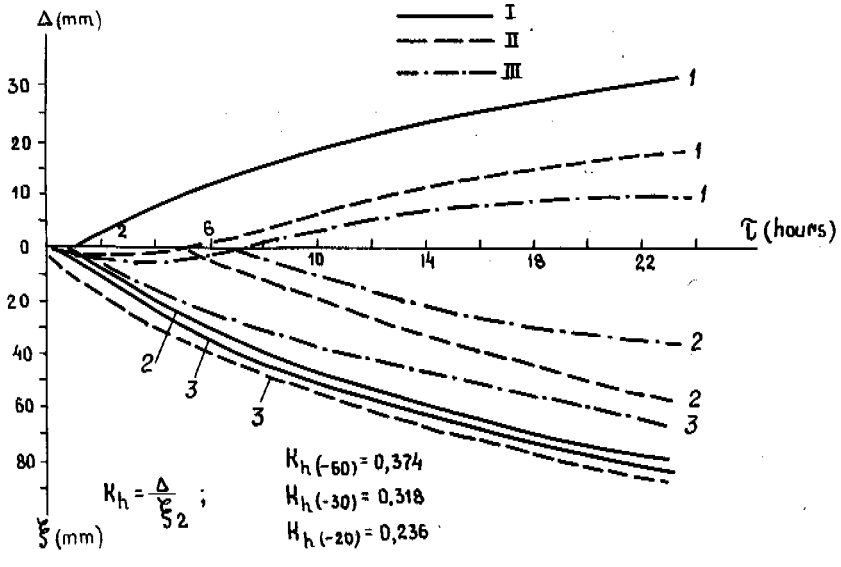

Fig.2 Dynamics of vertical displacement of the pipe (Δ) and freezing halo thickness below it (ξ) at -60°C, -30°C, and -20°C (curves with Roman figures I, II and III, respectively)

I - pipe displacement; 2 - change in the depth of freezing below the pipe upon the beginning of upward motion (ξ_2); 3 - total depth of freezing below the pipe.

Slusarchuk et al. (1978) described experimental investigations into the motion of 12 m-long and 1220 mm in diameter pipe sections when a frost-susceptible soil was freezing from the pipe. The heaving coefficient of pipe sections was 0.205-0.215, i.e. it was close to the values obtained by us in model studies.

When soil is freezing simultaneously from the surface and from the pipe walls (Fig.1d), the first thing that occurs is compaction of a layer of unfrozen soil under the bottom of the layer of seasonal freezing. The response of that layer significantly diminishes and (when it reaches a certain thickness) completely stops pipeline heaving until the time when the soil that is being frozen from the surface comes in contact with the frozen soil around the pipe. After that, when the soil is being further frozen from the surface, the pipeline will begin to move.

Thus, the method proposed here can predict the possibility and magnitude of displacement of underground pipelines when these interact with frost-susceptible soils. The relevant formulas involve the main characteristics of the state and properties of soils that control the intensity of pipe motion in a specific cross-section along the length of the pipeline. One of the tasks facing future studies is to conduct natural-size experiments in test areas in order to determine the coefficients of soil heaving for different pipe diameters, the effect of the motion of pipeline clamping in the soil, and the load due to the areas adjacent to the pipeline cross-section under consideration.

REFERENCES

Vetrov, Yu.A. & Kondra, A.S.(1972). Rezultaty issledovaniya lipkosti gruntov. Sb.: Gornye, stroitelnye i dorozhnye mashiny.Vyp. 14, pp.12-18. Kiev.

Kiselev, M.F. (1971). Meropriyatiya protiv deformatsii zdaniy i sooruzheniy ot deistviya sil moroznogo vypuchivaniya fundamentov, 102 pp. Moskva: Izdatelstvo Literatura po stroitelstvu.

Perelmiter, A.D. & Parmuzin, S.Yu.(1980). Vzaimodeistvie truboprovodov s puchinistymi gruntami. Sb.nauchnykh trudov VNIIST: Konstruktsii, metody rascheta gasoprovodov i sposoby stroitelstva, pp.57-68. Moskva.

Perelmiter, A.D., Parmuzin, S.Yu., Alekseyev S.I. & Spiridonov, V.V.(1981). Opredelenie peremeshcheniy i nagruzok, deistvuyushchikh na truboprovod v puchinistykh gruntakh. Nauchno-tekhnicheskiy referativny sbornik: Proektirovanie i stroitelstvo truboprovodov i gazopromyslovykh sooruzheniy. Vyp.14, pp.26-33. Moskva.

Rekomendatsii po opredeleniuy lipkosti gruntov v statsionarnykh laboratornykh i polevykh usloviyakh. (1983), 31 pp. Moskva: Stroiizdat.

Sirota, Yu.L. (1980). Issledovaniya prochnosti glinistogo grunta pri rastyazhenii. Nauchno-tekhnichesky referativny sbornik: Stroitelstvo i arkhitektura, Seriya 15: Inzhenernye izyskaniya v stroitelstve. Vyp.4. Otechestvenny opyt, pp.5-9.Moskva.

Slusarchuk, W.A., Clark, J.I., Nizon, J.E., Morgenstern, R.N. & Gaskin, P.N.(1978). Field test results of a chilled pipeline buried in unfrozen ground. Proc.3rd Int. Confr. on Permafrost, v.I, 877-884, Edmonton, Canada.

YUKON RIVER BANK STABILIZATION: A CASE STUDY

C.H. Riddle, J.W. Rooney and S.R. Bredthauer

R&M Consultants, Inc., Anchorage, Alaska 99503 USA

SYNOPSIS: Erosion on the right bank of the Yukon River above the Galena Airfield is caused by a combination of thermo-erosional niching of the frozen upper bank, causing massive block failures, and erosion of the failed material by river currents and natural thalweg migration. The average annual erosion rate is relatively uniform throughout the 8 km long bend upstream of Galena, ranging from 4-6 m per year. Subsurface investigations and geotechnical evaluation identified soil conditions, the extent of massive ground ice and other geotechnical parameters necessary for design and construction of bank protection. To limit continued erosion of the upper bank by thermo-erosional niching, alternative design concepts were prepared, each reflecting the different geotechnical and hydraulic conditions along the study reach. A conventional rock revetment was recommended for the more stable soil section. An insulated, rock protected revetment was suggested as an alternative for those areas found to have ice-rich soil and high thaw strain potential.

INTRODUCTION

Galena, Alaska is located on the north bank of an 11 km long meander of the Yukon River about 435 km west of Fairbanks (Fig. 1). The town of Galena was established around 1919 as a supply base for galena prospects in the vicinity. The Civil Aeronautics Administration constructed an airfield at Galena in late 1941 and the airfield was occupied by the military soon after. Although the site was known for periodic flooding, the military felt the Galena airfield could best fill their emergency needs at that time. Following an ice jam flood in 1971, which flooded the original townsite and nearly overtopped the flood control dike around the airfield, much of the civilian population relocated to a new townsite about 2.5 km upstream of the runway. The new townsite is also in the path of the migrating meander.

Since establishment of the airfield, several studies and projects have been completed by the U.S. Army Corps of Engineers (Corps) in efforts to control erosion in this area. Specific features within the project study area are shown in Fig. 1. Most of these actions have concentrated on protecting the airfield. In 1984 the exiting sheet pile hard point was in danger of being flanked due to erosion upstream of the piles.

Erosion at the old town site is primarily by wave attack of the upper bank, averaging 1.4-1.8 m per year. From the old town to slightly upstream of the Galena Airfield (points A to F on Fig. 1), the unprotected upper bank materials consist of unfrozen or relatively thaw stable frozen silt and sand. Upstream of the Galena Airfield and extending to near Beaver Creek (points F to J on Fig. 1), the shoreline generally consists of 4.5-7.5 m of frozen silt containing massive ice. In all cases, these materials overlie a typically frozen sand and gravelly sand deposit. This underlying granular material appears to be thaw stable, where frozen, representing a suitable foundation on which to place some form of embankment for upper bank slope protection.

Construction of longitudinal segments of bank protection was felt to be the most practical method of completing any significant portion of this project due to budget restrictions. A 656 m long section (identified as Phase I on Fig. 1), extending upstream from the sheet pile hardpoint, was constructed during the winter and spring of 1986. An additional 328 m long section (identified as Phase II on Fig. 1) located in front of the new town site is currently being completed by the Corps.

SITE CONDITIONS

General

Galena lies in a wide floodplain of the Yukon River. Sediments contained within the plain are Pleistocene or Holocene fine to coarse-grained deposits generally exhibiting distinct thin parallel stratification. The floodplain has four physiographic phases or units, each with distinct permafrost, drainage, vegetation, and engineering characteristics (Péwé, 1948). Each of these phases is temporary (relative to geologic time) and somewhat evolutionary in nature due to permafrost growth, flooding, river meandering, and associated changes in vegetation. These phases are readily identifiable from air photos, based on the shape and distribution of lakes and vegetation. The four phases in

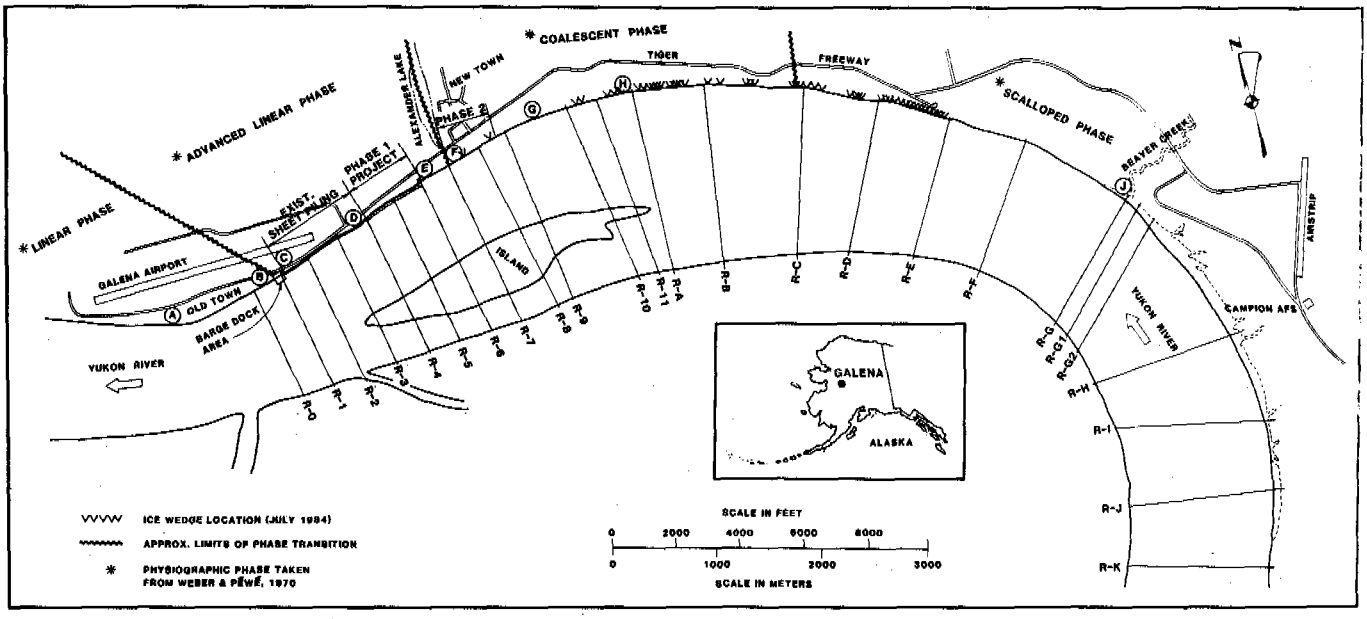

Fig. 1 Galena Bank Stabilization Site Plan

order of their ages (youngest to oldest) are the linear, advanced linear, coalescent, and scalloped phases (Weber and Péwé, 1970). Each phase and its relevance to the erosion control project are briefly discussed below. Fig. 1 also identifies the various physiographic phase transitions within the Galena vicinity.

Linear Phase

The linear phase is characterized by distinct linear lakes parallel to the river and one another. This phase is vegetated with grasses, alder, willows and cottonwood trees. Permafrost is generally absent or at depths of more than 6 m near the river's edge, but rises in elevation to 1-1.5 m depth at the inner phase boundary. Massive ground ice is generally absent in the linear phase. This unit is the lowest lying and forms the most active part of the floodplain. The linear phase lithology consists of well stratified micaceous silt, sand, and gravel. The thickness of the linear phase lithology is thought to be equal to the depths of the Yukon River channel.

Advanced Linear Phase

The advanced linear phase is characterized by distinct linear lakes parallel to predominant drainage trends. These lakes are becoming segmented by encroaching vegetation. Sediments composing this phase are found 1-2 m above river level and occur in thicknesses of 1.2-4.7 m. Soils composing this alluvial phase are generally micaceous silts with relatively rare occurrences of sand and gravel strata. Vegetation includes alder, birch and black spruce. Permafrost in this physiographic phase is generally present within the upper 1 m of the deposit, but is generally free of massive ice.

Coalescent Phase

Stunted spruce and birch forests, as well as developing peat moss tundra, are the primary vegetation on the coalescent phase of the floodplain. Linear lakes lying at various angles to the Yukon River become interconnected due to wave action and cave-ins. Soils encountered in the lithology of this phase are micaceous and organic silts. Permafrost generally occurs within 0.5 m of the ground surface. Massive ice is present, but polygonal ground patterns have not been observed.

Scalloped Phase

This phase is characterized by numerous irregularly shaped lakes, low vegetation on thick tundra and integrated drainage patterns. Some stunted black spruce, larch, birch, and willows are present. Permafrost occurs at 0.3 m below the ground surface in protected areas. Large ground ice masses are present in the silt and organic silt soils. Polygonal ground is apparent in this advanced phase of floodplain development.

DESIGN CONCERNS

Soil Assessment

Subsurface conditions along the Galena segment of the Yukon River have been defined in general terms during earlier studies completed by the U.S. Army Corps of Engineers, Péwé (1948) and Corps (1952; 1959) and more specifically in the study area identified as Phase I by R&M Consultants (1985). The latter subsurface investigation supported the design of the Phase I project and areas where subsequent slope protection were anticipated. This investigation included drilling and sampling

of 10 boreholes; 2 on top of the bank and 8 located at river level either near the shore or the thalweg. Generalized cross-sections showing soil and thermal conditions for Ranges 5, 7 and 8 are shown in Figs. 2, 3 and 4, respectively. These data indicated that the riverbank between Ranges 4 and 7 consists of approximately 4.5 to 7.5 m of frozen silt overlying sand and gravelly sand that is probably frozen inland from near the bank edge and intermittently frozen outward to the advancing river thalweg. The overlying frozen silt stratum encountered along the bank in TH-2 and TH-5 (near Ranges 5 and 7, respectively) contained a moderate to low ice content. Visual inspection of the exposed bank in 1984 indicated the general absence of large segments of massive ice within this area. Significant massive ice was observed in the overlying silt along the bank from roughly Range 7 to well beyond Range 11. These observations correlate with those compiled by Weber and Péwé (1970), where they observed that the coalescent and scalloped phases (lying east of roughly Range 7) were ice-rich and contained massive ice.

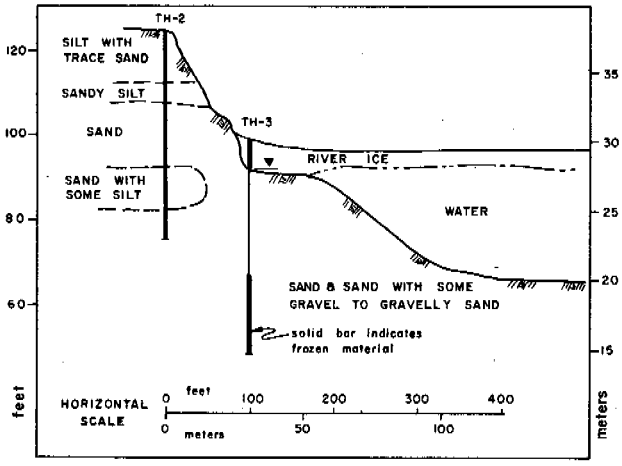

Fig. 2 Cross-Section Showing Soil and Thermal Conditions at Range 5 (March 1984)

Permanent thermistor strings were installed in two test borings. The temperature profiles identified the apparent variability in the advance of the thaw bulb into the sand stratum underlying the silt. Both borings were located within the coalescent phase of the floodplain approximately the same distance behind the top of river bank. Unfrozen conditions were found below a depth of 6.9 m in one test hole. On the other hand, the second test hole was completely frozen through its entire depth.

Based on the limited borehole information, it appears that underlying sands, gravelly sands and sandy gravels below elevation 30.5 to 33 m may be present at about the same level or slightly lower east of Range 7. While segments of the underlying granular material occurs unfrozen at some locations below the bank, it is anticipated that most of this material is frozen behind the bank face and

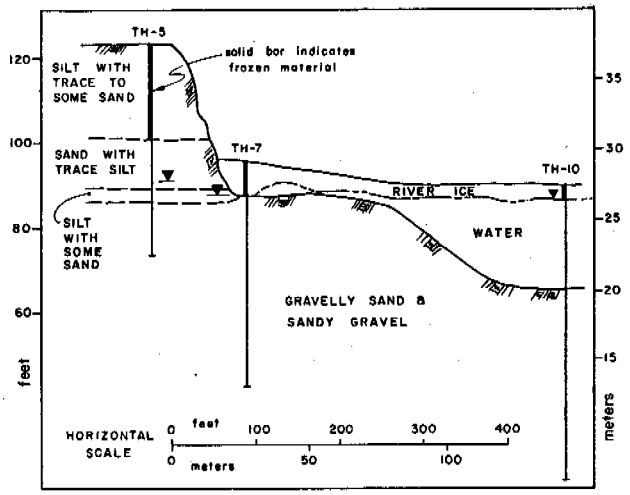

Fig. 3 Cross-Section Showing Soil and Thermal Conditions at Range 7 (March 1984)

will be mixed unfrozen/frozen out to the river thalweg. These conditions were noted in three borings drilled below the river bank where frozen ground was found at varying depths below the river ice. Penetration refusal at depth in other borings also indicated the presence of deeper lying permafrost below the river.

Because of the river bank erosion process and the relatively rapid northward advancement, the soil thermal state near the river bank itself was difficult to predict. Site studies and thermal modeling by Smith and Hwang (1973) on the Mackenzie River indicated that the long term thermal process involves a lag in talik formation with depth below the river along the cut bank side. They also indicate that the thermal affect of the river on the surrounding ground temperature field depends not only on the strength of the field source but also on

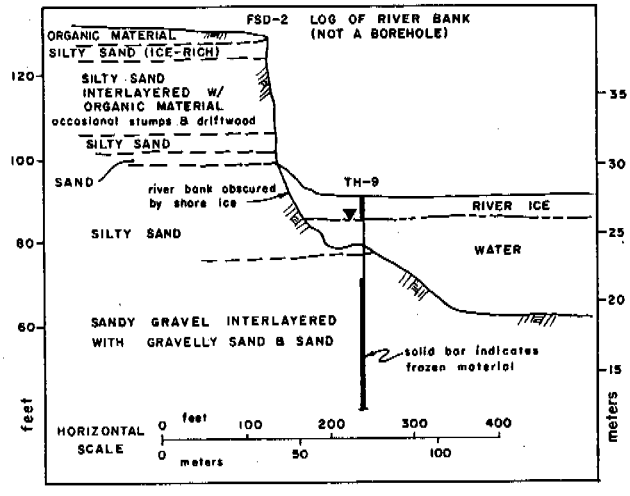

Fig. 4 Cross-Section Showing Soil and Thermal Conditions at Range B (March 1984)

the length of time available to the thermal process. Conditions found at Galena are similar to those reported by Smith and Hwang. The generalized soil profile developed along the bank indicated mixed frozen/unfrozen soil exists within the near shore below the river bank.

Thermal Assessment

Similar thermal erosion phenomena of the Coleville River delta has been reported by Walker (1983). However, published information on thermal performance of stabilized river banks with relatively high seasonal water level fluctuation is not available. Limited information on frozen reservoir embankments indicated that an uninsulated embankment segment of a dam remained frozen throughout the entire year (Fulwider, 1973 and R&M Consultants, 1986) . However, the influence of convection resulting from warm summer river temperatures and higher flow velocities and erosion conditions, such as occur at Galena, would not apply to that case. Various unpublished thermal studies by Alyeska Pipeline Service Company evaluated convection associated with frozen ground and thawing slopes. Because of modeling difficulties, the influence of convection was generalized by conservative assumptions for conduction to simplify the evaluation.

Experience gained by Alyeska in the use of insulation for thermal stabilization of slopes is useful. Two installations at major road cuts containing ice-rich soil along the Dalton Highway, one at Happy Valley on the North Slope (McPhail et al., 1975 and Brown and Kreig, 1983) and the other near Hess Creek north of Livengood (Rooney and Condo, 1984 and Mageau and Rooney, 1984), used insulation materials to retard thermal degradation and significant slope erosion.

Thermal Analysis

The modified Berggren equation was used to analyze the potential thermal performance of the embankment design shown in Fig. 5. The analysis considered the influence of uncertainty in estimated (silt) thaw strain and used a formulation which maintained consistency between thaw strain and latent heat in the silt. These results were, however, considered only suitable for a conceptual design. Any further analyses should be based on a more refined analysis using two-dimensional geometry to consider end and corner effects.

Results of the preliminary analysis are shown in Fig. 6. These results include estimates of the average thaw depth and average thaw settlement plotted as a function of thermal load (TL) for four insulation thicknesses: 0, 50, 100 and 150 mm. Two values of subgrade thermal conductivity (k) were used. Thermal load is plotted in Fig. 6 as a function of average surface temperature (ST) load and time. The need for insulation to minimize effects of thermal degradation is suggested by results presented in this figure.

Estimates of average thaw depth and thaw

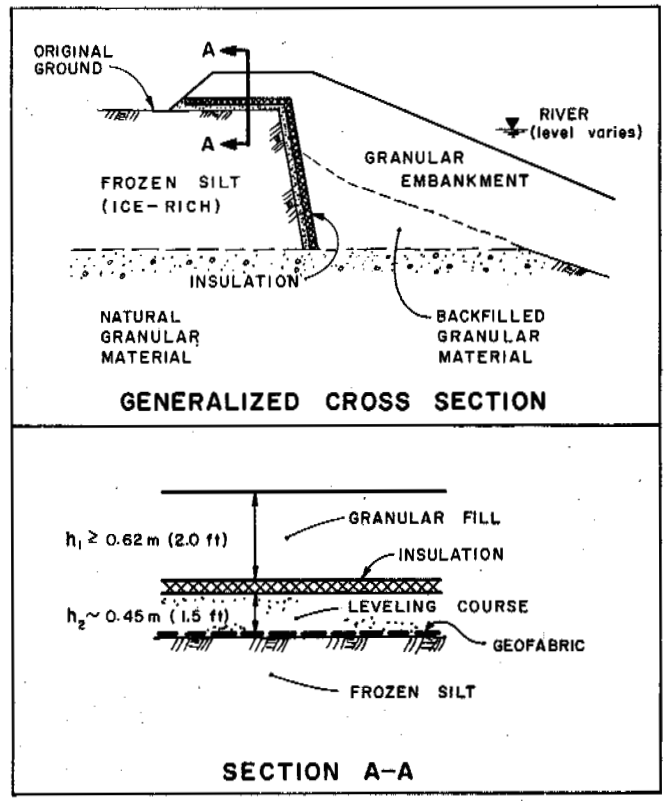

Fig. 5 Conceptual Insulated Embankment Section

settlement assume that the insulation maintains its structural and thermal integrity during the facility design life. Thaw settlement (TS) estimates in Fig. 6b are for average total settlement due to thaw; estimates are based on average thaw strain of 50%.

The dashed line estimates in Fig. 6b show thaw depth and thaw settlement using thermal conductivity values averaged between the estimates of k for silt = 1.0 W/mK and k for granular embankment material = 2.9 W/mK. These estimates represent possible thermal affects where large amounts of gravel (embankment) material are needed to fill thaw depressions in the embankment. In all cases thaw depth and thaw settlement estimates decrease with increasing insulation thickness. The thermal affect is very significant for no insulation whereas with as little as 50 mm of insulation this affect is considerably reduced. With 100 mm and 150 mm of insulation, the thermal affect is not as significant.

Design Interpretation

Fig. 6a shows three thermal loads: (1) a maximum thaw index based on CRREL Technical Report 102 (Aitken, 1963), (2) a 10-year thermal load, and (3) a 20-year thermal load. An equivalent average surface temperature, (ST) of -15.5°C was used for the 10 and 20-year thermal loads. This estimate of ST represents a conservative value for Galena appropriate for a surface thermal disturbance

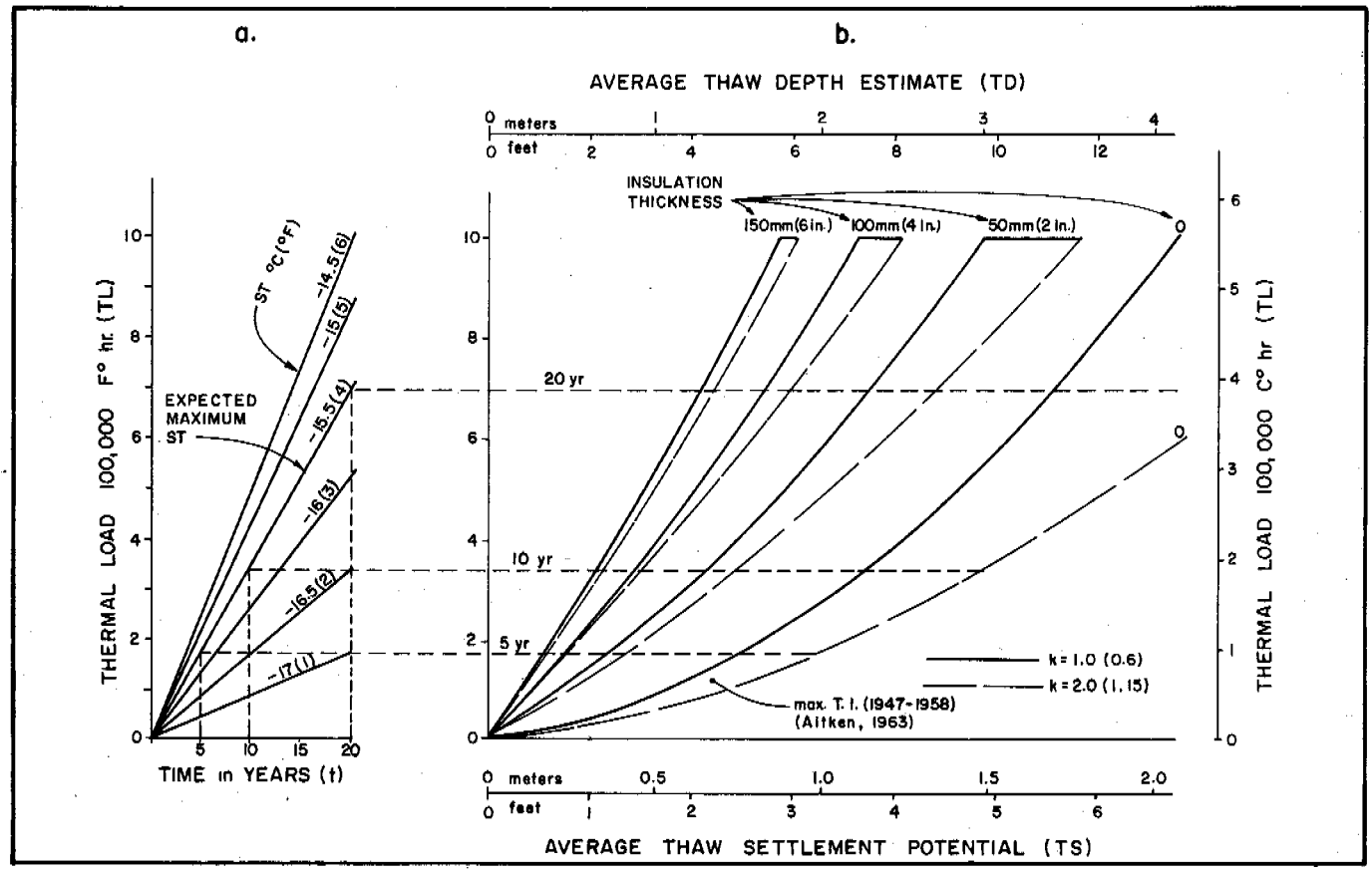

Fig. 6 Average Thaw Depth/Settlement Analysis and Interpretation

of (warm) permafrost existing at about -1°C. The corresponding estimates of average thaw depth and thaw settlement are shown.

Interpretation of the results based on a thermal load due to an average surface temperature of approximately -15.5°C give estimates of thaw settlement of the uninsulated silt embankment from about 1.7 m to more than 2 m in 20 years. Installation of 100 mm of insulation would reduce estimated thaw settlement in half; reducing the 20-year estimated thaw settlement to about 1 m; the 10-year estimate to about 0.5 m, and the 5-year estimate to less than 0.3 m.

Using the conceptual embankment design shown in Fig. 5 there are two alternatives: (1) use (polystyrene) insulation, and (2) do not use insulation. Insulation was recommended to provide adequate stability for any future bank protection projects located within either the coalescent or scalloped physiographic phases at locations where ice-rich and significant thaw settlement conditions are identified. A minimum of 50 mm but preferably 100 mm were suggested to reduce the rate and magnitude of thaw and resulting settlement. Geo-fabric was considered for placement on top of the bank. A minimum of .45 m of non-frost susceptible (NFS) granular fill was recommended for placement on top of the fabric. A minimum of .62 m of fill placed above the insulation would provide protection from subsequent construction and operational traffic loads.

Grading and drainage should be performed such that surface and melt water is diverted from the embankment. In particular, further design and maintenance efforts should attempt to minimize water from flowing under the embankment and insulation (either along or down the bank). Successful performance of the design assumes and requires ongoing maintenance of the embankment bench and adjacent bank. Lack of proper maintenance may result in undesirable damage to the proposed slope protection scheme and consequently to further deterioration of the river bank and protection system. If snow is removed or does not accumulate on the top of the embankment during winter, thaw and settlement rates and magnitudes will be reduced.

CONCLUSIONS

Bank protection solutions for the Yukon River at Galena, Alaska were developed to protect against upper bank thermo-erosional niching associated with hydraulic conditions. Conceptual designs accommodated for anticipated variability in both soil and permafrost conditions. Geotechnical consideration of thaw degradation and ground settlement were related to geologic deposits comprising four physiographic phases. Relatively conventional

bank slope protection was installed on a frozen bank section with low thaw strain potential. An insulated embankment design was developed for application along those sections of the bank where higher ice contents and thaw strain potential were encountered.

Construction of approximately 656 m of bank protection using the typical section shown in Fig. 7, was accomplished within the designated Phase I area (Fig. 1). The next segment, identified as Phase II on Fig. 1, is currently being constructed by the Corps using a typical section similar to that shown in Fig. 7. Fig. 8, is a conceptual typical section which has not been utilized in either construction phase since soil ice content has been relatively low within the bank sections considered to this time. Due to the limited thaw seasons since commencement of the phased construction project, performance data are not yet available.

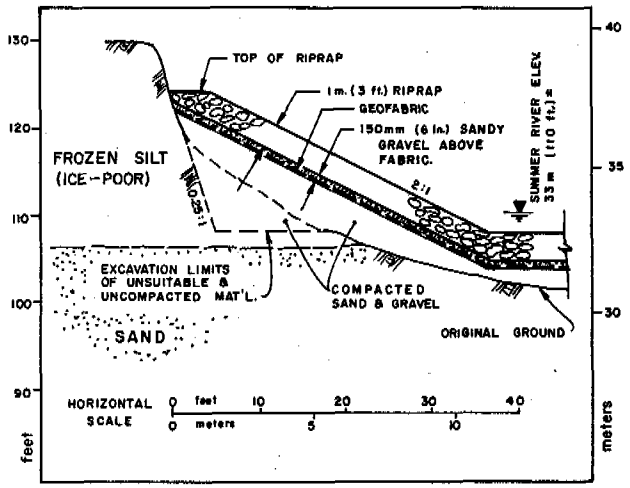

Fig. 7 Typical Embankment Section For Low Thaw Strain Soil

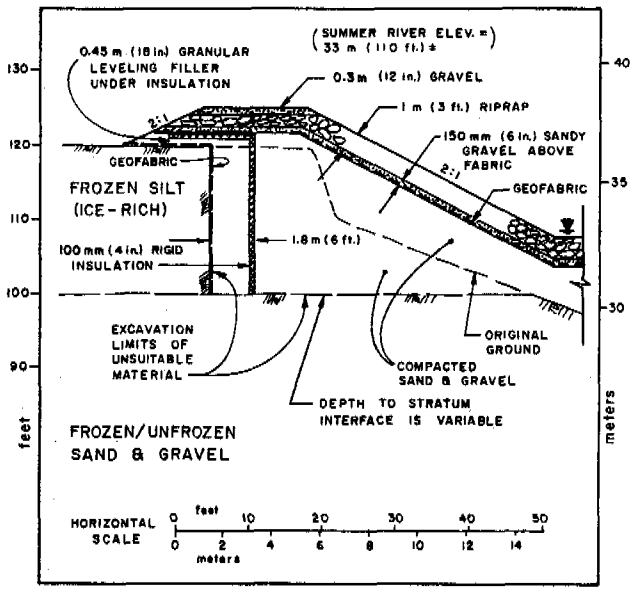

Fig. 8 Typical Embankment Section For High Thaw Strain Soil

REFERENCES

Aitken, G.W. (1963). Ground temperature observations, Galena, AK, U.S. Army CRREL, Tech. Report 102, 15p.

Brown, J., and Kreig, R.A., eds. (1983). "Guide to permafrost and related features along the Elliott and Dalton Highways, Fox to Prudhoe Bay, AK", Guidebook 4, 4th Intl. Conference on Permafrost, Alaska DGGS, 230 p.

Fulwider, C.W. (1973). Thermal regime in an arctic earthfill dam, Proc., 2nd Intl. Permafrost Conference, NAS, pp. 622-628.

Mageau, D.W. and Rooney, J.W. (1984). Thermal erosion of cut slopes in ice-rich soil, Alaska DOT/PF, Report No. FHWA-AK-RD-85-02.

McPhail, J. F., McMullen, W.B. and Murfitt, A.W., (1975). Design and construction of roads on muskeg in arctic and subarctic regions, 16th Annual Muskeg Research Conference, NRC of Canada, Montreal.

Péwé, T.L. (1948). Terrain and permafrost, Galena Air Base, Galena, AK: Progress Report 7, U.S.G.S. Permafrost Program, 52p.

R&M Consultants, Inc., (1986). Vortac dam and abutment repairs study, Prepared for City of Kotzebue, AK.

R&M Consultants, Inc., (1985). Galena bank stabilization, Prepared for Alaska DOT/PF, Project No. K-83513.

Rooney, J.W. and Condo, A.C. (1984). Hess Creek thermal erosion test site: Frozen cut slope surface treatments, 3rd Intl. Speciality Conference: Cold Regions Engineering, Vol. III., Edmonton.

Smith, M.W. and Hwang, C.T. (1973). Thermal disturbance due to channel shifting, Proc. 2nd Intl. Permafrost Conference, NAS, pp. 51-59.

U.S. Dept. of the Army. (1952). Preliminary study of erosion control Galena Airfield AK. Corps, Alaska District, Anchorage, AK.

U.S. Dept. of the Army. (1959). Foundation and materials investigations for erosion control of Yukon River, Galena Airport, AK.

Walker, H.J. (1983). Erosion in a permafrost-dominated delta, Proc. 4th Intl. Permafrost Conference, NAS, pp. 1344-1349.

Weber, F.R. and Péwé, T.L. (1970). Surficial and engineering geology of the central part of the Yukon-Koyukuk lowland, AK. U.S.G.S.,Map I-590.

AIRPORT RUNWAY DEFORMATION AT NOME, ALASKA

J.W. Rooney[1], J.F. Nixon[2], C.H. Riddle[1] and E.G. Johnson[3]

[1]R&M Consultants, Inc., Anchorage, Alaska 99503, USA
[2]Hardy BBT, Ltd., Calgary, Alberta, Canada T2E 6J5
[3]Alaska Dept. of Transportation & Public Facilities, Anchorage, Alaska 99519, USA

SYNOPSIS: The Nome Airport runways were constructed in 1942 on a mixture of dredged silts and sands, and non-dredged, generally frozen silts and organic silts. The dredged materials have remained unfrozen in many cases, whereas the non-dredged permafrost areas may contain significant excess ice. The runways were paved initially in 1943, and a continual history of vertical pavement movement has been recorded since. Subsurface investigation and geotechnical evaluation identified soil profiles, ground thermal regime and other geotechnical parameters necessary for conceptual design and construction considerations. All of this data, along with previous study results, were utilized to evaluate subsurface and pavement conditions and to develop alternative conceptual designs. Frozen natural deposits appear to be the major significant cause of ground settlement, whereas the embankment material composed of coarse tailings has a very high frost heave potential. Additionally, subsurface drainage systems were found to have an affect on the subsurface soil thermal state.

INTRODUCTION

The Nome, Alaska Airport was constructed by military contractors in 1942 as part of the Alaska-Siberia Lend-Lease (ALSIB) program. The airport was part of a system of airports used to ferry lend-lease airplanes to the U.S.S.R. during World War II. Much of the ground underlying both runways had been dredged and reworked during previous gold mining activities. Apparently, initial construction occurred only over areas that had previously been excavated using a bucket dredge and where ample dredge tailings were available for use as embankment material. The runways were obviously completed with haste and without utilization of modern methods of permafrost construction. The runway surfaces have experienced ongoing vertical deformation since original construction. Patching and major repairs have been required periodically over the more than forty year use of this facility. The runways were reconstructed in 1958-59 with installation of a major subdrain system. The runways were reconstructed again in 1973-74. Additional pavement repairs were made in 1984-85 (Fig. 1).

SITE CONDITIONS

Geologic Setting

The city of Nome is located on the south coast of the Seward Peninsula along Norton Sound, about 820 km west of Fairbanks and approximately 885 km northwest of Anchorage (Fig. 1). Bedrock consists of Paleozoic schist, gneiss, marble and metamorphosed volcanic rocks, all of which are cut by granitic intrusive masses (Sainesbury et al., 1972). Permafrost in the

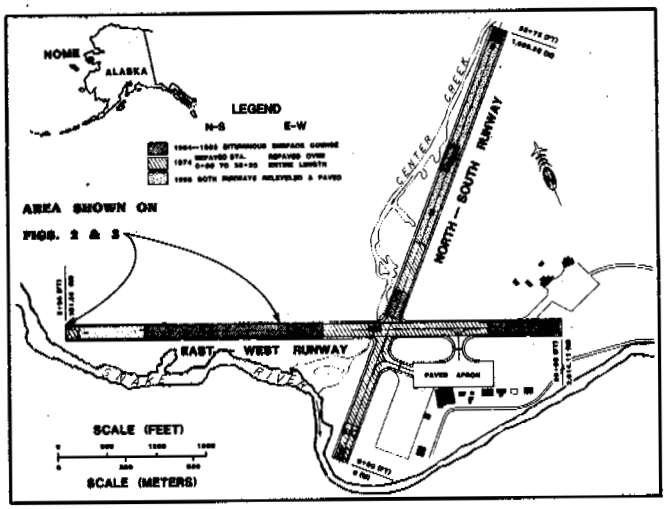

Fig. 1 Nome Airport Site Map

Nome area has been measured to about 27.5 to 36.5 m in thickness (AEIDC, 1976). Nome Airport is located about 1.6 km west of the town of Nome near the mouth of Center Creek where it converges with the Snake River (Fig. 1). Both Center Creek and the Snake River have been extensively re-routed into man-made channels in order to facilitate earlier dredging activities and subsequent airport improvements. Currently, Center Creek runs along the west edge of the North-South Runway and flows through a 1.2 m CMP underneath the East-West Runway before discharging into the Snake River (Fig. 1). Also, pipes for a subdrain system were installed in 1957 under much of both runways in order to drain shallow groundwater out of the runway embankment.

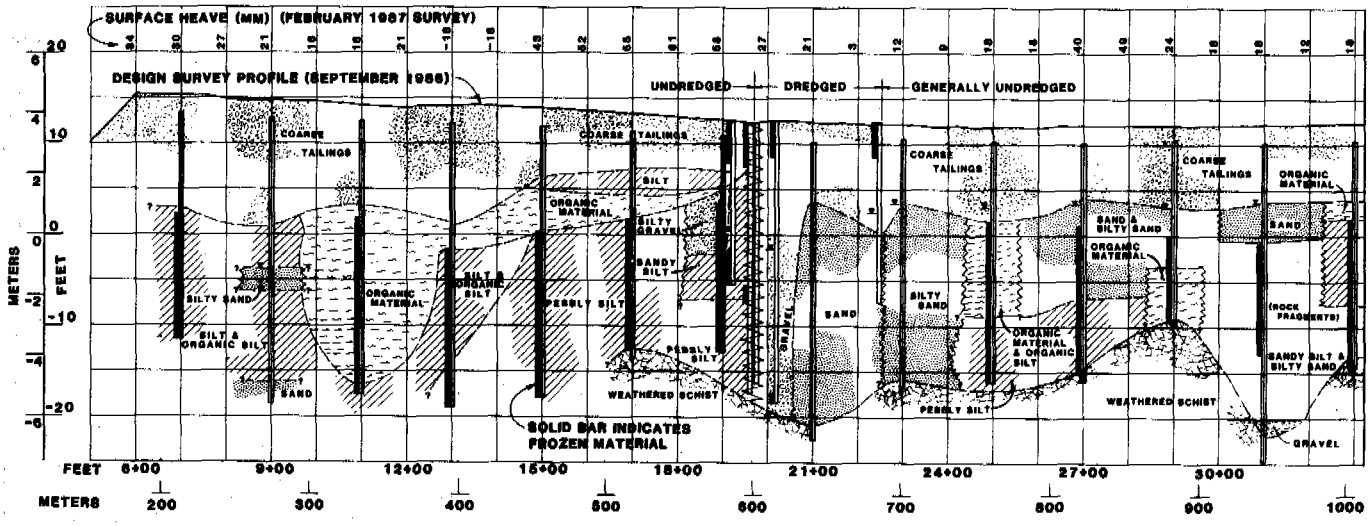

Fig. 2 Soil Profile - A Portion of East-West Runway Centerline

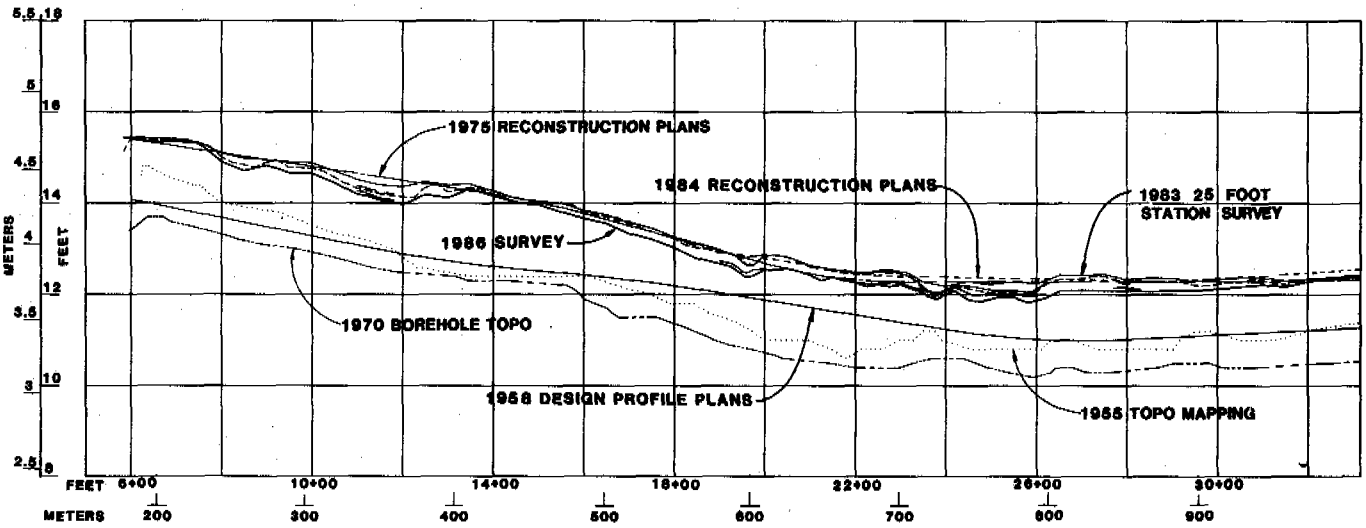

Fig. 3 Pavement Surface Surveys - A Portion of East-West Runway Centerline

Geologic profiles were prepared during the recent study (R&M Consultants, 1987) for both runways showing interpreted soil, bedrock, groundwater and thermal conditions. Additionally, topographic surveys were performed along both runways and plotted along with prior survey data. A portion of these centerline profiles for the East-West Runway are shown in Figs. 2 and 3.

Subsurface Soils

Much of the ground underlying both runways has been dredged and reworked during previous gold mining activities. The results of such dredging was to generally reverse the normal order of natural deposition. The surficial organic silts may now be found immediately overlying bedrock followed by sands and then coarse tailings at the surface. Undisturbed terrain soil consists generally of loess and colluvium covering Pleistocene till deposits. Outwash sand and gravel occur in the alluvial stream valleys. Marine sands and silty sands are interpreted to interfinger with the terrestrial deposits. Schist bedrock is generally encountered below about 7.5 m in depth.

Groundwater and Surface Drainage

Groundwater was encountered while drilling in many of the boreholes. Generally, borings that encountered no groundwater were located in undredged areas or occurred at locations where the borehole encountered generally frozen soil for the entire depth. Seasonal variations due to spring snow melt, rainfall or a rise in the levels of Center Creek and the Snake River may significantly alter the groundwater depth. In addition, because of the underlying permafrost layer, it is felt that the water level represents a "perched" water table that is highly influenced by the above-stated seasonal variations and ground thermal state. Periodically, storms on Norton Sound raise the level of the Snake River to within a meter of the runway

surface. This back charges the subdrain system and fills ditches adjacent to the runway. Groundwater flow velocities in some areas have been estimated to be above minimum values that make convective heat flow a significant thermal effect.

Permafrost

Permafrost was encountered in many of the test borings at depths ranging from 2.8 to 9.8 m. Massive ice was encountered in several borings located in non-dredged areas. In addition, from 2 to 10 percent visible ice was observed in numerous borings as random crystals, coatings on particles and stratified formations. Thermistor data shows that several intervals were observed to be below 0°C but the material clearly behaved as if unfrozen, based on blow counts, pushed samples, drilling rate, etc. In these situations, the unfrozen condition was thought to result from soil salinity freezing point depression or the convective influence of groundwater flow. Seasonal frost was observed to be on the order of 1.4 to 3.9 m deep with most borings showing 2.1 to 2.7 m of active layer. Little to no visible ice was encountered within the active layer.

DESIGN CONCERNS

Ground Thermal Behavior

A maritime climate provides cool, cloudy weather for Nome in summer, with frequent rain storms. In November, the climate changes from maritime to continental when the adjacent Norton Sound freezes. The average freezing index for 1951-1976 was about 2624°C-days, and the average thawing index was about 948°C-days, providing a mean air temperature of -4.1°C. The long term average prior to 1977 was about -3.9°C. However, during the seven year period from 1977 to 1983 inclusive, a series of anomalously warm years occurred, in which the mean annual temperatures remained consistently above the previous long term average in the range of -3.9 to - 0.3°C.

From the winter of 1984 to summer of 1985, readings were taken of air, pavement and gravel surface temperatures every 2 hours, and average daily and seasonal n-factors were calculated (Johnson, 1986). The summer n-factors were 1.63 and 1.32 for asphalt pavement and gravel, respectively. The winter n-factor for the pavement was 1.04. These values together with the actual mean monthly air temperatures were used in thermal simulations for the paved runways. It is important to note that all of the mean annual pavement surface temperatures, based on long term historical data and the above mentioned n-factors, are below 0°C. Calculations based on heat conduction will tend to predict stable permafrost in the long term under the paved runway.

Measurements taken in dredged and non-dredged areas reveal that ground temperatures in frozen areas are very close to the freezing point at depth with mean temperatures between 0 and -0.6°C. In unfrozen areas, the ground temperatures at depth are generally within 0 to 0.6°C. It should be noted that some isolated areas of significant salinity (2 to 18.8 ppt) were delineated. In general, however, salinities appear to be in the range of 0 to 3 ppt, which is less than one-tenth that of normal sea water.

An initial one-dimensional thermal simulation was carried out for the period 1942 to 1986, to determine the anticipated response of an unfrozen area of dredged tailings to long term seasonal freezing and thawing. The simulator includes phase change and thermal properties for several different soil layers. The surface air temperature was estimated from a series of mean monthly temperatures given as data to the program. The simulation predicted that freeze-back should have occurred in all dredged soil areas over the period studied. In fact, this has not happened in many areas, indicating that some convective heat flow component must be at work. The predicted ground temperature profiles agree quite closely with the actual temperature distributions measured in the upper 3 to 4.5 m in December, 1986. The simulation predicted that frost should have aggraded into the ground to a depth of 9 to 12 m.

Some dredged areas of the runway are in the process of freezing back. Examples of this may be seen on both runways. In the East-West Runway, a layer of dredged sand overlies a dredged sandy silt at depth for over a large proportion of its length. The upper layer of sand and silty sand appears in most boreholes to be unfrozen, whereas the deeper sandy silt material appears in most boreholes to be frozen. This upper cleaner sand layer appears to extend to a depth of 4.5 m or more. The lower sandy silt layer typically occurs about 4.5 m below pavement surface and continues to bedrock at a depth of 7.5 to 9 m. Therefore, it appears that the coarser-grained dredged materials are not freezing back, at least on a permanent basis, and may be thawing each year due to the action of convective groundwater flow. The finer grained dredged materials appear to have returned to the permafrost condition, and is likely due to a much lower potential for groundwater flow and consequent convective heat transfer.

From the pavement surface surveys conducted on the runways in the early and late winter of 1986/1987, the seasonal frost heave can, in part, be related to the material type present in the upper 3 m in the seasonal frost zone. Seasonal frost heave is most apparent in locations where the percentage of fine soil particles in the surface embankment tailings is higher. Also, in areas where the dredged sand comes right to the surface, the frost heave is a minimum. This suggests that the presence of the embankment tailings with the highest percentage of silt with some clay particles, corresponds to the area where frost action appears to be the most severe, as would be expected.

The maximum seasonal frost heave measured on the North-South Runway was approximately 140 mm, whereas on the East-West Runway the equivalent maximum seasonal frost heave was approximately 120 mm. On the North-South Runway, the area of highest seasonal frost

heave is at Station 40+00. This is an area of relatively thick embankment tailings, and the percentage of fines is around 24% (minus #200 sieve size). Frost heave tests confirmed the significant frost susceptibility of this material, even though the grain size curve does not suggest a particularly high degree of frost susceptibility.

In relatively impermeable soils, vertical heat flow by conduction is the primary mode of heat transfer causing seasonal freezing and thawing. In coarser grained soils, the possibility for near horizontal groundwater flow exists, and a new source of heat becomes available, should groundwater enter the freezing or thawing system at temperatures above freezing. As the dredged channels meander through the study site, and old river channels are present in the area, the potential for groundwater flow along coarse grained river channels or dredged areas is extremely high. In addition, a creek has been diverted through the East-West Runway by means of a 1.2 m diameter CMP near the intersection between the two runways. Assuming that the culvert entrance is not protected by impermeable soils, then it is very likely that a significant component of groundwater flow exists across the East-West Runway parallel to this CMP. In addition, the sub-drain system installed in 1957 provides further possibilities for lateral groundwater flow along old drain trenches, that have been backfilled with more permeable or looser backfilled materials.

In general, the influence of convection is to cause a positive inflow of heat into the system thereby slowing down or preventing long term freeze back of the affected soil, or alternatively, accelerating the depth of thaw. In view of the fact that the ground temperatures in this area are very close to the melting point, any small positive convective heat influx may be responsible for significant deviation in the depth of freezing and thawing predicted by purely conductive analyses. Convective heat flow is likely the explanation why some areas of dredged material have not frozen back in the 45 years since runway construction. Comparison of the pavement surface surveys carried out in late 1986 with earlier surveys (Fig. 3) confirms that settlement of the pavement surface has taken place over many years, at certain reasonably well identified settlement areas. These areas include the seven areas described in the ADOT/PF report (Johnson, 1986).

Frost Heave

A bulk sample of silty, sandy gravel tailings was collected for frost heave testing. The fine fraction of this material was comprised of micaceous platy particles. The grain size distribution indicated 11% finer than 0.02 mm, with 4% clay sizes (minus 0.002 mm). There was no change in grain size characteristics before and after the freeze thaw cycles carried out in this test series. This indicated that weathering was not continuing to take place in the sample due to freeze-thaw cycles in the laboratory. The initial water content of the soil was 10.8% and the final water content after four freeze thaw cycles was 8.3%. The sample was saturated throughout the test process. The Segregation Potential parameter varied from approximately 170×10^{-5} mm²/sec°C at a pressure of 43 kPa, to a value of 32×10^{-5} mm²/sec°C at the highest test pressure of 144 kPa. These values are indicative of a material of relatively high frost susceptibility. A description on the use of the Segregation Potential parameter in frost heave predictions can be obtained from Nixon (1987). The frost susceptibility decreases rapidly with increasing pressure. Therefore, this material can be expected to exhibit significant frost heave under conditions of low overburden pressure. However, as the degree of confinement or pressure in the ground increases, with depth, the degree of frost heave susceptibility can be expected to decrease significantly.

The tailings embankment material is more frost susceptible than would be expected from the grain size curve. It is strongly suspected that this is due to the mineralogy and platy nature of the silt and fine sand size particles. That is, material retained on the 200 mesh may have one dimension equal to the 200 mesh, but the other dimensions of the platy particles may be significantly less. Therefore, the smaller dimension could contribute to an increase in frost susceptibility.

In order to study the near surface seasonal frost heaving apparently taking place in the surface dredged tailings, another simulation was carried out as shown in Fig. 4. The profile assumed was 0.15 m of asphalt overlying 1.7 m of the coarse tailings at a water content of 6%. This upper layer was assumed to be non-frost susceptible, in view of the fact it is above the water table and likely unsaturated. Below the 2 m elevation, another layer of coarse tailings was assumed to be present to a depth of 3.4 m below pavement surface. Below this, a dredged sand/silt of 20% moisture content was assumed. Fig. 4 shows the predicted frost depth from 1969 to the present, and also shows the predicted seasonal frost heave that would take place as the result of the seasonal frost action.

The seasonal depth of frost is shown to vary between 3.4 and 4.4 m depending on the severity of the winter. The amount of seasonal frost heave occurring as a result of this is shown to vary from 30 to 50 mm, again depending on the severity of the winter. Considering that this is based on a single or average determination of the frost heave parameters, this appears to agree reasonably well with the average frost heave measured over the winter 1986/1987 by the topographic surveys (0-140 mm).

One option for stabilizing the runway surface may involve pre-thawing of currently frozen areas containing ice, and densifying the soil. One problem with this approach is the possibility of re-freezing and frost heave over a long period of time in the future after remedial action has been taken. The prediction carried out earlier used historical surface temperature data to predict long term frost advance. In order to project the future freezeback of a thawed area of silt or sandy silt, another freezeback simulation was completed using 30 year average surface temperatures, and assuming these would apply for the future. The same

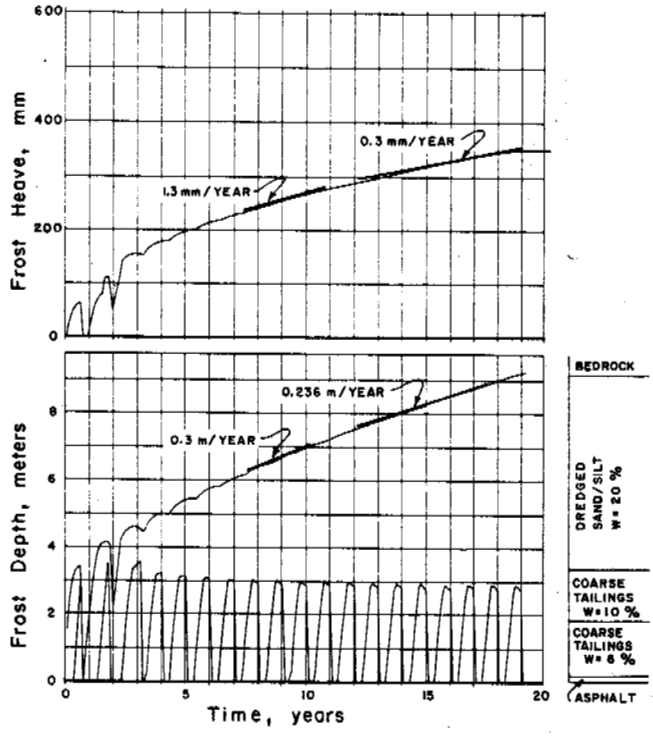

Fig. 4 Frost Heave Due to Freezeback of Prethawed Area

sequence of embankment tailings over dredged sandy silt was simulated, and the frost heave properties for both layers below 2 m were assumed the same. This simulation indicated that up to 0.3 m of frost heave could be expected over a 20 year period following the start of freezeback at depth. During the same period, a frost depth of around 9 m would be predicted. As no frost heave data are available for the lower sand/silt layers, this heave prediction may be on the high side. In addition, convective effects may reduce the rate of freezeback, or prevent it altogether. Considering that some of this frost heave would be of a relatively uniform nature and would be damped or smoothed out by the surface embankment layers, this was not felt to be a significant drawback to the pre-thawing and possible re-freezing option considered later. In either case, the predicted strain due to freezeback using these frost heave properties varies from about 4% to 2% at later times. This is considerably less than 10 to 20% thaw strain potential that is currently estimated for some frozen organic silt layers.

Consideration was given to the possibility of using a relatively thick layer of polystyrene insulation buried beneath the pavement surface for prevention of long term freezing and thawing effects. In order to understand the possible effects insulation would have on long term freezeback beneath a thawed or pre-thawed area, a simulation of an unfrozen subgrade was carried out, incorporating a 100 mm layer of insulation buried beneath 0.6 m of embankment fill and asphalt. This is the same profile and surface conditions as used in the previous analysis with the addition of the insulation layer.

For the first five years of the simulation, the frost depth increases but is thawed out each year. After this time, however, a continual but slowly aggrading permafrost situation develops. The rate of increase in the thickness of permafrost is approximately 0.2 m/year, and this is anticipated to continue for a further 10 to 20 years. Concurrently with this, the rate of frost heave of the pavement surface is predicted to be approximately 12 mm per year decreasing to 3 mm per year due to the increasing stress on the frost front with increasing depth. Therefore, it is anticipated that up to 150 mm of heave could occur over a 20 to 30 year period beneath a pavement and insulation layer. It is seen therefore that the use of insulation will not prevent gradual permafrost aggradation in these circumstances. However, the rate of frost advance and the rate of frost heave are reduced to some extent. This prediction is considered to be only valid in areas where there is almost no possibility of convective heat flow.

Thaw Settlement

Thaw settlement has been particularly apparent during the warm years that occurred in the period of 1977 to 1983 inclusive, and the mean temperatures were considerably above the long term average value. The locations of these settlement areas appear to correlate reasonably well with the presence of frozen organic silt, primarily within the undredged natural ground, having a reasonably high excess ice content. The thickness of coarse dredged tailings fill in these areas appears to be around 2.7 m. In order to study the historical response of this profile to the temperature fluctuations that have occurred in the last 20 years, a simulation of thaw depth with time was undertaken. The profile was assumed to be initially stable permafrost, exposed to the month-by-month temperature fluctuations. The moisture content of the coarse dredged tailings was assumed to be 5% to the 2.7 m depth, although slight variations in this value would not affect the outcome of the predictions to any great extent. The organic silt was initially frozen and had a water content of 50%.

Fig. 5 shows the predicted thaw depth versus time from 1967 to the present. During a typical year, the thaw depth is predicted to advance to the base of the coarse dredged tailings. The maximum predicted thaw depth during the years prior to 1977 is approximately 2.9 m. This implies that very little penetration of the thaw isotherm occurred into the organic silt. During the 7 warm years (1977 to 1983), the thaw line gradually increased to a maximum depth of about 3 m below ground surface, indicating an increase thaw penetration of approximately 0.2 m during this time period. The moisture contents and visible excess ice contents in this organic silt layer suggest that a typical thaw strain value of 10 to 15% is quite reasonable for this layer (see Hanna, et. al., 1983). If the incremental thaw depth of 0.2 m is multiplied by a thaw strain of around 15%, a thaw settlement of around 30 mm can be predicted.

It is worth noting that on the East-West Runway between Station 9+00 to 14+00, approximately

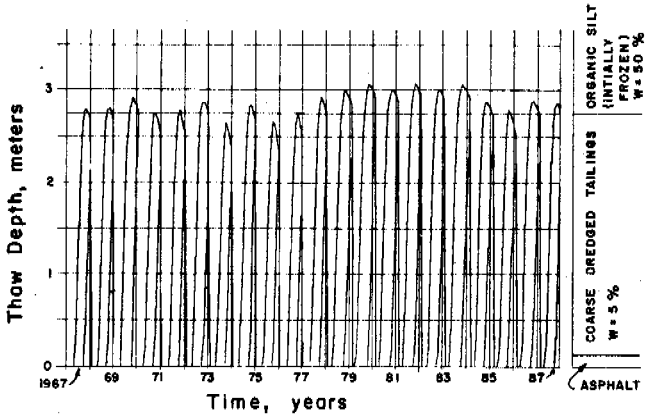

Fig. 5 Predicted Thaw Depth vs. Time (1967-1987)

30 mm of settlement occurred in the years 1983 to 1986. This, in part, can be explained by the increased thaw depth and thaw strain mechanism described above. It should be noted that all of the thaw strain will not necessarily occur in the season in which the incremental thaw occurred, due to time-dependent secondary consolidation in the organic silt deposit. It must also be acknowledged that some convective groundwater flow may have also contributed to settlement during the seven year warm period, together with other settlements occurring prior to that time. It appears that settlements that may cause noticeable distress to the runway, can be induced by increased thawing of as little as 0.3 m over a year or so.

In order to assess the effectiveness of using insulation to minimize thaw into the organic silt layer, a simulation was carried out involving a 50 mm layer of insulation and an organic silt permafrost layer overlain by 2.7 m of fill. This sequence was simulated over the period from 1967 to the present. The depth of thaw was found to vary between about 1.5 and 2.1 m, or about 1 to 1.5 m below the insulation layer. The depth of thaw did not penetrate to the organic silt layer, and the 50 mm insulation layer effectively reduced the thaw depths by about 1 m. The insulation is particularly effective in reducing the depths of thaw due to conductive action, and may be considered in areas where groundwater flow is not considered a significant heat transfer component.

CONCLUSIONS

Conceptual design alternatives to correct the deformation problems at the Nome Runway were presented in the order of increasing effort from minimum surface repairs to major improvement of the subsurface foundation soil and reconstruction of the runway surfaces and include the following (R&M Consultants, 1987):

1) Releveling the patching of surface depressions and constructing a new pavement section in selected areas. Leave the subdrain system as is.
2) Relevel and repave surface depressions after placement of insulation board. Place new pavement system in selected areas. Modify subdrain system where appropriate to enhance subsurface drainage away from runway. Relocate Center Creek which crosses the East-West Runway.
3) Thaw runway foundation soils to bedrock in designated areas (primarily undredged natural frozen ground). Relevel and construct new pavement structure. Modify drainage system as in Alternative 2. Relocate Center Creek.
4) Prethaw runway foundation soils to bedrock in designated areas, densify the designated areas to full depth utilizing dynamic compaction or controlled blasting techniques, fill to grade and construct new pavement structure. Remove existing subdrain system and replace with perimeter subdrains. Relocate Center Creek.
5) Same as Alternate 4 except densify full length of runways.
6) Same as Alternate 5 plus insulate full length of runways.

All six of the above alternatives will provide some improvement in runway performance. Alternates 1 and 2 are considered to present further temporary solutions that do not address the problems of time dependent subsurface foundation soil thaw subsidence or embankment frost heave. Alternates 3 through 6 address the poor foundation conditions and offer various methods for minimizing runway deformation.

REFERENCES

Alaska Department of Transportation and Public Facilities, (1985). Nome Airport layout plan, Internal Report.

Arctic Environmental Information and Data Center (AEIDC), (1976). Alaska Regional Profiles - Northwest Region, Volume V, Univ. of Alaska.

Brazo, G., (1982). Engineering geology and soils report, Nome Runway Repairs, Alaska DOT/PF.

Hanna, A. et al., (1983). Alaska Highway Gas Pipeline (Yukon Section) Thaw Settlement Design Approach, Proc. 4th Intl. Permafrost Conference, Fairbanks.

Johnson, E.G., (1986). Geotechnical report, investigation and analysis of the Nome Runway settlement problems, Alaska, DOT/PF.

Nixon, J.F., (1987). Pipeline frost heave predictions using the segregation potential frost heave method, Proc. ASME 6th Intl. Symposium on Offshore Mechanical and Arctic Engineering.

R&M Consultants, Inc. (1987). Nome Airport Runway Repair Study, Vol. I, II, III. Prepared for the Alaska, DOT/PF.

Sainesbury, C.L., Hummel, C.L., and Hudson, T., (1972). Reconnaissance geologic map of the Nome Quadrangle, Seward Peninsula, AK, U.S.G.S. open-file report.

PHYSICAL MODEL STUDY OF ARCTIC PIPELINE SETTLEMENT

T.S. Vinson[1] and A.C. Palmer[2]

[1]Oregon State University, Corvallis, OR 97331, USA
[2]Andrew Palmer and Associates Ltd., London, England SW1P 1QF

SYNOPSIS: A physical model study was conducted to investigate the effect of (1) arching and lateral load transfer, and (2) soil/pipe interaction phenomena on arctic submarine pipeline settlements. Typical field conditions were represented to be a 75 cm diameter pipeline, with a 1.6 cm wall, at a burial depth of 3.0 m, underlain by ice-rich permafrost at a depth of 8.5 m. With time, the warm oil in the pipeline may thaw the ice-rich permafrost to produce settlements of approximately 0.3 to 0.9 m. Based on an analysis of the test results obtained in the model study, pipeline displacements were observed to increase as the width of the settlement mass increased and the depth to the settlement mass decreased; centerspan displacements of the pipeline were substantially greater than quarterspan displacements; surface settlements directly above the pipeline were less than surface settlements over the settlement mass adjacent to the pipeline.

INTRODUCTION

It is likely in the future that submarine pipelines will be constructed offshore of the north coast of Alaska. One of the areas where pipelines may be needed is Harrison Bay. Surveys have shown that subsea permafrost exists under the bay out to a water depth of at least 25 m (some 20 km from the shoreline) and that the permafrost boundary may be as shallow as 5 m below the mudline. A pipeline to shore will be at a depth of approximately 3 to 5 m below the mudline to protect it from ice scour and the pipeline trench may be backfilled. Thermal calculations indicate that a warm pipeline may, in time, thaw permafrost several tens of meters below. If the permafrost is ice-rich, thaw settlement will occur and will be followed by deformations within the unfrozen seabed soil that surrounds the pipeline. The pipeline will deform with the soil, and there is a possibility that the deformation may be severe enough to damage the pipeline. To avoid damage to the pipeline it may be necessary to heavily insulate the pipeline, to prethaw the permafrost, or to support the pipeline independently, but these measures are likely to be expensive.

An analysis of the influence of thaw consolidation settlements on pipeline stresses and deformations will be part of the design process. It is essential that this analysis not be unduly oversimplified or overconservative. There is a risk that an oversimplified analysis may generate pessimistic conclusions which in turn would lead to the adoption of costly and difficult construction alternatives (such as prethawing). There is a secondary risk that regulatory authorities may adopt an unduly conservative design approach, and that it may become part of regulations.

One of the important factors in a pipeline settlement analysis is the extent to which the pipeline follows the thaw strain in the soil beneath. More directly, it is important to know if a thaw settlement of (say) 0.1 m in the thawed region necessarily induces 0.1 m movement in the soil immediately under the pipeline, or in the pipeline itself. Preliminary work by Walker et al. (1983), indicates there are several factors that mitigate the effect on the pipeline. For example, the frozen ice-rich region has a limited horizontal extent, and thaw consolidation leads to settlement in the zone above (surrounding the pipeline) which is partially constrained by the resistance to deformation of the soil to either side of the zone. This arching phenomenon transfers the weight of the pipeline and the soil around it laterally, so that vertical movements are smaller than they would be if the thawed region were of infinite extent. Further, the stiffness of the pipeline itself transfers loads horizontally, and further reduces settlement. Studies of the Interprovincial Norman Wells to Zama Lake pipeline (Nixon et al., 1984) have reached a similar conclusion.

OBJECTIVES AND SCOPE OF THE RESEARCH PROGRAM

The objective of the research program reported herein is to investigate the effect of (1) arching and lateral load transfer, and (2) soil/pipe interaction phenomena, on submarine pipeline settlements, using physical models tested on a centrifuge. The scope of the research program is limited to the results obtained in ten centrifuge tests conducted at the Cambridge Geotechnical Centrifuge Facility, Cambridge, England. The test results obtained in the program are reported herein. An analysis of the test results, including a comparison of the physical model results to the results of an analytical model, will be made in the future.

CENTRIFUGAL MODELING IN GEOTECHNICAL ENGINEERING

To accurately model soil/structure interaction phenomena, either analytically or physically, the stress-strain-strength dependency of the soil comprising the model on the overall stress state must be addressed. To accomplish this in a physical model study, a direct equivalence between the state of stress of a given soil element at corresponding points in the full-scale structure and the model must be achieved. This will not be the case in conventional small-scale modeling in a one gravity environment, if the same materials are used in the model as in the full-scale structure, unless a model the same size as the full-scale structure is constructed. Alternatively, the centrifugal modeling technique may be employed in which a physical model is constructed which represents the field or prototype condition (i.e., the same geotechnical material as the prototype, the same geometry, the same boundary conditions, etc.) to as great an extent as possible. Following fundamental principles, the model is constructed at a scale of 1 to n, so that the length, L, in the model corresponds to the length nL in the prototype. The physical model is then rotated in a centrifuge, with the model oriented such that the outward radial direction in the centrifuge corresponds to the vertical direction in the prototype, at an angular velocity chosen so that the radial acceleration in the model is ng, where g is the gravitational acceleration. Under this condition the stresses and strains induced in the model are the same as those in the prototype and the settlements or displacements are scaled in the ratio of 1 to n. Centrifugal modeling has firmly established its place in geotechnical engineering over the past 15 years and has been employed to study ice-structure interaction and ice ridge building (Vinson and Wurst, 1985; Clough, et al., 1986; Clough and Vinson, 1986; Palmer, et al., 1986), as well as a great number of conventional geotechnical engineering problems.

DESIGN CONSIDERATIONS ASSOCIATED WITH SUBMARINE SOIL/PIPE SETTLEMENT INTERACTION PHENOMENA

The design of submarine pipelines for settlements associated with thawing ice-rich subsea permafrost is based upon the maximum differential settlement that may occur at settlement transition zones in a submarine deposit. Differential thaw settlements in subsea permafrost deposits may be caused by (1) nonuniform thaw depths, or (2) variations in thaw settlement soil properties.

For long span settlement zones the maximum pipeline stresses are obviously located in the vicinity of the transition boundary; in the center of the settlement zone, distress to the pipe is minimized owing to the minimum curvature of the pipe in this region. As the settlement zone decreases in length, the pipe stiffness becomes increasingly more important. For short span settlement zones, the pipe can bridge the settlement trough and pipe distress will again be minimized. Allowable soil settlement is therefore unlimited for short spans. Between the long and short span condition there is a "critical" span, i.e., a span length for which distress to the pipeline is maximized owing to a maximum curvature of the pipeline. The minimum allowable settlement occurs at the critical span. An intermediate allowable soil settlement occurs at long spans. Nyman (1983) has determined that the minimum and intermediate allowable settlement, and the difference between the intermediate and minimum allowable settlement, increases as the soil cover over the pipe decreases. Also, the critical span increases as the depth of soil cover increases.

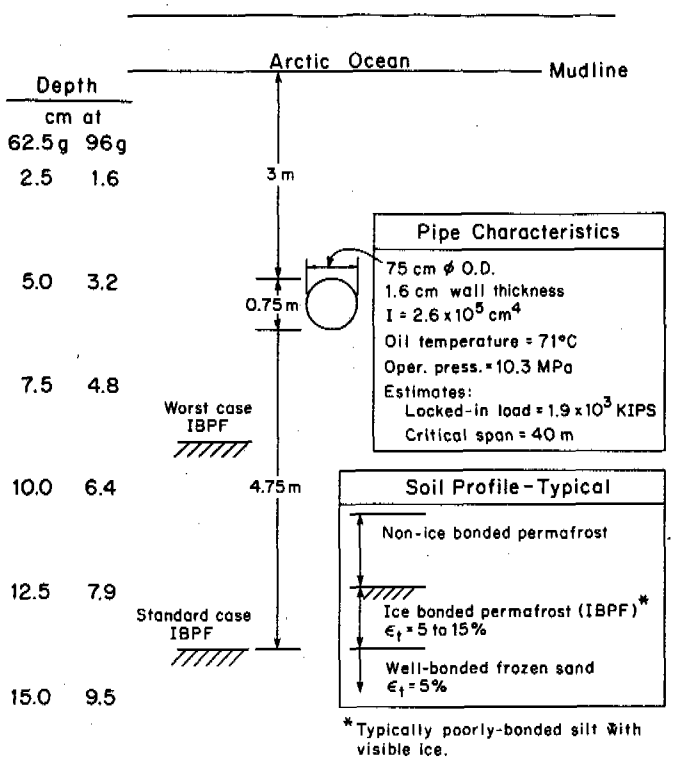

Fig. 1 Idealization of Field Conditions

IDEALIZATION OF FIELD CONDITIONS

An idealization of representative field conditions for arctic offshore pipelines is shown in Fig. 1. A typical pipeline may be 75 cm outside diameter with a 1.6 cm wall. The pipeline will carry oil at an operating pressure of 10.3 MPa. The pipeline will be buried at a depth of 3 m. The soil conditions at the site are typically non-ice bonded permafrost (typically silt) overlying poorly ice-bonded permafrost (typically silt with visible ice with thaw strains from 5 to 15%) overlying well-bonded frozen sands (with thaw strains of 5%). As a "worst" case the ice bonded permafrost may be as shallow as 5.5 m, but a more representative depth may be 8.5 m. The critical span for the pipeline is estimated to be 40 m. For settlements occurring at 8.5 m, the critical span length corresponds to an approximate settlement zone span length of 33.5 m (assuming a settlement spread of 0.7 (horiz.) to 1 (vert.).

Based on a preliminary analysis of the thermal regime associated with the condition represented in Fig. 1 the depth of the thaw bulb beneath the 5.5 m level will be 9 m after 20 years with 2.5 to 5.0 cm of insulation. If ice-rich permafrost occurs at 8.5 m with thaw strains from 5 to 15%, the settlement beneath the pipeline will be approximately 0.3 to 0.9 m. Surrounding the thawed mass is frozen ice-bonded permafrost and overlying non-ice-bonded permafrost. The pipeline, filled with warm oil, spans the mass of thawed ice-bonded permafrost, the length of which, along the axis of the pipeline, varies according to the actual geometry of the ice-bonded permafrost in the field. From the standpoint of pipeline design and analysis, the length of the thawed mass is presumed to be associated with the critical span for the pipe. Away from the settlement mass, the pipeline is considered to be infinitely long.

It is not possible to create a physical model that exactly duplicates the field condition described above. Consequently, it is necessary to idealize the field condition. It should be recognized a priori that only finite pipeline lengths can be employed in a centrifuge model container. Further, from an experimental standpoint, it would be difficult to create a mass of ice-bonded frozen material and thaw a portion of the mass with warm oil flowing through a model pipeline. In fact, from a phenomenological standpoint, it is not necessary to produce settlement beneath the pipeline with a thawed mass; it is only necessary to have a mass of material that will settle with time beneath the pipeline.

As a "first" physical model idealization of the field condition, the thawed mass may be represented with a compressible saturated clay block. The clay mass will settle with time under the high inertial accelerations created in the centrifuge. Also, the clay mass geometry is easily changed to allow different settlement mass geometries to be investigated in an experimental program. The incompressible frozen ice-bonded permafrost surrounding the settlement mass, and overlying non-ice bonded permafrost, may be represented with a cohesionless soil, for example, sand. Sand will experience only minor settlement under high inertial accelerations and will not settle with time. Further, sand is easily placed and saturated. The dimensions of the model pipe (i.e., diameter and wall thickness) must be scaled down by a factor "n". The model pipes should be made of steel to reflect the field condition and filled with oil. If the ends of the pipe are not fixed at a specified length in the model container, they will assume an unknown degree of fixity in the soil surrounding the pipe ends during an experiment. Recognizing that eventually the results from the physical model study may be used to validate an analytical model, it is desirable to set the conditions at the ends of the model pipe. The easiest condition to set is a fixed-end (i.e., no rotation of the pipe end).

CAMBRIDGE GEOTECHNICAL CENTRIFUGE FACILITY

The Cambridge Geotechnical Centrifuge Facility (CGCF) was constructed in 1974. The facility has been in continuous operation since that time. The general test procedure associated with a centrifuge model study involves building a model which represents the field situation as closely as possible. Next the model in a steel container is attached to the swinging bucket at a radius of 4 m from the hub of the centrifuge. Counterbalance weight is added to the bucket on the opposite end of the arm to maintain a gyroscopically balanced configuration. The centrifuge operator then accelerates the centrifuge to the revolutions per minute (rpm) corresponding to the desired inertial acceleration of the test. The instrumentation on board the model container is monitored remotely during the test.

The model container and test system employed in the research program is shown schematically in Fig. 2. The model container and test system consists of an 85 cm diameter, 40 cm high steel cylinder filled with saturated soil to a depth of 30 cm. The soil deposit is comprised of a gravel layer approximately 5 cm in depth underlying a fine sand approximately 25 cm in depth. Embedded within the fine sand are clay blocks, foundation plates, pipe clamps, and model pipes. Tubular stainless steel extension rods, 1.7 mm diameter, are attached to the model pipe, foundation plates, or settlement plates at settlement points. LVDTs were used to monitor model pipe soil surface settlement, and foundation plate movement. Druck miniature pore water pressure (pwp) transducers were employed to monitor pore pressure in the compressible clay blocks.

TEST RESULTS

Ten tests were conducted at the CGCF during the period March to August, 1984. To conduct a "modeling of models" study, two model pipe sizes were considered. Both 7.9 mm O.D. x 0.024 mm wall thickness and 12.1 mm O.D. x 0.04 mm wall thickness stainless steel tubular sections were commercially available. Given the representative field condition selected in the study (re Fig. 1) for which the full-scale pipeline is 75 cm O.D. x 1.6 cm wall thickness, the ratios of the full-scale to model pipeline dimensions suggest that inertial accelerations of 96 (re 7.9 mm O.D.) and 62.5 g (re 12.2 mm O.D.) would be appropriate in the test program. These levels of inertial acceleration further suggest the model depth scale given in Fig. 1. For the 7.9 mm model pipe, the depth of overburden is 3.2 cm and for the 12.1 mm, it is 4.9 cm.

An example of the test results from the research program is given in Fig. 3. During the conduct of a test, the following responses of the physical model were monitored: (1) model pipe displacements at center and quarterspan, (2) soil surface settlements, (3) porewater pressure dissipation in the clay blocks, (4) centerspan strains in the model pipe, and (5) inertial acceleration of the model.

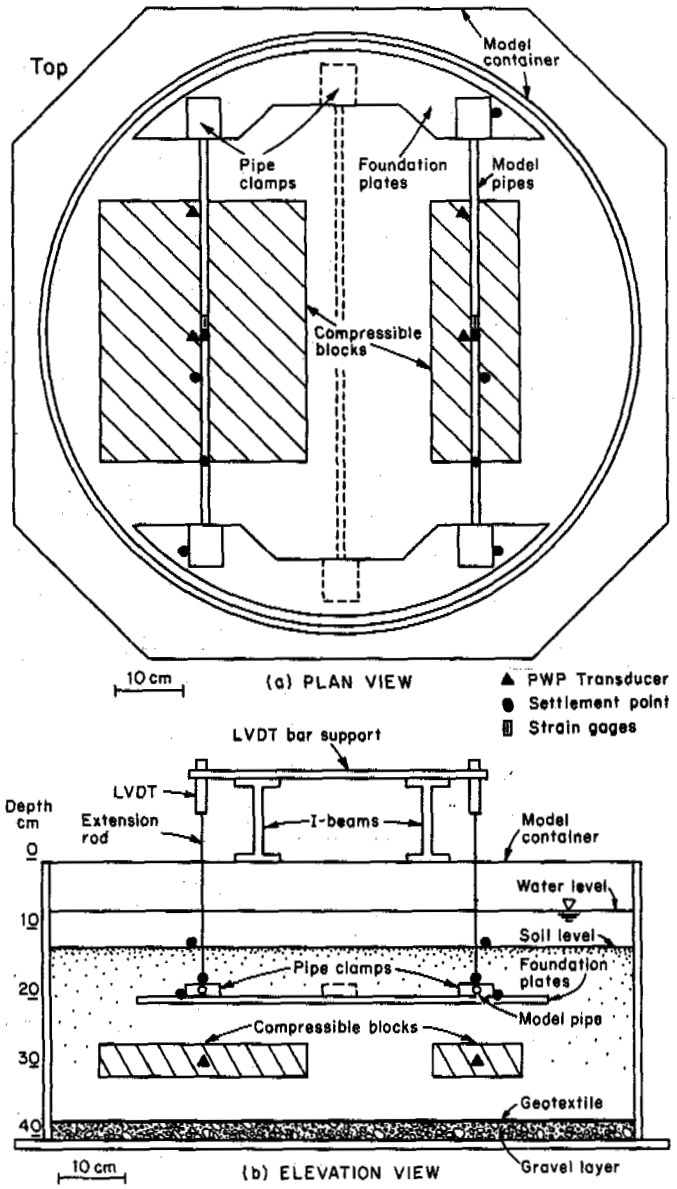

Fig. 2 Model Container and Test System

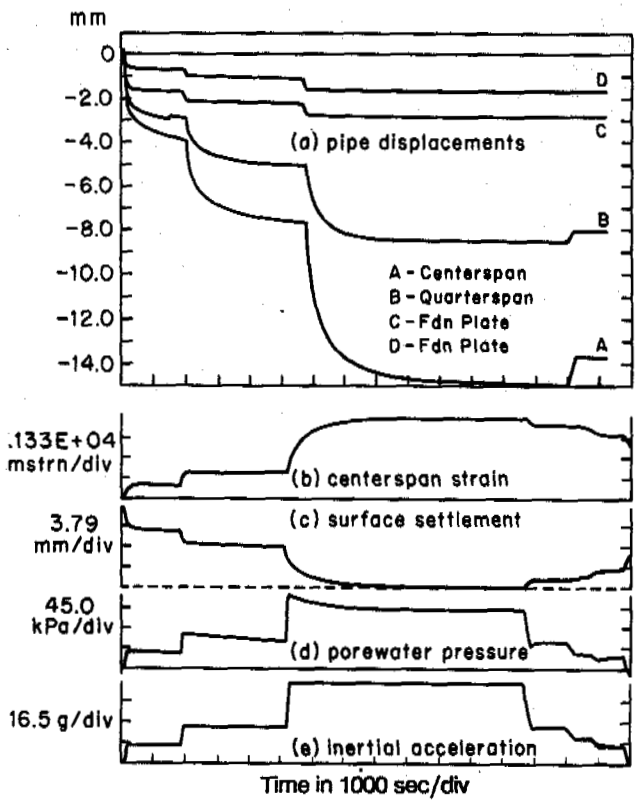

Fig. 3 Example of Test Results

QUALITATIVE EVALUATION OF TEST RESULTS

Test 1 was conducted to evaluate test system deflections, soil bed settlements and transducer performance under high inertial accelerations. The results from Test 1 indicate that approximately 2 mm displacement occurs for all components of the test system. Approximately 1 mm occurs from 0 to 20 g inertial acceleration and 1 mm occurs from 20 to 100 g. This magnitude of overall settlement is acceptable.

Test 2 was conducted to evaluate pipe deflections and fixity for free span conditions. Test 3 was similar but a surcharge was placed on the model pipes to simulate the field overburden condition. The physical model employed consisted of dry sand with three model pipes spanning an excavation in the sand. Knowing the span length and pipe stiffness, mass/unit length, and the pipe deflections at several inertial accelerations, it may be possible to determine the degree of fixity at the face of the excavation. Further, the results from the test provide information on pipeline response with no soil overburden load and no soil/pipe interaction phenomena in the settlement zone. The freespan test results appear to be reasonable. As expected, the net pipe displacements were appreciably less for the pipe with no surcharge compared to the displacements for the pipe with a surcharge. The post-flight stiffnesses of the pipes with the surcharges were approximately equal to the stiffnesses of the model pipes with no surcharge attached.

Test 4 was conducted to evaluate pipe deflections at critical span for two settlement mass widths, and the suitability of clay blocks to produce settlements beneath model pipelines. The physical model employed consisted of saturated sand with two 7.9 mm diameter model pipes. Compressible clay blocks were placed beneath the model pipes to produce settlements under the high inertial accelerations for the test. The wider clay block, 25.4 cm at 96 g reflected the approximate width of the thaw bulb that would occur for the representative field conditions (re Fig. 1). The narrow

block, 8.9 cm, reflected a width of block equal to the depth of overburden to the block level. A comparison of the pipe deflections for the two conditions allows a relative assessment to be made of arching phenomena at two feature widths, at critical span. Test 5 was conducted to evaluate pipe deflections at subcritical span for two feature widths. This test is essentially the same as Test 4 except 12.2 mm diameter model pipes were employed with a feature span length less than critical.

The compressible clay blocks employed in Tests 4 and 5 produced settlements under the model pipes, as anticipated. The overall duration of the flight was limited to 4 hours which proved very satisfactory with respect to conducting one test during one work day. For both tests, model pipeline displacements associated with settlements of wide blocks (approximately reflecting the width of the thaw bulb that would occur for the field conditions) may be compared to pipe displacements that are associated with settlements of narrow blocks. The test results suggest that over the range of widths considered, there is a minor reduction in pipeline displacement as the feature width narrows.

Test 6 was conducted to evaluate pipe deflections at critical span for two settlement mass widths and to verify reproducibility of the test results. The physical model employed consisted of saturated sand with two 7.9 mm diameter model pipes underlain by compressible clay blocks. The width and depth of one of the settlement masses, 8.9 cm, was identical to one of the masses employed in Test 4. The width of the other mass 4.5 cm was narrower than the widths considered in Test 4. The results of the test, when combined with Test 4, allow a relative assessment to be made of (1) arching phenomena at three feature widths, at critical span, and (2) reproducibility of test results.

The results from Tests 4 and 6 may be compared to assess the reproducibilitiy of the test results. At a feature width and depth of 8.9 cm, and length of 34.9 cm, Tests 4 and 6 indicated net maximum centerspan pipeline displacements of 11.3 and 10.9 mm, respectively. This close comparision is indeed encouraging. Also, pipeline displacements for an extremely narrow feature width considered in Test 6 may be compared to the results obtained in Test 4. As expected, net pipeline displacement continued to decrease as the feature width decreased. For feature widths of 4.5, 8.9, and 25.4 cm, net maximum centerspan displacements were 4.3, 11.1 (ave.), and 14.5 mm, respectively.

Test 7 was conducted to evaluate the influence of the fixity length on pipe deflections at subcritical span for a wide settlement mass. The physical model employed consisted of saturated sand with three 12.2 mm model pipes employed with a feature span length less than critical. Three pipe clamp grip spacings (52.8, 56.0, and 69.3 cm) were employed to determine if the grip spacing (i.e. fixity length) influenced pipe response. The 12.2 mm pipes at 62.5 g were considered to be a "worst case" condition. For this case, the fixity point is closest to the feature edge and, therefore, would have the greatest effect in pipeline response if, indeed, an effect was to be observed. With the 7.9 mm model pipes, the fixity point is further away from the feature edge and, as a consequence, if the fixity length was not important for the 62.5 g tests, it should not be important for the 96 g tests. Finally, in this test the drainage conditions for the clay blocks were changed from double to single drainage. This change results in a fourfold increase in the time required to achieve a given degree of consolidation in the clay block and, hence, settlement.

The results from Test 7 indicate that differences in the pipe clamp grip spacing do not have an appreciable influence on model pipe displacements. For the three grip spacings considered, the net maximum centerspan pipe displacements were 20.4, 21.5 and 19.6 mm, respectively. The use of a singly drained block resulted in extremely good control of the time rate of settlement of the clay block and they were used for the remainder of the test program.

Test 8 was conducted to evaluate pipe deflections at critical span at two feature depths for a given width. The physical model employed consisted of 7.9 mm model pipes underlain by compressible clay blocks at depths of 5.3 and 17.9 cm. The width of the masses, 8.9 cm was equal to the width of one mass used in Tests 4 and 6. Consequently, the test results, when combined with Tests 1 and 6, allow a relative assessment to be made of arching phenomena at three feature depths.

The results from Test 8, when compared to results from Tests 4 and 6 indicate that net centerspan pipeline displacements decrease with an increase in the depth of the feature. For feature depths of 5.3, 8.9, and 17.9 cm, net maximum centerspan deflections were 12.4, 11.1 (ave.), and 6.5 mm, respectively.

Test 9 was conducted to compare pipe deflections associated with settlement of ice-rich and clay blocks. The physical model employed consisted of saturated sand with two 12.2 mm model pipes underlain by a compressible clay block (Bay A) and an ice-rich block (Bay C). A heat plate was placed beneath the ice-rich block to thaw the block. It was recognized that the time rate and magnitude of settlement for the ice-rich block would be different than for the clay block. If observed pipe deflections were found to be equal at corresponding block settlements, then it may be concluded that the nature of the settlement mass (i.e. clay versus ice-rich block) does not influence arching phenomena in the zone of the pipeline. Settlement at the block level was not measured. Consequently, the best indicator of block settlement is the surface settlement measured over the block. At comparable surface settlements for the clay and ice-rich blocks, the net centerspan model pipe displacements were 4.0 and 5.0 mm, respectively. This comparison does not necessarily reflect the consequences of settlements that occurred owing to thaw of the ice-rich block prior to mounting the model container on the centrifuge.

Test 10 was conducted to compare pipe deflections at three span lengths for a wide feature. The physical model employed consisted of saturated sand with three 7.9 mm model pipes underlain by a large compressible clay block. The

settlement mass span lengths were 24.0, 46.0, and 34.9 cm. The test results allow an evaluation to be made of the critical span concept. Also the results at the assumed critical span for the pipeline, 34.9 cm may be compared to the wide feature, 25.4 cm results from Test 4 to allow an approximate assessment of the reproducibility of the test results to be made. Finally, the results from the shortest span length 24.0 cm may be compared to the results obtained in Test 5 to make an approximate assessment of "modeling of models" in the test program.

The results from Test 10 indicate that net maximum centerspan displacements are 8.2, 16.6, and 18.0 mm for feature lengths of 24.0, 34.9, and 46.0 cm, respectively. These results suggest that the "critical span" employed in the test program may not be correct. Further analysis of the results from Test 10 are necessary before a conclusive statement can be made.

At a span length of 34.9 cm, the results from Test 10 may be compared to the results from Test 4 to further assess reproducibility of the results. For a feature width of 25.4 cm (and span length of 34.9 cm), net maximum centerspan displacements were 14.5 mm in Test 4 compared to 16.6 mm in Test 10.

An approximate assessment of "modeling of models" may be made by comparing the results from Test 10 at a span length of 24.0 cm to the results from Test 5 at a span length of 37.6 cm and a feature width of 30.0 cm. At these model span lengths both tests reflect a span length in the field of 23 m. The ratio of net maximum centerspan displacements is 12.9 mm (@37.6 cm)/ 8.2 mm (@24.0 cm) = 1.57. This may be compared to the ratio of inertial accelerations, namely, 96 g/62.5 g = 1.54. Clearly, there is a very favorable comparison.

When the settlement was induced by consolidation at a shallow depth below the pipeline, the surface displacements immediately above the pipeline were less than the displacements on either side. The relative settlement profile is similar to the displacement profile that occurs when a pipe is pulled upwards out of the seabed. In both cases, the vertical force acting on the pipeline is much greater than the weight of a column of soil whose width is equal to the pipeline; this is well known in pipeline mechanics (Boer, et al., 1986; Palmer, 1972). The analysis required to determine the limiting vertical force, and therefore the moment induced in the pipeline, is similar to the analysis of breakout resistance of buried objects (Vesic, 1969).

CONCLUSIONS

Ten physical model tests were conducted at the CGCF to investigate the effect of (1) arching and lateral load transfer, and (2) soil/pipe interaction phenomena on arctic submarine pipeline settlements. Further development of the technique, and complementary finite-element analysis, follow from a more detailed understanding of the stress-strain behavior of the materials employed and of the interaction between the pipe surface and the soil.

The experience of this program reinforces confidence in the application of the centrifuge technique to soil-structure interactions created by thaw settlement, and to pipeline problems in particular. The technique not only gives a clear picture of the overall pattern of movements, but can be used quantitatively to assess pipeline strains. It can readily by extended to cover pipe deformation in the plastic range. This is important in practice because a marine pipeline is a robust structure which can withstand plastic deformations without distress, and a limitation to elastic behavior may be unnecessarily restrictive.

ACKNOWLEDGEMENTS

The authors thank Sohio Petroleum Company for their support of this program and David Walker, Andrew Schofield, and Malcolm Bolton for their helpful advice and use of the CGCF.

REFERENCES

Boer, B., Hulsbergen, C.H., Richards, D.M., Klok, A., and Biaggi, J-P. (1986), "Buckling Considerations in the Design of the Gravel Cover for a High-Temperature Oil Line," Proc., 18th OTC, Houston, TX, V 4.

Clough, H. and Vinson, T.S. (1986), "Centrifuge Model Experiments to Determine Ice Forces on Vertical Cylindrical Structures," Cold Regions Science and Technology, V. 12, N. 3.

Clough, H., Wurst, P., and Vinson, T.S. (1986), "Determination of Ice Forces with Centrifuge Models," Geotech. Test. J., ASTM, V. 9, N. 2.

Nixon, J.F., Stuchly, J., and Pick, A.R. (1984), "Design of Norman Wells Pipeline for Frost Heave and Thaw Settlement," Proc., ASME 3rd Intl. Symp. on OMAE, New Orleans, LA.

Nyman, K.J. (1983), "Thaw Settlement Analysis for Buried Pipelines in Permafrost," Proc., ASCE Spec. Conf. on Pipelines in Adverse Environments II, San Diego, CA.

Palmer, A.C. (1972), "Settlement of a Pipeline on Thawing Permafrost," ASCE, J. of the Transportation Div., V. 98, N. TE3.

Palmer, A.C., Schofield, A.N., Vinson, T.S., and Wadhams, P. (1985), "Centrifuge Modelling of Underwater Permafrost and Sea Ice," Proc., ASME 4th Intl. Symp. on OMAE, Dallas, TX.

Vesic, A.S. (1969), "Breakout Resistance of Objects Embedded in the Sea Bottom," ASCE, Civil Engineering in the Oceans II.

Vinson, T.S. and Wurst, P. (1985), "Centrifugal Modeling of Ice Forces on Single Piles," Proc., ASCE ARCTIC '85: Civil Engin. in the Arctic Offshore, San Francisco, CA.

Walker, D.B.L., Hayley, D.W., and Palmer, A.C. (1983), "The Influence of Subsea Permafrost on Offshore Pipeline Design," Proc., 4th Intl. Conf. on Permafrost, Fairbanks, AK.

BETHEL AIRPORT
CTB PAVEMENT PERFORMANCE ANALYSIS

C.L. Vita[1], J.W. Rooney[2] and T.S. Vinson[3]

[1]Engineering Reliability, Risk and Optimization, Woodinville (Seattle), Washington 98072, USA
[2]R&M Consultants, Inc., Anchorage, Alaska 99503, USA
[3]Dept. of Civil Engineering, Oregon State University, Corvallis, Oregon 97331, USA

SYNOPSIS: Long-term performance of the Bethel Airport pavement structure overlying permafrost is presented. The runway pavement structure, originally constructed in 1958 with an extension in 1971, consists of cement treated base (CTB) underlying asphalt concrete (AC). Soil cement usage in cold regions, particularly in permafrost areas such as Bethel Airport, is unusual, and thus provides the focus of interest in the Bethel project. Observations and analyses indicate use of CTB at Bethel Airport has been operationally successful. Compared to untreated crushed gravel base, CTB provides economically and structurally superior pavement performance. Current design practices for CTB appear suitable for cold regions. Good construction control and quality remain essential, as subsequent 1970 construction deficiencies at Bethel demonstrated. There seems to be no technological reason for inadequate performance of properly designed and constructed CTB in cold regions. In fact, the high quality of the 1958 CTB at Bethel has shown adequate performance for nearly 30 years, and the results of a mechanistic analysis indicates a very long remaining fatigue and rutting life for the current CTB pavement structure.

INTRODUCTION

Bethel Airport is located in western Alaska, approximately 650 km west of Anchorage. The pavement structure consists of cement treated base (CTB) underlying asphalt concrete (AC). Soil cement usage in cold regions, particularly in permafrost areas such as Bethel Airport, is unusual. Therefore, a study was undertaken to improve understanding of the application of soil cement in Alaska by evaluating the CTB pavement performance at Bethel Airport. The scope of the activities associated with the study which is summarized here included:

(1) Identification of pertinent aspects of the natural soil, thermal, groundwater and climatological factors;
(2) Identification of CTB construction history;
(3) A field and laboratory program to (a) measure pavement structure and thicknesses at selected sampling locations, (b) obtain AC, CTB, crushed gravel base (CGB) and subgrade samples of the pavement for laboratory testing, and (c) measure deflections at sampling points using Benkelman beam procedures; and
(4) Investigation of the relationship between pavement structural characteristics (as estimated from the field and laboratory program) and deflections using engineering analysis techniques.

Results from the study (Vita, et al., 1986) are summarized here.

BETHEL AIRPORT SITE CONDITIONS

Bethel Airport lies in permafrost composed of frozen Pleistocene delta deposits of silt and sand and Holocene floodplain alluvium from the Kuskokwim River. Frozen deltaic sediments are found to 130 m of depth in a nearby water well. With an average annual air temperature of -1.8°C, Bethel has an average freezing index of about 2440 C degree-days during a 196-day freezing season and an average thawing index of about 1720 C degree-days over a 169-day thawing season. The airport site is located 7.2 km west of the City of Bethel on a tundra covered sandy ridge lying above the Kuskokwim River active floodplain. Soil boring data presented on 1958 "as-built" drawings for the airport indicate frozen tundra or organic material overlying frozen silt, silty sand or sand to the maximum depth of exploration, 5.5 m below original ground surface.

CONSTRUCTION HISTORY

The present Bethel Airport (Fig. 1) was built to replace the aging and flood-prone Civil Aviation Airport located across the Kuskokwim River from the City of Bethel. Construction was phased to improve the facility as demands increased. Four construction phases are identified as follows.

Phase I: Initial site construction was begun in the summer of 1955 and continued through the summer of 1956. Excavation and subgrade preparation included stripping of surficial organic material to expose the underlying sandy material. Subsequent construction, into 1957, included continued excavation and grading to complete site rough grading for the runway, taxiway, parking apron and related support facilities.

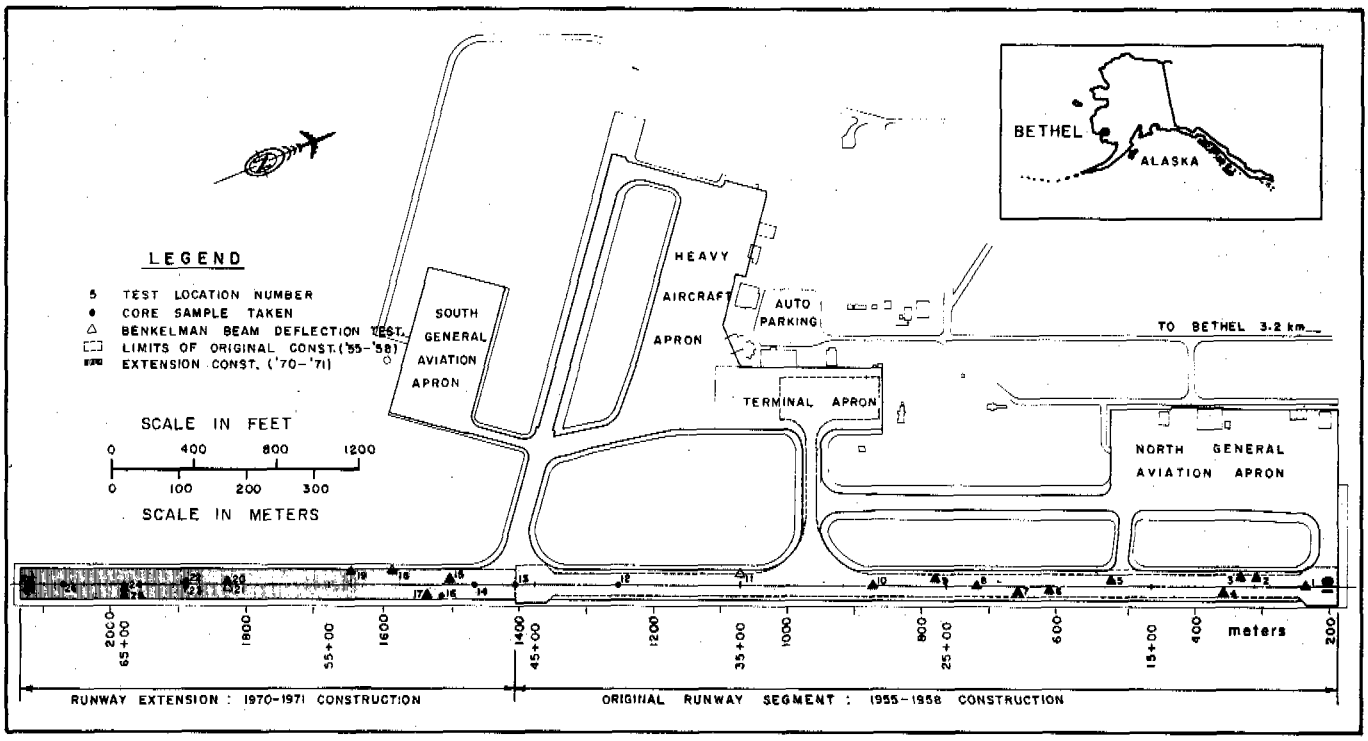

Fig. 1: Bethel Airport Site Map

Phase II: During July-August 1958 a 150 mm CTB was constructed over the initial 1,220 m runway and parking apron. The CTB was mixed in-place using natural sand-silt subgrade soil. Soils were placed in windrows. A Woods traveling mixer blended and redeposited the soil cement mixture. There was some difficulty keeping the sandy subgrade moist because of vertical drainage. Compaction was achieved using rubber-tired rollers. In some early construction locations inadequate CTB thickness was found in the center of the lanes. An extra 25 mm of AC was subsequently required where CTB thickness was considered inadequate. Areas of acceptable CTB thickness were given a 50 mm to 64 mm AC surface course; sections of thin CTB were given a 90 mm surface course. This completed the initial 1,220 m runway segment, hereafter referred to as the "1958" construction.

Phase III: Airport construction resumed in the fall of 1968 and included earthwork for a 747 m extension of the runway and an expansion of the parking apron.

The runway pavement condition was evaluated in 1969 to assess further CTB applications on the proposed runway extension. The pavement structure was reported to be in generally good condition with the principal defect being extensive cracking, mostly reflection cracks originating in the soil-cement base; surface condition and smoothness being good. Further, CTB was described as "constructed of good materials of consistent quality...of above-average compressive and flexural strength and not particularly susceptible to the ravages of freeze-thaw cycles." Average CTB thickness based on original construction records and the 1969 evaluation was 137 mm.

Phase IV: Construction began in August 1970 and consisted of (1) constructing a CTB for the 747 m runway extension, extending the main apron and widening the runway and taxiway, and (2) overlying the existing runway pavement and the new CTB with AC. A 190 mm CTB was specified for the runway extension and widening sections, with a 76 mm AC surface cover placed on the extension, and a 50 mm AC surface cover for the runway widening and overlay of the existing pavement. Using silty sand as aggregate, the CTB was mixed in a central plant, end-dumped, and spread to grade with a motor grader. CTB was placed between September 10-21, 1970.

At completion, it was apparent the CTB quality was highly variable and of questionable structural capacity and durability in many areas. Deficiencies were subsequently documented, as follows: (1) inconsistent cement content determined from coring and laboratory testing on 148 samples, indicating extreme variability in strength and durability of the base; (2) CTB surface conditions, grade and crown varied significantly; (3) surface roughness unsuitable for direct placement of the AC surface course; (4) soft pockets, scaled surface, dislodged and broken chunks of soil-cement were observed throughout the CTB construction area.

Portions of the 1970 CTB were removed and replaced with new CTB during the summer of 1971. Paving of the runway was completed August 21, 1971. Phase IV construction (with remedial efforts), hereafter termed "1971" construction, resulted in completion of the

main runway as it currently exists.

CEMENT-TREATED PAVEMENT MATERIALS

Cement stabilization involved mixing soil and measured amounts of cement and water, compacting, then letting the mixture harden by cement hydration. Cement stabilization of soils in roadway and airfield construction is common in temperate climates. In particular, because of economical increases in resistance to pavement fatigue and subgrade-rutting, CTBs are often used in asphalt and concrete pavement structures. Terrel et al. (1979) and Yoder and Witczak (1975) provide discussions on soil stabilization in pavements.

Yet in cold regions, cement stabilization is uncommon. This is due to limitations of portland cement availability in remote areas, and uncertainty about the economics and performance of the stabilized product that will result if construction (mixing, compaction, and curing) operations must be conducted under adverse weather conditions, particularly prolonged freezing temperatures.

Required Cement Content

Cement amounts required for soil-cement mixtures is established by durability tests or unconfined compression tests. Durability tests have historically been used to select cement content. Unconfined compression tests have recently become common.

Durability tests subject the soil-cement mixture to severe volume changes. In the standard test (PCA, 1971), duplicate samples are subjected to 12 cycles of wet-dry (W/D) and freeze-thaw cycling (F/T) and the weight loss after the cyclic conditioning is measured. The tests are not intended to simulate actual environmental conditions, but only cyclic volume changes. The most economical cement treatment level is the lowest percentage of cement which allows a stabilized mass to meet the maximum allowable weight loss criteria for an acceptable soil-cement mixture after 12 cycles of W/D and F/T tests.

Based on commonly acceptable criteria (PCA, 1971), cement-stabilized Bethel soils (1) should have a weight loss not exceeding about 10 to 14% and (2) would generally require a cement content of about 5 to 12% (by weight) to meet acceptable W/D and F/T weight loss criteria. Fig. 2 presents Bethel soil durability test data (R&M, 1972), and indicates a cement content somewhat exceeding 6% would meet acceptable W/D and F/T criteria. Fifteen Bethel CTB core samples were extracted and tested in this study. Cement contents averaged 7.7% ± 1.8% and ranged from 5.6% to 11.9%. Samples with these cement contents (all but one about 6.2%) would be expected to meet W/D and F/T weight loss criteria.

W/D and F/T tests may take up to a month to conduct. Consequently, "short-cut" test methods have been adopted by many agencies to determine the suitability of a soil-cement

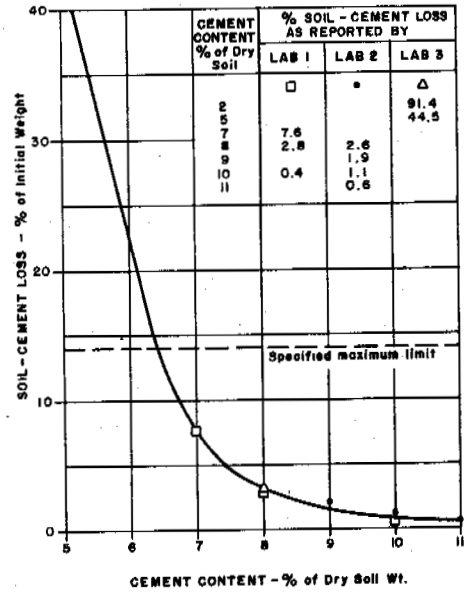

Fig. 2: Freeze and Thaw Test

mixture. The most common of these is based on the unconfined compressive strength of a 7-day moist-cured soil-cement sample (PCA, 1971). Minimum strength requirements for soil-cement mixtures range from 1585 kPa to 2068 kPa (PCA, 1971). Other agencies use generally higher (7-day) values. For example, Witczak and Yoder (1975) list California: 2,758 kPa (Class B) to 5,170 kPa (Class A), Texas: 4,825 kPa, British: 1,723 kPa (light traffic) to 2,758 kPa (heavy traffic). They state these requirements generally provide a durable mixture and only in extreme cases is it necessary to perform durability tests.

Fig. 3 presents 7-day and 42-day compressive strength data for cement-stabilized Bethel soils. Bethel soil cement contents somewhat exceeding 7%, giving a 7-day strength of about 2,068 kPa, would meet PCA unconfined compressive strength criteria. The 42-day strengths (ranging from about 4,825 kPa to 9,650 kPa at 8% cement content) indicate significant increases, by a factor of 2 to 4, over the 7-day strengths. The fourteen Bethel CTB samples taken from the in-service pavement and tested for this study show an unconfined compressive strength of 20,268 kPa ± 6,894 kPa with a range of 6,205 kPa to 29,437 kPa. The 20,268 kPa-average is about 2 to 4 times higher than the 42-day strength at 8% cement content and about 9 or 10 times higher than the 7-day strength at about 7% to 8% cement content. This data indicates large time-dependent strength increases for the Bethel CTB.

FIELD AND LABORATORY TESTING PROGRAM

As part of the current study, two field sampling and deflection surveys were made at the Bethel Airport main runway, the first conducted in October 1984. The subgrade was unfrozen. Twenty-six sampling locations were selected, as shown on Fig. 1. From these, 33

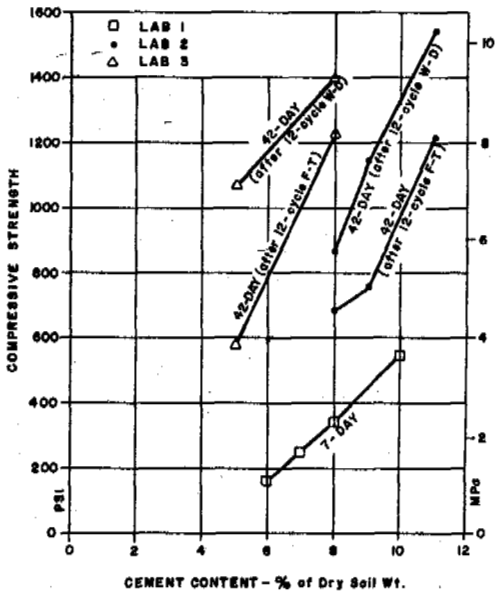

Fig. 3: Compressive Strength of Laboratory-Made Specimen

samples were recovered and 19 Benkelman beam measurements made. Laboratory tests were conducted on 12 AC cores, 15 CTB cores, one untreated CGB sample, and five subgrade samples. The second survey was conducted in May 1985 to obtain Benkelman beam measurements during the Spring break-up period, over a period of roughly maximum subgrade thaw-weakening. Data are summarized in Table I. Informal observations indicated the runway pavement was in generally good condition with some isolated areas showing signs of distress, particularly in non-CTB (gravel base) areas. Cracking was variable and included probable thermal and reflection cracks.

The laboratory test program was conducted to identify (1) index/physical properties of the AC and CTB cores and soil samples taken during the field program, (2) resilient moduli of the AC surface course, CTB material, aggregate base and subgrade soil, and (3) fatigue characteristics of the AC and CTB materials. Results are summarized in Figs. 4 through 6.

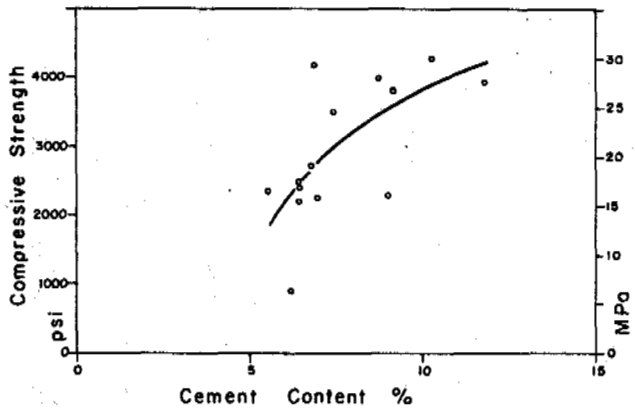

Fig. 4: Compressive Strength Versus Cement Content

Index/physical properties were made in accordance with the ASTM or AASHTO test procedures. Resilient moduli of the AC, CTB, CGB, and subgrade soils and fatigue characteristics of the AC were determined in accordance with Walter, et al. (1984). Sample location numbers are shown on Fig. 1.

The 1958 AC had higher average density (approx. 2,330 kg/m³) compared to the 1971 phase (approx. 2,275 kg/m³). The 1958 CTB had lower average density, cement content, and compressive strength (approx. 1,884 kg/m³, 7.1% and 19,365 kPa, respectively) compared to the 1971 phase (approx. 1,900 kg/m³, 8.3% and 21,165 kPa, respectively.) Compressive strength increases with increasing cement content as shown in Fig. 4. Compressive strengths (even compensating for the relatively long cure time) are well above strength levels considered acceptable to meet durability criteria (PCA, 1971).

Resilient moduli of AC cores were evaluated at -5°C, 10°C and 24°C. Results are summarized in Fig. 5. Resilient moduli for both the 1958 and 1971 cores decrease by nearly a factor of 10 over the 28°C temperature range (approx. 27,580 MPa at -4°C to approx 3,450 MPa at 24°C). The 1958 construction phase moduli are about 10% higher than the 1971 phase moduli. CTB resilient moduli are shown in Fig. 6. 1958 moduli are greater than the 1971 moduli. For practical purposes, CTB resilient moduli are temperature-independent.

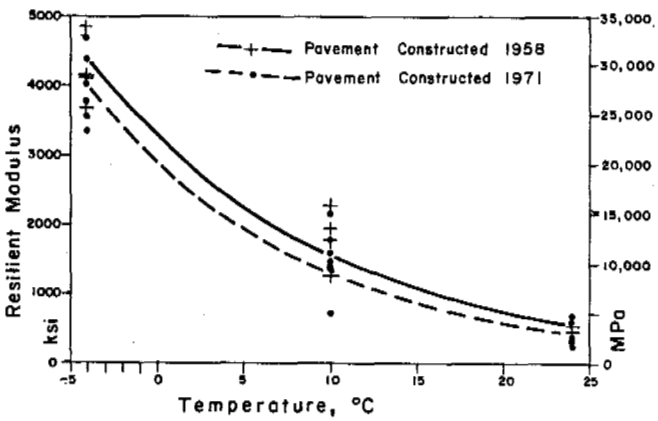

Fig. 5: Resilient Modulus Versus Temperature for Asphalt Pavements

PAVEMENT PERFORMANCE EVALUATION - MECHANISTIC APPROACH

Pavement structural performance analysis was based on the mechanistic approach (Mahoney and Vinson, 1983). Calculated strains at critical locations in the pavement structural section are limited to acceptable levels for a specified number of load repetitions (i.e., the design life). Two conditions are generally employed to define failure of the roadway structure: (1) tensile strain (or stress) at the bottom of the surface layer cannot exceed a maximum allowable tensile strain for a

specified number of load repetitions, and (2) vertical compressive strain at the top of the subgrade (supporting) layers cannot exceed a maximum allowable vertical strain for a specified number of load repetitions.

Reflection cracking of the CTB into and through the AC surface course is not analyzed as part of the mechanistic analysis. Cracking of a CTB (as with concrete pavements) is considered inevitable. The attempt is to control cracking and maintain pavement integrity by providing adequate AC thickness to limit reflection cracking, and then maintaining those cracks that do occur.

Stresses, strains and deflections in a pavement structure are predicted using pavement structure resilient moduli with multilayer elastic theory (Hicks, 1982). Validity is established by comparing observed pavement deflections with predicted deflections for equivalent loading conditions. To this end, a prediction was made of the surface deflections for the 1958 and 1971 pavement structure under the survey load vehicle. For the 1958 pavement, predicted surface deflection was 0.287 mm; observed average surface deflection was 0.279 mm. A similar comparison with the average 1971 CTB pavement structure indicated a predicted deflection of 0.266 mm and an average observed deflection of 0.279 mm. The close agreements for these cases support the use of material properties and the multilayer elastic model (program PSAD2A) to (approximately) assess stresses and strains in the Bethel Airport pavement structure for other pavement environmental conditions.

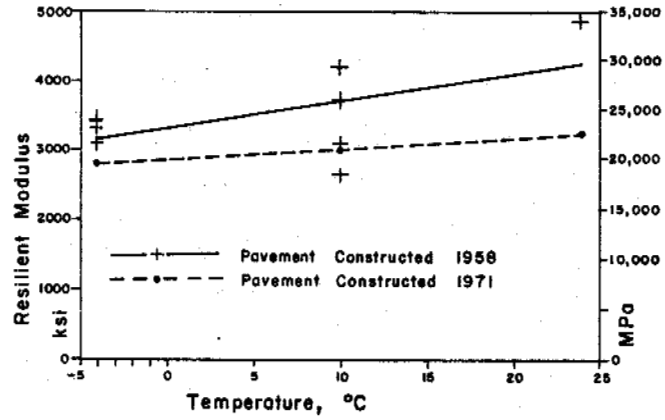

Fig. 6: Resilient Modulus Versus Temperature for Cement Treated Bases

Analysis of the pavement structure life for fatigue and rutting failure conditions was conducted at critical locations for Boeing 737 (B737) aircraft loading. Four thermal-environmental conditions were considered as follows:

1) Summer, Unfrozen: T=10°C in AC and CTB, unfrozen subgrade.
2) Winter, Frozen: T=-4°C in AC and CTB, frozen subgrade.

TABLE I

Asphalt and Cement Treated Base Core Index Properties

Location Number	Asphalt Thickness (mm)	Asphalt Density kg/m³	Base Thickness (mm)	Base Density kg/m³	Cement Content (%)	Strength (MPa) (-) Compressive (+) Tensile	Benkelman Beam Deflection September 1984 (mm)	Benkelman Beam Deflection May 1985 (mm)
1	147	2,300	132	1,863	6.45	1.32	.305	.305
2	135		135	1,911	6.45	-17.10	.406	.203
3	147		140				.305	.305
4	157		117	1,871	9.02	-15.72	.203	.305
5	150		114				.305	.254
6	165		127	1,879	5.56	-16.20	.305	.305
7	175		112	1,884	6.49	-16.48	.305	.203
8	175		114	1,874	7.48	-24.06	.305	.152
9	165	2,360	127	1,921		1.55	.203	.203
10	140		112	1,917	8.81	-27.34	.203	.457
11							.305	.203
12	137		170	1,829	6.83	-18.62		.203
13	91		302	1,938	10.36	-29.44		.102
14	91		213	1,969	9.23	-26.20		.508
15	102	2,290					.711	.610
16	57	2,347						.914
17	76		185	1,914	7.00	-15.44	.610	.610
18	62	2,276					.914	1.02
19	76	2,332					.610	.914
20	145		249	1,865	6.19	- 6.21	.203	.102
21	132		152				.406	.305
22	107		267	1,938	6.96	-28.75		.102
23	107		196	1,853	6.46	-15.10		.203
24	152	2,257	127	1,813			.203	.305
25	114	2,148	201	1,882		1.64	.305	.102
26	140		213	1,945	11.87	-27.03		.152

3) Spring-Breakup, Shallow-Thaw: T=2°C in AC and CTB, subgrade thawed to 0.6 m and frozen below.
4) Spring-Breakup, Deep-Thaw: T=2°C in AC and CTB, thawing subgrade to infinite depth.

AC and CTB moduli used in the multilayer elastic analysis were obtained from Figs. 5 and 6. Frozen soil moduli were increased by roughly 300% over unfrozen moduli and thawing soil moduli reduced to about 25% of the unfrozen moduli. Presentation of the results is given by Vita, et al. (1986). In summary:

1) At comparable thermal/environmental conditions surface displacements for the untreated CGB are about twice the displacements for the CTB sections.
2) Fatigue failure for the AC layer will not occur for any reasonable number of B737 loadings.
3) Rutting failure in the subgrade will not occur for any reasonable number of B737 loadings.
4) AC temperature does not appreciably influence the strain or flexural stress at the bottom of the CTB or vertical strain on the subgrade; AC temperature does influence the strain at the bottom of the AC layer.

SUMMARY AND CONCLUSIONS

Observations and analyses indicate that the use of cement treated base, CTB, at Bethel Airport has been operationally successful. Compared to untreated CGB, CTB gives economically and structurally superior pavement performance.

In all cases of CTB use, proper design and construction is essential to a successful product. Current design practices for CTB appear suitable for cold regions. Good construction control and quality are essential, as the 1970 construction season deficiencies at Bethel demonstrated.

There seems to be no special technological reasons for inadequate performance of properly designed and constructed CTB in cold regions. In fact, the high quality of the 1958 CTB at Bethel has shown adequate performance for nearly 30 years, and the results of the mechanistic analysis described above indicates a very long remaining fatigue and rutting life for the current CTB pavement structure.

Reflection cracking, a common and general condition of all CTB pavements, is generally controlled with adequate AC thickness to reduce surface cracking and crack sealing, as part of routine maintenance. Surface cracking on the Bethel Airport runway includes thermal cracking effects (similar to those found, for example, in the Fairbanks area) and CTB-induced reflection cracking. However, CTB reflection cracking does not appear to be a particular problem at Bethel.

The operationally successful use of CTB at Bethel provides support to the general use of CTB at other locations in cold regions. Of course, any given candidate location for CTB must be evaluated for case-specified conditions, needs, and constraints. For example, CTB does not have any special advantage in overcoming adverse effects of subgrade foundation thaw in areas of thaw-unstable permafrost. However, pre-thawing of subgrade permafrost several years in advance (as was done for the Bethel runway) may, in the right situation, improve foundation soil performance. Further, the performance of CTB in poorly draining soils (unlike Bethel soils) with a high groundwater table is unknown. Also, in cases where abundant crushed gravel is locally available, there may be no economic advantage to CTB. Finally, where a superior natural subgrade exists, there may be no advantage to CTB.

CTB experience at Bethel indicates that in poor subgrade areas where gravel is not economically available, CTB can provide a cost-saving solution which will contribute to high quality pavement performance. Following proper planning, design, construction and maintenance, CTBs can be used in cold regions to effect superior economy and long-term pavement performance.

CITED REFERENCES

Hicks, R.G. (1982). Use of Layered Theory in the Design and Evaluation of Pavement Systems, Report No. FHWA-AK-RD-83-8, Alaska DOTPF.

Mahoney, J. and Vinson, T.S., (1983). A mechanistic approach to pavement design in cold regions, Proc. 4th Intl. Conference on Permafrost, NAS.

Portland Cement Association (PCA), (1971). Soil-Cement Laboratory Handbook, Skokie.

R&M Engineering & Geological Consultants (R&M), (1972). Bethel Airport, Stage V Construction, Rept. to AK. Div. of Aviation.

Terrel, R.L., et al (1979). Soil Stabilization in Pavement Structures, A User's Manual, 2 vols., USDOT, FHWA-IP-80-2.

Vinson, T.S., Mahoney, J.P., and Kaminski, J.J. (1984). Cement stabilization for road construction in cold regions, Proc. 3rd Intl. Cold Regions Engineering Specialty Conference, Edmonton.

Vita, C.L., Vinson, T.S., and Rooney, J.W. (1986). Bethel Airport CTB-AC Pavement Performance Analysis, Report No. AK-RD-86-31, Alaska DOTPF.

Walter, J., Brickman, A.M., Hicks, R.G., and Vinson, T.S. (1984). Installation Operation and Maintenance Procedures for Repeated Load Triaxial and Diametral Test Systems, Transportation Research Report 84-1, Oregon State University.

Yoder, E.J. and Witczak, M.W. (1975). Principles of Pavement Design, 2nd ed., Wiley, New York.

A NEW METHOD FOR PILE TESTING AND DESIGN IN PERMANENTLY-FROZEN GROUNDS

Pile Testing, Relaxation, Permanently-Frozen Grounds, Pile Design, Variable Loading, Base Temperature

S.S. Vyalov[1] and Yu.S. Mirenburg[2]

[1]Moscow Engineering-Construction Institute, Moscow, USSR
[2]Northern Affiliate of Research Institute for Foundations and Underground Structures, USSR's Gosstroi, Vorkuta, USSR

SYNOPSIS Traditional methods of pile testing are very laborious and lengthy. A new, dynamometric method of testing has been developed, enabling testing time to be reduced and data to be obtained necessary for a long-term prediction of the carrying capacity of the pile and its settling under the impact of both constant and time-variable loading. Theoretical and experimental validation of the new method of testing, testing procedure and data processing, as well as pile design from the results of the tests.

INTRODUCTION

Tests on full-size piles prove to be a particularly reliable and trustworth source of data for predicting the settling and carrying capacity of pile foundations in frozen grounds. However, such tests are very long. Reduction of testing time can be achieved by going over from traditional tests by step-increasing loading to relaxation tests. One of such testing methods is the dynamometric method developed by the authors (Vyalov, Yeroshenko, Mirenburg, 1977).

DESIGN FORMULAE

To be able to obtain from test results a possibility for predicting the settling S and the carrying capacity F_u of piles for any variation of vertical loading $N(t)$ in time t we have worked out and employed a formula comprising instantaneous and time-varying strength F_{ut} and deformational A_{ut} characteristics of the pile foundation (Vyalov, Mirenburg, 1984).
For a constant load N this formula has the form:

$$S = A_o N + \frac{A_{ut} N}{1 - \frac{N}{F_{ut}}} , \qquad (1)$$

where the first term in the right-hand side stands for instantaneous settling linearly depending on the load, and the second term - the creep settling with the time-varying characteristics F_{ut} and A_{ut}, described by the universally-known dependences

$$F_{ut} = \frac{F_{uo}}{\ln t/t_o} , \qquad (2)$$

$$A_{ut} = A_u \left(\frac{t}{t_o}\right)^{\lambda} , \qquad (3)$$

where A_o, A_u, λ, F_o and t_o are parameters to be determined in the tests.
Dependence (1) reflects the physical essence of the pile settling process due to loading. Thus, as loading N approaches F_{ut} ($N \to F_{ut}$) the settling S increases without bound (fig.1-c). In accordance with the work (Gersevanov, 1917), this determines F_{ut} as a maximum resistance, thus enabling it to be represented in the form (2).

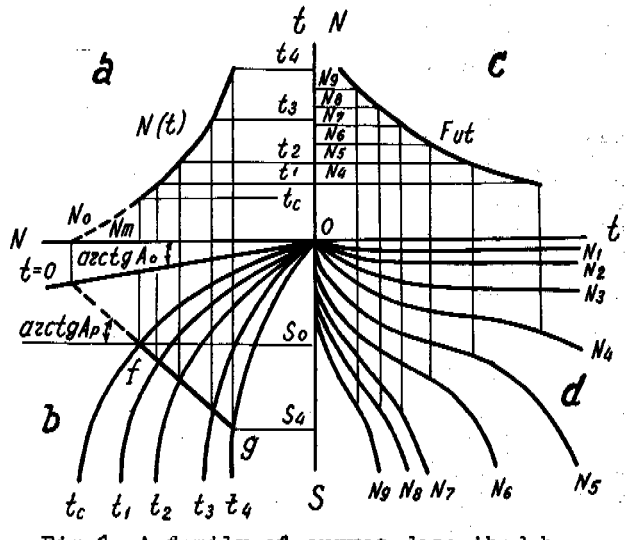

Fig.1 A family of curves described by the dependence (4):
a. Relaxation curve; b. Isochrones;
c. Long-term strength curve;
d. Creep curves.

Furthermore, in the limit $N \to 0$ the function (1) becomes linear with respect to loading N

$$S = (A_o + A_{ut})N \quad ,$$

which, to a certain extent, reflects a linear deformation of the base under small loads. Substituting (2) and (3) in (1) leads to a generalized dependence of settling upon loading

$$S = A_o N + \frac{A_u N}{1 - \frac{N}{F_{uo}} \ln \frac{t}{t_o}} \left(\frac{t}{t_o}\right)^{\lambda}. \quad (4)$$

The families of creep curves, isochrones and the long-term strength curve described by the expression (4), as seen from fig.1, correspond in shape to the experimental ones and, as revealed by our investigations, with an accuracy sufficient for practical calculations quantitatively reflect deformation processes and variations of strength characteristics of frozen grounds (Vyalov, Mirenburg, Fokin, 1979), bases of dies (Vyalov, Mirenburg, 1980) and piles (Vyalov, Mirenburg, 1984), as well as of the settling of buildings on these grounds (Mirenburg, Fedoseev, 1982).
This enabled the dependence (4) to be put at the basis of the elaborated procedure and the analysis of results of the dynamometric pile testing method.

TESTING PROCEDURE

The testing procedure divides into two stages (fig.2).
The first stage involves tests on the piles by a step-increasing load with a brief application (4-8 hr) of steps. In this case the loading is brought up to the values of N_m close to the maximum loading on the pile F_{ut}^m corresponding to the step duration t_c to be determined from the formula (2) for $t = t_c$

$$N_m = (0.7 - 0.9)F'_{ut} \quad . \quad (5)$$

The value of F'_{ut} will be determined during testing by plotting the variation of pile settling S at the end of the step versus the load N at this step in rectifying coordinates N/S-N (fig.3-a). As follows from the formula (1), the segment cut off by the plot at the x-axis determines F'_{ut}. On the y-axis, according to the same relationship (1), the plot cuts off a segment corresponding to the value of the inverse deformational characteristic A'_{ut} for the step duration t_c.
In the process of stage I, apart from the pile settling at the end of the step, instantaneous increments of pile settling ΔS_o and hydrojack piston run-out Δh_o during pile loading with the next step load are recorded. These data, as shown in fig.3-c, permit elastic characteristics of the setup A_o and of the pile foundation A_o to be determined.

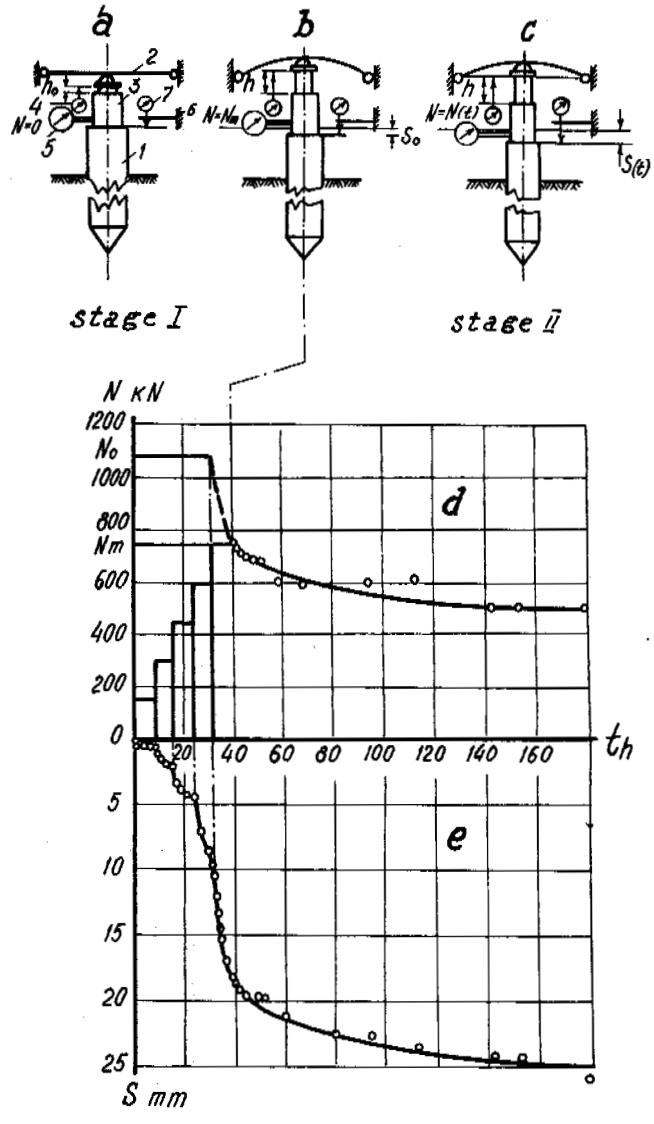

Fig.2 Deformation of testing set-up and pile during testing(a,b,c) and plotted variations of the load N(d) and progress of settling S(e) on a full-size pile №5.
1. Pile, 2. Bracing, 3. Hydrojack, 4. Hydrojack piston run-out meter, 5. Pressure gauge, 6. Reference system, 7. Pile settling meter.

Once the condition (5) has been fulfilled and the load N_m has been maintained during the time of a step t_c, oil feed to the hydrojack is terminated and testing continues at stage II with the hydrojak piston run-out height h fixed for the entire stage.

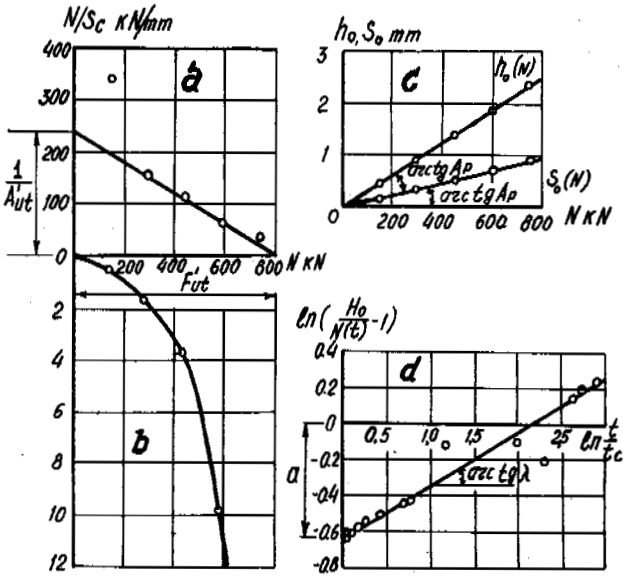

Fig.3. Processing of testing data for pile №5
a. Determination of F_{ut} and A'_{ut}; b. Isochrone t_c;
c. Determination of A_p and A_o;
d. Determination of λ and α.

In this case the progress of pile settling is due solely to the effect of elastic forces of the testing set-up. At testing stage II the measurement of the load on the pile with the pressure gauge 5 alone is obligatory. Measurement of the pile settling S and hydrojack piston run-out h are just checks. The length of testing stage I is determined by the minimal number of loading steps necessary for analysis. Given a correct choise of step magnitudes, their number is not more than 7-10, which corresponds to the time of 1-3 days.
The length of stage II is to be appointed on condition of obtaining a sufficient number of experimental points on the relaxation curve for analysis (fig.2-d) and, as a rule, does not exceed 3-6 days.

THEORETICAL VALIDATION OF DATA PROCESSING

For elaboration and validation of the procedure of data processing for dynamometric tests on piles let us examine the progress of pile settling and variations of loading on them in testing, as shown in fig.1-a,b. The properties of the pile-ground base in Fig.1-c are represented by a family of isochrones for time moments $t = 0$, t_c and $t_1 \div t_4$.
At the first stage of loading with a step-increasing load the progress of pile settling corresponds to the isochrone t at the stretch (of) up to the load N_m corresponding to the condition (5).
At testing stage II the pile settling occurs due to the effect of elastic forces of the "pile-brace" system and, therefore, the settling versus load relationship is linear with a proportionality coefficient corresponding to the brace rigidity A_p and is represented in fig.1-c by a straight line (fg) within the settling range $S_o - S_4$.
Extrapolation of this line segment as far as the isochrone $t = 0$ allows for the prehistory of loading at stage I and enables stage II to be examined separately, writing down the equation of settling progress, according to fig.1-c, in the form:

$$S = A_o N_o + A_p\left[N_o - N(t)\right] , \qquad (6)$$

An equation of the variation of loading in time N(t) at stage II will be obtained by substituting (4) in (6)

$$A_o N(t) + \frac{A_u N(t)}{1 - \frac{N(t)}{F_{uo}} \ln \frac{t}{t_o}} \left(\frac{t}{t_o}\right)^{\lambda} = A_o N_o + A_p\left[N_o - N(t)\right]. \qquad (7)$$

The formulae (2) and (3) will be used to find relationships between the values of F'_{ut} and A'_{ut} determined at stage I and the parameters A_u and F_{uo}

$$A_u = A'_{ut} \left(\frac{t_o}{t_c}\right)^{\lambda} , \qquad (8)$$

$$F_{uo} = F'_{ut} \ln \frac{t_c}{t_o} . \qquad (9)$$

Substituting these parameters in (7) will give after transformations the expression

$$(A_p + A_o)\left[N_o - N(t)\right] = \frac{A_{ut} N(t)}{1 - \frac{N(t) \ln t_o/t_o}{F'_{ut} \ln t/t_o}} \left(\frac{t}{t_o}\right)^{\lambda} . \qquad (10)$$

Our investigations and the comparison of fig.1-a with fig.1-c indicate that for practical calculations we may accept a prerequisite about the similarity of the efforts relaxation curve in the "pile-brace" system N(t) and the long-term strength curve F_{ut} with a similitude coefficient q

$$\frac{N(t)}{F_{ut}} = \frac{N(t)\ \ln t_c/t_o}{F_{ut}\ \ln t/t_o} = q = \text{const} . \qquad (11)$$

This leads to significant simplifications

$$(A_p + A_o)\left(\frac{N_o}{N(t)} - 1\right) = \frac{A_{ut}}{1-q}\left(\frac{t}{t_c}\right)^{\lambda} , \qquad (12)$$

enabling the plot of the expression (12) to be rectified in the coordinates

$$\ln\left(\frac{t}{t_c}\right) - \ln\frac{N_o}{N(t)} - 1 .$$

An in accordance with fig.3-d to determine λ and compute t_o from the formula:

$$t_o = \frac{t_c}{\exp\left[\dfrac{1 - \exp a}{\lambda\,(e-1)\exp a}\right]} , \qquad (13)$$

where a is a segment cut off by the plot in fig.3-d on the y-axis; e is the base of natural logarithms.
Parameters A_u and F_{uo} are to be determined from the expressions (8) and (9).
Thus, the proposed pile testing method permits all parameters in the formula (4) to be determined.

EXPERIMENTAL CHECK

In deducing design formulae of data processing for dynamometric pile testing some simplifications and assumptions were made for an experimental check on which in various years tests were made on one and the same piles by applying a step-rising load and dynamometrically. Comparison of these test results are listed in the Table.

TABLE

Comparison of the Length and Results of Tests by Stepped Loading and Dynamometrically

Pile №	Test length		Design maximally long loads on a pile according to testing data, kN			
			design with respect to carrying capacity (2)		design with respect to deformations (4)	
	stepped loading	dynamometrically	stepped loading	dynamometrically	stepped loading	dynamometrically
4	3600	206	453	420	491	490
5	3200	179	237	215	223	241
TC-1	336	192	246	260	197	180
TC-2	336	208	399	375	475	474

Design data with respect to carrying capacity in the Table have been determined from formula (2) for the service period t_s = 50 years. Design with respect to deformations was made from the formula (4) in which to determine the design loading the pile settling at the end of the service period t_s was assumed to be 15 cm, and for a comparison of design loads derived by calculation with respect to carrying capacity and deformations the latter, according to authorized requirements (Building Norms and Codes II-18-76) were multiplied by the safety coefficients γ_n = 1,2 and γ_g = = 1.1.
The tabulated data point to a close correspondance between test results obtained by applying a stepped-increasing load and dynamometrically. The latter is seen to be significantly more favourable as regards testing length, particularly in comparison with testing until an arbitrary settling attenuation 0.02 mm a day (piles №№ 4 and 5).

METHODS OF PILE DESIGN

The above formulae for the carrying capacity (2) and settling (4) of the pile enable variations in loading on the pile during service to be taken into account. To this end, the formula (2) is to be substituted in the equation of linear summation of damage (Vyalov, 1978), and the expression (4) is used in accordance with the phenomenological theory of non-linear hereditary creep

$$\frac{1}{t_o}\int_o^{t_s} \exp\left[-\frac{F_{uo}}{\gamma_g\,\gamma_n\,N(t)}\right] dt \le 1 \qquad (14)$$

$$S = A_u\left(\frac{t_o}{t_x}\right)^{\lambda} \Big/ \left[N(t_s) - \lambda t_o^{\lambda}\int_o^{t_s}\frac{d\nu}{(t_s+t_x-\nu)^{\lambda+1}N(\nu)} - \right.$$

$$\left. - \frac{1}{F_{uo}}\left(\frac{t_o}{t+t_x}\right)^{\lambda}\ln\frac{t_s}{t_o}\right] , \qquad (15)$$

where ν is the integration variable:

$$t_x = t_o\left(\frac{A_o}{A_u}\right)^{1/\lambda} . \qquad (16)$$

However, since the integral in (16) in a closed form cannot be taken, as a rule, by dividing the curve N(t) into portions where loading can be considered invariable, we should better use a simpler formula (Mirenburg,1984).

$$S = A_o N_{max} + A_u \sum_j^m \frac{(N_j - N_{j-1})\,\tau_j^{\lambda}}{\left(1 - \dfrac{N_j}{F_{uo}}\ln\tau_j\right)\left(1 - \dfrac{N_{j-1}}{F_{uo}}\ln\tau_j\right)} , \qquad (17)$$

where N_{max} is the maximum load on the pile;

$$j = \frac{t_s - j}{t_o} \qquad (18)$$

Using this relationship, we compared the progress of settling in tests on pile N.5 by applying step-increasing loading with its prediction from dynamometric test data. As evidenced by fig.4, the values of design settling not badly correlate with experimental data, particularly at loading range below the maximally-long design load, as determined in the table F_{ut} 250 kN.

Temperature variations can be approximately allowed for by introducing ficticious loads N_f in place of the actual ones N, the relationship between which is determined by the ratio of the carrying capacity of piles, as determined in compliance with SNandP P-18-76 under testing temperature F_{ux} and under the design temperature regime F_{ur}:

$$N_f = N \frac{F_{ur}}{F_{ux}} \qquad (19)$$

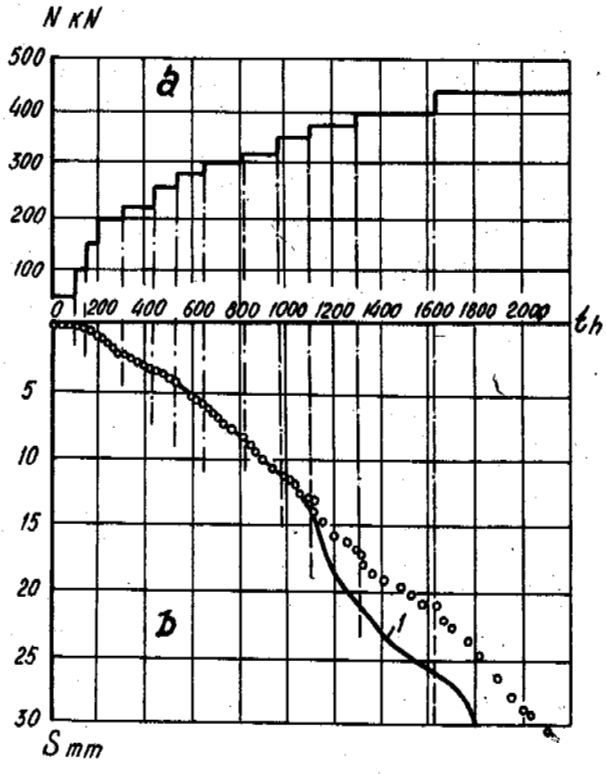

Fig.4. Comparison of full-size plot for settling progress on pile N.5 in stepped loading with that computed from dynamometric test data for the same pile.
a. Stepped variation of loading in tests; b. Experimental test data (1) and design plotted data (I).

CONCLUSION

The above releationships quite adequately and confidently describe the performance of piles in permanently-frozen grounds and can be used as a basis for predicting their settling and carrying capacity under constant and time-varying loads and temperatures.
The proposed dynamometric method of pile testing enables us to obtain within a relatively short period, 5-10 days, all relevant data for such a prediction.

LITERATURA

1. Gersevanov N.M. (1917). Opredelenie soprotivleniya svay. Zement, s. 9-11, Petrograd.
2. Mirenburg Yu.S., Fedoseev Yu.S. (1982). Prognoz osadki svaynih fundamentov v plastichnomerzlih gruntah. Reologiya gruntov i injenernoe merzlotovedenie. Nauka, s. 159-161. Moskva.
3. Mirenburg Yu.S., (1984). Uchet peremennoy nagruzki i temperaturi pri raschete fundamentov na vechnomerzlih gruntah. Osnovaniya, fundamenti i mehanika gruntov (3), s. 16-18.
4. SNiP P-18-76 (1977). Stroitelnie normi i pravila. Osnovaniya i fundamenti na vechnomerzlih gruntah. Stroyizdat, s.48.
5. Vyalov S.S., Eroshenko V.N., Mirenburg Yu.S. (1977). Sposob ispitaniya nesushey sposobnosti svay v gruntah. Avtorskoe svidetelstvo na izobretenie N 580268 Otkritiya. Izobreteniya n 42.
6. Vyalov S.S. (1978). Reologicheskie osnovi mehaniki gruntov. Visshaya shkola. s.447. Moskva.
7. Vyalov S.S., Mirenburg Yu.S., Fokin V.A. (1979). O vozmojnosti ispolzovaniya rezultatov ispitaniy merzlih gruntov na polzuchest dlya raschetov osnovaniya po dvum predelnim sostoyaniyam s uchetom reologicheskih svoystv gruntov. Gidrotehnicheskoe stroitelstvo v rayonah vechnoy merzloti i surovogo klimata. Energiya, s.27-31, Leningrad.
8. Vyalov S.S., Mirenburg Yu.S. (1980). Osadki i nesushaya sposobnost osnovaniy, slojennih slabimi gruntami s uchetom ih nelineynosti i polzuchesti. VI Dunaysko-Evropeyskaya konferenziya po mehanike gruntov i fundamento-stroeniyu, s.387-396, Varna, Bolgariya.
9. Vyalov S.S., Mirenburg Yu.S. (1984). Prognoz dlitelnih osadok svaynich fundamentov. Trudi instituta NII osnovaniy i podzemnih soorujeniy, vip.74, s.88-98.

CLASSIFICATION OF FROZEN HEAVE OF GROUND FOR HYDRAULIC ENGINEERING IN SEASONAL FROZEN REGIONS

Xie, Yinqi, Wang, Jianguo and Yian, Weijun

Heilongjiang Provincial Research Institute of Water Conservancy

SYNOPSIS In order to satisfy the requirements of hydraulic engineering, the frost heave property is classified into five types with absolute values of frost heave amount. On the basis of statistical analysis, the formulas are provided to calculate frost heave amount which is relative to the conditions of density, freezing index, ground water table and surcharge load.

PREFACE

In China, seasonal frozen ground mainly distributes in the south and north temperate zones and the mountain areas of the north subtropical zone (Xu and Wang,1983),of which the total area is about 5.137 million square kilometers and takes 53.5% of the area of China. In seasonal frost areas, frost heave of soil has caused a large number of damages in verying degrees for various engineering constructions, such as water conservancy project, bridge, highway, pipeline, railway, airport and other buildings.Classification of frost heave of soil, which ic called the evaluation of freezing sensitivity in some countries, reflects the research level and trend in some degree. Up to now, over one hundred kinds of classification methods of soil frost heave have been suggested in China and abroad, some of which have been brought into the relevant criteria (Ministry of Communication, PRC, 1975; National Construction Committee, PRC, 1974). In China, since 1960's, along with the development of economy, the problem of engineering freeze damage in seasonal frost area has been paid much attention. For various trades with the classification standards of frost heave in seasonal frost area were provided, but there is no any standard for water conservancy projects.

In recent years, in China and abroad a lot of research work and engineering practise have testified that frost heave of foundation soil is not only relative to the factors of soil particle size, water content and ground water table, but also closely related to engineering measures or conditions(Chen et al., 1978; Tong et al., 1985). For example, under the prerequisite of not changing the soil composition, both the ground ramming and the additional load of construction will greatly affect the frost heave property of ground. This shows that, if the ground soil is regarded as a system, ramming will change the inner texture of a system, which, in microscopic view, is that the increase of soil density changes the frost heave function of the system. The additional load, as the environmental condition, along with the conditions of temperature and water will also obviously change the frost heave function of the system.

The authors consider that a classification in frost heave should be faced on the following principles e.i. it should be able to reflect the features of speciality and engineering, its quantitative indexes should be clear and direct; these indexes should be easy to determine, and could be applied to engineering design practically, The main contents of classification should contain (1) classifying the frost heave, (2) the quantitative indexes of classifying frost heave, and (3) the determining method of quantitative indexes.

Selection on indexes for classification is one of the key problems. The current classification principles are mostly based on the average frost heave rate (in America) or the frost heave ratio (such as Ollove's classification in Soviet Union), the former must be specified in laboratory with special instruments and for the latter,the same frost heave ratio will have quite different frost heave amount in the areas of having different frozen depth. This will make the classification very confused. Although the absolute value of frost heave amount is not very large, it will be put into the class of strong frost heave because of the small frozen depth. In the opposite, although the absolute value of frost heave amount is very large, it will be put into the lower class of frost heave because of the large frozen depth.

It is obvious that the indexes of specifying frost heave classes must be clear, and should be able to directly and quantitatively reflect the possible degree of damage of ground frost heave to construction, that is, the "adaptation" degree for the permissible deforming of ground soil and constructions. Thus, it might be better to apply the absolute value of frost heave as the quantitative index for classification.

Considering that a same frost heave amount may cause various degrees of damages to different types of constructions, and even the sensitivities of different parts of a construction to

frost heave are not completely the same, so that the authors do not adopt the traditional terms, such as no frost heave, weak frost heave and strong frost heave, as the names of various classes, but classify frost heave into five classes from weak to strong.

Since the simulation law of model experiment of frost in laboratory have been not perfect, the authors took the indoor experiment as the means to examine the qualitative effect of various factors on frost heave, and took the frost heave amount obtained from field work as the quantitative basis, then proposed the engineering classification standard of ground frost heave property, which is suitable to the hydraulic structures in seasonal frost area. The analytical equations of claculating frost heave amount provided in this paper may also be regarded as the references of making engineering programme and frost heave forecast for the areas without observation data.

LABORATORY AND FIELD EXPERIMENTAL RESEARCH ABOUT THE BASIC RULES OF GROUND FROST HEAVE

In China and abroad, many scientists have made a lot of experimental research about unitary and multiple factors affecting frost heave of ground. For a certain kind of soil with certain texture, its frost heave amount h is the function of multiple factors:

$$h = f\ (F,W,Z,\gamma_d,P_i,\Delta S,H_f,V_f) \qquad (1)$$

where, F—freezing index;
W—prefreezing water content of soil;
Z—ground water table prefreezing;
γ_d—density of soil;
P_i—surcharge load;
ΔS—compress amount of underlain unfrozen soil;
H_f—frozen depth;
V_f—freezing speed.

For the fixed soil structure, W and γ_d are the major factors of internal structures of system (Xie, 1982); the environmental temperature F, the environmental water condition Z and the environmental engineering factor P_i are the main factors in environmental conditions, and frost heave, as a behavior of system, is controlled by the major structural and environmental factors as above. In order to provide reliable basis for the engineering classification of ground frost heave, the authors have continuosuly made experimental research on the basic rules of soil frost heave for eight years.

(i) The frost heave property of soil is closely relative to the particle size composition, only the fine grained soil possesses the mechanism of causing strong water migration. Based on the composition in particle size, soil can be classified into two groups.

Clayey soil: it consists of fine-grained soils and some sandy soils with a fine (<0.05 mm) content over 15% of total weigh.

Sandy soil: it consists of sandy soil with a fine content lower than 15% of total weight.

(ii) According to the frost heave amount distributing with depth, frost heave may be classified into three types: first, the frost heave is at the upper part of soil column; second, it is high at the lower part of soil column; and the third. it is homogeneuous through the whole column. In a close system, it can only be the first type.

(iii) An increase in density of clayey soil will obviously reduce the frost heave amount. The effect of density on frost heave can be expresses with the density reducing coefficient d_γ and calculated by means of Eq.(2),

$$d_\gamma = 1-EXP[-5.0(\gamma_d-1.35)] \qquad (2)$$

Eq.(2) adoptable to soils with a density $\gamma_d \geq 1.35$ g/cm^3.

(iv) Ground water table is one of major environmental factors affecting frost heave, which indicates the freezing type of system—close or open (Ding, 1983).Only for open system, the 1st and 2nd types of frost heave can occur. A saturated soil, freezing in an open system will form the strong frost heave.

(v) The surcharge load P_i, as a engineering factor in environmental condition, will strongly restrain the frost heave of ground. This action will be weakened with the increasing of density of ground soil. The reducing coefficient d_p may be calculated with Eq.(3).

$$d_p = 1 - e^{bP_i} \qquad (3)$$

Eq.(3) is adoptable to soils under a surcharge of $P_i \leq 3.0$ kg/cm^2.
where b is relative to soil density, and may be calculated with the Eq.(4).

$$b = -3.4EXP[-6.3(\gamma_d - 1.35)] \qquad (4)$$

The values of b also can be obtained from Fig.1.

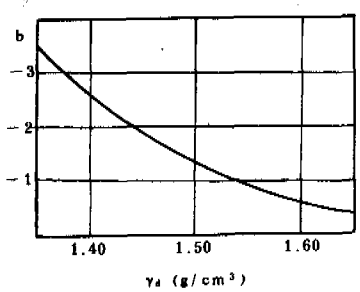

Fig.1 Dependence of Coefficient b on γ_d
b—coefficient related to density of soil

THE STATISTICAL ANALYSIS OF GROUND FROST HEAVE

A statistical analysis was made based on the basic rules of frost heave discussed above, the data presented at the previous Chinese National Conferences on Hydraulic Construction and Anti-freezing Technics and the National Conferences on Permafrost, and those obtained from 43 sites in the Heilongjiang Province. The extreme values of frost heave of clayey soil and sandy soil, 671 and 133 in number respectively, were selected for statistics. These data were from an area ranging from 36° to 50.2°N and 84° to 132°E, relative to Xinjiang, Qinghai, Gansu, Jingxia, Shanxi, Beijing, Hebei, Inner Mongalia, Liaoning, Jilin and Heilongjiang Provinces (or sity, autonomous region). 98% of the data were obtained from the testing sites of hydraulic construction.

Because the geographical range is just same with the seasonally frozen zone of China, and the data basicly come from the fields of hydraulic engineering, it is believed that the data used in this statistics can present nature of the whole region, with a sufficient, universality and reliability.

The results of correlation analysis of the extreme value of frost heave vs temperature and water, the major factors in environmental conditions and the quantitative calculation method are as follows:

(i) For clayey soil, the outer envelope line of the maximum frost heave values is conformed to the good random normal distribution vs freezing index and northern latitude, and the frost heave amount reduces exponentially with ground water table prefreezing, which can be expressed with the following equations,

(1) When north latitude D is known,

$$h'_{D,max}=\frac{1}{\sqrt{2\pi}\sigma_D}\ EXP[-\frac{(X_D-\mu_D)^2}{2\sigma_D^2}-bZ] \quad (5)$$

(2) When freezing index F is known,

$$h'_{F,max}=\frac{1}{\sqrt{2\pi}\sigma_F}EXP[-\frac{(X_F-\mu_F)^2}{2\sigma_F^2}-bZ] \quad (6)$$

where, $h'_{D,max}$ and $h'_{F,max}$ are the possible maximum value of frost heave (meter) corresponding to D and F for clayey soil; both σ_D and σ_F are characteristic constants and equal to 0.88654; μ_D and μ_F are also characteristic constants, and μ_D=10, μ_F=2.40; X_D and X_F are the conversion values of abscissa, and X_D=0.2222D, X_F=F/650; D denotes north latitude (degree); F denotes freezing index which can be one year observation value or the average value of years (in °C·day); b is a characteristic constant and b=-0.70; Z is ground water table prefreezing.

(ii) For sandy soil, the outer envelope line of the maximum frost heave values is also conformed to the random normal distribution vs north latitude and freezing index,

(1) When D is known,

$$h^c_{D,max}=\frac{1}{\sqrt{2\pi}\sigma^c_D}EXP[-\frac{(X^c_D-\mu^c_D)^2}{2(\sigma^c_D)^2}]-dZ \quad (7)$$

(2) When F is known,

$$h^c_{F,max}=\frac{1}{\sqrt{2\pi}\sigma^c_D}EXP[-\frac{(X^c_F-\mu^c_F)^2}{2(\sigma^c_F)^2}]-dZ \quad (8)$$

where, $h^c_{D,max}$ and $h^c_{F,max}$ are the possible maximum values of frost heave (in meter) corresponding to D and Z for sandy soil; σ^c_D and σ^c_F are characteristic constants, and σ^c_D=0.1773, σ^c_F=1.773; μ^c_D and μ^c_F are also characteristic constants, and μ^c_D=21.3, μ^c_F=4.53; X^c_D and X^c_F are the conversion values of abscissa, and X^c_D=0.5D, X^c_F=F/265; d is constant, and d=0.107; the meanings of D and F are same with those in Eq.(6).

(iii) By synthetical analysis of relations of $h_{F,max}$—F and $h_{D,max}$—D, it was found that the ground frost heave does not monotonously increase or reduce with the environmental factors F and D, but exist the "optimum" values of F and D for producing the maximum frost heave amount.

It is believed that the h will increase with F or D. However, as F or D comes up to a critical value, an increase in F or D will result in a decrease of h_{max}. This could be explained by the fact widly recognized that if the frost penetrating speed is much faster than the velocity of moisture migration, the frost heave would decrease.

(iv) The frost heave amount continuously changes in space (e.g.h_{max}—D), and changes with structure condition of soil (e.g.h_{max}—Z). To explore the inherent connection between the two changing types, the whole region is divided into three subregions for statistical analysis of maximum frost heave amount h_{max} of clayey soil vs Z.

(1) There are 208 samples when 42.5<D<47.5 degrees.

(2) There are 99 samples when 40.0<D≤42.5 degrees and 47.5≤D<50.0 degrees.

(3) There are 120 samples when 50.0≤D≤40.0 degrees.

The synthetical statistical analysis of the maximum value proved the existence of continuity between the maximum frost heave amount and regional factors and water condition.

Besides, for the three analytical subregions, water reducing coefficients b are all -0.7, this shows that at different geographical locations, the influence of water condition to frost heave is equivalent. This makes a basis for quantitatively evaluating the synthetical effect of latitude, temperature, and water on frost heave. Through the statistical analysis of the freezing and frost heave observational values in natural condition, the qualitative rules in laboratory may be quantitatively explained, and finally, the basis of engineering classification may be found out.

THE ENGINEERING CLASSIFICATION IN FROST HEAVE OF GROUND UNDER HYDRAULIC CONSTRUCTION IN EASONAL FROST AREA

Through the analysis as above, it could be considered that in seasonal frost areas, the frost heave of ground under hydraulic construction,in practise, can be divided into five classes, in which the absolute amount of frost heave is regarded as the classification index (Table I).

TABLE I

The Engineering Classification of Frost Heave in Ground Under Hydraulic Construction in Seasonal Frost Area

Standard of frost heave class	I	II	III	VI	V
Frost heave amount h (cm)	$h \leq 2$	$2 < h \leq 5$	$5 < h \leq 12$	$12 < h \leq 22$	$h > 22$

The reason without using the traditional names of classes, such as no frost heave, weak frost heave and medium or strong frost heave, is chiefly that the sensitivities of various structures to frost heave are quite different. For example, if the II class of frost heave is named as "weak frost heave", it is, perhaps, suitable to the structures of floodgate and U-shaped trough with good integrity, however, it may cause serious frost heave damage to the light structure such as the pavement of ditch. In addition, since most hydraulic constructions have sufficient water supply, and the absolute observational values in other engineering field, the traditional three names of "strong, medium and weak" are not sufficient to be used, which is the another reason of dividing five classes.

Using frost heave amount as the quantitative standard of determining frost heave class is clear and direct, and has the advantage of using corresponding technical measures according to the sensitivity of specific engineering to frost heave. To make the frost heave forecast of a construction and provide the basis of anti-frost heave designing for the areas without observational data, the authors provided the empirical formulas for determining classification indexes as follows:

(i) The calculation of frost heave amount for clayey soil

After knowing the annual freezing index, the ground water table in first 10 days, the prefreezing average density in frozen soil layer and the load born on ground, the following formula may be used to calculate frost heave amount

$$h = (1-d_p)(1-d_\gamma)\, h'_{F,max} e^{bx} = \frac{1}{\sqrt{2\pi}\sigma_F} EXP\{-\frac{(X_F-\mu_F)^2}{2\sigma_F^2} - 3.4P_i EXP [-6.3(\gamma_d-1.35)] - 5.0(\gamma_d-1.35) - 0.7Z\} \quad (9)$$

Eq.(9) is adoptable to the condition of $\gamma_d \leq 1.75$ g/cm^3 and $P_i \leq 3.0$ km/cm^2, where, d_p, d_γ, $h'_{F,max}$ may also be calculated by means of Eq.(2), (3) and (6) respectively.

If the value of F is difficult to obtain, frost heave amount may be calculated with the value of north latitude

$$h = (1-d_p)(1-d_\gamma)\, h'_{D,max} e^{bz} = \frac{1}{\sqrt{2\pi}\sigma_D} EXP\{-\frac{(X_D-\mu_D)^2}{2\sigma_D^2} - 3.4P_i EXP [-6.3(\gamma_d-1.35)] - 5.0(\gamma_d-1.35) - 0.7Z\} \quad (10)$$

Eq.(10) is adoptable to the condition of $\gamma_d \leq 1.75$ g/cm^3 and $P_i \leq 3.0$ kg/cm^2, where $h'_{D,max}$ may be calculated with Eq. (5).

(ii) The calculation of frost heave amount for sandy soil

When F and Z or D and Z are known, the frost heave amount for sandy soil may be calculated by means of Eq.(8) or Eq. (7), the suitable range of which is $h^c \geq 0$.

Making use of Fig.2 and Fig.3, the calculations of frost heave amount for clayey or sandy soil may be greatly simplified.

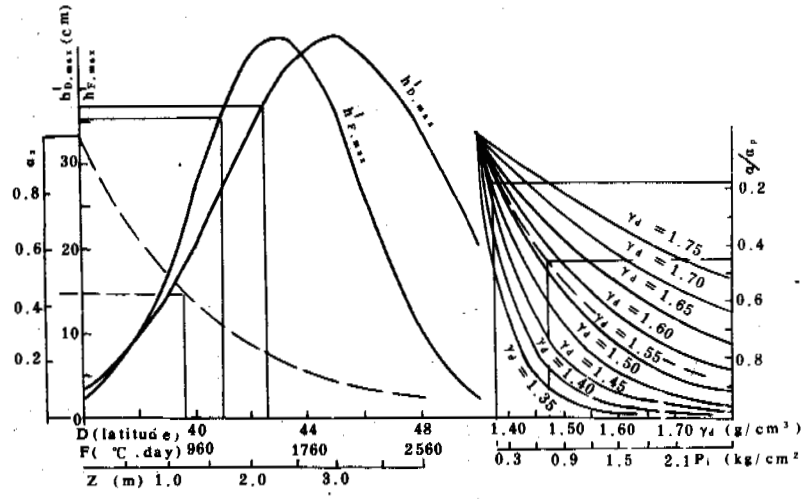

Fig.2 Normograph for Determining the Maximum Value of Frost Heave of Clayey Soil

$h'_{D,max}$, $h'_{F,max}$—maximum value of frost heave based on D (latitude, in degree) or F (freezing index, in °C·day);

γ_d—density of soil (in g/cm³).

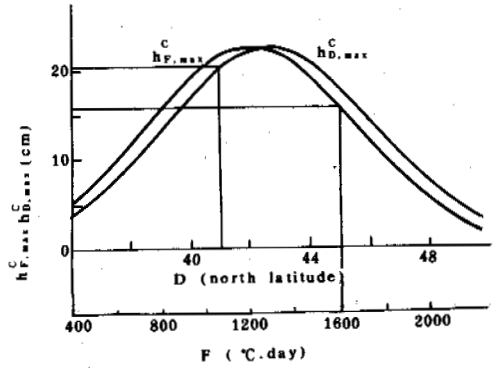

Fig.3 Normograph for Determining the Maximum Value of Frost Heave of Sandy Soil

REFERENCES

Chen Xiaobai, et al.,(1978). The preliminary study about the effect of loading on frost heave (abstract). Proc.Symposium on Glaciology and Cryopedology, (Cryopedology), 126-127, Lanzhou.

Ding Dewen, (1983). The calculation of freezing depth and moisture condition in open system. Proc.2nd Chinese National Conference on Permafrost. 191-196, Lanzhou.

Ministry of Communications, PRC,(1975).Standard of design of highway, bridge and culvert, People's Publishing House.

National Construction Committee, PRC,(1974). Standard of foundation design of industrial and civil architecture TJ7-74, Chinese Architecture Publishing House.

Tong Changjiang and Guan Fengnian, (1985). Frost heave of ground and the prevention and control of frost damage of construction. pp.265, Publishing House of Water Conservancy and Electric power, Beijing.

Xie Yinqi, (1982). The exploration of using prossed soil as the foundation of anti-frost have. Journal of Building Technics on Low Temperature, (1).

Xu Xuezu and Wang Jiacheng, (1983). Preliminary discussion on the distribution of frozen ground and its zonality in China. Proc.2nd Chinese National Conference on Permafrost, 3-12, Lanzhou.

RETAINING WALL WITH ANCHOR SLABS USING IN COLD REGION

Xu, Bomeng[1] and Li, Changlin[2]

[1]Northeast Design and Exploration Institute, Ministry of Water Resources and Electric Power, P.R.C., 74 Beian Road, Changchun, China
[2]Water Resources Institute of Jilin Province, P.R.C.

SYNOPSIS In recent years, we have conducted field test of horizontal frost heaving force on model retaining wall, as well as designed and constructed two retaining walls with anchor slabs in Jilin province being seasonally frozen area of our country. The tests and applications indicate that the anchored retaining wall has such advantages as very light in weight, economic in material, well flexible and adjustable to a certain extent to the frost heaving of soil and thus, is one of the fine structure types to prevent it damaging due to action of horizontal frost heaving force of soil behind the wall.This paper deals with the test results and the behavior of experimental walls.

INTRODUCTION

The retaining structure with anchor slabs consists of the wall face (including columns and panels), tie-rods, anchor slabs and soil between them as shown in Fig.1. Much has been done on the investigation and use of such structure in our country since 70's, however, limited basically to the railway and road engineerings of non frost areas. The retaining wall of anchor slabs, however, using in the hydraulic ingineering in seasonally frozen zones has some features of its own in addition to meet the common demands on this structure as follows:

(i) The soil behind the wall freezes in cold weather and thaws in warm seasons, thus, the internal stability of this structure must be satisfied under action of earth pressure in warm seasons and horizontal frost heaving force in winter.

(ii) The retaining structure works under high water table, the soil behind the wall has high moisture content. Thus the horizontal frost heaving force greater than that acting on the retaining wall using in other engineerings is resulted in. Therfore, it is nece ssary to seek effective measures to reduce the heaving force and correctly decide its value.

(iii) The retaining wall are often subjected to the influence of water flow, seepage and hydrodynamic pressure, which should be taken into account in the design.

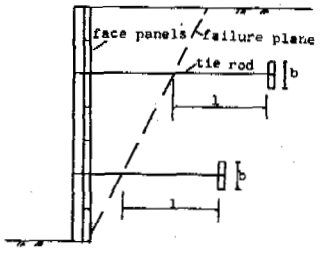

Fig.1 Schemtic Diagram of the Retaining wall with Anchor Slabs

STRUCTURE PATTERNS OF THE EXPERIMENTAL PROJECTS

According to the different characters of the experimental retaining structures, arched and smooth wall surface were adopted (Li Changlin, Xu Bomeng, Zhen Duo, 1986).

Dongala retaining structure with anchor slabs

The structure acting as the retaining wall of the intake pond of Dongala irrigation pump station was made in multi-arch shape composed of six individual arches with height of 4.6 m and intrados radius of 1.5 m (see Fig.2,3).

Daantun retaining structure with anchor slabs

This structure was set up at the inlet section of Daantun overflow earth dam, and so it works as a retaining wall on one hand, and functions as the guide wall.According to hydraulic theorie, the wall face composed of columns and retaining

panels were made smooth (Fig.4). This wall was 4 m high. The anchor slabs closer to the wall face were instaled within the freezing depth with the aim of bearing the frost heaving reaction force and aiding the stability against frost heaving force (Fig.5).

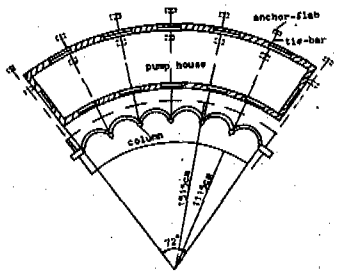

Fig.2 The Plane Figure of Donala Retaining Structure

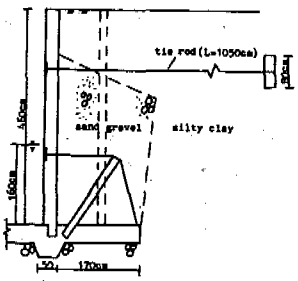

Fig.3 The Cross Section of Dongala Retaining Structure

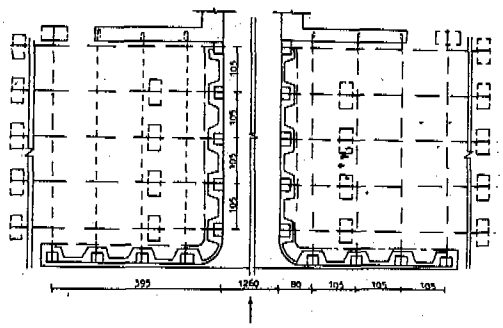

Fig.4 The Plane Figure of Daantun Retaining Structure

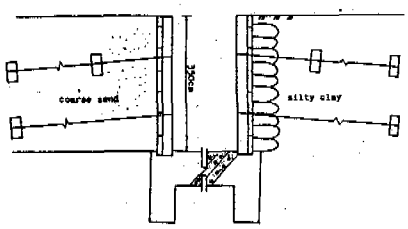

Fig.5 The Cross Section of Daantun Retaining Structure

HORIZONTAL FROST HEAVING PRESSURE ACTING UPON RETAINING WALL

Determination of horizontal frost heaving force under full confinement from in-situ tests

Horizontal frost heaving force occurs when the frost heaving of soil behind retaining wall is confined, as a result, its magnitude depends on the heaving properties of the soil and degree of confinement. To investigate the basic characters and design value of this force, the field tests on three model retaining wall were carried out.

The model walls were 2 m high and consisted of 10-layer reinforced concrete beams with total length of 3 m. In the course of test, the wall face was propped up to keep it from displacing forward. The properties and moisture content of soil behind the wall and the depth of the water table from wall top before freezing are listed in Table 1. The lowest temperature in the test area reached -25 to -30 ^{o}C and the freezing depth was 1.6-1.7 m.

The observed results indicate that the principal trend of horizontal frost heaving force distribution along the hight of the wall is as following: there is no or very little frost heaving pressure within a certain depth from the top of the wall being about 50-70 cm in this case; then, it increases with depth and reaches maximum value at certain height above the ground surface in the front of the wall being approximatly 40-50 cm under this circumstances; from then on it comes to decrease slightly towards the bottom of the wall (Fig.7).

This pattern of heaving pressure distribution is resulted from such factors as the temperature feature, the moisture state of soil behind the wall and the confinement condition of the soil heaving. The top layer of the soil behind the wall lies far from the water table and has low moisture content, moreover, it freezes from two directions with high speed, Thus,in general, the frost heaving of the soil may not occur, while the contraction of the soil body during freezing comes into being, resulting in cracking at the interface between the soil and wall back. For example, the soil behind model retaining wall No.A departed from the wall back 1.3 cm, 0.6 cm, 0.4 cm at depth 0-20 cm, 40-60 cm and 80-100 cm respectively. Subsequently, the horizontal frost

TABLE

Properties and Moisture Content(W) of the Soil, Depth of Ground Water(H)

Wall No.	Grain-size composition (%) 0.1-0.05 (mm)	0.05-0.005 (mm)	0.005 (mm)	r_d (g/cm^3)	W_p (%)	W_I (%)	I_p (%)	Soil classification	H (m)	W (%)
A	16	52	32	1.44	18.6	34	15.4	Silty clay(CI)	2.5	22.5
B	16	52	32	1.44	18.6	34	15.4	Silty clay(CI)	2.3	28.1
C	22	51	27	1.44	20.5	39	18.5	Silty loam(CI)	2.0	23.6

heaving force will be little or not in this layer. With the distance from ground surface increasing and being closer to the ground water level, and the confinement to the frost heaving of soil becoming stronger, the frost heaving pressure grows higher and higher. Nevertheless, at the bottom part of the wall, frost condition changes because of the influence of the ground before the wall, which leads on to decrease of the frost heaving force in this part.

Based on the results obtained from field tests and to simplify computation, the distribution pattern of horizontal frost heaving force versus the hight of the wall shown in Fig.7 may be adopted. Fig.7a is applicable provided that the frost depth of ground in front of the wall is less than that in backfill of the wall,otherwise the Fig. 7b can be used.

When using Fig. 7 to compute the horizontal heaving pressure, it is important to determine magnitude of the conditional depth without frost heaving force(h_1), frost-heaving areas (h_2, h_3) and the maximum frost heaving pressure (σ_{max}), the magnitudes of which all have to do with the water content, properties of the soil as well as the water table. The stronger the frost heaving of soil, the greater is the frost heaving pressure. Under the identical condition of soil property, as the water content and water table go up, h_2 and σ_{max} increase but h_1 decreases. Moreover, the higher the wall, the larger the value will be if other factors remain the same.

The results achieved so far have indicated that the ground would not heave before the water table reaches a certain distance from the ground surface which is defined as critical influential distance (H_c) and mainly dependent upon the capillary height. According to the existing research achievements (Xu Bomeng, Lu Xingling, 1986, Wang Xiyao, 1982), H_c varies from 1.5-2.0m for cohesive soil and 0.5-1.0 m for sandy soil. Therefore, under the circumstances of high water table, the following formulae can be used to decide the values of h_1 and h_2

$$h_2=H_c-Z \quad (1)$$

$$h_1=H-h_2 \quad (2)$$

where Z is the buried depth of underground water in front of the wall; H is the height of wall.

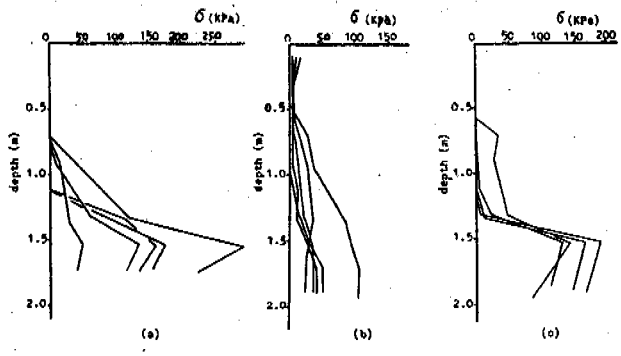

Fig.6 Distribution of the Horizontal Frost Heaving Pressure along the Height of the Wall

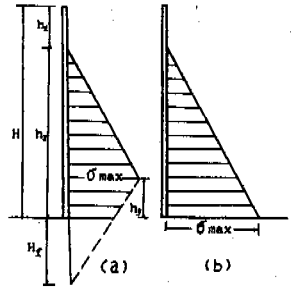

Fig.7 Diagram for Computing Horizontal Frost Heaving Pressure

In Fig.7a, the value of h_3 may usually be taken about 50 cm. The maximum horizontal frost heaving pressure observed appears at the lower part of the model retaining walls and has the value

generally from 220 to 240 KPa, However, the retaining wall must be designed to meet the requirements of stabilities against sliding and overturning, i.e. the most important to do it is to decide the magnitudes of the total frost heaving force and resultant moment. For this reason, taking the maximum horizontal frost heaving pressure σ_{max}=200 KPa, the critical influential distance H_c=1.6 m(Wang Xiyao, 1982), h_3=0.3 m in accordance with our field testing results and the measured value of the capillary rise, at the same time, using the distribution pattern in Fig.7, we have computed the maximum values of the total horizontal frost heaving force and resultant moment. The computed and observed results are listed in Table 2.

TABLE 2
Computed and Observed Values of the Total Horizontal Frost Heaving Force and Resultant Moment Acting on a Unit Width of the Model Retaining Walls

Wall No.	Total force (KN)		Resultant moment (KN)	
	observed	Computed	Observed	Computed
A	87.5	130	50.5	53.3
B	159.0	150.0	43.3	71.3
C	141.2	180.0	95.2	103.3

It can be seen from Table 2 that the computed values are generally conservative for the safty of the wall. Thus, it is adoptable to compute horizontal frost heaving force acting upon the retaining wall according to Fig.7 with taking 200 KPa as the maximum frost heaving pressure provided that the wall is under full confinement, the ground water level is relatively high and the soil behind the wall is cohesive.

Horizontal frost heaving pressure under the condition of wall deformation

As mentioned above, the horizontal frost heaving force has the maximum value while the frost heaving of soil is full confined. As the wall with anchor slabs has betterflexibility and deformability, the frost heaving force will to certain extent decrease. Based on the existing test data (Tong Changjiang, etc., 1985, Xu Zhenghai, 1986) and in consideration of the safty of structure, the horizontal frost heaving force under allowable deformation is calculated according to Fig.8 or formulae (3) and (4) in design.

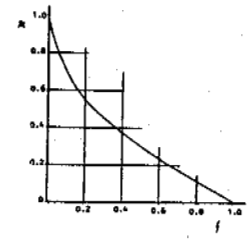

Fig.8 Relation between Allowable Deformation Rate and Reducing Coefficient of Heaving Force

$$m=1-f^{0.5} \quad (3)$$

$$\sigma=m\cdot\sigma_{max} \quad (4)$$

in which m is the reducing coefficient of the frost heaving force, i.e. the rate of frost heaving pressure corresponding to certain deformation and the maximum frost heaving pressure under full confinement; f is the allowable rate of deformation, i.e. the rate of the allowable deformation at a point and the freely frost heaving capacity of soil behind the wall.

Measures of reducing horizontal frost heaving force

In order to let the structures have greater safty factors, the measures of filling soil weak in frost heave and fabric bags filled with soil were used to reduce frost heaving force.

At Dongala pump station,the space between panels and excavation surface was partly filled with sand gravel. The lateral average width of the sand gravel layer was about 60 percent of the maximum frost depth.

The material behind right wall of Daantun project was silty clay which belongs to strong frost heaving one, so we built a 60 cm wide layer of geotextile bags filled with silty clay against the back of the wall (see Fig. 5). To prove the effect of this method, laboratory test on model retaining wall was carried out. The test results listed in Table 3 indicate that the tension of tie-rods when using geotextile bags filled with soil is about 28% smaller for the upper tie-rod and 11% smaller for the lower tie-rod than that without geotextile bags.

TABLE 3

Tensile Stress of Tie-Rods with and without Using Geotextile Bags (MPa)

With bags	Upper tie-rod	98.1
	Lower tie-rod	157.7
without bags	Upper tie-rod	136.6
	Lower tie-rod	177.8

DESIGN OF ANCHOR SLABS

The principle problem of anchor slab design is to decide the allowable pull-out force and then according to tie-rod tension to determine the area of anchor slabs and the section size of tie-rods. As the length of tie-rods is much greater than frozen depth, the pull-out strength of anchor slabs in seasonally frozen area is still dependent upon the resistance of the warm soil in front of the slabs. In accordance with the condition of the experimental projects, we conducted pull-out test on anchor slabs at the pump station of Dongala. Based on the results (see Table 4), we took 122.5 KPa as the allowable value in design.

TABLE 4

Pull-out Strength of Anchor Slabs in Clayey Soil

Size of anchor slabs(cm)	40x40	80x80
Ultimate pull-out force(KN)	39.2	156.9
Length of tie-rods(m)	6	6
Height of filled soil(m)	2	2
Dry unit weigth(g/cm^3)	1.6	1.6
Property of soil	Silty clay I_p=18.3	

OPERATION PERFORMANCE OF THE EXPERIMENTAL PROJECTS

Two experimental projects have been in proper operation for 3 and 4 years respectively and are still in good condition. Described in Fig.9 is the distribution of measured and design maximum values of the horizontal frost heaving pressure of Dongala retaining wall with anchor slabs along the wall height. It can be observed from the picture that the design approch described previously is of enough security.

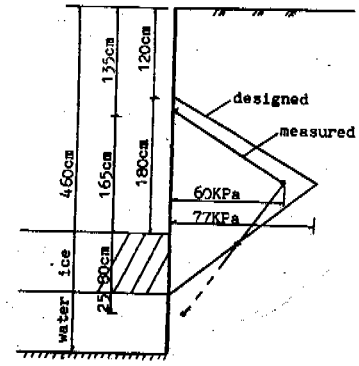

Fig.9 Distribution of the Measured and Design Maximum Values of the Horizontal Frost Heaving Pressure of Dongala Retaining Structure

SUMMARY

Many of retaining structures suffered heavy frost damage in cold north regions. The use of the retaining wall with anchor slabs provides a secure and feasiable new way for solving the frost damage.

The horizontal frost heaving force is the principle load acting upon the retaining wall of this type in seasonally frozen regions. It is feasible using Fig.7 to compute horizontal frost heaving pressure in design. The retaining structure with anchor slabs is a flexible one easily adjustable to frost heaving deformation, hence, it is feasible and secure to take the frost heaving force under certain displacement, in the meantime, to fill part of the soil weak in frost heaving or place geotextile bags filled with soil behind the wall to diminish the frost heaving force.

The test and applications of the retaining wall with anchor slabs indicate that such structure also has the advantages as less in masonry work, low in cost, high in speed of construction, able to be precasted and erected and so on.

REFERENCES

Wang Xiyao (1982). The frost heave and its distribution in different layers influened by shallow groundwater. Journal of Glaciology and Geocryology. Vol.4, No.2.

Xu Bomeng, Lu Xingling (1986) Influence of moisture condition on frost heave in clay. Journal of Glaciology and Geocryology. Vol.8, No.3.

Tong Changjiang, Guan Fengnian (1985) Frost heave of soil and treatment of frost damage of engineering structures. P.95.

Li Changlin, Xu Bomeng, Zhen Duo (1986). Experimenta of anchor slab retaining wall for hydraulic engineerings in seasonally frozen region. Journal of Northeast Hydraulic and Hydroelectric Engineering. No.11.

Xu Zhenghai (1986). Approximate calculation of the normal frost heaving force acting on the base of foundation. Journal of Glaciology and Geocryology. Vol.8, No.3.

THAW STABILIZATION OF ROADWAY EMBANKMENTS

J.P. Zarling,[1] W.A. Braley[2] and D.C. Esch[3]

[1]School of Engineering, University of Alaska Fairbanks
[2]Institute of Northern Engineering, University of Alaska Fairbanks
[3]State of Alaska, Dept. of Transportation & Public Facilities

SYNOPSIS The thermal degradation of permafrost beneath Alaskan roads leads to expensive maintenance and repair costs. This study evaluated two methods to stabilize the thaw. Snow sheds were built along two sections of roadways to shade the ground during summer and prevent snow from acting as an insulating blanket during winter. The second method consisted of removing snow during the winter months to reduce surface temperature. The results show that the snow sheds were more effective in decreasing the ground surface temperatures and, as such, the concept could be further developed.

INTRODUCTION

The existence of permafrost in northern regions has required highway engineers to carefully examine the effect of construction on the thermal regime of the ground. In both continuous and discontinuous permafrost areas, changing the ground surface condition can lead to thaw degradation of the underlying permafrost, and subsequent thaw consolidation and settlement in ice-rich soils. It is well established that in most northern locations, a .5°C to 5°C temperature difference exists between the mean annual air and ground surface temperatures. This difference is a function of slope and surface orientation, vegetative and snow cover, ground thermal properties, meteorological conditions, and surface and subsurface drainage. For example, shading the ground surface from the summer time sun and removing the insulating snow cover during the winter months should result in the mean annual soil surface temperature (MASST) approaching equality with the mean annual air temperature. If these modifications result in lowering the MASST below 0°C, permafrost will tend to be formed or thaw degradation of the permafrost will be prevented or stopped.

In the cooler Arctic regions the most common method of protecting a roadway constructed over permafrost against thaw settlement is through the use of gravel fill of sufficient depth to contain the active layer. As the MASST increases the required fill thickness increases. The use of fill becomes uneconomical as the MASST approaches 0°C. The fill thickness can be reduced through the use of rigid foam plastic insulation (Esch, 1973, 1983). Although the fill will protect the permafrost beneath the center of the roadway, the sloping of the fill to zero thickness at the toe of the embankment allows this region to experience thaw degradation. This is further exacerbated by plowing snow from the roadway during winter, which increases the thickness of snow cover on the side-slopes and the toe zone, further insulating the ground from the cold air. When the side slope thaw front penetrates into ice-rich permafrost, consolidation and thaw settlements occur. The effects of this settlement are sliding or rotation of the slopes and cracking of the surface.

Air duct systems (Zarling et al., 1983) have been used as an attempt to mitigate this problem. The concept is to bury a duct or pipe in each side-slope near the toe of the roadway with its ends open to the atmosphere. Cold air by either natural or forced convection will flow through the pipe, cooling and freezing the surrounding ground. Other alternatives have been the use of insulation placed in the toe of fill and construction of a berm at the toe of fill (Esch, 1983). However, none of these treatments have yet proven totally effective in preventing slope thawing and movements.

In discontinuous permafrost areas, the MASST of the paved roadway may be above 0°C. In this case, no amount of insulation or fill will prevent thaw degradation, only slow it down. Berg et al. (1983) have applied white and yellow paint and several other surface treatments to pavements in an attempt to lower the MASST. As their study demonstrated, a painted roadway surface does yield a lower surface temperature, but traffic quickly degrades the high solar albedo of the surface. Additionally, there are safety considerations when using painted roadway surfaces which become slippery when wet.

This study addresses two snow management schemes in an attempt to achieve colder roadway slope surface temperatures. The scope of the project was to build snow sheds along two sections and to remove the snow cover along one section of roadway embankments. The snow sheds were designed to shade the ground surface from the sun during summer and to prevent the snow cover from insulating the ground surface during winter.

THEORETICAL CONSIDERATIONS

A measure of the annual freezing or thawing potential at the surface of the ground is the surface freezing or thawing index. These indices are defined as the annual summation of the surface freezing or thawing degree days for the freezing or thawing season.

Because air temperatures and air freezing (A.F.I.) and thawing (A.T.I.) indices are generally available for most locations, empirical factors known as surface n-factors have been determined for many surfaces for both the freeze and thaw seasons in order to relate surface to air temperatures (Lunardini, 1981). Surface n-factors are defined as the ratio of the surface freezing or thawing index to the air freezing or thawing index. It can be shown that the mean annual surface temperature can be estimated as

$$MASST = \frac{n_t(A.T.I.) - n_f(A.F.I.)}{365} + T_f$$

Decreasing the surface thaw n-factor and increasing the surface freeze n-factor will yield a lower MASST. A measure of a system's performance in changing the MASST is directly related to the surface n-factors or surface freeze and thaw indices.

SITE LOCATIONS AND DESCRIPTIONS

The two sites selected for study were at Bonanza Creek, approximately 50 km west of Fairbanks, Alaska on the Parks Highway, and on Farmer's Loop Road, just west of the City of Fairbanks and adjacent to the University of Alaska Fairbanks campus.

In the vicinity of Bonanza Creek, the roadway alignment required an embankment ranging from 6.7 to 7.6 m in height over frozen muskeg. Overlying the permafrost at this site is a .3 to .6 m thick layer of peat moss, and scattered black spruce. Frozen organic silts were present beneath the surficial peat layer. Frozen water contents of the silt ranged from 30 to 380%, averaging about 100% by weight of the dry soil fraction. No massive ice was encountered in preconstruction borings. The design embankment height was initially believed sufficient to prevent seasonal thaw penetration into the underlying permafrost beneath the paved roadway. However, side slope thawing and related slope movements were anticipated. To retard these movements, three different experimental side slope modifications were selected for field evaluation when the road was constructed. Seven roadway sections with different combinations of berms, air ducts and insulation were constructed in 1974 and have been monitored since 1975. Vertical and horizontal thermocouple strings were installed and read monthly in each section, and slope movement reference stakes have been surveyed annually. Esch (1983) presented a detailed analysis of the three methods (insulation layers, air ducts and toe berms) based on extensive subsurface temperature and slope movement observations. After eight years of service, the embankment at this site was seriously distressed due to permafrost thaw and related slope movements. Lateral movements and vertical settlements of the slope reference stakes exceeded 1.5 m vertically and 1.8 m laterally in some places.

Portable recorders were installed in 1975 at the Bonanza Creek site to continually measure surface temperatures of the pavement and of the 2:1 side slopes which faced north and south. During four years of observation, the annual surface temperatures were .5°C for the pavement

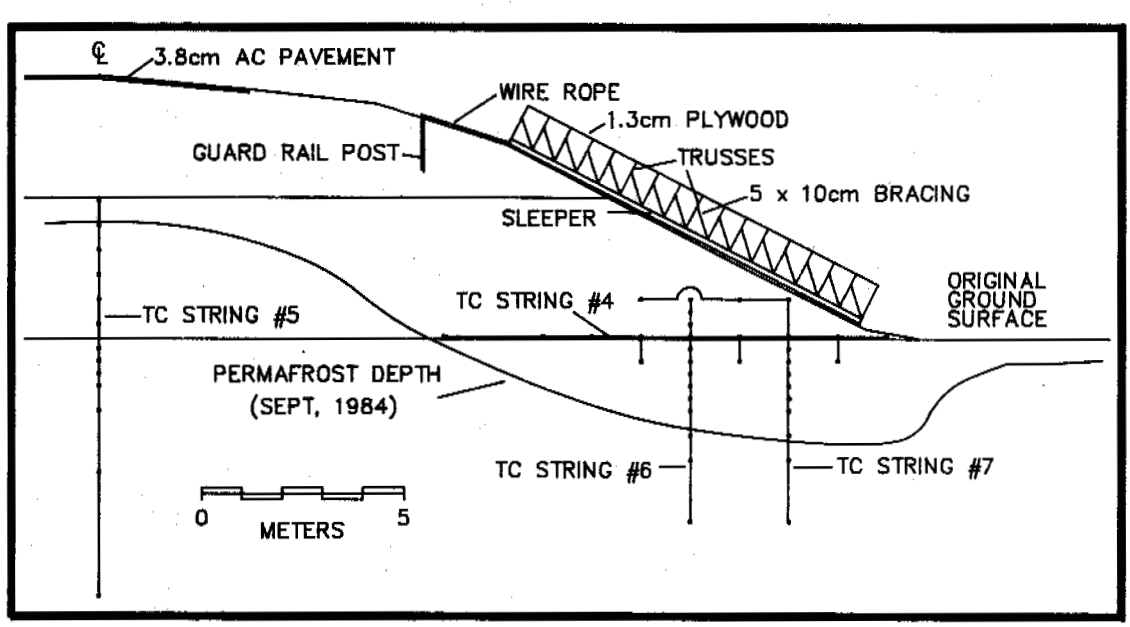

Figure 1. Cross-section view of roadway embankment and snow sheds at Bonanza Creek.

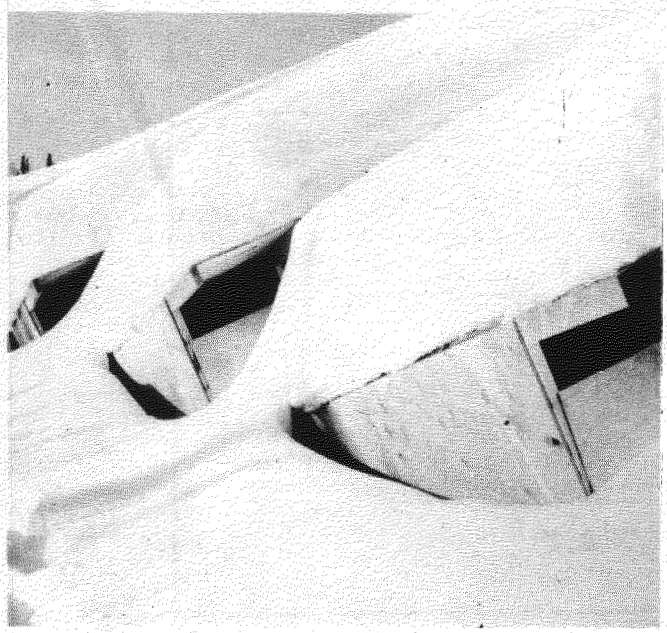

Figure 2. Pattern of snow accumulation on snow sheds at Bonanza Creek.

and 1.9°C and 5.0°C for the north and south facing slopes, respectively. Average surface thawing n-factors were 1.05, 0.40 and 0.45, respectively, for the three surfaces. The mean annual air temperature for this period was -2.7°C. Because none of seven original (1975) experimental treatment sections proved effective in preventing slope movements, the snow shed design was developed and constructed over the existing instrumented control section. Figure 1 shows a cross-section view of the embankment and of the annual 1984 thaw depth beneath the snow sheds. The section selected for snow removal had a 6.1 m wide toe berm and had also been instrumented and monitored since 1975.

At the Farmer's Loop site the four lane roadway was constructed in 1970 by widening an older two lane section, originally built in 1963, crossing a muskeg underlain by permafrost. The foundation soils at this location consist of ice-rich peat deposits underlain by gray organic silts with massive ice wedges. The peat deposits range in thickness from .6 to 3m. The peat is generally perennially frozen at a depth of .6 to 1.2 m below the original muskeg surface, except where heat gain by roadway side slopes has caused progressively deeper thawing.

THAW STABILIZATION METHODS

Snow Sheds

Seven snow sheds, each 9.8 m in length by 3.7 m in width, were constructed adjacent to one another at the Bonanza Creek site on the south facing embankment slope. The combined structure covered a total area of 251m^2 (25.6 x 9.8 m) and a length of 25.6 m of embankment slope. Roof trusses with a 3.7 m span, 1:4 pitch and .6 m overhang (eave) were constructed of nominal 5 x 10 cm lumber. The trusses were erected on .6 m centers and supported on sleepers placed on the ground running down the roadway side slope. The trusses were then decked with 1.27 cm thick plywood to form the roof. Plywood was also nailed on the upper and lower ends, and the longitudinal wall of the snow sheds. A gap was left open at the top of the longitudinal wall to allow adequate ventilation while avoiding snow accumulation within the shed. The sheds were oriented with ventilation gaps facing away from the direction of traffic, to prevent plows from throwing snow into the sheds. Following construction, the snow sheds were spray painted white to reflect solar radiation during the summer months. Figure 2 shows the pattern of snow accumulation on the sheds in March. Note the ventilation openings.

Eight thermocouples were installed to indicate air temperatures and ground surface temperatures inside and outside the snow sheds. Figure 3 shows the general location of these thermocouples. A Campbell Scientific Model 21X eight-channel portable data logger was located adjacent to the snow sheds to log temperature data. Once a month the temperature data were transferred to a cassette tape, and the lead acid battery powering the data logger was replaced with a fully charged one. The cassette data tape was then brought back to the University for data analysis on a microcomputer.

The snow shed constructed at the Farmer's Loop site measured 4.25 x 7.3 m covering an area of 31 m^2 as shown in Figure 4. For this installation, the trusses were erected perpendicular to the roadway with construction and materials similar to those used at the Bonanza Creek site. Air temperature was measured outside the snow shed in a weather shelter. Ground surface temperatures were measured at one location outside the snow shed and two points beneath the snow shed.

Snow Removal Area

A berm next to the embankment at the Bonanza Creek site was kept clear of snow during the winter of 1985-86. The size of the region cleared was 6 x 21 m or an area of 126 m^2. The snow was removed once a month if accumulation had occurred.

DATA ANALYSIS

Temperature data were recorded beginning in July of 1985 at the Bonanza Creek site and October of 1985 at the Farmer's Loop site. Temperature data were recorded for the entire thawing and freezing season between October, 1985 and October, 1986. The output of the thermocouples was sampled at 60 minute intervals, and then a daily average was calculated and stored by the data logger. A microcomputer was used to calculate mean monthly soil surface and air temperatures, and freezing or thawing degree days as appropriate. The ratio of surface freezing or thawing degree days to air freezing or thawing degree days were

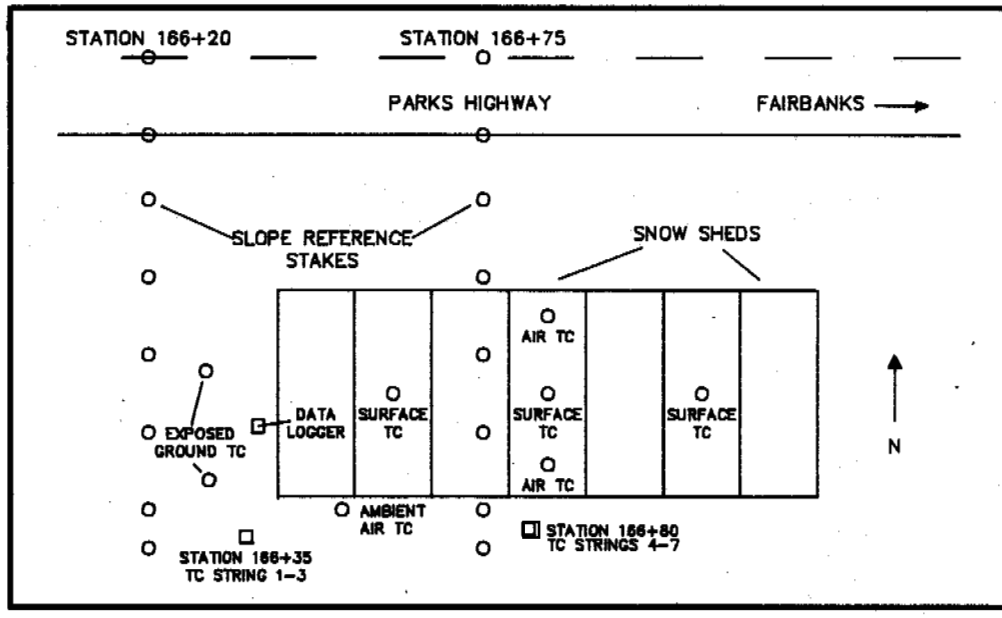

Figure 3. Bonanza Creek snow sheds showing thermocouple placement and slope reference stakes.

TABLE I

Temperatures at the snow sheds (°C)

Bonanza Creek						Farmers Loop			
	Air		Ground				Air	Ground	
Month	Ambient	In Shed	Exposed	In Shed	No Snow	Month	Ambient	Exposed	In Shed
08/85	12.1	11.3	15.1	8.3	---	11/85	-21.5	-3.2	-11.1
09/85	4.7	4.4	7.5	3.5	---	12/85	-15.2	-3.7	-9.8
10/85	-8.1	-7.7	-0.9	-2.1	---	01/86	-21.1	-5.7	-13.1
11/85	-20.2	-19.1	-4.8	-9.4	---	02/86	-16.7	-6.1	-12.2
12/85	-15.1	-14.2	-3.2	-8.5	---	03/86	-15.4	-6.7	-12.6
01/86	-20.4	-19.4	-4.7	-11.9	-8.7	04/86	-4.7	-3.1	-5.4
02/86	-14.9	-14.3	-4.9	-10.0	-10.0	05/86	8.9	7.8	4.1
03/86	-15.5	-15.6	-5.8	-11.8	-10.9	06/86	16.1	14.1	11.1
04/86	-5.6	-6.4	-0.1	-5.8	-4.2	07/86	16.9	15.4	13.7
05/86	8.0	6.7	10.1	1.9	8.1	08/86	11.8	10.8	9.8
06/86	16.2	14.5	18.4	7.7	---	09/86	6.7	6.2	5.7
07/86	17.3	16.1	20.7	11.0	---	10/86	-4.4	0.1	-0.7
AVG.	-3.5	-3.6	3.9	-2.3	---	AVG.	-3.2	2.1	-1.7

calculated for each month, as well as for the freezing and thawing seasons. The results of the data analysis are presented in Table I for the Bonanza Creek and Farmer's Loop sites.

Bonanza Creek Site

The data shown in Table I allows an evaluation of the performance of the snow sheds at the Bonanza Creek site in reducing the ground surface temperature. The maximum snow depth during the winter of the study period was 30.5 cm. The mean annual air temperature for the period of August 1985 through July 1986 was -3.5°C, while the average ground surface temperature beneath the sheds was -2.3°C or 1.2°C above air temperature. The mean annual air temperature for the four-year period beginning in 1975 for this site was -2.7°C, whereas the ground surface in the area where the sheds were subsequently located was 5.0°C, more than 7.7°C above mean annual air temperature. The long-term average maximum snow depth at a site near the study area is 56 cm. It is interesting to note that the mean annual ground surface temperature for 1985-86 was 3.9°C outside the snow shed on the south slope. Therefore, we conclude that the snow sheds have had a major effect on cooling the ground.

The n-factor data from 1975-79 and 1985-86 are summarized in Table II for the Bonanza Creek site. When compared to the undisturbed exposed slope, the snow sheds approximately doubled the surface freeze n-factor and halved the surface thaw n-factor. Improved protection for the underlying permafrost resulted from this

TABLE II

N-factor comparisons from the 1975-79 data and the 1985-86 data at Bonanza Creek.

	Exposed Slope 1975-79	Exposed Slope 1985-86	Snow Shed 1985-86	Air thawing and freezing indices 1985-86
n_t	1.72	1.25	0.55	1,767 C°-day
n_f	0.40	0.28	0.59	3,068 C°-day

increased winter cooling and reduced summer warming of the ground surface. The exposed embankment slope surface n-factors for the two observation periods differed significantly as shown in Table II. These differences in n-factors may be the result of different solar exposure due to vegetation growth differences and sensor positioning, and to differences in wintertime snow depths.

Farmer's Loop Site

Data were recorded at the Farmer's Loop Road snow sheds starting in August of 1985. At the completion of one annual temperature observations cycle, the n-factor data show the same trend as the data from Bonanza Creek. Table III summarizes this n-factor data.

TABLE III

N-factor data from the Farmer's Loop snow sheds.

	Exposed slope 1985-86	Snow shed 1985-86	Air thawing and freezing indices 1985-86
n_t	.88	.66	1,649 C°-day
n_f	.30	.67	2,976 C°-day

During the test period the mean annual air temperature, mean annual soil surface temperature-exposed, and mean annual soil surface temperature with snow sheds were -3.2°C, 2.1°C and -1.7°C, respectively. The maximum snow depth attained at the site during this period was approximately 30 cm while the long-term average maximum at a site near the study area is 61 cm. Again, the effect of the snow shed is to reduce the ground surface temperature, in this case by 3.9°C. The mean annual soil surface temperature beneath this snow shed is -1.7°C and as a result, refreezing and stabilization of the embankment slope should occur over a period of time. The surface thawing n-factor for the exposed slope is about one-half the value for the same parameter at Bonanza Creek. This is most likely explained by the heavier vegetative ground cover, the lower slope height and the less southerly exposure of the Farmer's Loop site.

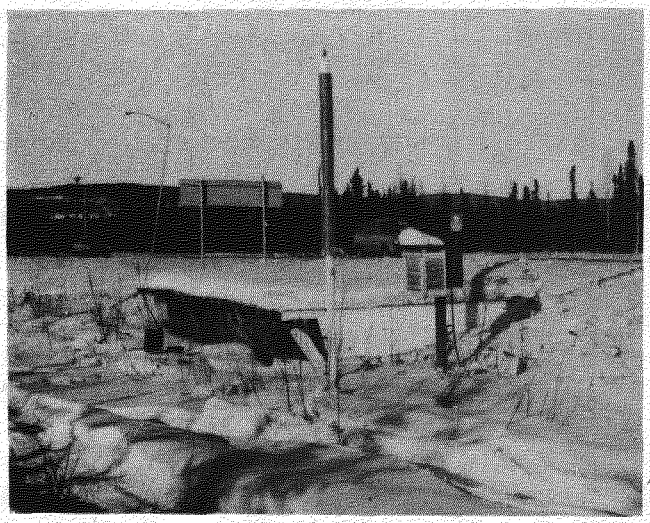

Figure 4. Farmer's Loop Road snow shed.

Snow Removal Area

The benefits of snow removal from the top of the section of the embankment berm were not nearly as notable as at the snow shed section. This is to be expected because the snow was only removed monthly and the treatment width was only 6.1 m. Removal of the snow from the 2:1 embankment side slopes was not found feasible due to the steepness and the presence of large rocks. Evidence of a benefit from the snow removal was found during the annual thaw depth probing surveys, done in late September of 1986. At that time a layer of residual frost approximately 15 cm in thickness was encountered beneath the snow cleared areas at a depth between 1.2 m to 1.5 m. Probing could penetrate this layer if considerable effort was expended. However, the presence of residual frost from the prior winter at this late date indicated that the snow removal had the effect of preventing the further progression of annual thawing into the underlying permafrost.

Temperatures recorded at the ground surface on the snow removal area did not cover the entire winter due to equipment problems. Data recorded are shown in Table I in the "no snow" column. Extrapolation of this data over the full season indicates that the freezing n-factor resulting from periodic snow removal was approximately 0.50 and that the average resultant mean annual surface temperature was very close to 0°C.

At both study sites during the winter season of the study period, the snowfall and the maximum depth of snow accumulation were approximately half of the long-term averages of these values. It could be expected that during a year of average snowfall the surface freezing index for exposed ground would be lessened due to the increase of the insulating ability of the snow cover. In this case the usefulness of snow sheds and snow removal in lowering the MASST would be accentuated when compared to an area retaining the natural snowfall through the winter.

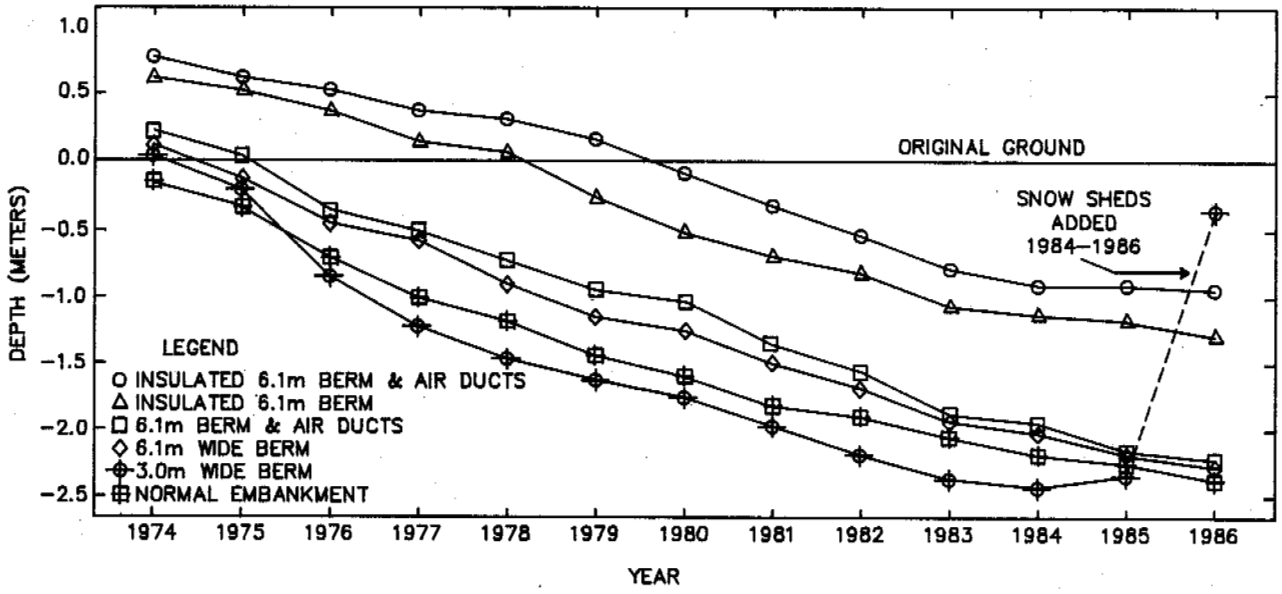

Figure 5. Maximum annual thaw depths versus time at a distance of 2.4 m inside of the embankment toe.

Observations of Thaw Depth and Slope Movement

At the Bonanza Creek site, the presence of previously installed subsurface temperature sensors permitted an analysis of the effects of the snow sheds on reducing the maximum thaw depth beneath the side slopes. Figure 5 shows the changes in thaw depth over time at a distance of 2.4 m inside of the embankment toe. Thawing at this location is especially critical as the embankment slopes and roadway shoulders are supported by the soil in this zone. It can be seen that the addition of the snow sheds resulted in a reversal of the previous trend toward deeper thawing each year. In 1986 the maximum depth of thaw beneath the snow sheds was observed to be approximately 2.0 m less than in 1985. This indicates that a thin layer of permafrost had been formed beneath the roadway side slope. Calculations indicate that the talik in this area would be returned to a permafrost state in six to eight years. The shed treatment was the only method found successful for preventing progressively deeper thawing beneath the lower embankment slopes.

The effectiveness of the sheds in slowing the slope movements was indicated by annual elevation surveys. Three of the four lower slope movement reference stakes showed no significant settlements between the 1984 and 1986 annual fall surveys. Movements of the roadway surface in this area were also observed to be significantly less than in adjacent areas without the sheds.

CONCLUSIONS

Two methods for reducing the thermal degradation of permafrost along roadways were evaluated. Snow sheds lowered the mean annual soil surface temperature to -2.3°C beneath the sheds as compared to 3.9°C for the exposed ground. A low-cost easily deployable system utilizing this concept should be developed to stabilize problem roadway sections built over non-thaw stable permafrost. Both man-made and natural (vegetative cover) systems should be reviewed.

ACKNOWLEDGMENTS

The State of Alaska Department of Transportation and Public Facilities supported this study.

REFERENCES

Berg, R.I. and Esch, D.C. (1983). Effect of Color and Texture on the Surface Temperature of Asphalt Concrete Pavements. Proc. 4th Int. Perfmafrost Conf., 59-61, Fairbanks.

Esch, D.C. (1973). Control of Permafrost Degradation Beneath a Roadway by Subgrade Insulation. Permafrost: North American Contribution (to the) Second International Conference, 608-621, Yakutsk, Siberia.

Esch, D.C. (1983). Evaluation of Experimental Design Features for Roadway Construction over Permafrost. Proc. 4th Int. Permafrost Conf., 283-288, Fairbanks.

Lunardini, V.J. (1981). Heat Transfer in Cold Climates, 731 pp. Van Nostrand Reinhold Co., New York.

Zarling, J.P., Connor, B. and Goering, D.J. (1983). Air Duct Systems for Roadway Stabilization over Permafrost Areas. Proc. 4th Int. Permafrost Conf., 1463-1468, Fairbanks.

METHOD FOR CALCULATING FROST HEAVE REACTION FORCE IN SEASONAL FROST REGION

Zhou, Youcai

Heilongjiang Provincial Institute of Low Temperature Construction Science Harbin, China

SYNOPSIS A method for calculating frost heave reaction force acting on enlarged pile foundation is discussed. According to the measured data from Yanjiagang Observation Station, it is obtained that the stress due to reaction force caused by tangential frost heave force is distributed as a power-function curve within the area of restrained width of the foundation. When the frost depth is approaching or equal to its maximum value, the restrained width of foundation is about 1.5 times the maximum frost depth. The author had derived 8 formulas for calculating frost heave reaction acting on enlarged pile foundation in various conditions.

INTRODUCTION

The enlarged pile foundation, which can bear frost heave reaction force with its enlarged head, suppresses the tangential frost heave force acting on the pile, so that it has an effect of self-anchor. It was generally recognized that the enlarged head was pressed downwards by the frost heave reaction force. This theory was put forward at first by B.E. dalmatov (1959). In recent years, the frost heave reaction force is being studyed by the Third Designing Institute of the Ministry of Railway and Heilongjiang Provincial Hydraulic Science Research Institute (Sui, 1985). But up-to-date, different views and calculating methods of the frost heave reaction force are existed.

For researching the methods of calculating the frost heave reaction force, experiments on the strong frost-susceptible soils in Yangjiagang Observation Station were conducted, where the terrain is flat and covered with the fine grained soil and the amount of the free frost heave is homogeneous. A test pile with the cross-section area of 30x30 cm was buried down to the depth of 130 cm in Oct. 1983 (Fig.1a), and 3 pile foundations with the cross-section area of 30x30 cm and the enlarged plates of 60x60, 90x90 and 120x120 cm, respectively, were buried down to the depth of 150 cm in July 1984 (Fig.1b,c and d). All of test foundations are made of relinforced concrete. Not only the frost heave forces are measured with dynamometers but also the deformations of the foundations and the ground surface in the constrained area of the foundation are measured. On the basis of analysing the measured data, 8 formulas are for calculating the frost heave reaction force deduced. Comparing with the formula proposed by B.E.Dalmatov, these formulas are with a higher accuracy.

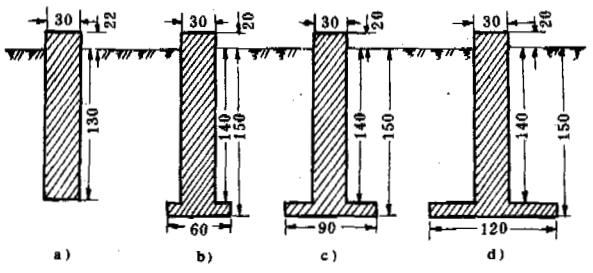

Fig.1 Schematic Diagram of Test Model Foundations

CALCULATION OF FROST HEAVE REACTION FORCE ON ENLARGED PILE FOUNDATION ACCORDING TO TANGENTIAL FROST HEAVE FORCE ON THE PILE FOUNDATION

In calculating it is assumed that the frost heave amount of any circular cross-section apart from the lateral surface of the foundation is equal in the constrained area; the constrained width (radius) around the foundation is equal along radius,and the soil, temperature and moisture condition are the same in the constrained range of the pile foundation.

According to the measured data in Yanjiagang Observation Station (Zhou, 1985) the frost heave amount of ground surface along the radial direction of a foundation within the constrained width is distributed as an increasing power function (see curve 1 in Fig.2).

which can be written as

$$Y = \Delta h(\frac{x}{L})^{\beta} \qquad (1)$$

where $\Delta h = \Delta H - \Delta H_1$

ΔH — free frost heave amount on the ground surface beyond the constrained area of foundation;

ΔH_1 — frost heave amount of the ground near the lateral surface of pile foundation;

L — constrained width of foundation, and

$\beta < 1.0$ — power relating to soil characteristic, free frost heave amount and the thickness of frozen layer.

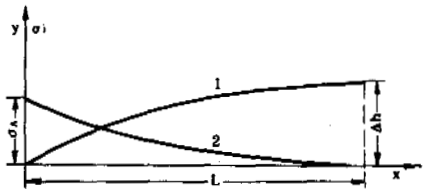

Fig.2 Curves of Frost Heave Amount on Ground Surface (1) and Vertical Frost Heaving Stress on Frost Front (2) Within the Constained Area of a Foundation

If not considering the self-weight of frozen layer, the vertical frost heave stress on frost front near the lateral surface of the pile foundation can be estimated by

$$\sigma_A = C\Delta h \qquad (2)$$

Within the constrained area of the foundation, the distribution of vertical frost heave stress (σ_i) on frost front can be described by decreasing power function (curve 2 in Fig.2):

$$\sigma_i = \sigma_A[1-(\frac{x}{L})^\beta] = C\Delta h[1-(\frac{x}{L})^\beta] \qquad (3)$$

where $C=\frac{T}{V}$ — coefficient of frost heave of base soil;

F — tangential frost heave force, and

V — reducing volume of the base soil within the constrained area due to frost heave.

Similar curves of frost heave amount and vertical frost heave stress around a foundation were observed by E.Penna (1974).

Calculation of frost heave reaction force of cricular enlarged pile foundation

The vertical frost heave forces on frost front acting upward and downward are equal in magnitude and opposite in direction. The frost heave reaction force is composed of the tangential frost heave force and the self-weight pressure of frozen soil layer. The tangential frost heave force equals the total amount of the vertical frost heave stress on frost front, i.e.,

$$T = 2\pi\xi F_p \qquad (4)$$

where F_p — vertical frost heave stress per unit length, and

ξ — coordinates of the center of gravity of the vertical frost heave stress diagram in X axis (see Fig.3).

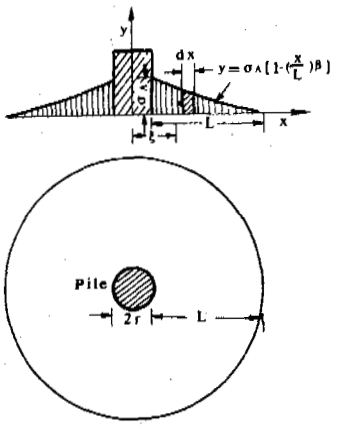

Fig.3 Diagram for Calculating the Tangential Frost Heaving Stress on a Circular Pile

They can be calculated as follows:

$$F_p=\int_0^L \sigma_A[1-(\frac{x}{L})^\beta]dx = \frac{\sigma_A\beta L}{1+\beta}$$

and $$\xi=r+\frac{1}{\frac{\sigma_A\beta L}{1+\beta}}\int_0^L[1-(\frac{x}{L})^\beta]xdx=r+\frac{(1+\beta)L}{2(2+\beta)}$$

Substitute F_p, ξ into eq.(4):

$$T = \pi\sigma_A\beta L\,(\frac{2r}{1+\beta}+\frac{L}{2+\beta}) \qquad (5)$$

where r is the radius of the pile.

The self-weight pressure of frozen soil layer can be evaluated by

$$M = L(2r + L)\,T^H \qquad (6)$$

where T is the unit weight of frozen soil.

From eq.(5), we have

$$\sigma_A = \frac{T}{\pi\beta L[\frac{2r}{1+\beta}+\frac{L}{2+\beta}]} \qquad (7)$$

Then, the maximum frost heave reaction force on frost front can by calculated by

$$P_{Amax}=\pi L\{\sigma_A\beta[\frac{2r}{1+\beta}+\frac{L}{2+\beta}]+\gamma_T H(2r+L)\} \quad (8)$$

The area of the enlarged plate is generally less than that of the constrained range of foundation, and the plate is buried bellow frost front. If the frost heave stress on freezing front transfers downwarde with the diffusion angle of $\theta°$, the width of distribution of frost heave reaction force at the depth of h from freezing front can be estimated by

$$L_h = L + h\mathrm{tg}\theta°$$

Substitute L_h for L and σ_a for σ_A, then eq.(5) becomes

$$T = \pi\sigma_a\beta L\ (\frac{2r}{1+\beta}+\frac{L_h}{2+\beta}) \quad (9)$$

This is the sum of the vertical stress of the frost heave reaction forces caused by the tangential frost heave force on the plane with the width of L and depth of h beneath freezing front.

If neglecting self-weight pressure of frozen soil layer, the vertical stress of the frost heave reaction force at the depth of h and near the lateral surface of the pile is

$$\sigma_a = \frac{T}{\pi\beta L_h[\frac{2r}{1+\beta}+\frac{L_h}{2+\beta}]} \quad (10)$$

On the plane at the depth of h, the vertical stress caused by the self-weight pressure of frozen soil layer per unit area is

$$\sigma_h = \frac{(2r+L)L}{\pi\beta L_h[\frac{2r}{1+\beta}-\frac{L_h}{2+\beta}]}\gamma_T H \quad (11)$$

where H is the thickness of frozen soil layer.

After knowing σ_a and σ_h the frost heave reaction force acting on the circular enlarged pile foundation below freezing front with a depth of h and verge length of t (see Fig.4) can be calculated by

$$P_A = 2\pi(\xi F_p + \xi_h F_h) \quad (12a)$$

where F_h—area of the reaction caused by the weight of frozen soil, and

ξh— coordinate of the center of gravity of the area in X axis.

For a curved quadrangle, F_p and ξ could be calculated as follows

$$F_p = \int_0^t \sigma_a[1-(\frac{x}{L_h})^\beta]dx=\sigma_a t[1-\frac{1}{1+\beta}(\frac{t}{L_h})^\beta]$$

$$= r+\frac{1}{F_p}\int_0^t \sigma_a[1-(\frac{x}{L_h})^\beta]xdx=r+\frac{\sigma_a t^2}{2F_p}[1-\frac{2}{2+\beta}(\frac{t}{L_h})^\beta]$$

Substitute F into the above formula, then

$$\xi = r+\frac{t}{2}\frac{1-\frac{2}{2+\beta}(\frac{t}{L_h})^\beta}{1-\frac{1}{1+\beta}(\frac{t}{L_h})^\beta}$$

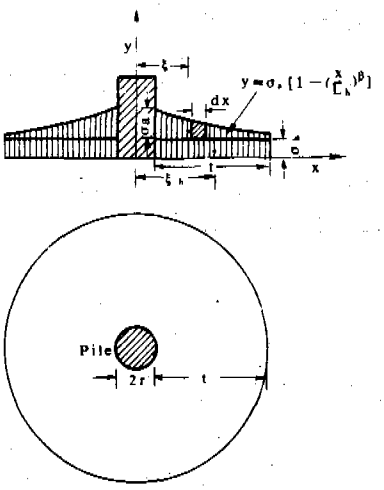

Fig.4 Diagram for Calculating the Frost Heave Reaction on a Enlarged Circular Pile Foundation

Substitute F_p and ξ into eq.(12a), we have

$$P=2\pi rt\{\sigma_a[1-\frac{1}{1+\beta}(\frac{t}{L_h})^\beta]+\sigma_h\}+\pi t^2\{\sigma_a[1-\frac{2}{2+\beta}(\frac{t}{L_h})^\beta]+\sigma_h\} \quad (12)$$

When the groundwater table is lower than the enlarged head, the reaction force equation should be written as

$$P_A=2\pi rt\{\sigma_a[1-\frac{1}{1+\beta}(\frac{t}{L_h})^\beta]+\sigma_h\}+\pi t^2\{\phi\sigma_a[1-\frac{2}{2+\beta}(\frac{t}{L_h})^\beta]+\sigma_h\} \quad (13)$$

where $\phi < 1.0$ is a reduction factor of the tangential frost heave force.

The formulas 12 and 13 show that the relation between the frost heave reaction force of the circular enlarged pile foundation and the length of verge board is of a parabola. When using the formulas 12 and 13 to calculate the frost heave reaction force on the enlarged head at freezing front, it is necessary to substitute L for L_h, σ_A for σ_a, $\gamma_T H$ for σ_h, i.e.,

$$P_A=2\pi rt\{\sigma_A[1-\frac{1}{1+\beta}(\frac{t}{L})^\beta]+\gamma_T H\}+\pi t^2\{\sigma_A[1-\frac{2}{2+\beta}(\frac{t}{L})^\beta]+\gamma_T H\} \quad (14)$$

$$P_B=2\pi rt\{\phi\sigma_A[1-\frac{1}{1+\beta}(\frac{t}{L})^\beta]+\gamma_T H\}+\pi t^2\{\phi\sigma_A[1-\frac{2}{2+\beta}(\frac{t}{L})^\beta]+\gamma_T H \quad (15)$$

Calculation of the frost heave reaction force on the square enlarged pile foundation

The tangential frost heave force of the square enlargel pile foundation is considered to be composed of the tangential frost heave forces at the straight line segments and at the conners of the square pile foundation. If not considering the vertical frost heave stress caused by the weight of the frozen soil layer, the tangential frost heave force on the straight line segments can be calculated by integrating formula (3) (areas of A in Fig.5); while the

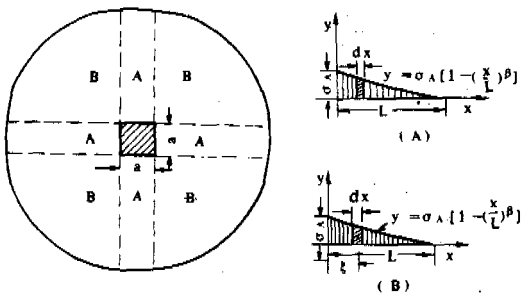

Fig.5 Diagram for Calculating the Tangential Frost Heave Force on a Square Pile Foundation

tangential frost heave force at the conners are formed a circle (areas of B in Fig.5). Which can be calculated with formula (4), but the item of r in the equation of (5) needs to be canceled, i.e.,

$$T=4a\int_0^L\sigma_A[1-(\frac{x}{L})^\beta]dx+2\pi\frac{\sigma_A\beta L}{1+\beta}\cdot\frac{(1+\beta)L}{2(2+\beta)}=\sigma_A\beta L[\frac{4a}{1+\beta}+\frac{\pi L}{2+\beta}] \quad (16)$$

where a — length of sides of the square enlarged pile foundation.

when not considering the weight of frozen soil layer, the vertical frost heave force close to the lateral surface of the pile on freezing front is expressed as:

$$\sigma_A=\frac{T}{\beta L[\frac{4a}{1+\beta}-\frac{xL}{2+\beta}]} \quad (17)$$

At a depth of h below freezing front the sum of the vertical stresses of the frost heave reaction force is:

$$T=\sigma_a\beta L_h[\frac{4a}{1+\beta}+\frac{\pi L_h}{2+\beta}] \quad (18)$$

where $L_h=L+h\,tg\theta°$ and σ_a is the vertical frost heave reaction stress close to the lateral surface of the pile, which can be calculated by

$$\sigma_a=\frac{T}{\beta L_h[\frac{4a}{1+\beta}+\frac{\pi L_h}{2+\beta}]} \quad (19)$$

At a depth of h below the freezing front the vertical stress of reaction force caused by the weight of frozen soil layer per unit area is:

$$\sigma=\frac{(4a+\pi L)L}{(4a+\pi L_h)L_h}\gamma_T H \quad (20)$$

Knowing σ_a and γ_h, we can calculate the frost heave reaction force on the enlarged square pile foundation at any depth below freezing front. This reaction force is made up of two parts: one is the reaction force for the straight line segment (areas of a in Fig.6) and another at the conners of the square foundation (areas of B om Fig.6).

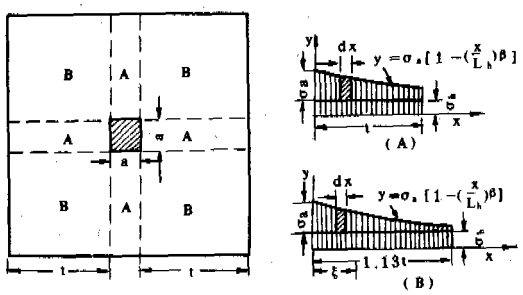

Fig.6 Diagram for Calculating the Frost Heave Reaction on an Enlarged Square Pile Foundation

The former can be calculated by integrating the vertical reaction stresses over the areas, and the latter can be considered as the reaction force acting on a square plate with the side length of 2t. For convenience it can be considered to be equivalent a circular plate with a radius of R, and on which the reaction force caused by the tangential frost heave force can be calculated with eq.(4). Thus, the total reaction force on the enlarged square foundation can be estimated by

$$P=4a\int_0^t\sigma_a[1-(\frac{x}{L_h})^\beta]dx+4at\sigma_h+2\pi\xi F_p+\pi R^2\sigma_h \quad (21a)$$

In which, R=1.13t; F_p and ξ can be calculated by

$$F_p=\sigma_a R[1-\frac{1}{1+\beta}(\frac{R}{L_h})^\beta]$$

and $$\xi = \frac{1-\frac{2}{2+\beta}(\frac{R}{L_h})^{\beta}}{1-\frac{1}{1+\beta}(\frac{R}{L_h})^{\beta}}$$

Substituting the expressions of R, F_p and ξ into eq.(21a), we have

$$P_A=4at\{\sigma_a[1-\frac{1}{1+\beta}(\frac{t}{L_h})^{\beta}]+\sigma_h\}+4t^2\{\sigma_a[1-\frac{2}{2+\beta}(\frac{1.13t}{L_h})^{\beta}]+\sigma_h \quad (21)$$

When the groundwater table is lower than the enlarged plate, eq.(21) becomes

$$P_B=4at\{\phi\sigma_a[1-\frac{1}{1+\beta}(\frac{t}{L_h})^{\beta}]+\sigma_h\}+4t^2\{\phi\sigma_a[1-\frac{2}{2+\beta}(\frac{1.13t}{L_h})^{\beta}]+\sigma_h \quad (22)$$

If using eqs.(21) and (22) to calculate the frost heave reaction force on freezing front it is necessary to substitute L for L_h, σ_A for σ_a and $\gamma_T H$ for σ_h in the two equation, i.e.,

$$P_A=4at\{\sigma_A[1-\frac{1}{1+\beta}(\frac{t}{L})^{\beta}]+\gamma_T H\}+4t^2\{\sigma_A[1-\frac{2}{2+\beta}(\frac{1.13t}{L})^{\beta}]+\gamma_T H\} \quad (23)$$

$$P_B=4at\{\phi\sigma_A[1-\frac{1}{1+\beta}(\frac{t}{L})^{\beta}]+\gamma_T H\}+4t^2\{\phi\sigma_A[1-\frac{2}{2+\beta}(\frac{1.13t}{L})^{\beta}]+\gamma_T H\} \quad (24)$$

COMPARISON BETWEEN THE MEASURED AND CALCULATED VALUES OF FROST HEAVE REACTION FORCE

The frost heave reaction forces were measured at the field test station in 1984-1985, when the maximum free frost heave amount is 26.78 cm and the maximum thickness of frozen layer is 147 cm. The observed values of the frost heave reaction for the three square test foundations with the verge length (t) of 15, 30 and 45 cm are 1.32×10^4, 3.10×10^4 and 5.25×10^4N, respectively.

As the groundwater table at the test site is lower than the bottom of the test foundations, the frost heave reaction force should be calculated with eq.(22). By using the parameters of $\beta=0.4$, $L_h=187.99$ cm, $a=30$ cm, $\gamma_T=0.0188$ N/cm^3, $\sigma_a=0.03696$ MPa, $\sigma_h=0.02555$ MPa and $\phi=0.908$, 0.817 and 0.725 for t=15, 30 and 45 cm, respectively, the frost heave reaction forces on the test foundations were calculated with eq.(22). The calculated results, together with the observed values, are shown in Table I. It is seen from the Table I that the calculated results are in a good agreement with measured values, indicating that the formulas for calculating the frost heave reaction presented are reliable.

TABLE I

Comparison Between the Calculated and Observed Values of Frost Heave Reaction for Various Foundations

Verge length of enlarged plate (cm)	Values of frost heave reaction, x10^4N		Error (%)
	Observed	Calculated	
15	1.32	1.34	+1.59
30	3.10	3.18	+2.78
45	5.25	5.41	+3.12

CONCLUSIONS

(i) When the frost heave reaction force on an enlarged foundation is calculated on the basis of tangential frost heaving force, the tangential frost heaving force should not be reduced if the groundwater table is higher than the enlarged plate, whereas it should be reduced according to the verge length of the enlarged head if the groundwater table is lower than the plate.

(ii) At the Yanjiagang Field Station where the maximum free frost amount is about 26-28 cm and the maximum frost depth is about 150 cm, the tangential frost heaving force will be completely balanced by the frost heave reaction when the verge length is not less than 55% or 40% of the thickness of frozen layer as the groundwater table is higher or lower than the enlarged plate.

(iii) Investigation shows that the relation between frost heave reaction and the verge length of englarged plate is parabolic.

REFERENCES

Cui Chenghan and Zhou Kaijiong, (1983). The experimental research of the frost heave reaction force, Proc.of Second National Conference on Permafrost, p.260-263,People's Publishing House of Gansu.

Dalmatov, B.E., (1959). The frost heave of soil acting on constructions, Book are translated by Harbin Industrial University, Construction-industrial Publishing House.

Panna, E., (1974). The frost heave force acting on the foundation of structures in frost soil, Canadian Geotechnical of Journal, Vol.11, No.3.

Sui Xianzhi, (1985). Calculation of frost heave reaction force on the enlarged pile foundation in seasonal frozen region, Journal of Glaciology and Geocryology, Vol.7, No.4.

Zhou Youcai, (1985), The calculation of frost heave force according to frost heave deformation in the constrained area of foundation, Journal of Glaciology and Geocryology, Vol.7, No.4.

COLD-MIX ASPHALT CURING AT LOW TEMPERATURES

A.N.S. Beaty and P.M. Jarrett

Royal Military College of Canada

SYNOPSIS

In July 1981 a series of cold-mix asphalt test sections were constructed at CFS Alert, situated at 82° N in the Canadian North West Territories. The performance of these test sections has been monitored with particular reference to the rate of curing, the change in strength with age and the long term effects of the asphalt pavement, both painted white and unpainted, on the permafrost régime. The observed data are presented and the performance of cold-mix asphalt in the environment of the high Arctic is discussed.

INTRODUCTION

Asphalt cold-mix is a mixture of unheated mineral aggregate and emulsified or cutback bitumen. Mixtures may be prepared either in a central plant or in place at the paving site using simple equipment.

The advantages claimed for cold-mix asphalt include:

- its adaptability to suit the requirements of a range of aggregate types in varying weather conditions.
- economy of production with simple equipment and unheated aggregate.

The most important of these advantages arise from not having to heat the aggregate. This makes the use of cold-mix asphalt particularly attractive at remote northern job sites where provision of heating would be difficult and expensive. The Asphalt Institute (1977) has suggested that cold-mix asphalt operations should be limited to temperatures above 10°C and to good weather conditions. In the high Arctic, road and runway pavements may have to be constructed at remote sites where neither the atmospheric temperature nor that of the aggregate will normally reach 10°C. However, Wocjik, Jarrett and Beaty (1983) and Jarrett, Beaty and Wocjik (1984) have shown that cold-mix operations can be succesfully carried out at temperatures approaching the freezing point.

The low temperature work referred to arose from a requirement to study viable methods for the stabilisation of the unbound aggregate runway at Alert, located at 82°30'N, 62°20'W in the Canadian North West Territories as shown in figure 1. In that study the general question of low temperature stabilisation was addressed using low temperature laboratory testing, pilot field trials and in 1981 a series of full scale trial sections at Alert.

The purpose of the present paper is to review the performance of the full-scale trial sections of cold-mix asphalt over the six years since they were laid and in particular to consider the following:

- rate of curing
- strength variation with time
- effect of asphalt on ground thermal régime
- general performance of the paved surfaces

FIELD TEST SECTIONS

In July 1981 a series of nine test sections was constructed on the runway apron at Alert. These consisted of a basecourse of crushed rock aggregate, compacted at a moisture content of 6% to a finished thickness of 8cm. Two low viscosity cut-back bitumens were used, these were an RC-30 and a primer, both produced by Gulf Oil. Using a range of binder contents, nine mixtures were made by mixing the binder with unheated crushed rock aggregate at about 4°C, in a Cedar Rapids pug mill having a capacity of 700 tonnes per hour. Binder contents ranged from 3.5% to 8.7% for the RC-30 mixtures and from 5.0% to 6.4% for those made with the primer binder. The mixtures were laid in four 3.8 metre wide lanes and compacted with a 9 tonnes vibrating roller. In order to investigate the effects of the construction on the permafrost régime approximately half the surface area was painted white and a series of thermistors were installed beneath the various

paved sections and the gravel runway to a maximum depth of 1.5 metres.

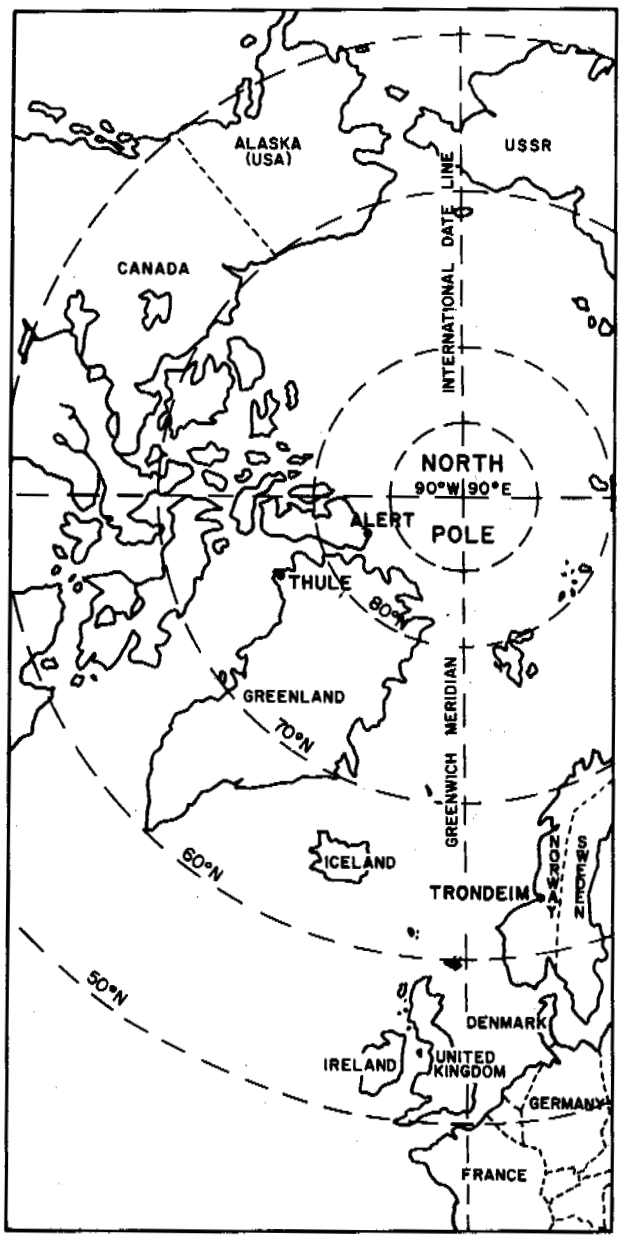

Figure 1 The location of Alert

LOW TEMPERATURE CURING

During mixing and laying, aeration of the mixture occurs and solvent is lost. At low temperatures this solvent loss during aeration must be limited in order to ensure that the mixture retains adequate workability for spreading and compaction. Based on a maximum viscosity, for workability, of 100 000 centistokes, suggested by Lefebvre (1966), a solvent loss of 43% could be allowed. However if the ultimate air voids content on completion of curing is not to exceed 6% as recommended by Field (1966), much less solvent loss during aeration can be permitted, in fact only 12%. Griffin, Miles and Simpson (1957) considered that 80% loss of solvent with mixtures made with RC-30 binder might constitute full curing. It may be that at the low ambient temperatures prevailing at Alert, full curing corresponds to even less than 80% solvent loss, in which case more than 12% loss could be permitted during aeration without increasing the final air voids content beyond 6%.

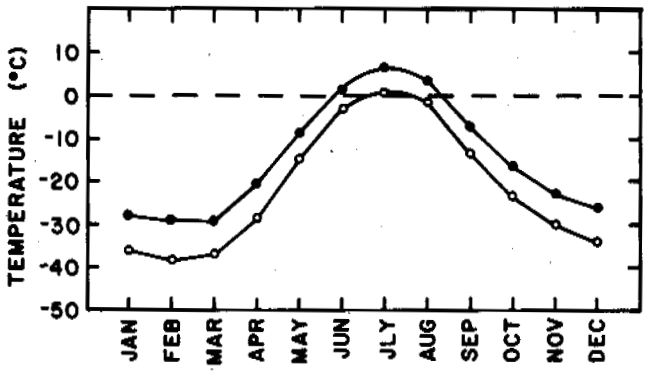

Figure 2 Mean of daily maximum and minimum air temperatures at CFS Alert

The mean daily temperature at CFS Alert is -18°C. The extreme values of temperature recorded are -49.4°C and +20.0°C. Figure 2 shows the mean values of daily maximum and minimum temperatures for each month. From this it can be seen that in an average year one might expect four frost-free weeks and a further seven weeks during which the daily maximum temperature is above the freezing point. During the brief construction season, the mean daily temperature is about 4°C. These are the ambient conditions in which curing of the asphalt takes place after laying and compaction.

The degree of curing was determined over a period of 60 days by direct weighing of laboratory Marshall specimens cured in a refrigerator at 4°C. In addition, samples were recovered from the field in 1984 and 1987 and the degree of curing under field conditions was determined by chromatography carried out by Gulf Canada.

These data are combined in figure 3, which shows, for the basic design mixture having an initial binder content of 5.1% by weight of RC-30, the degree of curing against time for the six years from 1981 to 1987.

On the assumption that no significant curing occurs at temperatures below 0°C, there are approximately 77 days per year during which curing may be expected to take place. Between construction in 1981 and sampling in June 1987, it is estimated that the curing period therefore corresponded to approximately 433 days. The figure indicates that some 70% of the initial solvent had been lost during this period. Griffin et al (1957) consider that 80% loss of solvent might constitute full curing for an RC-30 cut-back. Projection of the trend of figure 3 would seem to support this hypothesis.

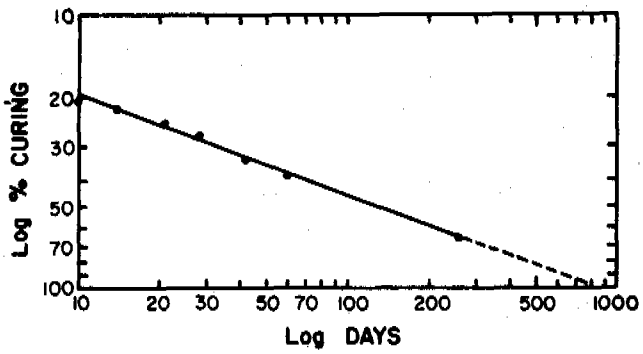

Figure 3 Degree of curing versus curing period

The degree of curing was also estimated for samples recovered in 1984 and 1987, from test strips constructed with a higher (8.7%) proportion of RC-30 cut-back binder. In this case the degrees of curing were 32% and 49% respectively, after three and six years. A sample recovered in 1984 from a test strip constructed with material having 3.5% of RC-30 cut-back as binder was estimated to be more than 90% cured. Thus it can be seen that the initial cut-back binder content significantly affects the curing rate.

STRENGTH DEVELOPMENT

Correlation between california bearing ratio and Marshall stability

Normally the development of the strength of asphalt during curing is determined by laboratory testing of samples recovered by coring. In the case of Alert, due to the remoteness of the site and the initial weakness of some of the cut-back mixtures this was not possible so it was decided to try to use the in situ CBR test as an indicator of strength. Kezdi (1979) has reported that Boromissza and Gaspar had shown a correlation between laboratory CBR values and Marshall stabilities, although the scatter was said to be excessive. Hitch and Russell (1976), however, concluded that although the CBR test might be appropriate for cement and some stabilised materials whose behaviour is essentially brittle, it was inappropriate for bituminous mixtures which behave viscoelastically. This observation was based on tests at 45°C for road bases in the tropics. The work of Gregg, Dehlen and Rigden (1967) showed that CBR values obtained on bituminous mixtures at 20°C were very much higher than those obtained at 40°C and 60°C as the binder viscosity is much increased at the lower temperature. They concluded that in situ strength of bitumen-sand bases could be measured with good repeatability using the CBR test. In the case of cold-mix asphalt one might expect more variability between individual test results due to the presence of larger aggregate particles in the mixture.

It should be noted that the strain rate in the CBR test is one-fortieth of that in the Marshall test and therefore the effective stiffness of the bitumen in the CBR test will be much lower than that in the Marshall test.

As the work at Alert was to be carried out at 4°C a laboratory study was made to determine whether CBR values correlated with Marshall stabilities measured at 4°C. For stabilities in the range 4000 to 6500 Newtons, the relationship:

Marshall Stability at 4°C = 36.5 CBR + 1925

where stability is in Newtons and CBR is a percentage was found to hold at 4°C with a correlation coefficient of 0.94.

In situ CBR tests

After construction and compaction of the test strips, in situ CBR tests were carried out over a period of 60 days and subsequently after one, three and six years in order to observe the relationship between strength and time.

Although there is considerable scatter in the results the general trend of increasing CBR with time can be clearly seen. Figure 4 shows CBR against curing time on a log-log basis for 3.5, 5.1 and 8.7% initial binder contents. The time plotted is not total elapsed time but estimated curing time taken as 77 days per year. This is the average number of days on which the minimum temperature at Alert exceeds 0°C.

It is believed that the technique of using in situ CBR tests to monitor the strength gain of asphalt cold-mix pavements could be further refined by the development of a family of temperature - CBR correlation curves. This would permit measured CBR values to be adjusted to a standard reference temperature. In the case of the work reported, the CBR-Marshall stability correlation was determined only at 4°C.

LONG TERM EFFECTS ON THE GROUND THERMAL REGIME

One critical aspect of pavement construction in permafrost areas is the effect of construction

on the ground thermal régime. This is of particular concern in the case of asphalt pavements due to their capacity for absorbing solar radiation. The deleterious effects on permafrost stability of the absorption of polar radiation have been reported by Herrion and Lobacz (1975) by Fulwider and Aitken (1962) and by others. One approach to minimising such heat absorption has been to paint the asphalt surface white in order to reflect rather than absorb heat. This is the case, for example, at the US Air Force Base at Thule (Berg and Quinn (1977).

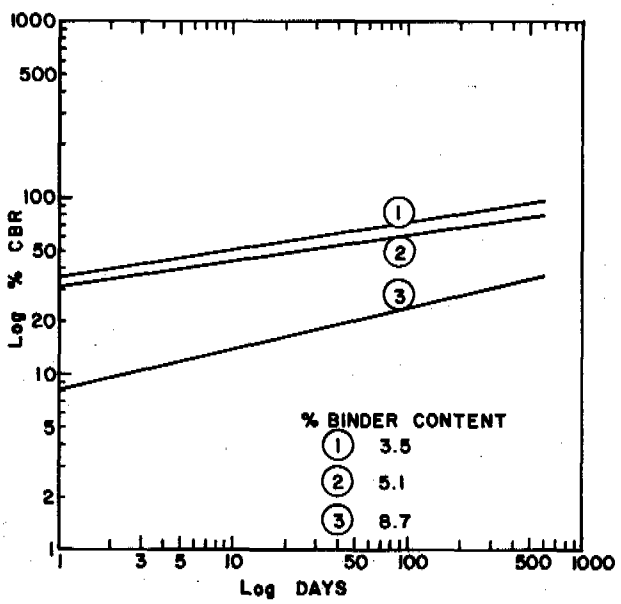

Figure 4 CBR versus curing time

In order to observe the long term effects at Alert, thermocouples were installed beneath the trial sections and in addition parts of the surface were painted white.

Figure 5 shows the profile of temperature with depth below the surface of the unpaved gravel runway at Alert, for four different dates during the Summer of 1981. Figure 6 shows temperature-depth profiles for unpaved, paved and painted, paved surfaces over the three years from 1981 to 1984. It can be seen that the depth of thaw penetration beneath the painted, paved surface was less than that under the gravel runway by about 10%. Furthermore, the depth of thaw beneath the painted surface remained remarkably constant over three years. On the other hand, the depth of thaw penetration beneath the unpainted, paved surface was generally greater than that under the gravel runway.

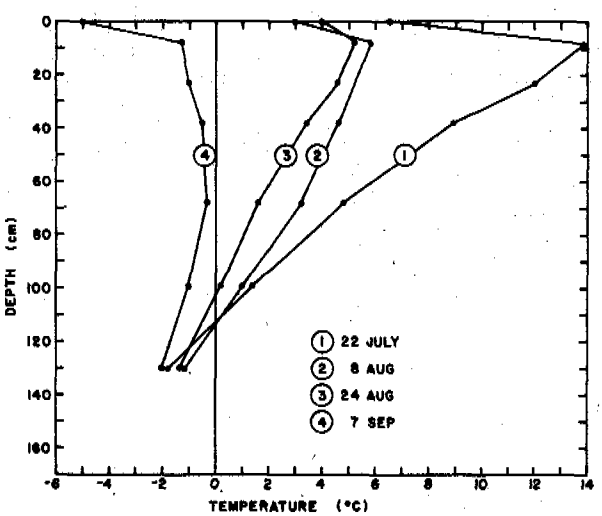

Figure 5 Temperature - depth profiles beneath unpaved runway in 1981

GENERAL PERFORMANCE OF STABILISED SECTIONS

The trial sections have been in place for six years, during which time they have been subjected to a limited amount of traffic. This has included use as a helipad, as a parking apron for Hercules transport aircraft and ground traffic associated with aircraft arrivals and departures. No systematic maintenance has been carried out. From visual inspection it appears that the sections at the design binder content of 5 to 5.5%, selectd on the basis of a modified Marshall method, Wojcik, Jarrett and Beaty (1983), have performed well and continue to do so. They appear to have sufficient strength to support the traffic and are not visibly deteriorating. The passage of a tracked vehicle over the strips shortly after their construction caused serious suface damage, but this would normally be avoidable. The lack of flexibility and cohesion of the leaner mixtures is beginning to show in the form of surface crazing. The rich mixtures containing more than eight per cent of RC-30 binder, even after six years are very soft and only half cured. They cannot support traffic in the short summer without rutting. The field performance of the test sections has shown that the binder content selected on the basis of the modified Marshall method has produced a pavement which has performed satisfactorily and has justified the use of the method.

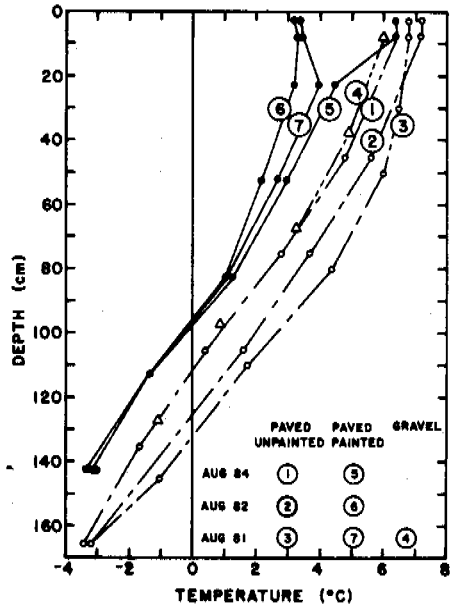

Figure 6 Temperature - depth profiles beneath unpaved, paved and painted paved surfaces

CONCLUSIONS

1. Observations of the behaviour over time of cold-mix asphalt in the extreme ambient conditions of 82° N have been presented.

2. Under these conditions the rate of curing of the mixtures is much less than that observed at higher ambient temperatures.

3. For a binder content in the range 5 - 5.5% full curing and associated strength gain has been observed to require from 6 to 10 years.

4. Curing is more rapid for lower binder contents and vice versa.

5. Although it is desirable to monitor strength gain on samples recovered by coring, at low temperatures the in situ CBR test may also prove useful.

6. Observation of temperatures beneath paved surfacing has confirmed that if the asphalt surface is painted white, thaw penetration is reduced. Conversely thaw penetration beneath the black asphalt surface was found to be greater than that under the untreated gravel runway. However, in the extreme climate of Alert the black surface does not appear to be inducing significant degradation of the permafrost.

7. The field performance of the trial sections made with the 5 to 5.5% optimum binder content as determined by the modified Marshall method has demonstrated the validity of the design approach.

REFERENCES

Asphalt Institute (1977). "Asphalt Cold-Mix Manual", MS-14, Asphalt Institute, College Park, Maryland.

Berg, R.L. and Quinn, W.F. (1977). "Use of a light coloured surface to reduce seasonal thaw penetration beneath embankments on Permafrost". Proc. 2nd. Int. Symp. on Cold Regions Engineering, Fairbanks, Alaska.

Field, F. (1966). "Mix design for bituminous pavements: method and interpretation", Proceedings, 11th annual conference, Canadian Technical Asphalt Association, v.XI, pp. 87-106.

Fulwider, C.W. and Aitken, G.W. (1962). "Effect of surface colour on thaw penetration beneath an asphalt surface in the arctic." Proc. 1st Int. Conf. on the Structural Design of Asphalt Pavements, Ann Arbor.

Gregg, J.S., Dehlen, G.L. and Rigden, P.J. (1967). "On the properties, behaviour and design of stabilised sand bases." Proc. 2nd. Int. Conf. on the Structural Design of Asphalt Pavements, Ann Arbor.

Griffin, R.L., Miles, T.K. and Simpson, W.C. (1957). A curing rate test for cut-back asphalts using a sliding plate viscometer", Proceedings, Association of Asphalt Paving Technologists, v. 26, pp. 437-467, Atlanta, Georgia.

Hennion, F.B., and Lobacz, E.E. (1973). "Corps of Engineers technology related to design of pavements in areas of permafrost." Proc. 2nd. Int. Conf. on Permafrost, Yakustk.

Jarrett, P.M., Beaty, A.N.S. and Wocjik, A.S.E. (1984). "Cold-mix asphalt technology at temperatures below 10°C", Proceedings of the Association of Asphalt Paving Technologists, Scottsdale, Arizona.

Kezdi, A. (1979). "Stabilised earth roads", Elsevier, Amsterdam.

Lefebvre, J.A. (1966). "A suggested Marshall method of design for cut-back asphalt-aggregate paving mixtures", Proceedings, 11th Annual Conference, Canadian Technical Asphalt Association, v. XI, pp. 135-181.

Wojcik, A.S.E., Jarrett, P.M. and Beaty, A.N.S. (1983). "Cold-mix asphalt stabilisation in cold regions", Proceedings IVth International Conference on Permafrost, Fairbanks, Alaska.

PROGNOSIS OF SOIL TEMPERATURE AT THE AREA UNDER CONSTRUCTION

A.L. Chekhovskyi

Research Institute of Engineering Site Investigations, Moscow, USSR

SYNOPSIS Methods and nomograms are proposed to estimate a two-three-dimensional stable temperature field when heat sources are freely arranged. To predict or to estimate a multivariate unstable temperature field with or without a change of soil phase is supposed to reduce to solvation of a one-dimensional problem. For this purpose a piecewise smooth function of boundary conditions is changed to a mean equivalent prescribed by the exponential law. The proposed approximate analytical method permits to estimate a multivariate temperature field for real conditions of town development.

From the very beginning of construction works engineering-geocryological conditions of the area under construction are exposed to great changes. This process continues when the construction works are completed.

From a thermophysical point of view an area under construction presents a combination of a number of areas with different heat release and heat absorption. A temperature field of every heat release or heat absorption area is formed under complex affects of natural and technogenic factors. If consider a city area as a whole its influence on a heat field of permafrost strata is estimated as hundreds metres and beneath individual districts and quarters of a city a depth of heat impulses penetration reaches dozens metres; under some buildings it exceeds 10-15 m a local temperature field of every specific point should be estimated with account of a temperature field of the area under construction as a whole.

To solve different engineering-geological or building problems of the area under construction it is necessary to estimate or to predict as a stable so unstable temperature field. A prognosis of a stable temperature field permits to determine a maximum depth of perennial thawing of soils under buildings and structures; to solve problems of underflooding the territory under construction; to estimate a bearing capacity of piles. An unstable temperature field permits to prognoze development of cryogenic processes; to select an engineering technology for buildings and structures, industrial sanitary communications, railways and motor roads.

Two-dimensional temperature field of a city development can be presented as a sum of integrals determined a temperature beneath a centre of the infinite band, i.e. $X_o=0$

$$T(Y_o)=\frac{Y_o}{\pi}\left[\int_{-\infty}^{m_1}\frac{T_o}{X^2+Y_o^2}\,dx+\int_{m_1}^{m_2}\frac{T_1}{X^2+Y_o^2}\,dx+\dots\right. \quad (I)$$

$$\left.\dots+\int_{m_n}^{\infty}\frac{T_n}{X^2+Y_o^2}\,dx\right]. \quad (I)$$

A surface temperature is prescribed as a piecewise smooth function $T(x)$ for every interval: $-\infty \div m_1$, $m_1 \div m_2$, $m_{n-1} \div m_n$, $m_n \div \infty$; Y_o- depth of a temperature control point; $T(Y_o)$ - ground temperature at point Y_o.

It follows from the foregoing equation that all the sources of heat release and heat absorption should be taken into account, but it presents some difficulties due to their great number. A computer-aided design shows that the remote heat sources and heat release can be neglected when measuring a temperature with an accuracy of 0.1°C and a building density varies from 0.2 to 0.8. There is a linear depen ence between a dimension of a design area (L) and a depth of a point dip (Y_o) where a temperature is measured. Function graphics $L = f(Y_o)$ for temperature differences in the intervals of the piecewise smooth function are presented in Fig. 1. For an effective design of a two-dimensional stable temperature field some nomograms are recommended (Fig.2). A procedure of a temperature measuring is as follows. The T_i^H values ("n" in number)are estimated depending on a depth of point Y_o dip; a distance from an origin of coordinates to m_i and a difference in temperatures (Δ T) at m_i point. Temperature at point Y_o can be deduced from the formula:

$$T(Y_o) = 0{,}318\sum_{i=1}^{n} T_i^H + \frac{T_o+T_n}{2} + g\,Y_o \quad (II)$$

where g - stands for a value of geothermal gradient, °C/m; for the values T_o and T_n see formula (I). Design of a three-dimensional

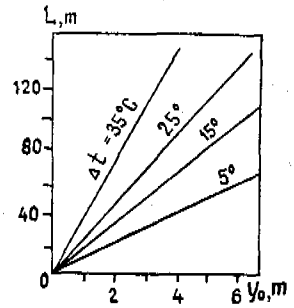

Fig.1 Dimension of a design area (L) depending on a difference in temperature ranges of a piecewise smooth function (Δ T) and a depth of Y_a point.

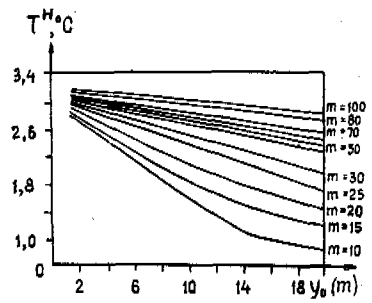

Fig.2 Chart for estimation of a two-dimensional stationary temperature pattern (Δ T = 2°C)

stable temperature field with an optional arrangement of heat sources and heat release is based on analytical methods proposed by Lachenbruch (1957), Balobaev, Shastkevich (1974), Sheikin (1976). Sheikin's method is based on solvation for a stable temperature (t_z) at a point of homogeneous ground semi-interval at depth Z under a centre of a circle-like source with R radius under a temperature within a circle countour, the temperature at this point exceeds the temperature within the rest surface by T°C. Then we have an equation: $t_Z = T\left(1 - \frac{1}{\sqrt{z^2+R^2}}\right)$. Proceed on the assumption that a temperature affect on the point at an adequate depth of some sources arranged at any area but a narrow enough concentric circular zone can be changed to an affect of an equivalent temperature (t_j). The t_j temperature is a result of arithmetic averaging temperature of all the sources with account of their area occupied in the circular zone under consideration.

In this case practical use of this method is rather difficult due to the fact that in order to determine t_j it is necessary to estimate an area occupied by every source in every circular zone. The method can be rather simplified if estimate circle stretches crossing a heat source instead of estimating the area. Circles cross a middle of every circular zone. Temperature t_j can be deduced from the following equation:

$$t_j = \frac{\sum ti \ lij}{\sum lij} \qquad \text{(III)}$$

where t_i - mean temperature of a heat source;

l_{ij} - length of a circle stretch crossing a heat source.

A number of calculations based on two methods of the t_j estimation for typical city buildings showed a difference in temperature t not more than 8-10% even under worse conditions (small-scale "mozaic" buildings). Due to simplified assumptions we succeeded in construction of nomograms provided an efficient design of a three-dimensional stable temperature field with an optional arrangement of heat sources (Fig. 3). By these nomograms

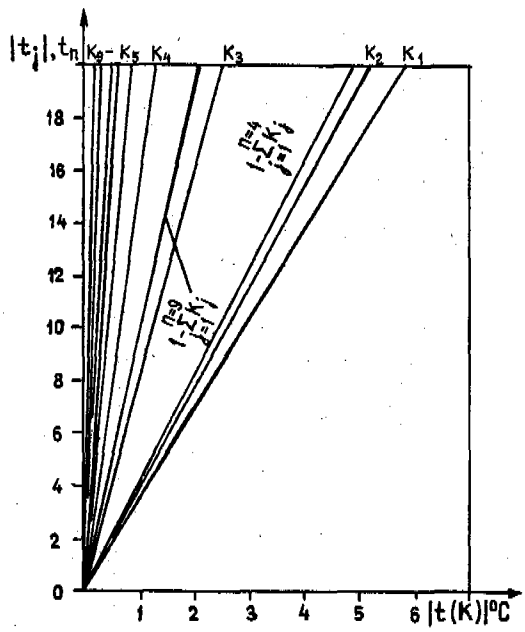

Fig.3 Chart for estimation of a three-dimensional stationary temperature pattern.

a temperature at the desired point can be deduced from the following formula:

$$t_z = \sum_{j=1}^{n-1} t(k) + \left(1 - \sum_{i=1}^{n-1} k_j\right) t_n + g_2 z \qquad \text{(IV)}$$

value $\sum_{j=1}^{n-1} t(k)$ is taken from the nomogram for

every circle and t(k) is found by equation III. Value $(1 - \sum_{j=1}^{n-1} kj)\, t_n$ is taken from the nomogram with account of a definite temperature t_n (temperature at point Z projected to the plane). Number of circles is 10 for an accurate design and 5 - for an approximate design.

Methods of prediction an unstable temperature field of areas under construction are subdivided to two groups. The first group envisages design problems of unstable temperature field without soil phase changes. The second group is known as Stephan's problem including design methods of an unstable temperature field with soil phase changes. In case of complicated distribution of surface temperature the design is reduced to solvation of a two-three-dimensional problem of heat conductivity.

As for a two-dimensional design area a band can be distinguished within the built-up territory; a width of this band is too small as compare to its length. Within this band the temperature distribution is a function of the X coordinate. Outside of the built-up area a temperature is constant and does not depend on coordinates. The problem is solved by usual methods under simple boundary conditions without soil phase changes. A two-dimensional problem of heat conductivity with a free prescribed function at the upper border of the half--plane was solved by S.S.Kovner. A problem of a half-plate and a two-dimensional plate was solved by A.V.Lykov (1967). But the solvations of the foregoing authors are so awkward that cannot be used in practical design. An approximate solvation of a two-dimensional unstable problem of heat conductivity with a prescribed piecewise smooth temperature at the upper region under examination was effected for the first time by L.N.Khrustalev (1971) by reducing a two-dimensional problem to one-dimensional. The authors of the present paper propose a method to solve a two-dimensional like as three-dimensional problems of unstable heat conductivity on the basis of solving one-dimensional problems with assumptions differ from those accepted by L.N.Khrustalev.

If a temperature is determined by Y coordinate for point x = o the area under examination can be rather accurately assumed as a terminal. Dimensions of the area are determined by a range variation of a temperature within the limits of the area under examination and a depth of the desired point. As a result, for the points depending on coordinate y, when x = o the one-dimensional problem of unstable heat conductivity can be solved with an accuracy sufficient for practice under condition when a temperature at the boundary of the area under examination is assumed constant and defined as T_{mean}.

So, the difficulty is a transition from a piecewise smooth function of temperature at the boundary of the area under examination to a constant temperature T_{mean}. With account of a degree of thermal effect of a heat source approximating zero when spreading at the boundary of the design area let's assume a law of decrease to be exponential. Mean temperature at the surface of the area under examination (T_{mean}) is prescribed in the following way:

$$T_{mean} = T_o + \frac{1}{2} \sum_{i=1}^{n} \Delta T_{exp}(-m_i/L_{/2} = m_i) \qquad (V)$$

where: T_o-temperature of the surface at point x = 0°C;

ΔT_i-difference in temperatures of the subsequent and previous interval at the point breaks in a piecewise smooth function, °C;

m_i-distance from point x = o to the i - interval;

L - dimension of a design area, m .

It follows from the proposed formula, if at centre of the design area within an interval ΔL a temperature is T_i and outside of this interval a temperature is constant T_2 then $T_{mean} \longrightarrow T_2$, if $\Delta L \longrightarrow 0$. If $\Delta L \longrightarrow L$, $T_{mean} \longrightarrow T_1$. A temperature at the desired point Y can be deduced from the well known formula:

$$T(Y,\tau) = T_{mean} + (T_n - T_{mean}) \operatorname{erf}(Y/2\sqrt{a\tau}) \qquad (VI)$$

where a - coefficient of temperature conductivity, m^2/h;

τ - time period, h.

Fig.4 represents a design, area for determination of T_{mean} when solving a three-dimensional problem of unstable heat conductivity.

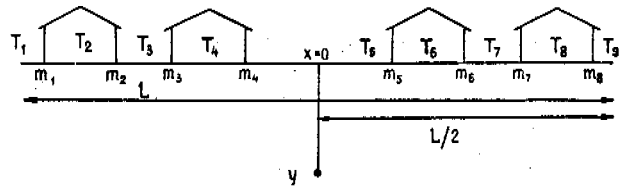

Fig.4 An example of a design scheme for estimation of T_{mean} when solving a two-dimensional problem of variable thermal conductivity.

A three-dimensional problem can be solved by reducing to one-dimensional. For this purpose it is desirable to find mean temperature on the surface of the design area (T_{mean} III). Value T_{mean} III depends on an area of heat absorption and heat release stretches; their tem-

perature on the surface and some other factors. T_{mean} III is determined in the following way (Fig. 5). All the heat sources and heat release sources of the design area are projected

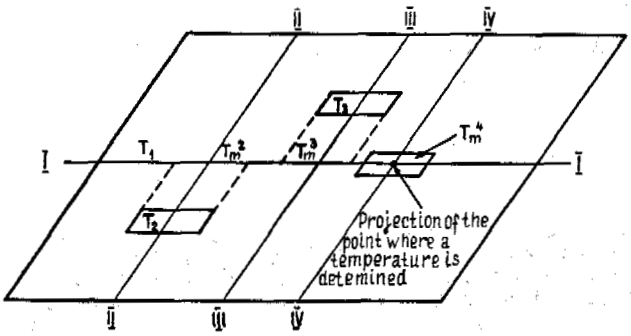

Fig.5 An example of a design scheme for estimation of T_{mean} III when solving a three-dimensional problem of variable thermal conductivity.

Projection of the point where a temperature is determined.

to line I-I. T_{mean} is deduced from formula V for lines II-II, III-III and IV-IV. Then deduce T_{mean} III from the following equation:

$$T_{mean}III = T^3_{mean} + \frac{1}{2} \sum_{i=1}^{n} \Delta T_{mean.i} \Big) \Big) \Big) \exp(-m_i/L_{/2} - m_1) \Big) \quad \text{(VII)}$$

A temperature at the desired point Y can be found by the following equation:

$$T(Y, \tau) = T_{mean.III} + (T^4_{mean} - T_{mean.III}) \operatorname{erf}(Y/2\sqrt{a\tau}) \quad \text{(VIII)}$$

Stephan's two-and-three-dimensional problem (non-stationary problem of heat conductivity with soil phase changes) is also solved by reducing to the one-dimensional problem. Mean temperature of the surface T'_{mean} is estimated by formulae V, VII. Then a positive temperature within the interval of positive values of the piecewise smooth function is changed to zero temperature since a major part of heat is consumed by thawing of frozen strata and the least quantity of heat is consumed by warm-up of the non-thawing permafrost. When a mean temperature on the surface of the design area is determined, a temperature at the desired point can be found by the well-known formulae:

$$T_i(Y, \tau) = T'_{mean}[1-\operatorname{erf}(Y/2\sqrt{a_i\tau})/\operatorname{erf}(\beta/2\sqrt{a_1})] \quad \text{(IX)}$$

$$T_2(Y, \tau) = T_o[1-\operatorname{erfc}(Y/2\sqrt{a_2\tau})/\operatorname{erfc}(\beta/2\sqrt{a_2})] \quad \text{(X)}$$

For practical design is deduced with an insignificant error from Stephan's simplified formula:

$$\beta = \sqrt{2\lambda_1 T'_{mean}/\rho w \gamma} \quad \text{(XI)}$$

where Y - depth of the desired point of the temperature design, °C;

T_1 - temperature within a thawing zone, °C;

T_2 - temperature within a permafrost zone, °C;

a_1 - coefficient of temperature conductivity of frozen ground, m^2/h;

T_o - initial temperature of top ground, °C.

To verify validity of the assumptions all the design results were compared on the basis of the foregoing methods and with the aid of computers. When solving two-dimensional problems the discordance does not exceed 10% and 15% - for the three-dimensional problems. The methods proposed to solve unstable problems of heat conductivity have no accurate theoretical grounds of course. It is evident that there exist temperature, ground and other limitation of the methods described. But their use for practical design and solvation of prediction problems is quite evident due to their simplicity and efficiency.

REFERENCES

Balobaev V.T., Shastkevich Ju.G. (1974). Raschet konfiguratsii talikovykh zon i statsionarnogo temperaturnogo polya gornykh porod pod vodoemami proizvoljnoj formy. Ozera kriolitozony Sibiri. 116-127. Novosibirsk, Nauka.

Lykov A.V. (1967). Teorija teploprovodnosti. c.c.1-600. Moskva. Vysshaja shkola.

Khrustalev L.N. (1971). Temperaturnyi rezhim vechnomerzlykh gruntov na zastroennoj territorii. c.c.1-168. Moskva: Nauka.

Sheikin I.V. (1976). Metod opredelenija statsionarnogo polja temperatur v gruntovom massive pri slozhnoj konfiguratsii istochnikov tepla na ego poverkhnosti. Inzhenerno-geologicheskie i geokriologicheskie issledovanija v Zapadnoj Sibiri. vyp. 49. 145-155. Moskva: Strojizdat.

Lachenbruch, A.H. (1957). Three dimensional heat conduction in permafrost beneath heated buildings Geol. Surv. Bull., 1052 13, 50-69.

PRESSURE IN RELATION TO FREEZING OF WATER-CONTAINING MASSES IN A CONFINED SPACE

M.M. Dubina

Permafrost Institute, Siberian Branch of the U.S.S.R. Academy of Sciences, Yakutsk, U.S.S.R.

SYNOPSIS Water-to-ice phase transition is accompanied by an abrupt change in density, which causes the volume of water-containing masses to increase as they are freezing. Such a process occurring in a confined space entails a pressure increase in the unfrozen phase as well as loading of the frozen phase and material that restricts a free deformation of the water-containing mass. The level of the stressed-deformed state during the course of freezing is able to reach a value sufficient for inducing failure of the material locking the mass. Obtaining quantitative estimates of the stressed-deformed state for such kind of processes is mandatory for purposes of tackling problems of maintaining safe servicing of engineering structures and describing the ice formation under natural conditions (Pekhovich, 1983; Dubina and Krasovitsky, 1983; Wood and Goodman, 1975). Previously documented cases of a manifestation of ice formation in confined cavities determine the upper bound on the magnitude of pressures of about two hundreds MPa, viz. under conditions of ice phase modification (Pekhovich, 1983). Under real conditions the pressures indicated are limited by the manifestation of a variety of thermal, physico-chemical and mechanical parameters of ice formation. This paper considers some results derived from mathematical simulation of the development of pressures of ice formation which yield computational relationships useful for making quantitative estimates.

FORMULATION OF THE PROBLEM

The following conditions may be categorized as ones forming ice formation pressures. First, it is the presence of a confined space that is filled with a water-containing mass increasing in its volume as it freezes. The second necessary condition implies satisfying thermodynamical conditions for ice formation, including the possible cooling of the water-containing mass and the dependence of the phase-transition temperature on the pressure and density of admixtures, in particular dissolved salts. We also take into consideration that, in cases of practical applications, the model of the process may be limited to the scope of axial and spherical symmetry when the freezing process is proceeding in the direction from the cooled outer walls of the space to its center.

In such a way, we consider the following specifying system of equations:

$$\frac{\partial T_i}{\partial \tau} = a_i\left(\frac{\partial^2 T_i}{\partial r^2} + \frac{\varepsilon}{r}\frac{\partial T_i}{\partial r}\right);\ 0 \le r < \infty;\ i = 1,2,3; \quad (1)$$

$$\left[\lambda\frac{\partial T}{\partial r}\right]_{r=S} = l\omega\rho\frac{dS}{d\tau};\ 0 \le a < S(\tau) \le S_0 < \infty; \quad (2)$$

$$T_i(r;0) = T_M(r);\ T_\varphi(0) = T_{\varphi 0};\ S(0) = S_0; \quad (3)$$

$$\lim_{r\to\infty} T_3(r;\tau) = T_M;\ \left.\frac{\partial T_1}{\partial r}\right|_{r=a} = 0;\ T_2(S,\tau) = T_1(S,\tau) = T_\varphi(\tau); \quad (4)$$

$$\frac{\partial C_i}{\partial \tau} = D_i\left(\frac{\partial^2 C_i}{\partial r^2} + \frac{\varepsilon}{r}\frac{\partial C_i}{\partial r}\right);\ 0 \le r \le S_0;\ i = 1,2; \quad (5)$$

$$\left[D\frac{\partial C}{\partial r}\right]_{r=S} = [C]_{r\le S}\frac{dS}{d\tau}; \quad (6)$$

$$C_1(r;0) = C_M(r);\ C_2(S,\tau) = kC_1(S,\tau); \quad (7)$$

$$\left.\frac{\partial C_1}{\partial r}\right|_{r=a} = \left.\frac{\partial C_2}{\partial r}\right|_{r=S_0} = 0; \quad (8)$$

$$\frac{M}{\rho_2}\left(\frac{\rho_2}{\rho_1} - 1\right)d\rho - Ml\frac{dT_\varphi}{T_\varphi} + Rd T_\varphi \ln\frac{1-C_1}{1-C_2} - RT_\varphi\left(\frac{dC_1}{1-C_1} - \frac{dC_2}{1-C_2}\right) = 0; \quad (9)$$

$$\Phi[\tau, \rho(\tau), S(\tau), S_0, a, E_i, \nu_i, \sigma_{pi}, \alpha_v, \gamma_i] = 0, \quad (10)$$

where ρ, T_i, a_i, and λ_i are density, temperature and the coefficients of temperature- and heat-conductivity; τ and r are time and spatial coordinate; S_0 and S are the original and current positions of the freezing front radius; l is concealed heat of phase transition; ω is total moisture content; $i = 1$, $a \le r \le S(\tau)$, and $i = 2$, $S(\tau) \le r \le S_0$ are the unfrozen and frozen zones of a freezing water-containing mass; $i = 3$ is the frozen zone that includes the space filled with a freezing mass; T_M is the natural, undisturbed temperature of frozen soil involving the space and the cooling temperature of a cylindrical (spherical) shell of radius S_0 involving the space, in which case $T(S_0,\tau) = T_M$; a is the radius of the inner shell placed at the center of the freezing mass ($0 \le a < S_0$), which occurs for certain variants of engineering practice; $T_{\varphi 0}$, $T_\varphi(\tau)$ is the original and current value of temperature of the water-to-ice phase transition; C_i and D_i are admixture salt concentration and its diffusion coefficient; k is the distribution coefficient describing the effect of partial **expulsion** of admixture salt ($0 \le k \le 1$); $C_M(r)$ is the initial distribution of admixture salt; $p(\tau)$ is the pressure in the given unfrozen zone that is unable to resist to shear deformations; M is the mass of 1 kilomole of solvent; R is a universal gas constant; E_i, ν_i, σ_{pi}, and γ_i are the elastic modulus, Poisson's coefficient, the yield point, and the angle of internal friction; $\alpha_v = 1 - \rho_2/\rho_1$ is the coefficient of **volume** strain of the freezing mass ($\alpha_v > 0$); and $\varkappa = 1$ is cylindrical symmetry and $\varkappa = 2$ is spherical symmetry.

The system (1)-(10) involves the following relationships: heat conduction equation (1); the Stephan condition at the front of a phase transition (2); initial and boundary conditions of the heat exchange problem (3) and (4); diffusion equation for admixture salt (5) and a relevant balance equation at the front of freezing (6); initial and boundary conditions for the admixture field concentration (7) and (8); Equation of ice formation phase diagram (9) obtainable from the equality condition for chemical potentials at the phase separation boundary; and a solution to the problem of the stressed-deformed state for the pressure of our interest in **supposed** liquid, unfrozen phase (10).

SPECIFYING THE MECHANICAL PART OF THE MODEL

The particular form of the relationship (10) involved in the system (1)-(10) is defined by the given particular case of geometry and the model used for mechanical behaviour of the medium. In the simplest case of freezing of the water-containing mass in between two coaxial and concentric shells the expression (10) has the form of an obvious relationship between the pressure and geometrical and mechanical parameters of the problem. Because these are trivial expressions and, therefore, we do not give them here.

For freezing in a cavility in the ground mass, we obtain the most simple solution for the mechanical part of the problem by assuming the strain distribution in the freezing mass to be hydrostatic. Such an approach provides a simple means to take into account elastic-plastic deformation of cavity-containing rocks, which seems to be done first in a paper of Wood and Goodman (1975). The elastic stage of deformation is limited by the pressure level which is calculated in the same manner as done by Dubina (1986) using the formula

$$p_e = \begin{cases} 2(1-\nu_3)\sigma_\infty + \dfrac{\sigma_{p3}}{2}, & \varkappa = 1; \\ \dfrac{3(1-\nu_3)\sigma_\infty}{1+\nu_3} + \dfrac{2\sigma_{p3}}{3}, & \varkappa = 2; \end{cases} \qquad (11)$$

where σ_∞ is rock pressure.

For the stage of elastic-plastic deformation of rocks, depending on the kind of a plasticity condition, the relationship (10) can be obtained in the form of a nonlinear algebraic equation for p. In the case of noncompressibility of a freezing mass and rigidity of its internal boundary in radius $r = a$ this equation simplifies to an explicit relation $p(S)$ which is given for the Mieses fluidity condition because the expressions for the Coulomb-Moore condition are unwieldy. According to Dubina (1986), for $p > p_e$, we have

$$p = \begin{cases} 2(1-\nu_3)\sigma_\infty + \dfrac{\sigma_{p3}}{2}\left\{1 + \ln\left[\dfrac{E_3\alpha_v}{\sigma_{p3}(1+\nu_3)} \times \right.\right. \\ \left.\left. \times\left(1 - \dfrac{S^2}{S_0^2}\right)\right]\right\}, \quad \varkappa = 1; \\ \dfrac{3(1-\nu_3)\sigma_\infty}{1+\nu_3} + \dfrac{2\sigma_{p3}}{3}\left\{1 + \ln\left[\dfrac{E_3\alpha_v}{\sigma_{p3}(1+\nu_3)} \times \right.\right. \\ \left.\left. \times\left(1 - \dfrac{S^3}{S_0^3}\right)\right]\right\}, \quad \varkappa = 2. \end{cases} \qquad (12)$$

Examination of (12) suggests an important conclusion about the limitedness of pressures in the cavity due to the quantity p_{mp} the expressions for which follow from (12) if it is assumed that $S \ll S_0$. The maximum pressure quantity p_{mp} is a mechanical property of rocks, i.e., some kind of their response to the process of solidification of the mass within the cavity. A similar effect of the existence of a pressure maximum has also been obtained for a viscous-elastic model of freezing reported by Dubina and Krasovitsky (1983) when the expression (10) has the form

$$p = \alpha_v\left[V(G_3 - G_2) + \int_0^\tau V(t)\left(G_3 R_3 - G_2 R_2\right)dt\right] + \sigma_\infty, \qquad (13)$$

where $G_i = E_i/[2(1+\nu_i)]$; $R_i(\tau,t)$ represents relaxation cores of the frozen phase (i = 2) and containing rocks (i = 3); $V(t) = 1 - S^2/S_0^2$ for $\varkappa = 1$; and $V(t) = (1 - S^3/S_0^3)\,4/3$ for $\varkappa = 2$.

REDUCTION TO ORDINARY DIFFERENTIAL EQUATIONS

The system (1)-(10) presented here is too complicated to be solved, even if proper allowance is made for simplifications to the mechanical part of variants (12) and (13) under consideration. Numerical estimates can, nonetheless, be obtained by further simplifying the formulation of the problem. Assuming the unfrozen zone to have no temperature gradient (i = 1) and the temperature distribution in the frozen zone to be quasi-stationary (i = 2) and by specifying the cooling temperature on the contour , we simplify considerably the heat exchange part of the problem statement. We also simplify the diffusion part assuming both regions of the freezing mass to have no gradient as well as the absence of admixture in surrounding rocks, and write the redistribution of admixture salt occurring at the front ( ), according to the concentration balance equation in the unfrozen zone, in the form

$$C_1 = C_0 \left(\frac{S_0^{\varkappa+1} - a^{\varkappa+1}}{S^{\varkappa+1} - a^{\varkappa+1}} \right)^{1-K}, \qquad (14)$$

where C_0 is initial concentration that is uniform throughout the entire freezing mass.

Bearing in mind all of the assumptions made, one is able to reduce the system (1)-(10) to two ordinary differential equations for an elastic-plastic model of the behaviour of rocks and for case of a freezing between two elastic shells (Dubina, 1986). Equation (9) is the first of these equations which should incorporate the second expression of (8), thus enabling the unknown C_2 to be eliminated. Besides equation (9) should include the explicit relation of $\rho(S)$ and $C(S)$ of the form (12) and (14). The second equation is known to have the form

$$\lambda(\theta_M - \theta_\varphi) = \begin{cases} -y\dot{y}\ln y, & \varkappa = 1; \\ y\dot{y}(1-y), & \varkappa = 2, \end{cases} \qquad (15)$$

where $y = S/S_0$; $\lambda = \lambda_2 T_{\varphi 0} \tau_0 / (\ell \rho_2 S_0^2)$;
$\theta_M = T_M / T_{\varphi 0}$; $\theta_\varphi = T_\varphi / T_{\varphi 0}$;
$\tau^0 = \tau / \tau_0$; and τ_0 is time scale.

In the case of a viscous-elastic model for deformation, with the exponential form of relaxation cores $R_i(\tau, t)$, the problem can also be reduced to solving ordinary differential equations (Dubina and Krasovitsky, 1985).

AN EXAMPLE CALCULATION

Figs 1-4 present the calculation results on the axisymmetrical case of a water solution of salt NaCl freezing in a space produced by an elastic shell of radius S_0 or a space in a natural rock which is considered for both an elastic and elastic-plastic model. In all examples, the following parameters are assumed constant: τ_0 = = 3600 s; $T_{\varphi 0}$ = 273 K; P_0 = 0.1 MPa (P_0 being the pressure scale); R = 8.32x10^3 J/(K·mole); M = 0.018 kg/mole; ℓ = 334·10^3 J/kg; λ_2 = 2.21 W/(m·K); ρ_1 = 1000 kg/m^3; ρ_2 = 910 kg/m^3; δ_{S0} = = 0.01 m; E_{S0} = 2·10^5 MPa; a = 0; S_0 = 1 m; and k_1 = k_2 = ∞ . The notation used is the following: δ_{S0} and E_{S0} are the thickness of the walls and the elasticity modulus of the shell that forms the space; and k_1 and k_2 are the volume elasticity modulus of the unfrozen and frozen phases of a freezing mass. The results of the calculation for the elastic space are marked by solid lines, and those for the elastic-plastic space are shown by dashed lines. Cases of the absence of salinization for the elastic-plastic space are marked by dash-dot lines. A total of seven calculation variants are shown in Figs 1-4. Variant 1 corresponds to curves 1.1-1.3 plotted for three values of initial mass concentration: x_0 = 2.5; 5; and 15 kg/m^3 for T_M = 263 K. Curves 2 and 3 correspond to G_3 = 1·10^3 and 0.3x10^3 MPa for T_M = 268 K and x_0 = 15 kg/m^3; curves 4 and 5 correspond to the same values of T_M and G_3 but with x_0 = 0. Plots 6 and 7 have been constructed for an elastic-plastic model of rocks involving the cavity, for the same θ_{03} = 1 MPa; G_3 = 5·10^3 MPa; and x_0 = 5 kg/m^3 for T_M = 268 and 263 K. Curves 1-5 also correspond to freezing in a single shell for which S_0 = 0.27 m and E_{S0} = 2·10^5 MPa, while the value of G_3 = = 1·10^3 MPa corresponds to δ_{S0} = 2·10^{-3} m and that of G_3 = 0.3x10^3 MPa corresponds to δ_{S0} = = 6.7x10^{-4} m. The qualitative implications of the analysis results regarding the calculations made in this paper may be summarized as follows.

CONCLUSIONS

1. Elastic-plastic treatment (Dubina, 1986).

In the case of the absence of salinization the water-containing mass either is able to freeze completely or the parameters S , ρ , and T_φ assume steady-state values on an infinite time interval. In the presence of salinization the parameters S , ρ , T_φ , and C_1 assume steady-state values on a finite time interval. In the case where the remaining conditions remain unchanged, salinization reduces the value of the pressure being evolved, in proportion to the degree of salinization but increases the strengthening of the material containing the freezing mass. Proper account of plastic deformations of rocks, with other conditions remaining unaltered, reduces considerably the level of evolving pressure. When the Coulomb-Moore fluidity condition is applied, an increase of the angle of internal friction of rocks, γ_3 , leads to an increase in pressures and time of freezing.

2. Viscous-elastic treatment (Dubina and Krasovitsky (1985).

When the variability of T_φ is taken into account, the process of freezing proceeds at lower rates. Without salinization, the water-containing mass freezes completely, with extrema of the parameters ρ and T_φ on the freezing interval. If the freezing of a viscous-elastic mass proceeds within an elastic space or between elastic shells, then the mass is able to

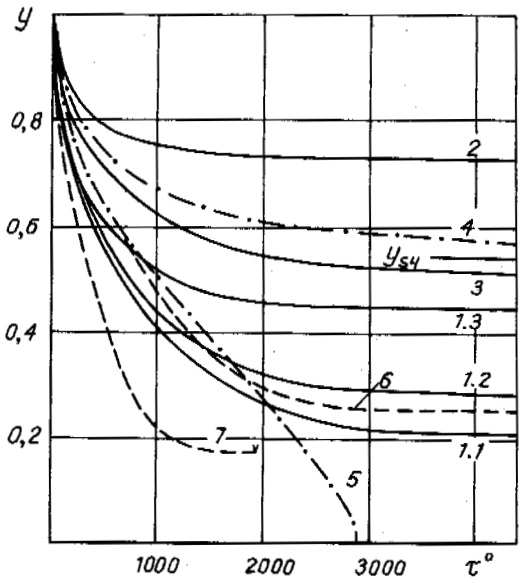

Fig.1 Behaviour of a Dimensionless Front of Phase Transition y as a Function of Time τ°.

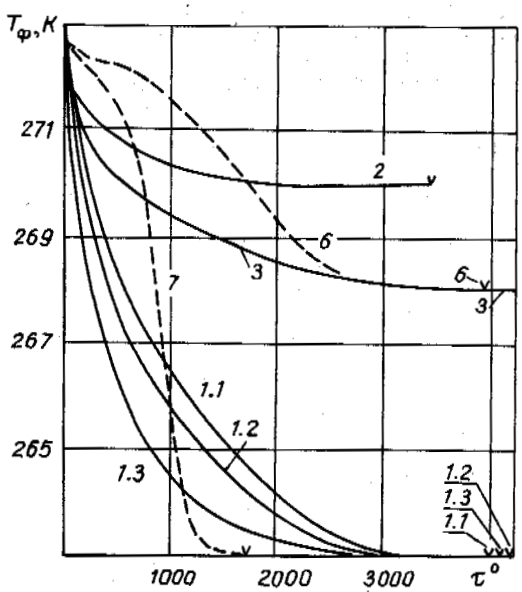

Fig.2 The Time Variation of Phase Transition Temperature $T_ф$.

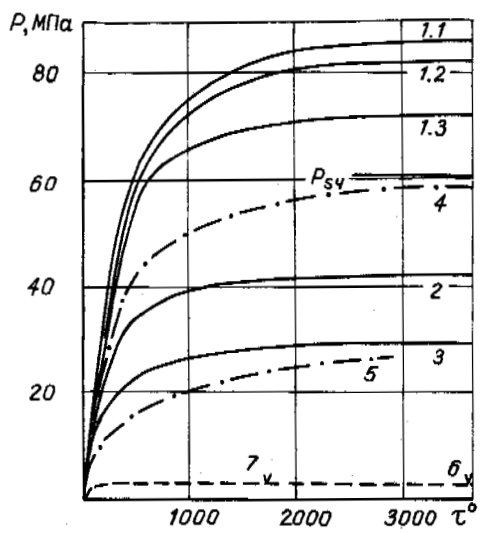

Fig.3 Growth Variation of Pressure ρ as a Function of Time.

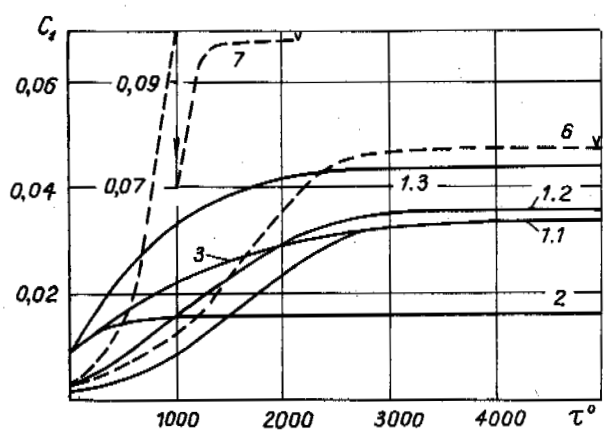

Fig.4 Behaviour of Admixture Concentration in the Unfrozen Zone C_i as a Function of Time.

freeze partially, with the parameters S , ρ , and $T_ф$ assuming steady-state values during a finite time interval. The presence of salinization leads to a partial freezing, with the manifestation of the remaining peculiarities mentioned above.

3. The estimating calculations we have carried out in this paper demonstrate the possibility of making a quantitative prediction of ice formation in confined spaces taking into account the degree of salinization as well as irreversible deformations of rocks, using a relatively simple technique.

REFERENCES

Dubina, M.M. and Krasovitsky, B.A. (1983). Teploobmen i mekhanika vzaimodeistviya truboprovodov i skvazhin s gruntami. 136 p., Novosibirsk.

Dubina, M.M. (1986). Priblizhenny raschet zatverdevaniya binarnoi smesi v osesimmetrichnykh yomkostyakh. ZhPMTF, No. 4, 79-83.

Dubina, M.M. and Krasovitsky, B.A. (1985). Zamerzanie taloi zony vokrug skvazhiny v merzlykh porodakh s uchetom zavisimosti temperatury zamerzaniya ot davleniya. IZhKh, v.X, 122-129.

Pekhovich, A.I. (1983). Osnovy gidroledotermii. 200 p., Leningrad: Energoatomizdat. Leningr.otd.

Wood, D.B. and Goodman, M.A. (1975). A mechanical model for permafrost freeze-back pressure behavior. SPEJ, v.15, No.4, 287-301.

ENVIRONMENT PROTECTION FOR MINING ENTERPRISES IN PERMAFROST REGIONS

E.A. Elchaninov

Skochinsky Institute of Mining, Moscow, USSR

SYNOPSIS Fast expanding and developing mining industry in permafrost regions puts forward a great number of environment protection problems. The degree of influence of the main technological processes in mining on natural complexes is defined and classified by investigations at the mining enterprises. The paper deals with some results obtained by the investigations of the polluted mine air, the pumped-out mine water, a great amount of waste rock piled on the surface, and surface subsidence caused by underground mining affecting natural complexes.

The entire complex of natural conditions under a wide influence of the technologic subsystems forms the background for the industrial activities during mining mineral deposits in the permafrost regions. The results of this interaction are determined by the character of the media transformed because of the activities of mining facilities. So there appears a necessity to find out what is being transformed and how it is being done. The insufficiently grounded solutions of imperfect technology for mining minerals may result in grave consequences or even irreversible disturbance of environment.

Let us consider the interaction between the environment and a mining facility i.e. a colliery.

When operating a coal-mining facility consumes a certain volume of fresh air for ventilation, takes water out of reservoirs for spraying system and fire-extinguishing pipelines for the sake of safety, obtains timber out of forests to proceed with mining operations in workings, extracts minerals and rock out of entrails of the earth, drains gas and water out of rock to provide for normal conditions of underground operations.

At the same time any mining facility cannot help being a source of polluted air containing gases, moisture and mineral particles, considerable amount of contaminated underground water with chemical and biological components, and finally great mass of barren rock is extracted from any mine and has to be dumped at some disposal area. Each such extraction of effluent represents a subsystem of mining facility - nature interaction.

In its turn each of the subsystems mentioned embarks on interacting with another or several other similar subsystems to form a whole system of influences upon the nature. Investigations have proved that the affects and influence of separate subsystems and - even less so - the interaction of the subsystems can be detected and found out but after a long time, sometimes 15-20 years and more.

By their degree of influence all the subsystems can be divided into the following:
- subsystems of limited influence (they cause mining subsidence, form rock spoil heaps, propagate karst and lakes, etc.)
- subsystems of regionsl influence (they give birth to the iffluents of gas, heat, condensate, etc.)
- subsystems of unlimited influence (they are responsible for the iffluents of dust and mine water).

The operational range of the subsystems of limited influence is restricted by the mine district or deposit. The subsystems of regional influence include the effluents liable to travel 50-60 km and more outside the limits of a mine district. The zone of influence of the subsystems of unlimited influence cannot be difined because their operational range is not restricted by any distance.

Let us consider briefly the mentioned subsystems.

Both development of mine workings to provide an access to a mineral and extraction of the mineral result in changing the landscape, i.e. they cause subsidence to form day falls, pits, faults, creeping wastes, ravines, etc. Upon appearing the falls and pits are suffused with water in rain and snow-melting seasons to form lakes, heat caverns and ravines.

At he same time as the mineral is mined the goaf and cavities are filled up with the gradually caving rocks. The height of rock caving and the degree of landscape disturbance and thus that of the geocryological situation

depend upon the depth of occurence of a mineral.

Provided the depth of mining does not exceed 60-90 m it leads to day falls with sheer brinks. When mining seams outcrops under overburden sediments the day fall depth can be as much as the thickness of the extracted mineral's seam. The day falls are filled up with top-soil together with trees and bushes. They are snowdrifted in winter and filled up with water in summer to from artificial lakes, and it deteriorates the permafrost with wash-out of their banks to follow. There are day fall areas from 3 to 15 thousand sq.m. registered at mining facilities with hillside landscape.

As the depth of mining increases up to 150-200 m terrain disturbances are come across rarer. In this case the geomechanical transformations of the surface lead to formation of moulds of subsidence accompanied with small falls-through, scarps and cracks. The moulds of subsidence represent a most typical form of the geomechanical transformation of terrain under the influence of mining. As a rule, their sizes correspond to those of the goaf, while the depth does not exceed the projection of the extracted mineral seam thickness on the vertical plane.

The small falls-through are developed provided the cave-in zone reaches the surface, i.e. the depth of mineral occurrence is less or equal to the thickness of caved rock layers.

$$H = \frac{M}{(K-1)\cos\alpha}$$

where
- M - is the mineral thickness extracted
- K - is the coefficient of filling the goaf with caved rock ($1.1 < K < 1.5$).

The size of a fall-through can be determined from the following relations:

$$L_f = M_v + 2 H_o \cdot tg\mathcal{E}$$

$$af = \frac{M_v^2 \cdot ctg\mathcal{E}}{2(M_v + 2H_o \cdot tg\mathcal{E})}$$

$$V_f = 0.5 \cdot L_f \cdot a_f \cdot L$$

where
- L_f - is the width of fall-through
- M_v - is the vertical thickness of mineral $= M/\cos\alpha$
- H_o - is the thickness of overlaying sediments over the mining operations
- α - is the angle of coal seam dip
- $\mathcal{E} = 45° - 0.5\varphi$.
- a_f - is the depth of fall-through
- V_f - is the volume of fall-through
- L - is the length of extracted part of the deposit along the strike.

With the exception of the zone of falls the maximums subsidence of surface in a displacement mould reaches 65-90 per cent of the summed-up thickness of extracted mineral. An average inclination of a displacement mould from its axis is 80-95 mm/m. Fissure gapping and degree of damage depend on the value of mould of subsidence. The first degree of damage is represented by the cracks and fissure gappings up to 30 mm wide, the second degree - up to 100 mm, the third degree - up to 250 mm, the fourth degree - up to 1000 mm, the fifth degree includes the cracks wider than 1000 mm and day falls.

For example, in a mine with the depth of mining up to 200-220 m and the summed-up thickness of coal seams about 12 m the maximum surface subsidence has reached 7.0 - 7.2 m. In another mine with the summed-up thickness of extracted coal seams 26-27 m the maximum depth of the mould of subsidence has reached 17.4 - 18.6 m. In the bottom of the mould one could observe some breaks of surface cover and cracks and fissure gappings of 0.3 to 2.15 m. which have collected the water of the season-melted snow and the slided-down top-soil peat layer, and it has lead to superfluous drainage and general thawing from 0.7 to 1.9 m. The disturbed area has reached 12 million sq.m. (fig. 1)

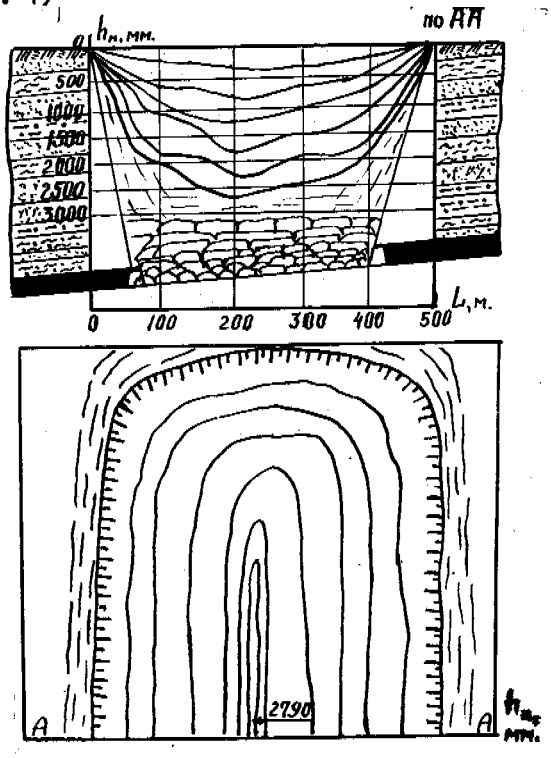

Fig.1. Scheme of surface disturbance above an extracted coal seam

Consecutive mining of several seams of a mi-

neral results correspondingly in successive repeated displacements of the total cover thickness. Each displacement changes the geocryological situation and it is caused by additional breaks of the surface and by a redistribution of strains and stresses.

The new moulds with cracks in bottom and walls are filled up with water. In case the water in the mould gets completely freezed in winter, then, there is formed an ice bowl with a lot of wedge-like ice veins penetrating the rock massif. At the same time it reduces the general temperature of the massif and the reduction reaches 0.6 - 1.0°C in two years. The radiation balance remains at the previous level. The vegetation cover around the ice lake remains unchanged, too. If the depth of a reservoir does not allow the water to get freezed to the bottom, then, under the bottom the permafrost begins melting to form slush which is quick to sink in the rock massif because of the water filling up the cracks and fissures. In the case the radiation balance around the reservoir undergoes sharp changes. The changes start from the mould edges with disturbed vegetation cover. In summer the radiation balance is as high as 32-37 kcal/sq. cm while usually it is 26-29 kcal/sq.cm. Every year the destruction wave expands along the edges of displacements to force teh vegetation cover to disappear and to develop thermokarst and ravines.

The started cryogenic processes caused by the mining operations lead to rather intensive and often fatal damage for the surface not only within the allotment, but on the adjacent areas, the rate of destruction exceeding that of the cryogenic processes outside the zone of mining operations by dozens of times.

In order to reduce the harmful influence of mineral extraction on the underworked surface there have been developed some technological schemes to mine coal seams without caving or to provide smooth rock lowering without visible breaks of the peat cover. All the technological schemes are divided into 14 groups and 5 types /1/ according to the geocryological and hydrogeological conditions with rock structure and technological conditions taken into account.

Resorting to the developed technological schemes has made it possible to reduce the damage of the surface by 75-90 per cent and to eliminate the formation of the artificial lakes thermokarsts and large day falls.

During opening, development and mining of a mineral a considerable amount of barren rock is delivered to the surface and has to be stored in waste dumps. Every year a mine is used to deliver 100-150 thousand cu.m. of barren rock to the surface to form enormous refuse heaps, each occupying an area of 10-15 thousand sq.m. Each refuse heap is surrounded with a protection zone of some 80-90 thousand sq.m. Without sanitary protection the top-soil cover of the surface is quickly destroyed, the permafrost is deteriorated, the rock of the refuse heap get sunk in the peat cover of the tundra to squeeze out a circular soil bank around itself thus providing the conditions for alternating the temperature mode of the next-to-surface layer. (fig. 2)

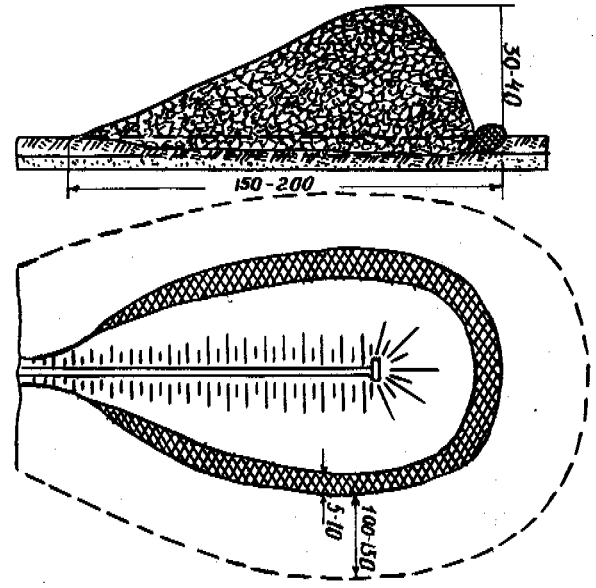

Fig.2. Scheme of surface disturbance with a waste dump

New refuse heaps alter the permafrost situations. The temperature mode of the refuse heaps depends on the air temperature and on the oxidation of sulphide inclusions come across in coal fines and rock. The oxidation and burning of refuse heap rocks provide an additional source of air pollution.

In order to reduce the volume of barren rock delivered to the surface there is a technology worked out to drive "in-seam" developments and to mine a mineral without extracting rock /2/. For the case when it is impossible to mine a mineral wothout extraction of barren rock and lifting it to the surface, there are given some technical solutions to utilize the barren rock as building material for road-building or as filling-up material in the goaf. For this purpose 1 cu.m. of out-of-mine rock is 2.0 - 2.5 times cheaper than that of building material specially produced at a quarry.

The effluent of ventilation air is accompanied with rock and coal flue dust escape, carbon dioxide, methane, oxides, moisture, heat etc. from the mine workings to the atmosphere. Its transparancy is being changed to blacken the snow cover at a radius of 35-50 km, or even 150 km in case of strong winds typical of Siberia and the Far North. About 0.1 - 1.5 per cent of total daily coal output turned into dust goes in the air to say nothing of 200-300 thousand cu.m. of methane, 36-65 thousand cu. m of carbon dioxide, several thousand cu.m of blasting oxides together with 180-360 thousand kJ of heat released. The spread coal dust has diminished the snow albedo by two-three times to absorb more solar radiation and to make the snow thaw 12-17 days earlier. It has resulted in deeper warming-up of top-soil and increas-

ing of the season's thawing from 0.4-0.6 to 0.9-1.1 m at a flat country and from 0.8-1.15 to 1.6-2.1 m at southern slopes. The century-settled heat balance has been upset to lead to greater swamping, thermokarsts, land slides, etc. Besides, the accelerated snow thawing caused greater inflow of polluted water into lakes and rivers used as water supplies. The water pollution has provoked some further changes to start other subsystems running. Fish spawnings and waterfowl nestings have been disturbed, certain plants have been substituted by other plants, i.e. sedge and willow-herb have substituted moss, cloud-berry and blueberry. Changes in the vegetative cover influenced migration of lemming, polar-fox and reindeer.

In order to reduce the harmful effect of the ventilation effluent we have developed a complex of technical means and measures including a reduction of effluent components by changing the moisture content and temperature of the air flow in workings, partial methane capture and dust collection to burn them later in boilers, utilization of the hot effluent to heat green-houses and buildings /3/.

When mining below permafrost layers the pressure subpermafrost water is often come across. The drainage to lower their level is carried out before development operations. This leads to depress the sub-zero isotherm, i.e. permafrost penetrates into the rock massif. The rock massif being undermined, the water-bearing level is subjected to destroying and water is collected in the goaf. As there is no circulation of water in the goaf the permafrost grows, in case the water circulation in the goaf the permafrost degrades.

The permafrost penetration into the rock massif depends on the temperature of the rock, the degree of mineralization of the interstitial water as well as on fissures and texture of the rock. It varies from 1.53 m to 2.17 m a year. As far as the permafrost degradation is concerned it spreads as fast as 5.75-8.29 m a year.

Both removal and discharge of the permafrost water exercise a great effect on the surface stability. Up to 50 thousand cu.m. of water are pumped out and discharged every day. The volume of the pumped-out water grows constantly as the minig operations become deeper and their inundation greater. Discharge of considerable volume of water leads to bank erosion and its pollution, to development of thermokarst, to disintegration of engineering structures, and to formation of vast icings at subzero temperatures.

Besides, fish spawnings and bird nestings are disturbed and food fish and game birds tend to disappear.

In order to reduce or completely eliminate the injurious effects of the water discharge on the environment there are several technical solutions worked out to change the approach to the water discharge and to utilize it either as technical, or even drinking water.

The presentday drainage methods are responsible for the fact that the mine water is combined with the inflow water to form the mine discharge water. The drainage water from the boreholes are directed to the workings to be mixed with water inflow in the water collectors and then to be pumped out to the surface where it is to undergo purification and be discharged.

In order to cut down the volume of discharge water to be purified there are interception schemes worked out to catch discharge water with the help of advance, raise and unloading boreholes, receiving it in special collectors and delivering it to the surface to be used for technical or drinking purposes without any additional purification. The discharge water requires aeration to release dissolved gases and iron dioxide. The drainage boreholes make it possible to intercept about 70 per cent of water inflow and only 30 per cent of it is pumped out as discharge water. Special conditions for removal of the discharge water are worked out. The discharge water is directed to the zone of natural talics wich are not the fedding zones for water-bearing subpermafrost horizones. In case there is no zones of natural open taliks the water is pumped down in the boreholes drilled below the deposit level. In order to heighten the filtration and absorption coefficient of the pumped-down water we resort do dispersed comouflet explosions in the boreholes. The discharge rate of the boreholes are determined accroding to the equation /4/:

$$Q = 2\pi c B \sqrt{\frac{P_o - P_1}{R_1^1 - R_{eq}^1}}$$

where
- c – is the coefficient for rock cracks
- B – is the thickness of the rock seam to pump water in
- $P_o - P_1$ – is the pressure differential
- R_I – is the borehole radius
- R_{eq} – is the equivalent radius of feed outline (fig. 3).

Comouflet explosions are carried out to heighten the debit of the boreholes. The cavity dimensions are determined from the equation:

$$D_{cav} = \frac{(3+4)\, d_{ch}}{k}$$

where
- d_{ch} – is the charge diameter
- k – is the coefficient of permeability.

The maximum radius of cracks (R_c) is calculated from:

$$R_c = k \cdot d_{ch}$$

Taking into account the hydrodynamic resistance of seam which depends on the radius of cracks the equivalent radius is determined as follows:

$$R_{eq} = 0.7\ R_c = 0.7\ k \cdot d_{ch}$$

At present some technical methods are being developed to use the water discharged from mine for transportation of extracted mineral, for operation of hydraulic turbines, for breaking rock and mineral, to control rock pressure and support a seam exposure or baring, etc.

Application of the developed technical methods has made it possible to completely eliminate (in some cases) or reduce by 50-60 per cent the harmful effect of the water discharge upon the environment.

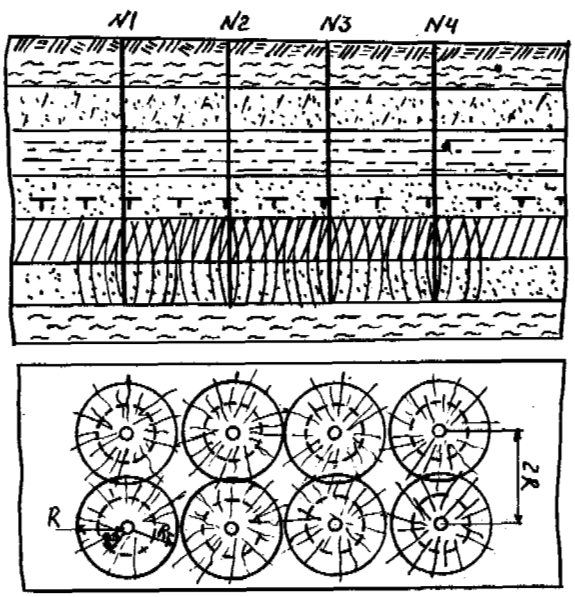

Fig.3. Scheme of water-collecting boreholes with artificially heightened crack formation

Not a less harmful effect on the environment is exercised by felling to satisfy the timber needs of a minning facility or that of the personnel employed by the facility. Under the permafrost conditions all the trees are undersized and it takes greater felling areas to satisfy the needs. Usually the felling areas are quite close to the mining facility. During last 25-30 years the felling area has reached several hundred sq.km. It would take a century or more to re-cultivate the trees under these conditions. As a rule, the forest-offence areas get covered with bushes, become bogged up with some kinds of plants substituted by the other types. In its turn it activates other subsystems such as flora, fauna, etc.

In order to exclude timber for support use at the mining facilities several measures have been developed to use instead of it the hydraulic, metal and powered supports as well as the rock-consolidating concrete and chemical mixtures, synthetic resins, cera-concrete, etc. Application of these substitutes and technical means has allowed a mining facility to reduce the timber requirements by 80-90 per cent.

With the type design practice for mineral mining technology being over according to a great many of factors of interaction to take account of the influence of technology upon nature and the nature's reaction and response to this or that technology, it confirms the idea of that the nature and a technology are the elements of a single system. Due to the fact it is necessary to resort to a systematic approach. The systematic approach allows to comprehensively understand the nature-technological and geotechnological systems the main elements of which are nature and technology.

This approach possesses a great potential it because it is directed at formation, first of all, of a single whole system without trying to "inscribe" separate technical solutions in the nature through a mining technology and to make their activities agree with the natural processes. Thus, at present the conditions have become imminent and urgent when it is necessary not only to establish a technology, but to design a geotechnological system to completely cooperate with the nature. It is the only appraoch that gives the opportunity to forecast if not all, then, a good many of the detrimental after-effects of a coal-mining technology on the natural environment as wll as to make arrangements to avoid or eliminate them.

REFERENCES

Provisional instructions for choosing supports of coal-mining workings under the permafrost conditions. Moscow, Scochinsky Institute of Mining, 1979, 40 pp.

Technical schemes for winning and development operations at the collieries of the production unit "Severovostokugol". Moscow, Scochinsky Institute of Mining, 1977, 84 pp.

Elchaninov E.A. State of art and ways to reduce the environmental disturbances during mining in permafrost regions. In: "Resistance of the surface against the technogenic activities in permafrost regions". Yakutsk, Siberian Department of the USSR Academy of Sciences, 1980, pp. 43-49.

Lovlya S.A., Gorbenko, L.A., Koplan B.L. Torpedoing and perforation of boreholes. Moscow, Gostechizdat, 1959.

ARCTIC MINING IN PERMAFROST

H.M. Giegerich

Cominco Alaska Incorporated, Pasadena, California, USA

SYNOPSIS This paper describes mine construction and operation in Arctic permafrost at three mining projects by Cominco Ltd. of Canada - the Black Angel Mine in Greenland, the Polaris Mine in Canada's arctic islands, and the Red Dog Project in Alaska. A major challenge in Arctic development is to overcome the problem of permafrost, or to use its unique engineering properties. At Black Angel, mining is not greatly affected by permafrost, as the rock is strong with little moisture. Building foundation design included construction on frozen glacial fill. The Polaris Mine has taken advantage of permafrost in underground extraction and support methods. Foundations for the major structures were frozen into place to give the stability normally supplied by conventional concrete. Permafrost at Red Dog is a technological problem, as it is relatively warm. The major design criteria are therefore to prevent thaw.

INTRODUCTION

Cominco Ltd. is a Canadian-based mining and metallurgical firm which has been developing and operating mines in northern Canada for 50 years, starting with the Con Gold Mine at Yellowknife, in 1938, and followed by the Pine Point lead/zinc operation in 1965. Both of these mines are in the Northwest Territories (Figure 1).

More recently, the Black Angel Lead/Zinc Mine started up in 1973, and the Polaris Lead/Zinc operation achieved commercial production in early 1982. Cominco is presently constructing the Red Dog Lead/Zinc/Silver Mine in Alaska, and this operation is scheduled to begin production in early 1990.

Developing an Arctic mine requires new and different approaches, to reduce the negative economic effects of climate and location. One of the major challenges is permafrost - either to overcome the related problems, or to utilize its' unique engineering properties. The physical characteristics of permafrost vary with soil type, moisture content, and temperature. Therefore, the relationship between these factors will determine if permafrost will be an asset or a liability.

Black Angel Mine (Underground Mine)

The Black Angel Mine is in Maarmorilik Fjord on the west coast of Greenland, at latitude 71° N, about 500 km north of the International Airport at Sondre Stromfjord. All personnel and air freight are moved between Sondre Stromfjord and the mine by helicopter. Figure 1 shows the location of airport and mine.

The Black Angel Mine began operation in 1973, at a mining rate of 600,000 tonnes of ore per year. Total project time from approval by Cominco to commercial production was 17 months.

The mine is in fjord country, with steep cliffs, and a plateau at about 1,000 m. elevation. The Greenland ice cap comes close to the edge of the plateau, and the glaciers discharge icebergs into the fjords. The ground is perennially frozen down to approximately 450 m., and rock temperatures in the mine are -10° to -12° C.

The Black Angel mineral zone is generally flat lying and outcrops about 600 meters above sea level, on the face of a steep cliff. Figure 2 is a photograph of the Black Angel Cliff.

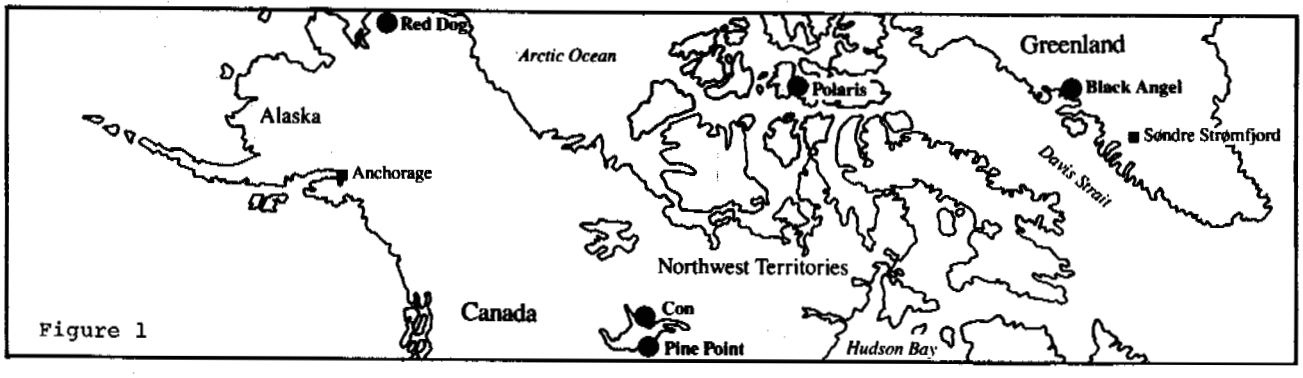

Figure 1

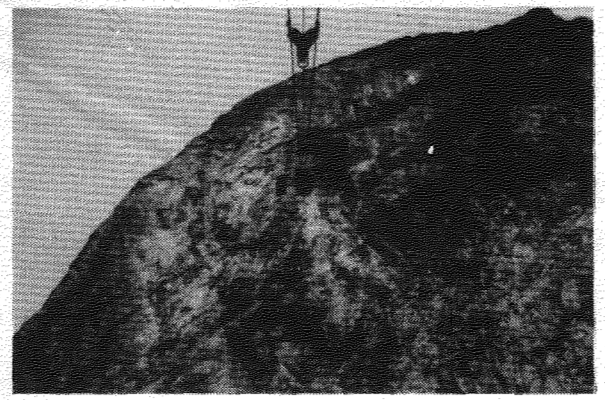

Fig. 2 - Black Angel Cliff

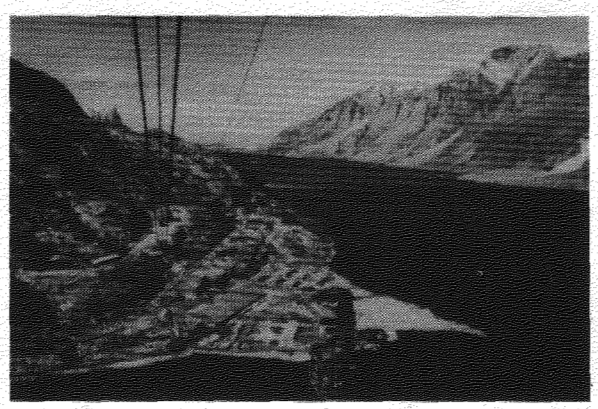

Fig. 3 - Black Angel Plant Site

Even though the mine itself is in permafrost, the ground is considered to be excellent, as it is composed primarily of marble and limestone, and with few faults. As a result, there was little moisture in the initial mining areas. However, as the mine advanced deeper into the cliff and under the ice cap, the development headings ran out of permafrost, and water was encountered in these areas. This caused some difficulties, as the water draining back through the existing workings in the permafrost created severe ice problems for access and equipment.

Another difficulty was in drilling, both core for exploration and percussion for production, as the normal method for cooling the bit, plus controlling dust and recovering the cuttings, is to use water. Due to the rock temperatures, a brine solution consisting of up to 7% calcium chloride was required, in order to have a drilling fluid that would not freeze. This created problems due to cost, as well as corrosion on equipment and skin rashes on people exposed to the brine. Otherwise, the operation of the mine was not particularly affected by permafrost. Very little backfill was used to replace the mined ore, although some consideration was given to the possibility of filling the open stopes with gravel or waste, and freezing. However, to date this has not been done to any great extent.

The ore storage bins, both in the mine and at the mill site, were excavated out of rock, which also was in permafrost. Again, due to the low water content, no significant freezing of the stored ore was encountered.

One of the design problems for the Black Angel plant was the limited area (12 ha.) across the fjord from the mine, on which the concentrator, power plant, service buildings, and accommodations are located (Figure 3).

Much of this site is covered with an unconsolidated glacial till, permanently frozen over a marble bedrock. The concentrator foundations were excavated out of rock because of the geotechnical concerns with building on a frozen base. The only concession to permafrost was to use a structural fill under the slabs-on-grade from which all material finer than 1 cm was removed in order to create voids which would serve as insulation. As well, rigid foam insulation was placed on top of the fill and under the slab, to ensure that any water on top of the slab would not freeze.

The service buildings at the Black Angel Mine which were built on the frozen glacial till consisted of either a pre-engineered industrial structure on a concrete slab, or a prefabricated accommodation unit on timber footings. The general method of construction was to excavate the permafrost to below the active layer (or depth of summer thaw), and then backfill with crushed and screened rock, as in the concentrator. Rigid foam insulation was also placed on top of the fill and under the concrete slabs. This is shown in Figure 4.

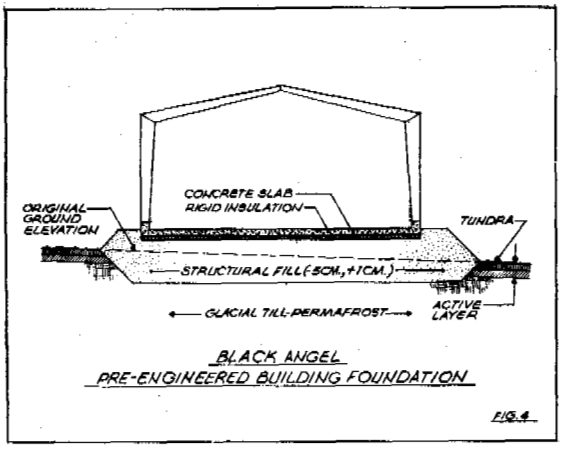

The prefabricated accommodation units constructed on permafrost were set on timber blocks placed directly on top of the structural fill, and an air space left under the buildings to ensure that heat could not pass into the fill. Figure 5 shows the foundation design. A total of 15 buildings were sited on the frozen till, using the methods described above, and of these, there was only one significant failure, due to a subsurface summer water course which was not detected during the excavation of the foundation.

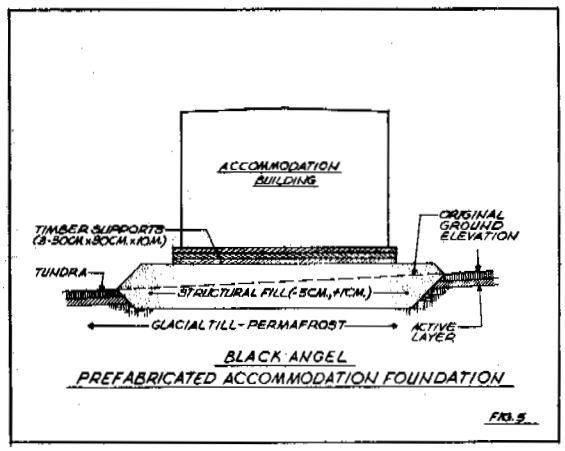

BLACK ANGEL
PREFABRICATED ACCOMMODATION FOUNDATION

FIG. 5

The other aspect at Black Angel which was affected by permafrost was water supply. All fresh water flows cease for five to six months during the winter. There are many fresh water lakes on top of the plateau, which could have been used as a water source, but the problems of constructing pipe lines down the steep cliffs made it difficult to ensure a dependable water system. Therefore, sea water was utilized in the process, and potable water was made in desalinators using waste heat from the diesel generator exhaust.

The Polaris Mine (Underground Mine)

The Polaris Mine in northern Canada (Figure 6) is Cominco's most recent operation in the Arctic, and is the most northerly metal mine in the world. Polaris is on Little Cornwallis Island, at latitude 76°, north of the Northwest Passage, and 1,500 km from the North Pole (Figure 1). Again, the mine is in permafrost, down to 400 meters below surface, with rock temperatures in the upper part of the ore zone in the range of -10° to -12° C, about the same as the Black Angel. The ore also goes down to about 400 m, so the bottom of the mine will be almost out of the permafrost.

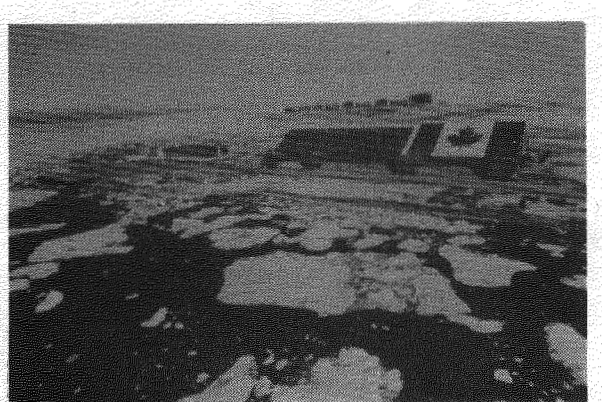

Fig. 6 - Polaris Mine

The deposit is much larger than the Black Angel Mine, with greater production. The Polaris Mine achieved commercial production in March, 1982, just 28 months after the "go-ahead" decision by Cominco, and is presently operating at 25% above design rates.

The topography of Little Cornwallis Island is rolling, with low relief. The highest point is 140 m above sea level, and several freshwater lakes are present, one of which supplies water for the operation.

Several innovative steps were taken at Polaris, including construction of the main plant facilities on a 30 m. by 130 m. barge in southern Canada. This was then towed for 5,000 km. up the west coast of Greenland and through the Northwest Passage to Little Cornwallis Island, where it was ballasted down in a permanent berth, and within two months of arrival was processing ore (Figure 7).

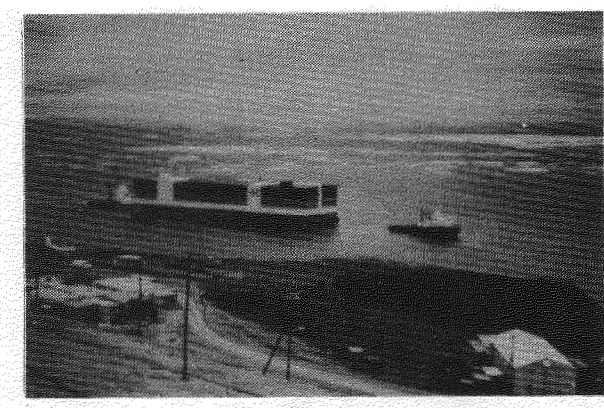

Fig. 7 - Polaris Process Barge

Other innovations to counteract permafrost, or to utilize the unique structural characteristics of permafrost, were also made. The mineral deposit itself consists of massive sulfide deposits in a karst formation in limestone, with many voids which are filled with ice. On average, the ore zone contains up to 5% ice by volume. Without permafrost, this would be a difficult orebody to mine, as the cementation provided by the ice is necessary to overcome the basic instability of the rock. The perennially frozen condition of the Polaris deposit is therefore a distinct advantage from the standpoint of mining, and it is essential that the mine be kept below freezing temperature at all times. This was a major concern during the conceptual design of Polaris, and after commencement of operation, it was found necessary to install a refrigeration plant in order to cool the ventilation air entering the mine during the three warm summer months.

The problems encountered at the Black Angel in using a brine solution for percussion drilling of the frozen ore were eliminated at Polaris by dry drilling. Cuttings are removed with compressed air, and a vacuum system on the drill machine collects dust. However, a brine solution is still required in diamond core drilling.

The mining of the underground ore at Polaris also benefited from permafrost and the cold winter temperatures. The basic mining plan is a "room-and-pillar" method, whereby the ore is removed in open stopes, with pillars of the same dimension left between the openings. The open area is then filled with waste material from the surface which contains about 10% natural moisture, partly as snow. This "backfill" is dumped down 2 m. bored fill raises and spread in the open stopes, and additional water is added to bring the total moisture content up to about 15%. The fill material is allowed to freeze for some months until it becomes strong enough to support the roof of the stope, and the intervening pillar can then be removed, with the frozen "backfill" supporting the mine. Figure 8 shows this stope and pillar layout.

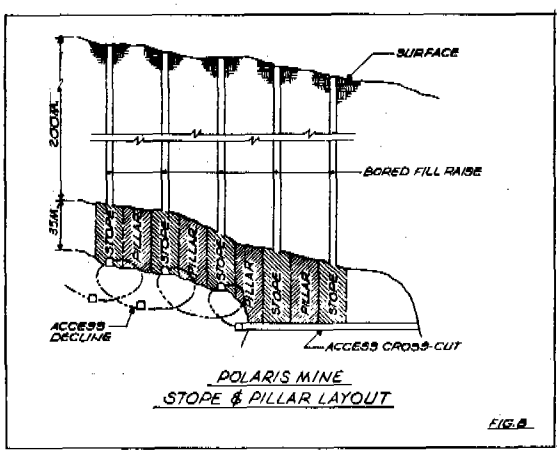

POLARIS MINE
STOPE & PILLAR LAYOUT

FIG.8

Advantage was also taken of permafrost in the foundations for the two main on-site structures. The accommodation foundations consist of pre-cast concrete pedestals, set in trenches dug into an area of weathered limestone. After the pedestals were positioned and aligned, the trenches were filled with the excavated material, sprinkled with water, and the foundations were frozen into place. Figure 9 shows the accommodation foundation scheme.

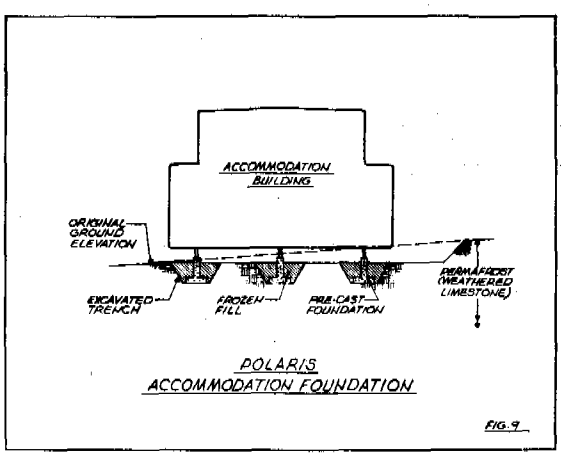

POLARIS
ACCOMMODATION FOUNDATION

FIG.9

The other major structure at Polaris is the concentrate storage building, which is 230 m. long, 55 m. wide and 30 m. high. Again, the permafrost was utilized by freezing in pre-fabricated footings for the foundations, so that very little expensive concrete was required. A method similar to the accommodations was applied, except in this case the foundations were a pre-built steel grillage set on the frozen bedrock. The trenches were then backfilled and watered, and the fill allowed to freeze in place, which gave the lateral stability required for the foundations. Figure 10 is a conceptual sketch of this foundation.

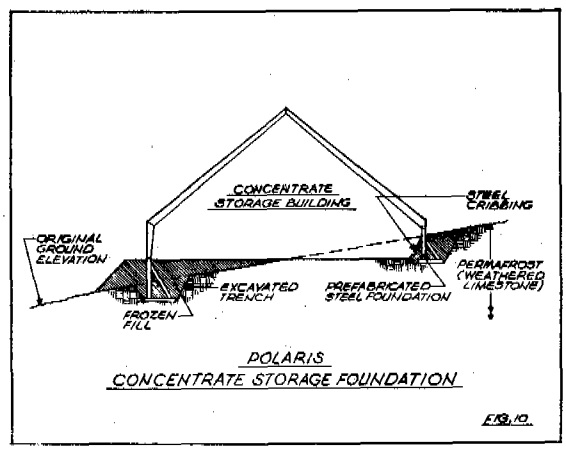

POLARIS
CONCENTRATE STORAGE FOUNDATION

FIG.10

The Polaris dock design was based on the engineering properties of permafrost. The major technical problem was the excessive pressure from multi-year ice, plus pressure ridges in the winter. Various designs were considered, including reinforced concrete and steel. Finally, it was decided to use the features in the Arctic that are most common -- cold and permafrost. The dock was built of sheetpile cells, with crushed rock fill. A circulating freezing system was installed in the fill, and over the following year, utilizing the winter cold, the broken rock was converted to permafrost.

The water supply system at Polaris is also affected by permafrost. The fresh water source is a lake two miles from the mine. There is no ground water inflow because of permafrost, and recharge depends on runoff only. Studies indicated that the watershed would normally have sufficient capacity for the mine requirements. In the event of a particularly dry period, the supply could be significantly augmented by the use of snow fences to collect and retain larger quantities of snow. To date this has not been necessary.

Red Dog Mine (Open Pit Mine)

The ore reserve at Red Dog dwarfs any other Cominco resource, with almost 17 million tonnes of Pb and Zn metal, and over 6 million kg. of silver.

Red Dog is in Northwestern Alaska, at latitude 67° north, and 90 km. inland from the coast of the Chukchi Sea (Figure 1).

The country around the mineral deposit is rolling hills, leading into mountains of up to 1,000 m. elevation. (Figure 11) The deposit is at an elevation of about 300 m., and is in permafrost, but different from that encountered in Greenland or the Canadian Arctic. The rock temperatures are only a few degrees below freezing, so the permafrost is relatively fragile, and can be fairly easily thawed, which adds cost to building roads and erecting structures.

Fig. 11 - Red Dog Camp

At Red Dog, in contrast to Polaris, permafrost is an engineering problem. For example, the mine is overlain with a combination of overburden and weathered mineral, ice-rich and unstable. As well, much of the surface soil consists primarily of colluvium (wind-blown fines), and this material serves to create additional instability. In the mine operation, the permafrost in the ice-rich surface material will require that this be mined only while frozen. The high moisture content would make handling this material difficult if allowed to thaw. This is particularly important with the surface mineralized areas, which are high in soluble heavy metals that have already created significant contamination in the area, and must be kept frozen so that additional leaching will not take place.

The plant site will be excavated down to good rock, to eliminate any concern in regard to the stability of the foundations, if thawed. The tailing dam will also be built on permafrost, but the dam design allows for the probability that a "thaw bulb" will form under the tailing pond and dam. Therefore, the design includes flat embankment slopes with facilities for removing any drainage water within the structure.

Another effect of the warm permafrost is on the road from the portsite to the mine. The majority of material underlying the road route is the ice-rich colluvium that can contain up to 30% ice, under 30 to 45 cm. of tussocky tundra. It is essential to preserve the tundra as an insulation so that the frozen soil will not thaw, and therefore the road is designed primarily as a built-up embankment. A minimum of 2.5 m. of fill will be placed on a geotextile mat which covers the width of the road. The purpose of the geotextile is to reduce the effect of rocks entering the voids between the tussocks, which could damage the roots and destroy the tundra (Figure 12).

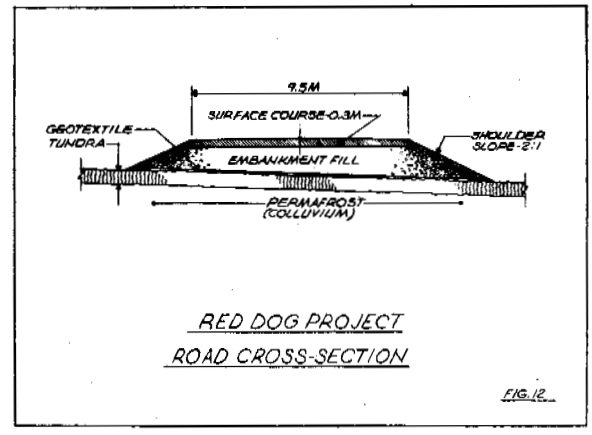

The other area of the road design that is affected by permafrost is the foundations for the bridges. These will be steel piles driven into the permafrost, with allowance for adjustment if any of the piles tend to "jack" under the effect of the seasonal freeze-thaw cycle in the active layer.

Fresh water flows at Red Dog cease for the colder months, similiar to the Black Angel and Polaris. To overcome this, a fresh water reservoir will be formed by an earth-filled dam which will be constructed in a drainage basin about 4 miles from the mine. As well, recycle of process water will be maximized, to reduce fresh water consumption and therefore the required size of the reservoir.

The final aspect of permafrost at Red Dog is at the portsite, where the onshore soils consist of about 15 m. of gravel, sand, and silt over bedrock, with up to 30% moisture as ice in the upper layers. The oil storage tank foundations consist of 2 m. of fill placed over the frozen ground, covered by 10 cm. of insulation, and with 0.5 m. of fine topping over the insulation (Figure 13).

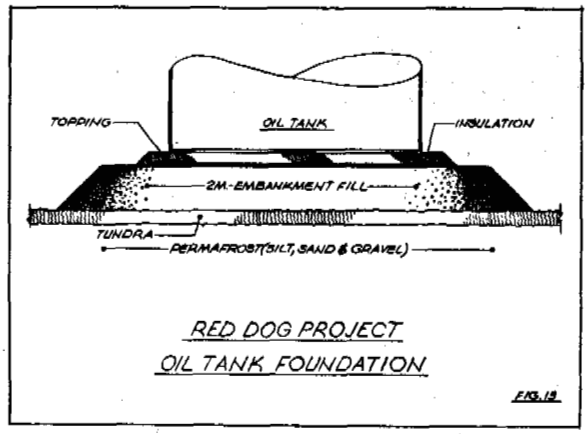

RED DOG PROJECT
OIL TANK FOUNDATION

FIG. 13

However, it is not possible to construct the large concentrate storage building at the shore because of probable creep in the ice-rich soils under the weight of the concentrate. Therefore, the concentrate storage building will be located 1,400 m. inland where there is bedrock under 3 m. of frozen overburden. The overburden will be removed and the concentrate storage building foundation will be sited directly on the rock.

Summary and Conclusions

This paper summarizes the construction and operation of three mining projects in the Arctic regions, and some of the practical aspects of dealing with permafrost. It is possible to take advantage of the engineering features of perennially frozen soil and rock. However, even if the permafrost is not an advantage, it must always be considered, as problems can be encountered if the characteristics of permafrost are ignored.

APPLIED STUDY OF PREVENTING STRUCTURES FROM FROST DAMAGE BY USING DYNAMIC CONSOLIDATION

Han, Huaguang and Guo, Mingzhu

Heilongjiang Provincial Low Temperature Construction Science Research Institute, Harbin, China

SYNOPSIS Some applied examples of subsoil treatment by using dynamic consolidation in buildings with shallow foundations, large tanks, road and sports ground engineerings have been introducted systematically in this paper. Our engineering practice shows that this treatment is a new technique for preventing structure from frost damage reliably and economicaly and can be used widely in future.

INTRODUCTION

Since 1982, a dynamic consolidation construction method has been used in Daqing, Harbin and other districts for treatment of frost susceptible subsoil, and lots of test engineerings were conducted at sametime, such as: industrial buildings, public and dwelling buildings with shallow foundation, large oil and gas tanks, water pools, pipe piers, pipe shelvers, road, large sports ground and so on. Our experimental results and operation condition of above various buildings for years were described and discussed in this paper.

APPLIED EXAMPLES OF ENGINEERINGS

Shallow foundation

Generally speaking, a main problem for large building set up on strong frost susceptible subsoil with shallow groundwater level is to prevent the buildings from frost damage. A dynamic consolidation method for improving subsoil such as silty clay with bog or pond was used in some engineerings. The brief conditions of test engineerings by using dynamic consolidation is shown in Table I.It is obvious that buildings with shallow foundation can be set up on strong frost susceptible subsoil as long as the dynamic consolidation technique is designed properly and coefficients are selected correctly.

Anti-heave practice for foundation of unheated open structures

This kind of structure with a deep frost depth under foundation, affected by air temperature directly, is easy to be suffered frost hazard, especially when the load up on foundation bed is not heavy and its construction is undertaken over winter or years. In order to prevent above structures from frost damage, a treatment of dynamic consolidation method has been used in the engineering base in the area of crude oil tanks. The conditions of dynamic consolidation used in crude oil tank area is listed in Table II. From Table II we know that even though the structures set up on the ground surface with frost susceptible subsoil, by using dynamic consolidation method, all of tanks have worked well. Meanwhile, a large amount of materials and money has been saved. What we have to point out is tank 76 and 77 started to work after construction for two years; tank 78 was set up in the next year after subsoil treatment by dynamic consolidation and started to work in third year; and all of the tanks were built in the subsoil with a middle sand or asphalt sand cushion with a thickness of only 0.3 to 0.45 m. Pipe piers and pipe shelvers were directly set up in spring in the pits with a depth of 1.2 m formed by dynamic consolidation. They, with a little load, have been worked well for years without any obvious frost heave and differential deformation caused by freeze-thawing cycles. As a conclusion, frost heave of subsoil can be completely controlled by using dynamic consolidation and the treatment subsoil may be constructed in frozen condition.

Prevention of frost heave and boil road

The subgrade, pavement, culvent, and bridge of road will be suffered frost damage in winter, and will be boiled or deformed differently in spring, which influences on transportation, construction serviously in cold regions. For preventing road engineering from frost damage, the dynamic consolidation method has been used for treatment of subgrade.

Test sections in two roads have been conducted in Daqing city. One of them named United road had a test length of 270 m and an area of 3300 m^2. The section was set up on the subsoil of clay and sandy clay with a sandy gravel pavement. It used to be stopped working because of frost heave and boil until rebuilding with a concrete pavement in 1984. The next section named Zhongqi road had a length of 100 m, an area of 2500 m^2, and was set up on the subsoil of sandy clay, silt and sandy, with asphalt pavement which replaced by concrete pavement in 1985.

The observation results in both test sections with or without treatment subgrade by dynamic

TABLE I

The Conditions of Test Engineering Base by Using Dynamic Consolidation

Projects	Engineering geologic conditions	Bearing capacity (MPa)		Frost susceptibility		Foundation depth (m)		Notes
		BR	AR	BR	AR	BR	AR	
dwelling building 82, 82* (six-storied	silty sandy clay:1 m thick groundwater: 0.5 m below the surface	0.08-0.12	0.25	strong	no	quarry stone strip footing 2.8-3.0	quarry stone strip footing 1.5	rammed in 1985
dwelling building 5-1, 2 (six-storied)	silty sandy clay of 0.5-1.0 m thick covered by fill soil of 0.8-1.2 m, groundwater talbe of 0.8 m below the surface	0.06-0.12	0.22-0.25	strong	no	quarry stone or reinforced concrete strip footing 3.0	quarry stone strip footing 1.5	rammed in 1984
laboratory (four-storied)	miscellaneous fill and silt of 1.0-1.5 m thick, groundwater of 0.5 m below the surface	0.06-0.10	0.15-0.16	heave	no	quarry stone footing 2.5	quarry stone footing 1.4	rammed in 1986
dorm building (five-storied)	fill soil of 0.8-1.0 m in the upper, silty sandy clay of 3-4 m below	0.08-0.10	0.18-0.20	strong	weak	quarry stone and reinforced concrete footing 4.0	quarry stone footing 1.5	rammed in 1986
training center building (seven-storied)	reed pond fill and silty sandy clay of 1.5-2.5 m thick underlain by silty sand, groundwater table of 0.8 m below the surface	0.06-0.10	0.16-0.18	strong	no	pile	reinforced concrete and quarry stone footing 2.0	rammed in 1985

Notes: BR = before rammed
AR = after rammed

consolidation method are listed in Table III, from which we know that the frost heave of subgrade can be reduced greatly after the treatment. Consquently, boiling can be avoided also.

MAIN PROPERTIES OF FROST SUSCEPTIBLE SUBSOIL AFTER A TREATMENT OF DYNAMIC CONSOLIDATON

The properties of subsoil will be changed greatly after a treatment of dynamic consolidation, because the subsoil layer will be compressed suddenly with a settlement of several to dozens centimeters while acted by kinetic energy of ram.

After dynamic consolidation, the density of subsoil will be increased with its porosity decreasing. The statistical results show that the dry density of subsoil is from 1.13 to 1.63 t/m^3 before the consolidation to 1.55 to 1.89 t/m^3 after the consolidation, and the void ratio is 0.55 to 1.42 before the consolidation and 0.45 to 0.75 after consolidation. The distribution of dry density and void ratio along depth is shown in Fig.1 and Fig.2.

Water content

After dynamic consolidation, the pore water pressure will be increased because the stress field of subsoil is changed. The cracks in soil mass will be occured while shock energy reaches a critical value which makes free water, capillary water and some weak bound water in soil expelled along the cracks. The experimental results show that water content is around 28 to 32% before the consolidation with a maximum of 64%, and 16 to 23% with a maximum of 28% after consolidation.

TABLE II

The Conditions of Crude Oil Tank Base by Using Dynamic Consolidation

Projects	Engineering geologic condition	Bearing capacity (MPa)		Frost heave		Foundation depth (m)		Notes
		before rammed	after rammed	before rammed	after rammed	before rammed	after rammed	
tank 76 steel tank	fill soil of 3-5m underlain by silty sandy clay and eroded by soil and acid	0.08	0.18-0.20	heave	no	2-3	0.3-0.45	rammed in 1984
tank 77 steel tank								rammed in 1984
tank 78 steel tank								rammed in 1984
pipe shelf 1-22	fill soil of 3-4 m underlain by silty sandy clay	0.08	0.15	heave	no	2-3	1.6	rammed in 1983
pipe pier 1-8								

TABLE III

The Conditions of Test Road Section by Using Dynamic Consolidation

Projects	Engineering geologic conditions	Pavement structure	Frost susceptibility		Notes
			unrammed	rammed	
Union road	subgrade was composed of sandy clay, groundwater table was 0.5 m below the surface;original sand and gravel pavement was broken by boiling	concrete pavement with thickness of 0.24 m underlain by sand and gravel	mean heave ratio of 69.4%	mean heave ratio of 3.77%	rammed in 1984
Zhongqi road	surface covered with sandy clay, silt sand; groundwater table was 0.5 m below the surface; asphalt pavement was boiled	concrete pavement of 0.24 m thick, underlain steel dregs, lime soil and white lime soil	100% (assumed)	decreased by 40-50%	rammed in 1985

Permeability and groundwater level

The observation results, obtained in door and in situ with tweleve engineering projects, show that the coefficient of permeability of soil decreases obviously after dynamic consolidation. In common case, the coefficient of permeability of clay after the consolidation is less than $1x10^{-6}$ cm/s with a minimum of $1x10^{-8}$ cm/s. Consquently, it is an impermeable layer within the subsoil without any sand intercalation. The groundwater level descends gradually from the beginning of ramming, and stays below the impermeable layer. Some observation results are listed in Table IV.

Frost susceptibility of foundation

In order to understand the frost susceptibility of subsoil after dynamic consolidation, some investigations in situ and frost susceptibility tests in laboratory have been conducted. The experimental results indoor are listed in Table V and the observation results in situ are listed in Table VI, from which the frost heave of subsoil might be reduced or eliminited by using dynamic consolidation. Our experimental results show that the relation between frost susceptibility of clayey soil after the consolidation and ramming energy per squre meter is very close. The more the ramming energy per meter is, the less the frost heave ratio of subsoil is (see Fig.3).

CONCLUSIONS

Our engineering practice and experimental results show that the frost susceptibility of

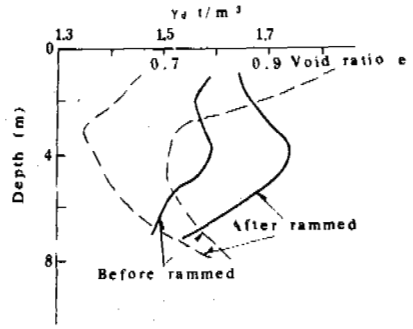

Fig.1 The Distribution of Dry Density and Void Ratio Along Depth for Dorm

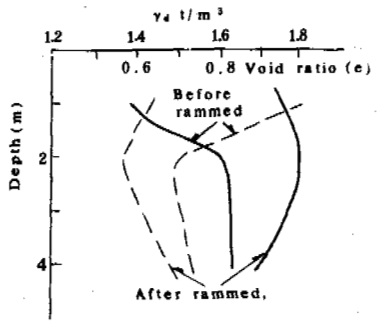

Fig.2 The Distribution of Dry Density and Void Ratio Along Depth for Dwilling Building

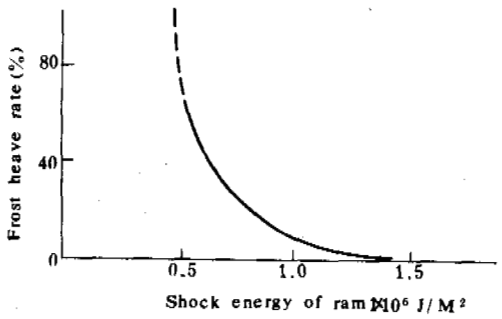

Fig.3 Frost Heave Patio vs Ramming Energy Per Squre Meter

TABLE IV

The Changes of Groundwater Level before and after Dynamic Consolidation

Projects	Groundwater level (m)	
	unrammed	rammed
Power plant	1.3	6.4
Stable crude oil tank area	1.5	6.0
Pipe shelf	1.5	5.6
Frozen ground testing station in Longfeng	0.3	4.8
Union road in Longfeng	0.3	3.0
Dwelling building	0.8	5.9
Office building	0.3	3.9
Dwelling building 82 and 83	0.5	6.2
Training centre	0.3	3.9
Daqing sports ground	0.6	3.7
Laboratory	0.3	3.9
Dorm	0.6	4.3

frost susceptible subsoil in seasonal frost regions may be reduced or eliminated after dynamic consolidation while the proper coefficient and ramming technology are selected reasonable with a given shock energy.

Analysing cryogenic texture of rammed soil frozen in open system with undirectional freezing, we know that the ice content was little without water accumulation and ice segregation in soil. Consquently, the treatment of subsoil by using dynamic consolidation is a new way for preventing structures from frost damage and increasing bearing capacity of subsoil. This construction method is very simple and can be used widely, so it is a valuable and practical technology.

ACKNOWLEDGEMENTS

The authors are grateful to the following coworkers: Mr.Tang Xiaobo, Mr..Wang Gongshan, Mr. Yu Guorong, Mr. Zhu Liping, Mr. Deng Runhui and Mr. Qi Huayi in Daqing Design Institute of Chemical Industry and Mr. Wang Zuerong in the First Architecture Company of Daqing city.

REFERENCE

Wu Ziwang and Zhang Uiayi, (1982). Strength of frozen soil and its destructive power, Proceedings of II National Conference on Permafrost, p.275-280.

TABLE V

The Results of Susceptibility Test in Laboratory

Projects		Sampling depth(m)	Number of test	Ratio of frost heave (%)	Mean frost heave ratio (%)
Daqing sports ground	Before rammed	0.5-1.1	2	19.0	20.5
			4	21.8	
			5	20.7	
		1.1-1.5	3		11.4
			6		
	After rammed	0.5-1.0	8		2.33
			9		
		1.0-1.5	10		3.03
			12		
			15		
		1.5-1.8	11	5.02	4.64
			13	5.07	
			14	3.20	
Dorm	Before rammed	0.1-0.3	1	14.8	19.7
		0.3-0.6	2	24.6	
	After rammed	0.3-0.5	3	0.85	2.0
			5	3.03	
		0.5-0.7	4	0.35	2.0
			6	3.60	
Dwelling building	After rammed	1.0-1.5	1	-1.2	0.1
			3	0.39	
			5	0.98	
		1.5	2	-0.64	-0.94
			4	-1.24	

TABLE VI

The Results of Frost Susceptibility Observation in Situ

Projects	Frost heave ratio (%)	
	Unrammed	Rammed
Frozen grouhd test station in Longfeng	9.3	0.8
Union road in Longfeng	6.94	3.77
Dwelling building	3.82	-1.4
Crude oil tank area	strong heave	-0.6

EFFECT OF HEATING ON FROST DEPTH BENEATH FOUNDATIONS OF BUILDING

Hong, Yuping and Jiang, Hongju

Oilfield Construction Design and Research Institute, Daqing Petroleum Administrative Bureau, Daqing, Heilongjiang Province, People's Republic of China

SYNOPSIS This study was started in 1960's and then continued at the beginning of 1980's. The purpose of this study was to determine the design values of Mt factor for eveluating the heating effect when the difference in elevation between indoor and outdoor surface (Δh) was great than 45 cm. The frost depth of 11 selected houses was detected and the Mt values were calculated for the houses with different values of Δh. The relationship between Mt and Δh was found to be in a linear function. The heating still significantly affected the frost depth both at the corner of outside walls and the middle section of north facing walls when Δh was less than 75 cm. The Mt values were close to one at northwest corner and in fraction at the middle section of northern wall when Δh was equal to 75 cm.

INTRODUCTION

The study of the effect of heating on frost depth in subsoils is of great significance for the stability of structure foundations in seasonal frozen regions. The economical and reasonable design and construction of foundations mainly depend on how well this study is carried out. Therefore, observations on the real structures have been started from 1960's and then continued in the period from 1981 to 1986. Some results have been brought into the Standard of Foundation Design in the Industrial and Civil Architecture (TJ7-74) and its revised edition in 1985. This paper is to discuss the elemental results of this study.

TEST AND OBSERVATION

To understand the effect of house heating on frost depth, the observations have been conducted on the selected houses under operation. The structure of those houses is made up of brick-wood or brick-concrete with single or multiple storeies, which is popular in China. This type of houses was usually using strip foundation and brick wall. Indoor floor was directly built on ground surface. Thermocouples or indicators of frost depth were buried beneath both inside and outside walls and around the foundations. The observations on the eleven selected houses lasted in a period of ten years from 1961 to 1965 and from 1981 to 1986 and a lot of reliable data were collected.

FEATURES OF EFFECT OF HEATING ON FROST DEPTH

From the observed data on the eleven selected test houses, the features of the effect of heating on frost depth could be summarized as follows:

Unevenness of frost penetration during freezing

The observed data show that the frost penetration of soils along the outside wall of foundation is developed unevenly. The base soils are firstly frozen beneath the four corners and beneath the middle section of the wall. The time reaching to the maximal frost depth is also different. In a testing house, for instance, the maximal frost depth was reached on Mar.28 at northwest corner, on Mar.20 at the middle section of the northern wall and on Feb.20 at the middle section of the southern wall, respectively. The frost penetration depth is the least at the middle section of the southern wall and its date reaching to the maximal frost depth is about one month earlier than that at the middle section of the northern wall. The difference of frost depth in soils between two adjacent observed points of the foundation reaches to the maximum in the middle ten days of Feb.when the frost depth of soils reaches to 90% as deep as its maximum

The thawing process of frozen soils around the outside wall foundation is opposite to the process of freezing. Thawing at the middle section of the southern wall occurs about two months earlier than that at the northern wall. Thawing occurred at the middle section of the wall is earlier than that at the corner, and thawing occurred at the northern corner is the latest with about three months later than that at the middle section of the southern wall.

Unevenness of the maximal frost depth around the outside wall foundations

The frost depth is deeper at four corners and much shallow at the middle of the foundation. The date reaching to the maximal frost depth changes with places. The observed data of a test house are shown in Table I. A significant

TABLE I

Maximal Frost Depth Observed at a Test House

Location	Southern wall			corner	middle of E.wall	NE. corner
No	I	II	III	IV	V	VI
hmax	160	135.3	153.1	176.7	145.9	170.20
D	Mar.5	Feb.20	Feb.23	Mar.10	Mar.5	Mar.20
Location	Northern wall			NW. corner	middle of W.wall	outdoor
No	VII	VIII	IX	X	XI	0
hmax	157.4	168.5	177.3	180.2	166.7	190
D	Mar.20	Mar.20	Mar.20	Mar.20	Mar.20	Mar.20

Note: hmax—the maximal frost depth,cm;
D—the date reaching to the maximal frost depth.

thaw depth has occurred at the southern wall when the maximal frost depth is just reached at the eastern, northern and western walls. The maximal frost depth of the test house is shown in Fig.1. It can be seen that the places with remarkable changes in frost depth are at eastern and western gables, and at both ends of southern and northern lengthwise walls with the distance of 4 m from the corners (especially, at the ends of corners in the southern wall).

Difference in the maximum frost depth between inside and outside of an outside wall foundation

Observations show that the frost depth at inside of an outside wall foundation is less than that at outside, and the difference in frost depth between inside and outside at corners of an outside wall foundation is less than that at the middle section of the foundation (see Fig.2). From the three features of frost depth mentioned above beneath foundations of the outside wall of a heating house, it is understood that the differential deformation of houses will be caused by frost heave and thaw settlement during freezing and thawing processes of subsoils. If the differential deformation of house exceeds a critical limit, the cracks in house will be caused. Therefore, it is necessary to know the three features in the study on the stability of foundations in the seasonal frozen ground.

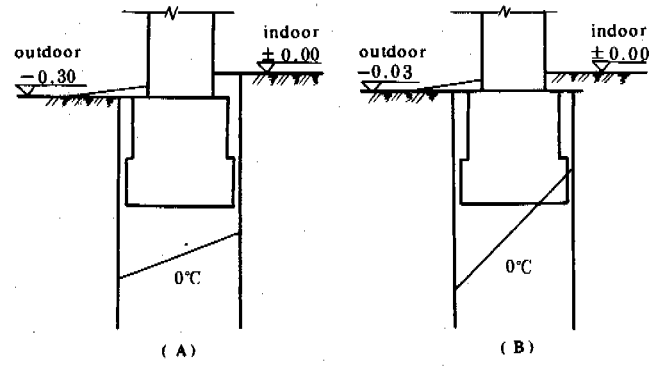

Fig.2 Difference of Frost Depth Between Inside and Outside of a Foundation
A: at the corner
B: at the middle section

DETERMINATION OF THE INFLUENCING COEFFICIENT OF HEATING ON FROST DEPTH

The frost depth of subsoils beneath foundation

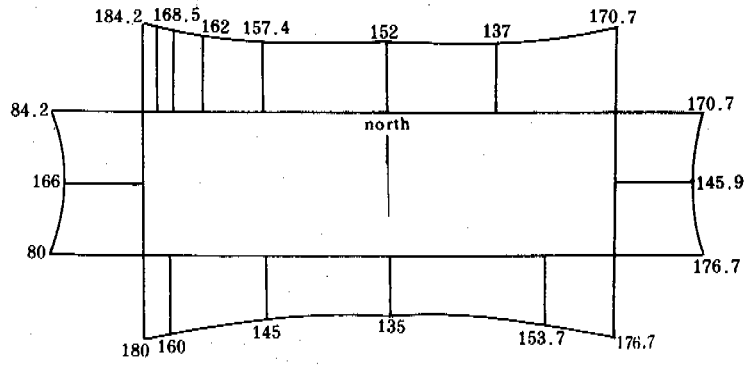

Fig.1 Maximum Frost Depth in cm for a Test House (determined on Mar.20,1963)

is reduced by the indoor heating of houses in winter. The reducing degree could be expressed as follows, which is so-called the influencing coefficient of heating on frost depth.

$$Mt = \frac{Hh}{Hn}$$

where Hh—the measured frost depth at the outside of the outside wall foundation of a building;
Hn—the frost depth of soils near by the building in natural conditions with the bear surface (without snow or vegetation cover). Note that Hh and Hn should be measured at the same time.

The value of Mt is influenced by the following factors:

Influence of the indoor temperature

For the unheated house, the Mt value at the corner of a house equals to one, or even slightly greater than one. But for the heated house, the frost depth of subsoils beneath the foundation is reduced. There are, for instance, two houses with the brick floor and the elevation difference of 30 cm between indoor and outdoor surface, the indoor temperatures of the two houses are 7.6 and 14°C (mean air temperature of Jan. and Feb.) respectively. The Mt values at northern corner of the houses are 0.94 and 0.84, respectively.

Influence of elevation difference between indoor and outdoor surface

As shown in Table II, the more the elevation difference (Δh) between indoor and outdoor surface, the greater the Mt value.

TABLE II

Values of Mt for Different Δh

Δh	0	30	50	70
Mt value	0.82	0.86	0.90	1.0

Influence of the location along a foundation

The values of Mt calculated from the data observed at a test house with Δh=30 cm in 1963-1964 are shown in Table III. As shown in Table III, the Mt value at the corner is greater than that at the middle section of a wall, and for the middle section, the Mt value at the northern wall is greater than that at the southern wall.

In determining the design values of Mt, the three factors mentioned above should be considered. But, for the general houses used for living and working, the indoor air temperature in winter is usually in the range of 15 to 18°C, i.e., the temperature difference is only 3°C, so that the influence of temperature on Mt value is insignificant. Therefore, the elevation difference (Δh) and the location along foundation are the more important factors for determining

TABLE III

Mt Values at Different Locations long a Foundation

Location	NW. corner	Middle of W.wall	SW. corner	Middle of S.wall
Mt value	0.84	0.62	0.80	0.50
Location	SE. corner	Middle of E.wall	NE. corner	Middle of N.wall
Mt value	0.69	0.55	0.77	0.65

Mt values.

For the engineering purpose, the two "representative" values of Mt are adequate. One is the Mt value at the northern corner and another at the middle section of the northern wall. To determine the values of Mt, the frost depth along the outside wall foundations of the eleven testing houses was observed. The calculated values of Mt were shown in Table IV. Fig.3 shows the relationship between the Mt value and the

TABLE IV

Calculated Values of Mt for 11 Test Houses

Δh (cm)	Type of floor	Indoor temp. (°C)	NW. corner	Mt Middle of N.wall	Year of observation	Type of house
0.00	concrete	10-18	0.82	0.50	1982-84	two-storey brick
30			0.94	0.77	1962-63	
30	brick	10-16	0.88		1962-63	single-storey
30			0.84	0.66	1963-64	brick-wood
50		9-17	0.84	0.66	1982-83	
50	concrete	9-17	0.98	0.79	1983-84	single-storey
75		10-19	1.01	0.62	1982-83	brick-concrete
75			0.94		1983-84	
75	concrete	13-18	0.93	0.70	1983-84	five-storey
75			1.00	0.73	1984-85	brick-concrete
75			0.93		1984-85	

elevation difference (Δh) between the floor and natural ground surface, which is plotted from the data shown in Table IV.

From figure 3 it can be seen tant the relationship between Mt and Δh is nearly linear. The higher the value of Δh, the greater the value of Mt. The heating influence on frost depth is very obvious when Δh is less then 75 cm. It is obvious at the middle section of the wall and less obvious at the northern corner when Δh is equal to 75 cm.

For the design value of Mt, it is described in the Standard of Foundation Design in the Industrial and Civil Architecture (TJ7-74) that the

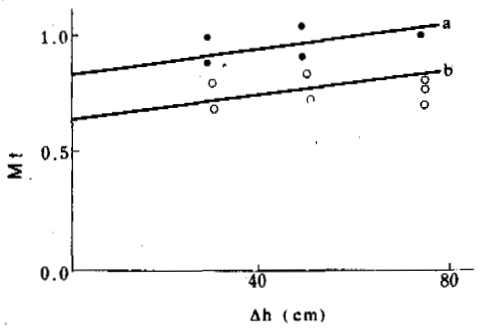

Fig.3 Relationship Between Mt and h

A: at the northwestern corner
B: at the middle section of the northern wall

value of Mt is equal to 0.85 at the corner of the outside wall and 0.70 at the middle section of the outside wall, respectively, when the house is directly built on ground surface. By using those stipulations, even if these houses are operated for a long period of ten years, they are stable, it proved that those stipulations are safe and reliable. According to the stipulations in the Standard TJ7-74. Mt value equals to one when the indoor temperature during heating is lower than 10°C and the elevation difference between indoor and outdoor surface is greater than 45 cm. But according to the data observed for several years(Fig.3 and Table IV), when Δh is in the range of 45 to 75 cm, the Mt values are in the range of 0.84 to 1.01 at the northern corner and 0.6 to 0.79 at the middle section of the northern wall, respectively. It indicates that heating still has considerable influence on frost depth when the value of Δh is in the range of 45 to 75 cm, so that the Mt values in the Standard TJ7-74 should be revised and the suggested values are shown in Table V.

TABLE V

The Suggested Values of Mt

Δh (cm)	Values of Mt at different locations	
	corners of outside wall	middle section of outside wall
≤30	0.85	0.7
=75	1.0	0.8
>75	1.0	1.0

Note: 1) Mt value could be taken by interpolation when values of Δh are in the range of 30 to 75 cm;
2) Mt values in Table V is available for the condition of the indoor floor directly built on the ground surface; (3) The division of the middle section and the corner is the same as the description in the remark of Table 19 in the Standard TJ7-74.

REFERENCE

The Standard of Foundation Design in the Industrial and Civil Architecture TJ7-74 (1974). Beijing, Publishing House of Architecture Industry.

PREDICTION OF PERMAFROST THAWING AROUND MINE WORKINGS

V.Yu. Izakson[1], E.E. Petrov[1] and A.V. Samokhin[2]

[1]Institute of Mining Engineering of the North, Yakutsk, U.S.S.R.
[2]Yakutsk State University, Yakutsk, U.S.S.R.

SYNOPSIS We have derived approximate formulae for prediction of the size of thaw areas of the mine working walls under the influence of warm air for positive and sign-varying thermal regimes. An analysis is made of the influence of a variety of factors upon thawing dynamics. The usefulness of heat insulation as applied depending on operating conditions for workings is shown.

Advantageous usage and design of the supports of mine workings within the permafrost are impossible unless thawing dynamics of the walls under the effect of a warm air is predicted. This question has been addressed by a number of papers having the same disadvantage in common, namely the analysis was made for conditions of a constant, positive temperature of the air in the mine.

For practical purposes, however, it is the results for variable temperatures which are required on most occasions because mine workings of all underground mining enterprises in the North-East of the U.S.S.R. operating throughout the year, are under conditions of a sign-varying heat regime.

Papers taking account of air temperature fluctuations are not numerous and are, basically, concerned with problem statements. Engineering prediction techniques (Izakson and Petrov, 1985) find a limited field of application and lack the analysis of thawing dynamics for positive and sign-varying heat regimes.

In the present paper this problem will be solved by a method of mathematical simulation on a computer by an algorithm reported in a paper of Izakson and Petrov (1986).

The algorithm solves multifront Stephan problems by the finite difference method via automatic sampling of the smoothing parameter. A large-scale computer simulation experiment has been conducted for the following variations of affecting parameters (Table I).

Mathematical simulation was carried out in two stages. The first stage involved selecting thermal characteristics of the problem (the heat exchange coefficient α, the heat conductivity and heat capacity coefficients for rock ground in unfrozen and frozen conditions λ_T, λ_M, $c_T\rho$, and $c_M\rho$, and moisture content of rock ground w) such as to achieve agreement between calculated and experimental results obtained under natural conditions (Dad'-kin et al., 1968) and laboratory experiments

TABLE I

Limits and Steps of Variation of Values in Mathematical Simulation

Parameter	Lower limit	Upper limit	Step
Natural temperature of a rock mass, T_o, °C	-6	-2	2
Yearly mean air temperature in the mine, t_{mean}, (t_{cp}),°C	-6	8	2
Yearly amplitude of air temperature fluctuations in the mine, A_t, °C	0	10	2
Service time of the working τ, months	1 1	48 240	0.1 0.25
Thermal resistance, R_u, $\frac{m^2 K}{W}$	0	3	0.5

(Izakson and Petrov, 1985). This was successfully obtained for α = 10 W/(m^2 · K), λ_T = = 1.6 W/(m · K), λ_M = 1.9 W/(m · K), $c_T\rho$ = = 640 W · hr/(m^3 · K), $c_M\rho$ = 480 W · hr/(m^3 · K), and w = 0.1.

In the second stage of mathematical simulation the variants were calculated using data in Table I. The calculation results were handled by the method of least squares. Although for each variant, we calculated the entire temperature field, we, nevertheless, investigated the behaviour of the main parameter of the temperature field, namely the size of the thaw area (ξ), whose boundary was taken to be the zero isotherm.

The case of heat exchange at constant, positive temperature was investigated on numerous occasions. The best representation of the dependence of the depth of thaw on the time of heat exchange is

$$\xi = a + b \lg \tau, \qquad (1)$$

where τ is the service time of the working (years).

For each variant, we determined the coefficients of equation (1), for each of which we chose a complex argument giving the best (in the sense of a minimum of standard deviation) representation of the dependences of the coefficients upon the affecting parameters. For the coefficient a, this is $\frac{t_{cp}}{|T_o - 1{,}8|(R_u+1)^3}$, and for b, $\frac{t_{cp}}{|T_o - 1{,}8|(R_u+1)}$. Representing the dependences of the above arguments may be characterized as being good (Figs 1, 2).

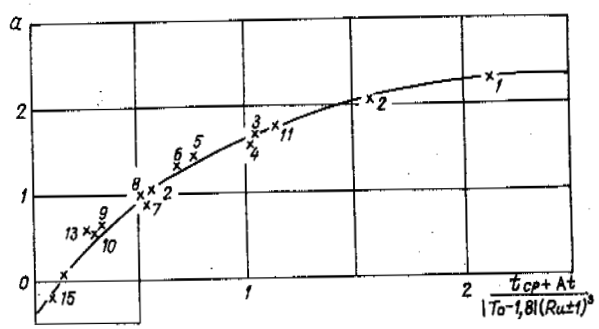

Fig. 1 The Dependence of the Coefficient Involved in Equation (1) upon Affecting Parameters. Mathematical Simulation Data are Numbered: 1st Figure t_{mean}, 2nd Figure, T_o, °C 8-2 (1), 6-2 (2), 4-2 (3), 6-4 (4), 6-6 (5), 4-4 (6), 2-2 (7), 4-6 (8), 2-4 (9), and 2-6 (10). Points 11-15 are obtained at t_{mean} = 6°C and T_o = -2°C, for heat resistances of 0.125; 0.4; 0.9; 1.3; and 1.53 W/(m^2 ·K), respectively.

The variable of air temperature of the mine was simulated using the relationship

$$t = t_{cp} + A_t \cos\left(\frac{\pi\tau}{6}\right),$$

where τ is time (months), i.e., allowance is made only for the annual cycle of temperature fluctuations and the beginning of heat exchange is accomplished with maximum yearly temperature.

In the case of a positive heat regime ($t_{mean} > 0$, $A_t \leq t_{mean}$), movement of the front of thaw is proceeding in the same manner as depicted in Fig. 3 which also shows the movement of the front of thaw at a constant temperature equal to t_{mean}.

The movement is oscillatory in character, i.e., the position of the front of thaw fluctuates

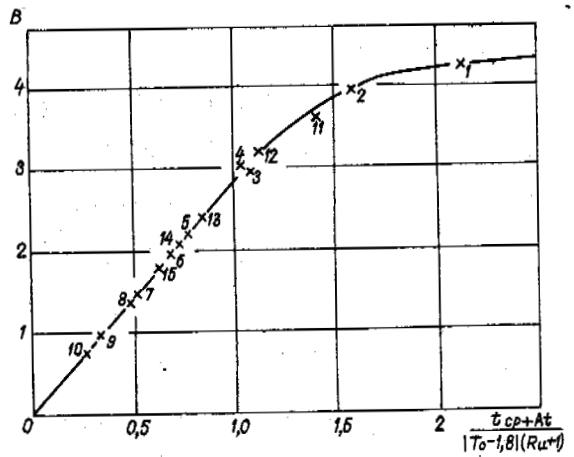

Fig.2 The Dependence of the Coefficient b; Point Numbering is the Same as Fig.1.

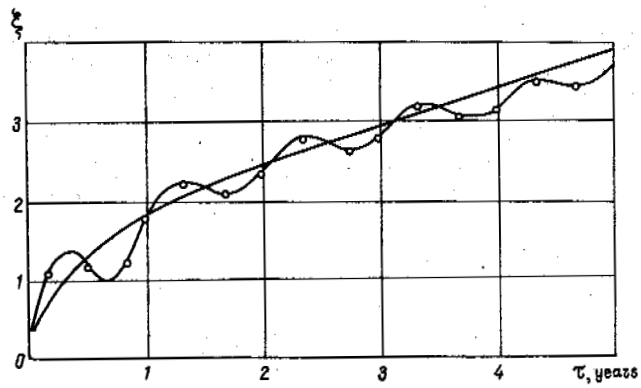

Fig.3 The Movement of the Front of Thaw in the Case of a Positive Heat Regime, °C: t_{mean} = 6, T_o = -2, A_t = 0(1), 6 (2).

The movement is oscillatory in character, i.e., the position of the front of thaw fluctuates about a position defined by equation (1). Following 4 or 5 cycles, the movement becomes a stationary one, pulsating toward the smaller side by 5 to 8% (the smaller is the yearly amplitude of air temperature fluctuations, the smaller is the deviation). Ignoring this, the size of the area of thaw at a variable, positive air temperature in the mine can be predicted using equation (1).

In the case of a sign-varying heat regime of the air inside the working, thawing dynamics are different for negative and positive yearly mean temperatures. When $t_{mean} \leq 0$°C, the movement of the front of thaw is pulsating in character (Fig. 4).

For prediction purposes as regards the greatest size of the area of thaw, for $\tau > 1$ year, we obtained the equation

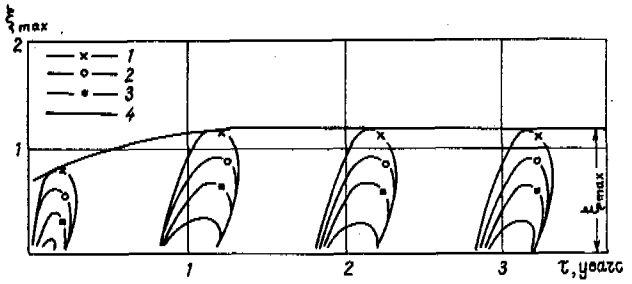

Fig.4 The Movement of the Front of Thaw in the Case of a Sign-Varying Heat Regime and Negative Yearly Mean Temperature, °C: $t_{mean} = -2$, $T_o = -4$, $A_t = 10$ (1), 8 (2), 6 (3), 4 (4).

$$\xi_{max} = \frac{22}{|T_o - 20|}\left[1{,}256 + 2{,}01\,\ell g\,\frac{t_{cp} + A_t + 2}{|t_{cp} - 8|(10R_u + 1)^{0{,}75}}\right] \quad (2)$$

The closeness of relation between equation (2) and mathematical simulation results is shown in Fig. 5.

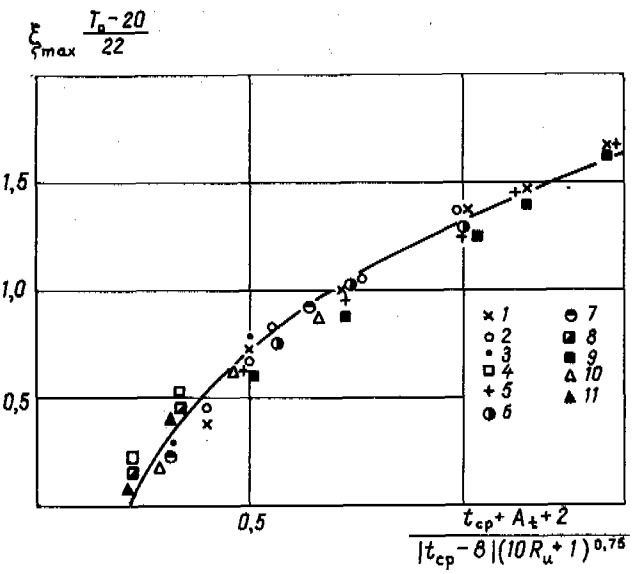

Fig.5 The Dependence of the Maximum Depth of Thaw upon Affecting Factors ($t_{mean} < 0$, $A_t > |t_{mean}|$). Mathematical Simulation Data are Numbered (1st Figure t_{mean}, 2nd Figure T_o, °C) 0-2 (1), -2-2 (2), -4-2 (3), -6-2 (4), 0-4 (5), -2-4 (8), 0-6 (9), -4-6 (10), -6-6 (11).

At positive, yearly mean temperature, thawing dynamics are more complicated. Let us denote by τ^* the time before which the condition $\xi_{max} < \xi$ is satisfied, where ξ is the depth of thaw at constant temperature (t_{mean}). It is evident that, when $\tau \leq \tau^*$, the thawing is pulsating in character, with the depth of thaw increasing from year to year and becoming stable when $\tau = \tau^*$.

Within this time range, as the amplitude of yearly air temperature fluctuations grows, the depth of thaw increases as well.

For $\tau > \tau^*$, this relationship is valid only for large amplitudes (A_t). If ($A_t - t_{mean}$) lies within the interval 0.5 - 2.5° (the interval becoming shorter with a decrease of the parameter $\frac{t_{cp}}{|T_o - 1{,}8|(R_u + 1)}$), then thawing dynamics show an unusual behaviour (curve 3 in Fig. 6).

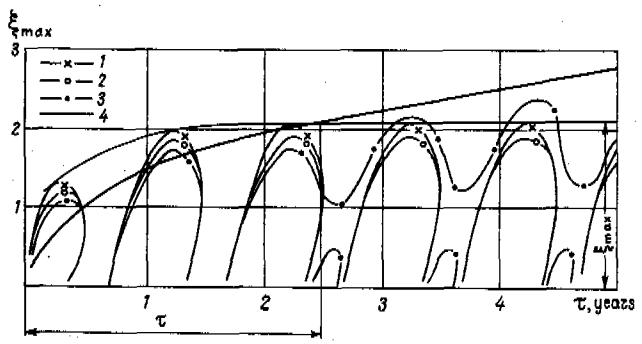

Fig.6 The Movement of the Fronts of Thaw in the Case of a Sign-Varying Heat Regime and Positive, Yearly Mean Temperature, °C: $t_{mean} = 4$, $T_o = -4$, $A_t = 10$ (1), 8 (2), 6 (3), 0 (4).

The outer front of phase transition that is situated farther from the working contour, displaces according to the relationship represented by a harmonic curve, whose ordinate of maxima and minima grows with the time remaining, however, smaller than the depth to which the mass would thaw out, provided that the temperature is constant.

The inner front of phase transitions appears during a 'cold' period of air temperature and, on some occasions, does not make contact with the outer front (Fig. 6).

For prediction purposes as regards the greatest depth of thaw, for $\tau \geq \tau^*$, we obtained the equation

$$\xi_{max} = \frac{22}{|T_o - 20|}\left[1{,}822 + 2{,}14\,\ell g\,\frac{t_{cp} + A_t}{|t_{cp} - 12|(10R_u + 1)^{0{,}75}}\right] \quad (3)$$

The quality of this dependence is illustrated by Fig. 7.

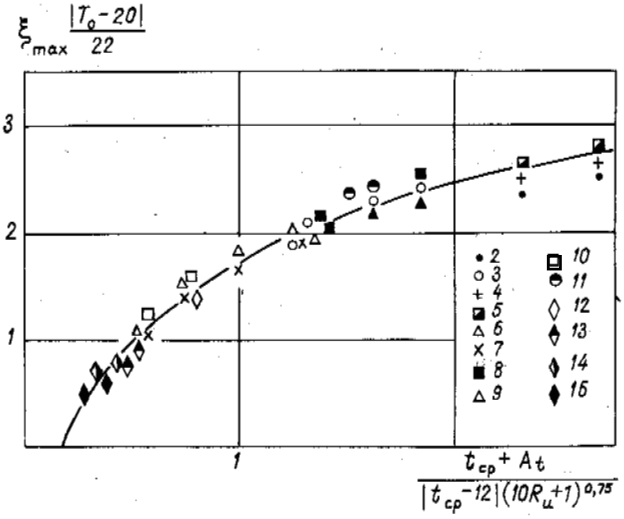

Fig.7 The Dependence of the Maximum Depth of Thaw upon Affecting Dactors ($t_{mean} > 0$, $A_t > t_{mean}$). Point Numbering is the Same as Fig. 1.

In order to calculate the value of τ^*, we may take advantage of the formula

$$\ell g\tau^* = \frac{\xi_{max} - \alpha}{\beta}, \qquad (4)$$

where ξ_{max} is determined by the expression (3), and the coefficients α and β are determined in Figs 1 and 2.

Let us analyze the results obtained. To begin with, it should be noted that the widely accepted point of view about the equivalence of the effects of a sign-varying cycle and the air temperature constant equal to t_{mean} is misleading. The depth of thaw in the first case is able to be both larger (when $\tau < \tau^*$) and smaller (when $\tau > \tau^*$) as compared with the second case.

In the case of a positive temperature regime and sign-varying temperature, but $A_t - t_{mean} \leq 2.5$, the depth of thaw can be predicted using formula (1) which may be transformed thus:

$$\xi = \beta\ell g\frac{\tau}{\tau_0}$$

where $\ell g\tau = -\frac{\alpha}{\beta}$ is the time of thawing onset after the warm air has affected the working walls. Note that heat insulation of the working walls has a larger influence upon the magnitude of the coefficient α (and hence upon τ_0) than upon the coefficient β in equation (1) because the argument of the dependence for α involves the value of thermal resistance to the 3rd power. Consequently, heat insulation effectively delays the onset of thawing and influences, to the same extent, the displacement speed of the front of thaw during a prolonged action of the warm air.

On the contrary, in the case of a sign-varying temperature regime, heat insulation effectively reduces the depth of thaw at prolonged service times of the working and has little effect during the first years because a high maximum temperature of the cycle comes into play.

In the case of sign-varying cycles the depth of thaw can be predicted with a reserve using formulae (2) and (3); however, with cycles with a positive, yearly mean temperature and short service times, the reserve may turn out to be considerable as well since formula (3) gives a value of $\tau \geq \tau^*$, and τ^*, at small values of $\frac{t_{cp}}{|T_0-1,8|(R_u+1)}$ may be large.

During the first year of service, thawing dynamics depends substantially upon the onset time of exploitation, i.e., on the period (win, ter, summer, spring, or autumn) during which the working is driven. During the second year and later on, this influence relaxes becoming of no significance. Fig. 8 gives example plots of thawing for four variants of the temperature regime. The type of scheme for air temperature variation is schematically represented by a circle diagram. A processing of the results derived from a mass computer experiment made it possible to obtain empirical formulae for the maximum relative depth of thaw during the first year of exploitation

$$\xi = \frac{22}{|T_0-20|}\left[C + B\,\ell g\,\frac{t_{cp}+A_t}{|t_{cp}-12|(10R_u+1)^{0,75}}\right] \qquad (5)$$

The coefficients B and C are given in Table II.

TABLE II

The Coefficients Involved in the Expression (1) as a Function of the Onset Time of Exploitation of the Working

No.	Variant (Fig.8)	B	C	Correlation ratio of the dependence
1	a	0.5869	0.6017	0.9928
2	b	0.8117	0.9037	0.9963
3	c	0.6154	0.6850	0.9924
4	d	0.7846	0.8734	0.9975

The relationship (5) is characterized by a very high closeness of relation because the correlation ratios are close to unity.

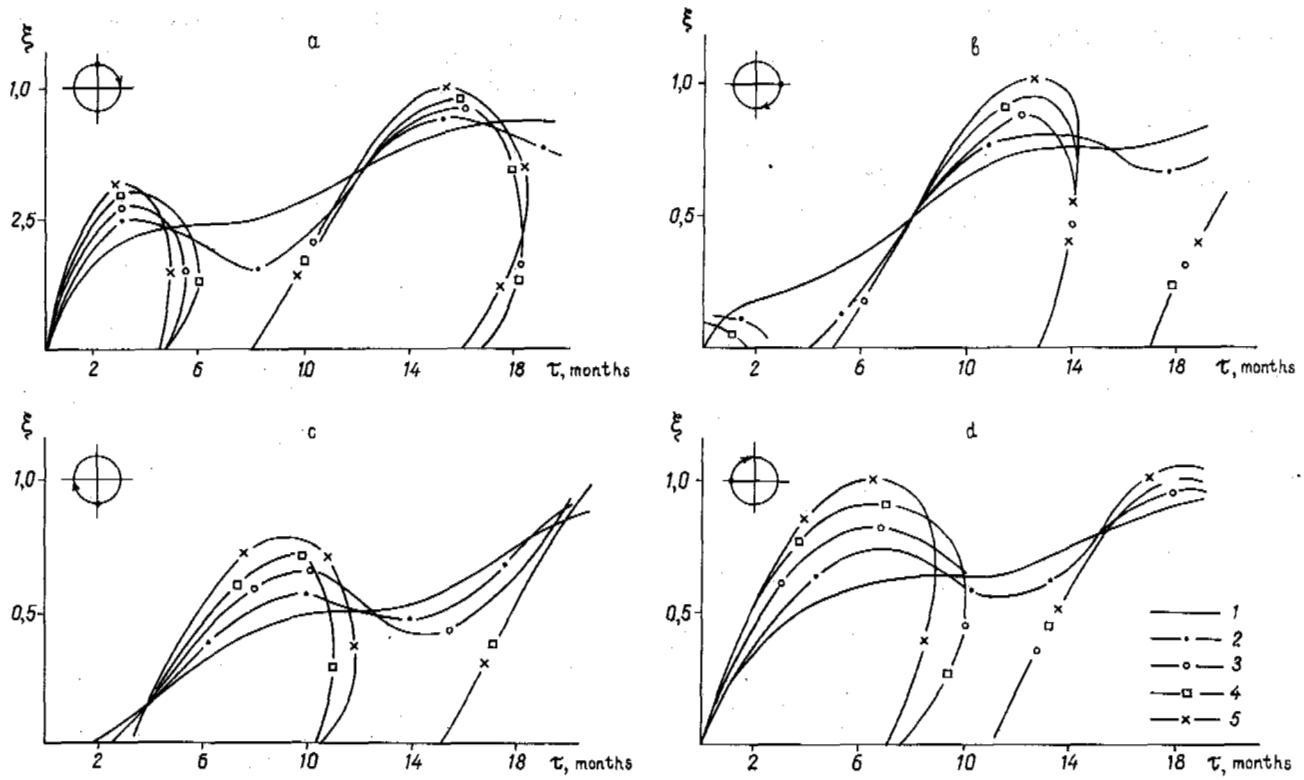

Fig.8 Examples of the Time Dependence of the Depth of Thaw for t_{mean} = 4°C, T_o = -4°C. The Amplitude of Yearly Air Temperature Fluctuations: 2° (1), 4° (2), 6° (3), 8° (4), 10° (5).

A maximum value is reached at different times with respect to the beginning of exploitation of the working (Table III).

TABLE III

Onset Times of Maximum Thaw with Respect to the Beginning of Exploitation (Months)

No.	Variant (Fig.8)	First maximum	Second maximum
1	a	3.1	15.1
2	b	12.6	24.6
3	c	9.3	21.3
4	d	6.5	18.5

By analyzing the results obtained, we are led to draw the following conclusions.

1. The onset time of heat exchange influences only the intensity of the first cycle of thawing and does almost not affect the simultaneity of the thawing and the air temperature variation (Table III). The time delay of the thawing with respect to the air temperature variation ranges from 10 to 20 days and seems to be of no practical concern.

2. The apparently unusual minimum of the depth of thaw for variant (a) is accounted for by the fact that the period of positive air temperature responsible for the first cycle of thawing is exceedingly short.

3. For the first year of exploitation of the working, heat insulation is a powerful remedy for the thawing - it can be avoided using heat insulation with a thermal resistance 3.....4 m^2K/W, which corresponds to 15.....20 cm thickness of foam plastic, for example.

4. The natural temperature effect of rocks is not as significant in the range studied - as T_o varies from -6° to -2°, the relative depth of thaw increases by 30%.

5. The results presented here may be useful for prediction purposes as regards the depth of thaw in the walls and the roof of the workings, as well as deciding upon the use of heat insulation and choosing temperature regime parameters of exploitation of the workings.

REFERENCES

Dyad'kin, Yu.D., Zilberbrod, A.F., and Chaban, P.D. (1968). Teplovoi rezhim rudnykh, ugolnykh i rossypnykh shakht Severa, Moscow: Nauka.

Izakson, V.Yu. and Petrov, E.E. (1985). Inzhenerny metod prognozirovaniya i regulirovaniya razmerov oreolov protaivaniya vokrug gornykh vyrabotok oblasti mnogoletnei merzloty, No. 5, FTPRPI.

Izakson, V.Yu. and Petrov, E.E. (1986). Chislennye metody prognozirovaniya i regulirovaniya teplovogo rezhima gornykh porod oblasti mnogoletnei merzloty, Yakutsk: Izd. YaF SO AN SSSR.

EXPERIENCE IN CONSTRUCTION BY STABILIZATION METHOD

L.N. Khrustalev[1] and V.V. Nikiforov[2]

[1]Laboratory of Engineering Geocryology, Faculty of Geology, Moscow State University
[2]Research Institute of Bases and Underground Structures, Moscow, USSR

SYNOPSIS The paper presents a new method for building foundations on perennially frozen grounds along with the assessment of the field of its possible application. Structural and technological designs of bases, foundations and cooling systems are described and the data obtained in the course of observations of the buildings built by this method are analyzed.

In permafrost regions all the areas under construction can be divided into two groups: areas with continuous or discontinuous perennially frozen grounds.

The former are most simple for development. Hence, the first principle of using grounds as a base is applied here: foundations are built in the permafrost; ventilated vaults or other cooling systems being arranged under a building. These systems help maintain a frozen state of the ground under buildings over the whole period of exploitation.

The latter are more complicated, since they require preliminary freezing or thawing of the permafrost to prepare a base for construction. Preliminary freezing artificially creates the conditions characteristic of the first group of areas, and then the ground of the base is used according to the first principle. The preliminary thawing creates conditions under which a further thawing of perennially frozen grounds under the action of heat generated by a building will not result in abnormal settlement of the foundations during the entire period of exploitation.

At present, a more economical way of constructing on permafrost of discontinuous type has been developed which envisages stabilization of the initial permafrost table over the whole period of a building exploitation. The idea of such a stabilization was proposed and protected by the authors' certificate granted to G.V.Porkhaev, L.N.Khrustalev, V.N.Yeroshenko and others (Avtorskoe svidetelstvo..., 1975).

The method of stabilization is applied at construction sites where the layer of seasonal freezing and thawing does not merge with the permafrost fully or partially within the area of a building, and the perennially frozen grounds are characterized by a considerable compressibility at thawing, and the overlying thawed grounds possess heaving properties during freezing.

The method involves maintenance of the initially prescribed permafrost table over the whole period of exploitation with the help of a ventilated vault arranged under the building. The bottom of the foundations is located in the layer of unfrozen ground between the permafrost table and the bottom of a seasonally or perennially frozen layer.

A mean air temperature close to zero is maintained in the vault for the whole period of exploitation to exclude the heat influence of a building on the underlying permafrost. In that case, the depth of seasonal or perennial ground freezing under the building becomes equal to that of seasonal or perennial thawing, producing a phase boundary of the stable maintenance of freezing temperature above the foundation bottom the year round. The second phase boundary is located at the top of the permafrost, and a layer of unfrozen ground, the "buffer layer", whose temperature gradients are equal practically to zero, and so, consequently, are the heat fluxes passing through it, is located between the phase boundaries. The buffer layer serves as a heat-tight curtain ensuring stabilization of the initial permafrost table and protecting the unfrozen ground from perennial freezing. The base of a building being protected from perennial freezing and thawing does not deform in the process of exploitation which ensures its stability.

In the construction and exploitation of buildings by the method of stabilization the following two modes of ventilated vaults operation: variable and permanent are possible.

The variable mode involves regulation of heat interaction between a building and its base in the process of exploitation and is aimed primarily at creating a special mode of the ventilated vault operation. It consists in maintaining 10-15 year periods of negative mean annual air temperature alternating with 2-5 year ones of positive mean annual air temperature in the vault.

Perennial freezing of ground occurs in the vault during the period of negative air temperature. The modulus of the vault ventilation

for that period is calculated so that the mean annual air temperature in the vault, taking into account probable deviations from the estimated values, should a fortiori be negative. The depth of perennial freezing at the base of a building is limited by the condition of the foundation stability against the action of heaving forces. Upon reaching such a depth, the perennial freezing is stopped by changing the air temperature in the vault from negative to positive.

The resultant perennially frozen ground layer thaws out during the period of positive air temperature in the vault, and the initial conditions are restored in the base of a building. This cycle recurs.

The operation mode of a ventilated vault is changed by opening and closing vantilation openings. Parameters of the vault design are assigned by calculations to ensure a positive mean annual air temperature with closed ventilation openings not less than the absolute value of the ambient mean annual air temperature in the region. This ensures a complete thawing of the short-term permafrost that forms during the period of negative mean annual air temperature in the vault at any temperature of the ground surface outside the contour of the building.

The alternation of control periods is carried out based on the results of temperature measurements in the base of the building in special thermometric boreholes. Such measurements are made once a year to determine the actual depth of perennial freezing or thawing in the upper layer over the entire area of the building so as to make a decision on the alternation of control periods.

In applying the stabilization method, a permanent mode of the ventilated vault operation is also possible. It is a particular case of the variable mode when one of the periods lasts for the whole term of exploitation of a building. An average mean annual air temperature in the vault is assigned to be close to 0°C (-0.5 to +2.0°C).

A method has been devised to calculate the main parameters of the base when construction is effected by the stabilization method. It implies calculation and specification of the following characteristics needed to design a building:

(1) depth of foundation and its carrying capacity;

(2) depths of the admissible perennial freezing of grounds at the base;

(3) resistance to the heat transfer of the floor over the ventilated vault and structures which surround it;

(4) areas of the vault ventilation openings;

(5) thickness of the protective unfrozen ground layer over the permafrost;

(6) distance between the ranges of monitoring thermometric boreholes.

The calculation is based on the method of the worst case. The essence of this method, as applied to the problem under consideration, is as follows.

Two conditional cross-sections are chosen in the base of a building to calculate the depths of perennial freezing and thawing for the whole period of exploitation. The calculation is performed for probable deviations of mean annual temperatures of the ground surface in the ventilated vault and outside the building from the mean values. In one of the cross-sections these temperatures are to be maximum, taking into account their probable deviations. The depth of perennial thawing of the underlying permafrost and the resultant settlement of the base and foundations are calculated for this cross-section. From the condition, limiting the settlement, the thickness of the protective unfrozen ground layer is determined. In the other section, the mean annual temperatures of the ground surface in the ventilated vault and outside the building, taking into account their possible deviations, are assumed as minimum. In this cross-section the depth of perennial freezing of the thawed layer around the foundations is calculated. Proceeding from the necessity of maintaining the stability of foundations in this cross-section from the action of tangential heaving forces in the course of perennial freezing, one has to determine their depth as well as permissible depth of perennial freezing of the unfrozen ground layer. In such a way, the thickness of the protective thawed layer, the depth of foundations, and the admissible depth of perennial freezing at the base both at permanent and variable modes of the ventilated vault operation are determined.

The parameters of the ventilated vault design (thermal resistance of the floor and enclosing structures, as well as the total area of ventilation openings) are specified from the following considerations.

Under the permanent mode of a ventilated vault operation, these parameters are determined by calculated mean annual temperature of the ground surface beneath the building which is a result of the calculation and the limitation of the perennial freezing of the unfrozen ground layer in the base.

Under the variable mode of operation of a ventilated vault, its design parameters are determined so as to ensure the desired calculated mean annual temperature of the ground surface under a building during warm and cold periods of exploitation.

The distance between the ranges of the monitoring thermometric boreholes under both modes of operation is specified by a special calculation depending on the width of the building, the inhomogeneity of the thermal regime in the vault, the admissible depth of perennial freezing, and accuracy of ground temperature measurements in the boreholes.

This calculation method of the main parameters of a base is described in detail in the recommendations on the application of the stabilization method (Khrustalev and Nikiforov, 1985).

At present, more than 30 appartment houses and public buildings have been built and successfully exploited in the northern European USSR by the stabilization method. Many of them were put into operation over 10 years ago. Therefore, to-day we can analyse the experience gained in the course of their construction and exploitation by this method.

The advantages of the stabilization method can be appreciated on the example of a residential micro-region (neighborhood housing unit) built in 1975-78.

Its geology is represented by deluvial and upper-morainic 0.5-5.0 m-thick loams overlying fluvioglacial deposits with a frequent interbedding of loams, loamy sands, coarse and fine-grained sands, and gravelly deposits with sand fill and some boulders.

The permafrost in this micro-region is characterized by great diversity and complexity. The sites of continuous permafrost occupy about 10%, those of shallow permafrost (less than 10-12 m) about 30%, and of deep permafrost (more than 12 m) about 60% of the area. The upper ground layer in the micro-region is distinguished by a greater thickness of the seasonally frozen layer which reaches 2.5-3.0 m. In addition, "pereletoks" (short-term permafrost extending down to 6-7 m) frequently occur here, covering more than a half of the area.

Due to the fact that the permafrost in this micro-region is of discontinuous type, the temperature at the depth of annual zero amplitudes is close to 0°C.

Loams in the upper layer of the geological section are subject to heaving during freezing. Perennially frozen fluvioglacial deposits are characterized by considerable shrinkage during thawing (over 5 cm/m). In this connection, it was decided to apply the method of stabilization when developing this micro-region.

Twenty six five-storied, large-panel appartment houses and public buildings with a total general useful area of 69,109 m^2 have been built in this micro-region. Friction piles, driven to a depth of 8-12 m, with a high foundation mat were used as foundation. Ventilated vaults were constructed beneath all the buildings of the micro-region. All sanitary engineering networks were concentrated in the technical floors which were located between the ventilated vault and the ground floor.

The stabilization method made it possible to minimize the preliminary preparation of the bases. The amount of preliminary thawing in the entire micro-region amounted to 36 thou. m^3, versus 1445 thou. m^3 envisaged by the second principle of construction. Pile foundations and considerable reduction of the volume of preliminary thawing and excavation work allowed us to industrialize the basement erection and to reduce the duration of construction by 3-4 months.

At all stages of designing and construction, the problems involved in town planning were solved jointly. Attention was focussed on laying sanitary-engineering communications within the micro-region and on their inlet-outlets in the buildings. This was accomplished by the same stabilization method using ventilated channels. Ground for the terrain leveling was transported from the outside. An efficient drainage was envisaged in the ventilated vaults to prevent flood and break-down water from penetrating into the ground. All these measures completely prevented penetration of heat from buildings and engineering communications into the ground.

The stabilization method permits free planning of housing construction. This has enabled to employ modern architectural designs. The three-dimensional unification of residential groups adopted in the project made it possible to use the front row of buildings as protection from wind and snow and thereby to increase comfort within the intrablock areas and density of construction, and to reduce the length of roads and underground sanitary-engineering networks.

All measures mentioned above have led to a considerable increase in the level of comfort in that area. The cost of housing construction in this micro-region has proved to be smaller than in the neighboring ones where other construction methods were applied. The estimates show that the stabilization method employment had decreased the cost of construction of 1 m^2 of useful area by 121.6 and 136.7 roubles as compared with Principle II, based on preliminary thawing, and Principle I, using preliminary freezing, respectively.

The status of the bases of buildings has been monitored since 1976 from the moment when the first of them were put into exploitation in this micro-region. The results of observing the bases of three buildings are given below by way of example.

The measurements involve air temperature regime in the ventilated vaults, ground temperature regime in the bases of buildings, and the foundation settlement.

Results of stationary observations of air temperature in the ventilated vaults of the three buildings in 1977-1981 show that average long-term values of this temperature are close to 0°C and are - 1°C in building 1, 0°C in building 2, and 0°C in building 3. The negative air temperature in the vault of building 1 can be explained by the increase of its socle height as compared with the projected one. The observations have also shown that in the ventilated vaults of these buildings there was an inhomogeneity of mean annual air temperature which occurred only along the length of the vaults, was random in character and its value did not exceed 1°C.

Ground temperature regime observations in the bases of three buildings show that a perennially frozen 3-5 m-thick layer formed and stabilized over the ten-year period of exploitation. Beneath the buildings, this layer is underlain by unfrozen ground wherein temperature gradients practically equal zero. The thawing of the underlying permafrost in the bases of the buildings has not been noted. This is indirectly evidenced by the small values of settlement

of the buildings under consideration not exceeding 5 cm for the period surveyed.

In addition to the stationary observations described, numerous urgent measurements of air temperature in the ventilated vaults and ground temperature in the bases of the majority of buildings in the micro-region were made during 1976-1986. Besides, measurements of the settlement of all the buildings were made on a regular basis.

The studies show that on the whole the air temperature regime in the ventilated vaults and grounds of the bases of the buildings corresponds to the estimated one. The mean annual air temperature in the ventilated vaults, depending on the mean annual ambient air temperature over the period surveyed, ranged from -1.0 to +1.5°C. The data obtained from practically all the thermometric boreholes indicate that a thawed-out protective layer with zero temperature and zero temperature gradients has formed in the bases. This layer is located between the bottom of seasonal or perennial freezing and the permafrost table. The thawing of the underlying permafrost has not been revealed from the data obtained in the thermometric boreholes. Perennial freezing was observed in the bases of some of the buildings at the beginning of exploitation. Its depth has already stabilized and does not exceed 5 m.

The absence of the underlying permafrost thawing and the super-admissible perennial freezing of grounds at the foundations is confirmed by the foundations leveling. For the period of investigations, the settlement of all the buildings in this micro-region has not exceeded 6 cm (the maximum admissible value being 15 cm).

Thus, the ten-year successful exploitation of the buildings in this micro-region has demonstrated the reliability of the stabilization method and the validity of theoretical notions on which the mentioned method is based.

REFERENCES

Avtorskoe svidetelstwo 480803 MKI^{2}E 02 d 27/32 (1975). Zdanie vozvodimoe na vechnomerzlykh gruntakh (G.V. Porkhaev, L.N. Khrustalev, V.N. Yeroshenko i dr. (SSSR) (Otkrytiya. Izobreteniya), N 30,str.90.

Khrustalev, L.N. & Nikiforov, V.V. (1985). Rekomendatsii po primeneniyu sposobov stabilizatsii vechnomerzlykh gruntov v osnovanii zdaniy, 44 str. Moskva: NII osnovaniy.

GEOCRYOLOGICAL STUDIES FOR RAILWAY CONSTRUCTION (STATE, PRIMARY TASKS)

V.G. Kondratyev, A.A. Korolyev, M.I. Karlinski, E.M. Timopheev and P.N. Lugovoy

Moscow State Design and Survey Institute of Transport Construction, Moscow, USSR

SYNOPSIS This report deals with the history of the problem; the experience of the Baykalo-Amurskaya Main Line (BAM) and, in particular, icing prevention are analysed here. A question is raised about fundamental changes of volumes, contents and quality of geocryological studies for railway construction purposes. The report gives characteristic of the object of investigations and general scheme of work, covering surveys, designing and construction of railways in permafrost zone. Geocryological problems and ways of their solution are considered on example of a new railway line Berkakhit-Yakutsk - one of the BAM Northern extensions.

First the necessity of clearing up of the geocryological conditions for railway construction appeared 100 years ago, when during surveys of Trans-Siberian Railway in Zabaykalye and Priamurye they came across permafrost, which strongly complicated designing and construction and later on - main line operation. Thus, Sumgin (1937, p. 41-42) wrote, characterizing 200-year history of permafrost investigation: "The permafrost soil investigation has considerably changed and advanced after construction of the Great Siberian Railway... The Problem of permafrost faced us in all its magnitude. It was necessary to give definite answers to practical requests... It is considered that only permanent repair of buildings and structures under deformations on Zabaykalskaya and Amurskaya railways has already cost the government 50 mln. gold roubles, not taking into account losses from driving offence on these railways". For the first time in Russia systematic studies of permafrost were carried out for grounding of Transsib construction for practical needs. The first in the world building on permafrost with aired cellar was built on the Mogzon station (Zenzinov, 1986). The first permafrost station was established on that railway in Scovordino in 1927. It did a lot for ensurance of transport construction in Siberia as well as for development of permafrost studies as a whole. In general, railway construction in Siberia, Canada, on Alaska and in China stimulated development of many problems of permafrost studies (Lvov, 1916; Pisarev and Datskiy, 1934; Bykov and Kapterev, 1940; Suhodolskiy, 1945; Nekrasov and Klimovskiy, 1978; Cornell, Law and Lake, 1973; Zabolotnik, 1983; Yusheng et al., 1983).

In this respect, the Baykalo-Amurskaya Main Line occupies a special place. Its surveys have been carried out with different intensity during several decades since 1932. At present its construction, begun in 1974, is completing. As long ago as in 1937 a specially organized geocryological expedition worked on the BAM; besides design and survey expeditions it fulfilled research works on investigation of permafrost regime. A powerful impulse in the geocryology development was observed in the 70-80s, when realization of the BAM project took place. This project was elaborated by Moscow State Design and Survey Institute (Mosguiprotrans) with participation of more than 200 research, design and survey organizations. Practically all leading permafrost centres of the country (institute of Merzlotovedeniya, Academy of Sciences of the USSR, Moscow State University and etc.) also took part in solution of the BAM geocryological problems and a special section for coordination and methodological management of permafrost investigations of different organizations on the BAM was organized in the Counsil of Earth cryology, Academy of Sciences of the USSR.

The BAM is a complicated technogenic complex, consisting of roadbed, embankments and cuts, bridges and tunnels, stations, settlements, towns, buildings, structures and communications of different purposes. The length of the main line is 3102 km, it has about 4200 buildings and structures, including 150 large bridges, over 30 km of tunnels, over 200 stations, over 20 large settlements; it lies in complicated nature conditions, is characterized by inclement climate, mainly by mountain relief, various geological structure, permafrost and high seismic activity of separate route sections. By the beginning of railway construction the degree of studying of natural conditions turned out to be uneven. Some factors, such as spreading, depositing conditions, temperature conditions, permafrost cryogenic structure turned out to be weakly studied. That is why their studying was to be fulfilled simultaneously with designing and sometimes during main line construction with the help of airphoto and spacephoto identification, engineering-and-geological survey, geophysical and drilling works. On the whole, the BAM engineering-and-geological conditions had been defined coredtly, however geocryological support of the BAM designing turned out to be insufficient in the

part of investigation of formation and development regularities of the route permafrost conditions in natural conditions as well as at technogenic loads in the process of the Main Line construction and operation. In this connection at present the problem of stability ensurance of railway installations becomes very urgent (Sobolev, 1984, 1985; Volkov, 1987).

The greatest difficulties during construction and temporary operation periods were made by icings. (Fig.1).

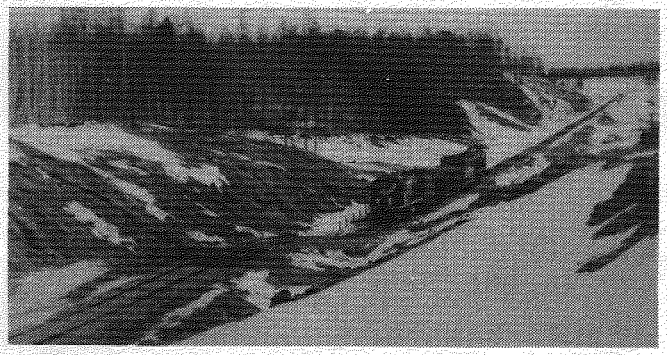

Fig.1 Railway track deformations at icing formation in cuts during the BAM construction.
Photograph by Vasilyev M.L., March 1983.

Thus, on section Tynda-Urgal, which length is 960 km, 160 icings were revealled during surveys directly on the route, 36 of which were attributed to dangerous. During elaboration of working drawings we had to change pipe culverts (envisaged in the project) for bridges, increase underbridge openings, embankment height and so on. As a result, after railway construction only 6 natural icings required special engineering solutions. As far as technogenic icings (which appeared as a result of changes of repmafrost-hydrogeological conditions) are concerned, they considerably complicated the Main Line operation. In all since 1979 up to 1985 dangerous icings appeared in 38 cuts and also on 11 sections of pipe culverts, low embankments and zero places. Since 1979 in order to protect cuts and semi-cuts we have to construct temporary structures: anti-icing fences made of boards and logs, warmed wooden chutes; to use cutting and removal of ice beyond the track limits, mounting and gauging of rail and tie skeleton, track laying round icing knobs and etc. (Fig.2).

Since 1982 we started construction of permanent anti-icing structures: permafrost belts, anti-icing banks, framed reinforced concrete warmed chutes, horizontal tube drainage. New methods of icing prevention such as deep water decrease (vertical drainage) and horizontal tubeless drainage carried out by drilling and blasting method were elaborated and successfully tested (Lugovoy and others, 1983). Even greater difficulties arise during Main Line operation as a result of roadbed deformations at permafrost degradation in the embankment foundation on "mari" and other sections of ice contenting soil. (Yuletskiy and Minaylov, 1984; Ivanov and Kozkevnikov, 1987).

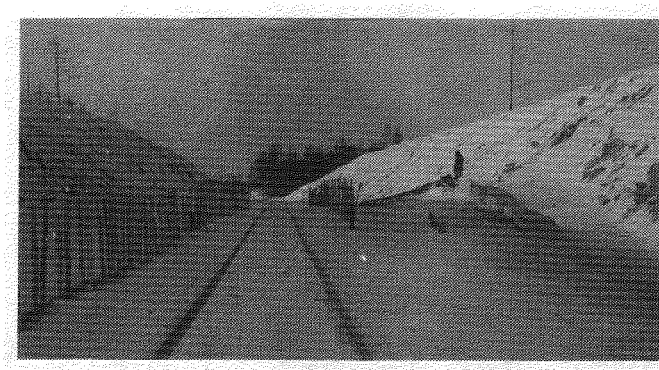

Fig.2 Temporary measures of railway track protection from icings in cuts during the BAM construction. Photograph by Aksenova N.M., January 1984.

Increasing volumes of railway designing and construction in permafrost zone require considerable volume, contents and quality changes of geocryological investigations at engineering-and-geological surveys for railway construction. It is already not enoph only to state the permafrost conditions on the routes and construction sites. In accordance with modern notions (Merzlotovedeniye, 1981) it is necessary to determine formation and development regularities of permafrost conditions, to forecast their changes during construction and operation of railway installations, work out recommendations on provision of optimum geocryological conditions for ensurance railway stability and reliability and also labour protection. The object of geocryological studies in this case can be determined as a nature-technogetic system: geological-geographical conditions on the construction route - permafrost conditions on it - railway Main Line (Table I). For all this, characteristics of geological-and-geographical conditions, permafrost conditions and railway Main Line are to be elucidate in space, time and intercommunication.

The Permafrost studies on the railway route are to be carried out during surveys as well as during construction and during the whole structure operation period, proceeding from specific features of permafrost conditions, consisting in its constant development and taking into account its functional intercommunication with complex of nature factors, which are changing at natural conditions as well as at technogenic actions. They must include permafrost survey, geocryological forecast and geocryological monitoring - systematic control of permafrost conditions dynamics during nature evolution and under influence of technogenic factors. It is necessary to carry out survey and forecast during surveying period and monitoring - during the whole surveying, construction and operation time of the Main Line. General scheme of works taking into account experience of analogous investigations for gas conduit construction purposes (Dubicov,

1978; Kondratyev, 1985) is as shown below (Table 2). In all, 3 periods of permafrost investigations are singled out, correspondingly: during surveying, construction and operation of the Main Line.

TABLE I

Object of Permafrost Investigations for Railway Construction Purposes

Geologo-geographical conditions on the railway route	Seasonaly frozen and permafrost rocks and connected with them cryogenic processes and phenomena	Interaction of railway Main Line and permafrost
Geological structure (age of rocks, genesis, composition and properties of rocks). Geomorphological structure (hypsometry of relief elements, exposure and gradient of slope). Hydrogeological conditions (propagation, depositing conditions, type, hydraulic features, conditions of power supply, transit and unloading, reserves, chemical composition, underground water temperature). Geobotanic conditions (type, species composition of vegetation, degree of covering or closing of top crowns). Climate conditions (radiation-and-heat balance of the surface; precipitation quantity, air humidity, annual average temperature and amplitude of annual air temperature variations, wind speed and direction, snow cover, height and density).	Temperature regime of rocks (annual average temperature and amplitude of its annual variations on the ground surface, on the base of seasonally thawed and seasonally frozen layers, on the layer base of annual temperature variations). Seasonal thawing and freezing of soils (type of seasonal thawing or freezing of soils, thickness, period and rate of seasonal thawing or freezing of soils; composition and cryogenic structure of seasonally thawed or seasonally frozen layer). Permafrost thickness of rocks (propagation, depositing conditions, thickness, composition, cryogenic structure, genesis, history of forming and development of permafrost thickness). Cryogenic processes and phenomena (forms, dimentions, structure, genesis, mechanism and conditions of phenomena forming, connection with geologo-geographical medium factors and permafrost conditions, paragenesis, dynamics, direction and potential possibilities of process and phenomena development).	Change of permafrost conditions in connection with Main Line construction (breakdown of geological-and-geographical conditions, change of rock temperature regime, depth and rate of seasonal freezing and thawing of rocks, development of parameters and of immerging permafrost, new permafrost formation and perennial thawing, development of cryogenic processes and phenomena). Change of permafrost conditions in connection with Main Line operation (constructive and technological pecularities of Main Line, forming of temperature regime of roadbed, soils, of its base and of right-of-way; layer forming of seasonal thawing or freezing of rocks, new permafrost formation and its degradation, development of cryogenic processes and phenomena). Influence of cryogenic processes on the Main Line operation (on track stability, on technological regime of Main Line operation).

During surveying investigations are carried out in 3 phases: feasibility study, project and working documentation of the railway construction. On the feasibility study phase it is expedient to carry out investigations in two stages: materials of the previous works and aero-visual examinations are analysed on the first stage, and on the second - investigations proper are fulfilled. Only one stage of works is singled out on other phases. The regularities of formation and development of permafrost conditions in natural conditions at Main Line construction and operation must be revealed during surveys as a result of permafrost investigations. The investigation activity must be enough for selection of optimum constructive and technological solutions and assigning of effective measures on control of permafrost conditions in order to ensure optimum construction and operation conditions for the railway line. A network of observation areas for investigation of permafrost condition dynamics in natural conditions must be made during surveys.

At present, as is correctly stated by Yu.F.Zaharov (1983), prospectors are unable to fulfill trustworthy quantitive engineering-and-geological forecast as a result of shortage of engineering survey volume (envisaged by the

TABLE II

Scheme of Works at Permafrost Investigations on Routes of the New Railway Lines

Period	Stage	Phase	Type	Purpose
Surveys	Feasibility study	I. Estimation of permafrost conditions of the supposed construction region	Collection and analysis of materials on geological-and-geographical permafrost conditions Airphoto and space-photo identification. Aerovisual and ground investigations.	Selection of route perspective directions.
		II. Works on route perspective directions in 10-20 km wide zone	Medium-scale aerial photography and identification of photographs Landscape zoning of the territory and selection of key areas Small scale permafrost survey is on Main Line linear part; medium slace survey is on station sections and transitions over large rivers and water sheds. Geocryological monitoring is in natural conditions. Natural-historical and general technogenic permafrost forecast.	Selection of route optimum direction Polygon selection for testing-and-experimental works Selection and basing of permafrost station location
	Project	III. Works on selected direction according to route alternatives in 10-20 km wide zone	Detailed aerial photography and identification of photographs. Medium scale permafrost survey is carried out on Main Line linear part and large scale survey on sections of operation points and barrier places Geocryological monitoring is carried out in natural conditions and on experimental areas Technogenic permafrost forecast Ingeneering-and-geocryological zoning	Selection of route optimum alternative, centre-line location, track schemes and structures
	Working documentation	IV. Works on route in 0.5-1 km zone	Large scale detailed permafrost survey is carried out on Main Line linear part, on sections of operation points and barrier places. Geocryological monitoring is made in natural conditions on experimental areas Technogenic permafrost forecast Elaboration of recomendations on permafrost condition control	Adoption of final constructive and technological solutions. Elaboration of measures on ensurance of Main Line stability and environment protection
Construction		V. Works in right-of-way	Control on execution of constructive measures on conservation or improvement of permafrost conditions Geocryological monitoring in natural conditions and in right-of-way Correction of measures on permafrost condition control	Ensurance of Main Line stability and environment protection
Operation		VI. Works in right-of-way	Control on execution of technological measures on conservation or improvement of permafrost conditions Geocryological monitoring of railway Main Line Correction of measures on permafrost condition control	Ensurance of Main Line stability and environment protection

normative documents) for complex action estimation on geological medium and its reaction on technogenic loads. Consequently, it is possible to form engineering-and-geocryological conditions at project realization and long structure operation, which essentially differ from the forecasted ones. That is why it is expedient to create a special permafrost service at board of directors of the constructed railway; it will fulfil: permanent permafrost control during construction and operation of the Main Line for accomplishing measures ensuring its stability and nature protection; regime observations of permafrost condition changes on the route under construction; study of cryogenic process effects on operation of railway installations and operative correction of measures on improvement of geocryological conditions of their operation and environment protection.

Proceeding from the abovementioned understanding of the geocryological provision essence for the railway construction, the primary tasks of the permafrost investigations on the Berkakit-Yakutsk railway line route (being one of the BAM sub-meridional developments) can be formulated in the following way: 1) carrying out of large-scale and detailed permafrost survey on section up to Tommot and medium-and large-scale permafrost survey on section Tommot-Yakutsk; 2) elaboration of technogenic permafrost forecast for drawing up of a project and working documentation of the railway installations; 3) elaboration of measures on permafrost condition control at the base of railway installations and on the adjacent territory for ensurance of optimum geocryological conditions of construction and operation of structures and environment protection; 4) organization of Main Line geocryological monitoring for permafrost condition permanent control and well-timed suppression or reduction of cryogenic process effects on structures; 5) study of the BAM and permafrost zone real interaction, generalization of engineering-and-geocryological investigation experience on the BAM with learning of necessary lessons, meaning improvement of normative-methodological base of surveys, railway designing and construction in the permafrost regions and elaboration of effective measures on "treatment of sore spots" of the Main Line.

At present Mosguiprotrans has come to solution of the first three problems with cooperation of the Moscow State University permafrost chair, of the Merzlotovedenije institute of the Academy of Science, of the Tynda permafrost station and the Novosybirsk branch of the Central Research Institute of Transport Construction within the programe limits of the engineering-and-geological surveys of the Berkakit-Tommot-Yakutsk railway line. A Programe of geocryological investigations and further BAM monitoring is also being elaborated.

So, only deep and well-timed study of formation and development regularities of permafrost conditions, systematic control of their dynamics at territory development and cryogenic effects on structures, realization of their permafrost protection measures will make it possible to realize stability and reliability of railways and also invironment protection in the permafrost zone.

REFERENCES

Bykov, N.I., Kapterev P.M. (1940). Vechnaya merzlota i stroitelstvo na ney. M.: Transzheldorizdat, 372.

Guletskiy V.V., Minaylov G.P. (1984). Bermy v konstruktsiyah nizkih nasipey na marevyh uchastkah. - Transportnoye stroitelstvo, N4, 9-10.

Dubikov G.I., (1978). Inzhenerno-geokriologicheskie issledovaniya dlya obosnovaniya lineynogo stroitelstva na Severe. Tr. PNIIS., vip. 52, 21-29.

Zaharov Yu.F. (1983). Problemy inzhenernogeologicheskogo prognozirovaniya v inzhenernyh izyskaniyah i projectirovaniye gazonefteromislovogo i truboprovodnogo stroitelstva. V kn.: Polysheniye effectivnosti inzhenernyh izyskaniy dlya stroitelstva v neftenosnyh rayonah Zapadnoy Sibiri. Tyumen, 34-36.

Zanzinov, N.A. (1986). Ot Peterburga-Moskovskoi do Baikalo-Amurskoi magistrali. M.: Transport, 216.

Ivenov M.I. (1987). Opyt obespecheniya stabilnosti nasypey na prosadochnyh osnovaniyah. Transportnoye stroitelstvo, N5, 6-7.

Kondratyev V.G. (1985). Merzlotnije issledovaniya v svyazi s proyektirovaniyem, sooruzheniy i ekspluatatsiey severnih truboprovodov. V kn.: Neft i gaz Zapadnoy Sibiri. Problemy dobychi i transportirovki. Tyumen, 216-217.

Lugovoy P.N.; Korolyev A.A.; Pozin V.A. i dr. (1983). Aktivniy metod borby s naledyami na BAMe. Transportnoye stroitelstvo, N12, 3-4.

Lvov A.V. (1916). Poiski i ispytaniya istochnikov vodosnabzheniya na Zapadnoy chasti Amurskoy zh.d. v usloviyah "vechnoy" merzloty pochvy. Irkutsk: MPS, 881.

Merzlotovedeniye (kratkiy kurs). Pod red. Kudryavtseva, V.A. (1981). M., Izdatelstvo Mosk. Ur-ta, 240.

Nekrasov I.A.; Klimovskiy I.V. (1978). Vechnaya merzlota zony BAM. Novosibirsk: Nauka, 115.

Pisarev G.F.; Datskiy N.G. (1934). Vechnaya merzlota i usloviya stroitelstva v Usinskom rayone Severnogo kraya. L: Izd. AN SSSR, 144.

Sobolev P.V. (1984). Ekspluatasiya zdaniy i sooruzheniy na verchney merzlote v usloviyah BAMa. Transportnoye stroitelstvo, N9, 23-24.

Sobolev P.V. (1985). BAM segodnya. Transportnoye stroitelstvo, N8, 8-9.

Suhodolskiy E.I. (1945). O sooruzhenii zemlyanogo zheleznodorozhnogo polotna v usloviyah severnih rayonov oblasty vechnoy

merzloty. Tr. In-ta Merzlotovedeniya im. V.A. Obrucheva, t.P.M.-L: Iz-vo AN SSSR, 5-120

Cornell, E.R.; Law, C.E.; Lake R.W. (1973). The Arctic railway - environmental aspects. - Eng. J., 56, 3, 23-27.

Zabolotnik, S.J. (1983). Conditions of Permafrost Formation in Zone of the Baikal-Amur Railway. Permafrost: Fourth internatoinal conference. Proceedings, National academy press. Washington D.C., 1451-1456.

Yusheng L.; Zhugui W.; and e.a. (1983). Permafrost study and railroad construction in permafrost areas of China: Fourth internationsl conference. Proceedings. National academy press, 707-714. Washington.

VENTILATED SURFACE FOUNDATIONS ON PERMAFROST SOILS
Permafrost, Soil Bed, Surface Foundation, Ventilated Through Space, Heat-Engineering Analysis

N.B. Kutvitskaya and M.R. Gokhman

The Gersevanov Research Institute of Bases and Underground Structures, Moscow, USSR

SYNOPSIS The main design solutions for ventilated surface foundations on permafrost soils and their advantages as compared to other types of foundations are considered. Principal propositions of the heat-engineering analusis of permafrost beds of ventilated surface foundations are presented. Results of the heat-engineering analysis of a bed of an industrial building rested on a ventilated plate-type surface foundation are given.

Ventilated surface foundations on permafrost soils are serving as both a supporting foundation construction and a soil cooling means. Such foundation furnishes a thin-walled reinforced concrete spatial system being mounted on a subbed which is prepared from plane plates, channeled or hipped plate elements, hollow volumetric blocks. Cooling of bed soils which yields creation and preservation of their specified temperature regime is brought about in winter period by the motion of the cold atmospheric air through spaces provided in a foundation. Ventilated foundations of a plate or strip type are empoyed depending on a character of loading transmitted from buildings or structures. Fig.1 shows examples of cross-sectional view of beds with a plate foundation (a) and a strip foundation (b).

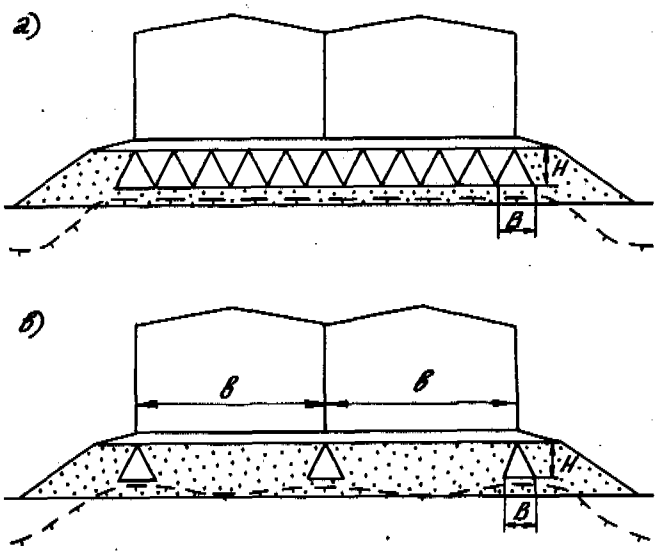

Fig.1 Cross-sectional views of beds with a plate foundation (a) and a strip foundation(b).

Compared to deep foundations (pile foundations, column pad foundations and others) the empoyment of ventilated surface foundations enables to eliminate almost completely the labour-consuming and expensive excavation of frozen soils and to reduce the consumption of building materials and electric energy. Surface foundations take loads transmitted to them by upper structures and distribute them along the soil surface beneath a building thus reducing the pressure on soil layers occurred below. Therefore this type of a foundation is advantageous to employ at sites built by salty high-temperature ice-saturated soils as well as by soils with cryopegs and underground ice. The bearing capacity of a soil bed of a ventilated surface foundation is defined essentially by physical and mechanical characteristics of bed upper soil layers which, in turn, depend on a thermal regime in a building and inside of foundation ventilated through spaces as well as on a thermal regime of a soil surface around a building. As a consequence the solution of a problem on conjugate heat transfer in a system "building-ventilated foundation-permafrost soil" enables to determin uniquelly the bearing capacity of a ventilated surface foundation bed. The analytical method of the heat-engineering analysis which was developed enables to select principal parameters of a foundation cooling system which ensure a required bearing capacity of a bed. With this aim in view, at given designs of a structure floor, subbed and ventilated foundation it is determined through the use of heat-engineering analysis a depth of seasonal thawing of soils beneath a structure and there are computed temperatures of permafrost bed - the maximum temperatures at a given depth z, T_m, and mean maximum temperatures along a depth z, T_e, according to a mean temperature for the ventilation period and an average annual temperature of foundation through space wall. Below is given the distribution of the mean for the ventilation period temperature, T_{hv}, of the foundation through space wall along the foundation axis y which was analytically obtained by Gokhman and Ivanov (1985) and grounded experimentally by Kutvitskaya (1978).

$$T_{hv} = T_{out.v}\left[\frac{1+\beta}{1+\eta}\exp(-a\gamma)-\beta\right] \qquad (1)$$

In the equation (1) the term T_{hv} depends on the mean temperature of the atmospheric air for the ventilation period, $T_{out.v}$, and the dimensionless complexes β, η and ay involving thermophysical properties of the soil and the air which moves along a foundation through space, geometrical parameters of subbed and foundation, an atmospheric air temperature and a temperature in a structure. These complexes are obtained in terms of analytical relationships and presented in the form of tables and nomographs. A value of the average annual temperature of the foundation ventilated through space wall, T_{ha}, is expressed in terms of the mean, within the boundaries of a structure outline, values of the system configuration function, $\bar{f}$, and the average annual temperature of the soil, T_o', which is obtained from the equation of heat balance in the system "structure-ventilated foundation" to be valid for the stationary-periodic regime of heat transfer.

$$T_{ha} = \left[T_o' - \frac{\lambda_{th}}{\lambda_f} T_{in}(1-\bar{f})\right] / \bar{f} \qquad (2)$$

In the equation (2) the terms λ_{th} and λ_f are the thermal conductivity of thawed and frozen soil respectively, T_{in} is the air temperature in a structure. The effect of geometrical parameters of a subbed and a ventilated foundation on the conjugate heat exchange in the system under consideration is taken into account in the equations (1) and (2) through the use of generalized characteristics of the stationary temperature fields and the heat flows - the form-factor of the system, φ, and the function of its configuration, f, (Gokhman,Ivanov, 1987). For the purpose of practical computations according to the equations (1) and (2) it was developed a procedure for determining φ and f by the method of electrical analogy based on the use of two-dimensional models made from the electroconductive paper and the electric integrator "EGDA". Simulation results for φ and f were obtained, tabulated and nomographed for the rectangular, triangular and trapezoidal cross-sections of the foundation ventilated through spaces. As an example, Fig.2 illustrates the simulation results for φ for foundation ventilated through spaces of the rectangular cross-section depending on the parameters H/B and b/H at $h_o/H = 1$ where $h_o = h - 0.5H$; h,H and B are the depth of the through space axis position, the height of the through space and the width of the through space respectively; b is the distance between the axes of the adjacent through spaces. The curves 1,2 and 3 conform to the values of the parameter H/B equal to 0.25;1;4 respectively. With the temperatures T_{hv}, T_{ha} and T_o' known, the computated temperatures of the soil are obtained by the superposition of the three-dimensional stationary temperature field and the two-dimensional stationary-periodic temperature field. The first

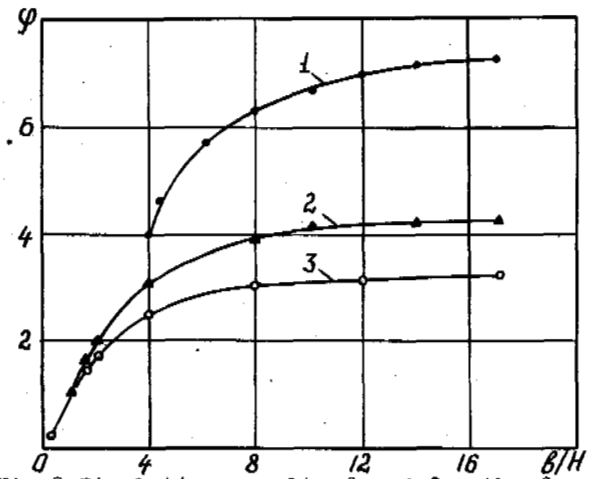

Fig.2 Simulation results for φ for the foundation ventilated through spaces of the rectangular cross-section at $h_o/H = 1$

one characterizes a steady-state distribution of the average annual soil temperatures beneath a structure with a ventilated foundation of corresponding configuration, while the second one describes seasonal variations of the bed soil temperatures from their average annual values. The equation for determination of the computated soil temperatures T_m and T_e may be represented in the following generalized form:

$$T_{m\varphi} = (T_o - T_o')\,k_{m\varphi} + \left(T_{ha} - \frac{\lambda_{th}}{\lambda_f} T_{in}\right) k^o_{m\varphi} + \frac{\lambda_{th}}{\lambda_f} T_{in} + T_{hu}\, k^u_{m\varphi} \qquad (3)$$

where

$$T_{hu} = T_{ha} - T_{out.u}\, T_{hv} / T_{out.v} \qquad (4)$$

T_o - the computed average annual temperature of the permafrost soil beyond the zone of the structure heat effect.

T_{hu} - the computated amplitude of seasonal variations of the temperature of the ventilated through space wall.

$T_{out.u}$ - the mean temperature of the atmospheric air in the most cold month.

$k_{m\varphi}$ - the coefficient of the structure thermal effect (Fedorovich,Gokhman,1985) tabulated as a function of the structure planform and the position of the bed point under consideration with respect to the structure centre.

$k^o_{m\varphi}$ - the coefficient of the thermal effect of the foundation ventilated through spaces tabulated as a function of their geometrical parameters and the position of the bed point under consideration with respect to the ventilated through space bottom.

$k^u_{m\varphi}$ - the coefficient of the seasonal temperature variation tabulated as a function of both the geometrical parameters of a bed and a fondation and the thermophysical

characteristics of the bed soils.

As an example, Fig.3 shows the coefficient k_m^u as a function of its parameters. Here, B is the

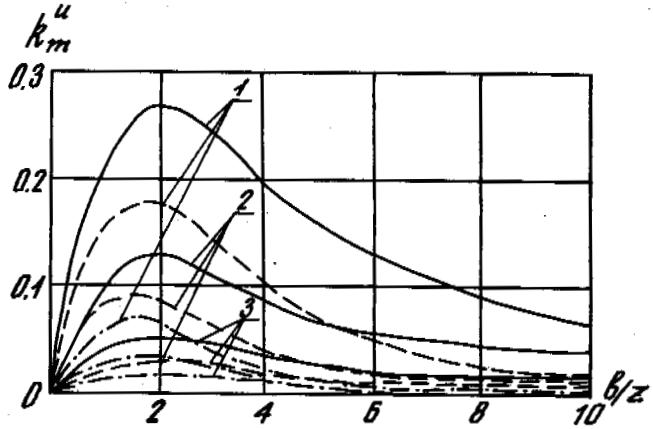

Fig.3 Coefficient k_m^u as a function of its parameters.

width of the ventilated through space bottom; b is the distance between the axes of the adjacent ventilated through spaces; C_f and a_f are the heat capacity per unit volume and the thermal diffusivity of the frozen soil respectively ($a_f = \lambda_f/C_f$). The families of curves 1,2 and 3 correspond to the values of the parameter B/b= 0.1;0.25;0.5 respectively. The solid, dotted and dash-dot lines correspond to the values of the parameter $z/\sqrt{a_f}$ = 25;50 and $100\,h^{0.5}$ respectively. Below are given main results of the heat engineering analysis of a bed of an industrial building which measures 24 x 48 m in plan and is constructed on a ventilated surface foundation rested on a fill. The analysis is made according to the methodology given above. The fill is prepared from sand soil exhibiting the total moisture content $W_{tot.p}$= 0.1 and the density ρ_{dfp} = 1.6 tons/m^3. As it is so, the heat conduction of the fill soil in a thawed and frozen state is λ_{thp} = 1.45 V_t/(m°C) and λ_{fp} = 1.62 V_t/(m°C) respectively. The bed soil is the sand exhibiting the temperature T_o= -0.5 °C; the total moisture content W_{tot} = 0.2 and the density ρ_{df} = 1.5 tons/m^3, the heat conduction of the bed soil in a thawed and frozen state is λ_{th} = 2.15 V_t/(m°C) and λ_f= 2.38V_t/(m°C) respectively; the heat capacity per unit volume of the soil in a frozen state is C_f = 2140 kJ/(m^3°C). The computed air temperature in the building is T_{in} = 18 °C, the mean wind velocity and the atmospheric air temperature over the ventilation period (t_v = 7 months) are V = 5.1 m/s and $T_{out.v}$ = - 18.6 °C respectively. The foundation is surface, ventilated, of plate type, built from prefabricated reinforced concrete elements and has the following parameters: the height H = 1.5 m; the width of the ventilated through space bottom B = 1.5 m; the thickness of the fill beneath the foundation underside level h_p = 0.5 m; the admissible depth of the seasonal thawing of the bed soils h_{th} = 0.9 m. According to the results of the analysis the required resistance to the heat transfer from the floor structure above the foundation ventilated through spaces is R_o = 3.2 m^2°C/ V_t and above the nonventilated through spaces it is R_n = 2.5 m^2°C/ V_t. In this case it is necessary to ventilate every third through space in the foundation (b = 3B = 4.5 m). The mean temperature over the ventilation period and the average annual temperature of the ventilated through space wall at the outlet (y = 48 m) are T_{hv} =-15.9 °C and T_{ha}= - 8.6 °C respectively. The computed depth of the seasonal thawing of the subsoil beneath the foundation through space bottom is equal to 0.7 m, the nonuniformity of thawing of the bed is δ = 0.9 - 0.7 = 0.2 m. Distribution of the maximum temperatures, T_m, of soil beneath the ventilated through space bottom in depth is given in Table I.

TABLE I

Distribution of maximum soil temperatures in depth

Depth, z, m	1	2	3	4	5
Temperature, T_m, °C	-1.45	-2.3	-2.78	-2.95	-3.05

CONCLUSIONS

Ventilated surface foundations allow for both transmitting of design loads to permafrost bed soils and ensuring its required bearing capacity.

The main parameters of the foundation cooling system, which ensure the required bearing capacity of the bed, may be selected on the basis of the proposed procedure for the heat-engineering analysis.

REFERENCES

Gokhman,M.R., Ivanov,M.M. (1985). Ustanovivshiysya teploobmen lineynih podzemnih soorujeniy s ottaivayushim (promerzayushim) gruntom. Ingenerno-Phizicheskiy Jurnal,(48),4, s.682,Moskva.

Gokhman,M.R., Ivanov,M.M. (1987). Analiticheskie i chislennie metody rascheta sopryajennogo teploobmena zaglublyonnih sooruzeniy s vechnomerzlimi gruntami.

Trudy Nauchno-Issledovatelskogo Instituta Osnovaniy i Podzemnih Soorujeniy, 81,ss. 76-81,Moskva.

Fedorovich,D.I.,Gokhman,M.R. (1985). Utochnenie raschetnih temperatur vechnomerzlih gruntov v osnovanii zdaniy i sooruzeniy.
Osnovaniya,Fundamenty i Mekhanika Gruntov,5,ss.22-24,Moskva.

Kutvitskaya,N.B. (1978). Teplotehnicheskiy raschet vechnomerzlih osnovaniy promishlennih zdaniy s ventiliruemymi kanalamy. Trudy Nauchno-Issledovatelskogo Instituta Osnovaniy i Podzemnih Soorujeniy,69, ss.117-126, Moskva.

RESULTS OF RESEARCHES AND EXPERIENCE OF HYDRAULIC MINING OF FROZEN ROCKS

N.P. Lavrov, G.Z. Perlshtein and V.K. Samyshin

All-Union Scientific Research Institute of Gold and Rare Metals, Magadan, USSR

SYNOPSIS Ice-rich fine-dispersed sediments may be successfully mined by a hydraulic method. In this report the newly determined regularities of hydrowashing of thawing rocks are given. The formulae for calculation of water temperature and density of heat flow into eroding rock massif are given. The dependence of intensity of erosion of loamy-sand and loamy rocks on their initial moisture is studied. The results of the researches are realized in some flow sheets of hydrowashing of permafrost placers.

There are thick ice-rich fine-dispersed sediments that are widely distributed through Arctic and Subarctic zones of permafrost. The problem of their mining by a hydraulic method is of great interest since the use of earth-moving equipment for this purpose does not assure good performance.

So called washing off works were mastered in Russia early in the 19th century at the Ural and Altai placers. To the end of the last century rock washing by pressure jets had got wide use at the Lena and Zabaikal placers. In the 40-es of this century hydraulic stripping operations were agreat success in permafrost placers near Fairbanks, Alaska. The hydraulic mining of placers in permafrost regions of the USSR was employed but in rare cases because of a defficient study of quantitative regularities of water flow interaction with eroding permafrost.

To fill up the gap the authors have carried out the whole complex of theoretical and experimental researches. The analysis of heat exchange in the system: thawing rocks - water flow - atmosphere was given. The water flow of a single width moving over the surface of the thawed rock layer of h thickness along x axis was considered.

The temperature changing through the flow length occurs under the influence of heat exchange with atmosphere and rock. It is supposed that owing to turbulent water mixing its temperature down the depth does not change. On the water surface there is a convective heat exchange with air (H_c) and energy exchange by evaporation or condensation (M). The water surface also receives radiant energy in the form of total shortwave radiation (Q_t) and longwave atmosphere (I_a) radiation. According to the surface albedo A the part of shortwave radiation of AQ_t quantity is reflected. Like any heated body water flow emits longwave energy (I_w) into space. We don't consider the radiant heat exchange below water surface as this practically has no effect on final results. Besides, the part of heat (q) is transfering through the thawed layer to permafrost surface.

As follows from the law of conservation of energy the changing of water flow heat content for an area of elemental length dx is equal to the algebraic sum of heat sourses acting on the area:

$$[Q_t(1-A)+I_a-I_w-H_c-M-q]\,dx=c\omega dT, \quad (1)$$

where c is the volume specific heat of water, $W \cdot h/(m^3 \cdot °C)$; T is the water temperature, °C; ω is a single consumption of water flow, $m^3/(m \cdot h)$.

The density of heat flow into thawing massif is defined from:

$$q = \lambda \frac{T_r}{h} = \alpha_f (T - T_r),$$

from which $$q = \beta T, \quad (2)$$

where $$\beta = \left(\frac{1}{\alpha_f} - \frac{h}{\lambda}\right)^{-1},$$

α_f is the coefficient of water flow heat exchange with underlying rocks, $W/(m^2 \cdot °C)$; T_r is the rock surface temperature, °C; λ is the thermal conductivity of thawing rocks, $W/(m \cdot °C)$.

The effect of water flow velocity on α_f at erosion of loamy-sand and loamy sediments is experimentally researched (fig.1).

Expressing the remaining constituents of heat exchange by the known physical lwas (Newton's, Stefan-Boltsman's) and using their linear approximations taking into account formula (2), let's present equation (1) as:

$$(q_0 - \alpha T)\,dx = c\omega\,dT, \quad (3)$$

where $$q_0 = (1-A)Q_t + I_a - I_0 + \alpha_h T_a + \alpha_e (e_a - e_0),$$

$$\alpha = \alpha_h + \beta \alpha_e + \alpha_r + \beta,$$

α_h is the coefficient of heat exchange between water flow and air, W/(m²·°C); T, T_a is the temperature of water and air, respectively, °C; α_e is the coefficient of evaporation (condensation), W/(m²·Pa); e_0, e_a are the elasticities of saturating vapour at 0°C and water vapours in air, respectively, Pa; β is the coefficient of linear approximation of the dependence of saturating vapour pressure on temperature, Pa/°C; I_0 is the heat radiation of surface at 0°C, W/m²; α_r is the coefficient of linear approximation of power law of heat radiation, W/(m²·°C).

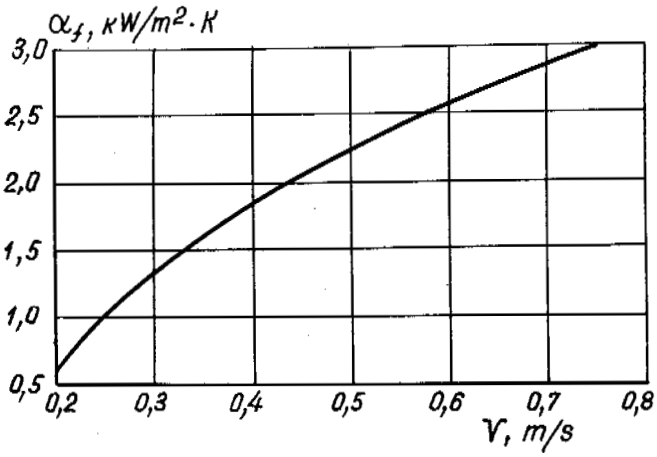

Fig.1 Dependence of the Coefficient of Heat Exchange (α_f) on Water Flow Velocity (V) when Eroding Loamy-Sand and Loamy Sediments

By solving equation (3) with boundary condition $T(0)=T_0$ we define the law of temperature change along water flow length:

$$T = T_0 - \left(T_0 - \frac{q_0}{\alpha}\right)\left[1 - exp\left(-\frac{dx}{c\omega}\right)\right] \quad (4)$$

It is interesting to note that as follows from formula (4) at the at the longest length of run ($x \to \infty$) directly down the frozen rocks surface the water temperature remains higher than 0°C by the $\frac{q_0}{\alpha}$ value, which is usually equal to 0.1-0.5°C.

The average density of heat flow (q_{av}) into thawing rocks at an area of ℓ length is:

$$q_{av} = \frac{\beta}{\alpha} q_0 \left[1 + \frac{1-m}{mn}(1-e^{-n})\right], \quad (5)$$

where $$m = \frac{q_0}{\alpha T_0}, \qquad n = \frac{\alpha \ell}{c\omega}.$$

For the climate conditions of the middle stream of Ichuveem river (q_0 =430W/m²; $\alpha_h + \beta\alpha_e + \alpha_r$ =39W/(m²·°C)) according to formula (5) we've calculated the heat coming into the rocks down the surface of which water flows at initial temperature 7°C, single water consumption 50m²/h, stream velocity 0.5m/s and its respective value of α_f =2000 W/(m²·°C). The coefficient of heat conductivity of thawed rock is 1.0W/(m·°C). The results of calculations are on fig.2.

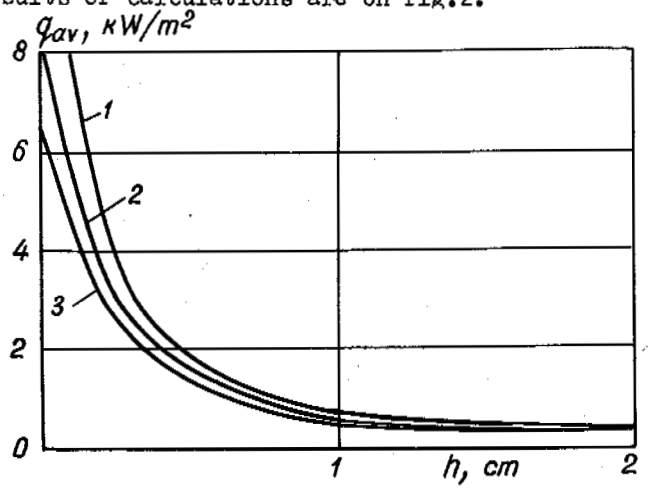

Fig.2 Dependence of Average Density of Heat Flow (q_{av}) into Thawing Massif on Thickness (h) of Thawed Layer at a Different Length (ℓ) of Water Run: 1-20m, 2-40m, 3-60m. The explanations are in the text

The attention is drawn to the fact of sharp decrease of q_{av} at increasing the thickness of accumulated thawed layer. So, at h =1cm and ℓ =50m the density of heat flow is approximately 10 times less than in case of limiting thermoerosion washing at which h =0.

From formula (4) it is not difficult to find the condition of water flow heating, i.e. its cooling action on underlying rocks. In the given example the thawed layer critical thickness at which water flow transfers to the regime of heating is 4.5cm.

In terms of stated it is obvious that at hydromonitor mining of thawed rock layers a water supply method is to assure the longest possible contact of flow with frozen surface. To realize this the hydraulic mining with gradual retreat of erosion front away from a transport trench was used. At a constant velocity of face advance for an ℓ distance the coefficient of heat-away is expressed by:

$$K_h = \frac{\alpha_f}{\alpha}\left[mn + \frac{1-m}{n}\left(e^{-n} + n - 1\right)\right]. \quad (6)$$

In the given case the coefficient of heat-away means the relation of the heat quantity absorbed by rocks to the initial heat content of water flow. When conducting the experimental works at a hydrowashing polygon quite satisfactory coinsidence of formulae (5);(6) with the results of observation is found. For example, the deviations of actual K_h values from the rated curves didn't exceed 10per cent (fig.3).

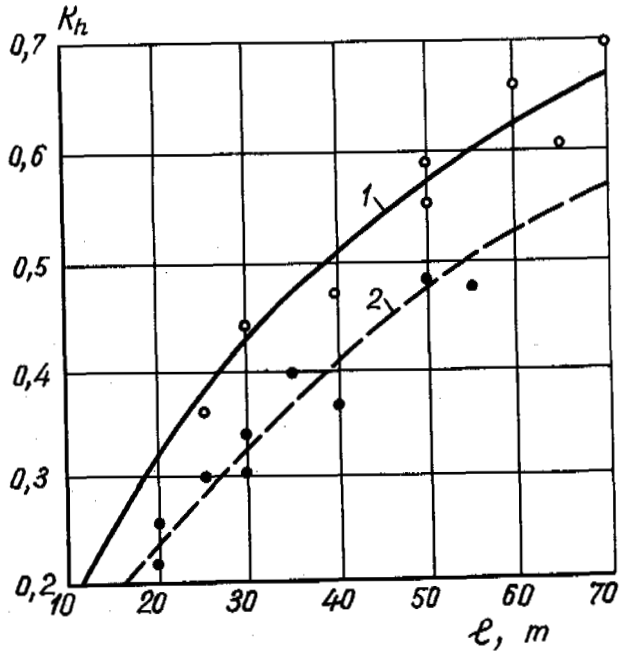

Fig.3 Relation between the Coefficient of Water Flow Heat-Away (K_h) and the Strip Width (ℓ) of Washing at a Single Consumption of 1 - 50m²/h, 2 - 70m²/h

When forcing frozen rocks by water flow and low-head jets the particles of already thawed layer are swept away. The layer's maximum thickness is determined by the relation of thawing velocity to the intensity of rock erosion at the given hydrodynamic characteristics and the temperature of flow.

Multiple laboratory experiments confirm the results of the preceding researches (Yershov a.o.,1979; Myrtshulava,1967): 1)the decrease of erosion intensity and the rise of non-eroding velocity in the range sand - loamy sand - loam; 2)sharp deceleration of erosion intensity increase at reaching some flow velocity corresponding to the beginning of limiting - thermoerosional regime.

The new data have been got concerning the connection of loamy sands and loams erosion ability with their total moisture content in unfrozen and frozen state (fig.4).

As for frozen rocks, the decrease of washing intensity in the left part of the curves can be explained by the deceleration of thawing velocity as the ice content grows. Further increase of the ice content to the right of the extreme is probably accompanied by fast weakening of structural links in the thawed non-eroded layer. As a result, its thickness sharply decreases,and according to formula(5) the density of heat flow into the rock and the thawing velocity increase. The same reason is for U growing at increasing the thawed rocks moisture in the range of high W values. The increase of the thawed rock erosion intensity as their initial moisture content is lowering to the left of the extreme point is difficult to explain otherwise than a "peeling" phenomenon under the influence of the gradient of capillary pression, which is the larger the lower the initial W value.

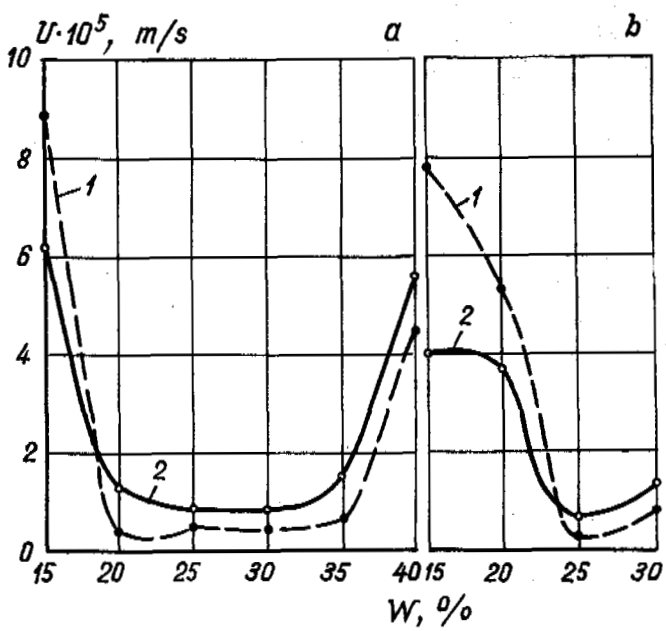

Fig.4 Correlation between Washing Intensity (U) of a) Loam Sands and b)Loams and their Initial Moisture Content(W): 1 - in Thawed State; 2 - in Frozen State

In natural conditions of Ichuveem river valley (West Chukotka) the observations were conducted for the earlier marked (Yershov a. o.,1979) perculiarities of erosion of frozen rocks of reticular cryotexture. The destruction of ice streaks at a direct contact with water flow was faster than the thawing of rock aggregates. The calculations show that to moment of full ice streaks thawing up to 80 per cent of rock aggregate volume remains in frozen state. Thanks to that the thawed rock, if it has water drainage, obtains the inherited fine-platy structure (fig.5).

Main technique for rock washing is a hydromonitor. Therefor its productivity was determined during operation by jets having most frequently used parameters (nozzle diameter is 70-75 mm, pressure is 0.6-0.65 MPa, water consumption is 500-550 m³/h). When hydromining heavy dusty loamy sand and broken stone loam it was noticed that at increasing the thawing depth from 2 to 25 cm there was steady productivity rise. The results of observations are expressed by the empirical formula:

$$P = P_0 + Sh^{2/3}. \qquad (7)$$

where P is the hydromonitor productivity for the accumulated thawed rock,m³/h; h is the thawing depth, cm; P_0, S are empirical parameters, respectively equal to 50 and 15 for loam, 40 and 30 for loamy sand.

Formula (7) is valid for the thawing depth up to 25 cm and for the rock of plastic consistansy.

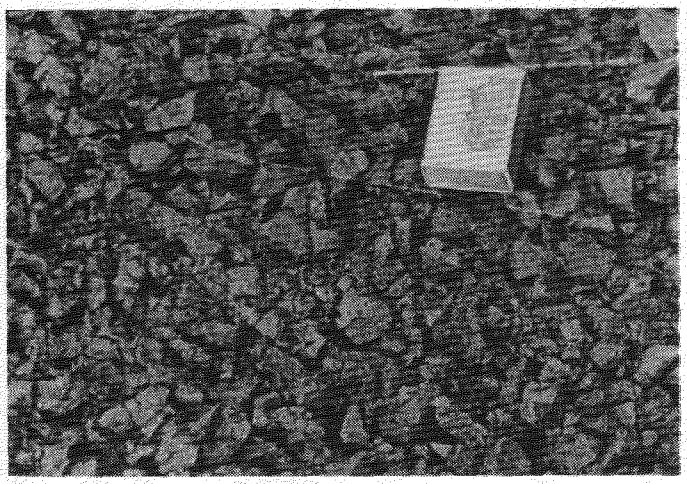

Fig.5 Inherited Postcryogenious Structure of Loam Sand and Loamy Sediments of Ichuveem River flood Land Facies

The conducted researches allow to choose rational technological parameters of hydrowashing. The necessary value of a day surface advance is determined on the base of initial requirements to the planned date of working out the placer of the given thickness. Then according to known calculation methods of radiation thawing (Pavlov,Olovin,1974) and formulae (5)-(7) they determine the optimum hydroerosion rate which assures sufficient intensity of mining operations and the best equipment productivity. After that the necessary quantity of hydromonitor installations for the entire mining area is determined.

The reseachers's results are realized in the range of flow sheets of hydrostripping works which have been employed over the past five years at placer deposits of the North-East of the USSR at different mining and geological and permafrost-climatic conditions. Hydromining was carried out by stationary and self-propelled hydromonitor units (fig.6,7,8) and also by sprinkling apparatus.

Depending on the type of a unit and the properties of eroding rocks water consumption was changed from 100 to 630 m^3/h, pressure from 0.2 to 0.8 MPa. Before starting hydrostripping operations the earthmoving machines removed moss and plant cover away from placer deposit surface, then washed out periodically the rock layer thawed down by the sun radiation heat; the said rock being transported to a hydrodump by running by gravity or by dredge pumps. If mined placer deposits contain plenty of large fragments, their moving through transporting trenches and piling was carried out by earthmoving equipment.

During hydrostripping operations next indices have been got:

specific consumption of electric power - 0.8-2.5kW•h/m^3
specific water consumption - 3-6m^3/m^3
hydromonitor productivity - 100-250m^3/h

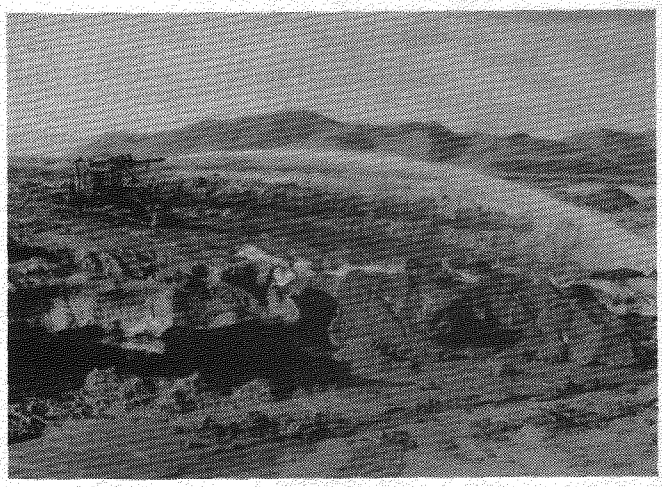

Fig.6 A Self-Propelled Hydromonitor Unit is Working on Erosion of Ice-Rich Rocks in the Basin of the Upper Current of Kolyma River

Fig.7 Bench Placer Mining by Stationary Hydromonitors

It should be noted that the proposed technology starts to compete against the most efficient conventional flow sheets beginning from 3 meter depth. The more the mining depth the best will be the efficiency of the method(Samyshin a.o.,1983).

While developing open-pit deposits containing large rock fragments the most effective are combined technologies including washing away a fine dispersed filler and transporting the remained rocks by earthmoving machines.

Nowadays the scales of hydromining use are quickly widening in the North-East of the USSR.

Fig.8 Polygonal Net Of Wedge Ice Stripped Out by a Self-Propelled Hydromonitor Unit in Ichuveem River Valley

REFERENCES

Yershov,E.D.,Kuchukov,E,Z.,Malinovskii,D.V. (1979).Razmyvaemost merzlykh porod i printsipy otsenki termoerosionnoi opasnosty territorii. Vestnik MGU,ser. geologia N@ 3,pp.67-76.

Myrtshulava,Tz.E. (1967).Razmyv rusel i metodika otsenki ih ustoichivosti.M,Kolos,p79

Pavlov,A.V.,Olovin,B.A.(1974). Iskusstvennoje ottaivanije merzlykh porod teplom solnechnoi radiatsii pti razrabotke rossypei. Novosibirsk,Nauka,p.182.

Samyshin,V.K.,Lavrov,N.P.,Perlshtein,G.G. (1983). Izyskanije ratsionalnykh parametrov gydrorazmyva ldistykh melkodispersnykh otlozhenii. V kn:Voprosy inzhenernogo merzlotovedenija pri razrabotke mnogoletnemerzlykh rossypnykh mestorozhdenii.Sb.nauchn.trudov/VNII-1,Magadan, pp.59-62

OFFSHORE SEAWATER TREATING PLANT FOR WATERFLOOD PROJECT, PRUDHOE BAY OIL FIELD, ALASKA, U.S.A.

V. Manikian[1] and J.L. Machemehl[2]

[1]ARCO Alaska, Inc., Anchorage, Alaska, U.S.A.
[2]Texas A&M University, College Station, Tx., U.S.A.

SYNOPSIS ARCO Alaska, Inc., along with consulting engineers and contractors, planned, designed, and constructed the largest civil engineering structure in the high Arctic Beaufort Sea. This structure, a barge-mounted plant longer than two football fields and taller than an eleven-story building, treats water from the Beaufort Sea for pressurization of the Prudhoe Bay oil field through waterflooding, to enable the recovery of an additional 160 million cu meters of oil. In the context of national energy production, this corresponds to about ten percent of estimated onshore undiscovered recoverable oil reserves in Alaska (Shell 1978, USGS 1975), and it is unlikely that the opportunity exists elsewhere in the U.S. to achieve with a single project the oil productivity of a Prudhoe Bay oil field waterflood.

As Prudhoe Bay oil production passes 500 million cu meters, injected water (known as waterflood) is needed to offset the pressure lost as the oil is removed. The construction of the Seawater Treating Plant with its innovative design provides the unique solution to the needs of industry and the local community.

INTRODUCTION

The barge-mounted Seawater Treating Plant is the first offshore facility in the high Arctic (Fig. 1). While the plant itself cost 385 million dollars, it is the cornerstone of a two billion dollar waterflood project which will enable ARCO Alaska, Inc., Standard Alaska Production Company, Exxon Company, U.S.A. and other owner oil companies to recover through this secondary recovery system the additional 160 million cu meters from the Prudhoe Bay oil field of Alaska.

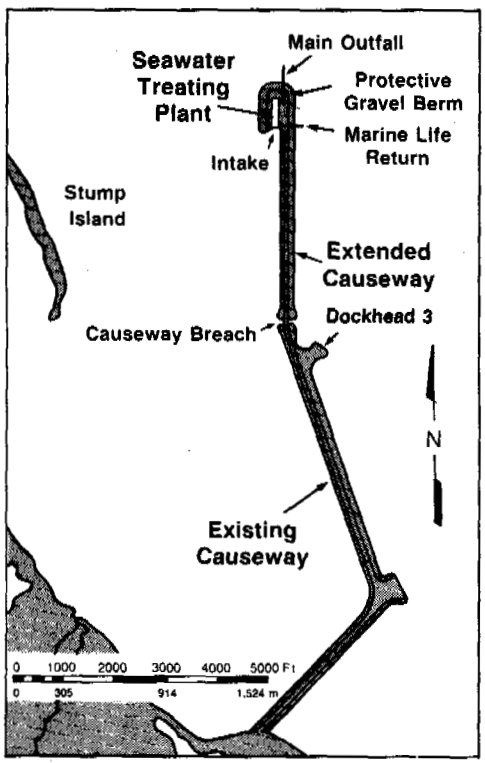

Fig. 1

Daewoo, Korea was chosen as the fabrication site for the 186 m long oceangoing barge and Seawater Treating Plant based on economic considerations and a study of available shipyard facilities. The fabrication started on January 4, 1982 and was completed in nineteen months on July 8, 1983. The barge was then towed 6,500 km to Prudhoe Bay to coincide with the 1983 summer open water sealift period, a short four- to six-week stretch when the ice floes recede and ships can get to Prudhoe Bay. The platform was positioned and set on a prepared offshore gravel foundation (Fig. 2) on the seabed by controlled ballasting on August 22, 1983. After mechanical completion and startup activities in Prudhoe Bay, the plant was put in operation on June 14, 1984 (Fig. 3). At the end of its expected service life of 25 yrs, the barge-mounted Seawater Treating Plant can be removed from its site by de-ballasting and towing.

The design of the Waterflood Project involved challenges and opportunities for innovation in the following areas: freeze protection and life support system, intake and marine life recovery system, ice criteria and protection, marine design, special materials and coatings, gravel foundation design, causeway and fish passage breach, buried pipelines, and slope protection.

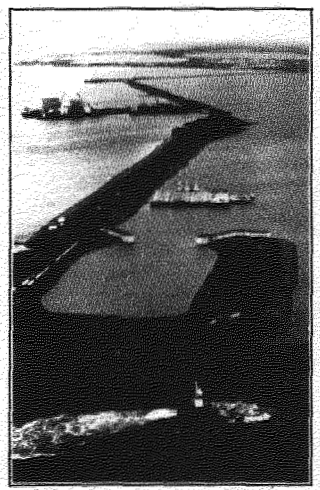

Fig. 2

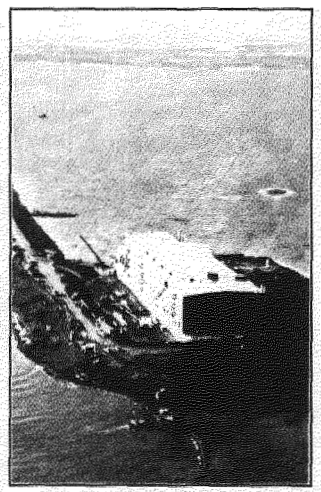

Fig.3

FACILITY DESCRIPTION

To maintain an adequate water supply even in winter, when sea ice can form to thicknesses of two meters or more, the Seawater Treating Plant had to be located at the end of the 1,200 m extension of an existing causeway, where water is 3.6 m deep (Fig. 1).

Seawater flows directly into the treating plant intake reservoir through ports in the shoreward end of the platform. The intake ports are located below winter ice and above the seabed to assure a reliable water source of good quality with minimum intake of marine organisms. Flow is then directed through angled screens which are part of a bypass system. Any incoming fish are diverted by the screens and returned to the sea. An untreated seawater spray will then remove any other debris from the screens. This debris will be collected and returned to the Beaufort Sea through the 61 cm main outfall line.

The seawater will then be pumped through in-line strainers to remove fibrous tundra particles. After straining, the seawater is heated to approximately 4.4°C to prevent freezing. The filtered seawater then flows through deaerators for dissolved oxygen removal. Finally, the treated water is pumped through pipelines to onshore injection plants, where it is pressurized and sent to designated injection wells in the oil field.

Processing removes suspended solids and dissolved oxygen for two reservoir operational requirments: (1) reduction of oxygen present in seawater to reduce corrosion to waterflood facilities, and (2) to eliminate the fines present in seawater that plug the pores within the reservoir formation. In addition, the processing provides heat for freeze protection in the low-pressure pipeline system of 1,690 K Pa.

The Seawater Treating Plant is protected from waves and ice by a gravel berm which is connected to the shore by a gravel causeway. Buried in the causeway are two large diameter supply pipelines that transport treated seawater to injection wells, conduits carrying the power distribution cables, and a fuel gas supply pipeline to the Seawater Treating Plant. The causeway also has a breach, spanned by a bridge, to minimize the impact of the causeway on free movement of marine life.

The environmental design criteria are summarized in the following TABLE I.

TABLE I
Environmental Design Criteria

Design Ambient Temperature:	−48°C
Water Depth:	3.6 m
Seawater Treating Plant Dimensions:	186 m (L) x 46 m (W) x 35 m (H)
Mean Draft:	3 m
Design Storm Surge:	+2.3 m, MLLW
Design Wave Height:	H_{sig} = 3.1 m, H_{max} = 4.6 m
Seawater Treating Plant Berm Height:	+ 8.7 m
Seawater Treating Plant Berm Side Slope:	1V to 5H

A 69 kV power system serves the facility. Other facilities in the Seawater Treating Plant include emergency power generators, fired heaters, elaborate fire protection and safety systems, maintenance shops, storage areas, offices, control rooms and emergency living quarters with on board desalination plant for potable water, a waste water and sewage treating plant, recreational facilities, kitchen and food storage facilities.

FREEZE PROTECTION

The Seawater Treating Plant is designed for an ambient temperature of −48°C. Life support systems (minimal lighting, heating system, elevators, fire protection and other basic facilities) have been designed with several levels of redundant power. On-board power generation is provided to back up the 69 kV power brought into Seawater Treating Plant from the on-shore facilities. The backup equipment consists of two turbine generators (dual fuel, gas or diesel) and one diesel generator. Any two generators can maintain minimum flow through the pipelines plus life support load at the facility, while any one generator can maintain the "life support loads."

Due to the Arctic environment a considerable freezing hazard exists if the discharge through the pipelines is significantly decreased. The insulation on the pipelines would keep the water above freezing temperatures for only a limited period of time.

The Seawater Treating Plant has been designed to maintain minimum flow through pipelines (usually 10% of design flow) to prevent freezing. As a last resort option, provisions have been made to evacuate the pipelines back into the ocean if the minimum flow could not be maintained.

INTAKE AND MARINE LIFE RECOVERY

Due to the large physical dimensions of the required integrated seawater intake, the early completion of its design was a key element in determining the overall size of the barge. Project planning considerations dictated that the barge dimensions be finalized early in the design effort. This, in turn, put a high priority on the intake design.

The design of the seawater intake, however, turned out to be very challenging. First, it had to meet specific hydraulic performance requirements for a broad range of anticipated water levels, sea states, and plant flow rates. Secondly, a serious ice particle ingestion problem required solution. And, finally, very stringent standards were established regarding minimizing harm to marine life.

Extensive analytical and physical modeling of the hydraulic performance of the eight bays comprising the intake was carried out. Ice problems at the intake included both the potential for clogging of the intake ports by accumulations of ice rubble and the ingestion of ice fragments into the intake. Design refinement, again with considerable model testing, was performed.

The intensive effort that went into the design and testing of the marine life recovery system will ensure that the Seawater Treating Plant will not disrupt the native fishery in the Prudhoe Bay area. This fishery is relied upon by North Slope natives for subsistence. Large numbers of fish (arctic and least cisco) feed during the summer in the Prudhoe Bay area. Alaska natives in coastal villages net these fish during the autumn.

The seawater intake was designed with low entrance velocities so that fish would not be drawn into the plant. Should fish swim or be drawn into the intake ports, the system will recover and divert them back to the ocean unharmed. This was achieved by designing a system that minimized thermal shock by specifying a maximum temperature rise in the fish diversion system (0.55°C) and by reducing mechanical damage by avoiding any contact of fish with moving parts of pumps. The system diverts fish from the main process flow by the use of angled screens and passages with gradually reduced cross sectional areas and returns them to the ocean with the help of jet pumps. Fish behavior tests, using live fish, were conducted before the system design was finalized. A series of closely spaced bars, positioned in the intake ports, will prevent marine mammals (e.g., seals) from entering the seawater intake.

ICE FORCE AND RIDE-UP PROTECTION

Ice Forces Criteria: The protective berm and the causeway were designed to resist ice loads of 655,000 kg/lin m of perimeter for the Seawater Treating Plant berm and 402,000 kg/lin m for the causeway. For the ice force design criteria see the following TABLE II.

TABLE II
Ice Force Design Criteria For Various Waterflood Activities

Causeway (From Shoreline to Dockhead 3)

Ice Force: 1800 K Pa x depth below MLLW x 110%
Frost penetration assumed 6 m below seabed under existing causeway.
Frozen gravel shear strength for local shear: 192 K Pa

Causeway Extension (From Dockhead 3 to Seawater Treating Plant)

Ice Force: 402,000 kg/lin m
Frost penetration assumed to be 1.8 m below seabed.

Seawater Treating Plant Berms

Ice Force: northern and eastern exposure - 595,000 kg/lin m
Ice Force: southern and western exposure - 402,000 kg/lin m
No frost penetration assumed below seabed.

Seawater Treating Plant Hull

Indirect ice load: N, E, W - 241 K Pa (223,000 kg/lin m)
Direct ice load: South - 402,000 kg/lin

Gravel fill weight above MLLW - 1,842 kg/cu m
Gravel fill weight below MLLW - 1,041 kg/cu m
Sliding Friction Co-efficient, Gravel/Soil - 0.5

Ice Forces Transmitted to Hull: A two-dimensional finite element analysis was conducted to determine pressure transmitted to the Seawater Treating Plant hull from migrating ice loads imposed through the protective berm in varying configurations of frozen and thawed conditions. It was determined that the resulting pressures on the hull were within the maximum allowables. The only direct exposure to the ice load was on the intake side of the Seawater Treating Plant. An integrated shear transfer system, including seven shear walls each 6 m high, 1 m wide, and 27 m long, were provided at the seawater intake to transfer direct ice forces into the main hull structure.

Ice Ride-Up Protection: Horizontal excursions by winter ice sheets constituted an ice "over-ride" threat. All structures projecting above the surface of the berm or causeway were placed sufficiently distant from the ocean to be beyond maximum anticipated ice movements.

MARINE DESIGN

The Seawater Treating Plant along with its intake structure and all the support facilities, was designed as an integrated facility with the barge. The plant consists of a marine hull and a superstructure. The hull is a doublewall and doublebottom construction. The 13 m high hull is divided into several watertight compartments to provide strength as well as damage survivability.

SPECIAL MATERIALS AND COATINGS

Due to the corrosive and electrolytic properties of the aerated seawater, special materials and coatings were used in the waterflood project. This was supplemented by cathodic protection measures. Also necessary was a galvanic corrosion protection design since a large corrosion potential existed due to use of various dissimilar metals.

GRAVEL FOUNDATION DESIGN

The Seawater Treating Plant foundation consists of a prepared gravel pad on the sea floor inside the protective berm. The foundation design was an area of considerable concern because very little geotechnical information was available on the offshore Arctic. The foundation also had to be built to very close tolerances ($\pm$2.5 cm) and required that the long term behavior of the foundation be predictable.

The top layer of the existing sea floor was silty material. This material was removed by dredging and replaced with gravel backfill. This provided a foundation of known uniform composition and of predictable behavior, which gave a higher degree of confidence in its integrity. After placement of the backfill the foundation gravel pad was brought up to final elevation and leveled. This leveling operation was carried out under water.

Backfill placed after the Seawater Treating Plant was in position would generate a higher loading condition than generated by the Seawater Treating Plant itself, which would result in an undesirable differential settlement between the center of the plant and the perimeter. Because of this consideration, a gravel preload was placed at the perimeter of the dredged and backfilled area to preconsolidate the foundation materials and eliminate the differential settlement. The preload material was placed one year prior to the Seawater Treating Plant installation. Preloading was used in lieu of mechanical compaction because settlement was expected to take place in the underlying materials. Mechanical compaction would only consolidate the gravel fill and not resolve the settlement problem.

Concern with offshore permafrost caused extensive thermal modeling of the Seawater Treating Plant hull to be conducted. In summary, the fact that permafrost is very deep at the Seawater Treating Plant site (more than 30 m), allowed the Seawater Treating Plant hull to be uninsulated at its bottom surface. (The hull is, however, insulated at the upper portions of its vertical surfaces to limit heat loss to the embankment.)

CAUSEWAY AND FISH PASSAGE BREACH

The berm surrounding the Seawater Treating Plant is connected to the shoreline with a gravel causeway, which provides a two-way vehicle access. Other major operational benefits of the causeway are the protection of, and ease of access to, the fuel gas line and the two large-diameter seawater supply pipelines buried in the causeway.

A fish passage causeway breach design was incorporated in the gravel causeway to intercept and allow fish passage through the causeway at a point where they are concentrated. The 16 m wide waterway opening is protected on its sides with sheet pile bulkheads driven into the seabed to an adequate depth below the worst case scour condition. The 46 m long bridge structure spanning over the breach area will accommodate loaded Euclid B-70 trucks with its load of 104,000 kgs, the set loading criteria for the bridge and the causeway. The bridge bottom of steel is 7.6 m above the mean-low water elevation to provide freeboard above storm surge, wave and winter ice sheets.

SEAWATER SUPPLY PIPELINES

The Seawater Treating Plant has two large diameter water pipelines to deliver treated seawater to the oil field for injection. These were insulated and buried within the causeway and are the first major underground pipelines ever constructed in the Arctic.

Treated water for ARCO and the Eastern Operating Area is pumped through an insulated 101 cm line. Treated water for Standard and the Western Operating Area is pumped through an insulated 91 cm line. The ARCO line has a design rate of 190,000 cu m/day and the Standard line has a design rate of 160,000 cu m/day.

Buried large diameter pipelines when subjected to Euclid B-70 impact loads can be subjected to ovalling deflections and excessive stresses. Calculations were conducted with special considerations to the pipeline sidefill resistance. The procedure models the soil-pipe interaction, characterizing the sidefill by an appropriate modulus value during winter or summer weather conditions. It was determined that with the available cover over the pipelines and under the design loading conditions the maximum pipe deflections were well below five percent of the diameter and the maximum pipe stresses below allowable values.

SLOPE PROTECTION

The Waterflood project was the first project requiring a decision on long-term slope protection in the Arctic Ocean. During its design, a management decision was made to allow the exposed berm and causeway slopes to erode. The decision to treat all exposed gravel surfaces as "sacrificial beaches" was based on a risk and economic analysis in which various slope protection alternatives were considered. The "sacrificial beach" concept allowed for estimated levels of beach erosion, thus, requiring restoration of the slopes after storms and on an "as-needed" basis. A program for future maintenance was found cost effective (i.e., substantially less expensive, on a "present worth basis") than other alternatives. The project will be monitored by the Prudhoe Bay Unit to ensure that the causeway and seawater treating plant can continue to function adequately with limited maintenance or down time.

CONCLUSIONS

The Seawater Treating Plant was a unique challenge requiring resolution of many complex problems. It was in many ways an unprecedented facility. We conclude that:

1. An offshore permanent industrial plant in the Arctic has proven to be technically feasible.
2. An integrated process plant and ocean-going vessel can be a viable cost-effective option in comparison to conventional modular construction.
3. It can be an attractive option when a complete plant is to be fabricated as a single transportable unit for remote locations.
4. This approach may be preferable for temporary process plant locations where marine access is available, or when a process plant has to be removed after completion of its assignment.
5. Process plant construction and shipbuilding techniques can be integrated with proper planning of engineering and construction. Experience gained on the Seawater Treating Plant project can be of tremendous value on similar projects in future.
6. Underwater foundations for large industrial plants can be prepared to close tolerances cost effectively.
7. A marine life recovery system can be designed without any moving mechanical parts coming in contact with the fish.
8. A "sacrificial beach" type of slope protection appears to be a viable alternative in the near-shore Beaufort Sea.
9. Providing pipeline access to an offshore site from the shoreline, by way of burial of the pipeline within a causeway, appears to be an efficient solution to many design problems including those related to subsea permafrost.

ACKNOWLEDGEMENTS

The permission of the Prudhoe Bay Unit owners to publish this paper is gratefully acknowledged.

Appreciation is extended to the following contractors and consultants that participated in the design and construction of the project: Alaska International Constructors, ARCTEC Engineering, Bechtel Petroleum, Daewoo Shipbuilding & Heavy Machinery, Dames & Moore, Harding - Lawson, Western Canada Hydraulic Laboratory, Woodward - Clyde.

REFERENCES

Shell, 1978. Shell: Alaska holds 58 percent of future U.S. oil finds. Oil and Gas Journal, November 20, 1978, p. 214.

USGS, 1976. Water resources data for Alaska, water year 1975. U.S. Geological Survey, Water-Data Report ALK-75-1, 410 pp.

DEVELOPING A THAWING MODEL FOR SLUDGE FREEZING BEDS

C. J. Martel

U.S. Army Cold Regions Research and Engineering Laboratory, Hanover, N.H. 03755-1290 USA

SYNOPSIS This paper presents the development of a model that can be used to predict the thawing design depth of a sludge freezing bed. A sludge freezing bed is a new unit operation for dewatering sludges from water and wastewater treatment plants. Preliminary results obtained from a pilot-scale freezing bed indicate that this model is valid.

INTRODUCTION

One of the main problems in sludge management is dewatering. Typically, sludges resulting from wastewater treatment processes contain only 0.25 to 12% solids (Metcalf and Eddy, 1979). Water treatment sludges may contain as little as 0.1% solids before thickening and perhaps 2.5% after thickening (Fair et al., 1968). In most cases, direct disposal of these dilute sludges is unacceptable because of the cost of transportation. In addition, the liquid in the sludge could pollute surface or ground waters, so some method of dewatering is usually required before disposal. Commonly used methods include filter presses, horizontal belt filters, centrifugation, and drying beds.

Selection of an effective dewatering method for facilities located in cold regions can be especially difficult. Because of the remoteness of many northern communities, parts and equipment are not easily obtainable. Most of these communities are small, and skilled operators are scarce or not available. Therefore, complex mechanical dewatering methods are often undesirable. Simpler methods such as drying beds and lagoons can be used but they are inefficient in cold regions because of the shortness of the drying season. Large storage facilities are often required to contain the sludge over the long winter and spring months.

A more efficient method of dewatering sludges in cold regions is to use natural freeze-thaw. Studies by Martel (1987) have shown that up to 2.0 m of freeze-thaw-conditioned sludges can be dewatered by this process. Some northern plants are already using natural freeze-thaw in their existing lagoons or drying beds. However, these operations are designed for drying sludge and are only deep enough to freeze 0.2 to 0.3 m of sludge. To optimize the natural freeze-thaw process, a specially designed unit operation is necessary.

A unit operation based on natural freeze-thaw conditioning has been proposed by Martel (1987). This unit operation is called a sludge freezing bed. A conceptual sketch of a sludge freezing bed is shown in Figure 1. In essence, the bed consists of a large in-ground concrete tank with a ramp on one side and an overflow gate on the other. The ramp is needed to allow vehicle access for sludge removal and to distribute the incoming sludge evenly within the bed. The overflow gate is provided in case of accidental overfilling and to draw off supernatant during thaw. The bottom of the bed is under-drained with wedgewire screen or sand to allow drainage of the filtrate. Both overflow and filtrate are collected in a sump and are pumped back to the plant. This concept is similar to the prototype freezing beds built at three small biological/chemical treatment plants in Sweden (Hernebring and Lagesson, 1986).

To use the bed the operator would apply sludge in layers during the winter months. Each layer would be applied as soon as the previous layer was frozen. At the end of the freezing season, applications would be terminated and the frozen sludge layers would be allowed to thaw. Under natural ambient conditions, thawing is expected to proceed from the top downward. Most of the supernatant would be drained away by removing stop planks from the overflow gate. When thawing is complete, any remaining liquid would be drained away through the wedgewire or sand bottom. If necessary the solids could be kept in the bed until the desired solids content is achieved. The operator would then remove the sludge with a front-end loader or other device. If sufficient warm weather remains, the operator could continue sludge dewatering by using the freezing bed as a drying bed.

As conceived, a sludge freezing bed could be used as a sole method of dewatering (Fig. 2a) or in combination with other methods such as drying beds (Fig. 2b). If it were used as the only method of dewatering, a storage facility would be needed to contain the sludge during the summer months. This storage facility could be a lagoon, tank, or even a digester if excess capacity were available. If used in

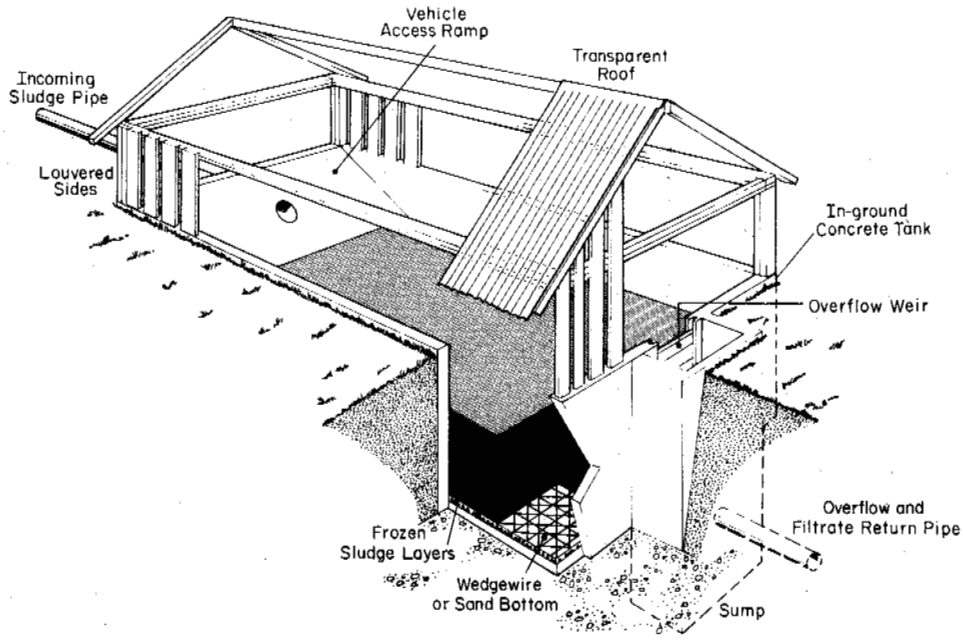

Fig. 1. Conceptual sketch of sludge freezing bed.

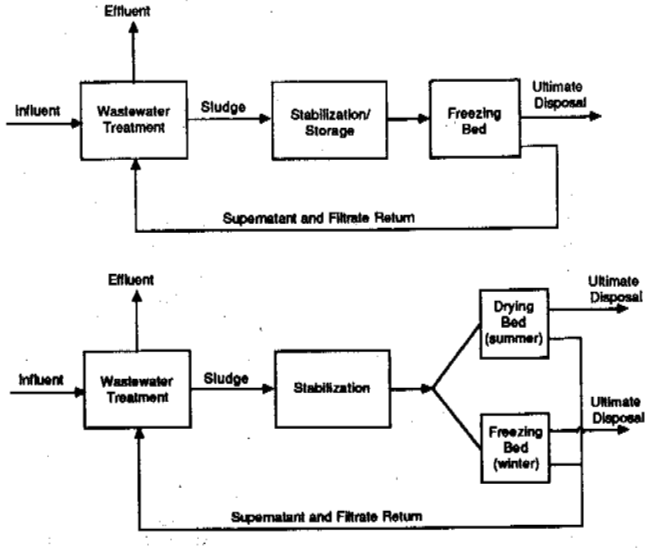

Fig. 2. Process flow sheets for sludge dewatering with freezing beds.

combination with drying beds, the freezing bed would be designed to handle the winter sludge production only. A freezing and drying bed combination is particularly attractive because both methods would be operating under optimum conditions.

The size of a sludge freezing bed depends on the depth of sludge that can be frozen and thawed at the proposed site. The lower of the two depths will be the limiting design depth. In permafrost areas the depth of thaw is limiting because of the short thawing season. This paper presents the development of a thawing model that can be used to predict this depth. Development of a freezing model can be found in Martel (1987).

DEVELOPMENT OF THAWING MODEL

Thawing proceeds downward from the surface and inward from the walls of the freezing bed. When the sludge thaws, the solids separate from the liquid and settle on the underlying frozen sludge. The depth of this settled solids layer increases as thawing progresses. This layer acts as an insulation between the warm ambient air and the frozen sludge, so the frozen sludge at the bottom of the bed will take longer to thaw than that at the top. The expected temperature profile in the bed during thaw is shown in Figure 3.

In this development it is assumed that most of the supernatant will be removed as quickly as possible. This can be accomplished by removing the stop-planks as thawing progresses. Leaving the supernatant in the bed decreases the thawing rate because of the added water layer.

Thawing occurs as a result of warm air passing over the settled solids layer and of solar radiation. The rate of heat transfer into the frozen sludge mass by both of these mechanisms must equal the rate of energy gain during the phase change from solid to liquid states. Thus, an energy balance per unit area at the solids/air interface yields

$$q_c + q_r = e \qquad (1)$$

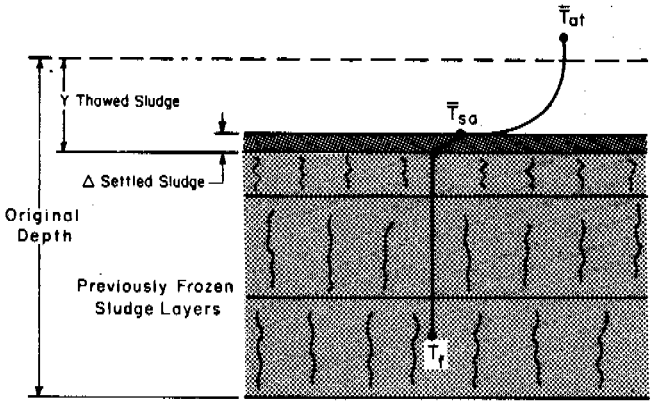

Fig. 3. Assumed temperature profile during thaw.

where q_c and q_r are the rates of heat transfer by convection and radiation respectively, and e is the rate of energy gain during the phase change.

The rate of heat transfer by convection (q_c) can be expressed as

$$q_c = \bar{h}_c A (\bar{T}_{at} - \bar{T}_{sa}) \quad (2)$$

where $\bar{h}_c$ is the average convective heat transfer coefficient (W/m²·°C), A is the surface area (m), $\bar{T}_{at}$ is the average air temperature during thaw (°C), and $\bar{T}_{sa}$ is the average temperature of the settled solids at the air interface (°C).

The rate of heat transfer by solar radiation (q_r) can be expressed as (Krieth, 1973)

$$q_r = \alpha\tau\bar{I}A \quad (3)$$

where α is the solar absorptance of the sludge (dimensionless), τ is the transmittance of the roof (dimensionless), and $\bar{I}$ is the average insolation during thaw (W/m²).

The rate of energy gain during melting can be calculated from

$$e = \rho_f LA \frac{dy}{dt} \quad (4)$$

where ρ_f is the density of frozen sludge (kg/m²), L is the latent heat of fusion (W·h/kg), and dy/dt is the rate of change in the position of the melting sludge interface.

Substituting Eqs. 2, 3, and 4 into Eq. 1 results in the following energy balance relationship:

$$\bar{h}_c (\bar{T}_{at} - \bar{T}_{sa}) + \alpha\tau\bar{I} = \rho_f L \frac{dy}{dt} \quad (5)$$

Another energy balance relationship can be obtained across the settled sludge layer. In this case the rate of heat transfer by conduction across the layer must also equal e. The rate of heat transfer by conduction (q_k) can be calculated from

$$q_k = \frac{AK_{ss}}{\Delta} (\bar{T}_{sa} - T_f) \quad (6)$$

where K_{ss} is the thermal conductivity of thawed sludge (W/m·°C), Δ is the thickness of the settled sludge layer, and T_f is the freezing point of sludge. Thus an energy balance across the settled sludge layer yields

$$\frac{K_{ss}}{\Delta} (\bar{T}_{sa} - T_f) = \rho_f L \frac{dy}{dt} \quad . \quad (7)$$

Neither Eq. 5 nor 7 is very useful because $\bar{T}_{sa}$ is difficult to determine. However, $\bar{T}_{sa}$ can be eliminated by solving Eqs. 5 and 7 for the temperature differences and adding them. This procedure results in the following expression in terms of $\bar{T}_{at}$ and T_f only:

$$\bar{T}_{at} - T_f = \left(\frac{1}{\bar{h}_c} + \frac{\Delta}{K_{ss}}\right)\rho_f L \frac{dy}{dt} - \frac{\alpha\tau\bar{I}}{\bar{h}_c} \quad (8)$$

Solving Eq. 8 can be simplified by assuming that the ratio of Δ to y is constant for all depths. Then Δ can be expressed as θy, where θ is the fraction of deposited solids per unit depth of thawed sludge. Substituting this expression into Eq. 8 and separating variables results in

$$\left(\bar{T}_{at} - T_f + \frac{\alpha\tau\bar{I}}{\bar{h}_c}\right) dt = \left(\frac{1}{\bar{h}_c} + \frac{\theta y}{K_{ss}}\right)\rho_f L dy \quad (9)$$

At t = 0, y = 0, and at t = t_{th} (time to thaw), y = Y (the total depth of thawed sludge). Integrating between these limits and solving for t_{th} results in the following equation for predicting thawing time:

$$t_{th} = \frac{\rho_f LY}{\bar{T}_{at} - T_f + \frac{\alpha\tau\bar{I}}{\bar{h}_c}} \left(\frac{1}{\bar{h}_c} + \frac{\theta Y}{2 K_{ss}}\right) \quad (10)$$

Eq. 10 can be solved for Y, the thawing design depth, by using the quadratic formula. This formula produces two values of Y but only the positive value is useful for engineering purposes. From this formula,

$$Y = \left(\left(\frac{K_{ss}}{\theta \bar{h}_c} \right) + \frac{2 K_{ss} t_{th}}{\theta \beta} \right)^{1/2} - \frac{K_{ss}}{\theta \bar{h}_c} \quad (11)$$

where β is equal to $\rho_f L/(\bar{T}_{at} - T_f + \alpha\tau\bar{I}/\bar{h}_c)$.

VALIDATION

To validate this model, 0.58 m of anaerobically digested sludge was frozen over the winter of 1986-87 in a pilot-scale freezing bed in Hanover, New Hampshire (Fig. 4). Thawing began on 18 March and was completed on 12 May for a total thawing time (t_{th}) of 1344 h. The average ambient air temperature ($\bar{T}_{at}$) and insolation ($\bar{I}$) during this period was 7.7°C and 149 W/m²·h respectively. The calculated average convection coefficient was 12.9 W/m²·°C based on the relationship $h_c = 5.7 + 3.8\ \bar{v}$ where $\bar{v}$ is the average wind velocity in m/s (Kreith and Kreider, 1978).

The thermal conductivity of the settled sludge (K_{ss}) was 0.20 W/m·°C according to measurements made in situ using a procedure developed by Atkins (1983). Drainage tests with this sludge indicated that θ, the fraction of settled solids per unit depth was 0.34. The freezing point (T_f) was found to be 0°C (Martel, 1987). Since sludge is mostly water, values of ρ_f and L were assumed to equal those of water, i.e. 917 kg/m² and 93 W·h/kg respectively. The transmittance (τ) of the transparent fiberglass roof was 0.9 and the absorptance (α) of the sludge was assumed to be 0.9.

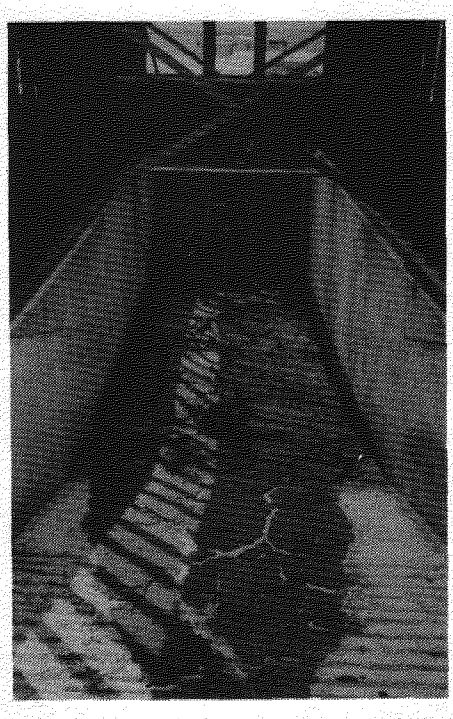

Fig. 4. Inside of freezing bed pilot plant after freeze-thaw of 0.58 m of anaerobically digested sludge.

Substituting these values in Eq. 11, the predicted depth of thawed sludge is 0.52 m, which is approximately 10% less than the actual thawed depth of 0.58 m. This small difference should not be significant for design. In addition, the equation predicted a lesser depth than the actual, which results in a more conservatively designed freezing bed.

A comparison of the $1/\bar{h}_c$ and $\theta Y/2K_{ss}$ terms in Eq. 10 indicates that the latter has a greater effect on thawing time. The value of $\theta Y/2K_{ss}$ is 0.493, which is 6.4 times greater than the value of $1/\bar{h}_c$. To reduce the value of this term it is necessary to either reduce the settled solids fraction (θ) or increase the thermal conductivity (K_{ss}). Although it would be difficult to increase the thermal conductivity, it can be prevented from decreasing by keeping the sludge saturated since water has a higher thermal conductivity than air. The settled solids fraction could be reduced by occasionally removing the solids during the thawing period.

The pilot-scale experiment demonstrated the beneficial effect of natural freeze-thaw. The anaerobically digested sludge, which originally contained only 6% solids, was dewatered to 40% solids after freeze-thaw. This represents an 81% reduction in water content. The sludge was easily removed from the bed with a front-end loader.

CONCLUSION

Natural freeze-thaw can effectively dewater sludges from most water and wastewater treatment facilities in cold regions. A new unit operation called a sludge freezing bed has been developed that can utilize this process. Preliminary results indicate that the model presented in this paper can be used to predict the depth of frozen sludge that can be thawed naturally during the spring and summer. More research is being conducted to further validate this model.

REFERENCES

Atkins, R T (1983).
In-situ thermal conductivity measurements. Final Report for the State of Alaska. US Army Cold Regions Research and Engineering Laboratory, Hanover, N.H.

Fair, G W, Geyer, J C & Okun, A D (1968).
Water and Wastewater Engineering, Vol. 2, John Wiley and Sons Inc., New York.

Hernebring, C & Lagesson, E (1986).
Conditioning of sludge by natural freezing (translation from Swedish). Report No. 27,

Institute for Urban Construction, Dept. of Water and Sewage Technology, University of Lulea, Sweden.
Kreith, F (1973).
Principles of Heat Transfer. 3rd Edition, McGraw-Hill Inc., New York.
Kreith, F & Kreider, J F (1978).
Principles of Solar Engineering, McGraw-Hill Inc., New York.
Martel, C J (1987).
Development and design of sludge freezing beds, Ph.D. Dissertation, Colorado State University, Ft. Collins.
Metcalf and Eddy, Inc. (1979).
Wastewater Treatment/Disposal/Reuse. 2nd Edition, McGraw-Hill Inc., New York.

TEST OF THE SHALLOWLY BURIED WATER SUPPLY PIPE

Meng, Fanjin

Oil Field Construction Design and Research Institute of Daqing Petroleum Administrative Bureau, China

SYNOPSIS In order to determine the proper buried depth for water supply pipes in cold regions the field full-scale tests were conducted in Daqing area for three winters. The temperatures at inlet and outlet of the pipe, the size of the melt ring and the ground temperatures at various points around the pipe were observed. The tests showed that the shallowly buried technique could be used in burial of water supply pipes. Based on the test resuls, 43 km water supply pipes were built in Daqing Oilfield with the buried depth of 1 m. No frost damage occured in three years.

INTRODUCTION

Daqing is in cold region, where winter is long and the ground is frozen as long as eight months. The lowest air temperature is -25.1°C in month average and -39°C in minimum. The deepest frost penetration is 2.2 meters.

The test was suggested based on the features of the water supply pipes and the actually productive conditions in the oil fields.

TEST CONDITION AND METHOD

Determination of the test parameters

The main purpose of this test was to investigate the behaviour of the water supply pipe that was buried above the lowest frost line and in different conditions, such as the pipe's length and diameter, water temperature in the supply inlet, flow and the property of the soil around the pipe, and to look for the allowable minimum buried depth of the pipe. The demands for this buried depth are: (a) water at the end of pipe should not be frozen during supply, (b) water in pipe should not be frozen in the allowable period of stopping water supply. Because it usually needs not more than 24 hours to maintain the supply pipe once, the time for stopping water supply in the test was decided to be 36 hours or more. Suitably buried depth is related with the pipe length and diameter, flow, water temperature and property of soil. These parameters were chosen as follows

A) Pipe length

In the oil field the supply stations' service radius is about 3 kilometers and the furthest point from the station is not more than 5 kilometers, among which the lengths of main pipes and branch pipes are 3.5 and 1.5 kilometers, respectively. Limited by test condition, the length of test pipe was chosen as 80 meters.

B) Water temperature

Water from different supply sources has different temperatures. Considering that the temperature of surface water is 0-1°C in the winter, and its amount is small, so it is not suitable to use surface water in the test. Ground water was used in the test and the water temperature is considered to be 9°C.

C) Soil property

The soils in the test site are light loam and sandy soil. Their thermal conductivity is 14 W/m³K.

D) Pipe diameter

According to the practical situation in the oil field, three kinds of pipes, ϕ114x4, ϕ88.5x4 and ϕ60x5 mm, were used in the test.

E) Flow

The flow in most branch pipes is about 3 m³/h and a few of that about 1 m³/h. All tests were conducted at two stages, i.e., "great flow" and "small flow" stage. In great flow stage, the test flows in the pipes of ϕ60x5, ϕ88.5x4 and ϕ114x4 mm are 2, 3 and 4 m³/h, respectively, whereas in small flow stage, they are 0.2-0.6 m³/h.

F) Buried depth of pipe

According to the standard, buried depth at the top of a pipe can not be less than 0.7 m and it is commonly designed lower than the maximum frost depth, that is 2.2 m in Daqing region. Buried depths (at the centre of a pipe) of test pipes were 1.5, 1.3 and 1.0 m for the pipes of ϕ60x5, ϕ88.5x4 and ϕ114x4, respectively.

Test method

When the ground temperature around the pipes were near the minimum, let the water run through

the pipes with a designed value of flow so as to form a melting ring around the pipes. At the same time, the soil temperatures around the pipes and air temperature were measured and recorded. As soon as the melting ring had been stable, water conveyance should be stopped immediately, but the temperatures at various point around the pipes should be observed continuously. The melting ring is considered to be disappeared when the temperature at the pipe wall becomes zero °C. According to the observed data, the magnitude of the melting ring and the time from stopping water supply to the disappearance of the melting ring were calculated, and the melting ring was drawn, as shown in Fig.1.

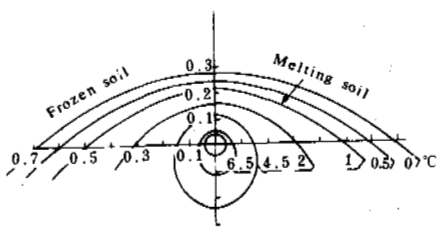

Fig.1 The Shape of the Melting Ring Around a Pipe

The test results obtained in three winters during 1978-1981 are shown in Table I.

the variation of ground temperature is slow the effect of short-term variation of air temperature on the temperature in deep soil layer is small, where the melting ring is comparativity stable once it has been formed.

Relationship between the magnitude of melting ring and the elapsed time of its disappearance

After water conveyance has been stopped, the melting ring will decrease in magnitude and finally disappear. The shape and magnitude of the ring change with the pipe's position in the soil.

If the pipe diameter, the flow and the buried depth are small, the ground temperature is low and the frost depth is great, the melting ring will be small in magnitude. In this case, the shape of the ring is a ellipse and the soil below the ring is frozen. It is easy for the melting ring to disappear after stopping water conveyance, so that the pipe is easy to be frozen. For the pipes with greater flow and big diameter, the melting ring is usually in parabolic shape and connect with underlying unfrozen layer. In this case, the elapsed time of disappearance of the ring is comparatively long and it is not easy to be frozen for water in the pipe. The elapsed time mentioned above is generally affected by the ground temperature, buried depth of the pipe and thermal conductivity and moisture content of the soil. If the soil thermal conductivity, moisture content and ground temperature are about the same, the greater the magnitude of the ring, the longer the elapsed time of disappearing the ring.

TABLE I

Observed Data in the Test

Pipe diameter mm	Buried depth m	Flow m^3/h	Radius of melting ring (upper/lower) m	Time for the disappearance of the ring h	Mean air temp. °C	Ground temp. at the depth of the centre of pipe °C	Depth of frost penetration m	Mean air temp. °C	Ground temp. at the depth of the centre of pipe °C	Depth of frost penetration m
60x5	1.5	3.1	0.3/0.63	110	-11.3	-2.3	1.85	-8.5	-1.6	1.87
60x5	1.5	0.24	0.25/0.6	110.5	-8.0	-1.1	1.67	-16.5	-1.1	1.72
88.5x4	1.3	20	0.28/0.75	500	-11.3	-4.3	1.85	07.0	-1.8	1.92
88.5x4	1.3	0.32	0.2/0.65	127	-10.6	-2.8	1.65	-16.1	-2.7	1.7
88.5x4	1.3	0.17	0.2/0.5	192	-16.9	-2.4	1.74	-12.8	-2.3	1.79
114x4	1.0	3.25	0.28/0.55	174.5	-11.3	-5.4	1.85	-8.5	-3	1.89
114x4	1.0	0.23	0.2/0.3	48	-15.4	-5.3	1.53	-14.5	-5.3	1.55
114x4	1.0	0.33	0.2/0.3	38	-10.6	-4.7	1.65	-10.6	-4.5	1.66
114x4	1.0	0.19	0.15/0.27	253	-14.0	-4.0	1.69	-21.0	-4.9	1.77

Influencing factors of the forming of melting ring

The developing speed and magnitude of the melting ring are mainly determined by the ground temperature, water temperature, the flow and the soil property. In the conditions of constant buried depth and flow, the higher the ground and water temperature, the greater the melting ring. When

Comparison between observed data and calculated results

The comparision shows that the calculated results are in a good agreement with observed data. The formula used in the calculation is as follows:

$$t_2=(t_1-t_g)EXP(-K\pi DL/GC)+t_g \qquad (1)$$

where t_2—water temperature at the outlet (°C);

t_1—water temperature at the inlet (°C);

t_g—ground temperature at the depth of the depth of the centre of pipe (°C);

D—the pipe's outer diameter (m);

K—average coefficient of thermal conductivity of soils around the pipe (Kcal/m²h°C);

C—specific heat of water (Kcal/kg°C);

G—water flow in weight (kg/h);

L—pipe length (m).

Example 1. Taking D=0.0885 m, G=3000 kg/h, L=80 m, t=-3°C, t=9°C, C=1 and K=3 Kcal/m²h°C). Then, the calculated result is t=8.73°C.

The difference between this result and observed data is only 0.03°C. According to Eq.(1), if the pipe length is 2000 m and water temperature at inlet is 7°C, the water temperature at outlet will be 2.72°C. The heat reduced from friction is not considered here.

The cooling time (T) for water in the pipe from stopping supply to freezing can be estemated by

$$T = T_o + T_3 \qquad (2)$$

where $T_o=\frac{D^2}{\alpha}(x+\frac{y}{N_\mu})\ln\frac{h}{D}$, and

$$T_3=100\frac{(D_T^2-D^2)n}{-\lambda_2 t_g m}\ln\left(\frac{4h}{D_T+D}+\sqrt{(\frac{4h}{D_T+D})^2-1}\right)$$

in which,

$$D_T=EXP\left(\frac{\lambda_2 t_g \ln D-\lambda_1 t_1 \ln(4h)}{\lambda_2 t_g-\lambda_1 t_1}\right)$$

is the diameter of the melting ring (m),

$$N_\mu=\frac{aD}{\lambda_2}$$

α—the coefficient of thermometric conductivity of soil (m²/h);

h—buried depth of pipe centre (m), =6-15 Kcal/m²°C h;

λ_2—thermal conductivity of frozen soil;

λ_1—thermal conductivity of melting soil;

m—the depth of frost penetration (m);

n—the volumetic moisture content in volume of soil;

x,y—parameters determined with Fig.2, in which;

Δt_1—the difference between water temperature in beginning and ground temperature (°C) and

Δt_2—the difference between water temperature at last and ground temperature (°C).

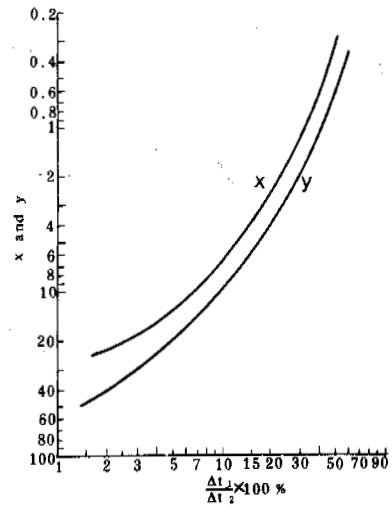

Fig.2 Determination of Parameters x and y

Example 2. Given the following data to calculate the sustained time of stopping water supply, T, on the assumption that the water temperature is allowed to be lowered to 0°C.

pipe diameter D=0.114 m,
Buried depth h=1 m,
Ground Temp. t_g=-4.3°C,
Moisture content of soil n=13%,
Specific gravity of soil=2.7,
Specific heat of soil c=0.6,
a=10 Kcal/m²°C h,
λ_2=2 Kcal/m²°C h, and
Water Temp. in beginning=8°C

With the equations shown above, it is calculated that

D_T = 0.9 (m)

T_o = 75.5(h), and T_3 = 52.5(h)

Thus, T = 128 (h).

CONCLUSIONS

Any water supply pipe that is in agreement with one of the following situations can be buried shallowly.

(i) The water supply pipe system is composed of many branchs;

(ii) The supply pipe system is netted but without dead water in any section of the system;

(iii) The diameter of industrial or civil water supply pipe is equal to or greater than 50 mm, the flow in it is greater than 0.1 m³/s, and the water supply will not cut off.

According to the test reults, 43 kilometers water supply pipe was constructed in Daqing Oil Field in 1983 with buried depth of 1 m. No frost damage has occured after three year's running. About 1000 kilometers water supply pipe has been buried shallowly in the soil field in recent years.

ROCK MECHANICS RELATED TO COAL MINING IN PERMAFROST ON SPITZBERGEN

A.M. Myrvang

The Norwegian Institute of Technology, NTH, 7034 Trondheim, Norway

SYNOPSIS This paper describes the results from rock mechanics investigations in permafrost in the Svea Mine, Spitzbergen. The investigations features in-situ measurements as well as laboratory testing, for the determination of the in-situ virgin stress, in-situ strength of coal, general mechanical properties of thawed and frozen coal and shale and deformational behaviour of the mine entries (tunnels) during actual mining.

INTRODUCTION

The Spitzbergen Islands (Svalbard) are situated approximately between 77° and 80°N. Thanks to favourable ocean currents the average temperature is higher than in comparable areas in the Arctic, but still the permafrost penetrates down to depths of approximately 300 m below surface. At present the Norwegian government owned company Store Norske Spitsbergen Kulkompani A/S (SNSK A/S) operates 3 coal mines on the island, but throughout the period from 1916, when SNSK A/S started its activities, the company has operated 8 mines. To date most of the mining operations have been in permafrost.

The design of the mining methods was traditionally based upon experience and/or trial and error approaches. In the late sixties the first rock mechanics investigations were carried out. From the late seventies quite extensive investigations have been initiated by the mine management, to get a better understanding of the mechanics associated with the coal mining. Rock mechanics programs have been carried out in the No. 3 mine, the No. 7 mine and the Svea Mine, with emphasis on the determination of in-put data for the design of the so-called room- and pillar system in the Svea Mine. This paper will concentrate on the results from the investigations in this mine.

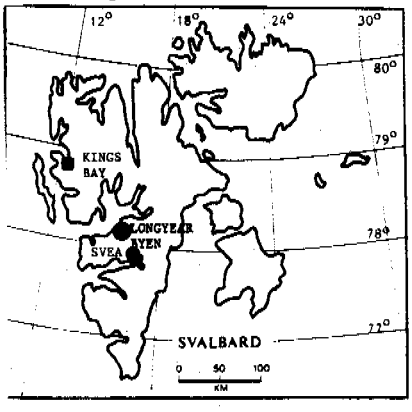

Fig.1 Location of Longyearbyen and Svea Mines on Spitzbergen

THE SVEA MINE

The Svea Mine is situated about 60 km SE of Longyearbyen, which is the "capital" of Svalbard and the location of the two other mines in operation (Fig. 1).

The Svea camp is served by a small commuter airplane from the main airport in Longyearbyen and also by snowmobiles during the winter season. Heavy equipment must preferably be brought in by ship during the shipping season, but to some extent equipment can be brought in by bulldozer sledges or helicopter.

As the other SNSK mines, the Svea Mine is also an adit mine situated in a valley side. The mining area is reached by a semi-horizontal adit (tunnel) from the valley side, and the coal seam itself is relatively flatlying. The coal seam is of tertiary age. The seam thickness is varying between approximately 2 m and 5 m. Major parts of the deposit contain intermediate bands of shale, which may have a thickness up to nearly 1 m. The roof is normally made up of fairly competent shales, while the floor in many cases consists of weak coal shale with bands of clay.

Fig. 2 gives a simplified cross section showing the lithology.

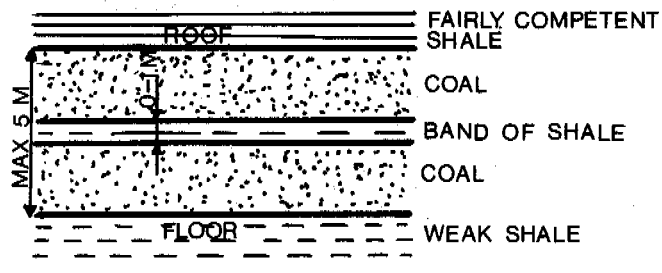

Fig.2 Simplified lithology

The variable conditions are not in favour of so called longwall mining (which is the major mining method in the No. 3 mine and No. 7 mine and in most European coal mines). It was therefore decided to develop a room- and pillar system as used in many U.S. coal mines. A room- and pillar system consists in principle of a number of panels or areas as indicated on Fig. 3.

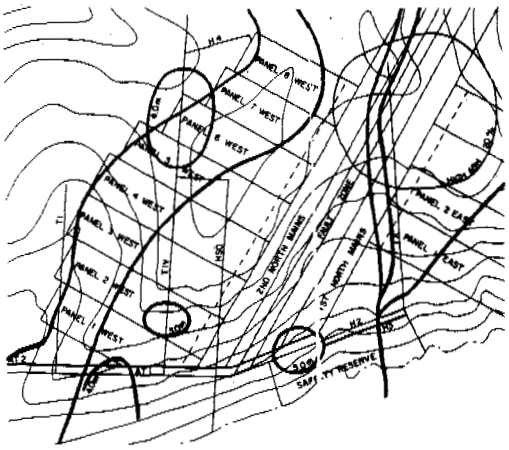

Fig.3 Panel lay-out

Each panel is first developed in a checkerboard pattern of rooms and pillars as shown on Fig. 4.

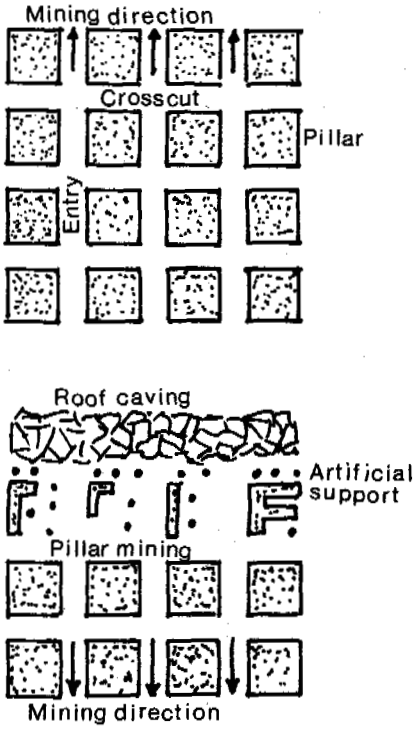

Fig.4 Simplified room-and-pillar mining

When a panel is developed, mining retreats while 40-70% of the pillars are removed. To manage this, it is essential that the roof of the mined out area caves gradually, Fig. 5.

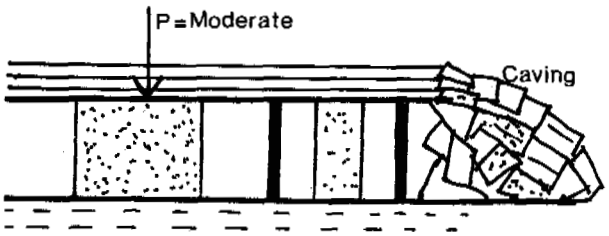

Fig.5 Simplified cross section showing successive, favourable caving

Successive, controlled caving of the roof will give moderately, increased load on the remaining pillars, allowing a major part of the coal in the pillars to be mined.

The geometry, the mechanical properties of the roof rocks and the in-situ stress conditions are important factors in this connection. Without caving of the roof, the remaining pillars will act as abutment for a "roof plate" which eventually can crush the pillars, or an uncontrolled, violent caving will occur when the span is large enough, Fig. 6.

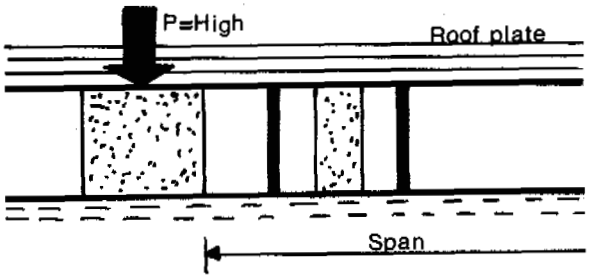

Fig.6 Situation without successive caving

During the first several years of mining the operations will be in permafrost. The average year-round temperature of the coal and surrounding rocks will be approximately -4°C. The intake ventilation air will always be above freezing temperature (artificially heated during the winter season). However, on its way to the mining panels the ventilations air will be cooled down, and in the mining panels the temperature will always remain below the freezing point as long as mining takes place in permafrost.

With increasing overburden the mining will eventually take place in thawed ground.

Rock mechanics data are vital in connection with the design of the room- and pillar lay-out. While the initial design was carried out by experienced American consultants; the necessary

rock mechanics data were provided by the Rock Mechanics Laboratory of the Mining Division, the Norwegian Institute of Technology (now part of SINTEF, Division of Rock and Mineral Engineering).

ROCK MECHANICS INVESTIGATIONS

Throughout the years 1978-87 investigations have been carried out during several periods. Both field and laboratory work has been included, featuring

- In-situ rock stress measurements.
- Sampling of material for laboratory investigations.
- Laboratory investigations including uniaxial and triaxial strength determination of coal and shale, determination of cohesion and friction angles and point load testing.
- In-situ mapping of joints and fractures.
- RQD (fracture index) determination of the roof rock based upon available diamond drill cores.
- Convergence measurements (change in roof to floor distance) during development of panels.

The Rock Mechanics Laboratory (RML) uses two methods for in-situ rock stress measurements, Fig. 7. In this case the two dimentional "doorstopper" method proved to be successful. The version used is developed by RML, and has been extensively used by RML for more than 20 years in a large number of mines and tunnels in Norway, Sweden, Finland, Spain and Greenland.

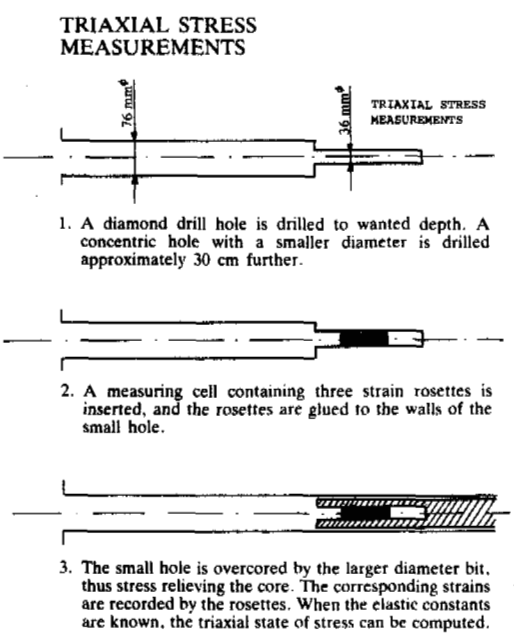

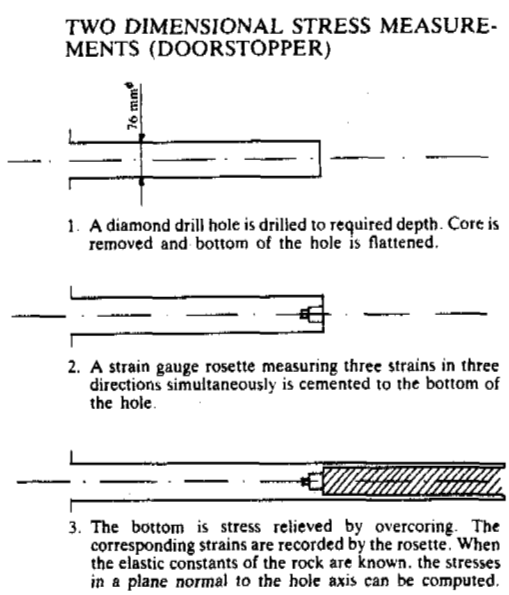

Fig.7 Rock stress measuring methods

To determine the in-situ stresses, measurements were carried out in the roof of entries at four different locations (Fig. 8). All measuring

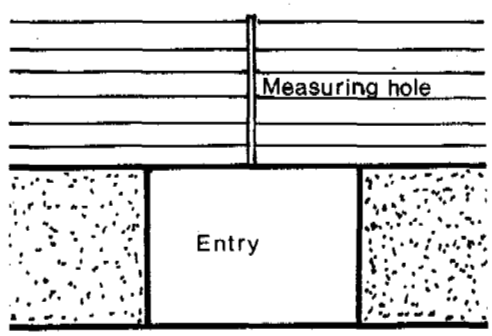

Fig.8 Measuring set-up

sites were in permafrost. No practical difficulties were encountered due to the permafrost. For the core drilling heated water was used to avoid freezing problems.

Assuming that the vertical stress is governed by the weight of the overburden (verified as the normal situation by numerous measurements throughout the world) the following stress pattern was determined:

- The vertical stress is in accordance with overburden i.e.

  $\sigma_v = \rho \cdot g \cdot h$

  where ρ = density $\simeq$ 2500 kg/m^3
  g = accelleration of gravity
  h = overburden

  By 300 m overburden $\sigma_v \simeq$ 7,5 MPa

- The measured maximum horizontal principal stress σ_{h1} is parallel to the mountain side and is equal to or slightly higher than the vertical stress. At the innermost measuring site σ_{h1} = 12 MPa.

- The measured minimum horizontal principal stress σ_{h2} is normal to the mountain side and is in the order of magnitude of the horizontal gravity induced horizontal stress given by

$$\sigma_h = \frac{\nu}{1 - \nu} \cdot \sigma_v$$

where ν = Poissons ratio

It is very important and interesting to note that even in these young tertiary rocks, there exist considerable "geological" stresses that superimpose the gravity stresses.

Considerable problems with so called floor heave and partly roof slabbing in some of the development entries are probably caused by high horizontal stresses normal to the axis of the entry combined with low strength of the rock, Fig. 9.

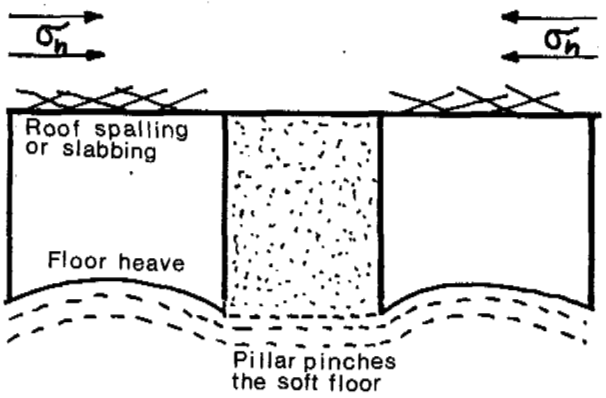

Fig.9 Floor heave and roof spalling

Floor heave is caused by buckling due to high horizontal stress or squeesing due to pillar penetration in the floor. The stiffer coal pillar pinches the soft floor causing the floor to heave. Roof spalling is shear failure due to high horizontal stress.

For the determination of in-situ strength of coal a test area pillar that showed quite heavy surface spalling and slabbing was selected. This indicates that the pillar stress is close to or over the in-situ strength of the coal. By taking stress measurements from the surface and into the pillar, the stress values will give an indication of the in-situ strength. Fig. 10 shows the measured stresses as a function of hole depth.

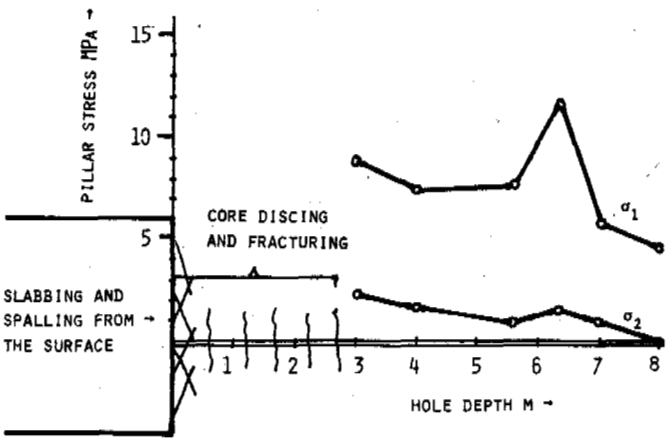

Fig.10 Measured stress as function of hole strength

The first successful measurement was taken at a hole depth of 3 m. Measurements at shallower depth were not possible due to core discing and fracturing. This indicates higher vertical stress near the surface of the pillar as would be expected, and that the stress here is close to the in-situ strength of the coal. The highest measured value is 11,6 MPa and for practical purposes it can now be assumed that the in-situ strength of the coal is close to that value. The laboratory determined uniaxial compressive strength is 16.3 MPa (se Table 1 on next page).

Sampling for laboratory testing has been extremely difficult, as both the coal and the shale disintegrates very easily. To obtain the best possible results, the laboratory testing should be carried out on frozen specimens, and the specimens should also be kept frozen all the time from the removal from the mine. The drill-cores were therefore kept in insolated polyuretan cases in the mine. Upon departure they were brought as hand baggage on the plane to Trondheim and immediately after arrival stored in a freezer with -4°C temperature. This proved to work out well, and the cores were still frozen upon arrival. The cores were then rapidly prepared (cut with a diamond saw) and again kept in the freezer until immediately before testing. Although this is not completely ideal, it is felt that the results are not very far from the real values. Table 1 shows the mechanical properties

of frozen coal and shale.

TABLE I Mechanical data for frozen coal and shale (based upon cores drilled out in the mine

Rock type	Youngs modulus GPa	Poissons ratio ν	Uniaxial compressive strength MPa
Coal	10,0	0,35	16,3
Shale ⊥ bedding	13,4	0,20	77,8
Shale ∥ bedding	17,0	0,20	86,4

Triaxial tests were carried out on thawed coal cored from blocks in the laboratory. The results are presented in Table II.

TABLE II Triaxial data for coal (thawed)

Failure stress σ_1 MPa	Confining stress σ_3 MPa
13,7	0
47,7	4,9
66,7	9,8
80,4	14,7

The uniaxial compressive strength is here 13,7 MPa vs. 16,3 MPa for frozen coal, indicating that the frozen coal is slightly stronger than the thawed coal. Fig. 11 shows the Mohr failure envelope for the coal. It will be noted that the envelope curve is not linear, which is the case for most rocks. For practical purposes in connection with pillar dimentioning the common Mohr-Coulomb failure criterion is often used assuming a straight line envelope curve.

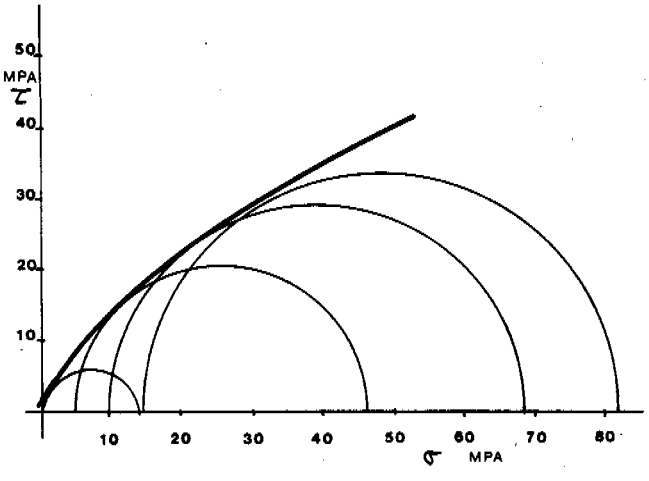

Fig.11 Mohr failure envelope for coal

A fitted straight line approach will give the following values for internal friction and cohesion:

- Internal friction angle $\Phi_i = 39,6^{\circ}$
- Cohesion $c = 4,5$ MPa

A general conclusion of the laboratory investigations is that the obtained values coicide well with values from coal fields other places in the world and that the permafrost as such does not seem to affect the material properties much.

The results from the in-situ measurements and laboratory tests have been used by the consultants as in-put data in empirically and computer based design of the room- and pillar systems. This resulted in 5 m wide entries and crosscuts, leaving 24 m x 24 m pillars.

A vital factor in the design is the ability of the roof rock to cave during pillar recovery. To get information about this several diamond drill holes were drilled 50-60 m vertically upwards in the roof, and the cores were mapped according to the so called RQD-system and also the Raith-Li-system.

The RQD (Rock Quality Designation) gives a measure of the fracturing of the rock mass, while the Raith-Li-system (developed mainly by the late professor Bjørn Li, Norwegian Institute of Technology) in addition also gives some indication of the strength of the rock mass. Both systems rate the rock in classes from "very bad" to "very good". In this case both methods in general indicated that the first 10-15 m of the roof was "bad". This in turn indicates that the caving ability of the roof is good.

Throughout the years from 1984 the development of the room- and pillar system has progressed. As mentioned earlier, considerable problems have been experienced with floor heave and sometimes also spalling from the roof. This is probably partly caused by high horizontal stresses. To map this more accurately, a convergence measuring program was started in late 1986.

EFFECT OF THAWING

The intake ventilation air to the mine is normally always above freezing point. During the winter season the air is artificially heated. The intake air is taken through the main adit. Throughout the years considerable stability problems have been experienced in the roof of the adit, as the roof shale gradually disintegrates. It is, however, not quite clear if this is due to thawing or a general effect due to exposure to air and/or humidity. It is known from other non-permafrost localities around the world that some sedimentary rocks tend to disintegrate when exposed to air and/or moisture. This is called slaking. In addition the effect of high horizontal stresses may also cause the roof to spall or disintegrate.

Normally, the roof was systematically rock bolted combined with steel net (Fig. 12a). In the main adit, the loosened chips of rock is collected by the net which would eventually bulge down by the weight as indicated on the figure. From time to time the net had to be opened to remove the debris. Because of this major parts of the adit is now supported by steel sets as indicated on Fig. 12b. Tests with shotcreate combined with rock bolts has proved to be quite successful (Fig. 12c). It seems that the thin layer of shotcreate seals the

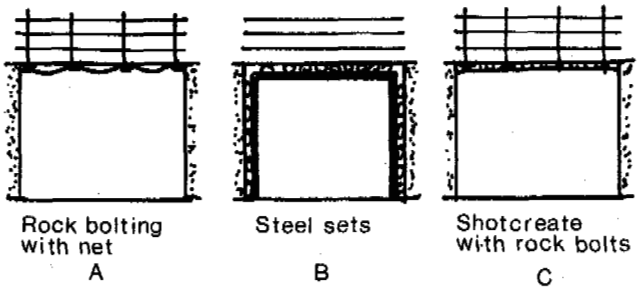

Fig.12 Different types of support used

rock from the influence of the air and a least delays the slaking process very considerably. This probably indicates that the deterioration is more an effect of air/moisture than thawing of the rock, as it must be assumed that the rock behind the thin shotcreate layer will also thaw eventually. In some areas exploration adits have been driven under the permafrost, and this has in many cases created quite serious water problems. Whereas "dykes" of ice with considerable thickness can be seen in the permafrost zone (and they normally not create problems), in the thawed zone the ice will inevitably be water with accompaning problems.

Traditionally, the entries and adits follow the fluctuations of the coal seam. The entries can therefore easily be flooded as indicated on Fig. 13. When the water reaches the permafrost it can eventually also freeze.

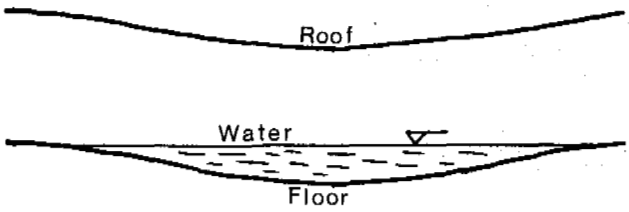

Fig.13 The entries follow the fluctuations of the coal seam

So both from an operational and a rock mechanics point of view, stable permafrost condition is seemingly to prefer versus thawed conditions.

Experiences from mining in crystalline rocks on Greenland also indicate that the stability and mechanical properties are noe much affected by the permafrost as such, but also here serious water problems have occured when going under the permafrost.

CONCLUSION

Rock mechanics investigations in permafrost in the Svea Mine indicate that the mechanical properties of coal and shale as such do not deviate much from those determined under non permafrost conditions other places in the world. The uniaxial compressive strength is probably slightly higher in permafrost than under thawed conditions.

Problems with deterioration of the roof in the main adit of the mine may or may not be due to thawing. Other factors like general influence from air and/or moisture and high horizontal in-situ stresses are probably as important. The major problem when mining takes place under the permafrost is water. From a practical and rock mechanics point of view stable permafrost conditions are therefore to prefer versus thawed conditions.

REFERENCES

Myrvang, A & Utsi, J (1987).
Evaluation of in-situ strength of coal from stress measurements in mine pillars. Proceedings 22.th Int.Conference of Safety in Mines. Beijing, China. Nov. 1987.

Myrvang, A (1983).
Report concerning rock mechanics investigation in the Svea Mine.
Report for SNSK A/S from the Rock Mechanics Laboratory, the Norwegian Institute of Technology. Trondheim, Norway.

Agapito, J F T (1983).
Room- and pillar plan for the Svea Mine.
Report for SNSK A/S from J F T Agapito & Associates Inc. Grand Junction, Colorado, USA.

SETTLEMENTS OF THE FOUNDATIONS ON SEASONALLY FREEZING SOILS

V.O. Orlov[1] and V.V. Fursov[2]

[1]All-Union Research Institute of Bases and Underground Structures, Moscow, USSR
[2]Tomsk Civil Engineering Institute, Tomsk, USSR

SYNOPSIS The development of vertical displacements of foundations to be built on seasonally freezing heaving soils are analyzed in this report. Results of long-term field tests with the use of shallow foundation-plates carried out in the Western Siberia are assumed as a basis for this study.

Till the present time it was not paid much attention to specific properties and to procedure of seasonally freezing soils testing, that is why problems of deformation development during thawing of seasonally freezing soils as well as sign-variable deformations occuring at long-term seasonal freezing and thawing of soils are studied unsufficiently. Solution to this problem was one of the aims of the investigations undertaken in Tomsk (Siberia) dealing with vertical displacements of shallow foundations which were carried out during the last 8 years on experimental sites with strongly heaved soils.

At experimental site the seasonally freezing layer consisted of quaternary loam deposits. The upper soil layer consisted of hardplastic and softplastic loams up to 1,2-1,5 m in thickness which were underlain by soils having the consistence ranging from softplastic to yield-plastic. The groundwater table was 1,8-2,8 m below the ground surface. On the whole the soils were represented by water-saturated soft silty loams.

In the tests there were used reinforced concrete foundation-plates of an area of 1 m^2 which transmitted pressure to the soil of 0; 0,1;0,2 and 0,3 MPa respectively. The foundation-plates were installed at a depth of 1,0 and 1,5m while the seasonal freeze and thaw norm depth was equal to 2,2 m. The side faces of the foundation-plates were isolated from the effect of tangent frost-heave forces, therefore during the tests the foundation-plates were displaced only as a result of seasonal freezing-thawing of soils beneath their underside level.

The analyse of testing results allowed to draw conclusions as to vertical displacements of the foundation-plates depending on the long-term seasonal freezing and thawing of soils and the pressure transmitted to them.

Unloaded foundation-plates (P=0) were heaved practically simultaneously with the beginning of soils freezing beneath their underside level and had the maximum displacements resulted from the effect of heaving soils deformations ($h_{fo}=h_f^{max}$). After thawing of soils they were descended to the initial position and their settlements were equal to their elevation at soils heaving ($S_o=h_{fo}$). Displacements of the loaded foundation-plates (h_{fo}) were less than the unloaded ones ($0<P<P_r$; $h_{fp}<h_{fo}$) where P and P_r are the pressures transmitted from the foundation-plate to the soil and the pressure of frost-heaving respectively. At thawing of base soils there were observed secondary settlements (S^∂), which were referred to as subsiding being equal to

$$S = S_o - H_{fp} \qquad (1)$$

Hence the total settlement of shallow foundation with consideration for deformations occured at seasonal freezing of soils during the past n -years may be determined according to the following equation:

$$S = S_p + \sum_{i=1}^{n} S_i^\partial \qquad (2)$$

where S_p - the stabilized settlement after loading of the foundation prior to the beginning of soil seasonal freezing, S_i^∂ - the secondary settlement to be a result of i - seasonal freeze-thaw cycle.

Figures 1 and 2 illustrate the development of vertical displacements of the foundation-plates and heave-measuring marks at different pressures on soil during the past 3 years of research.

At an increase of the load imposed on the foundation its displacements at the expence of frost heaving were increased at subsequent thawing. When the pressure at the foundation underside level became equal to the pressure of frost heaving, there was not observed the elevation of the foundation at freezing of soil beneath it. The settlements at thawing had maximum values ($P>P_r$; $h_{fp}=0$; $S^\partial = S_o$)

The maximum additional settlements were observed after the first seasonal freeze-thaw cycle. After the second cycle they accounted for 30-60% of the previous settlement and appeared to be reducing with time exhibiting a trend to be stopped at the expence of pro-

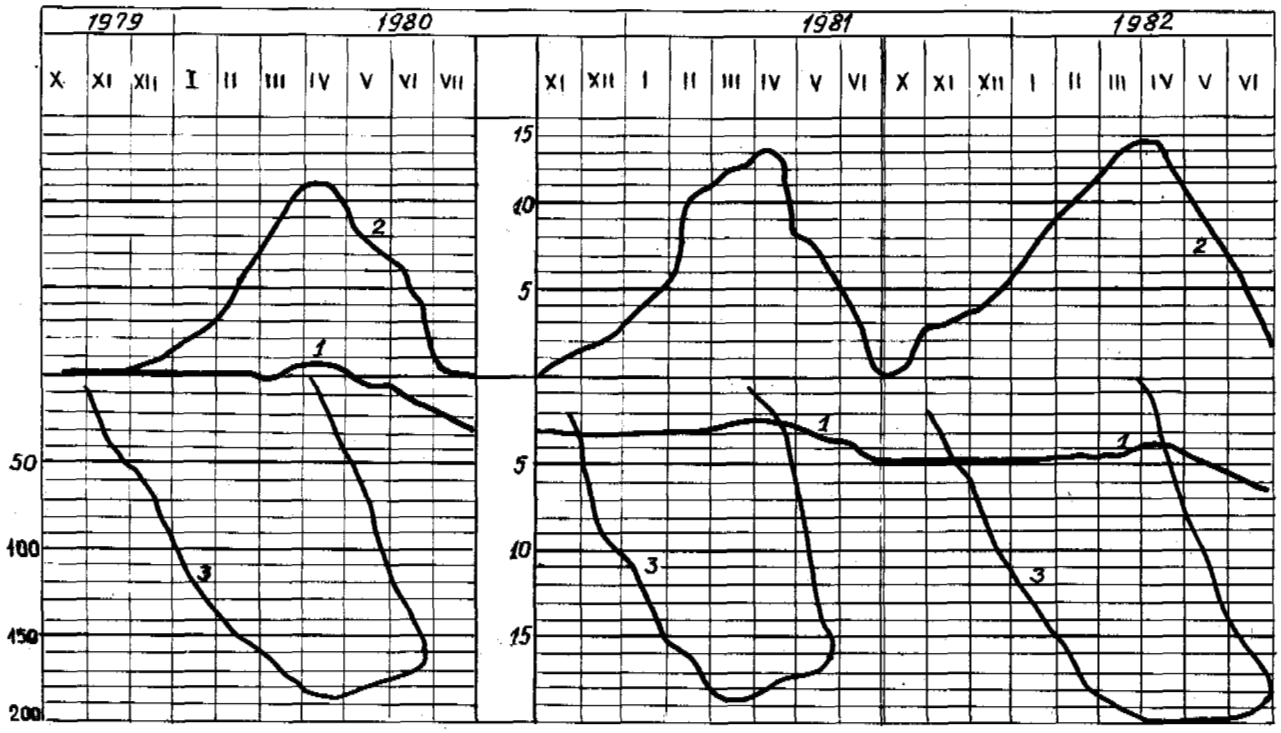

Fig.1 Vertical displacements of the foundation F_9 during freezing and thawing of soils
1 - foundation; 2 - surface mark; 3 - depth of seasonal freezing and thawing

gressive compaction and strengthening of the soil layer beneath the foundation underside level.

If to assume that koefficient (k_i) which characterizes the changes in secondary settlement at long-term cyclic freezing equals to

$$K_i = \frac{E_i^{\partial}}{E_1^{\partial}} \qquad (3)$$

then the experimentally determined relationship of this koefficient depending on number of cycles is expressed in terms of inverse function and is described by the following equation

$$K_i = \alpha + \beta \frac{1}{i} \qquad (4)$$

where E_1^{∂} and E_i^{∂} - the relative secondary settlements in the first and i - cycles respectively; α, β - the parameters depending on the consistence of soils; the pressure transmitted to the soils and the relative depth of the foundation deepening in the seasonal freezing layer.

Hence, the total secondary settlement (S_n^{∂}) resulting from the repeated seasonal freeze-thaw cycles for n -years may be determined from the equation

$$S_n^{\partial} = E_1^{\partial} (d_f - d) \left\{ n \cdot \alpha + \beta \left[C + \Psi_{(n+1)} \right] \right\}, \qquad (5)$$

where d_f and d - the depth of the seasonal freezing and the depth of the foundation deepening respectively; C - the Eiler-Maskerony constant; Ψ - the digamma function.

The results of comparison between calculated and experimentally determined values of secondary settlements of the foundation having 1,5 m in depth and exerting on base soils the pressure of 0,2 MPa during the seven-year test are illustrated by figure 2. The calculated values determined according to the above-mentioned procedure are accurate enough to be used in practice.

Laboratory investigations of soil deformations at freezing and thawing were carried out to ground the development of secondary settlements depending on the type of soil, pressure on the foundation-plate and the number of freeze cycles.

The work of shallow foundation was modelled in the refrigerator camera with the use of a heat-insulting chute made of acrylic plastic 500×500×700 mm in size. The dimensions of the foundation-plate model were determined on the assumption of geometric similarity to foundation model.

Linear scale of the model was 1:10, that corresponded to the area of square-shaped plate equaled to 100 sm^2. The tests were conducted on undisturbed samples of soil blocks and artificially prepared soil-bases at designed composition, moisture content and density.

Testing procedure was assumed to have in principle an analogy to field experiments and incorporated static test with consequent repeated cyclic freezing and thawing under pressure.

The tests conducted in the chute on different

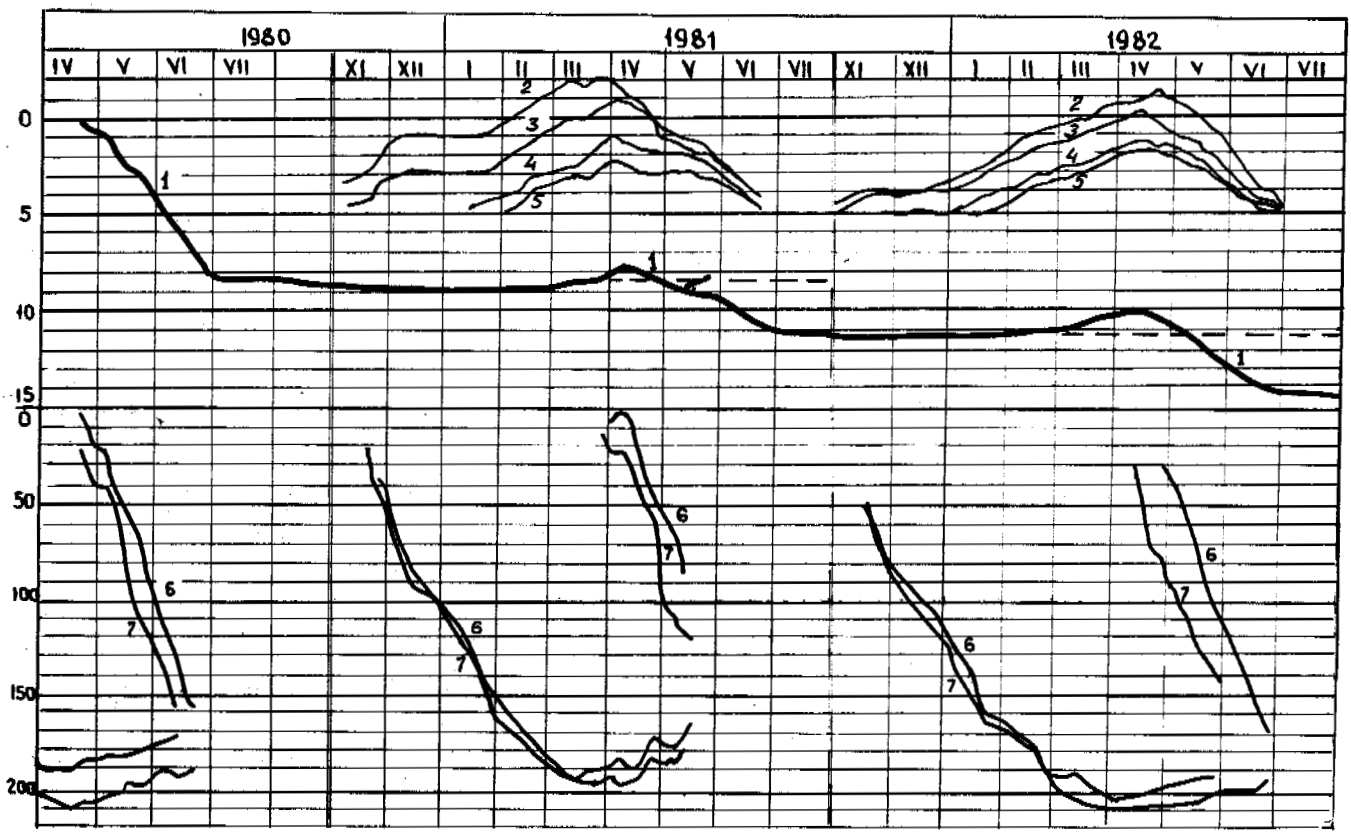

Fig.2 Vertical displacements of the foundation F_{10} (P=0,3 MPa, d = 1,5 m) and marks during freezing and thawing of soils.

1 - foundation; 2,3,4,5 - marks at points 0; 0,5; 1,0; 1,5; 6,7 - depth of seasonal freezing and thawing of soils on north and south sides of the foundation

types of soil showed that the greatest secondary settlements of plates were observed for loam bases and at the increase of moisture content of loam bases the secondary settlements grew at faster rate than frost heaving. Deformations of sand bases were mimimum and deformations of sandy loam bases were at the intermediate level between deformations of sand and loam bases. Tests data based on repeated freeze-thaw (up to 53 cycles) confirmed the results of 8-year field experiments that the maximum rate of secondary settlements occured after the first cycles and then appeared to be reducing with time and exhibited a trend to be stopped. The layer of compacted soil with small moisture content and improved mechanical characteristics is gradually being formed beneath the underside level of the foundation model.

The tests on compression with undisturbed samples of loams and sandy loams of basic regional types (59tests) conducted at repeated freezing- thawing under load in special oedometers made of acrylic plastic allowed to determine the calculated values of their additional compressibility at thawing. The relationships between a change in secondary settlements and a number of freeze-thaw cycles determined through the chute and compression tests correlate with the results of field experiments and are described by the equation (4)

Figure 4, for example, shows a graph of compression tests of silty loam (ρ_d = 1,57 g/sm^3, w = 0,22; w_L = 0,32; w_p = 0,18; S_r = 0,81) which was subjected to 8 freeze-thaw cycles under a pressure of 0,3 MPa. The relationships between relative values of deformations of silty loam and a number of freeze-thaw cycles is shown at figure 5. The relative frost heaving was ranging from 0,005 to 0,01 during the first four cycles of freezing as a result of soil compaction after thawing and an increase in its moisture content. The values of approximately 0,08 were observed during further freeze cycles. At the first thawing the relative secondary settlement had the maximum value E_1 = 0,024. At further thaw cycles the relative settlement was reduced significantly and had values ranging from 0,006 to 0,001.

The freeze-thaw process accompanied by transformation of structure and texture of silty-clayey soils leads to modification of their physical-mechanical properties as compared with the initial ones till freezing. At thawing it is observed the reduced values of strength, an increase in compressibility and acceleration of consolidation due to an increase in seepage capacity of soils as well as a change in water tightness of soil aggre-

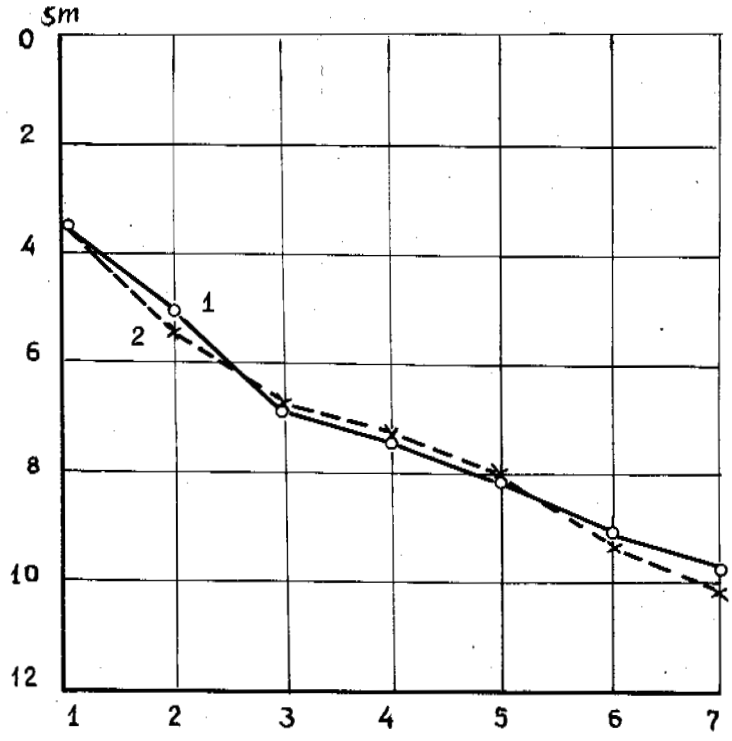

Fig.3 Relation between secondary settlement (sm) and number of cycles at long-term seasonal freezing and thawing in a base of the foundation F_9 (d = 1,5m, P = 0,2 MPa)
1 - experimental values; 2 - calculated values determined according to the formula (5)

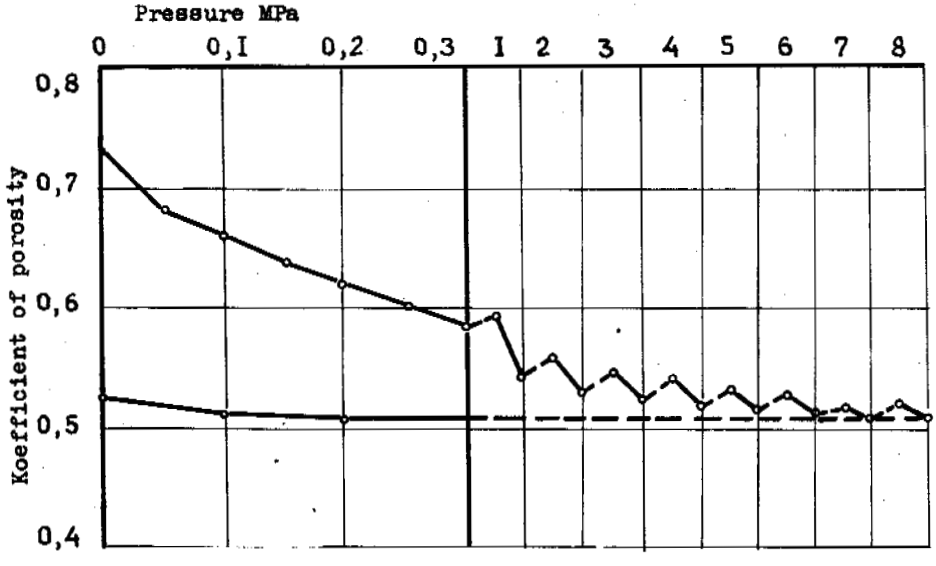

Fig.4 Freeze-thaw cycles

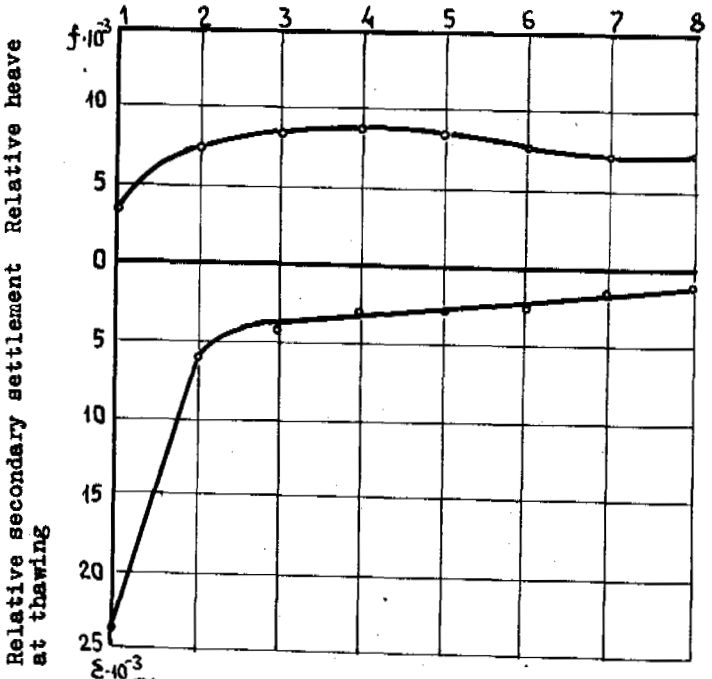

Fig.5 Compression tests of loams under load at repeated freezing-thawing

gates.
The above conclusions allow to make an approach to the problem of utilization of seasonally frozen soil layer as a natural base of shallow foundations on the basis of their calculations on deformations.

CONCLUSIONS

1. It is determined experimentally that a rate and amount of settlements of soils in bed of shallow foundations at seasonal thawing may considerably surpass the foregoing deformations caused by frost heaving of soils.
2. The settlements during thawing of seasonally freezing soil bases depend on the load transmitted by foundations and increase with the load increase.
3. The vertical displacements of shallow foundations in the process of long-term seasonal freezing and thawing of soils are developed due to an increase in total amount of secondary settlement for each year.
4. The greatest secondary settlements are observed after the first freeze-thaw cycle of soil under a load; after the second freeze-thaw cycle they are reduced by 2-3 times. In the course of long-term freeze-thaw cycles the settlement of the foundation exhibits a trend to be stopped due to the progressive compaction of soils beneath the foundation underside level.
5. The relationship of change in the amount of secondary settlement is expressed by an inverse function of the number of freeze-thaw cycles.

REGULARITIES OF THERMAL AND MECHANICAL INTERACTION BETWEEN CULVERTS AND EMBANKMENTS

N.A. Peretrukhin[1] and A.A. Topekha[2]

[1]TsNIIS Mintransstroy, Moscow, USSR
[2]Institute of Railway Eng., Khabarovsk, USSR

SYNOPSIS Data on railway embankment and track deformations in the limits of culverts under embankments location sites, as well as a regular relation of the deformations mentioned with seasonal vertical alternating displacements of the culvert sections, are presented in this report. Regularities of thermal and mechanical interaction between culverts and frostsusceptible soils surrounding sections and foundations of culverts, revealed on the basis of long-term investigations field conditions and theoretical generalization of measurement results of constructions deformations and soils temperature, are set forth. There are also some suggestions concerning the design of culverts and embankments within road sections located at frostsusceptible soils.

INTRODUCTION

The information concerning high deformability of railway track and highway bed in the zones of culverts locations in permafrost and deep frost penetration regions have been adduced in a number of publications (Jumickis,1973; Liverovsky,1941; Novozhilov,1963; Peckover,1978). However, there are no sufficiently substantiated data on causes and appropriate methods for prevention of deformations. In connection with activizing of road construction in northern regions, the provision of railway track and highway bed eveness in the zones of culverts locations have become an urgent necessity. Therefore special investigations of deformability and thermal regime of railway bed and culverts during freezing-thawing of soils, surrounding culverts and their foudations,have been carried out (Peretrukhin, 1967, 1982, 1983).

INITIAL CONDITIONS

Sections of various depth embankments with culverts in bounds of a railway, located in the regions of continuous permafrost, have been selected as objects for investigations (Peretrukhin, 1983, 1984).
Embankments near culverts at these sections have been constructed of frostsusceptible soils, namely loams and gravel sands with sandy loam, layers of which alternate at some sections. The fill depth above the culverts varies from 1.3 to 4.8 m. Soils of active layer are peats of 0.5 thickness, underlied in most cases by alternating layers of loam, sandy loams, as well as pebble with gravel and sand, often saturated with peat. Soils of active layer and embankment, with the exception of low-moist sands, used for upper part of some embankments, belong to the frostsusceptible ones by their composition and moisture. Bedrocks presented by sandstones and sandy clay-shales, lie under 3-4 m depth. There are six culverts within the embankment sections selected, including two rectangular culverts with apertures of 1.25 and 1.5 m, two ovoid culverts of 2 and 2.5 m and two circular ones of 1.5 and 2 m. All culverts have been constructed in 1948-1954 period. The foundation base of culverts sections and headwalls had been embedded into permafrost at the depth of 2-4.2 m from the earth surface. However, during investigations, the permafrost surface was at/or lower the foundation base level.

INVESTIGATIONS TECHNIQUE

Vertical displacements of the track, subgrade and culverts elements have been measured by means of technical levelling of marks located on the rail head and embankment shoulder above culvert, on both sides of the latter at 2, 4, 6,8,20-30 m distance from its axis, as well as on each section ends and heads of culvert. Bench marks made up of metallic rods and located beyond the embankment limits, were embedded into permafrost at the depth of 2-2.5 times greater than a local active layer thickness. A part of the bench mark roads within the active layer was enclosed into a vinil chloride tube and a space between the rod and tube walls was filled with a cup grease.
To measure the temperature near culverts 40 cased holes of 0.7 to 7.7 m depth were bored and by electric copper resistance thermometer sets equipped (Fig.1). Thermometers were located along the height with 0.2 up to 1 m intervals. More than half of all the holes were located at the rectangular reinforced concrete culvert with 1.5 m aperture. Here holes are located along the culvert axis and three lines parallel to the track and situated at the shoulder, the embankment slope and the slope base. The holes near the rest of culverts were located only at points which are significant by the thermal regime. Electrical resistance of thermometers was measured by a direct-current bridge. Measurements error, transfered in the temperature, amounted to $\pm 0.2^{\circ}C$.

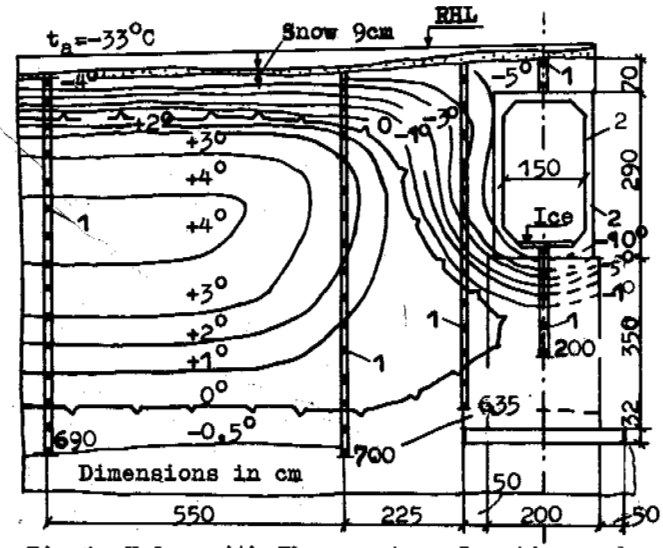

Fig.1. Holes with Thermometers Location and temperature Field within a Zone of 1.5 m aperture Culvert on Datum of 27 Nov Measurements: 1- Termometers, 2- Culvert

Measurements were conducted monthly during the period changing from one winter season to four years.

VERTICAL DISPLACEMENTS

The rail track, the embankment upper part above the culverts and all sections of the latter were deforming during the whole observation period: i.e. they rose in the time of soil freezing and subsided just as soil thawing. Under these conditions, in winter there appeared humps on the subgrade surface above culverts resulting in formation of track longitudal gradients, the algebraic difference of which above culverts ran up to 0.001–0.012 within adjacent 4–5 m long track sections. Accoding to current standards such distortion of the track profile is considered as an inadmissable one even for a train speed up to 50 km/h.

At the beginning of a winter period (October-November), before a culvert section rising start, the main cause of humps occurence on the embankment surface and a corresponding distortion of the track longitudinal profile above the culverts is different value of frost heaving of embankment soils above culvert and at some distance from the latter. Such difference is conditioned by simultaneous soil freezing above the culvert, from the embankment surface and from the culvert opening. As can be seen at Fig.2, during that period the embankment surface rise above culvert is more intensive (curve 1), than that at the distance of 30 m from the culvert axis (curve 2). After complete soil freezing above the culvert (December-January) the rise of embankment surface and accordingly railway track not ceased but lasted up to April (see Fig.2).Taking into account the approximate equality of rise values of both, embankment surface above the culvert and sections of the latter (curve 3), one can come to a conclusion that the humps occurence on the track at that period is conditioned by the culvert sections rise. During the winter period values of the sections rise of the rectangular culverts, located under 3.6 and 4 m high embankments, constituted from 63 to 77 % of the humps total height on embankment surface above culverts, i.e. the main part of the humps height.

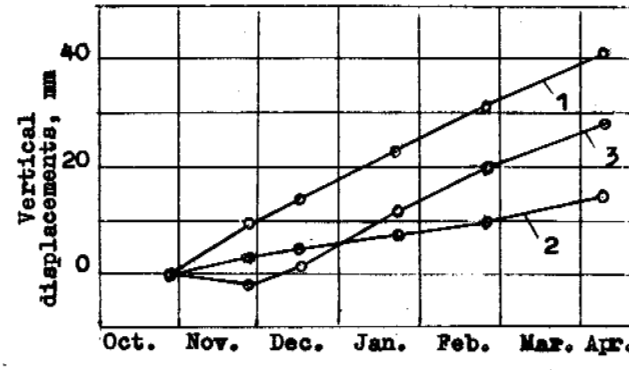

Fig.2. Rise of embankment Surface and Section of 1.25 m apertues Culvert: 1- Fill above Culvert, 2- Embankment at Distance of 30 m from Culvert, 3- Culvert section

Besides seasonal displacements, from year to year, residual unevennesses above all the culvert under investigation accumulated. Thus, there, for the two years, the hump height increased by 47 mm above an one of culverts. As a consequence of this the worst difference of local gradients of the track longitudinal profile above the culverts appeared at the end of the soil freezing period, when residual humps were increasing due to seasonal humps occurence. There were no humps on the track surface above a culvert, located under 8 m high embankment. According to the data obtained by other investigators (Liverovsky,1941) humps above culverts, stipulated by irregular freezing of embankment soils, not emerge, if the embankment height is equal or higher 5 m and the fill thickness above the culvert is more then 2.3 m.

THERMAL REGIME

Analysis of temperature measurement results allowed to reveal that soil,surrounding culvert, begins to freeze earlier and freezes more intensively, as compared with that of the embankment body beyond limits of the culvert thermal influence zone.

Thus temperature field, plotted according to measurement data on November 27 (see Fig.1), shows that freezing depth of soil around the rectangular reinforced concrete culvert is about 1.5–2 times more as compared to that of in the embankment body beyond the limits of the culvert thermal influence zone. Results of analysis of temperature fields in soils surrounding culverts, located under up to 5 m high embankments, allow to distinguish conditionally three stages of growth of a seasonally frozen soil halo around the culvert section. The first stage (Fig. 3,a) is characterized by the presence of initial freezing and heaving soil layers 1 around the culvert and at the embankment surface. It begins at a moment when the negative daily average air temperature becomes steady. The stage duration depends on the thickness of the fill layer over the culvert :

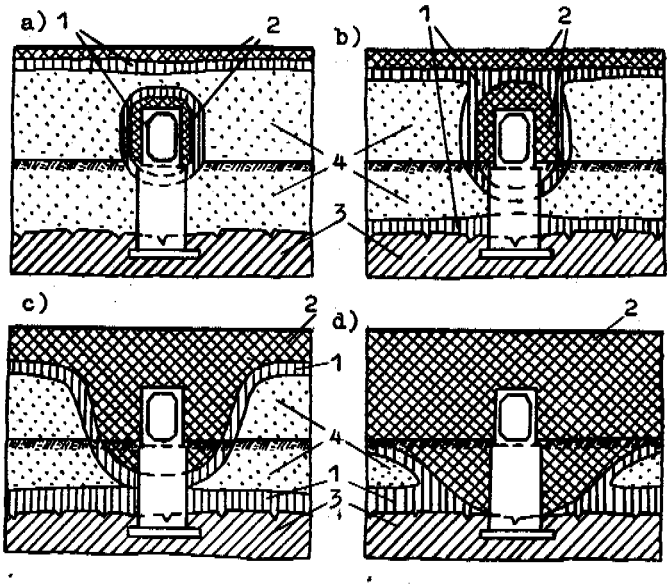

Fig.3. Freezing Stages of Soil around Culvert Sections: a- Stage 1, b- Start of Stage 2, c- Start of Stage 3, d- Finish of Stage 3: 1- Soil in initial Stage of freezing-heaving, 2- hard-frozen Soil, 3- Permafrost, 4- thawed Soil

it was equal to several days when thickness being 50-60 cm and to 2-3 decades for 1,5 m thickness. In the latter case there appears a hard-frozen soil layer 2 at cooling surfaces, thickness of whoch increases with time.
The first stage ends by the moment of closing of the two seasonal frozen ground layers, occured due to freezing of the fill from two sides, namely the embankment surface and the culvert orifice. After that moment the second freezing stage begins (Fig. 3,b) and further freezing of frozen soil continues up to reaching hardfrozen state. Besides, formation of a seasonally frozen soil layer from the underlying permafrost surface 3 takes place. The moment of that layer merging with seasonal frozen ground, generated from culvert orifice side, distinguishes the second stage completion (Fig. 3,c). By that time, soil near the middle part of the culvert foundation height is at initial freezing stage 1 and its temterature is higher than minus 2°C, while soil around culvert sections and the foundation top, being in a hard frozen state 2, has the temperature of minus 2°C and lower. Soil 4, beyond the culvert influence zone, is still in a thawed state. At this stage the freezing boundary is of a curved shape.
The third freezig stage is characterized by further cooling and thickness increasing of hard-frozen soil massif surrounding the culvert. By the end of this stage the process of soil freezing from the culvert orifice side finishes. Around the culvert a solid massif of seasonally frozen soil and permafrost forms, while beyond culvert thermal influence zone limits a layer of thawed soil can be remain (Fig. 3,d).

MECHANICAL INTERACTION

Frostsusceptible soil, freezing around the culvert, exerts a force influence on surface of the latter. A schematic notion on this influence one can imagine on the basis of the known regularities (Peretrukhin, 1967), taking into account analysed above freezing regime peculiarities of soils, surrounding the culvert. During the first stage of soil freezing (see Fig. 3,a) regelation of soil with lateral and upper culvert surfaces takes place (Fig. 4), whereas soil negative temperature dropping, the regelation strength increases.

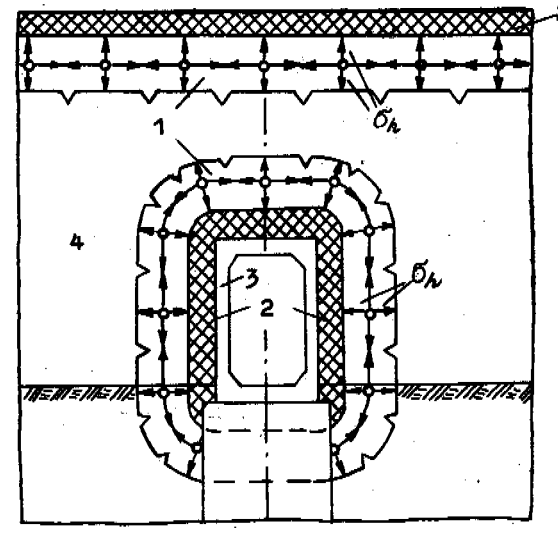

Fig.4. Scheme of heaving Forces acting within "freezing heaving Soil-Culvert Section" System during freezing Stage 1: 1- soil Layer in initial freezing-heaving Stage, 2- hard-frozen Soil, 3- Culvert Section, 4- Thawed Soil

Besides, there takes place a compression of culvert sections 3, as well as thawed soil layers 4, as a consequence of heaving force effect σ_h, i.e. internal stresses, generated in the soil layers 1 freezing around the culvert section and acting in the same direction as that of a thermal flow. The heaving force σ_h simultaneously generated in the soil layer 1, freezing from the embankment surface, causes rising of the overlaying hard-frozen soil layer 2 and compresion of underlaying thawed one 4. In the second stage of freezing (Fig. 3,b,c) the heaving force, generated in the layer of initial freezing-heaving 1 (Fig.5) is directed normally to an interface of this layer with the hard-frozen soil massif 2, but at an acute angle to the section lateral face3 and the foundation upper part 4 (see Fig. 5). Under such conditions the total heaving force may be decomposed into horizontal and vertical components. The horizontal one stipulates a lateral squeeze of the culvert sections and foundation, and increases contact ties of the regelation between hard-frozen soil and culvert, while the vertical one contributes to soil and culvert rise. Calculation results showed that for most of the standard culverts the total strength of soil regelation with the

culvert section surface exceeds the culvert weight. That's why the hard-frozen soil massif, surrounding culvert section, can rise only together with in-frozen culvert section. During the third freezing stage (Fig.3,d) the interface of hard and thawed soils within the thermal influence zone of culvert decreases, while the thickness of hard-frozen soil massif increases.

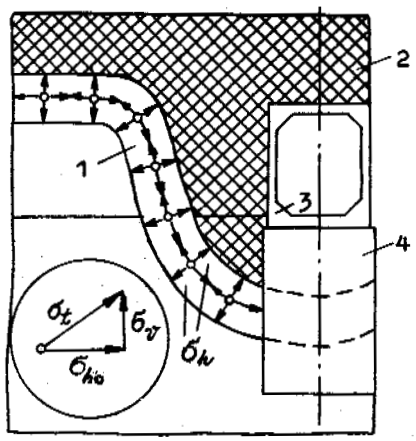

Fig.5. Scheme of heaving Forces acting within "freezing heaving Soil-culvert Section" System during freezing Stage 2: 1- soil Layer in initial freezing-heaving Stage, 2- hard-frozen Soil, 3- Culvert Section, 4- Foundation

So, the probability of hard-frozen soil rise together with culvert section decreases. In the light of the stated analysis the second stage of soil freezing around the culvert (Fig.3,c) should be considere as a basic one. Conditions, existing during that stage, should be taken as design ones (Fig. 5) when culverts standard structure developing and antiheaving measures selecting, as well as when determining culvert stability in case of heaving force effect, taking into account local natural conditions.
Peculiarities of thermal conditions of soils, surrounding road culverts, exclude the possibility of hard-frozen soil layers upward moving relatively to culvert sections. Therefore, the standard method for calculation of the construction foundation stability under the effect of heaving forces (SNiP, 1977) can't be used for road culverts stability estimation.

CONCLUSION

In the case of heaving soils utilization as a material or base for up to 5 m height road embankments, a special consideration should be given to the selection of culvert and embankment structures, taking into account peculiarities of their thermal and mechanical interaction. Standard culverts being used, antiheaving measures should be taken to reduce up to standard values or eliminate the probability of railway track or highway pawement unevenness occurence.
It is expedient to consider the use of thermal insulation within the zone of embankment and culvert contact as one of such measures. Consideration of versions of non-standard water-pass constructions, not affecting negatively on road embankments during the freezing-thawing process of frostsusceptible soils used, is a suggestive course as well.

REFERENCES

1. Jumikis A.R.(1973) The soil-culvert-temperature system upon freezing. Symposium on Frost Action on Roads. Report 1. Organization for Economic Cooperation and Development, Paris, pp. 235-248.

2. Liverovsky A.V., Morozov K.D.(1941) Stroitelstvo v uslovijakh vechnoy merzloty, Leningrad-Moskva, Stroyizdat.

3. Novozhilov G.F.(1963) Puchenie zemljanogo polotna na podkhodakh k iskusstvennym sooruzhenijam (Stroiteljstvo zheleznykh dorog):Sbornik Trudov, LIIZHT, Leningrad, Vypusk 203, ss.21-30.

4. Peckover F.L.(1978) Frostheaving of track-causes and cures. Bull.Amer.Railway Eng.Assoc., 79, N 666, pp.143-173.

5. Peretrukhin N.A.(1967) Vzaimodeistvie fundamentov s promerzajuschim puchinistym gruntom, v Sbornike Moroznoe puchenie gruntov i sposoby zaschity sooruzhenij ot ego vozdejstvija: Trudy TsNIIS, Vypusk 62, ss.74-99.

6. Peretrukhin N.A., Topekha A.A.(1982) O nerovnostjakh prodolnogo profilja zheleznodorozhnogo puti nad vodopropusknymi trubami. Transportnoe stroitelstvo, N 8, ss.7-8.

7. Peretrukhin N.A., Topekha A.A.(1983)Osobennosti teplovogo rezhima gruntov, okruzhajuscikh dorozhnye vodopropusknye truby. Transportnoe stroitelstvo, N 2, ss.8-9.

8. SNiP II-18-76 (1977) Chast II. Gl.18. Osnovanija i fundamenty na vechnomerzlykh gruntakh. Moskva, Stroyisdat.

METHODS OF QUANTITATIVE VALUATION OF REGIONAL HEAT RESOURCES FOR PREPARATION OF PERMAFROST PLACER DEPOSITS TO MINING

G.Z. Perlshtein and V.E. Kapranov

All-Union Scientific Research Institute of Gold and Rare Metals, Magadan, USSR

SYNOPSIS According to modern notions there are regional and microclimatic factors of heat exchange between rock surface and atmosphere. In the report it is offered to use three parameters for quantitative valuation of regional resourses of atmosphere heat: density of heat flow to the exposed surface of frozen ground, temperature of wet thermometer, and moist surface temperature. With the help of the data offered in the report the estimation is given to the natural heat resourses of some permafrost regions and the possibility of their use for water heat reclamation is considered.

Methods of thawing based on using solar radiation, atmosphere, and surface waters have got wide distribution in practice of permafrost placer deposits exploitation in the USSR and NorthAmerica. As a rule, the employment of every possible type of fuel and power installations turns out to be inexpedient because of high heat loss when conversing frozen rock into thawed state (20-60 $kW \cdot h \cdot m^{-3}$). The problems of efficiency and economy of thawing is especially acute for placer deposits of Siberia and the North-East of the USSR where preparation of some frozen grounds to excavation is being carried out in very large scales and influences decisively on the prime cost of mineral output. In connection with this the importance of workingout some reliable criteria allowing to value natural heat resourses of this or that region most completely from the point of view of permafrost thawing is evident. In Soviet literature similar valuations were made till recently by the sum of positive degrees-hours of air temperature drawing sometimes the data of radiation balance (Metodika...,1979). Besides, such important climatic factors as wind velocity, air moisture etc. were not taken into account. As for the temperature of surface waters it changes sharply depending on dimensions and local perculiarities of water course feed; therefore its use as a regional characteristic is not competent.

To our mind all the pointed drawbacks may be eliminated on the base of modern ideas about the dependence of temperature regime of different types of surfaces on outward heat exchange conditions (Kourtener, Chudnovskii, 1969; Pavlov, 1975; Perlshtein, 1979). In reference to the problem of radiation thawing (by Pavlov and Olovin) this question is thoroughly considered in works by Balobajev (1963), Lukjanov and Golovko (1957), Pavlov and Olovin (1974), Perlshtein (1979). Following them let's express the density of a heat flow (q, $W \cdot m^{-2}$) to a rock surface from the classic equation of radiation-heat balance:

$$q = Q_t(1-A) + I_a - I_s - H_c - M, \qquad (1)$$

where Q_t is total shortwave radiation; A is the surface albedo in shares of unit; I_a, I_s is longwave radiation of atmosphere and rock surface, respectively; H_c is the intensity of convective heat exchange with atmosphere; M is the heat loss for evaporation from the surface.

Using the linear approximation of surface temperature functions entering the known physical laws (radiation, cooling, and evaporation) let's express the values I_s, H_c and M by the following dependences:

$$I_s = \delta\sigma(T+273)^4 \approx I_0 + \alpha_r T, \qquad (2)$$

$$H_c = \alpha_h (T - T_a), \qquad (3)$$

$$M = \alpha_e [e_s(T) - e_a] \approx \alpha_e (e_0 + \beta T - e_a), \qquad (4)$$

where σ is Stephan-Boltsmann's constant, $W \cdot m^{-2} \cdot (°C)^{-4}$; δ is a relative radiating capacity of the surface in most cases approximated to 0.9; I_0 is the heat radiation of the surface at 0°C, ~ 288 $W \cdot m^{-2}$; α_h is the coefficient of convective heat exchange, $W \cdot m^{-2} \cdot (°C)^{-1}$; T_a is the temperature of air, °C; α_e is the coefficient of evaporation (condensation), $W \cdot m^{-2} \cdot Pa^{-1}$; $e_s(T)$ and e_0 is the pressure of saturating vapour at T temperature and 0°C, respectively, Pa; e_a is the pressure of water vapour in air, Pa; α_r is the coefficient of linear approximation of power radiation law, 4.6-4.8 $W \cdot m^{-2} (°C)^{-1}$; β is the analogous coefficient of the pressure dependence of saturating vapour on temperature, ~70 $Pa \cdot (°C)^{-1}$.

Taking into account expressions (2)-(4) let's express equation (1) as:

$$q = Q_t(1-A) + I_a - I_0 + \alpha_h T_a + \alpha_e (e_a - e_0) - \alpha T, \qquad (5)$$

where $\alpha = \alpha_h + b\alpha_e + \alpha_r$.

It is to be noted that the α_e/α_h ratio is constant ($1.56 \cdot 10^{-2} \cdot °C \cdot Pa^{-1}$). The α_h values depend on the wind velocity and may be expressed with a satisfactory approximation by the formula:

$$\alpha_h = \begin{cases} 6.16 + 4.19V & 0 < V < 5 \\ 7.56V^{0.78} & 5 < V < 30 \end{cases} \qquad (6)$$

where V is the wind velocity, $m \cdot s^{-1}$; the dimension of α_h is expressed in $W \cdot m^{-1} \cdot (°C)^{-1}$.

On exposing frosen rocks in warm period their surface gets the ice melting temperatures (0°C) nearly instantly. As follows from expression (5) the density of heat flow (q_o) from atmosphere is maximum at this moment and equal to:

$$q_o = Q_t(1-A) + I_a + I_o + \alpha_h T_a + \alpha_e(e_a - e_o). \qquad (7)$$

The right part of equation (7) includes the values depending on the regional perculiarities of climate ($Q_t, I_a, I_o, e_a, \alpha_h, \alpha_e$), and also on the physical constants (I_o, e_o). The exposed surface albedo of dispersed frozen rocks may also be considered as the constant approximating to 0.1. Thus, q_o is a regional characteristic taking into account all main sourses of natural energy which take part in forming heat flow to permafrost surface immediately after the thawed layer is removed. This value most fully characterises the heat potential of a region in relation to radiation thawing. All necessary data for its calculation may be found in climatic reference books.* It should be noted that in natural conditions the density of heat flow into thawing rocks during summer does not exceed 4-6 per cent of Q_t on an average. Unlike it, q_o value is, as a rule, 2-2.5 times more than Q_t . In connection with this the mistake of q_o calculation has a similar order with errors of definition of such quantities as Q_t , H_c etc. Table 1 gives the q_o values for three different regions of permafrost according to the average monthly data.

As one can see from the table, q_o varies widely reaching rather high values in the periods of maximum. It's enough to say that every square kilometer of exposed surfaces of frozen rocks in the upper Kolyma and Indigirka in July is influenced by the natural heat sourse equivalent in power to the Kolymskaya hydroelectric power station. If calculate q_o according to the data of fixed-term observations, one may be assured that the dayly course of q_o is close to a sine-shaped one. Between the midday and 3o'clock in the afternoon these values are 1.2-2.0 times higher than the average daily ones.

* Longwave radiation of atmosphere I_a is not measured directly at weather stations and may be calculated by the formula:

$$I_a = Q_r + \delta\sigma(T+273)^4 - Q_t(1-A),$$

in which the radiation balance Q_r and the rest measured values (Q_t, A, T) should relate to the same observation point.

TABLE 1

Heat Flow Density (q_o, $W \cdot m^{-2}$) of Solar Radiation and Atmosphere to the Exposed Surface of Frozen Rocks in the Period of Thawing

Region	May	June	July	August	September
The coast of the Arctic Ocean (Shmidt)	-	240	310	190	-
The upper Kolyma (Susuman)	150	420	500	350	90
Zabaikalje (Borzja)	350	620	720	605	300

As the thawed layer is accumulating, the surface temperature is raising and heat losses into atmosphere are increasing what causes quick decrease of heat flow density into thawing massif. The character of q changing on increasing the thawing depth is closely connected with the composition and thermophysical properties of rocks (fig.1).

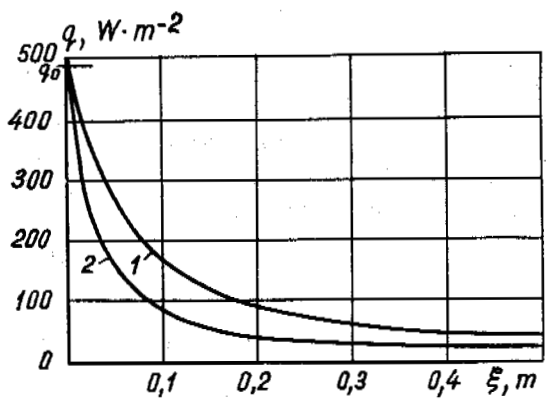

Fig. 1

Fig.1 Dependence of Heat Flow (q) Density into Thawing Massif on the Thickness (ξ) of Thawed Layer (July, the Upper Kolyma): 1- Gravel - Pebble Deposits; 2- Peat

It's clear that for the most effective utilization of natural heat resourses for purposes of radiation thawing of frozen rocks it is necessary to remove the thawed layer off its surface as often as possible. The given condition is fulfilled most easily when mining permafrost deposits with a bulldozer-scraper method which leading position in mining industry of the North-East of the USSR is

conditioned just by this fact

Such approach also allows to forcast the speed of snow and surface ice thawing in natural conditions and during the simplest operations of surface thermal reclamation. The calculations show that the thawing speed in May in the upper Kolyma increases 2.5-3.0 times as a result of soiling icings whereas it is only 25-30 per cent more in July. Such difference may be easily explained. In the summer when air temperature and moisture are high, the growth of absorbed radiation at the expence of surface albedo changing makes only little share in the positive part of the heat balance of ice surface.

As for hydraulic thawing the heat potential of the region is better to characterise by the two constants dependent on the complex of climate conditions - the temperature of wet thermometer (T_W) and the temperature of moist surface(T_m).

The notions of wet thermometer temperature are usefull when considering some questions of outward heat exchange in conditions of sprinkle thawing. Some works tell that water temperature is considerably raising during drops's flight in air (Veselov , 1959; Demidjuk,1961; Goldtman,1958). One cannot agree with this affirmation without serious provisors. Indeed, the temperature of flying drops (T_d) changes mainly as a result of turbulent heat mass exchange with air. The influence of radiation factors is negligibly little. The resulting density of heat flow (q_d) to a drop surface may be expressed by:

$$q_d = \alpha_h (T_a - T_d) - \alpha_e [e_s(T_d) - e_a] . \qquad (8)$$

It should be noted that the values of the coefficients α_h and α_e in formula (8) are quite high. So, for a spherical drop (of 1mm in radius) flying with 5m·s^{-1} speed $\alpha_h \approx 200$ W·m^{-2}.(°C)$^{-1}$ (Kutateladze,1971). However, the α_e/α_h ratio remains equal to 1.56·10^{-2}°C.Pa^{-1} It's clear that water heats if $q_d > 0$. Hence, the condition of drop heating in air is:

$$T_d < T_W \approx \frac{T_a + \frac{\alpha_e}{\alpha_h}(e_a - e_o)}{1 + \beta \frac{\alpha_e}{\alpha_h}} . \qquad (9)$$

Thus, T_W which serves as an integral characteristic of air temperature and moisture shows the possibility of heating or cooling drops in flight. On the territory of the North-East of the USSR water temperature is considerably lower than T_W only in the coldest small rivers and brooks.

More detailed analysis of heat mass exchange dynamics of water drops with air results in dependence:

$$T_d = T_W - (T_W - T_0)\, exp\left(-\frac{3at}{cR}\right) , \qquad (10)$$

where t is the time of drop flight,h; T_0 is initial water temperature,°C; c is the volumetric specific heat of water, W·h·m^{-3}·(°C)$^{-1}$; R is the drop radius,m; $a = \alpha_h + \beta\alpha_e$.

Formula (10) is meant for extremal valuations of temperature changing of water drops in air. Developing the proposed method one can easily calculate the maximum value of evaporation in sprinkling conditions what has a practical meaning for investigation of moisture balance while sprinkling arid earths.

The other parameter is T_m which presents the solution of equation (5) at q =0:

$$T_m = \frac{q_o}{\alpha} . \qquad (11)$$

Physical sense of T_m is the temperature which is attained by the moist surface in the given climatic conditions provided there is no heat outflow into an underlying layer. The temperature of shallow stagnant pools has the values close to T_m . As water temperature in rivers and brooks is, as a rule, considerably lower than T_m the question of the area of pools-heaters made for improving the hydraulic thawing effectiveness is of great interest.

Considering the heat balance of flowing water in interaction with atmosphere (neglecting heat flow into bottom deposits) we'll get an ordinary differential equation:

$$[q_0 - \alpha T(S)]dS = c\omega dT(S) ,$$

from which we'll find the dependence of water temperature T on the area and conditions of outward heat exchange:

$$T(S) = T_0 + (T_m - T_0)\left[1 - exp\left(-\frac{\alpha S}{c\omega}\right)\right] , \qquad (12)$$

where S is thearea of exposed surface,m^2; ω is watercourse debit,m^3·h^{-1}; the rest designations are the same. It is not difficult to see that at $\frac{S}{\omega} \to \infty$ (i.e. in a stagnant pool) $T(S) \to T_m$.

The calculations for the climatic conditions of July in the upper Indigirka are made by formula (12). The results are given in table 2.

TABLE 2

Rated Water Temperature in Shallow Pools-Heaters, °C

Initial water temperature, T_0 °C	Water temperature at different values S (m^2)				
	5	10	20	50	100
6	7.6	8.9	10.8	14.1	15.5
8	9.3	10.3	11.8	14.4	15.7
10	11.0	11.7	12.9	14.9	15.8
12	12.6	13.2	13.9	15.2	15.85
14	14.3	14.6	15.0	15.6	15.9

We'll point for comparison that T_m =16°C and actual water temperature, for example, in Bereljokh and Khatynnakh (Indigirka's tributary) rivers are 11.0 and 5.9 °C.Thus, the arrangement of shallow storage-ponds of 50-100m^2 in area for each 1m^3·h^{-1} of water-course debit will allow 1.4 and 2.5 times increase of water temperature and hence, hydraulic thawing speed, respectively.

The T_m value is subjected to rather sharp daily fluctuations. For instance, in inter-continental regions of the North-East of the USSR the average values of T_m in July in different day time change from 7 to 26°C(fig2).

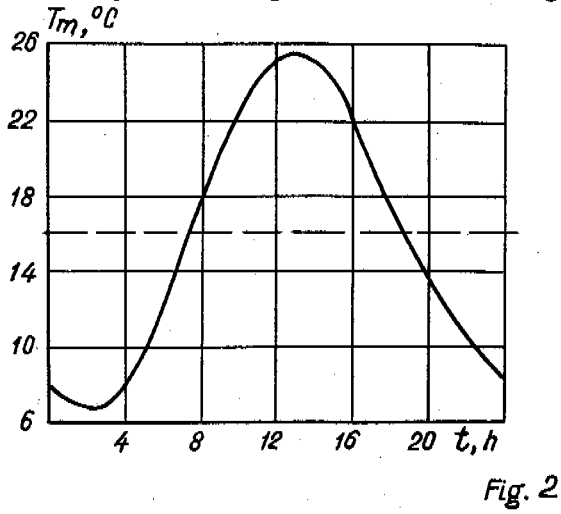

Fig. 2

Fig.2 Daily Course of the Temperature (T_m) of Moist Surface Calculated by the Data of Long Year Observations (July, the Upper Kolyma)

In the hottest days at bright sun shining T_m may be above 40°C. The calculations show that provided the surface evaporation and heat transfer into an underlying thick layer are excluded, the temperature of stagnant ponds at the warmest day hours may be increased to 65-70°C. These figures make oneself to search certain ways of accumulating and utilization of high potential heat energy which inexaustible reserves are presented in most regions of permafrost.

REFERENCES

Balobajev,V.T.(1963). Protaivanije merzlykh gornykh porod pri vzaimodeistvii s atmosferoi. V kn.: Teplo- i massoobmen v merzlykh tolshchakh zemnoi kory, pp.105-116.

Demidjuk,L.M. (1961). Effectivnoje ispolzovanije tepla solnechnoi energii pri primenenii dozhdevalno-drenazhnogo metoda ottaivania merzlykh gruntov. V kn.: Merzlotnyje issledovanija. Vyp.2,pp. 198-213.

Goldtman,V.G.(1958). Ottaika vechnomerzlykh gruntov dozhdevanijem oborotnoi vodoi. Tr.VNII-1, Magadan,t.7,razd.1. Merzlotovedenije,vyp.3, pp.1-16.

Kourtener,D.A.,Chudnovskii,A.F. (1969). Raschet i regulirovanije teplovogo regima v otkrytom i zashchishchonnom grunte. L.: Gidrometeoizdat, pp.184-226.

Kutateladze,S.S. (1971). Osnovy teplofiziki. Novosibirsk: Nauka, pp.229-231.

Lukjanov V.C.,Golovko,M.D. (1957). Raschet glubiny promerzanija gruntov.- M.: Transzheldorizdat, p.164

Metodika merzlotnoi sjomki. (1979). Pod.red. prof. V.A.Kudrjavtseva,M. Izd-vo MGU, pp.49-53.

Pavlov,A.V. (1975). Teploobmen pochvy s atmosferoi v severnykh i umerennykh shirotakh SSSR.- Yakutsk: Kn. izd-vo, p.303.

Pavlov,A.V., Olovin,B.A. (1974). Iskusstvennoje ottaivanije merzlykh porod teplom solnechnoi radiatsii pri razrabotke rossypei.- Novosibirsk: Nauka, p.182

Perlshtein,G.Z. (1979). Vodno-teplovaja melioratsija na Severo-Vostoke SSSR.- Novosibirsk: Nauka, p.304.

Veselov,V.V. (1959) Ottaika ekskavatornykh poligonov dozhdevanijem i gidroiglamy. Tr.VNII-1, Magadan,vyp.12,pp.223-243.

STABILITY OF ROAD SUBGRADES IN THE NORTH OF WEST SIBERIA

A.G. Polunovsky and Yu.M. Lyvovitch

Soyuzdornii, USSR

SYNOPSIS The report considers the peculiarities of natural and climatic conditions of West Siberia that should be taken into account at road design and construction. Principles of providing the stability of the embankments built of various soils are given. Structural solutions are proposed with the use of geotextile interlayers and heat-insulating materials.

The development of vast oil-and-gas regions in the North of West Siberia has required building a wide net of roads under complicated engineering-geological conditions. This network includes inter-and intrafield trunk roads of oil and gas producing regions, which are designated for heavy traffic (mainly from 200 to 1500 design vehicules per day).

Engineering solutions commonly used in road building practice are not applicable to this area due to the complex of unfavourable conditions which are as follows:

- the absence of construction industry base as well as natural resources of the rock, gravel, and sand soils with a filtration factor higher than 10^{-3}cm/s;
- short period of above-zero temperatures;
- excess moistening of the upper soil horizons;
- difficulties in construction of unshrinkable subgrades;
- deficit and high cost of labour resources.

A new approach to road building under such conditions provides structural-technological solutions aimed at maximum reduced volumes of earthworks and their execution on a round-the-year basis, stage road construction, the use of precast pavements from reinforced concrete slabs.

The region in the Ob-Enisey downstream interfluve is characterized by extremely unfavourable climatic, soil-hydrological and cryogenic conditions. The distinctive features of this area are excessive moistening and insufficient heat. Average annual air temperature is -3- -4°C in the south to -9- -12°C in the north of the area, a duration of frostless period is 60-90 days, winter temperature is up to -50°C, and the winds of 15-20 m/s blow frequently. Strong winds cause the snow transfer which is considerable due to a dry loose nature of the fresh snow with density 0.03-0.12 g/cm^3. A thickness of snow cover in the open tundra ranges from 20 to 100cm, an average one being 20-40cm. The relief is plane, slightly rugged and very poorly drained, absolute elevation marks range within 50-120m. The region is characteristic of extremely high swampiness and is very laky (up to 80%), there widely occur plane and convexo-hummock vast peat bogs with peat deposit depth from 1 to 4m (mainly about 2m).

As for soil conditions of the region, permafrost is most common. The latter, first of all concerns with the northen regions where separate taliks occur in the river valleys or near the lakes, with trough taliks being extremely rare. In the region of Nadym and Urengoi 25--30% of the interfluve area falls at the deposits thawed from the surface up to the depth 4-10m, which form the unmerged frozen masses. In the southern regions, development of the frozen masses occurs almost exclusively in the peat areas. A temperature of the rock at the depth of zero annual amplitude varies from -3-- -5°C in the north to above zero in the south; frozen ground becomes insular and the process runs more sluggishly with simultaneous reduction in the icity. Among the cover rocks a complex of sea deposits prevails with limited occurence of alluvial deposits in the flood plains and above-flood plain terraces. These rocks are mainly composed of clay soils-loam , sandy loam, clay, and more rarely by fine sands. In all the cases the content of silt particles is high ,up to 50-90%. In the thawed condition these rocks are characterized by unstable structure and are prone to the thixotropic fluidification under load application, especially under multiple loading or vibration. This is explained by high icity of the rock reduced from its surface down along the section. The moisture content of the frozen clay rocks is 25-65% and is higher than that of thawed ones, which is 25-40%. Sand soils of this region are referred to the fine silts of various icity and average moisture content of 20-30%. High degree of overwetting is, first of all, characteristic of the clay soils, but not seldom that is observed for the sandy soils. The

settlement of the clay soil depths on thawing varies depending on genesis, temperature climatic and hydrogeological conditions over a wide range up to 400 mm/m. Settelments on thawing of the sands are usually insignificant and admisi ble in terms of their use in the foundations and bodies of the road embankments at the loose-frozen state. The highest degree of the icity and subsidence is observed with the peat soils. The moisture content of the frozen peat not seldom is 300-400% at the voluminal icity 60-80%. Frost heave formations in the form of heave mounds several meters in height and 40--100m in plane occur in peat soils.

The icity and temperature of a soil influence not only its stability in the foundation and a degree of subsidence, but also, to a high degree, determine the conditions of working out the frozen soil and the possibility of using the material thus obtained either directly for embankment filling-up or after a preliminary technological treatment.

With due regard of the above peculiaries a number of basic principles of the design and construction of subgrades in the northern regions of West Siberia has been formulated.

According to the first principle the subgrade is designed on the embankments rather uniform in height (due to the smooth relief) and a reference mark is established with consideration of the snow-drifting. The latter is of special importance for a region that is characterized by frequent and strong winds, dry displacing snow, and a winter maintenance period up to 7-8 months each year. The absence of a special service of road operation during construction period as well as during the first years after putting a road into service should also be taken into account. That is why the subgrade design and the choice of reference mark is based on the criterium of the snow-drifting.

According to the snow-drifting condition the height of the embankment is designed on basis of a maximum height of the snow cover and climatic peculiarities of a region. Due to the absence of road network and the experience of its operation under winter conditions as well as difficuties of factual information gathering during winter investigations of a route, it is recommended to design the embankment height using a method of the Omsk Branch of Soyuzdornii by formula:

$$H = H_{sn}^{d} + K_1 \cdot \Delta h \qquad (1)$$

where H_{sn} = design maximum height of the snow cover from data of the nearest meteorological station;
K_1 = coefficient considering the influence of the relief, which is determined from Table 1;
Δh = minimum height of the embankment edge above the snow cover in the case of open horizontal section of the terrain, m.

TABLE I

Characteristic of the terrain	K_1
1	2
Highly rugged terrain covered with vegetation and forest massives	2.0
Leeward slopes of steepness 1:3 and more	1.8
Hilly rarely wooded tundra with underbrush	1.8
Hummocky tundra	1.7
Hilly tundra	1.6
Windward slopes of sttepness more than 1:3	1.3
Flat continental peat-moss tundra	1.2
Open frozen water surfaces (water areas) 1km and more in length	1.0-1.2
Near-shore tundra	1.0
Upland and watershed heads	0.8-1.0

When specifying the embankment height and structure, the second design principle should be followed which requires to determine the depth of thawing of the foundation under the embankment of a given height by means of heat-engineering calculations as well as to evaluate a probable settlement of the embankment foundation after thawing and the rate of settlement completion. To take into account a degree of soil thermosubsidence as well as an effect of the foundation settlement on the performance of a road the use is made of one of the two wellknown fundamentals (specified in construction norms) for designing the structures on thermosubsiding soils. In application to road construction conditions these fundamentals are interpreted by the following way: according to the first fundamental the thawing of the natural foundation underlying the embankment is inadmissible during the whole service life of a road; according to the second fundamental the thawing of soils in the embankment foundation is admissible through a design depth within which the settlement of the thawing layer does not exceed a permissible limit depending on conditions of the road pavement performance.

The third design principle is based on that the stability of the embankment itself built from a soil the moisture content of which is higher than an optimum one should be provided during thawing of the embankment or when the latter and its foundation is in the thawed state. The settlement on thawing of the embankment built in winter from icy lumpy soil is conditioned by the porosity of the soil itself and the secondary porosity of the lumps. This settlement should not exceed admissible limits depending on conditions of the pavement operation. When designing the embankment according to the second principle, total settlement of the embankment body and the thawing layer of the embankment foundation should be within the permissible limits.

Road design for the northern regions is recommended to carry out considering subsequently the above three principles. First of all, a reference mark of the embankment is established on the basis of snow-drifting condition.

With the embankment height obtained, the heat--engineering computations of a structure are performed and the depth of thawing of the embankment and its soil foundation is determined. For these computations a road is divided into typical lengths taking into account peculiarities of the relief, and soil-climatic conditions as well as composition, state and a degree of ice-cementation of the soil used for embankment construction. From data on thawing the embankment and its foundation, on physical-and--mechanical characteristics of the embankment and foundation soils the stability of a whole road structure (an embankment and road pavement) is assessed. The total settlement of the embankment and its foundation is calculated and compared with a permissible one, and the stability of the road structure as a whole after thawing is evaluated. At this stage of calculations the application of averaged data is allowable. When the embankment stability is not provided or the settlement exceeds an admissible limit the adjustment of the structure is performed. The adjustment may include the change of the embankment height, the change of the design principle (for instance, coming from the second principle to the first one), and the use of special materials (heat-insulating materials, geotextile) in order to regulate either thermal regime or stressed-strained state of the structure. Within the frames of alternate design various structural solutions can be considered not only as mutually complementary, but also as competitive ones from the engineering-economical point of view.

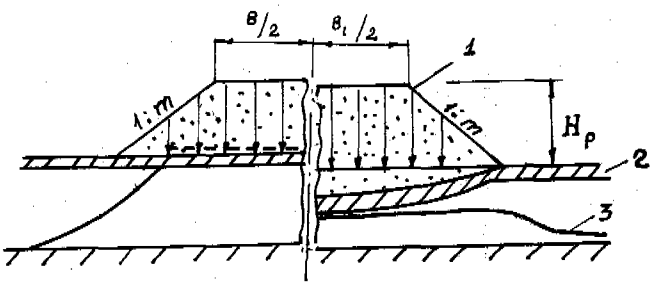

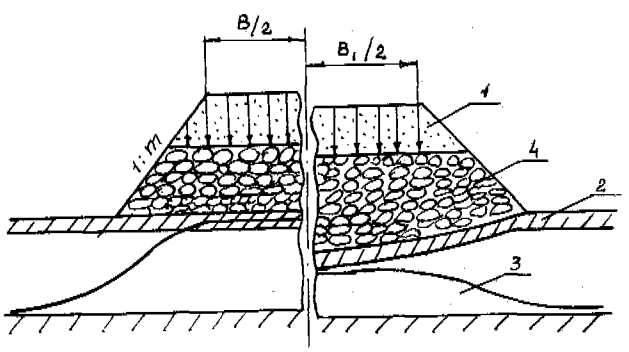

Fig.1a Design scheme for evaluation of the stability of the embankment made of incompressible soils and laid over the frozen foundation

Fig.1b Design scheme for evaluation of the stability of the embankment on the thawing foundation: 1- sand; 2- moss-peat layer; 3- the location of the upper boundary of the perennially frozen soils; 4- compressible-on-thawing soil

Fig.1c Design scheme for evaluation of the stability of the embankment over the frozen foundation, with the lower part of the embankment made of compressible soils

Fig.1d Design scheme for evaluation of the stability of the embankment on the thawing foundation (as in the case in Fig.1c)

Calculations for the road embankments on thermosubsident soils are performed on the basis of four basic schemes. The first two schemes (Fig.1) concern with construction of the embankments from sandy soils of admissible moisture content, and their design is performed according to the first or second fundumental, respectively, i.e. with inadmissible or admissible thawing of the foundation. Design schemes 3 and 4 (Fig.2) concern with embankment construction with the use of frozen lumpy soils in the lower part of the structure. Scheme 3 is applied to the embankment design according to the first principle, i.e. without thawing of the foundation and with location of a thawing horizon during a whole summer above the bottom of the embankment body. However in this case the settlement of the foundation is excluded because the embankment is built from soils unstable at thawing but deformations of the subgrade and road pavement are possible. Scheme 4 is applied to the design of the embankment according to the second design principle with a possibility of thawing of the foundation of the embankment built from soils unstable at thawing.

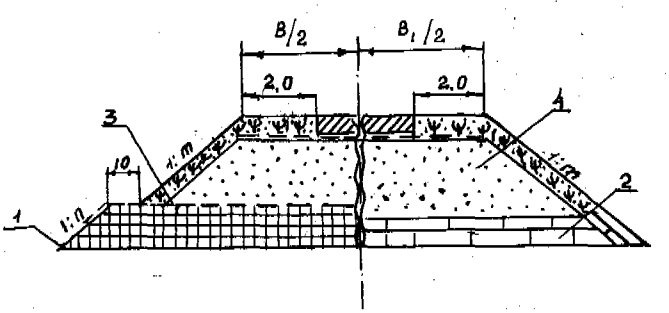

Fig.2 Structure of the embankment with heat--insulating layers in its foundation:
1- peat; 2- plastic foam; 3- geotextile;
4- sand

When designing road structures on the basis of the above four schemes, computations are performed which include the determination of magnitude of the final settlement of the embankment and its foundation active layer as well as duration of the consolidation settlement and terms of completion of the latter; before both these calculations the heat-engineering computations of the depth of the embankment and foundation thawing are carried out. An accepted method of the heat-engineering computations is based on the solution of a two-dimensional problem taking into account the non-uniformity of thawing across the embankment width due to an additional heat flow moving from the slope sides and the-near-slope band.

A computer software of the heat-engineering computations is worked out, which allows to car-

ry out a multifactor analysis of the influence of natural-and-climatic conditions of the area of the route alignment, of variants of the embankment heights and structures, of soil type, properties and state as well as the effect of interlayers from the artificial materials.

Final conclusions as to the possibility of the use of any particular structure may be drawn only on the basis of calculations of the embankment settlement and evaluation of possible pavement deformations. It should be taken into account that in the case of precast pavements there is a possibility of slab replacement and restoring the pavement evenness. According to this technology, which is essentially a variant of the two-stage construction method, at the first stage the pavement laying-down is permitted before completing the embankment consolidation. When the final settlement is achieved and there occurs settlement attenuation the second stage begins that includes slab dismounting, levelling and filling-up the subbase, and then slab relaying on the levelled surface.

To assess a magnitude of the final settlement of unstable, compressible-on-thawing soils of the embankment as well as its foundation it is recommended to use the following expression:

$$S_{total} = 0{,}001 \sum_{i=1}^{i=n} \ell_{p_i} \cdot H_i \ , \quad (M) \qquad (2)$$

$$\Sigma H_i = H_1 + H_2 + \Delta h$$

where S_{total} = total magnitude of the final settlement of road structure;
ℓ_{p_i} = modulus of settlement design layer, mm/m;
ΣH_i = thickness of a design comperrible-on-thawing layer in an "embankment-relief element system";
H_1 = thickness of unstable layer of the embankment;
H_2 = thickness of thawing active layer;
Δh = thickness of moss-peat cover.

Magnitude of the modulus of settlement of frozen lumpy soils on thawing, which are used for the lower layers of the subgrade is taken to be as follows: 100÷200mm/m for loose-frozen and dry-frozen sands, 300÷500mm/m for hard-frozen and plastic-frozen silty sands and sandy loams; 500-600mm/m for hard-frozen loams and clays, and 700÷800mm/m for frozen lumpy peats.

The modulus of settlement of soils in natural strata depends on the type of a soil in the active layer, its genesis, total moisture content, and a degree of the ice cementation (icity). Total values of the modulus of settlement at normal stress of 0.1g/cm^2 at the surface of a design compressible layer of soil are: 20÷60mm/m for sands, 100÷120mm/m for sandy loams, 120÷400mm/m for loams and clays, and 300--500mm/m for peats.

To determine a duration and time of completion of the settlement of compressible-on-thawing soil layer of the embankment and its foundation it is necessary to establish a period of consolidation in order later on to lay down a pavement, for instance, from precast reinforced slabs; because compressible (unstable) soil layer begins to deform under the load from the overlaying courses of the road pavement structure only after thawing or in the process of thawing, for rough computations it is possible to assume that the time and rate of consolidation is equal to the time and rate of thawing of the design compressible layer. Thus, it is proposed to consider the settlement and the time of consolidation of compressible layers together with the time and rate of thawing of compressible soils in the embankment and its foundation. For a given period of time t_i a thickness of thawing compressible layer H_i is found on the basis of heat-engineering computations and its settlement Δt_i at any given time is determined by formula (2). The time of achieving a final magnitude of the settlement corresponds to the time of complete thawing of a layer H_i. Of essential importance is thickness of the compressible soil layer, its total moisture content on thawing, its modulus of settlement and structure as well as a season of the embankment construction (summer or winter), the state of a soil used (thawed, frozen), a degree of fragmentation (lumpiness).

Indices of structural and physical-and-mechanical properties of the compressible-on-thawing soils of the subgrade influence the total value of settlement and a mode (non-uniformity) of settlement development which results in certain difficulties not only in providing the embankment stability but also in laying down the road pavement because the terms of construction of the latter depend on an admissible intensity of settlement development. In connection with the necessity to use compressible-on-thawing soils for the embankment construction, on the basis of the design schemes (Fig.1b,c,d) subgrade structures are developed which include elements made of geotextile and heat-insulating materials in order to compensate the non--uniformity of settlement development as well as to provide the structural stability and to regulate the congelation regime. Schemes of subgrade structures are given in Figures 2-5.

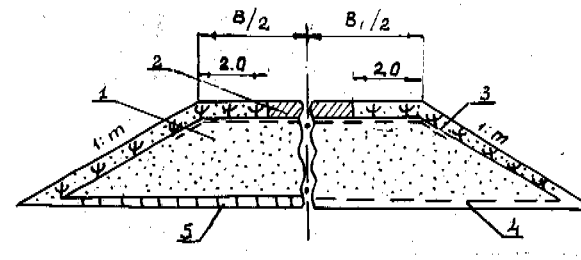

Fig.3 Structure of the embankment including a layer of compressible-on-thawing soil, with heat-insulating layer on the surface: 1- sand; 2- pavement slabs; 3- geotextile under the pavement slabs; 4- geotextile in the embankment foundation; 5- plastic foam of reduced thickness

In cases when it is necessary to preserve the embankment soil in the frozen state without an increase in the embankment height (design scheme 1) the use is made of the heat-insulating layers of artificial or natural materials (Fig.2) laid in the embankment foundation. To lower the non-uniformity of the embankment

settlement up to an admissible limit it is required to reduce either (1) a magnitude of the settlement or (2) a degree of its non-uniformity that is achieved, respectively, either by lowering a depth of thawing by means of heat--insulating interlayers or by reinforcing the embankment foundation by geotextile materials. This case corresponds with design scheme 2. When the lower layers of the embankment are built from hard-frozen soils compressible at thawing (design sohemes 3 and 4), geotextile envelopes or semi-envelopes combined (if required) with heat-insulating layers (design scheme 3) are used as structural elements (Figs.4 and 5).

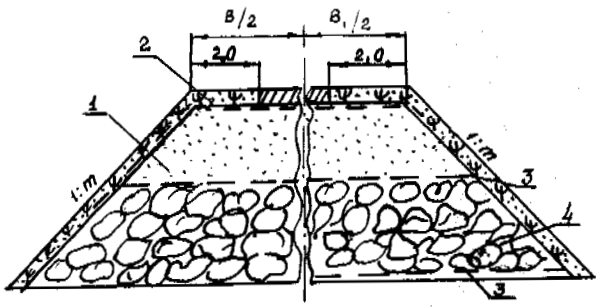

Fig.4 Structure of the embankment with geotextile interlayers and envelopes: 1- sand; 2- pavement slabs; 3- geotextile envelope; 4- frozen lumpy soil

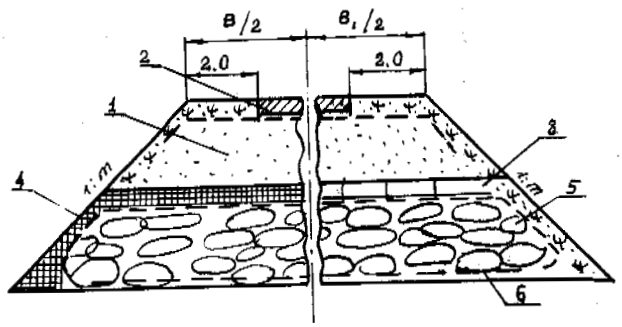

Fig.5 Structure of the sand embankment with heat-insulating interlayers and semi-envelopes of geotextile: 1- sand; 2- pavement slabs; 3- plastic foam; 4- peat; 5- geotextile semi-envelopes; 6- lumpy soil

CONCLUSIONS

Natural conditions of the northern regions of West Siberia are extremely unfavourable for road construction. The main difficulties are conditioned by a long cold period, the necessity to build the embankments from the frozen soil, considerable embankment settlements at thawing both filled-up soil and natural foundation. To raise the stability of the embankment in summer period without an increase in the earthwork volumes it is recommended to use heat-insulating layers as well as reinforcing and separating geotextile interlayers. The embankment height and structure are specified on the basis of computations according to the conditions of snow-drifting, thawing, admissible settlement, and stability of the embankment.

REFLECTION SEISMIC EXPLORATION AND DATA PROCESSING IN COLD REGIONS

F. Porturas

Division of Petr. Eng. and Appl. Geophysics, The Norwegian Institute of Technology, Norway

SYNOPSIS Today studies in cold regions are of great interest because of their potential economic resources. This paper presents an up-to-date analysis of multichannel seismic reflection methods and data processing problems. The application of reflection seismic methods meets particular difficulties which are not found elsewhere. The major question is how the frozen ground thickness and frost breaks affect the seismic sources and wave propagation. The frozen ground acts in the same way as weathering zones do on land seismics, or as a hard sea floor in marine operations, very similar to the exploration of transition zones. The seismic data processing is directed towards optimizing data quality where noise and spurious events, which tend to mask reflections of interest, must be attenuated. The success of any geophysical method in cold regions will rely on its ability to delineate boundaries and thickness of the frozen ground. Therefore the understanding of permafrost phenomena, glacial drift and related geological factors is necessary to achieve good results for resource exploration and engineering purposes.

INTRODUCTION

Increased attention is being focused on exploration in "frontier" areas of the world. These include regions which lie above high latitudes with permafrost and ice occurrence, here these zones are named "cold regions".

The most common methods applied in the evaluation of cold regions include reflection, refraction, spot bathymetric soundings and pulse techniques. Other sets of geophysical data have been obtained by airborne magnetometric, heat flow, gravimetric measurements, and limited shallow coring.
Radio echo soundings have been done in the Antarctic ice using very strong sources such as pulse-modulated radar. This method has limitations because the echos are affected by refraction phenomena on the ice surface, ice shelves, crevasses and cracks at the bottom of the ice. Recently, the measurements of ice thickness have been done using helicopters with a mounted impulse radar unit. The helicopter fly 3 to 5 m above the ice with a velocity of 5 to 10 knots. The energy is reflected partially by the ice and by the interface between the bottom of the ice and sea water. The difference between this technique and the seismic method is the nature of the energy source. Electromagnetic waves being used for the radar technique as opposed to sound waves for the seismic method.

In cold regions, the seismic data available is sparse because of the harshness of the environment and the unstable nature of the ice cover. Its discontinuity does not allow the use of land techniques and maneouvering of marine seismic vessels requires ice-breakers. Therefore seismic exploration in cold regions is a peculiar mix of land and marine operations.

The studies in cold regions deal with similar problems found when exploring transition zones. For instance, the areal extension of frozen ground and transition zones varies areally and depends largely on deposition environments, temperature (near the freezing point), salinity, history of burial and exposure, depth, proximity to surface, water saturation, lithology and stress factors. Seismic reflection techniques are a reasonable approach to the investigation of cold regions both in terms of economy and time. They provide useful information for estimation of ice thickness, ice bounded, and subsea permafrost extension. These data can be used for design and construction of mine shafts, designing suitable foundation sites, oil and gas facilities and to calculate the forces exerted by ice floes against structures such as platforms set on the seabed. Seismic exploration assists in the determination of compressional wave velocities and in acoustic log interpretation in permafrost.
The amount of work done in cold regions is large and most of the literature is scattered. In this paper a brief presentation of the main problems found both for data acquisition and during the seismic data processing is given. The examples presented include mostly synthetically generated data and they illustrate the main steps followed to process a seismic section.

SEISMIC DATA ACQUISITION

Seismic data acquisition programmes needs to be oriented towards solving the acoustic impedance problems encountered when dealing with ice covered and permafrost zones. The most important parameters to be considered are geophone or hydrophone spacing and signal frequency. The complexity of the subsurface will affect the source performance. Several energy sources such as airguns, explosives (dynamite, geoflex), sparkers and boomers have been applied. The basic criteria for selecting the energy source is its capacity to differentiate materials under the ice cover and permafrost, for instance they have different compressional velocities and when material become ice-bounded, the velocities will increase.
Tests using various volume charges of explosives have been performed. Normally, the explosives are placed beneath the ice or deep in the frozen ground with the purpose of maximizing the downward transmitted energy. This technique is prone to several difficulties. The holes usually refreeze, then the geophones are lost. The holes can cross and drain brine lenses, then seawater invades the hole and readily freezes and the geophone will be trapped. Experimental tests using dynamite charges of 10 lbs or greater detonated at depths less than 0.5 m shows a tendency to create ice breaks, fractures and frost breaks. The frost breaks constitute a major problem during data acquisition. They originate when exploding dynamite triggers, cracking the ice outwards from the detonation point. These minute cracks form in the ice of the permafrost and act as secondary sources of seismic energy which obliterate subsurface energy arriving at the same time. Experimental work has shown that volume charges between 1 to 2 lb and detonated between 5-10 m do not tend to create frost breaks.

The logistics for a seismic survey in cold regions are very important. For a 12 geophone trace and 24 channels group interval, 142 m spread, using a charge size of 25 lb, the energy necessary per mile of survey is 162.5 lbs of dynamite. From human safety and ecological considerations it is recommended to use small charges. Another difficulty encountered in cold regions is the ice flow camps power which restricts available sources. Noise results from water ground loops and due to mechanical vibrations of diesel or electric generators.
The receivers are a source of low frequency strumming noise. This is created by vortex shedding of water flowing fast suspended hydrophone cables. The hydrophones are prone to strum oscillations.
The recording systems used in the past were analogue. Today seismic data are gathered mostly digitally. Analogue methods have a seriously limited dynamic range. Digital single channel systems offer seismic records of poor quality and are not powerful enough to penetrate the structures sufficiently. Therefore multichannel systems are preferable. The only problem related to this way of recording seismic data is the often erratic direction of drift of the ice flows.
A standard magnetic tape format widely used to

SOURCES	ADVANTAGES/DISADVANTAGES	PROBLEMS	COMMENTS
- Sparkers	Faster for quick-look interpretation / No possibility to enhance data quality	Difficult to use in transition zones	- Only for seasonal operations. Requires good weather.
- Boomers	" "	"	
- Airguns up to 600 cu in Receiver either suspended or ice mounted.	- Susceptible to vibrational pickup from power generator and man-made camp noise	- Extreme cold can cause temperamental variations	- Needs proper maintenance
	- Heave - thumping instruments flexes the ice- Spoils data quality.	- Airguns do not work well if there is not enough good contact with water	- Very difficult to use seismic arrays.
	- Good data offshore seaward/ lesser depth; noise	- Offshore floating ice	
		- Cable towing	
- Explosives Receivers either suspended or mounted.	- Easy to drill on ice	- Trenching equipment	- Holes drilled on ice or charges placed in water
- Small charges up to 25 lbs	- For explorationists/environmentalists	- Frost breaks	- Charges preferable below permafrost
		- Ice fractures	
- 25' of 40 grain "Aquaflex"	- Ecologists/point source	- Ice breaks	- At least 10' below lower ice
	- Better onshore		
- Vibrators Onshore Deep water	- Disadvantage: direct coupling to the ice or frozen ground	- Flexural wave noise	- Inferior shallow data quality
- Weapons, 22 caliber rifle			Good data.

Fig. 1. Synopsis of seismic data acquisition parameters applied in cold regions.

record seismic data in cold regions is the format SEGA but other tape formats such as SEGB are also used. The energy source suitability depends on its ability to delineate permafrost, changes in lithology and lateral extension of the frozen ground. If data is not acquired properly, only limited improvement in resolution can be achieved during the processing. Figure 1 shows a synopsis of sources reported to be used in the seismic exploration of cold regions and Figure 2 shows the surface and subsurface coverage diagram of a seismic survey.

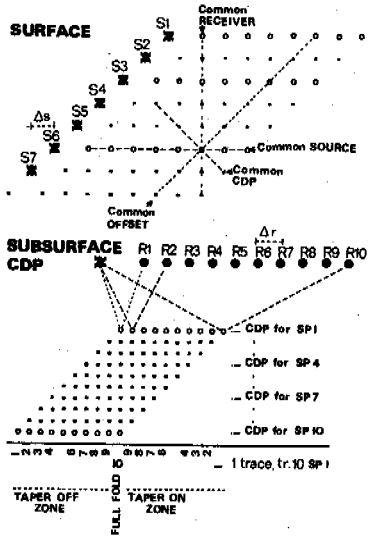

Fig. 2. Diagram showing surface and subsurface coverage for a seismic programme where $\Delta r = 2\Delta S$ and with 10 receivers.

DATA PROCESSING

The seismic data processing sequence for cold regions is similar to marine rather than land seismics, but it suffers the courses of both. Figure 3 shows a processing scheme adapted to treat data from frontier areas. The compulsory steps are illustrated using synthetically generated examples (Figures 4-10). The signal needs to be enhanced to a certain level of resolution, this is done at the processing center.

The primary goal in data processing is to enhance and discriminate primary reflections from unwanted noise events. By means of data processing, coherent and random noise must be removed from the seismic section. In ice-pack environments, the worst problem is multiples. Since the ice skin reflects the energy much more effectively than the water surface alone, multiple energy is effectively wasted energy. It is very complicated to design arrays for data acquisition in harsh environment areas. The additional amount of drilling would make it impractical, the random and coherent noise is treated in the processing center. At the processing center the raw data is demultiplexed and rearranged into Common Depth Point gather. Figure 4 shows a synthetic generated shot and its corresponding CDP gathers. During data processing, several algorithms are tested to find an optimal sequence for the survey.

Dealing with phase differences due to the different source signatures takes a good part of the time.

Decisions are taken at different parts in the processing sequence. When transition zones are invisible seismically and if cannot be well delineated on the basis of the seismic wavelet characteristics, it is recommended more testing to restore weak frequency components to a certain level of interpretability. A crucial step during the seismic data processing is the estimation of velocities for normal moveout correction. This done by interpreting the velocity spectra (Figure 6).

One important step is to test which gain function can be used to compensate for energy losses downwards. Figure 5 shows several gain functions, the purpose is to make the time series stationary previous to further processing.

The velocity analysis has a great deal of influence both on depth and velocity gradient estimations. It also influences the final stacked section. Figure 7 shows the velocity effects both on CDP's and in the stack. It is desirable to choose the most optimal velocities otherwise good resolution will not be achieved. In frontier areas the measurement of velocities are performed in temperatures ranging from 20°C to -36°C. In this range of temperatures the materials behave differently but as a rule the velocities in water saturated rocks will increase with decreasing temperature, while in dry rocks it is nearly temperature independent.
In the velocity spectra analysis the shape of the velocity function usually increase as a function of time and as a function of lithology in the underground. However it can be affected by numerous factors such as the inherent physical conditions of the frozen ground. When short arrays are used during data acquisition, poor resolution is expected. Source deconvolution algorithms are tested and designed to suppress the surface ghost and multiples, which tend to mask reflections of interest. This inverse filtering process must be adapted carefully to the problem in the case of transition zones. Migration is applied in order to move reflections to their correct positions. Figure 8 shows a stack response and its corresponding migrated section. Finally a good set of display parameters must be chosen for the final seismic section (Figure 9).

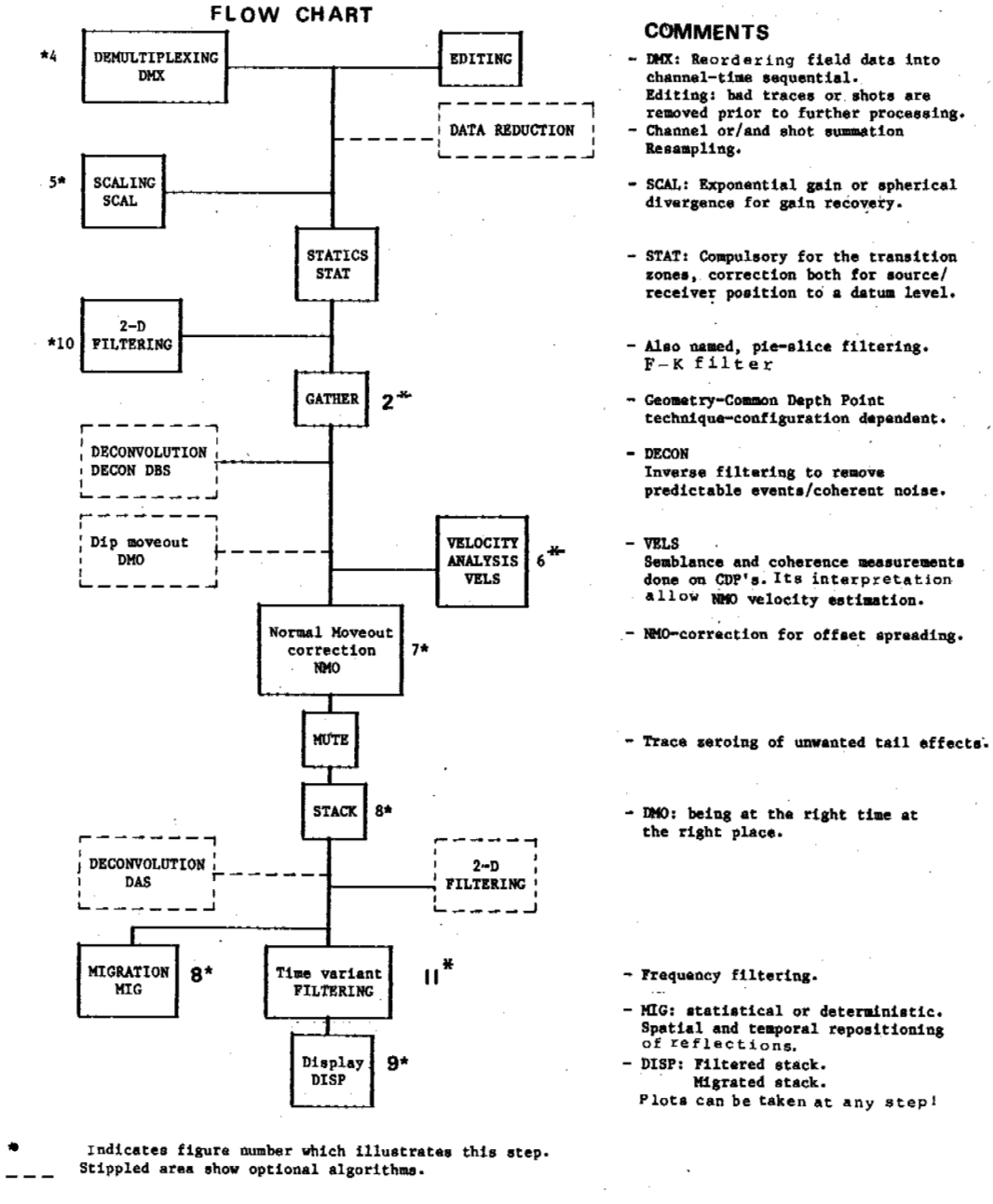

Fig. 3. Proposed seismic data processing scheme for cold regions.

EXPLORATION PROBLEMS

The reflection seismic method provides clues to the presence of frozen ground because of its characteristic high velocity. However the base of permafrost is difficult to observe if the quality of seismic data is not optimal. The thickness of the frozen ground has a special effect and acts as a variable statics anomaly which can lead to wrong interpretation. Methane hydrates may be concentrated at or near the base of permafrost zone, so delineation of the permeafrost is important, because of the potential danger inherent in drilling in hydrate zones.

The area and depth of permafrost can cause scattered and broadside noise. Good data can be acquired if the group intervals, geometry, and source are well designed.

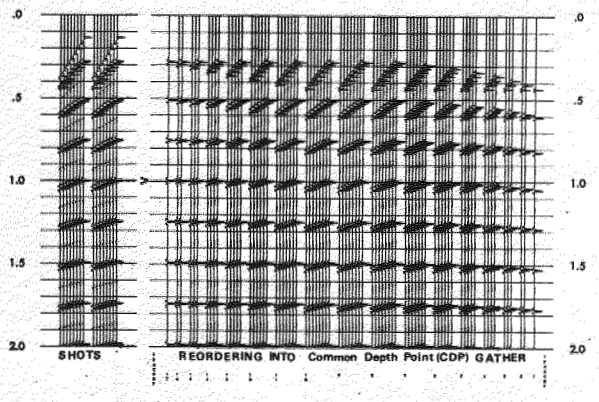

Fig. 4. Synthetic shots with 8 channels reordered into CDP gathers.

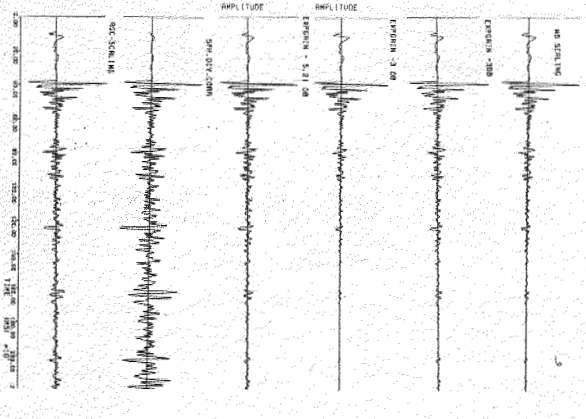

Fig. 5. Composite scaling tests used for gain compensation functions applied to the same single trace, displayed in true amplitude.

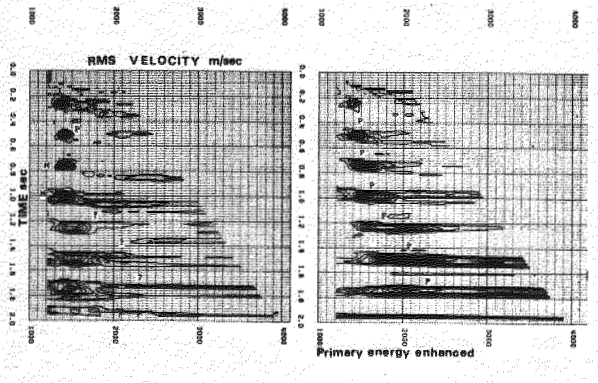

Fig. 6. Velocity spectra used for stack velocity estimations, left panel shows dominant multiple energy, obviously the wright panel is more interpretable.

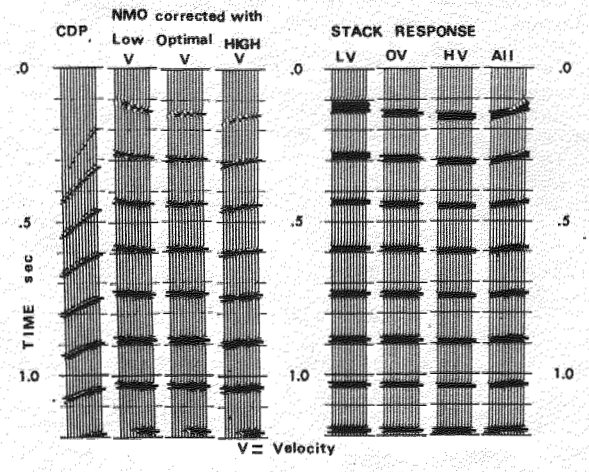

Fig. 7. Normal moveout correction options applied on a single CDP (left). Its effect on stack (wright). Note the dramatic effect when we combine all velocities, the stack shows dip which does not exist initially.

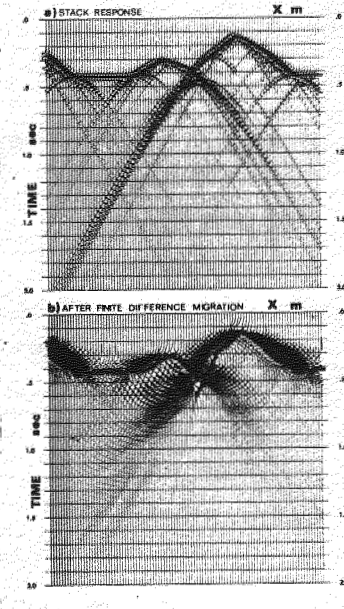

Fig. 8. Stack and migration responses on synthetic generated seismic data. Today migration is a compulsory step in any processing scheme.

Numerous locales of shallow gas bearing layers have been found offshore in several exploration areas. These are highly reflective horizons mostly followed by a low velocity layer. This fact leads to strong reverberation and shallow penetration of the underlying structure because of the lower transmition coefficients.

To deal with the complexity found in cold regions, the low frequency ground roll can be treated using multichannel filtering. This is the only way to discriminate signal from noise lying at the same frequency. Figure 10 shows an example of 2-D filtering. In other cases ice wave interference is greater than the reflected signal; therefore strong noise cancellation during processing is required. The final seismic section will in all cases be affected by significant residuals because of the intensity and local variability of the ice thickness which affects surface wave propagation.

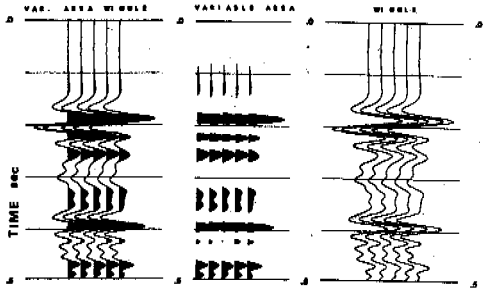

Fig. 9. Display types for seismic data. Variable area wiggle, variable area and wiggle traces only (from left to wright).

The subsea permafrost (high velocity media) acts as an efficient wave guide which produces strong reflected and refracted reverberation. Therefore, data processing needs special attention when applying deconvolution.

It should be noted that permafrost can vary in depth, and the upper section can be affected by seasonal variations and long term trends of regression and advance, (ice cover). Therefore extensive testing is necessary, since normal schemes will not generally work with this type of data.

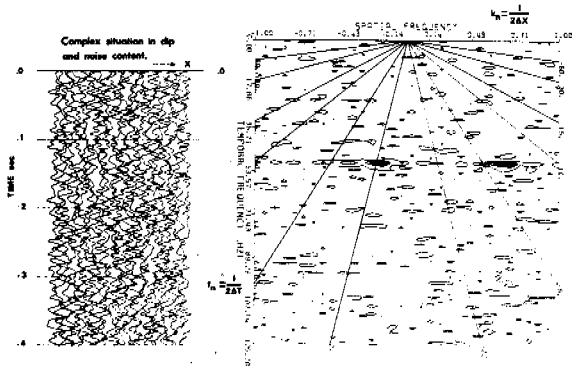

Fig. 10. Spectrum (wright) taken from a shot (left) to design a 2-D filter. Useful when random and coherent noise masks the seismic data.

It is all the time necessary to test at which frequency level the energy lies in the data. Figure 11 shows a filtering operation done on CDP's.

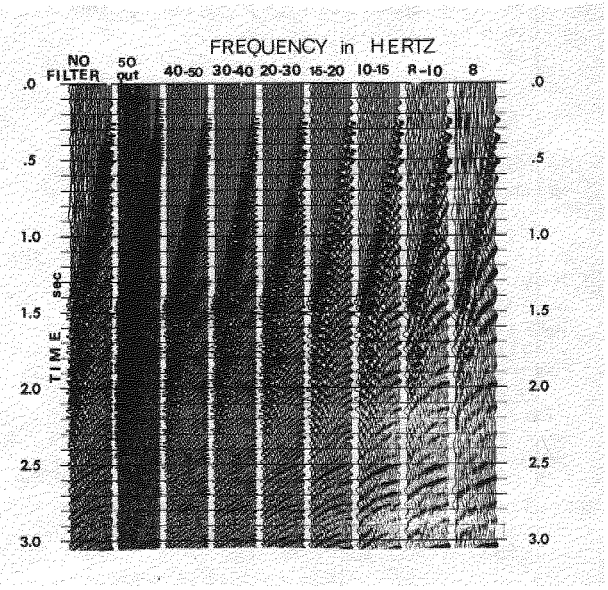

Fig. 11. Examples of filtering on a single CDP. Notice the improvement/damage to the seismic reflections.

Looking forward, experimental work related to the application of the reflection seismic method in cold regions, acoustic impedance variation as a function of offset remains to be done. Transition zones associated with permafrost are ideal candidates for observing effects of increased reflection coefficients and wave shape modification with offset.

CONCLUSIONS

In spite of the considerable research already done, cold regions still remain the least known. Technology is evolving which permits work in harsh environments; however, further advances must be made to acquire the comprehensive seismic data needed to develop its resources. Seismic exploration has been limited in quality, since it is only recently that array technologies have been used. Although coverage is sparse, future developments in remote sensing and submarine-mounted systems must be considered to solve the major constraints in acquisition and data processing. Finally, good data will be useful for producing more accurate interpretations and to provide a better insight into detection and location of potential drilling hazards and for site studies.

AKNOWLEDGEMENTS

I would like to thank Prof. Bjørn Ursin for the comments, GECO has provided computing facilities and to Anne-Lise Brekken for typing the manuscript. Finally to Prof. Jon Kleppe for his support.

REFERENCES

Baggeroer, A.B. & Duckworth, G.L. (1983). Seismic Exploration in the Artic Ocean. Geophysics: TLE, (2), 10, 22-27.

Brown, A. (1983). Seismic on the Pack ice. Geophysics: TLE, (2), 10, 12-16.

Harrison, C.H., (1970). Reconstruction of subglacial relief from radio echo sounding records. Geophysics, (35), 6, 1099-1115.

Justice, H.J. & Zuba, Ch. (1986). Transition zone reflections and permafrost analysis. Geophysics, (51), 5, 1075-1086.

Poulter, T.C. (1951). A discussion on seismic soundings of glaciers. Geophysics, (16), 535-537.

Proubasta, D. (1985). Ice saw - an incisive solution to seismic noise. Geophysics: TLE, (4), 10, 12-23.

Rackets, H.M. (1971). A low-noise seismic method for use in permafrost regions. Geophysics, (36), 6, 1150-1161.

Senneset, K. (1986). Landbasert virksomhet - utfordring fra permafrost. NORD-86.

Timur, A. (1968). Velocity of compressional waves in porous media at permafrost temperatures. Geophysics, (35), 4, 584-595.

PROBLEMS OF ARCTIC ROAD CONSTRUCTION AND MAINTENANCE IN FINLAND

S. Saarelainen and J. Vaskelainen

Technical Research Centre of Finland, Geotechnical Laboratory

PROBLEMS OF ARCTIC ROAD CONSTRUCTION AND MAINTENANCE IN FINLAND

SYNOPSIS. In the paper, the problems induced by the cold climate to road maintenance and construction in Northern Finland are described and discussed. Methods for the improvement of road on permafrost, frost heave, icing and snow accumulation are presented. According to the experimental design and construction, economical and technically feasible solutions can be achieved by the application of developed thermodynamic background.

1. INTRODUCTION

Finland is located between the latitudes 60 and 70 in the northern hemisphere. The mean annual air temperatures vary from + 6 °C in the south to -2...-3 °C in the north of Finland (fig. 1). The climate is heavily affected by the Golf stream, which smoothes the air temperature variation. In eastern parts of the country, the continental climatic effects are more distinct, and the seasonal temperature variations are relatively larger.

Due to the long cold period and relatively low mean temperature, the effects of frost and soil freezing are dominant in the behaviour of different structures exposed to freezing, i.e. soil structures, foundations, hydraulic structures and others. Due to the fact that the economical activity in the country is concentrated to the southern zone, the basic experience of construction and behaviour of structures is mostly based on practice in a relatively milder climate.

Because of the growing interest in cold regions engineering and the problems reported in the North, a development project was established to study the character and degree of the problems caused at the roads by extreme climatic conditions in Finland. This study was started with a general study on the problems involved in road construction and maintenance in Northern Lapland in 1985. The initiative and financial support were given by the Finnish Roads and Waterways Administration (TVH) and the Road District of Lapland. One responsible participant in the project was VTT, Geotechnical laboratory, which was responsible for the frost investigations and frost engineering design in the project, and other participants were the Road District of Lapland, which was responsible for site investigations, test construction and the monitoring of the behaviour of test structures, and Consulting Engineers Viatek Oy, which was responsible for the planning and road engineering design of the structures.

The goals of the project were to produce methods for road reconstruction feasible in these conditions to be used as a technical basis in the north, and to apply the modern cold regions engineering approach in the solution of these specific problems. From this point of view, if carried out on exact methods of analysis, the experience gained might be used to develop structures in other cold zones as well for the more southern zones as in the permafrost zone.

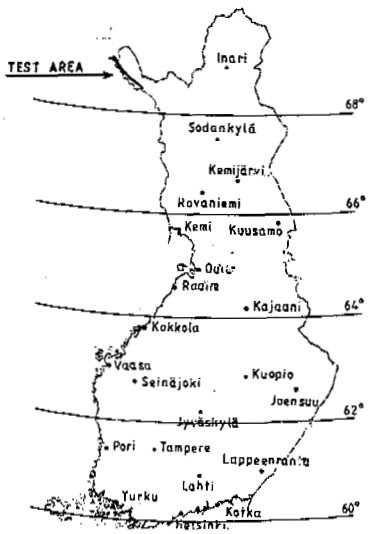

Fig. 1. Location of the investigation area.

2. PROBLEMS CAUSED BY THE COLD CLIMATE

According to the reports from the local road maintenance organization and the observations along the road line, some typical problems were found (Saarelainen & Vaskelainen 1986):

- excessive snow accumulation and snowdrift,
- aufeis formation due to the freezing of ground water and surface runoff at the road
- excessive uneven frost heave
- thaw settlement and damages of pavement on local palsa mounds (sporadic permafrost)
- slope slides at steep fjell slopes.

Most of the problems are connected to low winter temperatures. Some of the problematic processes are found in unconstructed terrain (palsas, ice formations, snow) while some problems result from human activity (frost heave, snow accumulation, slope processes, icing caused by frozen road embankment etc.). They are considered problems because of maintenance effort and costs.

Some problems arise in connection with strength losses of construction materials due to freezing. Some minerals expand when freezing, resulting in structural changes in the material, and a loss of strength.

3. PRINCIPLES OF THE TREATMENT OF THE PROBLEMS AND TEST CONSTRUCTION

3.1. Permafrost

Palsas were found generally at wetlands with peat cover along the road line (Fig 2). The palsa formation is caused by the difference in thermal conductivity of frozen and unfrozen surface peat, which eliminates the heating effect of solar radiation in summer on peatlands, and thus causes permafrost process at zones of mean annual air temperature close to -0 ^{o}C (e.g. Seppälä 1985, Keyser et al. 1984).

At the studied section of the highway two locations were found, where permafrost was underlying the road embankment. At these locations the road has originally been built on frozen ground with conventional methods, without any special measures due to the permafrost. The original route was a modest pathway, which was improved for car traffic during the World War II, and it was paved with emulsion pavement in the beginning of 60'ies. During the test construction it was found out that the road had suffered thaw settlement after paving about 1.8 m, which can be read from the successive repair pavement layers up to the total thickness of 1.8 m. During the soil investigations, laboratory tests on undisturbed samples of underlying, permanently frozen peat showed a total thaw compression of 70 % under overburden pressure. Roughly these figures show a mean annual thaw settlement about 60 - 70 mm, and mean annual thaw about 100 mm. The length of the palsa section was about 100 m, and the depth of the frozen core was 7 - 8 m.

Fig. 2. The palsa mound at Peera.

As to the principle of test construction it was decided to keep the permafrost in frozen state. This was realized by increasing the thermal resistance of the embankment with insulation above the frozen core, to minimize the heat exchange with the atmosphere, and to minimize the heat effect of solar radiation by using light-coloured pavement aggregate (white quartzite) to prevent the rise of surface temperature in summer. The design was based on thermal computer analysis considering actual material properties, limit conditions and the cycle of seasonal mean temperatures. As a result it was stated that the thickness of the insulation must be at least 100 mm to prevent thaw front from penetrating through the constructed layers into ice-rich subgrade (ADINA-T, Helander 1985). The time span of the analysis was 4 years (Fig. 3).

The test construction was started with the removal of old pavement in November 1986. The surface was kept snowless over the winter, and the insulated structure was constructed in April 1987. At the stage of construction the underlying active layer was observed to be frozen to the permafrost table. The completion of the road profile was carried in summer 1987 including the profiling of the slopes with peat and the construction of the new pavement. The structure is actually under monitoring of thaw depth, temperatures, frost heaves, settlements etc.

Comparing with the conventional solution of excavation and filling, the test structure was evaluated to save building costs under these conditions about 50 %. If the earlier observed settlement process is eliminated, the reduction in future maintenance and repair is expected to be remarkable.

3.2. Seasonal frost

On dry land areas at the site the ground freezes annually under the snow cover to the depth of 1-1,5 m. In the snowless areas the freezing depth may reach up to 2,5 - 3 m. The possibility of perennial frost is evident, because the variations of climate are rather considerable at these locations. At least according to the frost depth and temperature

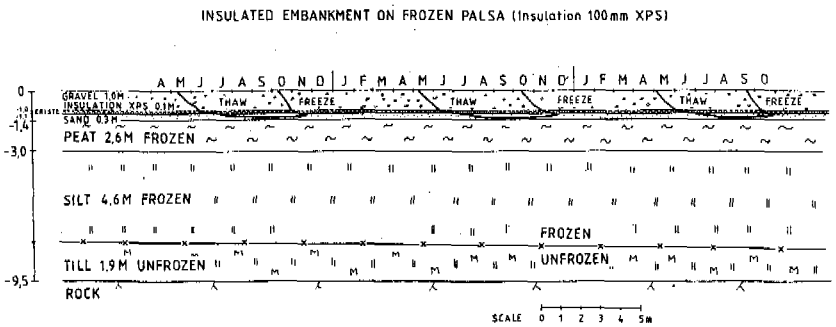

Fig. 3. Calculated seasonal thaw of the structure in Peera.

measurements in summer 1986, it can be supposed that the perennial frost was probable. The frost heave at the locations investigated was ranging between 0-270 mm with a considerable variation. The damages of pavement were found to concentrate at locations where the relative deflection of the pavement was larger than about 10 pro mille. The damages were mainly individual or systematic cracks and unevenness of the surface, and in minor amount netwise cracking, which is indicating loss in bearing capacity of the road structure.

The subgrade at the locations of problematic frost heave consisted mainly of alluvial or glaciolacustrine silts, sedimented in the depressions of the terrain and overlain with peat cover. The ratio between the frost heave and corresponding thickness of the frozen, frost susceptible soil was about 0,1-0,15. The segregation potential of the subgrade (Konrad & Morgenstern, 1981), determined by back-calculation on observed frost heave and frost depth was of the order of 4-5 mm^2/Kh. The analysis was carried out with a computer program based on the thermal balance at the freezing front, which takes into account besides real material properties, also the heat flow through the frozen layer, the heat release in in-situ freezing and frost heave and heat flow from underlying ground (Saarelainen 1987). In laboratory frost heave tests, the segregation potential was determined on a procedure similar to that of Konrad (Konrad & Morgenstern 1981), and the segregation potential was varying between 6,5-1,5 mm2/Kh when the load on the sample varied between 0-50 kPa. The same order of magnitude can be observed.

The test structure was designed on the basis of observed behaviour using the one dimensional program described above, with the maximum design frost heave of 50-70 mm, that can occur due to climatic variations once in ten years. The allowable design value is based on an asphalt pavement damage mapping earlier in Eastern Finland (VTT, 1984).

At Peera, the structural layers were compiled according to the principle of testing the usability of the local, abundantly present, slightly frost susceptible till. The till contains fines (fraction <0,074 mm) about 30 %, fraction <0,02 mm about 15 %, and practically no clay). For comparison, a section with full height gravel embankment was also constructed. (Figs. 4, 5). The capillary rise from beneath to the till was cut by 0,5 m thick isolation layer of gravel. To test the effect of the capillary cut on frost heave, the isolation was not constructed at one till fill section. The road structure was designed according to the Finnish road design guidelines (TVH, 1985) to reach reasonable bearing capacity at the pavement surface.

These test sections were constructed at Peera in August-October 1986. The monitoring of frost penetration and frost heave of the embankment, and the variation of moisture content and density of the materials in situ is carried out at two locations at each test section. The bearing capacity of the local till layer and the subgrade can be measured during thaw by loading plates installed in the embankment. According to the preliminary measurements, the frost heave varied in winter 1986-87 between 20-50 mm, when the frost index at the site corresponded to design winter (ca. 50 000 Kh; maximum in 10 years). According to the test loadings, the modulus of bearing capacity for the till corresponded with the values of non frost susceptible till, about 35 MPa.

Test construction has been continued at another section in summer 1987, and there the main emphasis has been to test different frost insulation structures. Besides the structures of local till and gravel, insulation has been constructed using extruded polystyrene, locally sprayed polyurethane, predrained and -compressed peat and local peat. In addition, the influence of artificial, geotextile-based capillary cut layer is investigated. The frost design has been carried out on the same procedure as that at Peera. The test structures are monitored in winter 1987-88.

3.3. Icing

The icing has been reported at sites, where the ground water flow from upper terrain has frozen at the upper slope of the road, and due to long freezing period, it has caused the risk of freezing of water flow to the pavement. The main reason seems to be the fact that the ground water flows through the road line during the warm season; during winter, the flow is dammed and forced to the surface due to the impermeable, frozen road base. In principle,

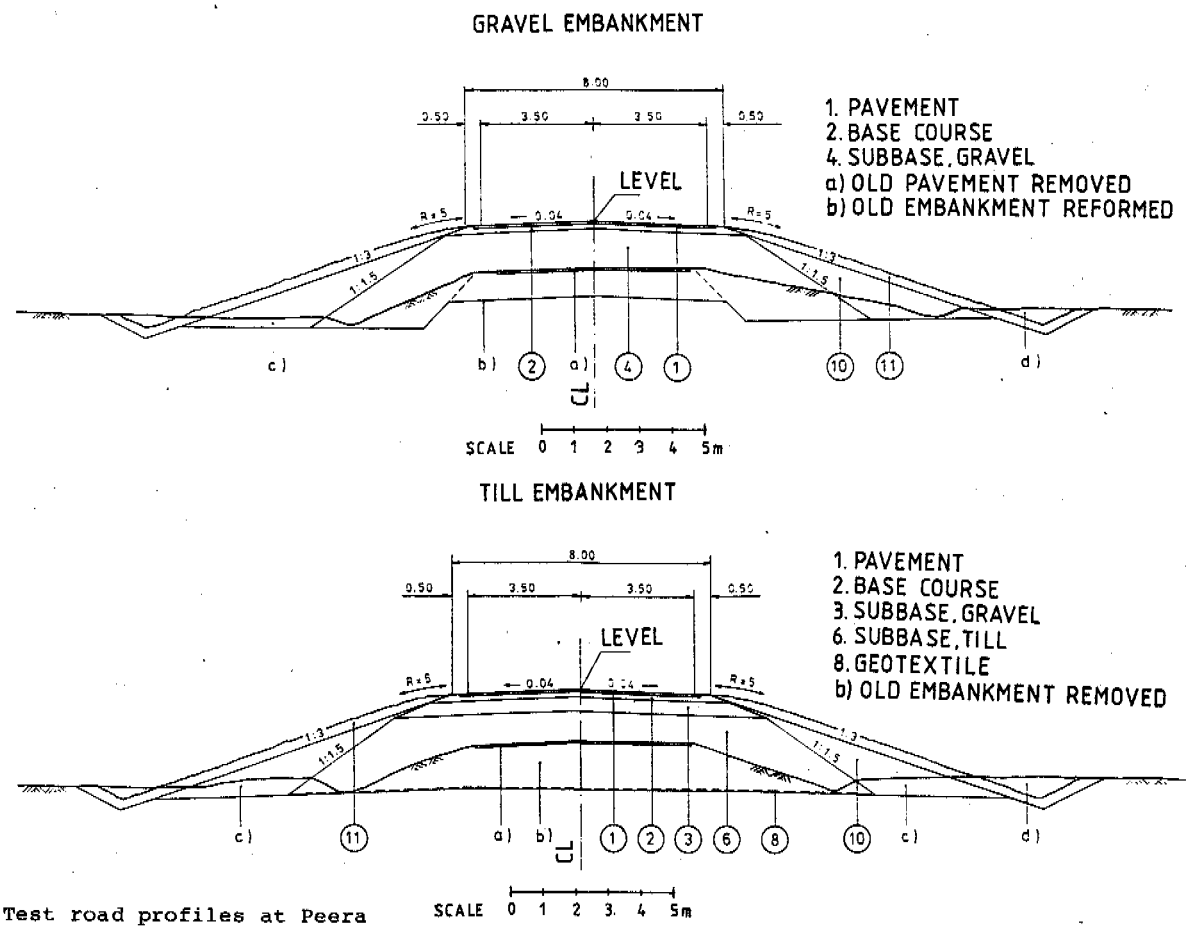

Fig. 4. Test road profiles at Peera

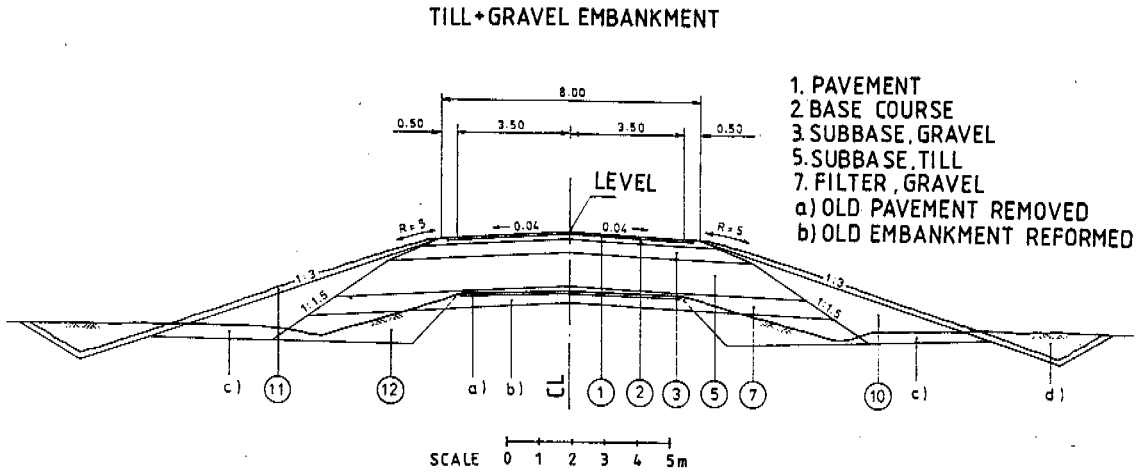

Fig. 5. Till embankment with gravel isolation.

the problem results from the inefficient winter drainage of the road. In the road district of Lapland there was carried out a study about the remedial maintenance measures against the icing, and in this study were listed different methods to prevent the freezing of culverts. Most of these seemed to be of temporary value, because they caused seasonal operation on the road line (insulation of the culvert ends, covers on the inflow, use of various thawing techniques etc).

After the local investigation, the following diagnosis could be made: the problems are basically caused by the ground water flow in winter at and across the road. The feasible solutions should include the maintaining of

positive temperature of the ground water flow across the road. This can be ensured by a winter culvert that should be kept unfrozen at frost free depth or by thermal insulation. The ground water should be collected in drains at upper terrain at a frost free depth and led to the winter culvert. The snowmelt that is the hydraulic design parameter, flows through the original large culvert. This is in spring time open and empty, if the winter flow is led via the winter culvert. The basic problem involved is to catch the ground water in the terrain before freezing and to let it cross through the road line unfrozen. The design should consider the frost depth under the snow cover in upper terrain, and the frost free depth and hydraulic design of the winter culvert.

This technique has been tested in 1986 at one location of ground water icing, and at one location of river icing. The structures needed proved to be relatively cheap, and according to the observation in winter 1986-87 they seemed to be effective, too.

Test construction was continued in summer 1987 at two other sites applying similar approach, but applying different drainage structures (i.e. vertical drainage mats instead of tubular drains). The behaviour will be monitored at least one winter to control the effect.

3.4 Snow control

The areas with snow problems are located at open tundra terrain, where the snow can flow freely with the eroding wind. According to literature information, the snow erosion starts as the wind velocity exceeds about 5 m/s, and it increases roughly proportional to the cubic of wind velocity (Galuzin 1980). The accumulation of snow, and the snow depth depends on the relative level of the location in reference to the surroundings.

The principle of design according to the snow depth is based on the finding that there is a reasonable correlation of snow depth at a location with snow depth at the closest climatic station with long term observations on snow depth variation (Bjalobzenskij 1983, Kuusisto 1984). Knowing the maximum depth at the location under study, the probability distribution of local snow depth can be constructed. In this manner it is possible to construct on a selected road line the design snow depth profile occurring at a certain probability, if the observations about maximum snow depth in one observation winter are available from the line in question. The design involves setting the level of the road above this level. If it is not technically possible, the snow accumulation can be limited with the aerodynamic form of the road profile, smooth cutting etc (e.g. Norem 1975).

The principle was tested at one problematic section. The snow depth was measured in a perpendicular profile with the observations of wind direction and speed at one point, and in a terrain profile along the road line (Fig. 6). According to the measurements and comparison with the observation series at the climatic stations at Kilpisjärvi and Muonio in Finland, it could be seen that the winter 1985-86 corresponded, considering the snow depth, to a winter repeated once in 10 years, and thus the observed snow depth profile is a representative design profile. At the test section this means an average snow depth of 800 mm, with local maximums up to 1200 mm.

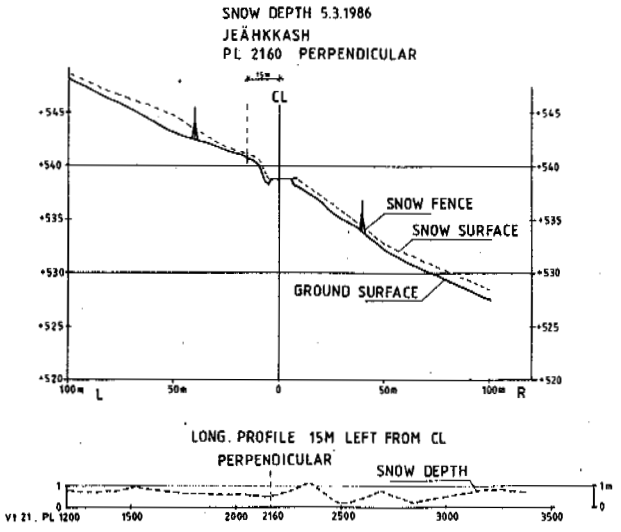

Fig. 6. The observed snow profile at Jeähkkash.

The test section was raised from the natural surface above the design level (Fig. 7). At one part it was not possible to keep the level proper due to a local mound, and here the road was cut to the hill side. the perpendicular profile was formed smooth with long slopes of 20 %. The shoulders of the embankment were rounded with a radius of 2 times the embankment height according to the Norwegian road design guidelines (Norem 1975).

The test section was constructed in summer 1987 with the length 800 m. The development of snow conditions, winds and the need of snow removal will be monitored over the coming winter to control the effect of the test design. The goal is to get rid of the snow fences earlier necessary on the line.

4. CONCLUDING REMARKS

The problems arising at a road line due to cold climate can be solved applying a sound thermodynamic approach. The applicability of the solutions depends strongly on the validity of design data about the local ground conditions, and the diagnosis about the reasons of the processes involved. In this study, the methods of design are of prototypic character, and in order meet to other climatic conditions, certain technical development must be applied to improve the economy of the solution and structures. It is evident, anyhow, that the basis of design can be used to solve similar problems in other parts of Northern Finland.

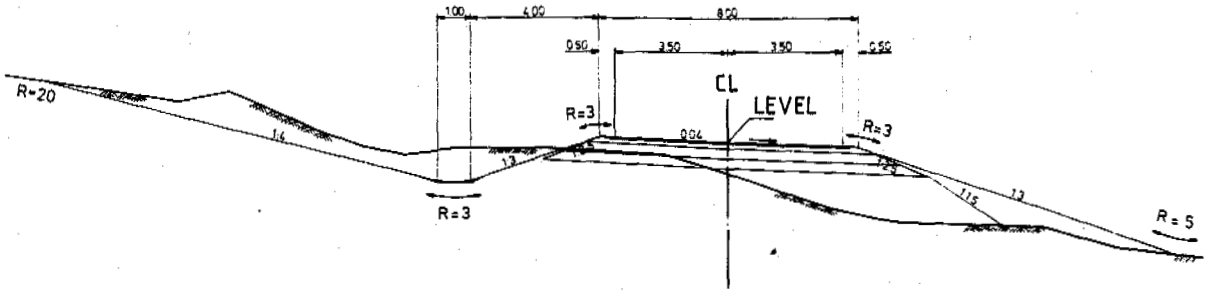

Fig. 7. The typical profile of the test road at Jeähkkash.

Because these problems can be recognized also in southern areas, the reasons may be of similar nature, but due to the different scale, the practical solutions that are effective enough, may be different. The design of structures in a cold climate must consider the winter behavior of structures more consciously than is being done today in the seasonal frost zone. In this respect the exchange of experience with the specialists of construction on permafrost might be fruitful. The soils are common, and the physical processes are in many cases similar. Difficulties lie mostly in proper techniques of investigations, and in the validity of the design models for the problems to be solved.

5. REFERENCES

Bjalobzenskij, G.V., Determination of snow cover thickness in the design of snow accumulation at road embankments (in Russian). Avtomobilnye dorogi (1983), No.10.

Galuzin V.M (ed.), Construction of streets in Northern conditions (in Russian). Strojizdat, Leningrad 1980. 136 p.

Helander R., The calculations for the thermal design of ground (in Finnish). Helsinki 1986. RIL, Publication K66-1986, p.23-66.

Keyser A., Hode J. & Laforte M.A., Road construction in palsa fields. Washington D.C. 1984. Transportation research record 978, p. 26-36.

Konrad J-M. & Morgenstern N.R., The segregation potential of a freezing soil. Canadian Geotechnical Journal, Vol. 18 (1981), p. 482-491.

Kuusisto E., Snow accumulation and snowmelt in Finland. Helsinki 1984. Vesihallitus, Publication 55. 149 p.

Norem H., Lokalisering og utforming av veger i drivsnoe-omrlder. Oslo 1975. Statens vegvesen, Veglaboratoriet, Meddelelse Nr. 49, s. 19-31.

Saarelainen S., Estimation model for evaluation of frost depth and frost heave (in Finnish). Helsinki 1987. RIL, Publication K78-1987, p.205-210.

Saarelainen S. & Vaskelainen J., Special problems in arctic road construction and maintenance in Finland. Proc Int Symp. CIB on Industrial planning, engineering and construction under extreme circumstances, Espoo, Finland May 19-23, 1986, pp.171-181.

Seppälä M., Palsa report (in Finnish). Preliminary work draft for the Arctic road-project 1985 (unpublished).

TVH Road structure (in Finnish). Helsinki 1985. The Finnish Roads and Waterways Administration, Instructions for the planning and design of roads, File B, Part IV.

VTT, 1984. The frost investigation at Karsikko and Opotta in Joensuu, Finland. VTT, Geotechnical laboratory, and Road and traffic laboratory, Espoo 1984 (unpublished).

SOME ASPECTS OF FREEZING THE ICE PLATFORMS

B.A. Saveliev[1] and D.A. Latalin[2]

[1]Research Institute of Engineering Site Investigations, Moscow, USSR
[2]Research Institute of Constructing Main Pipings, Moscow, USSR

SYNOPSIS A contemporary state of the problem of freezing the artificial ice platforms is elucidated. Special attention is given to the methods of calculating an artificial freezing of ice as well as to that of designing the artificial structures assuming their long-term operation.

One of the promising trends related to making a safe base to support drilling operations at the Arctic shelf is that of construction of artificial ice platforms allowing for their long-term operation. The experience in the USSR and abroad in application of large ice-soil masses as engineering structures enables to consider their wide application to be quite practicable (Saveliev et al., 1983; Latalin, Gagarin, 1984). Temporary platforms to support drilling operations are used by some firms in Canada and US (Cox, 1979; Ekelund, Masterson, 1981; Ice Platforms, 1974) but notwithstanding the progress achieved their application is presently limited for the purpose of exploration drilling and impossible for that of oil and gas exploitation due to a short-term period of operation.

A structure of ice and frozen ground which is constructed in Arctic regions should meet a number of requirements. Ice used as a building material should be sound and the structure should congeal to the reservoir bottom so that ice movements or flows might not transfer it somewhere else. The structure should be durable enough and the length of its existence period should not be limited by only a winter period.

Physico-mechanical properties of ice and its composition are governed by thermodynamic conditions of its formation. Therefore, all the methods to build-up the ice can be divided into three groups: successive flooding of layers of water, drop spraying and volume freezing of a water medium.

When freezing the ice by thin layers or by drop spraying the water the system "ice-brine" is somewhat of a closed type by its parameters. Generation and growth of crystals of fresh ice will result in an increase in brine salinity which cannot be eliminated with mass transfer. The ice produced will either contain a large amount of brine of higher concentration or possess a significant open porosity under drained conditions. Nevertheless, successive flooding and freezing of layers of water is one of the most efficient methods of producing an artificial ice. By successive flooding and freezing of layers of water a temperature condition of an artificial ice mass is affected by a number of factors main of which should be considered as follows: a rate of heat loss through cooling and freezing of a flooded water layer of a particular thickness towards the atmosphere and underlying ice mass as well as a time period and rate of cooling a frozen ice layer and underlying ice mass.

To build-up an ice mass with a pre-set temperature during the shortest time possible one should find an optimal combination of the given factors.

The formation of an ice mass by successive flooding and freezing of water layers of a particular thickness at its top surface is performed in two stages (Latalin, 1986).

1. Cooling of a frozen water layer and the whole of previously built-up ice mass consisting of i-layers during a time period, $\Delta\tau$ (Fig. 1).

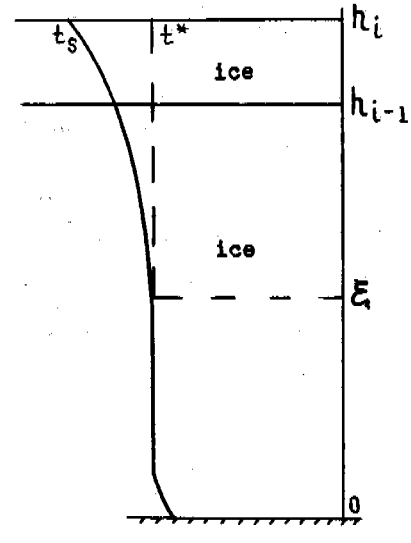

Fig.1 Temperature curve for a period of cooling an ice layer on an ice cover

2. Freezing of a water layer of $\Delta h = h_{i+1} - h_i$ thick flooded at an ice base of h_i thick (Fig. 2).

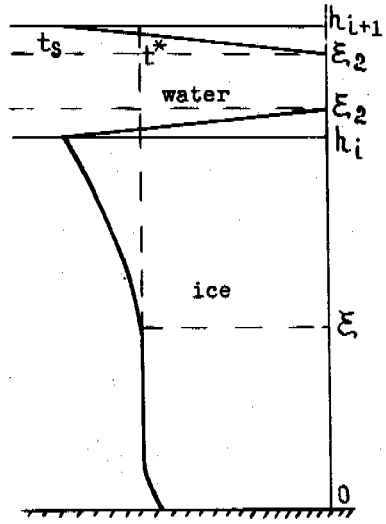

Fig.2 Temperature Curve for a Period of Freezing a Water Layer on an Ice Cover.

With a number of assumption the problem of flooding and freezing of water layers on an ice mass can be reduced to solution of the following two boundary problems:

I. $$\frac{\partial t_I}{\partial \tau} = a_I \frac{\partial^2 t_I}{\partial x^2}, \quad x \in [0, h_i], \quad i=\overline{1,n} \quad (1)$$
$$\tau \in [\tau_j, \tau_{j+1}]$$

$$t_I(x,0) = t_I(x) \quad (2)$$

$$t_I(h_i, \tau) = t_s \quad (3)$$

$$\lambda_I \operatorname{grad} t_I\Big|_{x=0} = 0 \quad (4)$$

II. $$\frac{\partial t_I}{\partial \tau} = a_I \frac{\partial^2 t_I}{\partial x^2}, \quad x \in [\xi_2, h_{i+1}]$$
$$\tau \in [\tau_{j+1}, \tau_{j+1} + \tau_\xi] \quad (5)$$

$$\frac{\partial t_I}{\partial \tau} = a_I \frac{\partial^2 t_I}{\partial x^2}, \quad x \in [0, h_1 + \xi_1] \quad (6)$$
$$\tau \in [\tau_{j+1}, \tau_{j+1} + \tau_\xi]$$

$$t_I(x,0) = 0 \quad (7)$$

$$\frac{\partial t_w}{\partial \tau} = a_w \frac{\partial^2 t_w}{\partial x^2}, \quad x \in [\xi_1, \xi_2] \quad (8)$$
$$\tau \in [\tau_{j+1}, \tau_{j+1} + \tau_\xi]$$

$$t_w(x,0) = 0 \quad (9)$$

$$\rho L \frac{d\xi}{d\tau} = \lambda_I \operatorname{grad} t_I\Big|_{\xi_1} \quad (10)$$

$$\rho L \frac{d\xi}{d\tau} = \lambda_I \operatorname{grad} t_I\Big|_{\xi_2} \quad (11)$$

$$t_I(\xi_j, \tau) = t_w(\xi_j, \tau) = 0, \; j = 1,2 \quad (12)$$

$$t_I(h_{i+1}, \tau) = t_s \quad (13)$$

$$\lambda_I \operatorname{grad} t_I\Big|_{x=0} = 0 \quad (14)$$

Here t_I - ice temperature; t_w - water temperature; t_s - temperature at the surface of the built-up ice; a_I - thermal diffusivity of ice; a_w - thermal diffusivity of water; L - heat of water-ice transformation; ξ_1, ξ_2 - position of a solidification front.

The above problem has been solved numerically using a finite difference method. Thermophysical properties of water and ice shown in Table 1 have been used for calculation. We have calculated temperature of an ice mass 1 m thick through flooding and freezing by layers of 0.01 m (100 layers), 0.02 m(50 layers), 0.03 m (33 layers), 0.04 m(25 layers), 0.05 m (20 layers) and during a total time period of cooling the ice massif being 25, 50 and 100 hours.

Table 1

Thermophysical Properties of Water and Ice Used in Calculations

Properties of water and ice	Water	Ice
Heat of water-ice transformation, kJ/m^3	336000	336000
Heat capacity per unit volume, kJ/(m^3.K)	4330	2090
Thermal conductivity, W/(m.K)	0.60	2.22

A surface temperature has been taken equal to -30°C. The results of simulation are tabulated in Table II. As seen from the table an average temperature of the ice mass decreases with an increase in a time period of cooling of frozen layers and increases with an increase in thickness of flooded layers. In practical work one can always select such a condition of flooding and freezing of water layers that an ice mass of a particular thickness and pre-set temperature be built-up during the shortest time possible.

The artificial structure having been built-up, the stability and length of its existence period depend on upkeeping a particular temperature condition. The temperature condition of the artificial ice-soil platform has been calculated using a finite element method (FEM). The method involves a substitution of a continuous function (in this very case - temperature) by a discrete model that is formed by a lot of piecewise-continuous functions determined from the finite number of elements.

Table II

Simulation Findings

Total length of cooling, hour	Thickness of layer, m / Number of layers	0.01 / 100	0.02 / 50	0.03 / 33	0.04 / 25	0.05 / 20
25	Length of cooling a layer, hour	0.25	0.5	0.75	1.0	1.25
	Average temperature, °C	-24.8	-12.2	-5.2	-4.6	-2.9
	Length of flooding and freezing cycle, hour	26.5	29.8	32.6	35.4	38.1
50	Length of cooling a layer, hour	0.5	1.0	1.5	2.0	2.5
	Average temperature, °C	-27.1	-18.1	-9.6	-7.7	-4.8
	Length of flooding and freezing cycle, hour	51.0	53.3	55.3	58.0	60.2
100	Length of cooling a layer, hour	1.0	2.0	3.0	4.0	5.0
	Average temperature, °C	-28.5	-23.0	-14.8	-12.5	-7.9
	Length of flooding and freezing cycle hour	100.0	100.8	101.8	103.2	104.8

Nodal values of temperature are so selected that the best approximation to its true distribution be ensured which is achieved by minimizing the functional related to the heat conduction differential equation. The process of minimizing is reduced to solving a system of linear algebraic equations relative to the nodal values.

A temperature profile of the artificial ice-soil structure is described by the heat conduction non-equilibrium equation

$$c\rho \frac{\partial t}{\partial \tau} = \frac{\partial}{\partial x}(\lambda \frac{\partial t}{\partial x}) + \frac{\partial}{\partial y}(\lambda \frac{\partial t}{\partial y}) + Q \; ; x, Y \in D \qquad (15)$$

provided that

$$\lambda \frac{\partial t}{\partial x} + \lambda \frac{\partial t}{\partial y} + q + \alpha (t - t_s) = 0 \qquad (16)$$

at G boundary

where t - temperature, τ - time, λ (X,Y) - thermal conductivity, C(X,Y) - heat capacity, ρ (X, Y) - density, α (τ) - coefficient of convective heat exchange, q(τ) - heat flux, t_s(τ) - surface temperature, Q (X,Y, τ) - heat sources.

Introducing a heat content (enthalpy) function:

$$H(t,X,Y) = \int_0^t (C(\theta)\rho + \rho L \delta(\theta - t^*)) d\theta \qquad (17)$$

where δ (θ - t*) - Dirac delta function

t* - phase transformation temperature.

The heat content function has a break in going through a temperature of phase transition, t*. Therefore for solving the problem a procedure of smoothing the heat content function about a certain critical temperature is carried out proceeding from the requirements of existence and continuity of the first and second temperature derivatives of the heat content functions.

The smoothing procedure having been employed, eqn. (15) takes the form:

$$\tilde{H}' \frac{\partial t}{\partial \tau} = \frac{\partial}{\partial x}(\lambda \frac{\partial t}{\partial x}) + \frac{\partial}{\partial y}(\lambda \frac{\partial t}{\partial y}), \quad x,y \in D \qquad (18)$$

The procedure of minimizing the functional related to differential equation (18) and boundary conditions (16) results in the following matrix equation (Zenkevich, 1975):

$$[K]\{T\} + [c]\left\{\frac{\partial T}{\partial \tau}\right\} + \{F\} = 0 \qquad (19)$$

where [K], [c], {F} are to be composed of element matrixes of the shape:

$$K_{ij} = \sum \lambda \iint_S \left(\frac{\partial N_i}{\partial x}\frac{\partial N_j}{\partial x} + \frac{\partial N_i}{\partial y}\frac{\partial N_j}{\partial y}\right) dD \qquad (20)$$

$$C_{ij} = \sum \iint_S N_i \tilde{H}' N_j \, dD \qquad (21)$$

$$F_i = \sum \int_l N_i (q - \alpha t_s) dG - \sum \iint_S N_i Q \, dD \qquad (22)$$

where N_i, N_j - shape functions.

Time sampling of matrix equation (19) has been achieved by Krunk-Nicolson circuit.

Computer-aided calculations of the temperature condition of the artificial ice-soil platform has been made. Boundary conditions have been specified as follows (Fig.3). Near the upper boundary the heat losses towards the atmosphere (boundary condition of the third order) has been specified. In the lower part of the plat-

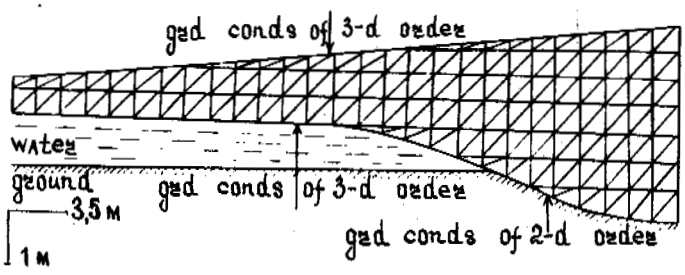

Fig.3 Dissection of the Region in Question into Finite Elements and Representation of Boundary Conditions.

form two boundary conditions have been specified, namely, the heat losses towards water (boundary condition of the third order) - at the contact of the platform and marine water and the geothermal heat flux (boundary condition of the second order) - at the contact of the structure and the sea bottom. Fig. 4 shows the results of numerical simulation of the heat condition of the ice-soil platform through initial distribution of the temperature obtained by the data of field investigations (Latalin, Gagarin, 1984). Results of numerical simulation enable to select such a temperature condition of the ice-soil structure that its heat stability during the most unfavourable periods of operation be ensured.

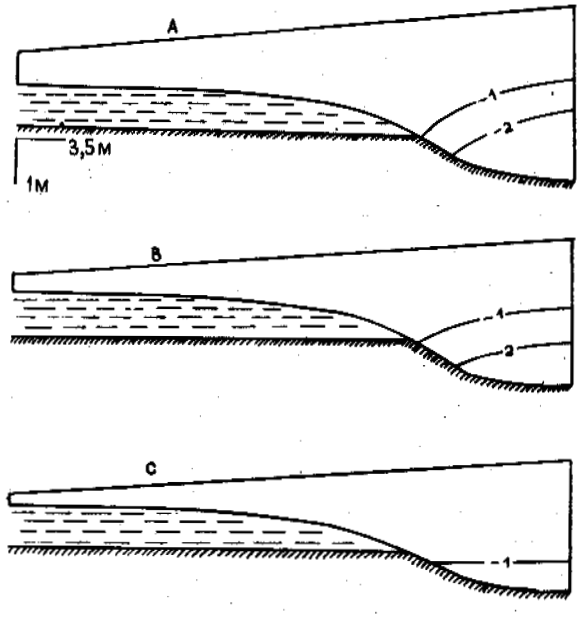

Fig.4 Prediction of the Temperature Condition of an Ice-Soil Platform.
A. - initial temperature
B. - position of isothermal lines in a month's time
C. - the same in two month's time.

REFERENCES

Zenkevich O. (1975). Metod konechnykh elementov v tekhnike. Moscow.

Latalin, D.A., Gagarin, V.E. (1984). Inzhenerno-glyatsiologicheskie aspekty sozdaniya iskusstvennykh ledyanykh platform v Arctike. Kn. "Inzhenerno-geocriologicheskie issledovaniya", 48-52, Yakutsk.

Latalin D.A. (1986). Ob optimizatsii posloinogo namorazhivaniya lida. Materialy glyatsiologicheskikh issledovanij. Khronika, obsuzhdeniya, N 55, 222-225, Moscow.

Saveliev, B.A., Latalin D.A., Gagarin V.E. et al. (1982). Sozdanie ledyanykh platform na arkticheskom shelife Materialy glyatsiologicheskikh issledovanij. Khronika, obsuzhdeniya, N 45, 166-168, Moscow.

Saveliev B.A., Gagarin V.E., Zykov Yu.D. et al. (1983). Fiziko-khimicheskie aspekty sozdaniya iskusstvennykh ledyanykh sooruzhenii iz morskoi vody. Kn. Problemy geokriologii, 113-118, Moscow.

Saveliev B.A., Latalin D.A. (1986). Iskusstvennye ledyanye platformy. "Okeanologiya", t.7, 191 p., Moscow

Cox G.F.W. (1979). Artificial ice island for exploratory drilling. 5-th Int. Conf. Port and Ocean Eng. Arctic Conditions, v.1, p.147-162. Norw.

Ekelund M.I., Masterson D.M. (1981). Floating Ice Platforms for Oil Exploration in the Arctic Islands. Arctic, v.33, N 1, p.168-183.

Ice Platforms, Subsea Methods Used for Arctic Ocean Well. (1974). World Oil, v. 179, N 1, p. 79-82.

SLOPE STABILITY IN ARCTIC COAL MINES

A.K. Sinha, M. Sengupta and T.C. Kinney

University of Alaska Fairbanks

SYNOPSIS: Permafrost soil slopes in arctic mines are susceptible to thaw induced instability. Such instability may jeopardize the safe working conditions of an open pit mine. The instability may also inhibit the safe operation of heavy machinery used in surface mining.

It has been demonstrated that covering the slopes with a suitable insulation material reduces or completely eliminates thawing of the soil slope. An approach for the calculation of the thermal conductivity of the insulation and its thickness is presented.

INTRODUCTION

Traditional slope stability analysis for a surface coal mine involves considerations of local geology, geotechnical properties of slope materials, groundwater condition and dynamic destabilizing forces that may influence the slope.

In arctic regions, however, the geotechnical engineer is faced with added complexities. Frozen ground adds another dimension to slope stability calculations. Frozen ground, consisting of natural earth materials may creep under its own weight as well as under externally applied loads. Due to surface disturbances, changing slope geometry, and thermal regime modifications, frozen ground may undergo thermal degradation and a mass movement may in turn lead to slope failure. Such movements in frozen soils have been reported by several investigators (McRoberts, 1978; Phukan, 1985).

STABILITY OF FROZEN SLOPES

The frozen rock and frozen soil slopes lend themselves to a limiting equilibrium analysis in context of mobilized strength of frozen ground and of tolerable deformation in terms of creep behavior just like slopes in temperate regions.

The strength characteristics of frozen soils depend primarily on the soil type, temperature, ice content, and strain rate.

Frozen soils exhibit creep behavior even at low stress levels at rates dependent upon ice content, temperature, and applied load. Generally, the creep behavior of ice-rich frozen soils is dominated by secondary creep with a short time interval for the primary creep. Ice-poor frozen soils may exhibit only primary creep.

STABILITY OF THAWING SLOPES

An infinite slope analysis approach may be applied to thawing slopes because the failure plane is approximately parallel to the surface of the slope. This approach is applicable to shallow instability problems, such as solifluction and bimodal flows. The factor of safety of such a slope has been discussed by Phukan (1985).

Thaw-Consolidation is a process where excess pore pressures are developed in soils upon thawing and subsequent consolidation. It can lead to slope instability and ground settlements. Solifluction and skin flow in permafrost slopes can be explained by the theory of thaw consolidation. The solution to some of the related problems has been presented by different researchers (McRoberts, 1978; Pufahl and Morgenstern, 1979).

PIT SLOPE STABILITY

For the stability analysis presented in this paper the open pit mining operation on the North Slope of Alaska in the area lying between Cape Lisburn, Point Lay, and Umiat, along the Colvile River, was selected (Paul, 1986). Three design alternatives were chosen using a finite element program as it allows:

(a). two-dimensional heat transfer modelling.
(b). simulation of multilayered systems, including rocks and insulation materials.
(c). surface energy balance calculations.

The strength of rocks change with temperature. Weathering may be induced due to exposure to repeated freeze-thaw cycles, but often rock slope stability can be investigated without detailed analysis of thawing if the rock has low porosity and low water content. However, rocks with high porosity and permeability may exhibit thermal characteristics similar to coarse grained soils and can be modelled accordingly.

Since, the rock in the area of concern is sandstone with high porosity, the slope model chosen for analysis consists of either fine grained or coarse grained soil. The classification of soil as fine and coarse, in this paper, is based on Kersten's thermal conductivity vs. water content charts Lunardini, 1981). The dry density of both fine and coarse grained soil was assumed to be 1281.49 Km/m^3 (80 lb./cft). Average published meteorolgical data for the environment of the area lying northeast of Cape Beaufort was used in the heat transfer calculation.

The criteria for choosing an insulation material are the thermal properties, the moisture absorption, and compressive strength, and the modulus of elasticity. Field and laboratory results indicate that extruded polystyrene (board type) has a combination of properties (viz. low thermal conductivity, low water absorption, and good performance in thaw/freeze cycles) that has made it more acceptable than other types of insulations in road embankment applications in Alaska (Olson, 1984). Expanded polystyrene has been successfully used as fill material as well as an insulating layer in Norway (Frydenlund, 1985).

Most of the insulation materials used for road embankments and slopes are either the formed in place type (e.g. urethane rigid Foam) or the board type (e.g. extruded polystrene boards).

Loose insulation materials such as cork, gravel, wood chips, etc. would limit the slope angle to their angle of repose, if spread out loosely on steep slopes, they may be contained in "geotextile bags", which in turn may be placed and anchored on the slope face. This process of using natural insulation material may, however, prove to be costlier than using synthetic insulation materials.

On steep slopes, insulation boards may be "sandwiched" between layers of geosynthetics to form insulation blankets which can be rolled down the steep slopes and anchored by gravel pad at the top and the bottom. A few long rock bolts may be required to firmly anchor the blankets to the slope face to avoid damage and swinging in high winds. Geosynthetics and laboratory results have shown that polyster geotextiles provided better performance under cold temperatures as compared to polypropylene type (Bell, et al., 1983).

RESULTS FROM THE GEODYNE MODEL

A two dimensional finite element model called GEODYNE was used to compute the thaw boundaries for both bare slopes and insulated slopes.

Bare Soil Slope

The slope, as shown in Figure 1, was considered to be a fine or coarse grained soil slope and the thaw depth penetration into the soil slope was calculated using GEODYNE. The slope is subjected to insulated boundaries on all sides, except for the slope faces exposed to air. This limitation of insulating boundary condition, assumed by the program unless a heat flux is mentioned for boundary conditions, is circumvented by choosing large slope dimensions.

Figure 2 illustrates the maximum thaw depth penetration at three different locations of the slope. All depths of thaw penetration are the maximum thaw depth for the summer season for the respective location.

The thaw depth in coarse grained soil is higher than that in the fine grained soil. This phenomena is due to the higher thermal conductivity of quartz, and other similar minerals, that dominate in a coarse grained soil, also, moisture content is higher in fine grained soils. As can be observed, the depth of thaw front penetration increases as the moisture content of the soil reduces.

Thus, the depth of penetration in the soil slope is from 0.61 m (2 ft.) to less than 1.2 m (4 ft.), the thaw depth being the highest along the sloping surface, depending on the soil type and the water content.

Insulated Slopes

The slope is assumed to be covered with certain thickness of insulation material, and the bench top and bottom are covered with a gravel pad to safeguard the insulation layer, (Figure 1). A 0.61 m (2 ft.) thick gravel layer was found satisfactory after considering the compressive strength of commercially available synthetic insulations and the potential compressive stress caused by a walking dragline of 25.23 m^3 (33 cu.yd.) bucket capacity.

The thermal conductivity of the insulations increases with the increase of water absorption by the insulation. In order to test the effectiveness of the insulation in the area of concern, a 0.076 m (3 inch) thick Polyurethane synthetic insulation was assumed to cover the slope surface. The properties of Polyurethane are tabulated in Appendix (1). The insulation layer water content has been raised from 0% to 400% and the thaw penetration calculated using GEODYNE. The results are shown in the Figure 3.

Figure 3 shows that a 0.076 m (3 inch) layer of insulation is sufficient to limit the thaw front from penetrating the soil slope even under extreme water absorption by the insulating layer. Along the sloping surface, the maximum depth of thaw is 0.074 m (0.24 ft.) (at 400% water content). As the insulation thickness is 0.076 m (0.25 ft.), the thaw front does not enter the soil.

Similarly, at locations A and C in the slope in Figure 4, maximum depth of thaw (at 400% water content) is about 0.65 m (2.13 ft.) below bench surface, whereas the combined thickness of the gravel pad and the insulation is 0.686 m (2.25 feet). Thus, the insulation limits the thaw front penetration in to the soil.

FIGURE:1

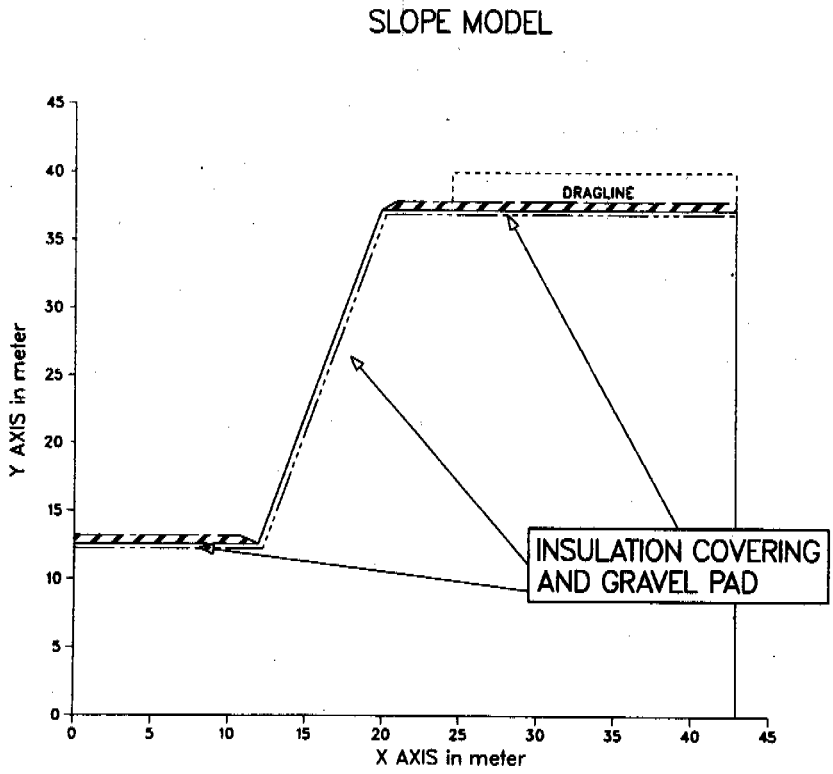

FIGURE:2

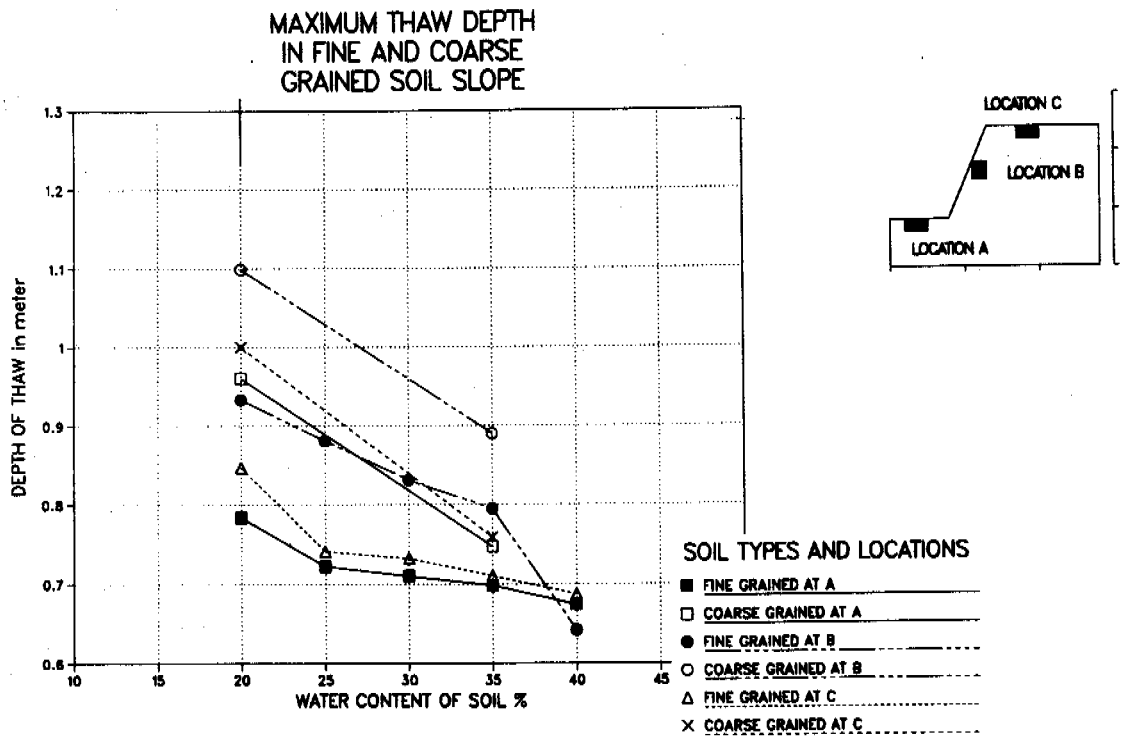

FIGURE: 3

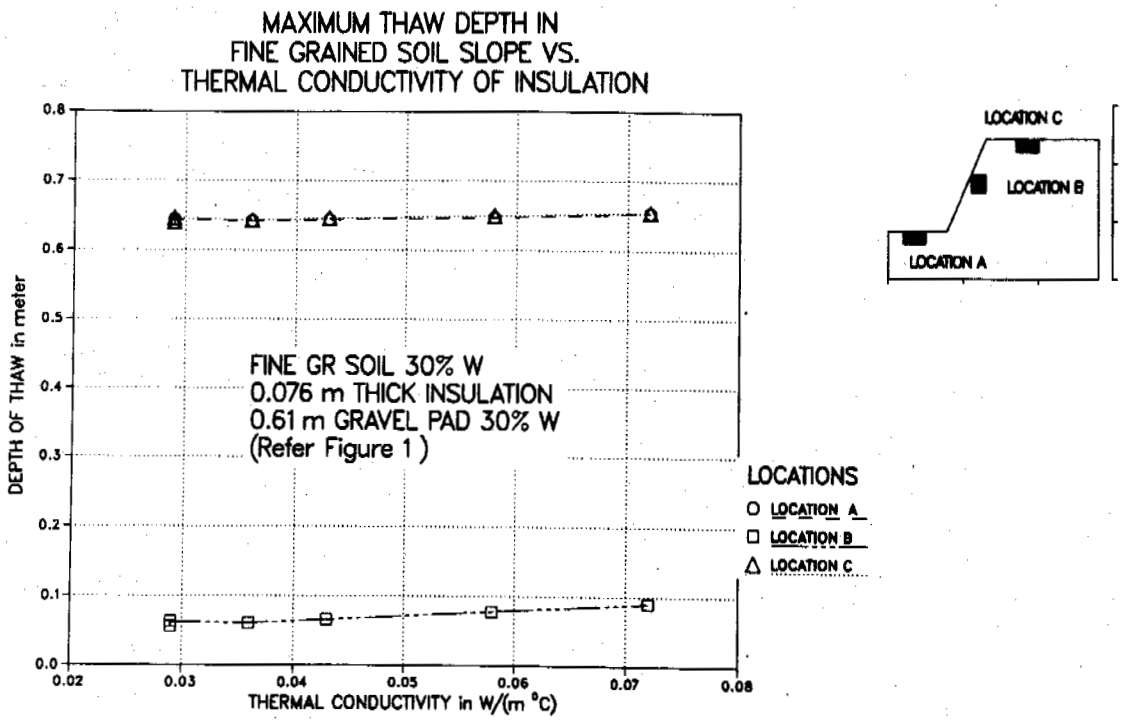

FIGURE:4

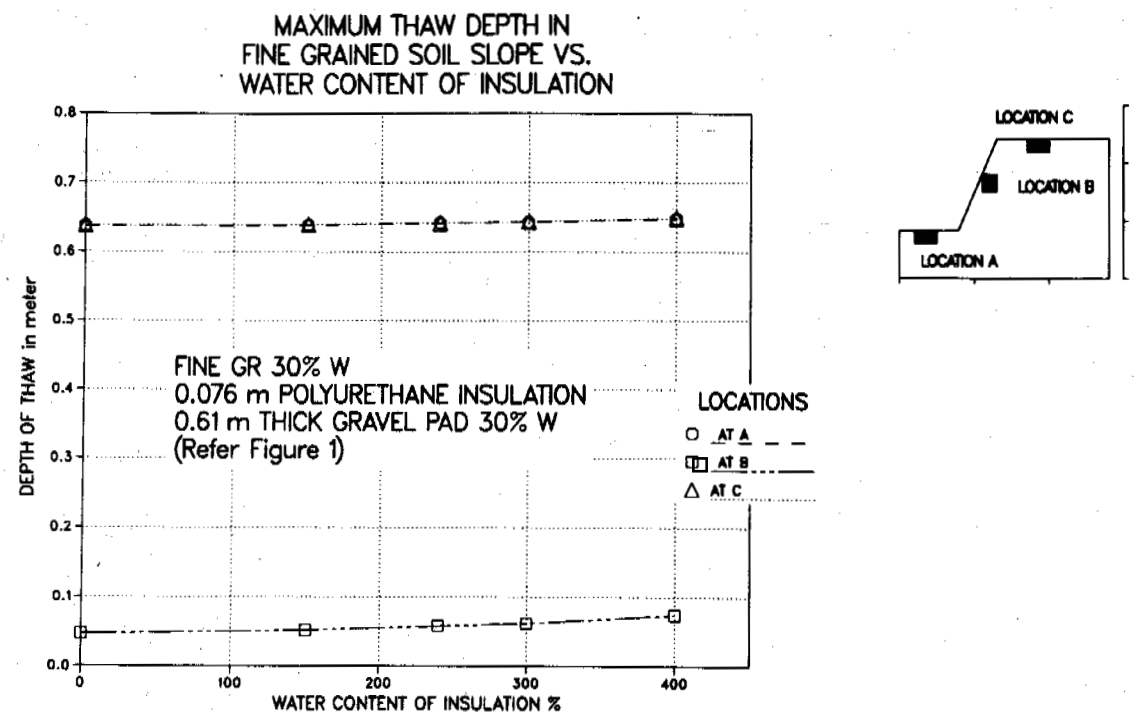

The thermal conductivity of the insulation layer forms another major design criterion. In order to determine a range of thermal conductivities suitable for the area of concern, insulation (water content 0%) with varying thermal conductivity was considered. The K value was raised from 0.0288 W/(m^{o}C) (0.20 Btu/sq.ft.-hr.-^{o}F) to 0.0722 W/(m^{o}C) (0.50 Btu/sq.ft.-hr-^{o}F). It might be observed that while a K value range of 0.0288 W/(m^{o}C) (0.20 Btu/sq.ft.-hr.-^{o}F) is close to extruded polysterene, a material widely recommended for road applications (Esch, 1978), that a K value of 0.0722 W/(m^{o}C) (0.50 Btu/sq.ft.-hr.-^{o}F), is close to that of wood chips.

The maximum thaw depth along the sloping surface, (Figure 4 - location B) is 0.089 m (0.29 ft.) below the slope surface at K = 0.0722 W/(m^{o}C) (0.50 Btu/sq.ft.-hr.-^{o}F), while the thickness of the insulation layer is 0.076 m (3 inch). The maximum depth of thaw at the locations A and B is about 0.65 m (21.5 ft.) below the bench surface respectively, while there lies a 0.65 m (2.25 ft.) thick combined layer of gravel pad and insulation. Hence, the insulation layer limits the thaw front penetration in to the soil, for locations A and C, but not B.

CONCLUSIONS

It has been successfully demonstrated that insulation cover on a slope face reduces the depth of thaw; the effectiveness of such a measure shall depend on site specific thermal and climatic conditions as well as on the type of the insulation material being used.

The model assumes homogeneity of the slope material as well as homogeneity of insulation cover, both of which are rarely present in the field. However, the model allows simulation of multilayered materials and, thereby, allows simulation of true insitu conditions.

In the case of the fine grained soil slopes in the general vicinity of the Deadfall Syncline area of North Slope, Alaska, an insulation cover of 0.076 m (3 inches) with a thermal conductivity in the range of 0.0288 to 0.0722 W/(m^{o}C)(0.20-0.50 Btu/sq.ft.-hr.-^{o}F) appears to be adequate to inhibit the thaw penetration, other conditions being as specified in the calculations. A 0.12m(4.5 inch) to 0.15m(6 inch) thick insulation cover will provide a non thawing slope, a measure that might be taken for safeguarding thawing slopes.

It has also been demonstrated that water absorption by the insulation cover, 0% to 400% in the simulations, for the area of concern, has an insignificant effect on thaw depth, other conditions being the same.

REFERENCES

Bell, J.R. et al 1983. Properties of Geotextiles in Cold Region Application. Proc. on Fourth International Conference on Permafrost, Fairbanks, pp. 123-160.

Berg, R.L. et al 1978. Thaw Penetration and Permafrost Conditions associated with Livengood to Prudhoe Bay Road, Alaska. Proc. of The Third International Conference on Permafrost, Edmonton, Canada, pp. 616-621.

Esch, D.C. 1978. Road Embankments Design Alternatives Over Permafrost. Proc. of Applied Techniques for Cold Environments, Anchorage, pp. 159-170.

Frydenlund, T.E. 1985. Soft Ground Problems. International Conf. on Plastic Foam in Road Embankments, Oslo, Norway.

Lunardini, V.J. 1981. Heat Transfer in Cold Climate. Van Nostrand Reinhold Company, NJ.

McRoberts, E.C. 1978 in Geotechnical Engineering for Cold Regions. McGraw-Hill, pp. 363-404.

Olson, M.E. 1984. Synthetic Insulation in Arctic Roadway Embankments. Proc.: Cold Regions Engineering Speciality Conference, pp. 739-751.

Paul, Jyoti Prakash 1986. Fragmentation System Design for an Arctic Surface Coal Mine. M.S. Thesis, University of Alaska, Fairbanks.

Phukan, A. 1985. Frozen Ground Engineering. Prentice-Hall International Series in Civil Engineering and Eng. Mechanics, NJ, pp. 200-500.

Pufahl, D.E. and Morgenstern, N.R. 1979. Stabilization of Planar Landslides in Permafrost. Canadian Geotech. J., vol.8, 558-580.

APPENDIX I

The GEODYNE is a two dimensional finite element model for time dependent analysis of freeze-thaw problems.

The two-dimensional form of the differential equation solved by the model can be written in Cartesian coordinates:

$$\underset{(1)}{\beta_1 \frac{\delta T}{\delta t}} + \underset{(2)}{\beta_2 \left(u \frac{\delta T}{\delta x} + v \frac{\delta T}{\delta y}\right)} - \underset{(3)}{\frac{\delta}{\delta x}\left(k_x \frac{\delta T}{\delta x}\right)} - \underset{(4)}{\frac{\delta}{\delta y}\left(k_y \frac{\delta T}{\delta y}\right)} + \underset{(5)}{w_{o_1}} - \underset{(6)}{w_{o_2}} = 0$$

where

T	=	temperature, ^{o}C
β_1	=	the average volumetric heat capacity of the soil mass (kJ/m^3); this term is temperature dependent
β_2	=	the volumetric heat capacity of water (kJ/m^3)
u,v	=	the components of Darcian water velocity in the x an y directions, respectively (m/hr)

K_x, K_y = thermal conductivity coefficients in the x and y directions, respectively (kJ/hr m ^oC); these terms are temperature dependent

w = the soil thickness normal to the x-y plane (m)

σ_1 = a thermal source or sink representing the effects of latent heat (kJ/hr m^3); this term is temperature dependent

σ_2 = a thermal source or sink term representing a thermal flux such as a surface heat flux or the flux resulting from the geothermal gradient (kJ/m)

Equation (1) represents a generalized, nonlinear statement of the equation describing the flow of heat in a saturated or unsaturated soil. In reviewing the equation, several comments concerning the assumptions made for each term are appropriate. First, in term (1) of Equation (1), the assumption is made that the heterogeneous soil-water matrix can be represented by a homogeneous approximation using a single volumetric heat capacity, β_1. In general, β_1 will be temperature dependent, and different values will be used if the local temperature is above or below the freezing temperature. In other words, β_1 is described in a stepwise fashion, with the step occurring at the phase transformation temperature.

Term (2) of Equation (1) represents the thermal effects of flowing water in the soil matrix, and is usually called the convection term. This term is derived directly from thermodynamic considerations and can have a profound effect on the behavior of a thermal regime. At the present time, it is assumed that all values of convective velocity are specified external to the model. If the temperature falls below freezing, the local water velocities are assumed to go to zero at that point. Terms (3) and (4) represent the diffusive transfer of heat according to the Fourier's analogy. As with the soil properties, the diffusion coefficients are assumed to be stepwise temperature-dependent at the freeze front. It is the analyst's responsibility to specify the correct properties for the soil mass above and below the freeze point. Also, while not a general situation, it is easily seen that Equation (1) is formulated to simulate anisotropic diffusion properties in the x and y directions. This may be of particular interest in axisymmetric problems. The fifth term of Equation (1) represents the effects of latent heat. Proper formulation of this term is essential to the solution of the freeze/thaw problem, and a large number of alternative formulations have been tested. At the present time, this term is formulated as:

$$\sigma_1 = \frac{\lambda}{\Delta t} (m_1 - m_0) \qquad (2)$$

where

σ_1 = the net effective heat source/sink term to represent the effects of the latent heat of fusion (kJ/hr m^3)

λ = the latent heat of fusion for the soil matrix (kJ/m^3)

Δt = some finite time interval between times t_0 and t_1 (hr)

m_1 = the unfrozen moisture content of the soil matrix at the end of the time interval Δt (fraction of total available unfrozen moisture for phase transformation)

$m_\emptyset$ = the unfrozen moisture content of the soil matrix at the beginning of the time interval t (fraction of total available unfrozen moisture for phase transformation)

Finally, it is assumed that the unfrozen moisture content of a soil, m can be approximated as a function of the soil temperature. This relationship has the form:

$$m = \lambda\left(\frac{\alpha}{\alpha + T_f - T}\right)^4 \quad \text{for} \quad T < T_f$$

$$m = 1.0 \quad \text{for} \quad T \geq T_f \qquad (3)$$

where

T = the local temperature (^oC)

T_f = the freezing temperature (^oC)

The last term of Equation (3) represents the effects of heat fluxes. Such fluxes may either be specified by the analysis (i.e., the geothermal flux), or may result from a calculation of a surface heat balance. When done as a surface heat balance, the net surface energy balance flux term is approximated by the relationship:

$$Q_{NET} = Q_{SW} + Q_{NLW} + Q_{TURB} - Q_{EVAP} \qquad (4)$$

where

Q_{SW} = transmitted shortwave radiation flux

Q_{NLW} = transmitted net longwave radiation flux

Q_{TURB} = turbulent heat transmitted across the surface

Q_{EVAP} = evaporative heat flux leaving the boundary surface

In general, the terms of Equation (4) are both surface temperature dependent and functions of one or more atmosphere variables.

THE RESISTANCE TO FROST HEAVE OF VARIOUS CONCRETE CANAL LINING

Song, Baoqing, Fan, Xiuting and Sun, Kehan

Qinghai Provincial Institute of Water Conservancy, Xining, China

SYNOPSIS Different types of canal lining were constructed in an observation station in an area subjected to seasonal frost. Linings included concrete plates with a trapezoidal section, ∏ shaped plates with a trapezoidal section, concrete plates set on beams with a trapezoidal section, overhead concrete plates with an arc bottom, an arch bar section, and a parabola shaped plate. The study included observations on the distribution of frost heave; frost depth and water content along canal sections; maximum heave displacement and residual frost heave; and the development of cracks. The results show that the complex concrete plates with an arc bottom was the best resistant to frost heave and the type of lining is suggested for use in regions subject to seasonal frost by the authors.

TEST PURPOSE, PROCEDURE AND METHODOLOGY

Introduction

Up to now, many engineers and scientists control frost damage of rigid canal linings by limiting the allowable displacement of the structure. However, what kind of rigid lining is most suitable to minimize frost heaving? This is what we want to discuss in this paper.

Based on frost heave distribution along a section of canal with various lining, we suggested some structures with flexible joints among each lining block in order to fit in with differential frost heave, and provided allowable maximum frost heave for different type of lining. After analysing the effect of anti-seepage, engineering cost and construction, the authors selected readily available rigid canal lining following observations in test sections.

Field test section

(i) Observation of test sections The field test setup had three main components:

A, Frost heave pool The pool had a depth of 3 m and an area of 600 m^2. It was lined on the inside surface with double plastic film. Water supply was runing through an arrangement of subsurface pipes surrounded by gravel (see Fig.1). The pool was filled with light loam with a dry density of about 1.52 t/m^3.

B, Water supply system The main pipe has a diameter of 4.2 cm and is connected to the branch pipes of the pool and is controlled by a valve. The pipes were full of water to supply water for the test. During freezing of the soil in winter, water was supplied from the supply system to the frost heave pool in order to keep the ground water level 40 to 60 cm higher than the pool bottom, that is 95 to 110 cm beneath the bottom of the canal linings.

C. Lining types Seven different types of canal lining were selected for test, each with an area of 5.1 to 5.25 m^2 and a depth of 1.5 m. The types of lining included:

(1) A concrete plate with trapezoidal section. The plate had a width at the bottom of 2 m, a slope of 1:1, a depth of 1.5 m and a width at the top of 5.0 m. The plate was constructed of cast-in-place concrete, with a thickness of 8 cm, and transverse construction joints at intervals of 3 m.

(2) A ∏ shaped plate with a trapezoidal section, similar to that described above. The plate at the bottom of canal was cast-in-place concrete with a joint at the centre for accommodating frost heave. The slope was lined by precast shaped concrete plates, with a length of 2.42 m, a width of 0.6 m and a thickness of 7 cm.

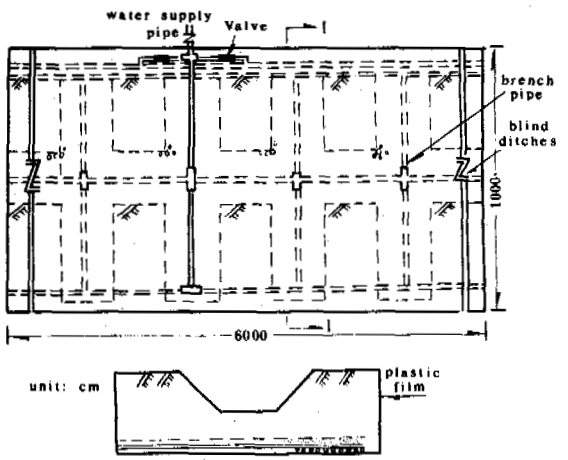

Fig.1 The Scheme of Frost Heave Pool

(3) A concrete plate set on beams with a trapezoidal section similar to that described in (1) above. A small beam with a section of 0.1x0.15 m was placed at intervals of 1 m. The concrete plate was cast-in-place above the beams in order to strengthen its rigidity.

(4) An overhead concrete plate, similar to that described in (1) above, supported on concrete beams. The precast beams were placed first, then the precast concrete plate were placed on the beams.

(5) A complex concrete plate with an arc bottom. The section was designed with a slope of 1:1, a depth of 1.5 m, a top width of 5.0 m, an arc radius of 2.5 m and a chord height of 0.5 m. The arc bottom was cast-in-place with a thickness of 8 cm and with a joint at its centre for accommodating frost heave. The side slopes were cast-in-situ or precast concrete plate with a ⊓ shape. A joint between the slope and the bottom was provided for accommodaing heave. An expansion joint was provided at intervals of 3 m.

(6) An arch bar with a radius of 2.7 m, a top width of 5.0 m and with a joint at the centre for accommodating heave. The bar was cast-in-place with a thickness of 8 cm. Expansion joints were placed along the canal at intervals of 3 m.

(7) A parabola shaped plate with a function of $Y=0.24\ X^2$, a depth of 1.5 m, a top width of 5.0 m and a thickness of 8.0 cm. A joint was constructed in the centre and expansion joints were provided at intervals of 3 m.

All seven types of test sections contained 8 parts (see Fig.2) were subjected to the same conditions, including canal gradient, climatic conditions, type of subsoil, and water supply.

(ii) Field observations Field observations including monitoring air temperatures, frost depths, water content of subsoils, frost heave of lining, development of crack on the surface of the lining and residual displacements. The layout of the moisture locations is shown on Fig.3.

RESULTS AND ANALYSE

Observation results

The minimum temperature was -16°C, and the maximum frost depth was 124 cm. Frost heave of the lining and frost depth were observed 29 times. The development of cracks on lining was described as they occurred. Pertinent observations are summaried in Table I and on Fig.4.

The soil water content as a function of depth was determined before freezing, at the moment of maximum frost depth and after thawing. These test results are summaried in Table II.

Analyse of results

(i) As indicated in Table II, the moisture distribution of subsoil along the section of canal was almost the same whatever in the condition before freezing, frozen or after thawing. Water content increased from the top to the bottom of the canal. In additions, the soil moisture content in north facing slopes was found to be higher than that in south facing slopes.

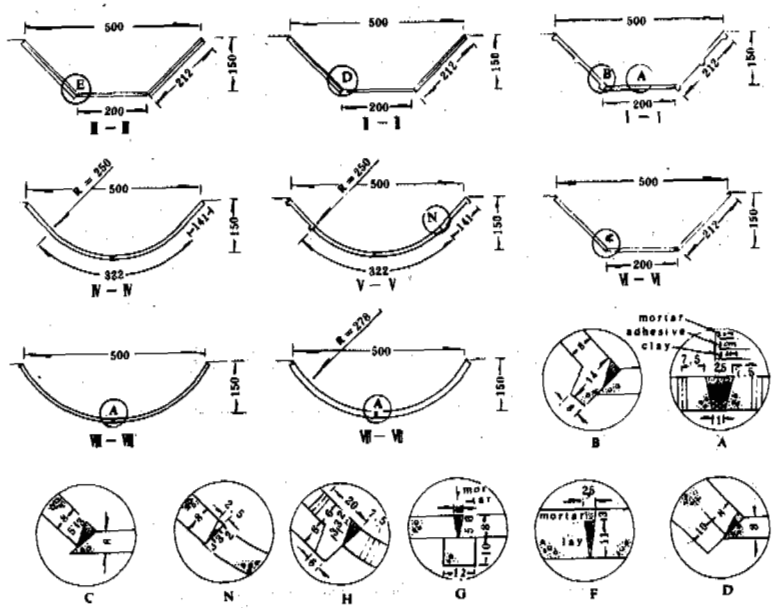

Fig.2 The Scheme of Different Types of Canal Structures

I-I Precast trapezoidal concrete plate
II-II precast ⊓ shaped concrete plate
III-III precast overhead concrete plate upon beams
IV-IV cast-in-place concrete plate
V-V complex concrete plate with an arch bottom
VI-VI complex cast-in-place concrete plate with an arch bottom
VII-VII cast-in-place arch structure
VIII-VIII cast-in-place parabola structure

TABLE I

Frost Heave of Lining with Different Structures

Lining type		Frost heave of lining (cm)										Max.displacement (cm)	Diff.coef.of heave				Development of crack
		1	2	3	4	5	6	7	8	9	10		1	2	3	4	
(1)	CH	0	0	0	0.5	2.3	1.5	1.1	0.8	0.3		2.3	0	1.9	0.41		A crack occurred at the centre of canal bottom with a width of 0.5 to 1.8 mm
	Max.C	0.7	0.7	1.0	2.8	4.5	4.0	4.8	3.1	1.4		4.8	0.17	1.8	1.9		
(2)	CH	0.1	0.8	0.8	2.3	4.6	4.7	3.3	2.6	2.1	0.7	4.7	0.41	2.7	1.6	1.1	A crack occurred at the canal bottom intersecting the centreline of canal at an angle of 63°
	Max.C	0.7	1.2	2.2	4.9	4.9	7.9	4.5	4.0	3.1	1.0	7.9	0.87	0	4.0	1.2	
(3)	CH																Significant frost heave occurred at the canal bottom
	Max.C	0.1	1.8	2.9	8.9	8.4	3.4	4.2	3.2	3.6	0.9	8.9	1.6	0.59	0.94	1.6	
(4)	CH																Significant frost heave occurred at the canal tottom
	Max.C	0.6	1.8	2.4	4.2	5.1	6.0	2.9	4.3	3.1		6.3	1.0	1.1	3.6	0.7	
(5)	CH	0.6	0.3	1.1	2.9	4.5	6.0	4.8	2.9	2.2	2.7	6.0	0.79	1.2	0.9	0.7	A crack occurred on the south facing slope, parallel to the direction of canal
	Max.C	0.6	0.3	1.1	2.9	4.5	6.0	4.8	2.9	2.2	2.7	6.0	0.79	1.2	0.9	0.7	
(6)	CH	0.3	0.2	2.8	4.1	4.4	3.2	1.2	0.3			4.4	1.3	1.5			A crack occurred on the south facing slope, parallel to the direction of canal
	Max.C	0.8	0.8	2.2	5.7	6.1	4.7	2.0	0.8			6.1	1.8	1.9			
(7)	CH	0.1	0.1	3.0	4.1	2.3	1.9	1.2	1.0			4.1	1.4	0.36			A crack occurred on the south facing slope, parallel to the direction of canal
	Max.C	0.3	0.4	5.1	6.3	5.1	3.5	2.2	0.6			6.3	2.2	1.6			

* CH—while crack happens; ** Max.C—while maximum crack occures.

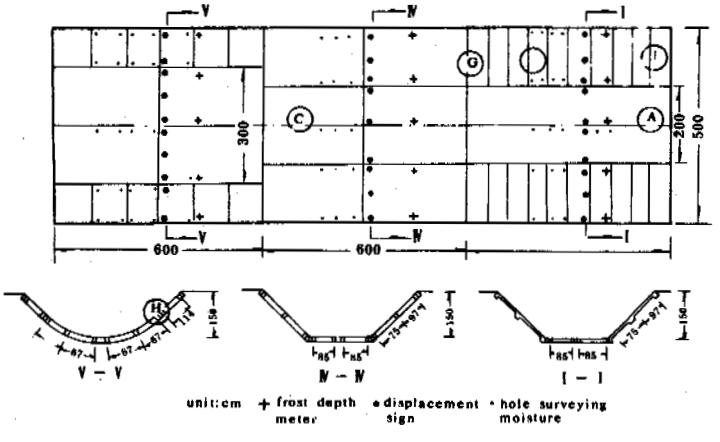

Fig.3 Layout of Moisture Locations

+ Frost depth measurements
• Frost heave displacements
· Water content measurements

TABLE II

Soil Moisture of Subsoil Under Canal

Lining type	No.	Average moisture (%)			Lining type	No.	Average moisture (%)			Lining type	No.	Average moisture (%)		
		BF	Max.F	AT			BF	Max.F	AT			BF	Max.F	AT
	1	11.6	15.2	16.1		1	17.5	19.6	17.0		1	10.2	11.5	15.8
	2	15.7	19.0	23.0		2	18.7	25.2	22.3		2	15.4	19.2	22.0
	3	24.0	22.3	21.5		3	21.1	27.3	23.9		3	16.3	22.5	20.5
(1)	4	21.8	25.8	21.5	(2)	4	20.8	28.7	25.6	(5)	4	15.5	28.9	23.1
	5	19.6	26.9	22.2		5	19.6	24.7	25.0		5	12.4	21.3	23.2
	6	16.1	17.5	20.8		6	14.5	20.6	23.5		6	11.8	16.2	22.5
	7	11.8	12.5	17.2		7	11.2	13.7	15.4		7	11.2	11.4	15.5

*BF—Before freezing; **Max.F—At the moment of max. frost depth; ***AT—After thawing.

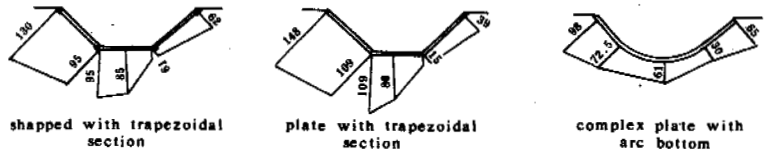

Fig.4 Distribution of Frost Depth along Canal Section

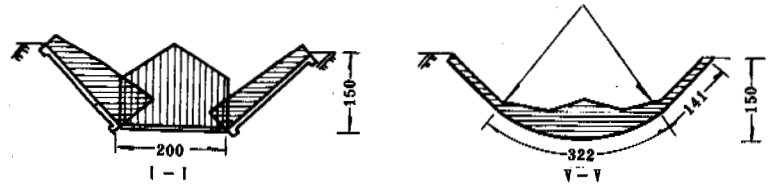

Fig.5 The Distribution of Frost Heave along Canal Section

The difference in soil water content before and after freezing between Π shaped plates and plates with a trapezoidal section is negligible. However, the water content under overhead plate was less about 3% than that above types.

The water content of subsoil before freezing in the complex plate section with an arc bottom is less than that in the trapezoidal section. But after freezing, the soil water content under the bottom was almost the same as that in the trapezoital one.

(ii) From Fig.4, we know that the distribution of frost depth along the canal sections is a maximum at the top. The frost depth below the north facing slope is greater than that below the south facing slope. The minimum frost depth for the trapezoidal section was at the toe of the south facing slope. The minimum frost depth of arc sections was at the middle of the south facing slope.

(iii) As indicated on Table I, the distribution if frost heave of lining along the sections is similar to the distribution of changes of soil water content. That is to say the frost heave at the top was the smallest and increased to a maximum at the bottom of the canal.

Based on observation results, we know that the direction of frost heave at the bottom was normal to the surface of the lining. However, the direction of the heave on canal sideslopes could be divided two parts, one being normal to the surface of slope and the other being vertical. The distribution of normal heave to the surface of lining for the section of Π shaped plate with trapezoidal section and for the complex plate with arc bottom section is shown in Fig.5.

From Fig.5 we see that the distribution of frost

heave in trapezoidal sections was like a "roof" at the bottom and like a trapezoid at the top. The distribution of heave along the complex plate with an arc bottom has the shape of a crescent Moon. Comparing the two types of frost heave distribution in Fig.5, it is obvious that the complex plate with an arc bottom is much more effecting to frost heave. The experimental results show that the maximum frost heave obtained from the curve sections (including the complex plate section with arc bottom, the arch bar section and the parabola section) is much less than that for the trapezoidal sections. As an example, the maximum heave of the complex plate section with arc bottom was 3.5 cm, when the maximum heave in the ∏ shaped plate with a trapezoidal section was 7.9 cm. The reason for this improved performance might be that under the action of frost heaving forces the arc bottom of the lining acts as an arch to resist upwards forces.

(iv) Frost depth and heave of the north facing slopes were found to be much larger than that in the south facing slopes. However, cracks in the lining usually occurred in the south facing slope first. The formation of cracks depends on not only the heave. The rate of crack development during subsoil freezing is much slower than that during thawing. Placing a joint in the centre of the canal bottom can improve reduce the number of cracks.

(v) From Table I we know that the resistance to frost heave of curve section is much better than that in trapezoidal section, and the best lining type in our test field is the complex plate with arc bottom, the next is arch bar. The third best is the parabola section, the 4th is the ∏ shaped plate with trapezoidal section, the 5th is the overhead plate with a trapezoidal section, the 6th is the plate set on beams with a trapezoidal section. The poorest resistance to heave was the concrete plate with a trapezoidal section. The maximum allowable frost heave of different types of lining structure is summaried in Table III.

Under the action of frost heave forces, the part of arc bottom in the complex plate lining was in compression zone, the joints in the centre of the canal bottom and between the slope plate and the arc bottom accommodating frost heave movements. Therefore, the structure of a complex plate with arc bottom performs extreme well against frost heave forces. The maximum allowable frost heave of a plate structure with a trapezoidal section is around 2 cm. The cracks in the plate structure therefore occurred under very small displacements.

The direction of frost heave at the top of canal slopes is not only normal to the slope but also vertical to the ground surface because of two dimensional freezing. The direction of frost heave at toe of the slope was normal to the slope and the frost heave amount at that point was much larger than that at the top of the slope. As a result frost heave forces subjected the slope plate to both tension and bending movements. Therefore, the cracking and frost damage on the slope of canals with trapezoidal sections usually occures at a depth which is 1/3 to 1/2 of canal height from the bottom. The construction of the arch bar section can prevent such damage.

(vi) After thawing of the subsoil, the displacement of concrete lining was partially recovered. The maximum residual displacement produced by frost heave are listed in Table IV: the maximum residual displacement occurred at the corner between the slope and the bottom of canal, for trapezoidal sections, or at the centre of the bottom of the canal for curve sections. Displacement recovery was greater for curve sections is compared to trapezoidal sections.

(vii) After analysing the results presented in Tables I and II and Fig.4, a relation between mean frost heave ratio and moisture content of the subsoil below the complex plate canal with an arc bottom was established as follows:

$$P = 0.56\ (W - 10.4)$$

where, P—the mean frost heave ratio, %;
W—the moisture content of the subsoil before freezing.

(viii) A review of the test data demonstrates that the structure of complex concrete plate with arc bottom performs the best with a strong resistance to frost heave and a good ability for recovering displacement. In order to provid a comparison from a cost and construction point of view, we have set up a test canal with a ∏ shaped lining of trapezoidal section (with a length of 2.6 km) and a test canal with complex plate lining with arc bottom (with a length of

TABLE III

Maximum Allowable Frost Heave of Various Linings

Lining type	Max.AFH (cm)	Diff.coef. of FH(x10)	Lining type	Max.AFH (cm)	Diff.coef. of FH(x10)
(1)	2.3	1.9	(5)	6.0	1.3
(4)	2.3		(6)	4.4	1.4
(3)	2.3		(7)	3.8	1.4
(2)	2.3	2.7			

Joints are important to reduce frost heave damage to the lining.

TABLE IV

Residual Displacement of Frost Heave with Different Lining Types

Lining type	Residual displacement (cm)	Lining type	Residual displacement (cm)
(1)	3.6	(5)	1.6
(2)	2.0	(6)	1.5
(4)	3.2	(7)	2.5
(3)	3.2		

1.4 km) in Daxia canal, Lodu county; a test canal with complex plate lining with arc bottom (with a length of 0.34 km) and U shaped section in Nanmenxia canal, Huzu county. Observations on these test sections provide the following conclusions:

A. Compared with trapezoidal and U shapped sections, the section of complex plate with an arc bottom is rather close to the economical one. Its perimeter is rather short, as an example, the perimeter is about 3% shorter than that of the trapezoidal section in Daxia test canal,and is about 5% shorter than that of U shaped section in Nanmenxia test canal.

B. The formwork for cast-in-place concrete for the complex plate with arc bottom is more simple and economic than that of U shaped section and precast ∏ shaped section.

C. Observation results in Daxia show that the cost of precast shaped lining is more expensive than a complex plate with a cast-in-place arc bottom.

D. Frost heave observations over a period of two years show that cracks occurred in more than 20 percent of the areas where lining consisted of ∏ shaped sections cracks occurred in only 0.4 percent of the areas where lining consisted of complex plate with an arc bottom. In conclusion, the complex plate with an arc bottom lining appears to cost the least and perform the best.

CONCLUSIONS

(i) The observation results show that the experimental test set up was suitable for testing the characteristics of different type of canal linings.

(ii) Observations of maximum allowable frost heave and residual displacement of different types of linings are useful for design and construction.

(iii) The test results showed that a lining consisting of a complex concrete plate with an arc bottom is host resistant to frost heave and most economical.

(iv) Construction joints should be used according to the distribution of potentail frost heave along canal sections.

THE BARROW DIRECT BURY UTILITIES SYSTEM DESIGN

J.E. Thomas, P.E.

North Slope Borough, Alaska, USA

SYNOPSIS: The Northern Eskimo community of Barrow, Alaska, USA began construction of the village wide underground Barrow Utilities System in 1981. In 1985 they decided to complete the unfinished portions of the utilities system using direct bury arctic pipes instead of the underground Utilidor used in previous phases of the project. This paper describes this Direct Bury Utilities System and discusses the unique features of the design. Design details, some advantages and a few problems associated with the design and construction of the project are presented.

INTRODUCTION

In 1981 the North Slope Borough began the design and construction of their aggressive underground utilities system to serve the 3000 residents in the Village of Barrow, Alaska, USA. This system was made financially possible by the development of the North Slope oil fields and the high price of oil during the late 1970's and early 1980's. The utilities system, commonly known as the Barrow Utilities System, represented a complete public works project whose main purpose was to provide a village wide underground utilidor containing water and sewer lines, cable TV, telephone, and future electrical service. In addition to the Utilidor construction, water pumping stations, sewage pump stations, a sewage lagoon, shop and warehouse facilities, and a village wide fire protection system were built. Roads were constructed or rehabilitated, a material site was developed and a long term solid waste disposal site was investigated. The entire project provided stable employment for the local villagers and in many cases training in some craft or skill.

In 1985 the North Slope Borough recognized that the entire project had grown in scope and could not be completed with the remaining monies set aside for the project. Wanting to honor their commitment to provide potable water and sewer service and fire protection throughout the village, the North Slope Borough decided to change the design from the well known "Barrow Utilidor" to a more cost effective Direct Bury System.

Frank Moolin and Associates, Inc. headquartered in Anchorage, Alaska, USA was contracted to perform the new Direct Bury System design since they had been the designers and project managers for the Utilidor System. It was felt they could complete the redesign quickly due to their intimate knowledge of the Utilidor System which was important since the North Slope Borough did not want to interrupt the established construction schedule for the entire project.

In June of 1985 work began on the redesign effort which would provide direct bury water and sewer service and fire protection to the areas not serviced by the utilidor. The author held the position of Senior Project Engineer for this project and was responsible for all portions of the technical design. Stanley Industrial Consultants, Limited of Edmonton, Alberta, Canada was contracted by the North Slope Borough to perform the design review and to provide technical assistance based on their considerable experience with utilities systems in the arctic. The resulting design successfully incorporated significant cost savings features, provided an easy to maintain system and was designed and constructed within the schedule constraints.

DESIGN PHILOSOPHY AND CRITERIA

Prefabrication

The North Slope Borough desired a high quality system which would provide water, sewer and fire protection to the unserviced portions of the village with the remaining Capital Improvement Funds. To achieve this goal it was decided that most of the system should be prefabricated in a shop environment with skilled labor. These prefabricated components would then be shipped to Barrow and assembled into the final operating system. The North Slope Borough indicated a desired to use on-site materials left over from the Utilidor project only if it was economically desirable. Some insulated piping and pipe fittings were utilized from these on-site materials.

Common Trench

The excavation and backfilling of the permafrost during the Utilidor installation proved to be one of the major expenses associated with the Utilidor construction. It was felt that a "common trench" design for the Direct Bury System should be used to reduce the excavation and backfilling costs. This common trench

approach did not meet the State of Alaska Standards for utility system installation and a variance allowing both the water and sewer lines to be placed in a common trench was needed.

Circulating Water Lines

Unlike the utilidor where the water lines were installed in pairs (one supply and one return line), the Direct Bury System's water lines would be configured in loops so that only one water line would be routed along any one street. The water would be made to circulate to prevent freezing during periods of low flow. Since the Utilidor was already operational in portions of the village, it would be used as the backbone of the Direct Bury System. All Direct Bury water loops would begin and end in the Utilidor.

Fire Flow

The North Slope Borough Fire Department required the Direct Bury System to provide a fire flow of 75 liters per second at all fire hydrants which established the system's peak flow rates. Stanley Industrial Consultants, Ltd. recommended that the system incorporate flow reversal in the water mains so the water could feed each fire hydrant from two directions as it does in the system they designed for Dawson City, Yukon, Canada. Flow reversal would allow for smaller diameter mainlines and associated cost reductions.

Maintainability

The existing Utilidor System provided the ultimate in access and ease of maintenance for a utility system in the arctic. The North Slope Borough desired to maintain this feature in the Direct Bury design. To satisfy this requirement all valving, fire hydrants, sewer clean-outs, heat trace panels, etc. were located inside surface accessible manholes.

SYSTEM COMPONENTS

The major components of the Barrow Utilities System were constructed between 1981 and 1985. These components included the Water Recirculation Plant, four sewage pump stations, the sewage lagoon and approximately five kilometers of utilidor. Only the extension of the mainline pipes from the Utilidor to the unserviced portions of the village was required in the design of the Direct Bury System. The major components of the Direct Bury System include:

1. The tie-in connections to the existing Utilidor water lines and gravity sewer lines.

2. The prefabricated manholes, which contain water valving, vents, drains, fire hydrants, sewer clean-outs, and heat trace panels.

3. The common trench, which includes insulated high density polyethylene piping, heat tracing, trench insulation and the backfill material.

4. The service connections, which included the mainline stub-out, the service connection piping and the belowground to aboveground connection box.

Details of these system components are discussed below. Included in the discussion are comments regarding the design, the fabrication and the installation of the components.

The Utilidor to Direct Bury Connections

Two methods of providing circulation in the Direct Bury System water loops were investigated, pumping and utilizing differential pressure at the Direct Bury water loop tie-in points. The use of circulating pumps was not selected because of their cost of installation and operation, the need for maintenance and the consequences of a broken pump resulting in the freezing of the water main. An in-depth hydraulic analysis indicated that circulation in all the direct bury loops could be easily provided by creating a 70 kPa pressure differential between the Utilidor's water supply and return lines.

Individual Direct Bury water loops were connected to the Utilidor water supply line using an isolation valve. The return end of each Direct Bury water loop was connected to the Utilidor's water return line with a check valve and circulation by-pass piping as shown in Figure 1. The circulation by-pass piping contains a flow balancing valve, a visual flow indicator and temperature and pressure indicators. By adjusting the flow balancing valve the desired flow velocity of 6 centimeters per second in the mainlines could be obtained. The in-line check valve provides the capability to reverse flow in the Direct Bury water line in the event of fire flow. When any hydrant is opened on a Direct Bury loop the pressure in the loop will be less than the Utilidor's water return line pressure and the check valve will open providing a reversal of flow in the line to the hydrant.

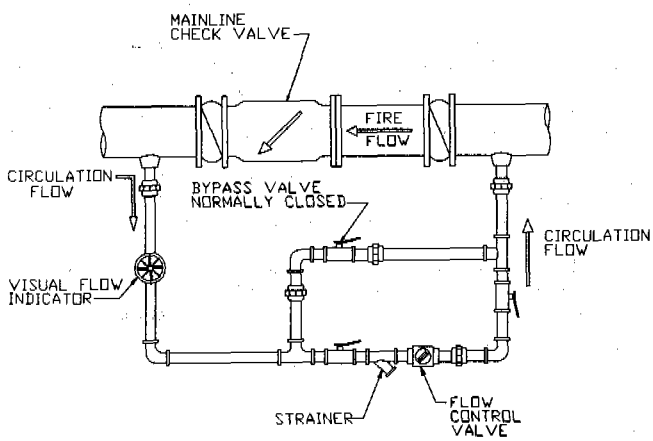

FIGURE 1 - FLOW REVERSAL PIPING

Maintenance is easy to perform on the flow control piping because it is located in the Utilidor where it can be inspected during the daily walk-through. Being inclosed in the warm Utilidor environment, the piping is not subject to freezing. There are no moving parts in the system except for the visual flow indicator

which allows the maintenance people to quickly verify that there is positive flow in each direct bury water loop.

The Manholes

The installation of the potable water and sanitary sewer piping in the same manhole is generally termed by the designer as the "common manhole" design. The common manhole design offers two major advantages over separate water and sewer manholes. First, the total number of manholes required when using common manholes is approximately one half of the number required if separate manholes were used. This reduces the construction cost significantly. Second, the fewer number of manholes also creates less interference with vehicle and foot traffic along the roads. This reduces the chance of damage to the manholes by snow removal equipment, public and private automobiles and recreational vehicles such as snowmachines and three wheelers.

The design of the direct bury manholes followed the basic design of the Utilidor's service box, a 1.9 meter diameter steel cylinder with a base plate, frost shield and a hatched lid. This design worked very well for the Utilidor service connections and it was felt the design would adapt very easily to the Direct Bury manholes. Each Direct Bury manhole was individually designed for a specific location. Figure 2 shows a typical manhole. The major components of the manholes are summarized below:

1. The manhole is made of a 1.9 meter diameter rolled steel shell with a 2.5 meter diameter steel base plate, a 0.6 centimeter thick steel lid, an access hatch, a ladder and an insulated frost shield located above the piping. The outside of the manholes is insulated with 7.6 centimeters of sprayed on urethane foam and sealed with 0.13 centimeters of waterproof coating.

2. The potable water piping is located 0.9 to 1.5 meters above the base plate. Necessary isolation valves, tees, ells, vents, drains and other pipe fittings are installed as needed for each unique manhole configuration.

3. Some manholes contained fire hydrant piping which includes an in-line tee base, the dry riser barrel and the hydrant head.

4. The gravity sewer piping includes sewer clean-outs and vents where necessary. The sewage piping is completely contained within a welded steel sewer enclosure with a gasketed and bolted lid.

5. The heat trace wiring connected to a control box.

The use of the steel sewer enclosure was in response to the State of Alaska Department of Environmental Conservation's concern over the possibility of contaminating the circulating water system if the sewer were to surcharge and leak into the manhole, eventually flooding the potable water piping. Both the water and gravity sewer piping are constructed of 860 kPa rated piping for added safety and the sewer

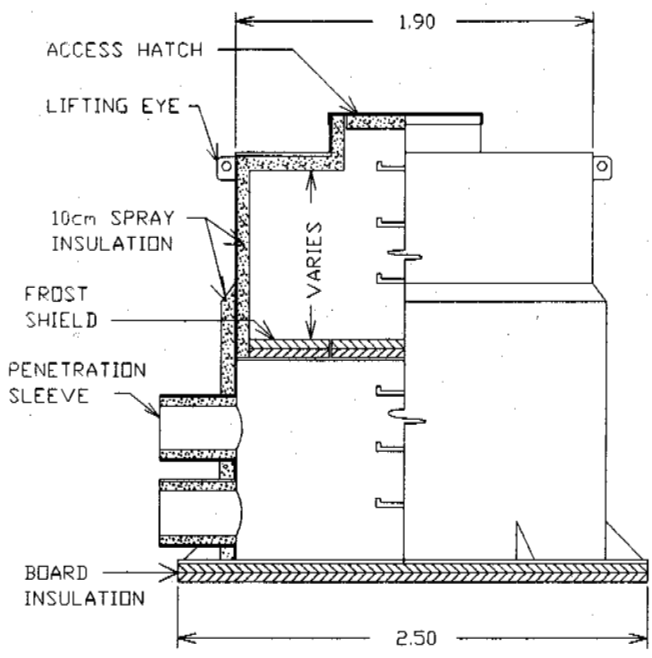

FIGURE 2 - MANHOLE DETAIL

enclosure provides additional assurance that cross contamination will not occur.

During the construction of the Utilidor all the basic materials for the system were shipped to Barrow and then assembled into their final configuration. This was necessary because of the nature of the Utilidor design and the desire to create jobs and job training in the village. With the need to reduce the overall cost of completing the utilities project, the direct bury manholes were totally prefabricated before being shipped to Barrow. Prefabrication of the manhole assemblies provided several advantages:

1. Higher fabrication standards could be met because the work was performed in a shop environment equipped for this type of work.

2. Shipping costs would be reduced because the number of pieces requiring handling, packaging and tracking was reduced.

3. Reduced installation costs at the construction site because all the manhole piping was pre-installed.

The Trench Configuration

The selection of the common manhole design simplified the use of a common trench design in which the water lines and the gravity sewer lines are installed over the top of each other. This approach provides considerable cost savings in the excavation of the trench and the installation of the mainline piping. Unfortunately, it makes the installation of the service connection piping more difficult because the water connection is located directly above the sewer line connection. A typical cross section of the Direct Bury

Utilities System trench is shown in Figure 3.

The trench width was fixed by the widest trench the Bortunco Roc-saw could cut with a single pass of its bar and chain. During the Utilidor construction the Roc-saw utilized a 40 centimeter wide chain to make the cuts in the permafrost. This 40 centimeter wide chain would produce a trench which was too narrow to allow proper backfilling of the mainline piping used in the Direct Bury System. Investigation into the maximum cutting width of the Roc-saw revealed that a 60 centimeter wide chain could be installed if minor modifications to the cutting bar were performed. A trench width of 60 centimeters provided 11.5 centimeters of clearance on both sides of an 20 pipe with insulation. This was enough clearance to allow the backfill material to fill the voids under the haunches of the pipe. Additionally, the few loops requiring a 25 centimeter pipe with insulation could be accommodated.

To facilitate the trench backfilling activities and to provide a more thermally stable installation, the non-frost susceptible (NFS) backfill material was placed in the trench as a slurry. Considerable effort was put into the thermal design of the Direct Bury Systems trench so a minimum burial depth could be utilized without compromising the integrity of the direct bury piping. Results of the thermal model indicated that backfilling with saturated NFS slurry would reduce the seasonal thaw depth in the trench during the first few years of operation. The frozen moisture in the slurry backfill would reduce the overall thaw penetration due to the increased latent heat of fusion in the slurry compared to that of dry NFS. Based on a -12 degree C soil temperature and a 5 degree C water temperature in the pipe, freezing times during no flow conditions were estimated to be 95 hours to frazzle ice formation in a 15 cm insulated pipe.

Tests performed during the Utilidor construction established that the dry NFS material was difficult to compact requiring several passes with a gasoline powered hand operated compactor. The use of a NFS and water slurry had several construction advantages over the placement of dry NFS in that it could be poured evenly into the trench from slowly moving mix-trucks, it would flow around the haunches of the pipe and it required no significant compaction effort. Cement vibrators easily settled the slurry around the pipes and moved the slurry along the trench to even out the thickness of the lift. The problems associated with buoyancy floating the piping in the wet slurry were solved by installing wood blocking across the trench at a selected spacing and predetermined elevations and then floating the pipe on top of the slurry until it was held in the proper position by the blocking. No attempts were made to remove the blocking since it would not effect the thermal stability of the trench.

The mainline piping in the trench consisted of 15, 20 and 25 centimeter diameter high density polyethylene pipes with 7.6 centimeters of spray applied polyurethane foam insulation and an extruded polyethylene jacket. This arctic pipe was identical to that used in portions of the Utilidor System where its historical performance was good. A heat trace channel and self regulating 20 kcal per meter heat trace was placed under the insulation for use during the loss of circulation to prevent freeze-up and to thaw frozen lines.

Board insulation was placed in most of the trenches to reduce the thaw penetration in the backfill material. When the pipe burial depth was shallow, insulation was placed across the width and vertically along the sides of the trench to prevent thaw penetration from both the sides and the top of the trench. At intermediate burial depths insulation was only placed across the trench width and at the deepest depths no trench insulation was needed. Five centimeters of extruded polystyrene board insulation was used in all cases since significant quantities were left over from the Utilidor project.

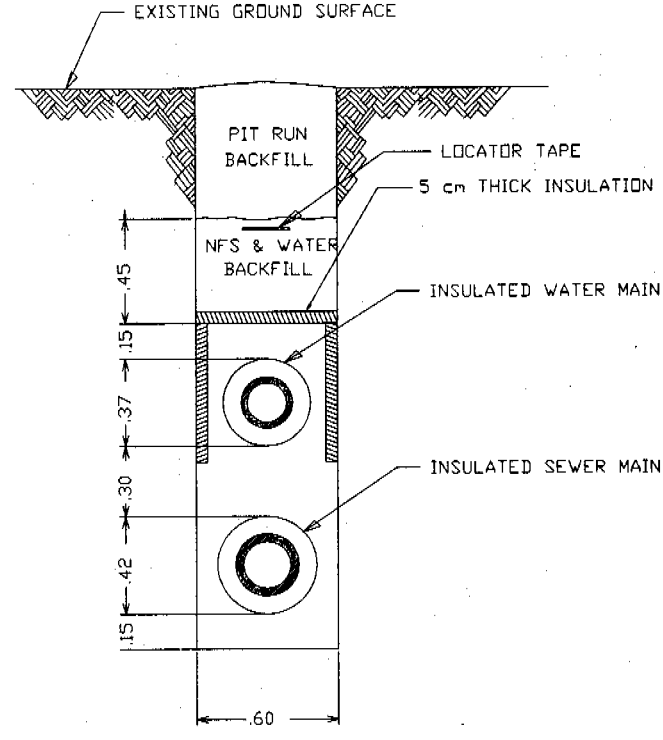

FIGURE 3 - TRENCH DETAIL

The State of Alaska Regulations require a separation of at least 3 meters between the water and sewer lines. Discussions with the Department of Environmental Conservation resulted in the agreement that the common trench design would have a very low cross contamination potential because the water and sewer pipes were made of high density polyethylene, insulated and covered with a seamless extruded jacket and the pipes were buried in a nearly impermeable saturated backfill.

Overall, this trench configuration provides good thermal integrity coupled with low con-

struction costs. The potential for contamination is remote and the ability to survive mainline freeze-ups is excellent.

Service Connections

The design of the service connection trench followed the approach used for the mainline common trench. The method of transitioning from belowground to aboveground at the building is similar to the method used for the Utilidor service connections. All Direct Bury service connections consist of a 10 centimeter insulated gravity sewer line installed in a common trench with a 10 centimeter insulated carrier pipe containing a 2.5 centimeter water supply line and a 2.0 centimeter water return line. Circulation in the water lines is developed by a small circulating pump located in the "connection box", the belowground to aboveground transition structure at the building.

Circulating the water in the service connection piping keeps it from freezing, however, heat tracing is installed inside the carrier containing the two water lines for back-up freeze protection. The insulated sewer line contains a heat trace channel and self regulating heat tracing for thawing purposes only. Under normal flow conditions the sewer should not freeze and the heat trace will be turned off. The heat trace cables and the circulating pump the are powered at the building from a dedicated electric meter since the costs associated with operating the circulating pump and the heat trace is built into the cost of the water. If a customer leaves the village for an extended period of time and has his house power turned off, the service connection will still operate.

During the mainline pipe installation prefabricated service connection stub-outs were installed at the building connection locations. When the time comes to connect a building to the mainlines, the service connection piping is fused on to the pre-installed stub-outs. This eliminates the need to excavate around the mainlines which would be difficult in the frozen soils. The water line stub-out is fabricated such that the two circulating water pipes are connected to the mainline pipe so they fit inside the 10 centimeter carrier pipe. This connection area is insulated, reinforced and made water tight with urethane foam and a fiberglass jacket. The sewer line service connection branch is constructed in much the same manor as the water line except that a single 10 centimeter fusion is made to the mainline instead of two 2.5 centimeter fusions. Figure 4 shows the prefabricated water stub-out.

SYSTEM PERFORMANCE

At the writing of this paper Phases I and II of the Direct Bury Utilities System had been constructed and were operating. Phase III is scheduled to be constructed during the winter of 1987-1988. The construction and operation of the first two phases has revealed a few problems which should be avoided in Phase III.

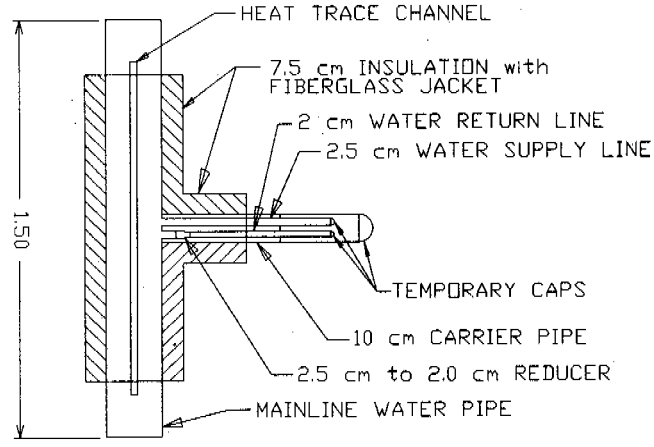

FIGURE 4 - PREFABRICATED WATER STUB-OUT

One significant problem encountered during the first two phases of construction was leakage during the pressure testing in the valve gaskets, at a few of the mainline pipe fusion joints and in the polyethylene pipe to steel pipe couplings. Poor installation practice accounted for the gasket and fusion joint problems. The leakage in the polyethylene to steel coupling was attributed to the cold temperatures causing the polyethylene to shrink to a much greater degree than the steel collar extruded around the polyethylene. Air escaped through the fitting which could not be prevented. Even though it was expected that these fittings would not leak when functioning at normal operating temperatures, the leaking fittings were replaced.

At the time of the initial system start-up only a few building were connected to the system. A single service could not generate enough sewage flow to keep the mainline sewers from freezing. Regular flushing of the sewer lines and operation of the backup heat trace was needed to prevent freeze-ups during the periods of low flows. As more buildings were connected to the system the problem of the freezing sewers disappeared.

Maintaining the proper hydraulic balance in the combined Utilidor and Direct Bury water loops normally requires very little action on the part of the system operators. However, the loops are finely balanced and any change in the pressures and flow rates in one part of the system will have an effect in all other parts of the system. Isolating certain loops of the network can cause zero flow conditions in other loops. For this reason it is important that the operators understand hydraulic principles and the relationships between the loops. Zero flow conditions have been encountered due to selected valving changes in the system. Fortunately, daily walk-throughs and visual inspections caught these conditions before a freeze-up occurred.

Gaining access to the sewer line clean-outs is difficult. The operators must open the manhole access hatch, remove the frost shield hatch,

climb under the potable water piping, unbolt the sewer enclosure lid and then remove the clean-out cap. The reverse process is performed when the inspection is completed. There is concern that the maintenance personnel will not replace the sewer enclosure lid with the required gasket and bolts because of the time consuming effort involved. Signs on the sewer enclosure lid pieces indicate the need to keep the lids bolted in place.

CONCLUSION

The Barrow Direct Bury Utilities System design offers a water and sewer distribution system which interfaces well with the Utilidor System. Efforts in the design stage to create a component type system which allowed for prefabrication and easy field installation, were successful. This approach to a utilities distribution system should be applicable to most arctic and sub-arctic villages where a buried system is desired. Utility system designers should visit the Barrow Utilities System to see first hand it's desirable features and to discuss the maintenance aspects of the system with the Direct Bury System operators. Hopefully, good engineering practice and quality construction have provided the community of Barrow with many years of reliable water and sewer service.

REFERENCES

Greenwood, W (1982)
Shallow Buried Insulated Water and Sanitary Sewer Systems in Permafrost Regions.

Martin, R & Sahlfeld, J (1984).
Sewer/Water Service Connections for Barrow Utilities System. Proc Cold Regions Engr, (1), 395-400

Shillington, E & MacKinnon, G (1987).
Barrow Utility System, Direct Bury System - The Alternative. Proc 2nd Conf on Cold Regions Envir Engr

Zirjacks, W & Hwang, C (1983).
Underground Utilidors at Barrow Alaska: A Two Year history. Proc IV Intl Conf on Permafrost

COLD CRACKING OF ASPHALT PAVEMENT ON HIGHWAY

Tian, Deting and Dai, Huimin

Heilongjiang Provincial Institute of Communications, Harbin, China

SYNOPSIS Based on field investigations on a asphalt-paved highway in Heilongjiang Province, Northeast China, features of the cold cracking of the road pavement were described, and its causes were analyzed as well. After intensively analyzing its influencing factors, measures for preventing the cold cracking were presented from various aspects including selection of pavement material, design of road structure and control of construction quality, etc.

INTRODUCTION

Cracking of road pavement caused by low temperature is a common phenomenon of frost damage in cold regions. It severely harms the normal operation of road and leads to a great increase in the maintenance cost. It was reported that the length of highway, which had been severely damaged by cold cracking, accounts for 17% of the total length of the highway in Japan. In China, because various kinds of oxide asphalts have been widely used in the construction of road pavement in recent years, cold cracking of the pavement becomes worse and worse.Therefore, more attention has been paid to the study on the cold cracking of road surface. This paper deals with the field investigation on the cold cracks occurred in the pavement of a second grade highway in Heilongjiang Province and their cures and prevention countermeasures.

TYPE AND FEATURES OF CRACKS IN PAVEMENT

The cracks in road pavement caused by cold contraction and frost heave can be classified as the longitudinal crack and crosswise crack.

Longitudinal crack

This type of crack is oriented along the longitudinal direction of a highway, i.e., most likely parallel to the direction of driving (Fig.1, photo). Field investigation shows that most of the longitudinal cracks are distributed at the central part of a road, and some at both sides of the vehicle runways or at the edges of the road. The longitudinal cracks are generally several meters, or several decades even hundreds of meters long, 1-5 mm (sometimes, 15-25 mm) wide and 5-40 mm deep.Usually the central cracks are wider and deeper, while the edgewise cracks are smaller and shallower.

The longitudinal cracks were caused by the uneven frost heave of subsoils. The severe cold cracking shown in Fig.1 occurred in the case

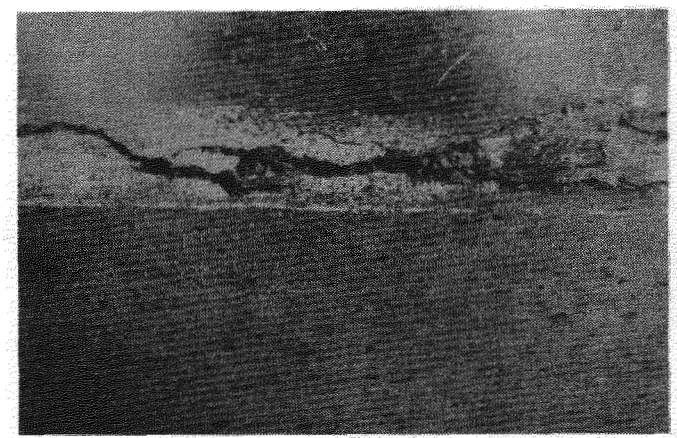

Fig.1 A Photo Showing Longitudinal Cracks Occured at the Central Part of the Highway

that the road was under the influence of flood before freezing. Field tests showed that the average water content of the roadbed within the depth of 20-80 cm beneath pavement was as high as 30.1% (for some places even up to 34.8%), which was higher than its liquid limit. The groundwater table there was also shallow. This allows lots of moisture migrating towards frost front and ice segregating during freezing. The ice segregation leads to a great amount of frost heave, and thus results in severe cracking of the pavement. Of course, the cracks could also be caused by the poor quality of the road construction.

Crosswise crack

This type of cracks were developed across a road. Some of the cracks may run through the road from one side to the other (Fig.2) and some may not (Fig.3). The former is wider, usually with a width of 3-10 mm (some up to 10-25 mm), and the latter is narrower but densely distributed, with a width of 2-5 mm in general.

Field investigation shows that some of the crosswise cracks may penetrate from pavement into

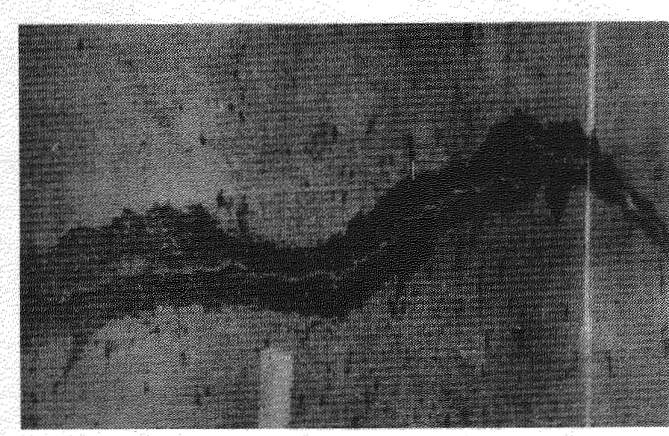

Fig.2 A Photo Showing a Crosswise Crack Running Through the Cross-section of the Highway

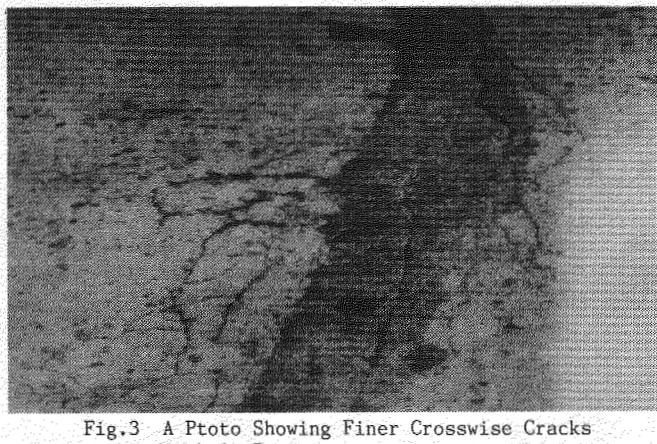

Fig.3 A Ptoto Showing Finer Crosswise Cracks in the Asphalt Pavement

roadbed, while some occur only in pavement. The crosswise cracks may be caused by cold contraction or short of the thickness of pavement and roadbed or excessive deformation of the underlying base soils.

MECHANISM OF THE COLD CRACKING

At present, there are two considerations dealing with the analysis on the mechanism of cold cracking. They are:

Stress analysis consideration

Because the asphalt pavement was cohered together with roadbed, the contraction deformation of the pavement due to cooling will be constrained by the cohesion and friction between the pavement and roadbed. Consequently, tensile stress will be produced in the pavement. The tensile stress will increase with decreasing temperature. As it excesses the peak tensile strength of the pavement material, tension fracture, and thus cracks will occur.

It is noted that the stress-strain behaviour of asphalt, the bonding component of the pavement mixture, is very sensitive to temperature. The higher the temperature, the higher the ductility. By contrast, the lower the temperature, the higher the brittleness of the material. Therefore, the environment temperature substantially affects the cold cracking of the asphalt road pavement.

From viewpoint of this consideration, the occurence of the cold cracks can be predicted by estimating the cracking temperature (i.e., the critical temperature for initiating cracking), which can be determined by comparing temperature stress (i.e., the tensile stress caused by cold contraction) in the pavement material with its tensile resistance.

Strain analysis consideration

It is considered from the strain analysis that with the decrease in temperature, the failure strain (i.e., the strain at which crack occurs) of asphalt mixture decreases, and as the total strain of cold contraction plus the strain caused by vehicle load of the pavement excesses its failure strain, cracking will occur. Of course, when the cold contracting strain is greater than failure strain, cracks will alos occur even if there is no action of vehicle load. Based on this, one could also estimate the cracking temperature by comparing the cold contracting strain with failure strain, and thus predict the occurence of cracking in pavement.

The cold cracks in asphalt pavement usually generate first at the surface and then penetrate downwards. This is due to the fact that the temperature in the surface is colder, as a rasult, it produces higher contraction stress and strain and makes the pavement material more brittle. Besides, it is also accounted for the ageing and fatigue of the surficial layer of the pavement. However, it there is a layer of lime-soil mixture directly underneath the asphalt pavement, which has a higher dry and cold contractibility, the cold cracks will initiate at the lower part of the pavement and penetrate upwards through the pavement.

INFLUENCING FACTORS OF COLD CRACKING

The main factors influencing the cold cracking of asphalt pavement include:

Temperature

Generally speaking, the colder the temperature, or the greater the temperature gradient, the more severe the cracking would be. Field investigation shows that the cold cracking is extremely serious particularly under the cyclic action of freezing and thawing during earlier winter and spring. As for the cracking temperature, it is reportedly, defferent (sey, -10°, -16° or -18°C) for different countries. According to the tests conducted at Harbin District, Northeast China, it also varies with the type of pavement. For example, it is about -7.5°C for the fine-grained asphalt-concrete pavement, -11°C for the medium-grained asphalt-concrete pavement and higher than -7.5°C for the lime-soil pavement. The minimum temperature in Northern China is lower than the above-mentioned cracking temperatures, so that the cold cracking is unavoidable there.

Trafic density

Field investigation shows that more cracks will occur as trafic density is less than 1000 vehicles/day. This is accounted for that the asphalt pavement can not be compacted to have a higher density under the repeated loading of lower trafic density.

Behaviour of asphalt and asphalt mixtures

It is easy to crack for:(1) the asphalt with lower penetration index, lower ductility and higher softening point,(2) the asphalt mixture with higher contractibility and greater rigidity modulus,(3) the asphalt containing less asphaltine,(4) the asphalt concrete with higher peeling ratio and lower void ratio,(5) the asphalt mixture containing more asphalt (thus, with higher contractibility), and (6) the asphalt mixture containing less finer particles (thus, with higher sensitivity to temperature, higher permeability and easy to be aged).

Effect of water

The accumulation and permeation of surface water and migration of capillary water from underlying groundwater will make the roadbed and subgrade very moist. When freezing, it produces a great amount of uneven frost heave, resulting in the severe cracking of pavement. Besides, when the asphalt pavement is wetted, the polar molecules of water will penetrate through asphalt film to the surface of mineral aggregates. It will peel off the surrounding asphalt film and decrease the bonding force between the cementing asphalt and aggregates, leading to cracking.

Effect of roadbed and subgrade material

The cold cracking of pavement on fine-grained subgrade is more severe than that on coarse-grained subgrade, because the fine-grained soil is favourable in water migration and ice segregation,and thus causing a great amount of uneven frost heave (Wu et al.,1981; Tong et al.,1985). However, cracking of the pavement laid on coarse-grained subgrade will aslo occur if the fine particle (<0.05 mm) content in the coarse soil excesses a certain limit (say, >15%).

The type of roadbed material also has a certain effect on cold cracking. Generally, various kinds of lime-soil mixture,which are of semi-rigid material with higher dry and cold contractibility, are easy to crack and lead to reflective cracks of pavement.

Grain composition of asphalt mixtures

Investigation shows that the coarse-grained asphalt concrete has a better behaviour of anti-cracking in comparison with the asphalt crushed stones; more cracks occur in the dense asphalt concrete with poor grain size distribution; and the cracking temperature for the medium-grained asphalt concrete is lower than that for the fine-grained one.

Effect of freezing index

It is obvious that the greater the freezing index, the deeper the frost penetration,and thus, the easier the cold cracking would be.The spacing of crosswise cracks depends upon cracking temperature.The lower the cracking temperature,the wider the spacing of the crosswise cracks. The further drop of temperature after initiation of cracking does not affect the spacing, but widens the cracks.

ANTI-CRACKING INDEX

The capacity of anti-cold cracking of asphalt pavement is generally characterized by the following indexes, i.e., rigidity modulus, cold contraction coefficient, split resistence and temperature stress.

The cold contraction coefficient (α) for different types of asphalt concrete measured by Tongji University and Heilongjiang Provincial Institute of Communications are shown in Table I. The values of splitting deformation (d) for various kinds of asphalt concrete observed by an institute in Beijing are shown in Table II. It is seen from Table II that the value of splitting deformation for the A-60 type of asphalt concrete is greater (about 1.58 times) than that for Vactory-100 asphalt concrete. It is, therefore, predicted that the colding cracking for the former is less serious than that for the latter. This is consistent with field observations.

Based on test results, the temperature stress (σ) as a function of temperature for asphalt concrete was formulated by Heilongjiang Provincial Institute of Communications and Tongji University, which was written as

$$\sigma = a - (a + bt)\exp(ct) \qquad (1)$$

where σ is the temperature stress in MPa, t is the absolute values of temperature in °C, and a, b and c are empirical parameters, having the values of a = 43.87, b = 0.5856 and c = 0.01467, respectively.

Eq.(1) can be used to accurately estimate the temperature stress for asphalt concrete within the range of temperature from 0° to -30°C and on the assumption that the longitudinal contraction is completely constrained and the crosswise contraction is free (i.e., one-dimentional stress state).

If the curves of σ vs t and σ_t/K vs t, where σ_t is the tensile strength and K is the correction factor taken a value of 2, are plotted in a diagram (Fig.4), then the cracking temperature (t_o) can be determined corresponding to the intercrossing point A of the curves.

The spacing of crosswise carcks (L) of asphalt-concrete pavement can be estimated by

$$L = \frac{1}{rf}\left[a-(a+bt)\exp(ct_o)\right] \qquad (2)$$

where r is the unit weight of the pavement material in KN/m^3, f is the friction coefficient at the interface between pavement and the underlying roadbed, generally taken a value of 0.2, and t_o is the cracking temperature in °C.

TABLE I

Values of the Cold Contraction Coefficient (α) for Different Types of Asphalt Concrete

Type of asph. concrete	Values of α ($\times 10^{-5}$) at the following ranges of temp. (°C)					
	0 — -5	-5 — -10	-10 — -15	-15 — -20	-20 — -25	-25 — -30
Medium-grained	2.38	2.22	2.10	1.98	1.79	1.64
fine-grained	2.32	2.18	2.04	2.03	2.00	1.95

TABLE II

Values of Splitting Deformation (d) for the Concrete Mixed with Different Types of Asphalt

Type of asphalt	Values of d (mm) at the following temps. (°C)						
	10	5	-0.5	-6	-10.5	-15	-20.5
A-60	0.65	0.48	0.36	0.32	0.30	0.24	0.18
Vactory-10	0.50	0.34	0.41	0.23	0.19	0.16	0.16

Comparison shows that the values of c calculated with Eq.(2) are in a good agreement with the observed values.

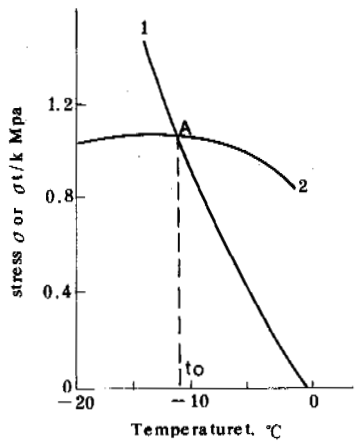

Fig.4 Determination of the Cracking Temperature (L_o) for the Medium-grained Asphalt Concrete: 1— σ vs.t, 2— σ_t/K vs.t.

CURE AND PREVENTION OF COLD CRACKING

Investigations and engineering practice show that cold cracking can be effectively prevented by the proper choice of pavement material and grain composition of mineral aggregates and the reasonable design of road profile.

Choice of pavement material

The behaviour of asphalt significantly affects the physical and mechanical properties of the asphalt mixtures, so that it is important to choose proper kinds of asphalt to construct road pavement for the prevention of cold cracking. Among the various types of existing asphalts used in road construction, the A-60, Vactory-100 and Jinxi-60 types of asphalt have a better behaviour of anti-cold cracking. It is, therefore, recommended to use the above-mentioned three types of asphalt in the construction of road pavement. Investigation shows that the behaviour of anti-cold cracking of asphalt can be greatly improved by mixing various kinds of asphalts, such as oil asphalt, natural asphalt and coal asphalt, together in a proper mixing ratio to make up a mixed asphalt or adding a certain amount of rubber, sulphur or asbestos fabric to the asphalt. For example, the results from the tests conducted at Dagang, Tianjin showed that the ductility of the asphalt with the additive of rubber is about twenty times as great as that without rubber.

Besides, mineral aggregates of the asphalt mixture also affect the anti-cracking behaviour of the pavement. It is better to use alkaline aggregates rather than acid aggregates to construct pavement, because the former has a higher coherence with asphalt, thus a higher capacity of anti-cracking.

Determination of grain distribution of aggregates

Test results show that the asphalt mixture with the grain distribution of aggregates listed in Table III is favourable in anti-cracking, so that it is recommended to the construction of road pavement. The ratio of asphalt to aggregates should be also considered in preparation of the pavement material. It is better to take the value of the ratio as 4.2-5.2. In addition, attention should also be paid to the ratio between mineral powder and asphalt. It can be determined through the split tests conducted at the lowest local air temperature, usually taking a value of 1.2.

Design of road profile

Practical engineering showed that to prevent cold craking, design of the road profile of an asphalt-paved road should be made in consideration of the operational performance of the road in cold climate. The following aspects should be particularly taken into account: (a) Reducing the difference in modula of pavement, roadbed and subgrade so as to avoid excessive consentration of tensile stress at the interlayers. (b) Under the prerequisite of meeting the needs of designed strength of pavement, cutting down the aggregate content to reduce the cold contraction of the pavement. (c) Thickening the roadbed and strengthening the coherence among pavement, roadbed and subgrade to avoid the underlying reflective cracks penetrating into pavement. (d) Increasing the strength pavement and roadbed. (e) Stabilizing the roadbed with various kinds of inorganic adhesives such as lime, cement and coal powder. The mixing ratios of the inorganic adhesives and soils recommended by the Beijing Institute of Municipal Engineering are show in Table IV. (f) Placing insulation layer (plastic film, earth fabric or sand and gravel) in roadbed to reduce the frost heave of the road. (g) Properly designing the water drainage and water proof system. In addition, carefully controlling the heating temperature and elapsed time of asphalt, ensuring the quality of construction and severely maintaining the road are also important for the prevention of cold cracking.

TABLE IV

Recommended Mixing Ratios of Inorganic Adhesives and Soils

Material	Mixing ratio
Lime: sand and gravel	5:95 or 7.93
Lime: fine soil: sand & gravel	1.8:13.2:85 or 2.4:17.6:80
Lime: coal powder: sand & gravel	5:15:80 or 3.75:11.25:85
Lime: sand and gravel	6.94

Cure of cracks

Once cracking occurs in pavement, proper cure measures should be taken. For those finer cracks which will be naturally closed in warm season, no treatment is needed at the moment. Whereas, for the wider and deeper cracks, proper treatment must be done in time. A commonly used measure is to fill the cracks with various sorts of pavement material such as rubber asphalt, resin asphalt, asphalt-cement-sand mixture. The choice of the material depends upon the size of cracks. Once cracks occured in a wide area on pavement, it is better to lay a thin layer (9-19 mm thick) of rubber asphalt, emulsified asphalt or foamed asphalt on the road surface covering the whole cracking area rather than to fill the cracks individually.

CONCLUSIONS

Investigation shows that the cold cracking of asphalt pavement depends upon cold condition (temperature and freezing index), physical properties of pavement materials (asphalt, mineral aggregates and other additives), moisture condition and type of roadbed and subgrade, structure of road profile and trafic density. After knowing the temperature stress and tensile strength of a pavement material as a function of

TABLE III

Recommended Grain-size Distribution of Aggregates in the Construction of Asphalt Road Pavement

Grain size, mm	25	20	10	5	2.5	1.2	0.6	0.3	0.15	0.075
% Finer by weight	100	82-95	50-65	30-50	22-35	—	15-28	10-25	4-12	3-7

temperature, cracking temperature of the pavement can be predicted. Cold cracking can be successfully prevented by correct choice of the pavement materials and their mixing ratios, reasonable design of road profile (pavement, roadbed, subgrade and insulation layer if necessary) and severe control of construction quality.

REFERENCES

Tong Changjiang and Guan Fengnian, (1985). Frost Heave of Soils and Prevention and Cure of Frost Damage of Structures. Hydraulic and Power Publishing House, 1985.

Wu Ziwang, Zhang Jiayi, Wang Yaqing and Shen Zhongyan, (1981). Experimental studies on frost heave of soils, Collected Papers of the Lanzhou Institute of Glaciology and Geocryology, Academia Sinica, No.2, pp. 82-96, Chinese Science Press, 1981.

AIRPORT NETWORK AND HOUSING CONSTRUCTION PROGRAMMES IN NORTHERN QUEBEC, CANADA

C. Tremblay[1] and G. Doré[2]

[1]Québec Department of Transport Quebec, Canada
[2]Service des Sols et Chaussées, Ministère des Transports du Québec

SYNOPSIS Some 750 000 square kilometers of Quebec territory are in permafrost zones. Northern Quebec is far from occupied Quebec, underpopulated and underdeveloped. In 1977, the native peoples (Cries, Naskapis, Inuit) Canada and Quebec signed the James Bay & Northern Quebec agreement. To fullfill their commitments governments are building housing units and establishing an air transportation network. In Quebec, there are greatly different approches to deal with northern construction programmes. The houses are built «on» frozen grounds; the airstrips are built «in» permafrost. So airport construction in a permafrost zone is ambitions and involves a great deal of technical considerations. Many constraints have to be taken into account when choosing an airstrip site; uneasy geotechnical conditions have to be dealt with by the designer. In Kangirsuk, Northern Quebec, such a situation occured; The one and only suitable site to locate the runway forced a 5 meter deep cut in ice - rich silty soil. Troubles were expected; our deficient experience in working in permafrost combined to a lack of relevant bibliographical references could not help us in evaluating their magnitudes. Monitoring the sensitive area was undertaken... Let us look at what we found in Kangirsuk since 1985.

Quebec is a large eastern Canada province. With more than 1 500 000 square kilometers its area is more than 15% of all canadian lands. Compare to european stantards its sizes are quite shocking; from south to north say from Montreal to Ivujivik the distance is more than 2 000 kilometers and Great White River on the west coast (Hudson Bay) is 1 200 kilometers away from the Gulf of St-Lawrence. Our Quebec alone is wider than all the nine EEC countries.

About one quarter of Quebec territory is in a continious permafrost zone, and about 50% approximately 750 000 square kilometers - in a discontinious permafrost zone.

FIGURE 1
Distribution of permafrost in Quebec

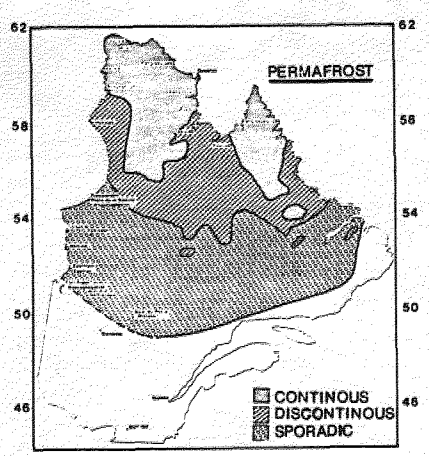

This vast northern area with its perennially frozen ground and subsoil is far from occupied Quebec, not very accessible, and virtually if not entirely uninhabited and/or developed. It is very appealing to the rest of Quebec because of its wealth of natural resources and the hydroelectric potential of all its fresh watercourses which flow towards the North, towards the Northern seas.

For centuries, the native people of those remote countries, for obvious historical reasons had very little social, commercial or administrative matters with both Quebec and Canada Governments. In early seventies the always increasing needs for energy and ressources moved up north southerners eager to exploid the huge potential of the barrens grounds of Northern Quebec - James Bay and Hudson Bay inhabited for long time by native Indians and Inuit. For the past 15 years or so these people have been at the heart of an innovative, original governement scheme which will have a great impact on resource development and, as a result, on infrastructures of all kinds.

In 1977, when the Canada and Quebec governments, the James Bay Crees, Quebec Naskapis and the Inuit of Nouveau-Québec signed the James Bay and Northern Quebec Agreement, all the parties to the contract were committing themselves to a vast undertaking on all northern coasts.

The James Bay and Northern Quebec Agreement is a sizable modern-type contract which the two (2) governments signed with the native peoples. It is contained in a book of six hundred-odd (600) pages broken down into thirty (30) highly-detailed chapters, and it touches upon all aspects of the life and development of the inhabitants of a specific area.

For the V International conference on permafrost, we have selected among several two (2) northern infrastructures improvement and development programs:

A- The construction of housing units for Inuit peoples living north of 55° latitude north;

B- The construction of a network of thirteen (13) airports to serve Inuit villages located north of 55° latitude north.

These two programs were chosen because they are examples of large-scale projects in a frozen region which use radically different building strategies and methods.

While the housing units built in the north by the Société d'Habitation du Québec (SHQ) were designed to avoid the permafrost without affecting it, environmental, physical, social and standardization-related constraints forced the designers and builders of the northern airports to «touch» the permafrost and deal with this formidable adversary.

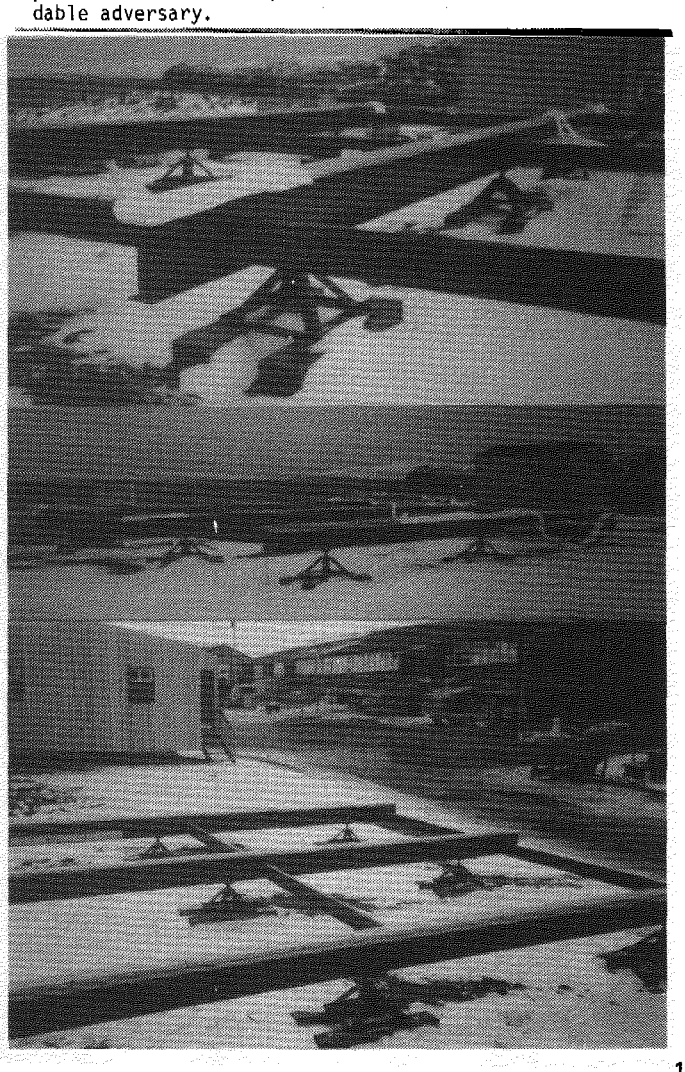

The SHQ built its structures on well drained, non-frost susceptible pads (granular material). Jacks were installed to support them and thereby alleviate all possibility of thermal bridges being created between the occupied areas of the buildings and the permanently frozen ground. The structures were reinforced in order to resist torsion, and the jacks are to be adjusted over the years to keep the buildings level. Services (sanitary tanks, drinking water tanks, etc.) were all located inside the units. You do not have to know much to realize that these construction techniques entail higher costs than conventional ones

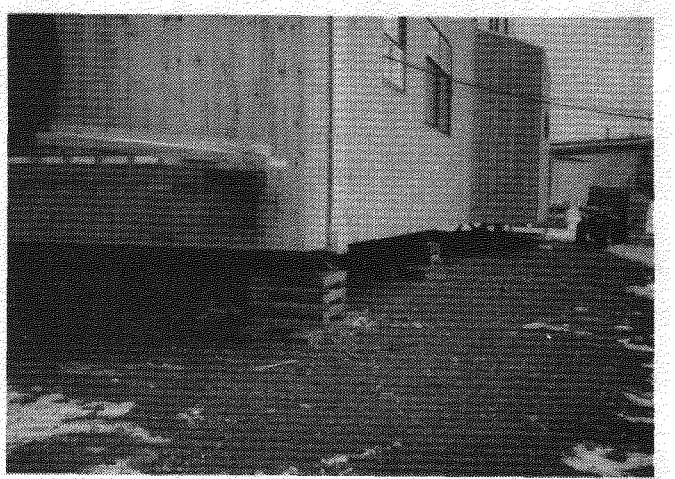

Over the past six (6) years, the SHQ has built or renovated six hundred eighty-seven (687) units and, by 1990, will spend about 65M$ on those projects that have already been approved to provide the thirteen (13) Inuit villages with some four hundred twenty (420) additional housing units.

The SHQ's policy with respect to permafrost is as follows: once new construction techniques that are practical and reliable have been perfected by researchers, an economic analysis will be conducted to decide whether intervention strategies in permafrost aeras should be altered.

In 1983, as part of the implementation of the James Bay and Northern Quebec Agreement, the Canada and Quebec governments concluded an umbrella agreement dealing with the construction of a network of thirteen (13) airports to serve the Inuit villages created and/or recognized by the first-mentionned Agreement.

This 100M$ project slated for completion in 1992 was initiated in 1984 with the construction of the Ivujivik airport - a typical airport with a gravel landing strip 1 070 metres by 30 metres (3 500' x 100'), a road from the village to the airport, a passanger terminal and a hangar for cargo, machinery, tools and vehicles. The runways are equipped with lights and electronic flight navigation aids. All the other villages will be provided with similar infrastructures with the same physical characteristics.

The summer 1986 construction context was especially eventful and interesting for the program engineers and designers.

Our first experience with the permafrost was at Kangirsuk on the western coast of Ungava Bay. In this particular case, we were glad that dedicated scientists had worked on finding logical and rational solutions to these sensitive problems and that we could still count on the determination of full teams of researchers to provide developers with techniques which greatly facilitate their task.

The second part of our presentation is a summary of a technical study conducted in order to guarantee the construction of a reliable landing strip at Kangirsuk and to improve upon the design of the projects slated for the other villages.

PART 2: Technical Considerations

1. Introduction: The context

It is quite a challenging experience working as a soil engineer and pavement designer for an airport building program in the north but, in some respects, not too rewarding a task. In fact, soils seem to be the last factor taken into account when choosing the site of an airfield. Social and environmental considerations are dealt with first as well as technical factors which are more closely related to aeronautics.

It then becomes a challenge to determine proper pavement design in view of the fact that gravel-wearing surfaces may not justify sophisticated and expensive design features such as insulation or thermo probes but do deserve good protection against poor performance due to the presence of permafrost in the underlying terrain.

One might think at first glance that a gravel surface requires very little design effort on account of the relatively low investment that it implies and of the easy and cheap maintenance it is liable to require. However, when ten airports involving a total investment of 100M$ are concerned, it becomes worthwhile to emphasize technical studies in order to optimize the structural designs and therefore long-term performance.

2. Development Limitations

Many factors are to be considered prior to the selection of an airfield site. Most of them are related to the needs of the community, aeronautical requirements, environmental considerations as well as the topographical and geological context. These factors make it very difficult to select a proper site even in a region as vast and little populated as northern Quebec.

Social Requirements:

The needs of the community are a key consideration. The airport has to be as close as possible to the village without aircraft takeoffs and landings constituting a danger or causing stress. Traditional hunting and gathering sites, graves, trails, reference points and archeological sites must also be protected.

Aeronautical Norms:

Strict longitudinal and traverse clearence norms have to be taken into account when designing the geometry of an airfield. Maximum slope and inflection standards must also be observed. The orientation of the runway can be determined only after due consideration to the direction of the prevailing winds.

Environment:

The arctic tundra constitutes a very sensitive environment. For instance, even a minor change in the thin organic layer, may leave scars that could never disappear. Archeological sites, nesting areas, vulnerable streams and visual aspects are some of the important points to be studied to evaluate the impact of the project.

Topography and Geology:

It is easy to figure out how cost and feasibility of a project can be affected by the relief of the terrain. It is however a little bit more difficult to determine the role played by geology. Two major problems have come up since the beginning of the airport programme. They are the rarity of granular materials and the difficulties occurring in cut sections on frost susceptible soils.

The geological context caused great difficulty to the engineers while prospecting granular materials and desigining foudations in cut sections on frost susceptible soils. Since in our mind the exploitation of sand or gravel pits would cause great harm to the environment and deprive Inuit communities of these scarce ressources, granular material was to be produced essentially from crushed stone. Besides, the lack of bibliographical references that deal with construction of gravel airfield pavements in permafrost areas and our own lack of experience in that field combined to the problems encoutered during the first excavation in frost susceptible soils, led to a specific study of the Kangirsuk airport.

3. Kangirsuk Research project

3.1 Introduction

The Kangirsuk airstrip is a typical example of a permafrost hazard. It required a 200m long excavation to a maximum depth of 5m that was done by blasting the grozen ground. Since no borehole had reached the sub-base level, very little was know about the soil and the permafrost at that point.

3.2 Geotechnical Context

Excavations and subsequent soil testing revealed that the granular pavement was to be placed on top of an ice-rich silty sand.

The problem area is charactarized by an outwashed glacial till (approx. 1m thick) on top of a fine-grain matrix till. Bedrock depth in the middle of the cut section is approximately 5.5m.

Soil at that point was constituted of up to 80% (in volume) ice lenses (average 50%) (figure 1). Results of testing showed fairly consistent water and fine-grain (<80M) content of respectively 30% and 40%. The active layer vary from 0.5, in fine grained soils to 2.5m in granular soils. The permafrost temperature is around -3°c.

FIG. 1 Ice rich silty soil at subgrade level

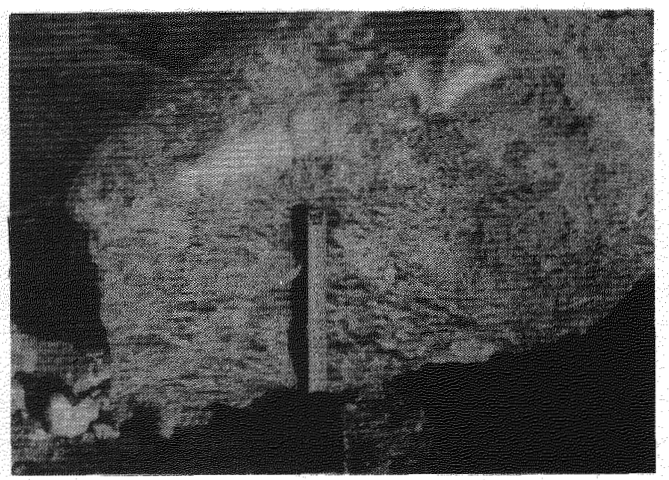

3.3 Pavement structure

Starting with a conventional pavement structure, alterations were made as problems occurred. The 70 cm thick structure was protected by a 15 cm sand pad over a permeable liner in order to protect the granular base from contamination by fine-grain soils. Moreover, the ditch was filled with a riprap and protected against solpe movement or erosion by a filtering barrier. This last feature was designed to ensure shoulder and slope stability while minimizing differential settlement and frost action (figure 2).

FIG. 2 Pavement structure in cut zone

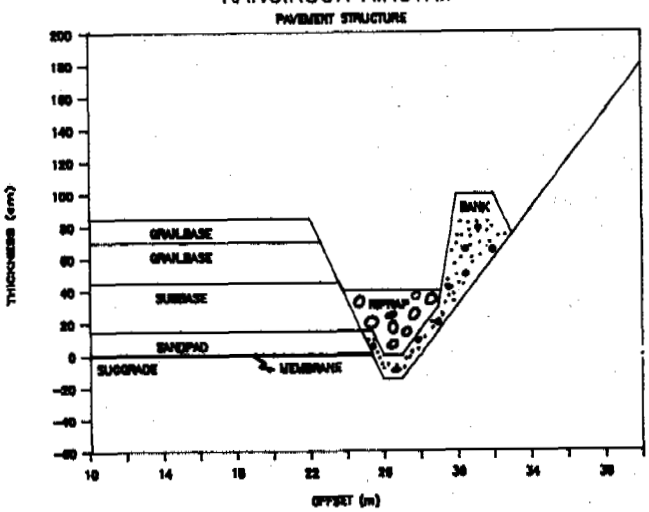

3.4 Evaluation Instruments

Five phenomena were to be observed during the first three seasons the airport was in operation. They were: penetration of the thaw line, long-term settlement trends, frost heave, bearing strength of the sub-base, and slope stability. Specially designed instruments were installed in the critical zone during the construction phase to measure specific parameters (figures 3 & 4)

FIG. 3 - Instruments illustration

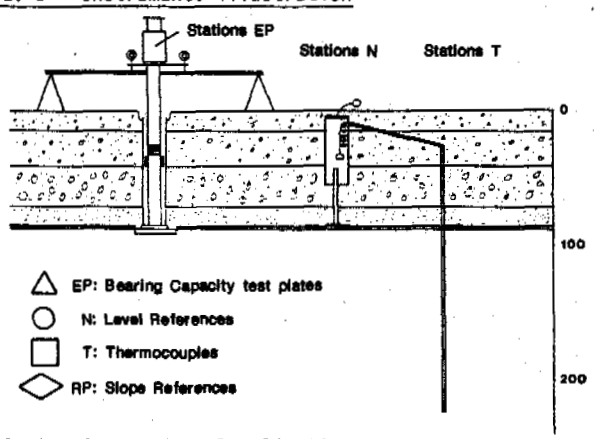

FIG. 4 - Instruments localisation

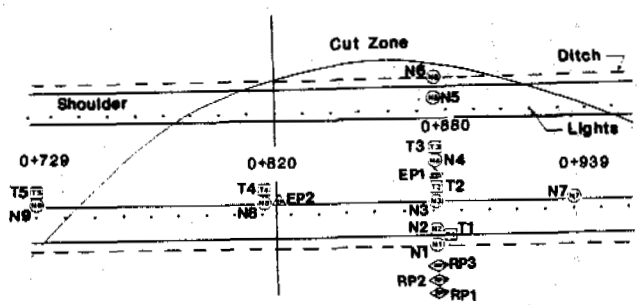

Thaw Line:

Five electronic thermometers were installed along a longitudinal and a transverse section on the runway. Each thermometer was constituted of six equally-spaced thermocouples on a 2.4 meter deep probe.

Settlement and Frost Heave:

These two parameters were to be measured by means of nine level references installed on the subbase surface. A metal rod protected by a metal cylinder enabled the reading of the reference marks installed in the pavement.

Bearing Strenght:

In order to measure the bearing capacity of soils in the active layer, two 30 cm plates were installed under the runway and protected by metal cylinders. They were left in place to be tested when the thaw line reached its maximum depth.

Slope Movement:

Three reference marks were placed on the slope along a cross-section where the cut was the deepest. These marks should make it possible to record the extent of slope movement due to solifluction or slumping.

3.5 Findings

After two seasons of thawing in Kangirsuk, data and observations were compiled to produce a preliminary report. The main findings of that first part of the study are as follows:

Active layer

After the first season of thawing, the active layer was 40 to 60 cm thick under the pavement structure while it reached 160 cm under the ditch. During the second season, the thaw line did not exceed the maximum depth reached the previous year (figures 4 & 5). Two factors could explain a thinner active layer during that second season. They are the possible colder summer and the addition of a 150 mm thick surface gravel layer at the end of the first season.

FIG. 4 Typical Thermocouple Record

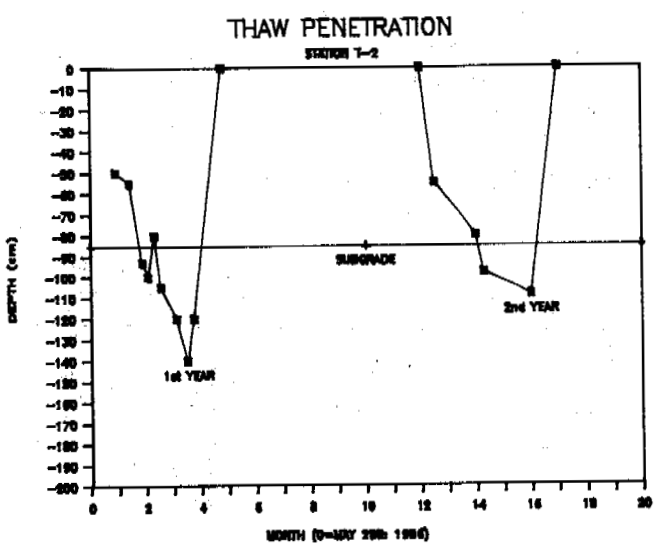

FIG. 5 Thaw Penetration during the first two years

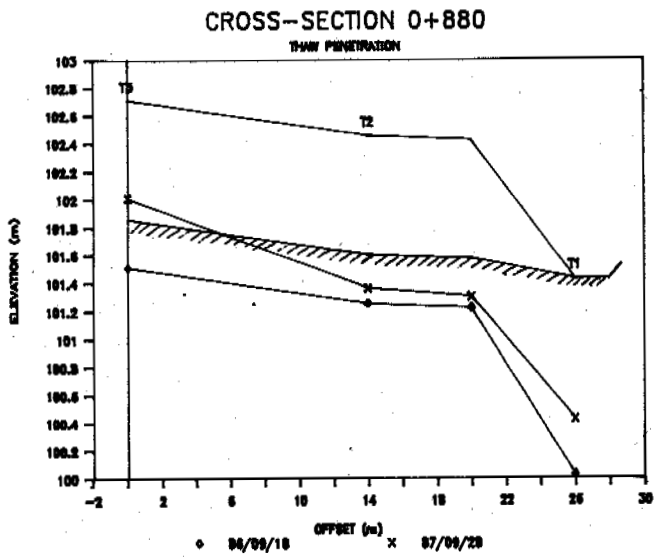

Settlement

The settlement was found to be very irregular. The average reading during the first reason was about 15 cm but it was as high as 23 cm at certain spots. During the second season, 1 to 5 cm of additional settlement was recorded in spite of the shallow active layer. Depressions were observed in the crown of the subgrade (figures 6, 7, 8, 9.)

FIG. 6 Typical Settlement record

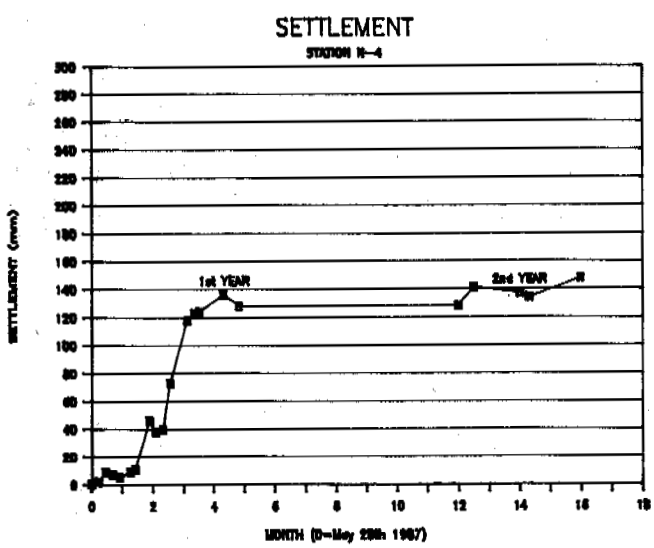

FIG. 7 Extreme Settlement Record

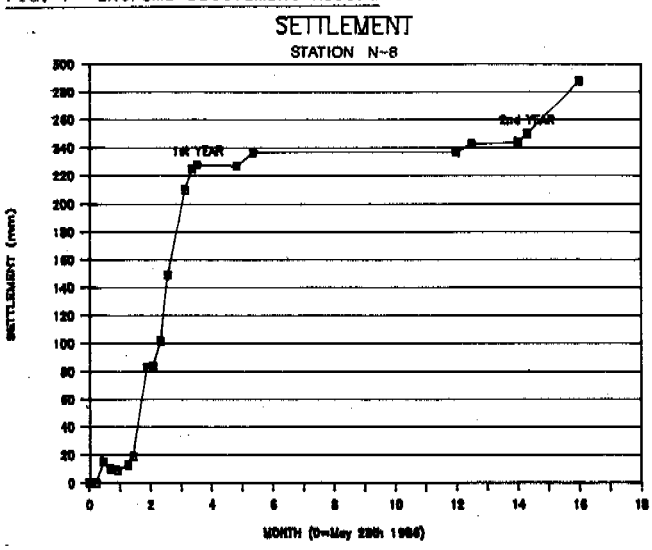

FIG. 8 Settlement: longitudinal section (1986 and 1987)

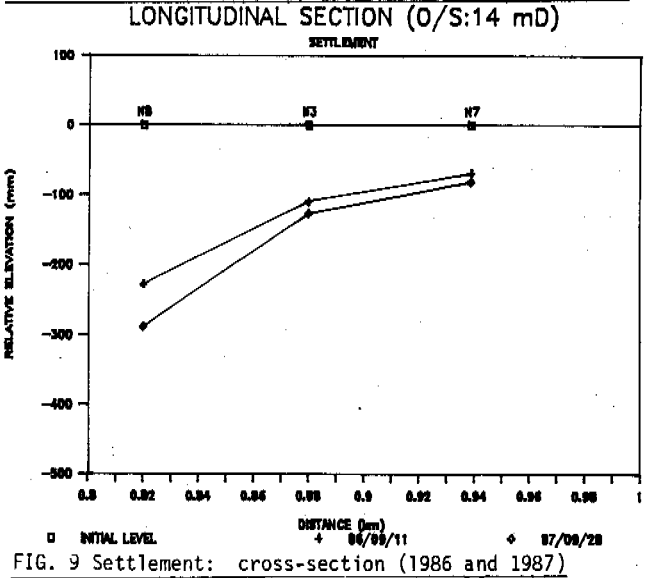

FIG. 9 Settlement: cross-section (1986 and 1987)

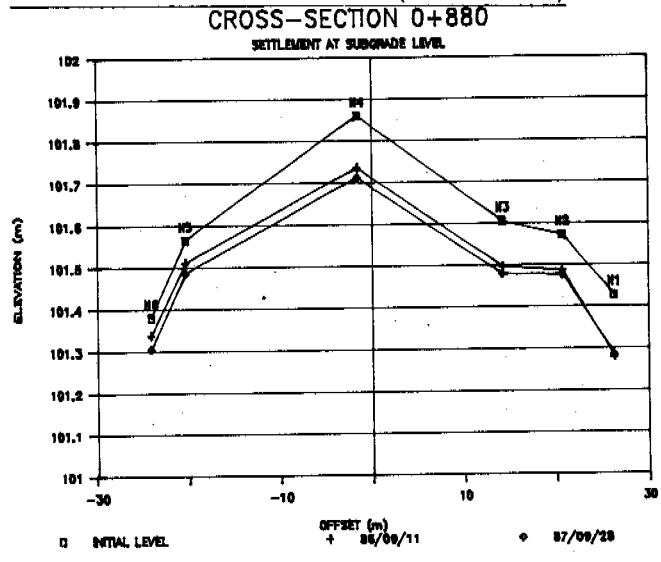

The addition of riprap in the ditch caused an additional settlement of 10 cm that kept the drainage point below the platform.

At this early stage of the study, no findings were as yet available on the extent of long - Term settlement Trends.

Bearing capacity

The bearing plate tests performed on the active layer after thawing and consolidation by the granular foundation, showed results slightly lower (10 to 15%). Than the predicted spring-reduced bearing strenght. It thus confirm that well drained soils in those conditions could regain expected bearing capacity.

Frost heave

During the only freezing season monitored so far, no significant heaving had occured. This might be related to the high thermic gradienter that probably lead to a fast freezing of the active layer.

Slope stability

The cut slope was affected by active erosion (figure 10) and by undefined solifluction movement. Big sinkholes (up to 60 cm deep) were also observed. The filtering bank was found to be efficient in controling eroded sediments altough overflowing occured in few spots.

FIG. 10: Active erosion in cut-slope

3.6 Recommandations

The first part of the study led to the proposal of the following preliminary design principles for future sites.

- If feasible cuts should be cuts should be avoided in frost susceptible soils.
- If a cut is unavoidable, the subbase thickness should be sufficient to minimize the penetration in subgrade and differential movement related to freeze-thaw cycles. A preliminary bibliographical approach would suggest a total granular thickness of 1,5 m protected against contamination, as being a proper foundation in such conditions (Laing,1983)
- If possible, excavation, preparation of the subgrade and placing the subbase should be performed early in the season while placing top layers of the

foundation should be done at the end of the thawing period. Such a method should result in a deep thaw penetration during the first year. The addition of the base layer later in the season would correct the first year settlement while it should ensure a shallower thaw penetration during the subsequent years.

- The crown should be accentuated to achieve a 3% traverse slope.

- The structural design should take into account a 10% to 15% additional reduction factor for the active layer bearing capacity.

- The drainage system should be protected against active sedimentation from cut slope erosion and solifluction - type landslides. Slope stabilisation should be strongly considered.

Conclusion

Considering all the money being invested in the northern Quebec airport programme, the Kangirsuk study is obviously worthwhile. Conclusions should lead to a better comprehension of permafrost and thereby improve our design and construction methods in that particular context. The long-term monetary as well as technical benefits should be profitable to the Inuit communities and to Quebec.

References

- Ouvrir le Nord à pas feutrés, Pilon J.A., Beaudoin A. Geos 1984/4.

- Road Construction in Palsa fields, Keyser J.H., Laforte M.A., Présentation du T.R.B. Washington, 1984

- Problèmes de conception des chaussées dans le Nord Québécois, Revue Routes et Transports, Printemps 1984

- Evaluation of experimental Design features for roadway construction over permafrost, Esch. D.C. Permafrost: fourth annual conference, Alaska 1983

- Determination of critical Height of railroad embankments in the permafrost regions of the Quinghai-Xizang Plateau, Xinoming H., Permafrost: fourth annual conference, Alaska 1983

- In situ Direct Shear tests at the freeze / thaw interface and in thawed soils, Zhiquan T., Permafrost: fourth annual conference, Alaska, 1983

- Infrastructure des Transports: les effets de gel et les moyens de Protection, Keyser J.H.

- Engineering in the North, Laing J.M., fifteenth musked research conference, may 1983

FROST DAMAGE OF ENCLOSURE AND ITS MEASURE FOR PREVENTING FROST HAZARD

Wang, Gongshan

Heilongjiang Provincial Low Temperature Construction Science Research Institute

SYNOPSIS The main reasons producing enclosure crack in seasonal frost region might be concluded as follows: the first is the deformation difference of foundation bed with various facing;the second is the difference of tangential frost heaving force around foundation; the third is the difference of normal frost heaving force acting on the bottom of foundation. Our observation results show that: the enclosure with an eccentrically loaded foundation can be able to reduce inclined degree about 92 to 97% caused by south facing;and the enclosure with a cone foundation is available for reducing the action of tangential frost heaving force on the lateral surface of foundation about 77%. Beside above, because the weakness of subsoil after freeze-thawing cycles will be happened, a weakness coefficient, less than 1, should be considered while designing the bearing capacity of subsoil if the foundation depth is less than the maximum frost depth.

INTRODUCTION

Up to now, more and more enclosures, with a simple and light structures, have been built in the areas with frost susceptible soils. However, they were broken in several years or sometimes in several months after building because of strong frost action. In order to explore the characteristics and mechanism of frost damage of enclosures and its preventation measures, we have investigated many phenomena about frost action on enclosures worked years and built some with various types of foundation for experiment in Yejiangan observation station during 1983 to 1986. After three freeze-thawing cycles test, some experimental results for preventing enclosures from frost damage have been got which were recommened in this paper.

MAIN REASONS ON FROST DAMAGE OF ENCLOSURE

The effect of direction on the stability of enclosure

The freezing and thawing speed in both sides of enclosure with a east-west direction is quite different because of various sunshine time. In winter, the frost penetration rate, the frost depth and frost heave amount of subsoil in the north facing side will be much larger than that in the south facing side. The angle deformation (Fig.1) produced by differential heave between north and south side can be expressed by

$$\theta_1 = \text{arc sin}(\Delta h_1/B) \qquad (1)$$

where B is the width of foundation. The centre of gravity of enclosure has been moved to the south. During spring, the thawing speed in the north facing side is rather slow. While the thawing depth is over to the bottom of foundation in the north side, there is a centain thickness of thawing layer under foundation in the south side. So the thawing settlement of the foundation in the south side will be certainly much larger than that in the north side, with a differential displacement of Δh_2, because of the

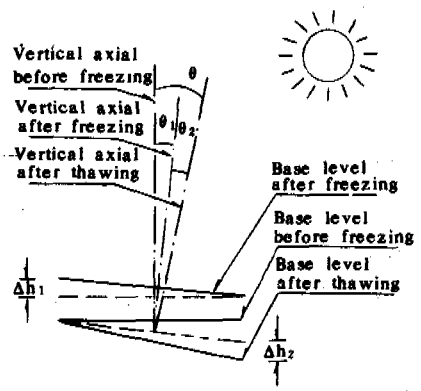

Fig.1 A Digram on Displacement Process of Enclosure

weakness of thawing layer and the movement of the centre of gravity of enclosure towards the south side, cause by differential heave which makes enclosure inclined to the south with an angle deformation θ_2 expressed by

$$\theta_2 = \text{arc sin}\ (\Delta h_2/B) \qquad (2)$$

After thawing, the total angle displacement of

enclosure to the south is $\theta = \theta_1 + \theta_2$. Meanwhile, the gravity can be divided two parts P_1 and P_2 which along the direction and normal to the direction of vertical axial of enclosure respectively

$$P_1 = P \cos \theta \quad (3)$$

$$P_2 = P \sin \theta \quad (4)$$

The eccentricity, e, will be increased with the increase of θ, so will be the P_2 which makes enclosure inclined, and even broken.

The effect of tangential frost heaving force on the stability of enclosure

Even if the foundation depth of enclosure is rather deep or deeper than the maximum frost depth, when the backfill around foundation is frost susceptible, the lateral surface of foundation is acted under frost tangential heaving force which makes foundation produced tansion crack and tansile failure with a direction to parallel to horizontal level near frost front.

The effect of normal frost heaving force on the stability of enclosures

When the foundation depth of enclosure is rather deep but less than maximum frost depth, the enclosure may be failed under the action of normal frost heaving force which causes differential heave. If the space between the bottom of bearing brick arch or concrete beam of enclosure and the ground surface is less than the maximum frost heave amount, the arch or beam will be acted under normal heaving force at the middle or the end of freezing period which, of course, makes enclosure cracked and broken also.

EXPERIMENT IN SITU

The experimental field is located in Yejianggan farm with yellow sandy clay in active layer, maximum frost depth of 1.2 to 1.4 m, and a homogeneous frost heave amount of 30.6 cm. The ground water level was always deeper than the frost penetration front, and was around -1.0 m in autumn and the deepest one of -2.15 m. The observation points of vertical deformation were set up at the both north and south sides of experimental enclosures, the displacement of ground surface and frost penetration depth were also conducted. However, the vertical angle deformation was calculated by the vertical differential deformation of both north and south sides, i.e.

$$\Delta h = h_N - h_S \quad (5)$$

and

$$\theta = \arcsin (\Delta h / L) \quad (6)$$

where, h_N—north vertical deformation of enclosure, cm;

h_S—south vertical deformation of enclosure, cm;

L—the distance between two observation points, cm.

EXPERIMENTAL RESULTS AND ANALYSIS

The relation of freeze-thawing penetration depth in both sides of enclosure vs elapsed time is shown in Fig.2. After analysing the observation results obtained in situ, some ideas might be made as follows:

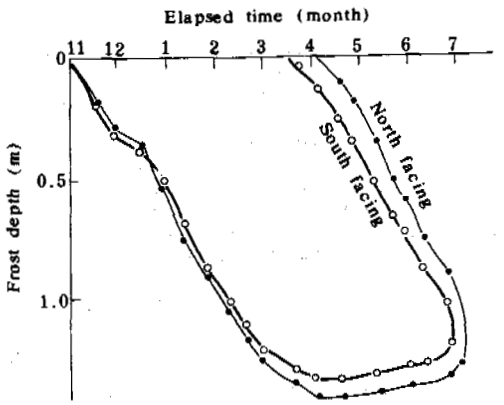

Fig.2 Frost Depth vs Elapsed Time in Both Sides of Foundation

1. Reducing incline of enclosure is an important measure for preventing structure from frost damage. Our results show that it is not necessary and not economy to make an enclosure produced no frost heave. If the anti-incline measure and settlement joint are set up reasonably, the enclosure will not be failure even though with a rather vertical displacement.

Because of a larger ratio of height and width of enclosure, and its higher centre of gravity, the effect of inclined angle of foundation on the stress distribution of subsoil is rather strong when the eccentricity of foundation is less than B/6, the stress of subsoil may be calculated as follows:

$$\sigma_{max} = N/F \, (1+6e/B) \quad (7a)$$

$$\sigma_{min} = N/F \, (1-6e/B) \quad (7b)$$

where, σ_{max}—the maximum stress of subsoil, P_a;

σ_{min}—the minimum stress of subsoil, Pa;

N—total load acting subsoil, N;

F—cross section of the bottom of foundation, m^2;

B—width of foundation bottom, m;

e—eccentricity, m, $e = h \cdot tg\theta$, h is the height of centre of gravity.

Our experimental results show that the compressive stress at the south bottom of type 1 foundation (Fig.3) was 7.23 times over that at the

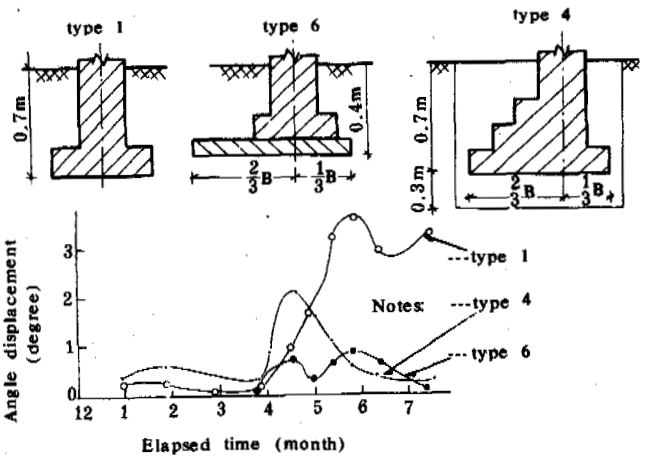

Fig.3 Angle Deformation vs Elapsed Time of Eccentrically Loaded Foundation

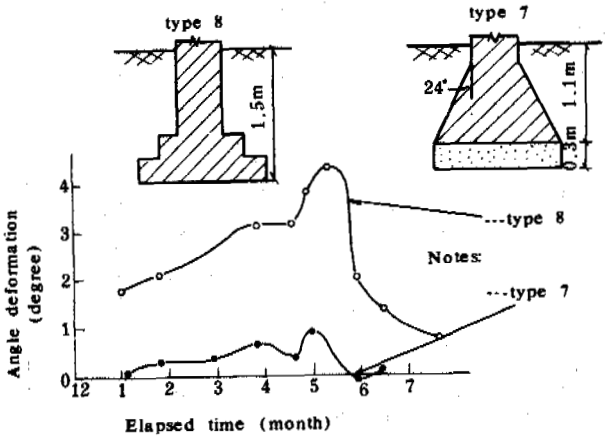

Fig.4 Angle Deformation vs Elapsed Time with Cone Shapped Foundation

north bottom after two freeze-thawing cycles which makes the enclosure of type 1 lain down after the three cycles. Type 4 and type 6 foundations have been added an eccentrical load with opposite direction before working in order to deal with the differential deformation problem. In this case, the compressive stress of subsoil at the bottom of foundation in the south side will be very small, so will be its deformation. We assume that the allowable stress of subsoil, σ, is given after thawing, the maximum incline angle θ_{max} can be calculated by formula (8),

$$\theta_{max} = \text{arc tg}\frac{B}{6h}(\sigma F/N - 1) \qquad (8)$$

The enclosure will be lain down while the inclined angle is more than the θ_{max}.

2. Reducing tangential frost heaving force is an effective way for preventing enclosure from frost damage. The enclosure with type 8 foundation (see Fig.4) has been lain down after two freeze-thawing cycles even though its foundation depth was over the maximum frost depth. Therefore, it will be not able to get a good result in the condition of only increasing the foundation depth, but never reducing the tangential frost heaving force. In order to reduce the effect of tangential heaving force, a test enclosure of type 8 (see Fig.4) with a cone shapped foundation, with a backfill of frost susceptible soil, has been conducted. Its experimental result was quite different from that of type 8. A space between frozen ground and cone foundation will be occured when surface part uplifts vertically under the action of frost heaving force, which will reduce the adfreezing area between frozen ground and the lateral surface of foundation. If the lateral deformation of frozen ground is so small that it is not necessary to be consisdered, which means that only the part of frost front connect to the surface of foundation. Therefore, the adfreezing area is so small that the connection is very easy to be broken. Thus, the space will be developed with the increase of frost penetration depth which is almost equal to the frost heave amount of subsoil (see Fig.5).

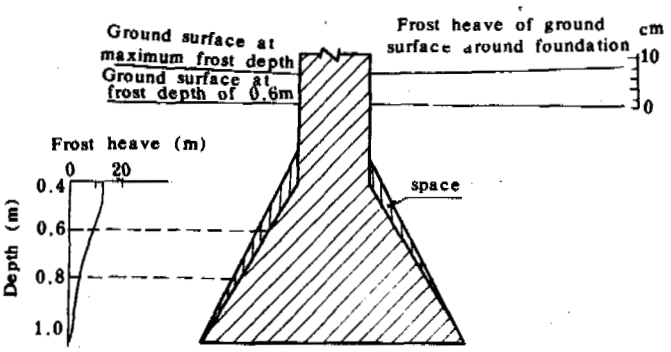

Fig.5 A Deformation Digram of Soil Block Around the Foundation with Cone Shapped

3. Weakness phenomena while thawing of frozen subsoil. If the plastic deformation of subsoil

during thawing does not happen, the foundation should be recovered to the origenal location after thawing. However, our experimental results show that the redusial inclined angle and total settlement will increase year by year. Based on the results of compressive test by Aoyama Kiyomichi* (see Fig.5), the strength of thawing soil will be lower than that of unfrozen soil, and it will be much strong for the subsoil with high water moisture. As a conclusion, the weakness of the subsoil after freeze-thawing cycles should be consisdered when the frost depth is over to the bottom of foundation. A weakness coefficient K after freeze-thawing should be decided before design of foundation. The K is a ratio between the ultimate strength of subsoil after thawing and the ultimate strength of subsoil before freezing with a value of less than or equal 1 which depends on the frost susceptibility of subsoil. In common case, K equals 0.4 to 0.6 for strong frost susceptible soil, 0.6 to 0.8 for middle frost susceptible soil, and 0.8 to 1.0 for slight or no frost susceptible soil respectively. Consquently, the subsoil strength of enclosure, changed with the facing direction, should be more than its maximum stress produced by loading.

$$[\sigma]\, K \geq \sigma_{max} \tag{9}$$

where, $[\sigma]$—allowable bearing capacity of unfrozen soil, Pa. Comparing formulas (5), (6), (7) and (9), we may have following expression:

$$[\sigma] \geq \frac{N}{KF}\left(1+\frac{6htg \arcsin\left(\frac{h_N-h_S}{B}\right)}{B}\right) \tag{10}$$

If there is no effect of the facing direction, formula (10) will be much simple:

$$[\sigma] \geq \frac{N}{KF} \tag{11}$$

CONCLUSIONS

1. The incline to the south of enclosure mainly occures in the thawing period of subsoil because the different thawing speed in each side of enclosure makes differential thawing settlement (see type 1 foundation). The incline degree can be reduce about 92% to 97% by using eccentrically loaded foundation (see type 4 and type 6 foundation).

2. For the enclosure of deep buried foundation without any anti-heave measure around its lateral surface, the frost heave of the enclosure will be happened under the action of tangential frost heaving force, and of course, its incline will occure during thawing. When the enclosure was set up with a cone shapped foundation with a cone angle of 24 degree, its incline degree can be reduced about 92%.

3. The weakness phenomena of subsoil during thawing should be considered while the foundation depth is less than the maximum frost depth. The bearing capacity of subsoil should be enough which can be got by using sand cushion base or eccentrically loaded foundation for reducing the effect of weakness phenomena (see type 4 or type 7).

4. Anti-heave measures of enclosure should be designed according to frost susceptibility of subsoil, direction, structure of enclosure, and landform etc.

ACKNOWLEDGEMENT

The authors appreciate the Chief Engineers Xia Yupu and Liu Hongxu for their instruction.

* The properties of freeze-thawing soil, "Soil and Foundation", 1977, No.7 .

APPLICATION OF LIME STABILIZATION ON HIGHWAY PERMAFROST REGION, QINGHAI-XIZANG PLATEAU

Wang, Qing-tu[1], Wu, Jing-min[2] and Liu, Jian-du[2]

[1]2nd Highway Eng. Bureau of the Ministry of Communication, Xian, Shaanxi, China
[2]The First Highway Survey and Design Institute of the Ministry of Communications, Xian, Shaanxi, China

SYNOPSIS Qinghai-Xizang Plateau is characterized by high altitude, low latitude, cold and severe weather, long frost duration and complex hydrogeological condition. Qingzang Highway runs through the hinterland of permafrost region where ground ice is well developed and buried very close to ground surface. It is difficult to get sand and stone for construction along the line under the threat flood from rivery water. So, the only way for preventing it from frost damage is to treat its subgrade with the lime stabilized soil(called "lime stabilization"). Since 1973, the First Highway Survey and Design Institute in co-operation with the Science Institute of the Ministry of Communications has done a series of tests on lime stabilization in laboratories and fields. A large number of data have been obtained from field observation and measurement at the tested subgrade with the length of kilometers. It is shown that the application of the lime stabilization on highway engineering in permafrost regions is quite good both in aspect of strength and of stability.

Introduction

Soils Stabilized with lime(called "lime stabilization") have been effectively applied as a kind of material for highway engineering widely in China, but it is still a new object of study on its application in permafrost regions, yet we have obtained a series of experience, successful in practices, at other regions in China. Qingzang Plateau is typical of permafrost table lands, spreading over a relatively large extent in region of moderate and comparatively low latitudes in Qinghai province and Tibet autonomous region, with the highest altitude in the world. It is a climatic region of bitter cold and arid. The freezing season is 7-8 mounths long and the annual mean atmospheric temperature is -4°C to -7°C there. The negative temperature has been recorded frequently at night, even in mounths, July or August with the highest average temperature yearly. It is lack of rainfall, the annual precipitation is about 300mm merely. Qingzang Highway is running through the hinterland of the permafrost region on the Plateau for 560 kilometres in length. The altitudes along the Highway 4500-5200 metres, the ground ices are very abundant everywhere. The major soil constituents in this region are silty and sandy soils or gravel soils. It is lack of stones and sands to be used for highway engineering all along the highway line. Therefore, we have no choice but have to make a trial to stabilize the natural subgrade soil of the highway with lime as fundamental layer of the pavement. Since 1973, the First Highway Survey and Design Institute in co-operation with the Communications Science Institute of the Ministry of Communications have conducted a good deal of simulated road tests, with typical soil samples under the climatic conditions which are analogous to that to be in region of the Plateau, in laboratories. More than ten segments of testing roads with a total length about 1.6k were erected separately in different types of lime stabilized soil subgrade and mat base structure at various testing fields and opened to traffic. Indices were drawn from a series of data which had been observed upon the strength, road stability and the pavement smoothness under traffic operating during seven years, which indicated that the "lime stabilization" is an effective approach to treatment for pavement in permafrost region of the Plateau.

The Phisical Properties of Soils and the Chemical Composition of Lime

The samples used for testing of lime stabilization were made of typical of soil, at our option, in various along the Highway, also with which was sampled at Barchal, for purpose to fulfill comparative tests. The physical characteristics of them are listed in table I

The physical properties of soil samples

Table 1

Sampling site	Soil	Plastic index	Liquid limit	Grain composition (%)								
				20~10	10~5	5~2	2~0.5	<0.5	>2	2~0.05	0.05~0.005	<0.005
All along The Qin-Zan Highway	Light clay soil	9	27						1 0	44 64	47 25	9 11
	Silty heavy clay soil	13	30							4	50	46
	Sandy loam	5	22						1	50	40	9
	Fine sandy loam	7	23							62	28	10
	Gravelly coarse sandy loam	5	16				16	39	45	47	1	7
	Gravelly light clayey loam	9	28						14	55	12	19
	Heavy clayey loamgravel	15	25	14	22	27	15	20	64	28	3	5
	Gravel-soil	13		9	21	29	4	1	59	33	4	4
	Debris-soil		19	15	16	28	17	36	51	40	4	5
	Silty light clayey loam	11	24									
	Silty heavy clayey loam	16	34							26	45	30

The contents of chemical composition in lime usefor soil stabilization in percentage by weight are: Cao, 60-84%; Mgo, 0.8-1.5%

The Strength of Soil structure Stabilized with Lime

We have made samples, with the typical of various soils, stabilized with various lime contents, cured under different curing conditions and with various curing periods, to study the strength developing with time during curing.

The rule of strength evolution during curing cycle under conditions of comparatively low temperature (+12°C).

The strength measured at various curing cycles, under the average temperature (+12°C) analogous to which during construction period (from May to September) at fields in the permafrost region of the Plateau, are listed in table II

The evolution of strength during curing at +12°C

Table-II

Sampling site	Soil specimen	Lime content %	curing	Curing cycle (day)	Compression strength without lateral restraining pressure (MPa) Unsaturated	Saturated	Hydrostability losses (g)
Cocksieloy	Sandy loam	10 10 10	water curing in air	14 28 60	0.05 0.07 1.52	0.19 0.27 0.77	0.30 0.31 0.61
	Light clay loam	10 10 10	water curing in moist sawdust	14 28 60		0.83 0.94 1.24	
	Debris-soil	5 5 5	water curing in moist sawdust	7 28 60	1.25 1.25	0.94 1.05 1.08	
Tsomall	Clay gravel	3 2 3 4 3	water curing in moist sawdust	14 28 28 28 60		0.52 0.89 0.81 0.82 0.72	
	Light clay loam	10 10 10	air curing	2 14 28		0.33 0.45 0.94	
River	Gravelly soil	5 3 5 7	water curing in moist sawdust	2 28 28 28		0.18 0.42 0.47 0.51	
Roadworks maintenance squad (NO.74)	Silty heavy clay loam	10 10 10 10	water curing in moist sawdust	7 14 28 60	0.38 0.86 0.90 0.75	0.98 0.19 0.32 0.51	0.28 0.30 0.48 0.89
Woodwlown	Debris gray soil	3 3 3	water curing in moist sawdust	14 28 60		0.28 0.48 0.47	
Barchol (Shaanxi province)	Silty light clay loam	10 10 10 10 10	water curing in moist sawdust	7 14 28 60 90	0.05 0.79 0.98 1.28 1.41	0.48 0.88 0.71 1.05 1.13	0.75 0.97 0.81 0.87 0.90
(Qinghai province)	Debris gray soil	5 5 5 5	water curing in moist sawdust	7 28 60 90	1.62 2.13 2.25 2.68	1.41 1.98 2.04 2.29	0.87 0.79 0.88 0.90

It is seen from table II, both the early strength of lime stabilized debris soil and that of the clayey loam are higher than those of other soils stabilized with lime. And the early strength of the lime stabilized sandy loam seems quite low. The key to the develping of the strength for lime stabilized soil structures lies in the chemical actions of the ion exchange and carbonation inside of them, which are directly in fluenced by the temperature. The chemical action develops more rapidly as the temperature is going up higher and higher, and correspondingly, the strength of the lime stabilized soil will increase quicker and quicker, but it would not increase any more, as the temperature has fallen below 0°C and the chemical action ceased at all. The Strength of any lime stabilized soils would increase with the days during curing. It is in general, the strength increasing is comparatively quicker within the curing period of 28 days, and it would slow down later on moreover, the strength of the stabilized soils which are alike in kind is closely correlated with the content of lime which has been added to the soil in percentage by weight, but the highest strength would be obtained at the optimum content only, and it is far from that the strength is proportional to the lime content added—the more the strength increases, the more the lime content has been added.

The evolution of strength during curing while the temperatures fluctuate between positives and negatives alternately.

Stabilized soil samples had been cured under temperature which had been made to fluctuate between positives and negatives alternately in accordance with that the negative temperatures often occurred at night in July and August of the warm season. The results of the tests are listed in table III and table IV respectively.

The evolution of strength during curing while the temperature had been made to fluctuate between positives and negatives alternately

Table-III

Sampling site	Soil specimen	Lime content (%)	Curing cycle (day)	Compression strength without lateral restraining pressure (MPa) saturated R	saturated w (%)	saturated r (g/cm³)	unsaturated R	unsaturated w (%)	unsaturated r (g/cm³)
Cocksieloy	Sandy loam	10	14	0.19	20.3	1.67	0.49	10.3	1.67
			28	0.25	20.5	1.67	0.66	8.0	1.67
			60	0.71	14.2	1.67	1.27	2.7	1.87

The strength evolution of unsaturated gritty soil stabilized curing at field in open air

Table-IV

Strength (MPa) / Lime content / Curing cycle (day)	3 %	4 %	5 %
14	0.93	1.21	1.38
28	1.71	1.87	2.01

It is seen from table III and IV, the strength of lime stabilization structure would evolve thoroughly too, while the sample was cured in positive and negative temperatures alternately. The strength increases with days of curing, but it is somewhat lower than what is cured in positive temperature with the same curing days. For example, the strength of the stabilized sandy loam is 20-30% lower, and that of stabilized gravel-soil is about 10% lower., However, they are all able to fulfill the quality requirements of design.

The Freezing Resistance and Hydrostability of Lime Stabilization Structure

Freezing Resistance

For verifying the evolution of strength of stabilized soil structure after it has been both frozen up and thawed out at -12°C--- -15°C for 16 hours, under dry, moist and saturated conditions separately. The evolution of strength of them after they underwent freeze-thaw processing 6 times again is shown in table V.

Moreover, both samples that of unsaturated and that of saturated after (which had) thawed were frozen at -5°C-- -20°C for 12 hours and thawed at +20°C for 12 hours and measured their strength at they were frozen-thawed 3,6,9,12 and 15 times over again, respectively. The evolution in

The evolution of strenght of stabilized soils frozen thawed many times over again

Table V

Sampling site			Cocksieley	Tsoumall River					Woodsolens
Soil specimen			Light clayey loam	Heavy clayey loam gravel			Light clayey loam	Gravelly soil	Debris-soil	
Content of line (%)			10	3			10	5	12	
Freezing proof agent (Mgcl2) added (%)				3						
Curing cycle (day)			28	60	28	14	28	60	28	28	14	28
Compression strength without lateral restraining pressure (MPa)	Cured sample without freeze-thaw processing		0.94	1.24	0.54	0.52	0.81	0.72	0.84	0.47	0.39	0.48
	Frozen-thawed 6 tiles over again	Frozen-thawed in dry air	0.76	1.02	0.54		0.62	0.62	0.82	0.41		0.37
		Frozen thawed in moistifying	0.62	0.86	0.51	0.25	0.32	0.53	0.77	0.29	0.25	0.28
		Frozen-thawed in saturation	0.59		0.42		0.27		0.68	0.27		0.16
Index of freezing resistance k		Frozen-thawed in dry air	0.81	0.82	1.00		0.86	0.86	0.98	0.87		0.92
		Frozen thawed in moistifying	0.66	0.77	0.95	0.47	0.52	0.74	0.91	0.62	0.63	0.71
		Frozen thawed in saturation	0.62		0.78		0.44		0.81	0.57		0.41

Note: curing in soil-1 cawhust, at temperature +12℃

strength which varied with times frozen and thawed over again is shown in figures as following.
It is seen in table V that the drop in strength of the stabilized soils has a natural relation with the times of frezen-thawed processing over.

(1) The frezen-thawed resistance of lime stabilized soils basically drops gradually with the increasing of times frozen-thawed. The strength drops abruptly in the beginning at frozen-thawed 3 times over, about 10--20%, and then drop slow down later gradually. The total amount of the dropo in strength at frozen-thawed 15 times over is about 30%. It is seen also from the graphs that the drop in strength will still go on, but decreases in amount more and more small slowly.
The drop in strength of the test roads seems to be on the fast side. For example, the strain of deflection "cup" of a double course lime stabilized pavement measured at Tsoumall River in 1976 was 0.31mm, and it was 0.46mm measured again at the same site in 1981, after the road had been opened to traffic for five years. In fact, the strength had decreased about 48%, but it was still within the allowance for working.

(2) It is seen from tests done, the freezing resistance of lime stabilized gravelly soil is quite better, that of the sandy loam is the next best and that of the clayey loam is relatively poor. But, since the early strength of the lime stabilized playey loam is quite higher, also, the strength, after the stabilized soils have undergone, frozen-thawed processing, is higher than that of stabilized sandy loam too, and on the other hand, the drop in strength, after the soils have been frozen-thawed 6 times over, is undistinguished, therefor, the lime stabilized clayey loam, to be sure, is a kind of material superior for use than the lime stabilized sandy loam, as it is judged by the strength that which is after frozen-thawed processing.

(3) Since the lime stabilization structures have a considerable drop in early strength after freezing-proof agent (Mgcl2) was added into the mixing of them, therefore, we wouldn't recommend to add the freezing-proof agent now, although the adding of the agent had led to an effect to slow down the drop in strength.

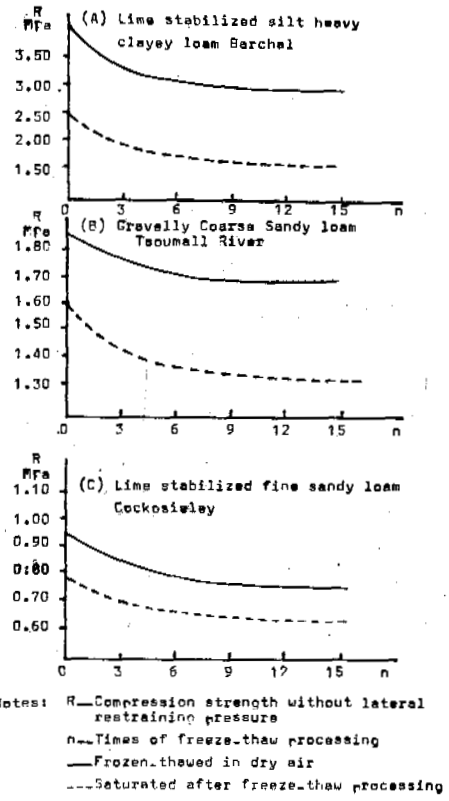

Notes: R—Compression strength without lateral restraining pressure
n—Times of freeze-thaw processing
——Frozen-thawed in dry air
---Saturated after freeze-thaw processing

Fig. 1

(4) The strength of the stabilized soils ceased from developing while the soils are being frozen up. The freezing resistance of the stabilized soils are in proportion to their curing days directly, and the longer they have been cured, the strenger the strength developed.

Hydrostableness

The hydrostableness of the lime stabilization struc ture is expressed by the ratio between the strength of unsaturated soil sample at certain curing period specified and that of the same curing period. The ratio of various soils which is so called as "hydrostableness index, P"is listed in table II. It is seen from table II that the lime stabilized soil structure with higher strength is more hydrostable.

Problems on Swell of Lime Stabilization
It is indicated by swell tests: the swell value in volume of the frozen lime stabilization increases with the increasing of water content in soil. The swell factors in volume for some

soils, while their water contents are 1--2% more than the optimum moisture contents respectively, are as following:

The swell factor for silty heavy clayey loam is 0.7--1.0%, that for fine sandy loam is 0.4--0.7% and that for lime stabilized gravelly soil is 0.1--0.2%.
In the light of above experimental data, it is clear, the influence of the swell on the stability of the whole pavement structure is very light and may be negligible, even the swell is at their utmost limits.

Some Aspects on the Application of Lime Stabilization as a kind of Paving Materials in Permafrost Region of Qingzang Highway

(1) The lime stabilization not only is a kind of materials to be able used for the base course and mat base of asphalt pavement, which is obtainable along the Highway everywhere in site, and it is an ideal material quite better in application comparatively.

(2) It is shown by indices of various lime stabilization on their strength, freezing resistance, hydrostableness and swell, that the lime stabilized gravelly soil and debris soil are more effective than other soils in application. But, as the silty clayey loam posses arelatively higher early strength which would be a favourable factor to put it in use fully by mixing certain amount of gravel (debris) or sandy gravel to improve its freezing resistance. The suitable amount of aggregates to be added in mixing is about 40% in volume.

(3) To plan a rational disposition of time limit for construction and its progress chart is a key link to quarantee fully developing of lime stabilization's strength. By meteorological observations and that of earth temperature within a depth of 0--20cm, it is seen that the ground temperature within the depth of 5--20cm remains at positives during the middle of May to that of October, even though, while negative temperatures may occure at night frequently. Therefore, it is suitable to fix up the time limit of construction in a period, from the beginning of May to that of September.

By the tests in laboratories and the investigations upon the lime stabilized soil base course in traffic operation on the test roads 50km in length, we have seen that the stabilized soil structures in permafrost region on the Plateau were plenty of consolidation and able to solidify out into block.
The pavement, paved with stabilized soil structures, as a whole was quite better in freezing resistance and in hydrostableness, therefore, its strength was able to satisfy the quality requirements in design. It is paved by practice now that the soil stabilization is quite feasible to apply on highway engineering in permafrost region on lateau. This is the conclusion of the author.

REFERENCES

Lanzhou Institute of Glaciology and Geocryology, chinese Academy of Sciences, 1978, Permafrost Soil along the Qingzang Highway.

Ministry of Communications of R.P.C. 1982, Specifcations for construction of lime-soil base course of highway pavement.

INVESTIGATION AND TREATMENT FOR SLOPE-SLIDING OF RAILWAY CUTTING IN PERMAFROST AREA

Wang, Wenbao

Qiqihar Railway Research Institute, Harbin Railway Administration Bureau

SYNOPSIS The slope-sliding is a special type of railway roadbed damages in the permafrost area of the Great Xingan Mountain. Through the exploration and engineering treatment for the sliding damages happened at the site of 440 kilometers of Yalin rail line, this report try to analyse in detail the processes of forming and developing of the damage, and discuss its features and reasons. The propping-seepage ditch of side slope, the block-seepage ditch and drain-seepage ditch compose a complete system and cure the damage permanently. This system possesses the functions of dredging skin-layer water, improving the drain-consolidation of soil, increasing soil strength and directly propping the soil-body of slope. In addition, it also has the action of frost-drain-consolidation. The engineering practice shows that the propping-seepage ditch on side slope is the key measure of treating damage, and its thermal effect does not influence the stability of the structure itself, therefore the method may be used to treat damages in roadbed engineering in permafrost areas.

DESCRIPTION OF THE DAMAGE

The damage section of railway line, from 440K+000M to 400M, is a road cutting, its left is river valley and right is mountain slope. This line runs basically from south to north. With the culvert as the boundary, located at the site of 440K+175M, the whole damage section can be divided into two subsections which are shown in Fig.1.

The first section is located from 440K+010M to 110M, and it is the old damage part. The soil-made cutting at the right side is 5 meters high. The gradient of the side slope is lower than 1:1.75. At the bottom of the slope within the section of 060 M to 110 M, there is a stone-cemented retaining wall; and at the top of the slope, there is a gutter.

Since 1965, two times of grave slope-sliding had occurred in August of 1970 and September of 1972 respectively. About one hundred cubic meters of soil collapsed down, which destroyed the retaining wall, washed it to roadbed and buried rails. In treating, we extended the retaining wall to the site of 010 M. Besides, on the surface of slope, we made the chip-stone checks and the sod bank protection. At the location of 055 M, we also made a dry-laid chip-stone handing ditch for draining the water of gutter. But after that the slope still considerably deformed. In autumn of 1980, the retaining wall in the section from 010 M to 030 M was collapsed.

The second section is located from 440K+240M to 340 M, and it is the late damage part. The soil-made cutting at the right side is 6 to 8

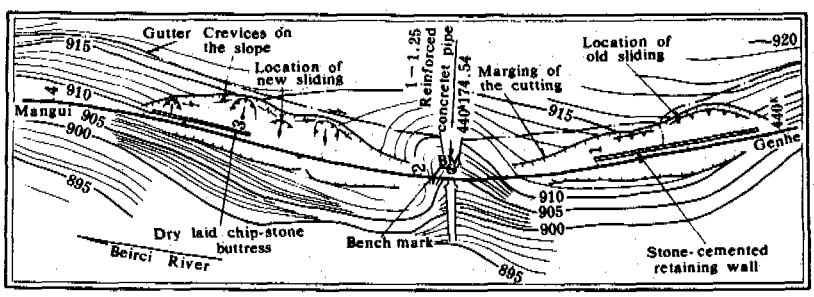

Fig.1 Topographic Map of the Slope-sliding in a Cutting at the Site of Yalin Railroad 440K

meters high, and the gradient of which is about 1:1.70. Along the right side of lateral ditch from 240 M to 290 M, there is originally a dry laid chip-stone platform which is 2.5 meters wide. At the bottom of side slope, there is a dry laid chip-stone bank protection with a height of 1.5 meters, and the upper of which is the bank protection of chip-stone checks. Along the right side of slope bottom, from 229 M to 345 M, there is a trapezoidal and dry laid chip-stone buttress-bottom-guard with a height of 1.5 meters. At the top of cutting, there are cemented chip-stone gutters, which are apart from the top of cutting over 8 meters. Most of the gutters are leaking because of the freezing-thawing action.

In this section, there was no deformation originally, however on September 21 of 1980, as the result of the continuous rain, the glide deformation simultaneously initiated on the slope surface of both the sites of 250 M and 275 M. It seemed being mudflow at the site of 250 M, and the right side rails were buried. At the latter site, it was the plastic sliding, and located on the platform outside of the lateral ditch.

At the site of 250 M, the slide-body was a long belt in shape, with 17 meters long and about 80 cubic meters in volume. The upper of which was wider, with 8 meters in average width, and the front edge of which showed like a tongue in soft-plastic and flowing state. At the upper edge of the slide-body, there was a steep wall with 1.3 meters high and water-seepage in many places. Its bottom was frozen. The thickness of the middle part of the slide-body is about 1.5 meters, and the gradient of its surface is 1:4. A birch on it had been moved about 7 meters. The maximum movement of the body may be up to 10 m.

At the site of 275 M, the slide-body was mound-shaped about 2 meters high and 10 meters wide. Its total volume was about 70 cubic meters. The original dry laid chip-stone bank protection was destroyed. The gradient of upper slide-body was about 1:25. There were crevices in the slide-body, from which water was leaked out, making the ground very moist. The crevices at the top of cutting was continuously distributed from 224 M to 340 M.

After 1981, at the site of 300 m, a new slope-sliding was formed. At the same time, the slope-sliding at the site of 250 M had beed developing. The arc wall at the top of the sliding was continuously nibbled and moved upward. The distance between the wall and gutter was reduced from 4 to 2.4 meters.

On August 18 of 1982, at the site of 300 M, a sliding of side slope suddenly happened. The developing process of the sliding was seen as follows.

In 12:30 of that afternoon, a few of laid stones on bank protection rolled down, which indicated that soil-body of the siding was beginning to creep and slid downward. But this phenomenon was not noted. In 13 o'clock, in the middle-lower part of the sliding, which was a little higher than the dry laid chip-stone buttress, the slope surface was raising. At the same time, mudflow was forming at the water-seepage place on the upper part of the sliding, and finally piled up on the middle platform. Following this, the soil-body at the middle part of the sliding obviously moved down, and its speed gradually increased. The whole slide-body pushed and pressed the lower slide slope and made it continuously raised and tumbled until the side slope was destroyed. After the slide-body (about 60 m) being separated from the slope surface,it rapidly advanced down with a largest speed of 5 meters per minute. Because of the obstruction of the dry laid chip-stone buttress, it was turned to south along the railway line, and finally piled up on the platform which is outside of the lateral ditch. Its front edge moved about 10 meters, and the gradient of its surface was 1:5. If there was no obstruction of the chip-stone buttress, it would had crossed surely the lateral ditch and buried the rails. Besides, the mud-flow directly rushed down to the lateral ditch and filled it up.

The slide-body was 7 to 8 meters wide, 11 to 12 meters long, and its average thickness was one meter. It looked like a inverse trapezoid. The wall of the sliding was one meter high and 15 meters wide, where the places of water-seepage was a wedge-like and raised upward. Because of the lateral press, in the middle part of the slope surface, a soil-ridge, which was less than one meter in height, was raised and buried a temperature observation hole. By inserting a trunck in the sliding we obtained that the depth on its upper edge was 0.8 meters, which was the average thawed depth of the sliding. On the next day, we measured the form of the section which was on the axis of the slide-body, and found that its surface was basically flat with a gradient of 1:4.2. The gradient of the sliding face below the sliding-wall was 1:2.75 (Fig.2). The whole process of the sliding lasted half hour, followed by the upper mud-flow which also lasted about half hour.

ENGINEERING GEOLOGICAL CONDITIONS

The left slope surface of the cutting is covered with broken stone of serious weathering, the outcrop of which extends down to the mountain from the left lateral ditch to the right in the slope of 1:2. The right side of the cutting is the soil sediments, which can be chiefly divided into three layers. The surficial layer is composed of yellowish-brown to greyish- brown sandy loam with 15-30% of crushed stone and gravel. Its water content is usually less than 20%,only on the skin and the gutters used for water-seepage, the water content is up to 25% to 30%. The thickness of this layer is generally less than 2 meters. The bottom of the layer tends to the railway line. In the second layer, the number of sandy-loam minilayers is gradually reduced, but minilayers of sand and gravel are increased. Its thickness is about 3 meters. The layer under the roadbed, the third layer,is chiefly composed of the interlayers and lensed of sand and gravel. The maximum gravel diameter is about 40 millimeters. The total thickness of the three layers is over 10 meters, and all the layers tend to railway line with the grad-

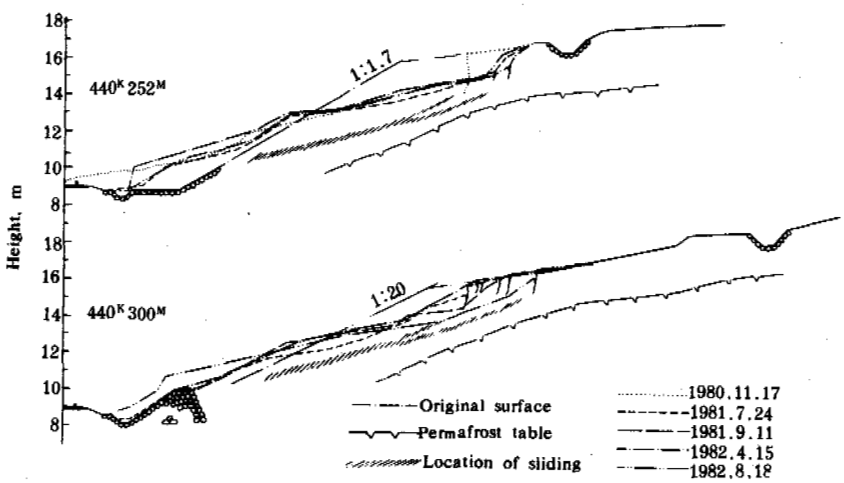

Fig.2 Process of Sliding on Two Slopes

ient of 1:10 to 1:20. The ground is frozen except the layer at the bottom of the slope.

The sandy loam is composed of 38% of gravel, 35% of sand, 25% of silt and 2% of clay. Thus, it is classified as the silty sand with gravels. The plastic limit is 18%; the liquid limit is 25%; the plasticity index is 7. It is from field investigation deduced that the stratum here may belong to the ice-water deposit.

The shear strength tests on the remolded silty sand were conducted. The result show that the angle of friction, ϕ, is less than 10 degrees and cohesion c=0.1 kg/cm^2 when water content W=20%, and they rapidly decrease with water content increasing.

In the warm season, water flows through gutters. Because of the freezing-thawing effect, many places in the gutters were deformed and broken, where water was leaked out from the slope surface. The locations of water-seepage were usually lower than the top of the cutting by 0.6 to 1.0 meters. This was the main water source of causing slope being moist and slope-sliding. The water in the soil also comes from rainfall and thawed snow.

The damage section is located in the central part of permafrost. According to the data obtained from the Mangui Observation Station, the annual mean air temperature is -4.7°C, the annual average thawing and freezing indexes are 1955 and 3600 °C·day, respectively.

The depth of permafrost table is between 1.7 and 2.5 meters at the top of the cutting with vegetation, greater than 2.7 meters on the slope surface without vegetation, and greater than 6.0 meters under the right lateral ditch and on the left side of the cutting.

FEATURES AND CAUSES OF THE SLOPE-SLIDING

Through observation and survey for two years and one time of witness, it is found that the sliding deformation of side slope has the following features and regularities:

1. The deformation of slope surface occurs in the whole warm-season from spring-thawing to freezing, and the process of the deforming is successive, which is showed in Fig.3.

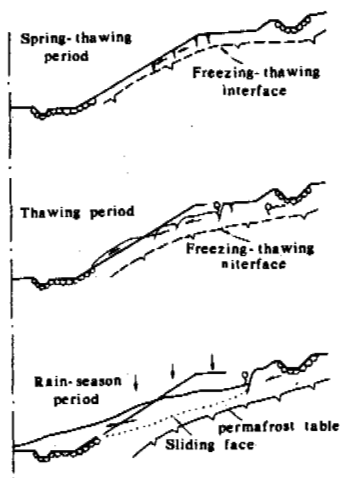

Fig.3 Schematic Drawing Showing the Development of a Slope-sliding

During spring-thawing, along with the gradually thawing of snow and frozen soil, slope deformation is chiefly the creep of surficial layer, which occurs everywhere and frequently. Simultaneously, crevices form at the top and on the slope surface of the cutting. In the warm-season, the layer of thawed soil gradually becomes thick, and the phreatic water and the leaking water from the gutter obviously act on the slope, so that the deformation becomes a small scale of mud-flow, which will form steep ridges at the places of water seepage on the cutting top edge, and continuously nibble and advance upward. Thus the area of the damage will be enlarged gradually. After enlarging a certain scale, and caused by a long time raining, the considerable scale's sliding of side slope may be happened above the freezing-thawing interface. In small water content, the sliding deformation may be showed as a hard-plastic stack sliding plastic sliding or soft-plastic mud-flow, respectively, which are all happened in the shallow layer and seasonally.

2. The deforming firstly occurs at the crevices of the cutting top. Since the thawed snow and surface water permeate into ground, the partial sliding deformation on the slope surface will be happened. When the platform or the water accumulation area are formed in the upper side slope, surface water will gradually permeate into the lower slope surface,which make the strength of the slope greatly reduced and can not bear its self-weight, thus the sliding deformation will be happened on the slope surface in a large scale.

3. The pattern of slope sliding is usually as follows. On the upper, there is an arc steep precipice or a slide-wall with one meter high; below that, there are water seepage exposures; in the middle part of slope surface, it is steps-like because of the breaking and separating of the soil-body; and in the lower part, there is an obvious tongue-like frontier, on which there exist arc wrinkles or crackles.

4. The sliding face is from the slide-wall or crevices on the top of the cutting edge to the lower part of the slope which is higher than the platform about 0.5 to 1.0 meters. Its middle part is controlled by the freezing-thawing interface, but located above it about 1.0 to 2.0 meters.

The side slope is mainly composed of silty sand with gravel, which possesses higher permeability and maintenance of water. It will have higher strength when the water content is lower, and the strength will be greatly reduced when it is rich of water. The existence of this kind of soil is the internal cause of the slope-sliding.

The thawed snow, the shallow phreatic water, and especially the leaking water of gutters are the mainly external causes for the sliding.

Furthermore, both the existence of permafrost and the freezing-thawing circles of active layer and its effect on soil structure and strength make the internal and external causes mentioned above interacted. This brings about the accumulation of the slope deformation and affects the integrity and stability of the soil-body of the slope. Thus, in rain-season, a certain scale of sliding on the slope may be caused and leads to a damage.

TREATMENT MEASURES

The guiding principles for prevention and cure of the slope sliding are: controlling and dredging the surface water and the phreatic water of surficial layer, increasing the degree of drain-consolidation and strength of soil,and constructing supporting structures. The measure, which has all the functions mentioned above, is to make propping-seepage ditches on the side slope surface, which.has been used in the treatment of the sliding discusses here.

The effects of the propping-seepage ditch in treating the slope-sliding in permafrost area are:

1. It directly blocks and dredges the phreatic water of surficial layer, eliminates the erosion action of water to slope surface and reduces the water content of surficial layer of the slope.

2. It increases the degree of drain-consolidation and the strength of soil of the slope.

3. It directly.props the soil-body of slope surface, thus increases its stability and protects the soil-body from sliding down.

4. It partly changes the temperature regime of permafrost and the freezing-thawing interface, which is favourable to the drain-consolidation of the soil-body of slope surface.

The propping-seepage ditch at the side slope, the block-seepage ditch on the top of cutting and other drain-seepage ditchs, form a perfect drain system, which plays a comprehensive effect of eliminating the damage of slope sliding.

TREATMENT EFFECTS

The treating engineering has experienced for four rain-seasons, which proved that the draining effect is good. The deformation and sliding of slope surface have been eliminated. Therefore, it is considered that the application of the propping-seepage ditch to the roadbed engineering in permafrost area is successful.

The observation of ground temperature indicates that the influence of propping-seepage ditch on permafrost is not obvious. It only limitedly increasse the thickness of active layer of the upper slope, which is favourable to the drain-consolidation of the soil. It also indicates that although the propping-seepage ditch is not located in permafrost layer, it still works well and is not destroyed by freezing-thawing effect.

CONCLUSIONS

(i) Using the original measure of dry laid chip-stone bank protection is not effective, the reason is that it is a king

of protectional measure for preventing the slope surface from washing and weathering peeling, and can not bear the frost heave force and pressure of soil. However, although the retaining wall and the dry laid chip-stone buttress are the passive measures, they still can control the area of the damage. The propping-seepage ditch, which has the effects of both drain-consolidation and propping-protection, is a good measure for treating the damage of slope-sliding.

(ii) In the central part of permafrost area, the propping-seepage ditch of side slope only partly changes the planar state of temperature field under slope surface, and its effects of drain-consolidation and propping-protection are identical to those in non-frost area.

(iii) The sliding face is from the place of water-seepage under the slide-wall to the slope surface which is higher than the platform, and the middle part of which is a gentle curved surface. Its gradient of upper part is close to 30 degrees at the upper part, about 12 to 15 degrees at the lower part, and 18 to 20 degrees at the middle part.

(iv) The sliding face is not the freezing-thawing interface, but about 0.8 meters higher than the interface,and it is not a smooth plane, but a layer or a band with the thickness of 0.1 to 0.5 meters.

(v) According to statistics, the sliding deformation usually occurs after a continuous rain about 20 days to one month.

(vi) Because of the thermal effect of the propping-seepage ditch, its foundation can not be set in permafrost layer.Thus, the foundation must be designed big and save enough based on the calculations on its mechanical stability.

ACKNOWLEDGEMENT

The author sincerely thanks Messrs Liu Shenjia, Xie Ruitang and Li Yingwu, who were involved in this work.

MODEL TEST TO DETERMINE THAWING DEPTH OF EMBANKMENT IN PERMAFROST REGION

Ye, Bayou, Tong, Zhiquan, Lou, Anjin and Shang, Jihong

Northwest Institute, China Academy of Railway Sciences

SYNOPSIS Model test is an indoor method used for simulating the temperature field in engineering structure in permafrost region. Contrasted with the engineering in situ the temperature distribution is almost the same with each other. Thus, the calculating formulas of the thawing depth obtained from the model test may be used for the practical engineerings.

MODEL DESCRIPTION

It is well known that there exists the interaction relationship (Ding Deweng, 1979) between time scale factor (C_τ) and geometric factor (C_L) of both the model and actual object namely $C_\tau = C_L^2$ if the model medium tested is the same as the actual one. That is, under this condition, the model temperature is the same as that of the actual object, whereas the time scale depends on the geometric scale. However, if the scale size of model is too small, the time scale is smaller, and then the changing amplitude of boundary temperature of model is much greater in a short time so it is not easy to be controlled. The variation law of model temperature field is also difficultly measured. When the model scale size is too big, the test cycle is long enough and the evaporation of water in model so large that it is difficultly controlled. According to the practice in the cool room, if time scale C_τ between model and the engineering in situ is 1:240, the geometric scale C_L is 1:15.49. So the time scale is one hour in model test equals to ten days in situ.

The model box, 2.2x1.41x2.0 m in size, can be directly assembled in the cool room. It is an insulated and sealed model box and can be devided into three parts, i.e. the temperature controlling chamber of bottom boundary of model, the temperature controlling chamber of top boundary of soil and the model soil chamber. The height of the soil chamber is 0.71 m which is corresponding to the height of foundation soil of embankment in situ. It can meet the needs of annual variation depth in situ. After the soil chamber is filled with earth taken from field, the embankment model is built. The electrical heater is installed in the top-boundary temperature-controlling chamber which is seperated with asbestos boards into five parts, road surface, sun-facing slope, shadow slope, berm of the sun-facing slope and berm of the shadow slope, and covered with rock wool to prevent warm air from rising which causes the surface temperature of emnankment not easy to be controlled (see Fig. 1).

The temperature of boundaries are controlled autometically by the temperature-controlling units. Thermistors are used to measure the temperature of boundaries and the electric heaters and fans at each boundary are controlled by the temperature-controlling units for heating or winding to keep the temperature needed at each boundary.

The temperatures are measured by the Universal Digetal Measuring Apparatus or Long-Figure Autometical Recorder and Thermocouples.

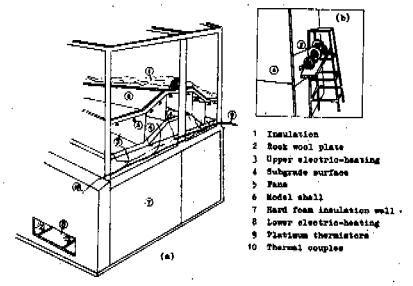

Fig.1 Test Equipment for Embankment Model
a. Before Assembling
b. After Assembling

COMPARISON BETWEEN MODEL TEST AND PRACTICE

In order to prove the accuracy of the test, we carry out the simulating about the temperature field variation of DK0+280 section of testing subgrade engineering on Qinghai-Xizang plateau. The model embenkment consists of two parts, one is the sandy-clay embenkment for simulating the engineering in situ, another is the coarse-grain soil embenkment. And 10 cm thick polystyrene hard foam is placed between them to eliminate the interaction.

Figure 2 shows the section type of embankment

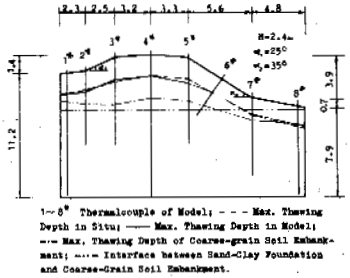

1~8° Thermalcouple of Model; - - - Max. Thawing Depth in Situ; —— Max. Thawing Depth in Model; -·- Max. Thawing Depth of Coarse-grain Soil Embankment; ·-·- Interface between Sand-Clay Foundation and Coarse-Grain Soil Embankment.

Fig.2 Embankment Model (DK0+280, Fenghuo Mt., Qinghai-Xizang Plateau), (m)

and the thawing depth after the model returns to its original condition. The embankment temperature field of model after returning is identical to that in situ. So the design, temperature-controlling instruments, measuring method and accuracy of model are dependable.

ANALYSIS OF TEST RESULTS

The embankment tests are carried out with three different heights, H=2m, H=3m and H=4m, respectively. The embankment section is shown in Fig. 3. The sand-clay and coarse-grain soil embankments for simulating are tested simutaneously for each height. Two different water contents are seperately simulated for each height. Each test continues for 6 cycles so there are 36 cycles totally. During analyzing and calculating the thawing depth of the embankments, the relative ice content, i, is 0.80 for sand-clay and 0.95 for coarse-grain soil.

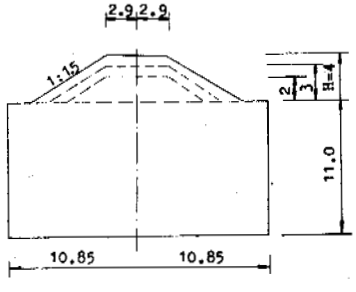

Fig.3 Embankment Section for Model (m)

Calculation of Thawing Depth at Subgrade Center----When the thawing Process Occurs in Embankment

Thermal physical parameters for soil of model are as following:

(i) sand-clay embankment

H = 2m
(1) γ=1650 W1=12 (0-1.0m) λ_1^+=1.37
W2=14 (1.0-2.0m) λ_2^+=1.41
(2) γ=1720 W =14.5 λ^+=1.55
H = 3m
(1) γ=1660 W =11 λ^+=1.32
(2) γ=1720 W =13 λ^+=1.47
H = 4m
(1) γ=1770 W1=11 (0-1.0m) λ_1^+=1.47
W2=13.5 (1.0-2.0m) λ_2^+=1.60
(2) γ=1650 W1=10 (0-1.4m) λ_1^+=1.26
W2=12 (1.4-2.0m) λ_2^+=1.34
section DK0+280
γ=1700 W1=10 (0-1.0m) λ_1^+=1.33
W2=12 (1.0-2.0m) λ_2^+=1.41

(ii) coarse-grain soil embankment

H = 3m
(1) γ=1430 W=4 λ^+=0.58
(2) γ=1400 W=4 λ^+=0.55
H = 4m
(1) γ=1400 W=4 λ^+=0.55
(2) γ=1450 W=4 λ^+=0.60
section DK0+280
γ=1420 W=5 λ^+=0.70

where γ = dry density (kg/m3), W = water content (%), and λ^+ thermal conductivity (kcal/m. hr.deg.).

It is assumed that the temperature on the embankment surface is F2 at the sun-facing slope center, F3 at the shadow slope and F1 at the top surface. According to the observation in situ, the temperature on the embankment surface is about 0.8 times as high as that of both the zero section and cut surface at the same section, but the maximum thawing depth at the embankment center is the same as or little larger than that of them, so that the heat quantity on both sides of the embankment has the influence on the thawing depth at its center. The thawing index at the embankment center might be:

$$S = \left[\left(\frac{F_2+F_3}{2}\right)\beta^2+F_1\right]\tau \qquad (1)$$

where: τ — thawing time lasted (hr.);

$\beta = \left(\frac{H}{b+H\,ctg\,\alpha}\right)$; H — embankment height; b — half width of road surface; α — slope angle. According to the observation data of test, the thawing depths of the embankment are shown in table I and II when the thawing index in equation (1) is taken. Based on them, relationship between thawing index S and thawing depth H is shown in Fig. 4 and 5. From them the following equations are obtained:

(i) sand-clay embankment

$$h = 0.87\sqrt{\frac{2\lambda_1}{Q_1}}\cdot\sqrt{\left[\left(\frac{F_2+F_3}{2}\right)\beta^2+F_1\right]\tau} \qquad (2)$$

(ii) coarse-grain soil embankment

$$h = 1.0\sqrt{\frac{2\lambda_1}{Q_1}}\cdot\sqrt{\left[\left(\frac{F_2+F_3}{2}\right)\beta^2+F_1\right]\tau} \qquad (2)$$

TABLE I

Thawing Depth of Sand-Clay Embankment (m)*

Embankment height (m) \ Thawing index S Sx10^3 (deg.hr.) / Thawing depth (m)	1	2	3	4	6	8	10	12	14	16	18	20	22	24	26	28
H = 2 β^2= 0.115	0.45	0.55	0.65	0.80	1.02	1.12	1.20	1.30	1.45	1.60	1.73	1.77	1.82	1.86	1.90	
	0.40	0.55	0.65	0.77	1.00	1.10	1.20	1.28	1.40	1.50	1.60	1.73	1.79	1.85	1.89	
H = 3 β^2= 0.164	0.47	0.60	0.65	0.70	0.87	1.07	1.20	1.30	1.40	1.55	1.68	1.78	1.88	1.94	1.98	
	0.50	0.60	0.65	0.75	0.88	1.08	1.23	1.30	1.37	1.53	1.65	1.80	1.90	1.92	1.95	1.99
H = 4 β^2= 0.202	0.45	0.55	0.65	0.72	0.85	1.08	1.22	1.30	1.40	1.46	1.57	1.70	1.86	1.95	1.99	2.04
	0.47	0.58	0.65	0.80	1.00	1.20	1.30	1.38	1.46	1.54	1.63	1.75	1.89	1.95	1.99	2.03
DKO+280 β^2= 0.106	0.45	0.55	0.65	0.80	0.97	1.15	1.25	1.40	1.50	1.60	1.70	1.80	1.90	1.95	2.05	

* The thawing index is calculated by equation 1.

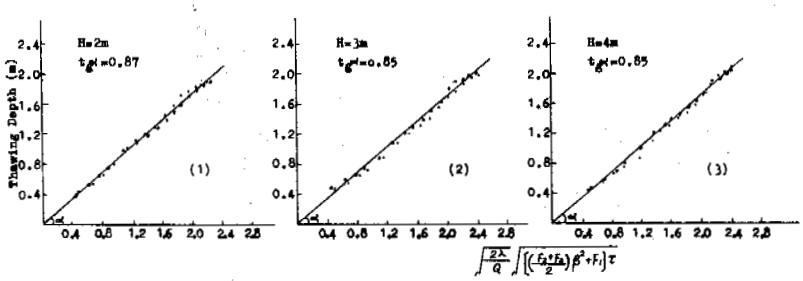

Fig.4 Relationship between Thawing Index S and Thawing Depth h of Sand-Clay Embankment

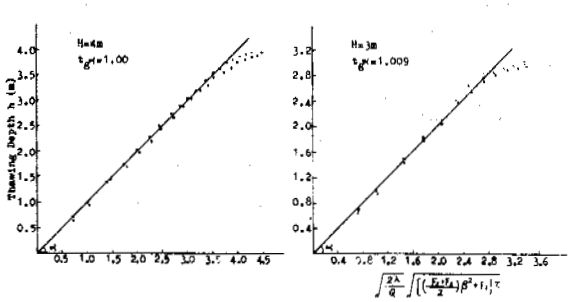

Fig.5 Relationship between Thawing Index S and Thawing Depth h of Coarse-Grain Soil Embankment

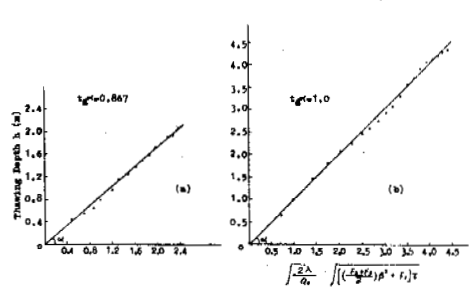

Fig.6 Relationship between Thawing Index S and Thawing Depth h of Understandable Section (DKO+280) Embankment
a. Sand-Clay Embankment
b. Coarse-Grain Soil Embankment

TABLE II

Thawing Depth of Coarse-Grain Soil Embankment (m)*

Embankment height (m) \ Thawing index S / Thawing depth (m)	Sx10^3 (deg.hr.)																		
	2	4	8	12	16	20	24	28	32	36	40	44	48	52	56	60	64	68	72
H = 4 β^2= 0.202	0.7 0.65	1.0 0.95	1.45 1.45	1.75 1.7	2.05 2.0	2.3 2.2	2.5 2.45	2.75 2.65	2.9 2.9	3.05 3.05	3.2 3.2	3.4 3.3	3.55 3.45	3.62 3.55	3.75 3.65	3.8 3.75	3.85 3.8	3.9 3.85	3.95 3.9
H = 3 β^2= 0.164	0.65 0.7	0.95 1.0	1.45 1.5	1.8 1.85	2.05 2.1	2.4 2.45	2.55 2.65	2.7 2.75	2.8 2.85	2.88 2.9	2.92 2.95	2.95 3.0	3.0						
DK0+280 β^2= 0.106	0.65	1.0	1.45	1.8	2.06	2.25	2.45	2.55	2.7	2.9	3.05	3.27	3.55	3.7	3.9	4.05	4.1	4.2	4.25

* The thawing index is calculated by equation 1.

where h is thawing depth at the center of the embankment (m); λ_1 is thermal conductivity of the soil in embankment (kcal/m.hr.deg.); Q_1 is latent heat of thawing of the soil in embankment (Q_1=80γw_1). The other signs are the same as before.

For the irregular embankment section (see Fig. 2, DK0+280), while calculating the value of β the filling height at the road center is taken as the embankment height H, and the average of both slope angles is taken as the slope angle, i.e. $\alpha = \frac{\alpha_1 + \alpha_2}{2}$. After dealing with as above we can use equation 2 and 3 to calculate the thawing depth of the irregular embankment (see Fig. 6).

Calculation of Thawing Depth at Subgrade Center ---When the Thawing Process Occurs in Foundation Soil of Embankment

When the embankment is not very high, the thawing occurs in the foundation of embankment. Such as the coarse-grain soil embankment in the test, when H=2m and H=3m, the foundation soil is thawed. The thermal parameters for coarse-grain soil and foundation soil are as following:

H = 2m
embankment
(1) γ=1450 W_1=3.5 λ_1^+=0.54
foundation soil
γ=1680 W_2=12.0 λ_2^+=1.38
embankment
(2) γ=1430 W_1=4.0 λ_1^+=0.58
foundation soil
γ=1680 W_2=12.0 λ_2^+=1.38

H =3m
embankment
(1) γ=1430 W_1=4.0 λ_1^+=0.58
foundation soil
γ=1680 W_2=13.5 λ_2^+=1.52

embankment
(2) γ=1400 W_1=4.0 λ_1^+=0.55
foundation soil
γ=1680 W_2=12.0 λ_2^+=1.38

From the observation to the test, the initial thawing time of foundation soil τ_1 and accumulated thawing index $F_1\tau_1$ of the embankment surface at this time can be determined. After this time, the difference Δs between the thawing index at time τ and $F_1\tau_1$ is $(F_1\tau - F_1\tau_1)$. Table 3 shows the thawing depth of subgrade at different Δss. Following is obtained from Fig. 7:

$$h = 1.06\left[\sqrt{\left(\frac{H}{K}\right)^2 + \frac{2\lambda_2}{Q_2} F_1(\tau - \tau_1)} - \left(\frac{1}{K} - 1\right)H\right] \quad (4)$$

where $K = \frac{\lambda_1}{\lambda_2}$; h is the thawing depth at the embankment center from the road surface (m); λ_2 is thermal conductivity of foundation soil in embankment (kcal/m.hr.deg.); Q_2 is the latent heat of thawing of foundation soil in embankment, (kcal/m^3); F_1 is the temperature of road surface ($^\circ$C); τ_1 is the total thawing hours in which the embankment at subgrade center thaws completely. It can be determined by equation 2 and 3; τ is the lasting thawing hours of subgrade ($\tau > \tau_1$). The other signs are the same as before.

In order to determine the minimum filling height, Hmin, of coarse-grain soil embankment, in equation 4 the maximum thawing depth H at the embankment center should be Hmin+hn, where hn represents the locally natual depth of permafrost table. Following is obtained after omitting the decimal terms:

$$H_{min} = 8.33hn - \left[(8.33hn)^2 + \frac{khn^2}{0.1272} - \frac{2k}{0.1132} \cdot \frac{\lambda_2 W_1}{Q_2}(\tau - \tau_1)\right]^{\frac{1}{2}} \quad (5)$$

TABLE III

Thawing Depth in Foundation Soil (m)*

Embankment height (m) \ Thawing index difference ΔS / Thawing depth (m)		ΔS = $F_1 - F_{1-1}$ (deg.hr.)										
		2000	4000	6000	10000	14000	18000	22000	26000	30000	34000	38000
H = 2	K=0.3913	2.07	2.12	2.15	2.22	2.28	2.36	2.46	2.57	2.66	2.75	2.80
	K=0.4203	2.04	2.06	2.12	2.25	2.35	2.50	2.60	2.70	2.75	2.80	2.86
H = 3	K=0.3816	3.05	3.10	3.15	3.22	3.27	3.30	3.40				
	K=0.3986	3.06	3.10	3.15	3.20	3.28	3.38	3.45	3.53	3.60	3.68	3.72

* Thawing depth includes the embankment height.

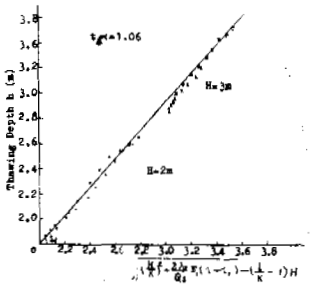

Fig.7 Thawing Depth h at Subgrade Center vs. Thawing Index Difference s

When calculating the minimum height of embankment by equation 5, the value of Hmin may be preestimated, τ_1 is determined by equation 2 or 3, and then Hmin is calculated by equation 5. Finally, τ_1 at Hmin can be determined after several calculations.

For example. in Fenghou Mt. region, Qinghai-Xizang plateau, hn=1.4m, λ_2^+=1.52 and Q_2=14515; for the coarse-grain soil of embankment, λ_1^+=0.58 and K=0.3816, its minimum height of the embankment determined is about 1.5m after calculation. Based on the model test, $F_1\tau - F_1\tau_1$=52000 (deg.hr.) might be determined, which is introduced into equation 5:

$$Hmin = 8.33x1.4 - \left\{(8.33x1.4)^2 + \frac{0.3816x1.4^2}{0.1272} - \frac{2x0.3816x1.5x52000}{0.1132x14515}\right\}^{\frac{1}{2}}$$

$$= 11.662 - 10.255 = 1.41 \text{ (m)}$$

Calculation of Thawing Depth at Slope Toe of Embankment

The berm at slope toe of embankment is commonly filled with sand clay. Following are the physical parameters for the berm at the slope toe on the section of sand-clay embankment:

H = 2m
γ=1680 W=10.5 λ^+=1.36
H = 3m
γ=1680 W=12.5 λ^+=1.43
H = 4m
γ=1790 W=12.5 λ^+=1.58

for the section of coarse-grain soil embankment:

H = 2m
γ=1790 W=10 λ^+=1.35
H = 3m
γ=1790 W=12 λ^+=1.56
H = 4m
γ=1760 W=12 λ^+=1.52

From the test data, the relationship between the thawing index ($\Sigma t\tau$) and the thawing depth h of slope toe (see Fig. 8 and 9) is obtained:

$$h = k_1 \sqrt{\frac{2\lambda}{Q}} \sqrt{\Sigma t\tau} \qquad (6)$$

where h is thawing depth of slope toe (m), λ is thermal conductivity of the soil in berm above 0°C (kcal/m.hr.deg.), Q is latent heat of thawing of the soil in berm (kcal/m), $\Sigma t\tau$ is thawing index of berm (deg.hr.), and k_1 is the correction for the sun-facing slope, shadow slope and soil properties. For the sun-facing slope toe of sand-clay embankment k_1 is 0.80; for the shadow slope k_1 is 0.78; for the sun-facing slope toe of coarse-grain soil embankment k_1 is 0.90; and for the shadow slope k_1 is 0.82

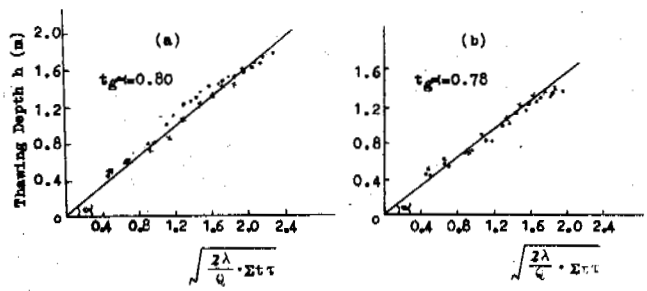

Fig.8 Relationship between Thawing Depth and Thawing Index at Slope Toe of Sand-Clay Embankment
a. Sun-Facing Slope Berm
b. Shadow Slope Berm

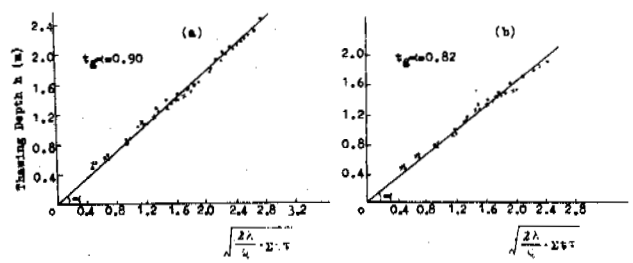

Fig.9 Relationship between Thawing Depth and Thawing Index at Slope Toe of Coarse-Grain Soil Embankment
a. Sun-Facing Slope Berm
b. Shadow Slope Berm

CONCLUSION

The result shows that a lot of data which are obtained difficultly in situ can be got through indoor test. This simulating test can provide the theoretical calculation bases for design and construction in field. But the observation to the water field and water supply is not enough.

REFERENCE

Ding Deweng and Luo Xuepo, (1979). Theoretical bases about model experiment of thermotechnique of permafrost. Scientific News, No.8, 624-632

STUDIES ON THE PLASTIC-FILM-ENCLOSED FOUNDATION OF SLUICE GATES AND ITS APPLICATION

Yu, Bofang, Qu, Xiangmin and Jin, Naicui

Heilongjiang Provincial Institute of Water Conservancy, Harbin, China

SYNOPSIS Based on the field experiments and engineering practice, a new type of soil foundation—The plastic-film-enclosed foundation was proposed and applied to the construction of water conservancy projects. Design and construction procedures of the foundation were described. To verify the reliability of the foundation proposed, three full-scale experimental projects (sluice gates) were constructed in seasonal frost regions. Observation results from the projects show that the proposed plastic film-enclosed foundation can successfully protect the structures from frost damage.

INTRODUCTION

To solve the problems of frost damage encountered frequently in the construction of hydraulic structures, a new type of soil foundation, i.e., the plastic film-enclosed foundation has been intensively studied in recent years. Field investigations and engineering practice proved that adopting this type of foundation could greatly reduce the frost heave of structures. Furthermore, it has the advantage of easy to construct and low cost. It is, therefore, an effective measure for preventing frost damage in the construction of the medium- and small-scale hydraulic projects in cold regions.

DESIGN OF THE PLASTIC FILM-ENCLOSED FOUNDATION

Basis of the design of the foundation

As well-known, frost susceptibility of soil depends chiefly upon moisture, freezing temperature and the type of soil. For a given temperature and soil, the frost susceptibility of the soil can be changed by its moisture condition. Investigations have shown that non or negligible amount of frost heave occurs during freezing when the water content in the soil is less than its initial water content causing frost heave, which is close to the plastic limit of the soil (Wu et al., 1981; Tong, 1982). Based on this fact, the frost heave of a soil can be eliminated or greatly reduced if the water content of the soil can be lowered and kept close to or less than its plastic limit. This is the scientific basis for the design of this type of foundation.

Choice of the enclosing material

At present, various kinds of impermeable films such as plastic film and variety of earth fabrics, which can be used as the enclosing sheet, are available. When choosing the enclosing material, one should consider its durability, impermeability, strength, cost and construction conditions. The commonly commercial polyvinyl chloride (plastic) film has the advantage of low permeability, soft, long running period, low cost, and easy to be constructed, so that it is a better choice to use this plastic film as the enclosing material for the construction of the enclosed foundation.

It is know that plastic film has been successfully used in canal construction for preventing seepage in Sweden and Norway for 30 years.plastic film has also been used in the construction of canal beds to prevent seepage in the Northest-Wang Farm, Beijing for more than 20 years. The buried (used) plastic film was sampled and tested in 1983. Test results (Table I) show that the tensile strength of the film does not decrease but increases after being used for 18 years. It is predicted from the test that its duration of service may be as long as 30-50 years. In addition, application of the plastic film to the hydraulic engineering at northeast and west China showed that its physical and mechanical behaviour could fairly meet the needs of engineering design. Based on these, it is decided to choose the polyvinyl chloride plastic film as the enclosing material (anti-permeating sheet) of the enclosed foundation in this study.

Design of the plastic film-enclosed foundation

To design the enclosed foundation on frost susceptible soils, it is necessary to know the maximum frost depth, maximum frost heave amount and frost susceptibility grade of the subsoils concerned, and then to determine the thickness (H) of the subsoils needed to be enclosed according to the thickness of the frost heaving soil as follows:

$$H \geq h - \alpha\delta \qquad (1)$$

where h is the thickness of the frost heaving soil, δ is the thickness of the foundation slab of a sluice gate and α is a reduction coefficient, having a value of 0.5 for a small slab (with its width less than frost depth) and 0.333

TABLE I

Comparison of the Tensile Strength and Ductility of Plastic Film before and after Being Used for 18 Years

Thickness mm	Tensile strength, MPa		Ductility (%)		Case
	Cross-sectional	Longitudinal	Cross-sectional	Longitudinal	
0.12-0.14	18.87	24.43	261.3	224	B
0.13-0.15	32.60	33.20	8-40	10-190	A
0.14-0.15	18.10	24.27	261.3	264	B
0.14-0.15	27.10	33.20	4-8	4-40	A

Note: B — Before buried in 1965, A — Sampling in 1983.

for a larger slab, respectively.

To eliminate the effect of frost heave caused by the subsoil around the foundation slab, the dimention at the top of the enclosed soil body must be greater than that of the slab base at least by 0.5 m at each side. The lateral surface of the enclosed soil body could be vertical or a slope of 1 on 1,depending upon the excavation stability condition of the pit.

The fill material could be any kind of fine-grained soils. But, its unit weight and water content must be carefully controlled during construction so as to meet the requirement of designed bearing capacity and allowable maximum frost heave of the subsoil.

In addition, it is better to seperate the enclosed soil foundation into several individual layers with plastic films in order to reduce moisture migration (thus the frost heave amount). The thickness of each layer is suggested to be not greater than 0.35-0.5 m.

The design of overlying structure is in principle the same as the design of usual sluice gate.But, the following two points should be taken into consideration: (1) The buried depth of foundation slab can be designed considering only the strength and stability of the structure itself, not the effect of frost heave. (2) Proper anti-frost heaving measures should be taken for the frost susceptible soil behind the side wall of the sluice gate to avoid the gate uplifting due to frost heave.

CONSTRUCTION OF THE PLASTIC FILM-ENCLOSED FOUNDATION

Excavation of pit

Procedure of the pit excavation for this type of foundation is the same as that for usual foundations and replacement. Configuration of the pit should be as accurate as possible, and the exposed surface should be as smooth as possible.

Placing of enclosing sheet

Before placing, the purchased small pieces of plastic film should be glued together with an overlapped width of 5-10 cm. When placing, all joints between the glued films need to be staggered with the width of 15-20 cm. To prevent the film from tearing by stone or tree roots, the exposed surface of the pit should be carefully cleaned before laying films.

Fill construction

The water content of the fill must be carefully controlled to meet the needs of design. Stones, hard piece of soil and other hard materials, which may tear the film, should be taken out from the fill. Fill materials should be compacted layer by layer with its unit weight meeting design value. Inter-layer insulating sheets will be placed during filling with their joints also staggered. As the height of the fill reaches its design value, the outer enclosing sheets are finally enclosed. By now the construction of the foundation is completed.

EXPERIMENTAL PROJECTS

Outline of the experimental projects

To test the reliability of the plastic-film-enclosed foundation, three experimental projects were constructed at Jidong County, Hailin County and Hulan County in Heilongjiang Province,Northeast China. For the convenience of discussion, they are numbered as No.1, No.2 and No.3 in this paper, respectively.

Some of the natural site conditions for the projects are shown in Table II. The dimention and form of the foundations and overlying structures for the test projects are the same. Drawings of the longitudinal section, airview and cross-section of the projects are shown in Figs.1,2 and 3, respectively, in which dimentions are in cm.

The excavation soil after sun-drying was used as fill material. Water contents of the fills are 23.8%, 15.9% and 23% for project No.1,No.2 and No.3,respectively.

Observations on the experimental projects

Frost depth, frost heave amount at ground surface and displacement of structures tested were observed once every five days during freezing period. The depth of groundwater table was also

TABLE II

Site Conditions for the Experimental Projects

Project No.	Annual mean air temp. °C	Minimum air temp. °C	Average frost depth cm	Maximum frost heave amount cm	Groundwater table cm	Type of soil
1	2.3	-38	170	22	-	Clay
2	2.5	-38.8	183	22	70	Loam
3	-	-	-	22	50	Loam

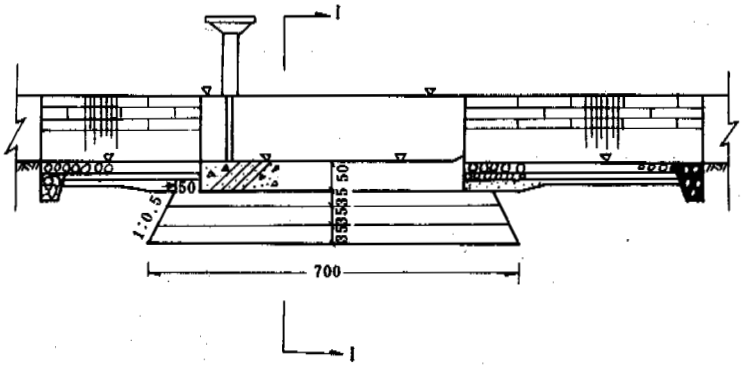

Fig.1 Longitudinal Section of the Experimental Project

∇ — levelling points

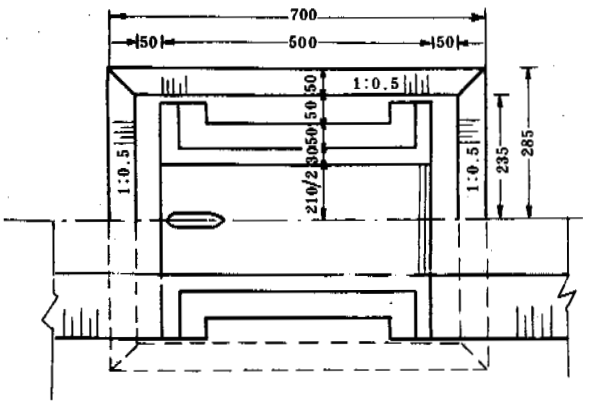

Fig.2 Airview of the Experimental Project

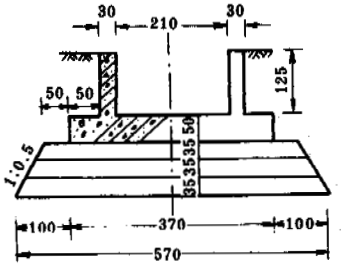

Fig.3 Cross-section of the Experimental Project

observed. A set of thermal couples were placed in the foundation of test project No.1 to monitor the actual frost depth of the foundation.

Observation results and discussion

Variations of the observed frost heave amount at ground surface, the displacement of structures and frost depth with time for the three projects were shown in Figs.4,5 and 6, respectively.

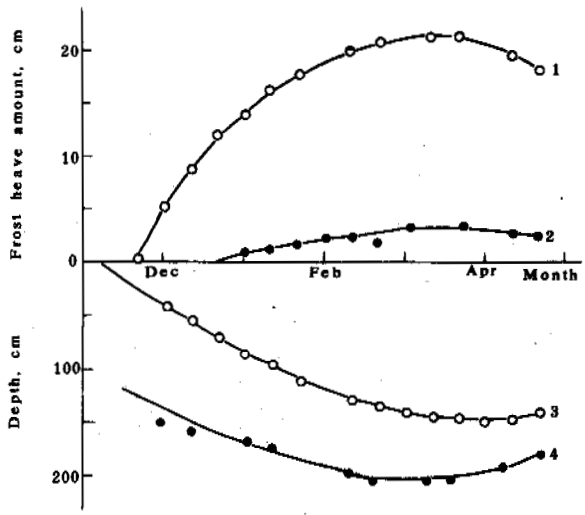

Fig.4 Curves of Frost Heave Amount at Ground Surface (1), displacement of Structure (2), frost depth (3) and Groundwater Table (4) vs Time for No.1 Test Project

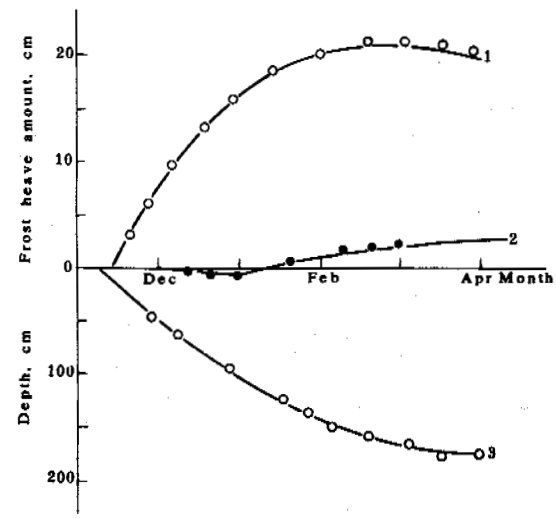

Fig.6 Curves of Frost Heave Amount at Ground Surface (1), Displacement of Structure (2) and Frost Depth (3) vs Time for Nor.3 Test Project

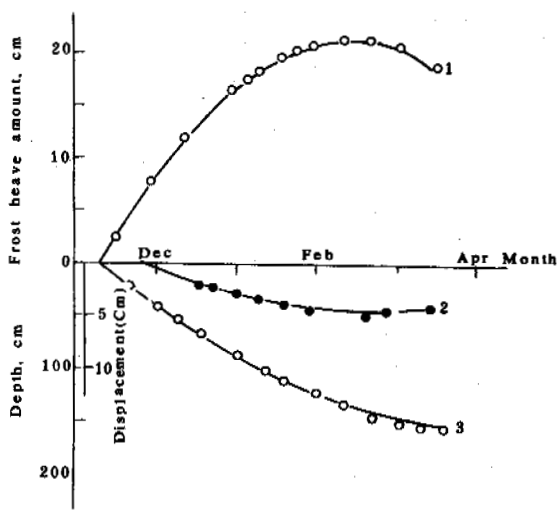

Fig.5 Curves of Frost Heave Amount at Ground Surface (1), Displacement of Structure (2) and Frost Depth (3) vs Time for No.2 Test Project

It is seen from Figs.4 and 6 that while the maximum frost heave amount at natural ground surface reaches up to 22 cm, the frost heave amount is only about 3 cm occuring in the ec-closed foundation soil (fill) with original water content of 23%, which is less than the allowable deformation of the structure. Fig.5 shows that there was no frost heave but a small amount of frost contraction occuring in the foundation soils of No.2 test project, for which the original water content is less than 17%.

Observations on the experimental projects were continuously made for four years. No damage has occured at all the three projects up to day, proving that the new type of foundation is reliable in application to hydraulic projects.

Observation shows that the plastic-film-enclosed foundation also has a certain effect of heat insulation. For example, the maximum frost depth observed at No.1 project is about 17% less than that at natural site.

CONCLUSIONS

Observations on experimental projects show that the plastic-film-enclosed foundation discussed here is obviously effective on anti-frost heaving. Besides, it has the advantage of easy to be constructed and low cost. It is, therefore, recommended that the plastic-film-enclosed foundation can be widely used in geotechnical engineering such as hydraulic project, airport, pipeline, road and civil engineering in cold regions. Test results show that the purchasable plastic (polyvinyl chloride) film can meet the needs of strength, ductility, impermeability and

durability for the foundation design, and it is also cheep, so that it is an ideal enclosing material for construction of this foundation.

REFERENCES

Tong Changjang, (1982). Frost heave behaviour of seasonally active layer in Fenghuo Mt. area on Qinghai-Xizang Plateau. Proceedings of the First National Conference on Glacier and Permafrost, Chinese Science Press,1982.

Wu Ziwang, Zhang Jiayi, Wang Yaqing and Shen Zhongyan, (1981). Experimental studies on frost heave of soils. Annals of Lanzhou Institute of Glaciology and Geocryology, Academia Sinica, No.2, pp. 82-96, Chinese Science Press, 1981.

GEOCRYOLOGICAL BLOCK OF OIL AND GAS PRODUCING AND TRANSPORTING GEOTECHNICAL SYSTEMS

Y.F. Zakharov[1], Y.Y. Podborny[2] and G.I. Pushko[2]

[1]Engineering-geological Department, TyumenNIIGiprogas, Tyumen, U.S.S.R.
[2]EGM Trust, Urengoi, U.S.S.R.

SYNOPSIS Safe running of oil and gas producing and transporting systems in permafrost zone is provided by progress in the design of hydrocarbon projecting and constant engineering-geological monitoring of its condition. To achieve this a special programme accounting to the changes in engineering-geological conditions of construction and running of the system was worked out in West Siberia. At the same time a special service was organized to control the system's condition, to predict and prevent hazardous changes in geological environment.

To provide prolonged and safe running of oil, gas and condensate producing and transporting systems in permafrost regions it is vitally necessary to maintain their design and management according to the requirements of system analysis. From the system analysis point of view oil and gas fields as well as trunk pipelines represent highly organized controlled geotechnical systems (GTS) with numerous feedforwards and feedbacks between their subsystems, blocks and elements. Apart from these internal relations GTS keep various outer connections with natural and manmade environment. In this multypurpose functional complexity of GTS especially in thr Northern regoins of West Siberia the main role belongs to geocryologic block of GTS geosphere. This most dynamic and vulnerable block determines the design character of its second subsystem - technosphere - and regulates the majority of technological and engineering-geological processes in GTS' functioning, which often progresses in extreme conditions. For instance, to prevent thawing of pipeline permafrost bedding and to avoid trunk subsidence it was considered necessary to equilize gas and ground temperatures and to apply special construction techniques and complex cooling devices in gas transport. If due to technological difficulties of GTS functioning prevention of permafrost thawing does not seem possible it will make sense to carry out the controlled thawing which reduces the negative sequences for geological environment and technosphere. Still, to achieve this one has to know the characteristics of geocryologic and geological processes in concrete engineering-geological conditions. Typical elements of GTS geocryological block are ice content, temperatures, seasonal thawing and freezing depth and velocity, cryogenic processes, thickness of permafrost and its interrelation with ground waters, cryopags. During construction and functioning of the GTS all these elements tend to alter under the direct effect of technospheric objects or throught the feedback impact after their action upon geological environment. For example, though it may seem unrelated with permafrost, prolonged exploitation of gas and condensate plays results in their compaction and leads to the subsidence of field's daylight area. This subsidence results in field's flooding and accumulations of water cause permafrost thawing.

When a large amount of heat emmitting con - structions and services (i.e. practically every modern oil and gas producing and transporting system) appears in permafrost zone this process results in largescale transformation of permafrost landscapes during GTS construction which causes permafrost degradation even in low temperature sections. Concrete parameters of GTS geocryologic block elements' alterations depend on engineering-geological structure, landscape and meteorologic conditions of the territory, sterngth of interconnections and character of acting factors. The above - mentioned alterations - as a result of human constructive and productive activity - in turn cause in GTS changes in objects of technosphere and in corresponding geological environmental masses (e.g. ground foundations subsidence, basement disruption, deformation of buildings, service lines and other structures, environment contamination, etc.). To prevent such dangerous effects in running oil and gas producing and transporting GTS the following is beneficial:

a) At a design stage of GTS creation consider its geocryologic block (despite of its complexity) in close connection with its inner and outer feedforwards and feedbacks with other GTS blocks; i.e. the design work should be based on complex engineering-geologic prediction of the consequences of GTS functioning, geocryologic forecast included.

b) While operating GTS constantly receive detailed information concerning current interaction between the objects and geological environment, especially frozen, freezing and thawing soils, which is vittally necessary for careful control over technological and engineering-geological processes.

A. Projection of oil and gas producing and transporting GTS in permafrost zone of West

Siberia is carried out with respect to antropogenic alterations of thermal conditions of seasonal freezing-thawing layer and considerable permafrost temperature rise in geospheres of oil and gas conditioning plants, compressor pumping and booster stations of pipelines, fields and pipelines infrastructure objects and accomodation camps. Initial engineering stage at the abovementioned sites usually causes the disruption of moss-lichen cover (its average thickness in GTS in question reaches I5-20 cm) and soil and vegetation. Thus, ground temperature rises by I-2°C simultaneously increasing thickness of seasonally thawing layer. Changes of permafrost temperatures caused by vegetation disruption is less pronounced Northward. Same thing happens with GTS surface flooding; if such is the case seasonal freezing depth decreases 2,5 times. On the other hand this depth rapidly grows at vegetation removal (low permeability sands freeze down to 4 m, clays and clayey silts freeze down to 3 m) and when high permeability soils are anchored on site by drainage. The latter may result in new permafrost formation - as it happens with drainage - and that must be taken into account while preparing the sites because draining may come out non-effective. Newly formed permafrost of antropogenic origin in South Arctic GTS are normally characterized by high ice content which is excessive compared to permeability of the ground in thaw. Similar changes in permafrost thermal condition result from such inevitable consequences of GTS running as snow removal, compaction or contamination.

Landscape transformation and direct thermal effect of oil and gas producing and transporting systems upon permafrost induces thermokarst and through feedback in GTS threaten system's safety. Most typical thermokarst symptom is funnel around the wellhead and rock settlement near heat emitting objects; also as a result of icy ground thawing caused by antropogenic influence. Maximal funnel dimensions are 6 m in diametre and I,5 m in depth. They may be easily cured by filling in draining earth material.

Because ice content of the majority of permafrost complexes in oil and gas producing and transporting GTS reaches 25-55%, thermal subsidence of thawing ground usually exceeds limits set for the objects of such GTS. That is why in the majority of GTS all the structures are built with preliminary thawing and only on piles foundation.

Since construction and running of the GTS usually change characteristics of surface covers, soil humidity and atmospheric heat exchange conditions, permafrost and seasonal thawing ground tend to heave. Most prominent manifestation of this process can be observed in pulverized loam and sandy loam, where total heave reaches I,5 m, with pile-ground adfreezing exceeding anchoring strength of the pile. To prevent heaving of piled foundations they have to increase the load on them which in turn threatens carrying capacity of the pile when/if unexpected thawing occurs. Sad experience of fighting the problem of foundation heaving on the initial stage of developing Medvejye and Vyngapurovskoye gas fields made it compulsory to take into account engineering-geological forecast at field projecting in West Siberia.

When ice-containing rocks and thawed permafrost freeze once again, thermokarst and heaving at drilling gas wells result in deformation of several drill strings under bearing stress. Curing of such serious problem demanded retrieving string parts and their complex repair. To prevent such dangerous consequences thorough geocryologic analysis of the territory is necessary to choose the location of well clusters, construction and technological changes and time definition for safe well shutdown. Site preparation and digging which brings to daylight area watery pulverized loam and peaty soils of Arctic regions of West Siberia, results in their frost fracturing. Originated thus stress reaches I6700 H (Geocryologicheskiye usloviya ... I983). Besides broken service lines, polygons of fracrures in 3-4 years transform into systems of polygonal wedge ice which hampers running of field and pipeline GTS. The only way to avoid destructive influence of the abovementioned cryogenic processes is tapping of surface and melt water from site.

To explore and develop Northern gas fields of West Siberia they have to build temporary winter roads - "zimniks" with crossings over frozen rivers and brooks. These elements of future GTS bring to life formation of icing in river valleys where it were not observed before. The only way to protect land and river vehicles, fishery and construction is to find less risky patches of the valley.

Landscape transformation in oil and gas producing and transporting GTS in Arctic regions of West Siberia resulting in vegetation layer removal stimulates slope solifluction and even rapid slides of earth masses. Such cryogenic processes normally take place on the slopes 3-4° steep most intensively when the dominant rock is pulverized loam or silty loam. Thawed ground mobility grows Northward and solifluction spreads over less steep slopes. Most effective way to prevent this is to control travel of track vehicles along tundra and to order digging and excavation in summer.

While thawing permafrost in oil and gas producing GTS of West Siberia, Yakutia and Far North of the European part of the U.S.S.R. lose almost completely its carrying capacity thus aggravating deformational properties. In frozen condition rocks are characterized by high values of these properties tens or even hundreds of times exceeding similar parameters of melt ground. The dependance of compression factors of frozen ground on changes of their physical properties and temperature was studied in the works of N.A.Zitovitch (I973) and others. Similar relationship for peaty soils was described by L.T.Roman (I98I).

Long time running of huge oil and gas producing and transporting GTS accompanied by intensive thermal action upon permafrost lessen the thickness of frozen layer which reaches 400 m in certain spots. Besides permafrost thawing due to direct thermal action and indirect influence of antropogenic activity upon subsurface permafrost layers, oil and especially gas extraction removes the screen en route of thermal flow from the depths and violates pressure and temperature balance, thus causing degradation of permafrost from beneath (Baulin, I985). Unfortunately, the

forecast of such slow process cannot yet be calculated with enough accuracy, that is why it is not taken into account at the designing of GTS.

B. To receive on-line information concerning dynamics of the processes in the abovement - ioned GTS for the most effective control over thermal and geomechanical interaction between objects and frozen, thawing and freezing rocks Ministry of gas of the U.S.S.R. organized in West Siberia special service of engineering-geological monitoring (EGM).* The main task of this service, apart from the stated, is generation of scientific recommendations and design decisions on soil rehabilitation, maintenance technology, etc. Among the latter most important are anchoring of the disruptured ground foundations, strengthening of the distorted foundations, contaminated soil rehabilitation, water wells regeneration, etc.
EGM service of technosphere objects comprises measuring subsidence, displacement, bending, curving, fracturing and fissure widening, corrosion degree. Geologic measurements include voltage values, change of phase, cryogenic processes dynamics, changes in strength, deformation and rheology of frozen, thawing and freezing soils and vibration of ground foundations of constructions with considerable dynamic load.
The theory and methodology of a new type of engineering activity - GTS engineering-geological monitoring - was worked out in Tyumen-NNGiprogas (Zakharov, I985; I986). Soviet scientists and technologists consider EGM the only positive way to oppose in full measure the aggravating condition of geological environment or running engineering objects as they grow old.

*Engineering-geological monitoring of the GTS concerns observation, evaluation, analysis and forecast of the current changes in geological environment and their negative consequences for the neighbouring objects; also scientific and technological basis for the accepted preventive and reconstructive measures, other regulations and their realization.

REFERENCES

Baulin, V.V. (I985). Mnogoletnemerzlye porody neftegazonosnykh rayonov SSSR., pp. I-I75. Moskva: Nedra.

Geocryologicheskiye uslovia Zapadno-Sibirskoi gazonosnoi provintsii. (I983)., pp. I-I98. Novosibirsk: Nauka.

Roman, L.G. (I98I). Phiziko-mechanicheskiye svoistva merzlych torfyanych gruntov., pp. I-I32. Novosibirsk: Nauka.

Zakharov, Y.F. Injenerno-geologicheskii monitoring objektov gazovoi promyshlennosti. (I985). Obzornaya informatsiya, ser. "Geol. i razv.gaz.mestorozhd.", vyp.I3, pp. I-77. Moskva: VNIIEGasprom.

Zakharov, Y.F. (I986). Injenerno-geologicheskii monitoring Zapadno-Sibirskich gazopromyslovych i gazotransportnych sistem i puti povysheniya ich nadezhnosti.Obz. inf-ya, ser. "Povysh.econom.obr.", pp. I-36. Moskva: VNIIEGasprom.

Zitovitch, N.A. (I973). Mechanika gruntov; pp. Moskva: Vysshaya shkola.

Author Index